Petros P. Xanthakos

BRIDGE SUBSTRUCTURE AND FOUNDATION DESIGN

- Introduction and General Principles
- Loads and Loading Groups
- Methods of Analysis and Design
- Piers for Conventional Bridges
- Piers for Special Bridges
- Wall Systems
- Abutments
- Footings
- Driven Piles
- Drilled Shaft Foundations
- Prismatic and Linear Foundations
- Strengthening and Rehabilitation

BRIDGE SUBSTRUCTURE AND FOUNDATION DESIGN

TRANSPORTATION STRUCTURES SERIES

Petros P. Xanthakos, Editor

Bridge Substructure and Foundation Design, *Xanthakos*
Bridge Strengthening and Rehabilitation, *Xanthakos*

BRIDGE SUBSTRUCTURE AND FOUNDATION DESIGN

Petros P. Xanthakos
Consulting Engineer

Prentice Hall PTR
Upper Saddle River, New Jersey 07458

Library of Congress Cataloging-in-Publication Data

Xanthakos, Petros P.
Bridge substructure and foundation design / Petros P. Xanthakos.
p. cm.
Includes index.
ISBN 0–13–300617–4
1. Bridges—Foundations and piers—Design and construction.
I. Title.
TG320.X36 1995
624′.257—dc20 94–40837
CIP

Acquisitions editor: Bernard Goodwin
Manufacturing buyer: Alexis R. Heydt
Compositor/Production services: Pine Tree Composition, Inc.

Prentice-Hall, Inc.
A Simon & Schuster Company
Upper Saddle River, New Jersey 07458

The publisher offers discounts on this book when ordered in bulk quantities.
For more information, contact:
Corporate Sales Department
Prentice Hall PTR
One Lake Street
Upper Saddle River, New Jersey 07458

Phone : 800-382-3419
Fax : 201-236-7141
E-mail : corpsales @prenhall.com

Printed in the United States of America

10 9 8 7 6 5 4 3 2 1

ISBN: 0-13-300617-4

Prentice Hall International (UK) Limited, *London*
Prentice Hall of Australia Pty. Limited, *Sydney*
Prentice Hall Canada, Inc., *Toronto*
Prentice Hall Hispanoamericana, S.A., *Mexico*
Prentice Hall of India Private Limited, *New Delhi*
Prentice Hall of Japan, Inc., *Tokyo*
Simon & Schuster Asia Pte. Ltd., *Singapore*
Editora Prentice Hall do Brasil, Ltda., *Rio de Janeiro*

To Eleni and Jay

Contents

Preface

Substructures and foundations constitute formidable components of bridges, and often represent more than half of the total bridge cost. The methods of analysis, design, and detailing are therefore important, and can influence the structural performance and project budget.

The current extensive body of knowledge documents the concerted efforts made to advance the theory and practice of bridge engineering. This progress has encompassed the design of piers, abutments, walls and foundations, and is also evident in our present understanding of soil-structure interaction. Notable improvements are reflected in the use of materials with better physical and structural characteristics, and in the rational and more explicit analysis of structural behavior.

In the present synthesis of the new and old concepts, traditional approaches have been integrated with recently evolved design philosophies, producing design options that enhance the field of structural analysis. Thus, the deterministic methodology represented in the past by the allowable stress design can now be supplemented or completely replaced by load factor design, a statistically-based probabilistic approach. Although many engineers believe that in this merge certain discernible gaps and inconsistencies are bound to remain for some time, the concensus of opinion is that in the field of bridge design there are now more workable alternatives that can be successfully applied to the entire structure and its foundation.

The introduction of load factor design is now a key feature of structural analysis in most areas of structural engineering and in most parts of the world. Whereas it draws from completed research as well as from judgment, it also signifies new provisions and major areas of change. It addresses load and force models, load factors, nominal resistance and resistance factors, limit states, and the soil-structure system on a global basis. A logical extension is the consideration of the variability in the characteristics of structural elements, which is treated as the variability in the loads. Thus, the underlying philosophy moves bridge design toward a more rational and probability-based proce-

dure, although the application of the working stress method is not excluded as an independent option.

The text is developed to achieve the following objectives: (a) present a systems study of substructure and foundation elements; (b) introduce an independent design methodology demonstrating compliance with AASHTO and other relevant specifications; (c) cover both the allowable stress method and the LRFD approach; and (d) include a sufficient number of design examples and case studies that show how to obtain credible solutions.

Chapter 1 provides a general review of pier types, abutments, wall systems, and foundation elements. Structure appearance and esthetics are discussed in conjunction with economic aspects. It appears that the process of selecting the visual characteristics of bridges and substructures represents largely an effort to create forms pleasing to the public in a format described in national terms, although bridge esthetics should also be examined in the context of structural requirements and budget constraints. Chapter 1 is completed with a discussion of subsurface explorations and foundation investigations, review of specifications and standards, and the fundamentals of cost relationship between superstructure and substructure.

Loads and loading groups are reviewed in Chapter 2. A comparison of design loads used in the United States and in other countries shows a broad variability in load models and magnitudes. However, the present AASHTO loads and forces have been expanded by the load models of the LRFD specifications, and these are intended to enhance the live load representation. As a logical exercise of resourceful judgment, the new loads could be scaled by appropriate load factors to be compatible with other load spectra.

Chapter 3 deals with methods of analysis and design, and articulates allowable stress and strength design procedures. A main concern is the reliability and uncertainty in the structural analysis. In routine practice, safety in working stress design is ensured by the application of a single factor of safety, usually taken as the ratio of design resistance to the design load. With the LRFD approach, reliability is ensured by treating both loads and resistances as random variables. Safety in the case is defined in terms of the probability of survival or the probability of failure.

Conventional piers are discussed in Chapter 4. This category includes piers for all-concrete slab bridges, concrete deck bridges on multi-beam systems, two-girder systems with floor beams and stringers, truss bridges, and bridges across waterways and rivers. Although the great variety of functional, structural and geometric requirements implies a corresponding variety of pier forms and configurations, this seeming multiplicity is reduced and consolidated to a discussion of pier selection criteria, load effects, column analysis, seismic considerations, structural capacity under combined axial compression and bending, section analysis, pier frame analysis, and piers integral with the superstructure. This chapter includes also a review of pier protection design provisions in navigable waterways.

Piers for special bridge types are discussed in Chapter 5. Piers and supports for arch bridges usually require the application of deflection theories based on elastic approach combined with appropriate software programs to give the general solution. Towers for suspension bridges are designed as columns to carry the vertical reaction of the cables and as cantilevers to resist any unbalanced horizontal tension. End anchorages are treated as part of the support system. Towers and pylons for cable-stayed bridges comprise the substructure and the tower proper extending above the roadway.

In a cable-stayed bridge the girders are supported at several locations, namely abutments and piers considered fixed and nonyielding supports, and at cable points with the cables emanating from the towers, considered yielding supports. A cable-stayed bridge can therefore be modeled as a continuous beam on both rigid and flexible supports. This articulation excludes an independent analysis of towers and pylons, and hence the design approach is to consider the cables, the stiffening girder and the pylons as an integrated system. Likewise, the design of piers for segmental bridges must distinguish certain functional and constructional requirements. Because these piers must resist final (service) loads as well as loads imposed during the construction stage, pier analysis must consider load and force effects during erection together with their explicit structural action. The review of piers for special bridges is completed with piers for movable bridges, and supports integral with the superstructure such as rigid frame bridges, piers with slant legs, and delta-leg piers.

Wall types are discussed in Chapter 6. They include conventional diaphragm walls built using the slurry trench process, anchored walls, post-tensioned walls, prefabricated panels, bored pile walls, and composite walls. Of special interest are mechanically stabilized earth walls and prefabricated modular walls, now included in standardized configurations in the AASHTO specifications. This chapter discusses also ground movement in excavations, lateral support systems, and design principles of the various wall types.

Chapter 7 reviews abutment types and configurations. These include conventional bridge abutments and wing walls, abutments on artificially stabilized earth walls, and abutments on modular systems. Of special interest are abutments for segmental bridges, arch bridges, and suspension bridges. The seismic design of abutments is discussed in detail in view of the recent guidelines and seismic criteria. Fully integrated continuous construction has been considered and accepted as a standard practice by many states, hence integral abutments are reviewed in the light of current principles.

Chapter 8 is the first of four chapters dealing with bridge foundations. Footings, also referred to as shallow foundations, are considered viable foundation systems, especially where settlement can be controlled or tolerated and where the foundation can be combined with ground treatment to improve soil strength. Of special interest is scour and its origin and effects. Interestingly, the bearing capacity theories first proposed in the 1940's have been expanded to an impressive body of knowledge which includes bearing resistance in soil and rock and a complete analysis of the settlement problem. This chapter is completed with a discussion of the structural action of footings and the associated design requirements.

Driven piles, treated in Chapter 9, have been traditionally a viable system used in deep foundations. As in shallow foundations the body of knowledge developed and disseminated in recent years is impressive and encompasses the soil-pile interaction, pile group action, settlement, and transfer of load. This chapter discusses pile types and selection criteria, design considerations, loads (including uplift and downdrag), and protection against deterioration. The design approach covers both allowable stress and load factor criteria with emphasis on movement and bearing resistance at the service limit state. Design procedures are formulated for axial loads, lateral loads, and uplift for the structural and geotechnical capacity of single piles and pile groups.

Drilled shaft foundations are discussed in Chapter 10. A relevant factor influencing the design is the assessment of construction methods, and practical considerations such as attainment of vertical alignment, quality control, and underreaming require-

ments. A major change in the design of drilled shafts relates to the prediction of the geotechnical strength. This is still the sum of the tip in shaft resistance but more reliance is now placed on the latter because it is mobilized at a much lower vertical movement and before any base bearing is developed. Topics discussed in detail are subsoil conditions favorable for drilled shaft foundations, and a generalized design approach that covers axial load, lateral load, bending moments, buckling of laterally unsupported shafts, structural capacity, and geotechnical strength.

Prismatic and linear foundations, discussed in Chapter 11, have been used in building construction and to a lesser extent in bridge work. The absence of standardized guidelines and explicit design criteria in specifications does not appear to deter their use. A main factor is, therefore, cost efficiency compared with other foundation options. As in drilled shafts, construction considerations and ground conditions can influence the geotechnical capacity, and because these factors can only be lumped in a single parameter, the usual design practice is to assume field quality controls that are explicitly devised and implemented. The procedures for the design of prismatic and linear elements outlined in this chapter reflect a combination of empirical data and theoretical concepts, and covers axial load, bending moments, settlement, and uplift.

Chapter 11 presents a brief outline of strengthening and rehabilitation procedures commonly used in substructures and foundations. In the context of this discussion, rehabilitation means the process of restoring a bridge element to its original service level, and strengthening is taken as an increase of the load-carrying capacity of a bridge component to a service level higher than originally intended.

In the last two decades, the vast development of software programs has changed the analysis of bridge structures significantly. This enhanced capability has, however, increased the importance of a synthesis in the design process. Thus, a profound understanding of structural behavior is the necessary first step in bridge design, and in keeping with this premise direct reference to computer usage has been avoided. Many detailed examples and case studies are included in each chapter, developed and presented as a teaching tool and as design aids to practicing engineers.

Direct reference is made to the AASHTO Standard Specifications of Highway Bridges (1992 Edition), also described AASHTO Specifications or simply AASHTO, and to the AASHTO LRFD Bridge Design Specifications (1994), also referred to as LRFD specifications or simply LRFD.

My deep appreciation is extended to my colleague Theodore Karasopoulos for the review of the entire text and his constructive comments. Special thanks are extended to my wife for the continuous support and help she provided as the book was prepared, including typing and proofreading.

Petros P. Xanthakos

About the Author Petros P. Xanthakos is a consulting engineer in Viriginia. A Ph.D. in civil and structural engineering, Dr. Xanthakos is widely considered a top authority in the technology of bridges and underground construction. His previous books include: *Slurry Walls*, 1980, McGraw-Hill, 680 pp.; *Ground Anchors and Anchored Structures*, 1991, Wiley, 685 pp.; *Theory and Design of Bridges*, 1994, Wiley, 1443 pp.; *Slurry Walls as Structural Systems*, 1994, McGraw-Hill, 855 pp.; *Ground Control and Improvement*, 1994, Wiley, 910 pp.

CHAPTER 1

Introduction and General Principles

1.1 BRIDGE ENGINEERING AND AESTHETICS

Evolvement of Bridge Engineering, Brief Review

Among the early documented reviews of construction materials and structure types are the books of Marcus Vitruvios Pollio in the first century B.C. The basic principles of statics were developed by the Greeks, and were exemplified in works and applications by Leonardo da Vinci, Cardeno, and Galileo. In the fifteenth and sixteenth century, engineers seemed to be unaware of this record, and relied solely on experience and tradition for building bridges and aqueducts. The state of the art changed rapidly toward the end of the seventeenth century when Leibnitz, Newton, and Bernoulli introduced mathematical formulations. Published works by Lahire (1695) and Belidor (1729) about the theoretical analysis of structures provided the basis in the field of mechanics of materials.

Kuzmanovic (1977) focuses on stone and wood as the first bridge-building materials. Iron was introduced during the transitional period from wood to steel. According to recent records, concrete was used in France as early as 1840 for a bridge 39 feet (12 m) long to span the Garoyne Canal at Grisoles, but reinforced concrete was not introduced in bridge construction until the beginning of this century. Prestressed concrete was first used in 1927.

Stone bridges of the arch type (integrated superstructure and substructure) were constructed in Rome and other European cities in the middle ages. These arches were half-circular, with flat arches beginning to dominate bridge work during the Renaissance period. This concept was markedly improved at the end of the eighteenth century, and found structurally adequate to accommodate future railroad loads. In

terms of analysis and use of materials, stone bridges have not changed much, but the theoretical treatment was improved by introducing the pressure-line concept in the early 1670s (Lahire, 1695). The arch theory was documented in model tests where typical failure modes were considered (Frezier, 1739). Culmann (1851) introduced the elastic center method for fixed-end arches, and showed that three redundant parameters can be found by the use of three equations of compatibility.

Wooden trusses were used in bridges during the sixteenth century when Palladio built triangular frames for bridge spans 10 feet long. This effort also focused on the three basic principles of bridge design: convenience (serviceability), appearance, and endurance (strength). Several timber truss bridges were constructed in western Europe beginning in the 1750s with spans up to 200 feet (61 m) supported on stone substructures. Significant progress was possible in the United States and Russia during the nineteenth century, prompted by the need to cross major rivers and by an abundance of suitable timber. Favorable economic considerations included initial low cost and fast construction.

The transition from wooden bridges to steel types probably did not begin until about 1840, although the first documented use of iron in bridges was the chain bridge built in 1734 across the Oder River in Prussia. The first truss completely made of iron was built in 1840 in the United States, followed by England in 1845, Germany in 1853, and Russia in 1857. In 1840, the first iron arch truss bridge was built across the Erie Canal at Utica.

The impetus of analysis. The theory of structures, developed mainly in the nineteenth century, focused on truss analysis, with the first book on bridges written in 1811. The Warren triangular truss was introduced in 1846, supplemented by a method for calculating the correct forces. I-beams fabricated from plates became popular in England and were used in short-span bridges.

In 1866, Culmann explained the principles of cantilever truss bridges, and one year later the first cantilever bridge was built across the Main River in Hassfurt, Germany, with a center span of 425 feet (130 m). The first cantilever bridge in the United States was built in 1875 across the Kentucky River. A most impressive railway cantilever bridge in the nineteenth century was the Firth of Forth bridge, built between 1883 and 1890, with span magnitudes of 1711 feet (521.5 m).

At about the same time, structural steel was introduced as a prime material in bridge work, although its quality was often poor. Several early examples are (1) the Eads bridge in St. Louis; (2) the Brooklyn bridge in New York; and (3) the Glasgow bridge in Missouri, all completed between 1874 and 1883.

Among the analytical and design progress to be mentioned are the contributions of Maxwell, particularly for certain statically indeterminate trusses; the books by Cremona (1872) on graphical statics; the force method redefined by Mohr; and the works by Clapeyron who introduced the three-moment equations.

The impetus of new materials. Since the beginning of the twentieth century, concrete has taken its place as one of the most useful and important structural materials. Because of the comparative ease with which it can be molded into any desired shape, its structural uses are almost unlimited. Wherever portland cement and suitable aggregates are available, it can replace other materials for certain types of structures, such as bridge substructure and foundation elements.

In addition, the introduction of reinforced concrete in multispan frames at the beginning of this century imposed new analytical requirements. Structures of a high order

of redundancy could not be analyzed with the classical methods of the nineteenth century. The importance of joint rotation was already demonstrated by Manderla (1880) and Bendixen (1914), who developed relationships between joint moments and angular rotations from which the unknown moments can be obtained, the so called slope-deflection method. More simplifications in frame analysis were made possible by the work of Calisev (1923), who used successive approximations to reduce the system of equations to one simple expression for each iteration step. This approach was further refined and integrated by Cross (1930) in what is known as the method of moment distribution.

One of the most important recent developments in the area of analytical procedures is the extension of design to cover the elastic-plastic range, also known as load factor or ultimate design. Plastic analysis was introduced with some practical observations by Tresca (1864), and was formulated by Saint-Venant (1870). The concept of plasticity attracted researchers and engineers after World War I, mainly in Germany, with the center of activity shifting to England and the United States after World War II. The probabilistic approach is a new design concept that is expected to replace the classical deterministic methodology.

A main step forward was the 1969 addition of the Federal Highway Administration (FHWA) "Criteria for Reinforced Concrete Bridge Members" that covers strength and serviceability at ultimate design. This was prepared for use in conjunction with the 1969 American Association of State Highway Officials (AASHO) Standard Specifications, and was presented in a format that is readily adaptable to the development of ultimate design specifications. According to this document, the proportioning of reinforced concrete members (including columns) may be limited by various stages of behavior: elastic, cracked, and ultimate. Design is considered as the action phase, and all calculated values derived from action loads are design values such as design bending moments, design axial loads, or design shears. Structural capacity is the reaction phase, and all calculated modified strength values derived from theoretical strengths are the capacity values, such as moment capacity, axial load capacity, or shear capacity. At serviceability states, investigations may also be necessary for deflections, maximum crack width, and fatigue.

Bridge types. A notable bridge type is the suspension bridge, with the first example built in the United States in 1796. Problems of dynamic stability were investigated after the Tacoma bridge collapse, and this work led to significant theoretical contributions. Steinman (1929) summarizes about 250 suspension bridges built throughout the world between 1741 and 1928.

With the introduction of the interstate system and the need to provide structures at grade separations, certain bridge types have taken a strong place in bridge practice. These include concrete superstructures (slab, T-beams, concrete box girders), steel beam and plate girders, steel box girders, composite construction, orthotropic plates, segmental construction, curved girders, and cable-stayed bridges. Prefabricated members are given serious consideration, while interest in box sections remains strong.

Bridge Appearance and Aesthetics

Grimm (1975) documents the first recorded legislative effort to control the appearance of the built environment. This occurred in 1647 when the Council of New Amsterdam appointed three officials. In 1954, the Supreme Court of the United States held that it is

Typical pier types that satisfy the warrants for construction at grade separations are shown in Figure 1–1. The general proportions and structure appearance are intended to give a pleasing scheme. Note that in all instances the bottom pier wall is extended 2 feet 4 inches minimum above the finish grade, and the minimum width of any pier cap is 2 feet 6 inches. This minimum dimension should be followed unless additional width is needed for the bearing seats.

Most engineers find the trapezoidal types shown in Figure 1–1(a) particularly pleasing and aesthetically adequate. In most grade separations, a pier type with two to four columns should accommodate the superstructure width. However, if the pier width exceeds 56 feet, additional columns should be considered. Trapezoidal piers are recommended with standard vaulted abutments (See also subsequent sections).

The hammerhead type shown in Figure 1–1(b) is often used with the standard pile bent abutment. Useful criteria are as follows:

- The single hammerhead type should be chosen with ratios $H/V \leq 2.25$.
- The double hammerhead type should be chosen with ratios H/V between 2.25 and 3.0, and with maximum $H = 40$ feet.
- The multiple hammerhead with three columns is recommended if H is in the range 40 to 54 feet, whereas the four-column pier is recommended if H is in the range 54 to 70 feet.

These criteria are based on V being in the range 13 to 17 feet, and for any extreme heights the ratio H/V should be reevaluated according to the design requirements.

Round and square columns. Piers with round and square columns have been used particularly in the past, the main reason being simplicity in detailing the reinforcement and the use of standard forms. Piers also may be detailed without cantilevered caps. Introducing cantilevers in the cap reduces the overall pier length and footing. The cantilever is also intended to reduce column distance in the pier frame and balance bending moments, although in some instances the cantilever moments may control the design.

Waterway Crossings

For waterway crossings, bridge designs should have reinforced concrete piers that can accommodate the practical site conditions. Special pier types should be considered at bridge sites that lend themselves to special architectural treatment.

On usual stream crossings, the solid pier can be used. The sides of solid piers up to 15 feet high may be straight, and the sides of those over 15 feet high may be battered. The minimum width at the top of a solid pier should be 2 feet. If the bearing seat requirements result in a wider cap, the design can be accommodated by a modified hammerhead pier; a wider cap is used, usually with cantilever as in the single hammerhead pier of Figure 1–1(b), with a narrower solid stem below. The ends of pier stems usually are rounded if the pier is located in the main stream.

For river crossings and major waterways, suitable pier types are shown in Figure 1–2. The pier type shown in Figure 1–2(b) is considered practical for low river heights, whereas the hammerhead type shown in Figure 1–2(a) is economical for high river clearance. A multiple-column pier such as the one shown in Figure 1–2(d) is practical on wide bridges where debris collection is not a problem. Invariably the hammerhead and

within the power of the legislature to determine that communities should be attractive as well as healthy, spacious as well as clean, and balanced as well as patrolled. The Environmental Policy Act of 1969 directs all agencies of the federal government to identify and develop methods and procedures to ensure that presently unquantified environmental amenities and values are given appropriate consideration in decision making along with economic and technical aspects.

Although in many civil engineering works aesthetics has been practiced almost intuitively, particularly in the past, bridge engineers have not ignored or neglected the aesthetic disciplines. Recent research on the subject appears to lead to a rationalized aesthetic design methodology (Grimm and Preiser, 1976). Work has been done on the aesthetics of color, light, texture, shape, and proportions, as well as other perceptual modalities, and this direction is both theoretically and empirically oriented.

Aesthetic control mechanisms are commonly integrated into the land-use regulations and design standards. In addition to concern for aesthetics at the state level, federal concern focuses also on the effects of man-constructed environment on human life, with guidelines and criteria directed toward improving quality and appearance in the design process. Good potential for the upgrading of aesthetic quality in bridge superstructures and substructures can be seen in the evaluation of structure types aimed at improving overall appearance.

Commentary. It appears that the process of selecting the visual characteristics of bridges and substructures is related largely to the effort to create forms pleasing to the public in a format described in rational terms. However, bridge aesthetics is not an isolated concept, and thus it should be examined in the context of structural requirements and budget constraints. In addition, engineers should also examine utilitarian aesthetics, which is a composition of physical factors and visual design aspects. With bridges, these considerations include location, site features, alignment, roadway details, bordering conditions, vistas and views, and the presence of open space and man-made complexes.

With substructure types certain common ideas are inherent in most choices. Tentatively, these are structure lightness and smooth lines, undistorted appearance but one that gives the composition of strength and structural adequacy, and a synthesis that considers harmony with the surrounding environment. Environmental fitness does not mean only physical harmony, but implies compatibility with the foundation conditions, wind forces, temperature variations, and the many factors that influence substructure design.

1.2 PIER TYPES

General

The common practice today is to build bridge piers with reinforced concrete, for reasons probably of economy and aesthetics. In some instances, innovative designs have been introduced and consist of segmental and posttensioned cast-in-place piers, but most states favor reinforced concrete piers in various configurations.

Piers are intermediate vertical supports that perform two main functions: transfer all vertical loads to the foundation, and resist all horizontal and transverse forces acting

on the bridge. Superstructures are normally placed on bearings that sit on pier caps and are capable of transmitting these forces. These connections can be fixed or expanded. In some instances the pier and superstructure may have a continuous connection with adequate reinforcement specially arranged to make framed corners. Alternatively, the pier can be cast monolithically with the superstructure yielding an efficient design where the frame incorporates a substructure stiffness that reduces superstructure moments. Monolithic construction reduces also the large substructure moments that result from a free-standing cantilever support, because a pier with moment restraints at top and bottom will have an inflection point where there is reversal of the bending moment direction.

Grade Separations

The design of grade separation is largely governed by bridge design standards relating to horizontal alignment and profile, clearances, location of substructure elements, roadway cross section, and framing plan. Bridges over waterways are governed mainly by vertical clearance, pier location, and horizontal clearance. Bridges in rural areas follow the geometric configuration of the main highway.

Various types of structures can be used to separate the grades of two intersecting highways, roads, or a highway and a railroad. The most suitable type should give the minimum sense of restriction since drivers usually react to sudden, erratic changes in speed and direction. Structures that avoid these problems have liberal clearance on the roadways at both levels. Thus, piers, abutments, walls, and the like are suitably offset from the traveled way. The structure should also conform to the natural lines of the roadway approaches in alignment, profile, and cross section. Although this relates to many variables, it does not preclude standardization, particularly in substructure location and type of structural element.

Typical examples of grade separation structures are single span bridges with full abutments, an arrangement generally pleasing and offering little sense of restriction; and bridges with open-end spans, in lieu of solid abutments and wing walls, with one, two, or three intermediate piers depending on the width of the median and on horizontal clearance requirements. The resulting scheme is a continuous superstructure or a series of simple spans.

Both AASHTO and state statutes have an explicit policy regarding vertical clearance. All new structures spanning the Interstate and Primary Systems must be proportioned to furnish a minimum vertical clearance of 16 feet 3 inches. Bridges spanning other systems must provide a minimum vertical clearance of 14 feet 6 inches. Through highway trusses must provide a minimum vertical clearance of 17 feet 3 inches. Structures over railroads must have a vertical clearance of 23 feet between the top of the rail and the underside of the deck.

Most states require a horizontal clearance between the right edge of through pavement and adjacent pier or abutment of at least 30 feet. The only exception to this policy is for very high unit cost bridges resulting from either extreme skews or from railroad loading. The minimum horizontal clearance between the left edge of pavement and adjacent pier on divided highways with medians ≥ 64 feet is often 30 feet. For medians less than 64 feet, the pier can be placed at the center of the median. Interpretation of these guidelines may result in a two-span structure with semifull abutments, or in a four-span structure with open-end bents.

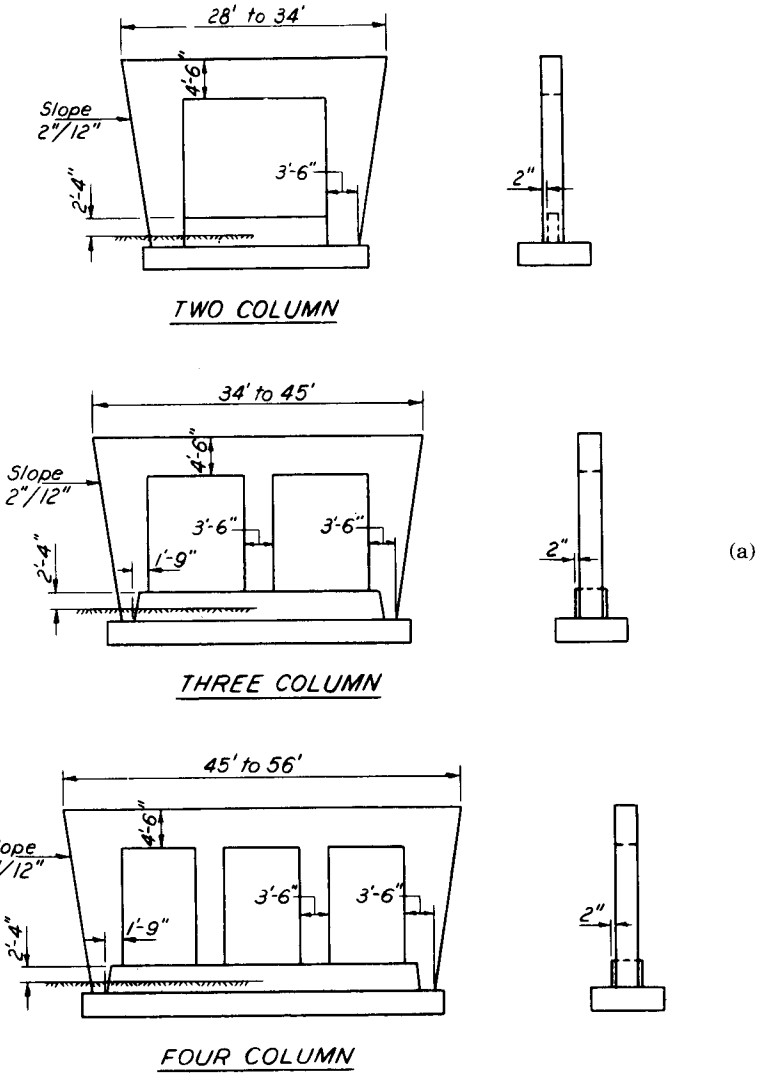

(a)

Note: For widths greater than 56 feet add columns as needed.

Figure 1–1 Typical pier types and proportions for grade separation structures; (a) trapezoidal piers; (b) hammerhead types. (*Source*: State of Illinois)

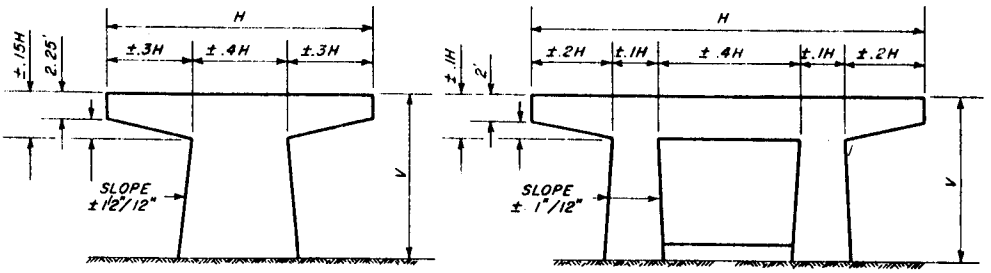

SINGLE HAMMERHEAD

STD. P-2
USE ONLY WHEN RATIO H/V ≅ 2.25

DOUBLE HAMMERHEAD

STD. P-3
USE WHEN RATIO H/V IS BETWEEN 2.25 AND 3.0 WITH MAX. H = 40'

(b)

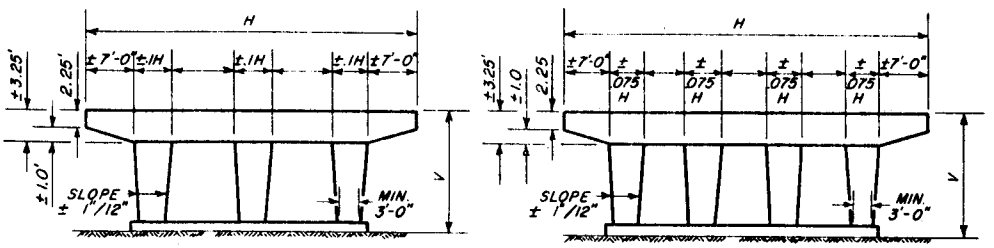

MULTIPLE COLUMN (3)

STD. P-5
USE H > 40' TO 54'

MULTIPLE COLUMN (4)

STD. P-6
USE H > 54' TO 70'

NOTE: RATIO'S BASED ON V OF 13'-17'
FOR ANY EXTREME HEIGHTS (V) THESE
RATIO'S SHOULD BE USED WITH CAUTION.

Figure 1–1 *(continued)*

multiple-column piers require a cap to receive and transfer the loads from the superstructure. Where the design selects a monolithic construction, pier caps must transfer moments to the columns by torsional action. With multigirder superstructure, more than one girder is framed into the cap or cross girder, hence the associated action requires a complex torsional analysis. The circular shaft pier shown in Figure 1–2(c) may be used where space limitations preclude other pier types, and provided the single-column substructure can ensure stability in both directions.

For high piers, consideration should be given to a battered shaft or to a stepped shaft as shown in Figure 1–2(e). However, pier stems with variable moment of inertia may complicate the analysis because of the difficulty of computing critical buckling

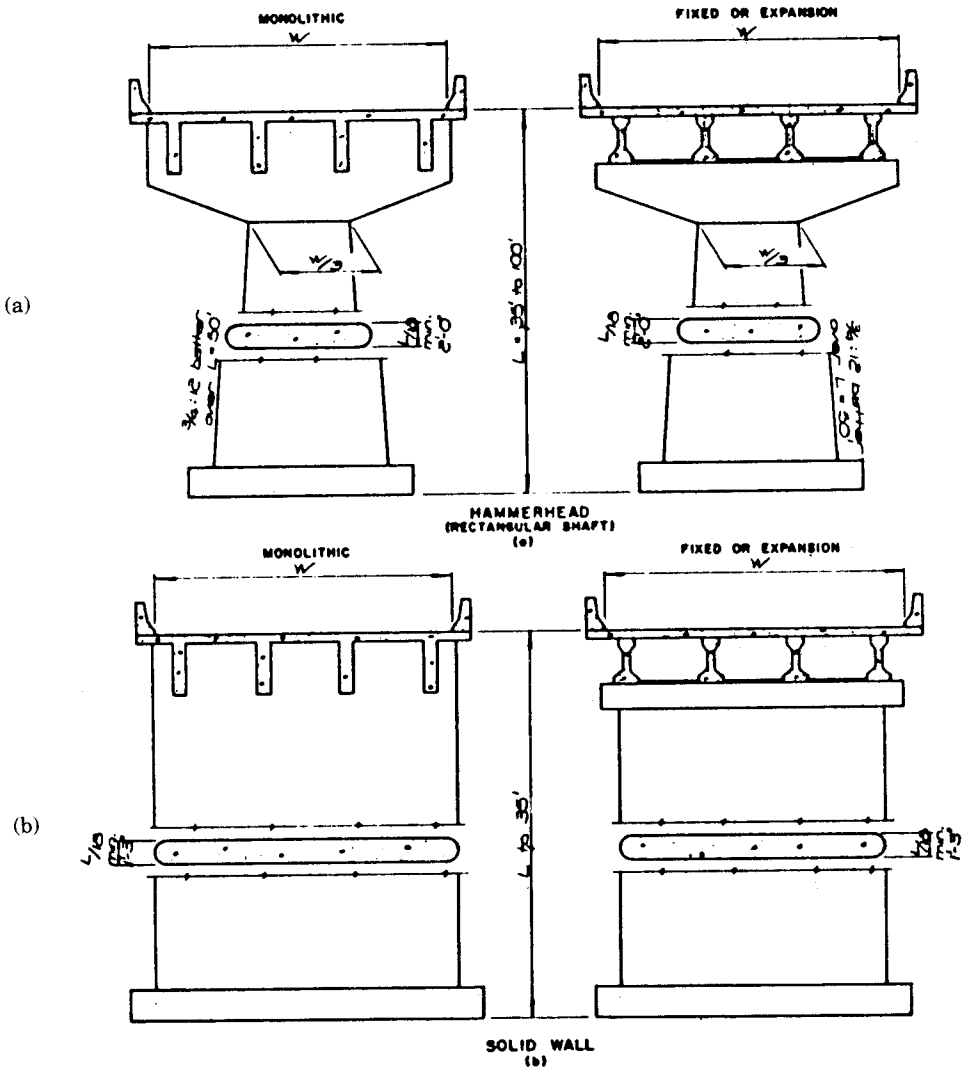

Figure 1–2 Typical pier types and configurations for river and waterway crossings.

loads, although they are more economical. Multistory frame piers offer good options for high piers, and should be considered for heights in excess of 100 feet.

For low and long bridges across waterways, a common pier is the pile bent. This combination results in economical designs, especially if the foundation cost justifies short-span structures.

Commentary

The dimensions at the bottom of the pier required for stability usually are larger than the top dimensions, resulting in pier sides that are appropriately battered. Normally the batter varies from 1/4 to 1 inch per foot.

The solid pier resists the forces acting on it by its massive configuration. Its design and construction is relatively simple, and the minimum required steel reinforcement is

(c)

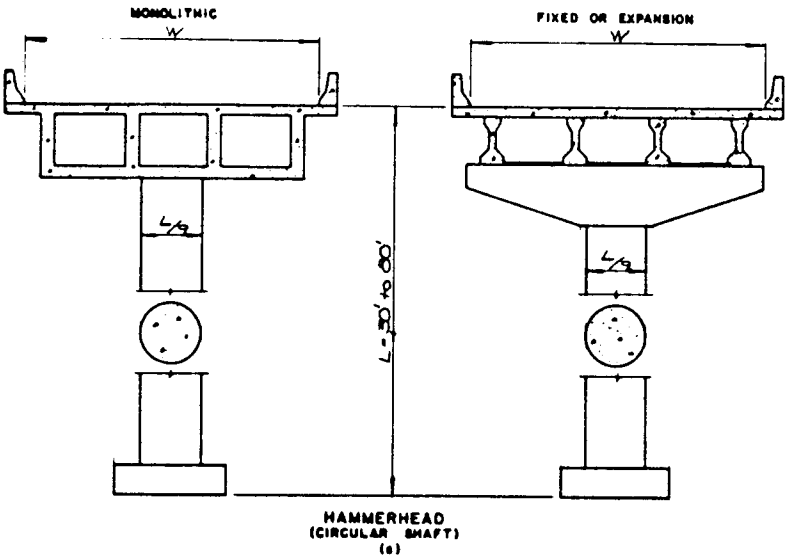

(d)

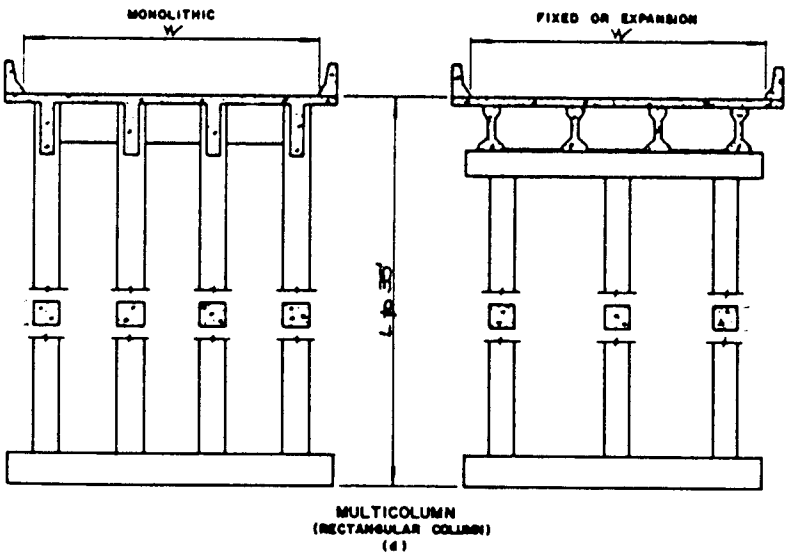

Figure 1–2 *(continued)*

controlled by applicable specifications. The main reinforcement consists of vertical bars placed along the perimeter to resist cantilever moments induced by forces acting at the top, perpendicular to the pier. Horizontal steel is provided to satisfy temperature and shrinkage requirements. The formwork is simple and economical, and allows rapid construction. Although the solid wall pier is practical for low heights, usually up to 25 feet, it has been used for taller structures. Where these considerations are not justified, the single hammerhead may be selected. This type can be used with superstructures con-

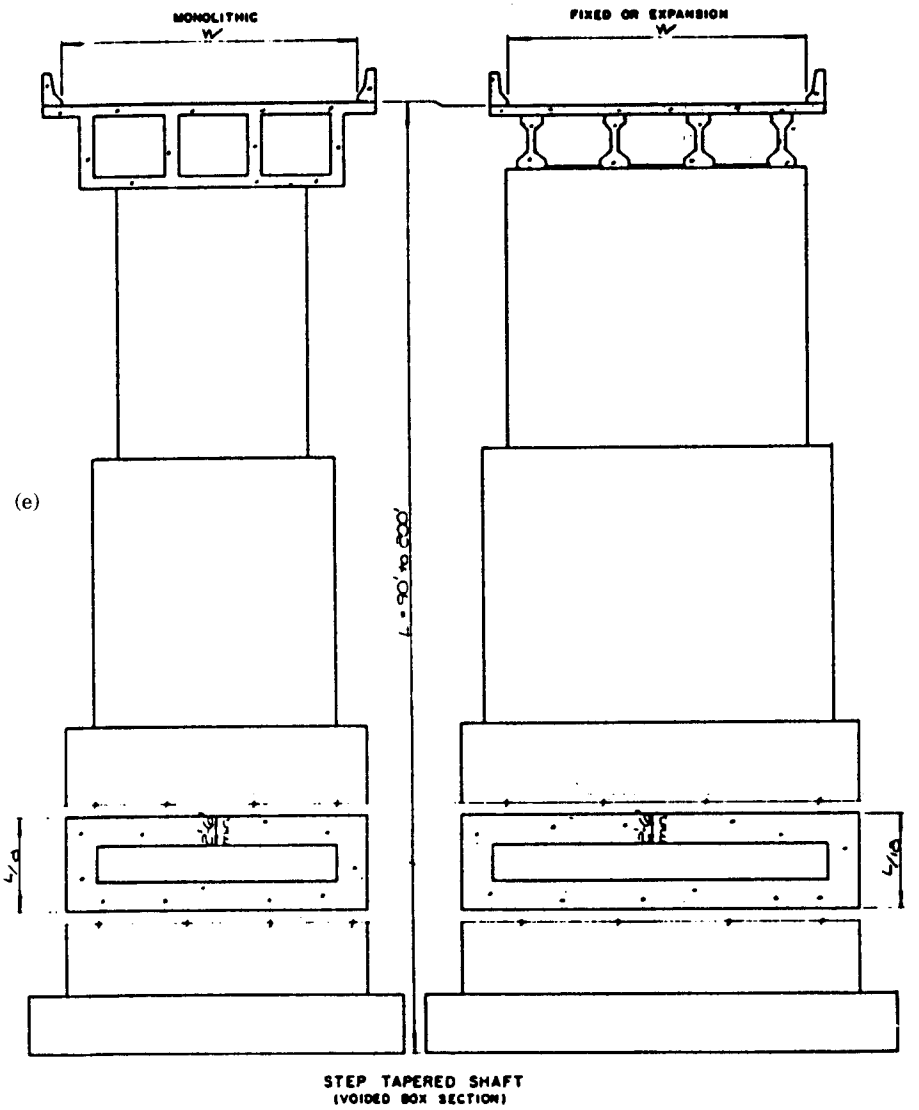

Figure 1–2 *(continued)*

sisting of multiple girder systems or two girders and two trusses. In the latter case the cantilever moments and shears are much higher.

Reinforced concrete rectangular shafts are more effective in terms of structural capacity than circular shafts, particularly when designed to resist moments, hence they work well with monolithic construction and rigid frames. There is some contention that circular shafts in rigid frames tend to attract more moment because of their stiffness, but lack the configuration to develop adequate resistance. However, they have certain advantages, such as ease in forming and additional confining strength associated with spiral reinforcement. The close spacing of spirals also ensures ideal buckling strength characteristics, and this is a definite advantage in resisting earthquake forces.

The dimensions and shape of a footing or pile cap for a hammerhead pier must be

selected to ensure stability in both directions. The main reinforcement is horizontal steel at the top of the head to resist cantilever moments and stirrups to resist shear. Vertical steel along the periphery of the shaft is also provided, treating the member as a tied column subjected to axial load and moments in both directions.

The hammerhead with a single circular shaft shown in Figure 1–2(c) has been found practical in California and other states, particularly in access ramps (entrance and exit) of complex interchanges. A popular design is the monolithic construction where circular shafts are combined with concrete box girders in the superstructure. With curved bridges, stability is enhanced in the transverse direction by the global resistance to overturning afforded by the curved plan of the piers. For very high bridges, such as in canyons, straight rectangular pier shafts are commonly integrated with the superstructure. Because of their height and slenderness, these piers can deflect with the superstructure while it expands and contracts as cantilevers restrained at the top and bottom; hence the prevailing mode of failure usually is associated with buckling under axial load.

Where the foundation conditions permit, or where the distance between columns is appreciable, the columns may rest on individual footings. Individual column footings can be designed for the actual moment and load effects induced in the columns, but the resulting scheme is better if the ground offers sufficient stiffness to justify fixed conditions at the base of the column.

In certain pile foundations, the piles can be left extended above ground to be connected with a reinforced pile cap (pile bent piers). These piers are economical for moderate heights and nominal transverse forces. Some of the piles can be battered for better resistance. Appearance and strength are enhanced if the piles are encased in concrete. Pile bent piers are often used with trestles, and are found useful for highway crossings over swamps, stagnant waters, and shallow waterways and lakes. In these cases superstructure-substructure interaction and cost optimization usually results in a bridge with relatively short spans.

Piers for Segmental Bridges

Segmental concrete bridges are covered in the 1989 AASHTO "Guide Specifications for Design and Construction of Segmental Concrete Bridges." This document is comprehensive in nature and represents several new concepts that may be considered as a significant departure from previous design and construction provisions. A complete treatment of segmental bridge construction is given by Podolny and Muller (1982). The topic is brought up to date by Xanthakos (1994a).

Segmental bridges require special pier types and foundations, particularly for spans erected by the balanced cantilever method. The substructure commonly consists of single shafts, double shafts, and moment-resistant piers. Both resistance and elastic stability of piers during erection require special analysis, and temporary piers or temporary strengthening of the permanent piers are commonly used singly or combined to satisfy construction requirements. However, the choice of piers that have adequate stability without temporary aids is generally favored. Piers of a box section, or twin flexible legs, either vertical or inclined, are equally desirable.

The use of full continuity in the superstructure means that the design must include features that allow for volume changes at the supports (shrinkage, creep, and thermal expansion). For example, segmental bridges on piers with flexible legs can accommodate full deck continuity and also provide frame action between deck and piers

without inhibiting free expansion or overexerting pier strength. Vertical parallel legs may be used on multispan structures since their additional flexibility can accommodate horizontal displacements. For longer structures, elastomeric bearings are used to enhance horizontal movement.

If single slender piers in the finished structure are designed solely for final bridge loads, they may not be adequate to resist unsymmetrical moments during cantilever construction, or with unbalanced segments and erection equipment. This implies that sophisticated temporary shoring is commonly needed, and at considerable cost. In some instances, the stability of the cantilever is ensured by the gantry used for placing the segments.

With double piers, the substructure elements consist of two flexible legs usually supported on a common footing. During construction, stability is maintained with relatively few additional measures and some extra bracing between the slender walls to prevent unstable conditions.

Unbalanced moments must be resisted at the pier by means of a temporary vertical prestress between the deck and the pier cap intended to develop a rigid connection. Where the ratio of span length to pier height is favorable, the rigid connection and the resulting frame action may be introduced permanently.

Piers for segmental bridges are not required to have solid massive sections. In fact, a box section such as the one shown in Figure 1–3 may be structurally more effective and also more economical. In some cases the tubular section can be replaced by an I-section, but caution is indicated to ascertain that the reduction of the torsional resistance is inconsequential. In other cases it may be desirable to precast the pier in tubular segments that are prestressed vertically to each other as well as to the foundation.

With continuous structures rigidly connected to short piers, length changes of the deck are combined with the effects of longitudinal prestressing to produce considerable moments eventually transmitted to the foundation. This action reverses the advantage of rigid superstructure-substructure attachment and suggests the use of supports that permit unrestricted longitudinal movement of the superstructure (neoprene pads, teflon, etc.). However, it is still necessary to ensure stability during cantilever construction. (See also Section 5.4)

Where clearance requirements permit, it is more economical to use a pier with inclined walls in order to reduce the moment eventually transmitted to the foundation. With the legs hinged at the superstructure and converging near the foundation level, the moments tend to diminish so that the load distribution is essentially uniform and occurs as a vertical reaction. Likewise, longitudinal forces on the superstructure are converted into axial forces (tension on one leg and compression on the other) as shown in Figure 1–4(a).

Another pier type suitable to cantilever construction involves a moment resisting system of two neoprene bearings as shown in Figure 1–4(b). Piers with double bearings respond in much the same way as piers with two legs. This arrangement ensures the benefits of pier rigidity during construction and allows free expansion of the completed structure.

Cable-Stayed, Suspension, and Movable Bridges

Cable-stayed bridges. Piers for this bridge type can have a configuration similar to pier types discussed in the foregoing sections for the portion below the superstructure, with a single or two vertical cantilevers to support the cable system. These piers are

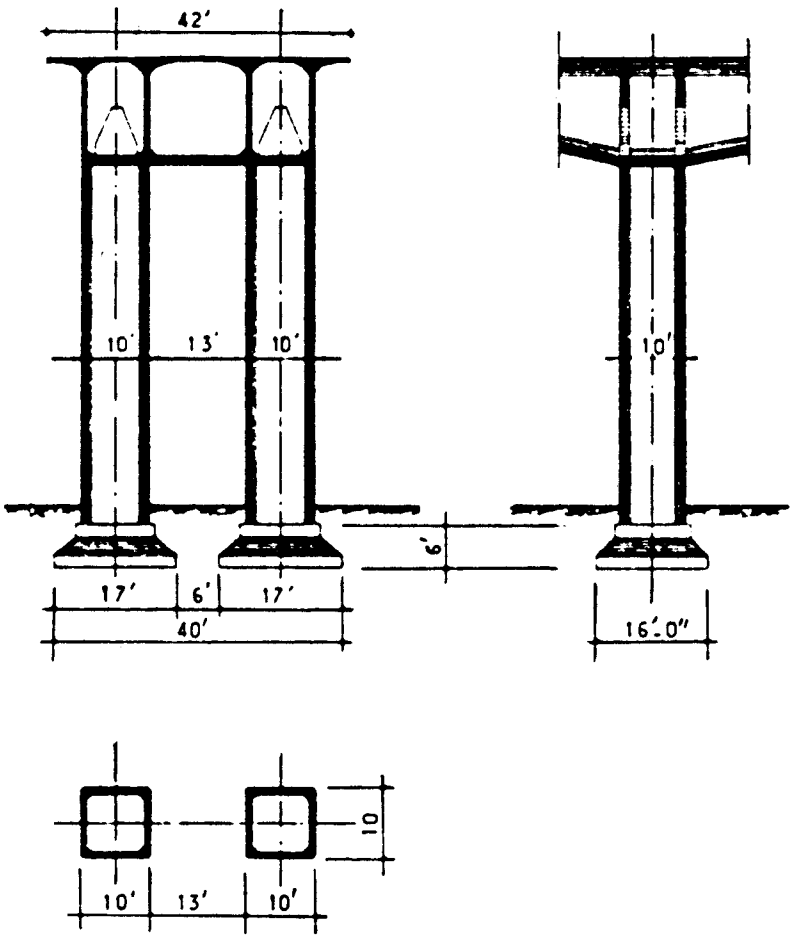

Figure 1–3 Pier example for segmental concrete bridges *(from Podolny and Muller, 1982).*

commonly referred to as towers or pylons. Other tower forms suitable for cable-stayed bridges are portal frames, and the configurations shown in Figure 1–5.

The modified A-frame shown in Figure 1–5(a) will accommodate a large vertical clearance below the superstructure, and provides sufficient pier width to support the two cable systems of the deck. The narrow diamond-shaped tower shown in Figure 1–5(b) is a variation of the A-frame; it can accommodate a large vertical clearance below the deck for a superstructure with one cable system at the center. The delta shape, or modified diamond, shown in Figure 1–5(c) can be used where a single-cable bridge does not require large vertical clearance below the superstructure.

In general, the towers consist of cellular sections that are fabricated from structural steel or reinforced concrete. There has been a trend to favor concrete towers, even with steel superstructures, because of the favorable response of concrete in compression. Tower height is determined from considerations such as relation to span length, deck width, and cable arrangement, and the aesthetics of the bridge as a whole.

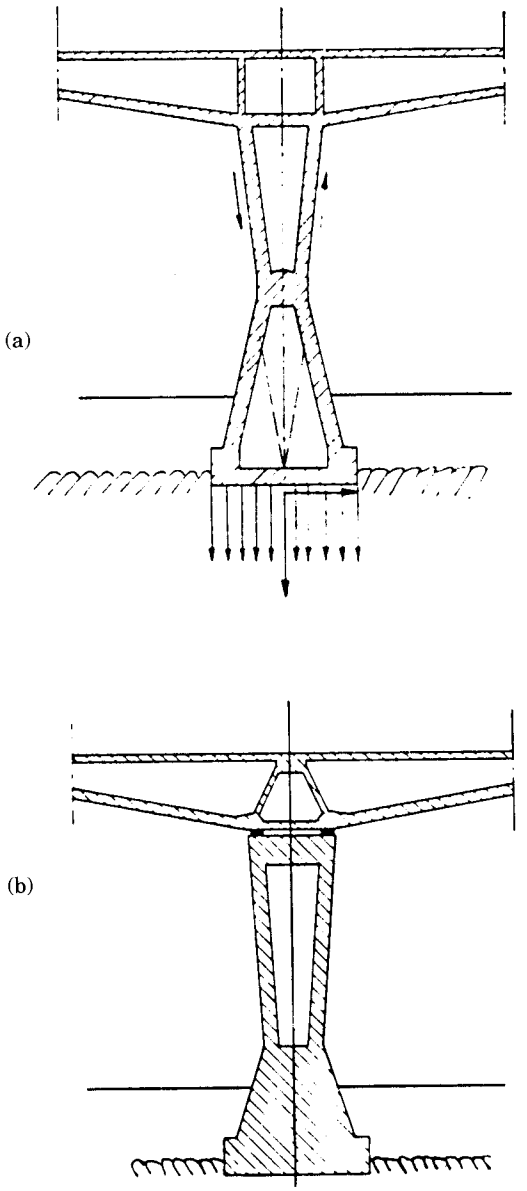

Figure 1–4 Pier details for segmental bridges; (a) piers with two inclined walls; (b) piers with two neoprene bearings.

Suspension bridges. As in some cable-stayed bridges, towers for suspension bridges may be considered as composed of two parts: the substructure or pier, and the tower proper extending above the deck and supporting the cables. The pier does not involve any special features that may differentiate it from ordinary bridge piers.

Towers must be designed so that they do not obstruct the roadway. A simple version is a column or leg for each suspension system. For lateral stability the tower legs are braced together with cross-girders and cross-bracing, or by arched portals. The sway and portal bracings are necessary to brace the tower columns against buckling, to take care of lateral components from cables, and to carry wind stresses down to the piers.

Tower legs must be designed as columns to withstand vertical reactions from the

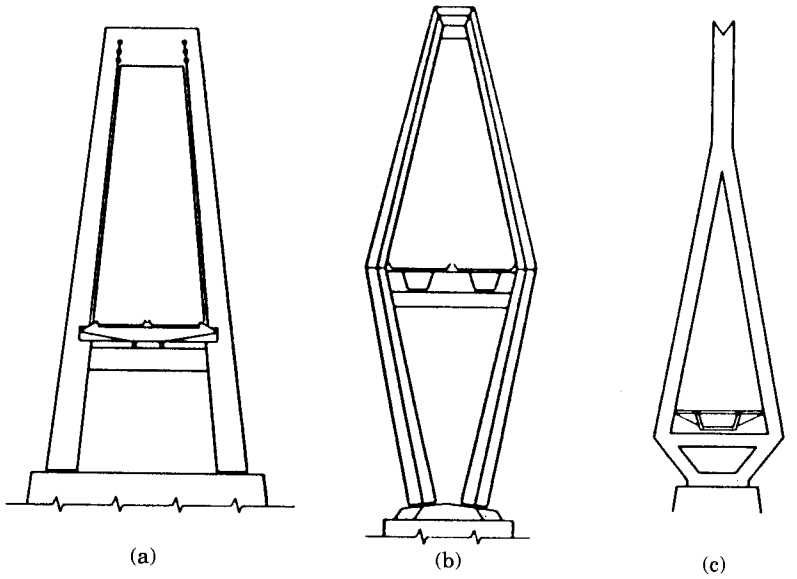

Figure 1–5 Tower types for cable-stayed bridges; (a) modified A-frame; (b) diamond; (c) modified diamond or delta.

cables, and also as cantilevers to resist any unbalanced horizontal tension. The latter will depend on the cable design, temperature and loading conditions, and cable geometry. Wind forces and aerodynamic stability must also be provided for.

Movable bridges. The three main types of movable bridges are (a) bascule bridges, (b) vertical lift bridges, and (c) horizontal swing bridges. The substructure elements must resist the stipulated load combinations with the movable span in the open and closed position.

A special loading feature relates to the mandatory introduction of counterweights. These are intended to balance the movable spans and their attachments in any position, except that there should be a small positive dead load reaction at the supports when the bridge is seated. Auxiliary counterweights usually are provided for vertical lift spans where vertical movement exceeds 80 feet. The design must also provide for unbalanced conditions of the machinery and power equipment. A swing span of unequal lengths or unbalanced machinery should be balanced by counterweights.

It appears from these brief comments that piers and foundations for movable bridges must be carefully selected and designed since any settlement, movement, or displacement may render the structure inoperable. Hence, special design precautions must be taken to prevent and exclude these effects. Load type, eccentricity, and intensity are frequently altered depending on the operating conditions of the movable span, and hence piers and their foundations should be capable of resisting torsional and horizontal force effects produced by this movement.

Other Types of Bridge Supports

Rigid frames with slant legs. A bridge type that has been found to be popular with many states (for example, Pennsylvania) is the so-called rigid frame with inclined or slant legs shown in Figure 1–6(a). This design treats the entire superstructure and sub-

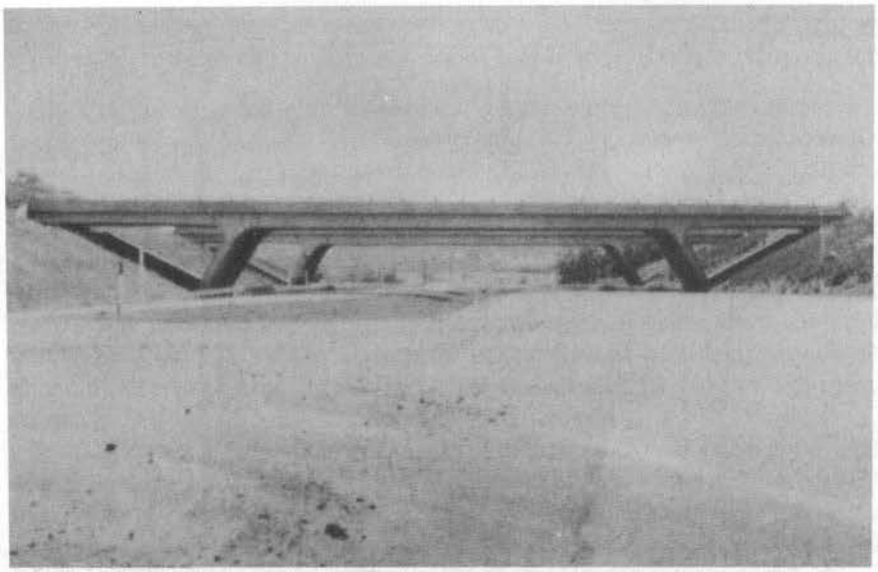

(a)

Figure 1–6 (a) Slant-legged bridge; (b) One-span rigid frame bridges.

structure as one unit. This type of construction eliminates the need for separate concrete piers, while positioning the supports away from the traveled roadway. The inclined legs interact structurally with the main longitudinal girders, and in fact, there is one leg for each deck girder; hence, each frame becomes indeterminate to the third degree. The associated response under a uniform dead load can be predicted using slope deflection or moment distribution methods. However, the analysis of moving live loads requires complex influence lines, the development of which is quite tedious and time consuming (Heins and Wang, 1976).

Alternatively, the inclined frame bridge may come within the definition of arches, even though the frames do not resist all the loads by compressive axial thrusts. The arch character of the slant-legged frame may be sustained by the fact that the supports are capable of developing lateral as well as normal reaction components.

Single-span, rigid frame concrete bridges. One-span rigid frame bridges were introduced in the 1920s, and demonstrated uninterrupted usage until the second World War. This type of bridge became popular on a regional basis, particularly for grade separations with favorable span-to-height ratios.

In structural terms, these bridges consist of horizontal members one span long, rigidly connected to the vertical supporting members. The latter have the lower ends designed and constructed in such a manner that they can resist horizontal thrusts produced by the frame action, and this brings them within the broad arch definition. If the base of either support is free to move horizontally, the structure is statically determinate.

A typical rigid frame one-span bridge is shown in Figure 1–6(b). In the upper sketch, the ends of the vertical members are hinged; hence they are restrained from any horizontal or vertical movement, but are free to rotate so that they cannot transfer moments to the foundation. Alternatively, the ends of the vertical members can be fixed to the foundation as shown in the lower sketch so that they can resist and transfer moments. A third condition is an intermediate response between hinges and full fixity.

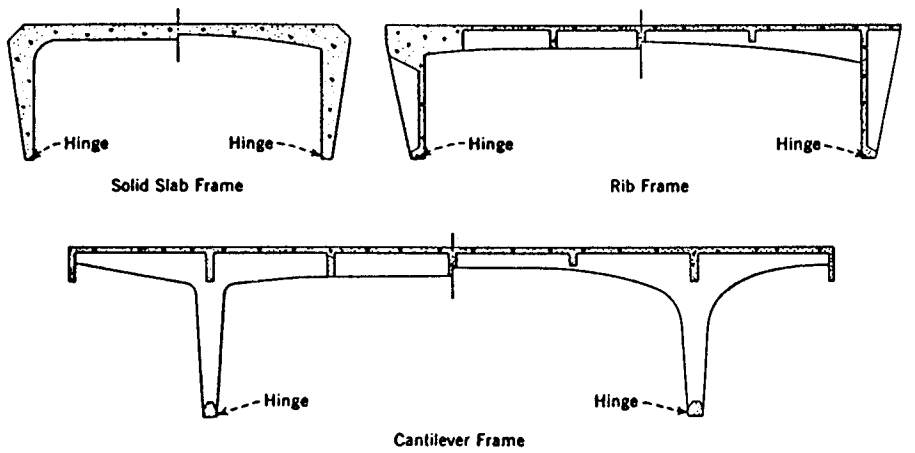

One Span Rigid Frames. Hinged Ends.

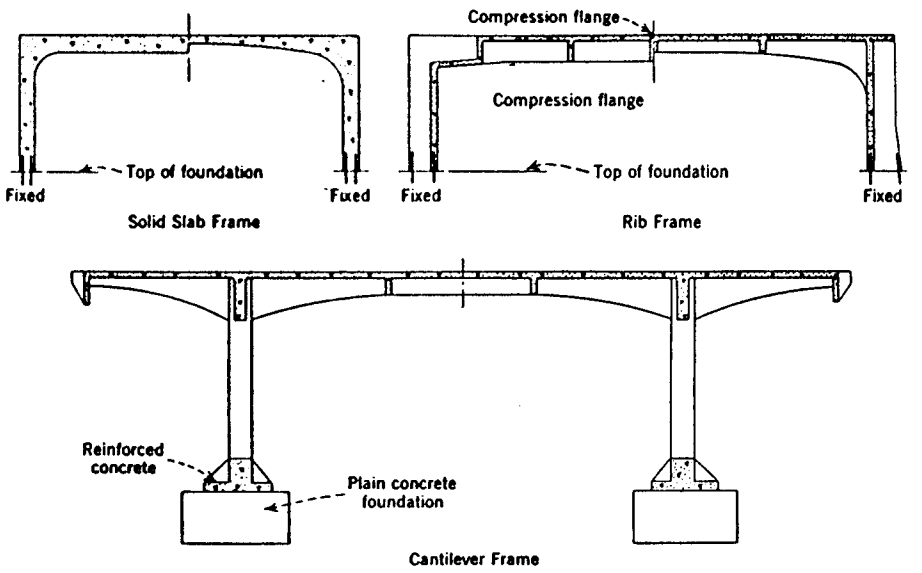

(b)

One Span Rigid Frames. Fixed Ends.

Figure 1–6 *(continued)*

Delta leg bridges. These are either all-concrete or all-steel bridges. The rigid delta legs at the piers are usually selected based on a comparative economic study and because they enhance appearance. As in the rigid frame types, an extensive use of computers usually is required in girder analysis and design, since the delta legs are integral with the superstructure.

Multiple-deck bridges. These are usually built in urban areas and along transportation corridors with limited right-of-way. They must satisfy operational and service conditions that often imply unique design requirements. The design must accommodate minimum vertical clearance between levels. The structure, including the support system, must occupy a minimum of space. Suitable supports are usually provided with portal

frames that require a minimum of space. The design of these frames requires explicit criteria because of the multipresence of live load and other relevant force effects.

1.3 ABUTMENT TYPES

General

Abutments are the end supports of a bridge, where it connects with the approach roadway. Their function is twofold: to transmit the reactions from the superstructure to the foundation, and to retain the earth embankment of the approach roadway. Thus the main loads on the abutment come from the superstructure or are induced as earth pressures.

Continuous bridges with several spans usually are designed with expansion ends, and therefore abutments are not required to resist longitudinal forces. Sometimes, the friction or shear force produced at expansion bearings on abutment seats may be considerable, and its inclusion in the analysis can thus have an additive effect on earth pressures and surcharge loads. Alternatively, for continuous bridges, the longitudinal forces can be transmitted at one location only provided that expansion and contraction are not restricted. In many instances the most suitable point of longitudinal restraint is at one abutment. Where abutments are massive and rigid, they are considered a suitable location to balance longitudinal forces from the superstructure. By the same rational approach, some engineers choose to resist lateral forces also at the abutments, and provide slender piers to carry vertical loads only.

A generalized version of various types of abutments is shown in Figure 1–7. The gravity abutment shown in (a) has a bridge seat, backwall and wing walls, and a common footing; this abutment responds as a gravity structure. The U-type shown in Figure 1–7(b) has wing walls perpendicular to the front wall, and this improves stability against overturning. The spill-through abutment shown in Figure 1–7(c) has the

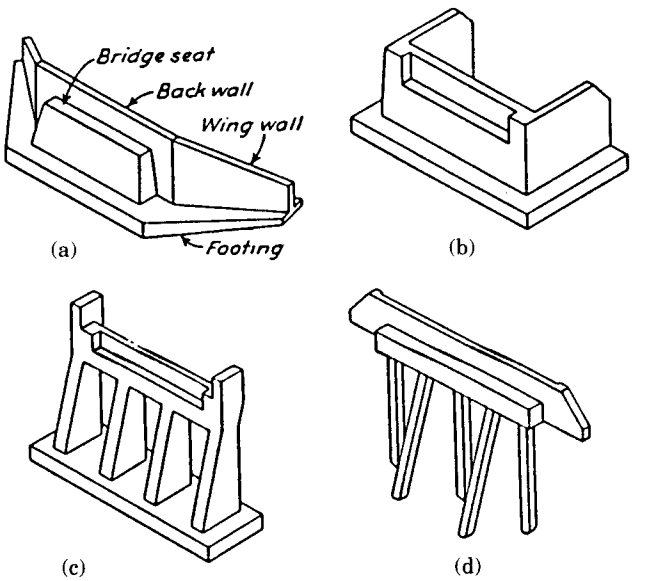

Figure 1–7 Various types of abutments; (a) typical gravity abutment with wing walls; (b) U-abutment; (c) spill-through abutment; (d) pile bent abutment with stub wings.

beam seat supported on counterforts resting on common footing. The pile bent abutment shown in Figure 1–7(d) has a pile cap that also provides the beam seat, and stub or inclined wings on piles. The latter are driven through precored holes if the distance from the bottom of the abutment to natural ground exceeds about 10 feet.

In general abutments cover two basic categories: pile bents or spill-through, and gravity types or full (closed) abutments. The closed design prevents the approach embankment from spilling out in front of the structure, and hence results in the shortest superstructure with the abutment placed to satisfy the horizontal clearance to the traveled roadway or shoulder. A pile bent abutment is considerably cheaper but requires a longer superstructure to allow for the embankment slope in front of the abutment, usually assumed at 2:1. Usually, the choice should be made after an economic comparison of the two schemes; in many instances, however, it is based on state standards. An intermediate solution is a partially closed abutment that allows a portion of embankment slope in front of the structure. The resulting bridge scenarios from these configurations may be a single-span, a two-span, or a four-span bridge.

Referring to the basic types shown in Figure 1–7, the main parts of an abutment are the bridge seat, the retaining backwall, the wing walls, and the footing or pile foundation. These are constructed to form an integral unit. The wing walls may be arranged parallel to the roadway, or placed at some angle. A proposed modification to the standard AASHTO Specifications articulates abutments into four types: stub abutments, partial depth abutments, full depth abutments, and integral abutments.

For conventional steel or concrete girder superstructures the abutment type should be independent of the structural system, with the choice dictated by the geometry, loads, slope arrangement, and economic considerations.

Pile Bent Abutments

Figure 1–8 shows a typical section of a pile bent abutment used in conjunction with conventional grade separation bridges. If the length of the abutment exceeds 90 feet, a 1-inch expansion joint should be used. The usual guidelines allow the base of an abutment under a superelevated roadway to be constructed level, if the difference between the low and high beam seat elevation is 1 foot 6 inches or less. If it exceeds this value, the abutment cap may be stepped with the reinforcement continuous through the transition. The height of the backwall depends therefore on the superstructure depth (deck, beams, bearings) and the roadway superelevation.

When natural ground is at or near the design elevation of the abutment base, consideration should be given to placing the cap on a spread footing in lieu of a pile bent. The minimum thickness of a spread footing is usually 2 feet, and the minimum thickness of a footing on piles is 2 feet 3 inches. If the footing is placed on rock, it should be keyed at least 6 inches into solid rock.

The dimensional layout of the abutment and the wing walls is the first step of the design. As shown in Figure 1–8, a berm is provided below the beam seat; usually it is extended about 9 feet from the back of the abutment. This dimension establishes the edge of the berm parallel to the abutment and the beginning of the 2:1 slope. The corresponding elevations of the berm and the shoulder line behind the abutment determine the length of the wing walls.

The width of the beam seat must be sufficient to accommodate the bearing plates under each beam, girder, or truss, and hence the width of the pile cap can be increased accordingly. The back wall keeps the soil under the approach roadway in place, and the

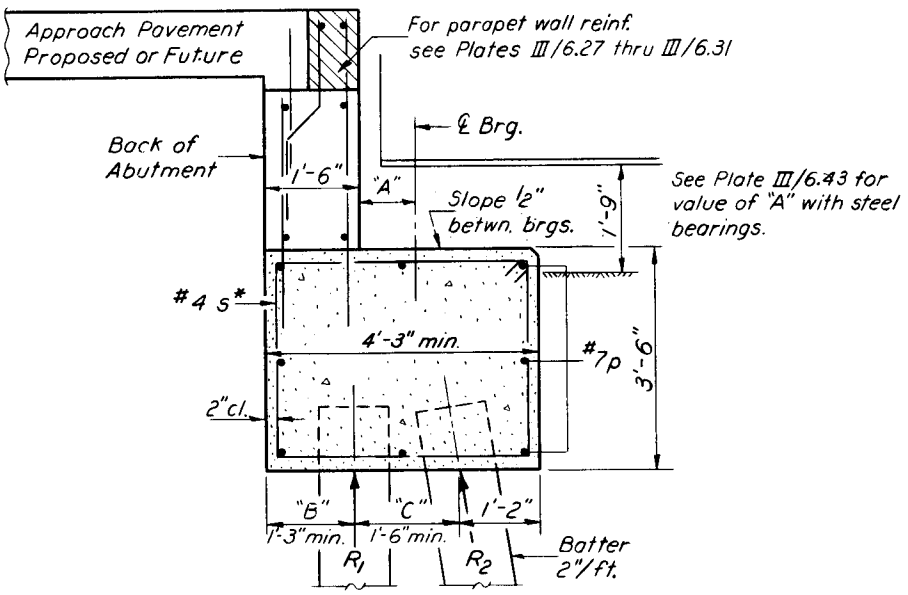

Figure 1–8 Pile bent abutment, typical details. (*Source*: State of Illinois)

approach slab rests on top of the back wall, as shown. If an approach slab is not provided, and there is a small settlement of the roadway at the edge of the back wall, the vehicular load is likely to induce a horizontal force component, which is generally indeterminate, as it impacts the back wall. Thus, an approach slab is recommended to eliminate the impact force and to maintain a smooth transition from the roadway to the bridge deck.

Closed (Full) Abutments

A typical section of a closed (full) abutment is shown in Figure 1–9. The footing may transfer the loads by direct bearing, or it may be supported on piles. The structure shown in Figure 1–9 is essentially a retaining wall subjected to vertical loads and lateral pressures. It is restrained at the top and bottom by the superstructure deck and the footing, respectively, so that it is laterally supported at the ends. The restraint at the bottom may range from a hinge condition to full fixity, depending on the rigidity of the footing and the supporting soil or pile system. The detail shown at the top suggests a hinge support, but can be converted to frame action with appropriate reinforcement and dimensions.

Closed abutments supporting simple spans may be restrained at both ends as shown in Figure 1–9 if the span does not exceed 45 feet. Although these structures are not necessarily integral abutments, a refined design should include provisions to resist or absorb creep, shrinkage, and thermal movement of the superstructure. In lieu of this analysis, some states stipulate a higher equivalent fluid pressure (probably 50 to 60 lb/ft^2) intended to reflect the possibility of earth pressures much higher than the active condition. Likewise if the approach roadway is a nonrigid type, its effect can be considered by adding an appropriate live load surcharge.

Wing walls for closed abutments should be of sufficient length to retain the road-

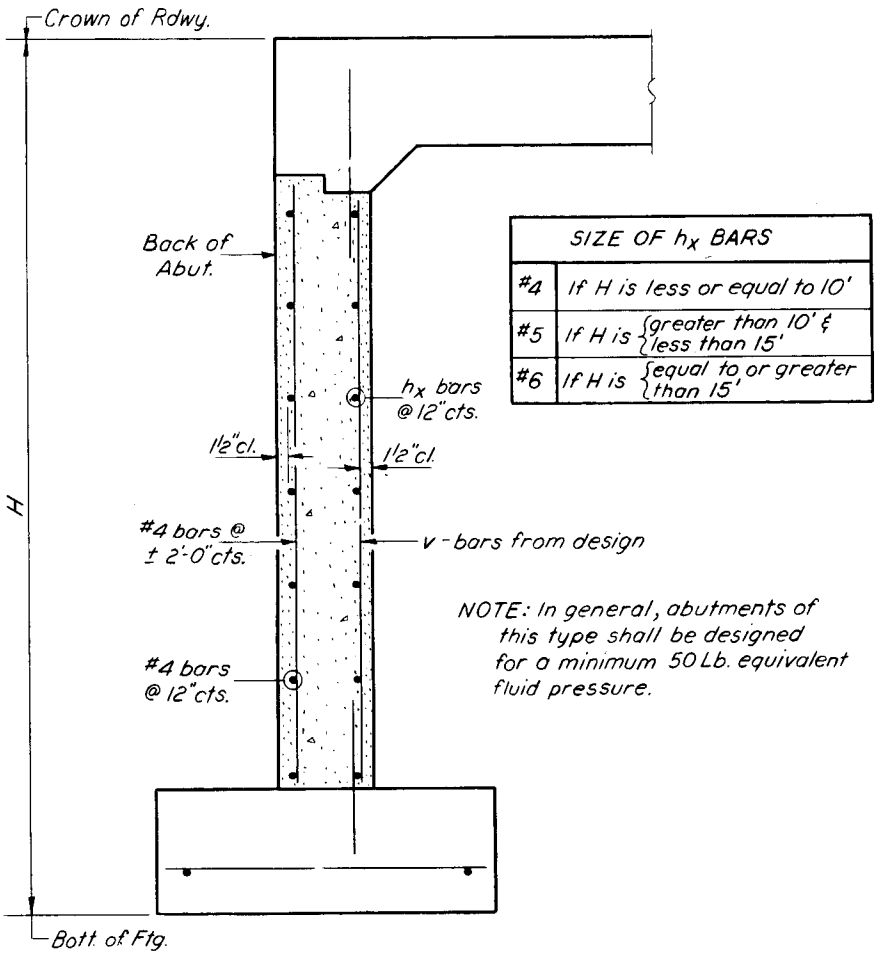

Figure 1–9 Typical section through a closed abutment. (*Source:* State of Illinois)

way embankment and to provide protection against erosion. The wing wall lengths are generally computed to accommodate the specified embankment slopes. These members can be placed on the same alignment as the abutment wall, on an alignment perpendicular to the abutment wall, or at an angle of 45°.

Closed abutments and their wing walls can be designed either as monolithic structures, or as separated with an expansion joint. In the latter case, the wing walls rest on footing that normally is continuous with and at the same elevation as the abutment footing. For normal embankment heights and slopes, the footing thickness and width can be constant, but for long wings the footing size may be reduced or stepped down to reflect the effect of reduced overturning moment.

The front face of wing walls usually is set back at the top 2 inches from the face of the abutment wall. Batter is placed on the front face up to a maximum of ½ inch per foot of height. If a greater wall thickness is required, the additional batter should be placed on the back face.

The top detail of the abutment shown in Figure 1–9 can easily be modified to support the approach slab by adding a bracket, and to accommodate fixed bearings of steel

or concrete girder superstructures. In the latter case a curtain wall is added at the ends to protect the beam seat area.

Cantilever type. If the bridge length for a simple span exceeds the limits up to which provisions for expansion are not necessary (usually 45 feet), the closed abutments can be fixed at one end and expansion at the other. For this situation both abutments should be designed as free cantilevers and provided with a foundation that is compatible with this condition. Design lateral earth stresses should be consistent with the expected movement.

As a guideline, a footing width about 0.55 times the distance from the crown to the bottom of the footing can initially be selected if there is no surcharge. Approximately one-half of the footing width should extend behind the wall.

Deflections of abutments may be critical because they can force the joints to close and thus induce unnecessary and undesirable forces in the superstructure. This implies that the design should predict these deflections in a controlled manner and ensure that the structure has adequate stiffness. Closed abutments with height exceeding about 20 feet should be designed with counterforts to increase structure stiffness.

Vaulted Abutments

This abutment type is a good alternative for the control of deflections in large abutments. It consists of two wing walls parallel to the roadway, a closed front wall, and a back wall resting on the embankment. A suitable deck system provides the traveled roadway, and is supported on the front and back wall. The embankment is then allowed to spill down inside the abutment so that the high lateral earth pressure is for the most part eliminated. This type is also called cellular abutment.

Figure 1–10 shows a configuration of a vaulted abutment utilizing precast prestressed beams to support the abutment span of the bridge. This abutment is generally used when the design span at right angles exceeds 21 feet. For shorter spans a reinforced concrete slab provides the deck. For either type, access to the inside of the vault must be provided. The front wall may be supported on piles or rest on spread footing. The rear wall is placed on top of the embankment and is supported on piles.

Integral Abutments

Integral abutments are structures connected to superstructure decks without joints, irrespective of the bridge length and the number of spans. The top detail of the abutment is essentially similar to Figure 1–9. The resulting restraining effect implies, therefore, that the abutment must be designed and constructed to resist and absorb any creep, shrinkage, and thermal movement of the superstructure.

In cold climates such as the northern United States, Canada, and northern Europe, integrated bridges are becoming attractive options because they can eliminate joint-related damage caused by the use of deicing chemicals and the restrained growth of rigid movement. However, the elimination of intermediate joints in multiple spans results in a structural continuity that may induce secondary stresses in the superstructure. Some of these stresses may be transmitted to the substructure. These stresses are

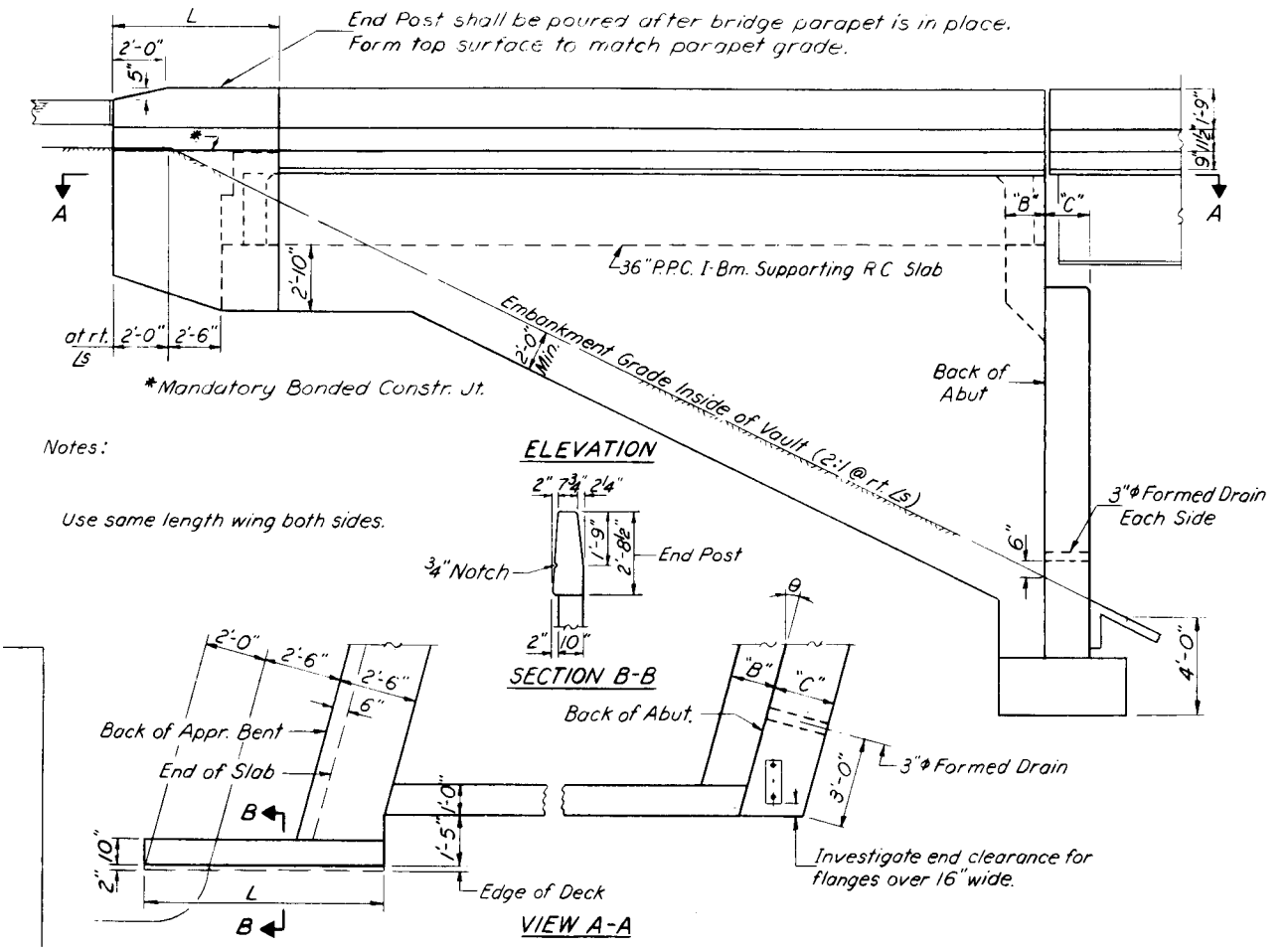

Figure 1–10 Details of vaulted abutment. (*Source:* State of Illinois)

caused by thermal expansion and contraction, moisture changes and gradients, substructure settlement, and posttensioning. If open joints are not provided at the ends, secondary stresses will be developed because of restraint introduced by abutment rigidity and foundations and backfill opposing cyclic movement of the superstructure. The choice of this construction can thus be justified if the design demonstrates that for short-to-medium span bridges of moderate length more damage and distress will be caused by the presence of deck joints than by exposing the superstructure to secondary stresses. Burke (1990) recommends accepting these stresses as part of the design requirements, since this may often result in simpler and probably less expensive schemes with enhanced integrity and extended durability.

Continuous and integral bridges. Continuity originated in the 1930s and received immediate impetus in design philosophies. Currently, some states have informative background material available on the movement toward the use of fully integrated continuous construction, leading the way in long span continuous bridges. A representative example is the Long Island bridge at Kingsport, constructed in 1980 as a series of

twenty-nine continuous spans without an intermediate joint. This bridge is 2700 feet long, but deck joints and movable bearings are provided only at the two abutments.

Currently, more than ten states have developed standards for continuous bridges with integral abutments for lengths up to 300 feet. Missouri reports examples of steel and concrete bridges with integral decks 500 and 600 feet long, respectively, and Tennessee reports examples of bridges 400 and 800 feet long for similar types.

Although the trend towards integral construction is documented, engineers should be cautioned that sections and components of such bridges may be subjected to high stresses that are not readily measured. A recent survey (Emanual et al., 1983) articulates the concern for potentially higher stresses that may develop in longer bridges. For example, abutments supported on a single row of piles may be flexible enough to accommodate longitudinal thermal cycling of the superstructure as well as dynamic end rotations under vehicular traffic. However, the piles may be subjected to axial and bending stresses that can approach or exceed yield stresses (Jorgenson, 1983).

Gamble (1984) considers restraint stresses for cast-in-place construction, and gives examples of cracking in continuous concrete frame bridges. In these cases the concrete stresses were below the yield strength, but the shear reinforcement was inadequate. Structural failure was attributed to stiffness and resistance to shrinkage or contraction of the bridge deck.

When precast concrete is used in the deck, the problems associated with initial shrinkage may be eliminated, but consideration should be given to subsequent thermal expansion and contraction as well as to long-term creep.

Integral abutment details. Abutment details for integral construction are shown in Figure 1–11(a) through (c) for Illinois, Tennessee, and Ohio, respectively. The integral joint connection is between the pile bent, the superstructure deck, and the approach slab. In all three details there is a horizontal construction joint between the pile bent and the end diaphragm wall. For the Illinois detail, this diaphragm is cast integrally with the deck, but for the Tennessee and Ohio standards there is another construction joint between the diaphragm and the deck slab.

The restraint provided by the passive pressure behind the wall of the bent as the bridge expands may be controlled by (1) limiting the bridge length, skew, and the vertical embedment of the bent into the embankment; (2) using select granular material and uncompacted backfill as shown in Figure 1–11(a) in conjunction with approach slabs that rest on the bent and thus inhibit surcharge loads; (3) using embankment trenches to shorten wing walls; and (4) using semi-integral abutments to eliminate passive pressure below bridge seats.

Further solutions that can be used to inhibit restraining effects at this location and thus make the abutment more compatible with longitudinal movement are

1. choosing the foundation of integral abutments to consist of a single row of slender vertical piles;
2. limiting the pile type;
3. orienting the weak pile axis of H-piles normal to the direction of movement;
4. using prebored holes filled with granular material;
5. providing an abutment hinge to control pile flexure; and
6. using semi-integral abutments for longer bridges as shown in Figure 1–12 to inhibit foundation restraint to longitudinal movement.

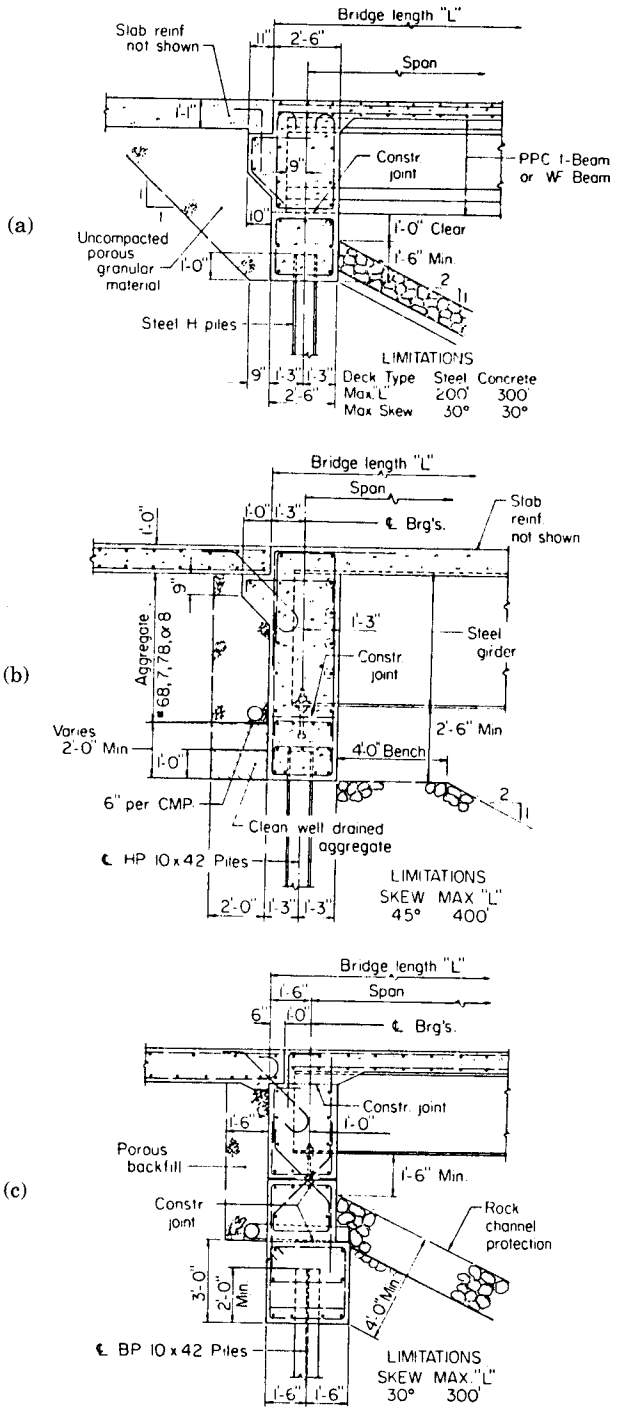

Figure 1-11 Abutment details in integral construction; (a) Illinois; (b) Tennessee; (c) Ohio.

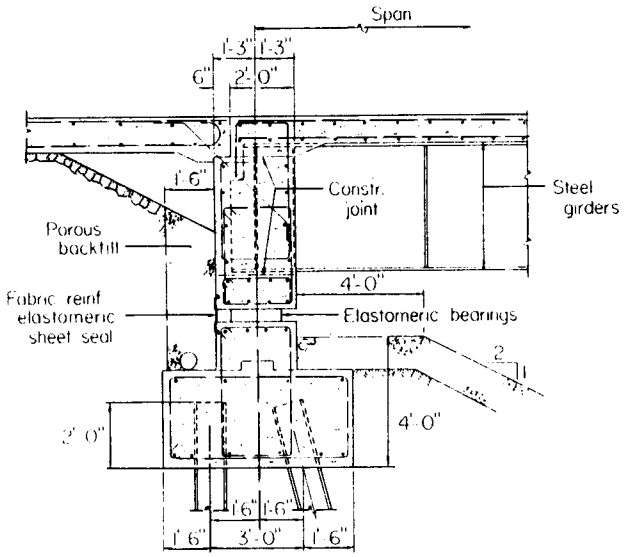

Figure 1–12 Semi-integral abutment details used in Ohio.

1.4 ABUTMENT WALLS

Alternative Retaining Walls

In this category we include embankment-type mechanically stabilized walls and precast concrete modular gravity walls, both built to retain fill and therefore suitable to confine approach embankments.

The first group is quite extensive, and examples are VSL retained earth, geotextile walls, geogrid walls, and welded wire walls. Prefabricated modular walls may be considered where conventional gravity, cantilever, or counterfort retaining walls are found suitable, but certain conditions apply. Examples of walls from both categories are shown in Figure 1–13.

Mechanically stabilized walls should be evaluated for internal failure by slippage or rupture of the reinforcements. A minimum panel thickness should be determined since these units are often used where the wall may be exposed to salt spray or other corrosive environments. The minimum panel thickness also reflects construction tolerances, and placement of reinforcement and connectors that can reasonably be conformed to in precast construction.

Prefabricated modular walls should not be used on curves with a radius less than 800 feet, unless the curve can be substituted by a series of chords. Likewise, steel modular systems should not be selected where the groundwater or surface runoff is acid, contaminated, or where deicing chemicals are to be used. Specific guidelines for the design of mechanically stabilized and modular walls are given by the LRFD specifications (see also subsequent chapters).

Walls Used as Abutments

In the context used herein these walls serve as ground supports and as end abutment walls in underpasses. These accommodate depressed motorways with a normal configuration and uniform cross section, having their grade usually lowered to provide mini-

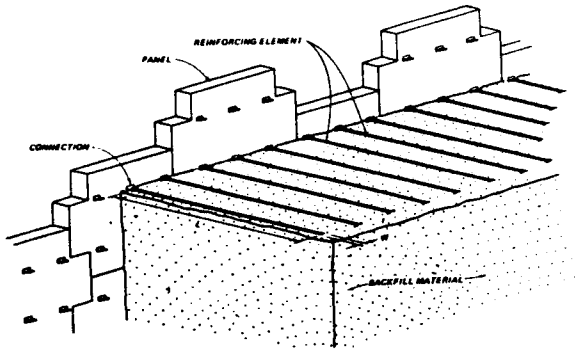

Schematic diagram of reinforced earth retaining wall

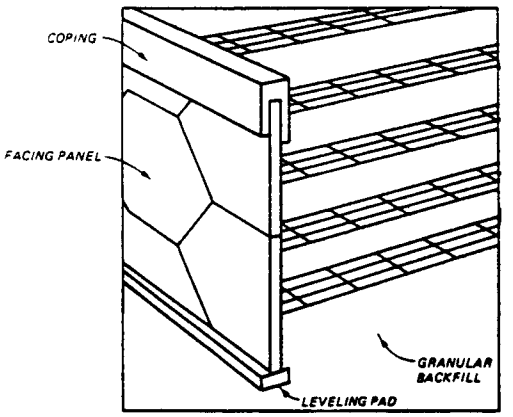

VSL retained earth retaining wall (adapted from VSL Corporation 1984)

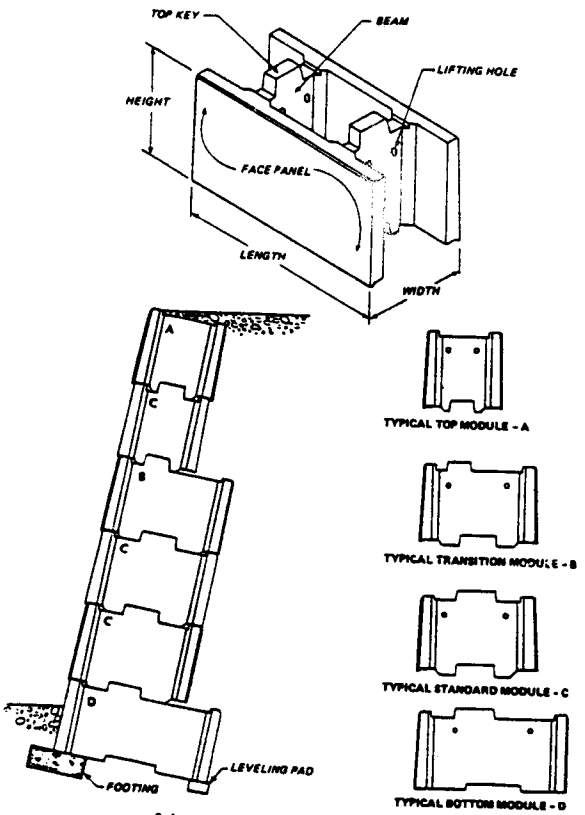

Schematic diagram of Doublewal retaining wall (after Doublewal Corporation 1984)

Figure 1–13 Mechanically stabilized earth walls and concrete modular wall *(from Corps of Engineers, 1989).*

mum vertical clearance. Since most of these intersections are in urban areas and carry heavy traffic, solutions that minimize traffic disruption during construction and also reduce construction time are favored. The use of slurry walls in this case as ground support and as substructure for the deck can offer considerable advantages.

Construction with cast-in-place walls. The four-lane roadway with safety walks satisfies the usual traffic standards in the United States and is also popular abroad. This scheme may require from 50 to 60 feet (15 to 18 m) face-to-face of walls. For a vertical clearance 14 feet 6 inches, the depth of excavation from street level is 19 to 20 feet, which is within the range of vertical cantilever walls (Xanthakos, 1994b).

Bridge concepts for traffic underpasses and depressed roadways are thus synthesized on the use of prefabricated elements for the deck (slab and box sections) and slurry walls for the substructure (Xanthakos, 1994a). In the covered (bridge) portion, the superstructure braces the walls laterally at the top, and usually it is placed before general excavation so that earth moving is done under cover while traffic is maintained on the street above. Provisions for temperature changes should be made when the span exceeds 40 feet to accommodate thermal movement and freedom of the system for end rotation under load. If such provisions are not made, both superstructure and substructure should be designed for the associated stresses as in integral bridges.

Unlike conventional abutment walls, slurry walls may be braced at the bottom against lateral movement by embedment into firm soil or by a base slab of sufficient rigidity. The load transfer is accomplished by direct bearing at the tip of the wall, by side shear, or both.

In the open (approach) segment of the underpass, the walls function as vertical cantilevers and should be checked not only for stability and flexural strength but also for maximum lateral movement. This movement may be controlled if some form of bracing is provided near the top and if the base slab is placed as soon as the excavation reaches the intended depth. A typical section for an underpass is shown in Figure 1–14 for the bridge and the approach section.

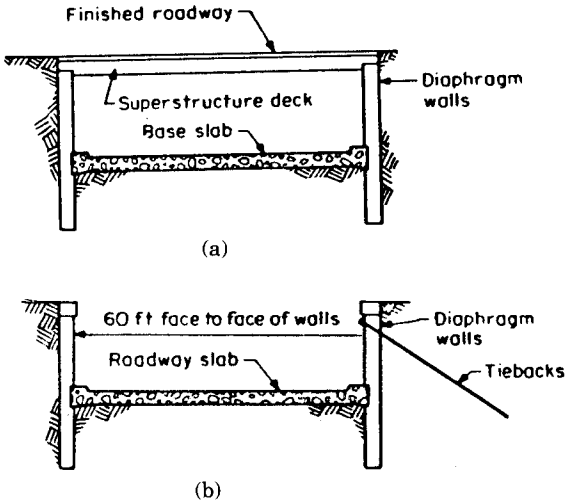

Figure 1–14 Diaphragm walls for traffic underpass; (a) covered section; (b) uncovered section for approach roadway.

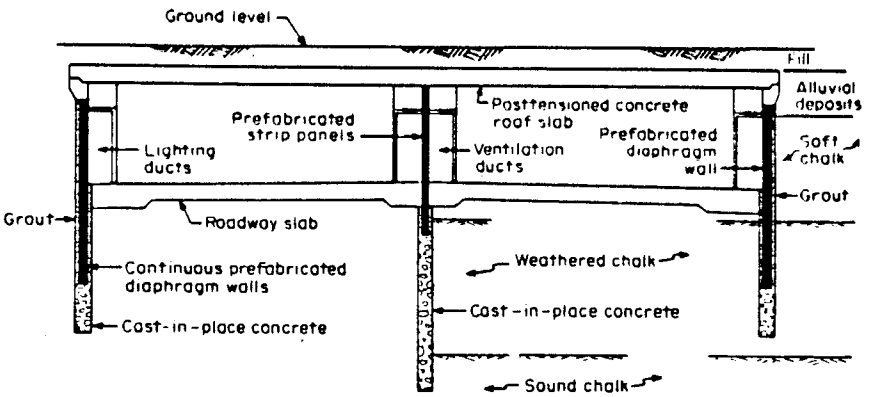

Figure 1–15 Cross section of a covered motorway built with prefabricated diaphragm walls *(from Leonard, 1974).*

Construction with a center wall. If the roadway width exceeds the single-span range, a center wall can be considered. This wall is also built from ground level, and since it will support heavier loads and reactions, it must be deeper. A suitable solution consists of strip panels capped with a continuous beam.

Construction with prefabricated panels. The advantages of precasting, mentioned for the deck, are also applicable to the walls. Usually the size of the job will offset the fixed costs of precasting; the uniformity of section geometry results in standard panel sections and configurations; sufficient space is available at the site as casting yard; and the smooth wall finish is acceptable as final face treatment.

Figure 1–15 shows a typical section for a depressed motorway. The exterior walls have continuous precast panels, and the center support consists of strip sections. When all supports were in place, the top slab was cast and posttensioned. Earth moving was carried out under cover.

1.5 FOUNDATION TYPES

Spread Footings

Spread footings (also referred to as shallow foundations) carry the loads from columns, walls, or other substructure elements and spread these loads laterally to the underlying soil so that the bearing pressure is reduced to a safe value. Alternatively, footings are proportioned to control settlement. In this case the two essential design requirements are that the total settlement of the structure must be limited to a tolerable amount and that differential settlement of various piers and abutments must be controlled or eliminated (see also subsequent sections).

Individual footings, usually rectangular in plan view, are the most common foundation type for columns, whereas strip footings are used to support walls. More complicated foundation members are those required to support several columns, and are usually referred to as combined footings. A combined footing may have a rectangular or trapezoidal shape or be a series of pads connected by narrow rigid beams referred to as strap footings. Footings for bridge piers and abutments are individual, strip, or combined.

Spread footings with tension reinforcement may be designed as two-way or one-way members depending on whether the steel bars used for flexure are placed in both or in one direction. Individual (square) footings are usually two-way slabs, and strip footings one-way slabs. Concrete is almost universally used for footing construction because of its durability and relative economy.

Single footings may have a uniform thickness or be either stepped or sloped. Stepped or sloped footings are used where they can produce considerable savings in the volume of concrete and where the footing is not reinforced.

Factors to be considered in selecting spread footings. Special attention should be given to footings placed on fills. Problems with insufficient bearing or excessive settlement in fill can be significant particularly in poor soil such as soft, wet, frozen, or non-durable materials and improperly compacted backfill. Such settlement around piers can result in considerable increase in footing loads caused by downdrag of friction forces exerted on the pier by the settling fill. Even properly placed and compacted fill is likely to undergo some form of settlement depending on the soil type, moisture conditions, method of placement, and degree of compaction.

Depth. The bottom of footing elevation should be determined with regard to the character of the foundation materials, considering also the possibility of undermining. Footings in waterways and stream crossings should be founded at a depth below the anticipated depth of scour. Footings that are not exposed to the action of stream current should rest on a firm layer below frost level. Special attention is given to footings on rock in conjunction with the effects of blasting, especially if this involves highly resistant competent rock formations that can result in some rock fracturing below the depth of the final rock surface. Blasting in this case is likely to reduce resistance to scour within the rock zone immediately below the footing level, and this operation should be carried out with care.

Frost penetration often occurs to different depths and in some instances erratically and with uncertainty. Where frost protection appears marginal or deficient, consideration should be given to the use of insulation to enhance frost protection.

Groundwater Effects. The design of footings should typically consider the highest anticipated groundwater table because of the obvious effect on the actual soil bearing strength. Evaluation of seepage forces and hydraulic gradients is essential in foundation excavations that extend below the groundwater table. Upward seepage forces in the bottom of excavations can result in piping in dense granular soil or heaving in loose granular soil. These problems can be controlled by adequate dewatering, often using wells or well points. However, dewatering of excavation in loose granular soils is likely to cause settlement of the surrounding ground, and if the associated damage is expected to be high, some form of protection should be considered.

Uplift. If in the final service the foundation is likely to be subjected to uplift forces, this effect should be investigated in the context of resistance to pullout and for structural capacity.

Adjacent Structures. Where substructure elements are placed near existing structures, the design should study the influence of the existing structure on the behavior of the foundation as well as the effect of the new foundation on the existing structure.

Driven Piles

Driven piles are basically deep foundations usually described as columnar elements inserted in the soil for the purpose of transferring loads from a superstructure to the ground. There are several good references, and among those to be mentioned are: Chellis (1961, 1962); NAVFAC DM 7.2 (1982); Fuller (1983); Tomlinson (1977); Vesic (1977); Canadian Geotechnical Society (1985); Carson (1965); Department of the Army (1992); and Prakash and Sharma (1990). These references classify piles in different ways that can be grouped into one of the following main categories:

1. Pile material
2. Method of pile fabrication
3. Extent of ground disturbance during pile installation
4. Method of pile installation into the ground
5. Method of load transfer

In this section we will consider only piles installed by driving. The classification is further narrowed down to types identified in terms of ground disturbance. Driven piles used in bridge foundations can be divided into two basic categories:

1. Displacement piles that have solid sections or hollow sections with a closed end. These displace the soil during installation involving driving, jacking, or vibration.
2. Nondisplacement piles that do not displace soil during their installation. The placement causes little or no change in lateral ground stress, and consequently, these piles develop less shaft friction than displacement piles of the same size and shape. Examples are H-piles and open-ended sections.

Pile types. Carson (1965) summarizes the various pile types in Figure 1–16. The maximum lengths are typical for the loadings frequently used in design. It is apparent from this brief review that no classification method is explicit in providing a complete description of the pile type and function. Hence, we choose to describe driven piles in terms of pile material, and articulate other pile characteristics according to their importance.

Timber Piles. These are the oldest type of pile foundations in bridge work. They are obtained from straight and slender sections of tree trunks with no defects and a uniform taper. Material deterioration and protection are essential. Timber piles situated wholly below the permanent groundwater table are resistant to fungal decay. However, when the project is above the groundwater, piles must be treated with preservatives to retard deterioration. The life of timber piles above the water table can be considerably increased by treating with creosote, oil-borne preservatives, and salt. Creosote application by pressure treatment is the most effective method of protection and almost the generally accepted preservation.

The advantages of timber piles are:

1. They are light and easy to handle
2. They have a high strength-to-weight ratio, and
3. They are durable when placed below the groundwater table

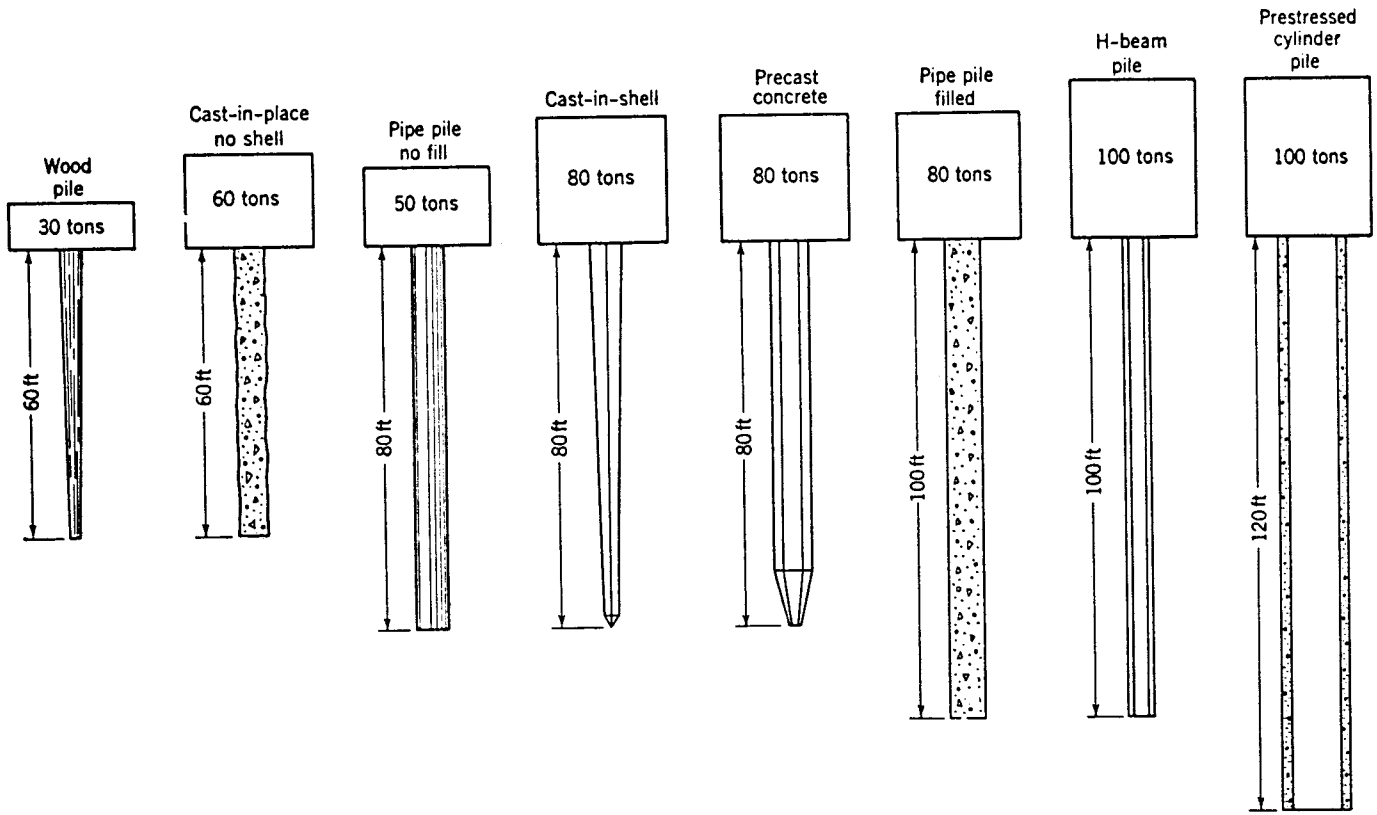

Figure 1–16 Summary of approximate maximum lengths of piles and unfactored loadings frequently used in design *(from Carson, 1965)*.

Conversely, their disadvantages are:

1. Their structural capacity is relatively low compared to other types
2. They are prone to damage during driving, especially in dense soil
3. They need protection when placed above the groundwater table, and
4. They are difficult to splice when extra length is needed

Concrete Piles. This type includes precast concrete piles, prestressed concrete piles, and composite versions. Precast piles are long slender units of reinforced concrete with square, octagonal, or circular cross section that must be designed to withstand handling and driving stresses in addition to service loads. They are made to carry a wide range of loads, typically up to 300 tons (2670 kN), and are reinforced for bending and uplift.

Prestressed concrete piles have steel rods or wires enclosed in a conventional spiral. They are further grouped into pretensioned and posttensioned piles. Possible length range is as much as 130 feet (40 m). Typical sections of pretensioned prestressed piles are shown in Figure 1–17.

Their advantages are:

1. They have relatively large axial capacity and suitability to soil and water conditions that require long piles
2. They have ability to withstand aggressive ground or marine environment with proper design
3. They offer resistance during hard driving, and
4. They also have all the advantages inherent in prestressing

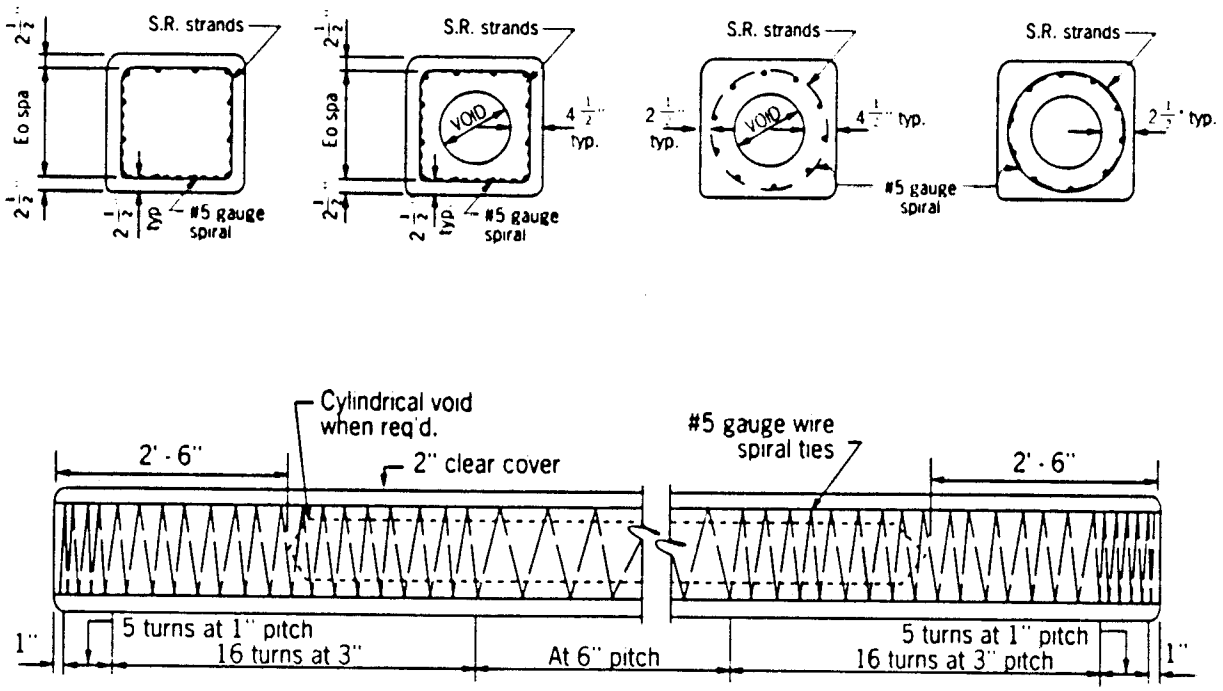

Figure 1–17 Typical design of a prestressed (pretensioned) concrete pile *(ASCE, Committee on Deep Foundations, 1984).*

Conversely, concrete piles may suffer damage during handling and driving, and cutting off excess length or splicing after driving is difficult and costly.

Composite versions are obtained either by encasing steel or timber piles by concrete in the zone susceptible to deterioration, or by making steel sections at the lower part where hard driving is anticipated.

Steel Piles. These include H-piles and steel pipe piles. Steel H-piles are suitable for penetrating rock and other hard and resistant materials. During driving they displace a minimum of soil mass, and therefore the operation does not cause heave. The usual load range is 40 to 120 tons (156 to 1068 kN), and the common length range is 40 to 100 feet (12 to 30 m). Preferably, the flange width should be at least 85 percent of the depth of the pile section to ensure comparable strength in the weak axis.

Steel H-piles have the following advantages:

1. They are robust and light
2. They come in various sizes and can easily be spliced
3. They provide ample axial capacity and resistance to buckling
4. They can penetrate hard layers, and
5. They accommodate situations with close pile spacing

Their inherent disadvantages are susceptibility to corrosion if left unprotected, small bearing resistance because of the small bearing area if left unplugged, and susceptibility to deflection if they hit hard sloping layers and obstructions.

Steel pipe piles can be driven with either open or closed ends, and may be used filled with concrete or unfilled. Unfilled open-end pipe piles are suitable if greater penetration depths are desired, since the soil inside can be removed during driving. Their advantages are:

1. They have small weight but sufficient stiffness to prevent damage during handling
2. They offer availability and variety of sizes that can easily be spliced
3. They have relatively high axial capacity and resistance to buckling
4. They conform to the loads and moments by varying pipe size and wall thickness, and
5. They allow easy inspection to detect deviations from intended alignment

However, like steel H-sections, steel pipe piles are prone to corrosion if left unprotected.

Composite Piles. Composite piles are shown in Figure 1–18. These are combinations of different pile types such as concrete and timber, concrete and steel, and concrete-filled steel pipes. Other combinations have also been used, the intent being to deal with difficulties arising due to the soil conditions. The structural capacity of these piles is determined by the weakest material. Certain types, such as timber-concrete, have been abandoned in North America because of the difficulty in forming good joints. High-capacity pipe and steel H-concrete composite piles do not present this problem and should be used when proven economical.

Factors to be considered in selecting piles. Driven piles should be considered when spread footings cannot be founded on rock or on solid earth material at reasonable cost. Piles may also be used as a protection against scour at sites where spread footings would be suitable but the potential of erosion exists. Other factors that will influence

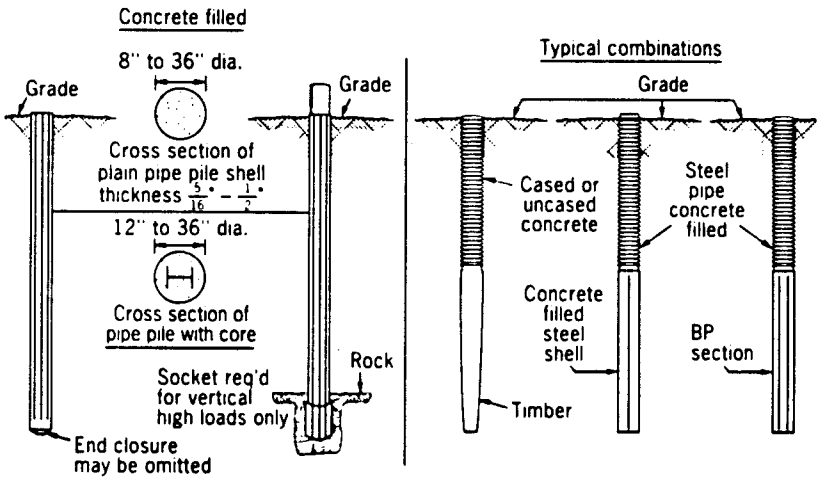

Figure 1–18 Typical sections for some composite piles *(Design Manual, NAVFAC DM 7.2. 1982).*

the selection of a pile foundation are the structural capacity of the pile, durability and resistance to handling, feasibility of splicing, ground displacement during driving, and penetrability.

Drilled Shafts

Drilled shafts, also referred to as drilled subpiers or caissons, are deep foundations installed by placing concrete in drilled holes. A typical drilled shaft is shown in Figure 1–19.

Construction methods. Drilled shafts may be installed in the dry, with casing protection, or under slurry, depending on the soil conditions and the presence of groundwater. Underreams or bells appear to have lost some popularity for several reasons:

1. Recent technological advances have demonstrated that straight shafts can be provided with sufficient geotechnical capacity for most conditions
2. The formation of underreams cannot be always ascertained, particularly in soils of low shear strength
3. The settlement often necessary to mobilize the capacity of the bells (base bearing) often exceeds the tolerable settlement of the structure, and
4. Underreams are difficult to reinforce.

Nonetheless, underreams are still favored regionally and in certain stiff soils, for example, London clay.

Installation in the Dry. This is feasible in soils above the groundwater table that are stable against caving. Examples are homogeneous stiff clays and sands with some cohesion. The method may also be used below the natural water table in soils of low permeability and where the seepage can be controlled.

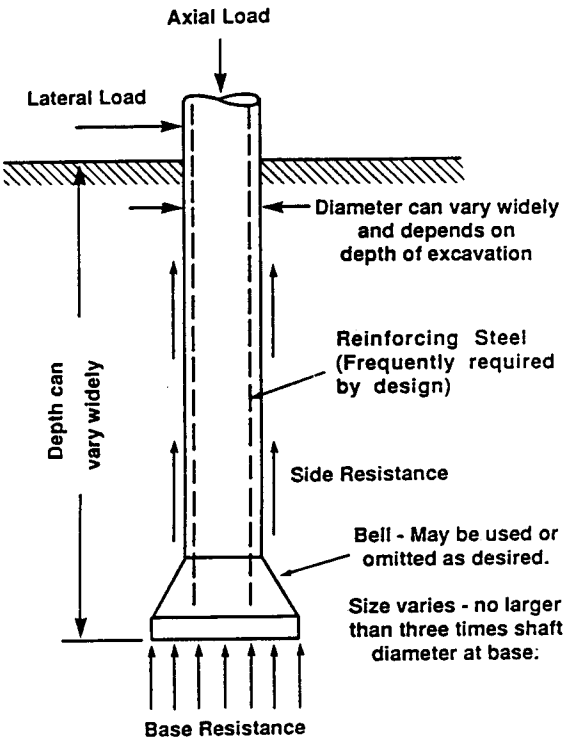

Figure 1–19 A typical drilled shaft *(from Reese and O'Neill, 1988).*

The excavation is carried out with suitable drilling equipment, usually truck-mounted for increased mobility or carried on crawler cranes and tractor trailers. Reinforcement may be placed in the entire depth of the hole, partly in the upper part, or omitted depending on the conditions of loading. The concrete is usually poured using tremie pipes, and exercising care not to strike the sides of the hole.

Installation with Casing. In water-bearing ground or in caving soil the hole almost invariably will not stand open, and in this case the use of a casing is mandatory.

Typical methods of advancing the hole with casing are described by Reese and O'Neill (1988). When the hole has been sufficiently excavated (usually under slurry), a casing is introduced as shown in Figure 1–20(a). This case involves an underreamed shaft drilled through a caving formation sandwiched between two competent soil layers. Once the casing is in place, the slurry is bailed out, and the excavation continues using a smaller drill that can pass through as shown in Figure 1–20(b). A belling tool forms the underream as shown in Figure 1–20(c), the reinforcing cage is inserted, and the hole is concreted as shown in Figure 1–20(d).

The seal at the bottom of the casing where it penetrates the lower impermeable stratum should be kept until the hydrostatic pressure of the fresh concrete can displace any slurry trapped behind the casing. As the latter is withdrawn, concrete flows around the base and displaces the slurry in the annular space. It appears, therefore, that the withdrawal of the casing is a critical part of the operation. If the concrete sets prematurely, it will move up with the casing, forming random cracks into which slurry can flow. The same situation can result with unworkable concrete. If the casing is pulled out prematurely, slurry is likely to flow in and mix with concrete.

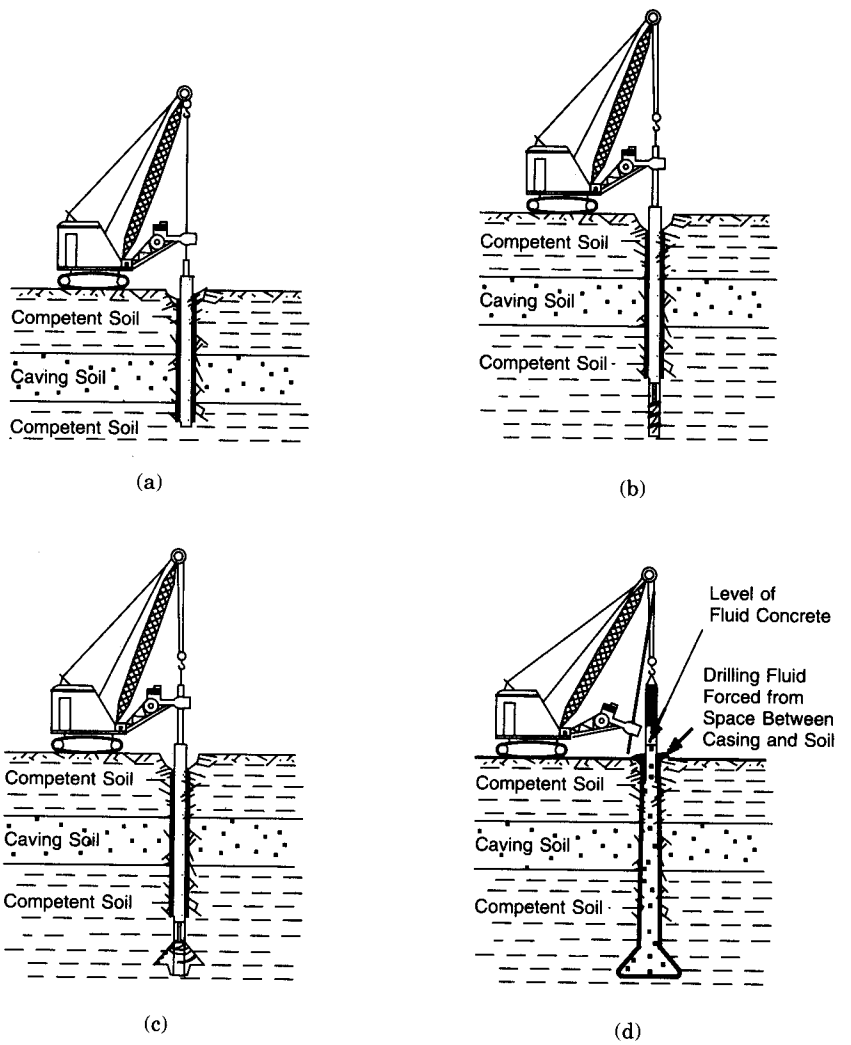

Figure 1–20 Advancing the hole with casing; (a) introducing the casing and removing the slurry; (b) drilling below the casing in competent soil; (c) forming the underream; and (d) removing the casing and concreting the hole *(from Reese and O'Neill, 1988).*

The Use of Slurry. Historically, the first significant applications of slurries occurred in connection with rotary drilling for large-diameter piles (Xanthakos, 1979). Initially the slurry was used to remove sand and cuttings from the excavation, but it soon became evident that it could improve the stability of the face, lubricate the tools thereby avoiding stuck-pipe problems, prevent formation fluids from entering the excavation, and keep the cuttings in suspension if pumping was stopped. With the extension of the foundation market, slurries were used in large-diameter holes, mine and access shafts, visual exploration holes, and eventually load-bearing elements.

The slurry is introduced into the hole as soon as an unstable formation is reached, and remains in the hole until the intended depth is reached. The drilling tool usually has a hollow stem or is provided with a suitable pressure relief device to allow the

slurry to flow through. Since multiple functions must be fulfilled by the slurry, stability controls are essential to check viscosity, pH, and density (Xanthakos, 1979). Some contractors use circular drills equipped with reverse circulation to remove excavated materials. Where local codes and standards require the hole to be drilled under slurry protection, the slurry control limits must also satisfy the requirements of tremied concrete.

Factors to be considered in selecting drilled shafts. These foundation elements should be considered when suitable soil does not exist for spread footings. As a deep foundation, drilled shafts should be compared for cost and feasibility with driven piles. In some cases they may be a viable choice where it is necessary to resist considerable lateral loads or uplift when deformation tolerances are limited by serviceability criteria. Invariably shaft embedment should be sufficient to ensure appropriate vertical and lateral load capacities and acceptable displacements.

An enlarged base, bell or underream, may be used in stiff cohesive soils to increase the base-bearing area or increase resistance to uplift. In this case the base resistance can be computed, assuming that the entire base area is effective in transferring the load, provided, however, that the bottom is cleaned and inspected before concrete placement.

Load Capacity. In drilled shafts, the load transfer capacity may be influenced by the method of construction (dry, casing, under slurry, or combination therefrom). This can affect particularly side resistance. Factors to be considered are the groundwater table, the division of load between shaft resistance and base bearing, and the consistency of installation procedures with material conditions. Any softening, loosening, or other change in soil and rock condition because of construction operations will most likely cause a reduction in load-bearing capacity.

In addition to normal vertical loads, downdrag forces may develop and should be considered. In general, a relative downward soil movement in the range of 0.1 to 0.5 inch is sufficient to mobilize downdrag loading on shafts.

Shaft Geometry. The center-to-center spacing of drilled shafts must be selected to avoid interference between adjacent elements (for example, hole stability, slurry communication, etc.). Usually this spacing is at least three times the shaft diameter. If closer spacing is required, interaction effects between adjacent shafts should be evaluated.

Batter shafts should be considered with great caution, since they give rise to special problems related to hole instability, installation and removal of the casing, installation of the cage, and concrete placement. If increased lateral resistance must be provided, a good alternative is to increase the shaft diameter or the number of shafts.

Uplift. The potential of uplift forces is a mandatory design requirement, particularly for shafts extending through expansive soils. This requires evaluation of the swell potential of the soil and the extent of the soil layers that may affect the shaft. A usual method for identifying swell potential is presented in Table 1–1 (Reese and O'Neill, 1988), and classifies swell potential as a function of the Atterberg Limits, soil suction, and percent swell from odometer tests. The thickness of the potentially expansive layer must be identified by examination of soil samples from borings and laboratory testing for determination of soil moisture content profiles.

Shafts in expansive soils should extend to a sufficient depth where moisture-stable soils are available to resist uplift. Sufficient clearance should be provided also between

Table 1–1 Method for Identifying Potentially Expansive Soils

Liquid Limit LL (%)	Plastic Limit PL (%)	Soil Suction (KSF)	Potential Swell (%)	Potential Swell Classification
> 60	> 35	> 8	> 1.5	High
50–60	25–35	3–8	0.5–1.5	Marginal
< 50	< 25	< 3	< 0.5	Low

(From Reese and O'Neill, 1988).

the ground surface and underside of shaft caps or beams to inhibit the application of uplift loads at this level because of swelling ground.

Potential construction problems. Potential construction problems related to installation deficiencies are presented in Figure 1–21. Possible remedies and solutions are summarized in Table 1–2 (Reese and Wright, 1977).

Linear and Prismatic Elements

These special-shape foundation elements are associated with the development of machines that can perform slot excavations under slurries, and hence are related to slurry wall construction (Xanthakos, 1979, 1994b). They may provide structural solutions that are not always feasible with driven piles or circular shafts. Typical configurations are shown in Figure 1–22. Variations from these sections can be worked out for unusual load combinations or for special classes of structures. In bridge work implemented with slurry walls this choice is logical and economical since it maintains construction consistency.

Linear or prismatic elements can replace a group of piles or shafts. This is particularly advantageous where heavy loads require unusually large monolithic structures, where the foundation is very deep or in difficult ground, and where large bending moments and lateral thrusts must be resisted. The flexibility inherent in prismatic panels regarding size, shape, and plan enhances their suitability for almost any type combination, and magnitude of loads.

The construction requires distinct phases and operations as follows:

1. Selection of suitable excavation equipment
2. Selection of a suitable slurry with appropriate checks and control criteria
3. Bottom cleaning and preparation of the base, and
4. Installation of the reinforcing cage and placement of concrete using tremie pipes.

These operations are described in detail by Xanthakos (1979, 1994b) and will not be repeated in this text.

An important advantage is the elimination of construction joints, round-end tubes, casings, and the associated appurtenances usually necessary with slurry wall construction. The result is a simplified construction and more efficient scheduling. A single element can be excavated and cleaned in one day, and reinforced and concreted the next day. If an airlift must be applied, it should be done just before concrete placement to

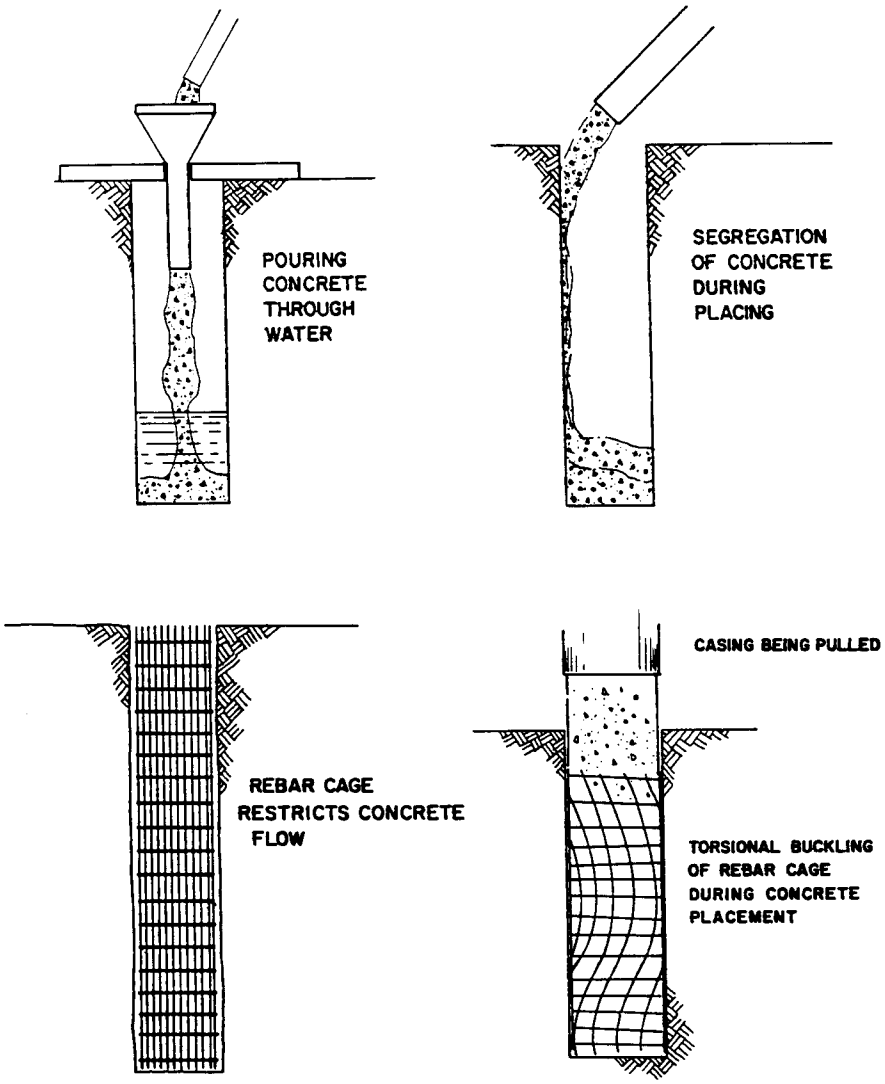

Figure 1–21 Construction deficiencies *(from Reese and Wright, 1977).*

prevent recurrence of cavitation and sloughing while the panel is open. As in conventional walls, the concrete pour should be continuous.

Potential Problems and Repairs. As in drilled shafts, possible defects of the finished structure and the conditions under which they occur can be summarized as follows:

1. Overstressing of soil beneath the foundation owing to insufficient bearing area or because of unconsolidated materials left at the bottom
2. Deformation of the walls or caving soil in the excavation space
3. Improperly tremied concrete causing voids and cavities in the finished foundation
4. Deviations from the true alignment causing local overstressing

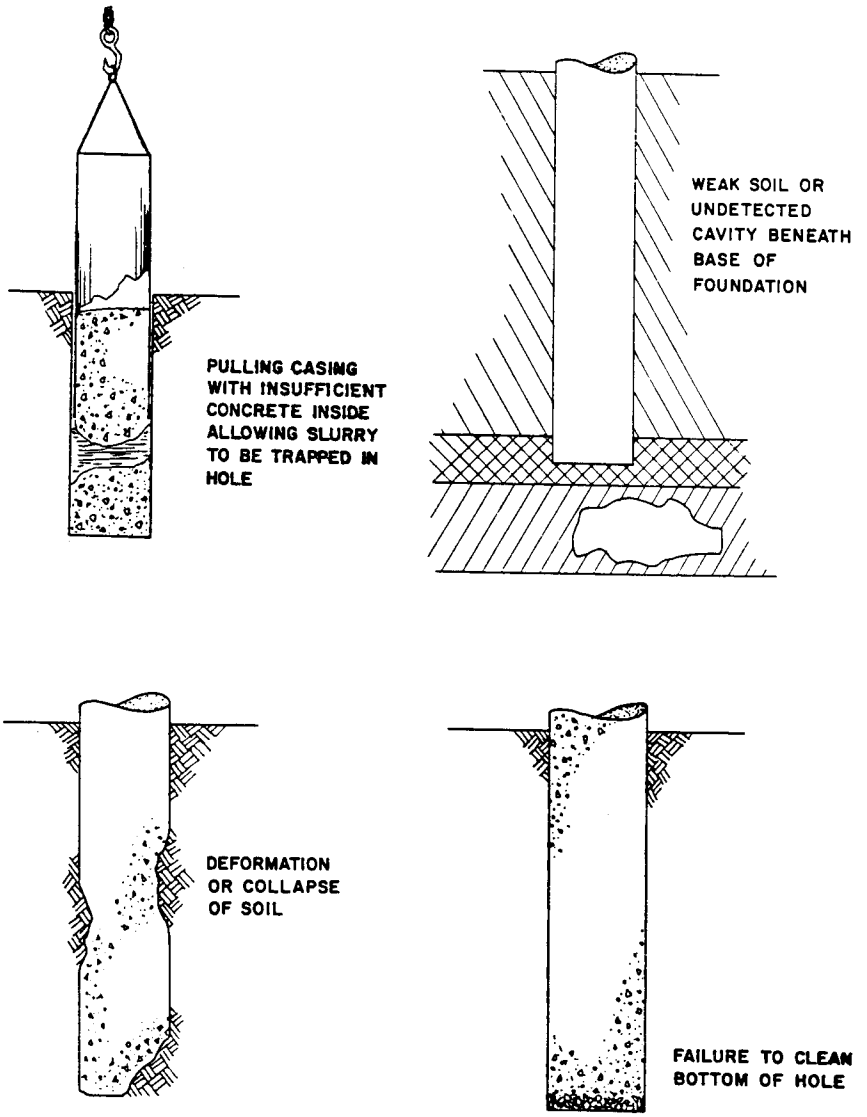

Figure 1-21 *(continued)*

5. Mixing with bentonite affecting the development of strength, and
6. Defects associated with restricted flow of concrete due to heavy cages and other obstacles impeding flow

Methods for checking and repairing defective elements are described by Xanthakos (1979).

Advantages and disadvantages of circular or prismatic shafts. Circular or prismatic shafts are deep foundations that must carry and transfer axial loads, lateral thrusts, and occasionally limit settlement to tolerable values.

Their advantages are summarized as follows:

Table 1–2 Possible Construction Problems with Drilled Shafts

Problem	Solution
Pouring concrete through water	Removal of water by bailing or use of tremie
Segregation of concrete during placing	If free-fall is employed, exercising care to see that concrete falls to final location without striking anything, or use of tremie
Restricted flow of concrete through or around rebar cage	Designing of rebar cage with adequate spacing for normal concrete (all clear spaces at least three times the size of largest aggregate) or use of special mix with small-sized coarse aggregate
Torsional buckling of rebar cage during concrete placement with casing method	Strengthening rebar cage by use of circumferential bands welded to lower portion of cage, use of concrete with improved flow charcteristics, use of retarder in concrete allowing casing to be pulled very slowly
Pulling casing with insufficient concrete inside	Always having casing extending above ground surface and always having casing filled with a sufficient head of concrete with good flow characteristics before casing is pulled
Weak soil or undetected cavity beneath base of foundation	Requiring exploration to a depth of a few diameters below the bottom of the excavation
Deformation or collapse of soil	Such problems are readily detected by even the minimum of inspection
Failure to clean bottom of hole	Modern construction methods permit all but a negligible amount of loose material to be removed by construction tools; inspection can be accomplished from ground surface

(From Reese and Wright, 1977).

1. Cost savings where a single element can substitute a group of piles
2. Excavation that can be extended to a greater depth, and through boulders, rock and hard strata, conditions that often inhibit pile driving
3. Less ground disturbance because of less soil displacement during installation, hence less heave and settlement
4. Less vibrations and noise associated with pile driving
5. Flexible geometry in plan and shape that allows field changes if needed
6. Ability to provide rock sockets to transfer heavier loads by base bearing

Disadvantages result from the following:

1. The work requires specialist contractors, and strict slurry controls
2. Whereas the action of pile driving in certain soils results in densification with associated strength improvement, slurry trench or shaft excavation may cause stress relief with possible expansion
3. The stability of the trench or hole must be maintained until completion; poor soils under artesian conditions tend to inhibit this method of construction
4. A single shaft or prismatic element used in lieu of a group of piles does not provide the redundancy associated with a multiple path system

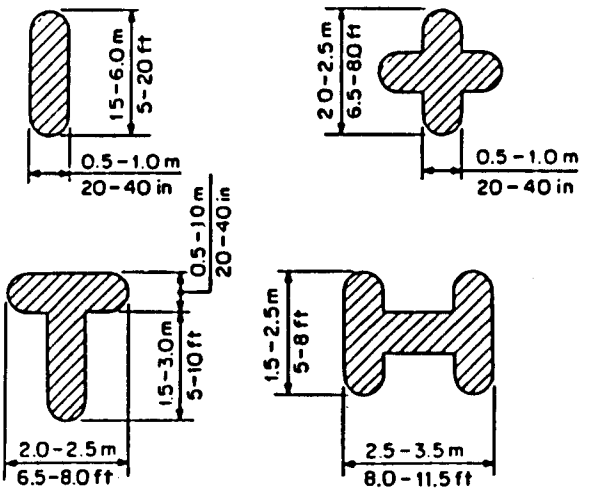

Figure 1–22 Cross sections of typical load-bearing elements.

1.6 SUBSURFACE EXPLORATION AND FOUNDATION INVESTIGATIONS

Foundation Investigations, General Considerations

Procedures and techniques for conducting subsurface investigations for substructure elements and foundations are outlined in the 1988 *AASHTO Manual on Subsurface Investigations.* This document sets forth procedures intended to carry the investigation from its original conception through the various phases of office, field, and laboratory work. Since there are an infinite number of conditions to be met, it is almost impractical to attempt to provide a set of guidelines for all possible cases. This leaves the opportunity for individual judgment and experience to be utilized.

In general, this program can be condensed into three main phases: (1) site reconnaissance and field survey; (2) main field investigation and laboratory testing; and (3) soils and foundation report.

Site reconnaissance and field survey. This phase is not intended to provide solutions to foundation problems, but rather focuses on the need to assess the general site conditions and to articulate the requirements of further investigations. The program addresses site topography, local geology, groundwater conditions, and relevant site characteristics and history.

Main field investigation. This begins with a boring plan prepared and detailed according to ground uniformity, expected substructure location, anticipated loads, and probable type of foundation. With erratic subsurface conditions the boring plan is more detailed and extensive. Where the size of the project and location warrant, the conventional boring program is supplemented by a geophysical survey consisting of cross-hole surveys, seismic exploration, electromagnetic subsurface profiling, and acoustic interpretation.

Foundation exploration implements the boring plan and provides pertinent samples. The wide divergence of geologic and soil conditions encountered in the United States does not warrant a practical and standard methodology in foundation explo-

rations. The objective, however, is the same: to obtain sufficient data regarding subsurface characteristics to expedite a safe and economical foundation design.

Laboratory testing is part of this phase, its main purpose being to verify soil classification and obtain engineering properties. The tests should also reflect the correlation between field work and foundation planning, and should be adequate in articulating the most severe design criteria. Laboratory tests for foundation analysis include mainly classification, strength, and compressibility tests. Dynamic testing of loose sands is indicated if liquefaction or excessive settlement is anticipated in areas of seismic activity and cyclic mobility.

Soils and foundation report. This report addresses the field exploration, laboratory investigations, site conditions, analysis of data, and foundation studies. Anticipated construction problems should be identified, and a firm basis should be established for estimating construction costs. The policy of releasing all available data is encouraged, but reliance upon this information should remain a matter of judgment. Since the associated legal ramifications are obvious, all information contained in the report should be as accurate as possible.

Subsurface Exploration

Objectives. In a typical subsurface exploration program the main objective is to obtain information in order to analyze foundation capacity, stability, and settlement with respect to the following: (1) nature of deposits, including the geologic origin; (2) extent, depth, thickness and elevation of soil and rock units; (3) engineering properties of soil and rock layers including unit weight, shear strength and compressibility; (4) groundwater conditions; (5) ground surface topography, and (6) pertinent information such as liquefiable, expansive or dispersive soil deposits, underground voids, slope instability potential, and chemical properties of soils and groundwater.

Borings are typically taken at pier and abutment locations to establish a reliable longitudinal and transverse substrata profile. Samples of materials are obtained and preserved for reference or testing; boring logs should be prepared in sufficient detail to indicate soil layers, results of penetration tests, and groundwater or artesian action. Care should be exercised to detect any narrow, soft seams that may be located at stratum boundaries.

The subsurface exploration should be extended to competent material of suitable bearing capacity where added stresses due to estimated footing load are less than 10 percent of the existing effective soil overburden stress. If bedrock is encountered at shallow depths, the boring should advance at least 10 feet into bedrock or to the proposed foundation depth, whichever is greater.

The foregoing guidelines articulate the scope of the exploration program but show also its dependence on many site-specific factors and on project requirements. Further useful guidelines have been developed by FHWA (1985), and are summarized in Tables 1–3 and 1–4.

Exploration techniques. Several techniques are available for exploring the subsurface environment at a given site. These differ mainly in the type of equipment or tools to be used and in the manner of advancing the hole. The choice depends largely on the depth

Table 1–3 Guidelines for "Minimum" Boring Programs

Geothechnical Feature	Minimum Number of Borings	Minimum Depth of Borings
Structure Foundation	1 per substructure unit under 100 ft in width 2 per substructure unit over 100 ft in width	Advance Boring: (1) through unsuitable foundation soils (such as peats, highly organic clays, soft clays, etc.) into competent materials of suitable bearing capacity and (2) to depth where added stresses due to estimated foundation load is less than 10% of the existing effective soil overburden stress or (3) minimum of 10 ft into bedrock, if encountered at shallower depth.
Retaining Walls	Borings spaced every 100 ft to 200 ft. Some borings should be in front and in back of wall	Extend borings to a depth of 2 times wall-height or minimum of 10 ft into bedrock.
Bridge Approach Embankments Over Soft Ground	When approach embankments are to be placed over soft ground, at least one boring should be made at each embankment to determine the problems associated with stability and settlement of the embankment. Typically, test borings taken for the approach embankments are located at proposed abutment locations to serve a dual function.	Same as established above for bridge foundation. Additional shallow exploration (hand auger holes) taken at approach embankment locations is an economical way to determine depth of unsuitable surface soils or topsoil.
Cuts and Embankments	Borings typically spaced every 200 ft (erratic conditions) to 500 ft (uniform conditions) with at least one boring taken in each separate landform. For high cuts and fills, should have a minimum of 2 borings along a straight line perpendicular to the centerline or planned slope face to establish geological cross-section for analysis.	*Cuts:* 1) In stable materials extend borings minimum 10 to 15 ft below grade. 2) In weak soils, extend borings below grade to: firm materials, or to the depth of cut below grade whichever occurs first. *Embankments:* Extend borings to firm material or to depth of twice the embankment height
Landslides	Minimum 2 borings along a straight line perpendicular to the centerline or planned slope surface to establish geological section for analysis. Number of sections depends on extent of stability problems. For active slide, place at least one boring above and below sliding area.	Extend borings to an elevation below active or potential failure surface and into hard stratum, or to a depth for which failure is unlikely because of geometry of cross-sections.
Materials Sites (Borrow Pits)	Borings spaced every 100 to 200 ft.	Extend exploration to base of deposit or to depth required to provide needed quantity.

(From Federal Highway Administration, 1985)

Table 1–4. Guidelines for Sampling and Testing Criteria

Item	Recommendations
Sand-Gravel Soils	SPT (split-spoon) samples should be taken at 5-ft intervals or at significant changes in soil strata. Continuous SPT samples are recommended in the top 15 ft of borings made at locations where spread footings may be placed in natural soils. SPT jar or bag samples should be sent to lab for classification testing and verification of field visual soil identification.
Silty-Clay Soils	SPT and 'undisturbed' thin wall tube samples should be taken at 5-ft intervals or at significant changes of strata. Take alternate SPT and tube samples in same boring or take tube samples in separate undisturbed boring. Tube samples should be sent to lab for consolidation testing (for settlement analysis) and strength testing (for slope stability and bearing capacity analysis). Field vane shear testing is also recommended to obtain in situ shear strength of soft clays, silts and well rotted peats.
Rock	Continuous cores should be obtained in rock or shale using double or triple tube core barrels. In structural foundation investigations, core a minimum of 10 ft into rock to ensure that it is a bedrock and not a boulder. Core samples should be sent to the lab for possible strength testing (unconfined compression) for foundation investigation. Percent core recovery and RQD value should be determined in field or lab for each core run and recorded on boring log. However, it would be easier in field to distinguish breaks caused by drilling operations.
Ground Water	Water level encountered during drilling, at completion of boring, and at 24 hours after completion of boring should be recorded on boring log. In low permeability soils, such as silts and clays, a false indication of the water level may be obtained when water is used as drilling fluid and adequate time is not permitted after hole completion for the water level to stabilize (more than one week may be required). In such soils a plastic pipe water observation well should be installed to allow monitoring of the water level over a period of time. Seasonal fluctuation of water table should be determined where fluctuation will have significant impact on design or construction. Artesian pressure and seepage zones, if encountered, should also be noted on the boring log. The top foot or so of the annular space between water observation well pipes and borehole wall should be backfilled with grout, bentonite, or sand-cement mixture to prevent surface water inflow which can cause erroneous groundwater level readings.

(From Federal Highway Administration, 1985)

and nature of the soil and the specified quality of soil samples. Details, uses, and limitations of these techniques are discussed in several good references: Sowers (1979), Tomlinson (1986), and *AASHTO Manual on Subsurface Investigations* (1988).

Laboratory Tests

The basic objective of these tests is to provide data with which to classify soils and to measure relevant engineering properties. They may be grouped into two main categories:

1. Classification tests, performed on either disturbed or undisturbed soil samples.
2. Quantitative tests to determine permeability, compressibility and shear strength.

These are generally performed on undisturbed samples, except for materials that are to be placed as controlled fill or materials that do not have an unstable soil structure. In these cases tests should be performed on specimens prepared in the laboratory.

Where rock strata are encountered, laboratory testing of rock samples has limited applicability, and is intended to give significant rock properties such as compressive strength, shear strength, hardness, compressibility, and permeability. The basic problem in this case is that rock samples small enough to be tested in the laboratory are usually not representative of the in situ rock mass.

In general, laboratory tests should be carried out conforming to relevant AASHTO or ASTM standards.

In Situ Tests

These tests are performed to obtain deformation and strength parameters of foundation soils or rock for analysis and design purposes. In general they are carried out according to relevant AASHTO or ASTM standards.

In situ soil tests. These include the following: (1) standard penetration test; (2) static cone test; (3) field vane test; (4) pressuremeter test; (5) plate bearing test; and (6) well (permeability) test. Certain features of common in situ tests are summarized in Table 1–5.

In situ rock tests. These are performed to obtain the following: (1) deformability and strength of rock by conducting an in situ compressive test; (2) data on direct shear strength of rock discontinuities; (3) modulus of deformation of rock mass using the flexible plate loading method; (4) modulus of deformation of rock mass using a radial jacking test; (5) modulus of deformation of rock mass using the rigid plate loading method; (6) stress and modulus of deformation determination using the flatjack method; and (7) stress in rock using the hydraulic fracturing method.

Special Investigations

Requirements for dynamic design. In addition to the normal exploration and investigation report, it may be necessary to extend this program to determine potential hazards and seismic requirements related to (1) soil strength that can be mobilized, (2) liquefaction, (3) settlement, (4) overall instability, and (5) increases in earth pressure, all as a result of earthquake motions.

Seismically induced slope instability in approach embankments or cuts may displace abutments, leading to differential settlement with associated structural damage. Liquefaction of saturated cohesionless fills or foundation soils can contribute to abutment instability and cause a loss of foundation-bearing capacity and lateral support. Because of the dynamic cyclic nature of seismic loading, the ultimate capacity of the foundation-supporting medium should be used in conjunction with the appropriate load combinations.

Table 1–5 In Situ Tests

Type of Test	Best Suited To	Not Applicable To	Properties that can be Determined
Standard Penetration Test (SPT)	Sand	Coarse Gravel	Qualitative evaluation of compactness. Qualitative comparison of subsoil stratification.
Dynamic Cone Test	Sand and Gravel	Clay	Qualitative evaluation of compactness. Qualitative comparison of subsoil stratification.
Static Cone Test	Sand, Silt and Clay		Continuous evaluation of density and strength of sands. Continuous evaluation of undrained shear strength in clays.
Field Vane Test	Clay	All Other Soils	Undrained shear strength.
Pressuremeter Test	Soft Rock, Sand, Gravel and Till	Soft Sensitive Clays	Bearing capacity and compressibility.
Plate Bearing Test and Screw Plate Test	Sand and Clay		Deformation modulus. Modulus of subgrade reaction. Bearing capacity.
Flat Plate Dilatometer Test	Sand and Clay	Gravel	Empirical correlation for soil type, K_e, overconsolidation ratio, undrained shear strength, and modulus.
Permeability Test	Sand and Gravel		Evaluation of coefficient of permeability.

(From Canadian Foundation Engineering Manual, 1985).

General comments on soil strength and stiffness mobilized during earthquakes, foundation uplift, lateral loading, and soil-structure interaction for substructure and foundations in seismic environments are provided in the AASHTO (1983) specifications for seismic design (included now in the 1992 standard specifications).

Relevant Soil Parameters. In most foundations, the amplitudes of dynamic motion and, consequently, the strains in the soil are usually small for machine effects but large for earthquakes or blasts.

The principal properties relevant to dynamic analysis of foundations include dynamic moduli, such as Young's modulus E and shear modulus G, with corresponding spring constants; damping parameters; and Poisson's ratio. The first two are dependent on the strain amplitude γ_2 since soil behavior is nonlinear. Several good references are available that describe laboratory and field methods used to determine dynamic soil moduli. Typical values of dynamic soil moduli and damping are given by Prakash and Sharma (1990).

Requirements for excavations under slurry. Routine chemical tests of groundwater will disclose conditions that may cause an unstable bentonite slurry. This problem may relate to excessive viscosity, flocculation, slurry loss, and spalling of the excavated face. Relevant factors are the pH and the presence of salt, calcium or organics in the soil. Simple tests may articulate anomalies and indicate the need for remedies. For a discussion of slurry controls necessary to ensure colloidal stability during excavation see Xanthakos (1979, 1994b).

Table 1–6 Correlation of Test Data

Simple Test	Possible Correlation
Water content	Shear strength of clay. Compression index of clay.
Grain size (D_{10}, D_{15}, C_u)	Permeability, strength, and drainability of cohesionless soils.
Liquid limit	Compressibility.
Plastic index	Swell-shrink, drained angle of shearing resistance of clay.
Void ratio, unit weight	Compressibility and shear strength.
Relative density (D_r)	Strength, compressibility of cohesionless soil.
Seismic velocity, (v)	Modulus of elasticity; strength of soil, rock.
Electrical resistivity	Water, clay, organic and salt content.
Penetration resistance, static and dynamic	Shear strength, relative density, modulus of compressibility.

(From Sowers, 1979)

Correlation with Engineering Properties

Several useful correlations have been established between the engineering properties of soils and indirect or classification properties. For initial or preliminary studies this information is reliable and is often used extensively. It may also supplement the source of design data. Sowers (1979) has compiled a summary of correlations of various tests with pertinent design properties, shown in Table 1–6. Equations for stress-strain relationships obtained by several methods are presented in Table 1–7 (Bowles, 1988). Other useful correlations are given in Figures 1–23 through 1–26.

Table 1–7 Equations for Stress-Strain Modulus, E_s by Several Test Methods

Soil	SPT*	CPT
Sand (normally consolidated)	$E_s = 500\ (N + 15)$ $E_s = (15000 \text{ to } 22000)\ \ln N$	$Es = 2 \text{ to } 4\ q_c$ $Es = (1 + D_r^2) q_c$
Sand (over-consolidated)	$E_s = 1800 + 750N$ $E_{sOCR} = E_{sNC}\ (OCR)^{0.5}$	$E_s = 6 \text{ to } 30\ q_c$
Gravelly sand and gravel	$E_s = 600\ (N + 6)\ N<15$ $E_s = 600\ (N + 6) + 2000\ N>15$	
Clayey sand	$E_s = 320\ (N + 15)$	$E_s = 3 \text{ to } 6\ q_c$
Silty sand	$E_s = 300\ (N + 6)$	$E_s = 1 \text{ to } 2\ q_c$
Soft clay	—	$E_s = 3 \text{ to } 8\ q_c$
Clay	expressed in terms undrained shear strength, s_u; and in same pressure units as s_u.	
	$I_p > 30$ or organic: $E_s = 100 \text{ to } 500$ su $I_p < 30$ or stiff: $E_s = 500 \text{ to } 1500$ su $E_{sOCR} = E_{sNC}\ (OCR)^{0.5}$	

Notes:* Units of E_s is in kPa (1 tsf = 100 kPa).
(Modified by Bowles, 1988)

(text continues on p. 53)

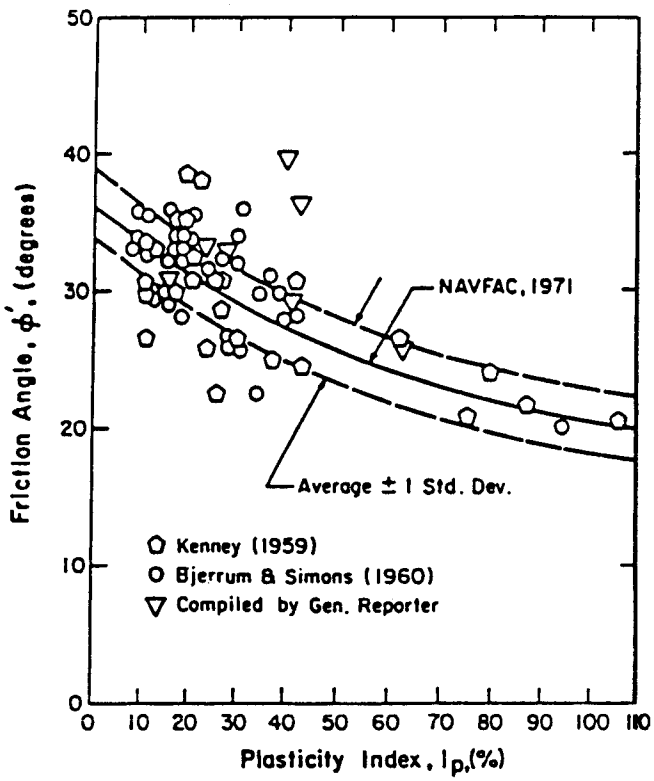

Figure 1–23 Correlation between peak effective friction angle and plasticity index for clays *(from Duncan et al., 1989).*

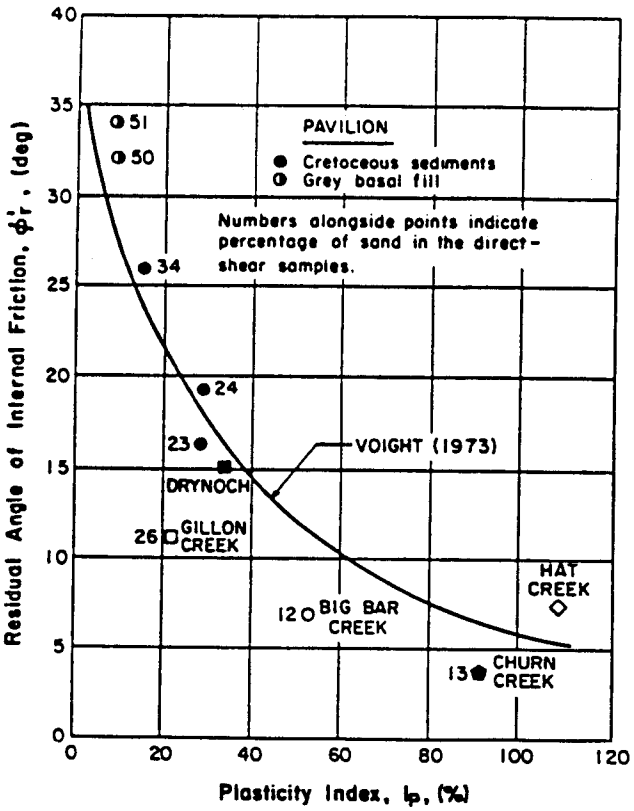

Figure 1–24 Relationship between residual angle of internal friction and plasticity index for clays *(from Duncan et al., 1989).*

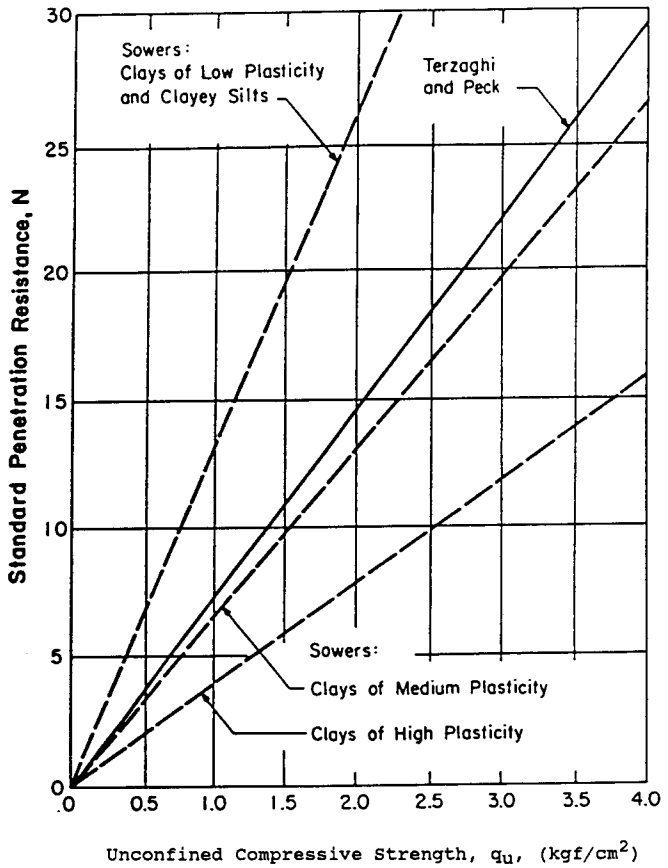

Figure 1–25 Relationship between standard penetration resistance, N, and unconfined compressive strength q_u *(from NAVFAC, 1982).*

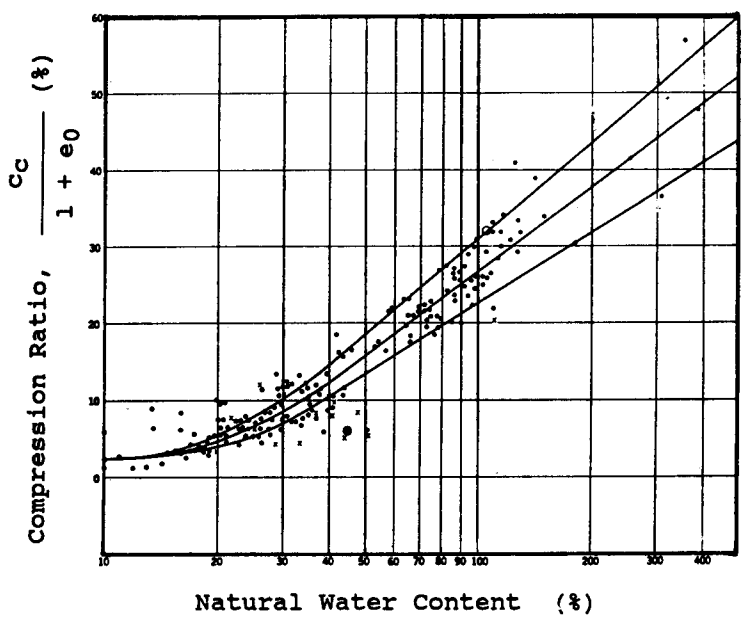

Figure 1–26 Relation between compression ratio and natural water content *(from Lambe and Whitman, 1969).*

Final Report and Recommendations

The data obtained from the exploration program and tests are usually presented in a graphical and tabular form. In addition, a final report is prepared with the intent to analyze and interpret these data, and also make specific design recommendations. Materials and conditions that may be encountered should likewise be discussed.

A typical report format is organized as follows:

1. Foundation studies (spread footing, driven piles, drilled piers, prismatic elements), with consideration of structural capacity, load transfer characteristics, settlement data, and probable cost
2. Pile supports
   - Method of support—friction or end bearing, in rock or in soil or both
   - Suitable pile types—reasons for particular choice or exclusion of types
   - Pile tip elevation (estimated, average values, range of variation). Also explain reasons, such as driving through fill, negative skin friction, scour, underlying soft layers, piles too long and therefore uneconomical, etc.
   - Allowable pile loads for ASD, nominal pile capacity for strength design
   - Settlement considerations, structural requirements versus soil conditions
   - Requirements for test piles and load tests
   - Effects on adjacent construction
   - Scour depth and protection
3. Spread footings
   - Footing elevation
   - Allowable soil pressure for ASD, and nominal bearing pressure for strength design. Tolerable settlement for serviceability states, considering soil, adjacent foundations, groundwater level, etc.
   - Overall footing stability, overturning, sliding, etc.
   - Materials on which footing is to be placed
   - Scour depth
4. Drilled pier foundations (also prismatic elements)
   - Method of load transfer, division between side resistance and base bearing
   - Straight shafts versus underreamed piers
   - Construction requirements (dry drilling, use of casings, use of slurry)
   - Allowable stresses (side shear, base bearing) for ASD, ultimate shear and base bearing for strength design
   - Downdrag forces and uplift
   - Settlement considerations
   - Comparison with other foundation types for cost and structural performance

1.7 SPECIFICATIONS AND STANDARDS

AASHTO Specifications and National Standards

The design philosophy used throughout this book is based on the current *Standard Specifications for Highway Bridges, Fifteenth Edition,* 1992, adapted by the American Association of State Highway and Transportation Officials (AASHTO). This document was initially compiled in 1921, and as design methodology it was gradually developed

and expanded. A complete specifications document was introduced in 1926, revised in 1928, and printed in 1931.

Following the first Standard Specifications published in 1931, the Association has provided revised editions in 1935, 1941, 1944, 1949, 1953, 1957, 1961, 1965, 1969, 1973, 1977, 1983, and 1989. The present fifteenth edition is the result of constant research and development in steel, concrete, and timber design, with an associated expansion of foundation types and support systems. It appears, therefore, that in terms of content and scope these specifications will continue as a developing document, revised from time to time to reflect new knowledge and continuing technical progress. Annual interim specifications are generally added to the document and supplement the contents. The intent of AASHTO is to provide a standard or uniform guide that best addresses the preparation of state standards and can be used as a complete reference by engineers.

In this context, the specifications provide explicit criteria and design methodologies, and stipulate minimum requirements that are consistent with current structural practice, but modifications are often necessary to accommodate local cases or special conditions. Since they apply primarily to the most common and usual bridge type, additional design guidelines may be necessary for unusual or very long bridges. Thus, in conjunction with the Standard Specifications, other relevant documents referred to in the course of this text are:

- *Manual of Subsurface Investigations* (1988), outlining the diverse techniques for conducting subsurface investigations for transportation facilities.
- *Foundation Investigation Manual* (1978), giving the sequential development of foundation investigation.
- *Guide Specifications for Seismic Design* (1983, and interim up to 1988), giving comprehensive guidelines that embody new concepts, now included in the 1992 standard specifications.
- *Guide Specifications and Commentary for Vessel Collision Design of Highway Bridges,* developing criteria based on observed performance during collision and on recent research (1991).
- *Guide Specifications for Design and Construction of Segmental Concrete Bridges,* articulating the new concepts in design and construction (1989).
- *Manual for Maintenance Inspection of Bridges* (1990), intended to provide uniformity in assessing the physical condition and maintenance need of bridges.

In addition, the text refers frequently to reports, studies, guidelines, and design documents prepared by the FHWA, to the current *Manual of Steel Construction* (AISC), to the current ACI *Concrete Code,* and applicable ASTM Standards. In neighboring Canada, important technical documents in bridge design include the *Ontario Highway Bridge Design Code,* and the publication *Design of Highway Bridges,* National Standard of Canada.

State Standards

Most states have bridge design manuals as part of a program to develop, maintain, and administer the policies that govern the design and preparation of plans and specifications for bridges. These manuals represent a compilation of design and plan presenta-

tion procedures, specification interpretations, standard practices, and details that constitute policy. Invariably, design policies are based on the AASHTO Standard Specifications with an attempt to unify and clarify design criteria, but they do not preclude justifiable exceptions that are based on sound engineering principles.

Likewise, the manuals are active in the sense that they are revised and expanded continuously as results from ongoing research and as new products become available. They cover planning, design, plan development, superstructure and substructure types, steel and concrete details, and foundations.

AASHTO LRFD Bridge Design Specifications (1994)

Until the early 1970s highway bridges in the United States were designed using working stress methods (also referred to as allowable stress design, ASD). In the mid-1970s AASHTO introduced load factor design, also known as ultimate strength design, as an alternative but equally approved method for designing the portions of a bridge above the foundation. An inherent inconsistency in this approach has been the fragmentation of the methodology whereby superstructures are designed using the ultimate strength approach, and foundations are proportioned using working stresses and service loads.

Recently, the underlying philosophy has been to move toward a more rational and probability-based procedure that can provide a formidable substitute for the deterministic nature of ASD. At the same time, the development of suitable load factor design criteria for bridge superstructures, substructures, and foundations would eliminate the previous inconsistencies and would ensure a rational and more efficient method of analysis.

The 1994 AASHTO LRFD Bridge Design Specifications is the result of research requested by AASHTO and initiated by the National Cooperative Highway Program (NCHRP) as Project 12-33. This document draws from completed and recent bridge research, and signifies new provisions and major areas of change. It addresses load models and modified load factors, structural analysis, concrete and steel structures, decks and deck systems, foundations, and bridge substructure elements. These specifications are interchanged and compared with ASD throughout this text.

Design philosophy. Bridges and their components must be designed for the specified limit state. All structural systems must be proportioned to reach the design failure mechanism before any other mechanism is developed. For example, unintended overstrength of a member or component where hinging is predicted should be avoided since it may result in the formation of a plastic hinge at an undesirable location and with adverse effects.

Service limit states represent restrictions on stress, deformations and crack width under normal service conditions. The non-strength status relegates function as main objective.

Fatigue limit states are selected as restrictions and limitations on the stress range under a single design truck to ensure structural safety within the expected stress range variations and cycles. The fracture limit state represents a set of material toughness requirements of the AASHTO Material Specifications.

Strength limit states are intended to provide structural strength and stability, partially or wholly, local or global, necessary to resist the statistically possible load combinations that may act on a bridge during its design life.

Extreme-event limit states relate to the structural survival of a bridge during a major earthquake, or when collided by a vessel, vehicle, or ice flow.

It appears that the basis of any design approach should be to ensure that (1) if loads, material strengths and stiffness, and the like, are as expected, the bridge will function satisfactorily within acceptable deformations, and (2) even if both loads and materials are significantly worse than expected (reach the worst credible values), there will still be sufficient (ultimate) strength to prevent structural collapse.

Whenever a bridge and its components reach a point where they no longer satisfy the design requirements, they are said to have reached a limit state. Limit states are classified as either ultimate stages associated with the worst credible values that the related parameters could reach, or serviceability limit states where the most probable (normal) values are used. In principle all limit states should be examined explicitly, but in practice only one may be more critical than the others.

In this context, a bridge, its foundation, and the ground on which it rests constitute a combined system of ground/structure whose implicit interaction must be recognized. Accordingly, an ultimate limit state is reached when (1) failure in the ground occurs without failure in the structure, involving loss of stability or causing substantial rigid body movement; (2) failure in the structure occurs with associated instability or structural fracture but without failure in the ground; and (3) failure occurs in the structure and ground together.

Serviceability limit states include (1) excessive deformation of the ground leading to excessive (unacceptable) differential settlement, heave, lateral movement, and so forth, of the structure; (2) excessive deformation (deflection) of bridge components; and (3) excessive cracking of the structure.

1.8 COST CORRELATION, SUPERSTRUCTURE VERSUS SUBSTRUCTURE

General

A suitable bridge type is one that satisfies function, aesthetics, structural requirements, and minimum cost. The selection of materials and structural forms for the superstructure is a complex procedure since it must consider all factors affecting design, including the relationship with the substructure and foundation, the cost of fabrication, construction procedures, ground conditions, bridge height, and erection constraints.

The relationship of span to structural type, and hence to substructure and foundation design, becomes obvious from an analysis of statistical data. Table 1–8 relates span length to superstructure type. The last column, showing the maximum span in service for the particular type, is probably the most significant indication of structural feasibility and its dependence on span length. In the medium-span range (400–700 feet or 120–210 m) the choice becomes broader in terms of structure type and materials, and is further enhanced in the small-span range.

Conventional grade separations. For grade separation structures discussed in section 1.2, the location of substructure elements is usually determined by intersection geometry, roadway cross sections and median width, embankment slopes, and horizontal clearance to traveled roadways. These considerations result in a fixed pier and abut-

Table 1–8 Span Length Range for Various Superstructure Types

Structural Type	Material	Range of Spans (ft)	Maximum Span in Service (ft)
Slab	Concrete	0–40	
Girder	Concrete	40–700	682, Bendorf
	Steel	100–860	856, Sava I
Cable-stayed girder	Concrete	<800	771, Maracaibo
	Steel	300–1100	1050, Knie
Truss	Steel	300–1800	1800, Quebec (rail) 1576, Greater New Orleans (road)
Arch	Concrete	300–1000	1000, Gladesville
	Steel truss	800–1700	1675, Bayonne
	Steel rib	400–1200	1200, Port Mann
Suspension	Steel	1000–4500	4260, Verrazano*

*Currently the Humber Bridge in England is the longest suspension span.

ment location, a predetermined pier type and abutment configuration, and a suitable foundation system. The superstructure is developed from a comparison of steel and concrete structural systems to accommodate the substructure location and the resulting span lengths. This procedure involves little, if any, correlation between deck and substructure types. In certain exceptions, alternative bridge systems may be compared for cost and function, for example, a four-span bridge with pile-bent abutments on fill versus a two-span structure with full abutments at grade level.

Congested sites. Likewise, in congested sites such as the four-level interchange shown in Figure 1–27, substructure elements (columns, single hammerheads, shafts, etc.) are determined by space availability, clearance, constructibility, and erection constraints. A superstructure scheme is developed to best accommodate the bridge supports in structural, functional, and esthetic terms.

Example of Cost Correlation

A cost comparison between superstructure and substructure can be made as in the example presented in this section. Typical unit prices for concrete and steel, the two predominant materials in bridge construction, are given in Table 1–9. These values are representative of a specific region, and are average for the year indicated. They cover a steel superstructure supporting a concrete deck, concrete piers, and concrete piles as foundation elements.

Based on these unit prices of steel and concrete, the superstructure cost for a simply supported composite girder bridge is given graphically in Figure 1–28. This bridge consists of cast-in-place deck carried on welded plate girders. The lower bound of the curves gives a linear variation of cost vs. span, expressed as

$$C_u = 1.5 + \frac{L}{20} \tag{1–1}$$

where C_u = superstructure cost, \$/sq. ft., and L = span length, ft.

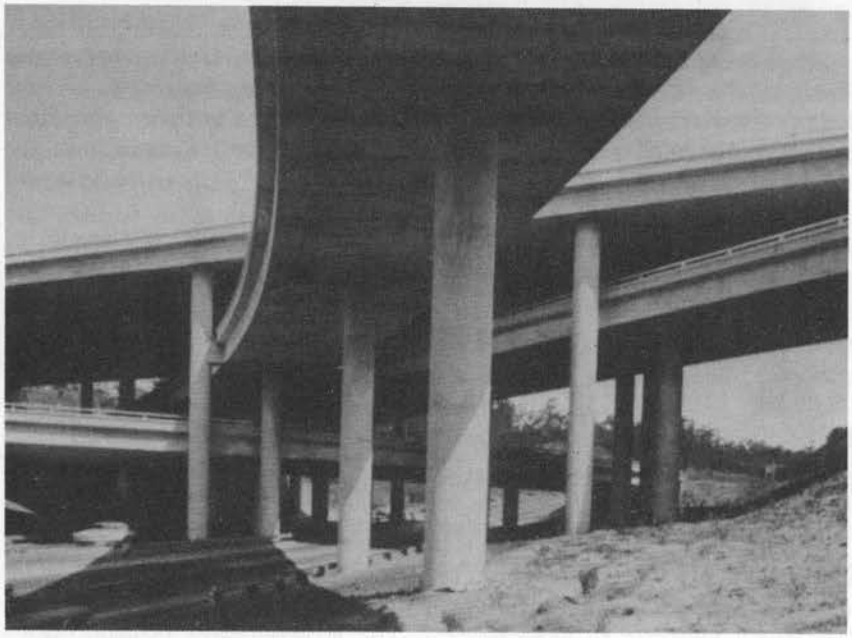

Figure 1–27 Four level interchange, San Diego, California. *(California Division of Highways).*

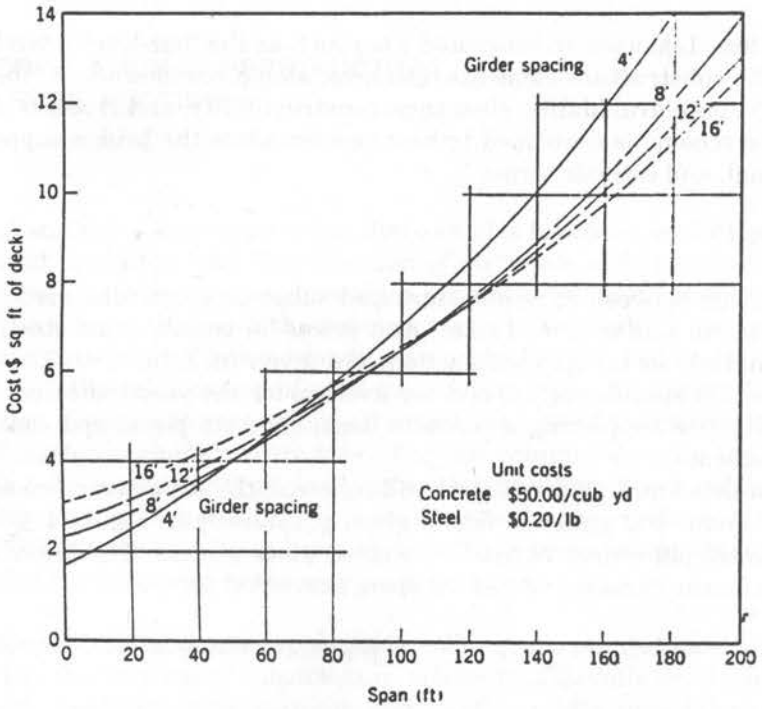

Figure 1–28 Theoretical costs (1969 dollars) of steel and concrete composite girder bridge.

Table 1–9 Unit Costs in Composite Steel and Concrete Bridge and Pile Foundation (1969 dollars)

Steel girder, in place	\$0.20/lb
Steel reinforcement, in place	\$0.20/lb
In situ concrete, in place	\$50.00/yd^3
Concrete in piles, in place	\$100.00/yd^3
Prestress	\$0.05/kip-ft

These costs are suitable for comparative purposes only. Current unit prices are much higher and may vary considerably in many parts of the world.

O'Connor (1971) has demonstrated that a computer program can be developed to give the cost of any pier, for example a pier with one, two, or three rows of circular prestressed concrete piles, a solid wall, and cast-in-place concrete pile cap, with its top at ground level. The bridge is assumed to have an infinite width and to consist of an infinite number of successive simply supported spans.

Using the unit prices of Table 1–9 the composite substructure/foundation cost per foot width of substructure is given graphically in Figure 1–29 for three pier heights, and evidently this cost increases linearly with span length but at a moderate rate. A 30 foot

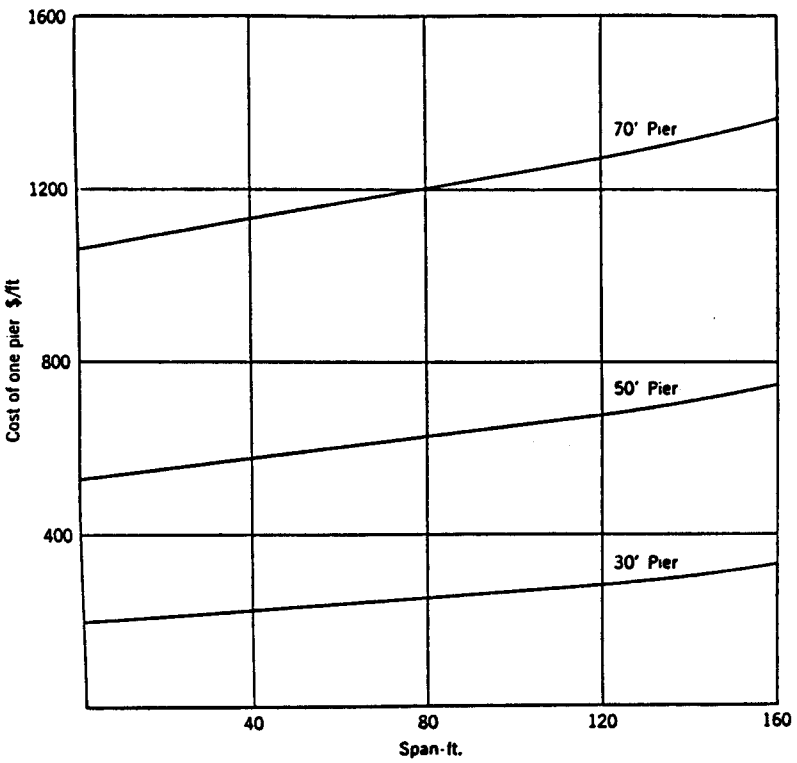

Figure 1–29 Foundation costs for bridges with various span lengths (1969 dollars).

pier has a cost of 200 + 0.7L (dollars). The corresponding surcharge to the superstructure cost per unit area of deck is this value divided by L, or

$$C_u = \frac{200}{L} + 0.7 \tag{1–2}$$

Superstructure and substructure cost for this example are given graphically in Figure 1–30. They are presented separately and in a composite form to obtain total bridge cost (O'Connor, 1971). Apparently, for each pier height there is an optimum span that may be computed as follows:

$$C_u = A_1 + A_2 L, \qquad C_L = A_3 + A_4/L \tag{1–3}$$

or

$$C = C_u + C_L = A_1 + A_2 L + A_3 + A_4/L \tag{1–4}$$

For the optimum condition

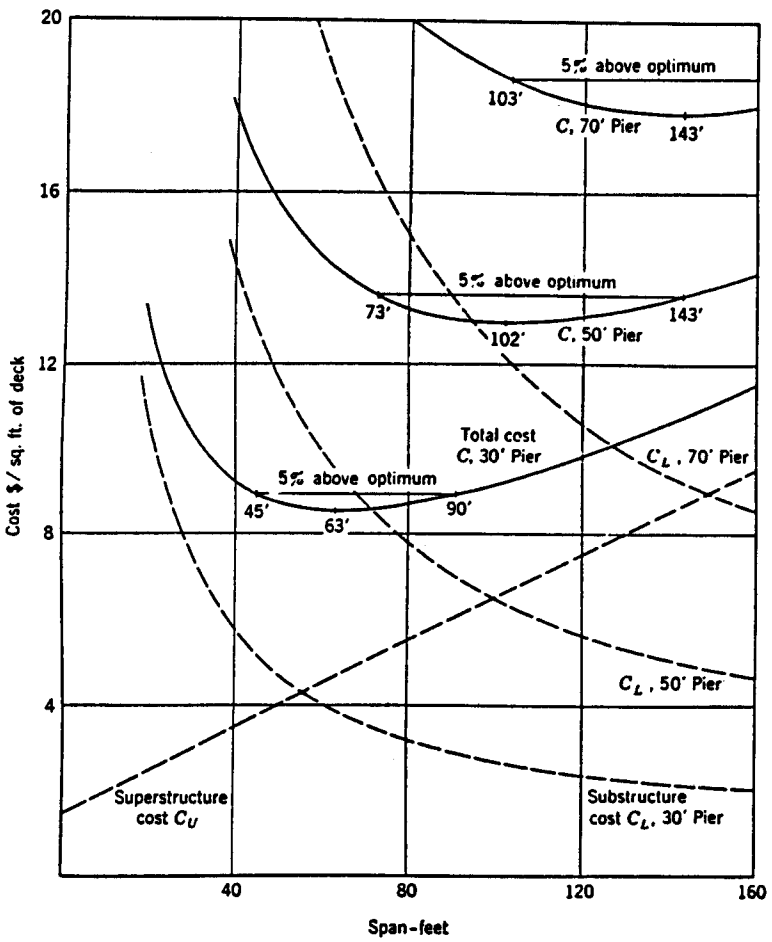

Figure 1–30 Superstructure, substructure, and total bridge costs for various spans (1969 dollars).

$$\frac{dC}{dL} = A_2 - \frac{A_4}{L^2} = 0 \tag{1–5}$$

which gives

$$L = L_0 = \left(\frac{A_4}{A_2}\right)^{1/2} \tag{1–6}$$

For a 30-foot pier, A_2 = 1/20 (Equation 1–1), and A_4 = 200 (Equation 1–2), we obtain the optimum length from Equation (1–6), or

$$L_0 = \sqrt{4000} = 63 \text{ ft}$$

which agrees with the value obtained from Figure 1–30.

From Equation (1–6) it follows that the optimum span varies as the parameter $\sqrt{A_4/A_2}$. Thus if the superstructure cost C_u and the substructure cost C_L are doubled or both reduced by one-half, the optimum span does not change. If the cost of the substructure is doubled, the optimum span increases by $\sqrt{2}$. If C_u and C_L have the simple form of Equation (1–3), the parameters A_2 and A_4 can be obtained from an exact design of any two spans.

The total bridge cost is rather insensitive to nominal deviations from the optimum span. For example, let us assume that the optimum cost C_0 corresponds to the optimum span L_0. Then

$$L_0 = \left(\frac{A_4}{A_2}\right)^{1/2} \quad \text{and} \quad C_0 = A_1 + A_3 + A_2L_0 + A_4/L_0$$

For the special case $A_1 + A_3 = 0$, $C_0 = 2\sqrt{A_2A_4}$

Let $L = KL_0$, then $C = A2L + A_4/L$

or $C = A_2KL_0 + \dfrac{A_4}{KL_0} = \left(K + \dfrac{L}{K}\right)\sqrt{A_2A_4}$

from which it follows that

$$\frac{C}{C_0} = \frac{C}{2\sqrt{A_2A_4}} = \frac{1}{2}\left(K + \frac{1}{K}\right) \tag{1–7}$$

The percentage deviation can be illustrated by a simple example. Consider the case C/C_0 = 1.05. Then K = 0.73 or 1.37; that is, for spans between 0.73 and 1.37 times the optimum span, the cost will not exceed the optimum by more than 5 percent. Referring to Figure 1–30, a 5 percent cost increase corresponds to a span range 0.71 to 1.43 times the optimum.

1.9 DESIGN EXAMPLE 1–1

Figure 1–31 shows the profile of the relocated Market Street in the city of Waukegan, Illinois. A preliminary study was made to address the following objectives:

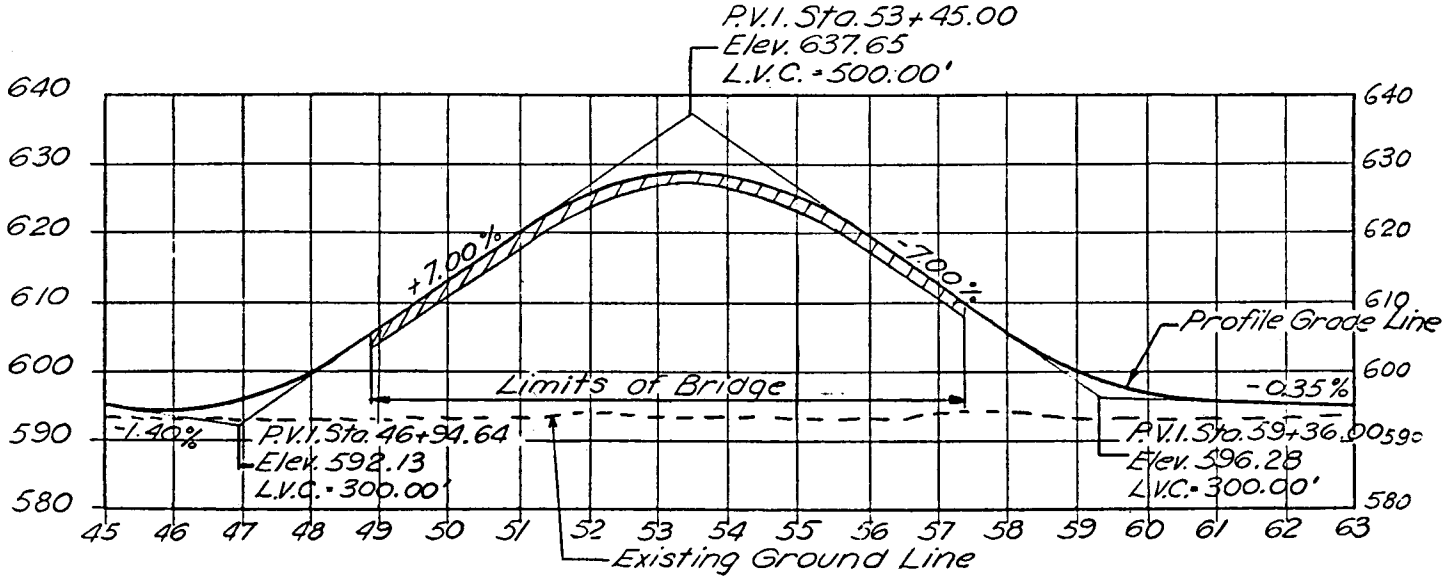

Figure 1–31 Profile of relocated Market Street.

Table 1–10 Unit Prices, Design Example

Concrete	$75.00/cu. yd.
Reinforcement bars	13¢/lb
Structural steel	16¢/lb
Aluminum handrail	$10.00/lin. ft
Protective coat	.83¢/lin. ft
Piles	$7.00/lin. ft.
Class A excav.	$3.00/cu. yd.
Embankment	$1.20/cu. yd.
Prestressed concrete beams	$21.00/lin. ft.
24′ Concrete pavement (total)	$50.00/lin. ft.

1. Compare the cost of retaining walls on one or on both sides of earth embankment, carrying the roadway for the relocated Market Street, with the cost of embankment with free slopes on both sides, and with the cost of a bridge structure (viaduct).
2. Establish the limits of these alternatives along the ends of the project.
3. Investigate various bridge types in conjunction with suitable superstructure and substructure systems, and establish optimum span and cost.

Unit prices for the main items entering into the analysis are shown in Table 1–10, and refer to the 1964 average price level in the region. The same example analyzed under current price trends would have essential similarities in terms of methodology, accepting the variations in the index of price increases between various items and materials. In addition, current analysis would also have to consider the entire range of alternative walls and foundation types discussed in the foregoing sections.

The design method is ASD, conforming to the 1961 AASHTO Standard Specifications in conjunction with Illinois standards and policies. Alternative schemes for the north and the south end of the project are shown in Figure 1–32(a) and (b), respectively. The feasibility of these schemes is consistent with the design requirements, and depends on cost, structural considerations, and geometry.

Optimization of bridge. For a 37-foot roadway width (0. to 0. of deck) shown in Figure 1–32, the analysis considered the optimum range of wide flange steel I-beams, namely W24 × 68, W24 × 76, W27 × 84, W33 × 118, W36 × 135, and W36 × 150, arranged at a spacing of 7 feet 3 inches within the 28-foot roadway, and a spacing of 4 feet under the sidewalk. For this investigation, the typical pier shown in Figure 1–33 was selected as the substructure element, with a spread footing approximately 10 feet below ground line. For each beam size, an analysis was then carried out for a typical 5- or 4-span continuous unit as follows:

W24 × 68 = 5-spans, lengths (ft)	= 27, 34, 34, 34, 27	total = 156 ft
W24 × 76 = 5-spans, lengths	= 30, 37.5, 37.5, 37.5, 30	total = 172.5 ft
W27 × 84 = 5-spans, lengths	= 33.5, 42, 42, 42, 33.5	total = 193 ft
W33 × 118 = 5 spans, lengths	= 45, 56.5, 56.5, 56.5, 45	total = 260 ft
W36 × 135 = 4 spans, lengths	= 56, 71, 71, 56	total = 254 ft
W36 × 150 = 4 spans, lengths	= 61, 77, 77, 61	total = 276 ft

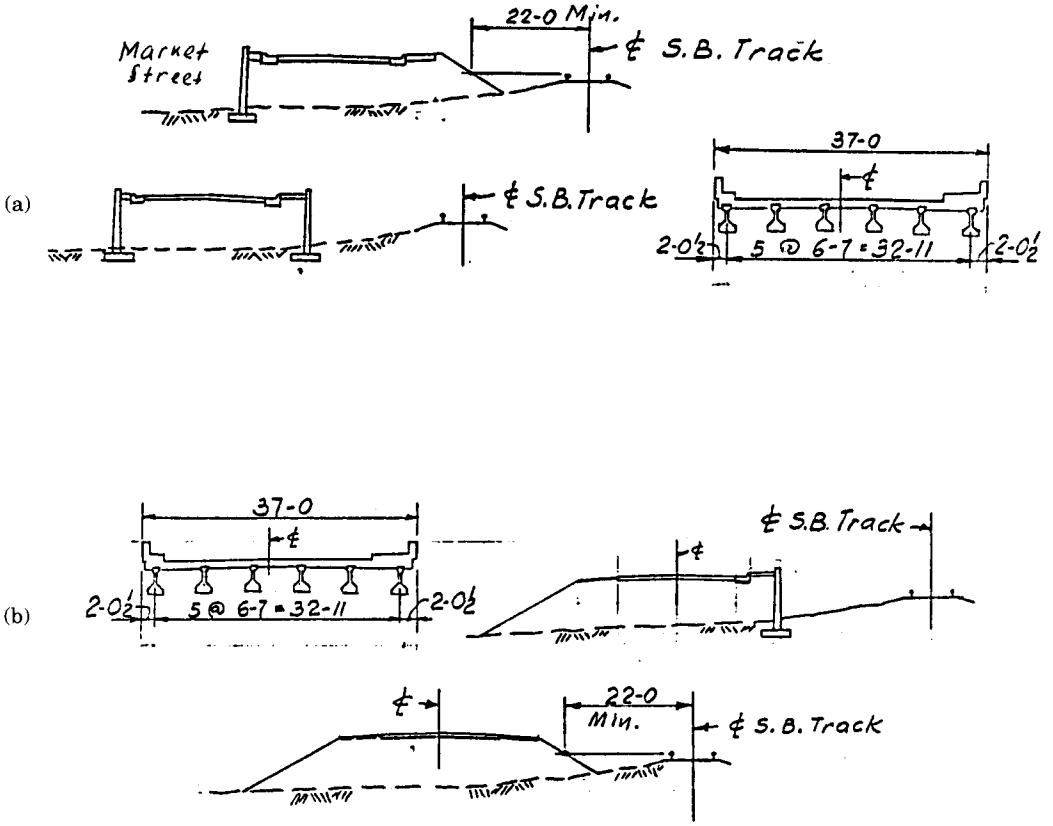

Figure 1–32 Alternative schemes, relocated Market Street; (a) north end (embankment with retaining wall on Market Street side and free slope on the other; embankment with retaining walls on both sides; bridge structure); (b) south end (bridge structure; retaining wall on railroad side; embankment on both sides).

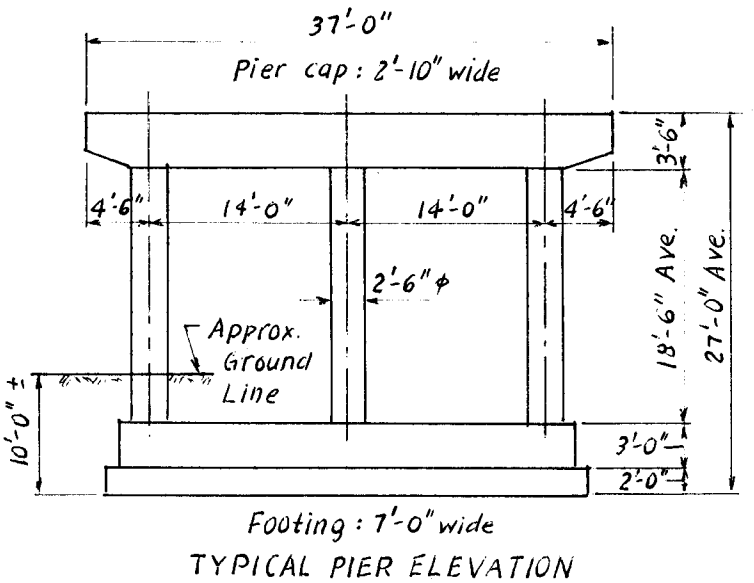

Figure 1–33 Pier type, proportions, and dimensions used for the superstructure analysis.

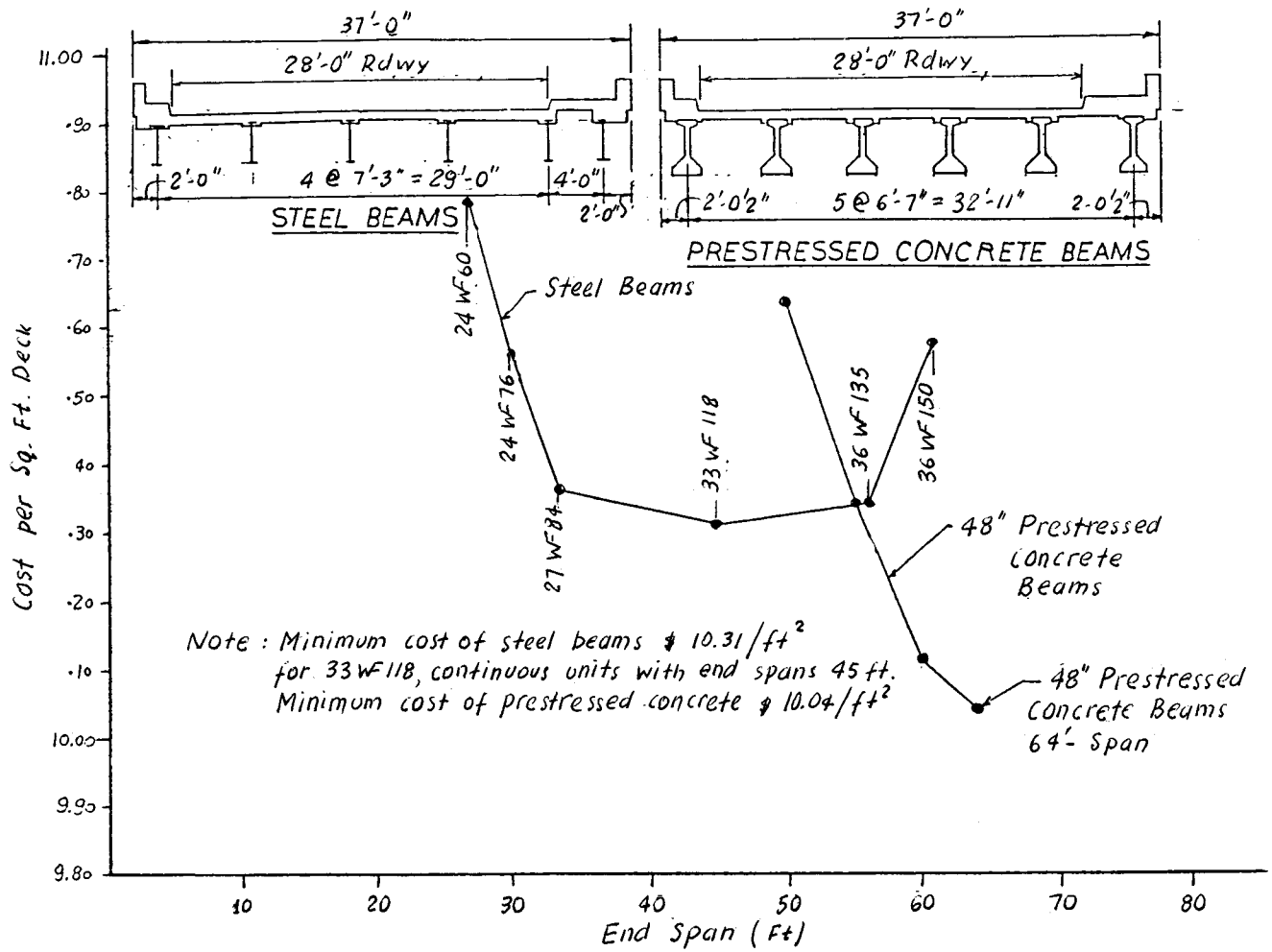

Figure 1–34 Total bridge cost of Design Example 1.1; steel beams versus prestressed concrete beams.

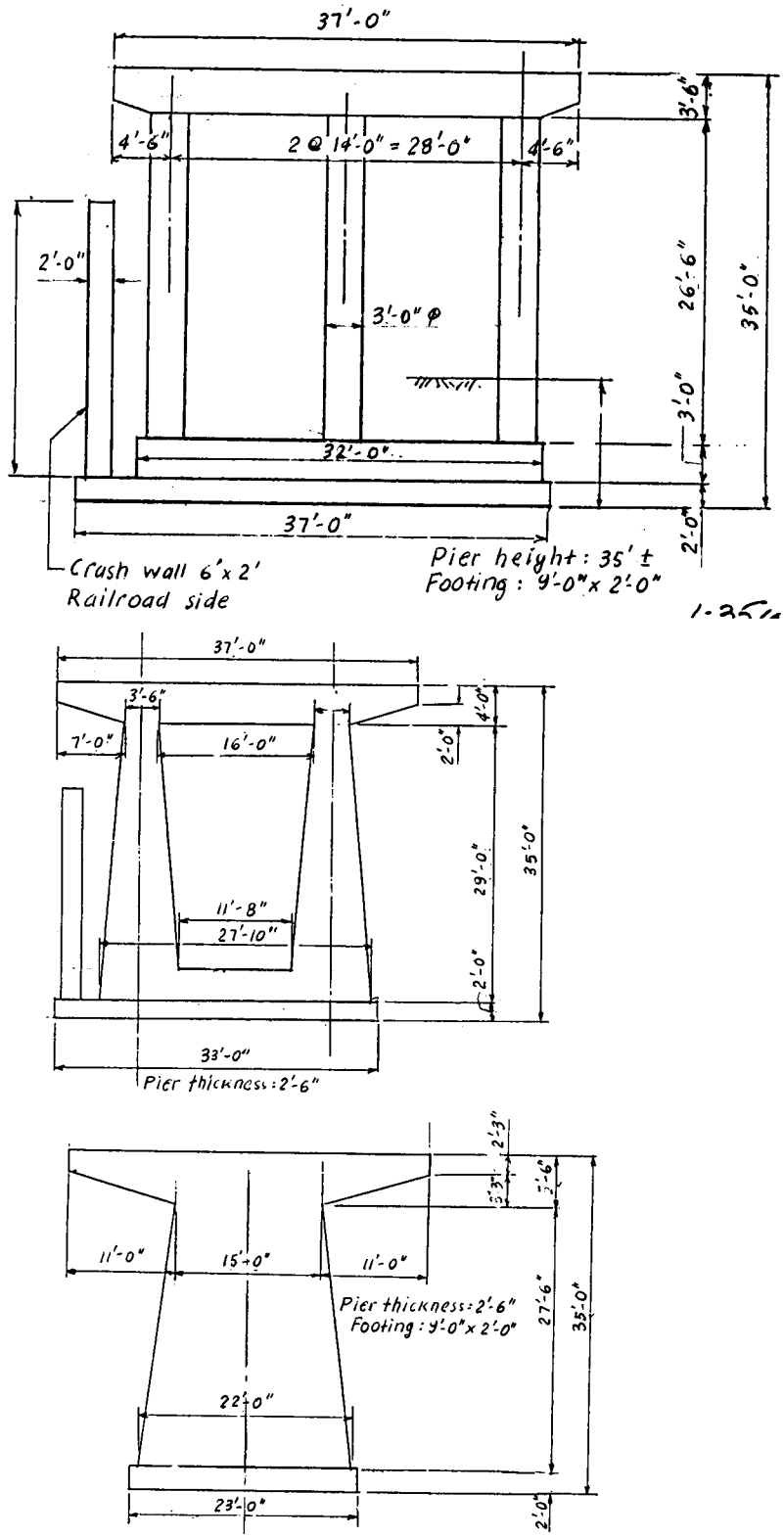

Figure 1–35 Pier types considered in final analysis, Design Example 1.1; (a) round-column pier; (b) double hammerhead; (c) single hammerhead.

For the purpose of obtaining total bridge cost, five piers were included in the 5-span continuous units, and four piers were added to the 4-span continuous units.

A similar analysis was carried out for typical (standard) 48-inch prestressed concrete beams, considering a span range of 50, 55, 60, and 64 feet. The upper limit of span length (64 ft) was established after fixed quotations from prestressed beam fabricators shows a unit price of $20/linear foot, up to 65 feet in length. Likewise, a number of piers equal to the number of spans was added to each bridge unit to obtain total (composite) cost.

The resulting costs from this analysis are presented in graphical form in Figure 1–34 for the steel beams and the prestressed concrete beams. The cost values shown are composite and include a 7-inch concrete slab, parapets, railing, supporting beams, concrete piers, class A excavation, and protective coat for the deck. This comparison suggests that prestressed concrete beams are in this case less expensive, and the cost difference represents a distinct advantage over other types.

The investigation was extended further to compare various pier types such as the initially selected round-column pier, versus a double hammerhead and a single hammerhead type, shown in Figure 1–35(a), (b), and (c), respectively. Note that for this com-

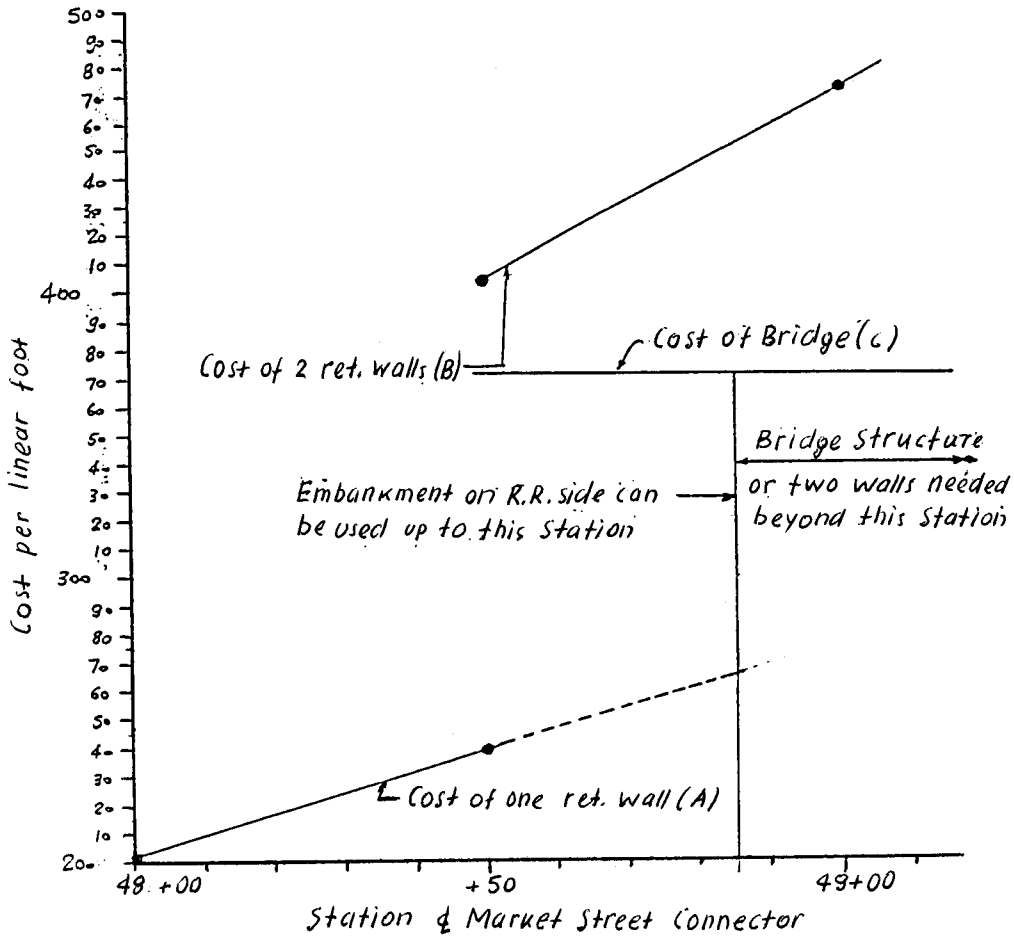

Figure 1–36 Cost comparison, Design Example 1.1, north end.

parison, the pier height is 35 feet, and column diameter is 3 feet. Note also that for the column and the double-hammerhead pier a crash wall must be provided on the railroad side as shown. This makes the solid pier of the single hammerhead type the most economical, with the double hammerhead and the column pier having a cost 5 percent and 16 percent higher, respectively.

Cost comparison, north end. Referring to Figure 1–32(a), studies were made for the following alternatives: (1) roadway with retaining wall on one side and free-slope embankment on the railroad side; (2) roadway with retaining walls on both sides; and (3) roadway on structure as optimized in first analysis. The associated costs are shown for each alternative in Figure 1–36. Alternative (2), two retaining walls, is more economical than alternative (3), bridge structure, up to a height h of 14 feet (where h is measured from the bottom of the wall footing to the finished roadway). Alternative (1) is found more economical than both (2) and (3) for h values up to 20 feet. However, alternative

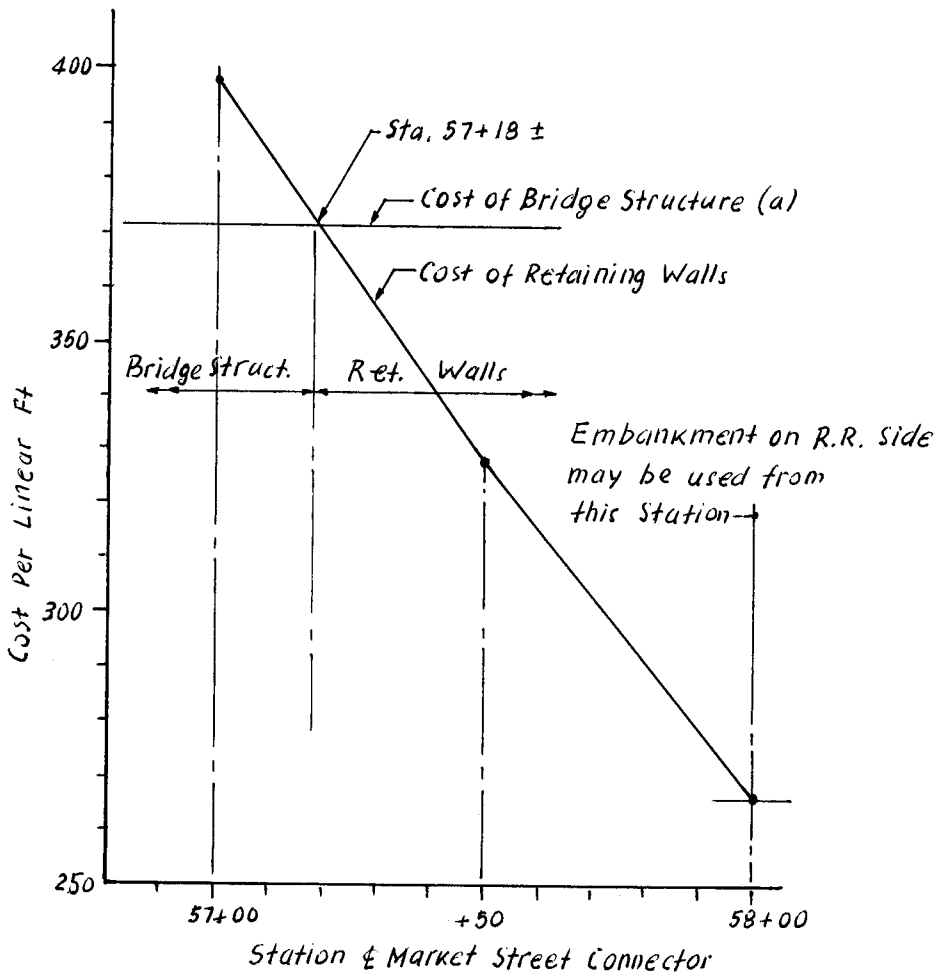

Figure 1–37 Cost comparison, Design Example 1.1, south end.

(1) must also satisfy the criterion of minimum horizontal distance of 22 feet (state standard) to the center line of the track, satisfied up to Station 49+00. At this point h is almost 19 feet, hence the bridge structure begins approximately at the same location.

For this analysis, studies were also made to establish the most economical foundation type for the retaining walls (spread footing versus piles). For small wall heights, spread footings are economical, although the results were not conclusive.

Cost comparison, south end. Referring to Figure 1–32(b), studies were made for the following alternatives: (1) roadway on structure as optimized in first analysis; (2) roadway with retaining wall on one side and free-slope embankment on the other; and (3) free-slope embankment on both sides. Likewise, the associated costs are shown in Figure 1–37 for alternatives (1) and (2), and these establish the limits of bridge structure as shown. Alternative (3), free-slope embankment on both sides, is feasible past Station 58+00 where the minimum horizontal clearance of 22 feet is satisfied.

REFERENCES

AASHTO, 1983: *Guide Specifications for Seismic Design of Highway Bridges,* American Association of State Highway and Transportation Officials, Washington, D.C.

AASHTO, 1989: "Guide Specifications for Design and Construction of Segmental Concrete Bridges."

AASHTO, 1992: *Standard Specifications for Highway Bridges,* American Association of State Highway and Transportation Officials, Washington, D.C.

AASHTO, 1994: AASHTO LRFD Bridge Design Specifications.

American Association of State Highway and Transportation Officials, 1988: *Manual on Subsurface Investigations,* Washington, D.C., p. 391.

BELIDOR, 1729: La Science des Ingenieurs, Paris.

BENDIXEN, A., 1914: Die Methode der Alpha-Gleichungen zur Berechnung von Rahmenkonstrukionen, Berlin.

BOWLES, J. E., 1988: *Foundation Analysis and Design,* 4th ed. McGraw-Hill Publ. Co.

BURKE, M., 1990: "Integral Bridges," Transp. Research Record 1275, TRB, *National Research Council,* Washington, pp. 53–61.

CALISEV, K. A., 1923: Technicki list, Nos. 1–2, and Nos. 7–21, Zabreb, Yugoslavia.

Canadian Geotechnical Society, "Canadian Foundation Engineering Manual," 2nd ed., Bitech Publishers Ltd., 1985, p. 460.

CARSON, A. B., 1965: "Foundation Construction," McGraw-Hill Book Co., New York, p. 424.

CHELLIS, R. D., 1961: *Pile Foundations,* McGraw-Hill Book Co., 2nd ed., New York.

CHELLIS, R. D., 1962: *Pile Foundations in Foundation Engineering,* Chap. 7, G. A. Leonards, ed., McGraw-Hill Book Co., New York.

CREMONA, L., 1872: Le Figure Reciproche nella Statica Grafica, Milan.

CROSS, H., 1930: "Analysis of Continuous Frames by Distributing Fixed-End Moments," *Proc. ASCE,* vol. 56, May, pp. 919–928.

CULMANN, K., 1851: "Der Bau der holzernen Brucken in der Vereinigten Staaten von Nordamerika," Allgemeine Bauzeitung, vol. 16, Vienna, pp. 69–129.

Department of the Army, "Design of Pile Foundations," 1992: *U.S. Army Corps of Engineers,* Washington, D.C. 20314-1000, Publ. No. EM 1110-2-2906.

DUNCAN, T. M, R. C. HORZ, and T. L. YANG, 1989: "Shear Strength Correlations for Geotechnical Engineering," Virginia Polytechnic Institute and State University, Blacksburg, VA.

EMANUAL, J. H., et al., 1983: "Current Design Practice for Bridge Superstructures Connected to Flexible Substructures," Univ. Missouri, Rolla.

Federal Highway Administration, 1985: Checklist and Guidelines for Review of Geotechnical Reports and Preliminary Plans.

FREZIER, 1739: Traite de la coupe des pierres, vol. 3, Strasbourg, France.

FULLER, F. M., 1983: *Engineering of Pile Installation,* McGraw-Hill Book Co., Chap 2, 3, & 6.

HEINS, C. P. and R. WANG, 1976: "Influence Lines for Slant Legged Rigid Frame Highway Bridges," *Civil Engineering Report,* Univ. of Maryland, College Park, MD, June.

GAMBLE, W. L., 1984: *Bridge Evaluation Yields Valuable Lesson,* Concrete International, June, pp. 68–74.

GRIMM, C. T., 1975: "Rationalized Esthetics in Civil Engineering," ASCE, *Journ. Struct. Div.,* vol. 101, No. ST9, Sept., pp. 1813–1822.

GRIMM, C. T. and W. F. E. PREISER, 1976: "Civil Engineering Esthetics," *J. Struct. Div. ASCE,* vol. 102, No. ST8, Aug., pp. 1531–1536.

KUZMANOVIC, B. O., 1977: "History of the Theory of Bridge Structures," *J. Struct. Div. ASCE,* vol. 103, No. ST5, May, pp. 1095–1111.

JORGENSON, J. L., 1983: "Behavior of Abutment Piles in an Integral Abutment Bridge," Transp. Research Record 903, TRB, *National Research Council,* Washington, D.C.

LAMBE, T. W. and R. V. WHITMAN, 1969: *Soil Mechanics,* Wiley, New York.

LAHIRE, P., 1965: Traite de Mechanique, Paris.

LAW, F. M., 1972: "Aesthetics—Part of Civil Engineering Design," Engineering Issues, *Journ. of Professional Activities,* ASCE, vol. 98, No. PP2, Proc. Paper 8850, April, pp. 275–285.

MANDERLA, H., 1880: "Die Berechnung der Sekundarspannungen," Allgemeine Bauzeitung, vol. 45, p. 34.

NAVFAC DM-7.2, 1982: *Foundations and Earth Structures,* Design Manual 7.2, Dept. of Navy, Alexandria, VA, Chap. 5, May.

O'CONNOR, C., 1971: *Design of Bridge Superstructures,* Wiley, New York.

PECK, R. B., HANSON, W. E., and THORNBURN, T. H., 1974: *Foundation Engineering,* 2nd ed., Wiley, New York.

PODOLNY, W. and J. M. MULLER, 1982: "Construction and Design of Prestressed Concrete Segmental Bridges," Wiley, New York.

PRAKASH, S. and H. D. SHARMA, 1990: *Pile Foundations in Engineering Practice,* Wiley, New York.

REESE, L. C. and WRIGHT, S. J., 1977: "Drilled Shaft Manual-Construction Procedures and Design for Axial Loading," Vol. 1, *U.S. Dept. of Transportation, Implementation Div.,* HDV-22, Implementation Package 77-21, July, p. 140.

REESE, L. C. and O'NEILL, M. W., 1988: "Drilled Shafts: Construction Procedures and Design Methods," FHWA Publ. No. FHWA-HI-88-042 or ADSC Publ. No. ADSC-TL-4, Aug., p. 564.

ROSE, S., 1970: "Toward A Stimulus-Response Theory of Environmental Design," *Proc. 1st Annual Environmental Design Research Assoc. Conf.,* School of Design, North Carolina State Univ., Raleigh, NC, p. 215.

SAINT-VENANT, B., 1870: "Memoire sur l'establissement des equations differentielles des mouvements interieurs operes dans les corps solides ductiles," Comptes Rendus, Academic de Science, vol. 70, Paris, p. 473.

SOWERS, G. F. 1979: *Introductory Soil Mechanics and Foundations: Geotechnical Engineering,* MacMillan Publishing Co., New York, p. 621.

STEINMAN, D. B., 1929: "A Practical Treatise on Suspension Bridges," Wiley, New York.

TOMLINSON, M. J., 1986: *Foundation Design and Construction,* 5th ed., Longman Scientific and Technical, London, England, p. 842.

TOMLINSON, M. J., 1977: "Pile Design and Construction Practice," *A Viewpoint Publication,* Cement and Concrete Association.

TRESCA, H., 1864: "Memoire sur l'ecoulements des corps solides," Comptes Rendus, Academie de Science, vol. 59, Paris, p. 754.

U.S. Army Corps of Engineers, "Engineering and Design Retaining and Flood Walls," Manual EM No. 1110-2-2502, Washington, D.C., Sept., 1989.

VAN DEN BROEK, 1948: *Theory of Limit Design,* Wiley, New York.

VESIC, A. S., 1977: "Design of Pile Foundations," *Transportation Research Board,* NRC, Washington, D.C., pp. 3–7.

WINKEL, G., MALEK, R., and P. THIEL, 1970: "A Study of Human Response to Selected Roadside Environments," *Proc. 1st Annual Environmental Design Research Assoc. Conf.,* School of Design, North Carolina State Univ., Raleigh, NC, p. 224.

XANTHAKOS, P. P., 1979: *Slurry Walls,* McGraw-Hill, New York.

XANTHAKOS, P. P., 1991: *Ground Anchors and Anchored Structures,* Wiley, New York.

XANTHAKOS, P. P., 1994a: *Theory and Design of Bridges,* Wiley, New York.

XANTHAKOS, P. P., 1994b: *Slurry Walls as Structural Systems,* McGraw-Hill, New York.

XANTHAKOS, P. P., Abramson, L., Bruce, D., 1994: *Ground Control and Improvement,* Wiley, New York.

CHAPTER 2

Loads and Loading Groups

2.1 GENERAL CONSIDERATIONS

The loads to be considered in the design of substructures and bridge foundations include loads and forces transmitted from the superstructure, and those acting directly on the substructure and foundation.

The governing specifications and standards usually specify minimum requirements for loads and forces, the limits of their application, and combinations to be considered in structural design for new bridges or for evaluation of existing bridges. When multiple performance levels are defined, the selection of the appropriate performance level is made by the supervising authority.

Quite relevant in many instances are the load factors for force effects that may develop during construction (for example, in segmental bridges). In addition to the standard loads, substructure and foundation design may be decisively influenced by force effects due to collision, earthquake, settlement, and structural distortion. Vehicle and vessel collision, earthquake, and aeroelastic instability result in force effects that largely depend on structural response, and hence these effects cannot often be quantified without appropriate analysis and testing.

For a rational design, it is necessary to develop explicit criteria on how loads are distributed and on how they should be applied to the various components of the substructure and foundation. For example, the assumption of fixity (restraint against longitudinal movement) at a given pier in a typical substructure scheme may imply that longitudinal forces must be resisted at this location. However, the assumption of frictional resistance at an expansion pier will imply that this element has an inherent capacity to resist longitudinal forces up to its friction potential.

The loads reviewed in this chapter are those stipulated by AASHTO, and those that represent the best estimates and criteria developed by task committees from joint ASCE-AASHTO effort. The text also introduces the load provisions, classification, and design methodology included in the LRFD specifications. The concept of safety through redundancy and ductility is emphasized, and special consideration is given to protection against scour and collision. In most instances, engineering opinion endorses current practice, while in others it appears to follow a radical departure from established codes and standards.

In general, loads must be considered together with allowable stresses or load factors. For instance, a moderate design load and a low allowable stress may be combined to yield a more conservative condition than the solution obtained with a heavy load and a higher allowable stress.

AASHTO loads. Section 3 of AASHTO specifications summarizes the loads and forces to be considered in the design of bridges (superstructure and substructure). Briefly, these are dead load, live load, impact or dynamic effect of live load, wind load, and other forces such as longitudinal forces, centrifugal force, thermal forces, earth pressure, buoyancy, shrinkage and long term creep, rib shortening, erection stresses, ice and current pressure, collision force, and earthquake stresses.

Besides these conventional loads that are generally quantified, AASHTO also rec-

Table 2–1 Loads and Their Designations, LRFD Specifications

Permanent Loads
DD = Downdrag
DC = Dead load of structural components and nonstructural attachments
DW = Dead load of wearing surfaces and utilities
EH = Earth pressure load (horizontal)
EV = Dead load of earth fill
ES = Earth surcharge load
Transient Loads
BR = Vehicular braking force
CE = Vehicular centrifugal force
CR = Creep
CT = Vehicular collision force
CV = Vessel collision force
EQ = Earthquake
FR = Friction
IC = Ice load
IM = Vehicular dynamic load allowance
LL = Vehicular live load
PL = Pedestrian live load
SE = Settlement
SH = Shrinkage
TG = Temperature gradient
TU = Uniform temperature
WA = Water load and stream pressure
WL = Wind on live load
WS = Wind load on structure

ognizes indirect load effects such as friction at expansion bearings and stresses associated with differential settlement of bridge components.

The LRFD specifications divide loads into two distinct categories: permanent and transient, as shown in Table 2–1. The grouping into permanent and transient loads is convenient and consistent with the scope of structural analysis. This grouping is retained in the text.

2.2 PERMANENT LOADS

Dead Load

This includes the weight DC of all bridge components, appurtenances and utilities, wearing surface DW and future overlays, and earth fill EV. Both AASHTO and LRFD specifications give tables summarizing the unit weights of materials commonly used in bridge work.

Earth Loads

From Table 2–1, these are earth pressure EH, earth surcharge ES, and downdrag loads DD.

In general, earth pressure depends on the type of soil, its water content and creep behavior, degree of compaction, location of groundwater table, soil-structure interaction, surcharge loads, and dynamic effects. Earth pressure acts against abutments, walls, and occasionally against piers. Walls that are expected to undergo little or no movement should be designed for the at-rest condition (for example, diaphragm walls in underpasses). Walls and abutments expected to move away from the soil mass usually are designed for earth pressures between active and at rest values.

Earth pressure and wall movement. The earth pressure acting on a wall or abutment will vary with wall displacement. When the wall moves away from the backfill, the earth pressure decreases; when it moves toward the backfill it increases. Movement required to reach the full active or the full passive condition is a function of wall height and the soil type. Typical values of these mobilizing movements have been obtained from experimental data and finite element analysis (Clough and Duncan, 1991), and are given in Table 2–2. If the backfill consists of cohesive materials, the effect of soil creep should be taken into consideration.

From Table 2–2 the following conclusions can be made:

1. The required movement for the extreme condition is approximately proportional to the wall height
2. The movement required to reach the maximum passive pressure is almost ten times that required for the minimum active pressure, and
3. The movement required to reach limit conditions for dense and incompressible soils is smaller than for loose and compressive soils.

The value of earth pressure coefficient varies with displacement, but after the limit value is reached these coefficients remain constant and independent of further dis-

Table 2–2 Approximate Magnitudes of Movements Required to Reach Minimum Active and Maximum Passive Earth Pressure Conditions

	Values of Δ/H*	
Type of Backfill	*Active*	*Passive*
Dense sand	0.001	0.01
Medium dense sand	0.002	0.02
Loose sand	0.004	0.04
Compacted silt	0.002	0.02
Compacted lean clay	0.01**	0.05**
Compacted fat clay	0.01**	0.05**

*Δ = movement of top of wall required to reach minimum active or maximum passive pressure, by tilting or lateral translation
H = height of wall

**Under stress conditions close to the minimum active or maximum passive earth pressures, cohesive soils creep continually. The movements shown would produce active or passive pressures only temporarily. With time the movements would continue if pressures remain constant. If movement remains constant, active pressures will increase with time, approaching the at-rest pressure, and passive pressures will decrease with time, approaching values on the order of 40% of the maximum short-term passive pressure.

(From Clough and Duncan, 1991)

placement. The rate of pressure change also varies so that the pressures in dense sand change more quickly with wall movement. These effects for sand are illustrated in Figure 2–1.

Compaction affects the lateral pressure. The heavier the equipment used to compact the backfill, and the closer it operates to the wall, the greater is the compaction-induced pressure. Figure 2–2 shows earth pressure coefficients for a backfill compacted to a medium dense condition (Clough and Duncan, 1991). Compared with the graphs of Figure 2–1, the curve is shifted upward and the required movement for the minimum active pressure is increased, while the movement necessary for maximum passive pressure is decreased. About 1 inch of movement in 20 feet produces active conditions, and 1 inch in 3 feet is necessary to bring the backfill to the passive state.

Pressure of water. Where possible, the development of hydrostatic water pressure behind walls or abutments should be predicted assuming a free-draining backfill or by providing adequate drainage through the use of weep holes and crushed stone, pipe drains, gravel drains, perforated drains or geofabric drains.

Pore pressure behind a wall may be computed by flow net analysis. When water is expected to pond, the wall should be designed to withstand the hydrostatic water pressure plus the earth pressure. Commonly, submerged (effective) unit soil weights are used to determine pressures below the groundwater table.

At rest pressure. In sedimentary (normally consolidated) soil, as the buildup of overburden continues there is vertical compression of material because of increase in vertical stresses, but there should be no significant horizontal compression. In this case the horizontal earth stress is less than the vertical, and for sand K_o (coefficient of pressure at rest) usually ranges between 0.4 and 0.5 (values of ϕ' between 27° and 34°). Thus, for

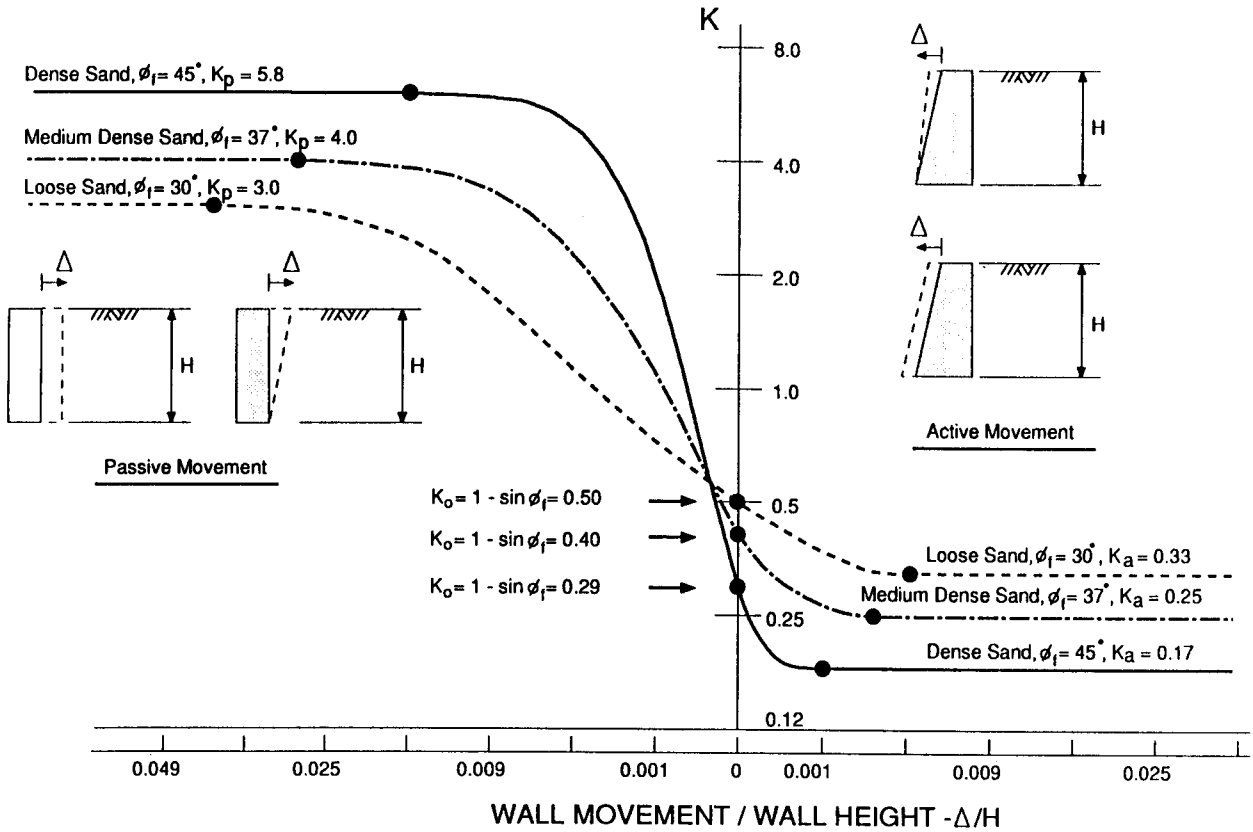

Figure 2–1 Relationship between wall movement and earth pressure *(from Clough and Duncan, 1991).*

initial loading, the expression proposed by Jacky (1944) is confirmed by Bishop (1958) so that

$$K_o = 1 - \sin \phi' \tag{2–1}$$

where ϕ' = friction angle (effective) of drained soil. Accordingly, the earth pressure p at depth z for a soil of unit weight γ is

$$p_o = K_o \gamma z \tag{2–2}$$

For overconsolidated soils, K_o is assumed to vary according to the overconsolidation ratio *OCR* or stress history (Mayne and Kulhawy, 1982). Values of K_{ou} may now be computed from

$$K_{ou} = K_o(OCR)^{sin\ \phi'} \tag{2–3}$$

where K_{ou} = coefficient of at rest pressure for overconsolidated soil; K_o = coefficient for normally consolidated soil = $1 - sin\phi'$; and *OCR* = overconsolidation ratio. Values of K_{ou} for various *OCR* ratios may be taken from Table 2–3 (Clough and Duncan, 1991).

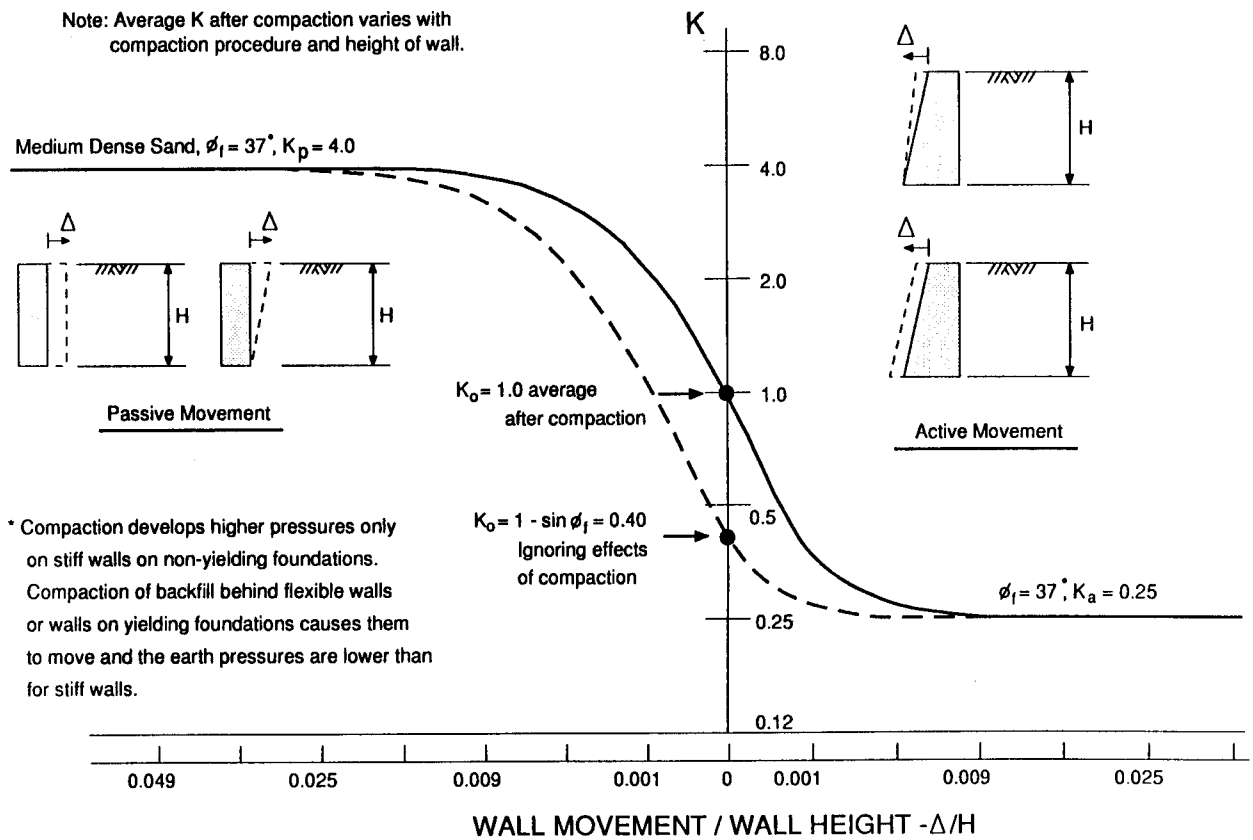

Figure 2–2 Relationship between wall movement and earth pressure for a wall with compacted backfill *(from Clough and Duncan, 1991)*.

Active pressure. For a normally consolidated soil in dry condition, the active pressure is given by

$$p_a = K_a \gamma z \tag{2–4}$$

where $K_a = tan^2(45 - \phi/2) = (1 - sin\ \phi)/(1 + sin\ \phi)$ = coefficient of active pressure.

Passive pressure. Likewise, the passive pressure is computed from

$$p_p = K_p \gamma z \tag{2–5}$$

where $K_p = tan^2(45 + \phi/2) = (1 + sin\ \phi)/(1 - sin\ \phi)$ = coefficient of passive pressure.

Limiting equilibrium theories. In general, these are formulated on the concept of soil strength expressed by the Coulomb-Mohr failure criterion, but they differ in the shape and location of the failure surface and in the application of statics. The Coulomb theory is based on the concept of a failure wedge with a planar surface that passes through the

Table 2–3 Typical Coefficients of Lateral Earth Pressure At-Rest, K_{ou}

Soil Type	Coefficient of Lateral Earth Pressure, K_{ou}			
	OCR = 1	*OCR = 2*	*OCR = 5*	*OCR = 10*
Loose sand	0.45	0.65	1.10	1.60
Medium sand	0.40	0.60	1.05	1.55
Dense sand	0.35	0.55	1.00	1.50
Silt (ML)	0.50	0.70	1.10	1.60
Lean Clay (CL)	0.60	0.80	1.20	1.65
Highly Plastic Clay (CH)	0.65	0.80	1.10	1.40

(From Clough and Duncan, 1991)

toe of the wall. A second assumption is that the thrust on the wall acts on some known direction, so that the resultant thrust can be determined by statics. A further assumption is that there is wall friction, that is, as the failure wedge moves with respect to the backface of the wall, a friction force is developed between wall and soil under a friction angle δ. The Rankine theory assumes no wall friction, so that the direct relationship between vertical overburden stress is $\sigma_v = \gamma z$, and the lateral pressure is expressed by Equations (2–4) and (2–5). Other theories are based on logarithmic spiral slip surfaces (Caquot and Kerisel, 1948), slip along a circular surface, and the concept of slices. In the Sokolovski (1965) method, the equations of equilibrium and the failure criterion are explicitly satisfied for each infinitesimal element responding to failure.

Active and passive states in soil with cohesion. The effect of cohesion on the passive thrust is assumed to occur at a rate that does not cause excess pore pressure. Setting $N_\phi = (1 + \sin\phi)/(1 - \sin\phi) = 1/\tan^2(45 - \phi/2)$, the following expression is derived:

$$Passive\ State: \quad p_p = N_\phi \gamma z + 2c\sqrt{N_\phi} \tag{2–6}$$

so that with cohesion c present N_ϕ is not the ratio of horizontal to vertical stress. The second term of Equation (2–6) has two components: a factor that has a linear variation with depth, and a factor that represents a constant stress with depth, so that the resultant thrust is located between the midpoint and the lower-third point.

$$Active\ State: \quad p_a = \frac{1}{N_\phi}\gamma z - 2c\frac{1}{\sqrt{N_\phi}} \tag{2–7}$$

Note that $1/N_\phi = K_a$

Although Equation (2–7) indicates a negative pressure near the top of the wall, meaning that the soil adheres to the interface, this adherence is doubtful in practice. It is better, therefore, to ignore cohesion and assume a fictitious triangular pressure using an arbitrarily selected friction angle.

The strain necessary to bring a clay to the limit state has been modestly investigated (see also Table 2–2). To produce the active state about 1 to 2 percent strain is required but much more is necessary to produce the passive state.

Analysis with friction. The foregoing apply to a horizontal backfill and to wall-soil systems without friction at the interface. However, two factors have a critical effect on the coefficient of earth pressure: wall friction and seepage pressure. The commonly used Rankine theory does not use wall friction and tends to be more conservative.

A complete evaluation of the active and passive states with friction becomes complicated because of the variation and pattern in the inclination of the slip planes. Solutions have been presented by Janbu (1957, 1972), and Sokolovski (1944).

Equivalent fluid method. For most practical situations and wall heights that do not exceed 20 feet, most states stipulate earth pressures based on equivalent fluid. Whereas this approximates earth pressure effects, it ensures uniformity and consistency in the analysis.

Useful data on this approach are given in Table 2–4. Values of the density of equivalent fluids are given for walls that can tolerate very little or no movement and for walls that can yield as much as 1 inch in 20 feet. The concept of equivalent fluid weight takes into account the effect of soil creep on walls. Soils designated as ML, CL and CH should not be used for backfill if free-draining granular materials are available.

Location of horizontal resultant. Data obtained from experimental investigations and field observations appear to confirm that the horizontal resultant pressure, commonly taken to be applied at the one-third point, has in reality a point of action above that point (Terzaghi, 1934; Clausen and Johansen, 1972).

These results suggest that the resultant lateral pressure may be from $0.4H$ to $0.43H$ from the bottom of the wall, where H is the wall height. Similar results are provided by Xanthakos (1979) for diaphragm walls braced at the top with bracing intended to prevent or minimize movement, based on a limited record of field studies.

Surcharge loads. Surcharge loads at ground surface include point, line, and strip loads. Where uniform surcharge is present, the effect is a constant earth pressure added to the basic earth pressure. The constant earth pressure is taken as

$$\Delta_p = K_s q_s \tag{2–8}$$

where Δp = uniform increase in lateral earth pressure; K_s = coefficient due to surcharge; and q_s = uniform surcharge applied to the upper surface of the active wedge. The coefficient K_s is taken the same as the lateral earth stress coefficient, that is, the same as K_a or K_o.

For point, strip, and line loads, the theory of elasticity is commonly used to analyze the associated effects, modified as necessary to account for the increased stiffness of rigid walls (Terzaghi, 1954; Spangler, 1951). Other investigators consider the soil elas-

Table 2–4 Typical Values for Equivalent Fluid Unit Weights of Soils

	Level Backfill		Backfill 2(H) on 1(V)	
Type of Soil	At-Rest γ_{eq}(PCF)	Δ/H = 1/240 γ_{eq}(PCF)	At-Rest γ_{eq}(PCF)	Δ/H = 1/240 γ_{eq}(PCF)
Loose sand or gravel	55	40	65	50
Medium dense sand or gravel	50	35	60	45
Dense sand or gravel	45	30	55	40
Compacted silt (ML)	60	40	70	50
Compacted lean clay (CL)	70	45	80	55
Compacted fat clay (CH)	80	55	90	65

(From Clough and Duncan, 1991)

Table 2–5 Equivalent Height of Soil for Vehicular Loadings

Wall Height	h_{eq}
10	4.2
20	2.1
30	1.4

tic, but introduce a modulus of elasticity increasing linearly with depth (Turabi and Balla, 1968). For solutions commonly used reference is made to the bibliography of this chapter.

The effects of vehicular loads should be considered only when highway traffic loads act on the surface of the backfill within a distance of one-half the wall height behind the wall. The wall height is taken as the distance between the surface of the backfill and the bottom of the footing.

The increase in horizontal pressure due to live load surcharge may be estimated from the following

$$\Delta_p = K\gamma h_{eq} \tag{2–9}$$

where Δ_p = increase (constant) in horizontal pressure due to the vehicular load; γ = unit weight of soil; K = coefficient of earth pressure (active or at rest); and h_{eq} = equivalent height of soil, to be taken from Table 2–5.

Reduction of effects because of earth pressure. In many instances, the inclusion of full lateral earth pressure may reduce effects (moments, shears, etc.) caused by other loads and forces. In this case, a reduction in the lateral pressure is admissible in the analysis, but to the extent that earth pressure can be expected to be permanently present.

Downdrag. This acts on piles, drilled shafts, and prismatic elements as a result of ground settlement around the element. Force effects due to downdrag are discussed in other sections.

The methods used to estimate downdrag are essentially similar to those used to calculate shaft resistance (friction or adhesion). An obvious distinction is that downdrag acts downward, and therefore it is a load. Shaft friction acts upward on the sides of the element and therefore it is a resistance.

2.3 TRANSIENT LOADS

Vehicular Live Load (LL)

Vehicle loading for short-span bridges. Considerable effort has been made in the United States and Canada to develop a live load model that can represent the highway loading more realistically than the H or the HS AASHTO models. Several states and provinces (California, Louisiana, Ontario) have proposed an alternate traffic loading which in some cases has been adopted by the supervising authority. Nonetheless, the consensus of opinion among engineers is that further documentation should be presented to warrant changes in the standard highway loading, and thus the current AASHTO model is still the applicable loading.

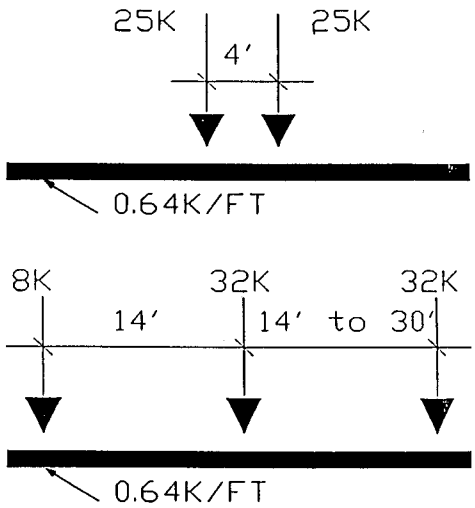

Figure 2–3 Live load models, LRFD specifications; axle loads. (Note: These models consider (a) effect of the design tandem combined with the effect of the design lane load; and (b) effect of design truck combined with the effect of the design lane load. The effects of an axle sequence and the lane load are superimposed to obtain extreme values. The lane load is not interrupted to provide space for the axle sequence, but interruption is needed only for patch loading patterns to produce extreme force effects). See also Article 3.6.1.3, LRFD specifications.

The LRFD specifications have introduced the vehicular live load shown in Figure 2–3. This consists of (1) design truck, (2) design tandem, and (3) design lane load. The design truck is the same as the HS 20 truck unit. The design tandem consists of a pair of 25-kip axles spaced 4 feet apart. The design lane load is similar to the standard AASHTO lane load and consists of a uniformly distributed load of 0.64 kips/ft. The live load is assumed to occupy 10 feet transversely.

The live load model, consisting of either a truck or tandem coincident with a uniformly distributed lane load, was developed as a notional representation of shear and moment produced by a group of vehicles routinely permitted on highways under various exclusions to weight limitations. Figure 2–4(a) and (b) show moment and shear ratios, respectively, of proposed models to HS 20 (truck or lane) or two 24-kip axles at 4 feet. The following nomenclature applies:

M POS .4L = positive moment at 0.4 point in either span
M NEG .4L = negative moment at 0.4 point in either span
M SUPPORT = moment at interior support
Vab = shear adjacent to either exterior support
Vba = shear adjacent to interior support
Mss = centerline moment in a simply supported span

The term "span" is the length of the simple span or one of the two continuous spans. A ratio greater than 1.0 indicates that the proposed model produces a larger load effect than the HS 20 or the two 24-kips axle loads at 4 feet. The total load effect to be used for design is also a function of the load factor, load distribution, and impact allowance.

The axle sequence and the lane load are superimposed to produce most critical results. This is a major departure from the traditional AASHTO approach where either the truck or the lane load with an additional concentrated load are used for extreme effects. The lane load is not interrupted to provide space for the axle sequence of the design tandem or truck; interruptions are needed only to patch loading patterns to produce extreme effects.

For reactions at interior piers of continuous bridges, the extreme force effect

(a)

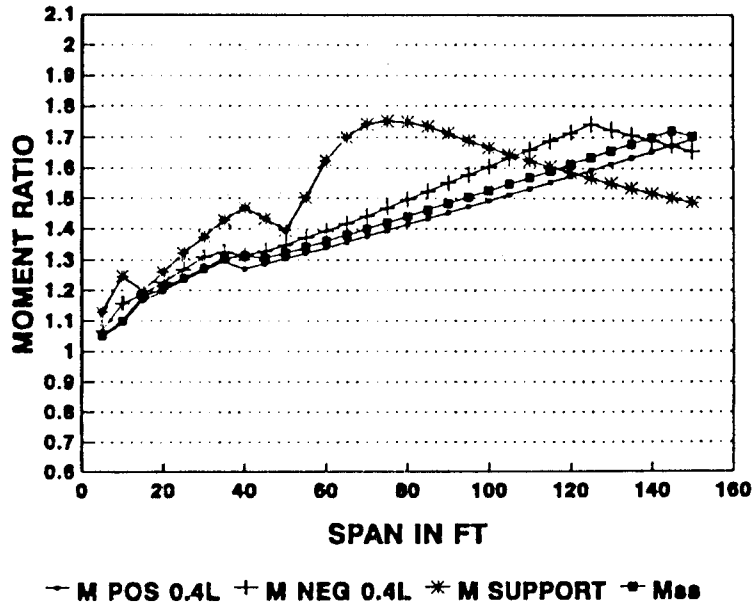

(b)

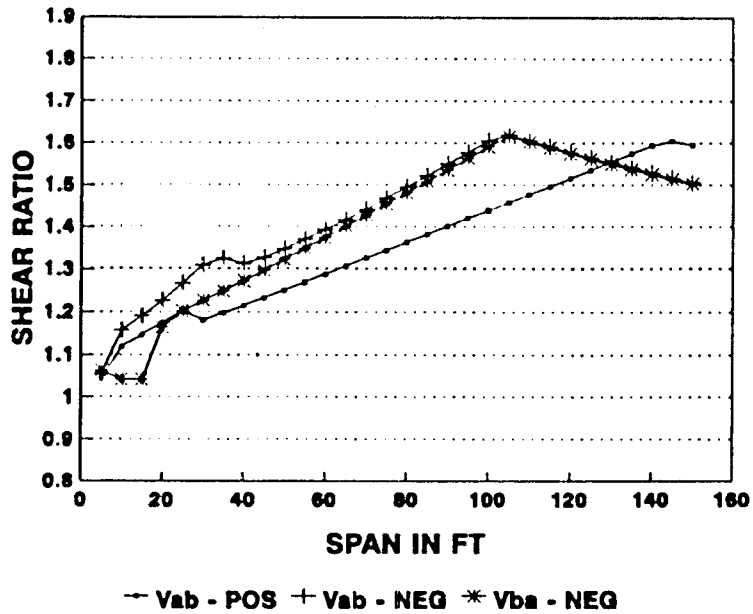

Figure 2–4 (a) Moment ratios—proposed models to HS 20 (truck or lane) or two 24.0-kip axles at 4.0 feet; (b) shear ratios—proposed models to HS 20 (truck and lane) or two 24.0-kip axles at 4.0 feet.

should be determined for the loading combination consisting of 90 percent of the effect of the two design trucks spaced at a minimum of 50 feet between the lead axle of one truck and the rear axle of the other truck, and 14 feet between the two 32-kip axles, combined with 90 percent of the effect of the design lane load. The design truck or tandem should be taken to coincide with the design lane load. Axles not contributing to the extreme force effect under consideration should be neglected, and the lane load should be positioned longitudinally for maximum effect.

Vehicle loading for long-span bridges. General guidelines for a rational design of long-span bridges are summarized by Xanthakos (1994a). The general conclusion is that little effort has been made to establish representative loads for bridge types outside the range of codes normally appropriate for a shorter bridge in the same conditions. Recommended design loads, consisting of a uniformly distributed load V and a single concentrated load P, are given by the ASCE Committee on Loads and Forces for Bridges (1981).

Impact and Dynamic Load Allowance (IM)

The intent of AASHTO is that impact should be included as part of the loads transferred from the superstructure to the substructure, but not in loads transferred to footings or to piles and columns that are below ground.

Among the many factors influencing the dynamic response of bridges is the condition of the bridge approach and the springing of the vehicle. Extremely large impacts can be induced due to initial vibration of the moving load if an area of settlement occurs in the roadway in advance of the bridge. However, the exclusion of abutments, walls, footings and other foundation elements indicates the intent to recognize the damping effect of soil when in contact with a structural component. A retaining type component is considered to be buried to the top of the fill.

Impact intensity. AASHTO gives the amount of impact as a fraction of the live load, to be determined as follows

$$I = \frac{50}{L + 125} \tag{2–10}$$

Measured impacts for short spans tend to be higher than those predicted by Equation (2–10), but for longer spans observed impacts are nearly the same as predicted.

Dynamic effects due to moving vehicles can be attributed to two main causes: (1) the hammering effect as the dynamic response of the wheel assembly to riding surface discontinuities such as deck joints, cracks, potholes and delaminations; and (2) the dynamic response of the bridge as a unit to passing vehicles.

The LRFD specifications stipulate that for all other components except deck joints, the dynamic load allowance should be as follows:

Fatigue and Fracture Limit State = IM = 15%
All other Limit States = IM = 33%

This allowance may be reduced if the design produces ample evidence from a dynamic analysis that the above values are not warranted. Dynamic load allowance need not be

applied to (a) retaining walls not subject to vertical reactions from the superstructure, and (b) foundation components which are entirely below ground level.

Centrifugal Force (CE)

The AASHTO stipulation to neglect lane load in computing the centrifugal force reflects the fact that spacing of vehicles at high speeds is large, resulting in a low density of vehicles following or preceding the design truck.

However, the LRFD specifications suggest that the combination of design truck and lane load represents a group of exclusion vehicles producing force effects at least 4/3 times those caused by the design truck alone. Thus, centrifugal forces are still applied to the axle weights of the design truck or tandem (neglecting lane load) but the factor 4/3 is retained. Thus, the factor C is given by

$$C = \frac{4}{3}\frac{V^2}{gR} \tag{2–11}$$

where V = design speed (ft/sec); g = gravitational acceleration = 32.2 ft/sec^2; and R = radius of curvature (ft).

Longitudinal (Braking) Force (BR)

There is indication that the longitudinal (braking) force that can be induced by one vehicle is at least equal to the weight of the vehicle, but it is also argued that the design truck may not exceed 100 percent friction because of restraints. Since it is unlikely that a large number of vehicles will exert the maximum braking force simultaneously, reduction in load intensity for multiple lanes is justified.

Interestingly, the 5 percent longitudinal load stipulated by AASHTO is much less than this type of load specified by other codes. For example, a comparison of this force for one lane 100 feet long gives the following:

1. AASHTO = 4.1 kips (18.2 kN) for HS 20 (lane load)
2. British Code = 100 kips (445 kN) for HA
3. Canadian = 101 kips (449 kN) for MS 250
4. French = 66 kips (294 kN) for Type B
5. Ontario = 23.6 kips (105 kN) for OHBD truck
6. ASCE = 57.6 kips (256 kN) for HS 20

The foregoing data, however, do not give an accurate comparison of load effects, since some of these loads are applied in combination of groups under a stress increase.

Alternatively, the LRFD specifications require a braking force 25 percent of the axle weights of the design truck or tandem per lane. This is based on energy principles with uniform deceleration. The braking force is

$$b = \frac{V^2}{2ga} \tag{2–12}$$

where a = length of uniform deceleration and b is the traction. Using a = 400 ft, and V = 55 MPH gives b = 0.253. Only the design truck should be considered as other vehicles, represented by the lane load, are expected to brake out of phase.

For the same lane 100 feet long, the design truck is one full HS 20, or 72 kips, giving a braking force $0.25 \times 72 = 18$ kips.

Given the weight of a vehicle W (kips), the change in velocity ΔV (ft/sec), and the time interval Δt (sec), the resulting braking (friction) force is

$$F = \frac{W}{g}\left(\frac{\Delta V}{\Delta t}\right) \tag{2–13}$$

For example, a truck of weight W moving at 60 MPH (88 ft/sec) and having the brakes suddenly applied will induce a longitudinal force that is dependent on the time necessary to change the velocity from 60 MPH to zero. If this time is taken as 6 seconds and the deceleration is assumed to be uniform, this force is

$$F + \frac{W}{32.2}\frac{88}{6} = 0.46W$$

However, if the time is taken as 11 seconds, the longitudinal force is $0.25W$, or the same as that given by Equation (2–12). The apparent shortcoming of both Equations (2–12) and (2–13) reflect the fact that a minor variability in the associated parameters causes a marked variation in the coefficients b and F; hence these solutions do not represent a rational approach to the braking force problem.

Friction (FR)

AASHTO stipulates that provisions should be made to transfer the forces from the superstructure to the substructure in a manner that relates the effect of friction at expansion bearings or shear resistance at elastomeric bearings. Friction forces are established on the basis of extreme values of the friction coefficient between the sliding surfaces, and where appropriate the effect of moisture should be considered.

Friction coefficients for sliding-type expansion bearings vary broadly. For example, Missouri, New York, and Iowa specify friction forces as 0.14, 0.15, and 0.25 of the dead load reaction, respectively, for steel bearing on steel. Recommendations on appropriate friction coefficients are predicted upon good maintenance procedures and inspection. Rusted or frozen bearings will develop a higher frictional resistance.

For sliding-type bearings, the longitudinal force due to friction recommended by ASCE (Committee on Loads and Forces on Bridges, 1981) may be based on the following fraction of the dead load reaction (ASD):

Steel bearing on steel	0.2
Steel bearing on self-lubricating bronze plate	0.1
PTFE on same or stainless steel	0.06
Elastomeric bearings	Shear as per AASHTO

For rocker-type bearings, friction should be taken as 20 percent the dead load on the pin, and then reduced in proportion to the radii of the pin and rocker as shown in Figure 2–5.

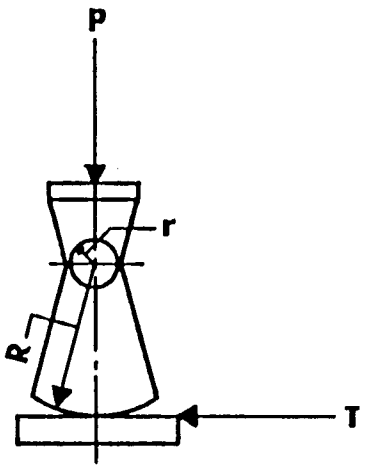

P = Superstructure DL

$T = (P \times 0.20)\ \frac{r}{R}$

r = radius of pin

R = radius of rocker

Figure 2–5 Forces on rocker bearings.

Friction can thus be considered a force effect or resistance. When designing expansion piers, for example, friction is a longitudinal force acting on top of the element, and should be applied with a load factor greater than 1.0. When designing fixed piers, the frictional resistance developed at the expansion bearings may be considered but with a resistance factor (smaller than 1.0), or may even be ignored completely (performance factor = zero).

Wind Load (WL and WS)

The wind forces specified by AASHTO and LRFD specifications are for wind velocities of 100 MPH. For substructure design, wind loads are developed as follows.

Forces from superstructure. These forces may be calculated for a wind at right angles to the bridge, and for a range of wind angles skewed off from this direction. The assumed wind direction should be that which produces maximum effects. The transverse and longitudinal forces should be applied simultaneously at the center of gravity of the exposed superstructure. The loads given in Table 2–6 are for Groups II and V. For Groups III and VI these loads may be reduced by 70 percent, but a load per linear foot should be added as wind load on moving live load as shown in Table 2–7.

For the usual girder and slab bridges with maximum spans 125 feet, AASHTO allows a simplified procedure for calculating wind effects from superstructure, as follows:

- Wind load on structure
  50 lb/ft^2, transverse
  12 lb/ft^2, longitudinal, applied simultaneously.
- Wind load on live load
  100 lb/lin ft, transverse
  40 lb/lin ft, longitudinal, applied simultaneously.

Table 2–6 Wind Loads for Group II and IV (AASHTO)

	Trusses		Girders	
Skew Angle of Wind	*Lateral Load*	*Longitudinal Load*	*Lateral Load*	*Longitudinal Load*
Degrees	PSF	PSF	PSF	PSF
0	75	0	50	0
15	70	12	44	6
30	65	28	41	12
45	47	41	33	16
60	24	50	17	19

Forces applied directly to substructure. For a 100 MPH wind, these forces are calculated from an assumed wind intensity of 40 lb/ft^2. If the wind direction is skewed to the substructure, this force is resolved into two components to the front and end elevation of the substructure element. These loads are for Groups II and V, and may be reduced by 70 percent for Groups III and VI (ASD).

Overturning forces. Provisions are made by AASHTO for the presence of an upward force applied at the windward quarter point of the transverse superstructure width. This force is 20 lb/ft^2 for Groups II and V, and 6 lb/ft^2 for Groups III and VI.

LRFD approach. Likewise the assumed wind velocity is V_B = 100 MPH, designated as base design wind velocity, giving pressures as shown in Table 2–8. For bridges or parts more than 30 feet above low ground or water, the design wind velocity V_{DZ} is obtained from

$$V_{DZ} = 2.5\, V_o \left(\frac{V_{30}}{V_B}\right) \ln\left(\frac{Z}{Z_o}\right) \tag{2–14}$$

where V_{30} = wind speed at 30 feet above low ground; Z = structure height above low ground > 30 feet; V_o = friction velocity taken from Table 2–9; and Z_o = friction length of upstream fetch, taken also from Table 2–9.

The parameter V_{30} may be established from (1) fastest-mile-of-wind charts for various recurrence intervals (ASCE 7-88); (2) site specific surveys; and (3) in the absence of better criterion, $V_{30} = V_B$ = 100 MPH.

Table 2–7 Wind Loads for Group III and VI (AASHTO)

Skew Angle of Wind	Lateral Load	Longitudinal Load
Degrees	*lb./ft.*	*lb./ft.*
0	100	0
15	88	12
30	82	24
45	66	32
60	34	38

Table 2–8 Base Pressures, P_B Corresponding to V_B = 100 MPH

Structural Component	Windward Load, PSF	Leeward Load, PSF
Trusses, Columns and Arches	50.0	25.0
Beams	50.0	NA
Large Flat Surfaces	40.0	NA

If justified by local conditions, a different base design wind velocity may be selected for limit states that do not involve live load. In this case the design wind pressure may be calculated as

$$P_D = P_B\left(\frac{V_D^2}{10{,}000}\right) \tag{2–15}$$

When vehicles are present, wind pressure should be applied to the vehicle, represented by an interruptable, moving force of 100 lb/lin ft acting normal to the roadway and 6 feet above the roadway.

When the wind direction is not normal to the bridge, the basic design wind pressure is resolved into two components as follows:

$$\text{Normal component } P_N = P_D \cos^2 \theta \tag{2–16}$$

$$\text{Parallel component } P_p = P_D \sin \theta \cos \theta$$

where θ = angle between wind direction and a normal to the bridge.

2.4 FORCE EFFECTS FROM SUPERIMPOSED DEFORMATIONS

These are internal forces induced by temperature changes, creep and shrinkage, and deformation and settlement.

Thermal Forces (TG)

Provisions for stresses or movements resulting from variations in temperature are essentially similar in both the standard AASHTO and LRFD specifications. The temperature range is articulated for moderate and cold climates. A moderate climate is determined by the number of freezing days per year. Freezing days are days when the average temperature is less than 32°F. If the number of freezing days is less than 14, the climate is considered moderate.

Internal stresses and structure deformations associated with both positive and negative temperature gradients should be analyzed in terms of the redistribution of reactive forces, both longitudinally and transversely. These effects are present in the bearings and substructure elements. Procedures are briefly discussed in chapter 3.

Table 2–9 Values of V_o and Z_o for Various Upstream Surface Conditions

Condition	Open Country	Suburban	City
V_o MPH	8.21	11.76	16.43
Z_o FT	0.23	1.00	2.63

Shrinkage (SH)

Shrinkage is associated with loss of moisture by evaporation. Differential shrinkage strains between concretes of different age or composition must, therefore, be evaluated since they can result in large internal stresses. These effects may be controlled to a certain extent by providing moist curing conditions. However, the larger the ratio of surface area to member cross section, the larger will be the resulting shrinkage.

Substructure elements seldom undergo uniform shrinkage. On the other hand, with reinforced concrete even uniform shrinkage causes stresses because of the internal restraint caused by the reinforcement. These stresses are compression in the steel and tension in the concrete.

A typical example of shrinkage effect is a multi-column pier with unusually long cap, shrinking differentially because of different construction times. This can induce large moments in the columns because of differential movement of the tops with reference to the fixed bases. These effects can be controlled in some instances by specifying appropriate construction joints in the cap and a closure pour.

Creep (CR)

Creep is strain increase with time under constant load. Factors tending to increase creep include loading at an early age, using concrete with high water-cement ratio, and exposing the concrete to drying conditions. Creep shortening of concrete under sustained loads is generally 1.5 to 4.0 times the initial shortening, depending mainly on concrete maturity at the time of loading.

Creep may be most critical and severe in superstructures where the associated effects can be transferred to the substructures, for example, in segmentally constructed bridges. Shrinkage and creep are reviewed in some detail in chapter 3.

Force Effects Due to Settlement (SE)

Force effects due to extreme values of differential settlement among substructures and within individual substructure units can be critical and must be considered. With the introduction of load factor design, the definition of the upper limit of tolerable movement is a serviceability limit state that imposes a specific design requirement. Whether the design approach follows ASD or LRFD, it is an essential task to ensure the ability of bridge superstructure to withstand movement (horizontal or vertical) without intolerable consequences. Thus, these force effects must be determined even though they do not relate directly to the structural capacity of substructures.

2.5 FORCES ON SUBSTRUCTURE

Vessel Collision

Recent incidents of bridge collapse caused by impact from vessels have prompted new design requirements, exemplified by the need to establish minimum impact criteria. The intent of vessel collision provisions is to prevent the risk of catastrophic failure of superstructures for bridges located on navigable waterways impacted by aberrant vessels. The collision impact forces represent a probabilistically based most severe head-on

collision as a vessel moves forward at high speed. AASHTO (1991) has developed comprehensive guide specifications and commentary for vessel collision design, and the requirements outlined in this section are based on this document, using Method II risk acceptance alternative.

Where vessel collision is anticipated, structures must be designed to resist the resulting force effects, or be adequately protected by fenders, dolphins, berms, islands or other works. Design vessels must be selected according to bridge importance classification, and vessel, bridge, and waterway characteristics. A probability-based analysis procedure is used in which the predicted annual frequency (AF) of bridge collapse is compared to an acceptance criterion.

For waterways whose width is less than six times the length overall (LOA) of the design vessel, the acceptance criterion for the annual frequency of collapse for each pier and span component must be determined by distributing the total bridge acceptance criterion (AF) over the number of pier and span components located in the waterway. For wide waterways with width greater than 6(LOA), the acceptance criterion for the annual frequency of collapse for each pier and span components is determined by distributing the total bridge acceptance criterion over the number of piers and span components located within the distance 3(LOA) on each side of the inbound and outbound vessel transit centerline paths.

Considerations to be included in the analysis of vessel collision include vessel frequency distribution, probability of aberrancy, geometric probability, probability of collapse, velocity distribution, transit velocity in the channel, collision velocity, and vessel collision energy.

Ship collision force on pier. The ship collision impact force is taken as (AASHTO Article 3.9 and LRFD Article 3.14.8)

$$P_s = \frac{220(DWT)^{1/2}V}{27} \tag{2–17}$$

where P_s = equivalent static vessel impact force (kips); DWT = deadweight tonnage of vessel (tonne); and V = vessel impact velocity (ft/sec). The effect of the impact load on the structure is complex, and depends on factors such as: (1) the structure type and shape of the ship's bow; (2) the degree of water ballast carried in the forepeak of the bow; (3) the size and speed of the ship; (4) the geometry of the collision; and (5) the geometry and rigidity of the pier. Typical ship impact forces computed using Equation (2–17) are shown in Figure 2–6.

Barge collision force on pier. AASHTO defines the standard hopper barge as in inland river barge that has the following characteristics (jumbo hopper):

Width	= 35.0 feet
Length	= 195 feet
Depth	= 12.0 feet
Empty draft	= 1.7 feet
Loaded draft	= 8.7 feet
DWT	= 1,700 tonne

The impact force for a standard hopper barge is taken as

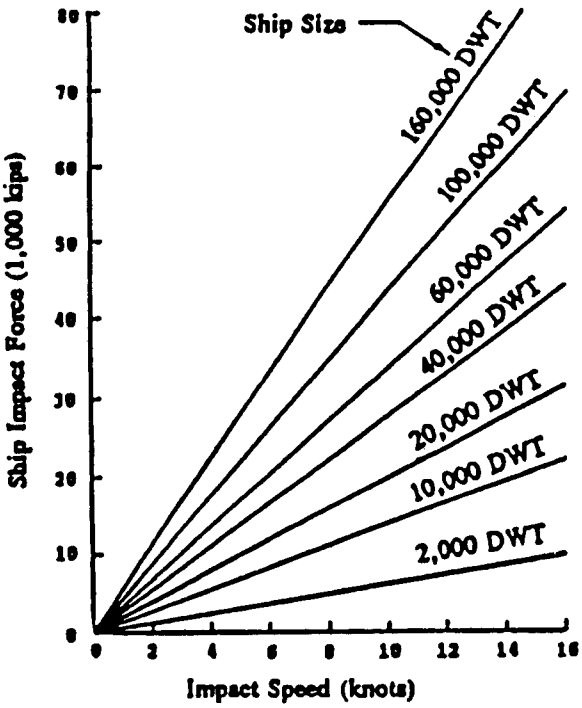

Figure 2–6 Typical ship impact forces.

$$\text{if } a_B < 0.34 \qquad P_B = 4112a_B \tag{2–18}$$

$$\text{if } a_B \geq 0.34 \qquad P_B = 1349 + 110a_B \tag{2–19}$$

where P_B = equivalent static barge impact force (kips), and a_B = barge bow damage length obtained from the following:

$$a_B = \left[\sqrt{1+\frac{KE}{5700}} - 1\right](10.2) \tag{2–20}$$

where KE = barge collision energy (kips-ft). The impact force for design barges larger than the standard hopper barge should be computed by increasing the standard hopper barge impact force by the ratio of larger width to the standard-barge width.

Typical barge impact forces using Equations (2–18) and (2–19) are shown in Figure 2–7.

Damage at the extreme limit state. The LRFD specifications permit damage or local collapse of substructure components provided that (1) sufficient ductility and redundancy of the remaining structure exists in the extreme event limit state to prevent global catastrophic collapse; and (2) damaged components can be inspected and repaired promptly. Alternatively, pier protection may be considered to prevent or minimize vessel collision loads to acceptable levels.

Application of impact forces. These forces are considered both parallel and normal to the centerline of the navigable channel. For substructure design, the design impact force should be applied as an equivalent static force as follows: (1) in a direction parallel

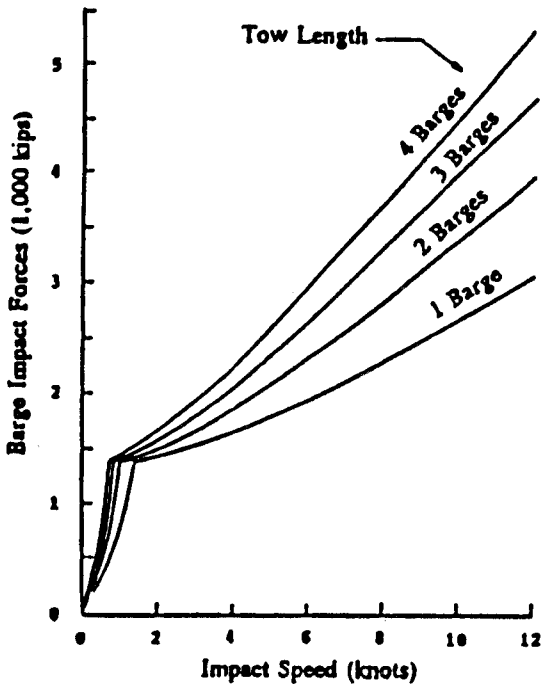

Figure 2–7 Typical hopper barge impact forces.

to the channel; and (2) 50 percent of that force in a direction normal to the channel. These forces should be applied separately.

Further design criteria are as follows:

1. For analysis of overall substructure stability, the design impact force should be applied as a concentrated force on the structure at the mean high water level of the waterway, as shown in Figure 2–8.
2. To design the pier and its components for local collision forces, the design impact force should be applied as a vertical line load equally distributed along the ship's bow depth, as shown in Figure 2–9. The ship's bow should be considered to be raked forward when determining the potential contact area of the impact force. For barge impact, the local collision force should be taken as a vertical line load equally distributed on the depth of the head block, as shown in Figure 2–10.

Water Loads (WA)

Static pressure. Static water pressure is assumed to act normal to the surface retaining the water. Extreme high water levels are usually provided as design criteria.

Buoyancy and uplift. This is the sum of the vertical components of static pressures. For substructures with cavities where the presence or absence of water cannot be confirmed, the condition producing the most extreme effect should be considered.

Stream Pressure. Flowing water acting in the longitudinal direction exerts a pressure as follows:

$$p = C_D V^2 \tag{2–21}$$

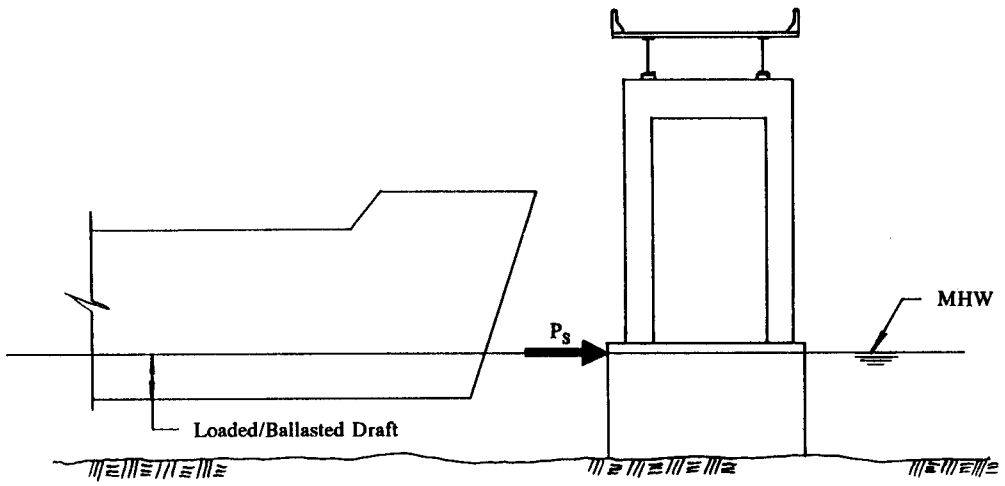

Figure 2–8 Ship impact concentrated force on pier.

where p = pressure (lb/ft^2); C_D = drag coefficient given in Table 2–10; and V = design velocity of water (ft/sec). The longitudinal direction refers to the major axis of a substructure unit. When a significant amount of driftwood and other debris is carried, allowance should be made for items lodged against the pier.

The lateral, uniformly distributed pressure on piers due to water flowing at an angle to the longitudinal axis of the pier may be computed as

$$p = C_L V^2 \tag{2–22}$$

where C_L = lateral drag coefficient given in Table 2–11, and all parameters are as shown in Figure 2–11.

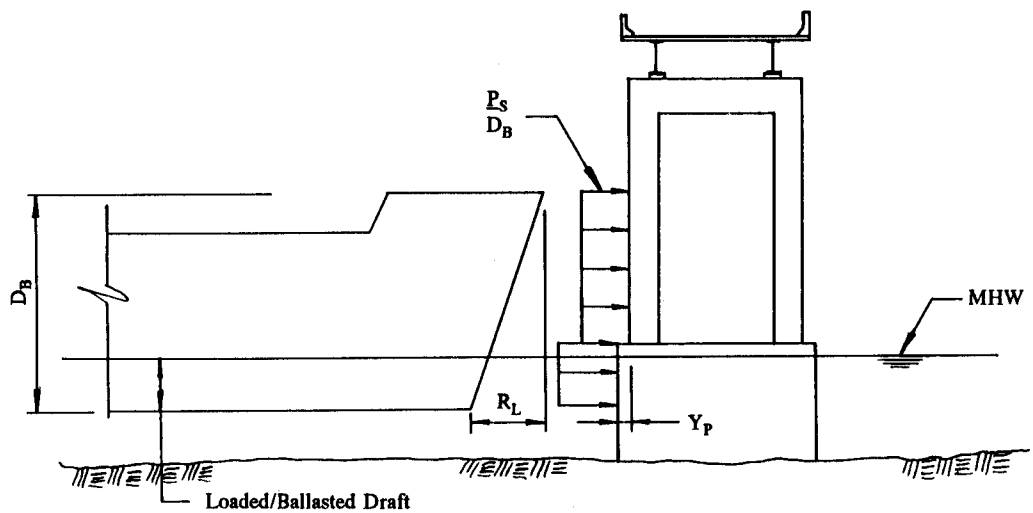

Figure 2–9 Ship impact line load on pier.

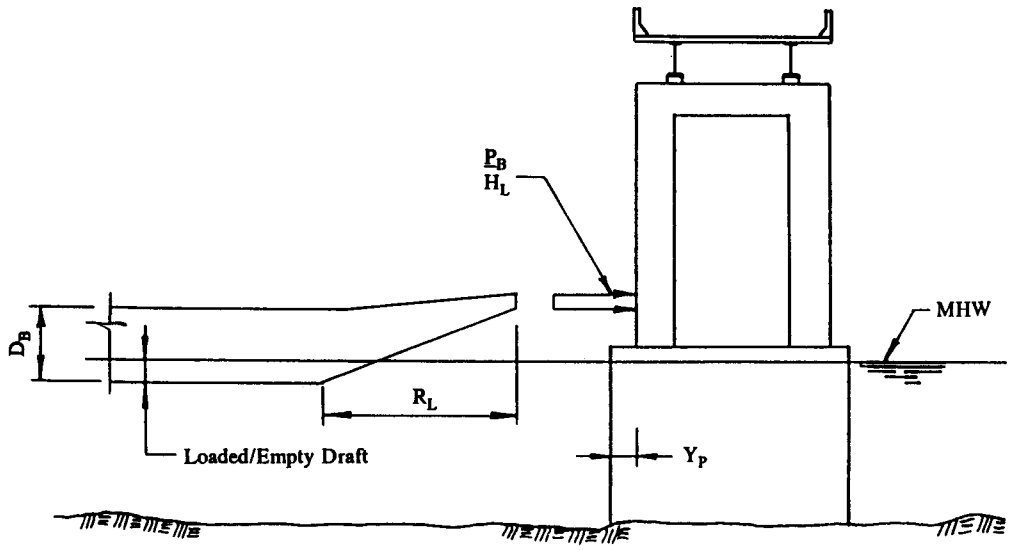

Figure 2–10 Barge impact force on pier.

Effects of scour. Scour is not a force or a resistance. However, scour is the most common cause of failure of highway bridges in the United States. By changing the conditions of the foundation, scour can alter the consequences and the process of force effects acting on the structure.

The design should consider the explicit consequence of changes in foundation conditions due to scour, resulting from the design-year flood at strength and service limit states. Scour is discussed in some detail in subsequent sections.

Ice Loads (IC)

Expected modes of action discussed by the standard AASHTO and LRFD specifications include the following:

1. Dynamic pressure due to moving ice sheets and ice floes carried by streams, wind, or currents
2. Static pressure due to thermal movement of ice sheets
3. Static pressure resulting from hanging dams or ice jams
4. Static uplift or vertical load from adhering ice in water of fluctuating level.

Table 2–10 Drag Coefficient

Type	C_D
semi-circular nosed pier	0.7
square ended pier	1.4
drift lodged against the pier	1.4
wedged nosed pier with nose angle 90° or less	0.8

Table 2–11 Lateral Drag Coefficient

Angle, θ, between direction of flow and longitudinal axis of the pier	C_L
00°	0.0
05°	0.5
10°	0.7
20°	0.9
≥30°	1.0

Considerable data on ice loads have been provided by Montgomery and Lipsett (1980), and have been incorporated in the specifications for ice loads prepared by the Canadian Standards Association (1988). Another useful source is Neill (1981). Articulating the two basic conditions producing ice forces on piers (dynamic and static), Montgomery and Lipsett (1980) provide the following comments, regarding ice failure.

Crushing. The ice fails by local crushing across the width of the pier, and crushed ice is continuously cleared from a zone around the pier as the floe moves past.

Bending. For piers with inclined noses, a vertical reaction acts on the ice floe and causes it to rise up the pier nose and fail by forming flexural cracks.

Splitting. When a small floe strikes a pier, stress cracks propagating from the pier into the floe cause it to split into smaller parts.

Impact. Small floes are brought to a halt while impinging on the pier nose before they fail by crushing over the entire width of the pier.

Buckling. For wide piers a large floe cannot clear the pier as it fails. In this case, compressive forces cause the floe to fail by buckling in front of the pier nose.

In bridge piers of usual proportions on large bodies of water, crushing and bending failures usually control the magnitude of the design dynamic ice force. On smaller streams that do not carry large ice floes, impact failure is the usual mode.

Static forces may be caused by thermal expansion of ice in which a pier is embedded, or by irregular growth of the ice field.

Dynamic ice forces. According to AASHTO standard specifications, horizontal forces resulting from the pressure of moving ice may be taken as

$$F = C_n ptw \tag{2–23}$$

where F = horizontal ice force on pier (lb); C_n = coefficient of nose inclination (from Table 2–12); p = effective ice strength (lb/in^2); t = thickness of ice in contact with pier (in); w = width of pier or diameter of circular shaft at the level of action (in).

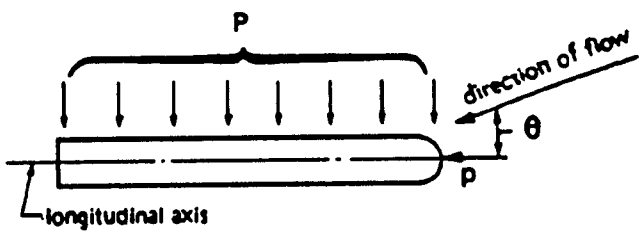

Figure 2–11 Plan view of pier showing stream flow pressure.

Table 2–12 Coefficient C_n for Nose Inclination for Dynamic Ice Force

Inclination of Nose to Vertical	C_n
0° to 15°	1.00
15° to 30°	0.75
30° to 45°	0.50

The effective strength p is normally taken between 100 and 400 lb/in^2 on the assumption that crushing or splitting of the ice occurs on contact with the pier. The value to be selected depends on an assessment of local conditions and previous experience. Refinements in Equation (2–23) have been introduced by the LRFD specifications (Article 3.9.2.2)

Thus, in the absence of more precise information the following values of the effective strength p may be used:

- 8.0 kips/ft^2 (55 lb/in^2) where break-up occurs at melting temperatures and the ice is substantially disintegrated in its structure.
- 16.0 kips/ft^2 (110 lb/in^2) where break-up occurs at melting temperatures and the ice is somewhat disintegrated in its structure.
- 24.0 kips/ft^2 (165 lb/in^2) where break-up or major ice movement occurs at melting temperatures, but ice moves in large pieces and is internally sound.
- 32.0 kips/ft^2 (220 lb/in^2) where break-up or major ice movement occurs at melting temperatures, averaged over its depth, measurably below the melting point.

Static ice forces. Ice pressures on piers from frozen ice sheets should be investigated when the ice sheets are subject to significant thermal movement, or under conditions producing substantial unbalanced forces on the pier. Only limited data are available for predicting static ice loads on piers. Under normal circumstances, the effects of static ice forces on piers may be strain limited, but competent advice should be requested if there are reasons for concern.

Hanging dams, ice dams, and vertical forces due to adhesion. The frazil accumulation in a hanging dam may be assumed to exert a pressure of 0.2 to 2.0 kips/ft^2 as it moves by the pier. An ice jam may be taken to exert a pressure of 0.02 to 0.20 kips/ft^2.

The vertical force on a bridge pier due to rapid water level fluctuation may be taken as follows:

$$\text{Circular pier } F_V = 21.0t^2\left(0.3+\frac{0.07R}{t^{0.75}}\right) \qquad (2\text{–}23a)$$

$$\text{Oblong pier } F_v = 0.2t^{1.25}$$

where t = ice thickness (ft)

R = radius of circular pier (ft)

2.6 EARTHQUAKE EFFECTS

The specifications for seismic design introduced by AASHTO are comprehensive and embody concepts based on both the observed performance of bridges during past earthquakes and on recent research here and abroad. They are supplemented by an extensive commentary documenting the basis for the design criteria, and contain appropriate examples.

However, these provisions apply to bridges of conventional steel and concrete girders, including box girder construction and trusses, with spans not exceeding 500 feet (152.4 m). Suspension bridges, cable-stayed bridges, arch type, and movable bridges are not covered in the main body, but general considerations are presented in the commentary.

A detailed seismic analysis is not required for single span bridges or for bridges in Seismic Performance Category A. Their connections must, however, be designed for specified forces, and must also meet minimum support length requirements.

The design earthquake motions generally should be based on a low probability of being exceeded during the normal life expectancy of a bridge. Bridges designed in this manner may suffer some damage, but should have low probability of collapse during a seismic event. These criteria incorporate the following principles:

1. Small to moderate earthquakes should be resisted within the elastic range of the structural components without significant damage.
2. Realistic seismic ground motion intensities should be relevant parameters in seismic design.
3. Exposure to shaking from large earthquakes should not cause partial or total collapse, and where damage occurs it should be readily detectable and possible to repair.

General Requirements

Acceleration coefficient. The coefficient A to be used in the application of AASHTO provisions is determined from appropriate contour maps, where the values are usually expressed in percent. The maps are based on a uniform risk model of seismic hazard.

Importance classification. This factor (also referred to as Importance Categories) is assigned to all bridges with an Acceleration coefficient greater than 0.29, for the purpose of determining the Seismic Performance Category (SPC) as follows:

1. Essential Bridges, IC = I
2. Other Bridges, IC = II

(Note: the LRFD specifications adds a third category: critical bridges).

Seismic performance categories. (Also referred to as Seismic Performance Zones). Bridges are assigned to one of four seismic zones according to the Acceleration coefficient. These reflect the variation in seismic risk and are used to determine the requirements for methods of analysis, minimum support lengths, column design details, and foundation and abutment design procedures.

Site effects. The effects of site conditions on bridge response are determined from the site coefficient based on specific soil profiles. AASHTO articulates three soil profile types, whereas the LRFD document has added a fourth type to include soft clays or silts greater than 40 feet in depth.

Elastic seismic response coefficient. According to the LRFD document, the elastic seismic response coefficient may be normalized during the input ground acceleration A and the result plotted against the period. An earthquake may excite several modes of vibration in a bridge, and the elastic response coefficient should be found for each relevant mode. Thus, for mode m, the coefficient can be taken as

$$C_{sm} = \frac{1.2AS}{T_m^{2/3}} \leq 2.5A \tag{2–24}$$

where T_m = period of vibration of the m mode (sec); A = Acceleration Coefficient; and S = Site Coefficient.

Earthquake loads are obtained as the product of the elastic response coefficient C_{sm} and the equivalent weight of the superstructure. The latter is a function of the actual weight and bridge configuration, and is automatically included in all methods of analysis.

Response modification factors. AASHTO stipulates that seismic design forces for substructures and connections of bridges with $A > 0.09$ must be determined by dividing the elastic forces by an appropriate Response Modification Factor R.

The current trend is to accept the philosophy that it is uneconomical to design a bridge to resist large earthquakes elastically. Thus columns may be assumed to deform inelastically when seismic activity exceeds the design level. The design level is established by dividing the elastically computed force effects by the appropriate R factor.

The LRFD specifications use a modified summary of R factors, taking into account the importance category of critical, essential, and other types of bridges. This document articulates also connections as those mechanical devices that transfer forces from one structural member to another. They include, but are not limited to, fixed bearings and shear keys. Monolithic joints between structural members are also connections, for example, column-to-footing connections. As any alternative to the R factor method, these may be designed to transmit the maximum force effects that can be developed by the inelastic hinging of the adjacent column or multi-column bent.

2.7 TRANSFER OF LOADS FROM SUPERSTRUCTURE TO SUBSTRUCTURE

Comments on Highway Loadings

Live load. To help the reader understand the adequacy of the AASHTO highway loading, Figure 2–12 summarizes examples of design loads used in other countries, involving both conventional and military loadings. In certain countries—for example, England—the inability of the railroad system to carry very heavy loads has prompted the adoption of unusually heavy highway loads. Whether the current AASHTO loading represents load effects realistically remains academic. The modified live load introduced by the LRFD specifications will enhance the live load representation. In practice, the selec-

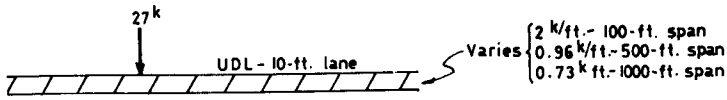

(a) British HA loading

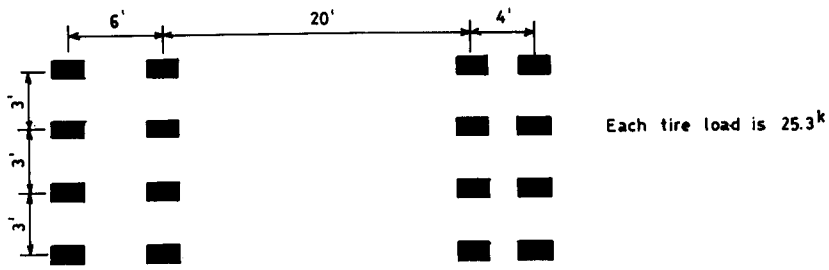

(b) British HB - Abnormal loading

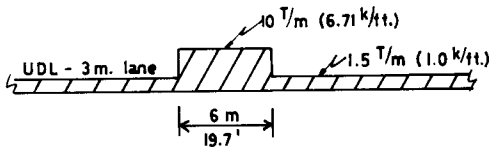

(c) German loading DIN 1078

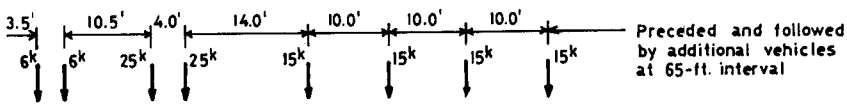

(d) Indian - Class A train of vehicles

Note :
A meaningful comparison would have to include dynamic allowance, multiple lane loading, distribution to structural elements, etc.

Figure 2–12 Design highway live loads for various countries.

tion of design criteria for a structural system should consider various factors. For example, bridges should not be expected to suffer damage as a result of normal traffic or because of an occasionally single overload. Serviceability is equally important, and bridge obsolescence due to heavy vehicle traffic should be deterred. It may appear, therefore, that the AASHTO loadings, combined with overload provisions and the alternate military loading, are sufficient for design purposes and represent a logical exercise of resourceful judgment. Where unusually long spans are involved, modified loadings may be considered.

Longitudinal (braking) forces. These are forces to be resisted solely by the substructures. Comparatively, the 5 percent provision of braking force may result in realistic predictions for long bridges, but may underestimate the braking effect on relatively short structures. For example, a 300-foot-long continuous bridge with two lanes in the same direction will have a longitudinal force according to AASHTO as $F = 0.05 \times 2 \times (0.64 \times 300 + 18) = 21.0$ kips. If a single truck (weight = 72 kips) moving at 60 MPH suddenly brakes, the longitudinal force computed from Equation (2–13) is $F = 0.46 \times 72 = 33.1$ kips.

Applying the LRFD criteria (all design lanes should be simultaneously loaded for bridges likely to become one-directional, and no reduction because of the multiple presence factor), two tracks can be placed on the bridge giving a braking force $F = 0.25 \times 2 \times 72 = 36$ kips.

The variability in the criteria for the longitudinal force is demonstrated by the state specifications. For example, the 1955 Ohio specifications stipulated that forces due to traction and momentum should be considered as longitudinal forces with a magnitude 10 percent the vertical live load on at least one-half but not more than two-thirds of the lanes, applied at the point of contact between superstructure and substructure.

Reduction in load intensity. According to AASHTO, if two or more lanes are loaded simultaneously to produce maximum effect on any member, the percentage of the resulting live load stress will be as follows:

Two lanes loaded	100 percent
Three lanes loaded	90 percent
Four or more lanes loaded	75 percent

Similar criteria are likewise provided by the LRFD specifications for multiple presence of live load. If refined methods are used, the factors given in Table 2–13 may be used to reduce calculated extreme force effects. The selected factor should be consistent with the number of lanes loaded for computing the extreme force effect.

Table 2–13 Multiple Presence Factors "m"

Number of Design Lanes	Multiple Presence Factors "m"
1	1.20
2	1.00
3	0.85
>3	0.60

This reduction reflects the improbability of coincident maximum loading, and applies to all live load reactions applied to substructure.

Dependence of Load Magnitude and Distribution on Bearing Type

Figure 2–13 shows four possible configurations for a typical four-span highway bridge. The scheme shown in Figure 2–13(a) consists of four simple-span units, with the fixed and expansion bearing located as shown. This may be a logical solution where seismic design is the controlling criterion, but it is highly undesirable because of the many expansion devices and open deck joints.

The solution shown in Figure 2–13(b) consists of a two-span continuous unit for the center spans and has simple units at the end spans. Normally, it would be selected if the center-to-end span ratio is unfavorable for continuity. Since the abutments have fixed bearings, the number of open deck joints is reduced from five to two. The four-span continuous unit shown in Figure 2–13(c) is probably the one to be selected under current criteria since it may give the most economical design. This scheme has, likewise, two open deck joints at the expansion (abutment) bearings.

Finally, the configuration of Figure 2–13(d) is an integral bridge with all five bearings fixed and no open deck joints.

Thus, although the bridge structure in all four schemes is essentially the same in plan, elevation, and structural capacity, the type and magnitude of loads to be transferred from the superstructure to each substructure element is markedly different, and depends mainly on the type and location of bearings.

Movement and load effects. Bridge movement may arise from a number of different causes, but thermal movement is of prime concern. The type, direction, and magnitude of movement must be accurately determined in order to design the bearing devices and to articulate the forces transferred to substructure. Simplified estimates, particularly for bridges of complex geometry, may lead to unrealistic and often unsafe design. Curved bridges and skewed bridges (see also following sections) may have transverse as well as longitudinal thermal movement in addition to creep and shrinkage. Rotations caused by permitted misalignment should also be provided for, and in many instances they may exceed live load rotations. Transverse movement of the superstructure rela-

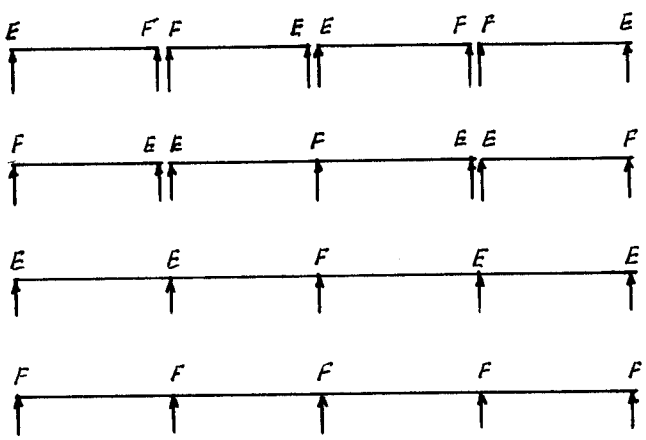

Figure 2–13 Configurations for a 4-span bridge.

tive to the substructure may become significant and have design implications on the substructure.

Any horizontal movement of the superstructure will be opposed by the resistance offered by the bridge bearings to movement and the rigidity or flexural resistance of substructure elements. The rolling resistance of rockers and rollers, the shear resistance of elastomeric bearings, or the frictional resistance of bearing sliding surfaces are typical examples of restraint to movement (Xanthakos, 1994a). In particular, rigidity of abutments and flexibility of piers of various heights and foundation types will affect the extent of bearing movement and the bearing forces opposing movement.

When horizontal movement at the ends of a superstructure is caused by volumetric changes, the forces generated within the structure in response to these changes are balanced. The neutral point can be located by computing these forces, taking into account the relative resistance of bearings and substructures to movement. For a curved superstructure laterally unrestrained by guided bearings, the direction at a bearing joint is commonly taken to be parallel to the chord centerline from the joint to the neutral point.

Effects from external action. Forces directly induced at bearing locations are from the longitudinal and transverse loads discussed in the foregoing sections. Among these, traction, wind, and centrifugal forces have a marked effect on substructure design.

Example of the Influence of Support Details

Support details for curved steel box girders must be designed to minimize horizontal restraint at the bearings. Since boxes are much stiffer in the lateral direction than plate girders, temperature changes will induce lateral forces at restraining points. Exempting friction, the ideal horizontal support system must be statically determinate and should not develop thermal forces. In a single continuous box, a statically determinate horizontal support is designed by fixing each of three supports in one direction only and freeing all other supports in all directions. One way is to fix one interior support in the tangent direction, the two end supports in the radial direction, and provide complete freedom at all other supports. If such a system is part of a multiple girder system where the girders interact with the deck and diaphragms, all other bearings in the remaining girders should be free in all directions to satisfy the statical determinancy of the bridge.

In any event, friction will upset the degree of statical determinancy, particularly with large reactions from dead loads, since this factor may cause bearings to respond as fixed while theoretically they are free to move. If this fixity is induced to the piers, it will cause them to deflect with corresponding force and moment effects. Most bearings will behave as fixed until friction is overcome and slip can occur.

Two different framing schemes can be used to transfer torque into the substructure. One way is to design the bearings so that the boxes are torsionally fixed at one or at all supports, merely by providing two shoes inducing a couple at each bearing line under each girder. For a single-box structure this degree of torsional rigidity is a primary requirement, especially with severe curvature, but may also be used in multiple-girder bridges.

The alternative is to allow torsional freedom at the bearings but connect the girders together by diaphragms at the supports, a solution applicable to multiple-girder bridges. Torsional freedom is ensured by a single bearing that can rotate radially. In effect, this arrangement converts torque at the supports into vertical reactions at the

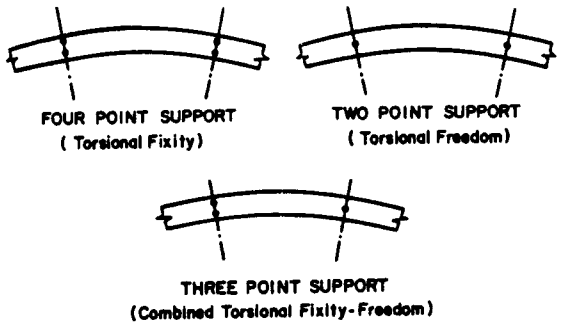

Figure 2–14 Bridge support options, curved steel box girders.

bearings rather than into couples. Various bridge support options are shown in Figure 2–14.

2.8 DISTRIBUTION OF LONGITUDINAL FORCES TO FIXED AND EXPANSION PIERS

Assumed Behavior

As mentioned, longitudinal forces at bridge bearings are induced by traction (acceleration or deceleration of live load), wind forces, and thermal movement. A frictional force may also be considered for rockers, rollers, and sliding-type expansion devices. The following distribution modes are often assumed.

1. Expansion bearings resist only thermal forces, while the fixed bearing resists all longitudinal forces associated with wind and traffic loads. This would place expansion piers under Groups IV, V, and VI in the standard AASHTO specifications.
2. Expansion bearings resist only thermal forces, but this resistance may suddenly be released at any expansion pier by live load vibrations. Thus, expansion bearings may become inoperable at some point and time, and the forces so released must be carried by the fixed pier.
3. A third approach assumes that expansion bearings will carry thermal forces as well as wind and live loads up to their frictional capacity, computed as the dead load reaction multiplied by a friction coefficient. This resistance continues until the longitudinal forces exceed the magnitude of friction and the bearing slips. At this point, any additional loads must be resisted at the fixed pier.

   (The third approach seems to be most rational, subject to the following comments: (a) AASHTO clearly stipulates that provisions must be made to reflect the effect of friction at expansion bearings or shear resistance at elastomeric bearings; (b) if friction is treated as resistance, it is omitted from group loads and group load applications; (c) designing an expansion pier for its full frictional capacity can give erroneous results unless the actual load acting at this bearing exceeds its friction; and (d) the percentage of stress to be used with friction is not specified, and therefore requires discretion.)
4. With massive, stiff abutments at the ends of a bridge, many designers choose to distribute longitudinal and lateral forces at these locations and design intermediate piers for vertical loads only.

It appears that none of the foregoing approaches is entirely acceptable because all are based on arbitrary, although convenient, assumptions. The rationalization of a design methodology is further complicated by the variability of friction coefficients. Other factors influencing the distribution of longitudinal forces to bridge bearings are the relative stiffness of substructure elements and their foundations, overall thermal movement, and relation of total longitudinal force to maximum resisting force available at expansion bearings. After a slip occurs, the remaining devices (fixed bearings and expansion bearings that have not slipped) will resist additional longitudinal effects.

Small-Scale Tests

These load effects on bridge bearings have been investigated in small-scale model tests by McDermott (1978), supplemented by a survey of two- and three-span bridges. Typically, these bridges have a ratio of design external force to internal resisting force at expansion bearings in the range 0.41–1.96, and a ratio of superstructure to substructure stiffness from 3 to 248.

For the model tests, the superstructure-to-substructure stiffness ratio was taken as 1.7 and 20.7 for the strong and weak pier axis, respectively. The induced forces and the range of externally applied loads are given in Table 2–14, and evidently three cases are considered: (1) internal force zero; (2) maximum expansion; and (3) maximum contraction. The desired range of external forces to maximum resisting forces was obtained by varying the external longitudinal load and the normal load at the expansion bearings. An additional test was carried out with all bearings fixed to determine the load distribution as a function of pier and abutment stiffness.

Details of the model structure are shown in Figure 2–15. The bearing devices consist of steel plates attached to the top of abutments and fixed pier. The plates at the abutments are allowed to slide to accommodate expansion. Thermal forces are simulated at these locations by turning the screw mechanism in Detail A until slip occurs. I-sections are used in the structural members, including the fixed pier where the bending axis is changed to study strong and weak axis effects. The abutments consist of steel pipes, fixed at the base as in the pier.

Table 2–14 Longitudinal Force Distribution Test

Induced Internal Forces	Applied Load	
	Normal Force, N	*Horizontal Force, F_L*
STRONG-AXIS TEST		
Zero Expansion Contraction	77 to 177 lb	25 to 150 lb
WEAK-AXIS TEST		
Zero Expansion Contraction	57 to 177 lb	50 to 150 lb

(From McDermott, 1978)

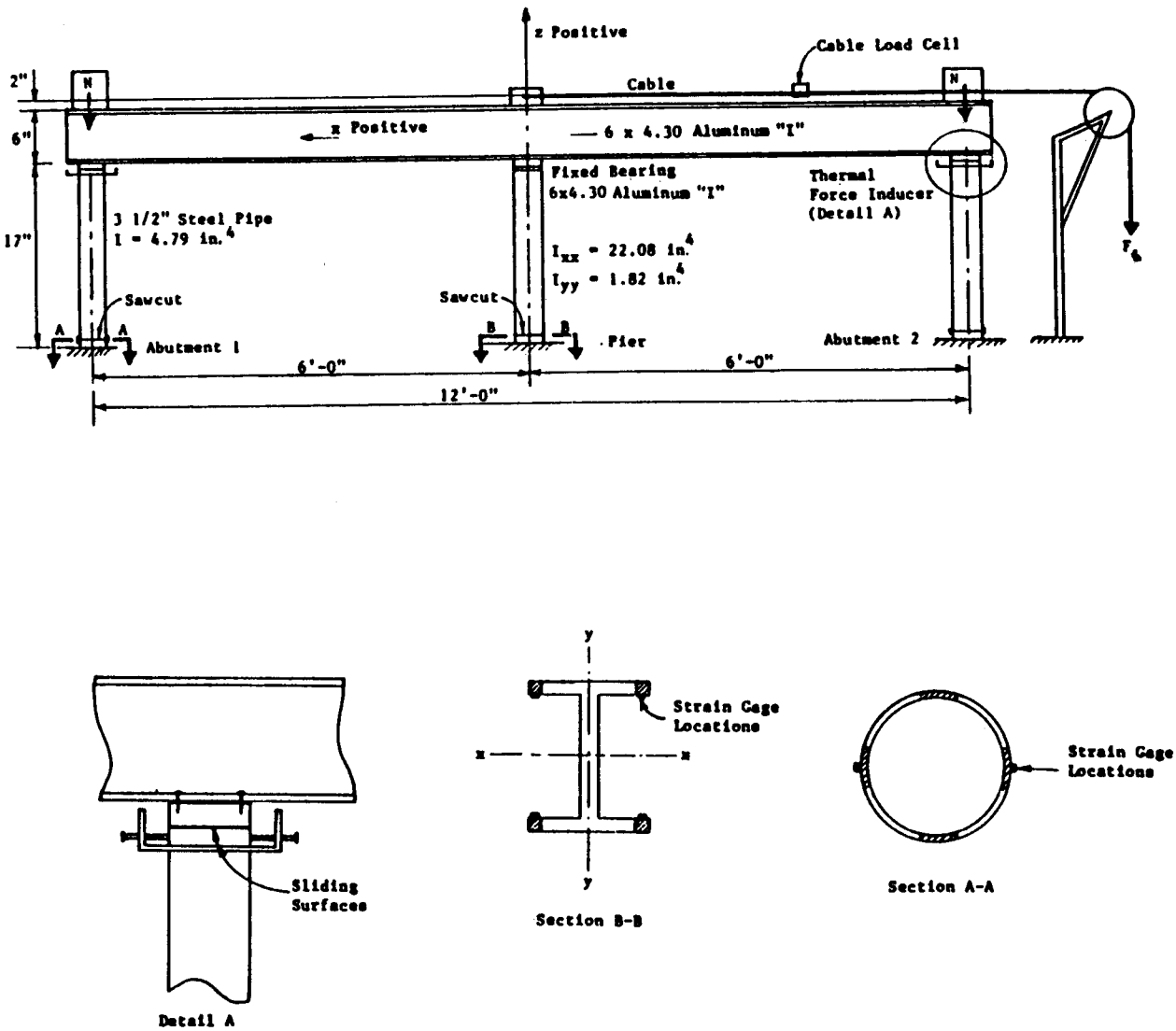

Figure 2–15 Test model structure; elevation and details *(from McDermott, 1978).*

For the test arrangement shown in Figure 2–16, a bending moment is introduced at the top of the pier with the application of force F_L. This moment is determined from the relative stiffness of the beam and column, maximum resisting force at expansion bearings, and point of application of force F_L. As a result, the moment at the pier base depends not only on pier height but also on factors affecting the top moment.

Test procedure. Resistance to horizontal loads was measured at all three supports. Readings were taken with no loads on the system, after a change in applied forces, following the application of vertical loads, horizontal loads and simulated thermal forces, and after removing these loads.

A vertical load placed over a bearing simulates dead load beam reaction and in-

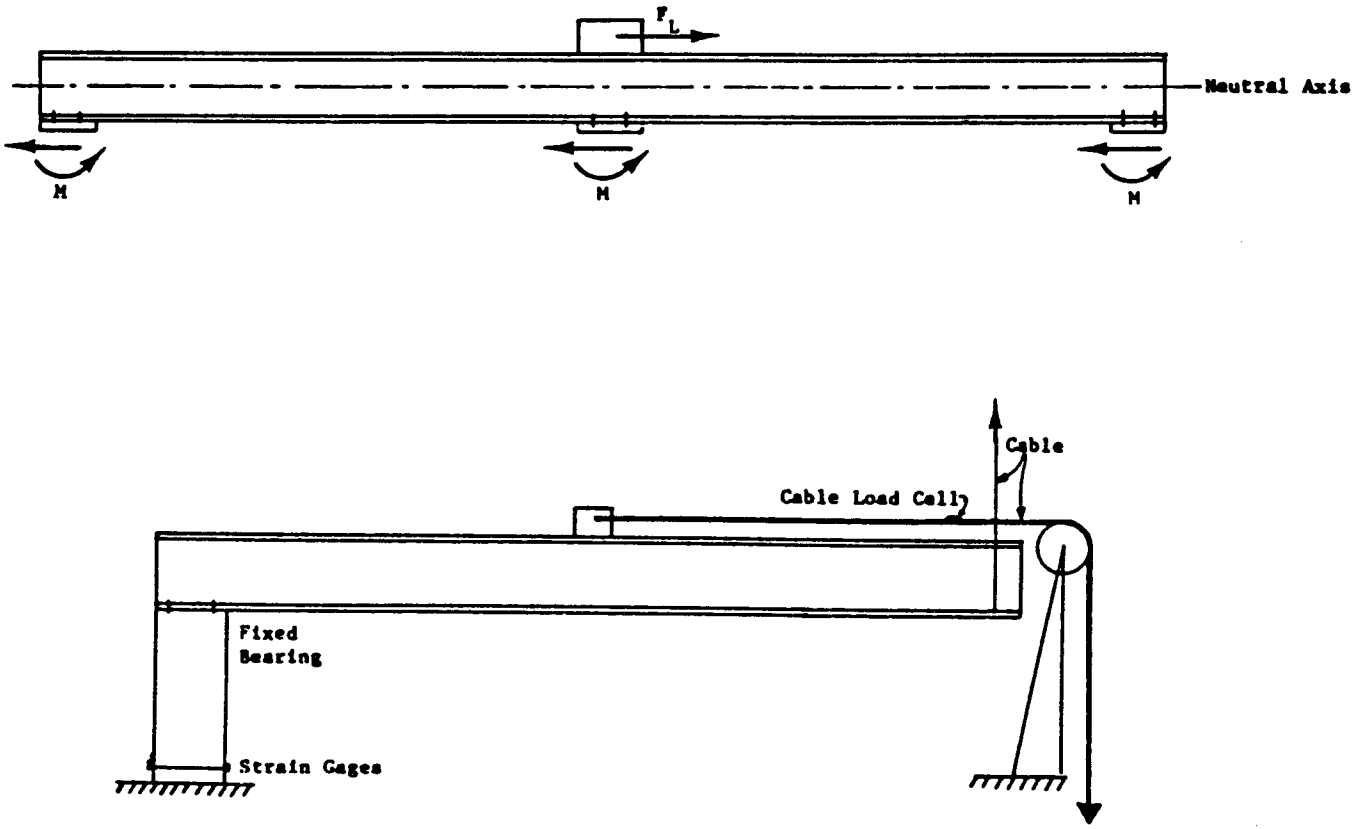

Figure 2–16 Simulation of bending moments in test model *(from McDermott, 1978).*

duces potential frictional resistance. Simulated thermal forces are introduced to a certain level before a horizontal force is applied. Because of the variability of the friction coefficient, induced forces are not linearly proportional to the normal (vertical) load. In order to satisfy static equilibrium, some force fraction must be resisted at the fixed pier even though no direct force is applied at this point. After the thermal force is induced, horizontal loads are applied over the center fixed pier 2 inches above the top flange of the beam. Longitudinal force distribution is then tabulated with the internal force and the longitudinal force in place. A partial summary of longitudinal force distribution is given in Table 2–15.

Variability of friction coefficients. These are calculated by dividing the induced (simulated) thermal force over the bearing by the normal load N, and are given in Table 2–16.

The wide variation range (friction coefficient 0.02 min., and 0.68 max.) is not explained by conventional theories. According to the test format, internal forces were induced until slip occurred, and at this stage the friction force was recovered and assumed to have its maximum value. Although no increase should be expected, it was observed at abutment 1 in compression and at abutment 2 in expansion after applying the longitudinal loads. Since the normal load did not increase, it means that the coefficient of friction is variable.

In practice, the performance of bearings can be affected by the presence of dust, humidity, rust, oxide films, temperature change, surface films, and extent of contamination. In theory, these factors cannot be singly or jointly considered, and care was taken to eliminate these effects during the tests. The suggestion is (McDermott, 1978) that some malfunctioning in the test and calibration procedures could have caused some discrepancies, and that the average friction coefficient for steel on steel is close to 0.4.

Theoretical Models

A suggested theoretical model is presented in Figure 2–17, and shows how the frictional forces at expansion bearings affect the distribution of longitudinal loads. The maximum resisting force at the expansion bearing is μN where μ = coefficient of friction. If μ can be assumed constant, the total frictional resistance of the system is $\mu\Sigma N$. Knowing the force at the expansion bearings (N), the force to be resisted at the fixed bearing is simply the difference $F_p = F_L - \mu\Sigma N$. This does not mean, however, that the force at the fixed

Table 2–15 Partial Summary of Longitudinal Force Distribution

Test	Vertical Load N (lb)	Applied Longitudinal Load F_h (lb)	Induced Lateral Force			Longitudinal Force Distribution		
			Abut. 1	*Pier*	*Abut. 2*	*Abut. 1*	*Pier*	*Abut. 2*
1A	77	−141.6	0.0	0.0	0.0	3.7	116.6	12.0
5A	127	−49.1	0.0	0.0	0.0	15.1	21.4	11.9
7A	77	−94.1	−24.8	2.7	16.7	9.6	60.5	17.3
$9A_E$	127	−61.5	−46.8	8.3	31.8	−23.3	48.9	32.4
2BB	127	−88.6	0.0	0.0	0.0	42.5	14.9	41.0
$6BB_C$	77	−90.3	16.6	8.0	−24.3	20.6	32.0	42.9
10BB	97	−91.1	0.0	0.0	0.0	44.6	16.1	40.9

(From McDermott, 1978)

Table 2–16 Apparent Coefficients of Friction

Test	Friction Coefficient when Slip Occurs[a]		Test	Friction Coefficient when Slip Occurs[a]	
	Abutment 1	*Abutment 2*		*Abutment 1*	*Abutment 2*
$7A_E$	0.32	0.22	$6BB_C$	0.22	0.32
	0.28	0.24		0.39	0.42
	0.31	0.26		0.30	0.37
$7A_C$	0.12	0.19	$7BB_E$	0.41	0.46
	0.03	0.24		0.41	0.42
	0.02	0.11		0.47	0.42
$8A_E$	0.28	0.28	$7BB_C$	0.36	0.37
	0.31	0.23		0.51	0.44
	0.34	0.25		0.40	0.33
$8A_C$	0.15	0.20	$8BB_E$	0.33	0.48
	0.16	0.24		0.44	0.42
	0.18	0.24		0.36	0.44
$9A_E$	0.37	0.25	$8BB_C$	0.20	0.40
	0.31	0.26		0.37	0.42
	0.30	0.21		0.32	0.31
$9A_C$	0.19	0.27	$11BB_E$	0.35	0.41
	0.13	0.07		0.48	0.68
	0.11	0.29		0.53	0.67
$6BB_E$	0.45	0.55	$11BB_C$	0.34	0.54
	0.44	0.56		0.35	0.42
	0.40	0.61		0.33	0.54

[a]Friction coefficient μ = Induced thermal force/N. (From McDermott, 1978)

bearing is zero until the difference $F_L - \mu\Sigma N$ becomes positive, since superstructure and substructure stiffness affect the distribution of F_L before expansion bearings mobilize their full capacity. When forces at expansion bearings are not sufficient to cause slip, a predictable percentage of longitudinal force is resisted at the fixed bearing. The force is a function of the ratio of pier-to-abutment stiffness, and increases as this ratio increases. If slip occurs at the expansion bearings, additional longitudinal forces are resisted at the fixed pier.

The foregoing highlight the behavior of the test model, in this case a two-span symmetrical bridge. For three or more spans, the fixed pier does not necessarily coin-

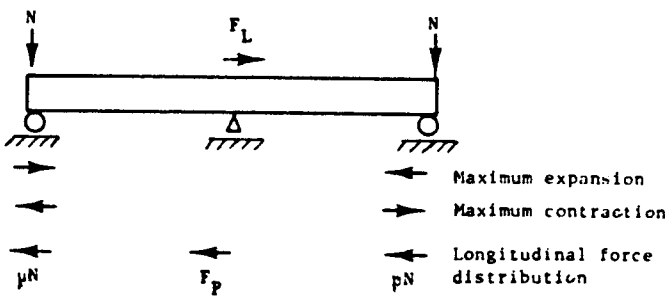

Figure 2–17 Magnitude and direction of longitudinal resisting forces on the test structure *(from McDermott, 1978).*

cide with the point of zero movement under thermal expansion and contraction. The analysis must now differentiate between actual applied loads (wind forces, traction, etc.) and forces manifested as movement (temperature changes).

A theoretical model for the distribution problem is shown graphically in Figure 2–18. Between points A and B, the distribution is essentially controlled by the relative stiffness of each substructure element, and a percentage of the longitudinal force F_L is always resisted at the fixed pier. The slope of line AB is influenced by forces initially present in the system (N) and by the coefficient μ. If the maximum thermal force is induced (just before slip occurs), the resisting force at expansion bearing is μN, but its direction depends on temperature change (expansion or contraction). Since one bearing is in the same direction as longitudinal resisting forces, it has no resisting capacity under any additional load that must now be resisted by the fixed and the expansion bearings in the opposite direction. These elements will receive the additional load in proportion to their relative stiffness. As the longitudinal force increases further, the resisting capacity manifested as friction will be depleted in the direction of load application, and at

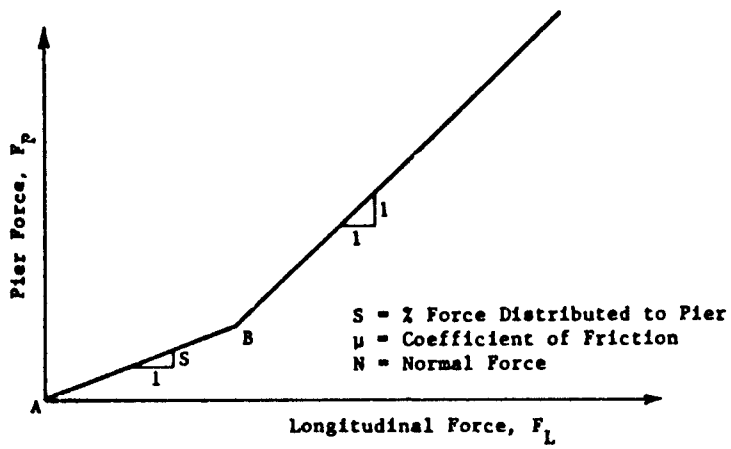

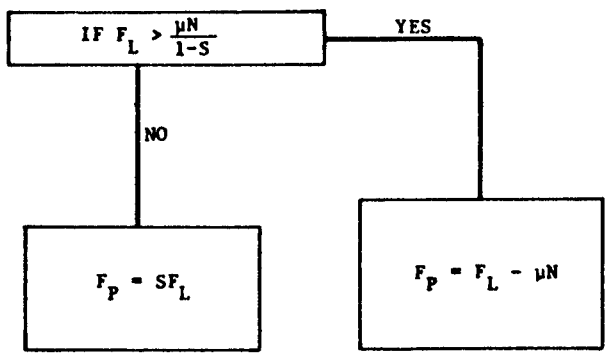

Figure 2–18 Theoretical distribution of longitudinal force *(from McDermott, 1978).*

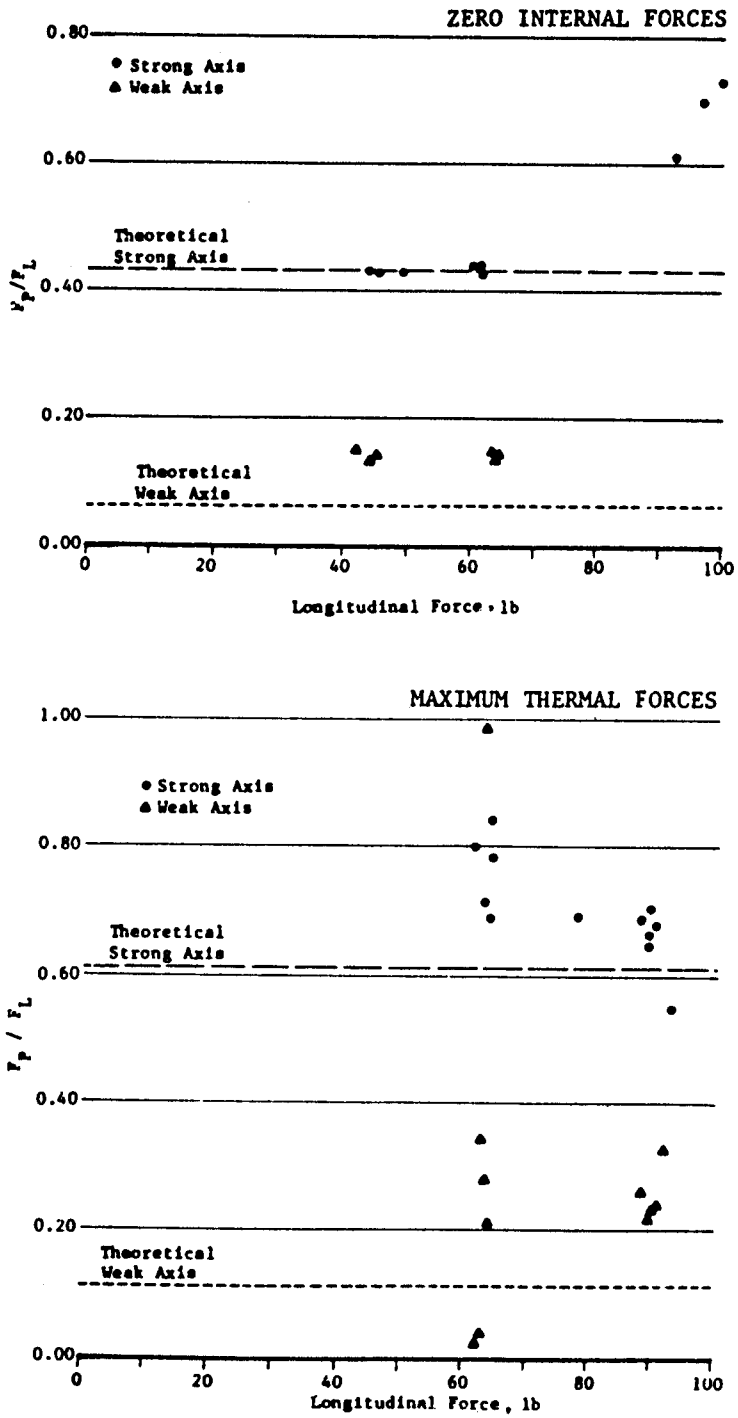

Figure 2–19 Force distribution to fixed pier *(from McDermott, 1978).*

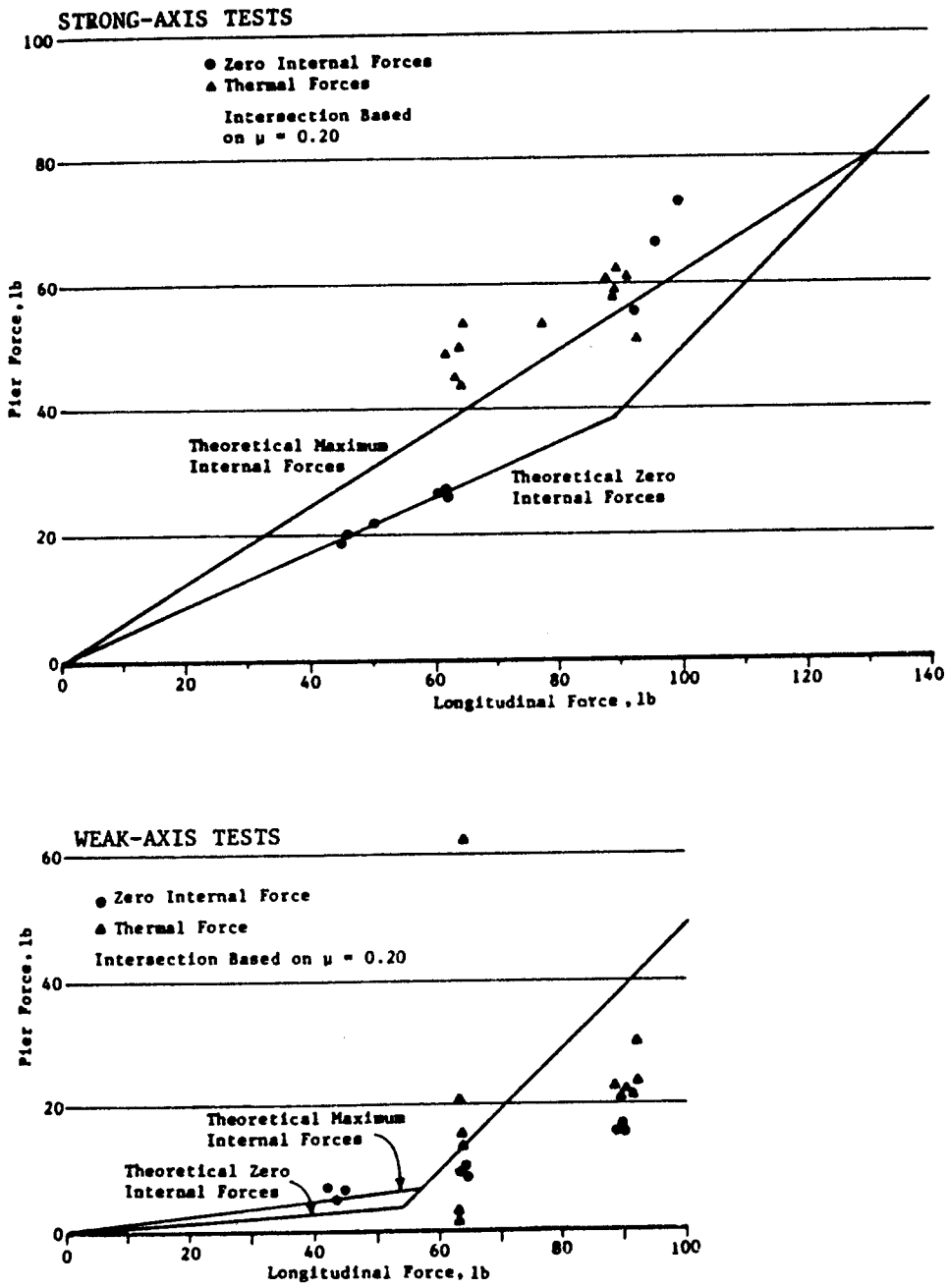

Figure 2–20 Fixed pier force; 127-lb normal force *(from McDermott, 1978).*

this point any additional load must be resisted at the fixed pier only. This behavioral model does not fully explain the effects of thermal expansion unless the analysis considers the point of zero movement. Furthermore, live load vibrations may release the thermal forces.

The Rationale of Load Action and Distribution

Figure 2–19 shows the percentage of force carried by the fixed pier; evidently this is a relatively constant fraction of the applied loads until slip occurs at the expansion bearings.

However, prediction of the distribution load beyond point B (Figure 2–18) is inconsistent because the variability of friction coefficients inhibits conclusion as to when bearing friction forces reach peak values. Figure 2–20 shows scattered data from the test for both the weak and strong axis versus the theoretical distribution lines. Two relations are plotted: (1) maximum initial internal force, where one abutment is effective in resisting longitudinal loads, and (2) zero internal force, where both abutments are effective. The theoretical line is plotted with average friction coefficients. The actual variability of friction coefficients may explain why the data do not coincide with the plot.

Design comments. A practical conclusion is that a bilinear relationship may be assumed between distribution of force to the fixed pier and applied longitudinal load, represented by the diagram of Figure 2–18. As the expansion bearing begins to slip, additional longitudinal load is carried by the fixed pier.

Abutments often are designed as massive structures with considerable rigidity and stiffness compared to piers. In this case it is very likely that initially a high percentage of force will be resisted at these locations before slip occurs, after which any additional force will be transferred to the fixed piers.

A bilinear relationship between pier force and longitudinal load is possible in bridges of equal spans, but may not exist in all bridges. For structures with unequal spans, the dead load reactions are different, changing the frictional capacity at the expansion bearings. In addition, thermal forces are different between spans, depending on span length and distance from point of zero movement. Slip is unlikely to occur simultaneously in all expansion bearings. If it occurs at one location before the other, more longitudinal load will be resisted by the other expansion bearings and the fixed pier. If slip occurs simultaneously at all expansion locations (this may be the case when the fixed bearing is at one end of the structure), all excess loads must be resisted by the fixed bearing. When designing a fixed pier, the possibility of friction force release at expansion locations should be considered, and the fixed pier may have to be designed to resist all longitudinal forces.

2.9 NUMERICAL EXAMPLES

Fixed Pier

The bridge shown in Figure 2–21(a) and (b) is a 4-span continuous steel plate girder superstructure with concrete deck. The span lengths are 50, 72, 72, and 51 feet, giving approximately a total bridge length 250 feet. From an analysis of the superstructure, the dead and live load reactions have been determined at each substructure element. The application of loads will be demonstrated for fixed pier 2. The special features of this

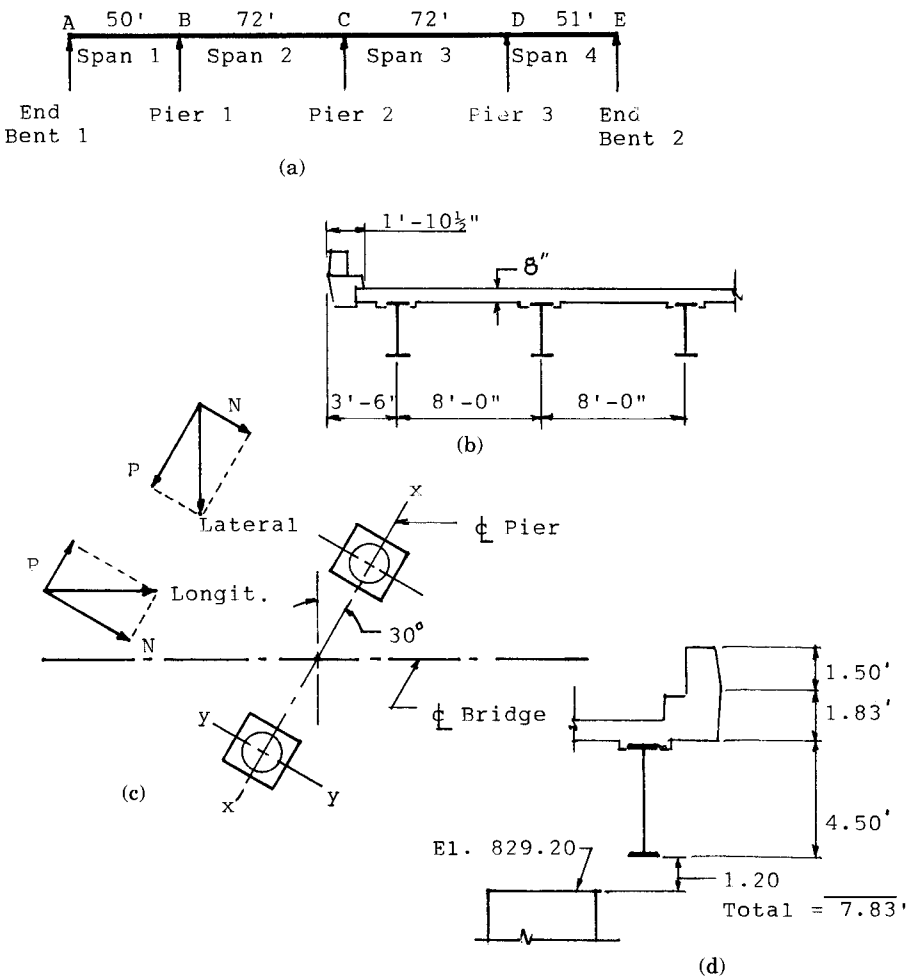

Figure 2–21 Part of I-75, I-275 4-level interchange; (a) I-75 bridge elevation; (b) partial deck cross section; (c) fixed pier plan; and (d) fascia detail.

bridge are reviewed and discussed in other sections. A basic feature of this structure is that the longitudinal deck beams frame into transverse box girders at the piers.

The transverse box girders at the piers are supported by two individual concrete columns on square spread footing transferring the loads to underlying rock. Special bearing devices allow rotation of the superstructure elements in both the longitudinal and transverse direction. The basic design philosophy was to design the fixed pier for all longitudinal forces plus a corresponding portion of the transverse loads. A basic pier plan is shown in Figure 2–21(c). The live load is HS 20.

1. *Dead Load Reactions* (obtained from superstructure analysis)

Interior Girders (5) = 110 × 5	= 550 kips
Exterior Girders (2) = 99 × 2	= 198 kips
Total D.L. (Superstructure)	= 748 kips
Weight of Box Girder	= 56 kips
Total DL	= 804 kips or 402 kips/column

2. *Live Load Reactions.* Again, from superstructure analysis we obtain directly Total LL = 154 × 0.9 = 139 kips/column where the coefficient 0.9 is applied to three lanes loaded.

Note that the pier is skewed at 30°, as shown in Figure 2–21(c). Hence all loads (longitudinal and transverse) are resolved into two components parallel and normal to the pier axis, P and N, respectively. For convenience, we write *sin* 30° = 0.500, and *cos* 30° = 0.866.

3. *Wind on Structure.* The exposed superstructure, as seen from an elevation parallel to the bridge, is shown in Figure 2–21(d) in relation to the pier top. According to relevant standards, the bridge is designed for wind velocity 84 mph, so that the wind intensity reduction coefficient is $84^2/100^2 = 0.71$. Both transverse and longitudinal wind is applied simultaneously at the elevation of the center of gravity of the exposed area of the superstructure. Since the maximum span lengths are less than 125 feet, Article 3.15.2.1.3 of AASHTO is applicable.

We now estimate the wind force on structure as follows:

		N	P
Lateral	$= 75 \times 7.83 \times 0.50 \times 0.71 = 20.8$ kips	10.4	18.1
Longitudinal	$= 250 \times 7.83 \times 0.012 \times 0.71 = 16.7$ kips	± 14.5	∓8.4

Keeping the lateral wind direction the same, and reversing the longitudinal wind direction, we obtain the following N, P combinations:

(a) $N = 10.4 + 14.5 = 24.9$ kips

$P = 18.1 - 8.4 = 9.7$ kips $\qquad \sqrt{24.9^2 + 9.7^2} = 27$ kips

(b) $N = 14.5 - 10.4 = 4.1$ kips

$P = 18.1 + 8.4 = 26.5$ kips $\qquad \sqrt{26.5^2 + 4.1^2} = 27$ kips

suggesting that for optimum design the footing must have a square shape.

4. *Wind on Live Load.*

Likewise, the wind on live load is computed using the simplified method.

			N	P
Lateral	$= 75 \times 0.10$	$= 7.5$ kips	3.8	6.5
Longitudinal	$= 250 \times 0.04$	$= 10.0$ kips	±8.7	∓5.0
		Total used	$N = 12.5$ kips	$P = 1.5$ kips

5. *Wind on Pier (one column).* Assume column height 23 feet, and column diameter 4 feet 6 inches.

	N	P
Lateral = 23 × 4.5 × 0.04 = 4.1 kips acting at El. 817.7	2.1	3.6

6. *Longitudinal Forces (one lane)* $\qquad N \qquad P$

One lane = 0.05(0.64 × 250 + 18) = 8.9 kips $\qquad$ 7.7 $\qquad$ 4.5

acting 6 feet above the top slab.

7. *Temperature Forces.* Assume that both bearings are fixed in the direction of the pier axis, and that the differential expansion temperature is 60°F. If the steel box girder expands and contracts in the direction of the pier, the associated elongation or shortening

will induce a corresponding force at the top of the columns. For a distance c. to c. of column = 46 feet, the total expansion per column is $0.5 \times 46 \times 12 \times 60 \times 6.5 \times 10^{-6} = 0.108$ inch. Ignoring the reinforcing steel, the moment of inertia of the column is $I = \pi d^4/64 = 417680$ in^4, and the force resulting from this movement is $F = 3EI\Delta/l^3$, = 19.3 kips acting at the top of the column.

Footing design. Other loads to be considered are the weight of the column = 55 kips; the weight of the footing = 45 kips (assumed 10 ft x 10 ft x 3 ft); and the weight of the earth on top of the footing, calculated as 30 kips. The bottom of footing elevation is taken as 803.20, giving a pier height 26 feet. The analysis is based on the standard AASHTO specifications.

Group I = D + L (CF = E = 0)

Dead Load = 402 + 55 + 45 + 30 = 532 kips
Live Load (3 lanes) = 139 kips
Total = 671 kips/footing

Group II = D + W (CF = E = B = SF = 0)

Wind on structure:	From N = 24.9,	$M_{x\text{-}x} = 0.5 \times 24.9 \times 31.10$	= 387 ft-kips
	From P = 9.7,	$M_{y\text{-}y} = 0.5 \times 9.7 \times 31.10$	= 151 ft-kips
Wind on column:	From N = 2.1,	$M_{x\text{-}x} = 2.1 \times 14.5$	= 30 ft-kips
	From P = 3.6,	$M_{y\text{-}y} = 3.6 \times 14.5$	= 52 ft-kips

Summary, Group II (one footing F = 532 kips, $M_{x\text{-}x}$ = 417 ft-kips, $M_{y\text{-}y}$ = 203 ft-kips

Group III = D + L + LF + 30%W + WL (CF = E = B = SF = O)

Dead Load + Live Load: F = 671 kips

Longitudinal forces:	From N = 7.7,	$M_{x\text{-}x} = 2.7 \times 7.7 \times 0.5 \times 37.8$	= 393 ft-kips
(three lanes)	From P = 4.5,	$M_{y\text{-}y} = 2.7 \times 4.5 \times 0.5 \times 37.8$	= 230 ft-kips
Wind on Live Load:	From N = 12.5,	$M_{x\text{-}x} = 12.5 \times 0.5 \times 37.8$	= 236 ft-kips
	From P = 1.5,	$M_{y\text{-}y} = 1.5 \times 0.5 \times 37.8$	= 28 ft-kips

Wind on Structure: For Group III, the wind should not be reduced. Thus the loads estimated for Group II are converted by multiplying by the ratio 1.0/0.71 = 1.41 or $N = 24.9 \times 1.41 = 35.1$ kips, and $P = 9.7 \times 1.41 = 13.7$ kips.

For 30% $N = 35.1 \times 0.3 = 10.5$,	$M_{x\text{-}x} = 10.5 \times 0.5 \times 31.10$	= 164 ft-kips
For 30% $P = 13.7 \times 0.3 = 4.1$,	$M_{y\text{-}y} = 4.1 \times 0.5 \times 31.10$	= 64 ft-kips
30% Wind on column	$M_{x\text{-}x}$ = 9 ft-kips	
	$M_{y\text{-}y}$ = 16 ft-kips	

Summary, Group III: F = 671 kips, $M_{x\text{-}x}$ = 802 ft-kips, $M_{y\text{-}y}$ = 338 ft-kips

Group IV = Group I + T: F = 671 kips, $M_{y\text{-}y} = 19.3 \times 26 = 502$ ft-kips

We should note that for Groups II and III, an overturning force should be added to the load effects, applied at the windward quarter points of the transverse superstructure width. For a bridge width 55 feet, this force is $55 \times 0.02 = 1.10$ kips/ft of length, and the force allocated to the fixed pier is $75 \times 1.10 = 82.5$ kips. The overturning moment is, therefore, $M_{OT} = 82.5 \times (55/4) = 1134$ ft-kips. Since the superstructure is not rigidly connected to the two-pier columns, this moment is resolved into two equivalent forces, one downward and one upward, acting on each column. The magnitude of this force is 1134/46 = 25 kips for Group II, and $0.3 \times 25 = 7.5$ kips for Group III, and may be neglected.

Soil pressure. For this example, the allowable soil pressure is q_{all} = 15 kips/ft^2 (ASD).

Group I. Soil pressure q = 671/100 = 6.71 kips/ft^2

Group III. Compute e_x = 802/671 = 1.20 ft, and e_y = 338/671 = 0.50 ft..
Then

$$q = \frac{\Sigma V}{B^2}\left(1 \pm \frac{6e_x + 6e_y}{B}\right) = \frac{671}{100} \times \left[1 \pm \frac{6(1.20 + 0.50)}{10}\right]$$

$$= 6.71 \times (1 \pm 1.02) = 13.6 \text{ kips/ft}^2 \text{ max.}$$

$$= -0.13 \text{ kips/ft}^2 \text{ min.}$$

The small negative value indicates that a very small area is in tension (no contact); for preliminary design this is acceptable. Whether the allowable soil pressure for this group should be taken as 15 × 1.25 = 18.75 kips/ft^2 is a matter of judgment and interpretation. In the context of the design philosophy, the allowable soil pressure for Group III should not exceed the basic 15 kips/ft^2.

Expansion Pier

For this structure, bearing devices at expansion piers and abutments are similar to the bearing detail shown in Figure 2–5. The effect of friction is in this case very small and can be disregarded.

1. *Dead Load Reaction.* (obtained from superstructure analysis).
   Interior Girders (5) = 112 × 5 = 560 kips
   Exterior Girders (2) = 101 × 2 = 202 kips
   Total D.L. = 762 kips
   Weight of Girder = 56 kips
   Total DL = 818 kips or 409 kips/column
   Weight of Substructure: Column = 57 kips
   Footing = 27 kips (assume 8.5ft × 8.5ft × 2.5ft)
   Earth = 27 kips
   Total = 111 kips
   Total Dead Load (One Column) = 409 + 111 = 520 kips

2. *Live Load.* This is the same as in fixed pier or 139 kips/column. Overall pier height is 26.5 feet, giving a column height 24 feet.

3. *Temperature Forces.* Both bearings are fixed in the direction of the pier. Hence, expansion or contraction of the steel box girder will induce the same movement in the top of the column, or 0.108 in/column. For a column diameter 4 feet 6 inches, and height 24 feet, the calculated force at the top induced by this movement is F = 17.0 kips. Then, $M_{y\text{-}y}$ = 17 × 26.5 = 451 ft-kips.

   The soil pressure is now as follows (for footing 8 feet 6 inches square):

   For Group I, total load F = 520 + 139 = 659 kips
   q = 659/8.5^2 = 659/72.25 = 9.1 kips/ft^2

For Group IV we first compute $e_y = 451/659 = 0.68$

$$\text{Then } q = 9.10 \times \left(1 \pm \frac{6 \times 0.68}{8.5}\right) = 9.10 \times (1 \pm 0.48) = 13.5) \text{ kips/ft}^2 \text{ max.}$$

$$= 4.7 \text{ kips/ft}^2 \text{ min.}$$

2.10 LOAD COMBINATIONS AND LOAD FACTORS

AASHTO Load Groups (1992 Standard Specifications)

The basic load group (N) may be expressed in the following form.

$$\text{Group (N)} = \gamma_N \Sigma \beta_i Q_i \tag{2–25}$$

where γ_N = group factor; β_i = load factor or coefficient for load component i; and Q = particular load among those included in the load summary. For allowable stress design (AASHTO service load method), the factor γ_N is 1.0 for all load groups. The coefficient β may be as low as 0.3 and as high as 2.0. For service load groups, the percentage of the basic unit stress depends on the load group, and may be from 100 to 150 percent.

For load factor design, the factor γ may be from 1.20 to 1.30, whereas the coefficient β can be as high as 2.20. Note that the stress percentage is not applicable since the stresses obtained from factored loads are compared to a factored ultimate resistance (or factored nominal strength).

Load groups and load factors are given in Table 2–17, taken from current AASHTO specifications. The types of loads included in each of the load groups are the same for service load (ASD) and load factor design. However, the two design approaches use different values of load factors and coefficients to calculate the design loads, and this difference is consistent with the allowable stress. Values for allowable stress design are more appropriate for serviceability states (for example, consideration of movement and settlement), whereas values for load factor design are consistent with conditions at failure.

LRFD Load Factors and Combinations (AASHTO 1994 Specifications)

In the LRFD approach, the basic load group (N) is expressed as

$$\text{Group (N)} = n \Sigma \gamma_i Q_i \tag{2–25a}$$

where $n = n_o n_R n_i > 0.95$
γ_i = load factor (a statistically based multiplier applied to force effects)
n_o = a factor relating to ductility
n_R = a factor relating to redundancy
n_i = a factor relating to operational importance
n = a factor relating to ductility, redundancy, and operational importance
Q = force effect

In the LRFD version, the γ, β factors of Equation (2–25) are lumped into one single parameter γ_i, and emphasis is on articulating ductility, redundancy and operational importance. This grouping is arbitrary, but constitutes a first effort of codification.

Table 2–17 Load Groups and Coefficients γ and β Standard Specifications

Col. No.		1	2	3	3A	4	5	6	7	8	9	10	11	12	13	14	
Group		γ	β Factors														
			D	$(L+I)_n$	$(L+I)_p$	CF	E	B	SF	W	WL	LF	R+S+T	EQ	ICE	%	
SERVICE LOAD	I	1.0	1	1	0	1	β_E	1	1	0	0	0	0	0	0	100	
	IA	1.0	1	2	0	0	0	0	0	0	0	0	0	0	0	150	
	IB	1.0	1	0	1	1	β_E	1	1	0	0	0	0	0	0	**	
	II	1.0	1	0	0	0	1	1	1	1	0	0	0	0	0	125	
	III	1.0	1	1	0	1	β_E	1	1	0.3	1	1	0	0	0	125	
	IV	1.0	1	1	0	1	β_E	1	1	0	0	0	1	0	0	125	
	V	1.0	1	0	0	0	1	1	1	1	0	0	1	0	0	140	
	VI	1.0	1	1	0	1	β_E	1	1	0.3	1	1	1	0	0	140	
	VII	1.0	1	0	0	0	1	1	1	0	0	0	0	1	0	133	
	VIII	1.0	1	1	0	1	1	1	1	0	0	0	0	0	1	140	
	IX	1.0	1	0	0	0	1	1	1	1	0	0	0	0	1	150	
	X	1.0	1	1	0	0	β_E	0	0	0	0	0	0	0	0	100	Culvert
LOAD FACTOR DESIGN	I	1.3	β_D	1.67*	0	1.0	β_E	1	1	0	0	0	0	0	0		
	IA	1.3	β_D	2.20	0	0	0	0	0	0	0	0	0	0	0		
	IB	1.3	β_D	0	1	1.0	β_E	1	1	0	0	0	0	0	0		
	II	1.3	β_D	0	0	0	β_E	1	1	1	0	0	0	0	0		
	III	1.3	β_D	1	0	1	β_E	1	1	0.3	1	1	0	0	0		
	IV	1.3	β_D	1	0	1	β_E	1	1	0	0	0	1	0	0		
	V	1.25	β_D	0	0	0	β_E	1	1	1	0	0	1	0	0		
	VI	1.25	β_D	1	0	1	β_E	1	1	0.3	1	1	1	0	0		
	VII	1.3	β_D	0	0	0	β_E	1	1	0	0	0	0	1	0		
	VIII	1.3	β_D	1	0	1	β_E	1	1	0	0	0	0	0	1		
	IX	1.20	β_D	0	0	0	β_E	1	1	1	0	0	0	0	1		
	X	1.30	1	1.67	0	0	β_E	0	0	0	0	0	0	0	0		Culvert

Not Applicable

$(L + I)_n$ - Live load plus impact for AASHTO Highway H or HS loading

$(L + I)_p$ - Live load plus impact consistent with the overload criteria of the operation agency.

*1.25 may be used for design of outside roadway beam when combination of sidewalk live load as well as traffic live load plus impact governs the design, but the capacity of the section should not be less than required for highway traffic live load only using a beta factor of 1.67. 1.00 may be used for design of deck slab with combination of loads as described in Article 3.24.2.2.

$$**\text{Percentage} = \frac{\text{Maximum Unit Stress (Operating Rating)}}{\text{Allowable Basic Unit Stress}} \times 100$$

For Service Load Design

% (Column 14) Percentage Basic Unit Stress

No increase in allowable unit stresses shall be permitted for members or connections carrying wind loads only.

β_E = 1.00 for vertical and lateral loads on all other structures.

For culvert loading specifications, see Article 6.2.

β_E = 1.0 and 0.5 for lateral loads on rigid frames (check both loadings to see which one governs). See Article 3.20.

For Load Factor Design

β_E = 1.3 for lateral earth pressure for retaining walls and rigid frames excluding rigid culverts.

β_E = 0.5 for lateral earth pressure when checking positive moments in rigid frames. This complies with Article 3.20.

β_E = 1.0 for vertical earth pressure

β_D = 0.75 when checking member for minimum axial load and maximum moment or maximum eccentricity . . . . . .For

β_D = 1.0 when checking member for maximum axial load and minimum moment . . . . . Column Design

β_D = 1.0 for flexural and tension members

β_E = 1.0 for Rigid Culverts

β_E = 1.5 for Flexible Culverts

For Group X loading (culverts) the β_E factor shall be applied to vertical and horizontal loads.

Basic Load Factors and Load Combinations. According to the LRFD approach, bridges and their components must be designed for the applicable combinations of factored extreme loads specified as follows.

STRENGTH I. This is the basic load combination that relates to the normal use of the bridge without wind effects.

STRENGTH II. This relates to the use of the bridge by permit vehicles without wind. The permit vehicle should not be assumed to be the only vehicle on the bridge unless traffic is controlled by an escort vehicle. If a permit vehicle travels unescorted, the other lane may be assumed to be occupied by the regular live load model.

STRENGTH III. This combination relates to bridges exposed to maximum wind velocity preventing the presence of significant vehicular traffic on the structure.

STRENGTH IV. This involves a load combination where the dead-to-live load ratio is very high. Since the main objective of the calibration process is to assess the possibility that prescribed service loads may be exceeded, the first logical conclusion is that a specified live load is more apt to be exceeded than a dead load that is largely fixed by the weight of the construction.

For this case, the calibration process has been carried out for a large number of bridges with spans not exceeding 200 feet, but spot checks have been made on several bridges up to 600-foot spans. For the primary components of large bridges, the ratio of dead-to-live load force effects is very high, and could result in a set of resistance factors different from those found acceptable and consistent for small- and medium-span bridges. Thus, load combination IV is expected to control when the dead-to-live load ratio of force effect exceeds about 7.0.

STRENGTH V. This involves a load combination of normal vehicular use of the bridge with wind velocity 55 MPH. Interestingly, the wind velocity does not relate to the normally expected maximum values, but represents a velocity beyond which vehicles become unstable.

EXTREME EVENT. This load combination relates to ice loads, collision by vessels, and certain hydraulic and earthquake events whose recurrence interval exceeds the design life.

The joint probability of these incidents is very low, and can be assumed to be applied separately. Under these extreme conditions, the bridge is expected to be subjected to considerable inelastic deformation so that locked-in force effects due to TU, TG, CR, SH, and SE will be relieved. The 0.5 live load factor reflects the low probability of the presence of maximum vehicular live load at the time when an extreme event is about to occur.

SERVICE I. This load combination involves the normal operational use of a bridge with 55 MPH wind. All loads are assigned nominal values, and extreme conditions are excluded.

SERVICE II. The intent of this combination is to prevent yielding of steel structures caused by vehicular live load, about halfway between Service I and Strength I limit state, and where the wind effects are insignificant. This load group corresponds to the overload provisions of the standard AASHTO specifications.

SERVICE III. This load group relates only to prestressed concrete structures with the main intent to provide crack control. The live load specified for this combination reflects current exclusion weight limits mandated by various jurisdictions. Vehicles permitted under these limits have been in service for many years. The statistical significance of the 0.80 factor on live load is that the event is expected to occur about once a year for bridges with two design lanes, and less often for bridges with more than two lanes.

FATIGUE. Fatigue and fracture load combination relates to gravitational vehicular live load and dynamic response, and hence BR and PL loads need not be considered.

Commentary. The load factors for the foregoing loads and load combinations should be as shown in Table 2–18. The larger of the two values shown for TU, CR, and SH should be used when computing deformations, and the smaller value should be used when computing other force effects. For a complete analysis, all relevant subsets of the load combinations should be investigated, and this should include both positive and negative extremes.

For permanent force effects, the load factor producing the more critical combination should be selected from Table 2–19. When the permanent load increases the stability or load-carrying capacity of a bridge component, the minimum value of the load factor should also be considered.

The intent of these provisions is to recognize that permanent loads may have an actual magnitude less than the specified nominal value, and this becomes important where the permanent loads reduce the effects of transient ones. Whereas creep and shrinkage are fairly stable, friction, settlement, and earth pressures are known to act with minimum and maximum values, and hence both effects should be investigated. Although limited data are available, it is known that the negative variability of permanent loads is less than the positive.

Table 2–18 Load Combinations and Load Factors LRFD Specifications

Load Combination Limit State	DC DD DW EH EV ES	LL IM CE BR PL LS	WA	WS	WL	FR	TU CR SH	TG	SE	Use One of These at a Time EQ	IC	CT	CV
STRENGTH-I	γ_p	1.75	1.00	—	—	1.00	0.50/1.20	γ_{TG}	γ_{SE}	—	—	—	—
STRENGTH-II	γ_p	1.35	1.00	—	—	1.00	0.50/1.20	γ_{TG}	γ_{SE}	—	—	—	—
STRENGTH-III	γ_p	—	1.00	1.40	—	1.00	0.50/1.20	γ_{TG}	γ_{SE}	—	—	—	—
STRENGTH-IV EH, EV, ES, DW DC ONLY	γ_p 1.5	—	1.00	—	—	1.00	0.50/1.20	—	—	—	—	—	—
STRENGTH-V	γ_p	1.35	1.00	0.40	0.40	1.00	0.50/1.20	γ_{TG}	γ_{SE}	—	—	—	—
EXTREME EVENT-I	γ_p	γ_{EQ}	1.00	—	—	1.00	—	—	—	1.00	—	—	—
EXTREME EVENT-II	γ_p	0.50	1.00	—	—	1.00	—	—	—	—	1.00	1.00	1.00
SERVICE-I	1.00	1.00	1.00	0.30	0.30	1.00	1.00/1.20	γ_{TG}	γ_{SE}	—	—	—	—
SERVICE-II	1.00	1.30	1.00	—	—	1.00	1.00/1.20	—	—	—	—	—	—
SERVICE-III	1.00	0.80	1.00	—	—	1.00	1.00/1.20	γ_{TG}	γ_{SE}	—	—	—	—
FATIGUE-LL, IM & CE ONLY	—	0.75	—	—	—	—	—	—	—	—	—	—	—

Table 2–19 Load Factors for Permanent Loads, γ_p LRFD Specifications

Type of Load	Load Factor	
	Maximum	*Minimum*
DC: Component and Attachments	1.25	0.90
DD: Downdrag	1.80	0.45
DW: Wearing Surfaces and Utilities	1.50	0.65
EH: Horizontal Earth Pressure		
• Active	1.50	0.90
• At-Rest	1.35	0.90
EV: Vertical Earth Pressure		
• Overall Stability	1.35	N/A
• Retaining Structure	1.35	1.00
• Rigid Buried Structure	1.30	0.90
• Rigid Frames	1.35	0.90
• Flexible Buried Structures other than Metal Box Culverts	1.95	0.90
• Flexible Metal Box Culverts	1.50	0.90
ES: Earth Surcharge	1.50	0.75

Load Factor versus Limit Analysis

Bridges, compared to other structures, are exposed to the most adverse environments of loading and climatic conditions. Although the traffic load application in the analysis is largely hypothetical, it is commonly taken as representative of the real loads on the structure. The live load on bridges is distinctly active as opposed to live loads in buildings usually made up of dead weights of desks and furniture. When this difference is considered, some yielding of bridge components because of overloading may not be as acceptable as it is in buildings in terms of performance and serviceability of moving traffic.

The load factor methodology is based on elastic analysis (no plastic redistribution) of the bridge, that is, the structure is analyzed to respond elastically to all applied loads. This philosophy is consistent with the intent to prevent undesirable effects of yielded bridge components. However, the capacity of bridge members for the elastically determined load and force effects is computed by ultimate behavior or strength criteria. Stated otherwise, structural components are proportioned by their strength to carry the elastically determined force effects. Thus it may be inconsistent to anticipate the structure to behave elastically while its components are proportioned by their ultimate capacity. The expected difference in the load factor approach and the ASD is that the service load unit stresses will not be as uniform in each component designed by load factor methods, but the strength of each member so designed will be more uniform in resisting the service load stresses (Porter, 1976).

The inconsistency has been suggested that, with stresses calculated assuming elastic distribution, in reality the stresses would have to be plastically redistributed in some structures to mobilize the strength of the member so proportioned. The counterargument in this case is that a structure designed by load factor methods is not intended to yield within its useful life expectancy. Furthermore, if plastic redistribution is as-

sumed, the structure must be capable of accomplishing it. With respect to substructure elements, special treatment of the concrete compression zone would be required to avoid crushing of the concrete (probably by limiting the critical strain). Since no load is ever intended to be applied that could remotely cause these conditions, these provisions may seem just as inconsistent with actual structural behavior as the load factor method seems with its strength provisions.

Convergence of the margin of safety. Allowable stress and load factor design may be compared by referring to the factor of safety. Safety is reflected in the two basic components of the analysis: (1) the variability of the predicted loads and the structural response to them, and (b) the strength behavior and importance of the component under consideration to the overall structural integrity.

Referring to Equation (2–25), the factor γ_N expresses the uncertainty associated with the particular group or load combination, and the coefficient β_i represents the variability of the load component Q_i within group N. The summary of the factored effects must be compared with the strength or structural capacity (see also subsequent sections) of the component expressed in terms of a capacity reduction factor ϕ_i.

With these definitions the factor of safety provided in load factor analysis may be understood. The uncertainty of predicting and applying the loads and the inability to precisely predict structural behavior are provided for by the load factors. The uncertainties of material strength, fabrication, manufacture, or in situ resistance, and strength predicted by analysis assumptions versus the real behavior of the ideal member, along with the normal experimental scatter of variation, the importance of the number to the overall capacity of the structure, and the type of failure (yield or sudden) should be reflected by the capacity reduction factor.

The overall load factor (for example, the factor γ_N) should reflect a function of the probability that the load combination at the stipulated load intensity and points of application will occur simultaneously and provide a factor of safety for the successful resistance by the structure. The load factor β_i applied to each load component should reflect a function of the probability of variation in the actual applied load in relation to the theoretical or assumed design load used to simulate it. In all load factors, the effects of simplified analysis and idealized techniques should also be included along with the normal variation expected between precise analysis and verification tests.

Likewise, the capacity reduction or performance is a factor of safety applied to structural materials and ultimate structural behavior. The statistical assessment of the performance factor deals specifically with quality control and sensitivity to variations from assumed ideal conditions at ultimate capacity. In arriving at a specific criterion it is necessary to ascertain the following: (1) using the capacity reduction factors, all component materials will be within the acceptable tolerances spelled out by the specifications; (2) the low or adverse side of the tolerance of each constituent allowed may occasionally occur simultaneously and lead to a weak spot in the structure; and (3) the performance reduction factor compensates for this condition.

The load factor analysis, however, goes beyond the strength considerations. Once a component is proportioned by strength criteria, it must be checked for serviceability conditions and levels of function associated with (1) deflections or deformations under live load; (2) elastic behavior under maximum expected overload; and (3) crack control in reinforced concrete.

Structural material behavior. The inconsistency between elastic analysis and inelastic behavior is addressed by the LRFD specifications. Thus, structural materials are considered to behave linearly up to the elastic limit and inelastically thereafter. Tests on concrete, however, indicate that in the elastic range of structural behavior cracking of concrete seems to have little effect on overall response and performance. This effect can, therefore, be neglected by modeling the concrete as uncracked for the purpose of analysis (King, Csagoly, and Fisher, 1975).

In the LRFD approach, extreme event limit states may be accommodated in both the inelastic and elastic ranges. Inelastic analysis may be applied to components that are innately ductile, or which can be made to behave in a ductile manner by confinement or other means.

If inelastic analysis is chosen, the associated behavior should be confirmed by physical tests or by a presentation of load-deformation behavior validated by tests. In the inelastic range only factored loads can be used, and without superposition of force effects. The sequence of load application should be consistent with the order on the actual bridge.

2.11 CASE STUDY, ICE LOAD ON BRIDGES

There has been concern among states that the ice forces obtained from Equation (2–23) in conjunction with an effective ice strength between 100 and 400 lb/in^2 often result in design requirements that are unduly severe. Similar concerns exist about the ice thickness and point of application, and about static ice pressure.

The values of the effective ice crushing strength introduced by the LRFD specifications are subject to the following comments. As a guide, the 8.0 ksf strength is appropriate for piers where long experience shows that ice forces are minimal, but some allowance is warranted to account for ice effects. The 32.0 ksf upper limit is considered reasonable based on the observed history of bridges that have survived ice conditions. The effective ice strength depends basically on the temperature and grain size of the ice. Laboratory measured compressive strengths at 32°F vary from 60 ksf for grain sizes of 0.04 in to 27 ksf for grain sizes of 0.2 in, and at 23°F these strengths are doubled. Unlike the compressive strength, the tensile strength is not sensitive to temperature. Because much of the ice failure is by splitting or by tensile failure, only crude approximations of ice strengths can be made.

An extensive ice load study by the Maine DOT supplemented by regional experience has produced a modified version of design guidelines for ice load effects (Chandler, 1981). In principle, the new proposal is simpler, having only one design pressure and two basic ice thickness categories. In addition, the point of application of the dynamic load has been changed from ordinary high water to the 50-year flood stage which seems to accommodate the local conditions. The coefficients for nose angle and pier width/ice thickness ratios given in the standard AASHTO specifications are retained and applied to the design ice pressure. According to the same philosophy, it is not necessary to design specifically for ice jams and ice uplift. The portions of river piers in water should be battered to minimize uplift effects. However, judgment reflecting a conservative design is suggested for bridge sites where ice jams are known to reoccur.

The relevant design criteria are summarized as follows.

Ice crushing strengths. A pressure of 100 lb/in^2 is selected for use with the 50-year flood stage (spring tide on coastal waters). This value represents appropriate conditions for spring ice. From research it appears that spring ice pressures are approximately one-half the value of winter ice. The underlying premise is that adequate safety factors exist to deal with unusually severe events of hard winter ice combined with high stages, hence it is not considered necessary to include the worst combination of all the criteria.

Rivers in Maine are relatively unpredictable with respect to time of ice break-up, so that it is impractical to design for several conditions such as a high pressure at a low elevation or a low pressure at a high elevation. The 100 psi criterion appears to be consistent with AASHTO and LRFD characterization of ice conditions for spring time. A further comment is that the somewhat more conservative values consciously adopted in the Canadian Code may be explained by the tendency to design relatively slender piers in that country.

Ice thickness. Ice thickness measurements at bridge sites in the Province of New Brunswick over a five-year period were analyzed and found to vary from 21 to 33 in, with an average of 27 inches. These sites are either in the colder zone or very close to it. Based on local experience and judgment, extrapolation of these data to the Maine conditions may suggest that values 6 inches less than found in New Brunswick would be appropriate, rounding up to 24 inches for the northern zone and rounding down to 18 in for the southern region. For rivers known to have severe ice conditions, the ice thickness is increased by 6 inches in both zones.

Point of application. The point of application of ice loads has been subject to considerable scrutiny and deliberation. Thus, ordinary high water may be considered too low and therefore unconservative, whereas the 50-year flood may appear to be too high and overconservative. A design compromise was reached by combining the 50-year flood stage level with the less conservative 100 psi ice pressure.

Transverse force. The general opinion is that it is difficult if not impossible to predict the skew of the stream relative to the pier direction. This skew often changes with different water elevations along the same stream. Considering also the fact that no universal procedure is known to determine the transverse force even when the skew is known, taking a percentage of the longitudinal force is appropriate for estimating the transverse load. This approach is consistent with AASHTO criteria. The percentage used in Maine is 30 percent, and independent of the skew.

Static force. The static force (magnitude and application) is based on studies and charts showing ice thrusts for expanding ice sheets at various latitudes and initial air temperatures. These data show that thrusts may vary from 4 kips to 15 kips per linear ft of pier, and are considered conservative because they are based on tests of samples of ice taken from lakes. A static value of 5 kips/lin ft is found adequate and consistent with criteria contained in the Finnish Design Code (FHWA Structural Engineering Series No. 1, Ice Loads on Piers).

The static force should generally be applied when ice can be expected to occur between two substructure units while having open water in an adjacent span. It is unlikely that an abutment toe slope, even with rough riprap, will provide enough resistance to an expanding ice sheet to cause a pier to fail. Static loads should be applied

separately and should not be combined with dynamic ice loads. The point of application of static loads may be taken as the ordinary high water.

REFERENCES

AASHTO, 1991: *Guide Specifications and Commentary for Vessel Collision Design of Highway Bridges,* American Association of State Highway and Transportation Officials, Washington, D.C.

AASHTO, 1994: AASHTO LRFD Bridge Design Specifications.

ARISTIZABAL, J. D., 1981: "Seismic Design Guidelines for Highway Bridges", ATC-6, *Applied Technology Council,* Berkeley, CA.

ASCE, 1981: "Recommended Design Loads for Bridges," *Committee on Loads and Forces on Bridges, Committee on Bridges of the Struct. Div., J. Struct. Div. ASCE,* Vol. 107, No. ST7, July, pp. 1161–1213.

BISHOP, A. W., 1958: "Test Requirements for Measuring the Coefficient of Earth Pressure at Rest," *Proc. Brussels Conf. Earth Pressure Probl.,* vol. 1, pp. 2–14.

Canadian Standards Association, 1988: *Specifications for Ice Loads,* Ottowa, Ontario, Canada.

CAQUOT, A., and J. KERISEL, 1948: 'Tables for the Calculation of Passive Pressure, Active Pressure and Bearing Capacity of Foundations," Gauthier-Villars, Imprimeur-Libraire, Libraire du Bureau des Longitudes, the L'Ecole Polytechnique, Paris, p. 120.

CLAUSEN, C. J. F., and S. JOHANSEN, 1972: "Earth Pressures Measured against a Section of a Basement Wall," *Proc. 5th Eur. Conf. SMFE,* Madrid, pp. 515–516.

CLOUGH, G. W., and J. M. DUNCAN, 1991: "Foundation Engineering Handbook," 2nd ed., edited by H. Y. Fang, Van Nostrand Reinhold, N.Y., pp. 223–235.

DUNCAN, J. M., G. W. CLOUGH, and R. M. EBERLING, 1990: "Behavior and Design of Gravity Earth Retaining Structures," *Proc. Conf. Design and Performance of Earth Retaining Structures,* ASCE, Cornell University, Ithaca, N.Y., June, pp. 251–277.

JACKY, J., 1944: "The Coefficient of Earth Pressures at Rest," *Journ. for Society of Hungarian Architects and Engineers,* Budapest, Hungary, Oct., pp. 355–358.

JANBU, N., 1957: "Earth Pressures and Bearing Capacity Calculations by Generalized Procedure of Slices," *Proc. 4th Int. Conf. Soil Mech. Found. Eng.,* (ISSMFE), vol. 2, pp. 207–212.

JANBU, N., 1972: "Earth Pressure Computations in Theory and Practice," *Proc. 5th Eur. Conf. Soil Mech. Found. Eng.,* Madrid, vol. 1.

KING, CSAGOLY, and FISHER, 1975: "Field Testing of the Aquasabon River Bridge," Ontario.

MAYNE, P. W. and F. H. KULHAWY, 1982: "K_0-OCR Relationships in Soils," *Journ. of the Geotechnical Engineering,* ASCE, vol. 108, No. GT6, June, pp. 851–872.

MCDERMOTT, R. J., 1978: "Longitudinal Forces on Bridge Bearings," FHWA Report No. FHWA-NY-78-SR58, National Tech. Inf. Service Springfield, VA.

MONTGOMERY, C. J. and A. W. LIPSETT, 1980: "Dynamic Tests and Analysis of a Massive Pier Subjected to Ice Forces," *Canadian Journ. of Civ. Eng.,* vol 7, No. 3, Ottawa, Ontario, Canada, pp. 432–441.

NEILL, C. R., 1981: "Ice Effects on Bridges," *Roads and Transportation Assoc. of Canada,* Ottawa, Ontario, Canada.

NEILL, C. R., 1976: "Dynamic Ice Forces on Piers and Piles. An Assessment of Design Guidelines in the Light of Recent Research," *Canadian Journ. of Civ. Eng.,* vol. 3, No. 2, pp. 305–341.

PORTER, J. C., 1976: *Load Factor Analysis for Design of Bridges,* ASCE Journ. of Struct. Div., vol. 102, No. ST5, May, pp. 891–897.

RITTER, M. A., 1990: "Loads and Forces on Bridges," Preprint 80-173, 1980, *ASCE National Convention,* April 14–18, Portland, Oregon, ASCE, N.Y., 1980.

SOKOLOVSKI, J., 1944: *Statics of Granular Media,* Pergamon, London.

SOKOLOVSKI, V. V., 1965: *Statics of Granular Media,* Pergamon, New York.

SPANGLER, M. G., 1951: *Soil Engineering,* art. 21.18, International Textbook, Scranton, PA.

TERZAGHI, K., 1934: "Retaining Wall Design for Fifteen-Mile Falls Dam," Eng. News-Rec., May, pp. 632–636.

TERZAGHI, K., 1934: Large Retaining Wall Tests," Eng. News-Rec.

TERZAGHI, K., 1954: "Anchored Bulkheads," Trans. ASCE, vol. 119.

TURABI, D. A., and A. BALLA, 1968: *Distribution of Earth Pressure on Sheet-Pile Walls,* ASCE Soil Mech. Found. Div., vol. SM 6, November.

XANTHAKOS, P. P., 1979: *Slurry Walls,* McGraw-Hill, New York.

XANTHAKOS, P. P., 1994a: *Theory and Design of Bridges,* Wiley, New York.

CHAPTER 3

Methods of Analysis and Design

3.1 GENERAL PRINCIPLES

Design Procedures

Both AASHTO Specifications and the ACI Building Code allow two alternate design procedures (see also section 2.10). In the service load design method (allowable stress design, ASD), working or unfactored loads provide the basis of concrete strength assessment. In flexure, the maximum elastically computed stress cannot exceed an allowable or working stress (usually taken 0.4–0.5 times the concrete and steel strengths).

The working stress method implies that the ultimate limit states are automatically satisfied if allowable stresses are not exceeded, but depending on the variability of loads and material strengths this is not necessarily true. Thus it is often necessary to consider the deflection limit state and the crack-width limit state. Inconsistencies associated with ASD have been pointed out by several investigators (MacGregor, 1976; Ellingwood, Galambos, MacGregor, and Cornell, 1980). The most serious drawbacks relate to the inability to account properly for the variability of resistances and loads, approximation of the actual level of safety, and inability to consider groups of loads where one increases at a different rate than the others. The last comment is particularly relevant when a relatively constant load (such as dead load) is used to counteract a highly variable load (such as wind or braking forces). In this case an increase in wind or braking force may cause a stress increase by a factor of 2, 3, or even higher.

Alternatively, strength design, discussed briefly in section 2.10, encompasses essentially limit states with emphasis on ultimate resistance while the serviceability limit states are checked after the original design is completed. According to this philosophy,

the required structural capacity of a member is the strength that must be developed to resist the factored loads and forces applied to the structure in combinations stipulated in relevant criteria. Thus, by definition, the required strength refers to the load effects computed from factored loads, or

$$\text{Required strength} = \gamma_N \Sigma \beta_i Q_i \tag{3–1}$$

where all the symbols correspond to the notation of Equation (2–25). Likewise, the design strength refers to the factored resistance, or

$$\text{Design strength} = \phi R_n \tag{3–2}$$

where R_n = nominal strength or resistance, and ϕ = performance or resistance factor. These topics are discussed in detail in subsequent sections.

Design Requirements

Expansion and contraction. AASHTO requires that provisions should be made for temperature changes for simple spans exceeding 40 feet. In continuous bridges, the design should consider thermal stresses unless thermal movement can be accommodated with rockers, sliding plates, elastomeric pads, or other means.

The coefficient of thermal expansion may be determined in laboratory tests on the specific mix to be used. In the absence of more accurate data, the coefficient of thermal expansion and contraction for normal weight concrete may be taken as 0.000006 per degree F.

Shrinkage and creep. Shrinkage and creep are superimposed deformations that can result in force effects (see also section 2.4). The shrinkage coefficient for normal weight concrete is usually assumed to be 0.0002 after 28 days of curing and 0.0005 after one year of drying. Both creep and shrinkage are variable properties depending on several factors, some of which may not be known at the time of design.

Modulus of elasticity. In the absence of more precise data, the modulus of elasticity E_c for concrete with unit weights between 90 and 155 lb/ft^3 may be taken as

$$E_c = w_c^{1.5} 33 \sqrt{f_c'} \tag{3–3}$$

where f_c' is in lb/in^2. For normal weight concrete E_c = 57000 $\sqrt{f_c'}$. Poisson's ratio may be assumed as 0.2.

The modulus of elasticity E_s for nonprestressed steel reinforcement may be taken as 29,000,000 lb/in^2.

Classes of concrete. Class A is generally used for all elements of structures including columns, except when another class is found more appropriate and specifically for concrete exposed to saltwater. Class B concrete is used in footings, pedestals, massive pier shafts and gravity walls. Class C concrete should be used in locations where the concrete will be exposed to severe or moderate weather (alternate freezing and thawing). Seal concrete should generally be used for concrete deposited in water, and Class P is used for prestressed concrete members when strengths in excess of 4000 lb/in^2 are required.

The proportioning of concrete mixes should be made to secure a workable, durable,

watertight, and wear-resistant finished product of the specified strength. Both AASHTO and the LRFD specifications give the content and ratio of constituent materials for the concrete classes, and these criteria are essentially the same with some variations.

3.2 SERVICE LOAD DESIGN METHOD (ALLOWABLE STRESS DESIGN, ASD)

Basic Allowable Stresses

For service load design, the allowable stresses in the concrete should not exceed the following:

Flexure. Extreme fiber stress in compression,

$$f_c = 0.40f'_c$$

Extreme fiber stress in tension, plain concrete,

$$f_t = 0.21f_r$$

Modulus of rupture, nominal weight concrete,

$$f_r = 7.5\sqrt{f'_c}$$

Shear. For beams, one-way slabs, and footings subjected to shear and flexure only, the allowable shear stress carried by the concrete may be taken as $0.95\sqrt{f'_c}$. A more detailed calculation of the allowable shear stress can be made from the following:

$$v_c = 0.9\sqrt{f'_c} + 1.100p_w\left(\frac{Vd}{M}\right) \le 1.6\sqrt{f'_c} \tag{3–4}$$

where M = design moment occurring simultaneously with shear V at the section considered, but with $Vd/M \le 1$, and p_w = reinforcement ratio.

For members subjected to axial compression, the allowable shear stress v_c carried by the concrete may likewise be taken as $0.95\sqrt{f'_c}$, or a more detailed calculation can be made using

$$v_c = 0.9\left(1 + 0.0006\frac{N}{A_g}\right)\sqrt{f'_c} \tag{3–5}$$

where N = design axial load acting simultaneously with shear V, A_g = gross area of section, and N/A_g is expressed in lb/in^2.

For members subjected to axial tension, shear reinforcement should be provided to carry the entire shear, unless a more detailed calculation is made using

$$v_c = 0.9\left(1 + 0.004\frac{N}{A_g}\right)\sqrt{f'_c} \tag{3–6}$$

where all symbols are as previously, and N is taken as negative for tension.

Bearing Stresses. In general the bearing stress f_b on the loaded area should not exceed 0.30 f'_c. However, when the supporting surface is wider on all sides than the loaded area, the allowable bearing stress on the loaded area may be increased by $\sqrt{A_2/A_1}$ but not by more than 2, where A_1 = loaded area, and A_2 = maximum area of the portion of the supporting surface geometrically similar to and concentric with the loaded area. When the loaded area is subjected to high edge stresses due to deflection or eccentric loading, the allowable bearing stress should be multiplied by 0.75.

Reinforcement. In general the tensile stress f_s in the reinforcement should not exceed the following:

Grade 40 reinforcement	$f_s = 20{,}000$ lb/in^2
Grade 60 reinforcement	$f_s = 24{,}000$ lb/in^2

Compressive, Tensile, and Shear Concrete Strength

The compressive strength of concrete f'_c represents the 28-day strength determined from a 6-inch round cylinder 12 inches long. For a maximum usable compressive strain 0.003, the specified concrete strength can vary from 3000 to 11,000 lb/in^2. Conventional reinforced concrete bridges and substructures usually specify 3000 to 4000 lb/in^2 for the concrete classes mentioned in the foregoing section, prestressed concrete members 5000 to 6000 lb/in^2, and special structures 6000 to 11,000 lb/in^2.

The tensile strength is essential since it affects the extent and frequency of cracking. This strength is relatively low, usually 10 to 15 percent of the compression strength and occasionally 20 percent, it is more difficult to measure, and the results vary more specimen to specimen than those from compression cylinders. The modulus of rupture as measured from standard 6-inch square beams appears to exceed the real tensile strength. The quoted value 7.5 $\sqrt{f'_c}$ is commonly used as the modulus of rupture.

The shear strength of concrete is considerable, usually 35 percent or higher of the compressive strength. The shear stress v can be computed from

$$v = V/b_w d \tag{3–7}$$

where V is the design shear force at the section considered, b_w is the width of the section, and d is the distance from the extreme fiber (compression) to the centroid of tension reinforcement. The real shear value is significant only in rare cases, since shear is ordinarily limited to much lower values in order to protect the concrete against diagonal tension stresses.

Flexure and Compression

For stress analysis at service loads, the straight line model of stress and strain in flexure is generally used with the following assumptions: (1) the strain in the steel and concrete is directly proportional to the distance from the neutral axis (except for certain deep flexural members); (2) in reinforced concrete members, the concrete resists no tension; (3) the modular ratio $n = E_s/E_c$ may be taken as the nearest whole number but not less than 6; and (4) in doubly reinforced flexural members, an effective modular ratio $2E_s/E_c$ must be used to transform the compression reinforcement for stress computations.

The combined flexural and axial load capacity of compression members should be taken as 35 percent of that computed according to applicable provisions, and slenderness effects must be included (see also the following sections).

Special Provisions for Footings

The shear capacity of footings in the vicinity of concentrated loads or reactions is governed by the more severe of two conditions: (1) Beam action, with a critical section extending in a plane across the entire width and located at distance d from the face of the concentrated load or reaction area. For this condition, the footing design for shear should be as outlined in the foregoing sections, except for footings on piles the shear on the critical section should be determined according to AASHTO Section 4. (2) Two-way action, with a critical section perpendicular to the plane of the member and located so that the perimeter b_o is a minimum, but not closer than $d/2$ to the perimeter of the concentrated load or reaction area. For this condition, the footing should be designed as follows:

The design shear stress should be computed from

$$v = V/b_o d \tag{3–8}$$

where V and b_o are taken at the critical section defined above. Furthermore, the design shear stress should not exceed v_c, unless shear reinforcement is provided, given by

$$v_c = \left(0.8 + \frac{2}{\beta_c}\right)\sqrt{f_c'} \le 1.8\sqrt{f_c'} \tag{3–9}$$

where β_c is the ratio of long side to short side of concentrated load or reaction area.

Shear reinforcement consisting of bars may be used in footings in conjunction with the following provisions: (1) shear stresses computed by Equation (3–8) should be investigated at the critical section defined above and at successive sections more distant from the support; (2) the shear stress v_c should not exceed $0.9\sqrt{f_c'}$ and v should not exceed $3\sqrt{f_c'}$; and (3) where v exceeds $0.9\sqrt{f_c'}$, shear reinforcement should be provided.

3.3 RELIABILITY AND UNCERTAINTY IN DESIGN

Sources of Uncertainties

In the design of substructures and foundations, uncertainties may unfold from four main sources: (1) uncertainties in estimating loads and their distribution; (2) uncertainties associated with the variability of soil conditions at each substructure location; (3) uncertainties in assessing in situ engineering properties of soils and rocks; and (4) uncertainties with regard to the degree to which the analytical model can predict the actual behavior of the soil-structure system. To a lesser degree uncertainties may relate to material properties and structural strength attained by the system components.

The uncertainties associated with the variability of soil conditions and assessment of soil and rock characteristics are probably the most critical and relevant to the design process. The main reason is simply the complexity of geological process associated with

the formation and deposition of soil and rock strata. This process results in inherent variability in the final structure of these materials.

The foregoing uncertainties are usually considered in the design in some quantitative form. Conversely, considerations related to design errors and omissions are seldom expressed in quantitative terms. They usually are lumped up in a safety factor, or accommodated by checking and independent review.

Probabilistic Analysis of Safety Factors

A design is considered safe if it ensures adequate structural capacity or resistance to carry and transfer the loads expected to act on it. The reserve capacity, in excess of the required capacity, is the safety margin and defines the factor of safety.

Let R denote resistance and S load effects in terms of a quantity, for example bending moments. For a given distribution of load effects, the probability of failure can be reduced if resistance is increased. Thus, the term $Y = R - S$ represents the safety margin. By definition, failure will occur if Y is negative. The probability of failure P_f expresses the chance that a particular combination of R and S will yield a negative Y.

The function Y has a mean value $\bar{Y}$ and a standard deviation σ_y. The parameter $\bar{Y}/\sigma_y$ is called the safety index. If Y follows a standard statistical distribution, and if $\bar{Y}$ and σ_y are known, the probability of failure is obtained from statistical tables as a function of the type of distribution and the value of $\bar{Y}/\sigma_y$. For a given value of the safety index, we can estimate the number of failures for x number of structures during their lifetime.

Because strengths and loads vary independently, it is expedient to have one factor or series of factors to account for variability in resistance, and a second series of factors to account for variability in load effects. These are referred to as resistance (or performance) factors ϕ, and load factors γ, β, respectively. The derivation of probabilistic equations for calculating values of ϕ and γ are based on the assumption that both the strength (resistance) and the load effects can be represented by log-normal distributions. The coefficient β is compared so as to differentiate the variability of load effects between different load types in groups. For example, for live load this coefficient is larger than for dead load because of the greater variability of the former. Engineers involved in analysis using strength methods normally would not compute values of ϕ, γ, and β because appropriate design codes specify the values to be used.

For example, for Group I loading AASHTO specifies the coefficient β for dead and live load as 1 and 1.67, respectively, where the load factor γ is taken as 1.3. This leads to a simple relationship between factored strength (resistance) ϕR_n and load effects (required strength) as follows

$$\phi R_n \geq 1.3[D + 1.67(L + I)] \tag{3–10}$$

Likewise the factor ϕ depends on the type of load effects (flexure, shear, axial load, torsion, etc.), and on the specific characteristics of the loaded medium (structural component, soil, rock, etc.).

The basis for establishing the values of design parameters and factors of safety is the underlying difference between the working stress method (allowable stress design, ASD), and the strength method (also load and resistance factor design, LRFD). The ASD approach is essentially a deterministic procedure, whereas strength design methods are based on probabilistic concepts and reliability analyses, often supplemented by judgment and previous experience.

Table 3–1 Safety Factors Customarily Used in Foundation Design

Failure Type	Failure Mode	Safety Factor*
Shearing	Bearing capacity failure	2.0–3.0
	Overturning	2.0–2.5
	Overall stability	1.5–2.0
	Sliding	1.5–2.0
Seepage	Uplift	1.5–2.0
	Heave	1.5–2.0
	Piping	2.0–3.0

*Note: The lower values are used when uncretainty in design is small and consequences of failure are minor; higher values are used when uncertainty in design is large and consequences of failure are major.

(From Terzaghi and Peck, 1967)

Safety Factors in Working Stress Design (WSD)

The working stress theory treats loads and resistances (strengths) as deterministic parameters, characterized in calculations by a single (most probable) value usually called the nominal value. In working stress design, this is either the mean value, or a somewhat more conservative value. In selecting nominal values, the random nature of loads and resistances is not taken into consideration.

The selection of nominal values is a critical step in design. Dead loads are usually predicted with sufficient accuracy and certainly more accurately than live loads, often determined by codes, standards and experience. For problems involving soil-structure interaction, the selection of appropriate soil parameters requires careful consideration of soil conditions in conjunction with the intended structural use.

In routine practice, safety in WSD is ensured by the application of a single factor of safety, also referred to as the "global" safety factor. In this case, the safety factor is defined as the ratio of design resistance to the design load, and appropriate values are chosen considering the uncertainties of design in conjunction with the consequences of failure. Typical values of safety factors used in underground construction work and foundation design are given in Tables 3–1 and 3–2, taken from two different sources. Since these are not determined consciously by the use of probabilistic methods, they merely represent the results of experience and engineering judgment.

Table 3–2 Typical Safety Factors in Foundation Design

Failure Type	Item	Safety Factor*
Shearing	Earthworks	1.3 to 1.5
	Earth retaining structures, excavations	1.5 to 2.0
	Foundations	2.0 to 3.0
Seepage	Uplift, heave	1.5 to 2.0
	Exit gradient, piping	2.0 to 3.0

*The lower values are used when uncertainty in design is small and consequences of failure are minor; higher values are used when uncertainty in design is large and consequences of failure are major.

(From Meyerhof, 1984)

Reliability of LRFD Approach

Load and Resistance Factor Design (LRFD) has been developed recently based on probability and reliability theories. Both loads and resistances are treated as random variables characterized by probability density functions as shown in Figure 3–1. Safety is defined in terms of the probability of survival or the probability of failure, so that the design can be based on some acceptable probability of failure.

For given distributions of load and resistance the probability of failure can be explicitly defined as shown in the foregoing sections. For example, for the combined distribution of resistance minus the load shown in Figure 3–2 the probability of failure p_f is defined as the area under the shaded region. Partial safety factors are introduced to ensure that this probability is within acceptable limits. These partial safety factors are the load and performance (resistance) factors γ and ϕ, respectively, as shown in Figure 3–1. The load factor γ (usually larger than unity) accounts for the uncertainties of loads and the probability of group occurrence. The performance (resistance) factor ϕ is intended to

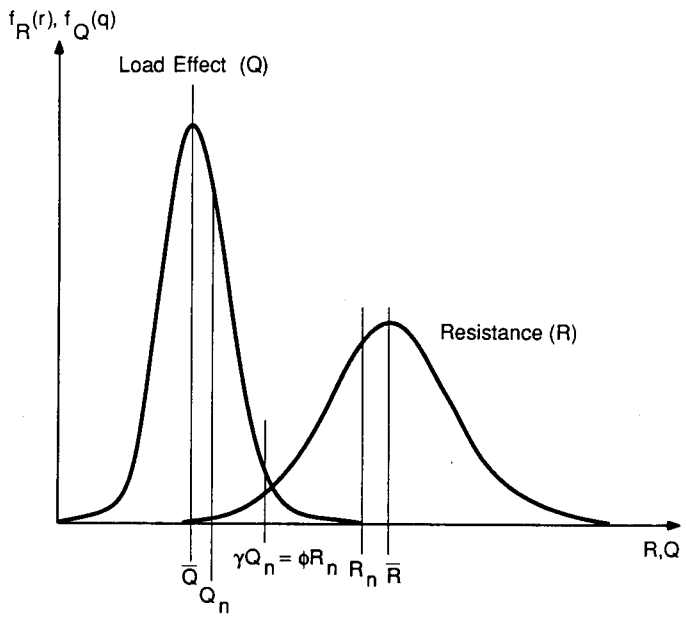

Notation:

$\bar{Q}$ = mean of load
$\bar{R}$ = mean of resistance
Q_n = nominal value of load
R_n = nominal value of resistance
$f_R(r)$ = probability density function of random variable R
$f_Q(q)$ = probability density function of random variable Q
γ = load factor
ϕ = performance factor

Figure 3–1 Load and resistance factor design.

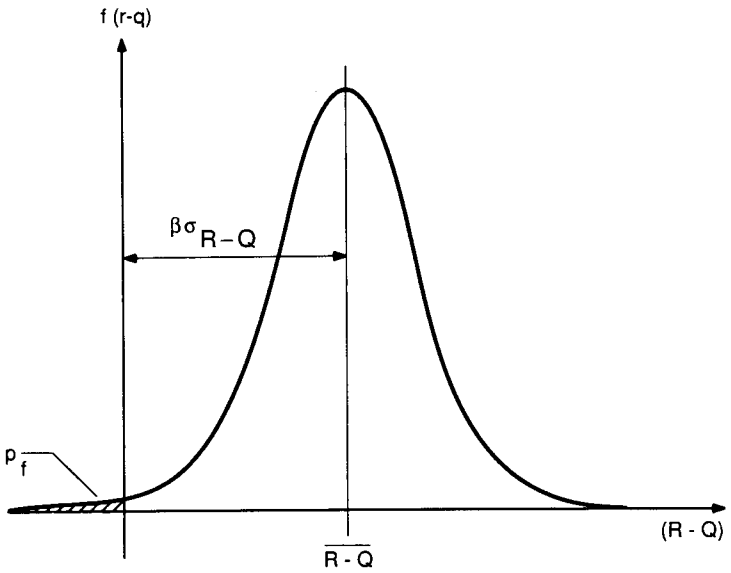

Notation:

R = resistance
Q = load effect
β = safety index
p_f = probability of failure
σ_{R-Q} = standard deviation of random variable, R - Q

Figure 3–2 Definitions of probability of failure and safety index.

account for the variability of strength (nominal or ultimate) in structural members and in soil. The resulting relationship is as follows:

$$\phi R_n \geq \Sigma \gamma_i Q_i \tag{3–11}$$

where ϕ = performance factor; R_n = nominal resistance (strength); Q_i = load effect due to load component i; and γ_i = load factor for load component i (see also section 2.10).

Values of load and performance factors are commonly given by AASHTO and LRFD specifications (for example, Tables 2–18 and 2–19), based on target values of reliability or on the best estimate of judgment, and are revised from time to time as new data become available. Because these values are interrelated, consistent sets must be used in the design, generally taken from the same or related source.

3.4 ALTERNATE APPROACH TO LIMIT STATES

General Principles

In the context of the soil/structure system, a limit state is said to have been reached when the system reaches a point where it no longer satisfies the requirements for which it was designed. From this broad definition, limit states are further classified as ulti-

mate limit states where account is taken of the worst credible values that the associated variables could take, or serviceability limit states where the most probable values are used. Although in principle all limit states should be examined explicitly, in practice only one may be more critical than the others.

Soil-structure system. This approach is applied to the combined system of soil and structure, and hence the interaction between them must be considered and the soil-structure system defined quantitatively.

Ultimate limit states. These are manifested by (1) failure in the soil without failure in the structure, involving loss of stability or causing considerable movement; (2) failure in the structure resulting in loss of structural capacity, without failure occurring in the soil; and (3) failure occurring in the structure and soil together.

Serviceability limit states. These are assumed to have been reached if the following occur: excessive deformation and ground settlement, heave, lateral displacement, and the like, transferred to the structure or adjacent structures.

Note that the ultimate limit states as defined herein correspond to the limit states of the LRFD specifications mentioned in section 1.7, but are not as explicitly defined. The serviceability limit states represent non-strength conditions and emphasize function as the main objective.

Loads and load effects. A load is considered as an external action applied to the soil/structure system; an example is dead, imposed, and wind loads acting on the structure, or gravitational forces and surcharges acting on the soil.

Load effects are necessarily internal to the soil/structure system. In this context, internal forces (axial, shear, etc.) and moments are considered load effects. For overall stability (overturning, etc.), the total disturbing moment or force is load effect.

Characteristic values. These are not intended to have direct significance. The term is merely a convenient reference item that may have a specified minimum value, a statutory value, or an average value based on testing.

Characteristic Loads. For dead, imposed, wind load, and so on, the characteristic values should be taken as defined in the specifications.

Characteristic Material Properties. These involve strength, stiffness, unit weight, and so on. For concrete and steel, they are designated by the specifications. For soils, the characteristic value of any material property is the best estimate of the in situ value. The assessment of test results relates to the reliability and number of tests in conjunction with the variability of in situ conditions. If sufficient reliable results are available, the characteristic value may be taken as the mean of the results. This is justified since failure in the soil requires the development of limiting states of stress over a significantly large area over which the assumption of average values is reasonable.

Characteristic In Situ Values. For the soil system, the first requirement is to establish the initial pore water pressure. Characteristic initial vertical stresses may be derived from unit weight and pore water pressure. It may also be necessary to establish the characteristic initial horizontal stress. Interestingly, soil pressures acting on a structure are not classified as loads, although they may be considered load effects.

Most probable values. These are defined as either: (1) for variables that are constant with time (for example, dead loads and certain material properties), the most probable values are the best estimates of in situ values; or (2) for variables that change with time (for example, live load, wind load, and soil strength), the most probable values are the best estimates of the extreme values that will occur during the life of the structure.

The most probable values of the different variables are obtained by applying partial factors to the characteristic values, and in most instances these factors are close to unity. Exceptions are structural material strengths where the characteristic values are defined in terms of specified minimum strength rather than mean values.

Worst credible values. For loads and material properties these have an accepted very small probability of being encountered. As a criterion, the probability should notionally be set at 0.1 percent. The worst credible value of any variable will be either the maximum or the minimum value depending on whether the effect is beneficial or adverse.

The worst credible load effects will be the worst credible combinations of the effects of different variables. Allowance can be made for the reduced probability of the worst credible values of the individual variables occurring together.

For variables such as dead, live, and wind load and structural material strengths, the worst credible values may be obtained by applying partial safety factors to the characteristic values. However, the methodology is not suggested for soil strengths. For variables such as pore pressure, material stiffness, and initial stresses, the partial factor approach is considered impractical. When partial factors are not to be applied, worst credible values should be evaluated directly from the available information (Note: the exclusion of soil characteristics and parameters articulates the principal difference between this approach and the more conventional strength methods).

Structural Factors and Limit State Requirements

Partial safety factors. These are intended to reflect the effect of various uncertainties inherent in design and construction.

Load Factors γ_{f1} and γ_{f2}. The load variation factor γ_{f1} takes account of the possibility of unfavorable deviations of loads from their characteristic values (this is equivalent to the load coefficient β). The load combination factor γ_{f2} accounts for the reduced probability of loads, stochastically independent, occurring at the same time (hence, it is equivalent to load factor γ).

Structural Performance Factor γ_p. This factor takes account of the following effects: (1) inaccurate assessment of loads and unforseen stress redistribution within a system; (2) deviations in construction accuracy; (3) the importance of the limit state under consideration; and (4) some systems may provide a warning of approaching a limit state, while others may reach it suddenly.

Partial Materials Factor γ_m. This factor reflects the effect of the following: (1) materials in the system may have a strength lower than indicated by samples; and (2) the structure may be weaker because of construction imperfections.

For ultimate limit states the factors γ_{f1} and γ_{f2} should be applied to the characteristic values of the loads, giving the worst credible loads or load combinations. The worst credible material strengths can be obtained in the same manner by dividing characteristic strength by γ_m.

Ultimate limit state requirements. These are satisfied if

$$\frac{\text{Worst Credible Resistance } R}{\text{Worst Credible Load Effects } S} \geq \gamma_p \tag{3–12}$$

where R and S are calculated using the worst credible values and combinations of loads and material strengths. The term γ_p is the structural performance factor.

Serviceability limit state requirements. These are satisfied if movement, distortion, and cracking of the combined structural system is acceptable (including surrounding structures). The most probable values should be assumed, except when the consequences can be serious and the associated effects sensitive to variations, in which case more conservative values may be assumed. Where structural elements are considered, the limit state for service conditions will often be assumed to be satisfied once ultimate limit state checks have been made.

For movements in the soil, two approaches are suggested, and both can be combined to provide a basis for design. Thus, it will be necessary to calculate the most probable settlement, heave, and movement from theoretical considerations; and correlate the results with data from experience under similar conditions to demonstrate that equilibrium and stability can be maintained.

The alternate approach reviewed briefly in this section has been used in certain European countries and Canadian provinces. It is presented to demonstrate the different scenarios of strength design and for comparison with load factor methodologies introduced in the United States.

3.5 AASHTO STRENGTH DESIGN METHOD, REINFORCED CONCRETE STRUCTURES

Basic Philosophy

The load factor equations simply state that the design strength (nominal strength R_n multiplied by strength reduction factor ϕ, also referred to as resistance or performance factor) must exceed the required resistance (factored load effects). The proportioning of a member is controlled, however, by various stages of behavior: elastic, cracked, and ultimate. The latter may have to be altered when the limiting stages are the elastic and cracked conditions for working loads, but these proportions should not give a resistance less than the ultimate state. A member is thus structurally sound if its proportions satisfy the various limiting stages under the worst credible loading conditions. In this context, member response is better weighted throughout the various stages of behavior, and ensures a more uniform structural safety.

At the ultimate stage, load effects are resisted by the tensile yield strength of the reinforcement and by the compressive strength of concrete. Where high-yield strength steels are used and flexural behavior is involved, excessive crack widths and deflections may develop and thus require additional controls. Serviceability must therefore be considered in strength design, and includes limitations with reference to structural fitness at overload conditions, and safety against excessive cracking, deflections, vibrations and permanent set, and fatigue of materials.

Design Strength and Performance Factors

The load magnification coefficients β and the overall load factors γ are applied to the computed load effects (working), and are taken from AASHTO Table 3.22.1A (our Table 2–17). These factors are derived taking into account the probability of a limiting stage such as accidental damage, possible load increase, construction defects, and possible stress redistribution. The load factors are modified for different loading groups, and for substructure and foundation design the controlling group is not known until the analysis is completed.

For long span bridges designed by the load factor method, AASHTO allows discretion in increasing the γ and β factors if the expected loads, service conditions, or construction materials are different from those commonly specified.

Typical values of strength reduction factors ϕ are shown in Table 3–3. These values may be increased linearly from the value for compression members to the value for flexure as the design axial load ϕP_n decreases from its designated value to zero.

Fatigue and crack control. In investigating stresses at service loads to satisfy fatigue and crack control requirements, the straight line theory of stress and strain applies.

The fatigue strength of reinforced concrete members is more relevant to superstructures, and some of the damage mechanisms are distinctly related to overload. Progressive overload-induced damage to concrete decks has been documented in the field, and often includes interaction with other effects such as corrosion. Fatigue problems in substructures are less likely to arise, and may appear mainly in members (for example, pier caps) subjected to an unusually high frequency of repeated loads.

For crack control under flexure, AASHTO provides criteria for the distribution of reinforcement if $f_y > 40{,}000$ lb/in^2. Crack control is better provided if the reinforcement bars are well distributed over the effective tension area of concrete surrounding the tension bars and having the same centroid. For a given area of concrete around a bar, flexural crack width is independent of bar diameter, but crack spacing and width decrease as the thickness of concrete cover decreases. It follows, therefore, that cracking is inhibited if the volume of concrete around each bar is minimum and the steel tensile stress is low.

Design Assumptions

The strength design for flexure and axial loads involves the application of the conditions of equilibrium of internal stresses and compatibility of strains. Thus, the following assumptions are made: (1) the strain in reinforcement and concrete is directly proportional to the distance from the neutral axis; (2) the maximum usable strain at the ex-

Table 3–3 Strength Reduction Factors*

(a) Flexure	$\phi = 0.90$
(b) Shear	$\phi = 0.85$
(c) Axial compression with	
spirals	$\phi = 0.75$
ties	$\phi = 0.70$
(d) Bearing on concrete	$\phi = 0.70$

*From AASHTO Article 8.16.1.2

treme concrete compression fiber is 0.003; (3) the stress in reinforcement below the specified yield strength, f_y, will be E_s times the steel strain, but for strains greater than those corresponding to f_y the stress in the reinforcement will be independent of strain and equal to f_y; (4) the tensile strength of concrete is neglected in flexural calculations; and (5) the concrete compressive stress/strain distribution may be assumed to be a rectangle, trapezoid, parabola, or any other shape that reflects results of comprehensive tests.

Special Provisions for Footings

These address the shear strength of footings in the vicinity of concentrated loads or reactions. The design must consider two conditions: (1) beam action with a critical section extending in a plane across the entire width and located at distance d from the face of the concentrated load or reaction area; and (2) two-way action, with a critical section perpendicular to the plane of the member. These provisions are the same as in ASD.

The design of cross sections subjected to shear must satisfy the following:

$$V_u \leq \phi V_n \tag{3–13}$$

where V_u = factored shear force at the section considered, and V_n = nominal shear strength computed from

$$V_n = V_c + V_s \tag{3–14}$$

where V_c is the nominal shear strength provided by the concrete and V_s is the nominal shear strength provided by the shear reinforcement.

3.6 LRFD PRINCIPLES OF STRENGTH DESIGN (AASHTO, 1994 SPECIFICATIONS)

Strength Limit States and Resistance Factors

The strength limit states consider the factored resistance, which is the product of nominal strength and a resistance factor. For flexure and bearing the ϕ factors are the same as in Table 3–3. A resistance factor 0.90 is stipulated for shear and torsion, and a factor 0.70 is applied to compression in anchorage zones of strut-and-tie models.

Structures as a whole and their components should be proportioned to resist sliding, overturning, uplift, and buckling. The latter is particularly critical for compression members subjected to lateral eccentricity of loads. In addition, structures should be proportioned to resist collapse due to extreme events.

Design Considerations

Effect of imposed deformations. A mandatory requirement is the investigation of effects of imposed deformations due to shrinkage, temperature change, creep, and support movement. In relatively long column piers, experience shows that the redistribution of load effects because of shrinkage and creep can be considerable.

In monolithic frames, moments in columns and pier caps resulting from prestressing the superstructure may be computed based on the initial elastic shortening.

Strut-and-tie models. These are conceptual models used to proportion reinforcement and concrete sections in regions of concentrated loads and supports, and by extension in areas of geometric discontinuities. Where conventional methods are not adequate because of nonlinear strain distribution, the strut-and-tie model can provide an acceptable solution in approximating load paths and force effects.

Strut-and-tie models should be considered in the design of deep footings and pile caps where the distance between the applied load and the supporting reaction is less than about twice the member thickness. This topic is discussed in more detail in subsequent sections.

Design for flexure and axial forces. The design assumptions are articulated for service and fatigue limit states, and for strength and extreme event limit states. For the latter condition the design assumptions are essentially the same as in section 3.5. Thus, for usual designs a rectangular stress distribution may be used as defined in AASHTO Art. 8.16.2.7.

Control of Cracking. The provisions for crack control apply to all concrete components where service loads cause tension in the gross section exceeding $0.22\sqrt{f'_c}$. Noting that crack width is inherently subject to wide scatter, satisfactory control is ensured when the steel reinforcement is well distributed over the zone of maximum concrete tension. Thus, several bars at moderate spacing are more effective in controlling cracking than one or two larger bars of the same area.

Compression members. The effects of axial loads, variable moment of inertia on member stiffness, fixed-end moments, deflections on moments and forces, and the duration of loads should be considered in the analysis. In lieu of this exact procedure, nonprestressed columns with $Kl_u/r < 100$ may be designed by approximate procedures. In this relation, K = effective length factor, l_u = unsupported length of compression member, and r = radius of gyration.

According to current codes, the area of longitudinal reinforcement for compression components should be not less than $0.01A_g$. Since the proportioning of columns is controlled primarily by bending, this limitation does not account for the influence of the concrete compressive strength. In order to include this factor, the minimum reinforcement in columns subjected to flexure should be proportional to f'_c/fy, with relevant criteria expressed quantitatively.

Shear and torsion. Regions of members, where it is reasonable to assume that plane sections remain plane, should be designed for shear and torsion by one of the following methods: the sectional model, or the strut-and-tie model.

The sectional model is appropriate for components where the assumptions of beam theory are valid. This implies that the response at a particular section depends only on the calculated force effects (moment, shear, axial load, and torsion), and does not consider how these effects were introduced. While the strut-and-tie model can be applied to flexural regions, it is more appropriate to regions near discontinuities where the actual flow of forces must be considered in more detail.

Where the plane section assumptions of beam theory are not valid, the section should be designed using the strut-and-tie model. In determining the shear resistance of footings in the vicinity of concentrated loads, the analysis may consider beam action or two-way action, as in the standard AASHTO documents.

For footings supported on piles, shear on the critical section for column or wall loads should be taken as: (1) entire section from any pile whose center is located $d_p/2$ or more outside the critical section should be considered as producing shear on that section; (2) reaction from any pile whose center is located $d_p/2$ or more inside the critical section may be neglected when computing shear on that section; and (3) for intermediate positions of pile center, the portion of the pile reaction to be considered as producing shear on the critical section should be based on linear interpolation of the criteria in (1) and (2). In this case d_p is the diameter of a round pile or depth of an H-pile at footing base.

For footings supporting columns carried on metal base plates, the face or the perimeter of the concentrated load should be taken as halfway between the face of the column and the edge of the base plate.

3.7 DESIGN FOR THERMAL EFFECTS

Thermal effects are manifested by short term (daily) as well as by lengthy (seasonal) temperature changes. Several factors influence the longitudinal deformation of a bridge, but these effects are more severe where thermally induced movement is restrained, that is, in integral bridges.

Euberg and Emanuel (1967) have produced a survey that reviews the problems associated with thermal movement of bridges. There is a tendency to consider these effects more frequently in steel than in concrete bridges, but the general attitude is towards a rational method that will account for thermal effects.

In general certain conclusions can be drawn: (1) thermal stresses can cause damage in many bridges if they are ignored in the design; (2) adequate provisions can be made as for live and dead load; (3) temperature criteria can address equally safety and structural damage; (4) if provisions are made for expansion, the effect of temperature change is friction at the expansion bearings; and (5) an alternative to providing for free movement is to design the bridge to resist thermally induced stresses.

Thermal strain occurs without stresses if the bridge is completely free to move, and thermal stress occurs without strain if the bridge is completely restrained from movement. Stress and strain are usually combined since most bridges have partial restraint against movement.

Bridge temperature. The bottom elements of a bridge ordinarily have the same air temperature, but the upper (including the exterior beams) have a temperature that depends on the amount of solar radiation, the wind, and precipitation. The result is a temperature lag or differential that may reverse its sign and vary its magnitude, introducing a variety of temperature distributions.

Results of test on concrete samples show a variation of 22 percent above and 64 percent below the higher value of the thermal coefficient. Most codes including AASHTO stipulate an average thermal coefficient 0.000006 per degree F, which is the coefficient commonly used to calculate thermal expansion and contraction of bridges.

Emerson (1979) introduces the concept of "effective" temperature of a bridge. This is the temperature that governs the longitudinal movement of the bridge deck and can be derived by considering both the product of the areas between isotherms and their mean temperature divided by the total area of cross section of the deck.

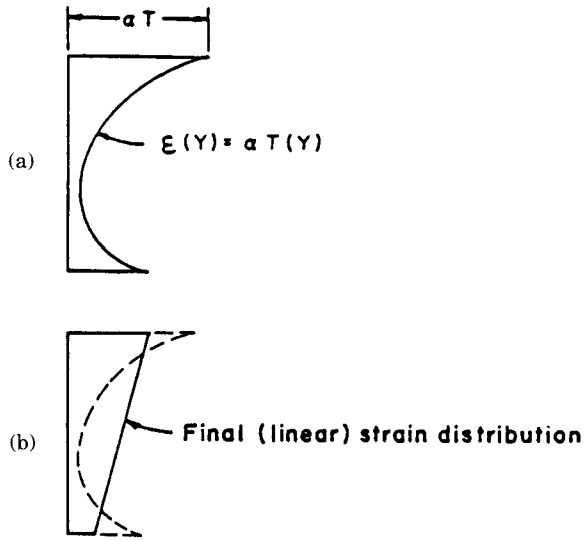

Figure 3–3 (a) Temperature-induced strain distribution assuming that the section's fibers have no influence on each other; (b) final temperature-induced strain distribution.

Longitudinal effects. If an arbitrary unrestrained cross section is subjected to a temperature field which is not plane, its fibers will tend to deform as shown in Figure 3–3(a). However, this strain distribution violates the condition of equilibrium, and since only a portion of the temperature field is responsible for the section deformation, the final strain profile is linear as shown in Figure 3–3(b).

The composite diagram of Figure 3–4 illustrates the strain difference resulting in the self-equilibrating stress. Beginning with the strains resulting from the free expansion of the section fibers and the strains in the resultant plane section, we superimpose the difference between them, and the result is the self-equilibrating stresses shown.

For the bridge member shown in Figure 3–5, the temperature varies only in the vertical direction. At the ends of the member full restraint is provided by a bending moment M and an axial force P. For a nonlinear temperature-induced strain, the longitudinal stresses are

$$\sigma_t(Y) = E\alpha T(Y) \tag{3–15}$$

where $\sigma_t(Y)$ = longitudinal stress at a fiber at a distance Y from the c.g. of the cross section; α = thermal coefficient; and $T(Y)$ = temperature at depth Y. The stress associated with the axial force P acting on the cross-sectional area A is

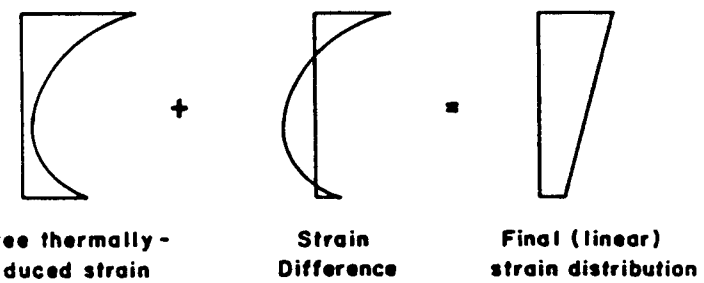

Figure 3–4 Strain difference that articulates the results and yields the self-equilibrating stress condition.

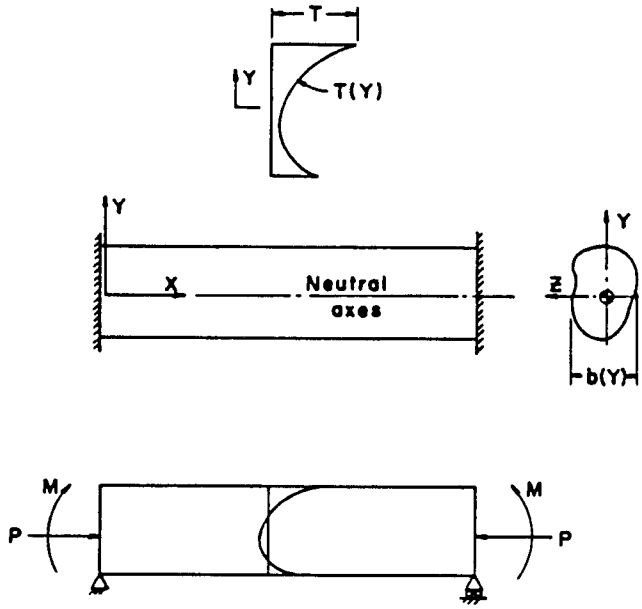

Figure 3–5 Member restained at the ends, with arbitrary cross section and vertical temperature distribution.

$$\sigma_p(Y) = P/A \tag{3–16}$$

whereas the longitudinal stress associated with the bending moment M is

$$\sigma_M(Y) = MY/I \tag{3–17}$$

For a long thin member without end restraints, the longitudinal self-equilibrating stress is derived if we apply the restraining axial force P and the restraining end moment M to the stress distribution given by Equation (3–15), or

$$\sigma(Y) = EaT(Y) - (P/A) - (MY/I) \tag{3–18}$$

This process and the resultant stress are shown graphically in Figure 3–6. It should be noted that if the temperature variation is linear, self-equilibrating stresses are not necessary.

These principles may be applied to analyze the effect of vertical temperature gradients on superstructure movements and accompanying restraints imposed on substructures.

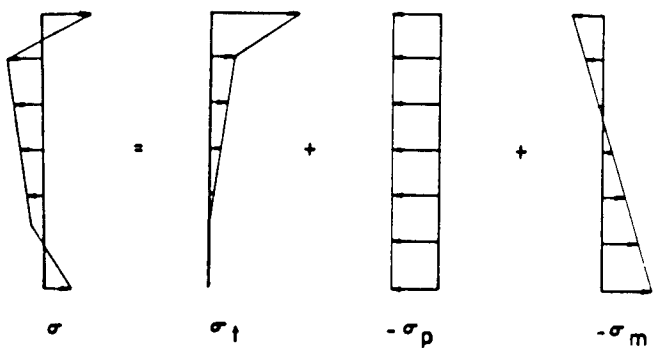

Figure 3–6 Distribution and resultant of self-equilibrating stresses.

Suggested guidelines. The TRB-NCHRP Report 276 (1985) gives design guidelines for thermal effects in bridges with concrete superstructures. These effects result from time-dependent fluctuations in the effective bridge temperature or from temperature differentials. Reference to the same report is made by AASHTO for segmental concrete bridges, but it is also recognized that additional field research is needed to verify the temperature gradient range.

LRFD specifications. This document analyzes thermal effects by considering the response of a bridge to a multilinear temperature gradient to consist of three phases: (1) axial expansion; (2) rotational deformation equivalent to self-equilibrating stresses; and (3) resultant internal thermal stresses. If the structure is externally unrestrained (i.e., simply supported or cantilevered), no force effects are developed, although deformations are produced.

The axial strain and curvature are then used in both flexibility and stiffness formulations, resulting in internal stresses as expressed by Equation (3–18).

The temperature gradient (TG) and the uniform temperature (TU) are included in various load combinations in Table 2–18. However, this does not necessarily imply that temperature forces should be investigated for all types of structures. There may be cases where experience demonstrates that neglecting the temperature gradient in the design of a particular structure or component does not lead to structural distress, or may not be the controlling load combination. Multiple-beam superstructures are an example for which judgment and past experience may provide formidable criteria.

Temperature effects should be considered in integral bridges, at expansion piers where the bearings carry considerable dead load reactions, and for relatively long and short multi-column piers where there is a temperature differential between the top cap and an embedded pier footing.

3.8 SHRINKAGE AND CREEP (LRFD SPECIFICATIONS)

Creep

Current methods for determining creep and shrinkage are taken from Collins and Mitchell (1991). These methods are based on the recommendations of ACI Committee 209 and modified by recently disseminated data. Other applicable references include Rusch, Jungwirth, and Hilsdort (1983), Bazant and Wittman (1982), and Ghali and Favre (1986).

The creep coefficient may be computed from

$$\psi(t,ti) = 3.5k_c k_f \left(1.58 - \frac{H}{120}\right) t_i^{-0.118} \left[\frac{(t-t_i)^{0.6}}{10.0+(t-t_i)^{0.6}}\right] \qquad (3\text{–}19)$$

where H = relative humidity (%); k_c = a factor for the effect of the volume-to-surface ratio of the member, taken from Figure 3–7; k_f = a factor for the effect of concrete strength; t = maturity of concrete (days); t_i = age of concrete when load is initially applied (day); $\psi(t,t_i)$ = creep coefficient. The factor k_f may be taken as

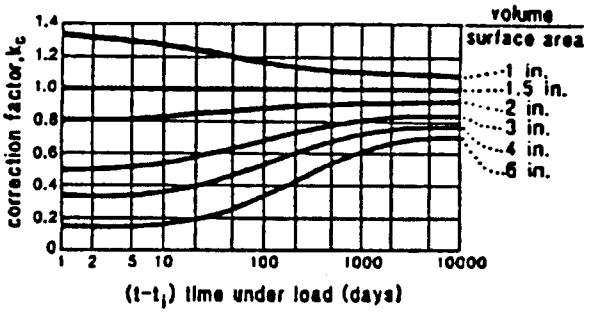

Figure 3.7 Factor *kc* for volume to surface ratio.

$$k_f = \frac{1}{0.67 + \left(f_c'/9\right)} \tag{3–20}$$

In determining the maturity of concrete at initial loading t_i, one day of accelerated curing by steam or radiant heat may be taken as equal to seven days of normal curing.

The surface area used in determining the volume-to-area ratio should include only the area that is exposed to atmospheric drying. For poorly ventilated enclosed cells, only 50% of the interior perimeter should be used in calculating the surface area.

Shrinkage

For moist cured concrete, devoid of shrinkage-prone aggregates, the shrinkage ε_{sh} at time t may be taken as

$$\varepsilon_{sh} = k_s k_h \left(\frac{t}{35.0 + t}\right) 0.51\left(10^{-3}\right) \tag{3–21}$$

where t = time over which the concrete has been exposed to drying (days); k_s = size factor taken from Figure 3–8; k_h = humidity factor taken from Table 3–4.

If the moist-cured concrete is exposed to drying before five days of curing have elapsed, the shrinkage from Equation (3–21) should be increased by 20 percent.

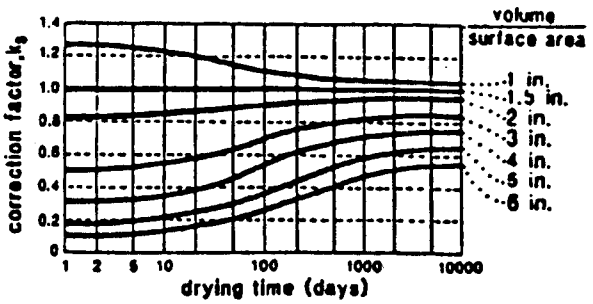

Figure 3–8 Factor *ks* for volume to surface ratio.

Table 3–4 Factor k_h for Relative Humidity*

Average Ambient Relative Humitidy	k_h
40%	1.43
50%	1.29
60%	1.14
70%	1.00
80%	0.86
90%	0.43
100%	0.00

*The annual average ambient relative humidity may be obtained from charts or from local records.

3.9 DESIGN FOR VESSEL COLLISION

Protection Options of Substructures

The development of substructure protection alternatives for vessel collision generally is based on three approaches: (1) reduction in the annual frequency of collision events by imposing, for example, navigation aids near a bridge; (2) reducing the probability of collapse by imposing, for example, vessel speed restrictions in the waterway; and (3) by reducing the disruption costs of collision using physical protection and motorist warning systems. In most instances modifications to navigation aids and standards in waterways and vessel operating conditions are beyond the design options and difficult to implement, hence the primary area of substructure protection may focus on physical protection and motorist warning systems.

Protection may be provided to minimize or even eliminate the exposure of bridge substructures to vessel collision. Physical protection systems include fenders, pile clusters, pile supported structures, dolphins, islands, and combinations thereof. Severe damage or even collapse of the protection system can be allowed to occur, provided that the system has stopped the vessel prior to striking the pier or has redirected the vessel away from the pier.

The current design practice of protective structures is almost invariably based on energy considerations. A common assumption is that the loss of kinetic energy of the vessel is transformed into an equal amount of energy absorbed by the protective structure. The kinetic impact energy is dissipated by the work done in bending, shear, torsion, and displacement of components interacting in the collision event.

The design is usually an iterative process where a trial configuration of the protective structure is initially developed. For the trial structure, a force-versus-deflection diagram is developed through analysis or with the help of physical testing and modeling. The area under the diagram is the energy capacity of the protective system. The forces and energy capacity of the protective system is then compared with the design vessel impact force and energy to confirm that the vessel loads have been resisted.

Acceptable damage. Where damage or local collapse of substructure components is permitted, the design must ensure that the structure does not collapse by providing redundancy or ductility. Since these concepts involve consideration of plastic behavior, and since little information is available on this topic for the type of dynamic impacts associated with vessel collision, assumptions based on experience and sound practice should be substituted.

Local collision forces. In designing bridge substructures for vessel collision, two cases must be investigated: (1) overall stability of the combined substructure-foundation system where the vessel impact is a concentrated force at the waterline; and (2) the ability of each member to withstand local collision effects resulting from collision impact (see also Figures 2–8, 2–9, and 2–10).

The need to apply the local collision forces mentioned in section 2.5 on bridge piers and substructures exposed to contact by overhanging portions of a ship or barge's bow is documented by accident case histories. An example is the Sunshine Skyway Bridge in Tampa Bay, which collapsed in 1980 as a result of a ship's bow impacting a pier column 42 feet above the waterline. Ship and barge bow rake lengths are often large enough so that they can even extend over protective fender systems to engage vulnerable substructure elements. Typical bow geometry data are given by the AASHTO (1991) *Guide Specifications and Commentary for Vessel Collision Design.*

Design Collision Velocity

Velocity distribution. The design collision velocity or impact speed V (see also Section 2.5) for each exposed bridge component should be based on (1) the vessel transit velocity V_T within the navigable channel limits; (2) the minimum velocity V_{min}; (3) the distance to the location of the component from the center line of vessel transit path, x; and (4) length (LOA) of the design vessel. This distribution is shown in Figure 3–9 where V = design impact velocity (ft/s); V_T = typical vessel transit velocity in the channel (ft/s); V_{min} = minimum design impact velocity (ft/s); x = distance to pier from channel center line; x_c = distance to edge of channel; and x_L = distance equal to three times the length overall of the design vessel (ft).

The triangular distribution is chosen because of its simplicity and because it gives reasonable results in modeling the aberrant vessel speed situation. Historical accident data indicate that aberrant ships and barges that collide with bridge piers further away from the channel are moving at reduced speeds compared to those hitting piers closer to the navigable channel limits. The use of the distance 3(LOA) in Figure 3–9 to define the

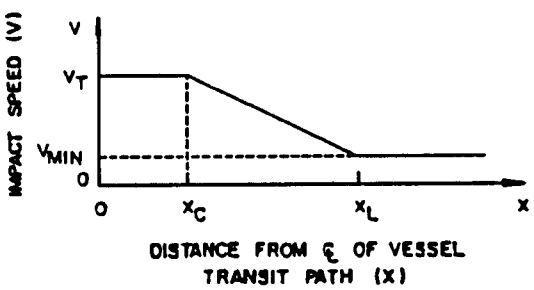

Figure 3–9 Impact velocity distribution.

limits at which the design speed becomes the same as the water current is based on the observation that very few accidents have occurred beyond that boundary.

Transit velocity. The vessel transit velocity in the channel, V_T, represents the velocity at which the design vessel is transiting the channel or waterway under normal conditions. Since the selection of the design impact speed is one of the most important design parameters, it should reflect a typical transit speed of the design vessel under typical conditions of wind, current, visibility, opposing traffic, waterway geometry, and so on.

In general, the design speed should not represent extreme values of extreme events, such as flooding and other extreme environmental incidents. Vessels transiting under these conditions cannot represent annual average situations that reflect typical transit conditions.

Vessel Collision Energy

A moving vessel releases a certain kinetic energy that must be absorbed during a non-eccentric collision with a bridge pier. This energy (AASHTO Article 3.8) is

$$KE = \frac{(C_H)(W)(V)^2}{29.2} \tag{3–22}$$

where W = vessel displacement tonnage (tonne); C_H = hydrodynamic mass coefficient; and V = vessel impact velocity (ft/s). Equation (3–22) is the standard version $MV^2/2$ of kinetic energy after appropriate conversion of units and incorporation of the parameter C_H to account for the influence of surrounding water on the moving vessel. Procedures for estimating C_H are based on work done by Saul and Svensson (1980) and data published by PIANC (1984). This coefficient may be computed as follows:

If underkeel clearance is large ($\geq 0.5 \times$ Draft), $C_H = 1.05$
If underkeel clearance is small ($\leq 0.1 \times$ Draft), $C_H = 1.25$

The underkeel clearance is taken as the distance between the bottom of the vessel and the bottom of the waterway. For intermediate values, C_H may be estimated by interpolation.

3.10 BASIC PHILOSOPHY OF SEISMIC DESIGN

Design Approaches

There are two seismic design approaches, conceptually different but both based on the "force design" principle: the current New Zealand and CalTrans criteria.

The New Zealand Code accepts the philosophy that it is uneconomical to design a bridge to resist a large earthquake elastically. Thus bridges are designed to resist small-to-moderate earthquakes in the elastic range, but for large earthquakes the intent is to make bridges ductile where possible. Flexural plastic hinging in columns is acceptable but significant damage to foundations and other joints is not. Accordingly,

forces resulting from plastic hinging in columns are determined, and the capacities of connections to columns are checked to confirm that they can resist these forces. Hence, critical bridge components must be designed to resist the maximum forces to which they will be subjected during a large earthquake event.

In the CalTrans approach, component forces are determined from an elastic design response spectrum for a maximum credible earthquake. The design forces for each member are then obtained by dividing the elastic forces by a reduction factor Z (between 1.0 and 0.8 for hinge restrainers and shear keys, respectively). These components are therefore designed for expected and greater-than-expected (in the case of shear keys only) elastic forces resulting from a maximum credible earthquake. Well-confined ductile columns have a Z factor from 4 to 8, that is, they are designed for lower-than-expected forces from elastic analysis. This assumes that the columns can deform plastically when the seismic forces exceed these lower design forces.

Although the two approaches are conceptually different, the end results are basically similar. However, experience from past earthquakes in Alaska, California, and Japan indicates that loss-of-span type failures are associated with relative displacement effects. Usually, these arise from out-of-phase motion of different parts of a bridge, from lateral displacement or rotation of the foundations, and differential displacement of abutments. Thus, stipulating minimum support lengths at abutments, columns and hinge seats is essential. Special attention to the problem of relative displacement is necessary for bridges with high columns or piers.

The AASHTO philosophy combines in part the New Zealand and CalTrans force-design approach, but equally addresses the relative displacement problems. Four additional concepts addressed in the document are as follows:

- First, minimum requirements are stipulated for support lengths of girders at abutments, columns, and hinge seats to account for relative displacement that cannot be calculated by current methods. A somewhat similar criterion is included in current Japanese Standards (JSCE, 1977).
- Second, component design forces are computed to account for the directional uncertainty of earthquake motions and the simultaneous occurrence of earthquake forces in two perpendicular horizontal directions.
- Third, design requirements are intended to inhibit foundation damage that is not readily detectable.
- Fourth, the underlying principle is to develop standards that are applicable to all regions of the United States, by articulating the seismic risk and by defining four Seismic Performance Categories (SPC).

Thus, for bridges classified as SPC A (Acceleration Coefficient ≤ 0.09), the essential requirement is to prevent superstructure collapse by specifying support lengths for girders at abutments, columns, and expansion joints. In addition, the design of connections of superstructure to substructure must consider a force 0.20 times the dead load reaction.

For bridges classified as SPC B ($0.09 <$ Acceleration Coefficient ≤ 0.19), the design is based on the CalTrans approach, whereby elastic member forces are obtained from a single-node analysis and then are divided by the response modification factor R to obtain the design forces (see also section 2.6). Values of factor R are shown in Table 3–5. For columns and piers, R varies between 2 and 5, resulting in design forces lower than predicted by elastic analysis. Therefore, the columns are expected to yield when subjected to the forces of the design earthquake. This yielding in turn implies relative dis-

Table 3–5 Response Modification Factor (R)

Substructure[1]	R	Connections	R
Wall-Type Pier[2]	2	Superstructure to Abutment	0.8
Reinforced Concrete Pile Bents		Expansion Joints within	
a. Vertical Piles Only	3	a Span of the Superstructure	0.8
b. One or more Batter Piles	2	Columns, Piers or Pile Bents	
Single Columns	3	to Cap Beam or Superstructure[3]	1.0
Steel or Composite Steel		Columns or Piers to Foundations[3]	1.0
and Concrete Pile Bents			
a. Vertical Piles Only	5		
b. One or more Batter Piles	3		
Multiple Column Bent	5		

[1]The R-Factor is to be used for both orthogonal axes of the substructure.

[2]A wall-type pier may be designed as a column in the weak direction of the pier provided all the provisions for columns in Chapter 8 are followed. The R-Factor for a single column can then be used.

[3]For bridges classified as SPC C and D it is recommended that the connections be designed for the maximum forces capable of being developed by plastic hinging of the column or column bent as specified in Article 4.8.5. These forces will often be significantly less than those obtained using an R-Factor of 1.

tortions of the structural system that must be considered. Requirements necessary to ensure sufficient ductility capacity of columns classified as SPC B are specified but are not as stringent as for classifications C and D. Foundations are designed for twice the seismic design forces of a column or pier.

The seismic design of bridges with SPC C and D follows the same general principles, but includes additional requirements. Thus columns must be capable of developing the required ductility capacity, and the recommended design forces for connections and foundations are based on the maximum shears and moments that can be developed by column yielding. Horizontal linkage and tie-down criteria at connections are also provided.

Seismic Ground Motion Accelerations

Selection of the seismic ground motion to be used is based on the criteria provided by the Applied Technology Council (1978) also known as ATC-3-06. These maps are based on (1) a realistic assessment of expected levels of ground motion shaking; (2) approximately the same probability that the design ground shaking will be exceeded for all regions; and (3) the frequency of occurrence of earthquakes in various parts of the country. The AASHTO specifications use the same criteria, but the ATC map has been replaced by a more recent map produced by the U.S. Geological Survey in 1988 (Algermissen, Perkins, Thenhaus, Hanson, and Bender, 1990). For locations near active faults, a qualified expert should be consulted to determine an appropriate value of the Acceleration Coefficient A.

Effects of Soil Interaction

The effect of soil conditions on ground motion may be considered in one of the following approaches:

- This interaction may be based on the concept of potential resonance of a structure with the underlying soil. The *SEAOC* (1975) code for seismic design gives the seismic site-structure resonance coefficient from 1.0 to 1.5 depending on the ratio of the fundamental building period to the characteristic site period.
- In the second approach, the computer program SHAKE (Schnabel, Lysmer, and Seed, 1972) was used by CalTrans to develop soil amplification factors for design criteria. The program analyzes a one-dimensional soil column for shear wave motions propagating from the rock level to the top of the soil column. This approach, however, is limited because only vertically propagating one-dimensional soil effects are considered, and parameters that might have marked effects are not. These parameters include surface waves, oblique transmission of waves through the soil, and the effects of reflection and refraction at the interface of different material layers.
- The third approach is developed by ATC-3-06 to determine corresponding values of effective peak ground acceleration and smoothed spectral shapes for three typical site conditions (AASHTO Art. 3.5). Representative ground spectral shapes were modified based on a study of ground motions recorded at locations with different site conditions, and coefficients were obtained for each of the three typical sites. This approach is incorporated in the current AASHTO specifications.

Response Modification Factors

Response modification factors R shown in Table 3–5 are intended to modify the component forces calculated from elastic analysis for SPC B, C, and D. These values imply that columns may yield when subjected to forces induced by the design ground motions, but connections and foundations must accommodate the same effects with little, if any, damage.

The rationale used in developing the R factors for columns, piers, and pile bents involved consideration of redundancy and ductility provided by the various supports. The wall-type pier is judged to have minimum ductility capacity and redundancy in its strong direction, and is assigned an R factor of 2. A multiple-column bent with well-detailed columns is considered to have good ductility capacity and redundancy, and is given an R factor of 5. The ductility capacity of single columns is the same as in multiple-column piers, but because a single column has no redundancy, a lower R factor of 3 is assigned. Since little information is available on the performance of pile bent abutments in actual earthquakes, the R factors are based on judgment of potential performance in comparison to other structural types. In the same context, pile bents with batter piles are judged to have some reduction in ductility capacity, and hence are assigned lower R factors.

3.11 REQUIREMENTS OF REINFORCED CONCRETE IN SEISMIC DESIGN

Ductility in Reinforced Concrete

The intent to provide ductility in reinforced concrete is initially part of the safety requirements, but deserves consideration of technical aspects. Ductility implies that strength is maintained while sizable deformations and deflections occur. Combined with

redundancy, ductility allows a heavily stressed component to continue to carry its capacity load while deforming enough to bring lesser stressed neighboring members into the resistance pattern. When energy must be absorbed, as in blasts and earthquakes, ductility is particularly important.

In beams and slabs ductility is ensured (a) by introducing reinforcing steel bars to carry the tension and (b) by limiting the amount of steel so that this reinforcement will yield before the concrete reaches the catastrophic strain and crushes in compression. Reinforced concrete columns are basically brittle under vertical load, but spiral columns can introduce limited ductility. Under lateral loads (sidesway) considerable ductility can be built into columns by proper detailing and the use of spirals. The detailing of reinforcement at the joints between caps and columns is particularly important in ensuring ductility and capacity to survive a shock loading. The structural capacity is thus based on the logical criterion to absorb earthquake energy rather than on strength alone, and is markedly increased with ductile concrete as compared to brittle material.

Where ductility cannot be achieved in design or in detailing, additional strength may be necessary to ensure that potential failure will still be initiated at a section that is more ductile or is expected to respond in a ductile manner. This approach is shown, for example, in choosing more conservative performance factors ϕ, and in specifying longer bar laps for tension splices.

Ductility factor. A simple load-displacement curve is shown in Figure 3–10. Referring to this diagram, the ductility factor is defined as the ratio of the maximum permissible or useful inelastic deflection or displacement to the initial yield deflection. This factor is, therefore, the ratio b/a. A recommended minimum ductility factor for buildings in earthquake areas is from four to six. The determination of the value of the ductility factor for a reinforced concrete frame is a complex problem involving bending and shear deformations of heterogeneous members consisting of concrete and ductile reinforcing steel.

Applied in conjunction with elastoplastic behavior, the ductility factor μ_u is the ratio of maximum deformation prior to failure to the deformation at initial yield. It is interesting to note that the maximum deformation may be established by direct stress, by secondary stress, by buckling, by local failure, or by whatever condition or combination of conditions leads to the minimum value. Where there is indeterminacy or there are multiple stress paths in a frame, there may be local failure at one or several points, but the overall force-deformation characteristics may not be at the initial yield.

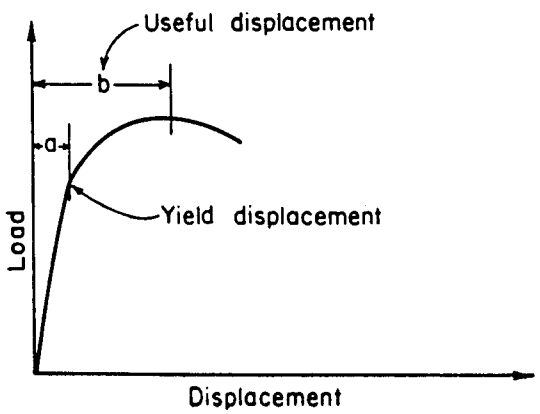

Figure 3–10 Load-displacement curve.

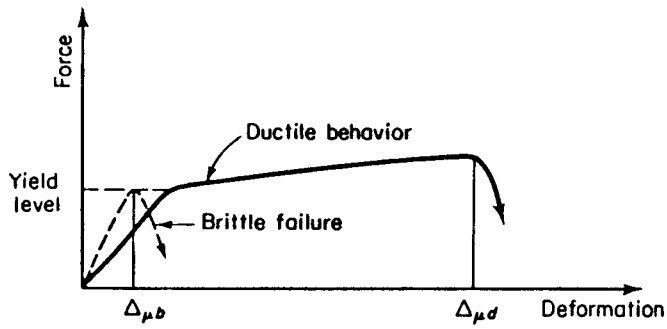

Figure 3–11 Capacity of brittle and ductile elements; subscripts b and d denote brittle and ductile element, respectively.

Relationship to energy absorption. Figure 3–11 indicates conceptually the relative work capacities of two hypothetical elements of structures, each with the same yield strength. The area under the curves respectively represents work capacity, which is much greater for the ductile element along with the probability of survival in a strong earthquake.

The curves of Figure 3–11 show how the energy absorption capacity is related to the ductility. However, ductility alone is not adequate for energy reconciliation, since there could be a large value of μ associated with a small force and the area under the curve would be inadequate. At the other extreme, a very great force could develop sufficient energy in the elastic range or at values of μ between 0 and 1.

Ductility and energy absorption capacity are important in seismic design because (a) it is economically impractical to design structures to resist the maximum expected earthquake forces within the elastic stress range; and (b) it is difficult to predict the character of the earthquake motion that will occur at a given site.

Guidelines for ductile concrete design. Among the many useful publications on the design of ductile concrete, reference is made to Blume, Newmark, and Corning (1961) and SEAOC (1966) with subsequent revisions. These documents combine theory, illustrations, and code terminology.

Ductile concrete design entails additional steps in the design process. Deformation or ductility and work capacity is an added dimension to strength. A logical approach is to design according to traditional strength requirements and then to provide for ductile concrete as a final procedure. Alternatively, the basic ductile concrete requirements may serve as a basis to establish concrete dimensions, and then detail the reinforcing steel selection.

In general, concrete sections may tend to be slightly larger, especially columns, and main reinforcement steel areas may be somewhat less. Web reinforcement and transverse column reinforcement tend to be more in total volume especially near and at the joints.

AASHTO Requirements

These requirements are intended to ensure that the design of components for bridges, particularly those classified as SPC C and D, is consistent with the overall design philosophy. Columns must be designed to yield in flexure with a reasonable ductility capacity, whereas the potential for shear, compression of loss of anchorage failure, is also minimized. The additional design requirements for piers provide for some inelastic capacity, but this is markedly less than that of columns.

As mentioned, the actual ductility demand on a column or pier is a complex function of several variables such as earthquake characteristics, design force level, period of the structure, shape of the inelastic hysteresis loop of the column, elastic damping coefficient, contribution of foundations and bearing compliance to structural flexibility, and plastic hinge length of the column. The damage potential of a column is also related to the ratio of the duration of strong motion shaking to the natural period of the bridge. This ratio indicates the probable number of yield excursions, and hence of the cumulative ductility. The latter is considered a more relevant index than the peak ductility level.

Both service load and load factor methods are allowed, but the load factor method is recommended because it is consistent with the ultimate load capacity concept used in determining the design forces. When service load design is used, the allowable stress can be increased by 33 percent.

Seismic performance, categories A, B. For category A, special seismic design requirements are not necessary because of the low level of seismic risk and the low probability that a column will be subjected to seismic forces large enough to cause yielding.

Bridges classified as SPC B may be subjected to seismic forces that will cause yielding of the columns. The columns must, therefore, be provided with some ductility capacity in terms of the transverse reinforcement requirements in order to prevent buckling of the longitudinal steel and provide confinement for the core of the column. The maximum spacing at the transverse reinforcement is, however, increased to 6 inches.

Seismic Performance Categories C and D

Column requirements. The minimum vertical reinforcement is 1 percent, and reflects traditional concern for the effect of time-dependent deformations as well as the intent to avoid a difference between the flexural cracking and yield moments. The 6 percent maximum steel ratio is selected to remedy congestion and to permit anchorage of the longitudinal steel. Specified yield strength f_y should be limited to 60,000 lb/in^2 because higher strength steels may not have the yield plateau needed for ductility. Thus, the use of higher grade steels may result in inadequate ductility when the column is strained into the plastic range.

Flexural Strength. Columns must be designed biaxially and checked for both the minimum and maximum axial forces. If the maximum axial stress exceeds 0.20 f'_c, the strength reduction factor ϕ is reduced to 0.50. This requirement was added because of the trend towards a reduction in ductility capacity as the axial load increases. Columns with axial stresses exceeding 0.20 f'_c are not prohibited, but are designed for higher force levels (i.e., lower ϕ factor) in lieu of the lower ductility capacity.

Column Shear and Transverse Reinforcement. The AASHTO criteria are intended to minimize the potential of shear failure in a column. If a column fails in shear, the potential of superstructure collapse will exist.

Columns may yield in either the longitudinal or transverse direction. The shear force corresponding to the maximum shear developed in either direction (noncircular columns) should be used to determine the transverse reinforcement.

The concrete contribution to shear cannot be considered within the plastic hinge

zone, particularly at low axial load levels, because of full section cracking under load reversal. Hence, this contribution is neglected for axial load levels less than $0.10 f'_c A_g$. It is probable that using $v_c = 0$ for low load levels is overconservative, but limited test data presently available inhibit a reasonable alternative.

Transverse Reinforcement for Confinement of Plastic Hinges. Plastic hinge regions are generally located at the top and bottom of columns and pile bents (see also sections 4.5 and 4.7).

The main function of the transverse reinforcement is to ensure that the axial load carried by the column after spalling of the concrete cover will be at least the same as before spalling, and buckling of the longitudinal reinforcement is prevented.

The equation for the ratio of spiral reinforcement to total volume of concrete core is based on the arbitrary concept that, under axial compressive loading, the maximum capacity of the spirally reinforced column before loss of cover concrete is equal to that with the cover concrete destroyed and the spiral reinforcement stressed to its useful limit. The toughness of the spiral column under axial load is not directly relevant to its function in earthquake-resistant structures where toughness or ductility is likely to be related to performance of the column under large reversal of moments and axial loads. Thus, without implicit technical incentives the basic spiral reinforcement equation has not been modified for seismic design other than adding a second equation to provide for a lower bound to the amount of transverse reinforcement. These criteria are expressed by AASHTO Equations (8–1) and (8–2).

The confinement requirements for rectangular columns were developed from the criteria for spiral columns (ACI *Manual of Concrete Practice,* 1972). Referring to Figure 3–12, the confining force P provided by the spirally reinforced column is

$$P = rsD = 2A_s f_{yh} \tag{3–23}$$

where r = confining pressure; s = spacing of spiral reinforcement; D = core diameter of column; A_s = area of spiral reinforcement; and f_{yh} = yield strength of spiral reinforcement. From Equation (3–23) we obtain

$$r = \frac{2A_s f_{yh}}{sD} \tag{3–24}$$

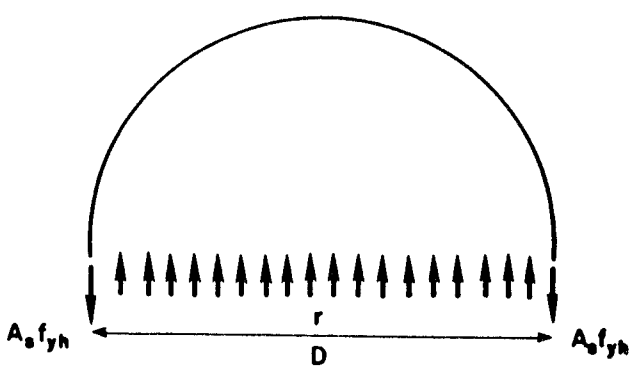

Figure 3–12 Confining pressure provided by a spirally reinforced column.

The volumetric ratio p_s of the spiral reinforcement is

$$p_s = \frac{4\pi DA_s}{\pi D^2 s} = \frac{4A_s}{Ds} \tag{3–25}$$

Substituting Equation (3–25) into Equation (3–24),

$$r = \frac{p_s f_{yh}}{2} \tag{3–26}$$

Referring to Figure 3–13, the confining force provided by the rectangular column is

$$P = rah_c = \Sigma A_s f_{yh} \tag{3–27}$$

where a = spacing of the hoop reinforcement, and h_c, $\Sigma A_s f_{yh}$ are as shown. Therefore

$$r = \frac{f_{yh}\Sigma A_s}{ah_c} \tag{3–28}$$

If the two columns provide equal confining pressure r, it follows that

$$\Sigma A_s = ah_c p_s/2 \tag{3–29}$$

We also recall that for spiral columns

$$p_s = 0.45\left[\frac{A_g}{A_c} - 1\right]\frac{f_c'}{f_{yh}} \tag{3–30}$$

Then by substituting Equation (3–30) into Equation (3–29),

$$\Sigma A_s = 0.225ah_c\left[\frac{A_g}{A_c} - 1\right]\frac{f_c'}{f_{yn}} \tag{3–31}$$

The 0.225 coefficient for a rectangular column corresponds to the coefficient 0.45 of Equation (3–30) for a spiral column, determined experimentally. Since limited data were available, a rectangular column was not judged as effective as a spiral column, hence the coefficient was increased to 0.30.

Figures 3–14 and 3–15 show the detailing of reinforcement in rectangular columns based on Equation (3–31) with the 0.30 coefficient. It should be noted that A_s, the total

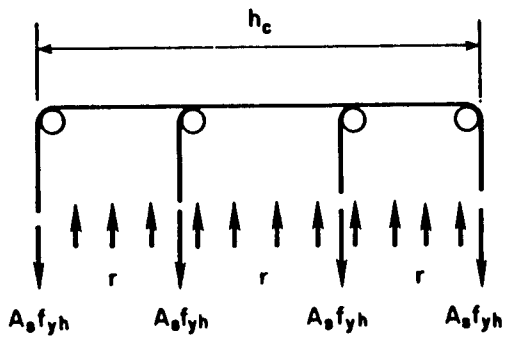

Figure 3–13 Confining pressure provided by a rectangular reinforced column.

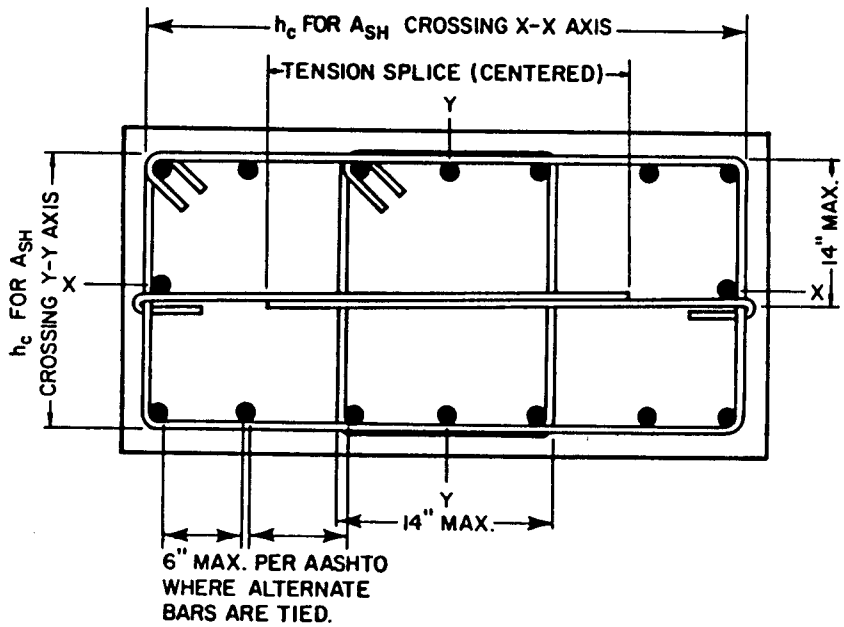

Figure 3–14 Column tie details.

area of hoop reinforcement, should be calculated for both principal axes and the maximum value should be used.

Loss of concrete cover in the plastic hinge zone, resulting from spalling, requires special detailing of the confining steel. Lapping the steel only is not adequate, since the spiral will tend to unwind if the concrete spalls. The problem can be remedied by providing full strength lap welds. Likewise, rectangular hoops should be anchored by bending ends back into the core as shown in Figure 3–15.

While either spirals or ties are allowed for transverse column reinforcement, the use of spirals is recommended as the more effective and economical solution. When more than one spiral cage is used to confine an oblong column core, the spirals should be interlocked with longitudinal bars as shown in Figure 3–16. Spacing the longitudinal bars at a maximum of 8 inches is also recommended to enhance confinement of the core.

Splices. It is often good practice to lap longitudinal reinforcement with dowels at the column base. However, this detailing is undesirable for seismic performance because of two reasons: (1) the splice is located in a potential plastic hinge region where bond requirements are critical; and (2) lapping the main reinforcement will tend to concentrate plastic deformation close to the base and reduce the effective plastic hinge length as a result of stiffening of the column over the lapping region (this may result in a severe local temperature demand).

Commentary on inelastic behavior of reinforced concrete. The ductility of various types of joints has been demonstrated in tests. Figure 3–17 shows a specimen (beam-column member), and the loading and reaction points. Figure 3–18 shows the force-deformation for the test specimen of Figure 3–17 under cyclic loading (Bennett, Hanson,

(text continues on page 161)

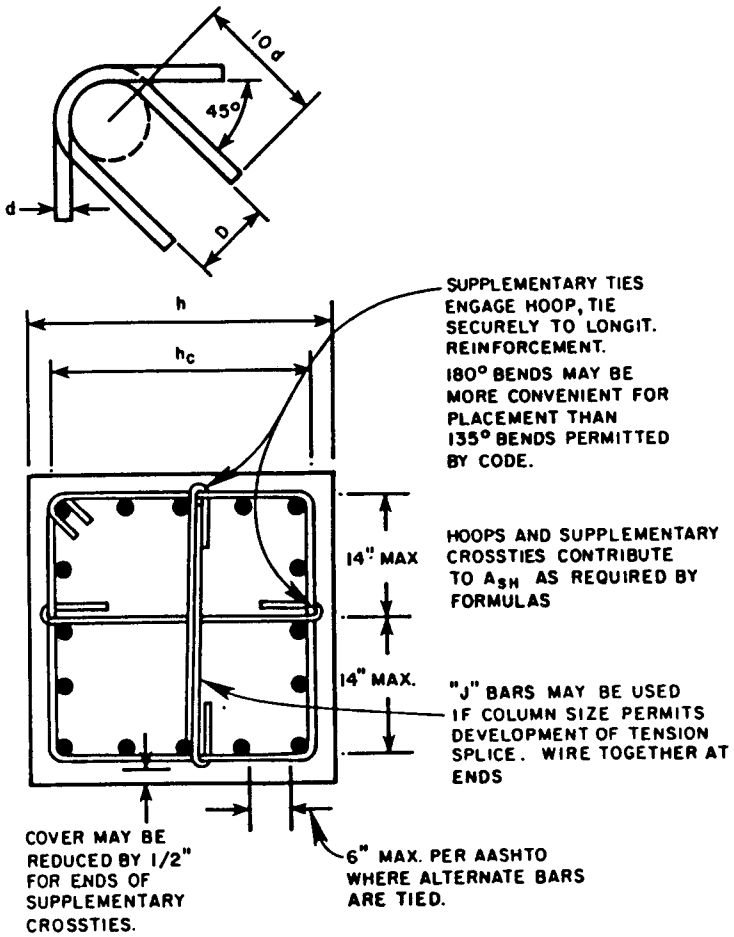

Figure 3–15 Column tie details.

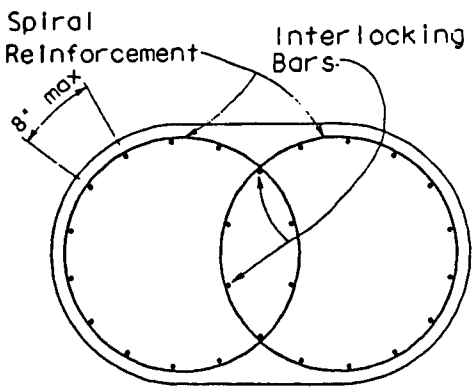

Figure 3–16 Column interlocking spiral details.

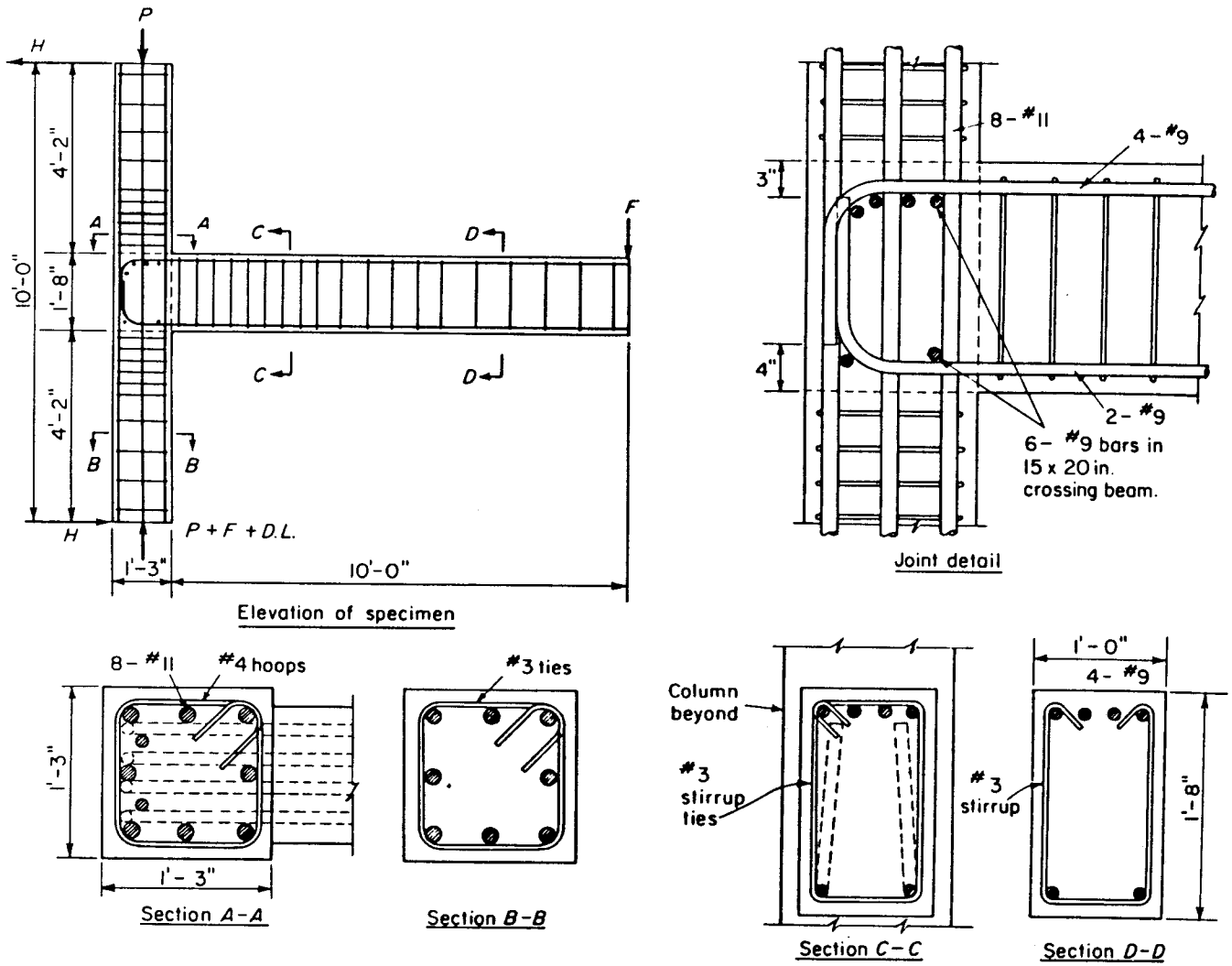

Figure 3–17 Details of a test beam-column member *(from Bennett, et al., 1965).*

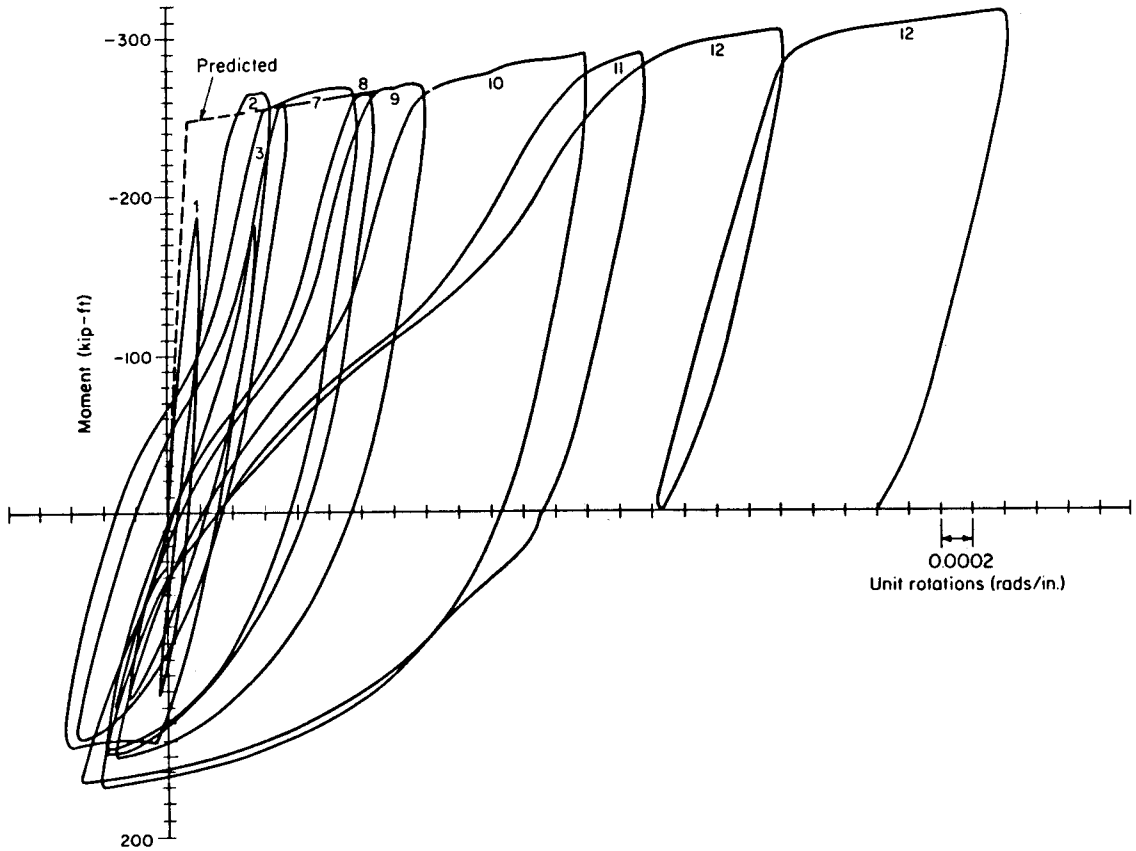

Figure 3–18 Test results for specimen VA *(from Bennett et al., 1965).*

Parme, and Sbarounis, 1965). The ductility is good in spite of several specimen details that do not fully comply with the best recommended practice. The test is intended to be severe and to reveal any weakness in laterally unrestrained exterior joints of a concrete frame under cyclic loading. The results show that ductility and energy-absorbing capacity can be provided even at unfavorable joints and under severe column axial loading. A free-standing exterior beam-column joint (such as a column-pier) requires some joint hoops to resist internal tensile forces in the joint.

Columns are basically subjected to compressive axial load, although considerable moment and shear can be present especially under earthquake motion. Thus, in addition to interaction of moment and axial load, as in normal concrete design, the matter of "confinement" must be included in consideration of column force-deformation characteristics. If a column loaded in axial compression is restrained from bulging outward, or is confined, the load capacity and the allowable deformation before failure are markedly increased. This is demonstrated in Figure 3–19, showing data from tests of plain concrete cylinders with varying confining fluid pressure (Blume et al., 1961). In lieu of fluids, transverse hoop or spiral reinforcement is provided to confine the core concrete. The shell concrete outside the transverse reinforcement is of no value under severe loading conditions, and is ignored. Thus, for any given column section, the ductility available

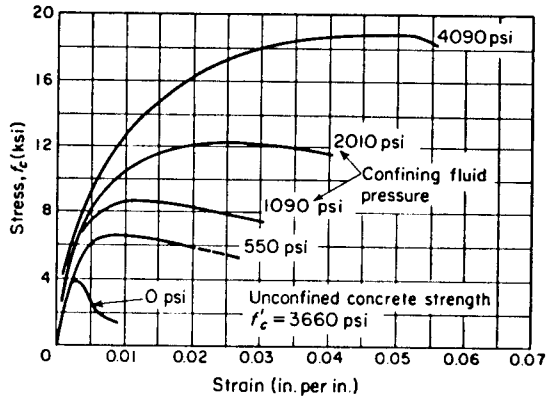

Figure 3–19 Stress-strain curves from compression tests of confined concrete cylinders *(from Blume et al., 1961).*

under axial force and moment will depend upon the force-moment interaction as well as upon the capacity of the transverse reinforcement to confine the core concrete. A confined concrete section has much greater ductility below the balance point than does the unconfined section.

Figure 3–20 shows interaction curves for a specific concrete section, and Figure 3–21 presents the ductility ratio for curvature for the same section in the confined and unconfined state and under various column load ratios (Blume et al., 1961). Columns generally have less ductility than horizontal members, and cost more if they are de-

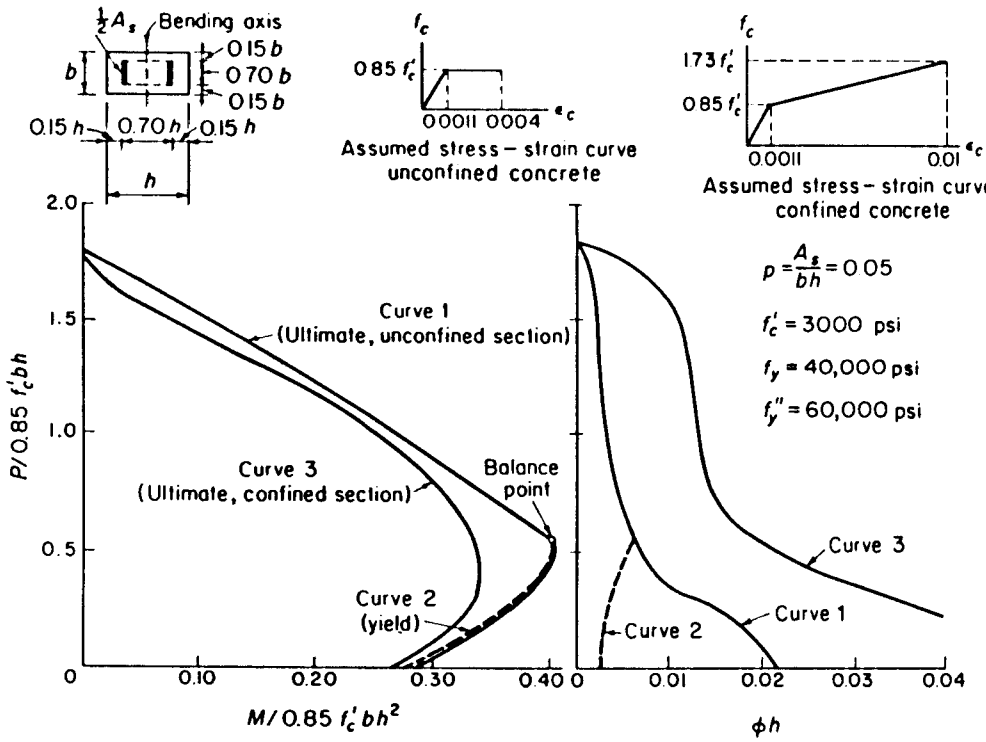

Figure 3–20 Interaction curves for a rectangular section having a confined concrete core *(from Blume, et al., 1961).*

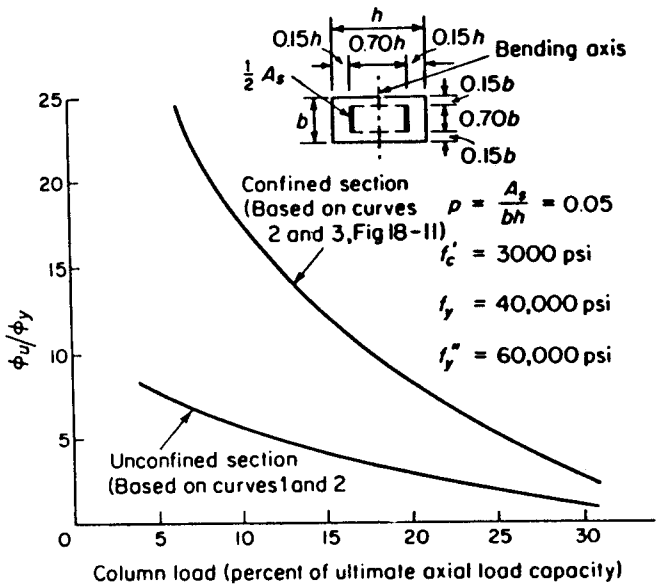

Figure 3–21 Variation of ϕ_u/ϕ_y for tied columns of unconfined and confined concrete in respect to axial load *(from Blume et al., 1961).*

signed to have equal ductility. For this reason, it is often desirable to proportion a frame so that plastic hinges will develop in the horizontal rather than in the vertical members under severe lateral loading.

Beams (or pier caps) are made ductile by proportioning the reinforcement so that concrete shear failure and compression failure in flexure are not possible. What preceeds collapse, therefore, is stretching of the tension steel, hence the members are intentionally underreinforced.

Joints are subject to moment, shear, and axial forces, and sometimes torsion as well, imposed by the columns and the intersecting horizontal members. Although the internal stresses follow a complex pattern, they can be resolved by rational methods if required. Empirical data from tests confirm that intersecting horizontal members and continuous bars increase the joint strength under most conditions so that plastic hinges develop outside the joint. Exterior joints require transverse ties to resist internal diagonal tension, a practice often extended to interior joints as well.

In summary, reinforced concrete can be made to have adequate ductility and reserve energy absorption capacity by: (1) preventing shear failure; (2) confining any compression failure; and (3) forcing local failures under severe loading to occur mainly by local stretching of tensile steel.

Pier requirements. The provisions for pier design are based on limited data on pier behavior in the inelastic range. Consequently, the factor of 2 for piers in Table 3–5 is based on the assumption of minimal inelastic behavior.

One of the main requirements pertains to the vertical reinforcement ratio; this should be equal to or in excess of the horizontal reinforcement ratio in order to prevent the case of inadequate web reinforcement in piers that are short. Splices should be staggered to avoid concentrated weak sections. The requirement for a minimum of two layers of reinforcement in walls subjected to considerable shears is based on the criterion that two curtains of reinforcement will tend to envelop the concrete and maintain the integrity of the wall after cracking. Also, under typical construction conditions the pos-

sibility of maintaining the location of a single layer of reinforcement near the middle of the pier is low.

Column connections. Column connections are vertical extensions of the column area into adjoining members such as pier caps, pile caps, and spread footings. The integrity of these connections is, therefore, essential to develop their flexural capacity. The longitudinal reinforcement must develop its overstrength capacity of $1.25 f_y$, while the transverse confining reinforcement of the column must be continued a sufficient distance into the joint to avoid a plane of weakness at the interface.

For column connections in a pier cap, evaluation of existing and new data on the joint strength under moment reversals indicates that the strength of the joint is relatively insensitive to the amount of transverse reinforcement (provided there is a minimum amount), and that a limiting shear stress of 12 $\sqrt{f'_c}$ for unconfined joints may be used for normal weight concrete. For lightweight concrete the allowable stress for the joint is reduced to 75 percent.

Construction joints in piers and columns. Where construction joints must be provided, they must be designed to resist the design seismic force at the joint. Where shear is resisted at a construction joint solely by dowel action and friction on a roughened concrete interface, the total shear force across the joint cannot exceed the value

$$V_j = \phi(A_{vf} f_y + 0.75 P_n) \tag{3–32}$$

where A_{vf} = total amount of reinforcement normal to construction joint; and P_n = minimum axial load for columns or piers.

The derivation of Equation (3–32) is based on current ACI principles on shear friction along interfaces between members that can slip relative to one another. These interfaces include a surface formed by placing one layer of concrete on top of an existing

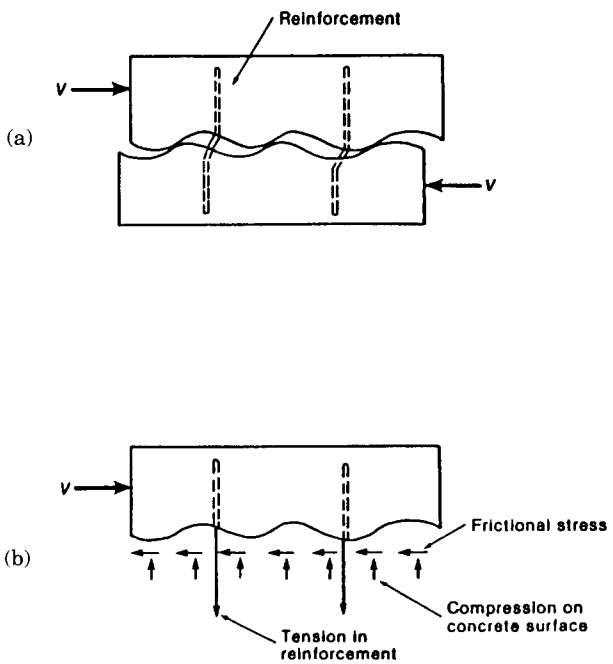

Figure 3–22 Shear friction analogy.

hardened layer. Under the action of a shear force V slip of the layers can cause the separation of the surfaces as shown in Figure 3–22(a). If there is reinforcement across the interface, it is elongated by the separation of the surface and hence it is stressed in tension. For equilibrium a compressive stress is needed as shown in Figure 3–22(b). Shear is now transmitted across the interface by (1) friction resulting from the compressive stresses, and (2) the interlock of aggregate protrusions combined with dowel action.

Because the reinforcement is assumed to yield in order to develop the necessary forces, the yield strength of the steel is limited to 60,000 lb/in^2. Each bar must be anchored on both sides of the interface to develop its strength. The reinforcement must be placed uniformly across the shear plane so that all parts of the interface are clamped together. Permanent net compressive force across the interface can be considered as directly additive to the force $A_{vf}f_y$. These considerations lead to the development of Equation (3–32) under appropriate load and resistance factors.

3.12 TOLERABLE DIFFERENTIAL MOVEMENT AND SETTLEMENT OF BRIDGES

General Principles

Settlement can occur as a result of foundation movement, or it may be caused by excavation (for example, to build an underpass). For almost any type of ground support, movement and settlement due to excavation will depend on the soil characteristics and the groundwater conditions, the size of the excavation and particularly the depth, the type of support system, the details and sequence of the bracing, and the general workmanship of construction. From these brief remarks, it follows that bridges may settle (uniformly or differentially) because of adjacent excavation, or the settlement may relate mainly to the foundation system.

The settlement caused by open-cut excavation that a structure can withstand is less than the settlement that the same structure can undergo without damage under the effect of its own weight. Settlement caused by subway construction may occur rapidly and produce erratic effects. Damage to nearby structures will depend first on the type, foundation, age, and general condition of the structure. The first comprehensive summary of settlement that may be damaging to surroundings was provided by Skempton and MacDonald (1956), and involved mainly buildings. Useful classifications of allowable and detrimental settlements in various conditions are also given by Sowers (1962) and by Grant, Christian, and Vanmarcke (1972).

Differential movement, also expressed as angular distortion, is of much greater concern than uniform settlement or tilting. It can be considered by computing theoretical settlements for various points such as corner, center, or beneath lightest and heaviest loaded footings to obtain the geometry of composite settlement. If a bridge moves vertically the same amount or rotates as a plane rigid body, this will not generally cause structural problems. For example, if a structure settles 1 inch at one end and 5 inches at the other end with linear settlement variation between the two points, except for some aesthetic effects, structural damage is unlikely to develop. In this case, the structure will have settled 1 inch, and tilted an amount $z = (5–1)/L$. Local settlements below the tilt line between the two ends may cause some distress. These local settlements below either the settlement or the tilt line are the differential settlements that

the foundation design must control, since they can determine the serviceability of the structure.

Differential settlements can be computed as the difference in settlement between two adjacent points.

Nature and Causes of Foundation Movement

Components of bridge settlement. The settlement of a bridge can be divided into three components: uniform settlement, tilt (or rotation), and nonuniform settlement. These are illustrated in Figure 3–23.

Uniform settlement represents a condition where all foundations beneath the bridge settle uniformly and by the same amount. Since composite settlement is seldom uniform, it is only a hypothetical possibility. However, this type of settlement often constitutes a component of more complex settlement patterns. In structural terms it does not cause distortion of the bridge superstructure (Stermac, 1978; Yokel, 1990), although it may cause some problems at the junction of the bridge with the approach slabs if it becomes excessive (Wahls, 1990). Other problems associated with excessive settlement relate to drainage at the end of the bridge and vertical clearance at underpasses.

Uniform tilt or rotation corresponds to a uniform angular rotation. All settlements at pier footings vary linearly along the length of the bridge. This pattern of settlement

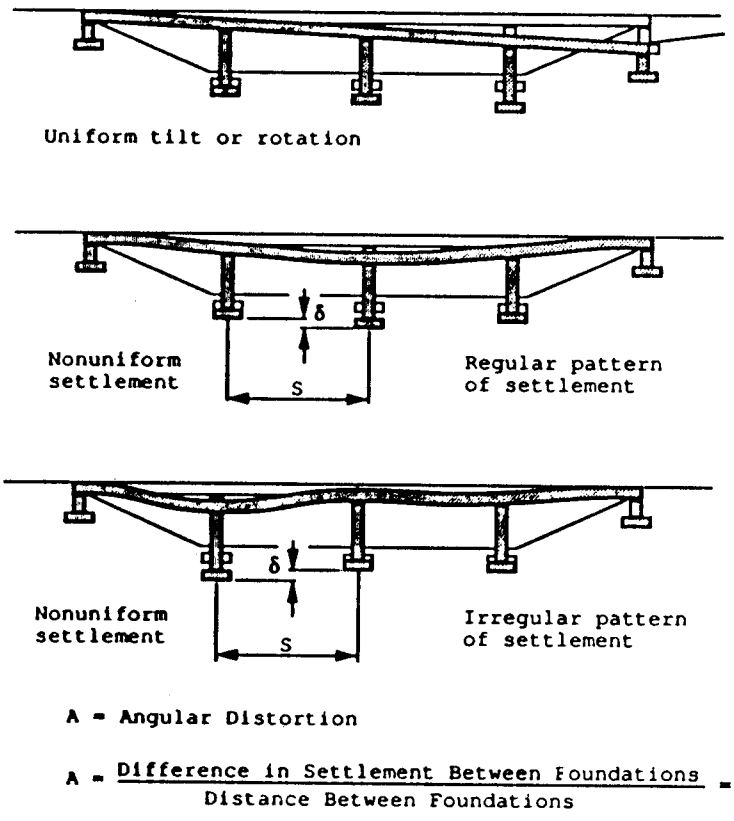

Figure 3–23 Components of settlement and angular distortion in bridges.

is likely for bridges with very stiff superstructures, and is probably the only settlement mode of single-span bridges. Although distortion effects are absent in the superstructure, it could result in the same approach slab, drainage, and clearance problems. Some distortion is also possible where the bridge superstructure connects to substructures or foundation elements that cannot rotate with the superstructure.

Nonuniform (differential) settlement results in deformation of the superstructure if the bridge is continuous over three or more supports. Two distinct types of nonuniform settlement are mentioned (Figure 3–23). In the first, the pattern of settlement is regular (increasing towards the center from the ends); in the second, the pattern is irregular (settlements vary erratically along the bridge). Both types result in distortion of the superstructure in continuous spans. Considering equal settlement magnitudes, an irregular settlement pattern would be expected to cause amplified distortion of the superstructure, mainly because the differential settlement between adjacent supports would be greater.

Likewise, nonuniform settlement can cause the same grade problems at the junctions with approach slabs and between adjacent spans, drainage problems, clearance problems, and in addition structural distress associated with larger support reactions and internal stresses.

Usual causes of settlement. Foundations commonly load the soil underneath. Elastic deformation occurs quickly, it is usually small, and is normally neglected in design. Changes in volume associated with reduction in the water content of the subsoil (usually referred to as consolidation) can be estimated and measured. Consolidation settlement occurs in all soils. In cohesionless soils, consolidation occurs quickly and is normally not distinguishable from the elastic deformation. In cohesive soils it can be a long-term process.

Various loads may have significant effects on the magnitude of settlement or lateral displacement of a soil. Among the factors influencing this process are: (1) the ratio of sustained load to total load; (2) the duration of sustained loads; and (3) the time interval over which settlement or lateral displacement occurs.

Consolidation settlements in cohesive soils are time-dependent, so that transient loads have negligible effect. In cohesionless soils, however, and especially where the permeability is high, elastic deformation of the subsoil due to transient loads can occur rapidly. Since deformation in cohesionless soils takes place also during construction as the loads are applied, part of the overall settlement can be accommodated by the structure to an extent compatible with the construction method. In the same context, settlements due to transient loads may be significant in cohesionless soils.

Problems Caused by Settlement of Abutments and Foundations

It follows from this brief review that uneven movement of bridge supports can affect the serviceability of the structure, bridge appearance, the structural integrity of the system, and, at the extreme, the structural safety. The severity of these consequences increases as the movement pattern and magnitude are amplified, particularly if the supports shift laterally.

Moulton, GangaRao, and Halvorsen (1985) note that even completely uniform settlements without distortion effects can reduce clearance at grade separations. Differential settlement between bridge decks and approach slabs is a typical cause of grade

bumps. Similar problems arise when one span settles differently from the adjacent spans, producing the condition of "faulting at expansion joints" (Keene, 1978).

Differential settlement between supports causes redistribution of moments and shears over the supports and at the spans, resulting in increased support reactions and higher internal stresses in the superstructure framing. These effects have been documented and quantified (Emanuel, 1978; Grover, 1978). These investigators have also suggested that uneven settlements can reduce the level of comfort on the part of the user, and may even affect driving safety. Conversely, Moulton et al. (1985) tend to discount the likelihood of rider discomfort, so that this criterion is not likely to control the selection of tolerable movement. Thus, foundation movement would become intolerable for other reasons before reaching a level that would create rider discomfort. Hence, it follows that if a tolerable movement range is established with regard to structural consequences, it will be acceptable in the context of serviceability and safe vehicle operation.

A general agreement indicates that horizontal movement can be more critical in terms of structural problems than settlement in the same context, and this philosophy is shared by most investigators (Keene, 1978; Walkinshaw, 1978; Bozozuk, 1978; Moulton et al., 1985; Wahls, 1990). The problems articulated as a result of differential horizontal movement between decks and abutments, or between adjacent spans, focus on the following: (1) shearing of anchor bolts; (2) excessive opening of expansion joints; (3) complete closing of expansion joints and jamming of bridge decks into abutments; (4) shifting of abutments when expansion joints jam; (5) severe damage of abutment walls, approach slabs, or bridge decks associated with jammed joints; (6) distortion and structural damage to bearing devices; and (7) damage to bridge parts such as railings, curbs, parapets, and sidewalks.

Dependable procedures are available for estimating settlements. However, probable horizontal movement can only be predicted from experience and judgment, referring to case histories. Refined methods based on finite element analysis are available but they are complex, time-consuming, and costly (see also subsequent sections).

Criteria for Tolerable Settlement

Upper limits for the magnitude of settlement to be used as criteria for the boundary between tolerable and intolerable performance have been suggested by several investigators (Walkinshaw, 1978; Bozozuk, 1978; Grover, 1978; and Wahls, 1990). However, owing to the complexity of settlement patterns, no single measure of settlement or distortion can serve as a sole indicator of potential damage to a bridge. For example, settlements may be considered tolerable even though they may have a pattern and magnitude that can cause some degree of damage.

Bozozuk (1978) divides settlements and horizontal movements into three categories: (1) those that are not harmful; (2) those that are harmful but tolerable; and (3) those that are harmful and intolerable. Likewise, Moulton et al. (1985) define intolerable movement as follows: Movement is not tolerable if the associated damage requires costly repairs or maintenance, and a more expensive construction to prevent this would have been preferable.

It appears that intolerable settlement has not been defined in explicit terms, but is highly subjective and depends on factors other than the physical condition of a bridge. Cost and practical problems in repair and maintenance are part of the definition. The investigation conducted by Moulton et al. (1985) involves more data, and it seems ap-

propriate to emphasize the results and conclusions of that study with regard to what constitutes tolerable movement.

Criteria for settlement of bridges, expressed as a function of the magnitude of settlement, are given in Table 3–6, and it appears that they are reasonably consistent. The smallest value (2 inches or 51 mm) was suggested by Bozozuk (1978) as not harmful on the basis of a survey of the performance of actual bridges. Grover (1978), Bozozuk (1978), and Wahls (1990) recommend 4 inches (102 mm) as the settlement that may cause some damage, although still tolerable.

The criteria in Table 3–6 do not articulate the type or size of bridge. Although this may be an oversimplification, the data still have some direct applicability since they represent experience with actual bridges.

Criteria for settlement of bridges in terms of angular distortion are given in Table 3–7. Referring to Figure 3–23, angular distortion is expressed as

$$A = \frac{\delta}{S} \tag{3–33}$$

where δ = differential settlement (difference in settlement) between the foundations at the two ends of a span, and S = span length.

Moulton et al. (1985) consider angular distortion a good basis for establishing tolerable movement magnitude, and suggest the criteria presented in Table 3–7. These results are also supported by Yokel (1990) and Wahls (1990) as reasonable criteria for tolerable settlement. The values of angular distortion given in this table are based on data for 56 simple-span bridges and 119 continuous-span bridges.

A data summary from these studies that articulates the most critical conditions in establishing tolerable settlement criteria is shown in Table 3–8. These data show that 96 percent of 119 continuous span bridges sustained angular distortions as large as 0.004 without suffering damage that might be considered intolerable. As the upper bound of angular distortion was increased to 0.005, the percentage of acceptable incidents fall to 92%. Accordingly, the limit of tolerable settlement recommended by Moulton et al. (1985) is $A = 0.004$, and is based on a 96% acceptability rate. If all bridges were considered, this rate would probably be higher, because the data base included only bridges that had moved, excluding those that had not moved.

For simple span bridges, 56 cases were documented and provided the basis for establishing angular distortion criteria. A value of $A = 0.005$ is recommended as the upper limit of tolerable angular distortion, and this corresponds to a 98 percent acceptability rate among the bridges studied. However, an analysis of these data may indicate that this criterion may be too conservative. For example, for one bridge a value of $A < 0.001$

Table 3–6 Settlement Criteria for Bridges Expressed in Terms of Settlement Magnitude

Settlement Magnitude (mm)	Basis for Recommendation	Recommended By
51	Not harmful	Bozozuk (1978)
63	Ride quality	Walkinshaw (1978)
>63	Structural distress	Walkinshaw (1978)
102	Ride quality and structural distress	Grover (1978)
102	Harmful but tolerable	Bozozuk (1978)
>102	Usually intolerable	Wahls (1990)

Table 3–7 Settlement Criteria for Bridges Expressed in Terms of Angular Distortion

Angular Distortion δ/s	Basis for Recommendation	Recommended By
0.004	Tolerable for multiple-span bridges	Moulton, et al. (1985)
0.005	Tolerable for single-span bridges	Moulton, et al. (1985)

was associated with intolerable behavior, and it seems reasonable to exclude this bridge from the data input since no other structure with $A < 0.005$ suffered intolerable damage, so that this bridge clearly represents an aberrant case. With this exclusion, the percentage of bridges with acceptable behavior is shown in parenthesis in Table 3–8. Using these values, 95 percent of the bridges sustained angular distortions as large as 0.008 without damage that might be considered intolerable.

In summary, the following values of angular distortion are recommended as criteria of acceptable behavior (Duncan and Tan, 1991).

Continuous bridges, $A \leq 0.004$ is acceptable
Simple span bridges, $A \leq 0.008$ is acceptable

AASHTO criteria. AASHTO recommends criteria consistent with the function and type of bridges, anticipated service life, and consequences of unacceptable movement.

Tolerable movement criteria for foundation settlement are based on angular distortions according to the recommendations by Moulton et al. (1985). Thus, the angular distortion is limited to 0.004 for continuous-span bridges, and to 0.005 for simple-span bridges.

Likewise criteria for horizontal displacement are based on the potential effects of

Table 3–8 Data Used by Moulton et al. (1985) to Establish Criteria for Magnitudes of Angular Distortion

Value of Angular Distortion	Percent of 119 Continuous Span Bridges for Which this Amount of Angular Distortion was Considered to be Tolerable	Percent of 56 Simple Span Bridges for Which this Amount of Angular Distortion was Considered to be Tolerable*
0.000 to 0.001	100%	98% (100%)
0.001 to 0.002	97%	98% (100%)
0.002 to 0.003	97%	98% (100%)
0.003 to 0.004	96%	98% (100%)
0.004 to 0.005	92%	98% (100%)
0.005 to 0.006	88%	96% (98%)
0.006 to 0.008	85%	93% (95%)

*Values in parentheses exclude one bridge, for which a value of angular distortion < 0.001 was associated with "intolerable" behavior. This bridge was excluded for the purpose of calculating the values in parentheses because it is considered likely that, in this particular case, the intolerable behavior was not the result of the very small angular distortion that was experienced by the bridge.

combined horizontal and vertical movement. Where combined horizontal and vertical displacement is possible, horizontal movement should be limited to 1 inch. Where vertical displacement is small, horizontal displacement is limited to $1^1/_2$ inches. If estimated or actual movements exceed these levels, special analysis or measures are necessary to rectify the problem.

Criteria for Tolerable Horizontal Movement

Criteria for tolerable horizontal movement are shown in Table 3–9, based on observations of actual bridge performance. Two categories can be distinguished: not harmful, and harmful but tolerable. The lower bound is suggested by Bozozuk (1978) with less than 1 inch considered not harmful, and up to 2 inches considered harmful but tolerable.

The data summarized by Moulton et al. (1985) show that horizontal movement tends to be much more damaging when it is accompanied by settlement. These investigators found that horizontal movement less than 1 inch is invariably reported as tolerable, but movement exceeding 2 inches is most likely to be considered intolerable. On this basis, the recommendation is to limit horizontal movement to 1.5 inches. Likewise, Walkinshaw (1978) and Wahls (1990) suggest 51 mm (2 in) as the magnitude of horizontal movement as a condition that might indicate intolerable performance.

It may appear that a movement of 1.5 inches may be set as a reasonable value. Closely related to this value is the amount of movement at abutments and walls necessary to reduce earth pressures to design values (see also subsequent sections).

Methods for Assessing Structural Consequences

Differential settlement and movement are in reality imposed deformations that change the geometry of a structure. The resulting effects are in principle changes in shear forces and bending moments. In many cases, the degree of sensitivity can be assessed and evaluated on the basis of a single-step approximation such as the moment magnification factor method. In other cases, a complete second-order analysis is necessary. Where bridges and bridge components are flexible, the omission of deflection and distortion limits will indicate a trend to make the traditional boundary between small- and large-deflection analysis less distinct. Where the deformation of a structure is expected to result in a significant change in force effects, a new condition of equilibrium should be considered.

A properly formulated large deflection analysis will in this case provide all the

Table 3–9 Horizontal Movement Criteria for Bridges Expressed in Terms of Movement Magnitude

Horizontal Movement mm	Basis for Recommendation	Recommended By
25	Not harmful	Bozozuk (1978)
38	Tolerable in most cases	Moulton, et al. (1985)
51	Structural Distress	Walkinshaw (1978)
51	Harmful but tolerable	Bozozuk (1978)
51	Usually intolerable	Wahls (1990)

force effects necessary for the assessment. Further application of moment magnification factors may not be required. Where compressive axial forces are present, they will tend to amplify both out-of-straightness of a component and the deformation due to nontangential loads, thereby increasing the eccentricity of the axial force. The simultaneous effect of this interaction is an apparent softening of the component, that is, a loss of stiffness. As axial compressive stress becomes a significant percentage of the Euler buckling stress, this effect becomes more significant and must be considered.

Second-order effects arise from the translation of applied loads creating new eccentricity. They are geometric nonlinearities, and are typically addressed by solving the equilibrium equations, or by using geometric stiffness terms in the elastic range. Useful data on the characteristics of the elements employed, assumptions on which they are based, and numerical procedures are given by White and Hajjar (1991). Although these references are related to metal structures, the underlying theory has general applicability.

Since the large deflection analysis is inherently nonlinear, the loads are not proportional to the displacements, thus excluding the use of superposition. The order of load application is important, and influence functions are not directly applicable. As the deformation occur, the dead load is present, but the live load will generally be applied on the deformed structure.

Empirical Assessment. The foregoing procedure can result in overly conservative results, indicating that considerable overstress can be caused by small deformations. This is contrary to the general experience that shows that considerable deformation can be tolerated with minor distress in a great number of cases. This has been demonstrated, for example, in buildings and is documented in the references mentioned at the beginning of this section. Field data indicate that framed building structures can withstand considerably greater differential settlement than would be inferred from structural analysis.

There is a tendency to extend this rationale to the settlement effects on bridges. Interestingly, a simplified analysis of a specific example will demonstrate this approach. Consider the tolerable distortion of a reinforced concrete deck in a two-span continuous bridge, and assume that the deck settles an amount δ relative to its ends. The bending stress induced in a simple rectangular reinforced concrete slab by this settlement can be expressed as

$$f_{\max} = \frac{\delta}{S}\left(\frac{3E}{2} \cdot \frac{t}{S}\right) \tag{3–34}$$

where f_{max} = maximum bending stress induced by settlement; δ = differential settlement between center pier and abutments; E = modulus of elasticity; t = thickness of deck; and S = span length.

To prevent cracking, the maximum tensile flexural stress should not exceed the tensile strength of the concrete, f_t. The requirement $f_{max} = f_t$ yields

$$\frac{\delta}{S} = \frac{2f_t S}{3Et} \tag{3–35}$$

The concrete has $f'_c = 4000$ lb/in^2, $E_c = 3.6 \times 10$ lb/in^2, and the S/t ratio is 24. The value of f_t is calculated as $7.5\sqrt{f'_c} = 475$ lb/in^2. For these parameters we calculate $\delta/S = 0.0021$.

This simplified analysis indicates that if the angular distortion reaches 0.0021, the consequences will be cracking in the concrete, and this is contrary to the conclusions drawn from field results.

Experience and field data show, therefore, that bridges can accommodate more settlement than traditionally allowed or anticipated in design. This behavior is accompanied by creep, relaxation, and some redistribution of force effects. The studies mentioned in this section have been used to arrive at a reasonable criterion for settlements and angular distortions expected to be tolerated. Lesser values may be introduced after consideration of (1) cost of mitigation, through increased foundations, realignment or overbuilding; (2) ridability; (3) aesthetics; and (4) safety.

3.13 DESIGN EXAMPLE 3–1, SETTLEMENT

Three-Span Continuous Bridge

Figure 3–24 shows a three-span continuous bridge with spans of 75, 120, and 75 feet. The structure has four supports: two abutments on spread footings, and two piers on piles. The objective is to estimate tolerable differential movement.

One approach is to use the criteria established by Moulton et al. (1985) regarding tolerable angular distortion. For a continuous bridge the maximum tolerable distortion is 0.004. If this is used as a basis for computing the maximum tolerable settlement, the shortest span governs. In this example the shortest span is the end span of 75 feet. Accordingly, the maximum tolerable differential settlement is

$$\delta = (0.004)\,(75) = 3.6 \text{ inches}$$

This is the maximum tolerable differential settlement over the length of the end spans.

Differential settlement can be calculated by structural analysis as the difference between the settlements at two adjacent locations, that is, the abutment and the pile foundation. This will involve consideration of soil properties, and solutions are demonstrated in subsequent sections. The difficulty of this approach is that calculations are associated with a level of uncertainty in estimating the real settlement for either the abutment or the pier foundation. Accordingly, the calculated value of the differential settlement, obtained as the difference between the abutment and pier settlement, has inherently the same level of accuracy or uncertainty. Furthermore, the actual differential settlement may exceed the calculated value (even if the settlement at the ends is computed with reasonable conservatism) merely because one support may settle less

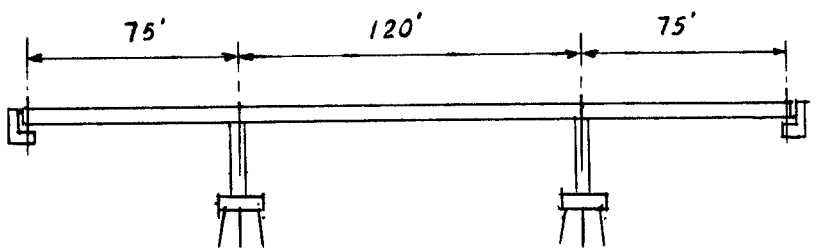

Figure 3–24 Three-span continuous bridge, design example.

than predicted while the other settles the estimated amount. Taking this possibility into account provides an upper limit of differential settlement.

The variability of settlement in two adjacent supports suggests the possibility of different scenarios of differential settlement between the same two points. A reasonable and generally accepted procedure is suggested by Duncan and Tan (1991), and requires the following steps: (1) Use conventional methods to compute the settlement of all foundations; (2) the settlement of any foundation in the same structure could be as large as the value calculated; and (3) assume that at the same time the settlement of the adjacent foundation could be zero.

Under these assumptions the probable maximum differential settlement is the largest settlement calculated for the foundation at either end of the span. This procedure is reflected in Figure 3–23, where maximum tolerable settlement is inferred directly from the value of maximum tolerable angular distortion.

The differential settlement thus obtained may be checked using the criteria of Table 3–6. These would indicate a tolerable differential settlement of the order of 4 inches. The two procedures give equivalent results for spans of 83 feet ($L = 400/48 = 83$ ft). For spans exceeding 83 feet, the 0.004 angular distortion controls, and for spans less than 83 feet the criteria of Table 3–6 control.

The maximum tolerable horizontal movement can be inferred from the data of Table 3–9. These indicate that the bridge could tolerate a horizontal movement of about 1.5 inches.

Three-Simple-Span Bridge

In this example we consider a bridge consisting of three simple spans, each 75 feet long. The bridge has two abutments in special footings and two piers supported on piles, as in Figure 3–24.

Using the Moulton et al. (1985) criteria for simple-span bridges, the angular distortion that this structure can tolerate is 0.008. For spans 75 feet long, this corresponds to a differential settlement

$$\delta = (0.008)\,(75) = 7.2 \text{ inches } (180 \text{ mm})$$

or almost 80 percent higher than the values shown in Table 3–6. Interestingly, a number of bridges surveyed by Bozozuk (1978), which were used to provide the data of Table 3–6, actually settled more than 8 inches without undergoing intolerable damage. A few of these bridges settled more than 1 foot without intolerable damage. Thus, while an 8-inch settlement in simple span bridges does not appear to be structurally critical, serviceability requirements related to ridability, aesthetics, and safety may be the governing considerations.

Settlement Beneficial to Structural Performance

The structure carrying Southwest Highway (Route 7) over B and O.C.T. Railroad, Melvina and Stony Creek was assessed (Xanthakos, 1981) for structural damage, rehabilitation, and remedial work. The bridge consists of 25 simply supported spans, generally 50 feet long, with an overall length approximately 1270 feet back-to-back of abutments. The substructure consists of reinforced concrete multicolumn rigid frame piers, except for one location where the pier is a steel bent encased in a concrete wall above ground

level. According to the original structure plans, all piers and abutments are supported on treated timber piles, ranging in capacity from 10 to 18 tons (see also section 12.10).

An extensive rehabilitation and retrofitting program was carried out as a result of this investigation, and is briefly mentioned in chapter 12. A structural consideration of obvious importance was the condition of the foundation. It appears that the intent of the initial design was to keep the tops of the timber piles below the groundwater table, and in this respect most piers have the bottom of their footings more than 10 feet below ground level.

From a detailed survey it became apparent that the bridge had settled nearly uniformly by almost 10 inches to 1 foot, following a gradual groundwater lowering and long-term consolidation. Several borings taken at critical substructure locations indicated that this consolidation resulted in considerable increase in soil strength, with a probable design soil pressure from 2 to 2.5 kips/ft^2 for a factor of safety between 2.5 and 3.0 (working stress method).

Thus, the analysis of the foundation stability included an estimation of the loads carried by the piles, with the bridge in its initial configuration and after rehabilitation and retrofitting. The adequacy of the foundation was also checked assuming that the piles had become severely damaged or completely inoperable, using an allowable pressure according to strength parameters obtained from the borings. The significant conclusion was that, in the event of complete pile failure (accepted as a precondition for assessing the structural capacity of the bridge), the footings could transfer the loads by direct bearing with an acceptable factor of safety.

3.14 CASE STUDY, FORCES INDUCED BY SETTLEMENT

Analytical Concepts

Bishara and Jang (1980) introduced a methodology whereby a reinforced concrete flexural member is idealized as a viscoelastic beam. Referring to Figure 3–25, showing an n-span continuous beam, we can write for elastic analysis

$$[M] = [k][\theta] + [q] \tag{3–36}$$

where $[M]$ = member force matrix; $[k]$ = element stiffness matrix, which is a diagonal matrix with individual stiffness matrices as its constituents; $[\theta]$ = element deformation matrix; and $[q]$ = total effect matrix with fixed-end moments. In this expression, $[M]$ and $[q]$ are constants, and E_c is replaced by the relaxation modulus $Y(t)$ so that $[\theta]$ is time dependent. The foregoing yield.

$$Y(t) = E_c/[1 + \alpha(t)] \tag{3–37}$$

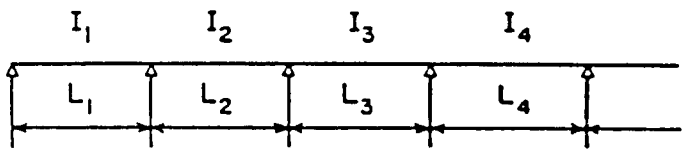

Figure 3–25 Continuous beam with n spans.

where $\alpha(t)$ = long time deflection multiplier. Long time deflections are caused principally by the effects of shrinkage and creep. Shrinkage causes stresses similar to those due to temperature changes, although these are not related to the effects of differential settlement. Hence, the latter are excluded so that the dominating factor in $\alpha(t)$ is creep. Solutions are given by Bishara and Jang (1980).

Settlement rate and induced forces. Predictions on the rate, type, and amount of settlement are discussed in subsequent sections, and are usually made considering the type of foundation and soil characteristics in soil-structure interaction analysis.

In this study, settlement-induced forces are articulated for continuous nonprestressed concrete bridges such as slab, T-girder, and box girder cast-in-place decks. For these bridge types either the interior or the exterior girders of the superstructure may be treated as continuous beams on simple supports because the relative stiffness of the column bent is small and should not affect the analysis. Referring to Fig. 3–25, if the beam undergoes a set of immediate foundation settlements $\Delta_1, \Delta_2, \ldots\ldots \Delta_{n+1}$ under supports 1 through $n+1$, we can write

$$[n] = [k][\theta] + [R] \tag{3–38}$$

where $[R]$ is a function depending on Δ_i, I_i, and E_c (Bishara and Jang, 1980).

If a set of settlements imposed at $t = 0$ are held constant, the displacements of all points and all strains are the same as in the corresponding elastic bean (Flügge, 1975). The stresses are derived from those of the elastic problem by multiplying by $Y(t)/E$ where E is the modulus of elasticity of the viscoelastic material.

We can now write

$$[M]^v = \frac{Y(t)}{E_c}[M]^e \tag{3–39}$$

where $[M]^e$ = elastic solution of the forces induced on the joints of the structure by a set of foundation settlements, and $[M]^v$ = corresponding viscoelastic solutions of settlement-induced forces, varying with time.

From elastic analysis, we obtain

$$M_i^e = \sum_{j=1}^{n+1} 6\, E_c \phi_j \Delta_j \tag{3–40}$$

where ϕ_j = constants in terms of stiffness of the superstructure, and Δ_j = foundation settlements. Thus, for the general case

$$M_{ij}^e = 6E_c\phi_j\Delta_j \tag{3–41}$$

and substituting (3–41) into (3–39) we obtain

$$M_{ij}^e = 6Y(t)\phi_j\Delta_j \tag{3–42}$$

where M_{ij}^e = elastic bending moment at *ith* support due to settlement at *jth* support.

The relaxation modulus $Y(t)$ can be expressed as

$$Y(t) = E_c\left[\frac{10 + (t - t_u)^{0.6}}{10 + W_u(t - t_u)^{0.6}}\right] \tag{3–43}$$

Combining Equations (3–42) and (3–43) gives

$$M_{ij}^{v} = 6E_c\phi_j\Delta_j\left[\frac{10+(t-t_u)^{0.6}}{10+W_u(t-t_u)^{0.6}}\right] \tag{3–44}$$

where

$$W_u = 1 + 1.25\,C_cK_rC_ut_u^{-0.118} \tag{3–45}$$

and C_c = ambient condition factor; K_r and C_u are constants; and t_u is an intermediate time between t_o and t.

The viscoelastic solution of settlement-induced forces may be derived by a numerical approach based on the concept of hereditary integral (Bishara and Jang, 1980).

Example

For the two-span continuous reinforced concrete girder bridge shown in Figure 3–26(a) the following data are given: Average I_{eff} = 789,610 in^4; concrete weight = normal and moist cured; f_c' = 3000 lb/in^2; f_y = 60,000 lb/in^2; date of falsework removal = 28 days after casting; C_c = 1.0; K_r = 0.80.

The elastic solution for Δ_1, Δ_2, and Δ_3 gives 2.0, 1.5, and 0.5 inches, respectively, and these values are summarized in Table 3–10. The force induction factors are estimated from a numerical analysis. The elastic moment is also shown.

Figure 3–26(b) shows the variation of M_2^v (viscoelastic moment at pier 2) with time. Evidently the rate of settlement of pier 2 influences markedly the determination of $M_2^v(t)$. Case A, where the rate of settlement is slower than in case B and C, results in a smaller value of M_2^v maximum (about 47 percent of M_2^e) at a longer time (390 days) after loading. This is explained by the slower rate of settlement for pier 2, allowing the settlement of abutments 1 and 3 to result in larger negative moments to counteract the positive moment induced by the settlement of pier 2, in addition to longer time of stress relaxation in the concrete in the superstructure.

Case B has a rate of settlement comparatively faster than case A, and shows a higher value of M_2^v maximum (about 80 percent of M_2^e) occurring 92 days after loading. Case C has a rate of settlement much faster than both cases A and B, and also compared to abutments 1 and 3. The maximum M_2^v in this case is close to 1.3 M_2^e.

3.15 DESIGN REQUIREMENTS FOR BRIDGES IN WATERWAYS

A general hydraulic analysis should consider, among other aspects, stream or waterway stability, bridge waterway requirements, and effects on bridge foundations.

Stream Stability

A study is generally necessary to evaluate the stability of the waterway and to assess the impact of construction. It should address the following:

1. Whether the stream reach is degrading, aggrading or in equilibrium.

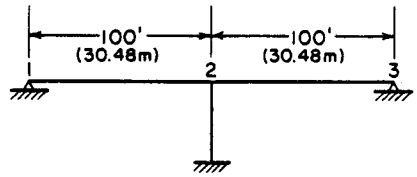

(a)

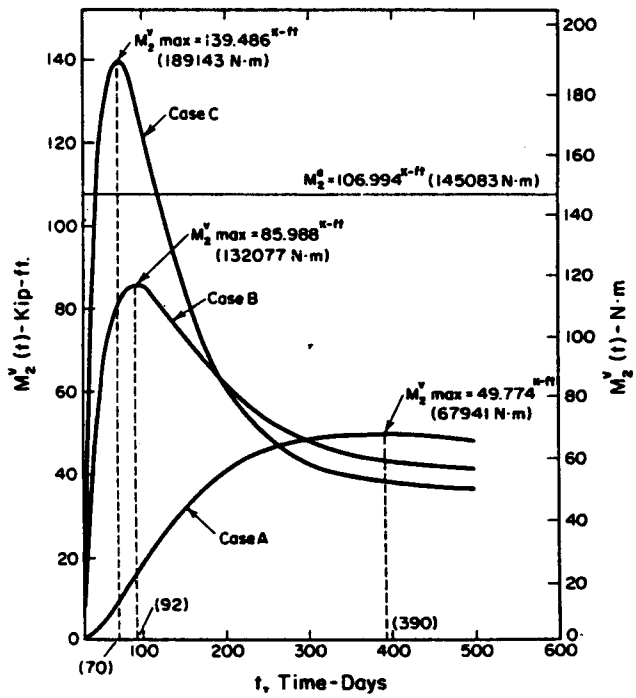

(b)

Figure 3–26 (a) Two-span reinforced concrete girder bridge; (b) variation of $M_2^v(t)$ with time.

2. Favorable crossing locations for the stream, considering the stream alignment and the need to protect the substructure and foundation from existing or anticipated future stream conditions.
3. The effect of natural geomorphic stream pattern changes on the proposed structure.
4. The effect of geomorphic changes on existing structures in the vicinity of the proposed bridge.

For unstable streams or flow conditions, special studies are warranted to assess the probable future changes to the stream's plan form and profile and to determine countermeasures to be included in the design.

Bridge Foundations

Several design concepts may be considered to reduce the exposure and vulnerability of a bridge to damage from scour and hydraulic loads. Suggested countermeasures are the following:

Table 3–10 Elastic Solutions for the Example of Figure 3–26

Δ_f, in inches (millimeters)	M_2^e, in kip-feet (Newton • meters)
2.0, 0, 0	–427.979
(51,0,0)	(–580,339.5)
0, 1.5, 0	641.969
(0, 38, 0)	(870, 509.9)
0, 0, 0.5	–106.996
(0, 0, 13)	(–145,086.6)
2.0, 1.5, 0.5	106.994
(51, 38, 13)	(145, 086.6)

(From Bishara and Jang, 1980)

1. Set bridge profile as high as practical for the given site conditions to minimize inundation by floods. Where bridges are expected to be subject to this effect, provide for overlapping of roadway approach sections and streamline the superstructure to minimize the area to be exposed to hydraulic loads, ice, debris and drifts.
2. Utilize relief bridges, guide banks, dikes, and other devices to reduce the turbulence and hydraulic effects on bridge substructures.
3. Select continuous span units, with the superstructures anchored to the substructures where hydraulic loads, buoyancy, ice, and debris impacts are expected, and provide an effective drainage system.
4. Where practical, limit the number of piers in the channel, streamline pier shapes, and align piers with the direction of flood flows. Avoid pier types that collect debris.
5. Locate abutments back from channel banks and where significant problems should not be anticipated.
6. Design piers on flood planes as river piers with foundations of the appropriate depth.
7. Use debris racks or ice booms to stop ice and debris before they reach the bridge substructure. Where significant ice and debris accumulation is unavoidable, it should be considered in determining foundation depths.

Bridge Scour

Statistically, a majority of bridges that have failed in the United States and elsewhere have failed because of scour. Three types of scour in a waterway are shown in Figure 3–27 (Sowers, 1962). The type of scour shown in (a) is due to the lateral shifting of the channel. Continuous scouring occurs at the outside of each bend in a meandering river because of higher velocity of the stream, whereas sedimentation takes place at the inside of each bend. The abutment close to the outside of a bend should be protected from undermining by the placement of concrete or asphaltic mats over the river bank. Alternatively, the abutment may be founded below the lower depth of possible scour.

The second case shown in Figure 3–27(b) is caused by river erosion occurring during periods of high flow. High-velocity flows remove bed materials so that the river bed is lowered. The scouring action is particularly severe if the width of the flow path is narrow. The normal scour generally is proportional to the rise of the water surface. Using

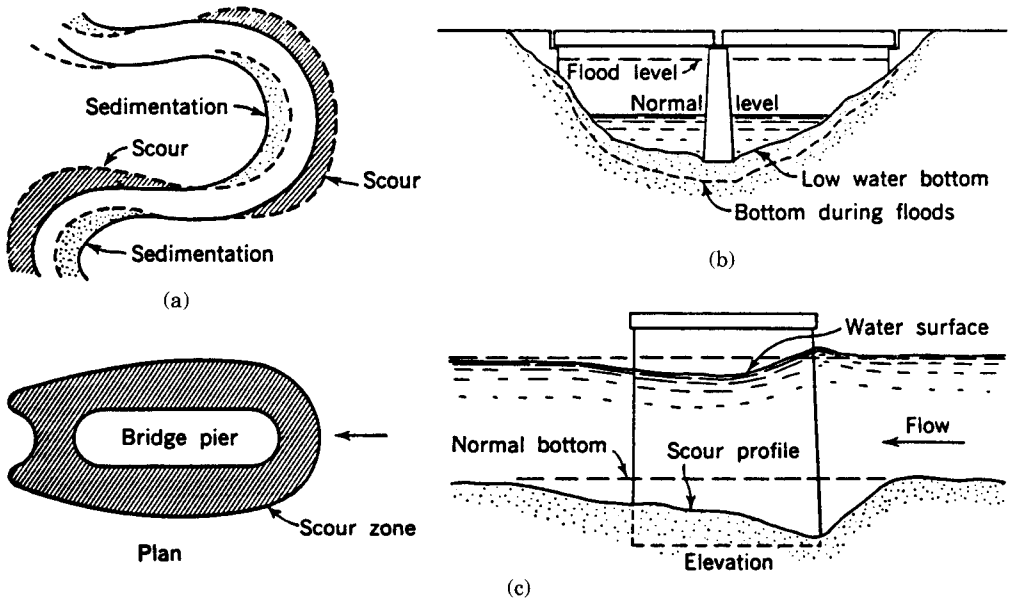

Figure 3–27 Forms of scour in rivers; (a) lateral shift of a stream caused by bank erosion and deposition; (b) normal bottom scour during floods; and (c) accelerated scour caused by a birdge pier *(from Sowers, 1962)*.

this as a criterion, the maximum scour depth may be estimated by observing the river bed during periods of high flow.

The third case of scour, shown in Figure 3–27(c), is a localized but accelerated scour that results from river obstructions such as bridge piers causing contraction of the channel cross section and generating higher flow velocities. The scour depth in this case depends on pier configuration and inclination with respect to flow, the contraction of the waterway, and the volume of debris that may be accumulated at the bridge.

The general approach to the scour problem involves certain simple design guidelines as follows:

1. Estimate the long-term channel plan form changes for the service life of the bridge.
2. Adjust existing channel and flood plain cross-sections upstream and downstream to reflect anticipated changes in channel profile and plan form.
3. Articulate the combination of existing or likely possible future conditions and flood events expected to result in the deepest scour for design purposes.
4. Determine the extent of contraction scour and local scour at piers and abutments.
5. Carry out a scour analysis considering the variable parameters, the available information, and past experience with existing structures during similar floods. Consider present and future flow patterns in conjunction with the presence of a bridge.

Where necessary, bridge modifications may include (1) relocation or redesign of piers and abutments to avoid areas of deep scour or overlapping scour holes from adja-

cent foundation elements; (2) addition of protective works to ensure smoother transition of flow and to control lateral movement of the channel; (3) enlargement of the waterway area; and (4) relocation of the crossing to a more desirable site. Scour is discussed also in subsequent sections in conjunction with particular bridge components, also in chapter 4 in connection with pier design in waterways, and in section 12.4 in connection with remedial and corrective measures taken to repair scour damage.

REFERENCES

AASHTO, 1994: AASHTO LRFD Bridge Design Specifications.

ALGERMISSEN, S. T., D. M. PERKINS, P. C. THENHAUS, S. L. HANSON, and B. L. BENDER, 1990: "Probabilistic Earthquake Acceleration and Value Maps for the United States and Puerto Rico," *Miscellaneous Field Studies,* Map MF-2120, U.S. Geological Survey, Reston, VA.

Applied Technology Council, 1978: "Tentative Provisions for the Development of Seismic Regulations for Buildings," ATC Report No. 3-06, Berkeley, CA., June.

BARBER, E. S., 1957: "Calculations of Maximum Pavement Temperature From Weather Reports," Bull. 168, Hwy. Research Board, pp. 1–8.

BASE, G. D., J. B., REED, A. W., BEEBY, and H. P. J., TAYLOR, 1966: "An Investigation of the Crack Control Characteristics of Various Types of Bar in Reinforced Concrete Beams," Research Report No. 18, *Cement and Concrete Association*, London, Dec.

BAZANT, Z. P. and F. H. WITTMAN, 1982: *Creep and Shrinkage in Concrete Structures,* Wiley, New York.

BEEBY, A. W., 1983: "Cracking Cover and Corrosion of Reinforcement," *Concrete International: Design and Construction*, vol. 5, No. 2, Feb., pp. 34–40.

BENNETT, W. B., J. M. HANSON, A. L. PARME, and J. A. SBAROUNIS, 1965: *Laboratory Investigation of Reinforced Concrete Beam-Column Connections Under Lateral Loads,* Chicago: Portland Cement Assoc., September.

BISHARA, A. G. and S. Z. JANG, 1980: "Settlement Induced Forces in Concrete Bridges," *J. Struct. Div., ASCE,* vol. 106, No. ST7, July, pp. 1423–1436.

BLUME, J. A., N. M. NEWMARK, and L. H. CORNING, 1961: *Design of Multistory Reinforced Concrete Buildings for Earthquake Motions*, Chicago, Portland Cement Association.

BOZOZUK, M., 1978: "Bridge Foundations Move," Transportation Research Record 678, *Tolerable Movements of Bridge Foundations, Sand Drains, K-Test, Slopes, and Culverts, Transportation Research Board,* Washington, D.C., pp. 17–21

Bridge and Structural Committee, 1977: *Japan Society of Civ. Eng.*, "Earthquake-Resistant Design of Bridges."

CHAPMAN, H. E., 1979: "An Overview of the State of Practice in Earthquake Resistant Design of Bridges in New Zealand," *Proc. of a Workshop on Earthquake Resistance of Highway Bridges,* Applied Technology Council, Berkeley, CA., January.

CLOUGH, R. W., 1966: "Effect of Stiffness Degradation on Earthquake Ductility Requirements," Report No. 66-16, Structural Engineering Laboratory, Oct., Berkeley, University of California.

COLLINS, M. P., and D. MITCHELL, 1991: "Prestressed Concrete Structures," Prentice Hall, Englewood Cliffs, N.J.

DUNCAN, J. M., and C. K. TAN, 1991: *Engineering Manual for Estimating Tolerable Movement of Bridges,* NCHRP 343, TRB, Washington, D.C.

EUBERG, M., and J. H. EMANUEL, 1967: "Thermal Movement of Bridges: A Survey," University of Missouri-Rolla, October.

ELLINGWOOD, B., T. V. GALAMBOS, J. G. MACGREGOR, and C. A. CORNELL, 1980: "Development of a Probability Based Load Criterion for American National Standard A58," NBS Special Publ. 577, National Bureau of Standards, U.S. Dept. Commerce, Washington, D.C.

EMANUEL, J. H., 1978: Discussion of "Survey of Bridge Movements in the Western United States," by J. L. Walkinshaw, Transportation Research Record 678, *Tolerable Movements of Bridge Foundations, Sand Drains, K-Test, Slopes, and Culverts*, Transportation Research Board, Washington, D.C., pp. 11–12.

EMERSON, M., 1979: "Bridge Temperatures for Settling Bearings and Expansion Joints," TRRL Suppl. Report 479, Dept. of Transport, Berkshire, England.

FLÜGGE, W., 1975: *Viscoelasticity,* Blaisdel, Waltham, Mass.

FUNG, G., R. F. LEBEAU, E. D. KLEIN, J. BELVEDERE, and A. G. GOLDSCHMIDT, 1971: "Field Investigation of Bridge Damage in the San Fernando Earthquake," *Bridge Dept., Div. of Highways, Calif. Dept. of Transportation*, Sacramento, CA.

GATES, J. H., 1979: "Factors Considered in the Development of the California Seismic Design Criterion for Bridges," *Proc. of a Workshop on Earthquake Resistance of Highway Bridges,* Applied Technology Council, Berkeley, CA., January.

GERGELY, P., and L. A. LUTZ, 1968: "Maximum Crack Width in Reinforced Concrete Flexural Members," *Causes, Mechanism and Control of Cracking in Concrete,* SP-20, American Concrete Institute, Detroit, pp. 87–117.

GHALI, A., and R. FAVRE, 1986: "Concrete Structures, Stresses and Deformations," Chapman Hall, London, Appendix A.

GRANT, R., J. T. CHRISTIAN, and E. H. VANMARCKE, 1972: *Differential Settlement of Buildings*, ASCE, J. Geotech. Div., Sept., pp. 973–991.

GROVER, R. A., 1978: "Movements of Bridge Abutments and Settlements of Approach Slabs in Ohio," Transportation Research Record 678, *Tolerable Movements of Bridge Foundations, Sand Drains, K-Test, Slopes, and Culverts, Transportation Research Board*, Washington, D.C., pp. 12–17.

HOUSER, G. W., 1956: *Limit Design of Structures to Resist Earthquakes,* Proc. 1st World Cong. on Earthquake Engineering.

JIRSA, J. O., 1979: "Applicability to Bridges of Experimental Seismic Test Results Performed on Subassemblages of Buildings," *Proc. of a Workshop on the Earthquake Resistance of Highway Bridges*, Applied Technology Council, Berkeley, CA., January.

JSCE, 1977: "Seismic Design Guidelines," *Japanese Society of Civil Engineers,* Toyoko, Japan.

KEENE, P., 1978: "Tolerable Movements of Bridge Foundations," Transportation Research Record 678, *Tolerable Movements of Bridge Foundations, Sand Drains, K-Test, Slopes, and Culverts*, Transportation Research Board, Washington, D.C., pp. 1–6.

MACGREGOR, J. G., 1976: "Safety and Limit States Design for Reinforced Concrete," *Canadian Journ. Civ. Eng.*, vol. 3, No. 4, Dec., pp. 484–513.

MAHER, D. R. H., 1970: "The Effects of Differential Temperature on Continuous Prestressed Concrete Bridges," *Civ. Eng. Trans.*, Instit. Engineers, vol, CE12, No. 1, Paper 2793, pp. 29–32. Australia.

MEYERHOF, G. G., 1984: "Safety Factors and Limit States Analysis in Geotechnical Engineering," *Canadian Geotechnical Journal,* Toronto, Ontario, Canada, vol. 21, pp. 1–7.

MOULTON, L. K., H. V. S. GANGARAO, and G. T. HALVORSEN, 1985: *Tolerable Movement Criteria for Highway Bridges,* Report No. FHWA-RD-85-107, Federal Highway Administration, Washington, D.C., p. 118.

NCHRP, 1985: "Thermal Effects in Concrete Bridge Superstructures," *NCHRP Report 276,* TRB, Washington, D.C.

PIANC, 1984: "Report of the International Commission for Improving the Design of Fender Systems," *Permanent International Association of Navigation Congress*, Brussels, Belgium.

Permanent International Association of Navigation Congresses (PIANC), 1984: "Report of the International Commission for Improving the Design of Fender Systems," Brussels, Belgium.

PRIESTLEY, M. J. N. and I. G. BUCKLE, 1979: "Ambient Thermal Response of Concrete Bridges," *Road Research Unit Bull. 42,* Bridge Seminar, vol. 2, Road Research Unit, New Zealand.

PRIESTLEY, M. J. N., and R. PARK, 1979: "Seismic Resistance of Reinforced Concrete Bridge Columns," *Proc. of a Workshop on the Earthquake Resistance of Highway Bridges*, Applied Technology Council, Berkeley, CA., January.

RUSCH, H. D. JUNGWIRTH and H. K. HILSDORT, 1983: *Creep and Shrinkage*, Springer Verlag, N.Y.

SAUL, R. and SVENSSON, H., 1980: "On the Theory of Ship Collision against Bridge Piers," *IABSE Proc.*, pp. 51–82.

SCHNABEL, P. B., J. LYSMER, and H. B. SEED, 1972: "SHAKE—A Computer Program for Earthquake Response Analysis of Horizontally Layered Sites," EERC Report No. 72-12, *Earthquake Engineering Research Center,* Univ. of California, Berkeley, CA.

SKEMPTON, A. W. 1951: *The Bearing Capacity of Clays,* Build. Res. Congr. Lond. pap. Div., L., pp. 18–189.

SKEMPTON, A. W., and D. H. MACDONALD, 1956: *The Allowable Settlement of Buildings*, Proc. Inst. Civ. Eng. Lond., vol. 5, pt. III.

SOWERS, G. F., 1962: *Shallow Foundations,* McGraw-Hill, N.Y.

STERMAC, A. G., 1978: Discussion of "Bridge Foundations Move," by M. Bozozuk, Transportation Research Record 678, *Tolerable Movements of Bridge Foundations, Sand Drains, K-Test, Slopes, and Culverts, Transportation Research Board*, Washington, D.C., pp. 17–21.

Structural Engineers Association of California, 1966: *Seismology Committee.* Recommended Lateral Force Requirements.

Structural Engineers Association of California, 1975: "Recommended Lateral Force Requirements and Commentary."

TERZAGHI, K., and R. B. PECK, 1967: *Soil Mechanics in Engineering Practice,* Sec. Ed., Wiley, New York.

WAHLS, H. E., 1990: "Design and Construction of Bridge Approaches," National Cooperative Highway Research Program Synthesis of Highway Practice 159, *Transportation Research Board,* National Research Council, Washington, D.C., 45 pages.

WALKINSHAW, J. L., 1978: "Survey of Bridge Movements in the Western United States," Transportation Research Record 678, *Tolerable Movements of Bridge Foundations, Sand Drains, K-Test, Slopes, and Culverts, Transportation Research Board*, Washington, D.C., pp. 6–11.

WHITE, D. W., and J. R. HAJJAR, 1991: *Application of Second-Order Elastic Analysis in LRFD, Research to Practice*, Eng. Journ., American Institute of Steel Construction, vol. 28, No. 4.

XANTHAKOS, P. P., 1981: "Investigation and Structural Report, Bridge Carrying Southwest Highway (Route 7) over B & O.C.T. RR, Melvina and Stony Creek," Chicago, Ill., Ill. DOT.

YOKEL, F. Y., 1990, "Proposed Design Criteria for Shallow Bridge Foundations", *Depart. of Commerce, National Inst. of Standards and Technology*, Gaithersburg, MD, p. 50.

ZUK, W., 1965: "Simplified Design Check of Thermal Stresses in Composite Highway Bridges," *Hwy. Research Record,* No. 103, pp. 10–13.

ZUK, W., 1965: "Thermal Behavior of Composite Bridges—Insulated and Uninsulated," *Hwy. Research Record,* No. 76, pp. 231–253.

CHAPTER 4

Piers for Conventional Bridges

4.1 PIER TYPES

The term "conventional bridges" as used here refers to the following bridge types: (1) all concrete slab bridges; (2) concrete deck bridges supported on multi-beam systems such as concrete beams and girders, box girders, prestressed concrete beams, steel beams and plate girders, steel box girders, orthotropic systems, and curved systems; (3) two-girder systems with floor beams and stringers, and double-truss bridges; and (4) bridges with similar configurations and structural systems, built across waterways and rivers. Excluded from the review are piers for arch bridges, towers for suspension bridges, piers for segmental bridges, piers for movable bridges, and towers for cable-stayed bridges, discussed in chapter 5. However, similarities in the structural action and analysis may exist and they are pointed out.

From these brief comments it follows that pier types may take the following forms and configurations:

1. Trapezoidal piers and hammerhead types shown in Figure 1–1, usually for bridges separating the grades of two intersecting highways and roads, or a highway and railroad.
2. Multicolumn piers with square or round columns and a pier cap, with similar functions as the piers shown in Figure 1–1.
3. Piers for waterway or river crossings, shown in Figure 1–2(a) and (b).
4. Piers consisting of a single shaft with a hammerhead or with the superstructure integrally connected, as shown in Figure 1–2(c).

5. High piers, usually built in river crossings where high vertical clearance is required, as shown in Figure 1–2(e).
6. Pile-bent piers (or trestles) for low and long crossings of waterways.
7. Single columns supporting one girder, or two individual columns supporting a two-girder or a double-truss system, with or without a common pier wall or footing.
8. Single columns supporting a cross girder into which the longitudinal main girders are framed.
9. Bents consisting of steel columns and transverse girders.
10. Bents with steel columns encased in concrete.

Any of the foregoing pier types is chosen based on functional, structural, and geometric requirements, and after a cost optimization in conjunction with a suitable superstructure type. In the context of analysis and design, the seeming multiplicity of pier forms and configurations is reduced and consolidated to the topics discussed in the following sections.

4.2 CRITERIA FOR PIER SELECTION

Quite frequently, pier types are mandated by state or local standards. Examples are the trapezoidal piers shown in Figure 1–1, and the typical multiple round-column piers with a cap. With multiple-column types, pier walls are usually required in river crossings and for substructures adjacent to railroads, where they serve as protection against impact and collision forces. A low pier wall is often recommended in conventional grade separations (see also Figure 1–1) as protection. A pier wall extended above the finish grade is also dictated in many cases as a means of reducing differential thermal expansion and contraction between the top cap and the base of the pier, which may induce considerable stresses in the columns, particularly with long piers in skew crossings. Useful guidelines for these pier types are given in section 1.2.

The solid wall pier shown in Figure 1–2 is essentially a gravity pier. This pier resists all forces to which it is subjected by its global mass. It is simple in design and construction and generally is used for low heights, usually 15 feet. For higher structures, the pier may be battered or converted into multiple columns above the base wall. Alternatively, the hammerhead type may be substituted for the solid pier. The structural action is the same as in the gravity pier, but the selection results in less concrete, and thus less weight on the foundation. The hammerhead type can be used favorably with multiple-beam superstructures, but is also suitable with superstructures consisting of two girders or two trusses, although in the latter case the cantilever moments and shear on the head are much higher.

When the economical height of single solid piers and hammerheads is exceeded, the design should consider the rigid frame pier shown in Figure 4–1. The rigid frame pier can satisfy stability by structural frame action. This type is found also suitable for superstructures of two girders or trusses, with the top of the columns centered under the bearings and the vertical geometry sloped or tapered to accommodate the desired footing dimensions. The legs may have constant thickness as shown in the side view of Figure 4–1, or a small batter if structurally necessary. One or more horizontal struts should be spaced to tie the columns and satisfy slenderness requirements. When several

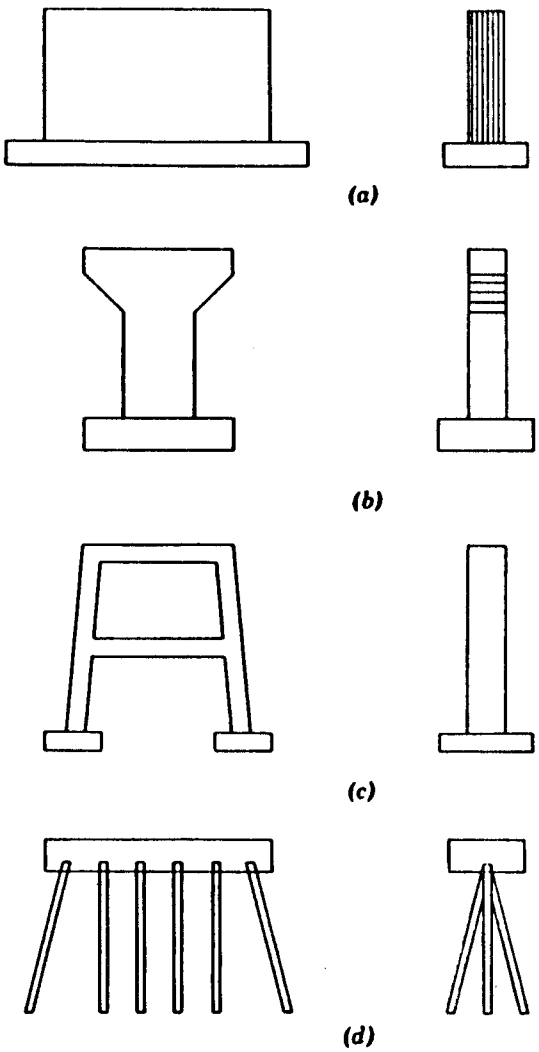

Figure 4.1 Common types of piers; (a) gravity pier; (b) hammerhead pier; (c) frame pier; (d) pile bent pier.

piers of varying height are present in a bridge, strut spacing and column sizes should be selected to provide uniformity of appearance.

Most pier shaft configurations have rectangular or circular shapes. Often, however, more unusual configurations are selected to satisfy aesthetic requirements. Examples are the Linn Cove Viaduct shown in Figure 4–2, and the CTA Englewood extension in Chicago where the piers have a diamond shape.

In river and waterway crossings, rectangular shafts are often modified with rounded ends to improve stream flow characteristics.

Pier footings can be proportional and designed as spread footings on firm soil or rock, or as members transferring the loads to piles, drilled shafts, and prismatic elements (see also chapters 8 through 11). The design of pier frames may be based on the assumed boundary conditions and may involve pin-ends, fixed ends, or partially restrained column bases.

Excepting cases where pier types and proportions are detailed by state policies and standards, the first step is to select piers that are the most likely to be suitable in terms

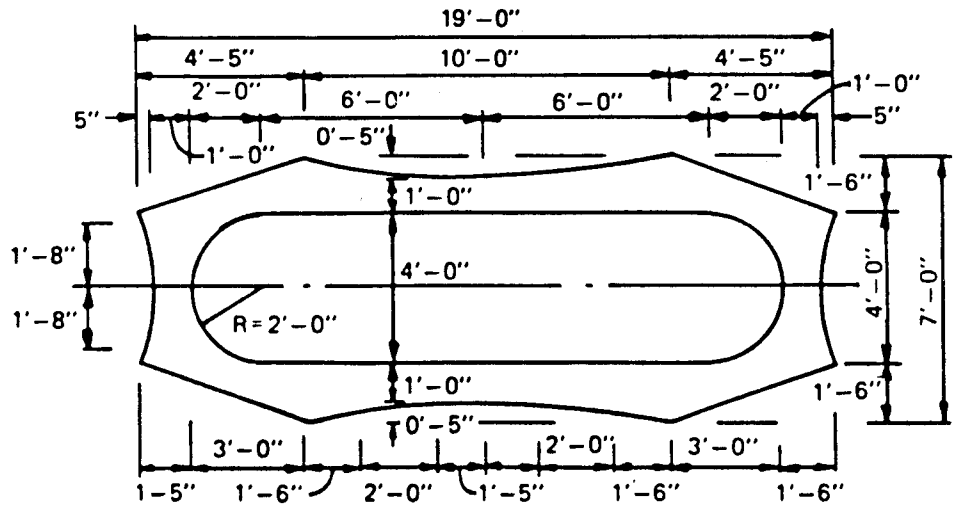

Figure 4–2 Pier section, Linn Cove Viaduct.

of economics and appearance. Soil and foundation conditions are most relevant to pier design, and often a determining factor in pier selection. Hence, before a pier design is undertaken, it is essential to have the results of a soil investigation. For long bridges, optimum location and pier type is routinely based on cost and structural optimization of superstructure and substructure analyzed as one unit. Further comments on pier functions and selection criteria are found in section 1.2.

4.3 LOADS AND MOMENTS ON PIERS: END CONDITIONS

Forces Acting on Vertical Supports

Piers are commonly subjected to forces and loads transmitted from the superstructure, and forces acting directly on the substructure. Forces and loads from the superstructure include

1. vertical reactions due to dead and live load;
2. dead load of the pier, which for high and solid piers may form a considerable part of the total load;
3. longitudinal forces (traction);
4. for curved bridges, centrifugal forces;
5. transverse and longitudinal wind acting on the superstructure and the live load; and
6. friction, manifested as a reaction to the longitudinal loads and thermal expansion effects.

Force effects may also be present because of shrinkage, creep, and settlement.

Forces acting directly on the substructure include wind, vessel collision impact, and water and ice loads. Of special concern are earthquake effects. A detailed descrip-

tion of these loads is given in sections 2.2 through 2.6. Piers may also be subjected to uplift because of the hydrostatic action of water.

The effect of temperature changes and shrinkage of the superstructure needs to be considered when the superstructure is rigidly connected with the supports. Where expansion bearings are used, forces caused by temperature changes to be provided for may not exceed the frictional resistance of the bearings.

Uplift due to hydrostatic pressure of the water should be taken into account only when its effect on the stability of the pier is unfavorable, but it should not be considered as a permanent effect that reduces the maximum foundation pressure or pile load. When conditions warrant, a proportion of the total hydrostatic pressure to be considered as active uplift may be determined from a rational analysis.

End Conditions

An important assumption to be made when analyzing a pier involves the degree of fixity for the foundation conditions. The same problem arises in the analysis of rigid frames, discussed in section 5.6, and several assumed conditions are shown in Figure 5–43. The literature contains limited information and data in determining end fixity and restraint. An exact analysis may be carried out, considering the soil type and stiffness, type of foundation, and soil-structure interaction. Such analysis is not warranted, however, and may give results as approximate as those obtained from simplified assumptions. Pier stiffness, as it relates to foundation stiffness, may be determined as suggested by FHWA (1969), summarized in Table 4–1.

For the usual pier types and foundation conditions, the following guidelines are recommended in lieu of a more elaborate analysis.

1. Piers on multiple rows of piles or on two or more rows of drilled shafts and prismatic elements may be considered to have a fixed base.
2. Piers on a single row of piles or drilled shafts may be considered as pinned at the pile connections to the footings.
3. Piers on spread footings with an allowable foundation pressure (ASD) of 3 to 6 tons/ft^2, may be assigned a 30 percent fixity at the bottom of the footing.
4. Piers on spread footing with an allowable foundation pressure (ASD) of 6 to 9 tons/ft^2, may be considered 40 percent fixed at the bottom of the footing.
5. Piers on spread footing with an allowable foundation pressure (ASD) of more than 9 tons/ft^2 (competent rock) may be considered 100 percent fixed at their bottom.

Table 4–1 Foundation Fixity Parameters

G_B	
1.5	Footing on rock anchored
3.0	Footing on rock not anchored
5.0	Footing on soil
1.0	Footing on piles (add 10 ft (3.05 m) to the effective length)

$$G_B = \frac{EI/L \text{ columns}}{EI/L \text{ members resisting column bending @ } B \text{ end of column}}$$

Hinge Details to Reduce Moment at Column Bases

The degree of fixity at the base of a column is particularly critical in seismic regions where columns must be designed to withstand the plastic hinge moments that develop at their base. Various hinge details for column bases have been proposed, with the inherent basic concept being to provide a reduced moment capacity in the plastic hinging regions. A usual procedure is to place a layer of easily compressed material at the base to introduce a partial discontinuity between the column and the footing or pier wall. This discontinuity results in a smaller cross section at the base, and hence a reduced hinge capacity.

Lim, McLean, and Henley (1989) have provided results of experimental investigations on small-scale specimens, with different moment-reducing hinge details, subjected to increasing levels of cycled inelastic displacements under constant axial load and deflected in single curvature.

Hinge details. Figure 4–3 shows hinge details investigated in this program. The detail marked CA is a hinge providing only horizontal discontinuity. The detail marked WA incorporated both vertical and horizontal discontinuity. These discontinuities are ensured by a layer of easily compressed material at the base of the column. Because only horizontal discontinuity is provided in detail CA, the plastic hinging action in the column will be largely concentrated along a horizontal plane at the interface between the column and the footing. The presence of both horizontal and vertical discontinuity in detail WA has the result of distributing the plastic stresses over a greater vertical section at the base.

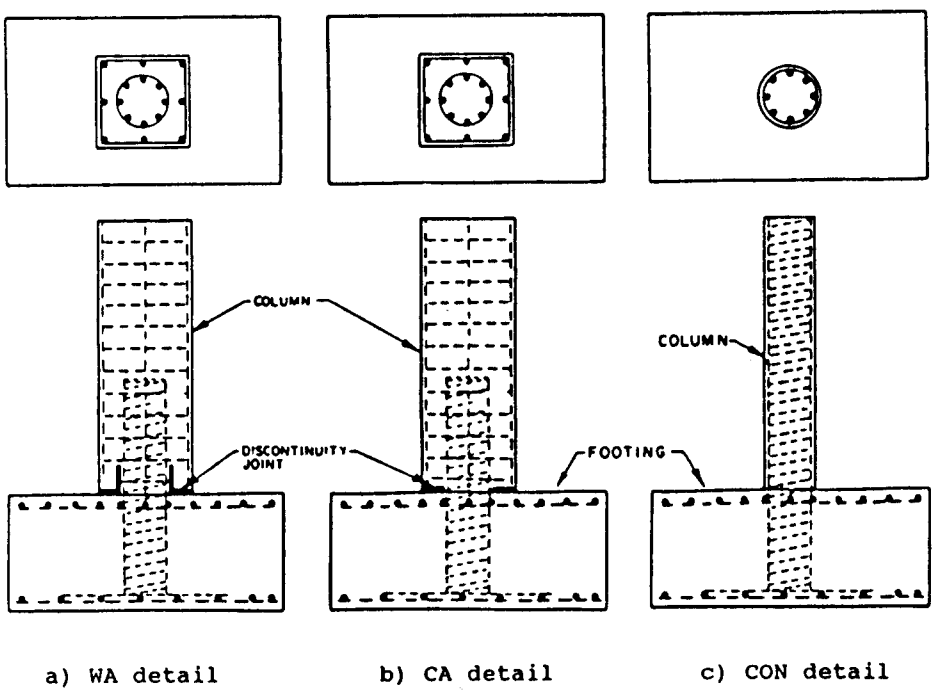

Figure 4–3 Hinge details investigated.

The column detail marked CON in Figure 4–3 has the same dimensions and reinforcement as the first two details but no joint discontinuity. Dimensions and reinforcement for a typical column specimen are shown in Figure 4–4.

The column height-to-width ratio of these specimens is 1.25 and 2.5, hence these are short columns. Two levels of axial compression were applied: $P/(f'_c A_c) = 0.24$ and 0.35 where A_c is the cross-sectional area of the column measured out-to-out of the spiral. A hinge longitudinal reinforcing ratio of 7.2 percent and a hinge spiral reinforcing ratio of 1.5 percent referenced to the area of the hinge connection were used in all specimens.

The thickness of the horizontal discontinuity is 0.5 inch, and for the WA detail the vertical discontinuity joint is 6 inches high. Following results from small-scale tests, the horizontal joint thickness was increased to 1 inch at the outer edges of the column to allow hinge rotation without contact between column and footing. A summary of the specimen details is given in Table 4–2, together with test results and relevant data.

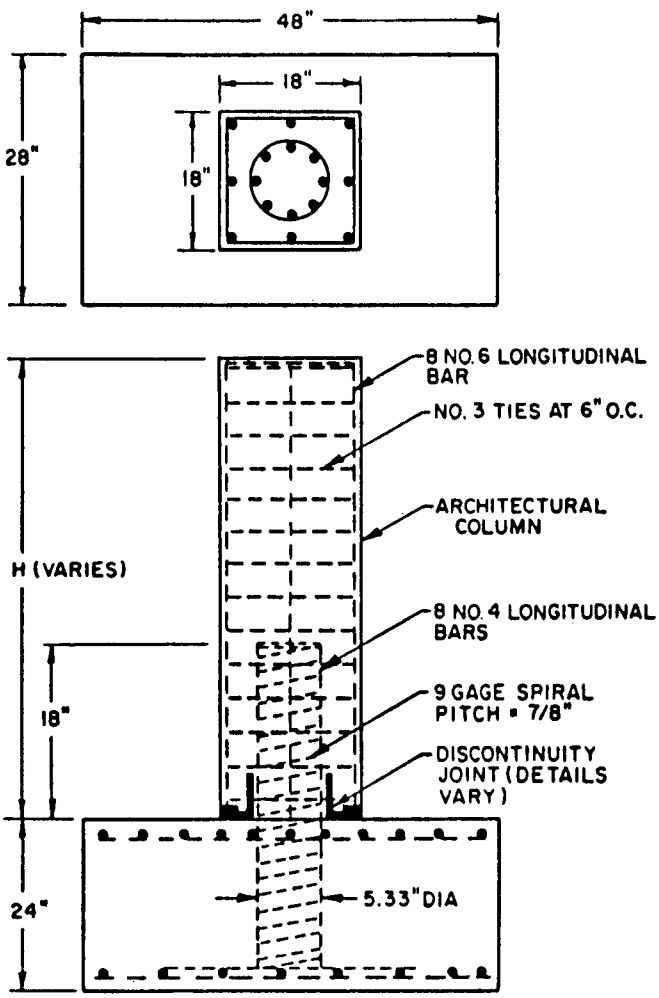

Figure 4–4 Typical dimensions and reinforcement of the column specimens.

Table 4–2 Summary of the Testing Program

Specimen No.	Variable Studied	Aspect Ratio (H/D)	Axial Load (P/f'_cA_c)	Yield Displacement (in.)	Measured Yield Moment (in.-kips)	Measured Peak Moment (in.-kips)	Maximum Applied Shear Load (kips)
CA1	aspect ratio	2.50	0.24	0.30	181	270	6.0
WA1	"	2.50	0.24	0.30	133	212	4.7
CON2	hinge detail	*	0.24	0.15	93	209	9.3
CA2	"	1.25	0.24	0.15	162	279	12.4
WA2	"	1.25	0.24	0.15	142	250	11.1
CA3	axial load	1.25	0.35	0.15	166	277	12.3
WA3	"	1.25	0.35	0.15	135	240	10.7
CA4	low-cycle fatigue	1.25	0.24	0.15	138	271	12.0
WA4	"	1.25	0.24	0.15	130	236	10.5

*circular control column with the same height as Units CA2 and WA2

Test results. Column performance is evaluated with respect to the moment capacity and displacement ductility, overall hysteresis behavior, and degradation and energy dissipation characteristics.

Figure 4–5 shows the plots of the shear strength envelope curves, obtained by plotting the maximum shear force attained at each peak displacemening level with respect to the same displacement. Unit WA2, CA2, and CON2, corresponding to the details of Figure 4–3, are subjected to an axial load of $0.24\ f'_cA_c$, and have an aspect ratio of 1.25. The hysteresis curves for all three specimens show excellent stability even at displacement levels of $\mu = 12$. No evidence of any sudden drop is observed, and the plastic hinges continue to absorb energy.

From Figure 4–5 it is evident that unit CA2 exhibits the greatest stiffness and

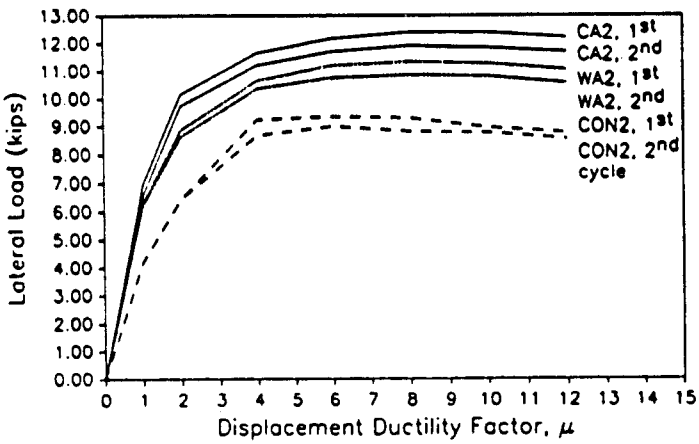

Figure 4–5 Shear strength envelope curves for Units CON2, WA2, and CA2.

unit CON2 the least stiffness. Some degradation can be seen in unit CON2 beginning after $\mu = 4$. The difference in stiffness between these specimens may be attributed to two reasons. First, the elastic stiffness of the control column is less than that in the architectural column with the moment-reducing details. Second, the moment-reducing details may have the effect of "pinching" the rebar crossing the interface between the column and the footing, thereby introducing larger strains in the longitudinal reinforcement of the moment-reducing details.

Effect of column aspect ratio. The effect of the column aspect ratio on the behavior of the modified hinges is shown in Figures 4–6 and 4–7, showing hysteresis for units WA1 and CA1 (aspect ratio 2.5), respectively. These results are compared with hysteresis curves for units WA2 and CA2 (aspect ratio 1.25). The hysteresis curves for specimens with higher aspect ratios are essentially similar to those for shorter specimens, indicating that flexure dominates behavior in both cases. However, the curves for unit WA1 are somewhat narrower than for unit CA1, meaning decreased energy dissipation characteristics in the column with the CA detail.

Effect of axial load level. Units WA2 and CA2, and units WA3 and CA3, were tested with axial load levels of $0.24\ f'_cA_c$ and $0.35\ f'_cA_c$, respectively. The results show that there is only a small difference between the behavior of specimens with the WA detail and virtually no difference in the curves for the specimens with the CA detail for the two different load levels.

The shear strength envelope curves for units WA2 and WA3 and units CA2 and

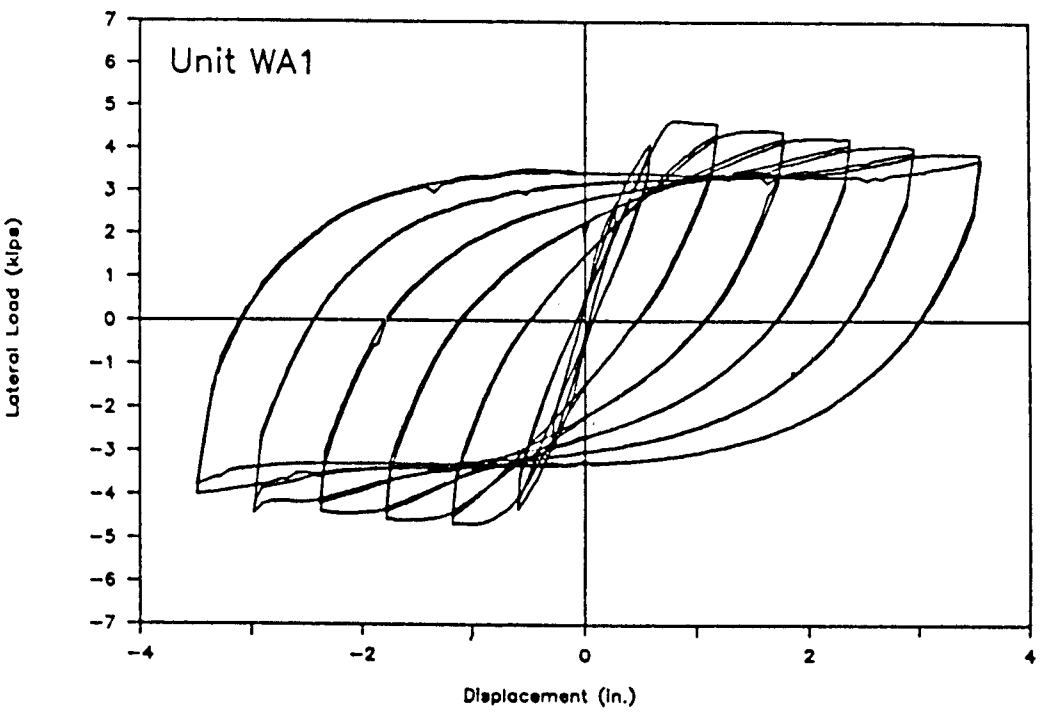

Figure 4–6 Lateral load-displacement hysteresis curves for Unit WA1.

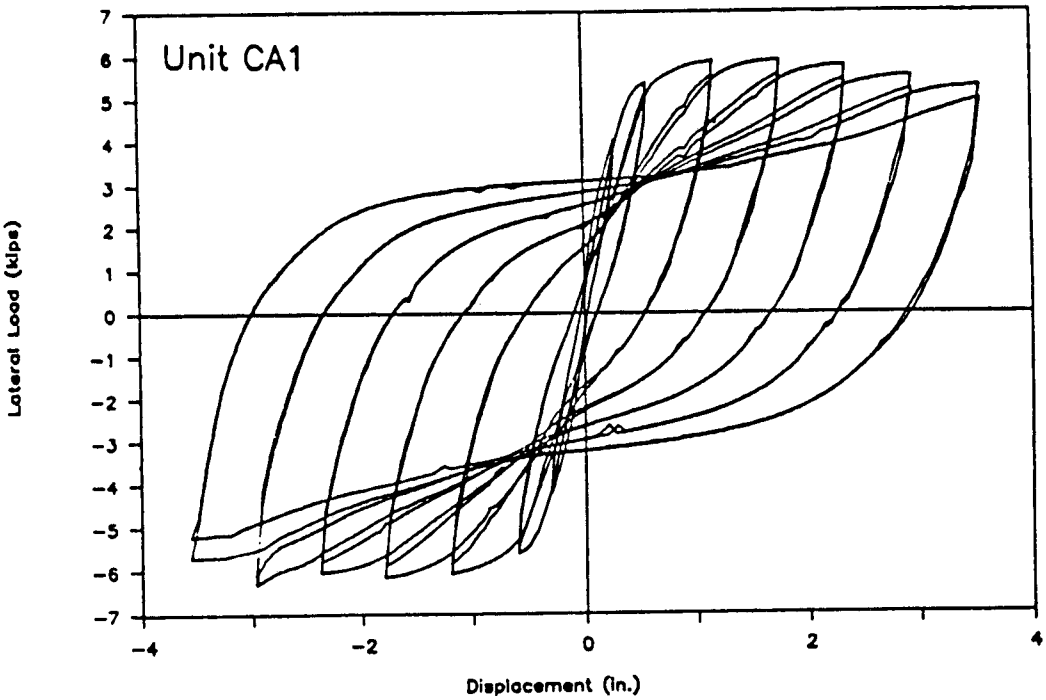

Figure 4–7 Lateral load-displacement hysteresis curves for Unit CA1.

CA3 are shown in Figures 4–8 and 4–9, respectively. For the columns with the WA detail, the larger load results in a greater drop in strength. For the columns with the CA detail, the axial load seems to have little effect on strength. The reason that these columns are almost unaffected by the axial load level may be the considerable confining effect provided around the hinge region by the outer architectural detail, particularly with the CA detail.

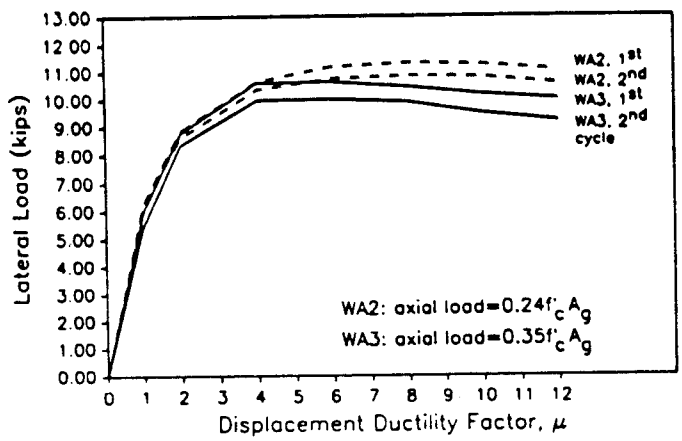

Figure 4–8 Shear strength envelope curves for Units WA2 and WA3.

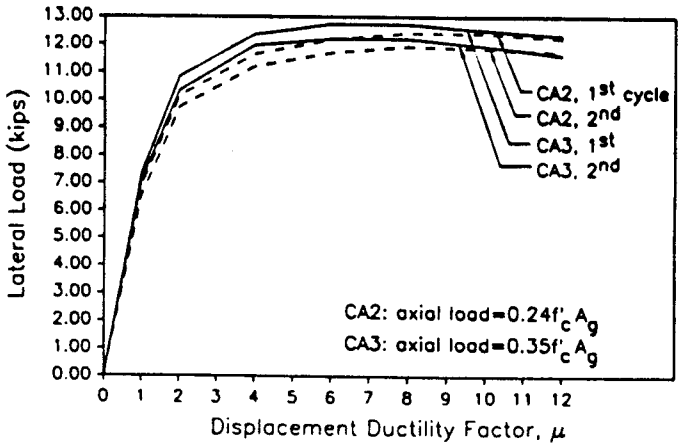

Figure 4–9 Shear strength envelope curves for Units CA2 and CA3.

Effect of low-cycle fatigue. Units WA4 and CA4 (see also Table 4–2) were tested to evaluate the low-cycle fatigue characteristics of the moment reducing hinge detail. Both units were cycled to a displacement level of $\mu = 10$ and then subjected to multiple cycles at this displacement level. The hysteresis curves for these units show that very little degradation occurred after the completion of the second cycle at $\mu = 10$. The hinges continued to exhibit stable plastic behavior even after being cycled up to sixteen times at this displacement level.

Repeatability of results. Units WA4 and CA4 were constructed to be identical with units CA2 and WA2. The two sets of columns were also loaded identically through two cycles of loads to the displacement ductility level of $\mu = 10$. Comparison of the results provides a measure of repeatability in behavior. The shear strength envelope curves for units WA2 and WA4 and units CA2 and CA4 are shown in Figures 4–10 and 4–11, respectively. These curves show close agreement between the two sets.

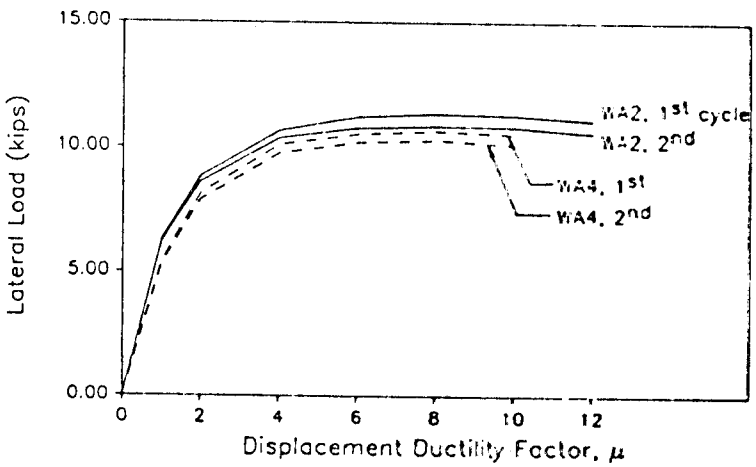

Figure 4–10 Shear strength envelope curves for Units WA2 and WA4.

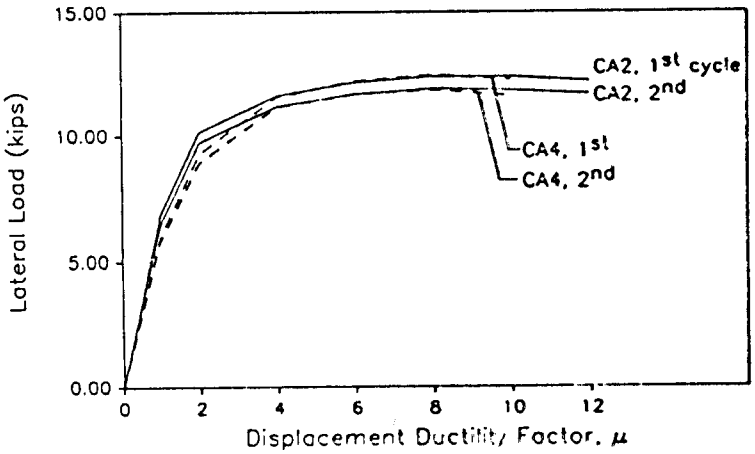

Figure 4–11 Shear strength envelope curves for Units CA2 and CA4.

Comparison of energy dissipation characteristics. The energy dissipated by a column by a particular load cycle is represented by the area enclosed by the load-displacement hysteresis curve. The energy dissipated by a perfectly elastoplastic system during a complete displacement cycle is the area of parallelogram BCDE in Figure 4–12. For a given displacement ductility factor μ, the ideal plastic energy E_p dissipated in the processes can be computed as

$$E_p = 4\,(\mu - 1)V_p\,\Delta_y \tag{4–1}$$

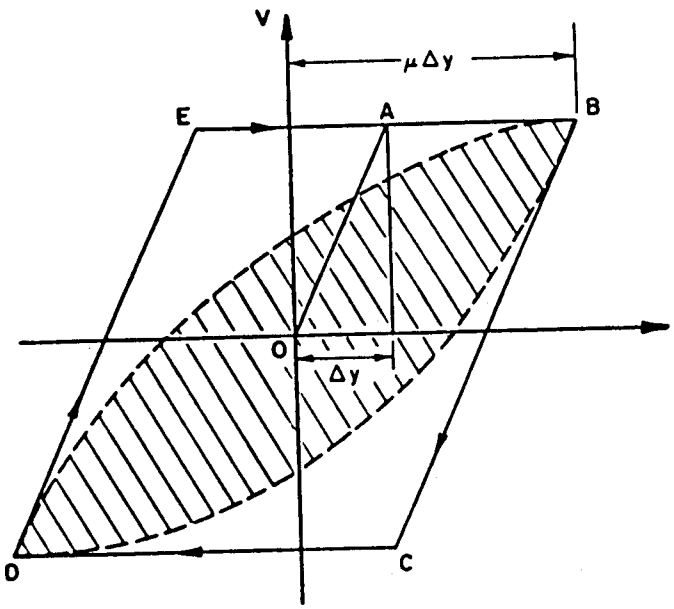

Figure 4–12 Actual and idealized perfectly elastoplastic hysteresis curves.

where V_p is the maximum shear force attained at the corresponding displacement level (Ang, Priestley, and Pouley, 1985).

The energy dissipation capability of the various hinge details may be expressed quantitatively by dividing the measured energy dissipation by the E_p value of the column for the same displacement ductility factor. This ratio is referred to as the relative energy dissipation index. Plots of the E/E_p ratio versus the displacement ductility factor μ for units WA2, CA2, and CON2 are shown in Figure 4–13. The low value of E/E_p at $\mu = 2$ and $\mu = 4$ for the control column (CON2) are probably attributed to the inexactness in defining the actual yield displacement in the different columns, with the result that the response of unit CON2 is still largely elastic at these displacement levels. From Figure 4–13 it is evident that the energy dissipation effectiveness is greater for unit CON2 and the least for unit CA2. The reduced effectiveness in columns with moment-reducing details may be explained by the confinement of the plastic action (i.e., length reduction over which the plastic hinge is developing) at the base of the column, particularly for the CA detail.

Conclusions. Lim, McLean, and Henley (1989) summarize the following conclusions:

1. When subjected to cycled inelastic displacement under constant axial load, columns with moment-reducing plastic hinge details (WA or CA) display a hinge behavior essentially similar to that of an unmodified column with the same dimension and reinforcement.
2. Columns with the CA detail develop larger strains in the longitudinal bars for the same level of displacement than do columns with the WA detail or the unmodified (control) detail. Also, columns with the CA detail have lower energy dissipation effectiveness compared with columns with other details.
3. Flexure dominates the behavior of all columns, including those with aspect ratio of 1.25. The lower aspect ratio, however, results in a larger drop of strength between the first and second cycle of loading in the column with the WA detail.
4. Increasing the axial load by 50 percent results in a slightly larger degradation of

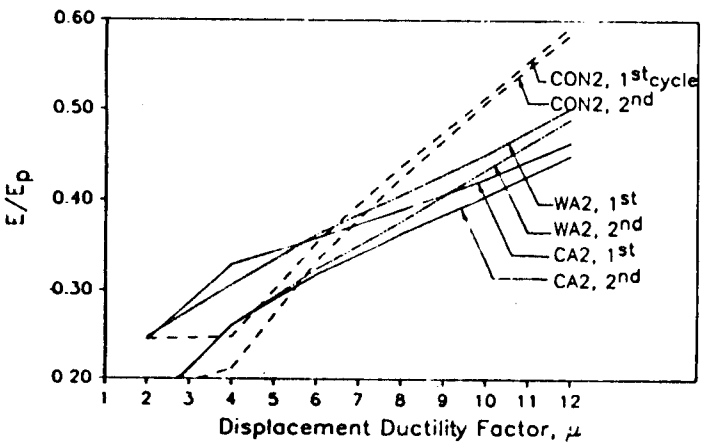

Figure 4–13 Relative energy dissipation index curves for Units CON2, WA2, and CA2.

shear strength in columns with the WA detail, whereas columns with the CA detail are unaffected by the increased axial load. The absence of the effect is attributed to the confinement around the hinge provided by the outer architectural column.

5. In the low-cycle fatigue tests, no evidence of distress was detected in columns with WA or CA detail when units were cycled up to 16 times at a displacement level of $\mu = 10$.

Restraint at Pier or Column Top

The top of a pier or column may be restrained by: (1) attachment to the superstructure whereby the pier responds consistently to the deformation of the superstructure in the direction of the bridge (any rotation of the superstructure is transmitted to the top of the pier); (2) by rigid-frame action (multiple-column pier) between columns and pier cap in the direction of the pier; and (3) by restraint against movement induced by the presence of fixed bearings or by frictional forces at expansion bearings. The first two effects involve a structural interaction discussed in some detail in the following sections. The last effect is related to the action of bearings, and a brief review is presented in this section.

Basic types of bearings. Bearing types and design requirements are reviewed by Xanthakos (1994), and include the provision of the standard AASHTO specifications and the proposed LRFD guidelines.

Essentially, bridge bearings are mechanical devices that transmit the loads to substructure elements. Bearings must also provide for expansion of the superstructure. The four basic types of bearings are (1) fixed bearings; (2) hinged bearings; (3) sliding or expansion bearings; and (4) hinged, linked, and roller-jointed devices. A fixed-end bearing is an attachment that can supply a vertical and a horizontal reaction plus a restraining moment. Considering the expense of fixing a heavy steel member at the ends, such a bearing is not usually considered practical for bridges. A hinged bearing permits rotation of the ends of the member, and this is usually accomplished by a pin. Hinges carrying heavy vertical loads are normally provided with lubrication systems to reduce friction and ensure free rotation without excessive wearing.

Expansion bearings permit rotation as well as movement of the superstructure resulting from temperature change, shrinkage, and deflection. These articulations are usually provided in two forms: the sliding joint and the roller joint. With the introduction of new materials and fabrication methods, sliding joints can accommodate longer spans and heavier loads. Devices classified as expansion generally induce only friction or longitudinal shear from the movement of the bearing during longitudinal expansion and contraction, but occasionally must also transmit lateral thrust in the transverse direction between the superstructure and the substructure.

A combination of hinge and roller bearing accommodates a normal reaction but without lateral restraint. The hinge permits rotation and the roller allows expansion. For articulations within a truss or a heavy girder, hinges are provided by a pin or a link with two pins. A pin permits rotational movement and also transmits horizontal and vertical reactions. A link transmits force only along its length and thus controls the direction of the reaction.

The span beyond which the simple bearing plate is unsatisfactory is largely a mat-

ter of judgment and experience. Most guidelines allow bridges with spans less than 50 feet to be designed without provisions for deflection, arranged merely to slide upon metal plates with smooth surfaces. Curved sliding surfaces (spherical bearings) accommodate deflection and rotation in the longitudinal and transverse direction. These devices usually consist of two metal parts with matching curved surfaces and a low-friction sliding interface.

In general, bearings should be designed to provide sufficient restraint to maintain the stability of the superstructure. The location of fixed and expansion piers and abutments is a matter of overall bridge design, and relates to the type of superstructure, the rigidity of substructure elements, stiffness of the foundation system, and the requirements for horizontal thermal movement.

The dependence of load magnitude and distribution on the bearing type is demonstrated in section 2.7, and a typical example is the bridge configuration shown in Figure 2–13. Furthermore, any horizontal movement of the superstructure will be opposed up to the resistance offered by the bearings and the rigidity or flexural resistance of substructure elements. Thus, an expansion bearing will restrain movement up to the point where its friction is overcome, and a fixed superstructure-substructure attachment will have minimum effects on superstructure movement if the supports consist of very slender columns that can deflect and move with the thermal expansion and contraction of the deck. An example of the influence of the support details is shown in Figure 2–14.

The distribution of longitudinal forces to fixed and expansion bearing is discussed in section 2.8, together with the distribution modes commonly assumed.

4.4 EFFECT OF TEMPERATURE CHANGE AND SHRINKAGE

General Principles

In section 2.7, it was pointed out that bridge movement may arise from a number of different causes, but thermal movement is of prime concern. In addition, when horizontal movement at the ends of a superstructure is caused by volumetric changes, the forces generated within the structure in response to these changes must be balanced. The neutral point (zero movement) may be determined by computing these forces, taking into account the relative resistance of bearings and substructure to movement.

Consider, for example, the five-span bridge shown in Figure 4–14, where substructure and superstructure are rigidly connected. Expansion and contraction due to thermal changes will produce moments in all members of the frame. Shrinkage may be considered together with temperature fall because their effects are similar. However, temperature changes produce moments in a frame only when they cause either horizon-

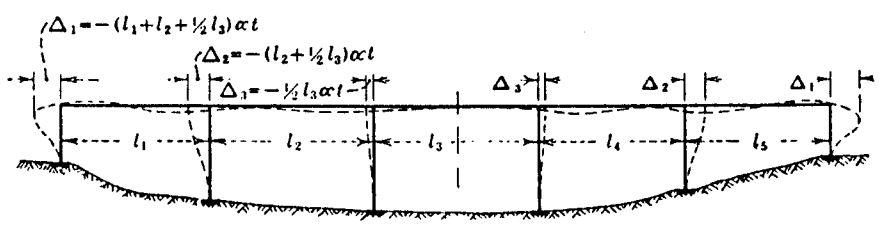

Figure 4–14 Movements of column heads due to rise of temperature.

tal or vertical movements of its column heads while at the same time the bottoms of the vertical members remain stationary. To simplify the analysis, the effects of horizontal and vertical movement of column heads are considered separately. The problem of determining thermal effects is then reduced to finding the magnitude of movement for each column head, and determining moments in the frame corresponding to those movements.

Horizontal movement. The extent of horizontal movement of column heads due to temperature changes depends not only on the number, length, and disposition of spans, but also on the end conditions to the extent they may affect expansion or contraction.

When conditions at both ends are the same, a symmetrical frame will extend and contract symmetrically on both sides of its line of symmetry, also referred to as the line of zero movement. Referring to Figure 4–14, the movement Δ_l of any column head at distance l from the line of zero movement is simply $\Delta_l = \alpha + l$ where α is the coefficient of thermal expansion and t is the temperature change.

The dash lines in Figure 4–14 show the exaggerated deflection of the frame after expansion. Columns 1, 2, and 3 move to the left, while columns 4, 5, and 6 move to the right. The movement Δ_3 of column 3 is due to the expansion of one-half of the center span l_3, and the movement of column head 1 (end support) is due to the expansion of two and one-half spans. For temperature fall and shrinkage the movement is reversed.

For unsymmetrical frames, the position of the point from which expansion or contraction begins must be determined from an analysis of the rigidity of both ends of the frame. A reasonable assumption is that the location of the point of zero movement is such that the work required to move the column heads at either end is the same. The problem becomes, however, more complicated when the end conditions are different (for example, one abutment is firmly placed against rigid embankment while the other end is free to move). In this case, it may be necessary to assume that one end is completely restrained, and expansion will take place only in the direction of the free end.

Vertical movement. Likewise, under the effect of temperature changes, the whole frame moves bodily up and down. When the height (length) of all vertical members is the same, the vertical movement of the column heads is the same, and no moments are induced. For unequal column height, the longer columns have larger head movement vertically, and the result is bending moments induced in a manner similar to the effect of differential foundation settlement.

Actual versus theoretical movement. Fall of temperature causes opening of construction joints and produces a number of incipient cracks distributed along the length of the member. Hence, the final movement of the column head is reduced by the aggregate width of the cracks, resulting in actual moments less than those computed.

The expansion of a bridge structure may be affected by the end conditions. If the bridge frame is connected at the end with abutment walls subjected to earth pressures, active or passive pressure may prevent the expansion, partly or wholly. Temperature rise will induce compressive stresses that must be resisted by the horizontal members in addition to the flexural stresses caused by vertical loads. These effects influence the final moments at the column heads, but the actual solution is a highly indeterminate problem.

A usual procedure for estimating the effect of temperature changes involves the following steps:

1. Establish the temperature variation from relevant specifications.
2. Compute the horizontal movement of each column head, based on the actual point of zero movement.
3. Analyze the effect of a condition whereby only one head moves horizontally while all other column heads remain stationary. There will be as many moment diagrams produced in this manner as there are columns in the frame whose heads have moved.
4. Combine the moment diagrams for all the individual movements of column heads, to obtain a composite diagram which represents the total effect of all movements.

With suitable software programs the foregoing steps can be consolidated into one routine analysis.

Example

Figure 4–15 shows an elevation of a two-span bridge designed and constructed as a rigid frame. The assumed range of temperature changes to be provided for is ± 30°F. Shrinkage may be expressed by a temperature fall of 15°, so that the effect of temperature fall plus shrinkage is 45°F.

The coefficient of expansion is $\alpha = 0.000006$ per degree F. The concrete strength is $f'_c = 3500$ lb/in^2, so that $E_c = 57{,}000\sqrt{f'_c} = 3{,}375{,}000$ lb/in^2. Because of symmetry, the center column head remains stationary during expansion and contraction of the bridge frame. For a fall of temperature of 45°, each end column moves toward the center column by an amount

$$\Delta_l = (0.000006)(45)(80) = 0.022 \text{ ft}$$

From reference to Figure 4–15, the following are also given:

$$h_1 = 24.0 \text{ ft and } I_h = 12.0 \text{ ft}^4 \text{ (moment of inertia of column)}$$

Next, we compute the term

$$\frac{6E_cI_h\Delta_l}{h_1^2} = \frac{(6)(144)(3{,}375{,}000)(12)(0.022)}{24^2} = 1{,}336{,}000 \text{ ft-lb}$$

With this term computed, the moments at the top and bottom of the column may be determined by deflection theories and moment distribution or by appropriate formulas.

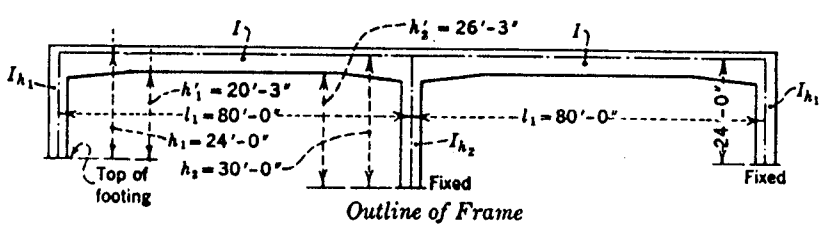

Figure 4–15 Elevation of bridge for design example.

The moment at the top is computed as M_T = 806 ft-kips. Likewise, the moment at the bottom is M_B = 1031 ft-kips. There is also a horizontal thrust at each end column producing direct tension in the horizontal member that must be resisted by additional longitudinal reinforcement.

For a rise of temperature, the signs of the bending moments are opposite to those for the fall of temperature. The moment values obtained previously are simply multiplied by the ratio 30/45 = 0.67. Appropriate formulas for computing moments directly will be found in Taylor, Thomson, and Smulski (1958) or PCA (Continuous Concrete Bridges, Second Edition).

4.5 SEISMIC DESIGN CONSIDERATIONS FOR PIERS AND COLUMNS

Design Forces for Seismic Performance Category C and D

In Article 4.8.2, AASHTO stipulates the forces resulting from plastic hinging at the top or bottom of a column, and presents two procedures. One is for a single column hinging about its two principal axes, generally applicable for piers and bents acting as single columns. The other procedure is for a multiple column bent in the plane of the bent. The forces are determined according to the potential overstrength capacity of the material, and to be valid the design details must be developed as specified in Section 7 and 8 so that plastic hinging of the column can occur. The overstrength capacity follows actual material strength (steel yield strength, concrete compressive strength) being greater than the minimum specified, a situation that must be accounted for when forces generated by yielding of the column are used as design forces.

The shear mode of failure in a column or pile bent is likely to result in a partial or total collapse of the structure, requiring the design force to be calculated conservatively, including potential locations of plastic hinges. For flared columns, these may occur at the top or bottom of the flare. For multiple column bents with a partial-height wall, the plastic hinges will probably appear at the top of the wall unless the wall is structurally separated from the columns.

For columns connected to deeply embedded foundations, plastic hinges may develop above the foundation mat or pile cap. For pile bents the plastic hinge may occur above the assumed point of fixity. Because of the serious effects of a shear failure, the location of possible hinges should be determined in a manner such that the smallest potential column length is used with the plastic moments to obtain the largest potential design shear force.

The design forces specified in AASHTO Article 4.8.3 reflect the design philosophy of the guidelines: the design moments are specified on the assumption that the columns are expected to yield when subjected to the forces of the design earthquake. The axial forces that control both the flexural and shear design requirements are either the maximum or minimum of the unreduced design forces or the values corresponding to the plastic hinging of the columns. In most cases, the latter will be lower than the unreduced design values. The design shear forces are specified with the intent to minimize the possibility of shear failure in the column.

The pier design forces specified in AASHTO Article 4.8.4 are developed on the assumption that a pier has low ductility capacity and no redundancy. Accordingly, a low Response Modification Factor of 2 is used in estimating the reduced design forces, assuming that only a small amount of inelastic deformation will occur when a pier re-

sponds to the effects of the design earthquake. When a pier is designed as a column in its weak direction, then both the design forces and design requirements of Article 4.8.3 and Section 8 are applicable.

The recommended column and pier connection design forces in AASHTO Article 4.8.5(c) are intended to ensure that column connections are designed for the maximum forces that a column can transmit to the connection. These forces are therefore calculated after the column design is complete and the overstrength moment capacities have been obtained.

Design Displacement Criteria

Seismic Performance Category A and B. Bridges classified as SPC A should meet the requirements shown in Figure 4–16. Bearing seats supporting the expansion ends of girders must be designed to provide a minimum support length N measured normal to the center line, calculated as follows:

$$N = 8 + 0.02L + 0.08H \text{ (in)} \tag{4–2}$$

where L = length (ft) of the bridge deck to the adjacent expansion joint, or to the end of the bridge deck; and H = column or pier height (ft).

For SPC B, the seismic design displacements may be as specified for SPC A or in accordance with AASHTO Article 4.3.

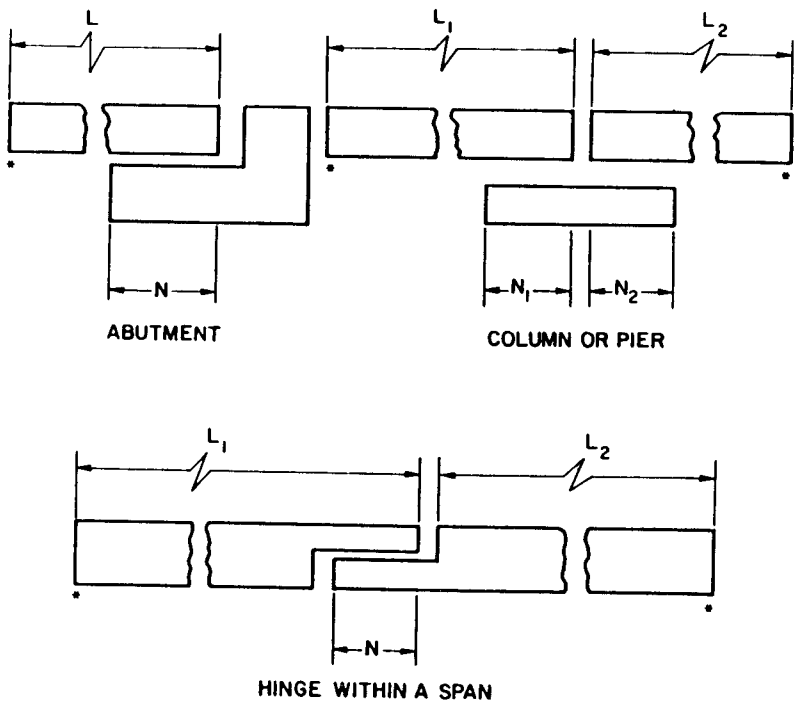

Figure 4–16 Dimensions for minimum support length requirements *(from AASHTO).*

Seismic Performance Category C and D. In this case Equation (4–2) is modified as follows:

$$N = 12 + 0.03L + 0.12H \text{ (in)} \qquad (4\text{–}3)$$

The length of support provided by the foregoing procedures is intended to accommodate displacements resulting from the overall inelastic response of the bridge, possible independent movement of different parts of the substructure, and out-of-phase rotation of columns resulting from traveling surface wave motions (Hall and Newmark, 1979).

Because the current state of the art precludes a good estimate of differential column and abutment movement expected when a bridge is subjected to an earthquake, it is necessary to specify minimum support lengths to provide for the foregoing effects. If the displacements resulting from an elastic analysis (Article 4.3) exceed the values specified in Equations (4–2) and (4–3), the values obtained from the elastic analysis should be used.

Methods of Analysis

The multimode response spectrum analysis discussed in AASHTO Article 5.4 should be performed with a suitable space frame linear dynamic analysis computer program. Currently available programs with capabilities are listed in Article C 5.4.1.

The intermediate columns or piers should also be modeled as space frame members. For short, stiff columns with length less than one-third of either of the adjacent span, intermediate nodes are not necessary. Long, flexible columns should be modeled with intermediate nodes at the third points in addition to the joints at the ends. Foundation conditions at the column base may be modeled using equivalent linear spring coefficients.

Special Requirements

The basic philosophy of seismic design is outlined in section 3.10. Section 3.11 summarizes the requirements of reinforced concrete in areas of seismic activity.

The provisions of this section apply to the design for the strong direction of a pier. The weak direction may be designed as a column under the provisions of AASHTO Article 8.4.1 with the Response Modification Factor as in Article 4.8.1. The minimum reinforcement ratio both horizontally, p_h, and vertically, p_n, in any pier should not be less than 0.0025, and the reinforcement spacing in either direction should not exceed 18 inches. The reinforcement for shear should be continuous and uniformly distributed.

4.6 STRUCTURAL CAPACITY UNDER COMBINED AXIAL COMPRESSION AND BENDING

Commentary

The current emphasis on load factor methods for the design of columns subjected to combined axial loads and bending moment probably reflects a strong opinion that the service load provisions (ASD) are overly conservative and somewhat unrealistic. We recall that in strength design, three parameters become relevant: the factors β, γ, and ϕ.

The parameter β is commonly called the load magnification coefficient, and the parameter γ is usually referred to as the overall load factor (see also section 3.5). The parameter ϕ is the strength and performance factor applied to the nominal strength to obtain the factored strength.

The application of strength design enhances the comprehension of the entire structure at various stages of structural behavior. For example, for a bridge deck supported by one-shaft piers, the ratio of footing cantilever length to footing thickness tends to be large. Any unsymmetrical application of live load with respect to the pier shaft will cause uneven soil pressure or pile loads. Deformation of the supporting soil and deflection of the footing may induce pier rotation and consequent lateral deflection of appreciable magnitude. For a continuous bridge, this deflection may have to be considered. The effect of overloads may magnify these results and may change the structural fitness. These events may necessitate modification and adjustments in the design until the overall behavior is acceptable.

Comparison of Working Stress and Load Factor. Consider a situation involving dead load, live load, and impact (Group I). The load factors γ and β are 1.3 and 5/3 = 1.67. If a member in flexure is analyzed, the section of the number will have to resist at least

$$\frac{1.3D + 2.17\,(L + I)}{\phi}$$

meaning that the factored loads cannot exceed the factored strength. Taking $\phi = 0.9$ we compute the ratios

$$\gamma/\phi = 1.3/0.9 = 1.44, \quad \text{and} \quad \gamma\beta/\phi = 2.17/0.9 = 2.41$$

For the same member, the working loads at working stress and the factored loads at yield strength may be related as

$$\frac{[D/(L + I)] + 1}{f_s A_s jd} = \frac{[1.44D/(L + I)] + 2.41}{f_y A_s d[1-(a/2d)]}$$

For a small bridge, the live load plus impact predominates. Assuming that the ratio $D/(L + I)$ is about 0.25, the ratio $[1 - (a/2d)]/j$ will be approximately 1.06. The foregoing yield a relationship of yield strength to safe stress

$$f_y/f_s = 2.10$$

In the working stress method, this relationship is

60/24 = 2.50 for Grade 60 reinforcement
and 40/20 = 2.00 for Grade 40 reinforcement

When considering possible increase in the live load, the overall factor of safety of 2.10 compares favorably with the factors of safety in ASD. In longer spans (in excess of 120 feet) the ratio dead load/live load approaches 3 or more. In this case the ratio f_y/f_s is close to 1.60. The smaller factor of safety is admissible in view of the smaller variability in the magnitude of dead load, and consistent with the concept of the overall responses and with the level of uncertainty in predicting maximum loads.

AASHTO Requirements

Service load design. AASHTO offers two design procedures: service load and load factor. Interpretation of Article 8.15.4 dealing with compression members indicates that when column design is considered under service load, the column analysis must be based on capacity, and that this should not exceed 35 percent of that computed in accordance with the provisions of Article 8.16.4 (compression members under strength design method). Slenderness effects must be evaluated according to Article 8.16.5, and the term P_u in AASHTO Equation (8–41) is replaced by 2.5 times the design axial load. The coefficient ϕ is taken as 1.0.

The service load procedure also accounts for moment magnification as part of the approximate analysis of slenderness effects outlined in Article 8.16.5.2 for load factor design.

Strength Design (Load Factor) Method. In Article 8.16.4 AASHTO introduces the more traditional ultimate design procedures for columns where two different values of ϕ are assigned to the nominal strength P_n. Thus, the design axial load strength ϕP_n is obtained using $\phi = 0.75$ for spiral columns and $\phi = 0.70$ for tied columns. The specifications (Article 8.16.1.2) also allow for the value of ϕ to be linearly increased from the value stipulated for compression members to the value specified for flexure as the design axial load ϕP_n decreases from $0.10 f'_c A_g$ or ϕP_b, whichever is smaller, to zero. In this case P_b is the nominal axial strength of a section at balanced strain conditions (Article 8.16.4.2.3). Most bridge pier designs fall within this range.

Although there are no provisions for computations at the service load stress level, many designers pursue pier analysis at the service load as a routine practice. Special serviceability criteria are not outlined, but some consideration should be given to piers in water or buried in the ground where they may be exposed to cyclic freezing and thawing. In this context it may be reasonable to assume a maximum permissible crack width of 0.006 inch when applying appropriate formulas for crack-width determination.

It should be noted that the AASHTO requirements for axial and flexural analysis must be supplemented or modified as provided for in the AASHTO guidelines for seismic design (see also section 3.11).

LRFD Specifications

These specifications require provisions to transfer force effects from compression components, adjusted for second order moment magnification, to adjacent components. When the connection is by a concrete hinge, longitudinal reinforcement should be centralized within the hinge to minimize moment strength, and should be developed on both sides of the hinge interface.

Appropriate limits are stipulated for the maximum and minimum area of longitudinal reinforcement in noncomposite compression components. Referring to current ACI codes stipulating an area of longitudinal reinforcement of not less than $0.01 A_g$, it is pointed out that the dimensions of pier columns are primarily controlled by architectural criteria and bending. This limitation does not account for the influence of the concrete compressive strength. To account for this factor, the minimum reinforcement in flexural members is shown to be proportional to f'_c/f_y (compressive strength of concrete/yield strength of reinforcing steel).

Slenderness effects are likewise evaluated as in AASHTO Article 8.16.5. For rectangular compression members, the radius of gyration r may be taken as 0.30 times the overall dimension in the direction in which stability is analyzed. For a circular compression member, r may be taken as 0.25 times the diameter (see also AASHTO Article 8.16.5.2.2).

Moment Magnification

The design of compression members must be based on forces and moments determined from an analysis of the structure. Such an analysis should include the influence of axial loads and variable moment of inertia on member stiffness and fixed-end moments, the effect of deflections on moments and forces, and the effect of the duration of loads.

This general AASHTO criterion suggests several modes of analysis. First-order loads and moments may be computed on the basis of elastic analysis where the stress below the specified yield strength is E_s times the steel strain. With regard to stiffness assumptions, an uncracked cross section may be assumed neglecting all reinforcement, or a transformed cracked section throughout. The column ends may be assumed fixed, free, or partially restrained. The most correct representation of the ultimate state, however, may be obtained using moment-curvature relationships. Reasonable results can be expected if EI values are assumed to be equal to $E_c I_g(0.2 + 1.2\, p_t\, E_s/E_c)$ for piers and to $0.5\, E_c I_g$ for superstructure stiffness, where I_g = gross moment of inertia, $p_t = A_s/A_g$, E_s = 29,000,000 lb/in^2, and $E_c = 57{,}000\sqrt{f'_c}$ lb/in^2. An important assumption involves the degree of fixity for the assumed foundation conditions, discussed in section 4.3.

In lieu of an exact second-order analysis that can realistically represent the foregoing effects, the results may be approximated by the use of the moment magnifier method. Referring to Figure 4–17, the primary deflection Δ_1 caused by the end moment M_1 is

$$\Delta_1 = \frac{M_1 L^2}{8EI} \tag{4–4}$$

The secondary deflection Δ_2 caused by the axial load influence is

$$\Delta_2 = \frac{0.10P(\Delta_1 + \Delta_2)L^2}{EI} \tag{4–5}$$

From the critical Euler load $P_{cr} = \pi^2 EI/L^2$, we obtain

$$\frac{L^2}{EI} = \frac{\pi^2}{P_{cr}} \tag{4–6}$$

Substituting this term into Equations (4–4) and (4–5) yields

$$\Delta_1 = \frac{M_1}{8}\left(\frac{\pi^2}{P_{cr}}\right) \tag{4–7}$$

and

$$\Delta_2 = 0.10P(\Delta_1 + \Delta_2)\left(\frac{\pi^2}{P_{cr}}\right) \tag{4–8}$$

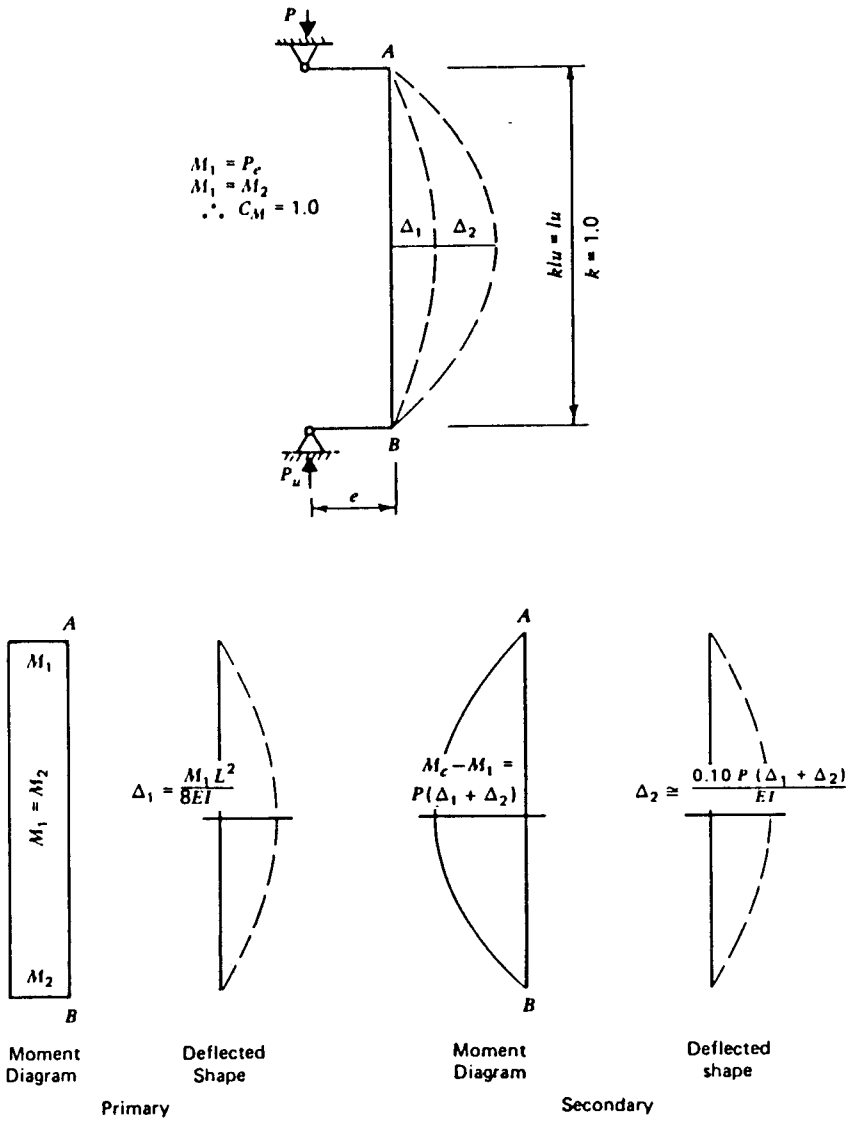

Figure 4–17 Deflection shapes of columns.

Summing up $\Delta_1 + \Delta_2$ we obtain

$$\Delta_1 + \Delta_2 = \left[\frac{M_1}{8} + P(\Delta_1 + \Delta_2)(0.10)\right]\left(\frac{\pi^2}{P_{cr}}\right) \tag{4–9}$$

Noting that $M_c = M_1 + P(\Delta_1 + \Delta_2)$, yields

$$M_c = M_1 + P\left(\frac{\pi^2}{P_{cr}}\right)\left[\frac{M_1}{8} + P(\Delta_1 + \Delta_2)(0.10)\right]$$

or $$M_c = M_1 + \left(\frac{P}{P_{cr}}\right)[M_1 + P(\Delta_1 + \Delta_2)]$$

and $$M_c = M_1 + \left(\frac{P}{P_{cr}}\right)[M_1 + M_c - M_1]$$

which is reduced to $$M_c = \frac{M_1}{1-(P/P_{cr})} \tag{4–10}$$

Setting $M_c = \delta M$, where δ is the moment magnifier factor, we obtain

$$\delta = \frac{1}{1-(P/P_{cr})} \tag{4–11}$$

The specifications introduce the factor ϕ to give

$$\delta = \frac{1}{1-(P/\phi P_{cr})} \tag{4–12}$$

which is AASHTO Equation (8–41a). We should note that Equation (4–12) applies to moment M_{2s} caused by lateral loads or gravity loads that result in appreciable sidesway, defined by a deflection Δ_2 greater than $l_u/1500$ where l_u is the unsupported column length. A second magnifier factor applied to moment M_{2b} caused by gravity loads results in no appreciable sidesway.

The derivation also assumes columns with pinned ends, single curvature, and equal end moments. Therefore the column design must be modified by the effective length factor κ to give an equivalent pinned-end column with single curvature. In this case the critical load is expressed as

$$P_{cr} = \pi^2 EI/(\kappa l_u)^2 \tag{4–13}$$

Effective length factors may be determined from Figure 4–18, and for framed structures from the Jackson-Moreland Charts (CR-CEF, 1960) shown in Figure 4–19. These charts use the parameter

$$G_x = \frac{\sum (EI/L)_c}{\sum (EI/L)_{mc}} \tag{4–14}$$

where $\Sigma(EI/L)_c$ is for columns, and $\Sigma(EI/L)_{mc}$ is for members resisting column bending at x end of column.

The same parameters can be introduced in the equations suggested by Granston (1972) for braced columns, where

$$\left.\begin{aligned} \kappa &= 0.7 + 0.05\,(G_A + G_B) \le 1.0 \\ \kappa &= 0.85 + 0.05\,(G_{\min}) \le 1.0 \end{aligned}\right\} \tag{4–15}$$

(where κ is the smaller of the two values). The same parameters may also be used for unbraced columns as suggested by Furlong (1971) as follows:

Effective length factors, K						
Buckled shape of column is shown by dashed line	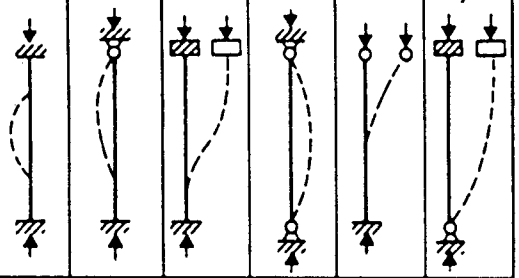 (a) (b) (c) (d) (e) (f)					
Theoretical K value	0.5	0.7	1.0	1.0	2.0	2.0
Design value of K when ideal conditions are approximated	0.65	0.80	1.2	1.0	2.1	2.0
End condition code		Rotation fixed Translation fixed Rotation free Translation fixed Rotation fixed Translation free Rotation free Translation free				

Figure 4–18 Effective length factors, K.

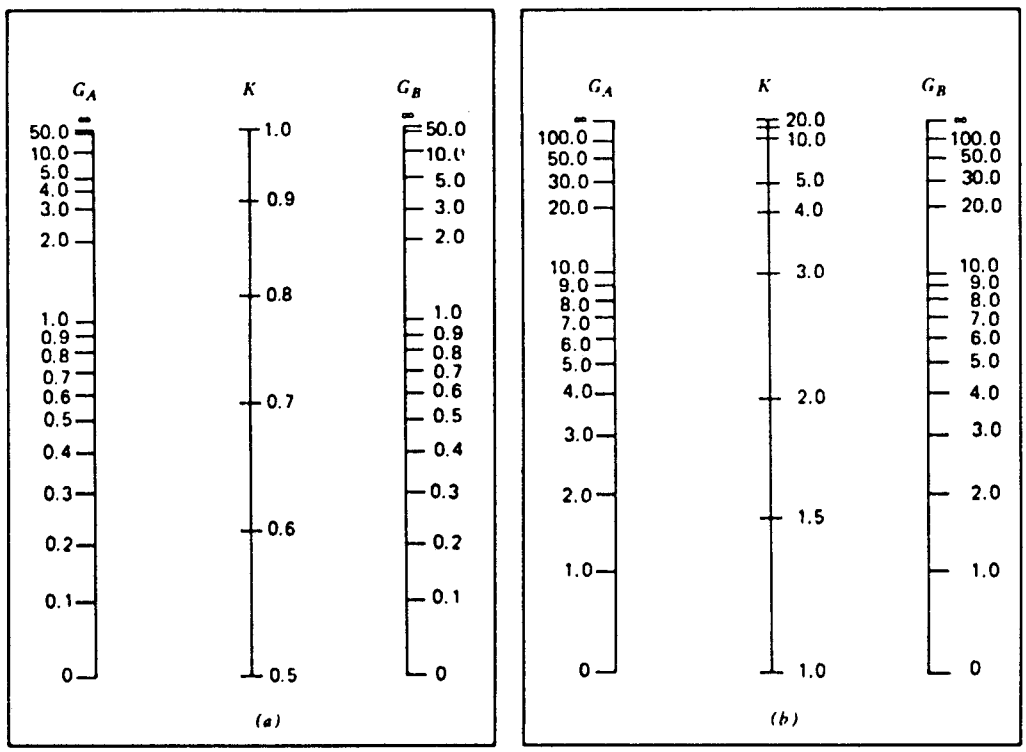

Figure 4–19 Alignment charts for effective length of columns in continuous frames; (a) sidesway prevented; (b) sidesway permitted.

For $$\text{For } G_{av} < 2 \quad \kappa = \frac{20 - G_{av}}{20}\sqrt{1 + G_{av}} \tag{4–16a}$$

and for $$G_{av} \geq 2 \quad \kappa = 0.9\sqrt{1 + G_{av}} \tag{4–16b}$$

The value of G to be selected for various foundation conditions may be taken from Table 4–1.

An important influence on the effective length factor is the presence of bracing against sidesway. Piers may be designed for the unbraced condition. A braced condition should be considered only in a case similar to a row of columns in a bent strutted with a large wall of considerable stiffness against lateral movement in the transverse direction.

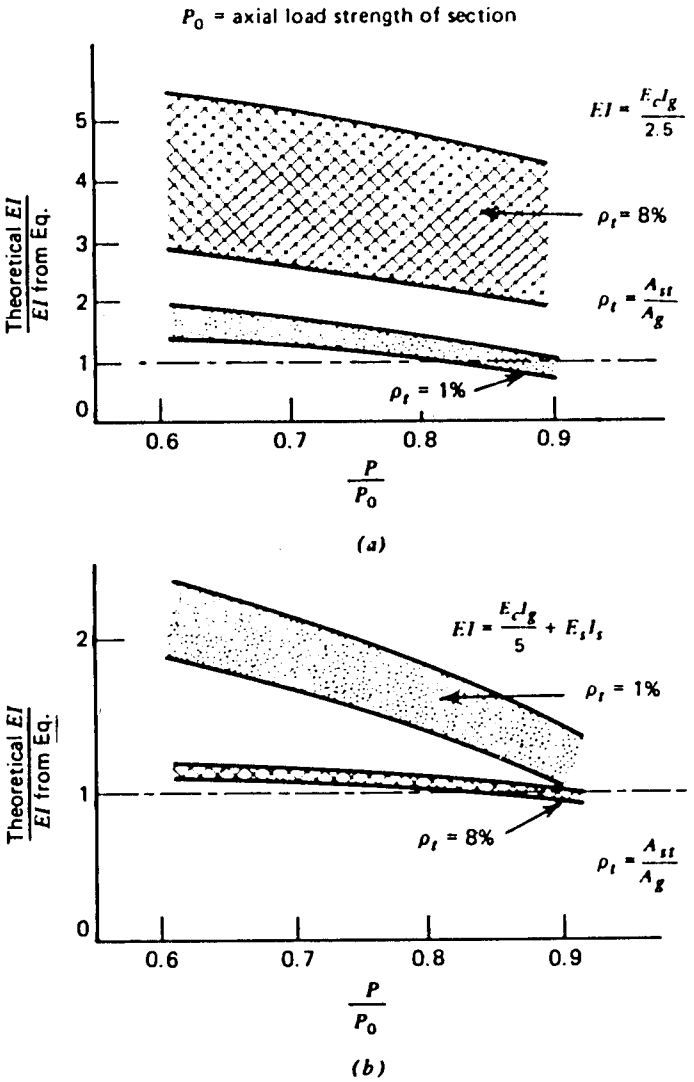

Figure 4–20 Comparison of equations for flexural stiffness with theoretical values from moment-curvature diagrams.

In computing the critical buckling load from Equation (4–13), or AASHTO Equation (8–42), the formulas for EI were developed using the data shown in Figure 4–20. These curves are plots of the ratio of the theoretical to the specifications EI for different ratios and percentages of reinforcement. They show that using $EI = E_c I_g/2.5$ is extremely inaccurate for high percentages of reinforcing steel, whereas $EI = E_c I_g/5 + E_s I_s$ is somewhat inaccurate for low percentages.

A recommendation that emerges from these results is to use $EI = E_c I_g/2.5$ for the design of piers with reinforcement 2 percent or less, and $EI = E_c I_g/2.5 + E_s I_s$ for the design of piers with reinforcement more than 2 percent. These guidelines are related to AASHTO Equations (8–43) and (8–44), to be applied only in computing the critical buckling loads. These equations contain also the expression $(1 + \beta_D)$ where β_D is the ratio of maximum dead load moment to the maximum total load moment, taken always positive. This factor accounts for the effect of creep due to sustained loads. The value of $(1 + \beta_D)$ decreases EI and thus increases the moment magnification.

The foregoing analysis is for buckling loads of columns of a constant moment of inertia. Quite often, however, pier columns or shafts are tapered. In this case, the critical buckling load may be computed by reference to the charts shown in Figure 4–21 and Table 4–3 (Newmark, 1942). A numerical procedure is also available (Newmark, 1942) for computing buckling loads for columns and piers with variable moment of inertia.

When a series of piers with variable stiffness is attached to the superstructure

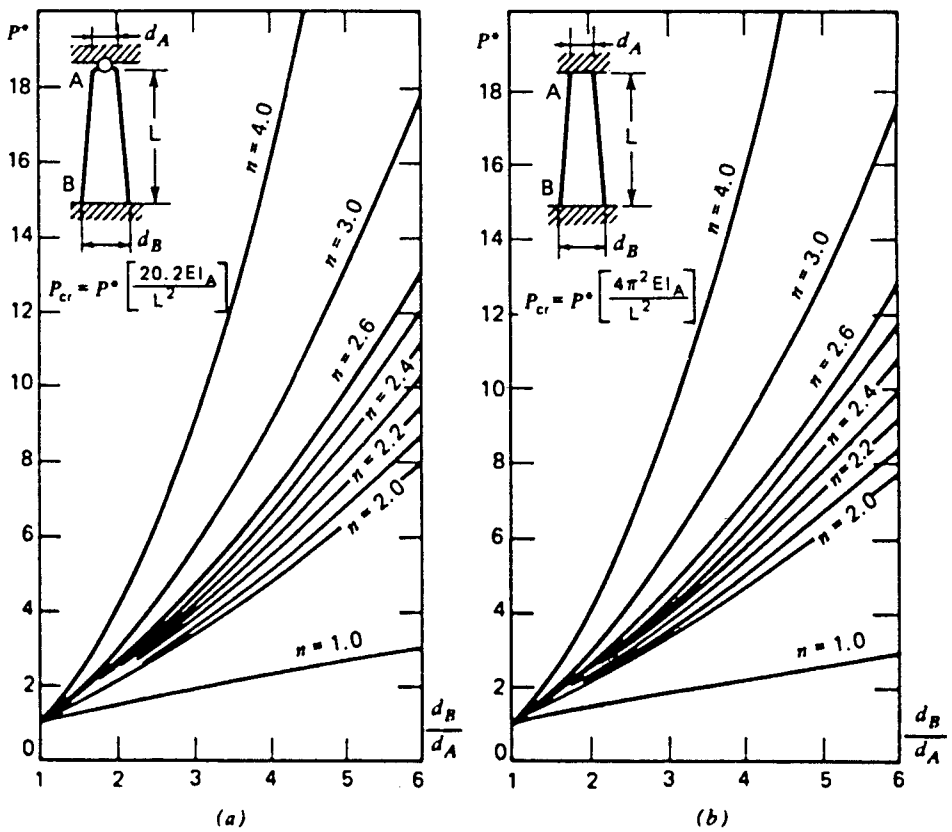

Figure 4–21 Critical buckling loads for tapered shafts; (a) Case 3 column, fixed-pinned ends; (b) Case 4 column, fixed ends.

Table 4–3 Shape Factors

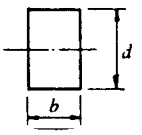	Solid, rectangular section Constant width b Varying depth d Buckling about horizontal axis	$n = 3$
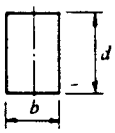	Solid, rectangular section Constant width b Varying depth d Buckling about vertical axis	$n = 1$
	Solid, circular section Varying diameter d	$n = 4$
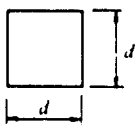	Solid, square section Varying dimension d	$n = 4$

(continuous frame), it is expedient to evaluate the buckling strength of the entire unit. Yura (1974) has developed a procedure which involves transmitting lateral thrust through the superstructure to provide additional lateral strength to the more flexible piers (see also Xanthakos, 1994).

4.7 SECTION ANALYSIS

Pier or column sections are typically analyzed for the most critical loading conditions and load combinations. The anaysis involves computations of stresses for conditions under serviceability and load capacity criteria. Because pier shafts and columns frequently have unusual shapes to satisfy architectural requirements, an analysis must often be made for irregular and unsymmetrical sections.

In most routine designs pier sections are governed by moments and not axial load. Hence, the most critical condition is associated with the load combination producing the largest moment about the weak pier axis. For loads inducing similar moments with variations in load, the load producing the maximum eccentricity will usually control.

Besides pier shafts and columns, other components that are commonly subjected to combined axial load and moment are driven piles and drilled shafts. Methods for analyzing the structural capacity and for computing the resulting stresses are discussed in sections 9.12 and 10.17.

Interaction Diagrams

Strain compatibility solution. Although it is possible to develop a system of equations to evaluate the strength of columns subjected to combined bending and axial load, the procedure is tedious and time consuming. Instead, interaction diagrams for columns are

usually produced assuming a series of strain distributions, each corresponding to a particular point on the interaction diagram, and computing the corresponding values of P and M. Once enough points have been computed, the results are plotted to produce an interaction diagram.

The calculation process is illustrated in Figure 4–22 for a maximum compressive strain of 0.003, corresponding to failure of the section. The resulting stress block is shown in Figure 4–22(c) and the forces in the steel and concrete are shown in Figure 4–22(d). The axial force P_n is computed by summing the individual forces in the concrete and steel, and the moment M_n is found by summing the moments of these forces about the centroid of the section. The values of P_n and M_n thus obtained represent one point on the interaction diagram.

Figure 4–23 shows a series of strain distributions and the resulting points on the interaction diagram. Strain distributions A and point A represent pure axial compression. Point B corresponds to crushing at one face and zero tension at the other. If the tensile strength of cracking is ignored, this marks the onset of cracking on the bottom face of the section. Points lower than this represent cases where the section is partially cracked. Point C corresponds to a maximum compression strain of 0.003 and the yielding strain in the steel, hence it represents the balanced condition. Point D corresponds to the strain distribution shown, and point E represents pure bending.

Alternatively, a strain compatibility solution may be obtained assuming a nonlinear stress-strain relationship. This will require, however, typical stress-strain curves.

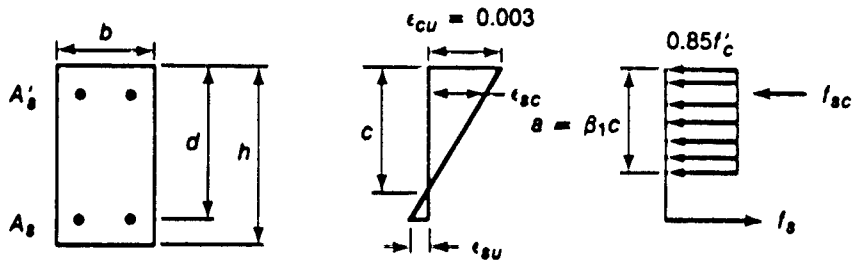

(a) Section. (b) Strains. (c) Stresses.

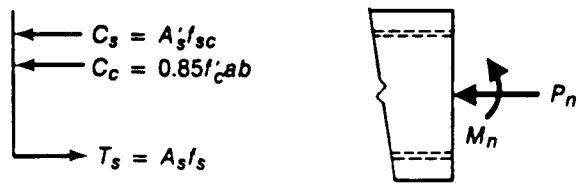

(d) Internal forces. (e) Resultant forces.

Figure 4–22 Calculation of P_n and M_n for a given strain distribution.

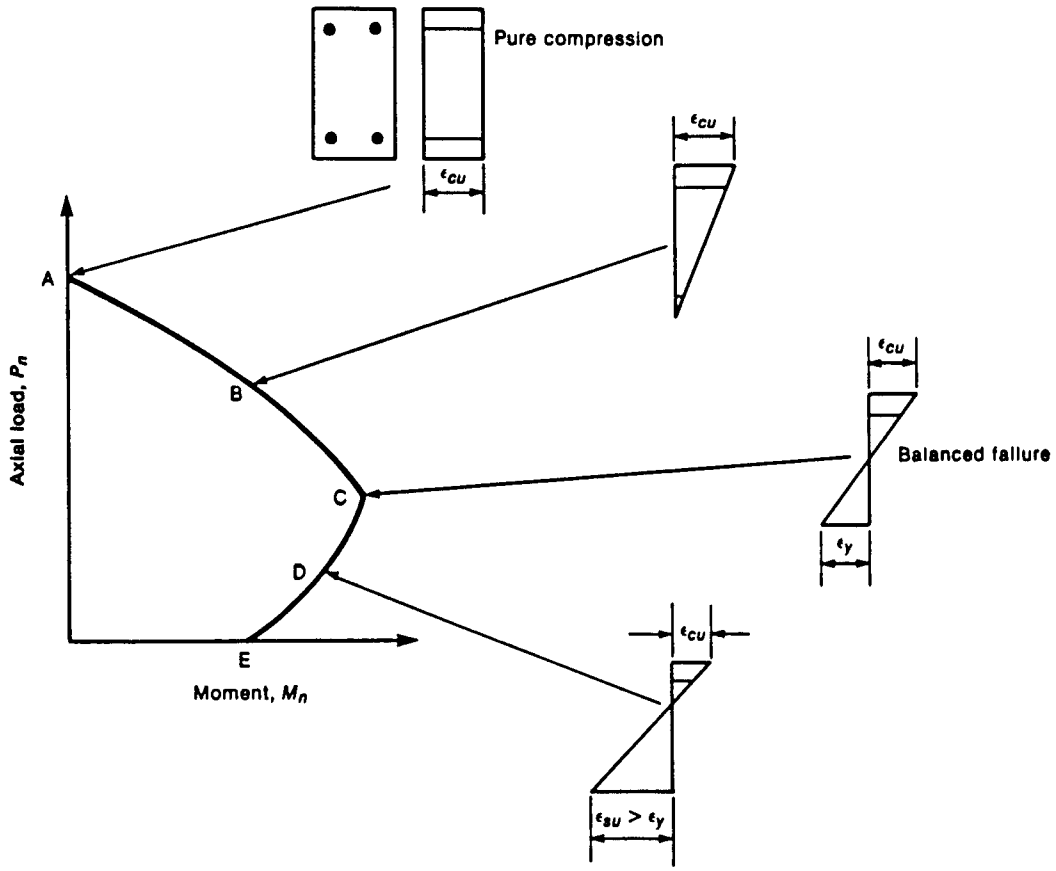

Figure 4–23 Strain distributions corresponding to points on interaction diagram.

Biaxial Bending

Procedures for computing stresses in piers have been proposed by Goodall (1948) and Hu (1955). These methods do not account for double compression in the reinforcing steel, hence are conservative in relation to stress.

The AASHTO design specifications stipulate that biaxial bending and axial load should be analyzed for ultimate load, based on stress and strain compatibility, or, in lieu of a general section analysis, by one of the following approximate expressions

$$\frac{1}{P_{nxy}} = \frac{1}{P_{nx}} + \frac{1}{P_{ny}} - \frac{1}{P_o} \tag{4–17}$$

when the factored axial load is $P_u \geq 0.10 f'_c A_g$,

or

$$\frac{M_{ux}}{\phi M_{nx}} + \frac{M_{uy}}{\phi M_{ny}} \leq 1 \tag{4–18}$$

when the factored axial load is $P_u < 0.10 f'_c A_g$. Equation (4–17) was originally presented

by Bresler (1960), and appears in several codes. Other procedures used to design rectangular columns subjected to biaxial loads are as follows:

1. The biaxial eccentricities e_x and e_y may be replaced by an equivalent uniaxial eccentricity e_{ox}, and the column designed for uniaxial bending and axial load (MacGregor, 1973). This procedure is limited in application to columns that are symmetrical about two axes with a ratio of side dimensions x/y between 0.5 and 2.0. The reinforcement should be in all four faces of the column.
2. Charts or relationships may be used for the 45° section through an interaction surface. The design is then based on straight-line approximations to horizontal slices through the interaction surface. This method is described by ACI (1978) and by Gouwens (1975).

Alternatively, the axial load capacity can be estimated by considering a uniform strain between the extreme concrete fiber and reinforcing steel locations at which the maximum allowable concrete strain is 0.3 percent (Heins and Lawrie, 1984). Because most columns fall in an area below the balance point on the interaction curve, it is reasonable to compute two steel strains, one at the balance point of 0.207 percent and the other at about 0.5 percent. By connecting these two points on an interaction diagram, a reasonable approximation is obtained of the axial load capacity of the most common pier shafts and columns. Computation of the biaxial load capacity requires only evaluation of the two uniaxial capacities and the rotation of a curve between the points.

Commentary. Referring to Equations (4–17) and (4–18), it may be noted that at ultimate analysis of bridge pier columns, P_u is usually less than $0.10 f'_c A_g$. However, there are situations where the service load (35 percent ultimate) will cause P_u to be greater than $0.10 f'_c A_g$, and this would require the use of Equation (4–17), also referred to as reciprocal load equation. In practice, it is possible to simulate the stress and strain compatibility analysis during a PCA computer program, based on the work of Parme, Nieves, and Gouwens (1966) and Gouwens (1975). Alternatively, it is reasonable to use the elliptic equation

$$\sqrt{\left(\frac{M_{ux}}{\phi M_{nx}}\right)^2 + \left(\frac{M_{uy}}{\phi M_{ny}}\right)^2} < 1 \qquad (4\text{–}19)$$

(Furlong, 1979). A simulation of the interaction surface, produced by a stress and strain compatibility analysis, is shown in Figure 4–24. In this case, an interaction diagram is drawn for axial load and bending about either axis. These two diagrams form the two edges of an interaction surface for axial load and bending above two axes. The calculation of each point on such a surface involves a double iteration: (1) the strain gradient across the section is varied, and (2) the angle of the neutral axis is varied. The neutral axis will generally not be parallel to the resultant moment vector. Further discussion on the interaction diagrams for biaxially loaded columns is provided by Brondiem-Nielsen (1982).

Two inaccuracies may be noted in the biaxial bending-direct load analysis:

1. The approximation of the true shape of the compression block by a rectangular block over a portion of the compression area tends to underestimate the capacity.

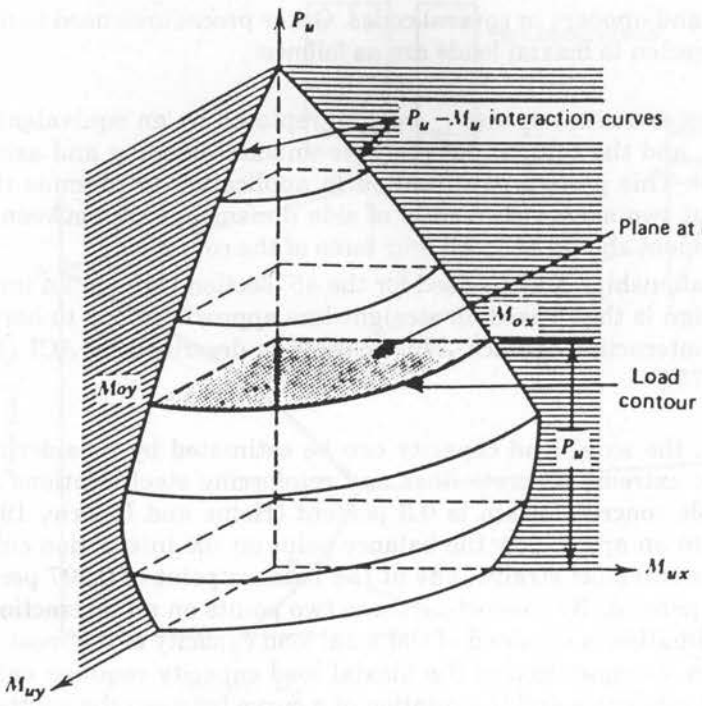

Figure 4–24 Interaction surface for axial load and biaxial bending.

2. There is experimental evidence suggesting that in some instances a strain of 0.4 percent will be reasonable as a limiting value before the concrete is assumed to deteriorate (see also Xanthakos, 1994).

The strength analysis of irregular and unsymmetrical shapes involves problems essentially similar to the problems associated with biaxial bending, but limited research has been carried out in pier analysis. An example of irregular sections is shown in Figure 4–25, modeled by Marin (1979) mathematically. Experimental tests should be forthcoming to verify the results, with emphasis on the requirements for shear and lateral reinforcement.

There are some questions regarding the variations in the requirements for hoops, ties, and spirals. Lateral reinforcement has a limited function before initial concrete deterioration, but thereafter its action becomes significant. Experience shows that spirals perform better than hoops and ties, mainly because of the better confining capability developed by the circular hoop tension. Studies by Potangaroa, Priestley, and Park (1979) and by Gill, Park, and Priestley (1979) have shown that column ductility may be greatly improved by using closely spaced hoops, ties, and spirals in potential plastic hinge areas (see also section 3.11). AASHTO stipulates that in seismic zones where major damage could be expected from earthquakes, lateral reinforcement for column piers should be designed and detailed to provide adequate strength and ductility (Article 8.18.2.4), but does not articulate what "adequate" means. The LRFD provisions are more specific, and in seismic zones C and D they require the spiral reinforcement to extend from the footing or other support to the level of the lowest reinforcement in the members supported above.

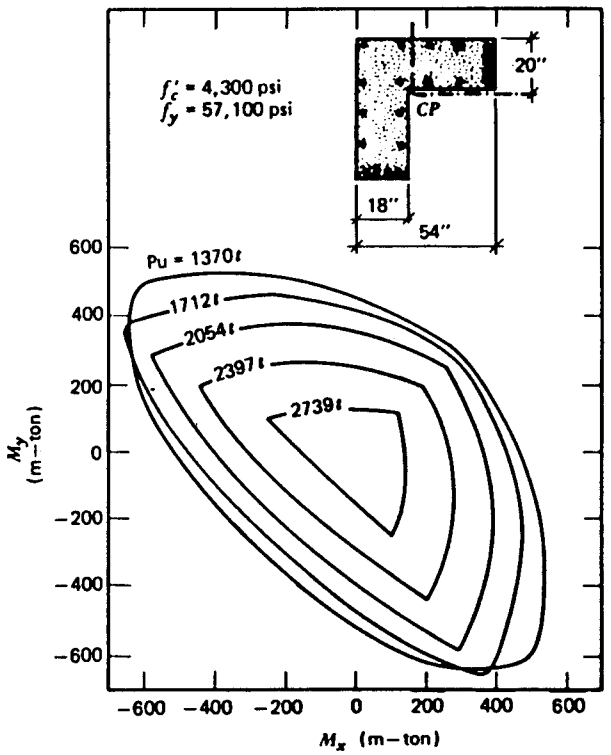

Figure 4–25 Isoload diagram for L cross section. Developed by Marin.

4.8 STRUCTURAL CAPACITY OF COMPOSITE COLUMNS

Concrete-encased steel columns are often used in connection with large-capacity steel piles. The piles are merely extended above ground level, and the above-ground section is encased in concrete. Column bending moments applied in any direction may be efficiently resisted by a circular array of longitudinal bars placed away from the column center. Large axial forces can be accommodated by increasing the cross-sectional area, or the longitudinal bars. Whereas the vertical load in the steel pile section and in the composite section is essentially the same, this design implies that the moments above the ground (in the column length) are considerably larger so that the structural capacity in the column section must be enhanced by concrete encasement and reinforcing steel.

A procedure for computing the ultimate strength of circular concrete columns containing symmetrical steel I-sections and steel bars enclosed with helical reinforcement is developed by Brettle (1973).

Properties of Composite Columns

Both the ACI and the Australian building code include recommendations for the elastic or allowable stress design of composite columns, consisting of a structural steel core surrounded by longitudinal reinforcement and spiral encased in concrete.

Because of the large number of variables affecting a composite column, the development of a practical method of analysis becomes difficult. The variation range can, however, be reduced by assigning constant values to several variables and by using

nondimensionalized ratios. This approach is consistent with the use of steel sections in which the nominal flange width is about equal to the nominal depth. The dimensions of such composite columns are nondimensionalized by dividing them by their nominal flange width b'. For a column diameter b, the nominal flange width is taken as $b' = 0.45b$. The longitudinal bars are placed along a circle of diameter $0.8b$. A steel ratio p_b of 0.01 is used, but the number of bars for the usual composite columns is taken as twelve for the charts developed for preliminary analysis.

The Method of Partitioning Cross Sections

The composite section, subjected to axial load and biaxial bending, is assumed to fail when a combination of axial force P_u and bending moments about two axes is applied. Using axes through the plastic centroid, the eccentricities e_x and e_y refer to the point of application of P_u, and are as shown in Figure 4–26(a). The moments at failure are,

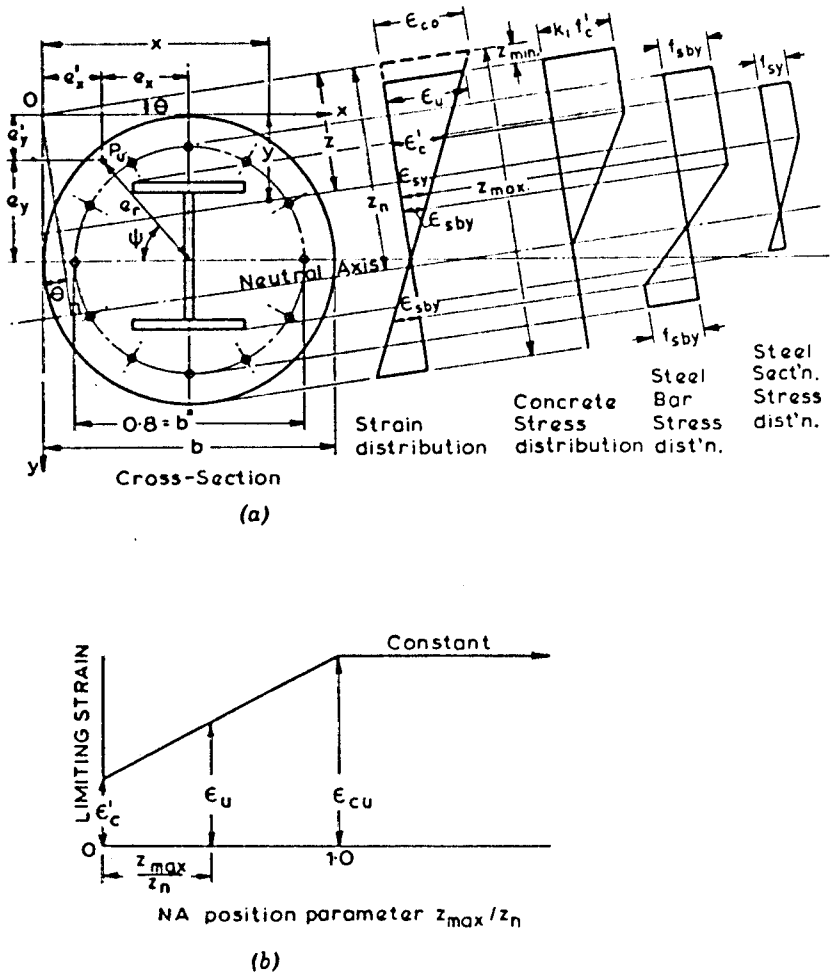

Figure 4–26 Relation between neutral axis location and stress and strain distributions.

therefore, $P_u e_x$ and $P_u e_y$. The analysis requires the summation of stresses multiplied by the areas over which they act in the longitudinal direction of the column, and the summation of the first moment of the resulting forces about both axes.

The process of summing the forces acting on the small elements is ideally suited for computer solutions. Collapse of a section is assumed to occur when the concrete extreme fiber strain ε_{cu} attains an upper limiting value (by the usual bridge standards 0.003). However, the eccentricity of loading and the section properties cause the neutral to be inclined at some angle θ to the steel section major axis at failure, so that the position of the fiber sustaining maximum compressive strain moves around the concrete periphery. The solution can be simplified if this point of maximum compressive strain remains stationary.

The cross section of a circular concrete area can be subdivided into small elemental areas by means of a square grid. An elemental area may be considered effective if its centroid is within the circular area, and can be ignored if its centroid is outside the circular area. Obviously the concrete area can be more closely approximated by increasing the fineness of the grid mesh.

Ultimate strength analysis. The area of the steel section is taken as 5 percent of the total cross section, although most codes permit a steel ratio much higher. The longitudinal steel is enclosed by a spiral, hence the composite column is assumed to be a reinforced concrete column and the relevant collapse criteria are applied. The strain distribution is assumed to be linear up to failure. The derivation of equations expressing equilibrium conditions is provided by Brettle (1973), and will not be repeated here.

Design charts have been developed correlating the ratio P_u/P_o with the ratio e_r/b, where P_o = load at failure with zero eccentricity; P_u = load at failure with loading point eccentric to one or both principal axes; e_r = resultant eccentricity = $\sqrt{e_x^2 + e_y^2}$; and b = overall diameter of circular column. Two values of critical strain were used, 0.002 and 0.0035. The charts are also developed to accommodate the concrete strength and yield strength commonly used in the structural steel and reinforcing bars for bridges in the United States. For the use of these charts, reference is made to Brettle (1973).

Commentary. Specifications for the design of composite columns were modified along with slenderness provisions for columns in the 1971 edition of the ACI code.

Column strength depends on two basic properties: (1) the load capacity of the cross section, and (2) the overall slenderness of the compression member. Both the ACI and AASHTO consider failure imminent at a strain of 0.003. According to the foregoing section, slenderness effects may be considered in terms of moment magnification. The ACI code requires a cage of reinforcement around the structural core. The structural capacity of a composite concrete column can be described with a thrust-moment interaction graph, any point of which is cumbersome to evaluate. An alternate procedure is to use moment magnifier, but this is also tedious. Because column design usually requires some iteration on possible cross sections, tabulations of both strength and slenderness data must be available.

Furlong (1974) has derived representative design tables for structural shapes of A36 steel with nominal depth of 6, 8, 10, 12, and 14 inches. The tables are for encasement consisting of concrete with f'_c = 3000 lb/in^2. The sections are dimensional to allow at least 1-3/4 in of concrete cover over any edge of the encased structural shape.

The capacity of a cross section is assumed to have been reached at a strain of

0.003. Skew bending capacity may be estimated by means of the reciprocal thrust, Equation (4–17). The strength tables give values of thrust capacity for each cross section. The appropriate eccentricity for use of the tables will be the ratio between moment and thrust. For major axis bending, the eccentricity $e_x = M_{ux}/P_u$ should be used to determine P_x. Likewise, the ratio $e_y = M_{uy}/P_u$ should be used for determining P_y. For the use of these tables reference is made to Furlong (1974).

4.9 DESIGN EXAMPLE 4–1: SINGLE-SHAFT PIER (LOAD FACTOR DESIGN)

The pier shown in Figure 4–27 is the center support of a single-lane bridge supported at the left support and cantilevered to the right of the pier, as shown in Figure 4–27(b), where the pier is designated as *BD*. The design load is HS 20, with no overload provisions. The pier shaft will be analyzed by load factor method.

Loads and moments are tabulated in Tables 4–4 and 4–5 for the top and bottom of the shaft, respectively. M_L and M_T denote longitudinal and transverse moments, respectively. These various loads are grouped and factored according to AASHTO Table 3.22.1A. The factor β_D is applied as stipulated, that is, $\beta_D = 0.75$ to reduce axial load and produce maximum eccentricity, and $\beta_D = 1.0$ for moments.

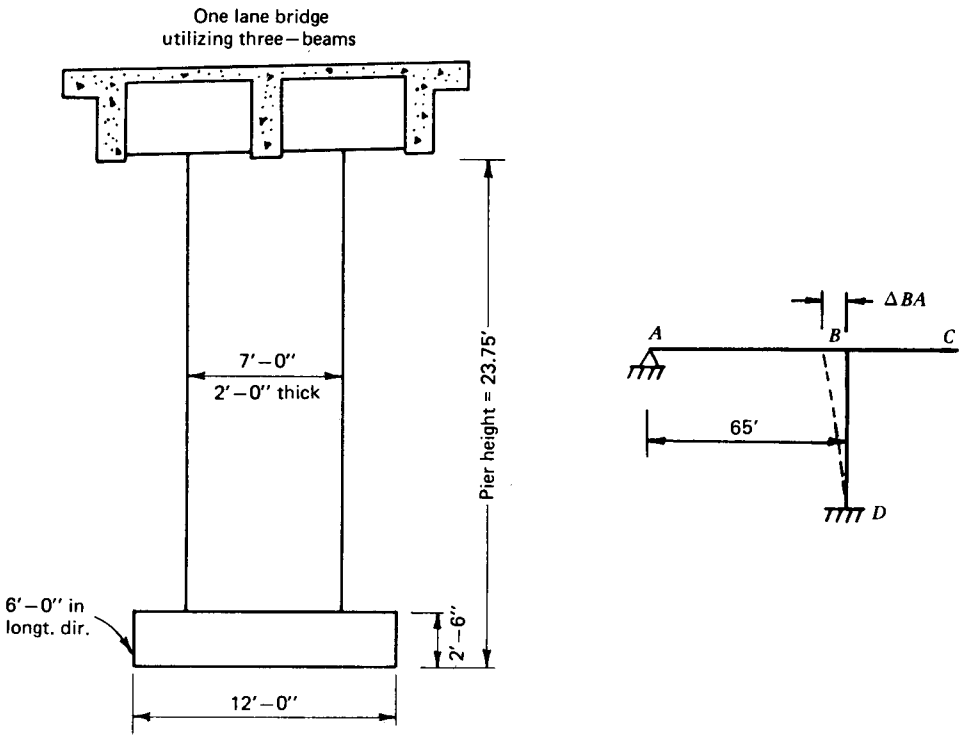

Figure 4–27 (a) Pier elevation of design example; (b) rigid frame of bridge elevation.

Table 4–4 Loads and Moments at *BD* Top Pier (HS 20)

LL Case		Case IB			Case II		
Group	*Loading*	P	M_L	M_T	P	M_L	M_T
I	$\beta_D D$	226.4	+430		226.4	+322	
	$1.67(L + I)$	97.5	+578	391	150.3	−364	601
	Σ	323.9	+1008	391	376.7	−42	601
	$1.3 \times \Sigma$	421.1	+1310	508	489.7	−55	781
II	$\beta_D D$	226.4	+430		+226.4	+322	
	$W + OT$			94			94
	Σ	226.4	+430	94	+226.4	+322	94
	$1.3 \times \Sigma$	294.3	+559	122	294.3	+419	122
III	$\beta_D D$	226.4	+430		+226.4	+322	
	$L + I$	58.4	+346	234	90.0	−218	360
	$0.3W$						
	$0.30T$			28			28
	WL						
	Σ	284.8	+776	262	+316.4	+104	388
	$1.3 \times \Sigma$	370.2	+1009	341	+411.3	+135	504
IV	$\beta_D D$	226.4	+430		+226.4	+322	
	$L + I$	58.4	+346	234	90.0	−218	360
	$S + T$		+227			−556	
	Σ	284.8	+1003	234	316.4	−452	360
	$1.3 \times \Sigma$	370.2	+1304	304	411.3	−588	468
V	Σ Group II	226.4	+430	94	+226.4	+322	94
	$S + T$		+227			−556	
	Σ	226.4	+657	94	+226.4	−234	94
	$1.25 \times \Sigma$	283.0	+821	118	+283.0	−292	118
VI	Σ Group III	284.8	+776	262	+316.4	+104	388
	$S + T$		+227			−556	
	Σ	284.8	+1003	262	+316.4	−452	388
	$1.25 \times \Sigma$	356.0	+1254	328	+395.5	−565	485
VII	$\beta_D D$	226.4	+430		226.4	+322	
	EQ			0			
	Σ			Neglect			
	$1.3 \times \Sigma$						

Section capacity. The analysis follows the procedure discussed in section 4.7. We assume that the requirements for capacity are below the balance point on the interaction curve. Therefore, the capacity is computed about each axis for a concrete compressive strain of 0.003 and a compressive steel strain of 0.00207 at the balance point. Next, we compute the direct load and moment capacity for a concrete compressive strain of 0.003 and a steel compressive strain of 0.005, which are close to a level at which the direct load is very small or close to zero. The capacity interaction curve is approximated by a straight line between these two points. In Figure 4–28 the reinforcement bars are located and numbered on the cross section. The strain diagrams are drawn next in a position that is a direct projection from the column section.

The strain diagrams of Figure 4–28 are used with a maximum strain of 0.00207 to compute the capacity in direct load and bending about the *Y-Y* axis. The reinforcement bars are located with reference to the centroid of the section. The strains at each bar lo-

Table 4–5 Loads and Moments at *DB* Bottom Pier (HS 20)

LL Case		Case IB			Case II		
Group	*Loading*	*P*	M_L	M_T	*P*	M_L	M_T
I	$\beta_D D$	254.9	+149		254.9	+112	
	$1.67\,L + I$	97.5	+194	391	150.0	−125	360
	Σ	352.4	+343	391	404.9	−13	360
	$1.3 \times \Sigma$	458.1	+446	508	526.4	−17	468
II	$\beta_D D$	254.9	+149				
	W			317			
	OT			94			
	Σ	254.9	+149	411			
	$1.3 \times \Sigma$	331.4	+194	534			
III	$\beta_D D$	254.9	+149		254.9	+112	
	$L + I$	58.4	+116	234	90.0	−75	360
	βW			95			95
	$0.30T$			28			28
	WL			170			170
	Σ	313.3	+265	527	344.9	+37	653
	$1.3 \times \Sigma$	407.3	+344	685	448.4	+48	849
IV	$\beta_D D$	254.9	+149		254.9	+112	
	$L + I$	58.4	+116	234	90.0	−75	360
	$S + T$		+229			−560	
	Σ	313.3	+494	234	344.9	−223	360
	$1.3 \times \Sigma$	407.3	+642	304	448.4	−290	468
V	Group II	254.9	+149	411			
	$S + T$		+229				
	Σ	254.9	+378	411			
	$1.25 \times \Sigma$	318.6	+472	514			
VI	Group III	313.3	+265	527	344.9	+37	653
	$S + T$		+229			−560	
	Σ	313.3	+494	527	344.9	−523	653
	$1.25 \times \Sigma$	391.6	+617	659	431.1	−654	816
VII	$\beta_D D$	254.9	+149				
	EQ			1161			
	Σ	254.9	+149	1161			
	$1.3 \times \Sigma$	331.4	+194	1509			

cation are taken from the strain diagram and are given a + sign for compression and a − sign for tension. Stresses in the bars are computed from the corresponding strain using E_s = 29,000 ksi, and f_y = 60 ksi as maximum stress. The resulting force in the bars is the stress multiplied by the bar area A_s. The moments induced by these forces are then taken around the centroid. These forces and moments are added to give the balance load and moment, P_b and M_b. The entire procedure is shown in tabulated form in Table 4–6 for the relevant capacity reduction factors ϕ. The procedure shown in Table 4–6 is repeated for an intermediate point with 0.005 as the maximum tensile strain in the reinforcement, and 0.003 strain in the concrete, and the results are tabulated in Table 4–7.

The values obtained in Tables 4–6 and 4–7 are plotted in Figure 4–29, with the most critical cases obtained from the table of ultimate loads and moments. These values are shown for bending about the *Y-Y* axis.

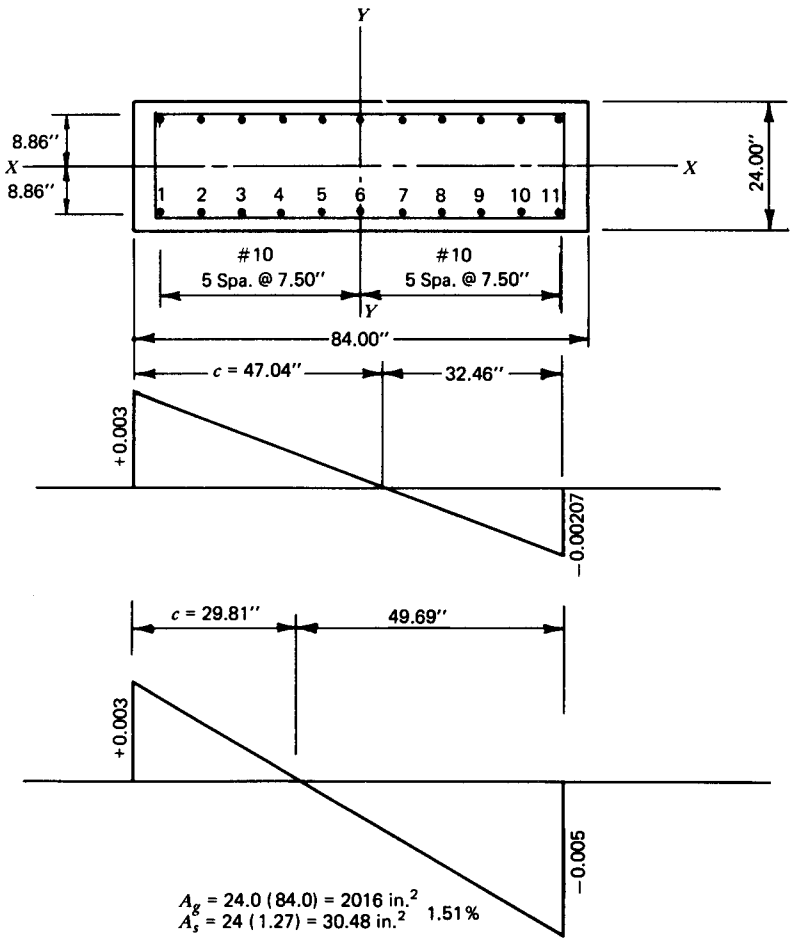

Figure 4–28 Reinforcement arrangement and strain diagrams in the transverse direction.

Using the same procedure, the analysis is repeated for the section capacity about the x-x axis (longitudinal direction), and the related data are shown in Tables 4–8 and 4–9 and in Figure 4–30. These values are likewise plotted, in addition to the ϕP_o term, and are shown in Figure 4–31.

The critical loading is selected next and compared with a simulated interaction plane, using the elliptic Equation (4–19), or the AASHTO expressions, Equation (4–17) or (4–18). For this example, the most critical condition is Group I loading at the top of the shaft.

Section capacity analysis, top of shaft. From Table 4–4, the case that controls is Group I, Case IB, with biaxial bending. The relevant parameters are

$$P_u = 421 \text{ kips}, \quad M_{u(x\text{-}x)} = 1310 \text{ ft-kips}, \quad M_{u(y\text{-}y)} = 508 \text{ ft-kips}$$

Moment magnification is considered in the transverse direction only, because the shaft is braced longitudinally against sidesway by the frame action and the stiffness at the

Table 4–6 Pier Capacity Analysis $\epsilon_s = 0.00207$ (Axis Y–Y)

Reinforcing Location	Distance R/F to Centroid	Reinforcing Area A_s	Strain at R/F	Stress in R/F	Force in R/F		Moment (kip-ft)
1	37.50	3.81	+0.00271	+60.00	+228.6		714
2	30.00	2.54	+0.00223	+60.00	+152.4		381
3	22.50	2.54	+0.00176	+51.04	+129.6		243
4	15.00	2.54	+0.00128	+37.12	+94.3		118
5	7.50	2.54	+0.00080	+23.20	+58.9		37
6	0	2.54	+0.00032	+9.28	+23.6		0
7	7.50	2.54	−0.00016	−4.64		−11.8	7
8	15.00	2.54	−0.00064	−18.56		−47.1	59
9	22.50	2.54	−0.00111	−32.19		−81.8	153
10	30.00	2.54	−0.00159	−46.11		−117.1	293
11	37.50	3.81	−0.00207	−60.00		−228.6	714
					+687.4	−486.4	2719

$c = 47.04 \qquad \beta_1 = 0.85$

$\beta_1 c = 39.98$

$A_c = 960$

$C = 0.85(3250)(960) = 2652$ kips

$M_c = 2652[42.0 - (39.98)/2](\frac{1}{12}) = 4864$ kip-ft

$\phi P_b = 2652 + 687 - 486 = 2853$ kips
$\phi M_b = 2719 + 4864 = 7583$ kip-ft
} $\phi = 1.0$

$\phi P_b = 2568$ kips
$\phi M_b = 6825$ kip-ft
} $\phi = 0.90$

$\phi P_b = 1997$ kips
$\phi M_b = 5308$ kip-ft
} $\phi = 0.70$

superstructure. For a minimum value of e of 1/10 the pier depth, or $e = 7 \times 12/10 = 8.4$ inches, $M_{u(y\text{-}y)} = 421 \times 8.4/12 = 295$ ft-kips (minimum eccentricity does not control).

The EI stiffness value is calculated next for the critical buckling loads, and moment magnification is applied in the transverse direction only. The section properties are as follows:

$$E_c = 3{,}250{,}000 \text{ psi} \qquad \text{For creep } \beta_D = 0 \qquad E_s = 29{,}000{,}000 \text{ psi}$$

$$I_y = 24 \times 84^3/12 = 1{,}185{,}410 \text{ in}^4$$

$$I_s = 4(1.27)(7.5^2 + 15.0^2 + 22.5^2 + 30.0^2) = 8572$$

$$= 6(1.27)(3.75^2) = 10{,}716$$

Total $I_s = 8572 + 10{,}716 = 19{,}288$ in^4

From AASHTO Equation (8–43)

$$EI = \frac{E_c I_g/5 + E_s I_s}{1 + \beta_D} = 1.33 \times 10^{12} \text{ lb-in}^2$$

For the critical buckling load, we use $\kappa = 2$ (From Figure 4–18), then

Table 4–7 Pier Capacity Analysis $\epsilon_s = 0.005$ (Axis *Y–Y*)

Reinforcing Location	Distance R/F to Centroid	Reinforcing Area A_s	Strain at R/F	Stress in R/F	Force in R/F		Moment (kip-ft)
1	37.50	3.81	+0.00255	+60.00	+228.6		714
2	30.00	2.54	+0.00179	+51.91	+131.9		330
3	22.50	2.54	+0.00104	+30.16	+79.6		144
4	15.00	2.54	+0.00028	+8.12	+20.6		26
5	7.50	2.54	−0.00047	−13.63		−34.6	−22
6	0	2.54	−0.00123	−35.67		−90.6	0
7	7.50	2.54	−0.00198	−57.42		−145.8	91
8	15.00	2.54	−0.00274	−60.00		−152.4	190
9	22.50	2.54	−0.00349	−60.00		−152.4	286
10	30.00	2.54	−0.00425	−60.00		−152.4	381
11	37.50	3.81	−0.00500	−60.00		−228.6	714
					+457.7	−956.8	2854

$c = 29.81$

$\beta_1 c = 0.85(29.81) = 25.34$ in.

$A_c = 25.34(24.0) = 608$ in.^{2}

$C = 0.85(3250)(608) = 1680$ kips

$M_c = 1680[42.0 - (25.34)/2](\frac{1}{12}) = 4106$ kip-ft

$\phi P_n = +457.7 - 956.8 + 1680 = 1181$ kips
$\phi M_n = 2854 + 4106 = 6960$ kip-ft
} $\phi = 1.0$

$\phi P_n = 1063$ kips
$\phi M_n = 6264$ kip-ft
} $\phi = 0.90$

$\phi P_n = 827$ kips
$\phi M_n = 4872$ kip-ft
} $\phi = 0.70$

$$P_{cr} = \frac{\pi^2(1.33 \times 10^{12})}{(2 \times 23.75 \times 12)^2} = 38{,}400 \text{ kips}$$

The magnification factor δ is computed using $\phi = 0.77$, established from capacity charts. Because the column is in the unbraced condition, $C_M = 1.0$.

From Equation (4–12)

$$\delta = \frac{1.0}{1 - 421/(0.77 \times 38{,}400)} = 1.014$$

Therefore, the load and moment conditions are

$$P_u = 421 \text{ kips} \qquad M_{u(x-x)} = 1310 \text{ ft-kips}$$
$$M_{u(y\text{-}y)} = 508 \times 1.014 = 515 \text{ ft-kips}$$

Scaling directly from the capacity curves, we obtain

$$\frac{M_{ux}}{\phi M_{nx}} = 0.88 \quad \text{and} \quad \frac{M_{uy}}{\phi M_{ny}} = 0.10 \text{ (from plots)}$$

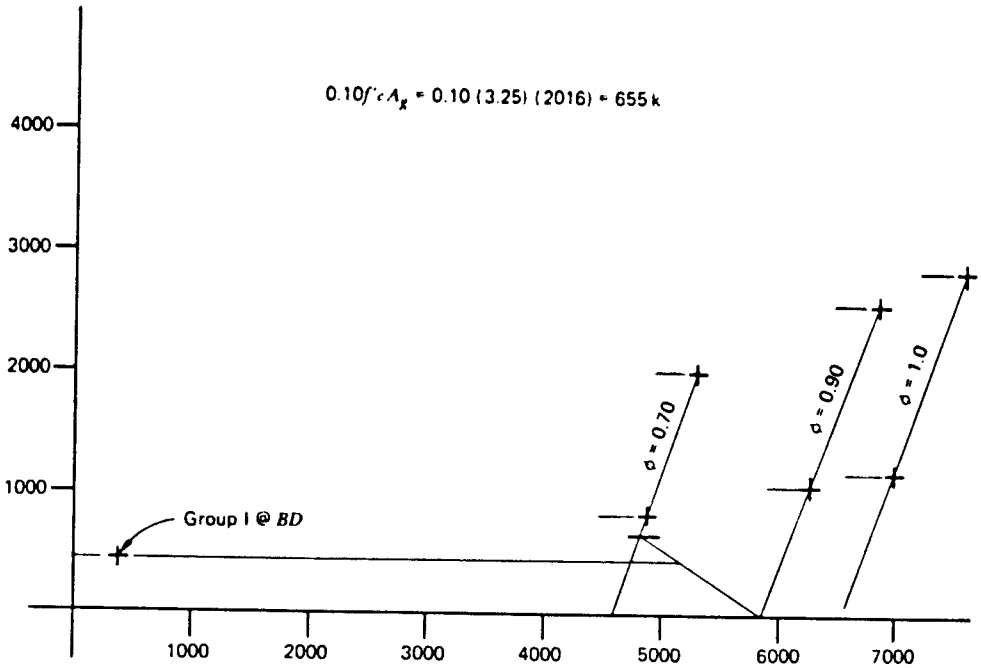

Figure 4–29 Procedure for pier section analysis; axis *Y-Y* (transverse direction).

Table 4–8 Pier Capacity Analysis $\epsilon_s = 0.005$ (Axis *X–X*)

Reinforcing Location	Distance R/F to Centroid	Reinforcing Area A_s	Strain at R/F	Stress in R/F	Force in R/F		Moment (kip-ft)
1	8.86	13.97	+0.00180	+52.20	+729.2		538
2	0	2.54	−0.00160	−46.40		−117.9	0
3	8.86	13.97	−0.00500	−60.00		−838.2	619
					+729.2	−956.1	1157

$c = 7.82$

$\beta_1 c = 0.85(7.82) = 6.65$

$A_c = 6.65(84.0) = 558$

$C = 558(3.25)(0.85) = 1542$ kips

$M_c = 1542[12.0 - (6.65)/2](\frac{1}{12}) = 1115$ kip-ft

$\phi P_n = 1542 - 729.2 - 956.1 = 1315$ kips
$\phi M_n = 1115 + 1157 = 2272$ kip-ft
} $\phi = 1.0$

$\phi P_n = 1184$ kips
$\phi M_n = 2045$ kip-ft
} $\phi = 0.90$

$\phi P_n = 920$ kips
$\phi M_n = 1590$ kip-ft
} $\phi = 0.70$

Table 4–9 Pier Capacity Analysis $\epsilon_s = 0.00207$ (Axis X–X)

Reinforcing Location	Distance R/F to Centroid	Reinforcing Area A_s	Strain at R/F	Stress in R/F	Force in R/F		Moment (kip-ft)
1	8.86	13.97	+0.00224	+60.00	+838.2		619
2	0	2.54	+0.00008	+2.32	+5.9		0
3	8.86	13.97	−0.00207	−60.00		−838.2	619
					+844.1	−838.2	1238

c = 12.34 in.
$\beta_1 c$ = 0.85(12.34) = 10.49
A_c = 84.0(10.49) = 881
C = 881(3.25)(0.85) = 2434 kips
M_c = 2434[12.0 − (10.40)/2]($\frac{1}{12}$) = 1370 kip-ft

ϕP_b = 2434 + 844.1 − 838.2 = 2440 kips
ϕM_b = 1370 + 1238 = 2608 kip
} ϕ = 1.0

ϕP_b = 2196 kips
ϕM_b = 2347 kip-ft
} ϕ = 0.90

ϕP_b = 1708 kips
ϕM_b = 1826 kip-ft
} ϕ = 0.70

The biaxial capacity may now be checked according to two criteria.

1. According to AASHTO, by applying Equation (4–18)

$$\frac{M_{ux}}{\phi M_{nx}} + \frac{M_{uy}}{\phi M_{ny}} < 1, \text{ or } 0.88 + 0.10 = 0.98 < 1.0, \text{ OK}$$

2. According to Furlong, by applying Equation (4–19)

$$\sqrt{(0.88)^2 + (0.10)^2} = 0.88 < 1.0, \text{ OK}$$

Analysis by the Hu method. This procedure, mentioned briefly in the foregoing section, is used to compute stresses at a given column section. It involves the following steps.

1. Compute the section constants. These are: A_c = gross area of cross section; A_s = area of steel reinforcement; I_x^s = moment of inertia of steel about x-x axis (nontransformed section); I_y^s = moment of inertia of steel about y-y axis (nontransformed section); I_x^c = moment of inertia of gross section about x-x axis; I_y^c = moment of inertia of gross section about y-y axis.

Also
$$np = \frac{nA_s}{A_c} \qquad nq_x = \frac{nI_x^s}{I_x^c} \qquad nq_y = \frac{nI_y^s}{I_y^c}$$

where n is the elastic constant ratio.

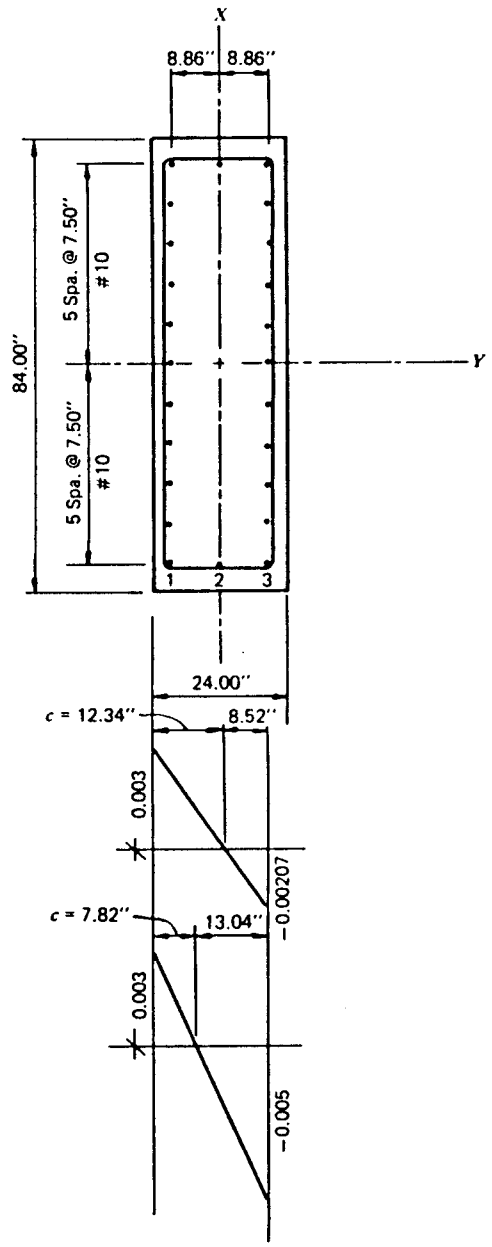

Figure 4–30 Reinforcement arrangement and strain diagrams, longitudinal direction.

2. Compute the load constants. These are as follows:

$$e_x = \frac{M_x}{Nd} \qquad e_y = \frac{M_y}{Nb} \qquad m_z = \frac{e_x}{e_y}$$

where M_x = bending moment about x-x axis; M_y = bending moment about y-y axis; N = total direct load; d = length of section normal to x-x axis; b = length of section normal to y-y axis.

3. Compute the value Q from section and load constants. This value is

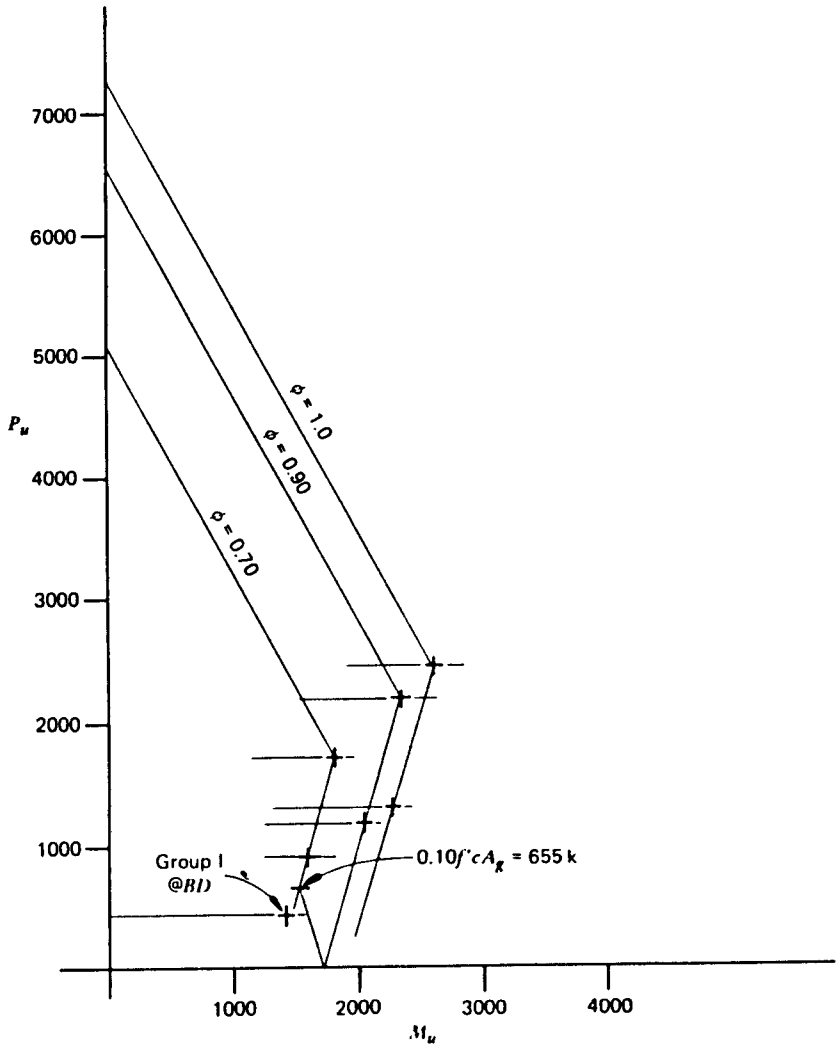

Pier section capacity: axis X-X (longitudinal moment.

$$\phi P_0 = [(0.85)(f'_c)(A_g - A_{st}) + A_{st} f_y]\,\phi;$$

$$\phi P_0 = [(0.85)(3.25)(2016 - 30.48) + 30.48(60)]$$

$\phi = 7314$ k $\quad \phi = 1.0,$

$= 6582$ k $\quad \phi = 0.90,$

$= 5120$ k $\quad \phi = 0.70.$

Figure 4–31 Procedure for pier section analysis; axis X-X (longitudinal direction).

$$Q = (nq_y + m^2 nq_x)/np$$

4. Obtain the values of N/bdf_c and κ by reference to Figure 4–32. An interpolation is usually necessary between the charts for both np and Q as computed from step 3. Note that the e_x and e_y axes are not consistent in these charts. The values of Q may be kept within the chart range by a proper selection of x and y axes. The values of np in the chart may be expected to fall within most practical ranges.
5. Obtain the concrete stress by making use of N/bdf_c. The steel stress is computed from

$$f_s = nf_c\left(1 - \frac{1-a_x}{h} - \frac{1-a_y}{k}\right)$$

where $h = \kappa/m$, and a_x and a_y are the clearances to the center lines of bars in the x

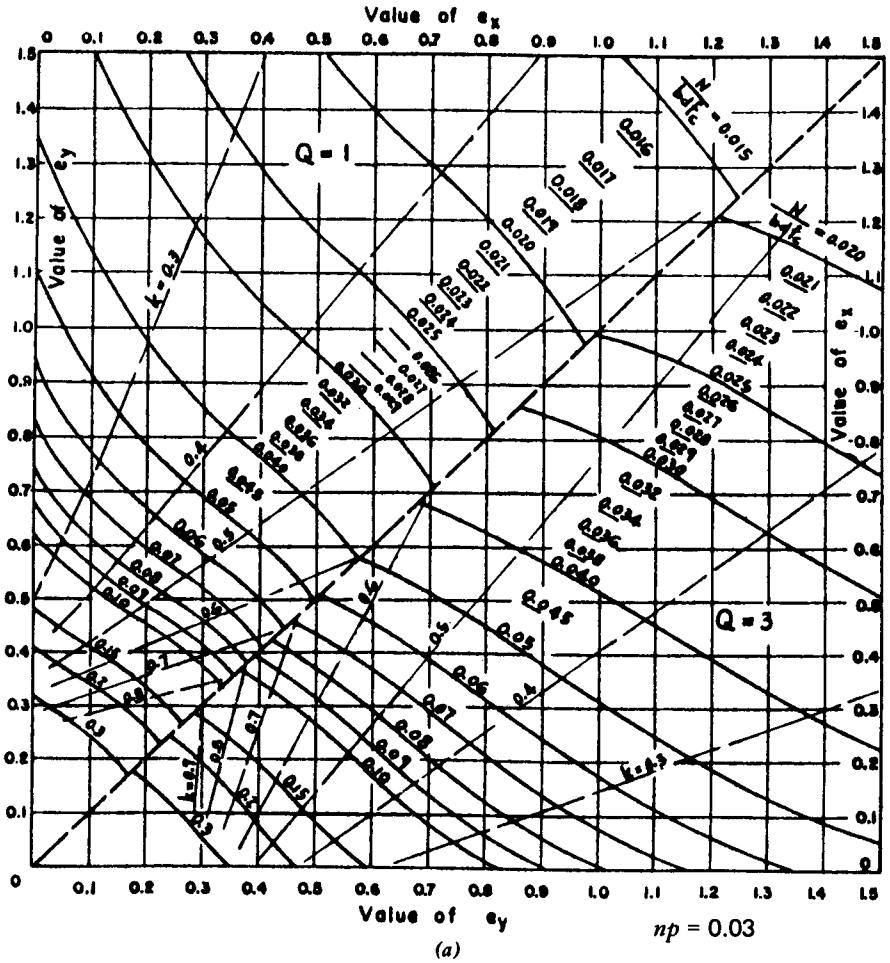

Figure 4–32 Charts and bending curves for section analysis, biaxial bending *(from Hu, 1955)*.

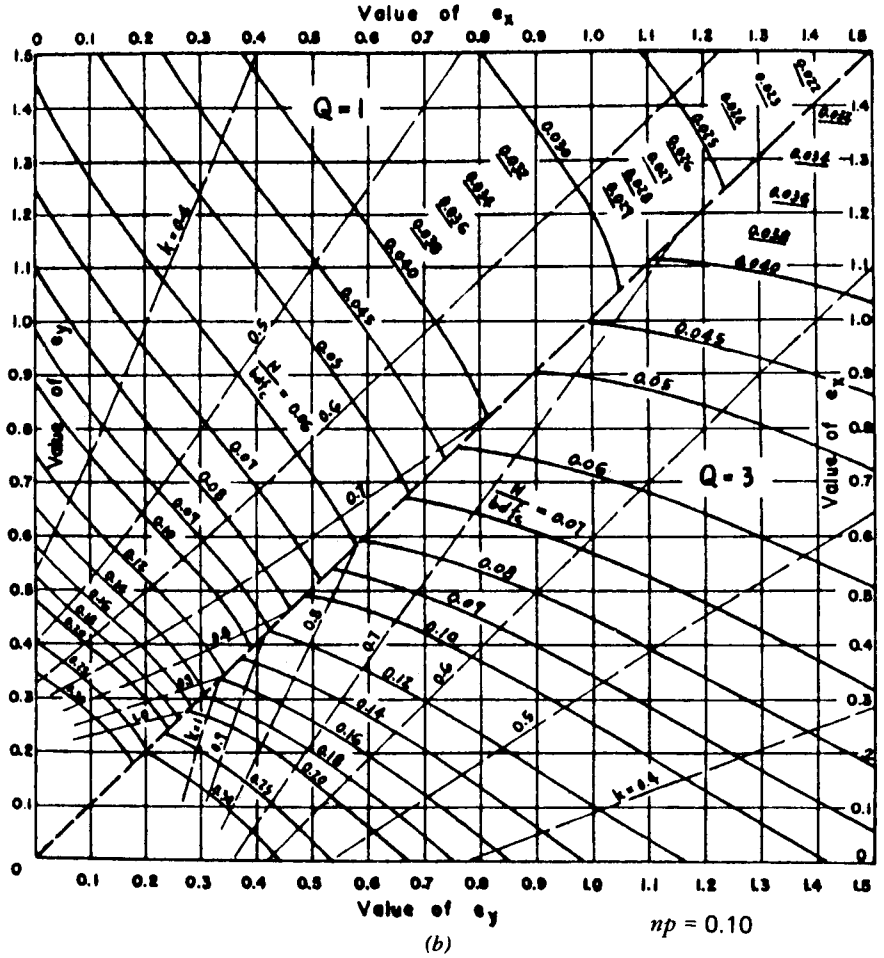

Figure 4–32 *(continued)*

and y directions, respectively, expressed as a fraction of the section dimensions in the same direction.

For the column top section and reinforcement details shown in Figure 4–28, the stresses will be checked under service loads. These loads are

$$P = 360 \text{ kips} \qquad M_y = 776 \text{ ft-kips} \qquad M_x = 234 \text{ ft-kips}$$

Also $$A_s = 30.48 \text{ in}^2 \text{ and } A_c = 2016 \text{ in}^2$$

The following parameters are computed

$$I_x^s = 4(1.27)(7.50)^2 + 4(1.27)(15.00)^2 + 4(1.27)(22.50)^2$$
$$+ \ 4(1.27)(30.00)^2 + 6(1.27)(37.50)^2 = 19{,}298 \text{ in}^4$$

$$I_x^c = 24.0(84.0)^3 / 12 = 1{,}185{,}400 \text{ in}^4$$

$$I_y^s = 2(11)(1.27)(8.86)^2 = 2193 \text{ in}^4$$

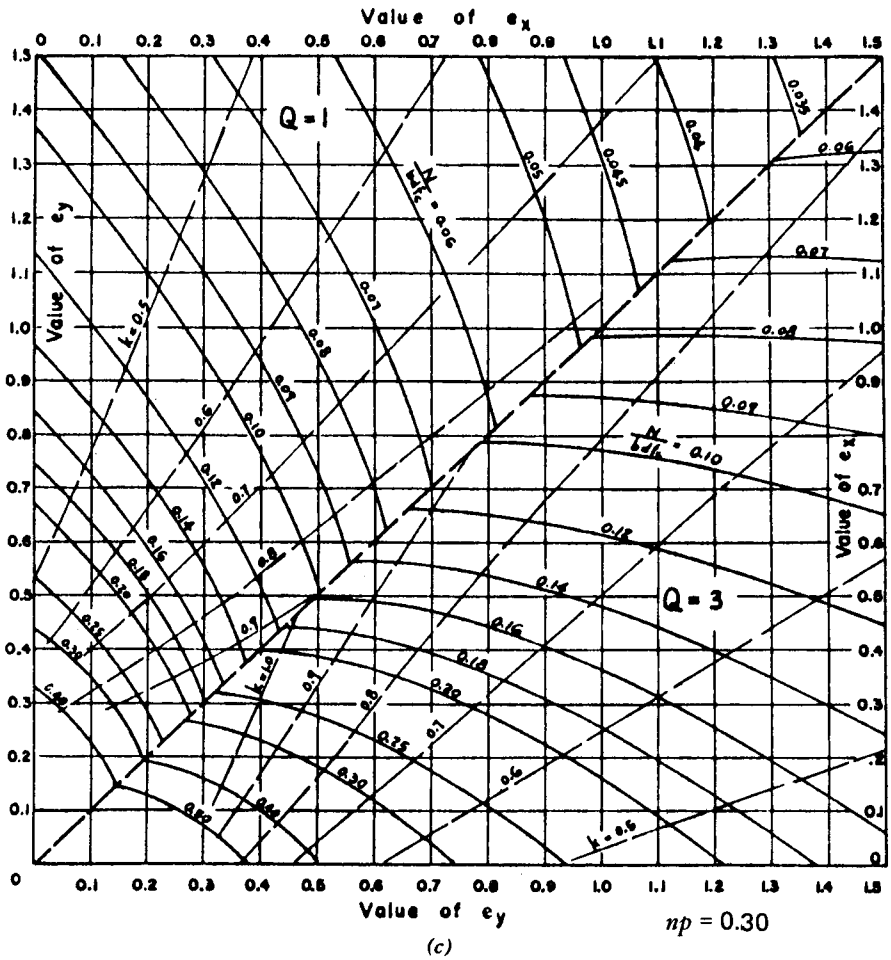

(c)

Figure 4–32 *(continued)*

$$I_y^c = 84(24.0)^3 / 12 = 96{,}768 \text{ in}^4$$

$$np = 9(30.48)/2016 = 0.1361$$

$$nq_x = 9(19{,}284)/1{,}185{,}400 = 0.1464$$

$$nq_y = 9(2193)/96{,}768 = 0.204$$

$$e_x = (234)/(360.2)(7.00) = 0.0928$$

$$e_y = (776)/(360.2)(2.00) = 1.077$$

$$m = 0.0928/1.077 = 0.086$$

$$Q = \frac{0.204 + (0.086)^2(0.1464)}{0.1361} = 1.51$$

The values of N/bdf'_c are computed by interpolation as shown in the following tabulation:

	$np = 0.10$		$np = 0.30$	
	N/bdf'_c	k	N/bdf'_c	k
$Q = 1$	0.072	0.35	0.115	0.45
$Q = 3$	0.115	0.38	0.205	0.52
$Q = 1.51$	0.083	0.36	0.138	0.47

from which the following are obtained

$$np = 0.1361 \quad N/bdf'_c = 0.093 \quad \kappa = 0.38$$

The factors h, a_x, and a_y are computed as: $h = 0.38/0.086 = 4.42$; $a_x = 4.5/84.0 = 0.0536$; $a_y = 3.14/24.0 = 0.1308$.

The stresses in the concrete and the steel are computed as follows:

$$f_c = \frac{N}{bd(0.093)} = \frac{360{,}000}{(24.0)(84.0)(0.093)} = 1920 \text{ lb/in}^2$$

$$f_s = 9(1920)\left(1 - \frac{1-0.0536}{442} - \frac{1-0.1308}{0.38}\right) = 26{,}000 \text{ lb/in}^2$$

The shaft should also be checked for serviceability requirements with respect to crack width, computed as follows (Kaar and Mattock, 1963). For the top of the column, $A = 2(3.14)(7.5) = 47.1$ and $w = 0.115 \sqrt[4]{47.1} \times (26.0) \times 10^{-3} = 0.0078$ in < 0.008 in.

Commentary. The LRFD specifications contain provisions for special crack width control, applied to concrete members subjected to flexure, or flexure and axial load, or axial tension. For column without tension in the cross section, these provisions do not apply.

Crack control is indicated for piers exposed to moisture, and freezing and thawing. An expression giving the probable maximum crack width at the tension face of a flexural member is (Gergely and Lutz, 1968)

$$w = 0.076 \, \beta f_s \sqrt[3]{d_c A} \tag{4–20}$$

where w = expected maximum crack width (0.001-in units); β = ratio of distances to the neutral axis from the extreme tension fiber and from the centroid of A_s; d_c = cover of outermost bar of A_s measured to the center of the bar; A = tension area per bar measured as specified by ACI Code.

The ACI code applies Equation (4–20) with $\beta = 1.2$ as a basis for computing limiting values of $f_s \sqrt[3]{d_c A}$, which are set as 175 kips/inch for interior exposure and 145 kips/inch for exterior exposure. These values give $w = 0.016$ and 0.013 inch, respectively.

The LRFD specifications address the control of cracking in the context of bridges subjected to normal exposure. Control of surface cracking is particularly important for reinforcement with yield strength exceeding 40,000 lb/in^2. There appears to be little or no connection between surface crack width and steel corrosion, and thicker or additional cover can result in greater surface crack widths. Structures subjected to very aggressive exposure are beyond the scope of the provisions, but for bridge piers positioned in water or buried in the ground, the recommended limiting maximum crack width is 0.006 inch.

4.10 DESIGN EXAMPLE 4–2: HAMMERHEAD PIER

Two typical hammerhead pier types are shown in Figure 1–1(b), and include the single hammerhead usually chosen with H/V ratios less than 2.25, and the double hammerhead usually recommended for H/V ratios between 2.25 and 3.0 and with a maximum H = 40 feet. For H values exceeding 40 feet, the multiple hammerhead with three or more columns may be chosen, but in this case the pier type should be classified as multiple-column pier. These guidelines are based on V being in the range of 13 to 17 feet, which is the usual pier height for conventional grade separation structures. For extreme heights the single hammerhead is a viable choice.

Design Procedure

The design procedure may be summarized in the following sequence of steps:

1. Determine general dimensions from geometric and structural considerations.
2. Calculate the loads and forces acting on the pier, and their point of application.
3. Check the overall pier stability under all applicable group loadings. This involves primarily overturning and resistance to sliding.
4. Determine the required reinforcing steel for flexural, shear, and axial capacity.
5. Adjust dimensions, if necessary, to attain the necessary convergence in the calculations and assumptions.

Initially the pier dimensions follow the dimensions of the bridge and the geometry of the superstructure. The pier height is controlled by the bridge profile and the elevation at the bottom of the footing. The minimum width of the pier may be dictated by the space necessary for the bearings. For single bearings and nominal skews, a usual thickness is 2.5 to 3.0 feet, with 2 feet as minimum.

The pier head may be detailed as shown in Figure 1–1(b), with a minimum depth at the outer edge of 2.25 feet. This depth is usually increased at a slope pleasing to the eye. A suggested depth at the junction with the shaft is 0.15 H. Evidently, this depth may also be controlled by shear and moment requirements where the projecting portion is treated as a cantilever beam.

The shaft or main hammer may be detailed with a minimum slope or batter as shown in Figure 1–1(b). The overall width at the base (top of footing) may be dictated by stability considerations (overturning of the pier in the transverse direction) or by the size of footing necessary to accommodate the allowable soil pressure or the number of piles.

Interestingly, whereas Group I will normally control the design of the pier head (cantilever portion), Group II or III may control stability against overturning and the design of the foundation. These AASHTO groups may also govern the design of the pier in the direction of the bridge.

Design Data

The pier for this example is one of the intermediate supports for a three-span bridge simply supported. The superstructure consists of a 7¼-inch concrete slab on steel beams spaced at 6 feet 9 inches in centers. The beams have fixed bearings at the abut-

ments. It appears from this configuration that one of the piers has two expansion bearings, and the second pier has one fixed and one expansion bearing.

The concrete for the pier has f'_c = 3000 lb/in^2, and reinforcing steel grade 40. Rock exists approximately 40 feet below the slab level, and has a design allowable bearing of 8 kips/ft^2. The pier is assumed to be 4 feet thick. A partial pier end view in the direction of the bridge is shown in Figure 4–33(a), and includes the position of a wheel line for maximum live load reaction. The bridge is placed at zero skew.

Design of Pier Head (ASD)

Figure 4–33(b) shows a partial pier elevation. Also shown are the beam locations, the position of live load with maximum eccentricity to produce maximum moment and shear in the cantilever, and the unit dead load from the superstructure.

Figure 4–34 shows the detail of the pier head with the position of the live load for maximum eccentricity. Also shown are the dead load reactions, and the live load reactions (without impact) for the loading position (truck) shown in Figure 4–33(b). These reactions are distributed to the beams assuming the slab acts as a simple beam between longitudinal beams.

From Figure 4–33(b) we obtain

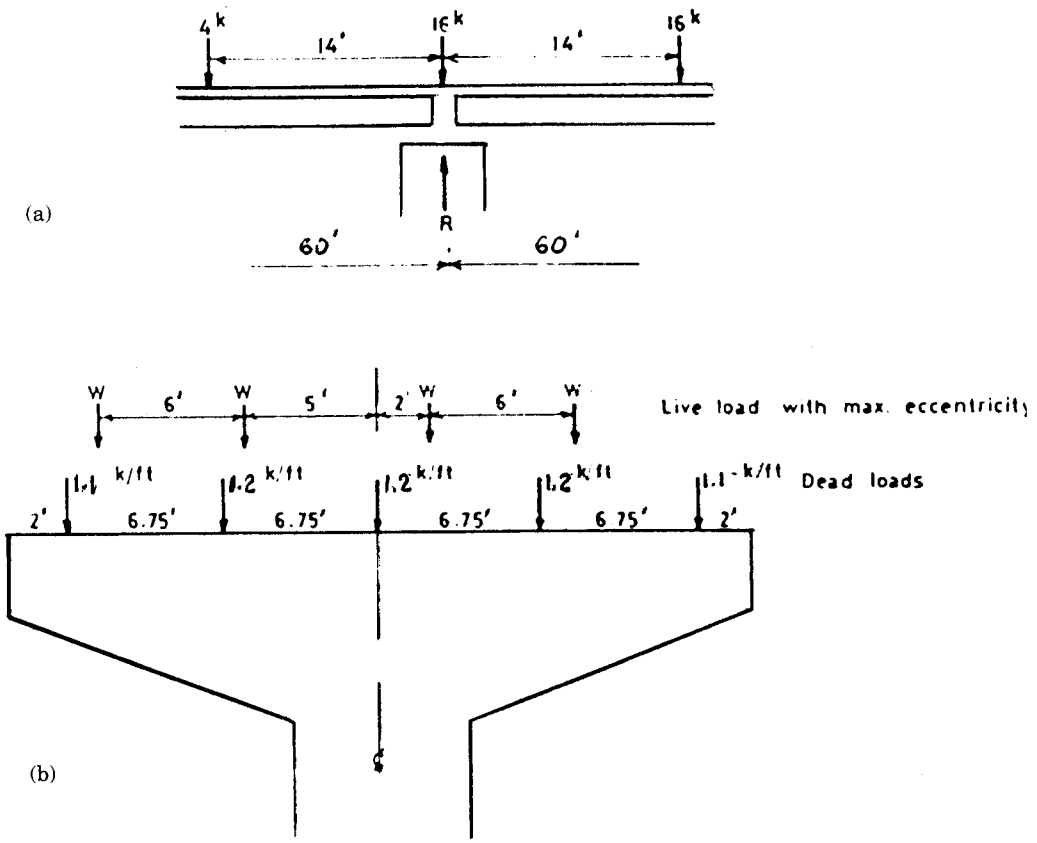

Figure 4–33 (a) Live-loading reaction at pier; (b) live-loading on pier.

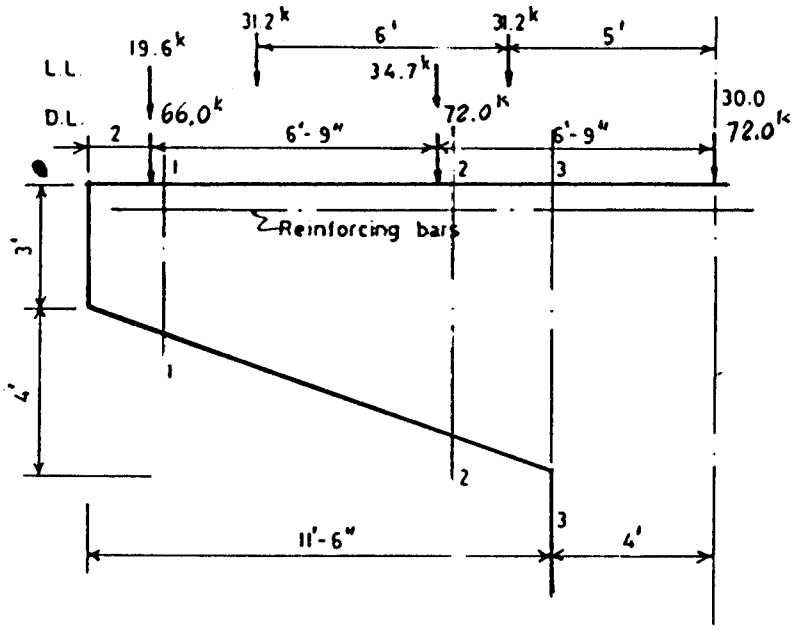

Figure 4–34 Pier-head loading.

$$R = W = 16 + \frac{46}{60}(20) = 31.4 \text{ kips}$$

The dead load reactions are as follows:

$$\text{Interior beams} = 60 \times 1.2 = 72.0 \text{ kips}$$
$$\text{Exterior beams} = 60 \times 1.1 = 66.0 \text{ kips}$$

Shear. At section 1–1 (D = 4 ft), Figure 4–34

$$V = 19.6 + 66.0 + 4(3)(3.5)(0.15) = 91.9 \text{ kips}$$

For D = 48 in, d = 45 in, and

$$v = \frac{V}{bd} = \frac{91900}{48 \times 45} = 43 \text{ lb/in}^2$$

Allowable $v_c = 0.95\sqrt{f'_c} = 52 \text{ lb/in}^2 > 43$ OK

Note however that a more detailed calculation of shear may be made by using AASHTO Equation (8–4).

At section 2–2 (D = 6 ft), reactions from two beams

$$V = 85.6 + 106.7 + 4(9)(4.5)(0.15) = 216.6 \text{ kips}$$
$$v = \frac{216600}{48 \times 69} = 65.4 \text{ lb/in}^2, \text{ stirrups are required}$$

At section 3–3 (D = 7 ft)

$$V = 192.3 + 4(11.5)(5)(0.15) = 226.8 \text{ kips}$$

$$v = \frac{226800}{48 \times 81} = 58.3 \text{ lb/in}^2$$

Where stirrups are required, the spacing is

$$s = \frac{A_u f_s}{(v - v_c)b}, \text{ AASHTO Equation (8–7)}$$

For #4 stirrups, v = 65.4 lb/in^2, and v_c = 52 lb/in^2

$$s = \frac{0.40(20{,}000)}{(65.4 - 52)(48)} = 12.4 \text{ in, say 12 in}$$

Stirrups or ties are, however, recommended throughout the length of the pier head, or #4 @ 12-in centers.

Moment. The moment is computed at section 3–3, or

$$M = 85.6(9.5) + 106.7(2.75) + 20.7(5.75) + 13.8(3.83) =$$
$$= 813.2 + 293.4 + 119.0 + 52.9 = 1278 \text{ ft-kips}$$

Assuming a 2-inch cover and #10 bars, d = 84 − 2.63 = 81.4 inches. Assume j = 7/8 = 0.875, then

$$\text{Required} \quad A_s = \frac{1278(12)}{(0.875)(81.4)(20)} = 10.8 \text{ in}^2$$

Number of bars (#10) = 10.8/1.27 = 8.5, say 9 bars, spaced at about 5½-inch centers. The reinforcement for the pier head is arranged as shown in Figure 4–35. Note also that 4 #5 bars are provided at the bottom, and 3 #4 bars along each face. The stirrups are used in pairs, and several configurations may be necessary to fit the increase in the depth. Although experience indicates that the concrete stress is unlikely to control, it will be computed as follows:

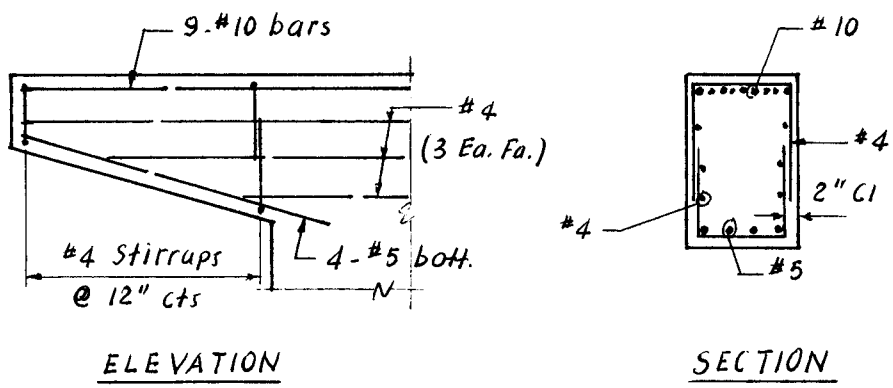

Figure 4–35 Top of pier details, Design Example.

$$f_c = \frac{2(1278)(12)}{48(81.4)^2(3/8)(7/8)} = 290 \text{ lb/in}^2 < 1200$$

Pier Stability

Group I. Referring to Figure 4–36, the total dead load from the superstructure is 348 kips, concentrically applied. The live load is 31.2 × 4 = 125 kips, applied with an eccentricity of 1.5 feet as shown. The weight of pier is computed as follows:

$$W_1 = (31\times3 + 11.5\times4 + 29.7\times8)(4)(0.15) = 226 \text{ kips}$$
$$W_2 = 14\times10\times4\times0.15 = 84 \text{ kips}$$

Total vertical load = 348 + 125 + 226 + 84 = 783 kips
Overturning moment = 125 × 1.5 = 188 ft-kips
Balancing moment = 783 × 7 = 5481 ft-kips
Factor of safety FS = 5481/188 = 29

The pier must be designed to resist overturning with a factor of safety at least 2.0, and sliding with a factor of safety at least 1.5 (see also section 7.4).

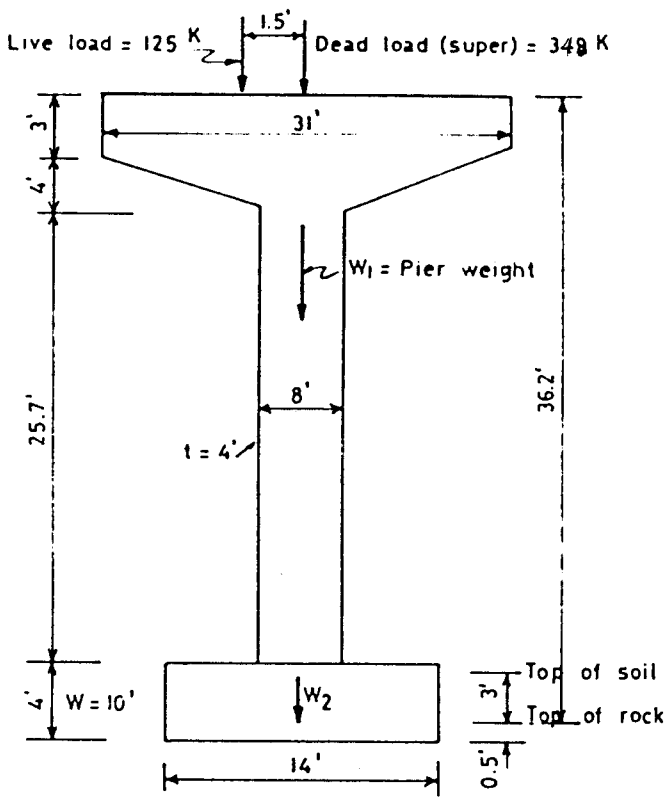

Figure 4–36 Pier elevation, dimensions, and loads, Group I.

With one lane loaded, total load P = 720 kips, and overturning moment M = 499 ft-kips, giving a factor of safety FS = 10.1.

Group II. (D + W), 125 percent stress. Figure 4–37 shows elevation of the bridge. The symbols F and E indicate fixed and expansion bearing, respectively. Because the pier analysis for Group II involves the action of transverse and longitudinal forces, besides vertical loads, it is necessary to define the design criteria with regard to the distribution of these forces to fixed and expansion bearings. An explicit assumption is that the expansion bearing can resist longitudinal forces up to its frictional capacity. Assuming 10 percent friction, the resisting force is 0.5 × 348 × 0.10 = 17.4 kips. For a total superstructure depth of 5 feet 6 inches (including curb, parapet and railing), the longitudinal wind from half span is (5.5)(30)(12) = 2 kips. In effect, this means that both fixed and expansion bearings resist the longitudinal wind equal, hence the designs of pier 1 and 2 for Group II are identical.

With the superstructure in place the forces and loads are computed as follows:

Lateral wind force = 5.5× 60 × 0.05 = 16.5 kips (acting 41 ft above base of footing)
Longitudinal wind force = 5.5 × 60 × 0.012 = 4.0 kips
Uplift wind = 32.2 × 60 × 0.02 = 38.6 kips (acting at the quarter point)
Wind on substructure, lateral = 33.2 × 4 × 0.04 = 5.3 kips
Computation of moments:

From lateral wind on superstructure,	M = 16.5× 41	= 677 ft-kips
From uplift	M = 38.6 × 8.1	= 313 ft-kips
From wind on pier	M = 5.3 × 20.2	= 107 ft-kips
Total lateral overturning moment		= 1097 ft-kips
From longitudinal wind on superstructure	M = 4.0 × 41	= 164 ft-kips

Total vertical force = 348 + 226 + 84 − 39 = 619 kips

The resultant overturning moment from the lateral and longitudinal forces is, therefore,

$$M = \sqrt{1097^2 + 164^2} = 1109 \text{ ft-kips}$$

The resultant overturning moment has a direction very close to the lateral direction, hence overturning may be assumed about the short axis of the footing. Then, the balancing moment is 619 × 7 = 4333 ft-kips, and

$$FS = 4333/1109 = 3.9 > 2$$

Group III. Referring to Figure 4–37, the following assumptions are made:
(1) the right expansion bearing at pier 1 becomes frictionless and cannot resist longitudinal forces; and (2) the expansion bearing at pier 2 continues to provide frictional resis-

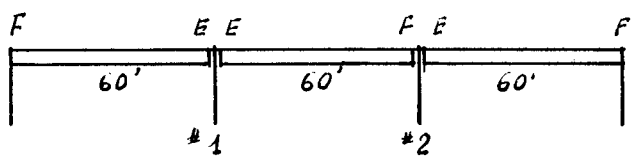

Figure 4–37 Bridge elevation, Design Example.

tance and can resist longitudinal forces up to its frictional capacity. Consequently, the design of pier 2 will be different from the design of pier 1, and will normally govern. This pier must be designed to resist all longitudinal forces from the center span, and one-half of the longitudinal forces from the end span.

The longitudinal forces are computed as follows:

Wind on live load = $60 \times 1.5 \times 0.04 = 3.6$ kips
Wind on superstructure = $60 \times 1.5 \times 5.5 \times 0.012 \times 0.3 = 1.8$ kips
Traction (2 lanes) = $(0.64 \times 90 + 18) \times 2 \times 0.05 = 7.6$ kips

The lateral forces are likewise computed assuming that the pier resists lateral effects from one span, as in Group II.

Superstructure lateral wind	$= 16.5 \times 0.3$	$= 5.0$ kips
Uplift wind	$= 38.6 \times 0.3$	$= 11.6$ kips
Wind on live load	$= 60 \times 0.1$	$= 6.0$ kips
Wind on pier	$= 5.3 \times 0.3$	$= 1.6$ kips

Traction forces and wind loads on live load are assumed to act 6 feet above the deck floor, although some states choose to transfer these forces at the bearing level.

The lateral overturning moment is

$$M = 1097 \times 0.3 + 6 \times 46 = 329 + 276 = 605 \text{ ft-kips}$$

The longitudinal moment is the summation of the following:

Wind on live load $M = 3.6 \times 46$		$= 166$ ft-kips
Wind on superstructure $M = 1.8 \times 41$		$= 74$ ft-kips
Traction $M = 7.6 \times 46$		$= 350$ ft-kips
Total longitudinal moment M		$= 590$ ft-kips

In addition, a live load reaction may be considered as in Group I, but one lane with the same eccentricity. This reaction is 63 kips, giving a moment of 499 ft-kips, to be added to the lateral moment. The Group III load-moment summary is, therefore,

$$P = 709 \text{ kips, Lateral } M = 1104 \text{ ft-kips,}$$
$$\text{Longitudinal } M = 590 \text{ ft-kips}$$

A suggested approach for checking the stability against overturning in either direction is to compute the resultant moment $M = \sqrt{1104^2 + 590^2} = 1252$ ft-kips and compare it with the balancing moment in the lateral direction. In this case

$$FS = \frac{709 \times 7}{1252} = 3.96 > 2$$

Footing

For footings subjected to eccentric loading about one or both principal directions, an effective footing size may be obtained as discussed in section 8.3, and expressed by Equation (8–5) and (8–6). The reduced dimensions represent an equivalent uniform bearing pressure and *not* the actual contact pressure distribution beneath the footing. This equivalent pressure may be multiplied by the reduced footing area to obtain the ultimate load Q_{ult} from the standpoint of ultimate capacity. This yields Equation (8–7). The actual contact pressure distribution (usually trapezoidal) should be used to check moments and shears. For ASD, the maximum contact pressure (occurring at one corner of the footing) may be compared with the allowable soil pressure.

The initial dimensions for the footing of this example are as shown in Figure 4–38. Referring to this detail,

M_y = transverse moment about y axis, $e_x = M_y/P$
M_x = longitudinal moment about x axis, $e_y = M_x/P$

The soil pressure may be computed from the following

$$q = \frac{P}{BL}\left(1 \pm \frac{6e_x}{L} \pm \frac{6e_y}{B}\right) \tag{4–21}$$

where all notation corresponds to Figure 4–38.

Group II. Given P = 619 kips, M_y = 1097 ft-kips, M_x = 164 ft-kips
We compute e_x = 1097/619 = 1.77 ft e_y = 164/619 = 0.27 ft

$$q_{max} = \frac{619}{14 \times 10}\left(1 + \frac{6 \times 1.77}{14} + \frac{6 \times 0.27}{10}\right) = 4.42(1 + 0.76 + 0.16) = 8.5 \text{ kips/ft}$$

$$< 8.0 \times 1.25, \text{ OK}$$

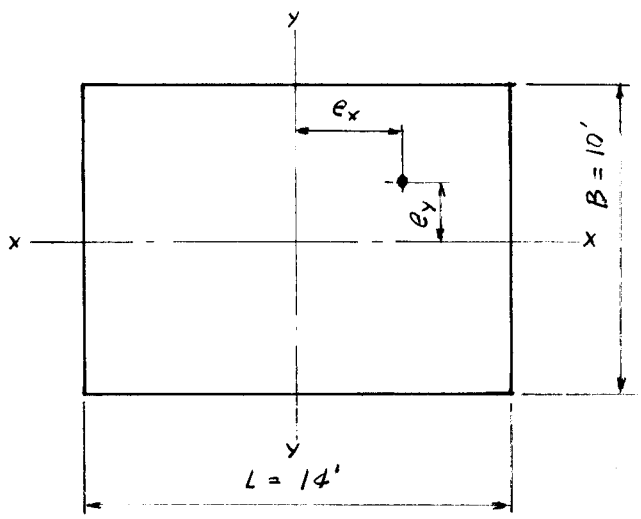

Figure 4–38 Footing plan and dimensions, Design Example.

Wind force applied directly to the pier may also be assumed in a direction skewed to the pier. This wind may be resolved into two components perpendicular and parallel to the main pier direction, and then applied simultaneously with the wind loads from the superstructure. Referring to Figure 4–36, this wind force is computed as 15 kips, resulting in a moment of 375 ft-kips. The assumed direction is taken as 30° from the line normal to the pier. This moment is resolved into two components as follows:

$$\text{lateral moment} = 375 \times 0.5 = 187 \text{ ft-kips},$$

$$\text{longitudinal moment} = 375 \times 0.866 = 325 \text{ ft-kips}$$

For this condition the loads and moments for Group II are

$$P = 619 \text{ kips} \qquad M_y = 1177 \text{ ft-kips} \qquad M_x = 489 \text{ ft-kips}$$

Likewise, we compute $e_x = 1177/619 = 1.90$ ft,

$$e_y = 489/619 = 0.79 \text{ ft}$$

The pressure is now

$$q = \frac{619}{140}\left(1 \pm \frac{6 \times 1.90}{14} \pm \frac{6 \times 0.79}{10}\right) = 4.42(1 \pm 0.80 \pm 0.47)$$

Because there is a negative pressure (indicating tension), the footing must be revised. We select new dimensions $L = 16$ feet, and $B = 12$ feet. The pressure is computed as

$$q = \frac{619}{192}\left(1 \pm \frac{6 \times 1.90}{16} \pm \frac{6 \times 0.79}{12}\right) = 3.22(1 \pm 0.71 \pm 0.39) =$$

$$= 6.8 \text{ kips/ft}^2 \text{ max.}$$

$$= -0.3 \text{ kips/ft}^2 \text{ min.}$$

A negative pressure of 0.3 kips/ft^2 is acceptable, and it means that actual soil pressures in the tension zone are redistributed so that the average pressure from the direct load is somewhat increased.

The analysis of the shaft must be performed for axial load and biaxial bending, and involves procedures discussed in the foregoing sections.

4.11 DESIGN EXAMPLE 4–3: STEEL BENT CAP

Figure 4–39 shows a typical steel bent pier, part of a long viaduct. The superstructure consists of simple spans, concrete decks on composite steel girders for the longer spans, and steel rolled beams for spans between 50 and 60 feet long. The bents supporting the girders are built of steel, with one, two, or three columns depending on the length of the bent and its location. As can be seen in Figure 4–39 the bent caps are raised because they encroach on usable roadway where minimum vertical clearance must be provided. The beam seat support details are, therefore, part of the bent cap framing. The two simple spans adjacent to this bent are 59 feet 5 inches long on either side, and simple supported.

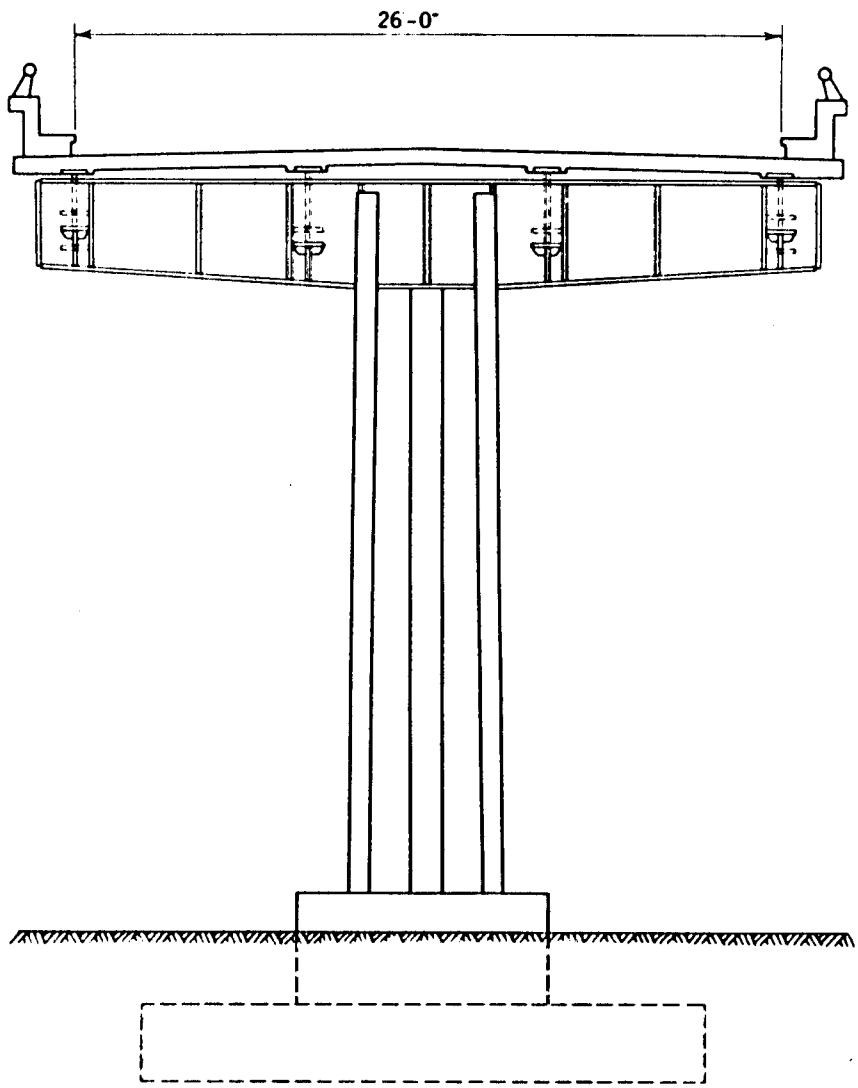

Figure 4–39 Bent elevation of design example.

Loads on Bent

The dead load reactions are 82 kips for the exterior girders, and 60 kips for the interior girders. The live load is HS 20. The live load reaction is checked for truck loading and lane loading. For one truck, the live load reaction is

$$32 + \frac{45.4}{59.4}(32 + 8) = 62.6 \text{ kips}$$

Likewise, the live load reaction for lane loading is (one lane)

$$26 + 0.64 \times 59.4 = 64.0 \text{ kips (controls)}$$

Because the girders frame into the bent cap through the direct support, impact will be used. According to AASHTO the impact factor is

$$I = 50/(50.4 + 125) = 0.27$$

Live load plus impact = $1.27 \times 64 = 81.4$ kips (one lane)

The cap configuration with the outline of the deck slab and the reactions from the girders are shown in Figure 4–40. The steel is A36.

Moments and Shears

The dead load shear is computed as follows:

Reaction from girders	= 59.5 + 81.5	= 141.0 kips
Weight of cap	= 0.32 × 11.75	= 3.8 kips
	Dead load shear	= 144.8 kips

Likewise the live load plus impact shear is 81.4 kips, and need not be resolved into two components representing the beam reactions.

Dead load moment $M_{DL} = 59.5 \times 2.08 + 81.5 \times 10.75 + 0.32(11.75)^2/2 = 1023$ ft-kips

Live load plus impact moment $M_{LL+I} = 81.4 \times 5.75 = 468$ ft-kips

Summary: Total moment $M = 1491$ ft-kips,

Total shear $V = 226$ kips

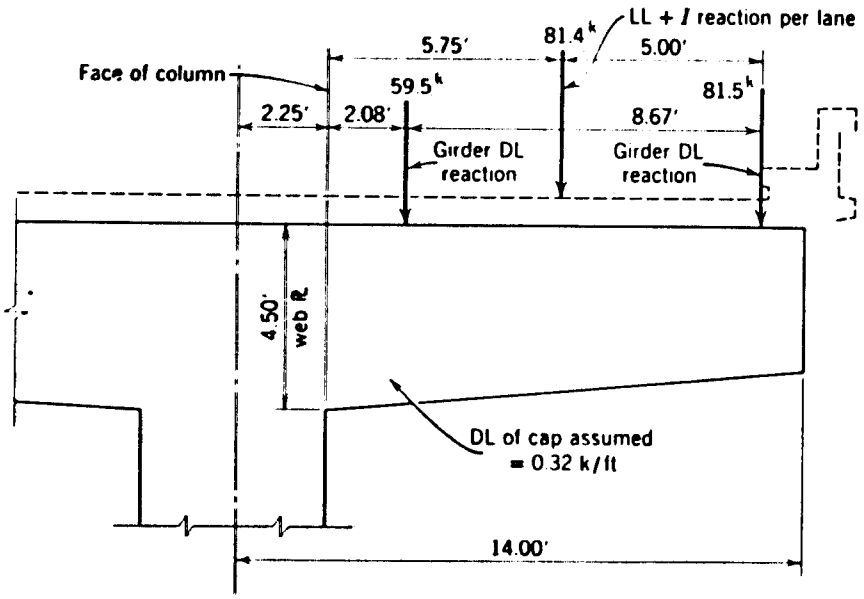

Figure 4–40 Partial bent view and loads.

Design of Section

The cap will be designed for moments and shear at the face of the column. Because both maximum moment and maximum shear occur simultaneously at this section, the analysis should consider principal tensile stresses. Allowable compression stresses should also be checked in the lower flange.

Because of erection requirements the upper flange for the cap is made narrower to provide enough clearance when the longitudinal girders are lowered into position on their respective beam seats. Figure 4–41 shows the trial section with steel plates of equal areas, but different dimensions, for the top and bottom flanges. For simplicity, the neutral axis is assumed at the middepth of the web plate, but in reality it is slightly above this point.

The section properties are computed next:

I of web $= 5740 \text{ in}^4$

I of flanges $= 2 \times 18 \times 27.6^2 = 27{,}470 \text{ in}^4$

Total I $= 33{,}210 \text{ in}^4$

Maximum tensile stress

$$F_s = \frac{1491 \times 27 \times 12}{33{,}220} = 14.5 \text{ kips/in}^2 \quad F_{all} = 20 \text{ kips/in}^2 \text{ OK}$$

The statical moment of the flange about the neutral axis is $Q = 18 \times 27.75 = 500 \text{ in}^3$. The shear stress is therefore

$$F_v = \frac{VQ}{It} = \frac{226.2 \times 500}{33{,}210 \times 0.438} = 7.8 \text{ kips/in}^2$$

The maximum diagonal tension is computed from

$$F_{\max} = \frac{F_s}{2} + \sqrt{\left(\frac{F_s}{2}\right)^2 + F_v^2} \quad \text{or}$$

$$F_{\max} = \frac{14.5}{2} + \sqrt{(7.25)^2 + (7.8)^2} = 17.9 \text{ kips/in}^2 < 20$$

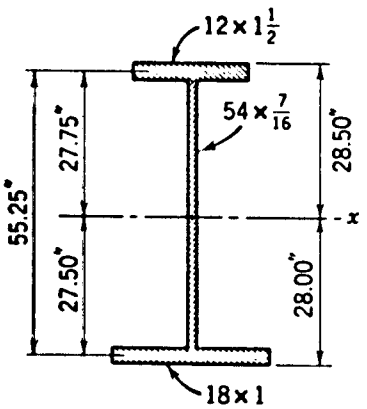

Figure 4–41 Trial section for maximum moment.

The shear in web is

$$F_v = \frac{226.2}{54 \times 0.438} = 9.56 \text{ kips/in}^2, \text{ allowable } 12 \text{ kips/in}^2$$

Likewise, the maximum compressive stress in the bottom flange is

$$F = \frac{1491 \times 28 \times 12}{33{,}210} = 15.0 \text{ kips/in}^2$$

For a partially supported or unsupported compression flange, the allowable stress is

$$F_b = \frac{50 \times 10^6 C_b}{S_{xc}} \left(\frac{I_{yc}}{l}\right) \sqrt{0.772 \frac{J}{I_{yc}} + 9.87 \left(\frac{d}{l}\right)^2} \leq 0.55 F_y \qquad (4\text{–}22)$$

where C_b = $1.75 + 1.05 (M_1/M_2) + 0.3 (M_1/M_2)^2 \leq 2.3$; where M_1 and M_2 is the smaller and larger end moment of the unbraced segment, respectively;

l = length (in) of unsupported flange between points of support;

I_{yc} = moment of inertia of compression flange about the vertical axis in the plane of the web, in^4;

d = depth of girder (in);

$J = \frac{(bt^3)_c + (bt^3)_t + Dt_w^3}{3}$, where b and t are the flange width and thickness of the compression and tension flange;

D,t = web depth (clear distance between flanges) and thickness, respectively. F_b in this case exceeds actual F, hence the section is satisfactory.

Load Factor Design AASHTO Standard Specifications

The strength design method is an alternate approach for the design of steel beam and girder structures of moderate length. The steps involved in this analysis are as follows:

1. Check the steel section to ensure that it satisfies the compact section requirements stipulated in AASHTO Article 10.48.1.1.
2. Compute the plastic modulus Z of the section.
3. Compute the moment capacity of the section as $M_u = F_y Z$.
4. Compute the factored load moment (required strength) and compare it to the moment capacity obtained in step 3. Fabricated girders not meeting the requirements for compact sections may be checked for load factor, but the moment capacity is now $M_u = F_y S$ where S is the elastic section modulus. There are two different design criteria, for braced and unbraced sections, respectively.

   Compact section requirements:

   (a) Projecting compression flange element
   $b'/t = 8.78/1.0 = 8.78$, $2055/\sqrt{36{,}000} = 10.8$ OK

   (b) Web thickness $D/t_w = 54/0.438 = 116$,
   $19230/\sqrt{36{,}000} = 101$ NOT OK

   Braced non-compact section requirements:
   $8.78 < 2200 \sqrt{F_y} = 11.6$

Web thickness $D_c/t_w = 27/0.438 = 62$,
$15400/\sqrt{36{,}000} = 81$ OK

The nominal moment strength is, therefore, $M_u = 36 \times 1208/12 =$
$= 3625$ ft-kips

Required moment strength $M_u = 1.3 \times 1023 + 2.17 \times 468 =$
$= 2346$ ft-kips OK

Note, however, that the diagonal tension of 17.9 kips/in^2 controls the design.

4.12 DESIGN EXAMPLE 4–4: STEEL BENT CAP FOR TORSIONAL LOADING

In the foregoing example the bent cap receives loads from two adjoining equal spans of the same structural and geometrical configuration; hence, under dead load alone the cap girder is subjected to moment and shear only. With live load, however, acting on one span only, the live load reaction is eccentrically applied, and even though this eccentricity is relatively small, it may cause the girder to twist about its original axia. A member subjected to a torsional moment develops shear stresses. A flat section or open section provides very little resistance to twisting effects. For the structure shown in Figure 4–39, the longitudinal beams in the main deck are simply supported at the ends and are free to rotate without transferring deformation effects to the cap girder.

In general, torsional resistance is markedly improved with the use of torsionally rigid sections. Three basic procedures are available for the best utilization of steel where torsional loads are present.

1. Use closed sections (boxes) where possible.
2. Introduce stiffeners and diagonal bracing.
3. Make rigid end connections.

The solid or tubular round closed section is ideal for torsional loading because the shear stresses are uniform around the circumference of the member. A second choice is a closed square or rectangular tubular section. For a member consisting of plates with uniform thickness as shown in Figure 4–42(a), the torsional resistance factor R is given by

$$R = \frac{2b^2d^2t}{b+d} \tag{4–23}$$

If the section consists of plates with different thickness as shown in Figure 4–42(b), the torsional resistance factor is

$$R = \frac{2b^2d^2}{\frac{b}{t_b} + \frac{d}{t_d}} \tag{4–24}$$

Members of a box section, butt-welded directly to a primary component, have the fully rigid end connections required for high torsional resistance.

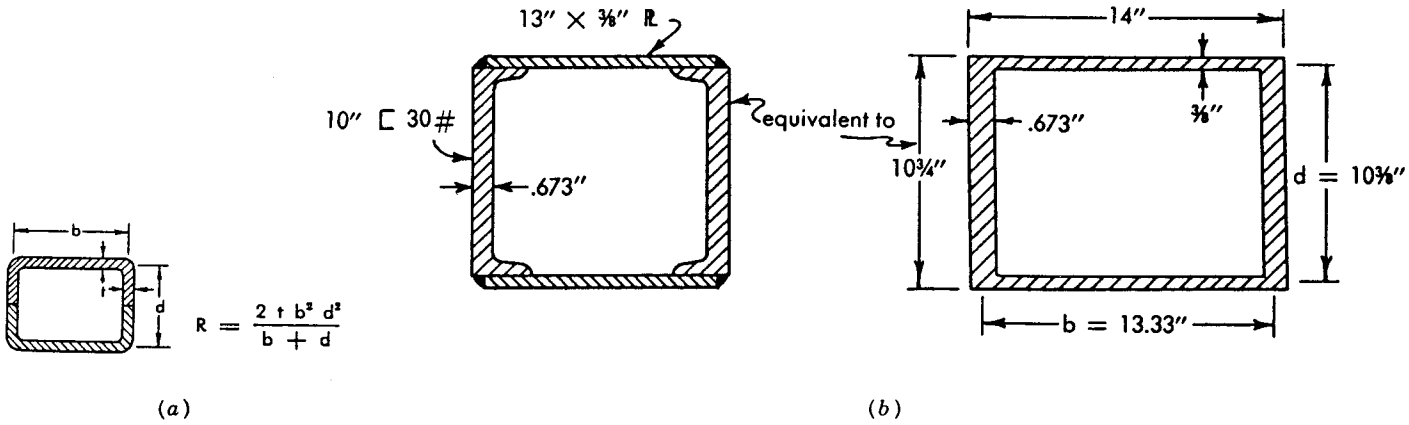

Figure 4–42 (a) Rectangular section with plates of uniform thickness; (b) rectangular box with plates of different thickness.

Applications

The torsional theory may be applied to the analysis of the bent girder shown in Figure 4–43(b). The bent is an interior support component for the bridge shown in Figure 4–43(a), and consists of a closed steel box section supported on two individual columns marked as supports A and B in Figure 4–43(b). A typical section of the bent box girder is shown in Figure 4–43(c).

The longitudinal girders are welded to the box girder, hence rotation at their ends is restrained, as in continuous beams. The ends of the box girder are assumed fixed against rotation, restraining the box section from twisting under deformation effects induced by the longitudinal girders. Furthermore, the load from either span is assumed to be applied sequentially, resulting in a differential response.

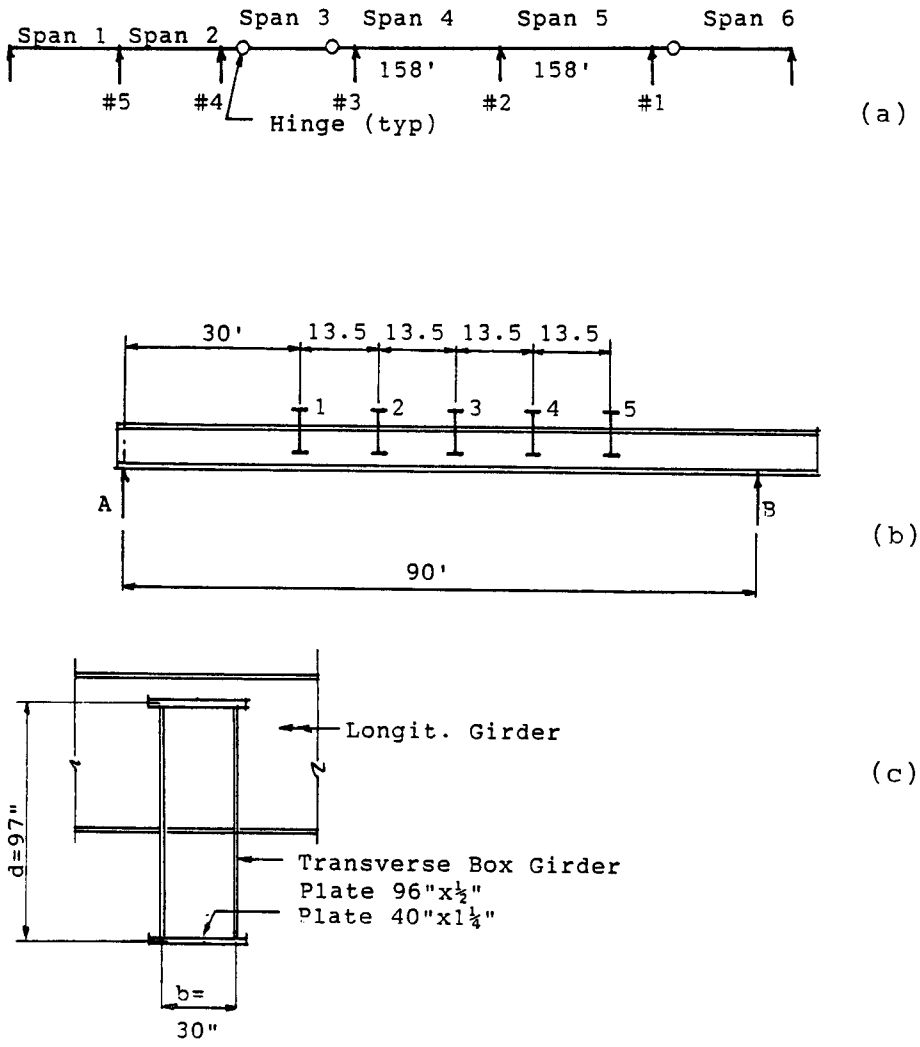

Figure 4–43 (a) Typical girder elevation, ramp C, I–75/I–275, four level interchange; (b) box girder elevation at pier 3; (c) box girder section.

From Figure 4–42(b) the torsional resistance factor is computed as

$$R = \frac{2 \times 30^2 \times 97^2}{(30/1.25) + (96/0.5)} = 78{,}408 \text{ in}^4$$

The torque in the central portion of the box girder is caused by the deformation of the longitudinal connection girders as they deflect under load. Each longitudinal girder carries a uniform dead load of 1.5 kips/ft = 125 lb/in, and has an average moment of inertia I = 50,000 in^4. Referring to Figure 4–43(a), girder 3-2 in span 4 is considered first as simply supported and then with its ends restrained against rotation. As simply supported, girder 3-2 has zero end moment and an end rotation

$$\theta_e = \frac{wL^3}{24EI} = \frac{125 \times 158^3 \times 12}{24 \times 30 \times 10^6 \times 50{,}000} = 0.024 \text{ radian}$$

For the same girder restrained against rotation at the end (θ_e = 0), the end moment is

$$M_e = \frac{wL^2}{12} = \frac{1.5 \times 158^2}{12} = 3120 \text{ ft-kips}$$

It is possible to calculate the torque that must be applied at each beam location along the box girder to cause it to twist by θ_e = 0.024 radian. This torque T_i applied at a point i to cause a rotation θ_i is found from the expression

$$\theta_i = \frac{T_i ab}{LE_s R}, \quad \text{or} \quad T_i = \frac{\theta_i E_s RL}{ab} \tag{4–25}$$

where all notation refers to the configuration of Figure 4–44, for a member of length L fixed at the ends against twisting.

For girder 1, $T_1 = \dfrac{(90 \times 12) \times (12 \times 10^6)(78{,}408)(0.024)}{(30 \times 12)(60 \times 12)} = 7800$ ft-kips

For girder 2, T_2 = 6970 ft-kips
For girder 3, T_3 = 7450 ft-kips
For girder 4, T_4 = 10,260 ft-kips
For girder 5, T_5 = 27,900 ft-kips
(using $E_s = 12 \times 10^6$ lb/in^2)

The resulting relationship is shown in a moment-rotation chart in Figure 4–45. The straight lines through the origin ($M = \theta = 0$) represent the applied torque T and angular notation θ at each girder line in the central portion of the box girder. A straight line in the opposite direction represents the end moment M = 3120 ft-kips and the rota-

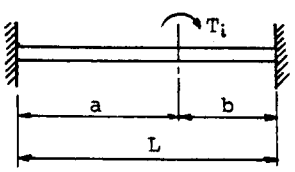

Figure 4–44 Rotation and torque for box girder, restrained at the ends against twisting.

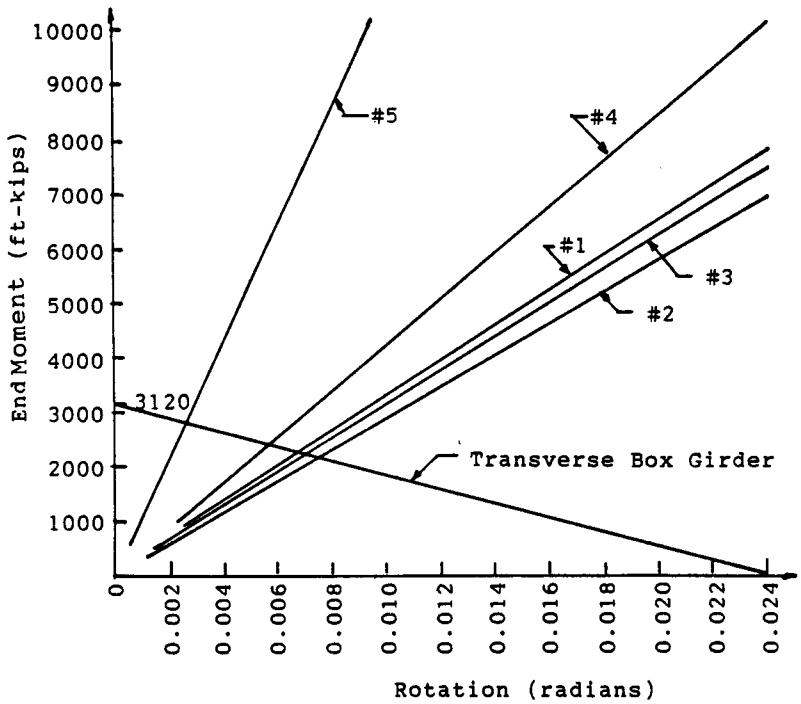

Figure 4–45 Moment-rotation chart, box girder of Figure 4–43.

tion $\theta_e = 0.024$ radian. The intersecting points define the actual end moment or torque T and the corresponding rotation (twisting) at the point under consideration. These torques are obtained graphically as

$$T_1 = 2300 \quad T_2 = 2200 \quad T_3 = 2250 \quad T_4 = 2450$$
$$T_5 = 2850 \text{ (ft - kips)}$$

Referring to Figure 4–43(b) the end torque at support B, assumed torsionally fixed, is

$$T_B = 2850 \times \frac{84}{90} + 2450 \times \frac{70.5}{90} + 2250 \times \frac{57}{90} + 2200 \times \frac{43.5}{90} + 2300 \times \frac{30}{90} = 7830 \text{ ft-kips}$$

Torsional shear stresses in box girder. The shear stress in the flange is

$$t_b = \frac{T}{2[A]t_b} = \frac{7830 \times 12 \times 1000}{2 \times 97 \times 30 \times 1.25} = 12{,}900 \text{ lb/in}^2$$

where $[A] = bd$ (Figure 4–43c).

Likewise the shear stress in the web is

$$t_d = \frac{7830 \times 12 \times 1000}{2 \times 97 \times 30 \times 0.50} = 32{,}250 \text{ lb/in}^2 > \text{ allowable}$$

Because the design is not satisfactory, the following solutions may be considered: (1) convert the initial scheme into simple span units as in the example of section 4.11; (2)

provide a roller-type bearing at supports A and B of the box girder; (3) minimize the occurrence of differential loading by proper construction sequence; and (4) increase web spacing and thickness in the box girder to enhance its torque capacity. A spherical bearing satisfies the functional requirements by allowing rotation in both directions.

4.13 GENERAL PRINCIPLES OF PIER FRAME ANALYSIS

In general, pier frames are analyzed and designed with the help of computer programs, available with a wide variety of mathematical capabilities. Computer-aided analysis and design has become an essential part of structural work because of the considerable mathematical process. Because pier frames are commonly represented by a continuous beam line with columns below having continuity with the beam line, several analysis program options are possible:

1. A single-story beam line program
2. A multistory frame program
3. A general planar frame program
4. A general space frame program

Column piers usually fall within the category of planar frames that may have pinned, fixed, or roller supports. It is quite essential that the designer understands the program's capability to consider the analytical behavior relevant to the conditions of the frame. Thus accurate modeling is necessary to describe a structure properly before a computer analysis is carried out. In general, the program considers both axial and flexural deformation of all frame members and gives moments, shears, and thrusts. With proper input, a computer program can also carry out the design by selecting member sizes and reinforcement.

A computer program may also be used to generate an analysis that is used as a basis for designing the members of a pier. Concerns about effective lengths, bracing, stress level, material strengths, and load distribution are always present. The analysis results usually present only numbers based on a fully elastic first-order analysis, and often without regard to stress level, buckling considerations, or pattern and magnitude of deflections. Thus, it may be necessary to pursue a more sophisticated analysis before design can proceed, especially with the more complex pier types and configurations. Interactive design procedures are often chosen by designers, which also include documentation of the results.

Methods of Analysis

Continuity affects moments and shear in a pier frame much as does the member stiffness. Typically, the analytical model considers the relevant factors in the proper order: method of analysis; a consideration of the physical constants; and a consideration of application of these values to design.

Pier frames are statically indeterminate structures, hence they are analyzed by compatibility or by equilibrium methods.

Compatibility method of analysis. This method, also referred to as the "force method" or the "flexibility method," is based on the solution of a set of equations that express compatibility relationships throughout the structure. Where several redundant forces are present, a number of compatibility equations must be solved simultaneously. Because there are several acceptable patterns for the selection of the redundant forces, there is no unique formulation of the problem. This variability is a detriment to computer formulation, because it is not possible to automate the procedure for generating the compatibility equations.

An example is the three-moment equation, particularly useful in determining the internal support moments of a continuous beam. Because the solution of the resulting compatibility equations yields member-end moments, the shear and moment diagrams are easily constructed.

Compatibility equations by energy methods generate solutions for indeterminate beam- and frame-type structures. Castigliano's second theory is employed in the form

$$\frac{\vartheta U}{\vartheta P_i} = \Delta_i \tag{4–26}$$

where U is the total strain energy for the structure, and P_i and Δ_i represent the ith applied load and its companion displacement, respectively. In this case, the strain energy results from flexure. Where both flexure and axial load are present, as in pier columns, the strain energy for each member results from summing the individual strain energies.

Equilibrium method of analysis. This procedure, also referred to as the "displacement method" or the "stiffness method," is conceptually straightforward and has advantages for certain types of structures. It is based on the solution of a set of equations that express the equilibrium requirements. Unlike the compatibility method, all the kinematic degrees of freedom are taken as redundant displacements and this facilitates the automation necessary in computer programming.

An example is the slope deflection equation that accounts for flexural deformation but ignores axial and shear deformation. It may be used to determine the end moments for statically indeterminate beams and frames.

Matrix methods. A more generalized approach to the problem of analysis is to establish a complete interactive relationship between member-end forces and the associated member-end displacements. In matrix form, if $\{F\}$ is the vector of member-end forces and $\{\delta\}$ is the vector of member-end displacements, then

$$\{F\} = [\kappa]\{\delta\} \tag{4–27}$$

where $\{\kappa\}$ is the member stiffness matrix. The details concerning the determination of the stiffness coefficients are covered in appropriate references. Likewise, the force-deformation relationship can take the form

$$\{\delta\}_r = [f]\{F\}_r \tag{4–28}$$

where $\{\delta\}_r$ and $\{F\}_r$ are reduced versions of the displacement and force matrices, respectively, and $[f]$ is the member flexibility matrix.

When equilibrium methods are formulated in a general matrix format, the resulting equations contain the structure stiffness matrix, derived from the synthesis of the

individual member stiffness matrices. In this respect, the matrix method as an equilibrium approach is referred to as the "stiffness method." When compatibility methods are expressed in a general matrix formulation, the corresponding equation involves the structure flexibility matrix that results from a synthesis of the individual member flexibility matrices. In this case the matrix method is called the "flexibility method."

The foregoing brief comments clearly give a crude definition and a mere outline of the methods of structural analysis. The matrix approach is particularly suited to computer applications that must process a large number of reiterative calculations. In addition, the direct stiffness method is becoming the most common analytical solution because of its generality and ease of programming. For a detailed study, see West (1989), Arbabi (1991), and Armenakas (1991).

The Moment Distribution Method

Since its initial conception and formulation by Cross (Cross and Morgan, 1932), this method has been used widely in the solution of continuous beams and frames. An iterative-type procedure is carried out with emphasis on the physical process of alternatively clamping and releasing joints until equilibrium is established. The method allows the determination of moments, shears, and reactions for a given set of loads. Before the analysis can proceed, the designer must compute the following: (1) the moments developed at the ends of loaded spans considering these ends fixed (FEM); (2) the resisting moment developed at a joint on the end sections of members connecting at the joint; and (3) the resisting moment developed at the fixed end of the beam by action of a moment applied at the other end that is not fixed.

Consider the beam shown in Figure 4–46, where point B is clamped and therefore temporarily restrained against rotation. First, we calculate the end moments on the two fixed-end beams for this condition shown on the sketch as fixed-end moments. Evidently, point B is unbalanced because there is a counterclockwise moment of 50 on the left side and a clockwise moment of 80 on the right, giving an unbalanced moment of 30 clockwise. Upon releasing the joint, it will rotate clockwise until the moments on both

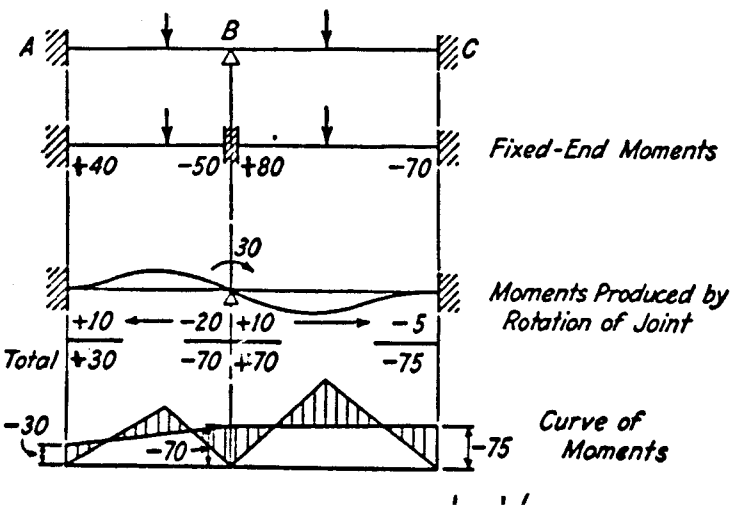

Figure 4–46 Application of the method of moment distribution.

sides balance. The moment of 50 will be increased by some amount, say 20, and the moment of 80 will be decreased by 10, so that $50 + 20 = 80 - 10$, or $50 + x = 80 - (30 - x)$, so that the sum of the changes in moments on the two sides of the joint will be the initial unbalanced moment of 30. This moment at B is therefore distributed between the connecting beams in a proportion to the moment necessary to rotate each beam through a given angle at B. This distribution is a function of the relative member stiffness.

Referring again to Figure 4–46, we note that when a positive moment rotates beam AB at B, a negative moment is introduced at A, as evidenced by the curvature of the beam. Likewise, when a negative moment rotates beam BC at B, a positive moment is produced at C as shown. It follows, therefore, that fractions of the distributed moments are carried over to the other ends of the beams with the same sign and according to a carry-over factor.

Fixed-end moments, stiffness, distribution factors, and carry-over factors. Fixed-end moments may be computed for any conditions of end restraint, and type and distribution of loads. Design aids usually include graphs and tables. The term "stiffness" is used to mean the moment needed at the end of a beam simply supported at this end, and rigidly fixed at the other, to produce a unit rotation at this end. This definition is interpreted from Figure 4–47, and implies no relative linear displacement of the two ends of the member. Because this stiffness varies as I/L, the latter is usually taken as the relative stiffness and is designated by the factor K. If the far end of a member is hinged, rather than fixed, the moment it exerts on the locked joint is the moment at the fixed end of a beam hinged at the other end. Hence, for computing distribution factors, the stiffness of a member with the far end hinged is $K = 0.75\ (I/L)$ rather than $K = I/L$ for far end fixed.

For several members meeting at a joint, and having stiffness factors $K_1, \ldots . K_i$, the distribution factors are $K_i/\Sigma K$. The carry-over moments at the far ends are one-half of the distributed moments, that is, the carry-over factor is one-half.

Moment distribution for frames with joint displacement (sidesway). The general outline of the method discussed in the foregoing section allows the determination of load effects in structures whose joints, although rotated, are not linearly displaced (translated) under load. It applies, therefore, to continuous beams without vertical support displacement and to pier frames where the vertical loads are acting symmetrically about the structure. Piers, however, are typically subjected to horizontal loads in their main direction and to loads from the superstructure unsymmetrically applied. In this case the pier frame moves slightly to either direction, and this displacement produces additional moments in the frame members. A horizontal force may act on the pier, resulting from transverse wind on the superstructure or from longitudinal and transverse forces on skew bridges. Where the top and bottom column conditions are not the same, differential expansion and contraction from thermal changes may cause length changes in the

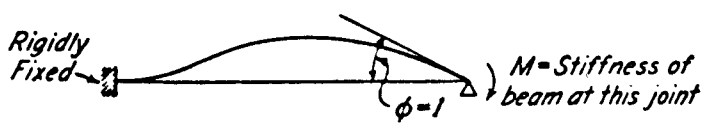

Figure 4–47 Stiffness of a beam.

pier cap with corresponding joint displacement. The moments induced in this manner must be computed and considered for the appropriate group loading.

As an example, consider the frame shown in Figure 4–48. With the horizontal force acting as shown, the frame will deflect an amount d. The magnitude of this deflection may be determined from the slope deflection method. Even though in actual design the horizontal force is usually known (say, wind pressure), it is more convenient in moment distribution analysis to proceed in the reverse order.

The frame is given an arbitrary displacement d of a convenient magnitude. Next, the moments due to this displacement and the force required to produce it are computed. Let the force corresponding to d be h and the moment m. For an actual horizontal force H, the actual moment is

$$M = m\frac{H}{h} \tag{4–29}$$

To compute, m and h, the joints B and C in Figure 4–48 are first locked against rotation, and they are given an arbitrary displacement d, causing moments m' to occur at A, B and C (D being a hinge in this example). Leg AB, with parallel tangents at both ends, bends with a double curvature. For a given displacement d the moments are

$$m'_{AB} = m'_{BA} = 6EK\theta_A = 6K\frac{Ed}{l_1} \tag{4–30}$$

which is true for the bottom of the column fixed.

Column CD is hinged, hence the moment is

$$m'_{CD} = 3EK\theta_c = 3K\frac{Ed}{l_3} \tag{4–31}$$

Next, the temporarily locked joints are released, and the moments m corresponding to the actual configuration of the frame are computed by distributing the moments m'. The horizontal reactions h_A and h_D are determined from the equilibrium of each leg, or

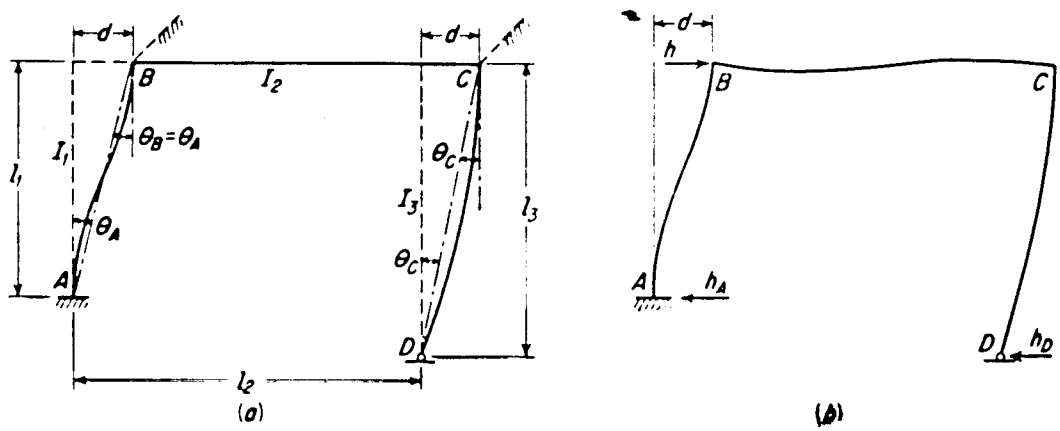

Figure 4–48 Deflection of rigid frame under horizontal load.

$$h_A = \frac{m_{AB} + m_{BA}}{l_1} \quad h_D = \frac{m_{CD}}{l_3} \tag{4–32}$$

The total horizontal force corresponding to the arbitrary displacement d is, therefore,

$$h = h_A + h_D \tag{4–33}$$

Illustrative example. Figure 4–49(a) shows a frame with a load of 16 kips eccentrically applied as shown. The stiffness for all members is calculated as $K = I/l$ except for member DE, $K = 0.75\ I/l$. Next, the distribution factors are computed for all members at joints B, C and D. Relative stiffness and distribution factors are shown on the computation sketch, Figure 4–50(a). The fixed-end moments for span BC are obtained from reference tables.

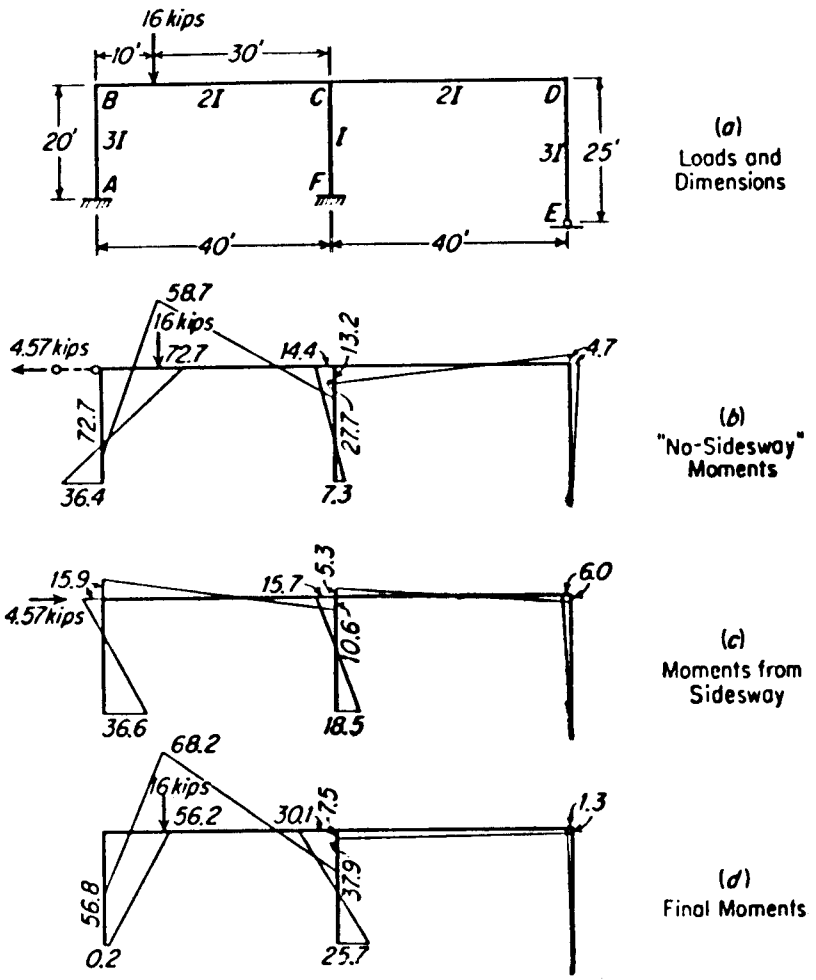

Figure 4–49 Effect of sidesway on moments in rigid frame.

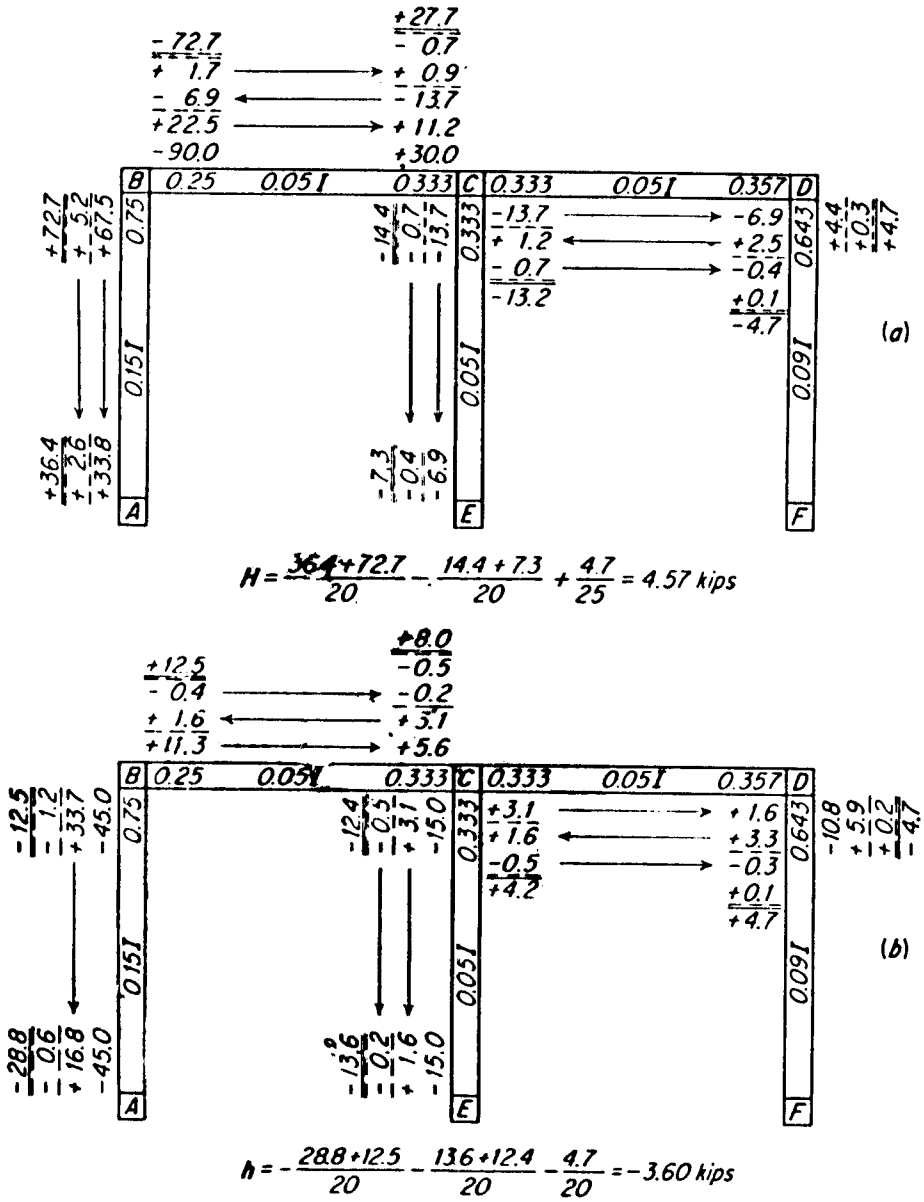

Figure 4–50 Computation sketches of moment distribution.

Step 1. With these data the moment distribution is carried out in the usual way with no sidesway, and this procedure is tabulated in Figure 4–50(a). The distribution is started by unlocking joint B and then successively C and D. The completion of the first cycle in each column of figures is indicated by the dashed line. The second cycle is carried out in the same sequence. A third cycle would probably contribute about 1 percent to the accuracy of the results, hence it is not considered necessary.

The computation of shears at the bottom of the three columns produces an unbalanced force $H = 4.57$ kips, meaning that the frame would be in equilibrium only if a hor-

izontal support was present to prevent sidesway and to supply a horizontal reaction of 4.57 kips.

Step 2. This step is carried out to give a sidesway correction, hence it applies a force equal and opposite to H. This amounts to removing the fictitious support at D, thus allowing the natural sidesway to occur. The sidesway moments caused by H may be superimposed on those of Figure 4–48(b) to give the corrected moments.

To compute these moments, joints B, C, and D are locked and given an arbitrary horizontal displacement, chosen to produce moments of convenient magnitude. Using $Ed = 1000$ is reasonable. The corresponding end moments for legs AB and CE are computed from Equation (4–30), and for the hinged leg DE from Equation (4–31). These moments are applied and distributed in the same manner, as shown in Figure 4–50(b). For $Ed = 1000$, the moments are -45.0, -15.0, and -10.8 ft-kips, respectively. Horizontal shears are computed again, giving a total horizontal force $h = -3.60$ kips, corresponding to $Ed = 1000$. From these results it follows that the actual sidesway moments are 4.57/3.60 times those of Figure 4–50(b). The moment diagram for these sidesway moments is shown in Figure 4–49(c).

Step 3. The final moments are obtained merely by adding the moments of Figure 4–49(b) and (c), resulting in the final moment diagram shown in Figure 4–49(d).

Step 4. Where an actual horizontal force H must be considered, such as wind load or traction, the moments are simply $H/4.57$ times those shown in Figure 4–49(c), or by analogy $H/3.60$ of those determined by the distribution of Figure 4–50(b). Where the effects of expansion and contraction must be considered, the resulting moments may likewise be computed by considering the ratio of $E\delta/Ed$ where δ is the actual joint displacement due to thermal changes

The frame in the foregoing example has columns with two distinct conditions or restraints: bottom end of the column fixed, and bottom end of the column hinged. Other

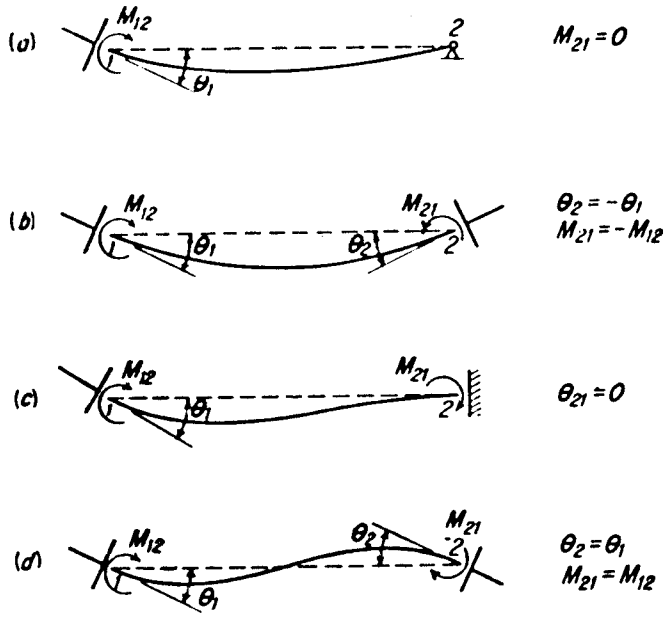

Figure 4–51 Various conditions of end restraint for columns.

Table 4–10 Moments for Different Conditions of Restraint

Case (see Fig. 4–51)	Relation Between θ Angles, No Load on Span	Moment at Near End in Terms of θ_1, No Load on Span	Moment at Far End in Terms of θ_1 and θ_2, No Load on Span	Moment at Near End in Terms of θ_1, Intermediate Loads on Span	Moment at Far End in Terms of θ_1 and θ_2, Intermediate Loads on Span
a Far end hinged	$\theta_2 = -1/2\theta_1$	$M_{12} = 3EK\theta_1$	$M_{21} = 0$	$M_{12} = 3EK\theta_1 - \left(M_{12}^f + \frac{M_{21}^f}{2} \right)$	$M_{21} = 0$
b Symmetrical bending	$\theta_2 = -\theta_1$	$M_{12} = 2EK\theta_1$	$M_{21} = -2EK\theta_1$ $M_{21} = 2EK\theta_2$	$M_{12} = 2EK\theta_1 - M_{12}^f$	$M_{21} = -2EK\theta_1 + M_{21}^f$ $M_{21} = 2EK\theta_2 + M_{21}^f$
c Far end fixed	$\theta_2 = 0$	$M_{12} = 4EK\theta_1$	$M_{21} = 2EK\theta_1$	$M_{12} = 4EK\theta_1 - M_{12}^f$	$M_{21} = -2EK\theta_1 + M_{21}^f$
d Antisymmetrical bending	$\theta_2 = \theta_1$	$M_{12} = 6EK\theta_1$	$M_{21} = 6EK\theta_1$ $M_{21} = 6EK\theta_2$	$M_{12} = 6EK\theta_1 - M_{12}^f$	$M_{21} = 6EK\theta_1 + M_{21}^f$ $M_{21} = 6EK\theta_2 + M_{21}^f$

possible conditions are symmetrical bending, and far end fixed. All four possible cases are shown in Figure 4–51. Note that leg *AB* in Figure 4–48 was assumed to bend antisymmetrically as in Figure 4–51(d). Moments for the four conditions or restraints are summarized in Table 4–10.

4.14 DESIGN EXAMPLE 4–5: MULTIPLE COLUMN PIER

Multiple column piers are usually selected for bridges in conventional grade separations where the decks are unusually wide or the bridge is skewed, resulting in relatively long piers of average-to-medium height. General guidelines regarding the number of columns and the proportions of the structure are provided by states, and are intended to produce uniformity and architectural harmony. Round and square columns are equally popular in lieu of columns with variable sections, the reason being simplicity in detailing and the use of standard forms. The use of a cantilever in the pier cap reduces column distance and balances moments, although in some instances the cantilever moments may control the design. This configuration results also in a shorter pier length and footing.

Many designers often choose to place the columns so that one beam is directly above one column and the next beam is between two columns. This arrangement reduces the shear in the cap but increases the moments, both positive and negative. For unusually long piers an open joint is usually provided in the cap to accommodate stresses due to thermal changes. For the same reason it is good practice to extend the pier wall above the ground line as shown in Figure 1–1(b), particularly for long piers of moderate height where differential thermal expansion between top and bottom can induce considerable moments in the columns. These effects are less severe in tall piers, such as the structures shown in Figure 1–2(d) where differential expansion is better absorbed by the slenderness of the column.

Design Procedures

The design procedure is essentially similar to that for hammerhead piers and involves the following steps:

1. Establish the number of columns, considering the pier dimensions and the advantages of cantilevered caps.
2. Establish explicit criteria regarding the distribution of forces and loads from the superstructure, and the division of these forces between fixed and expansion bearings.
3. Compute the dead and live load transmitted by each beam or girder to the pier cap. The truck or lane load may be placed within the lane limits specified by AASHTO but in different positions to produce maximum effects. For each position the live load reactions in each beam may be computed assuming the deck slab acts as simple beam.
4. Check overall pier stability of the pier under the applicable group (usually Group II or III). This will involve computing the resistance against overturning and sliding.
5. Carry out a frame analysis for each loading. This articulation is particularly neces-

sary when load factor is used. Compute moments, axial loads, and shears, adjusted for sidesway.

6. Check the allowable stress or the structural capacity after selecting a tentative reinforcing scheme, and repeat the analysis to obtain the necessary convergence.

For pier column on base walls and common footing, the base restraint may be taken as shown in Figure 4–51(c), that is, full fixity with zero rotation, and consistent with Case C of Table 4–10. For columns resting on footing only, the end restraint may be assumed as in Figure 4–51(d) and consistent with Case D of Table 4–10. For columns on individual footings, the base restraint may be decided according to the criteria established in Table 4–10. Therefore, it may be a hinge, partial restraint, or full fixity. We should note that the column deformation models shown in Figure 4–51 do not have to correspond to the buckled shapes of Figure 4–18, which apply only to the critical buckling load under axial load only.

The forces acting normal to the main pier axis may be assumed to be resisted equally by all columns. The final load effect on the columns includes an axial load, a moment in the direction of the pier, and a moment in a direction normal to the pier.

Design Data for Example

The bridge shown in Figure 4–52(a) has span lengths as shown, determined by satisfying the geometric requirements of support locations. Possible configurations include a four-span continuous unit as shown in Figure 4–52(b). Note that the center pier is made fixed, and all other supports are made expansion. This is usually a good solution, but in this case problems will arise from the extreme span ratio of 67/30 = 2.22, causing uplift at the end supports. A second solution, shown in Figure 4–52(c) consists of a two-span continuous unit and two end simple spans, with fixed and expansion bearings placed as shown. A third solution would involve a four-span continuous unit with integral abutments tied to the superstructure, heavy enough to resist the live load uplift. A fourth solution represents conversion to a two-span unit by eliminating supports B and D and moving the end abutments to reduce the span lengths.

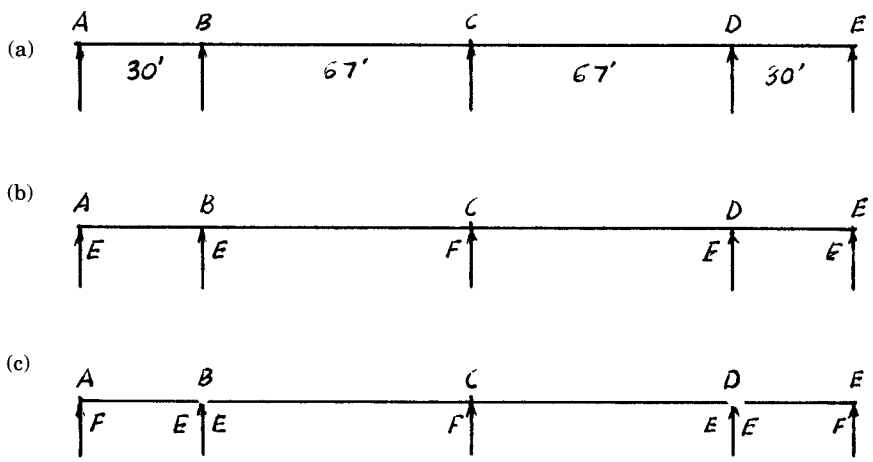

Figure 4–52 Span bridge; possible configurations.

The selected design is the scheme shown in Figure 4–52(c). Because there are no requirements for end rotation at the abutment bearings (fixed), the approach slabs may be cast against the deck slab. The expansion joints are in this case only two as in the four-span continuous unit, although in different locations. The bridge is assumed at zero skew.

A typical deck transverse section with the pier elevation is shown in Figure 4–53. The columns are spaced at 12-foot centers so that one beam is exactly at the center line of a column, as shown. The pier has a spread footing without walls. The longitudinal forces may be assumed to be distributed to the fixed end expansion bearings according to one of the models discussed in section 2.8. The distribution we assume in this analysis is that expansion bearings may resist longitudinal forces up to their frictional capacity, but friction may be released, making the bearing inoperable so that all longitudinal forces must be resisted at the fixed pier. As mentioned, when a fixed pier is analyzed in conjunction with an expansion pier, the friction at the latter represents resistance, hence it must be considered with a resistance (performance) factor, usually less than 1.0. However, when the expansion pier is analyzed, the friction is an active force and must be included with a load factor more than 1.0.

Loads and Forces Acting on Fixed Pier

Dead load. The curb and parapet section of the deck is placed after the main slab is poured, and is assumed to be distributed equally to all beams. This gives a uniform dead load unit weight of 0.84 kips/ft, and includes the weight of the beam. From tables, the reaction at the fixed pier is

$$R_{DL} = 0.84 \times 1.25 \times 67 = 70.4 \text{ kips/beam}$$

Live load. Live load reactions may be obtained from influence lines for one lane (truck or lane loading).

Truck loading	$R_{LL} = 32 + 8 \times 0.944 + 32 \times 0.944 = 69.8$ kips/lane
Lane loading	$R_{LL} = 0.64 \times 1.25 \times 67 + 26 = 79.6$ kips/lane, controls

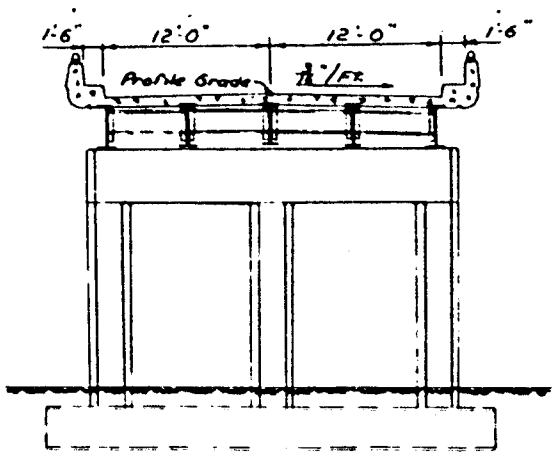

Figure 4–53 Transverse deck section and pier elevation.

Weight of cap. Assume cap dimensions 3 ft × 3 ft, unit weight 3 × 3 × 0.15 = 1.35 kips/ft

Reactions, at interior columns $D_L = 1.1 \times 1.35 \times 12 = 17.8$ kips
at exterior columns $D_L = 0.4 \times 1.35 \times 12 = 6.5$ kips (approximately)

Wind on Superstructure. Assume superstructure depth = 6.25 ft

Lateral wind = 6.25 × 1.25 × 67 ×0.05 = 26.1 kips
Longitudinal wind = 6.25 × 67 × 2 × 0.012 = 10.0 kips

Wind on Live Load

Lateral wind = 1.25 × 67 × 0.10 = 8.4 kips
Longitudinal wind = 67 × 2 × 0.04 = 5.4 kips

Overturning force = 67 × 1.25 × 29 × 0.02 = 48.6 kips

Longitudinal Forces. One lane LF = (0.64 × 134 + 18) × 0.05 = 5.2 kips

Temperature Forces. In the longitudinal direction, the fixed pier may be assumed the point of zero movement. However, because the base of the column is in the ground, a differential expansion and contraction is assumed between top and bottom. This differential expansion is based on an assumed temperature difference of 35°F. The tops of the exterior pier columns may be deflected and amount $\delta = 12 \times 35 \times 12 \times 0.000006 = 0.03$ inch.

Pier Frame Analysis

Typically, the analysis of a pier frame includes the dead load from the superstructure, live load beam reactions for the truck or lane loading positioned within the individual traffic lanes, the weight of the cap, transverse forces applied at the top of the pier in the main axis, and force effects associated with the displacement of the column tops. These effects are combined with the forces acting normal to the pier. The design of columns is usually controlled by the base conditions, and involves biaxial bending, axial load, and shear. The axial load is the reaction obtained from frame analysis for the actual beam location and loads carried by each beam, hence is different for exterior and interior columns. However, when computing soil pressures underneath the footing, this distinction is no longer made, and all loads are considered as a resultant force assuming the footing is stiff enough to induce a uniform pressure distribution. A different structural action of the footing should be considered where columns are spaced far apart resulting in pressure concentrations under the column tributary zone (see also section 8.11).

Moment distribution. A frame elevation is shown in Figure 4–54. The dimension from the top of the footing to the underside of the pier cap is 14 feet 6 inches. Both columns and the pier cap have a square section 3 ft × 3 ft, and the footing is assumed to be 2 feet 6 inches thick. The frame height is taken as the distance between the geometric center of the cap and the footing, or 17.25 feet.

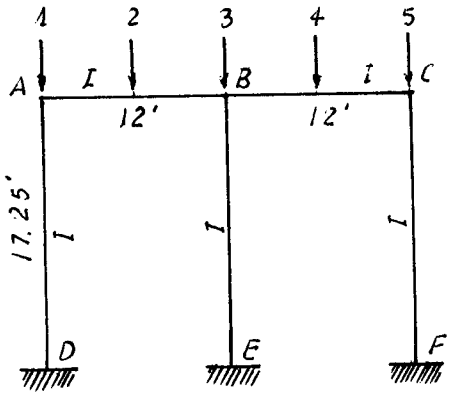

Figure 4–54 Frame elevation of design example.

The stiffness factors K are computed assuming the far end fixed, and are shown in the sketch of Figure 4–55 as a function of I. The distribution factors are computed as follows:

$$D_{AD} = \frac{0.083}{0.083 + 0.058} = 0.59 \qquad D_{AB} = 0.41 \qquad D_{CF} = 0.59$$

$$D_{CB} = 0.41$$

$$D_{BE} = \frac{0.058}{0.083 + 0.083 + 0.058} = 0.26 \qquad D_{BA} = D_{BC} = 0.37$$

Four separate analyses are necessary: (1) dead load from beams 2 and 4; (2) live load from beams 2 and 4 unsymmetrically placed; (3) a horizontal force acting at the top

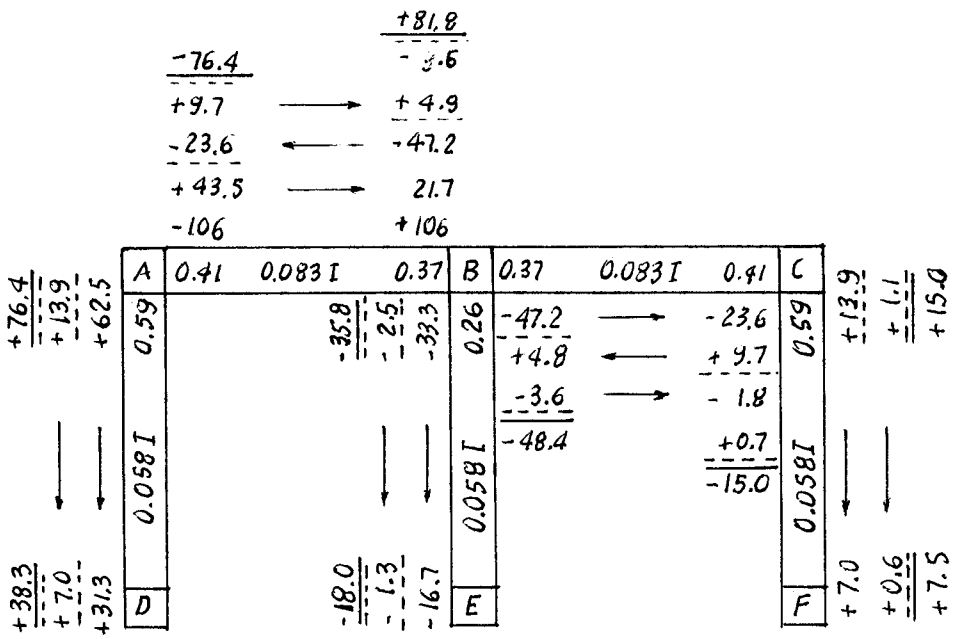

Figure 4–55 Moment distribution, design example.

of the frame; and (4) for a top displacement of points A and C caused by thermal changes.

Dead Load From Beams 2 and 4. Because of symmetry only one panel (AB) is considered loaded. The results with panel BC loaded will be similar and can be superimposed to obtain the total effects. For a dead load reaction (beam 2) of 70.4 kips, the fixed-end moments are

$$FEM_{AB} = 0.125 \times 70.4 \times 12 = -106 \text{ ft-kips}$$
$$FEM_{BA} = +106 \text{ ft-kips}$$

The moment distribution is carried out precisely as in the example of Figure 4–50 using a two-cycle procedure. If necessary, a third cycle would contribute further corrections to the final moments. The effect of beam 4 acting in span BC is exactly the opposite, so that the results are merely superimposed on the first analysis. Sidesway corrections will be necessary for unsymmetrical live loads. The effect of a horizontal force and column top displacement are computed in the manner described in the foregoing sections. Figure 4–55 shows the tabulation of the moment distribution.

4.15 DESIGN EXAMPLE 4–6: PIER INTEGRAL WITH SUPERSTRUCTURE

Design Data

The bridge pier shown in Figure 4–56 is one of two interior supports for a three-span continuous concrete slab bridge with spans 34 feet, 44 feet, and 34 feet. The roadway width is 30 feet, with a curb and railing along each side, giving an out-to-out bridge deck width of 33 feet. The slab is locally thickened at the bent cap as shown, and the columns are rigidly connected to the superstructure. The analysis will focus on the design of columns.

From previous superstructure analysis the reaction from the deck slab for the interior column is computed as 152 kips. For the same column, other loads are as follows:

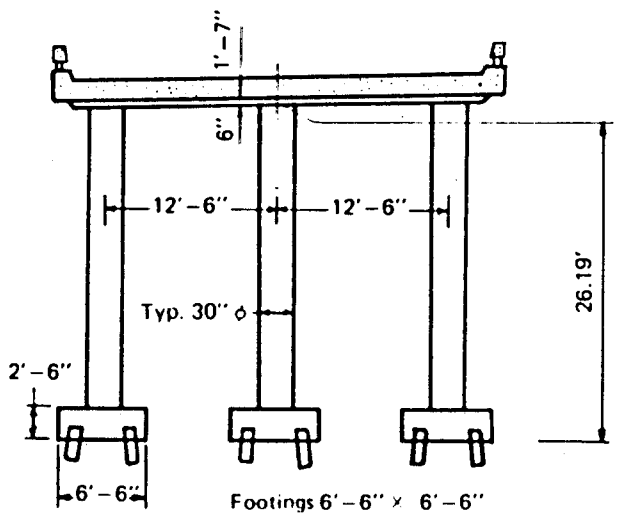

Figure 4–56 Pier elevation and deck cross section, design example.

Column dead load = $(3.14)(1.25)^2(23.69)(0.15)$ = 17.4 kips
Footing = $(6.5)(6.5)(2.5)(0.15)$ = 15.8 kips
Earth (3 ft on top of footing) = 13.4 kips
For column design $R_{DL} = 152 + 17.4 = 169.4$ kips
For footing design $R_{DL} = 169.4 + 15.8 + 13.4 = 198.6$ kips

The design live load is H 15, and by inspection it is obvious that the interior column will carry the most load and moment from the superstructure. For this condition, the live load is placed as shown in Figure 4–57, and for this position the live load reaction at the interior column is

$$R_{LL} = 2.96\ W$$

where W is the reaction at the pier obtained for one wheel load with the truck positioned longitudinally.

Because the superstructure is relatively shallow, the wind effects are minimal and are not expected to control the design. Hence, group loadings II, III, V, and VI are neglected. However, the effects of thermal changes in the bridge axis are significant and must be considered. Assuming a temperature change of 40°, a coefficient of shrinkage 0.0002, and the point of zero movement at midpoint of the center span, we compute the following:

Temperature change $\Delta = 0.000006 \times 40 \times 22 \times 12 = 0.064$ in
Shrinkage $\Delta = 0.0002 \times 22 \times 12 = 0.053$ in
Total = 0.117 in = 0.0097 ft

Because the pier is rigidly connected to the superstructure, for a given displacement Δ at the top, the fixed end moment is obtained for Case d of Table 4–10 as

$$M^F = 6K\ \frac{E\Delta}{l} = \frac{6EI\Delta}{l^2},\quad M^F_{BE} = 93 \text{ ft-kips} = M^F_{CF}$$

In the foregoing equation for M^F, E = 57,000 $\sqrt{4000}$ = 519,100 kips/ft^2 and l = 26.19 ft. The moment distribution of these fixed end moments is carried at the other end as in previous examples. The temperature rise movements and resulting moments are proportional and of opposite sign to the temperature drop plus shrinkage moment. The frame elevation for the bridge with dimensions and distribution factors is shown in Figure 4–58.

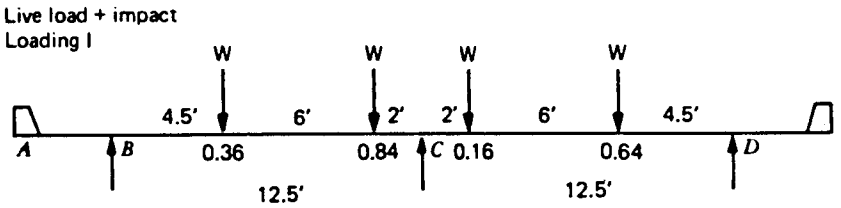

Figure 4–57 Position of live load for maximum interior column reaction.

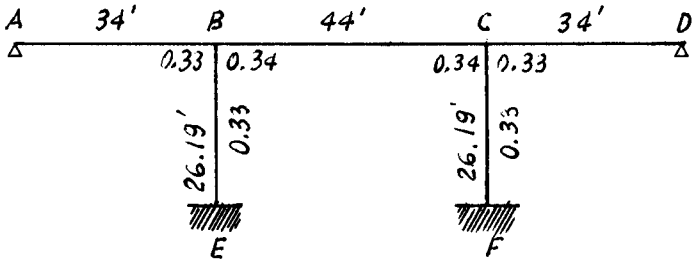

Figure 4–58 Bridge frame elevation.

The distribution is shown in Table 4–11, and is self-explanatory. The shear at the base of the column is computed as

$$V_{EB} = (57 + 77)/26.19 = +5.1 \text{ kips, and}$$
$$V_{FC} = -(57 + 77)/26.19 = -5.1 \text{ kips (no unbalanced shear)}$$

Design criteria. Because the design live load is H 15, only Group IA load factors for live load are used (AASHTO Table 3.22.1A). Groups to be considered are I, IV, and VII. Group I should be checked because live load may produce significant moments at the column tops. Group IV includes temperature effects in the longitudinal direction, hence it induces moments as shown in Figure 4–58 and Table 4–11. Group VII is significant where earthquake forces must be considered. Transverse moments are not included, because transverse load effects from wind are insignificant. If transverse forces were to be included, they would be combined with longitudinal forces and resolved in a moment for column analysis. The γ and β_D factors are given values as per AASHTO standard specifications. Thus γ is taken as 2.20 for LL + I, whereas β_D is taken as 0.75 when checking for minimum axial load and maximum moment or maximum eccentricity, and as 1.0 when checking the maximum axial load and minimum moment for column design.

For column loads and moments, three cases of live load positions are considered longitudinally, identified as Cases III, IV, and VI. These cases are shown in Figure 4–59(a), (b), and (c), respectively.

Case III. This is intended to produce maximum negative moment M_{BA} resulting from the H 15 truck load. This loading should also produce the maximum positive moment in column *BE* (see also Figure 4–58).

Table 4–11 Moment Distribution for Temperature

		B		E	F		C	
	BA	BC	BE	EB	FC	CF	CB	CD
	0.33	0.34	0.33			0.33	0.34	0.33
FEM	–	–	+93	+93	–93	–93	–	–
DISTR.	–31	–31	–31			+31	+31	+31
		+16		–16	+16		–16	
	– 5	– 6	– 5			+ 5	+ 6	+ 5
Σ	–36	–21	+57	+77	–77	–57	+21	+36

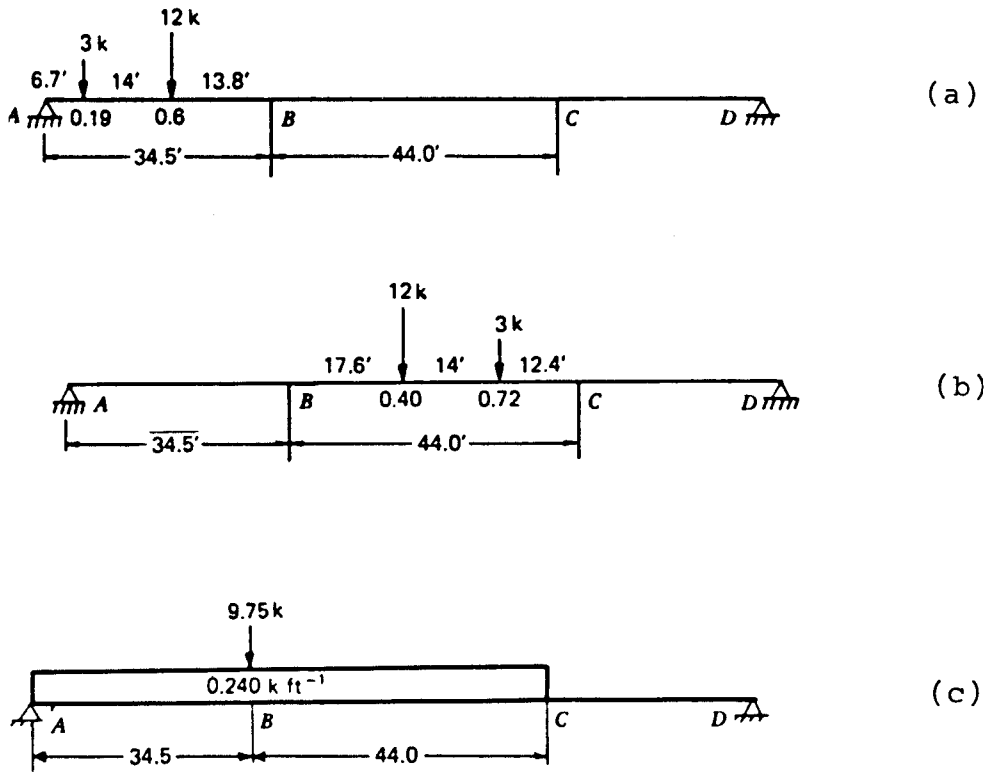

Figure 4–59 (a) End span maximum live load moment loading case III (negative); (b) interior span maximum live load moment loading case IV (negative); (c) lane loading for maximum reaction at B, case VI.

Case IV. This case is intended to produce the maximum negative moment M_{BE}, which results from the H 15 truck load positioned as shown in Figure 4–59(b). This loading also produces the maximum negative moment in column *BE*.

Case VI. This case results in maximum reaction at *B* for the lane loading shown in Figure 4–59(c). This maximum reaction is $R_B = 20.7$ kips per line wheels.

The moments for dead load and live load for the three cases mentioned are tabulated in Table 4–12 for the top and the bottom of the interior column, based on previous analyses.

Load Factor Design

The section capacity is determined as in the example of section 4.9, except that the analysis considers the properties of segments of a circle. An obvious conclusion is that bending will control the design so that it can be assumed that the critical loadings will fall below the balance point and below 10 percent of the critical load ($0.10\, f'_c A_g$) on the interaction curve. For this condition the capacity about each axis is computed for a concrete compressive strain of 0.003 and a steel compressive strain of 0.00207 at the balance point. The properties of segments of a circle may be taken from Figure 4–60. A direct load and moment capacity are also computed for a concrete compressive strain of

Table 4–12 Column Moments (Top and Bottom), Design Example

LL Case		Case III			Case IV			Case VI		
Group	*Loading*	M	M_L	M_T	M	M_L	M_T	M	M_L	M_T
@ Column *BE*										
I	$\beta_D D$	115	−26		115	−26		115	−26	
	$2.20L + I$	88	+185		75	−262		176	−57	
	Σ	203	+159		190	−288		291	−83	
	X 1.3	264	+207		247	−374		378	−108	
IV	$\beta_D D$	115	−26		115	−26		115	−26	
	$L + I$	40	+84		34	−119		80	−26	
	$S + T$		+60			−24			−24	
	Σ	155	+118		149	−169		195	−76	
	X 1.3	202	+153		194	−220		254	−99	
VII	$\beta_D D$	115	−26							
	EQ		−163							
	Σ	115	−189							
	X 1.3	150	−246							
@ Column *EB*										
I	$\beta_D D$	128	−12		128	−12		128	−12	
	$2.20\,L + I$	88	+20		75	−88		176	−37	
	Σ	216	+8		203	−100		304	−49	
	X 1.3	281	+10		264	−130		395	−64	
IV	$\beta_D D$	128	−12		128	−12		128	−12	
	$L + I$	40	+9		34	−40		80	−17	
	$S + T$		+67			−27			−27	
	Σ	168	+64		162	−79		208	−56	
	X 1.3	218	+83		211	−103		270	−73	
VII	$\beta_D D$	128	−12							
	EQ		−162							
	Σ	128	−174							
	X 1.3	166	−226							

0.003 and a steel compressive strain of 0.005, which is close to a level where the direct load is small or close to zero.

The relevant portion of capacity interaction curve may be approximated by a straight line between the two points, as shown in Figure 4–61. The necessary computations are as follows:

First we draw a half-column section as shown in Figure 4–61 with the reinforcing steel spaced around the face. The two strain possibilities considered are projected from the half section and the necessary dimensions are computed. The capacity is determined for the strain condition at the balance point of 0.00207 steel strain and 0.003 concrete strain. First the reinforcing is located in relation to the centroid of the section, and the strain at each bar is computed on the basis of its location in the assumed strain diagram. This strain is converted into stress by multiplying by E_s = 29,000 kips/in^2 using the yield strength of 60 kips/in^2 as a maximum stress. These stresses are converted into forces by multiplying by the steel area, and moments are obtained by multiplying the bar force by its distance from the centroid. The results are tabulated in Table 4–13.

According to AASHTO Article 8.16.2.7, the size of the compression block is computed using β_1 = 0.85 (valid for f'_c up to and including 4000 lb/in^2), whereas the area of the block is computed using the data of Figure 4–60 from which the centroid of the block

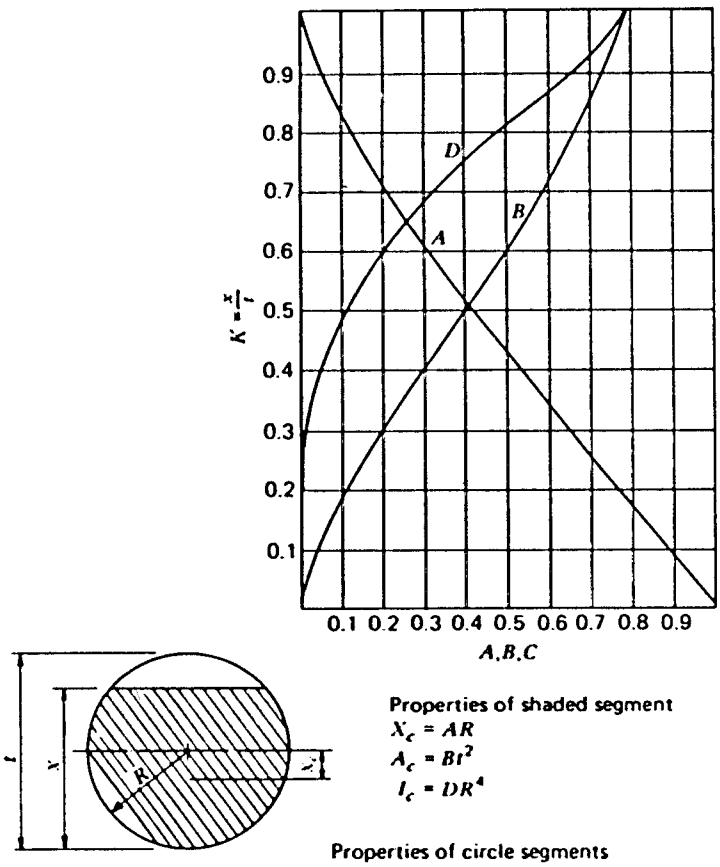

Figure 4–60 Properties of circle segments.

is also taken. The force in the compression block and its moment about the centroid are then computed. All forces and moments are added to give the capacity values P_b and M_b and are shown for different values of the performance factor ϕ, namely 1.0, 0.90, and 0.75.

The same procedure is repeated to compute the capacity values for P and M for a concrete strain of 0.003 and a steel strain of 0.005, and the results are tabulated in Table 4–14.

A moment magnification factor is computed and applied to the different loading conditions. Computations for effective length factors are based on the unbraced condition and the data of Figure 4–19.

Group I, case IV, top of column. The factored load and moment are

$$P_u = 247 \text{ kips}, \quad M_u = 374 \text{ ft-kips}$$

The modulus of elasticity is

$$E_c = 57{,}000\ \sqrt{4000}\ = 3{,}605{,}000 \text{ lb/in}^2$$

The moment of inertia of the column is (30-inch diameter)

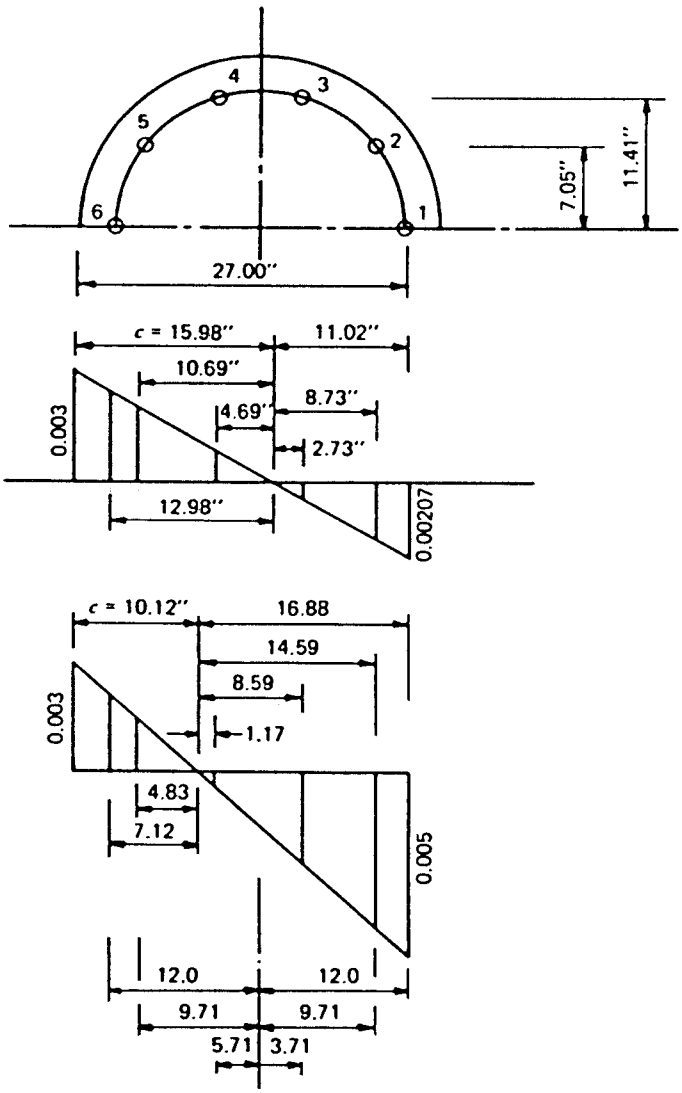

Figure 4–61 Column strains.

$$I_g = 0.049087 \times 30^4 = 39{,}760 \text{ in}^4$$

The factor β_D, ratio of dead load moment to total moment (see also section 4.6), is $\beta_D = 26/288 = 0.0903$. The stiffness EI for critical buckling is computed from AASHTO Equation (8–44), or

$$EI = \frac{3{,}605{,}000(39{,}760)}{2.5(1.0903)} = 5.259 \times 10^{10} \text{ lb/in}^2$$

From the charts of Figure 4–19 we obtain directly the stiffness parameter for the top and bottom, or

Table 4–13 Maximum $\epsilon_s = 0.00207$

Reinforcing Location	Distance R/F to Centroid	Reinforcing Area A_s	Strain @ R/F	Stress in R/F (kips)	Force in R/F (kips)	Moment (k-ft)
1	12.00	0.79	−0.00207	−60.00	−47.4	47
2	9.71	1.58	−0.00164	−47.56	−75.1	61
3	3.71	1.58	−0.00051	−14.79	−23.4	7
4	3.71	1.58	+0.00088	+25.52	+40.3	12
5	9.71	1.58	+0.00201	+58.29	+92.1	75
6	12.00	0.79	+0.00244	+60.00	+47.4	47
					+179.8 −145.9	249

c = 15.98 in.

$\beta_1 c$ = 0.85(15.98) = 13.58 in.

$k = \dfrac{\beta_1 c}{t} = \dfrac{13.58}{0.30} = 0.453$

B = 0.345 (Figure 4–60) $A_c = 0.345(30)^2 = 310$ in.^{2}

C = 0.85(4000)(310) = 1054 k

A = 0.475 (Figure 4–60) $x_c = 0.475(15.0) = 7.12$ in.

for C $M_c = 1054\left(\dfrac{7.12}{12}\right) = 626$ k-ft

P_b = +179.8 − 145.9 + 1054 = 1088 k
M_b = 249 + 626 = 875 k-ft } $\phi = 1.0$

P_b = 979 k
M_b = 787 k-ft } $\phi = 0.90$

P_b = 816 k
M_b = 656 k-ft } $\phi = 0.75$

$$G_{TOP} = (0.971)/(0.990 + 0.947) = 0.501$$

$$G_{BOTT} = 1.0 \text{ (From Table 4–1, footing on piles)}$$

The effective length factor is $\kappa = 1.2$, and the critical buckling load is computed as (Equation 4–13)

$$P_{cr} = \frac{3.14^2(5.259 \times 10^{10})}{(1.2 \times 26.19 \times 12)^2} = 3649 \text{ kips}$$

The moment magnification factor, Equation (4–12), is now computed using $\phi = 0.75$, or

$$\delta = \frac{1.0}{1 - 247/(0.75 \times 3649)} = 1.099 = 1.10$$

Then, for ultimate load capacity analysis,

$$P_u = 247 \text{ kips} \quad M_u = 374 \times 1.10 = 411 \text{ ft-kips}$$

Group VII, top of column. The factored load and moment are P_u = 152 kips, M_u = 246 ft-kips

Table 4–14 Maximum $\epsilon_s = 0.005$

Reinforcing Location	Distance R/F to Centroid	Reinforcing Area A_s	Strain @ R/F	Stress in R/F (kips)	Force in R/F (kips)		Moment (k-ft)
1	12.00	0.79	−0.00500	−60.00		−47.4	47
2	9.71	1.58	−0.00432	−60.00		−94.8	77
3	3.71	1.58	−0.00254	−60.00		−94.8	24
4	3.71	1.58	−0.00035	−10.15		−16.0	−5
5	9.71	1.58	+0.00143	+41.47	+65.5		53
6	12.00	0.79	+0.00211	+60.00	+47.4		47
					+112.9	−253.0	243

$c = 10.12$ in.

$\beta_1 c = 0.85(10.12) = 8.60$ in.

$k = \dfrac{\beta_1 c}{t} = \dfrac{8.60}{30} = 0.287$

$B = 0.182$ (Table 4–60) $\quad A_c = 0.182(30)^2 = 164$ in.^{2}

$C = 0.85(4000)(164) = 558$ k

$A = 0.665$ (Figure 4–60) $\quad x_c = 0.665(15.0) = 9.98$ in.

for C $M_c = 558\left(\dfrac{9.98}{12}\right) = 464$ k-ft

$P_n = +112.9 - 253.0 + 558 = 418$ k
$M_n = 243 + 464 = 707$ k-ft $\Big\}$ $\phi = 1.0$

$P_n = 376$ k
$M_n = 636$ k-ft $\Big\}$ $\phi = 0.90$

$P_n = 314$ k
$M_n = 530$ k-ft $\Big\}$ $\phi = 0.75$

Likewise we compute $\beta_D = 26/189 = 0.138$

$$EI = 5.259 \times 10^{10} \times \frac{1.0903}{1.138} = 5.040 \times 10^{10}$$

$$P_{cr} = \frac{3.14^2(5.040 \times 10^{10})}{(1.2 \times 26.19 \times 12)^2} = 3498 \text{ kips}$$

$$\delta = \frac{1.0}{1 - 150/(0.75 \times 3498)} = 1.06$$

For ultimate load capacity analysis,

$$P_u = 152 \text{ kips.} \qquad M_u = 246 \times 1.06 = 261 \text{ ft-kips}$$

The magnified moments and loads are plotted in Figure 4–62, and both Group I Case IV, and Group VII satisfy the strength requirements.

Serviceability requirements. Cracking is discussed in section 4.9 in conjunction with relevant specifications and conditions requiring crack width control, applied to concrete members subjected to flexure. In this example, the first step is to compute the service

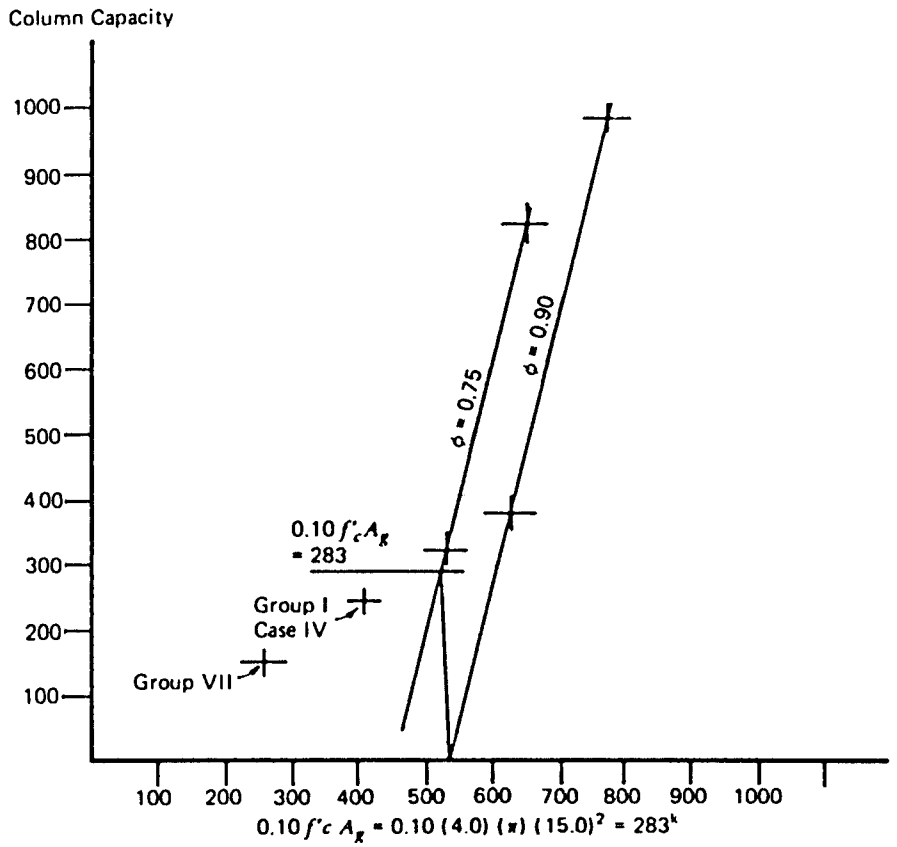

Figure 4–62 Column capacity.

load level forces and moments at the top and bottom of the column and then select the most critical loading. The steel stress is computed as suggested by Toprac (1959), and then converted to a crack width for comparison with the allowable of 0.006 inch. The method for computing stresses is basically and elastic analysis for a transformed reinforced concrete section. This procedure applies the properties for circular segments shown in Figure 4–60 and uses double compression in the reinforcing steel. The associated terminology is defined in Figure 4–63. Groups I, IV, and VII are obtained for a service load level, and the results are tabulated in Tables 4–15 and 4–16. The loads and moments for each group loading are summed and divided by the allowable overstress.

Referring to Figures 4–60 and 4–63, the procedure involves iteration of the assumed locations for the neutral axis. A neutral axis location is assumed and another neutral axis location is computed to check this assumption. If the comparison is not satisfactory, the next trial is made by assuming the neutral axis is approximately where it was computed during the preceding trial.

For this analysis, Group VII is selected, and a steel area of 1 percent is assumed. The notation is as shown in Figure 4–63. The steel area is

$$A_s = 0.01 \times 3.14 \times 15^2 = 7.07 \text{ in}^2, \text{ select } 10 \#8 \text{ bars}$$

$$A_s = 7.90 \text{ in}^2$$

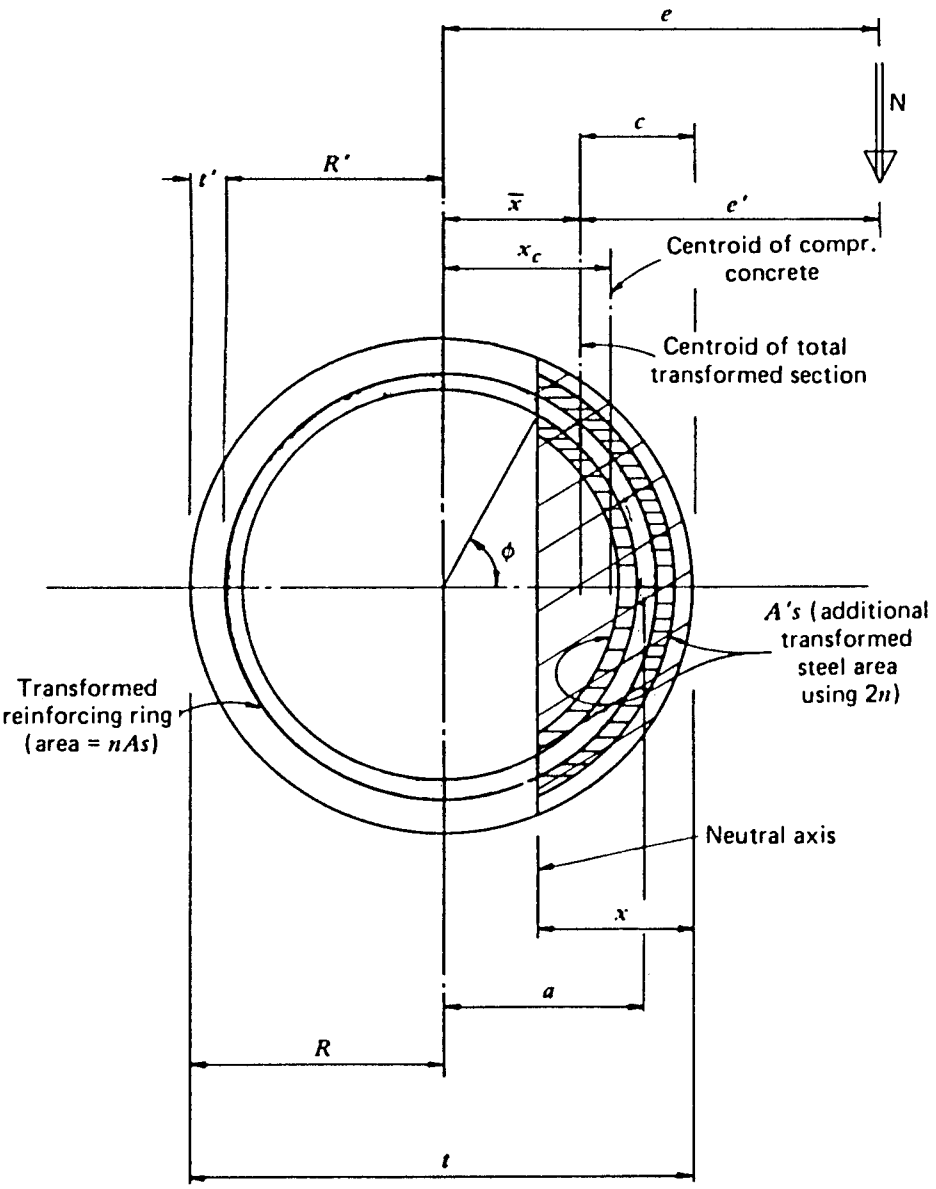

Figure 4–63 Notations for stress analysis of circular column.

This area is assumed to be a continuous ring, as shown in Figure 4–63. Using the proper notation, the relevant data for Group VII are

N = 115 kips,	M = 142 ft-kips	e = 14.82 in
t = 30.0 in	t' = 3.00 in	d = 27.00 in
A_g = 707 in^2	A_s = 7.90 in^2	p = 0.0112
n = 8	R = 15.0 in	R' = 12.0 in

Assume x = 12.60 inches, then $\kappa = x/t$ = 12.60/30.00 = 0.42

Table 4–15 Bent No. 1: Column Loads and Moments (Interior Column). Service Load Level

		Case III			Case IV			Case VI		
Group	Loading	N	M_L	M_T	N	M_L	M_T	N	M_L	M_T
@ *BE*										
I	*D*	153	–26		153	–26		153	–26	
	L + *I*	40	+84		34	–119		80	–26	
	Σ	193	+58		187	–145		233	–52	
IV	Group I	193	+58		187	–145		233	–52	
	S + *T*		+60			–24			–24	
	Σ	193	+118		187	–169		233	–76	
	÷ 1.25	154	+94		150	–135		186	–61	
VII	*D*	153	–26							
	EQ		–163							
	Σ	153	–189							
	÷ 1.33	115	–142							

Next, the area of concrete in compression is computed using the data of Figure 4–60:

$$B = 0.31 \quad A_c = 0.31 \times 30^2 = 279 \text{ in}^2$$

The transformed steel area for the ring is

$$nA_s = 8 \times 7.90 = 63.20 \text{ in}^2$$

From Figure 4–63 the angle ϕ to the compressive reinforcement with $\cos \phi = 1 - a/R'$ is computed as

$$a = 12.60 - 3.0 = 9.60 \text{ inches} \quad R' = 12.0 \text{ inches}$$
$$\cos \phi = 1 - (9.60)/(12.0) = 0.200, \quad \phi = 78.5°$$

Table 4–16 Bent No. 1: Column Loads and Moments (Interior Column). Service Load Level

		Case III			Case IV			Case VI		
Group	Loading	N	M_L	M_T	N	M_L	M_T	N	M_L	M_T
@ Column *EB*										
I	*D*	170	–12		170	–12		170	–12	
	L + *I*	40	+9		34	–40		80	–17	
	Σ	210	–3		204	–52		250	–29	
IV	Group I	210	–3		204	–52		250	–29	
	S + *T*		+67			–27			–27	
	Σ	210	+64		204	–79		250	–56	
	÷ 1.25	168	+51		163	–63		200	–45	
VII	*D*	170	–12							
	EQ		–162							
	Σ	170	–174							
	÷ 1.33	128	–131							

The angular fraction of a half-circle is $\lambda = \phi/180 = 78.5/180 = 0.436$. The area of the additional compressive reinforcement resulting from the use of $2nA_s'$ is computed as

$$A_s' = \lambda(nA_s) = 0.436 \times 63.20 = 27.55 \text{ in}^2$$

The total transformed steel area is then

$$A_{ST} = nA_s + A_s' = 63.20 + 27.55 = 91 \text{ in}^2$$

so that the total transformed area is

$$A_T = A_c + A_{ST} = 279 + 91 = 370 \text{ in}^2$$

Then

$$\frac{N}{A_T} = \frac{115}{370} = 311 \text{ lb/in}^2$$

Referring again to Figure 4–60, the centroid of the compressed concrete is obtained as follows:

Coefficient $A = 0.51$, $x_c = 0.51 \times 15.0 = 7.65$ inches

and the centroid of the compressed steel A_s' is computed by using

$$x' = 57.3\, R' \frac{\sin \phi}{\phi}$$

or

$$x' = 57.3(12.0)\frac{\sin 78.5}{78.5} = 8.58 \text{ inches}$$

The centroid of the entire transformed section is computed by summing moments about the column axis

$$A_c = 279 \times 7.65 = 2134$$
$$A_b = 27.55 \times 8.58 = 236$$
$$2370, \text{ or } \bar{x} = 2370/370 = 6.41 \text{ inches}$$

Similarly, other relevant dimensions with respect to the centroid at the transformed section are

$$x_c - \bar{x} = 7.65 - 6.41 = 1.24 \text{ inches}$$
$$x' - \bar{x} = 8.58 - 6.41 = 2.17 \text{ inches}$$
$$c = 15.00 - 6.41 = 8.59 \text{ inches} \quad e' = 14.82 - 6.41 = 8.41 \text{ inches}$$

The moment of inertia of the compressed concrete is computed from the graphs of Figure 4–60:

$$\text{Coefficient } D = 0.062 \quad I_c = DR^4 = 0.062 \times 15^4 = 3139 \text{ in}^4$$

The moment of inertia of the reinforcing ring nA_s is

$$I_s = \frac{A_s(2R')^2}{8} = \frac{63.20 \times 24.0^2}{8} = 4550 \text{ in}^4$$

Because of its eccentricity, the additional moment of inertia of the compressed concrete is

$$A_c(x_c - \bar{x})^2 = 279 \times 1.24^2 = 429 \text{ in}^4$$

Likewise, because of its eccentric location the reinforcing ring has an additional moment of inertia

$$nA_s\bar{x}^2 = 63.2 \times 6.41^2 = 2597 \text{ in}^4$$

The additional compressive reinforcing steel has a moment of inertia because of its eccentricity

$$A_s'(x' - \bar{x})^2 = 27.55 \times 2.17^2 = 130 \text{ in}^4$$

The total moment of inertia is

$$I_T = I_c + I_s + A_c(x_c - \bar{x})^2 + nA_s x^2 + A_s'(x' - \bar{x})^2 = 10{,}845 \text{ in}^4$$

Next we compute the stresses $Ne'c/I_T$ and $Ne'(R' + \bar{x})/I_T$

$$\frac{Ne'c}{I_T} = \frac{115 \times 8.41 \times 8.59}{10{,}845} = 766 \text{ lb/in}^2$$

$$\frac{Ne'(R' + \bar{x})}{I_T} = \frac{115 \times 8.41 \times 18.41}{10{,}845} = 1642 \text{ lb/in}^2$$

The maximum concrete stress is

$$f_c = \frac{N}{A_T} + \frac{Ne'c}{I_T} = 311 + 766 = 1077 \text{ lb/in}^2$$

whereas the maximum tensile stress in the steel is

$$\frac{f_s}{n} = \frac{N}{A_T} - \frac{Ne'(R' + \bar{x})}{I_T} = 311 - 1642 = -1331 \text{ lb/in}^2$$

which gives $f_s = -8(1331) = -10{,}600$ lb/in^2

The foregoing results must be checked for the initial assumptions by examining the value of x:

$$x = d\frac{f_c}{f_c + f_s/n} = 27 \times \frac{1077}{2408} = 12.08 \text{ inches}$$

which is fairly close to the assumed x = 12.60 inches. For 10 #8 bars at 9.4-inch centers we compute

$$d = 3.0 \text{ inches} \quad A = 2 \times 3 \times 9.4 = 56.5 \text{ in}^2$$

Rather than using Equation (4–20), the crack width is computed from

$$w = 0.115\ \sqrt[4]{A}(f_s)(10^{-3})$$
$$= 0.115\ \sqrt[4]{56.5}(10.6)(10^{-3}) = 0.0033 \text{ in} < 0.006, \text{ OK}$$

4.16 PIER TRESTLES

Trestles, as described here, consist of decks supported by pile bents or by piers built on piles. They are used extensively for highway as well as for railroad crossings of low profile over swamps, stagnant waters, and shallow lakes.

Pile Bents

A pile bent consists of several precast concrete piles driven into the ground and connected at the top by a reinforced concrete cap. The piles may have octagonal or rectangular cross section with chamfered edges. The main reinforcement of a pile consists of longitudinal bars with a steel area not less than 1.0 percent of the pile cross section. The dimensions of the pile depend on the loads to be carried and on the unsupported length (see also section 9.6 and 9.7).

For bridges with roadway width up to 30 feet, four piles per bent are usually sufficient. For greater roadway widths, additional piles are necessary. The piles may be vertical, but the outside piles may be battered to increase lateral stability.

The longitudinal spacing of pile bents is decided from a cost analysis of superstructure and substructure. Where long piles are needed and the driving is difficult, the economical spacing is larger than for short piles. The bent spacing may also be affected by the type of superstructure. For example, if simple slabs are used for the superstructure, the bent spacing should be close to 20 feet. If the decision is to use precast deck units, the bent spacing may depend on the available facilities for handling and erection.

Caps. Piles composing a bent are connected at the top by a reinforced concrete cap, cast in place after the piles are driven and cut off to proper grade. The vertical pile reinforcement usually is extended into the cap to provide a rigid connection, and the piles are allowed to extend into the cap from 6 to 12 inches, thus stiffening the connection.

When the deck consists of a concrete slab, the caps must be treated as continuous beams supported by the piles. Moments resulting from the slab loads (dead and live) may also be distributed to the piles that must be designed for this condition. With deck construction consisting of a concrete slab and beams or girders, each beam is placed directly over a pile, eliminating cap moments from deck loads. Longitudinal and lateral forces will still act, however, on the deck and will produce moments in the piles.

Double Bents

For relatively long trestles, the bridge is considerably strengthened longitudinally by double bents placed over three to four spans. The deck may be rigidly connected at the double bent. In this manner all longitudinal forces may be resisted at the double bent location. Moments are converted into axial loads, and horizontal forces are resisted by the extra stiffness of the double bent.

4.17 PIER PROTECTION DESIGN PROVISIONS IN NAVIGABLE WATERWAYS

General Considerations

Vessel collision forces and design considerations were briefly discussed in sections 2.5 and 3.9, respectively. These aspects were considered in conjunction with AASHTO Method II, which is essentially a risk analysis method that transforms a large body of data into a series of computations based on statistical and probability procedures. Values of the various parameters must in this case be determined using the designer's judgment as the primary basis for the estimate.

This section focuses briefly on the requirements for the design of physical protection systems to prevent the collapse of piers and spans due to vessel collision. These are structures provided to absorb the impact loads fully or partially. Protective systems may be located directly on the bridge piers (such as a fender), or independent of the bridge (such as a dolphin). Their geometric configuration can be worked out to deflect or redirect the aberrant vessel away from the bridge. This configuration should be developed to prevent the rake (overhang) of the design vessel's bow from striking and causing damage to any exposed portion of the bridge above the protective structure, with the latter in its deflected or collapsed position.

The intent of the AASHTO (1991) specifications is to provide two basic protection options. The first involves designing the bridge to withstand the impact loads in either the elastic or plastic range. With plastic design, it is necessary to ensure that the superstructure does not collapse by incorporating redundancy in the system, or by other means. The second protection option allows the designer to provide a system of fenders, pile supported structures, dolphins, islands, and so on, as physical protection to either reduce the magnitude of impact loads to within the allowable strength of the bridge, or to protect the bridge elements independently.

Fender systems

Timber fenders. Timber fenders consist of vertical and horizontal timber members in a grillage geometry attached to the face of the bridge pier or erected as an independent structure adjacent to the pier. Energy is absorbed by elastic deformation and crushing of the timber members.

Timber fenders are also placed on most other types of protection systems to provide a rubbing and anti-sparking surface to avoid metal-to-metal contact with steel hulled vessels.

Rubber fenders. Rubber fenders are commercially available in a wide variety of shapes. The high elasticity inherent in rubber allows a relatively high energy absorption characteristics through elastic deformation either in compression, bending and shear, or a combination of all three.

Concrete fenders. Concrete fenders are hollow, thin-walled concrete box structures attached to the bridge pier. Usually, a timber fender is also attached to the outer face of the concrete box fender.

These systems offer an effective method of absorbing vessel collision energy. A

wide range of energy absorption capabilities can be achieved by varying the box dimensions, wall thickness, and geometric layout of interior walls and diaphragms. However, a primary drawback is the difficulty in analyzing the energy absorption characteristics of the structure while undergoing plastic deformation.

A crushed concrete box fender with timber facing is shown in Figure 4–64. Crushing of the hollow concrete box is the primary mechanism of energy absorption of this fender.

Steel fenders. Steel fenders are thin-walled membranes and bracing elements that can be developed in various box-like arrays and assemblies attached to the bridge pier. Impact energy is likewise absorbed by compression, bending, and buckling of the steel elements in elastic and plastic deformations. Primary disadvantages are their susceptibility to corrosion in saltwater environments and the possibility of metal-to-metal contact with steel-hulled vessels. Timber facing, concrete encasement, and special coatings may be considered to reduce those problems.

Pile Supported Systems

Pile supported structures can be used to absorb collision impact loads. One method is to provide pile groups connected by a rigid cap, but free-standing piles or piles connected by flexible caps can also provide a high level of protection resistance. The pile group may consist of vertical piles, which absorb energy primarily by bending, or batter piles which absorb energy by bending and compression. Because of the high impact loads induced by vessel collision, plastic deformation and crushing of the piles is permitted, provided that the vessel is stopped before striking the pier, or the remaining impact force is below the resistance of the pier and its foundation.

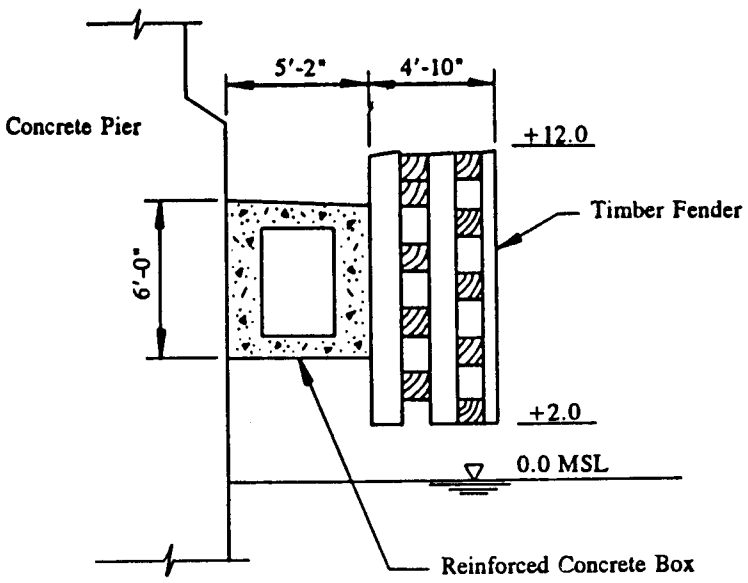

Figure 4–64 Crushable concrete box fender on the Francis Scott Key Bridge main piers, Baltimore, Maryland.

The pile protection system may be either free-standing or attached to the pier. Occasionally fenders are attached to the pile structure and help resist a portion of the impact forces. The choice of pile may include timber, steel, or concrete sections.

An example of a pile-supported protection system is the Tasman Bridge in Australia (Maunsell and Partners and Brady, 1978), shown in Figures 4–65 and 4–66. This system consists of 10-foot diameter prestressed concrete piles tied together by a rigid concrete cap beam. During the design impact of a 35,000 DWT ship at 8 knots, the piles would form plastic hinges at the top and bottom to absorb the impact energy through rotational deformation.

A dynamic analysis of pile protection systems has been performed by Derucher (1981) assuming that the piles and fender remain in the elasetic range, and that a ship is a non-deformable rigid body. The pile/ship system is modeled as a spring and weight, and a distribution factor *DF* is introduced into the spring constant to account for the influence of waters and adjacent piles in the structure, as shown in Figure 4–67. Assuming a fender attached to the pile structure, the analysis yields

$$P = KYC \tag{4–34}$$

$$K = \frac{(K_p)(K_f)}{(K_p + K_f)} \tag{4–35}$$

where P = applied force to structure (kips); K = equivalent spring constant of pile and fender (kips/in); K_p = spring constant of pile; K_f = spring constant of fender; Y = maximum system deflection; and C = vessel coefficient. The stiffness of a cantilevered pile with a unit lateral load at the top is

$$K_p = 1/\Delta_p \tag{4–36}$$

where Δ_p is the pile deflection given by

$$\Delta_p = \frac{L^3}{3EI_p}(DF) \tag{4–36a}$$

where L = length of pile above assumed fixed point; E = modulus of elasticity; I_p = moment of inertia of pile; and DF = distribution factor.

The vessel coefficient C accounts for the eccentricity, configuration, and hydrody-

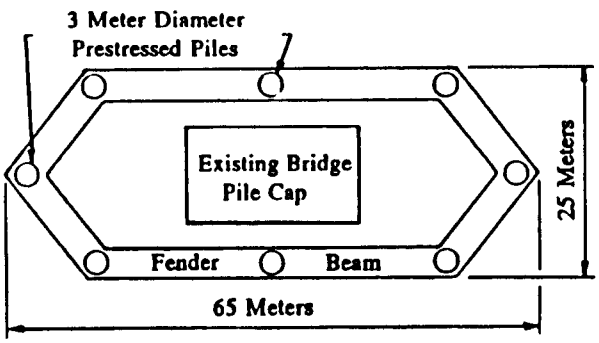

Figure 4–65 Plan of pile supported pier protection system evaluated for the Tasman Bridge, Australia.

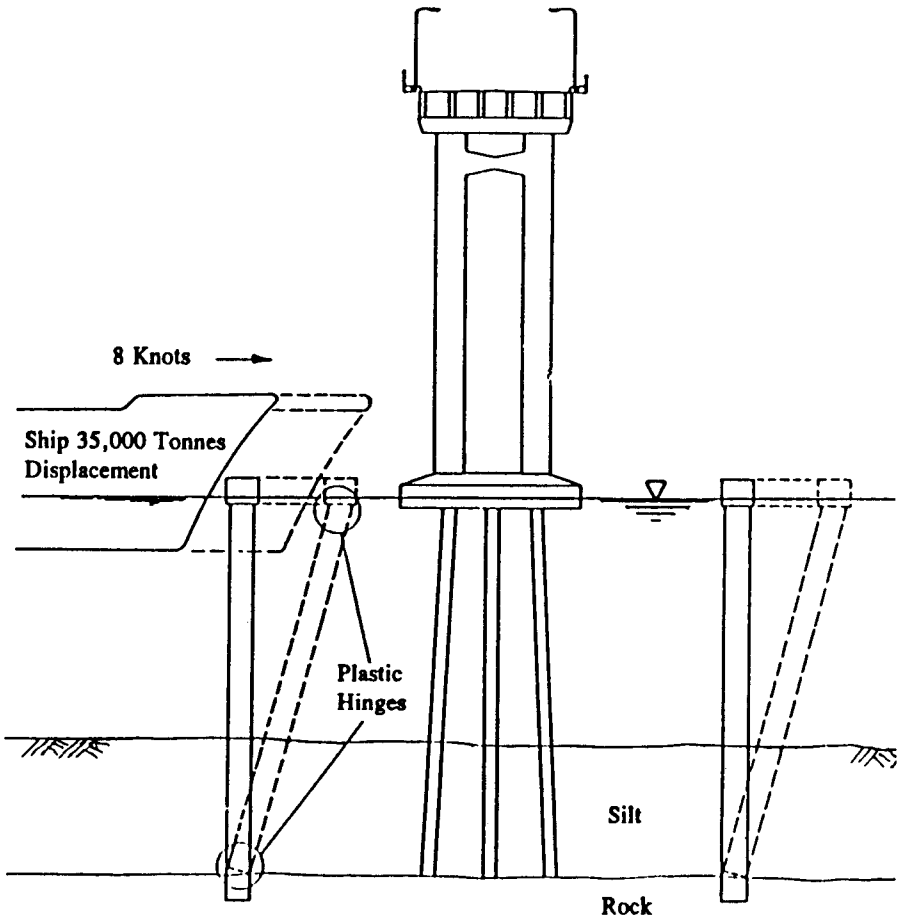

Figure 4–66 Section of pile supported pier protection system evaluated for the Tasman Bridge.

namic mass coefficient of the vessel. For head-on impact, $C = C_H$ as defined in section 3.9. The distribution factor DF may be computed as proposed by Derucher (1981), or

$$DF = (-6.0 \times 10^{-7} D_x + F) L^{-0.006} \tag{4–37}$$

where

$$F = -3.5 \times 10^{-13} D_y^2 + 3.1 \times 10^{-7} D_y + 0.335 \tag{4–38}$$

where D_y = vertical stiffness = EI_p / S_p;
S_p = vertical pile spacing;
D_x = horizontal stiffness = EI_w / S_w;
S_w = horizontal waler spacing;
I_w = waler moment of inertia.

The maximum system deflection Y and period λ can be computed as

$$Y = V/\lambda = (K/M)^{1/2} \tag{4–39}$$

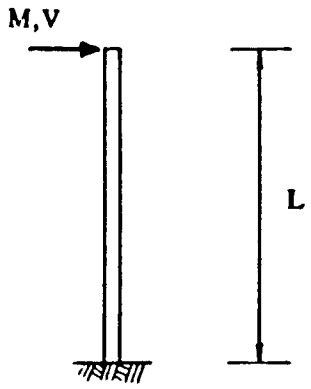

a. Single Pile Elevation.

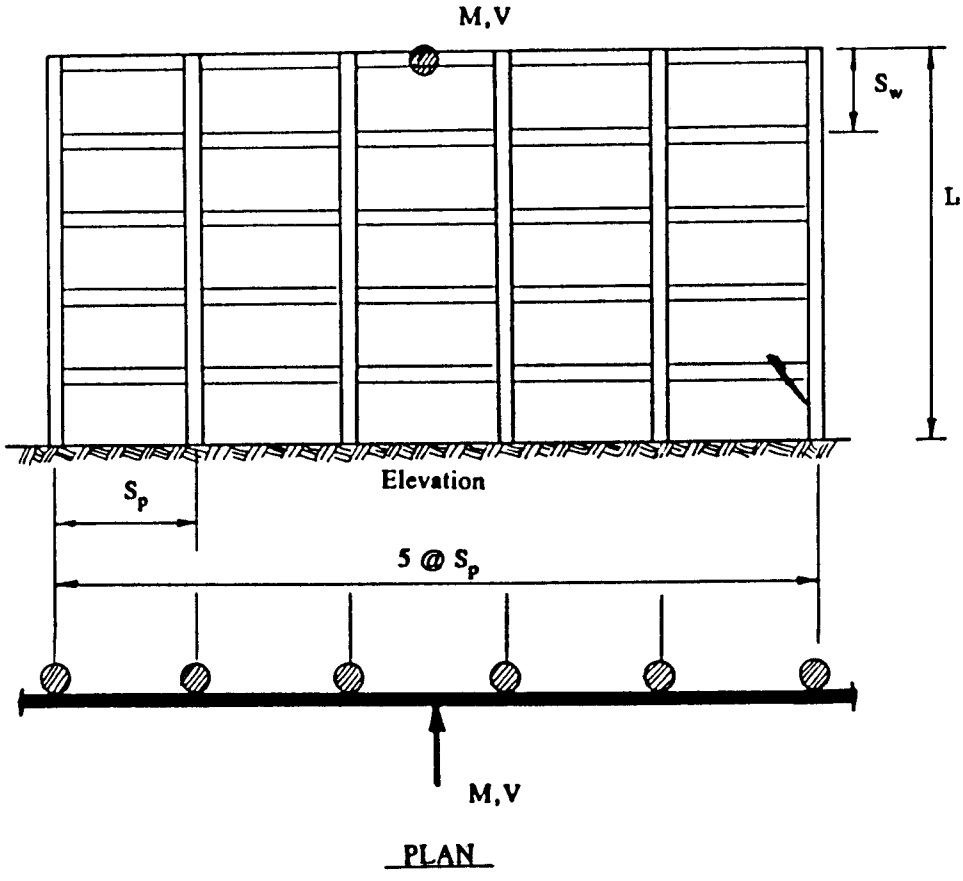

b. Multiple Pile Fender Structure.

Figure 4–67 Typical pile structure geometry for Derucher's Dynamic Analysis.

where V = impact velocity, and M = mass of vessel. The acceleration a and stopping time t may be determined as follows:

$$\alpha = V\lambda \tag{4–40}$$

$$t = (\pi/2\lambda) \tag{4–41}$$

Dolphin Protection

Large diameter dolphins may be used to protect bridge piers. Dolphins are circular cells constructed of driven steel sheet piling and filled with rock or concrete. A concrete cap is placed on top. Alternate construction includes precast concrete sections and driven piles.

The circular shape of the dolphins deflects aberrant vessels away from the pier. The cell should, however, be designed for the maximum loading case of head-on impact. If the dolphin is stronger than the vessel, the latter will absorb most of the impact through crushing of its bow. If the dolphin is weaker than the vessel, it will absorb most of the energy. A balance between cost and safety associated between these two conditions is the usual design practice. Figure 4–68 shows the case where the collision energy is absorbed by both the cell and the ship. Where large plastic deformations are permitted, the maximum displacement of the top of the dolphin should be limited to one-half of the cell diameter under the design impact. In addition, the sheet piling should be embedded a sufficient distance below the waterway base to increase its resistance to pull-out.

Design considerations are usually based on the energy changes that take place during an impact. Force-displacement relationships are typically developed for the following forces:

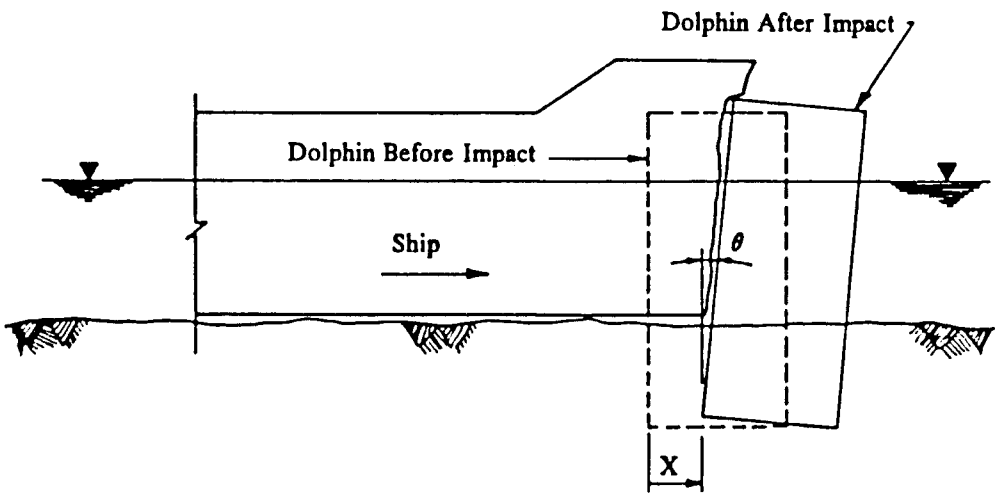

Figure 4–68 Collision energy absorbed by dolphin rotation and sliding, and by crushing of vessel bow.

- Crushing of the vessel's bow
- Lifting of the vessel's bow
- Friction between the vessel and the dolphin
- Friction between the vessel and the bay bottom
- Sliding of the dolphin
- Rotation of the dolphin

The area under the force-displacement diagram is equal to the energy absorption capacity of the item, and it may be assumed that the deformation of the ship/dolphin system will follow a path of least energy. Deformation stops when all the impact energy has been absorbed.

Island Protection

Protective islands are highly effective around vulnerable bridge piers. The island geometry is developed according to the following criteria: (1) Vessel impact force transmitted to the bridge pier should not exceed the lateral capacity of the pier and its foundation; and (2) island dimensions should be such that vessel penetration into the island will not result in physical contact between the vessel and the pier.

Design methodologies usually involve a combination of mathematical modeling and scale physical model tests, with results from the latter used to calibrate the theoretical assumptions. Fletcher, May, and Perkins (1983) describe the following items that dissipate or redistribute energy during a vessel collision with an island:

Ship. Change in potential energy of the ship due to change in the vertical position of its center of gravity, or crushing of the hull of the ship.

Water. Change in potential energy of the water displaced by the ship, or generation of water waves and turbulence.

Island. Change in potential energy of island material; displacement, shear, and compaction of the island material; friction between the ship and the island; generation of shock waves within the island; crushing of particles of island material.

Because the inclusion of these items in mathematical form is difficult and complex, simplifying assumptions, supplemented by model tests, are necessary.

Planning Guidelines

AASHTO Section 8 provides useful guidelines for bridge protection based on case histories and accident data. It may be expected that the application of these guidelines will result in relatively long span and high clearance bridges to reduce the incident risk and consequences of vessel collision. The higher cost of longer spans with a lower present worth of avoidable disruption costs must be balanced against the lower cost of a shorter span with a higher present worth of avoidable disruption costs. The optimization of these two conditions yields the bridge solution for vessel collision.

4.18 DESIGN EXAMPLE 4–7: BRIDGE PROTECTION IN WATERWAYS

Figure 4–69 shows the profile of a hypothetical suspension bridge. Using Method II risk analysis procedures, we will evaluate the following: (1) the annual frequency of collapse AF of one of the main piers; and (2) if AF is unacceptable, the level of impact forces to be used in developing pier protection alternatives.

Waterway characteristics. The following waterway data are assumed:

- Navigable channel is 800 feet wide.
- Two-way traffic for merchant vessels applies, hence the center line of vessel transit is located 200 feet on each side of the channel center line.
- At the main piers the water depth is more than 65 feet.
- Annual mean water current is approximately 0.3 knots (V_{min} = 0.5 ft/s).

Bridge characteristics. For this analysis, the structure characteristics are as follows:

- Pier width is 60 feet
- Pier resistance to impacts is equal to 20,000 kips
- Bridge importance classification = critical

Vessel Frequency. The bridge will be evaluated for a period of 50 years assuming that the number of vessels using the waterway increases annually. The forecasted vessel traffic data for the merchant fleet for the 50-year span are shown in Table 4–17 beginning with the year 1990. Using the 50-year forecast for the number of vessel transits will result in a conservative estimate of the current risk.

Vessel characteristics. The vessel characteristics are shown in Table 4–18, and were developed using AASHTO criteria and data.

The LOA dimension required for the impact speed and geometric probability distribution represents a vessel selected using Method I criteria. For this example, a maximum of fifty ships will control. Counting back fifty ships from the vessel distribution in Table 4–17 results in a 150,000 DWT vessel with LOA = 1030 feet. This is considered a constant and applies to all vessel classifications according to AASHTO.

Design impact speed. For the bridge location, data provided by relevant merchant associations indicate a typical transit speed V_T of 13 knots (22 ft/s). From Figure 4–70, the design impact speed V for the main pier is computed as

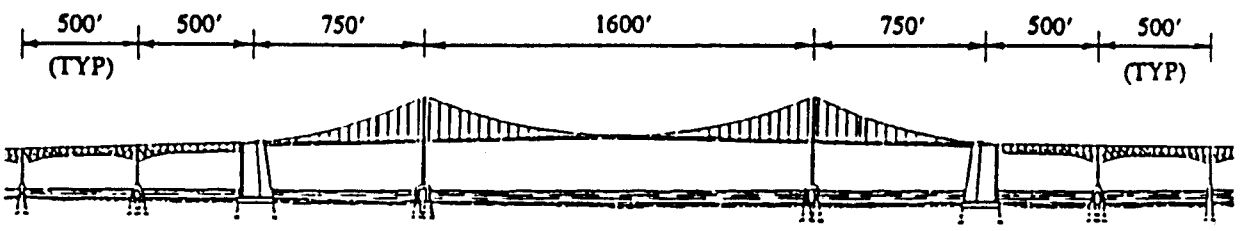

Figure 4–69 Bridge profile for Design Example 4.7.

Table 4–17 Ship Frequency Data (Yr. 2040)

Size(DWT)	Type*	No. of Passages N (per year)
10,000	F/C	3,000
20,000	F/C	2,000
40,000	B/T	100
60,000	B/T	100
80,000	B/T	300
100,000	B/T	100
150,000	B/T	60
TOTAL		5,660

*F/C = Freighter/Container Vessels
B/T = Bulk Carrier/Tanker Vessels

$$V = 22.0 - \left[(800 - 400)\left(\frac{22.0 - 0.5)}{3090 - 400}\right)\right] = 18.8 \text{ ft/s}$$

Probability of aberrancy. The probability PA of vessel aberrancy is estimated from the following equations

$$PA = (BR)(R_B)(R_C)(R_{XC})(R_D) \tag{4–42}$$

where BR = aberrancy base rate; R_B = correction factor for bridge location; R_C = correction factor for current acting parallel to vessel transit path; R_{XC} = correction factor for crosscurrents acting perpendicular to vessel transit path; and R_D = correction factor for vessel traffic density. For this example, $BR = 0.6 \times 10^{-4}$ for ships; $R_B = 1.0$ because bridge is in a straight region; $R_C = 1 + (0.3/10) = 1.03$ for $V_C = 0.3$ knots; $R_{XC} = 1.0$ (no cross-current at the site); and $R_b = 1.6$ for high density vessel traffic. Hence,

$$PA = (0.6 \times 10^{-4})(1.0)(1.03)(1.0)(1.6) = 1.0 \times 10^{-4}$$

Geometric probability. The normal distribution shown in Figure 4–71 is used to compute the geometric probability PG of ship collision. The standard deviation of the normal distribution is σ = LOA = 1030 feet. For the 150,000 DWT vessel with $B_M = 146$ feet, the value of PG is computed from normal distribution tables as follows:

Table 4–18 Ship Characteristics

Size(DWT)	Type	Length, LOA (ft)	Beam, B_M (ft)	Draft, D_L (ft)
10,000	F/C	472	64	26.9
20,000	F/C	643	91	34.4
40,000	B/T	682	99	37.4
60,000	B/T	771	109	40.4
80,000	B/T	850	120	43.3
100,000	B/T	902	138	52.8
150,000	B/T	1,030	146	59.1

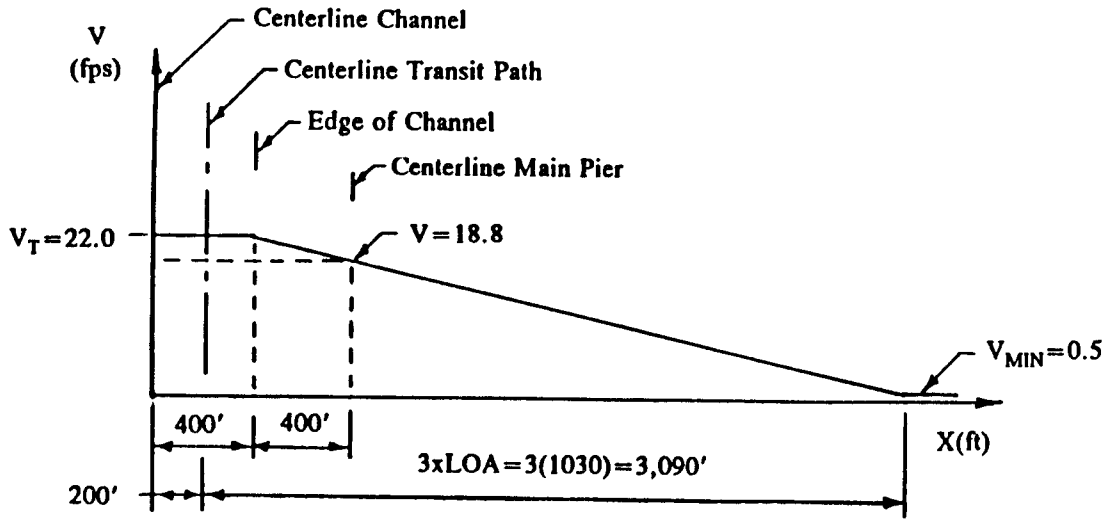

Figure 4–70 Main pier design impact speed.

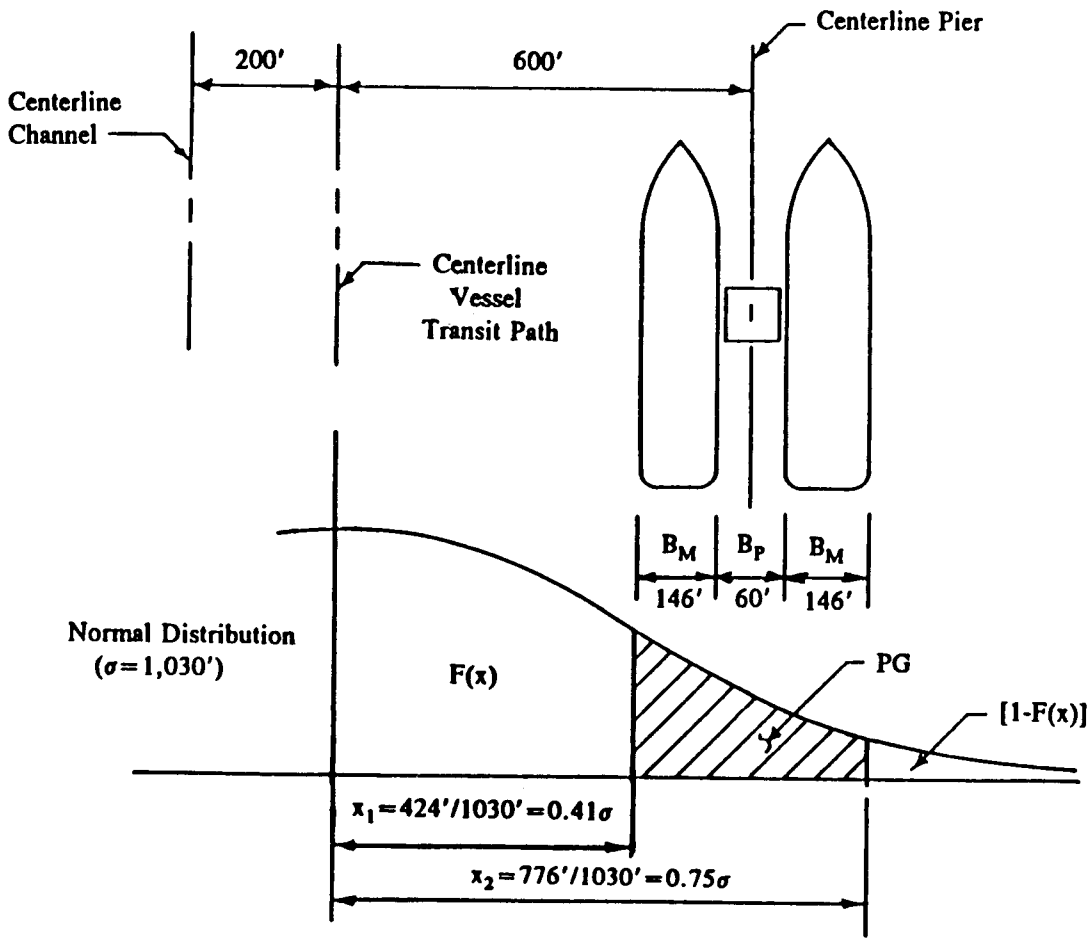

Figure 4–71 Geometric probability of vessel collision with main pier.

$$At \quad x_1 = (0.41)\sigma \quad 1 - F(x_1) = 0.3409$$
$$At \quad x_2 = (0.75)\sigma \quad 1 - F(x_2) = 0.2266$$

Hence $PG = [1 - F(x_1)] - [1 - F(x_2)] = 0.3409 - 0.2266 = 0.1143$.
Values of PG for each vessel classification are summarized in Table 4–19 for H_p = 20,000.

Ship collision force. The ship collision forces are computed from Equation (2–17). For a 80,000 DWT Bulk Carrier/Tunner colliding at the design speed V = 18.8 ft/s, the impact force is $P_s = 220\ (80{,}000)^{1/2}\ (18.8)/27 = 43{,}330$ kips.
Ship collision forces are summarized in Table 4–20 for each vessel classification.

Probability of collapse. The ultimate lateral resistance of the main pier, H_p, is 20,000 kips. The probability of collapse PC is computed from

$$PC = (1 - H/P)/9$$
$$H_p/P_s = 20{,}000/21{,}664 = 0.923, \text{ and} \qquad (4\text{–}43)$$
$$PC = (1 - 0.923)/9 = 0.0086$$

A summary of PC values for each vessel classification is shown in Table 4–21.

Annual frequency of collapse. The annual frequency of collapse, AF, may be computed from

$$AF = (N)(PA)(PG)(PC) \qquad (4\text{–}44)$$

where N = annual number of vessels classified by type, size, and loading conditions that can strike the bridge element; PA = probability of vessel aberrancy; PG = geometric probability of a collision between an aberrant vessel and a bridge pier or span; and PC = probability of bridge collapse due to collision with an aberrant vessel. The results of computations for each ship classification along with the pier total are summarized in Table 4–19. The ship sizes are arranged in decreasing order from the largest (150,000 DWT) to the smallest (10,000 DWT). This ordering permits a quick determination of the impact of vessel size on the ΣAF, and for comparison against the acceptable annual frequency AF_p.

From Table 4–19, the ΣAF for all ship classifications is 0.000508. The main pier return period of collapse, RP, becomes

$$RP = 1/AF = 1/0.000508 = 1968 \text{ years}$$

Table 4–19 Annual Frequency of Main Pier Collapse (H_p = 20,000)

Ship(DWT)	N	PA	PG	PC	AF	ΣAF
150,000	60	1.0×10^{-4}	.1143	.0737	.000051	.000051
100,000	100	1.0×10^{-4}	.1076	.0652	.000070	.000121
80,000	300	1.0×10^{-4}	.0973	.0598	.000175	.000296
60,000	100	1.0×10^{-4}	.0906	.0519	.000047	.000343
40,000	100	1.0×10^{-4}	.0839	.0386	.000032	.000375
20,000	2,000	1.0×10^{-4}	.0772	.0086	.000133	.000508
10,000	3,000	1.0×10^{-4}	.0607	.0000	—	—

Table 4–20 Ship Collision Forces

Size(DWT)	(Type)	P_a(kips)
10,000	F/C	15,319
20,000	F/C	21,664
40,000	B/T	30,637
60,000	B/T	37,523
80,000	B/T	43,327
100,000	B/T	48,441
150,000	B/T	59,328

Risk acceptance criteria. For a critical bridge, the total bridge acceptance annual frequency of collapse, is 0.0001 (AASHTO Article 4.8.2). This total acceptance must be distributed among the exposed bridge elements within a distance 3(*LOA*) on each side of the inbound and outbound vessel transit paths. For the suspension bridge shown in Figure 4–69, the distance from the center line of the channel to the edge of the analysis area is

$$x = 200 + 3(LOA) = 200 + 3 \times 1030 = 3290 \text{ feet}$$

Within this distance are five piers on each side of the channel center line for a total of ten piers. The distribution of AF_c among these ten piers must be determined by the design, and a convenient approach is to spread the acceptable risk equally among these elements. However, this is not desirable because it does not take into account the importance and higher cost associated with the main pier of this bridge, hence a better method is to apportion the risk to each pier based on its percentage value of the replacement cost of the structure in the central analysis area. For this example, the two main piers represent 50 percent of the replacement cost of the bridge in the central analysis area. Each main pier is, therefore, assigned 25 percent of the total acceptable annual frequency, or

$$AF_p = 0.25\ (AF_c) = 0.25 \times 0.0001 = 0.000025$$
$$RP_p = (1/AF_p) = 1/0.000025 = 40{,}000 \text{ years}$$

A comparison of the allowable value of AF_p = 0.000025 with the actual value of ΣAF = 0.000508 in Table 4–19 indicate that under these future year traffic conditions the pier will be vulnerable to catastrophic vessel collision. It can also be seen that even the 150,000 *DWT* vessels with AF = 0.000051 exceed the acceptable criteria.

Table 4–21 Probability of Collapse

Size(DWT)	(H_p/P_s)	PC
10,000	1.306	0.0000
20,000	0.923	0.0086
40,000	0.653	0.0386
60,000	0.533	0.0519
80,000	0.462	0.0598
100,000	0.413	0.0652
150,000	0.337	0.0737

Table 4–22 Annual Frequency of Main Pier Collapse (H_p = 46,000)

Ship(DWT)	N	PA	PG	PC	AF	ΣAF
150,000	60	1.0×10^{-4}	.1143	.0250	.000017	.000017
100,000	100	1.0×10^{-4}	.1076	.0056	.000006	.000023
80,000	300	1.0×10^{-4}	.0973	.0000	—	—
60,000	100	1.0×10^{-4}	.0906	.0000	—	—
40,000	100	1.0×10^{-4}	.0839	.0000	—	—
20,000	2,000	1.0×10^{-4}	.0772	.0000	—	—
10,000	3,000	1.0×10^{-4}	.0607	.0000	—	—

Revised annual frequency. Possible alternatives are to revise the pier strength in order to meet the acceptance criteria, or determine an impact force (neglecting the cost-effective procedure) in conjunction with developing a pier protection system to protect the main pier.

These options are analyzed in a trial and error process in which values of H_p are assumed, new AF's are computed, and a comparison with AF_p is made. As a first trial, we assume H_p = 46,000 kips, which is approximately the impact force P_s of a 90,000 DWT ship. The revised annual frequency of collapse is shown in Table 4–22.

The new ΣAF = 0.000023 is less than the AF_p = 0.000025 acceptance criteria. Hence, a 90,000 DWT design vessel would be required for the design of a pier protection system for the main pier.

4.19 DESIGN EXAMPLE 4–8: PIER STABILITY UNDER STREAM FLOW

The pier of Figure 4–36 is built in a stream, and is subjected to the forces of stream flow. The water is 10 feet deep, and flows at a rate of 5 ft/s.

The pressure exerted by the stream is computed from Equation (2–21). The drag coefficient C_D is obtained from Table 2–10 for square-ended pier, or C_D = 1.4. Therefore,

$$p = 1.4 \times 5^2 = 35 \text{ lb/ft}^2$$

Total lateral force $SF = (35 \times 4 \times 10) = 1.4$ kips
Moment at the bottom of the footing

$$M_{SF} = 1.4 \times 9 = 12.6 \text{ ft-kips}$$

The weight of the pier is reduced by the buoyant effect of the water. This uplift is

$$(8 \times 4 \times 10 + 14 \times 10 \times 4)(0.063) = 55 \text{ kips}$$

Recall from Design Example 4.2 that the overturning moment is:

Wind on superstructure	=	677 ft-kips
Wind uplift	=	313 ft-kips
Stream flow	=	13 ft-kips
Total	=	1003 ft-kips

Total vertical force = 619 − 55 = 564 kips
Balancing moment = 564 × 7 = 3948 ft-kips

$$FS = 3948/1003 = 3.9, \text{ ample}$$

Other cases to be considered include Group III, and full wind on the portion of the pier above the water surface. In both these cases, the pier has ample stability.

REFERENCES

AASHTO Manual on Foundation Investigations, American Association of State Highway and Transportation Officials.

AASHTO, 1991: *Guide Specification and Commentary for Vessel Collision Design of Highway Bridges,* American Association of State Highway and Transportation Officials, Washington, D.C.

AASHTO, 1994: AASHTO LRFD Bridge Design Specifications.

ACI, 1978, Committee 340: *Design Handbook in Accordance with the Strength Design Method of ACI 318-77,* vol. 2, Columns, ACI Publications SP17A(78), American Concrete Institute, Detroit, pp. 214.

ACI-ASCE COMMITTEE 327, "Report on Ultimate Strength Design," *Proc. ASCE,* vol. 81, Oct. 1955, Paper 809. See also ACI Journ., Proc., vol. 2, No. 7, January 1956, pp. 505–524.

ANG, B. G., M. J. N. PRIESTLEY, and T. PAULEY, 1985: *Seismic Shear Strength of Circular Bridge Piers,* Research Repo. 85-5, Dept. of Civ. Eng., Univ. of Canterbury, Christchurch, New Zealand, July.

ARBABI, F., 1991: *Structural Analysis and Behavior,* McGraw-Hill, New York.

ARMENAKAS, A. E., 1991: *Modern Structural Analysis: The Matrix Method Approach,* McGraw-Hill, New York.

AUSTIN, WALTER J., 1961: "Strength and Design of Metal Beam-Columns," *Proc., ASCE, Journ. Struct. Div.,* vol. 87, No. ST4, April, pp. 1–34.

BEAUFAIT, F. W., 1977: *Basic Concepts of Structural Analysis,* Section 8.1 through 8.3, Prentice-Hall, Englewood Cliffs, N.J.

BRESLER, BORIS, 1960: "Design Criteria for Reinforced Concrete Columns under Axial Load and Biaxial Bending," *ACI Journ., Proc.,* vol. 57, No. 5, Nov., pp. 481–490; Discussion, pp. 1621–1638.

BRETTLE, H. J., 1973: "Ultimate Strength Design of Composite Columns," *Journ. Struct. Div.,* ASCE, vol. 99, No. ST9, Sept., pp. 1931–1951.

CRANSTON, W. B., 1972: *Analysis and Design of Reinforced Concrete Columns,* Research Rep. 20, Paper 41.020, Cement and Concrete Assoc., London.

CROSS, H., and N. D. MORGAN, 1932: *Continuous Frames of Reinforced Concrete,* Wiley, New York.

CR-CEF, 1960: *Guide to Design Criteria for Metal Compression Members,* Column Research Council Engineering Foundation.

DERUCHER, K. N., HEINS, C. P., 1979: "Bridge and Pier Protective Systems," Marcel Deckker, Inc., New York.

DERUCHER, K. N., 1981: "Bridge Protection Systems and Devices—Final Report," *U.S. Coast Guard, Office of Navigation,* Report No. CG-N-1-81.

ENGLOT, J. P., 1988: "Collision Protection of Arthur Kill Bridges," *New York ASCE Section Structures Conf. Proc.,* ASCE, May.

FEDERAL HIGHWAY ADMINISTRATION, 1983: "Pier Protection and Warning Systems for Bridges Subject to Ship Collisions," *Technical Advisory T5140.19,* Washington, D.C., February 11.

FHWA, 1969: *Strength and Serviceability Criteria, Reinforced Concrete Bridge Members,* Ultimate Design, FHWA, October.

FLETCHER, M. S., R. W. P. MAY, and J. A. PERKINS, 1983: "Pier Protection by Man-Made Islands for Orwell Bridge, U.K.," *IABSE Colloquium,* Preliminary Rep., pp. 327–333.

FURLONG, R. W., 1974: "Concrete Encased Steel Column-Design Tables," *Journ. Struct. Div.,* ASCE, vol. 100, No. ST9, Sept., pp. 1865–1882.

FURLONG, R. W., 1974: "Column Slenderness and Charts for Design," *J. Am. Concr. Inst.,* 68(1) 9–17, January.

FURLONG, R. W., 1979: "Concrete Columns under Biaxially Eccentric Thrust," *J. Am. Concr. Inst.,* October.

GERE, J. M. and W. O. CARTER, 1962: *Critical Buckling Loads of Tapered Columns,* ASCE Struct. J., February.

GERE, J. M., and WEAVER, W., JR., 1965: *Analysis of Framed Structures,* Chapter 4, Van Nostrand, Princeton, N.J.

GERGELY, P. and L. A. LUTZ, 1968: "Maximum Crack Width in Reinforced Concrete Flexural Member," *Causes, Mechanism and Control of Cracking in Concrete,* SP-20, ACI, Detroit, p. 87.

GERSTLE, K. H., 1974: *Basic Structural Analysis,* Chapters 10, 11, and 12, Prentice-Hall, Englewood Cliffs, N.J.

GILL, W. D., R. PARK, and M. J. N. PRIESTLEY, 1979: *Ductility of Rectangular Reinforced Concrete Columns with Axial Load,* Research Rep. 79-1, Dept. of Civ. Eng., Univ. of Canterbury, February.

GOODALL, DAVID M., 1948: *Analysis of Rectangular Reinforced Concrete Sections Subjected to Direct Stress and Binding in Two Directions,* Public Roads Magazine, June.

GOUWENS, ALBERT J., 1975: "Biaxial Bending Simplified, 1975: Reinforced Concrete Columns," *ACI Publ. SP-50,* American Concrete Institute, Detroit, pp. 233–261.

Greiner Engineering Sciences, Inc., 1983: "Study of Pier Protection Systems for Bridges," prepared for Maryland Transportation Authority, Baltimore, Md.

Greiner Engineering Sciences, Inc., 1985: "Pier Protection for the Sunshine Skyway Bridge Replacement—Ship Collision Risk Analysis," prepared for the Florida Dept. of Transportation, December.

HALL, W. J. and N. M. NEWMARK, 1979: "Seismic Design of Bridges—An Overview of Research Needs," *Proc. of a Workshop on Earthquake Resistance of Highway Bridges,* Applied Technology Council, Berkeley, Ca., January.

HAVNO, K., M. KNOTT, 1986: "Risk Analysis and Protective Island Design for Ship Collisions," *IABSE Symp. on Safety and Quality Assurance of Civ. Eng. Structures,* Tokyo, Japan, Sept. 4–6.

HEINS, C. P., and R. A. LAWRIE, 1984: *Design of Modern Concrete Highway Bridges,* Wiley, New York.

HSIEH, YUAN-YU, 1970: *Elementary Theory of Structures,* Chapter 9, Prentice-Hall, Englewood Cliffs, New Jersey.

HU, LU-SHIEN, 1955: "Eccentric Bending in Two Directions of Rectangular Concrete Columns," *J. Am. Concr. Inst.,* May.

KAAR, P. H., and A. H. MATTOCK, 1963: *High Strength Bars as Concrete Reinforcement, Part 4, Control of Cracking, PCA Development Dept.* Bulletin D59 (see also Journ. of PCA Research and Development Laboratories, 51(1) 15, January.

KARDESTUNCER, H., 1974: *Elementary Matrix Analysis of Structures,* Chapter 5 through 10, McGraw-Hill, New York.

KNOTT, M., 1986: "Pier Protection System for the Sunshine Skyway Bridge Replacement," *Proc. 3rd Annual Intern.* Bridge Conf., Pittsburgh, Pa., June 2–4.

LAURSEN, H. I., 1966: *Matrix Analysis of Structures,* Chapter 3, McGraw-Hill, New York.

LIM, K. Y., D. I. MCLEAN, and E. H. HENLEY, 1989: *Plastic Hinge Details for the Bases of Bridge Columns: Small-Scale Model Study.* Interim Project Rep., Washington State Dept. of Transportation, Olympia, April.

LIM, K. Y., D. I. MCLEAN, and E. H. HENLEY, 1990: "Moment Reducing Hinge Details for the Bases of Bridge Columns," TRB 1275, *National Research Council,* Washington, D.C.

LIVESLEY, R. K., 1964: *Matrix Method of Structural Analysis,* Chapter 4, Pergamon Press, MacMillan Co., New York.

MACGREGOR, JAMES G., 1973: "Simple Design Procedures for Concrete Columns," Introductory Report, *Symp. on Design and Safety of Reinforced Concrete Compression Members,* Reports of the Working Commissions, vol. 15, Intern. Assoc. of Bridge and Structural Engineering, Zurich, Apr., pp. 23–49.

MARIN, J., 1979: "Design Aids for L-Shaped Reinforced Concrete Shapes," *J. Am. Concr. Inst.,* November.

MAUNSELL, PARTNERS, and BRADY, P. J. E., 1978: "Second Hobart Bridge—Risk of Ship Collision and Methods of Protection," *Technical Rep. prepared for Dept. of Main Roads,* Tasmania, Australia.

MCGUIRE, W., and R. H. GALLAGHER, 1979: *Matrix Structural Analysis,* Chapters 3 through 5, Wiley, New York.

NEWMARK, N. M., 1942: *Numerical Procedure for Computing Deflections, Moments, and Buckling Loads,* ASCE Proc., May.

Notes on Load Factor Design for Reinforced Concrete Bridge Structures with Design Applications, Portland Cement Assoc.

OSTENFELD, C., 1965: "Ship Collisions Against Bridge Piers," *Publications IABSE,* pp. 233–277.

PARK, R., and R. W. G. BLAKELY, 1979: *Seismic Design of Bridges: Bridge Seminar,* Summary vol. 3, Structures Committee, Road Research Unit, National Roads Board, New Zealand.

PARME, A. L., J. M. NIEVES, A. GOUWENS, 1966: "Capacity of Reinforced Rectangular Columns Subject to Biaxial Bending," *J. Am. Concr. Inst.,* September.

PCA: *Continuous Concrete Bridges,* Second Edition, Portland Cement Association, Skokie, Illinois.

POTANGAROA, R. T., M. J. N. PRIESTLEY, and R. PARK, 1979: *Ductility of Spirally Reinforced Concrete Columns Under Seismic Loading,* Research Report 79-8, Dept. of Civ. Eng., Univ. of Canterbury, February.

PRIESTLEY, M. J. N., and R. PARK, 1987: *Strength and Ductility of Concrete Bridge Columns Under Seismic Loading,* ACI Structural Journ., Jan.–Feb.

RAMA, H. E., 1981: "Pier Protection of Staten Island," *Bridge and Pier Protective Systems and Devices Conf. Proc.,* Stevens Institute of Technology, pp. 125–129, December.

RUBINSTEIN, M. F., 1966: *Computer Matrix Analysis of Structures,* Chapter 9, Prentice-Hall, Englewood Cliffs, New Jersey.

TAMBS-LYCHE, P., 1983: "Vulnerability of Norwegian Bridges Across Channels," IABSE Colloquium, Preliminary Rep., pp. 47–56.

TAYLOR, F. W., S. F. THOMSON, and E. SMULSKI, 1958: *Reinforced Concrete Bridges,* Wiley, New York.

TOPRAC, A. A., 1959: *Circular Reinforced Concrete Columns Subjected to Direct Stress and Bending,* Public Roads Magazine, December.

TROELS BRONDIEM-NIELSEN, 1982: "Ultimate Limit States of Cracked Arbitrary Concrete Sections under Axial Load and Biaxial Bending," *Concrete International: Design and Construction,* vol. 4, No. 11, Nov., pp. 51–55.

WERNER, S. D., L. C. LEE, L. H. WONG, and M. D. TRIFUNAC, 1977: "An Evalution of the Effects of Travelling Seismic Waves on the Three Dimensional Response of Structures," *Agbabian and Associates,* El Segundo, Ca., October.

WERNER, S. D., L. C. LEE, L. H. WONG, and M. D. TRIFUNAC, 1979: "Effects of Traveling Waves on the Response of Bridges," *Proc. of a Workshop on Earthquake Resistance of Highway Bridges,* Applied Technology Council, Berkeley, Ca., January.

WEST, H. H., 1989: *Analysis of Structures,* Wiley, New York.

XANTHAKOS, P. P., 1994: *Theory and Design of Bridges,* Wiley, New York.

YIU, C., 1981: "Innovative Fender Design," *Bridge and Pier Protective Systems and Devices Conf. Proc.,* Stevens Institute of Technology, pp. 161–174, Dec.

YURA, JOSEPH A., 1974: *The Effective Length of Columns in Unbraced Frames,* AISC Eng. J., April.

CHAPTER 5

Piers for Special Bridges

5.1 STRUCTURAL INTERACTION OF ELASTIC PIERS IN MULTI-SPAN ARCH BRIDGES

Basic Principles

The formulation of theories for the analysis of single-span arches is based on elastic principles that correlate loads and the resulting deformations. The associated elastic equations are added to the equations of static equilibrium to give a mathematical system normally sufficient for the determination of all unknown reaction components. The same method of analysis can be expanded to include an arch of any number of spans and support conditions; for example, intermediate pier supports that can undergo elastic yielding under load.

Consider the two-span arch bridge shown in Figure 5–1. The end skewbacks are supported by rigid and unyielding abutments. The center pier is also rigid, but slender so as to yield or distort elastically under load. In this case, the analysis can proceed, considering the three sets of unknown reaction components at the three support locations, for a total of nine, namely,

H_1, V_1, and M_1
H_2, V_2, and M_2
H_3, V_3, and M_3

Three equations are written from statics, and the other six can be obtained as elastic equations for deflections, noting that the movement of point a must be exactly the

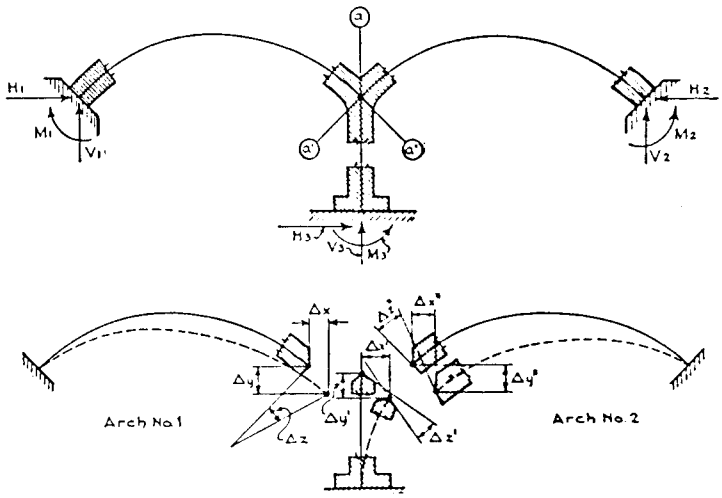

Figure 5–1 Two-span arch bridge; elastic equilibrium.

same when (1) regarded as the righthand terminal point of arch 1, (2) regarded as the lefthand terminal point for arch 2, and (3) regarded as the upper terminal of the pier.

Next, the complete elastic system is divided into three components by means of sections $a - a' - a''$, and the following equations are written:

From statics: three equations

also

$$\left.\begin{array}{lll} \Delta_x = \Delta_{x'''} & \Delta_y = \Delta_{y''} & \Delta_z = \Delta_{z''} \\ \Delta_x = \Delta_{x'} & \Delta_y = \Delta_{y'} & \Delta_z = \Delta_{z'} \end{array}\right\} \tag{5–1}$$

giving a total of possible independent equations equal to nine. This is the same as the number of unknowns; hence, a complete solution is possible.

Figure 5–2 shows a three-span arch bridge. For the computations of moments and reactions at the supports, there are twelve unknown reaction components as indicated.

For the two end arches we can write the following expressions

$$\begin{array}{lll} \Delta_x = \Delta_{x'} & \Delta_y = \Delta_{y'} & \Delta_z = \Delta_{z'} \\ \Delta_{x'''} = \Delta_{x^{IV}} & \Delta_{y'''} = \Delta_{y^{IV}} & \Delta_{z'''} = \Delta_{z^{IV}} \end{array} \tag{5–2}$$

These six expressions, together with the three static equations, provide nine independent equations, leaving three equations yet to be evolved.

Now let Δ_x^{II}, Δ_y^{II}, and Δ_z^{II} denote the deflection components in the central arch span caused solely by the distortion in the arch rib. We can now write three additional elastic equations by simply equating the movement of one end span or one pier to the cumulative movement of the other two, namely:

$$\left.\begin{array}{l} \Delta_{x'''} + \Delta_{x''} = \Delta_x \\ \Delta_{y'''} + \Delta_{y''} = \Delta_y \\ \Delta_{z'''} + \Delta_{z''} = \Delta_z \end{array}\right\} \tag{5–3}$$

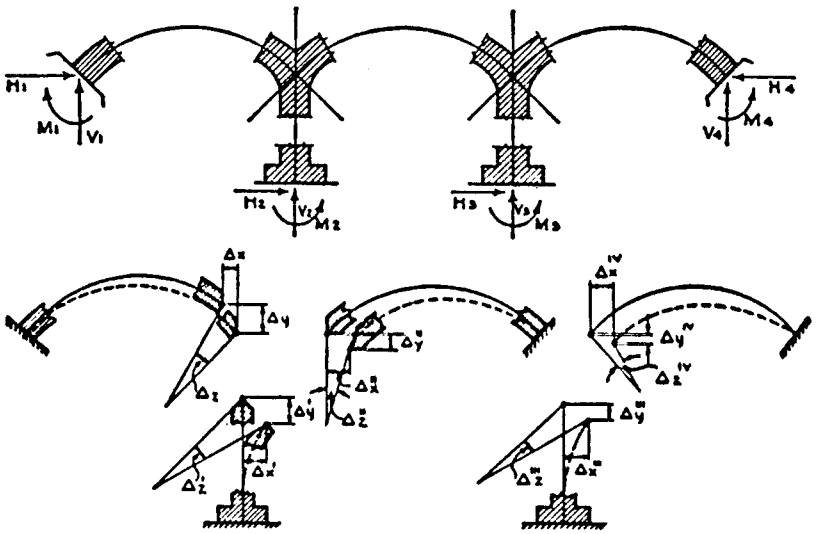

Figure 5–2 Three-span arch bridge; elastic equilibrium.

The total independent equations are now twelve and obviously sufficient for a complete determination of the twelve unknown reaction components.

It should be pointed out that the twelve equations developed in the foregoing analysis constitute the maximum number of independent equations that are possible with this problem. Other expressions may be derived from substitutions, but they do not bring new conditions into the compatibility of the structure.

What determines the number of independent equations for a given number of spans and support conditions may be inferred from a considerations of statics and deflection pattern. For a given arrangement of arch spans on rigid and unyielding end abutments, the total movement from end to end of the span is zero, that is, the interior distortion components must balance or neutralize each other since the end supports undergo no displacement. This being the case, we may select any point in the structure and equate the algebraic sum of the displacement components to zero. Thus, for any point the following is true

$$\left.\begin{aligned} \Delta_{x(R)} + \Delta_{x(L)} &= 0 \\ \Delta_{y(R)} + \Delta_{y(L)} &= 0 \\ \Delta_{z(R)} + \Delta_{z(L)} &= 0 \end{aligned}\right\} \tag{5–4}$$

These three equations, together with the three equations of static equilibrium, provide six expressions for any arch system. In addition, three equations may be written for each pier from the condition that the displacement of the pier at the junction with the arch must be exactly the same as the displacement, at the same point, of the arch rib on either side of the pier.

The total number of independent equations that are possible for any case is therefore $3N + 6$ where N is the number of piers, so that a complete solution is always possible. Deflection theories based on the elastic approach may be combined with appropriate software programs to give the solution of the system of equations, and the complete determination of the external reaction components at the piers and end supports.

Method of Substitute Elastic Voussoir

It is apparent from the foregoing discussion that arch spans supported on piers that are relatively high and slender are under the effect of elastic distortions that can markedly modify the load stresses. The general effect of elastic yielding of the piers is a decrease of the horizontal thrusts, an increase in the crown moments, and corresponding adjustments of load effects in adjacent spans and intermediate piers. Interestingly, the quantitative determination of stress induced by pier elasticity is comparatively recent, although the actual use of arch span groups is by no means new.

Basic principles. Consider the ordinary fixed arch (single span) shown in Figure 5–3(a). If at either end the rib is assumed to be split into two separate elements, as shown in Figure 5–3(b), and extending up to any two sections such as *a-a* and *b-b*, the same method of analysis would still apply. With this transformation taken one step further, the same approach would apply if the two component segments were extended to form an intermediate pier and an additional span as shown in Figure 5–3(c). In this substitution the original righthand voussoir (from section *a-a* to the skewback) is replaced by a curved composite voussoir as shown in Figure 5–3(d).

If the elastic displacement of the pier and span combination (cross-hatched in Figure 5–3(d) under a given load F is the same as the arch block from which it was developed, the elasticity of the central segment *a-a* to *b-b* is not changed but remains the same in both cases. It appears, therefore, that a suitable method of analysis is simply this development in reverse. This would involve the determination of the elastic displacement of each pier and rib combination, beginning at either end, and the replacement of this combination by an "ideal" or "substitute" voussoir section having an equivalent elastic displacement. For a complete analysis, the work must be carried one step

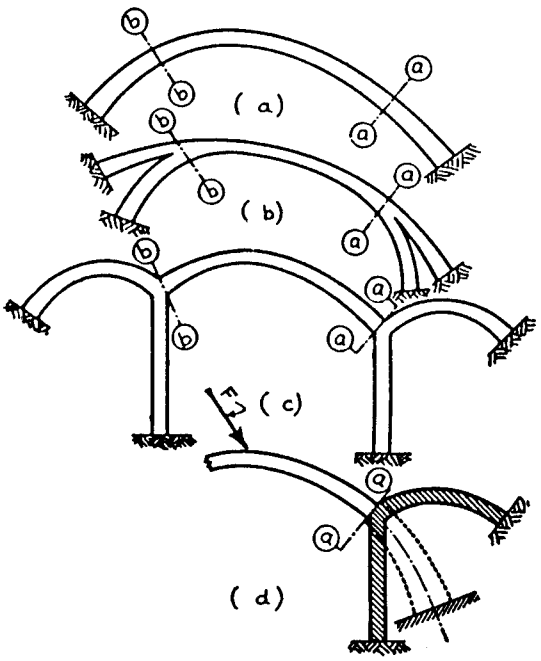

Figure 5–3 Conversion of a single fixed rib arch into a multispan arch.

further, since the above procedure can only determine stresses in the central rib induced by a load acting on the same rib. In addition, it is necessary to determine what portion of a load applied on any one of the spans is transferred to adjacent spans, and what portion is carried down through intermediate piers.

Although the analysis is tedious and time consuming, with shortcuts and approximations it is possible to pursue a complete set of calculations from which to plot the necessary influence lines. Alternatively, a computerized procedure will save considerable time and provide the advantage of parametric solutions.

The steps involved in the analysis of an elastic arch group over three spans are discussed by Xanthakos (1994). The initial elastic system is transformed and eventually replaced by an ideal or substitute single voussoir. The same method of analysis can be extended to include any number of spans and intermediate piers. With proper substitutions, the original n-span group may be replaced and broken up into n equivalent single systems.

5.2 TOWERS FOR SUSPENSION BRIDGES

Configurations

Towers for suspension bridges may be considered as composed of two parts: the substructure or pier, and the tower proper extending above the roadway and supporting the cables or chains. The pier does not involve any special features that might distinguish this structure from ordinary bridge piers.

Towers must be designed so as not to obstruct the roadways. They usually consist of a lower leg for each suspension system or a column. For lateral stability the tower legs are braced by means of cross-girders and cross-bracing, or by arched portals. The sway and portal bracing are necessary to brace the tower columns against buckling, to accommodate the lateral components from cradled cables or chains, and to carry wind stresses down to the piers.

The design of towers must be compatible with the structural materials. These may consist of masonry, reinforced concrete, and more commonly steel. With masonry construction, the towers may consist of shafts springing from a common base beneath the roadway and connected together at the top with arched members. For smaller spans the towers may consist of two separate tapering shafts. Resistance to transverse forces is better provided if the towers taper toward the top, and this shape is also accepted as a fine architectural treatment.

The tower legs are designed as columns to carry the vertical reaction of the cables, and as cantilevers to resist any unbalanced horizontal tension. The latter will depend on the saddle design (fixed or movable), the temperature and loading conditions, and the difference in inclination of the main and the side span cable tangents at the saddle. Provisions must also be made to resist forces due to wind pressure on the cables, towers, and deck trusses or girders.

The use of steel in towers offers several advantages. A greater height is possible, and this ensures a more favorable sag-ratio. The thermal expansion of the steel towers balances the movement of the suspenders, and this minimizes temperature effects present with indeterminate types.

Steel tower columns are made up of plates and angles to form either open or closed sections. The sides may be either latticed or closed with cover plates. These members

are proportioned according to the design requirements of compression members and slender columns. Typically the cross section is enlarged near the base, and outside stiffening webs may be added. The base must be anchored to resist the horizontal forces.

Tower details. Rocker towers, with a pin bearing at the base, usually provide the most economical and structurally adequate design for bridges of longer spans. They eliminate the stresses from unbalanced horizontal forces without requiring movable saddle construction. However, where rockers are adopted, the towers must be temporarily secured against overturning during erection.

Figure 5–4 shows an example of a tower 230 feet high. The legs are battered, from a top width of 33 feet 6 inches to a width of 55 feet 6 inches at the base. The width at the top corresponds to the spacing of trusses, with the cables hanging in vertical planes. The advantage of this detail is that the truss and road deck runs through the tower portal without interference from the tower legs. An added advantage is the increased transverse stability that is especially important for narrow bridges.

The two legs of this tower are braced with rigid diagonal and transverse members, including a transverse distributing girder at the top, a transverse reaction girder supporting the stiffening truss, and a transverse portal girder immediately above the stiffening truss portal. The legs are made up of a double box section with a maximum longitudinal width of 8 feet and a constant transverse width of 3 feet 6 inches. Transverse stiffening diaphragms are provided at intervals, two in each column section.

The tower is designed for a maximum horizontal component reaction of 3860 kips in each cable, resulting in a maximum vertical reaction of 3790 kips per column. This is supplemented by the vertical reactions of the stiffening truss and approach span (240 and 300 kips, respectively), which affect only the lower sections of the tower. In addition, the tower top is subjected to a maximum lateral pull of 75 kips per tower from wind forces transmitted through the cables, whereas at the bottom the tower receives the lateral reactions (190 kips) from the trusses. These force effects are taken into account in proportioning the tower columns and the transverse bracing. Unbalanced cable pull at the top of towers is accommodated by the rocker feature.

The rocker base details are also shown in Figure 5–4. The pedestal or base casting rests on the concrete piers, and is terminated to a base bearing plate 7 feet × 8 feet. The maximum vertical reaction on each rocker bearing is 2420 tons or 4840 kips. Assuming a concrete strength $f_c' = 2500$ lb/in^2 for the piers, the allowable bearing is $0.3f_c' = 750$ lb/in^2 compared with an actual bearing stress of $4840/56 \times 144 = 600$ lb/in^2.

Erection

The towers may be erected simultaneously with the construction of the anchorages and end supports. A common procedure for erecting tower columns is by means of derrick platforms adapted to travel vertically up the tower as the erection proceeds. Each platform projects out from the face of the tower and is supported by two brackets. The tipping moment is resisted by two pairs of rollers or wheels, one at each column, engaging vertical edges of the projecting middle portion of the column.

For handling and erection purposes, the columns are divided by transverse and longitudinal field splices to give sections of convenient size. Each tower column is finished with cap section upon which the saddle is set.

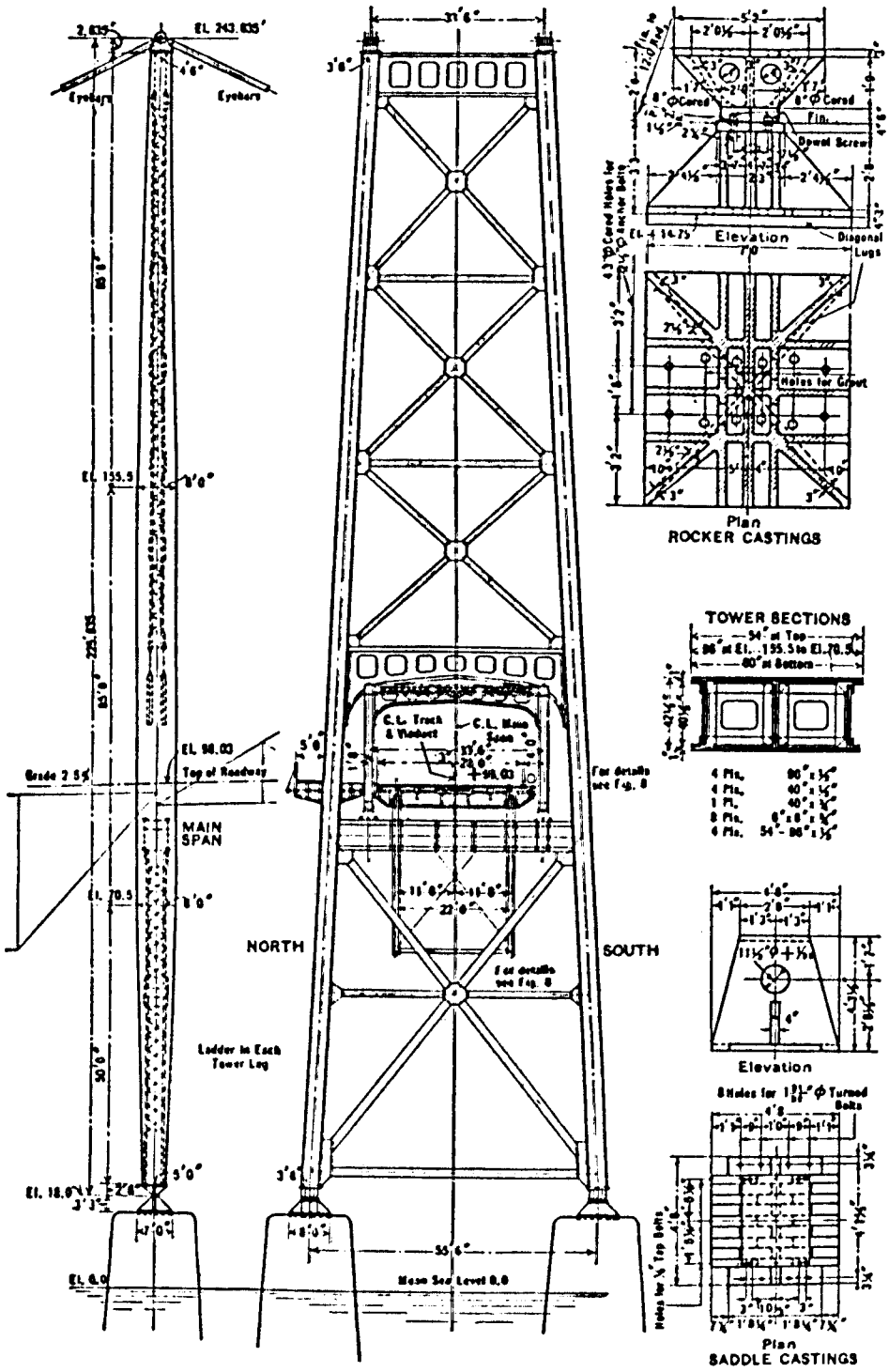

Figure 5–4 Tower details for suspension bridge.

Design Example

A two hinged suspension bridge with supported side spans has the following data:

Main span l = 1080 feet
Side span l_1 = 360 feet, span ratio $r = l_1/l = 1/3$
Distance, tower to anchorage = 400 feet
Cable sag in main span f = 108 feet ratio $n = f/l = 1/10$
Cable sag in side spans f_1 = 12 feet ratio $n_1 = f_1/l_1 = 1/30$

Each tower consists of two columns of box section, stiffened with internal diaphragms and rigidly tied together with transverse bracing in a vertical plane. Each tower column is 225 feet high and consists of a double box section 42.5 inches wide. The dimension parallel to the stiffening truss is 4 feet at the top and increases to 9 feet at the base. The walls are 1 1/4 inches thick and the vertical transverse diaphragms are 5/8 inch thick. Splices are provided at suitable intervals to keep individual sections within the size limitations specified for shipment and erection. Horizontal diaphragms are provided at splice locations and at 10-foot intervals.

The tower columns are battered to clear the trusses. They are spaced 42.5 feet center-to-center at the top, and 53.5 feet center-to-center at the base.

Movement of tower top. The towers are assumed fixed at the base and the cable saddles immovable with respect to the tower.

The maximum stress in the tower columns occurs with the live load covering the main span and the farther side span at maximum temperature. Under this condition of loading, the top of the tower will deflect toward the main span as a result of the following deformations: (1) an upward deflection Δf_1 at the center of the unloaded side span; (2) the elongation of the cable between the anchorage and the tower, caused by elastic response to the applied loads; and (3) the elongation of the cable caused by thermal expansion.

These deformations may be calculated as follows:

For a uniform live load p' = 860 lb/ft, the corresponding horizontal tension in the cables is computed as H = 1050 kips (with the live load covering all three spans). With the live load covering two spans, H = 1040 kips. It should be noted that the live load reflects the design criteria applicable when this bridge was constructed, and does not represent the vehicle loading currents recommended for long-span bridges.

Upward Deflection Δf_1. For cables assumed to be parabolic, the loads acting on them must be uniform per horizontal unit length. If the panel points are spaced uniformly (horizontally), the suspender forces must be uniform throughout, acting downward on the cable. The cable maintains equilibrium between the horizontal tension H, resisted by the anchorages, and the downward acting suspender forces. If the suspender forces per horizontal linear unit are denoted by s, they may be computed from

$$s = H\frac{8f}{l^2} \tag{5–5}$$

where all the parameters are as defined. Accordingly

$$s = \left(\frac{8}{10}\right)\left(\frac{1040}{1080}\right) = 770 \text{ lb/lin ft per truss}$$

The upward deflection Δf_1 is found by considering the unloaded side span as a simple beam subjected to an upward loading s. Hence

$$\Delta f_1 = \left(\frac{5}{384}\right)\left(\frac{sl_1^4}{EI_1}\right) \tag{5–6}$$

Substituting the numerical values for the parameters in Equation (5–6) we obtain

$$\Delta f_1 = 0.428 \text{ ft}$$

Elastic Elongation of Cable. The elastic elongation of the cable in the side span is based on stress-strain considerations. A convenient expression is

$$\Delta L = \frac{Hl}{EA}\left(1 + \frac{16}{3}n^2\right) \tag{5–7}$$

where E is the modulus of elasticity and A is the cross section of the cable, and other parameters are as previously defined. Substituting the numerical values for the parameters in Equation (5–7), the elastic elongation is calculated as

$$\Delta L_1 = 0.192 \text{ ft}$$

Temperature Expansion. The temperature expansion of the cable in the side span may be estimated by reference to Figure 5–5, where l_1 represents the horizontal length of the side span. The true vertex of the curve or lowest point V will generally be found to be outside point D. The exact length of curve will be VA-VD, or the difference between two semiparabolas, each of which may be easily calculated. An approximate value of the curve may be obtained by taking the closing chord $AD = l_1 \sec \alpha_1$ and adding the parabolic curvature correction. This will yield

$$\text{Curve } DA = L_1 = l_1\left(\sec a_1 + \frac{8}{3}\frac{n_1^2}{\sec^3 \alpha_1}\right) \tag{5–8}$$

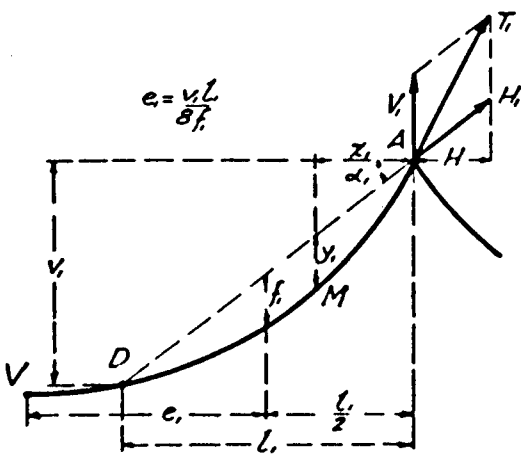

Figure 5–5 Parabolic cable in side span.

where $n_1 = f_1/l_1$ as previously defined. For a change in temperature of t degrees, coefficient of expansion w, the change of cable length is

$$\Delta L = wtL \tag{5–9}$$

where $t = \pm 60°F$. The temperature expansion of the cable in the side span is now computed as

$$\Delta L_1 = (0.156)(1.037) = 0.162 \text{ ft}$$

From Equation (5–8) we also obtain

$$\frac{\Delta L_1}{\Delta l_1} = \cos\alpha_1 + \frac{8}{3}n_1^2\left(2\cos^3\alpha_1 - 3\cos^5\alpha_1\right) = 0.964$$

and

$$\frac{\Delta L_1}{\Delta f_1} = \frac{16}{3}\frac{n_1}{\sec^2\alpha_1} = 0.160$$

The deflection of the top of the tower is given by

$$y_o = \Delta l_1 = \frac{\Delta l_1}{\Delta L_1}\frac{\Delta L_1}{\Delta f_1}\Delta f_1 + \frac{\Delta l_1}{\Delta L_1}\Sigma(\Delta L_1)$$

and substituting the values just computed,

$$y_o = \left(\frac{0.160}{0.964}\right)(0.428) + \left(\frac{1}{0.964}\right)(0.192 + 0.162) = 0.439 \text{ ft}$$

Forces acting on tower. The deflection $y_o = 0.439$ ft may be considered as a displacement produced by an unbalanced horizontal force P applied at the top of the tower. If the sectional properties of the tower are known, this force may be computed from elastic theory. Accordingly,

$$y_o = \frac{P}{E}\Sigma\left(\frac{x^2}{I}\Delta x\right) \tag{5–10a}$$

For this example previous analysis gives $\Sigma\dfrac{x^2}{I}\Delta x = 1740$. Hence,

$$P = y_o\frac{E}{1740} = 17{,}200y_o = 7550 \text{ lb/column}$$

Other loads acting on the tower are the vertical reaction V at the saddles, and the end shear V_1 at the point of support of the stiffening truss. The saddle reaction may be computed from $V = 2H\tan\phi$, where ϕ is the inclination of the cable at the given section or $V = (2)(4340)(0.40) = 3470$ kips/column.

The truss reaction, with all spans loaded and maximum temperature rise, has been computed from previous analysis (not shown here), and is

$$V_1 = 99 \text{ kips/column}$$

with one side span unloaded and the same assumptions,

$$V_1 = -52 \text{ kips/column}$$

The inaccuracy introduced by neglecting the uplift $V_1 = 52$ kips will be on the safe side; hence the structural adequacy of the column may be estimated only for the horizontal load P and the vertical load V.

At any section x of the tower, the horizontal deflection y from the initial vertical position of the axis is given with sufficient accuracy by the expression for the elastic curve of the cantilever or

$$y = y_o\left[1-\left(\frac{3}{2}\right)\left(\frac{x}{h}\right)+\left(\frac{1}{2}\right)\left(\frac{x}{h}\right)^3\right] \tag{5–10b}$$

where h = height of tower = 225 feet.

Tabulation of stresses. The resulting extreme fiber stress at any section of the tower is

$$F_s = \frac{V}{A}+\frac{Pxc}{I}+\frac{V(y_o-y)c}{I} \tag{5–10c}$$

with the section properties and dimensions computed from a separate analysis, the stresses are tabulated at 25-foot intervals and are shown in Table 5–1.

Wind stresses. Stresses due to wind forces must be superimposed on the stress produced by live load and temperature, shown in Table 5–1, to obtain total stresses.

The truss wind load is taken as 400 lb/lin in, and produces a horizontal reaction at each tower computed as

$$360\frac{l}{2}+400\frac{l_1}{2} = 266 \text{ kips}$$

acting at joint No. 4 (x = 100 ft).

Table 5–1 Stress Summary for Design Example

Joint No.	x ft.	y_0–y ft.	$d = 2c$ ft.	A sq. in.	I in.^{2} ft.^{2}	$\frac{x^2}{I}$	$\frac{V}{A}$	$\frac{P_{xc}}{I}$	$\frac{V(y_0-y)c}{I}$	Combined Stresses lb./sq. in.
0	0	0	4.0	280	560	0	12,400	0	0	12,400
1	25	.068	4.5	295	730	.86	11,800	500	700	13,000
2	50	.134	5.0	310	940	2.66	11,200	900	1100	13,200
3	75	.197	5.5	325	1170	6.40	10,700	1200	1600	13,500
4	100	.254	6.0	340	1440	6.94	10,200	1500	1800	13,500
5	125	.305	6.5	355	1740	8.98	9,800	1600	2000	13,400
6	150	.348	7.0	370	2080	10.80	9,400	1800	2000	13,200
7	175	.380	7.5	385	2460	12.42	9,000	1900	2000	12,900
8	200	.400	8.0	400	2880	13.88	8,700	1900	1900	12,500
9	225	.408	9.0	430	3850	13.20	8,100	1800	1700	11,600
						$\Sigma = 69.54$				

The depth d of the stiffening truss is 22.5 feet. The deflection of the truss under wind produces a horizontal reaction at the top of each tower of 40 $l/2$, whereas the wind on the surface of the cables produces an addition to this reaction equal to 10 ($l/4 + l_1/2$). The total reaction at the tower top is 26 kips.

The wind acting directly on the tower is taken as 25 lb/ft^2 of vertical elevation. At each tower joint, this action produces an equivalent concentrated load equal to (25)(25d). The resulting bending moments are divided by the moment arm to obtain the column force. This force divided by the column cross-sectional area gives the unit stress caused by the wind effect. The results are tabulated in Table 5–2.

Commentary. The use of construction materials is justified in economic terms by the introduction of stresses for which the materials are suitable. Considering the restrictive criteria and stress limitations applied to compression members, the cables of suspension bridges, subjected primarily to tension, justify the economic use of steel. The choice may also be justified in terms of (1) the direct stress paths from the points of load application to the points of supports; (2) the high ultimate resistance of steel cables; and (3) the associated structural redundancy: If a member tends to fail, the rest of the structure is likely to remain unaffected so that the damaged member can be repaired or replaced.

The simplest form of a suspension bridge is a simple span, classified as 2F, or 3F. A bridge with classification 3F has a stiffening truss, it is non-continuous, it has the side span free, and is three-hinged. The classification 2F means the same configuration and structural details, except that the bridge has no center hinge. Suspension bridges classified as 3S and 2S are essentially similar except that the side spans are suspended. The bridge of the foregoing example is type 2S.

Design of an anchorage. Figure 5–6 shows the anchorage structure for a suspension bridge. Anchorage end blocks are also discussed in section 7.15, and details are shown in Figures 7–38 and 7–39 for the Humber suspension bridge. The anchorage shown in Figure 5–6 is a reinforced concrete structure.

The principal forces acting are the cable pull and the weight of the anchorage, including any superimposed loads. For this example, the cable pull is estimated as 7800 kips. The weight of the anchorage and the superimposed loads is 30,000 kips. This

Table 5–2 Wind Stresses for Design Example

Joint No.	x ft.	d ft.	Wind Load kips	Shear kips	Moment ft. kips	Column Dist. ft.	A sq. in.	Stress from W.L. lb./sq. in.	Stress from L. L. + Temp. lb./sq. in.	Total Stress lb./sq. in.
0	0	4	26+1	0	0	42.5	280	0	12,400	12,400
1	25	4.5	3	− 27	− 675	43.5	295	100	13,000	13,100
2	50	5	3	− 30	− 1,425	44.5	310	100	13,200	13,300
3	75	5.5	3	− 33	− 2,250	46.5	325	100	13,500	13,600
4	100	6	266+4	− 36	− 3,150	48.5	340	200	13,500	13,700
5	125	6.5	4	−306	−10,800	49.5	355	600	13,400	14,000
6	150	7	4	−310	−18,550	50.5	370	1000	13,200	14,200
7	175	7.5	5	−314	−26,400	51.5	385	1300	12,900	14,200
8	200	8	5	−319	−34,375	52.5	400	1600	12,500	14,100
9	225	9	3	−324	−42,475	53.5	430	1800	11,600	13,400

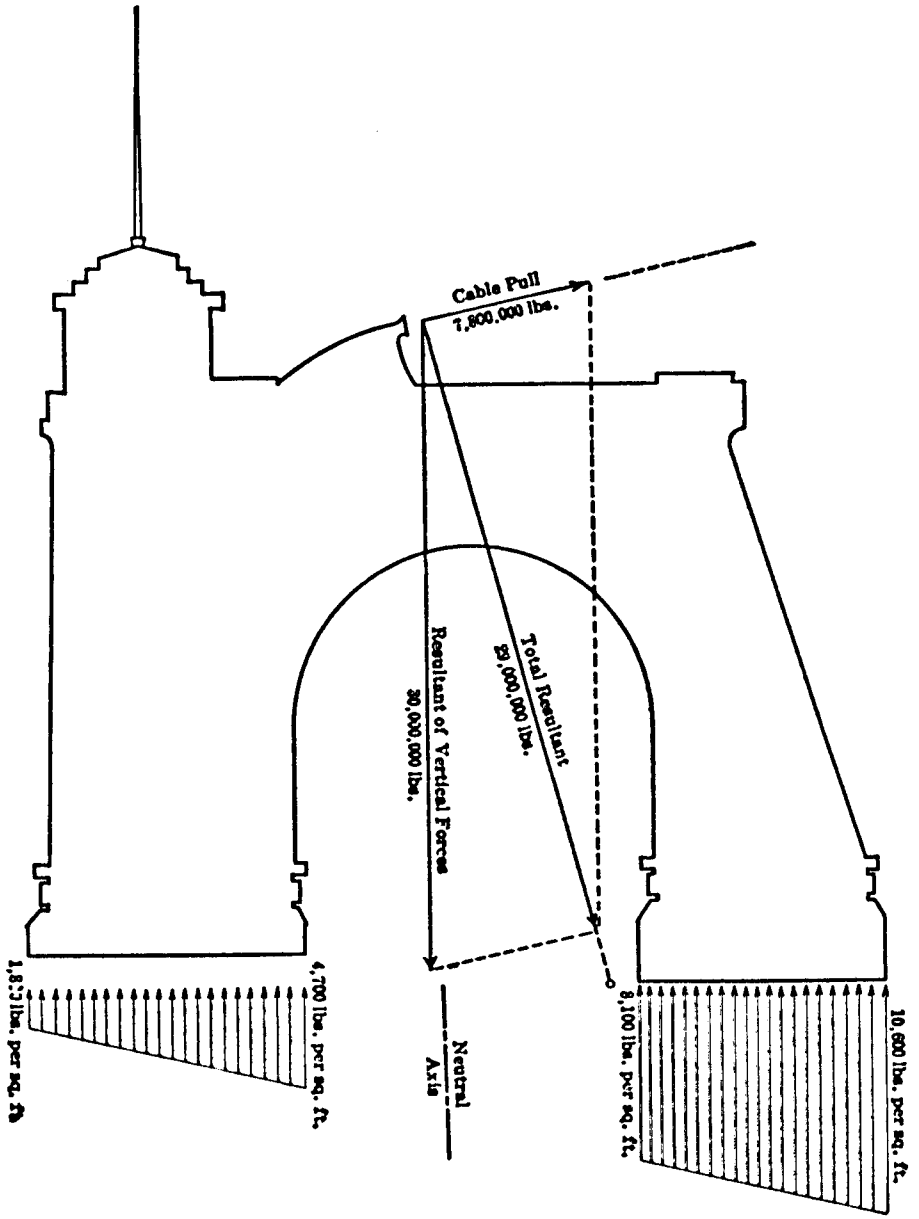

Figure 5–6 Anchorage detail.

weight is represented in the diagram as a vertical force through the center of gravity of the anchorage and the applied loads. The total resultant and its direction is found from the parallelogram of forces. Its magnitude is 29,000 kips. If its inclination from the vertical is less than the friction angle, the anchorage is safe against failure by sliding.

In order to investigate the stability against tilting, the line of action of the resultant is extended until it intersects the base. Its vertical component V = 28,000 kips is considered an eccentric load applied at the intersection point. The toe and heel pressures are given by

$$p = \frac{V}{A} \pm \frac{Vec}{I}$$

where A is the area of the base, I is the moment of inertia, and e is the eccentricity of V with reference to the centroid of the base. The pressures are then obtained as 10.6 kips/ft^2 at the toe, and 1.8 kips/ft^2 at the heel. The allowable foundation pressure (ASD) is 6 tons/ft^2, hence the anchorage is safe against overturning. The analysis should be completed by estimating the maximum settlement and comparing it with the tolerable value.

5.3 TOWERS AND PYLONS FOR CABLE-STAYED BRIDGES

Historical Data

Simple examples of cable-stayed bridges have been found in remote areas of the world. Kavanagh (1973) mentions a footbridge of iron built in 1857 near Pieter Maritzburg in South Africa. A bridge more than 120 years old has been found in Singapore.

Recently built bridges provide data on the validity of the economic span range, at one time suggested as 500 to 1200 feet. Thus single pylons supporting an asymmetric main span of 320 m (1050 ft) actually correspond to a main span of over 600 m (1970 ft) in a symmetrical bridge with pylons on each side of the main span. Leonhardt and Zeliner (1972) have proposed that for spans of 750 m (2460 ft) to 1500 m (4920 ft) the cable-stayed system is technically and economically superior to the classical suspension scheme, especially with respect to aerodynamic stability, provided certain basic factors are considered in the design.

These considerations are probably more relevant in the United States where bridges over waterways and large bodies of water are often built. Contrary to these requirements, the German practice involves a practical limit of about 300 m (1000 ft), which is the typical span for bridges across a main river, such as the Rhine. Optimum span range in this case may be imposed by physical factors rather than by technical and economic considerations.

The trend toward asymmetry of the bridge with respect to the towers is documented by lower Elue span in Hamburg, the Deggenau Bridge over the Danube, the Rhine Bridge at Speyer, the new Rheinbridge at Dusseldorf-Oberkassel, the North Bridge at Mannheim, the Knee Bridge at Dusseldorf, and the proposed bridge across Charles River in Boston. Other recent tendencies have been noted toward the use of A-type towers (pylons), reminiscent of the early Severin Bridge over the Rhine at Cologne. The inclined cables leading from the apex or legs of the A-frame form a space structure of considerable torsional rigidity which increases the resistance to aerodynamic effects.

Distinctive components. The four basic cable configurations are shown in Figure 5–7. The radiating type shown in Figure 5–7(a) is a converging system whereby the cables intersect or meet at a common point at the top of the tower. The harp configuration has the cables parallel and spaced along the girder and the pylon as shown in Figure 5–7(b). The fan arrangement shown in Figure 5–7(c) combines the radiating and harp types, whereas in the star configuration shown in Figure 5–7(d) the cables are placed along the pylon and converge at a common point on the girder. Variations are possible from the four basic types.

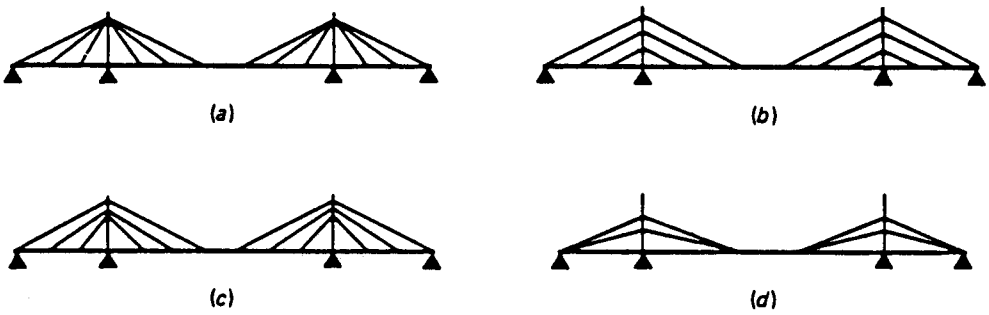

Figure 5–7 Longitudinal cable configuraiton: (a) radiating; (b) harp; (c) fan; (d) star.

In the transverse direction two basic arrangements are generally available: those where the cables are arranged in two planes, and those where the cables are arranged in a single plane. The basic arrangements may have variations represented by the types shown in Figure 5–8.

In type (a) (Figure 5–8) the single-plane configuration has one vertical plane, usually on the longitudinal centerline of the structure. A feasible variation is type (b), where the vertical plane of the cables is positioned laterally from the longitudinal centerline of the bridge. In types (c) and (e) the double-plane arrangement has two planes of cables located outside the roadway, either vertical or sloping and intersecting on the bridge center. Type (d) consists of a V-shaped double plane system, used to reduce the tower height without changing the height ratios, avoiding the stay concentration of the tower top and eliminating the lateral sway of the girder deck.

Basic Tower and Pylon Types

As in suspension bridges, the towers or pylons comprise the substructure or pier, with the tower proper extending above the roadway and supporting the cables. Because the pier segment does not involve any special features and structural behavior that may

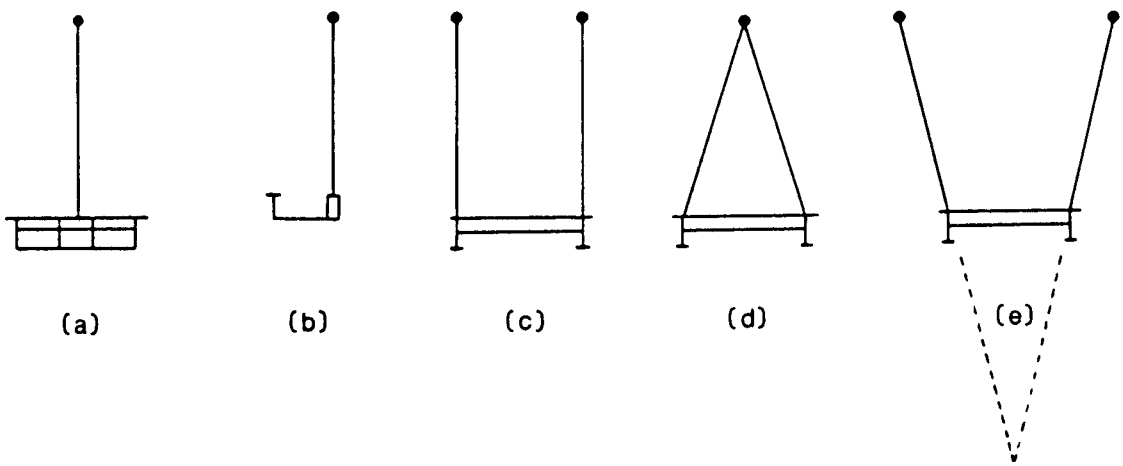

Figure 5–8 Transverse cable arrangement; (a) single-plane vertical; (b) single-plane vertical/lateral; (c) double-plane vertical; (d) double-plane sloping; (e) double-plane V-shaped.

distinguish this member from ordinary bridge piers, we will consider the tower proper as the subject of this analysis.

Towers, often referred to as pylons, may have the simple form of a single cantilever for a single-plane arrangement, or may consist of two cantilever members for a double-plane cable structure. The towers may be hinged or fixed at the base, depending on the magnitude of the vertical loads and distribution of cable forces along the tower height. Base fixity induces considerable bending moments in the pylon, but this disadvantage is offset by the increased rigidity of the structure as a unit. A fixed base is also practical for erection purposes, and may cost less than a heavy pinned bearing.

Alternatively, the tower may have the shape of a transverse A-frame (mentioned in the foregoing sections) fixed or pinned at the base as shown in Figure 1–5(a). Other shapes and configurations are the diamond form shown in Figure 1–5(b) and the delta-type shown in Figure 1–5(c). When several large spans are contemplated, two A-frames or two or more portal frames may be placed in the plane of the cables and joined transversely at the top by a portal beam.

Factors affecting the selection of a proper tower type include the vertical clearance required below the structure. In this respect the standard A-frame has a disadvantage because it requires a large pier to accommodate the legs.

The towers are normally constructed of cellular sections fabricated from structural steel or made with reinforced concrete. Concrete towers are selected where steel is in short supply and the choice involves natural materials. Recent trends show, however, a preference for concrete because of the inherent resistance of this material in compression.

The height of the tower is determined from relevant considerations, such as the relation to span length, cable arrangement, and overall aesthetic proportions.

Special Pylon Types

Column pylons fixed to pier. A pylon fixed to the pier at the base will be subjected to much less horizontal displacement, but requires larger cross-sectional areas to limit displacement to the value obtained with a fixed-cable system. Two equal-fan systems with one-sided loading are shown in Figure 5–9. The upper system has a vertical support at the right and therefore contains a fixed cable, whereas the lower system is connected to a moment-rigid pylon assumed to have a constant section.

The horizontal movement of the pylon top may be expressed as

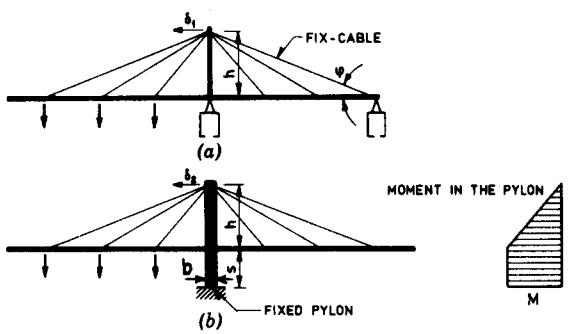

Figure 5–9 Fan-shaped cable systems with one-sided loading: (a) cable system with fixed-cable; (b) cable system connected to fixed pylon.

$$\delta_1 = \frac{h}{\sin\phi\cos\phi}\frac{\sigma_{fc}}{E_c} \tag{5–11a}$$

$$\delta_2 = \frac{2h^2 + 6sh + 3s^2}{3b}\frac{\sigma_{pb}}{E_p} \tag{5–11b}$$

where δ_1 and δ_2 is the horizontal displacement for the upper and lower system, respectively. Also, σ_{fc} is the tensile stress in the fixed cable, E_c is the modulus of elasticity of the cable, σ_{pb} is the bending stress in the lower part of the pylon, and E_p is the modulus of elasticity of the pylon. Other parameters are as shown in Figure 5–9.

Equal stiffness under one-sided load implies $\delta_1 = \delta_2$. Selecting the following practical values $s = h/2$, $\phi = 20°$, $E_c\sigma_{pb}/E_p\sigma_{fc} = 0.5$, the condition $\delta_1 = \delta_2$ yields $b = 0.31h$. This value of b is in practice unattainable. For example, a bridge with 800 foot main spans is likely to have pylon heights $h = 135$ feet. For a moment-rigid pylon, this bridge would require a width $b = 40$ feet to give the same stiffness effect provided by the fixed cable. By comparison, the same 135-foot pylon in a two-span or three-span bridge usually has a width of 6 to 9 feet.

Triangular pylon structures. A longitudinally A-shaped frame can be used to achieve sufficient horizontal stiffness in a fixed pylon, with reasonable dimensions of members. Figure 5–10(a) shows the vertical force induced in the pylon top by a symmetrical load. A one-sided load induces a vertical and horizontal force at the pylon top and a horizontal force in the stiffening girder, as shown in Figure 5–10(b). The horizontal force is equal to Pa/h giving a bending moment equal to Pa at the girder level. Based on these moments, the pylon configurations shown in Figure 5–11 are suitable solutions. In this case, the moments acting on the pylon structure are converted into axial forces in individual members. At the same time, flexural deformations of the vertical members provide a horizontal flexibility of the tower part, and this accommodates the application of continuous stiffening girders as a workable concept.

The two isometric projections shown in Figure 5–12 are pylons with the tops longitudinally fixed. For the left structure, the upper part consists of two free-standing triangular pylons, and the lower part consists of two wall-shaped pier shafts. Heavy transverse girders are placed between the pylon legs under the bridge deck as shown and ensure lateral stability. The pylon structure shown on the right of Figure 5–12 has a pyramidal configuration, with four legs comprising the lower part. In this manner the

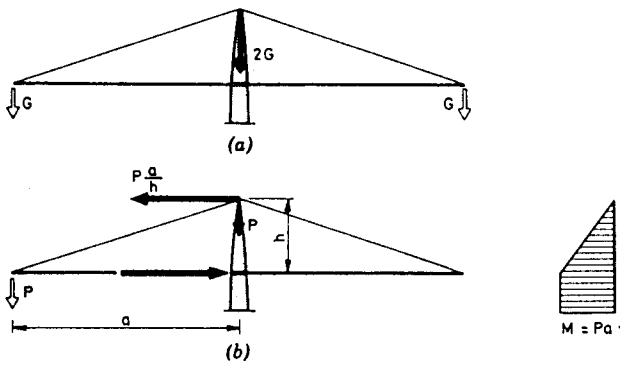

Figure 5–10 Forces acting on fixed pylon: (a) symmetric load; (b) one-sided load.

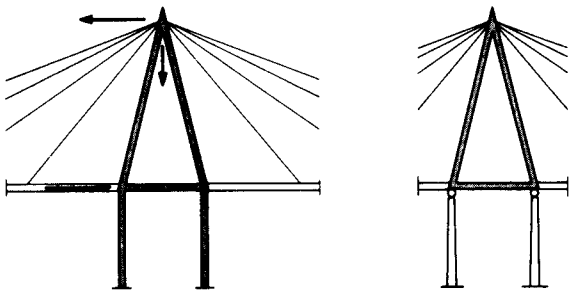

Figure 5–11 Triangular pylon structures.

pylon is fixed in all directions. Horizontal legs are placed at the bottom of the pyramid in both the longitudinal and transverse directions.

Applications. Most cable-stayed bridges have two or three spans which are sufficient to accommodate the usual navigable waterways. In these cases the horizontal displacement of the pylon is controlled by a fixed cable, that is, an upper side span cable anchored to the stiffening girder at the end support, as shown in Figure 5–9(a).

In stayed bridges with several equal spans, the inner cable systems do not contain inclined fixed cables, and thus an efficient horizontal fixing of the pylon top is not feasible. With one-sided loading with reference to the inner pylons, the result is rotation of the inner cable systems, inducing considerable vertical deflection of the stiffening girder as shown in Figure 5–13. The solutions and special pylon structures shown in Figures 5–11 and 5–12 may be considered in this case.

The importance of a connection transmitting horizontal forces from the stiffening girder to the pylon structure is demonstrated in the two structural systems shown in Figure 5–14. System I has no direct connection between the stiffening girder and the pylon, whereas in system II such a connection is available and allows the transfer of horizontal forces. In both systems the ends of the stiffening girder are supported on longitudinally movable bearings.

Under a symmetrical load such as dead load, both systems have identical deflections. For one-sided load, however, their structural action is markedly different. In system I the stiffening girder moves longitudinally toward the unloaded span, and this reduces the action of the stays, with the result of increased vertical deflection. In system II the longitudinally fixed stiffening girder inhibits changes in geometry, and this re-

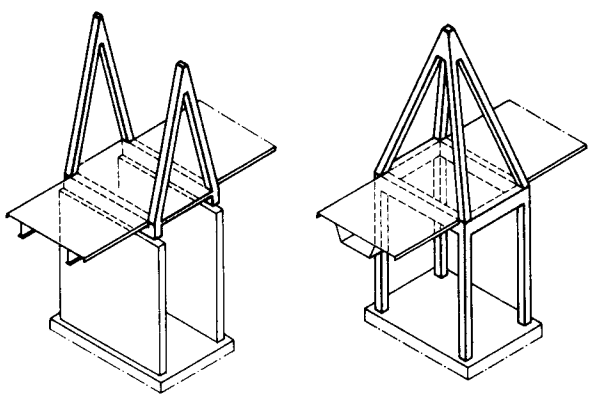

Figure 5–12 Isometric projections of triangular pylon structures.

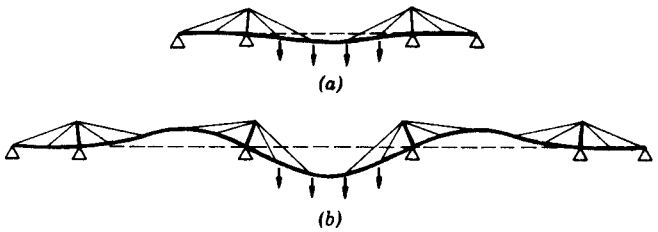

Figure 5–13 Deflection of stayed girder bridge with: (a) one main span; (b) three main spans.

duces the vertical deflection almost by one-half. The bending moments in the girder and the variation of cable forces in the system are structurally more favorable.

Erection and Fabrication

Fabrication and erection procedures for towers and pylons are closely related to the erection of the bridge as a completed structure. In general, the trend is to fabricate and erect components as large as possible for simplified construction. There are three basic methods for erecting cable-stayed bridges: the staging method, the push-out method, and the cantilever method.

The staging method is most often used with a low vertical clearance requirement, and where temporary bents will not interfere with traffic below the bridge. The associated advantages are control of geometry and grade, and a relatively low cost. An exam-

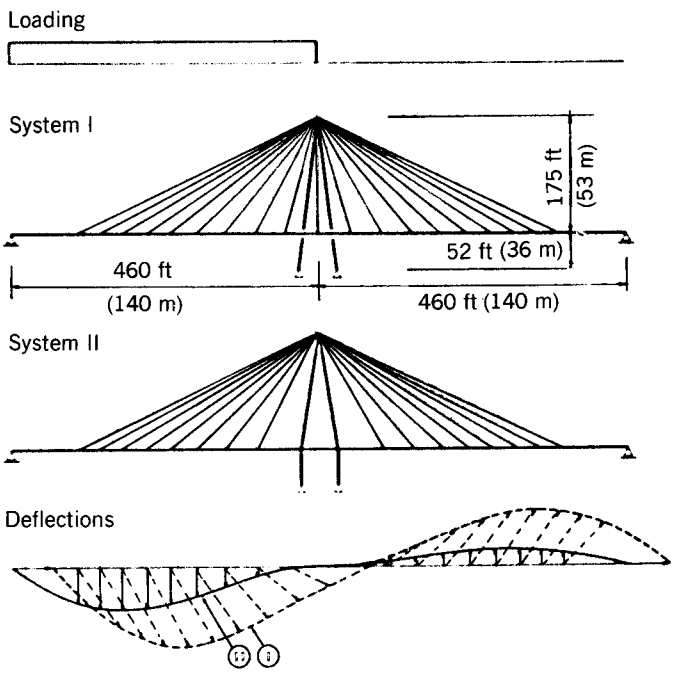

Figure 5–14 Deflections of two different stayed girder bridges under one-sided loading.

ple is construction that begins with an abutment on two temporary land piers, and then proceeds by shore cantilevers to rest on a temporary river pier and then the permanent tower pier.

The push-out technique has been used successfully in Europe but is relatively new to the American practice. It allows construction without interfering with traffic below the bridge, and where cantilever construction is impracticable. Large sections on the bridge deck are pushed out over the piers on rollers or sliding teflon bearings. The deck is pushed out from both abutments toward the center, and occasionally from one abutment to the other.

The cantilever erection method is used when temporary supports are necessary. In this context, it may require heavier sections to accommodate larger moments and shears that may act temporarily during erection. The principal advantage is again the absence of interference with the traffic below the bridge.

Example. The Lake Maracaibo Bridge, Venezuela, is 5.4 miles long, and has five main navigation openings consisting of prestressed concrete cable-stayed structures with suspended spans totaling 771 feet (235 m). The cantilever span is supported on four parallel X-frames, and the cable stays are supported on two A-frames with a portal connection at the top. There are no connections between the X- and the A-frames. Typical details are shown in Figure 5–15. The pier cap consists of a three-cell box girder with the X-frames continued up to the girder to act as transverse diaphragms, as shown in Figure 5–16. When the pier was completed, service girders were raised into position to be used in the construction of the cantilever arm. Because an additional moment was introduced during this construction stage, additional concentric prestressing was required in the pier cap (Figure 5–16).

The erection and concrete pouring sequence for the X-frames is shown in Figure 5–17. The concrete for this frame and the lower half of the A-frame was poured simultaneously. Before concreting section 4, inclined braces were installed in each leg as shown until section 8 was completed (Figure 5–17). After completion of section 13 and before pouring section 15, the X-frame outer legs were tied together by six prestressed 1-inch diameter high-tension steel bars.

The legs of the A-frame tower have variable dimensions in the cross section, tapering from bottom to top. Because of this variation, the formwork and reinforcement required frequent checks on alignment, and similar bracing was added as in the X-frame. The legs of the X-frames were erected before the legs of the A-frame, and were used to frame the latter. The erection sequence of the A-frame is shown in Figure 5–18. After erection of section 5, a longitudinal and a transverse brace were installed between the X- and the A-frame. Upon completion of section 9, transverse sections were installed at the section. After segment 15 was completed and the permanent longitudinal and transverse beams were in place, transverse bracing was installed at section 15. After completion of section 18, additional transverse bracing was installed at the same elevation.

Analytical Concepts

In a cable-stayed bridge, the girders are supported at several locations, namely abutments and piers, usually considered as fixed and nonyielding supports, and at cable points with the cables emanating from the towers. The latter are yielding supports as

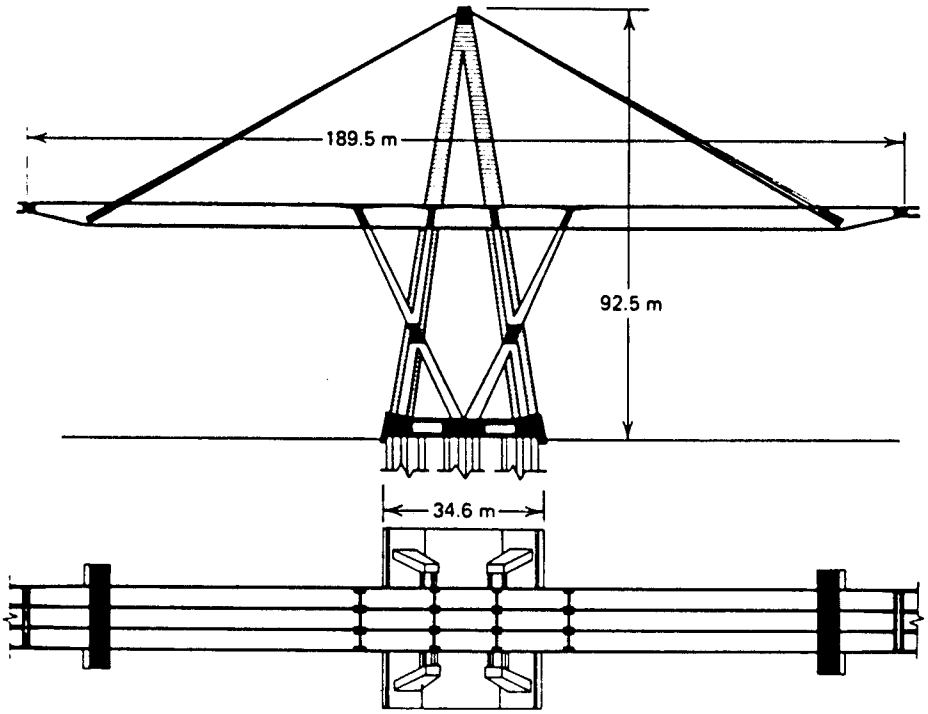

Figure 5–15 Lake Maracaibo Bridge, main span tower and X-frames.

the cables change length under load and also because the towers are flexible and can move. A cable-stayed bridge can therefore be modeled as a continuous beam on both rigid and flexible supports. This articulation excludes an independent analysis of towers and pylons; hence, a rational approach to analysis considers the cables, the stiffening girder and the pylons as an integrated structural system.

Experience shows that the effect of deflection in producing nonlinear behavior is relatively small. Felge (1966) reports that this effect on girder bending moments may be of the order of 6 to 12 percent. A nonlinear analysis may thus be carried out in the following sequence: (1) complete a linear analysis using nominal geometry to obtain the deflections; (2) use these deflections to calculate the revised geometry; and (3) apply the revised geometry to a second linear analysis.

Mixed Method of Analysis: Single Plane

According to this approach (Smith, 1967, 1968; Podolny and Scalzi, 1986), the general behavior is determined by superimposing the action of tower rotation, stay elongation, and tower shortening. This interaction evolves into a mixed-force displacement analysis where appropriate modifications are introduced to account for each action. Further modifications are added to reflect the effect of bending of the towers, base fixity of the towers, shortening of the girder, twist or torsion of the girder, and so on. The compati-

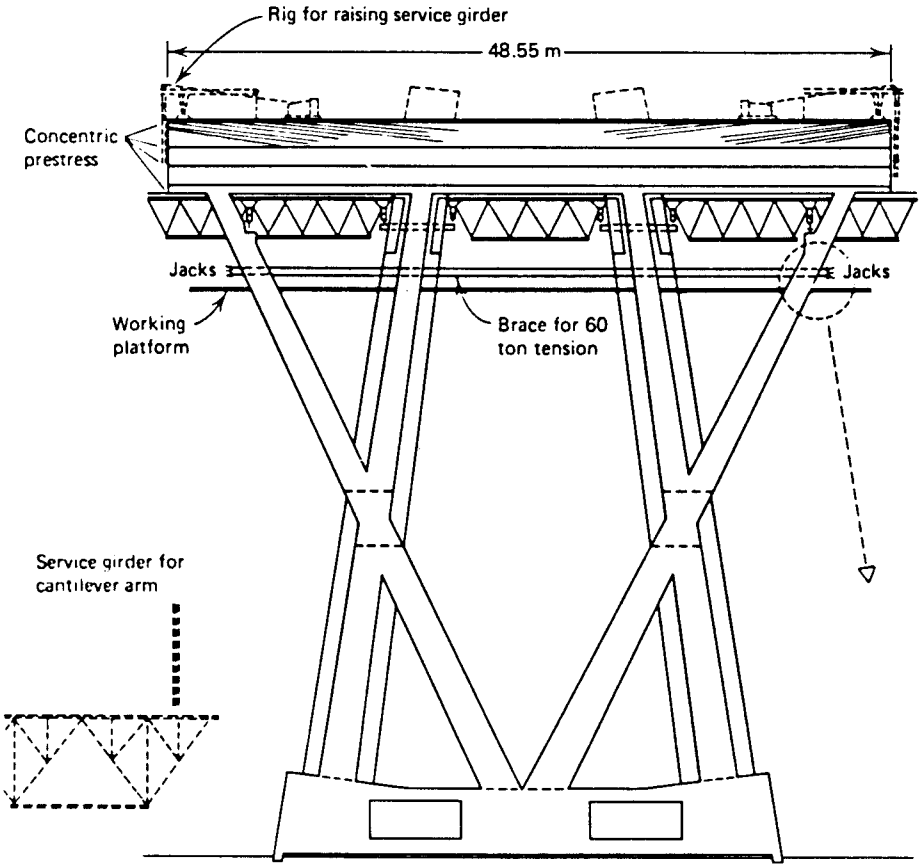

Figure 5–16 Lake Maracaibo Bridge, pier cap of a main span and service girder.

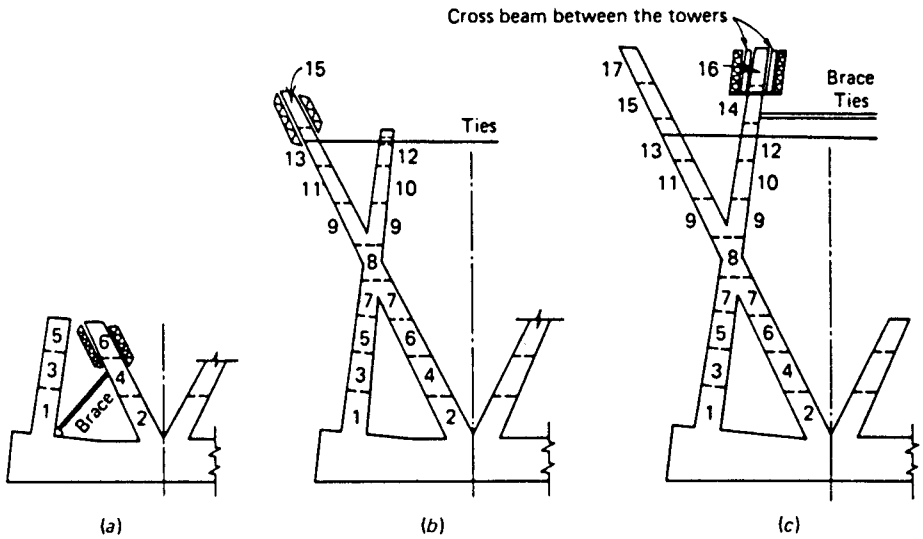

Figure 5–17 Lake Maracaibo Bridge, erection sequence at X-frames.

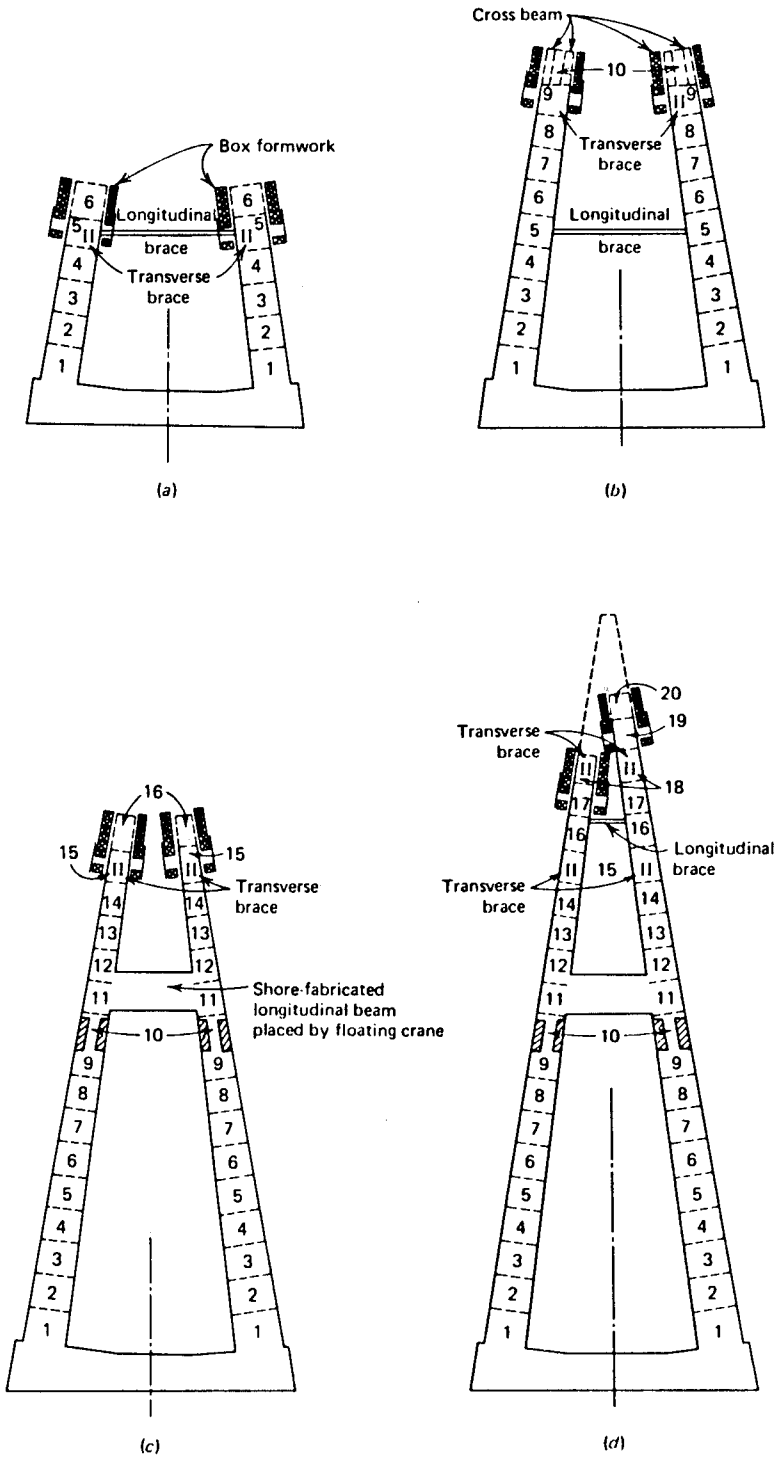

Figure 5–18 Lake Maracaibo Bridge, erection sequence of A-frames.

bility equations are thus adjusted and the equilibrium conditions formulated to give a single mixed matrix for the total structure.

The method is essentially linear because it assumes that deflections are proportional to the load at all portions of the structure and for the structure as a whole. The overall response is predicted by the general technique of consistent deformations. The positions or locations of the cables serve as restraints or supports, assumed to act as springs dependent on the induced forces and geometry.

A generalized solution includes the various influences from the cables and the towers. The following phases are considered and superimposed on these effects: (1) rigid supports at tower locations; (2) elastic cable effects of supports; (3) tower shortening; (4) tower rotation; and (5) combined effects. Because the text is essentially on substructures, the discussion is confined to items 1, 3, and 4.

Rigid supports at tower locations. Consider the structure shown in Figure 5–19. The double cable system has an applied load P as shown. The tower is pinned at point 2, and the cables are extended to points 1 and 3, also assumed pinned to the girder. In Figure 5–19(b) the cables are replaced by supports, and the resulting system is indeterminate to the third degree. Removing the redundant reactions R_1, R_2, and R_3 as shown in Figure 5–19(c) yields a determinate system. However, the associated deformations Δ_1, Δ_2, and Δ_3, caused by removing the reactions R_1, R_2, and R_3, must be zero in the real structure. Essentially, the solution involves the determination of the values of R_1, R_2, and R_3 necessary to maintain compatibility, or $\Delta_n = 0$. These reactions are calculated considering the effect of individual unit reactions on the system. This is shown in Figure 5–19(d) where $R_1 = 1$ induces deflections δ_{11}, δ_{21}, and δ_{31}. Likewise, $R_2 = 1$ and $R_3 = 1$ are applied separately at points 2 and 3, respectively, as shown in Figure 5–19(e) and (f). The summation of the combined deformations gives

$$R_1\delta_{11} + R_2\delta_{12} + R_3\delta_{13} = \Delta_1 \tag{5–12a}$$

$$R_1\delta_{21} + R_2\delta_{22} + R_3\delta_{23} = \Delta_2 \tag{5–12b}$$

$$R_1\delta_{31} + R_2\delta_{32} + R_3\delta_{33} = \Delta_3 \tag{5–12c}$$

Tower shortening. The vertical component of the cable force causes the tower to shorten as shown in Figure 5–20. If these components are R_1 and R_2 for the cables connected at nodes 1 and 3, respectively, the total shortening is

$$\Delta v_T = (R_1 + R_3)\frac{L_T}{A_T E_T} \tag{5–13}$$

where A_T and E_T denote the cross-sectional area and elastic modulus, respectively, for the tower.

This effect can be expressed in the following equations:

$$R_1\delta_{11} + R_2\delta_{12} + R_3\delta_{13} = \Delta_1 - \Delta v_1 - \Delta v_T \tag{5–14a}$$

$$R_1\delta_{21} + R_2\delta_{22} + R_3\delta_{23} = \Delta_2 \tag{5–14b}$$

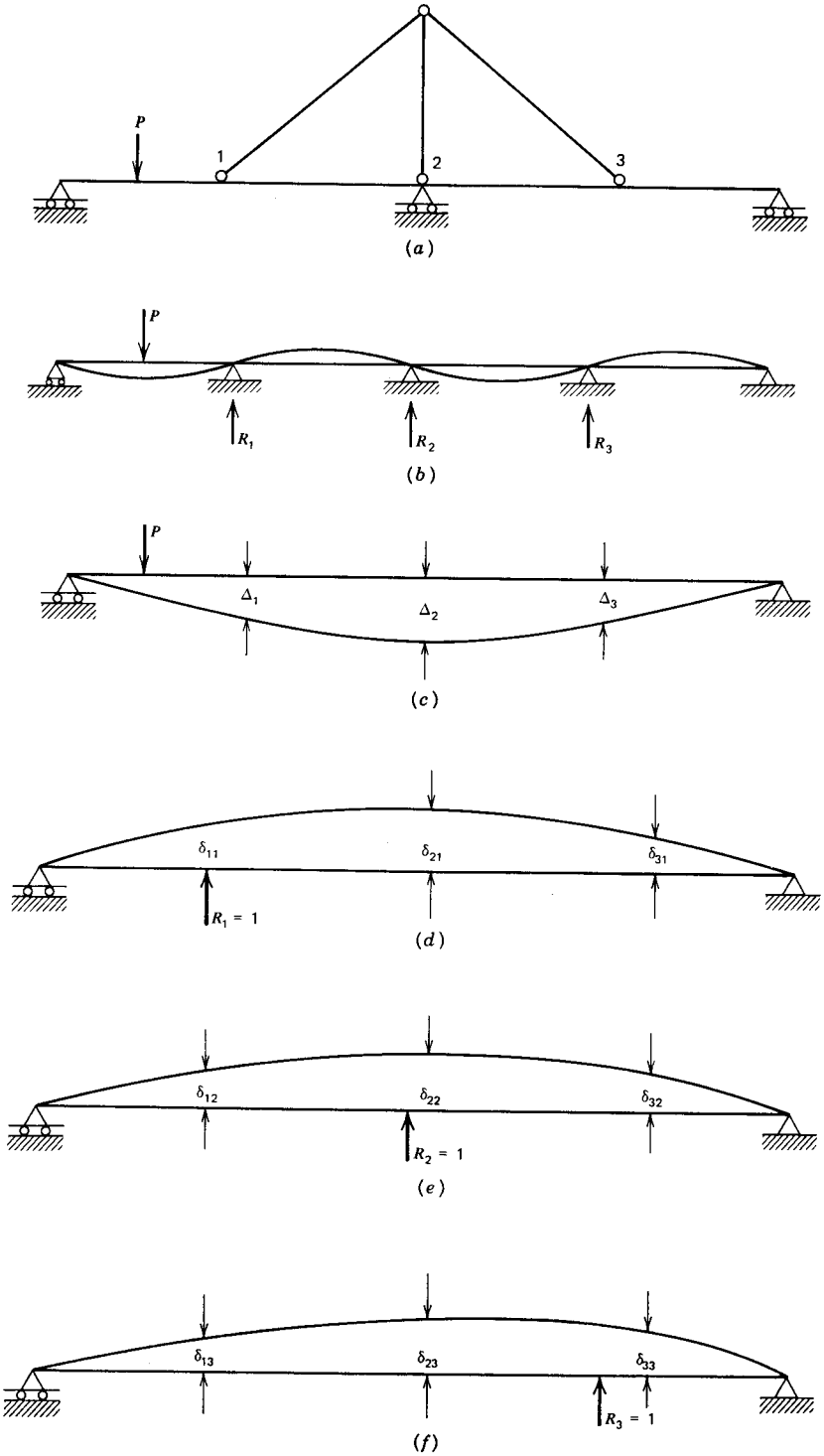

Figure 5–19 Example of double-cable systems: (a) original double-cable bridge; (b) equivalent continuous span; (c) simple span, P loading; (d) simple span, unit loading R_1; (e) simple span, unit loading R_2; (f) simple span, unit loading R_3.

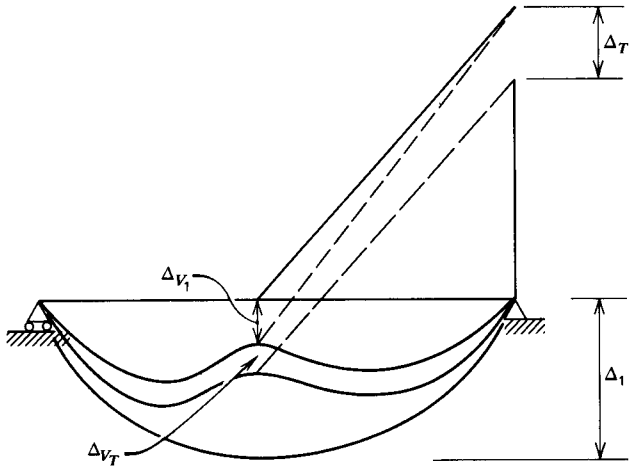

Figure 5–20 Tower shortening and effects on bridge girder.

$$R_1\delta_{31} + R_2\delta_{32} + R_3\delta_{33} = \Delta_3 - \Delta v_3 - \Delta v_T \tag{5–14c}$$

Tower rotation. For a load applied asymmetrically about the tower, the latter will rotate as shown in Figure 5–21 causing a vertical displacement Δ_ϕ in the girder expressed as

$$\Delta_\phi = \phi h_1 \tag{5–15}$$

This effect is added to (5–14) to give

$$R_1\delta_{11} + R_2\delta_{12} + R_3\delta_{13} = \Delta_1 - \Delta v_1 - \Delta v_T - \phi h_1 \tag{5–16a}$$

$$R_1\delta_{21} + R_2\delta_{22} + R_3\delta_{33} = \Delta_2 \tag{5–16b}$$

$$R_1\delta_{31} + R_2\delta_{32} + R_3\delta_{33} = \Delta_3 - \Delta v_3 - \Delta v_T + \phi h_3 \tag{5–16c}$$

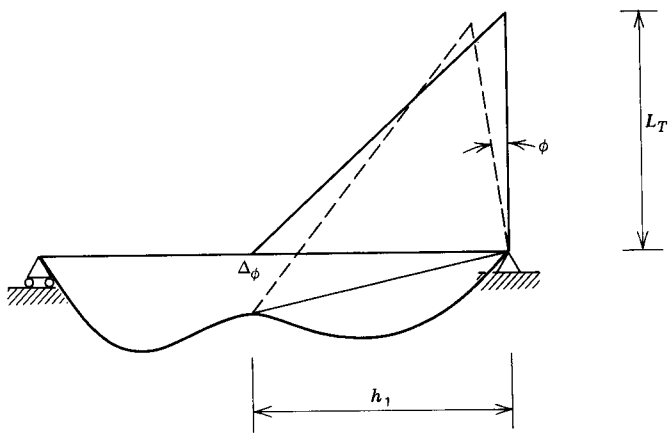

Figure 5–21 Tower rotation and effects on bridge girder.

Effect of other actions. The horizontal components of the cable forces will induce an axial compression force in the girder. This will cause elastic shortening of the girder, the extent of which depends on the axial force and the section properties. The effect of elastic cables at supports may be considered, assuming that the tower does not rotate or shorten. Another action is from clamped cables attached to the tower at different heights, and a pair of cables that are carried by saddles or rollers at the tower. All these factors must be accommodated by appropriate adjustment of the flexibility matrix to obtain the combined effect.

Mixed Method of Analysis: Double Plane

A-frame tower. An A-frame tower with a double plane of cables is shown in Figure 5–22. Because the cables are concentrically connected, the separate tower rotations will become one single rotation ϕ as shown. The rotational equilibrium for the combined tower depends on the horizontal components of all the cables in the system. The equilibrium condition may be expressed in matrix form by a single equation (Podolny and Scalzi, 1986).

Portal tower. An example of portal tower arrangement is shown in Figure 5–23. The relative rotation of the system is limited, resulting in increased resistance, but this effectiveness is not as great as in the A-frame of Figure 5–22. Because complete rigidity of the portal frame is not possible, it is necessary to include the effect of out-of-plane warping of the tower.

Consider, for example, a load P eccentrically applied to one of the stiffening girders between points A and D as shown in Figure 5–23. The corresponding differential rotation of the towers will cause the portal beam to twist, and the towers to rotate counterclockwise. The resistance provided by the portal beam to the differential rotation of the towers is a function of the bending and torsional stiffness of the portal columns and beam, and partly due to the degree of fixity against twist available at the base of the towers.

If the base of the towers is free to twist, the induced deformation will be as shown in Figure 5–24, where the columns are subjected only to bending and the beam only to torsion. For this condition the out-of-plane deflection at the top of the tower is

$$\delta_f = (X_d \cot\theta_d - X_e \cot\theta_e)\bar{X} \tag{5–17}$$

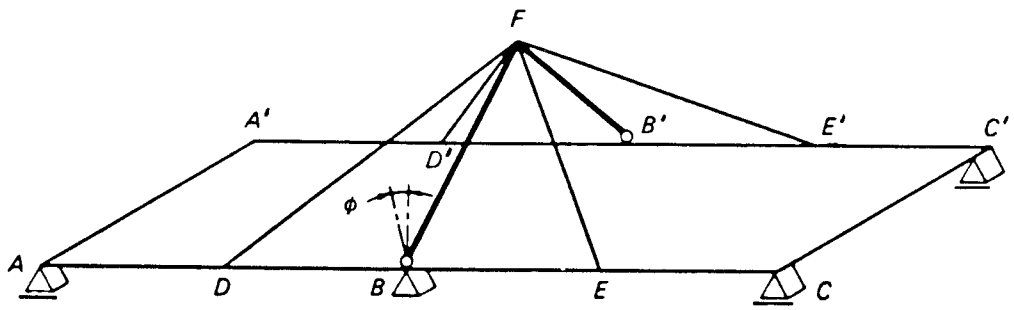

Figure 5–22 Bridge with A-frame tower.

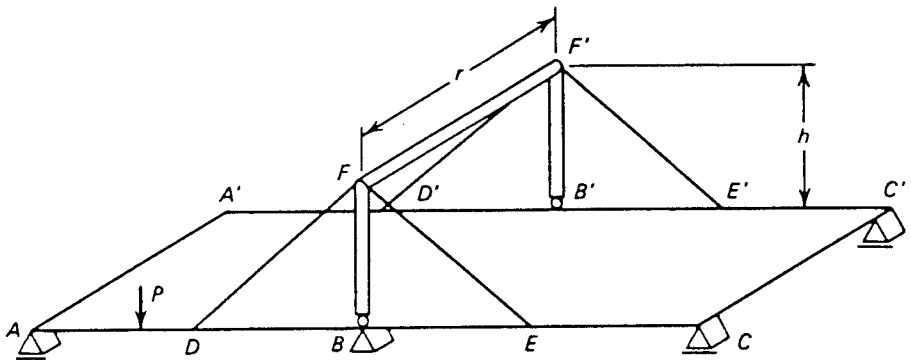

Figure 5–23 Bridge with portal tower.

where

$$\overline{X} = \left[\left(\frac{h^2 r}{2GJ_2}\right) + \left(\frac{h^3}{3EI_1}\right)\right] \tag{5–18}$$

where all notation corresponds to Figure 5–24. These warping deflections plus or minus δ_f at F and F' result in a downward deflection at D and an uplift at D' equal to $\delta_f l_{bd}/h$ and producing a twist to the girder at D given by

$$\psi_{df} = \frac{2(X_d \cot\theta_d - X_e \cot\theta_e) l_{bd} \overline{X}}{hr} \tag{5–19}$$

Similarly, the twist at E is

$$\psi_{ef} = \frac{-2(X_d \cot\theta_d - X_e \cot\theta_e) l_{be} \overline{X}}{hr} \tag{5–20}$$

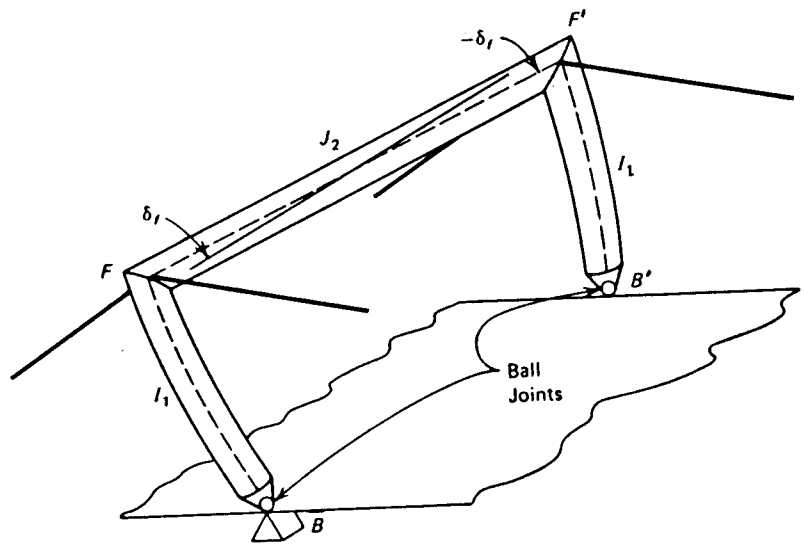

Figure 5–24 Portal columns in bending only; portal beam in torsion only.

The behavior of this system is the same as that for the double-plane, single tower structure except for the portal warping effect. Therefore, the matrix formulation for this structure is the same as in the A-frame tower provided the coefficients for X_d and X_e are modified. These necessary modifications include the addition of the terms $2l_{bd}\cot\theta_d\overline{X}/hr$ and $-2l_{bd}\cot\theta_e\overline{X}/hr$, and also the terms $-2l_{be}\cot\theta_d\overline{X}/hr$ and $2l_{be}\cot\theta_e\overline{X}/hr$. In this manner, the torsional compatibility at D and E is maintained.

When the base of the towers is restrained against rotation in the horizontal plane, the resulting deformed portal is shown in Figure 5–25. In this condition the portal columns and the portal beam are subjected to bending and torsional moments. Using energy methods, it can be shown that the twist at D and E, respectively, may be expressed as

$$\psi_{df} = \frac{2(X_d\cot\theta_d - X_e\cot\theta_e)l_{bd}}{hr}\frac{\overline{X}\overline{Y}}{(\overline{X}+\overline{Y})} \tag{5–21}$$

$$\psi_{ef} = \frac{-2(X_d\cot\theta_d - X_e\cot\theta_e)l_{be}}{hr}\frac{\overline{X}\overline{Y}}{(\overline{X}+\overline{Y})} \tag{5–22}$$

where $\overline{X}$ is as previously, and

$$\overline{Y} = \left[\left(\frac{r^2h}{4GJ_1}\right)+\left(\frac{r^3}{24El^2}\right)\right] \tag{5–23}$$

and the coefficients for X_d and X_e in the original matrix must again be modified for the torsional compatibility at D and E.

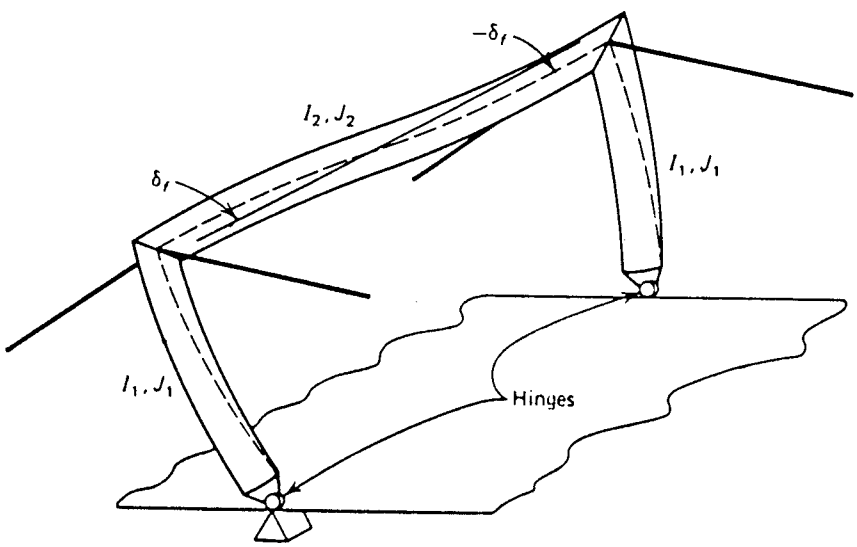

Figure 5–25 Portal columns in bending and torsion; portal beam in bending and torsion.

Multitower continuous girder. For multitower structures the procedure is likewise to release all interior supports and thus produce a simple beam for which the free deflections and twist can be calculated. Compatibility and stability equations are appropriately modified and formulated to produce a single mixed matrix for the entire system.

Comments on the mixed method. The overall behavior of the cable-stayed system is determined by superimposing the various actions. This consideration evolves into a mixed force-displacement analysis where modifications are necessary to account for each action. The result is a single mixed matrix for the total structure.

The method is essentially nonlinear because it assumes that the deflections are proportional to the load for any member and the structure as a whole. Since nonlinearity is not considered, the analysis is restricted to elastic behavior. Suitable two-dimensional plane frame or three-dimensional space frame programs are available with current software capabilities and can be appropriately modified to accommodate varying conditions.

Nonlinearity

Nonlinear behavior may be exhibited in three parts of the bridge, namely the girder, tower, and cables. Nonlinearity effects are present in the girder and the tower when subjected to compressive loads and moments simultaneously. Their extent is largely determined by the relative magnitude of the compressive load compared with the critical Euler value and by the magnitude of the deflection caused by bending. Normally, these effects may be expected to be small and inconsequential, but for slender girders and pylons an analytical assessment is indicated for extreme loading conditions.

Nonlinearity in the cables occurs as the load increases and the cable sag decreases producing an increase in cable chord length with an associated elongation of the cable. From the practical standpoint, the nonlinear effects for the cables may be ignored if an equivalent E is used. When all the details of the design are specified and expressed in a final mathematical form, a nonlinear analysis may be carried out using a preselected overload.

Nonlinear analysis is suggested by the ASCE Task Committee on Cable-Suspended Structures (1977) to study and determine the effects of cable sag and girder-pylon deformations caused by combined moments and axial forces.

Buckling Considerations

Buckling considerations are important because both the girder and towers may be subjected to large compressive forces. Overall buckling may be analyzed by various methods. Tang (1976) proposes an energy method to calculate the buckling load. Because the cables, the girder, and the towers are all interconnected, the entire structure is treated as one system.

Analytical procedure. If the buckling mode is known, the critical buckling load can be estimated with sufficient accuracy using an energy method whereby the external energy is equated to the internal energy. However, for a complex structure such as a cable-stayed bridge a reasonably good approximate mode shape is difficult to obtain.

For a cable-stayed bridge, the external energy due to the axial force P_s is

$$V_e = \frac{1}{2}\int P_s W'^2 ds = \frac{1}{2}\int \xi_x P_o W'^2 ds \tag{5–24}$$

Likewise the internal energy due to flexural bending and cable tension is

$$V_i = \frac{1}{2}\int EIW''^2 ds + \frac{1}{2}\Sigma\varepsilon_c^2 E_c A_c l_c \tag{5–25}$$

where W = deflection of the girder and towers; E = modulus of elasticity; A = cross sectional area; and l_c = cable length; and the subscript c denotes cables. The variable $\xi = P_s/P_o$ expresses the distribution of the axial forces in the girders and towers. At buckling load, $P_o = P_c$, and the external energy equals the internal energy, from which we obtain

$$P_c = \frac{\int EIW''^2 ds + \Sigma\varepsilon_c^2 E_c A_c l_c}{\int \xi W'^2 ds} \tag{5–26}$$

The accuracy of the critical load P_c depends on how well the mode of buckling is predicted. Unacceptable deviations may be avoided by grouping together several possible curves to form curves for the approximation by linear combinations

$$W = A_1 W_1 + A_2 W_2 + \ldots\ldots = \Sigma A_i W_i \tag{5–27}$$

where the coefficients A_i can be determined according to the Ritz method. Differentially the critical load by the coefficient A_i results in a homogeneous equation system

$$\frac{\vartheta P_c}{\vartheta A_i} = 0, i = 1,2,3,..... \tag{5–28}$$

Combining the foregoing relations and partial differentiating according to Equation (5–28) yields the characteristic equation for buckling

$$C - \lambda B = 0 \tag{5–29}$$

where $\lambda = P_c$ is the eigenvalue. The elements in matrix C are

$$C_{i,j} = \int EIW_i'' W_j'' ds + \Sigma\left(e_i e_j E_c A_c l_c\right) \tag{5–30}$$

and the elements in B are

$$b_{ij} = \int \xi W_i' W_j' ds \tag{5–31}$$

The Ritz method requires that each curve W_i satisfies the geometric boundaries of the bridge, and this can be ascertained by using actual deflection curves of the structure under various loading conditions. About ten to twenty curves are sufficient for a reasonably good approximation (Tang, 1976).

Critical load. Because the axial load P_s varies along the girder and towers, a precise definition of the critical load is not possible. The value of P_c is obtained as an eigenvalue depending on the variable ξ. If the latter changes, that is, the axial forces in different portions of the bridge change in relation to each other, the value of P_c will also change. Thus, the critical load is not a single parameter but a group of loads in a fixed relationship, increasing or decreasing in the same proportions.

Tang (1976) proposes to predict the factor of safety against buckling for a given group of loadings than to estimate the buckling load. The factor of safety v is the ratio

$$v = P_{cr}/P_{exist} \tag{5–31}$$

where P_{cr} and P_{exist} are the critical and existing loads, respectively. From the foregoing we obtain

$$v = \frac{\int EIW''^2\, ds + \Sigma\varepsilon_c^2 E_c A_c l_c}{P_o \int \xi W'^2\, ds} \tag{5–32}$$

Design approach. Although conclusive recommendations regarding the application of load factor may not be forthcoming for some time, for concrete members with axial load P and bending moment M, the design may consider the load P and a magnified moment

$$M_{mag} = \delta M = \frac{C_m M}{1 - \dfrac{P_u}{\phi P_c}} \tag{5–33}$$

where ϕ = strength reduction factor; $P_c = \pi^2 EI/(kl)^2$ = critical load of an idealized column with two pin-end supports. The ratio P_c/P_u may be replaced by the factor v, so that

$$\delta = \frac{\phi v}{\phi v - 1.0} \tag{5–34}$$

As an example, for $\phi v = 5.0$ and $\phi = 1$, $\delta = 1.25$, that is, the bending moment will be increased by 25 percent.

The value of C_m is difficult to define and should be determined by means of a detailed nonlinear analysis. In lieu of this Tang (1976) proposes to use $C_m = 1.0$.

The foregoing approach applies to towers made of reinforced concrete. For steel pylons, Tang (1976) proposes the same analytical procedure in conjunction with the effective slenderness ratio.

5.4 PIERS FOR SEGMENTAL CONCRETE BRIDGES

Section 1.2 gives a brief review of pier types for segmental concrete bridges, and distinguishes certain functional and design requirements. Because piers must resist final (service) loads as well as loads imposed during the construction stage, a brief reference to the basic construction methods is necessary in order to understand their influence on pier performance and the associated structural action.

Basic Construction Methods

Under the current AASHTO specifications (1989), segmental bridges are articulated as those erected by the following methods.

1. Balanced cantilever
2. Span-by-span with truss or falsework
3. Span-by-span lifting
4. Incremental launching
5. Progressive placement

The designer may choose between cast-in-place and precast construction depending mainly on local conditions and size of job, available construction time, accessibility to site, environmental constraints, and equipment locally available.

Balanced cantilever. The procedure was also mentioned in conjunction with cable-stayed bridges. Suitable segments are simply added from a pier in a cantilever fashion, and a closure is made with a previous half-span cantilever from the preceding pier. This process is repeated until the structure is completed. It follows, therefore, that unless symmetrical segments are simultaneously added, the pier will be out of balance by one segment, and its design must accommodate the temporary moments thus induced. Alternatively, temporary shoring may be used.

For cast-in-place construction, the movable formwork is supported from the previously erected segment or from a movable form traveler while the new segment is being formed, cast, and stressed.

Span-by-span construction. This is used mainly in long viaduct structures with relatively short spans. In this process, the superstructure is constructed in one direction span-by-span using a form traveler, with construction joints or hinges located at the points of contraflexure. The form carrier in effect is a factory-type operation suited to the job site. It may be supported on the piers, from the edge of the previously completed construction, at the joint location, or from one pier.

Although this method was initially intended to accommodate cast-in-place construction, it is also applied to precast segments assembled on a steel truss to make a complete span. Prestressing tendons ensure the assembly of the various segments in one span while maintaining full continuity with the preceding span, as shown in Figure 5–26.

Incremental launching. This process, shown schematically in Figure 5–27, is also referred to as push-out construction. Bridge segments 30 to 100 feet long are cast in stationary forms located behind the abutments. Each individual unit is cast directly against the previous unit, and after it attains the necessary strength it is posttensioned to the previous unit. The assembly is then moved forward, and the same steps are repeated for the succeeding unit.

The forward movement of the superstructure is facilitated by special low-friction sliding bearings at the piers, provided with suitable lateral guides. The main objective is to estimate and overcome the frictional resistance induced by the weight of the superstructure assembly.

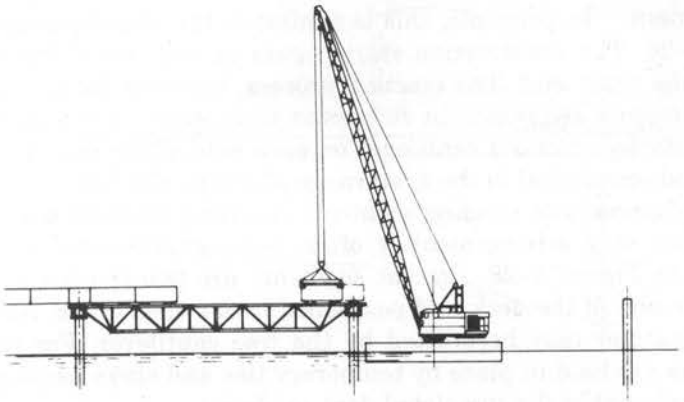

Figure 5–26 Span-by-span assembly of precast segments with truss.

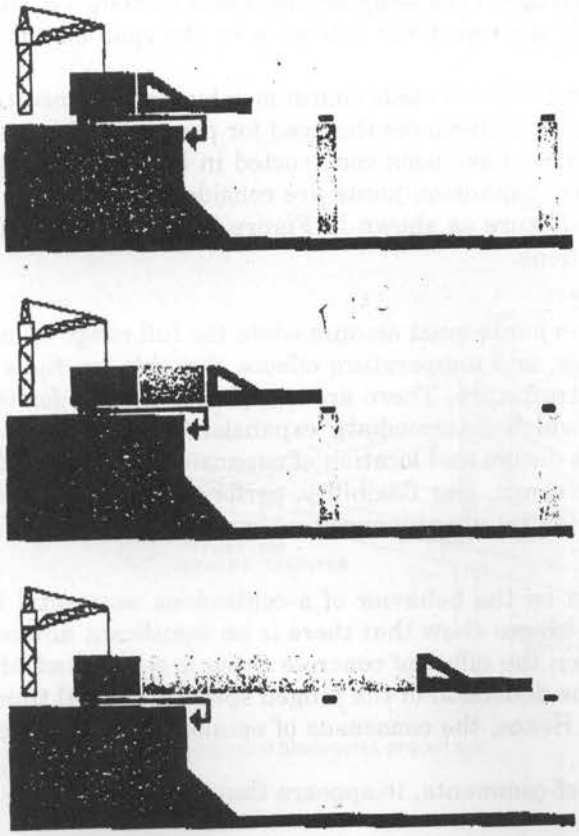

Figure 5–27 Incremental launching sequence.

Progressive placement. In principle, this is similar to the span-by-span construction shown in Figure 5–26. The construction starts again at one end of the bridge and is completed toward the other end. The erection process, however, follows the cantilever concept. Precast segments are placed in successive cantilevers on the same side of the same pier rather than by balanced cantilever on each side of the pier. The method appears practicable and economical in the span range of 100 to 300 feet.

Because of the appreciable bending moments resulting from the cantilever length, a movable temporary stay arrangement is often necessary to control the cantilever stresses, as shown in Figure 5–28. Precast segments are transported along the completed portion to the end of the deck and positioned by a swivel crane. About one-third of the span from the pier may be erected by the free cantilever. For the remaining length, the segments are held in place by temporary ties and stays passing over a temporary tower and anchored in the completed deck as shown.

Span Arrangement and Details

Span lengths. With the balanced cantilever method, the segments are placed symmetrically about the pier. For a three-span bridge, the recommended length for the end spans should be two-thirds of the main span in order to shorten the deck portion for the abutment closure as shown in Figure 5–29(a), since this cannot be erected as a balanced cantilever.

When the span lengths vary, a compromise solution is to introduce an intermediate span with lengths the average of the two flanking spans as shown in Figure 5–29(b). This restores compatibility of the cantilever concept with the span on either side of the intermediate span.

Individual cantilever sections are made continuous by tendons inserted in positive moment areas upon closure. This alleviates the need for permanent hinges at midspan. Continuous decks without joints have been constructed in bridges up to 2000 feet long (integral construction). Where expansion joints are considered necessary, they may be placed near points of contraflexure as shown in Figure 5–29(c) to avoid slope changes that may occur at other locations.

Deck expansion. Expansion joints must accommodate the full range of movements resulting from creep, shrinkage, and temperature effects. Suitable locations are at piers, abutments, or points of contraflexure. There are no specific criteria for the maximum continuous length beyond which intermediate expansion joints should be provided. Given the type of bridge, the design and location of expansion joints should be based on factors such as temperature range, pier flexibility, performance of expansion bearings, details of deck joints, and potential maintenance problems.

Structural continuity. Data on the behavior of a continuous segmental bridge and a structure with intermediate hinges show that there is no significant difference between the two types. However, when the effect of concrete creep is considered, the two structures respond differently. The deflection of the hinged spans is several times the deflection of a continuous bridge. Hence, the consensus of opinion is that full continuity improves bridge performance.

From the foregoing brief comments, it appears that the construction method and

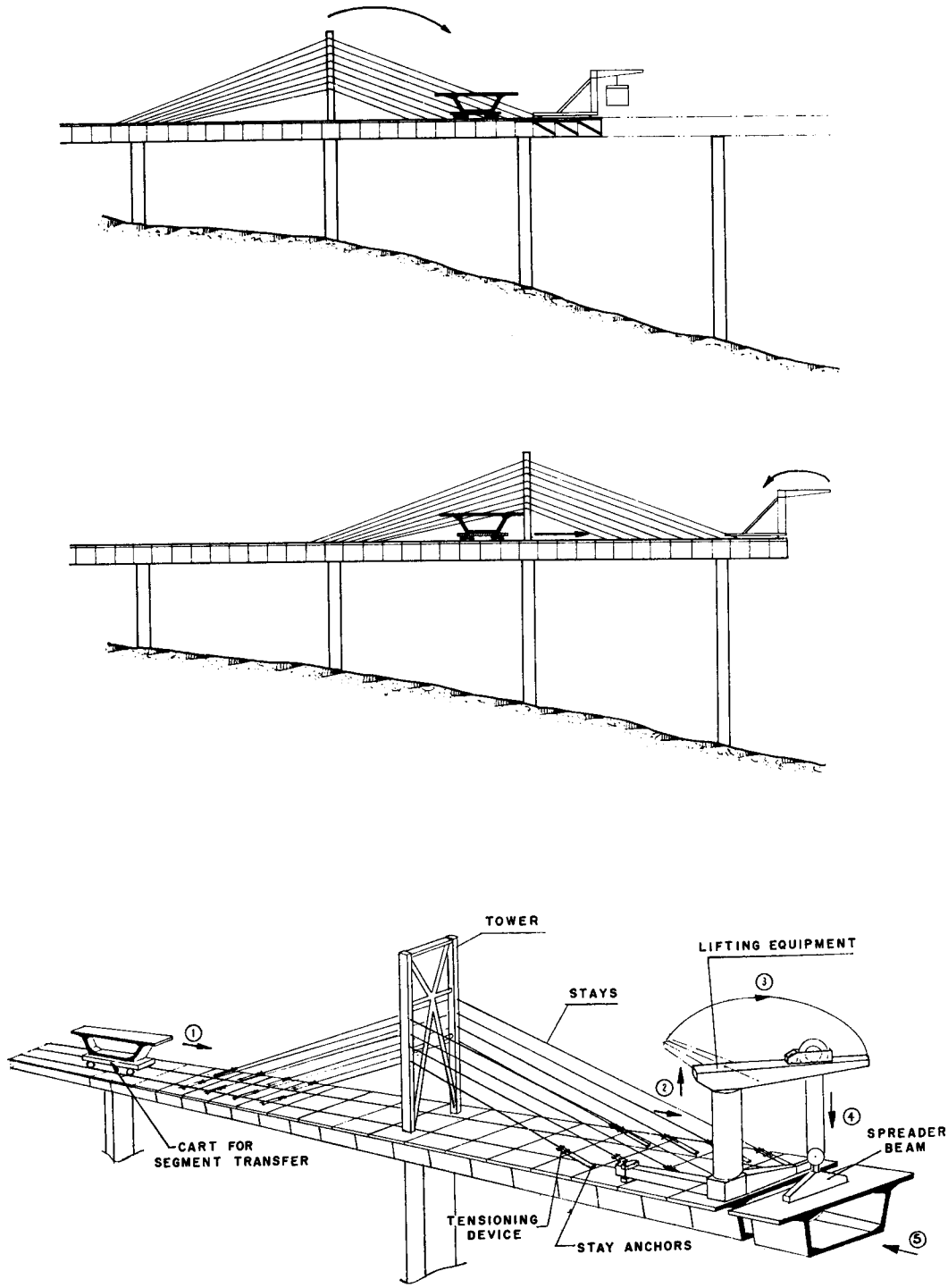

Figure 5–28 Progressive placement procedure.

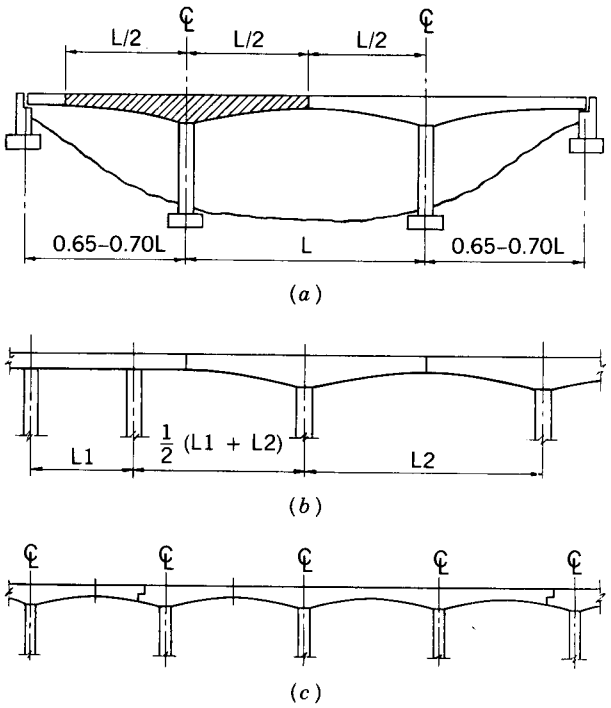

Figure 5–29 Balanced cantilever construction showing effects on span lengths and location of expansion joints.

span configuration have a marked effect on the selection of pier types and the design approach.

Load Factors and Load Combinations

Loads. In addition to the loads and loading groups discussed in chapter 2, AASHTO articulates erection loads, comprising all loadings in connection with the anticipated system of temporary supporting works and special erection equipment consistent with the assumed construction sequence and schedule. Thus, the assumed erection loads and acceptable closure forces due to misalignment corrections should be shown on the plans. An allowance should be made for the effects of any changes of the statical structural scheme during construction associated with the application or removal of temporary supports or action of special equipment that may result in residual "built-in" forces, moments, deformations, creep, shrinkage, and any other strain-induced effects.

These requirements imply that all elements of the bridge, including the substructure, must be designed for the assumed construction scheme, and any subsequent changes in the construction method should be checked for design compatibility.

In addition to the standard AASHTO Load Groups IV, V, and VI at service load, the following thermal loading combination should be considered

$$\text{Group} = (DL + SDL + EL) + \beta_E E + B + SF + R + S + (DT) \qquad (5\text{–}35)$$

with 100 percent allowable stress, where DL = dead load, structure only; SDL = superimposed dead load; EL = erection load (final stage); R = creep effects; DT = thermal differential; and other loads are as per AASHTO.

Construction load combinations. Erection loads are stipulated by AASHTO as follows:

1. Dead load of structure. These are the same as in conventional bridges.
2. Differential load from one cantilever. This applies only to balanced cantilever construction, and its magnitude is 2 percent of the dead load applied to one cantilever.
3. Superimposed dead load. Normally, this does not apply during construction, but if it does, it should be considered part of the dead load.
4. Distributed construction live load. This represents miscellaneous items of plant and equipment in addition to the major specialized construction equipment.
5. Specialized construction equipment. Examples include a launching gantry, beam and winch, and truss or similar major items. In general, this load represents the maximum construction loads applied to the structure by the main equipment during the lifting of segments.
6. Impact load from equipment, usually taken as 10 percent.
7. Segment unbalance, relevant primarily to balanced cantilever construction. This load can also be extended to include any unusual lifting sequence, or it may be the result of any out of balance condition.
8. Wind uplift on cantilever.
9. Accidental release or application of a precast segment load, or other sudden impact from an otherwise static load A. Impact force = $2A$.
10. Creep, shrinkage, and thermal forces.

AASHTO Table 8–1 articulates the foregoing loads and gives a summary of construction load combinations and allowable stresses (ASD). If more unfavorable conditions should occur with a particular construction system, they should be considered. The maximum allowable compressive stress under construction loads is $0.5f'_c$

Load factor design for construction conditions need not be considered except for certain load combinations. When this approach complies with AASHTO Art. 8.3, the strength provided by any member should not be less than the following load combinations:

$$\text{For maximum forces and moments} = 1.1\,(DL + DIFF) + 1.3CE + 2A \qquad (5\text{–}36)$$

$$\text{For maximum forces and moments} = DL + CE + 2A$$

where DL = dead load, structure only
$DIFF$ = differential (unbalanced) dead load from one cantilever
CE = weight of specialized construction equipment
A = static segment weight

LRFD specifications. These reflect essentially the 1989 AASHTO Guide Specifications. The span length to which these provisions apply is about 800 feet. Bridge designs should allow the contractor some latitude in choosing construction procedures. To ensure compatibility of the design feature and details with proposed construction methods, the contractor should be required to prepare working drawings and design calculations based on the chosen method.

Special provisions for bridge types. Precast segmental bridges are normally erected by balanced cantilever, by use of erection trusses, or by progressive placement. Precast sections should be no less than fourteen days old at the time of erection in order to limit construction deflections to values consistent with the design.

Cast-in-place segmental bridges may be erected on falsework, by free cantilever methods, using span-by-span lifting procedures of spans cast at the bridge site, or by incremental launching. The form traveler weight assumed in stress and camber calculations should be identified in the design.

For construction implemented with incremental launching, the design should articulate loads and stresses during this phase, moments due to construction tolerances, and combinations of construction tolerances and temperature gradient. Piers and superstructure diaphragms at piers should be designed so that during all launching stages, as well as after launching for the installation of permanent bearings, the superstructure can be lifted with hydraulic jacks. Pier designs should consider frictional forces during launching according to the following criteria:

- The friction on launching bearings may be assumed to vary between 0 percent and 4 percent, according to the hold-back or pushing forces.
- The upper value of friction may be reduced by 0.5 percent if the pier deflections and the launching jack forces are monitored.
- The design should reflect the fact that inclined launching bearings create additional forces at the launching jacks and at the pier tops.
- For bridges built by the incremental launching method, provisions should be made to have the deflection of the pier tops continuously monitored. Monitoring devices are recommended with automatic switch off devices for the launching equipment in case the permissible pier deflections are exceeded.

Commentary on erection loads. Erection loads may be imposed on opposite cantilever ends by use of a form traveler, diagonal alignment bars, a jacking tower, or by external weights. In addition, AASHTO stipulates a concrete weight of 155 lb/ft^3, intended to provide for more heavily reinforced sections than would be anticipated in more conventional concrete superstructures. These requirements result in special pier types and foundations, particularly where the erection loads control the design. Some of these types were discussed in section 1.2, and examples are shown in Figures 1–3 and 1–4. Pier types are reviewed in more details in the following sections.

Design Considerations

In addition to the pier types suggested in section 1.2, another solution is to use piers with twin flexible legs. The transmission of horizontal loads in the direction of longitudinal axis is accommodated by the flexibility of the legs. These piers provide three advantages: (1) structural fixity of the superstructure to the substructure with regard to vertical loads, feasible with the action of the separate supports; (2) large flexibility in the horizontal plane, relative to the displacements parallel to the longitudinal axis of the superstructure, compatible with the expansion of the continuous structure; and (3) stability of the superstructure during erection by adding simple temporary bracing.

In terms of the design requirements pier types may be classified as follows:

1. Moment-resisting piers either fixed or hinged to the superstructure.
2. Moment-resisting piers with double neoprene bearings.
3. Piers with flexible legs.
4. Conventional flexible piers, combined with temporary supports during construction to resist unbalanced conditions.

Pier section flexibility. Considering the loads and force combinations discussed in the foregoing sections, piers must respond to the following structural actions:

1. When a frame rigidity is introduced between superstructure and piers, the latter must withstand and transfer moments particularly under unsymmetrical loading. The piers are an integral part of the entire system and their flexibility or stiffness must be quantified and incorporated in the overall analysis. Figure 5–30 shows the structural parameters that define the flexibility of a pier in conjunction with the basic applied loads M, Q, and N, and the corresponding deformations θ, u, and v. The four flexibility coefficients must include the components of the pier and its foundation, that is, supporting soil or piles, footing, pier shaft, neoprene bearings, and so on.

Special structural action of piers may be caused by: (A) close proximity to an expansion joint (usually at the point of contraflexure) and under the effect of appreciable bending moments because of hinge relaxation and live load on the cantilever; and (B) loads applied to the structure by the construction equipment.

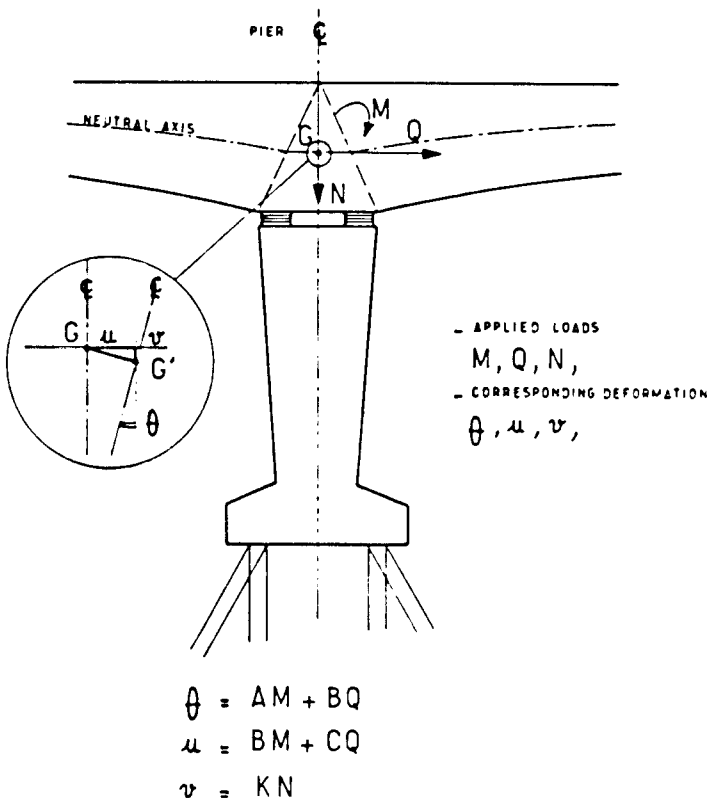

Figure 5–30 Basic components of pier flexibility.

2. In precast construction with segments placed with a launching gantry, the gantry leg reactions are applied to a temporary static scheme and released in another static scheme when the continuity between two adjacent cantilevers is restored. With cast-in-place construction, the weight of travelers is applied to the free cantilever but is removed when continuity is achieved. For long spans the effect on the deck is usually favorable although large moments may be induced simultaneously.

3. Volume changes due to creep, shrinkage, and thermal variations induce moments and horizontal loads that must be considered.

Piers Designed to Resist Moments

Monolithic piers. The Brotonne viaduct bridge is supported on two main cylindrical piers, 41 feet in diameter, hollow inside, with a maximum wall thickness of 9.3 feet. A thick concrete mat covers the entire bottom. The piers are extended 115 feet (35 m) below ground level, and are founded on limestone overlain by alluvium, silt, and gravel beds (Podolny and Muller, 1982). The maximum load at the tip of the pier is 19,000 tons (metric). At the foundation level, the limestone bed has the following strength parameters: angle of internal friction, 20°; cohesion, 5 tons/ft^2; and a pressure limit of 45 tons/ft^2, based on triaxial tests.

The main pier foundation column is subjected to a bending moment applied at the top, a vertical load, and a horizontal force, as shown in Figure 5–31. If the assumption can be made that the pier is a short rigid shaft, it may rotate about a pivot point as shown in Figure 10–19. The discussion presented in section 10.16 is relevant in this case, and if the rigid pier can be idealized with a rotation center, the toe and heel pressures will be as shown in Figure 10–19. Interestingly, the length-to-diameter ratio is 115/41 = 2.8, or close to the ratio assumed to produce the soil-structure interaction shown in Figure 10–19.

The pier has been analyzed as a rigid body under the applied loads, and the resulting lateral reactions and base pressures are as shown in Figure 5–31, conceptually compatible with the pressure diagrams of Figure 10–19. Values of the lateral and vertical reactions were obtained for the various soil layers, and equilibrium was checked assuming the rigid body to rotate about point *C*. The coordinates of this point were determined as follows: vertically, it represents the level where lateral reactions from the soil change sign (change from passive pressure on the front face to counter passive reaction at the back face); horizontally, point *C* is the position of the neutral axis for the base pressure.

The maximum pressures (lateral and bearing) are shown in Figure 5–31 together with diagrams for the bending moments along the pier shafts. Without lateral support (passive resistance), the bending moment at the base would be 370,000 ft-kips compared with the actual moment of 130,000 ft-kips. Accordingly, the extreme fiber stress is less than 24 tons/ft^2, whereas the average bearing pressure is 14.3 tons/ft^2. These data give a factor of safety against bearing capacity failure between 3 and 4, depending on the assumed soil conditions.

It may appear that the load-bearing capacity of the pier shaft is based on base bearing alone, and that shaft resistance has been ignored. Because no further data are available regarding this analysis, it is not possible to predict the vertical settlement necessary to mobilize base bearing other than making a crude estimate based on the theory presented in sections 9.5 and 10.13.

The piers were installed in the dry inside a cofferdam made up of a continuous

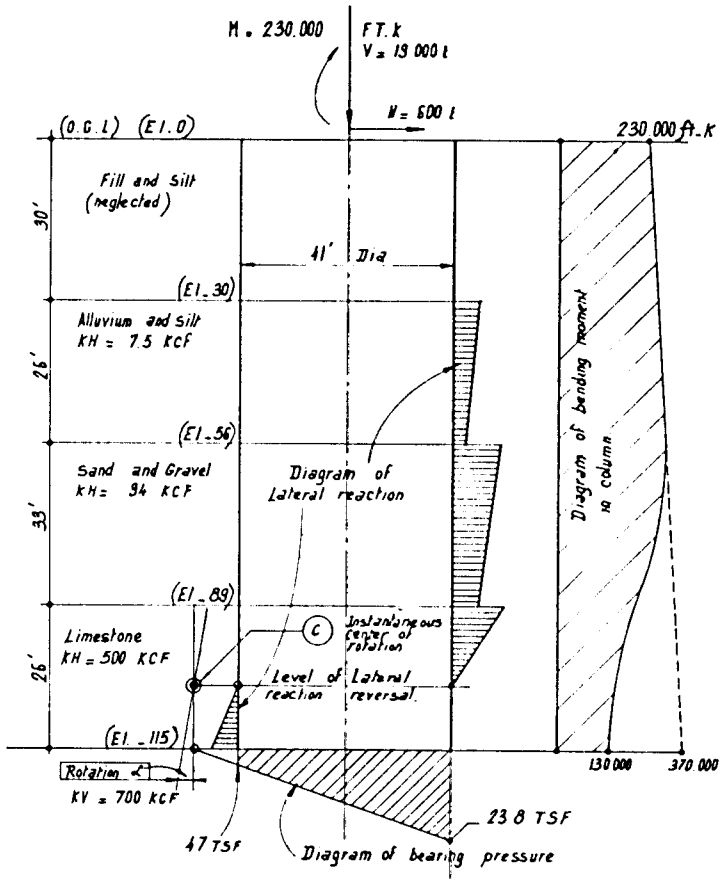

Figure 5–31 Brotonne Viaduct, loads and soil reasctions on column of main foundations.

slurry-trenched concrete wall extended to the limestone layer. Grouting of the base allowed complete dewatering after excavation to inspect the foundation material and verify the soil characteristics by in situ tests. The reinforced concrete mat was placed in the dry, and the cofferdam was then flooded to prevent the risk of footing failure under the exterior water head. The pier shaft was given the shape of an octagon. Since the completion of the bridge, regular survey measurements at the site have been made to monitor vertical movement, and the results show the settlement has been stabilized and is within acceptable values.

Assembled piers. A special construction procedure and use of materials is reflected in the scheme shown in Figure 5–32. The piles for this pier are steel tubes concreted after driving. The tubes have a diameter of 27.5 inches (700 mm), and a thickness of 0.4 inch (10 mm), and are 98 feet (30 m) long. Each pier is supported on 24 piles. In situ tests confirmed the pile capacity in compression and tension. When all piles were installed, the template trough was filled with tremie concrete around the pile tops up to the upper edge of the template.

The template is shaped like a circular slab surrounded by an annular trough pro-

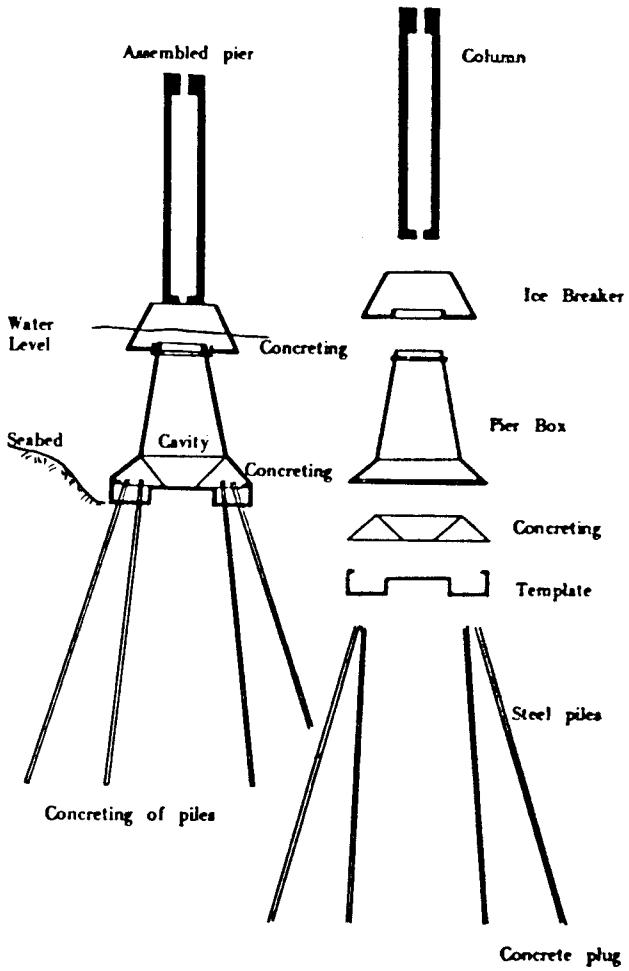

Figure 5–32 Sallingsund Bridge, schematic of substructure.

vided with holes for the piles. It was transported to its exact location by floating crane and set on three temporary vertical piles. Its bottom is set about 52.5 feet (16 m) below the water level.

The pier box, shown in Figure 5–32, is shaped like a truncated cone about 39 feet (12 m) high. It was precast in three lifts to accommodate progressive sinking. A reinforced concrete ring structure was made by connecting the pile tops to the pier box by reinforcing and concreting the space between them. The shell for the icebreaker is a reinforced concrete box precast near the site, and transported to the exact location by floating cranes. With the box in place, the piles were filled with concrete, and the pile tops and lower part of the pier box were cast together. Then, the cavity of the icebreaker was filled with concrete.

The pier columns were cast in place in lifts 10 feet (3 m) high using climbing forms. Lateral forces are resisted by the batter piles, and bending moments are converted into axial loads. Under these loading conditions, the piles may be subjected to tension or compression, hence their capacity is derived partly by base bearing and partly by shaft resistance.

Piers with Double Elastomeric Bearings

General principles. The concept of the double row of elastomeric bearings, mentioned briefly in section 1.2 and shown in Figure 1–4, was initially developed to restore compatibility between two converging structural actions that previously had contradictory requirements: flexural rigidity necessary to resist moments, and horizontal flexibility to accommodate volumetric changes of the superstructure. Since its initial conception, the solution has been applied to many bridges.

The working principle of two rows of bearings is demonstrated in Figure 5–33. For the service load condition, shown in Figure 5–33(a) and under the effect of unsymmetrical loads, the upper and lower flanges of the superstructure are subjected to tension forces T_L and T_R and compressive forces C_L and C_R, respectively. With vertical diaphragms placed over each row of bearings, the center portion of the top flange of the pier segment must accept the tension force $T_L - T_R$, in order to maintain equilibrium. However, this solution is not satisfactory because the thickness of the flange and the necessary reinforcement may have to be excessive between the two rows of bearings. In addition, there is the risk of cracking.

These problems are avoided by placing the diaphragms inclined and converging at the level of the top flange as shown. The differential tension $T_L - T_R$ is divided into two force components C and T, compression and tension, respectively, along the plane of diaphragm. At the same time, the tension force may be accommodated by prestressing the diagonal bracings. A further function of the pier segment design involves unbalanced loading developing at the bottom flange from the unequal reactions R_1 and R_2 at the bearings, requiring a careful stress analysis of all loading stages.

For the temporary construction phase, the superstructure-pier connection is detailed as shown in Figure 5–33(b). Because the pier must accommodate an unbalanced moment resulting from the erection procedure, the pier segment is supported on four temporary bearings of steel or concrete, denoted as ①, and temporarily fixed by prestressing to the top of the pier, denoted as ②. After achieving midspan closure, the joint is unlocked by releasing the prestressing. Flat jacks are then activated to substitute the permanent bearings for the temporary bearings.

Structural response of piers with a double row of bearings. Consider the pier arrangement shown in Figure 5–34. The pier has a constant section, and the following properties: height h, crosssectional area A_p, moment of inertia I, and modulus of elasticity E. The pier is further assumed to be fixed at the base in a completely rigid foundation. Next, we consider the following elastic coefficients:

$$A = \frac{h}{EI}, \quad B = \frac{h^2}{2EI}, \quad C = \frac{h^3}{3EI}, \quad K = A - \frac{B^2}{C} = \frac{h}{4EI} \tag{5–37}$$

With elastomeric bearings placed between the pier and the deck, the associated change in elasticity of the system must be taken into account. The presence of two rows of bearings spaced at distance d introduces a partial fixity of the superstructure to the pier. The bearings influence the deformation of the pier by their normal force $\pm M/pd$ produced by the moment M, as shown in Figure 5–34(c).

The moment M applied at the top of the pier may be divided into components f and m in the bearings, as shown in Figure 5–34(d), such that

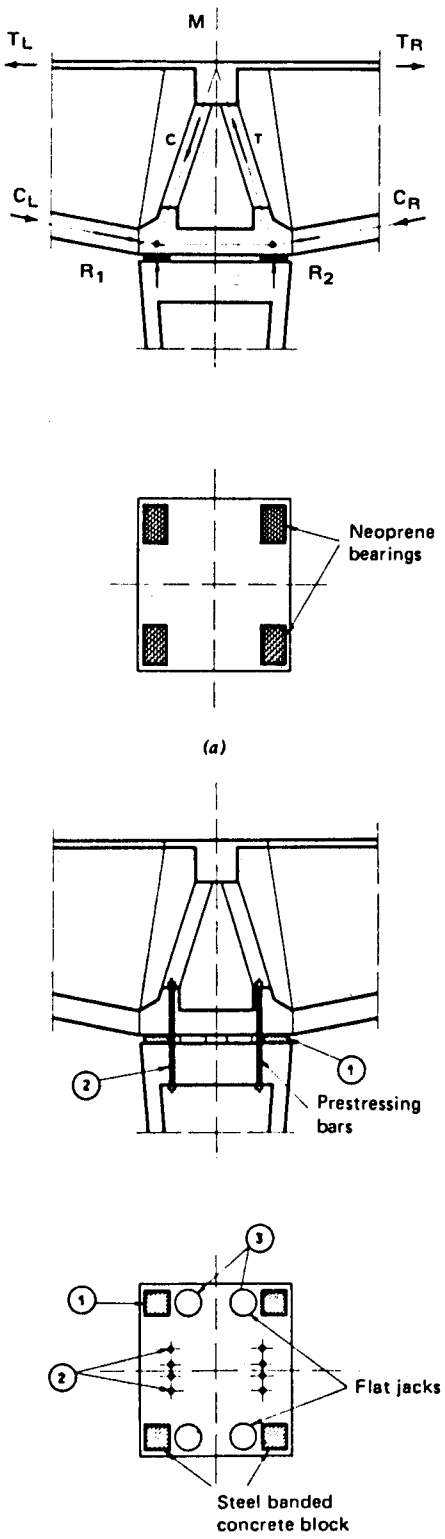

Figure 5–33 Connection of superstructure and pier; (a) in service; (b) in temporary construction phase.

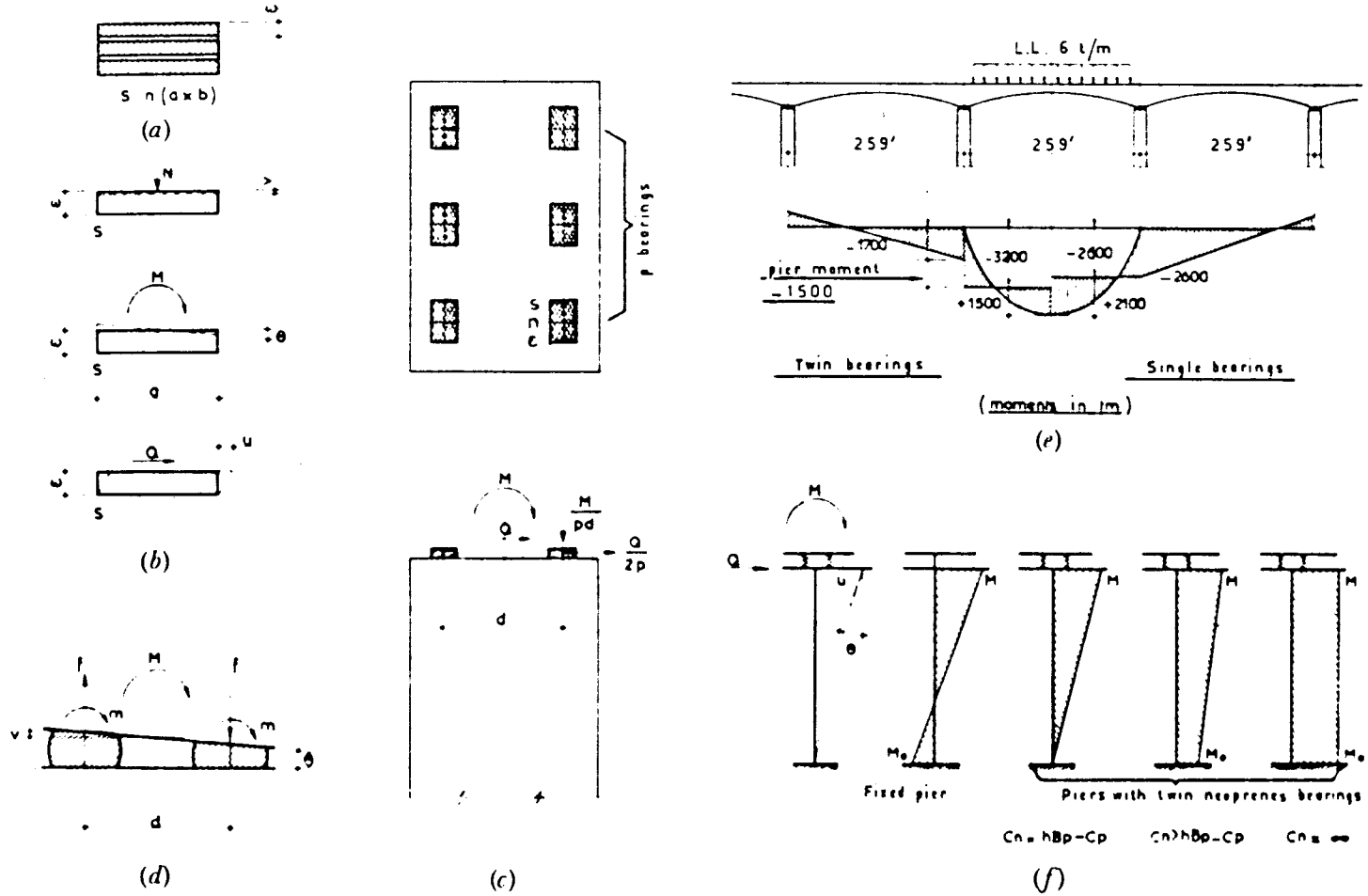

Figure 5–34 Piers with double row neoprene bearings (Oleron Viaduct). The most widely used polychloroprene is neoprene.

$$M = fd + 2m,\ \theta = 2v/d \tag{5–38}$$

setting

$$m = \frac{GA_b pa^4}{C' nt^3}\theta$$

and

$$f = \frac{GA_b pa^2}{Cnt^3}v$$

yields

$$M = \frac{pGA_b a^2}{nt^3}\left(\frac{d^2}{2C} + \frac{2a^2}{C'}\right)\theta \tag{5–39}$$

In most cases, $2a^2/C'$ is small relative to $d^2/2C$.

As an example, we consider dimensions of the elastomeric bearing 600 × 600 mm, and the spacing between the axes d = 2.4 m. We calculate b/a = 1, C = 2.37, C' = 86.2. Then

$$M = \frac{pGA_b a^2}{nt^3}(1.215 + 0.008)\theta$$

The second term in parenthesis may be neglected (the rotational stiffness of the elastometer may be taken as zero). We obtain

$$\theta = \frac{2nCt^3}{pGA_b a^2 d^2}M \tag{5–40}$$

The flexibility coefficients of the elastomeric bearings may, therefore, be written as

$$\begin{aligned} A_e &= C\frac{2n}{pd^2}\frac{t^3}{GA_b a^2} \\ B_e &= 0 \\ C_e &= \frac{n}{2p}\frac{t}{GA_b} \\ K_e &= \frac{n}{2p}\frac{t}{EA_b} \end{aligned} \tag{5–41}$$

where p is the number of elastomeric bearings per row. Then, if the flexibility coefficients of the pier shaft are denoted by A_p, B_p, C_p and K_p, the total flexibility coefficients are

$$A = A_p + A_e,\qquad B = B_p,\qquad C = C_p + C_e,\qquad K = K_p + K_e \tag{5–42}$$

The foregoing analysis suggests that piers with a double row of elastomeric bearings behave similarly to piers with flexible legs: They ensure an effective fixity under

load effects while allowing free thermal expansion of the superstructure. This fixity reduces the bending moments in the spans without significantly increasing the moment at the bearings, as can be seen from Figure 5–34(e).

By a proper choice of elastomer thickness it is possible to reduce the bending moment eventually transmitted to the foundation. Consider, for example, a pier with a double row of bearings supporting a continuous superstructure. For a moment M at the top of the pier, and without horizontal displacement, the moment transmitted to the base of the pier is, in Figure 5–34(f),

$$M' = M + Qh$$

where h is the pier height. Because $u = 0$, $BM + CQ = 0$, or

$$Q = -\frac{BM}{C}$$

and

$$M' = \left(1 - \frac{Bh}{C}\right)M = \left(1 - \frac{B_p h}{C_p + C_e}\right)M = \phi M \tag{5–43}$$

The coefficient ϕ varies with the thickness of the elastomeric pads. If the requirement is $M' = 0$ (no moment transfer to the foundation), then $\phi = 0$, from which

$$C_e = hB_p - C_p \tag{5–44}$$

Conversely, if the bearing thickness becomes very large, ϕ approaches unity, and in this case $M' = M$ as shown in Figure 5–34(f).

Example. A pier with a constant moment of inertia, fixed at the base, has a double row of elastomeric bearings that support a maximum reaction of 1000 tons.

A box section is assumed with external dimensions 5.0 × 3.0 m and a wall thickness 0.30 m, $h = 33$ m, $I = 7$ m^4. We compute the following coefficients

$$EA_p = \frac{h}{I} = \frac{33}{7} = 4.71, \quad EB_p = \frac{h^2}{2I} = 77.7, \quad EC_p = \frac{h^3}{3I} = 1715$$

Four elastomeric bearings are arranged in two rows, spaced at 2.4 meters longitudinally. The dimensions of each bearing are 600 × 400 × 3 (12 + 2). These dimensions correspond to the following notation:

a and b	= plan dimensions of bearing
n	= number of elastoner sheets
t	= thickness of one elastoner sheet
$2e$	= thickness of the internal steel sheet (twice the external)
$A_b = ab$	= area of bearing

so that the dimensions are $abn\ (t + 2e)$

The flexibility of the elastomeric bearings is determined as follows: $b/a = 1.5$, C = 1.7, $A_b = 0.24\ m^2$, $n = 3$, $p = 2$, $t = 1.2 \times 10^{-2}$m, $G = 160$ t/m^2, $E_c = 3.9 \times 10^6$t/m^2. Then

$$EA_e = EC\frac{2n}{pd^2}\frac{t^3}{GA_b a^2} = 0.97, EB_e = 0$$

$$EC_e = E\frac{nt}{2pGA_b} = 915$$

Total flexibility of pier:

$EA = 4.71 + 0.97 = 5.68$, $EB = 77.7$, $EC = 1717 + 915 = 2630$

Elasticity of pier in the structure:

$$EK = E\left(A - \frac{B^2}{C}\right) = 5.68 - \frac{77.7^2}{2630} = 3.38$$

Elasticity of pier without elastomers

$$EK = E\left(A - \frac{B^2}{C}\right) = 0.25\frac{h}{I} = 1.18$$

Coefficient of moment transmission in the pier:

$$\phi = 1 - \frac{Bh}{C} = 1 - \frac{77.7 \times 33}{2630} = +0.03$$

For these conditions, the bending moment M' transmitted to the base is very small, about 3 percent of M. For the moment M' to be zero, the following must be satisfied:

$$EC_e = EC_p/2 = 860$$

Then, the corresponding thickness of the elastomeric bearing is

$$nt = \frac{2(EC_e)pGA_b}{E} = \frac{(2)(860)(2)(160)(0.24)}{(3.9)(10^6)} = 0.034 \text{ m} = 34 \text{ mm}$$

Design example. A three-span continuous bridge is supported on two identical piers. The bridge consists of a box girder with variable moment of inertia and spans 44 meters, 70 meters, and 44 meters. The bending moments in the superstructure and piers are calculated assuming the following conditions: (1) superstructure fixed at the pier; and (2) superstructure partially fixed elastically at the pier, with elastomeric bearings with the varying lamina of 1, 2, 3, 6, or 9 (thickness 12 mm). The superstructure/pier supports are assumed simple.

The loading conditions are as follows:

- Uniform superimposed dead load q = 1.9 t/m
- Deck expansion at a rate of 2×10^{-4} corresponding to an increase in temperature of 20°C.
- Shrinkage of the deck at the rate of 2×10^{-4} corresponding to a decrease in temperature of 20°C combined with creep.
- Applied loads: S_2 = 4.5 t/m center span; S_1 = 6.8 t/m end spans.

- Braking force $F = 15\ t$ on the superstructure, corresponding approximately to 1/20 of the structure dead load. (These loads are not necessary AASHTO models, but reflect criteria applied abroad).

Tables 5.3a and b give a moment summary for the top and base of the pier, respectively. Table 5–3c gives a moment summary in the superstructure. The following comments are appropriate:

1. The moments in the superstructure vary little with the number of elastomer laminations. When this number increases from one to six, the maximum bending moment at the support decreases only by 4 percent, whereas the maximum positive moment in the span increases by 10 percent. The extreme case of 9 laminations should be avoided because of risk of instability evident by the tall stack or elastomers ($a/nt < 5$). Compared with the effect of simple supports, the presence of a double row of bearings benefits the system by a considerable decrease in the positive span moment for a relatively smaller increase in the negative moment.
2. For the pier moments, there is an optimum thickness of elastomer at which the moment transferred to the foundation becomes a minimum. For this example, the optimum thickness is three laminations of 12 mm.

Piers with Twin Flexible Legs

Piers with twin flexible legs were first used in France, and then Europe and the United States. Several examples are described by Podolny and Muller (1982), hence this section deals primarily with analytical and design considerations.

Table 5–3a Bending Moment at the Top of the Pier as Function of the Bearing Thickness[a]

	Number of Elastomer Lamina					
Loading	*0 (Fixed Pier)*	*1*	*2*	*3*	*6*	*9*
Superstructure D.L., $q = 1.9$ t/m	+ 124	+ 106	+ 93	+ 84	+ 68	+ 58
Deck expansion, $+2 \times 10^{-4}$	+ 92	+ 68	+ 53	+ 43	+ 27	+ 19
Deck shrinkage, -4×10^{-4}	− 184	− 36	− 106	− 86	− 54	− 38
Σ moments (no L.L.) $+M$	+ 216	+ 174	+ 146	+ 127	+ 95	+ 77
Σ moments (no L.L.) $-M$	− 60	− 30	− 13	− 2	+ 6	+ 20
L.L in center span, $S_2 = 4.5$ t/m	+1700	+1440	+1270	+1150	+ 930	+790
L.L. in end spans, $S_1 = 6.8$ t/m	−1420	−1240	−1120	−1030	− 850	−740
Braking force, $F = 15$ t	± 101	± 97	± 93	± 90	± 80	± 74
Maximum moments $+M$	+2017	+1711	+1059	+1367	+1105	+941
Maximum moments $-M$	−1581	−1367	−1226	−1122	− 924	−795

[a]Values have been calculated at the intersection of the axis of the pier with the center of gravity of the superstructure.

Table 5–3b Bending Moment at the Base of the Pier as Function of the Bearing Thickness

Loading	Number of Elastomer Lamina: *0 (Fixed Pier)*	*1*	*2*	*3*	*6*	*9*	*Simple Support, t = 24mm*
Superstructure D.L., q = 1.9 t/m	− 62	− 31	− 15	− 4	+ 13	+ 20	0
Deck expansion, $+ 2 \times 10^{-4}$	− 202	−157	−129	−111	− 77	− 60	−130
Deck shrinkage, $- 4 \times 10^{-4}$	+ 404	+314	+258	+222	+154	+120	+260
Σ moments (no L.L.) $+M$	+ 342	+283	+243	+218	+167	+140	+260
Σ moments (no L.L.) $-M$	− 264	−188	−144	−115	− 64	− 40	−130
L.L in center span, S_2 = 4.5 t/m	− 820	−435	−198	− 47	+176	+265	0
L.L. in end spans, S_1 = 6.8 t/m	+ 197	− 74	−207	−265	−380	−400	0
Braking force, F = 15 t	± 159	±163	±167	±170	±180	±186	(±520)
Maximum moments $+M$	+ 698	+609	+577	+558	+527	+591	+780
Maximum moments $-M$	−1243	−786	−518	−550	−624	−626	−650

Equilibrium and deformability characteristics. Referring to Figure 5–35 the following notation is introduced:

M, Q, N	= moment, horizontal load, vertical load, respectively, acting at point 0,
m, t, n	= components of load acting at the top of pier leg, oriented to the axis of the leg (Fig. 5–35c)
$\theta, u, v,$	= displacements corresponding to M, Q, N at point 0
ω, α, β	= displacements corresponding to m, t, n at the top of the pier leg
E	= modulus of elasticity of the concrete leg
l	= length of leg between points A and B (Fig. 5–35c)
$2d$	= spacing of legs at the top between points A and A′

Table 5–3c Maximum Bending Moments in the Superstructure as Function of the Bearing Thickness

Loading		Number of Elastomer Lamina: *0 (Fixed Pier)*	*1*	*2*	*3*	*6*	*9*	*Simple Support,*
Moments at support	Center span	−3125	−3060	−3020	−2985	−2925	−2895	−2660
Moments at support	Side span	−3105	−2960	−2845	−2770	−2635	−2545	−2055
Moments in span	Center span, $(0.5\, l_2)$	+ 910	+ 960	+ 990	+1015	+1060	+1090	+1270
Moments in span	Side span, $(0.4\, l_1)$	+ 890	+ 935	+ 965	+ 980	+1020	+1040	+1200

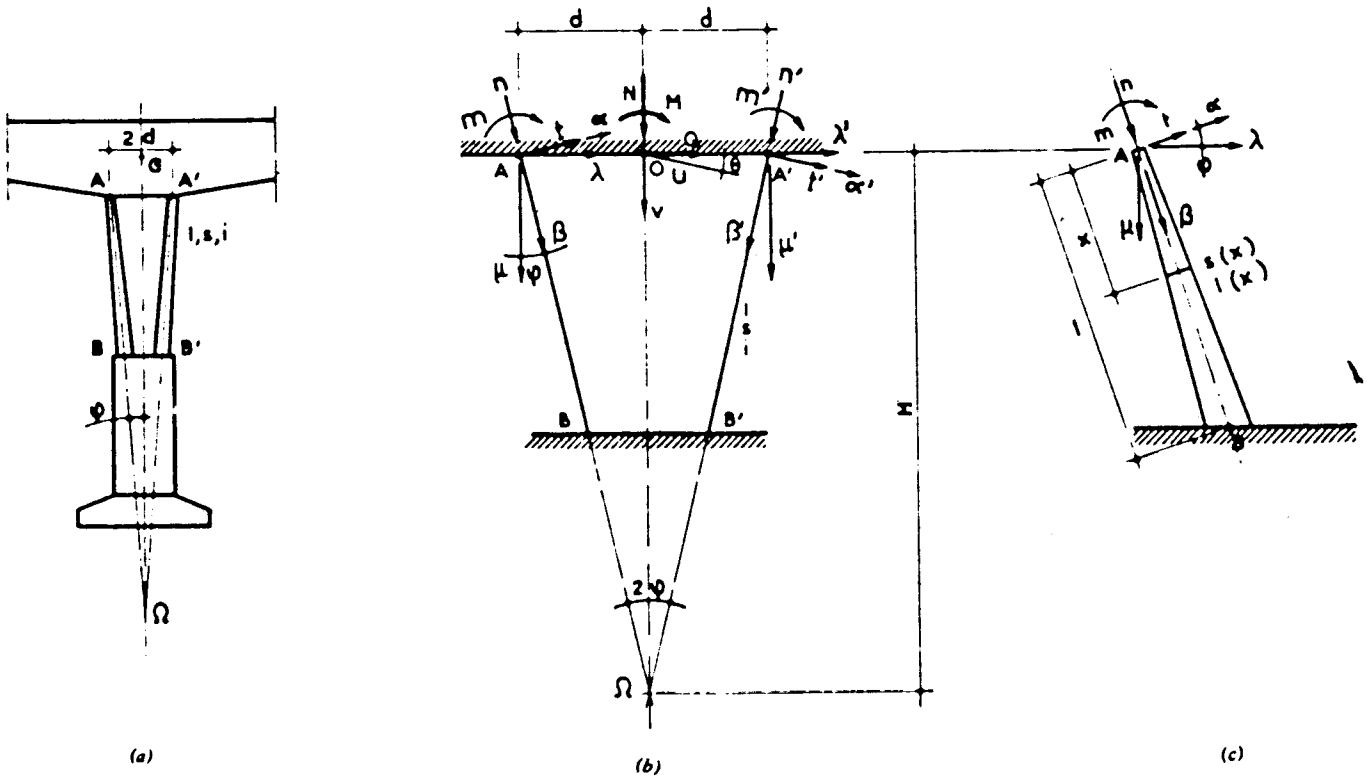

Figure 5–35 Piers with flexible legs, notations.

a = cross-sectional area of leg
i = moment of inertia of one leg
$P_o = ad^2/2i$ = dimensionless coefficient
ϕ = angle of inclination of the legs with the vertical

Identical and symmetrical legs of length l are arranged as shown in Figure 5–35(a). The cross-sectional area and moment of inertia of each leg at a distance x from the top A or A' are $a(x)$ and $i(x)$, respectively.

An equivalent area of the leg is designated by σ, so that

$$\frac{1}{\sigma} = \frac{1}{l}\int_o^l \frac{dx}{a(x)} \tag{5–45}$$

Also, U, V, and W are the characteristic integrals, or

$$U = \int_o^l \frac{dx}{i(x)} \quad V = \int_o^l \frac{xdx}{i(x)} \quad W = \int_o^l \frac{x^2dx}{i(x)} \tag{5–46}$$

At the superstructure level AA', the combined area and moment of inertia of the two legs is A and I, respectively, so that

$$A = 2a \text{ and } I = 2i + 2ad^2$$

where $2d$ is the distance between the two legs (Figure 5–35a). Setting $p_o = \alpha d^2/2i$, the combined moment of inertia of the two legs is $I = 2i(1 + 2p_o)$.

The deformations of the pier are expressed by linear equations relating the displacements θ, u, v, to the applied forces M, Q, N. Legs AB and $A'B'$ are connected at their ends by two rigid underformable sections AA' and BB'. Section BB' is assumed fixed against translation, and the deformation equations are given by

$$\theta = AM + BQ \qquad u = BM + CQ \qquad v = KN \tag{5–47}$$

where A, B, C and K represent deformation coefficients for the legs.

The force components M, Q, N acting at point 0 (center of AA') are the resultant of the external forces applied to the pier. The parameters θ, u, v are the corresponding displacements of section AA' at point 0 (Figure 5–35b).The forces m, t, n and m', t', n' in the legs at A and A' may be determined considering the expressions of equilibrium, deformation, and compatibility.

Equilibrium Equations. The system is in equilibrium about point 0 if

$$\left.\begin{aligned} M &= m + m' + d\sin\phi\left(t + t'\right) - d\cos\phi\left(n - n'\right) \\ Q &= \left(t + t'\right)\cos\phi + \left(n + n'\right)\sin\phi \\ N &= -\left(t - t'\right)\sin\phi + \left(n + n'\right)\cos\phi \end{aligned}\right\} \tag{5–48}$$

Deformation Equations. The displacements ω, α, β and ω', α', β' at points A and A' with respect to the axis of the legs are given by

$$\omega = \omega_0 + \int_0^l \frac{m + tx}{Ei} dx = \omega_0 + \frac{mU}{E} + \frac{tV}{E}$$

$$\alpha = \omega_0 l + \int_0^l \frac{m + tx}{Ei} x\, dx = \omega_0 l + \frac{mV}{E} + \frac{tW}{E} \qquad (5\text{–}49)$$

$$\beta = \frac{n}{E} \int_0^l \frac{dx}{a} = \frac{nl}{E\sigma}$$

where ω_0 is the rotation of the leg AB and B, and E is the modulus of elasticity of the concrete. Similar equations give the displacements ω', α', β' at point A'.

The displacements of points A and A' with respect to the pier axis, θ, λ, μ and θ' λ', μ' are obtained as

$$\begin{aligned} \theta &= \omega \quad \lambda = \alpha\cos\phi + \beta\sin\phi \quad \mu = \alpha\sin\phi + \beta\cos\phi \\ \theta' &= \omega' \quad \lambda' = \alpha'\cos\phi + \beta'\sin\phi \quad \mu' = \alpha'\sin\phi + \beta'\cos\phi \end{aligned} \qquad (5\text{–}50)$$

Compatibility Equations. Compatibility of displacements of points A, A′ and O requires the following:

$$\begin{aligned} \theta &= \omega = \omega' \left(\text{if there are no hinges at A and A}'\right) \\ u &= \lambda = \lambda' \quad \mu = v - d\theta \quad \mu' = v + d\theta \end{aligned} \qquad (5\text{–}51)$$

The foregoing equations are sufficient to determine θ, u and v in terms of the applied actions of M, Q and N.

In practice, it is necessary to consider four possible cases: (1) legs fixed at both ends; (b) legs fixed at the superstructure and hinged at the base; (c) legs hinged at the superstructure and fixed at the base; and (d) legs hinged at both ends. For any of these cases, the legs may have constant or variable cross section, and be either inclined or vertical. A comprehensive analysis has been made by Mathivat (1966, 1974), and includes complete derivations of mathematical relationships applying to each case.

A practical case involves twin vertical walls with constant cross section, for which the foregoing equations are greatly simplified. A summary of flexibility coefficients for this case is given in Table 5–4. It should be noted that the expression $p_o = ad^2/2i$ becomes $p_o = 6\,(d/h)^2$ with $2d$ being the distance on centers of both legs, and h being the wall thickness. Usually p_o should be expected to vary between 30 and 80.

A pier with twin legs behaves in much the same way as a conventional pier of a cross-sectional area A and a moment of inertia I, with respect to the effect of vertical loads and moments on vertical displacements and rotation. However, the behavior is completely different with respect to the horizontal displacement caused by the application of horizontal loads (bracing force or thermal expansion. The elasticity coefficient $C = l^3/3EI$ in this case is multiplied by the dimensionless factor $1 + p_o/2$ for vertical walls fixed at the top and bottom, and by $(1 + 2\,p_o)$ for walls hinged at one end.

The elasticity coefficient approaches infinitely large values for vertical walls with both ends hinged. The lack of restraint in this case simply implies that horizontal loads must be resisted through other arrangements.

Table 5–4 Flexibility Coefficients of a Pier with Twin Vertical Walls of Constant Cross Section[a]

Flexibility Coefficient	*Multiplier Coefficient*	End Conditions for Legs			
		Fixed Top and Bottom	*Fixed Top Hinged Bottom*	*Hinged Top Fixed Bottom*	*Hinged Top and Bottom*
Exact Formulas					
A	$\frac{l}{EI}$	1	$1+\frac{1}{2\rho_0}$	$1+\frac{1}{2\rho_0}$	$1+\frac{1}{2\rho_0}$
B	$\frac{l^2}{2EI}$	1	$2\left(1+\frac{1}{2\rho_0}\right)$	0	0
C	$\frac{l^3}{3EI}$	$1+\frac{\rho_0}{2}$	$\left(1+\frac{1}{2\rho_0}\right)(3+2\rho_0)$	$1+2\rho_0$	∞
Approximate Formulas[b]					
A	$\frac{l}{EI}$	1	1	1	1
B	$\frac{l^2}{2EI}$	1	2	0	0
C	$\rho_0\frac{l^3}{3EI}$	0.5	2	2	∞

[a]Notation: $I = 2i(1 + 2\rho_0)$, equivalent global inertia of twin walls. $\rho_0 = ad^2/2i = 6(d/h)^2$, with $2d$ distance between walls, h wall thickness.

[b]When $1/\rho_0$ is negligible with regard to 1.

Example. The associated structural action of pier legs with various end restraints is demonstrated in Table 5–5, which presents results of a study for the Choisy-le-Roi Bridge considering (1) legs fixed at both ends, (2) legs hinged at both ends, and (3) legs fixed at the top and hinged at the base. The same study considered also the flexibility of the body of the pier to the base of the foundation, where M_0 = bending moment of the superstructure at the pier section (side of the center span); M_1 = bending moment in pier (top section); and Q = horizontal reaction in the pier.

From these results, the following conclusions are appropriate:

1. For this example, the superstructure is efficiently restrained (fixed) over the river piers by the twin inclined wall system. The end moment for the center span totally fixed at both ends would be 255, compared with the actual end moment computed between 230 and 232.
2. The elastic behavior of the pier has a minor dependence on the conditions of fixity of the walls at the top and bottom (variation from 0.92 to 1.03).
3. The position of the point of contraflexure in the pier varies only little with the pier subjected to moment, but this position is considerably more sensitive to the presence of a horizontal load.
4. The horizontal rigidity of the pier varies considerably with the degree of fixity of the legs.

Elastic stability. The elastic stability of twin flexible legs imposes certain limitations, because there must be an ample margin against buckling. For a given horizontal force, a bridge superstructure tends to move an amount u, but resistance to this displacement is provided by the pier rigidity including the bending resistance of the legs. The minimum vertical reaction for which the imposed displacement shows no tendency to dimin-

Table 5–5 Choisy-le-Roi Bridge: Behavior of River Piers under Horizontal and Vertical Loads[a,b]

Type of Legs	Flexibility Coefficients			Elasticity	Unit Vertical Load in Center Span		Unit Horizontal Load Applied to Deck		Unit Volume Change		
	A	B	C	E_k	M_0	M_1	M_0	M_1	M_0	M_1	Q
Fixed	4.06	54.6	973	0.92	−232	−157	+3.4	+5.7	+7.4	+24.7	2.4
Fixed/hinged	12.7	234	4670	0.98	−231	−154	+5.1	+8.7	+6.4	+21.5	1.3
Hinged	—	—	—	1.03	−230	−150	+6.3	+10.7	+5.9	+19.7	0.9

[a]Notation: A, B, C = flexibility coefficients of pier. E_k = global elasticity of pier. M_0 = end moment of center span (in tm). M_1 = bending moment at pier top (in tm). Q = horizontal reaction in pier.

[b]Units: All coefficients in metric system. A uniform vertical load of 1 t/m is applied over the center span. A unit horizontal load of 1 t is applied at deck level. A unit shortening of the deck is applied such that $E\,\Delta = 10^3$.

ish until the cause inducing it no longer exists represents the critical buckling load. This critical load is generally smaller than with the legs isolated and subjected to the same load conditions.

The deformations (θ, u) produce internal reactions (m, t, n and m', t', n') as shown in Figure 5–35(b) in the top of the legs A and A', requiring the following conditions:

$$m_1 = m_1' \quad t_1 = t_1' \quad n_1 = -n_1' \tag{5–52}$$

Now, let R_θ represent the rigidity of the superstructure against rotation and R_u against longitudinal displacement. Also let M and Q represent the moment and horizontal force transmitted to the pier. Then

$$\left.\begin{aligned} M &= -R_\theta \theta f(m_1, t_1, n_1) \\ Q &= -R_u u g(t_1, n_1) \end{aligned}\right\} \tag{5–53}$$

These equations may be modified to substitute the deformations of the superstructure, θ, u for those of the legs, or

$$\left.\begin{aligned} & R_\theta w f'(m_1, t_1, n_1) \\ & R_u(\alpha \cos\phi - \beta \sin\phi) g'(n_1, t_1) \end{aligned}\right\} \tag{5–54}$$

with $aw = \alpha\sin\phi + \beta\cos\phi$, and $\beta = (l/E\sigma)n_1$.

The initial load condition, expressed by n_0, is modified for the case of the displacement imposed to the structure. The new condition is

$$\begin{aligned} \text{Nominal force} &= n_o + n_1 \\ \text{Bending moment} &= m_1 \\ \text{Transverse force} &= t_1 \end{aligned}$$

The additional forces m_1 and t_1 may be expressed as a function of the leg displacement, ω, α, and the initial force n_0. When these forces are substituted into Equations (5–54) as functions of α and ω, a new system of linear equations is obtained with three unknowns n, α, ω.

Assuming that the displacements α, ω are not zero when the cause of the displacement is not present, the determinate form of the three equations is nil, and this allows to obtain the value of critical load n_{1c}.

The critical buckling force of one pier leg is expressed as

$$n_{cr} = r^2 \frac{E_i}{l^2} \tag{5–55}$$

where r is a dimensionless coefficient related to the usual Euler formula. Accordingly,

$$n_{cr} = \pi^2 \frac{E_i}{\lambda^2} \tag{5–56}$$

where λ is the effective length. Therefore, the equivalent buckling length of one leg considered part of the total pier is

$$\lambda = \frac{\pi l}{r} \tag{5–57}$$

Example. The Choisy-le-Roi Bridge is again considered as an example. The analysis included seven typical cases with vertical and inclined legs and different end restraints. The horizontal restraint of the bridge at the abutments was also varied. The results are presented in Table 5–6, for the following parameters:

Wall length l = 8.50 m, center-to-center spacing $2d$ = 2.00 m
Area a = 6.40 m^2, moment of inertia i = 0.085 m^4
Elastomeric pads over the abutments: area A_b = 1.28 m^2, E/G = 20.000

The first six cases in Table 5–6 are design options analyzed for comparison with case 7, the actual configuration of the bridge. The following are relevant conclusions:

1. Three main factors have an obvious effect on the elastic stability of the pier: inclination of the legs to the vertical; horizontal rigidity of the elastomeric bearings at the abutments; and fixity conditions at the ends of the pier legs.
2. The difference between case 2 and 6 in Table 5–6, articulated by the factor of

Table 5–6 Choisy-le-Roi Bridge: Elastic Stability of Twin-Flexible-Legged Pier for Various Support Conditions

Case Number	Conditions of Legs at River Piers	Support Condition at Abutments	$\frac{\lambda}{l}$	Factor of Safety
1	Hinged vertical legs	Rigidity neglected	∞	0
2	Vertical legs hinged at the base and fixed at the top	Rigidity neglected	2.00	1.1
3		Five neoprene pads	1.20	2.8
4		Three neoprene pads	1.00	4.0
5	Vertical legs fixed top and bottom	Rigidity neglected	1.00	4.0
6	Legs inclined 6.5%, hinged at base, fixed at top	Rigidity neglected	0.88	5.2
7	Legs inclined 6.5%, hinged at base, fixed at top (actual case of Choisy-le-Roi)	Three neoprene pads	0.97	4.8

safety, reflects the arch effect of inclined legs in case 6. Horizontal displacement of the substructure does not occur without mobilizing the bending stiffness mechanism of the pier. For case 2, elastic stability relies solely on the bending stiffness of the legs, so that the buckling force is the same as for a beam fixed at one end and free at the other.

Stability of Flexible Piers during Construction

The pier types considered in the foregoing sections have sufficient flexural capacity to resist construction moments without additional strengthening. Alternatively, a pier may be designed to receive the loads from the superstructure through a single row of bearings. In this case, stability during cantilever erection may require temporary supports, or a modified design that includes procedures for increasing pier stability.

Structures with temporary supports. Figure 5–36 shows the erection sequence for the Paris Belt Bridge, together with the temporary support. Because of the limited dimensions of the pier shafts and the associated marginal flexural capacity, a temporary support was used until deck continuity was achieved. This support was placed on one side of the pier within the space available inside the temporary cofferdam. The lever arm is in this case only 8.5 feet (2.40 m), imposing a heavy reaction on the temporary support.

The maximum loading conditions are for the case of one precast segment out of balance as shown, including the erection equipment. With provisions for random (unexpected) loads and the added reaction of the temporary prestressing, the maximum reaction for the temporary support was 2030 tons (1840 metric tons). Each temporary support consisted of (1) a 40-inch (1 m) steel pipe filled with concrete resting on the spread footing of the permanent pier, and (2) a V-shaped concrete frame placed upon the pipe and allowing the deck reaction to be transferred directly from the box section webs to the pipe.

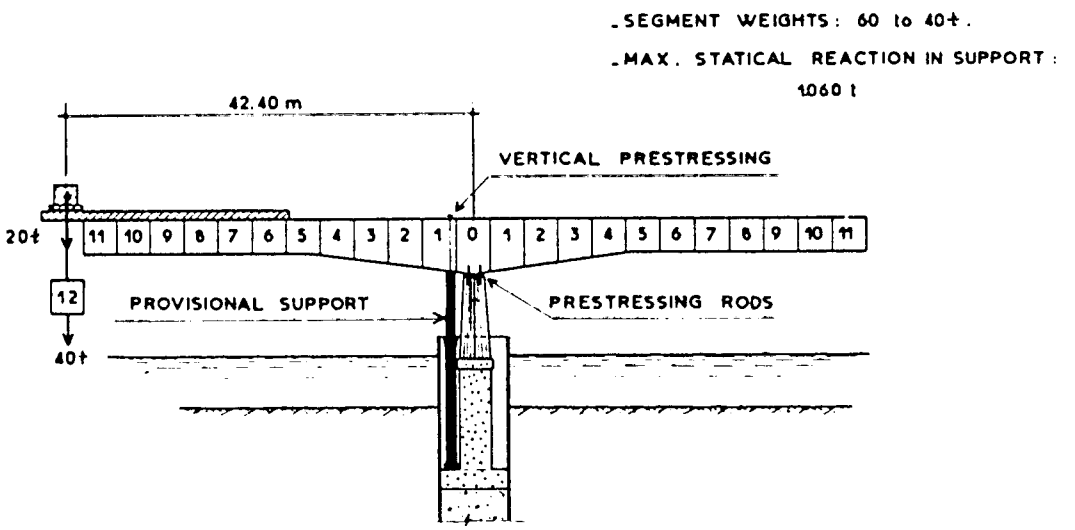

Figure 5–36 Downstream Paris Belt Bridge, schematic of temporary support and stability of river pier during construction.

A second example is the Saint Jean Bridge in Bordeaux, France. This structure is supported by relatively slender pier shafts, founded on an open-dredged concrete caisson anchored in a bed of dense sand and gravel. Construction of the piers called for the use of an auxiliary floating platform that could be raised on eight temporary pipe piles, as shown in Figure 5–37. The reinforced concrete caisson was floated into place, suspended from the platform resting on its legs, and incorporated into the permanent structure. As the caisson was lowered to its final elevation, precast segments were added to bring the structure to the required height.

The cofferdam for the pier shaft was made up of temporary additional caisson rings stacked upon the permanent caisson and firmly connected. This cofferdam was used during construction of the deck to resist unbalanced loads from the erection process, and as a substitute to the flexible permanent pier. During construction, the deck was therefore resting only on the cofferdam and the lower caisson through two temporary caps, providing a stable base for any unbalanced loading, as shown in Figure 5–38.

After construction was finished and deck continuity was achieved, flat jacks were introduced to transfer the deck load from the temporary cofferdam and caps to the permanent pier. All the temporary ring segments above low water were removed.

Comparison of methods of pier stability during cantilever construction. Pier stability during construction may be maintained through the use of several methods, used singly or in combination.

Temporary Eccentric Prestress. For an unbalanced cantilever erection process, the resulting unbalanced moment varies between zero and Wd, where W is the weight of the segment and d is the distance from the pier centerline as shown in Figure 5–39(a). If a temporary vertical cable, anchored in the foundation of the pier, is provided for this unbalanced loading configuration, it may be stressed to a load P such that

$$P\delta = \frac{Wd}{2} \tag{5–58}$$

The unbalanced moment in the pier becomes now one-half, or $Wd/2$, so that the actual flexural capacity of the pier is doubled. In practice, this is not a fixed gain because it is not expedient to change the tendon prestress each time the segment moves further, hence a proper temporary connection between pier foundation and deck must be always present. It should be noted that the foundation must be designed for the extra load effects and the resulting additional pressure because of the temporary unbalanced moment. This condition may control the size and configuration of the foundation.

Unsymmetrical Pier Segments. If the pier segments are erected eccentrically with respect to the pier centerline, as shown in Figure 5–39(b), a permanent moment is induced in the pier when an even number of segments is placed on the deck. The segment dimensions may be selected such that the maximum unbalanced moment due to one segment (placed on the proper side of the pier) will result only in one-half applied to the pier. This, however, may cause serious complications in the layout of the prestressing tendons.

Both methods described thus far have a common disadvantage: The deck cantilever is never balanced over the pier, and becomes more complicated as the erection continues according to the geometry of the deck.

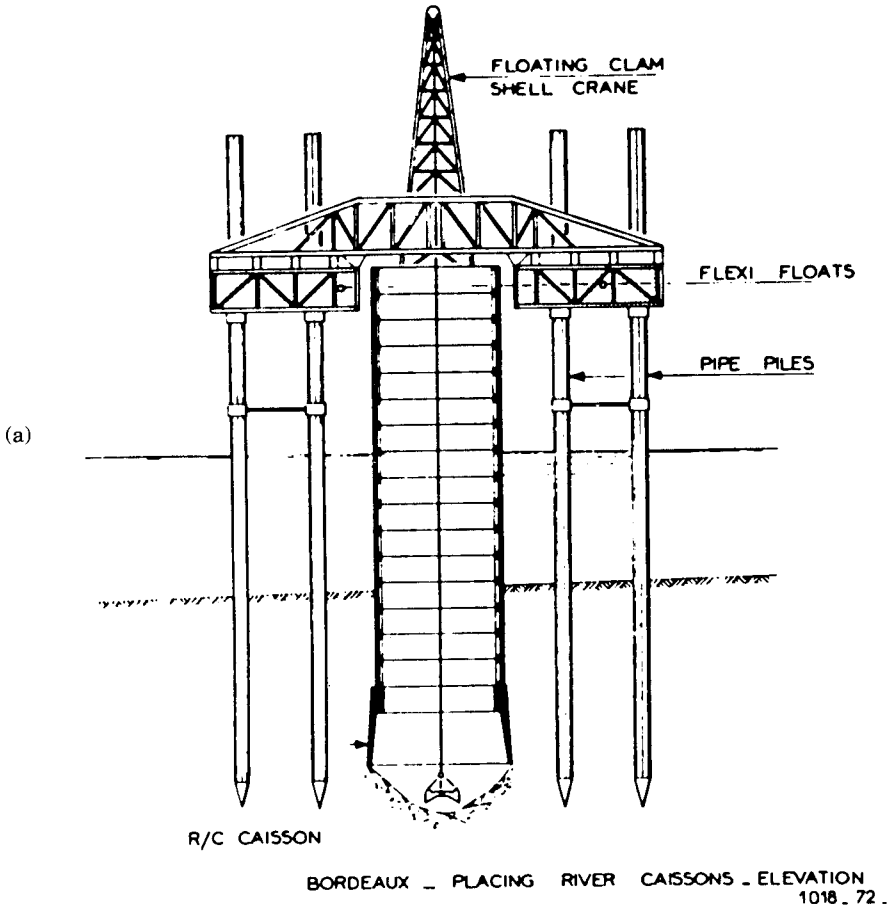

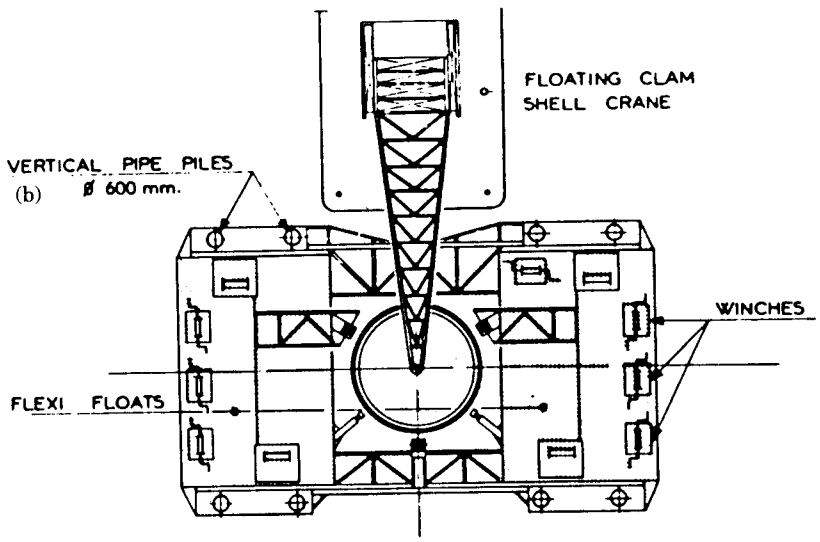

Figure 5–37 St. Jean Bridge, Bordeaux, France; schematic presentation of river piers; (a) elevation; (b) plan.

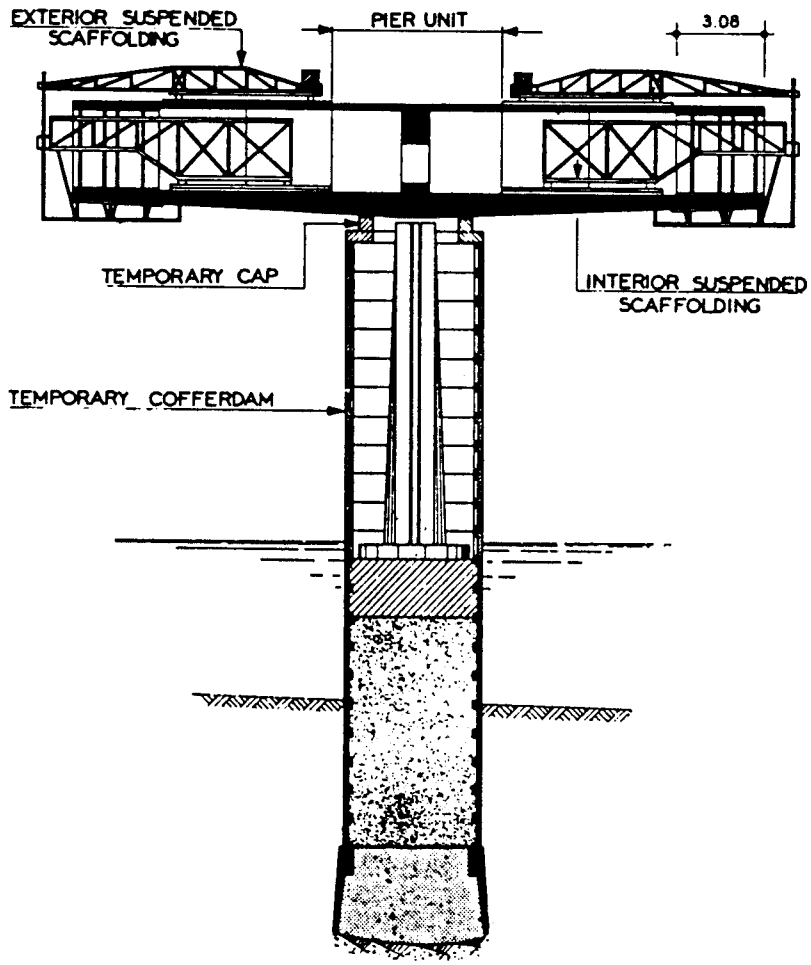

Figure 5–38 St. Jean Bridge, Bordeaux, France; temporary arrangement of piers for deck cantilever construction (cofferdam and deck support).

Stability with Erection Equipment. Cantilever stability may be maintained with the use of the construction equipment. Several typical examples are shown in Figure 5–39(c), and may apply to either cast-in-place or precast construction. The stability of the cantilever is achieved by an overhead truss or a launching gantry. Examples are mentioned by Podolny and Muller (1982), and include projects in the United States.

Temporary Supports. A temporary support may be placed on the side of the unbalanced segment (response is in compression) or on the opposite side (response is in tension). Consider a single temporary support placed as shown in Figure 5–39(d) on one side only. The following reactions are developed:

$$\text{At pier} = V - M/a$$
$$\text{At temporary support} = M/a$$

If two symmetrical temporary supports are used, both placed at distance a, the system becomes statically indeterminate and the actual distribution of the reactions

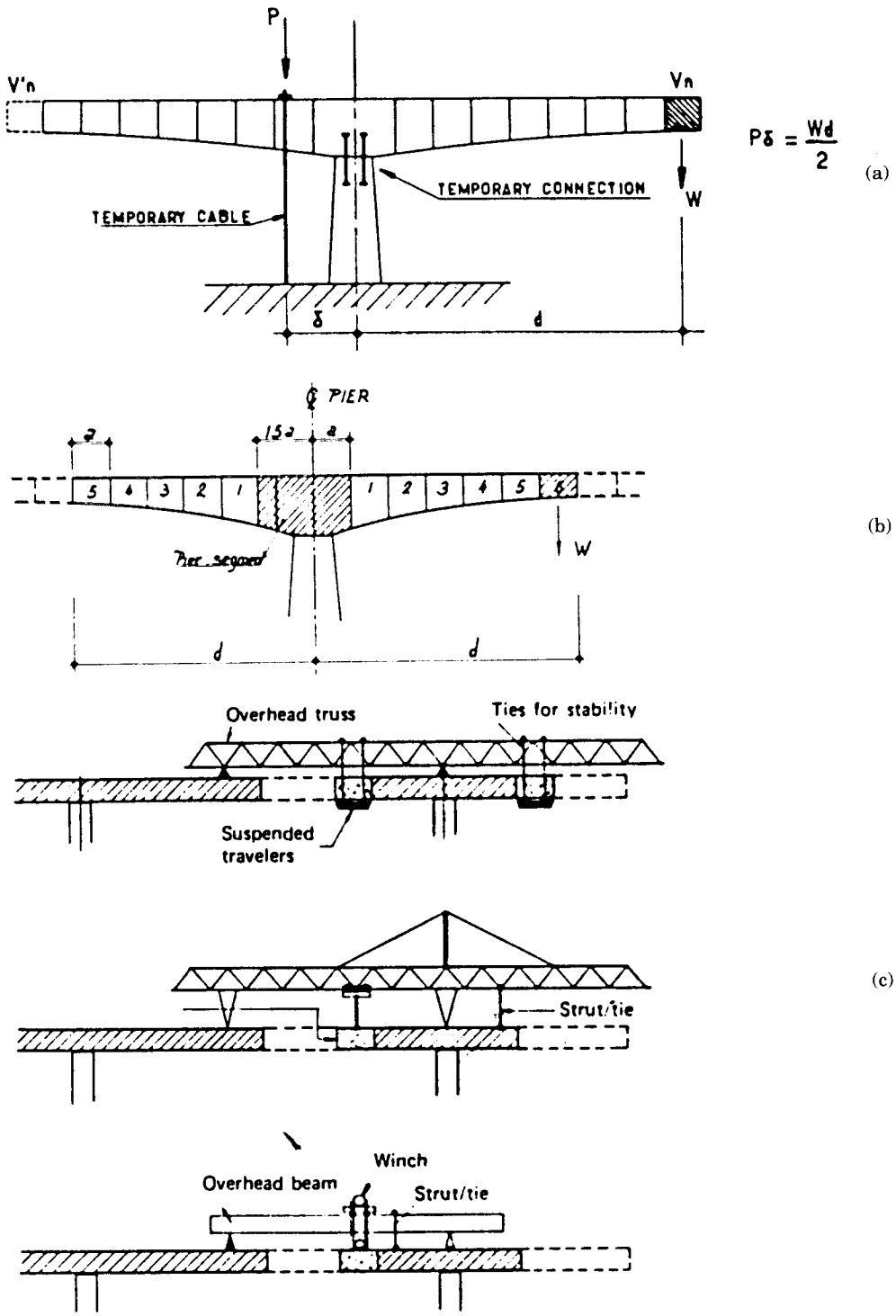

Figure 5–39 (a) Temporary stability of deck and pier during construction by prestressing tendon; (b) unsymmetrical pier segment; (c) cantilever stability by deck construction equipment; (d) cantilever stability by temporary supports; (e) cantilever stability by temporary stays.

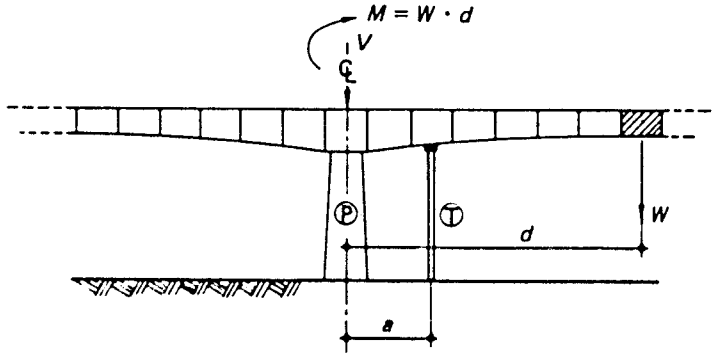

(d)

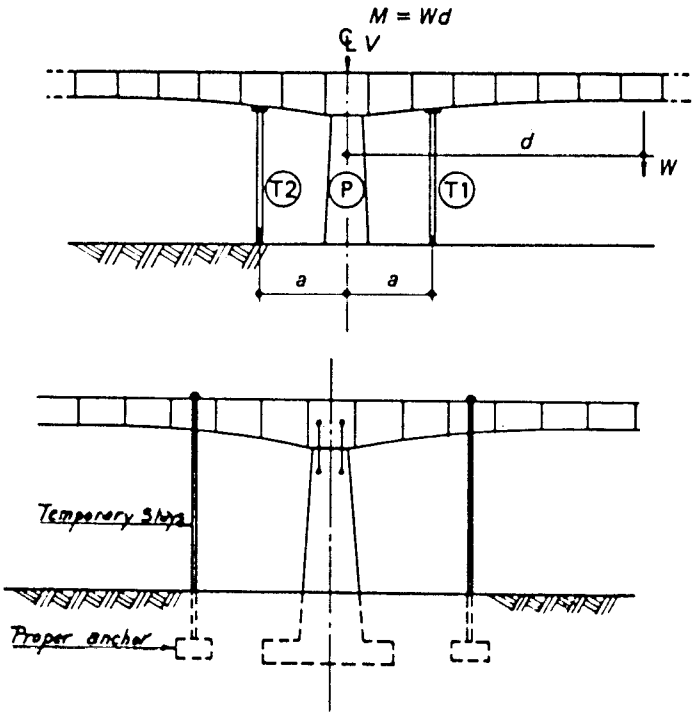

(e)

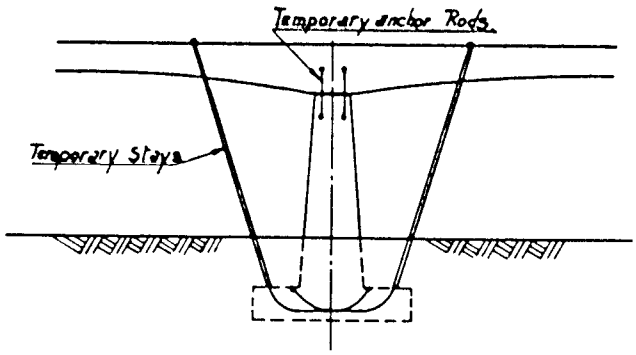

Figure 5–39 *(continued)*

will depend on the relative stiffness of the pier and the supports. The load distribution is as follows:

	Temporary Support, T_1	Pier, P	Temporary Support, T_2
Effect of vertical load V	ρV	$(1-2\rho)V$	ρV
Effect of moment M	$-\frac{M}{2a}$	0	$+\frac{M}{2a}$
Total	$\rho V - \frac{M}{2a}$	$(1-2\rho)V$	$\rho V + \frac{M}{2a}$

If the criterion is to inhibit uplift in any of the temporary supports, the support stiffness must be such that a sufficient fraction of the vertical load reaches the temporary supports to compensate the effect of the unbalanced moment. Then, the minimum value of p must be such that

$$pV - \frac{M}{2a} \geq 0 \quad \text{or} \quad p \geq \frac{M}{2a}$$

In this case the maximum reaction at support T_2 becomes at least equal to M/a, which is the value of the reaction for a single support with the same loading configuration. It follows, therefore, that the double support system has twice the cost of a single support system. Its only advantage is that it allows the construction of the deck to proceed indifferently from either side of the pier, or to maintain an equal safety level if an error should occur in the sequence of operations for the case of a single support.

Temporary Stays. In some instances, stability during construction has been provided with the use of temporary vertical stays or inclined stays anchored in special foundations, such as blocks, or in the permanent pier footing, as shown in Figure 5–39(e). The latter system is simple, particularly when its feasibility is ascertained. The temporary stays are usually made of simple prestressing tendons and are much less costly than rigid temporary supports. The associated structural action requires, however, strong connections with the deck and adequate bearing capacity at the footing-soil level.

5.5 PIERS FOR MOVABLE BRIDGES

Movable bridges are grouped into three main types: bascule, vertical lift, and horizontal swing bridges. The type to be used depends largely on the horizontal and vertical clearance requirements. Whether the choice should focus on a low-level movable bridge or a high-level fixed bridge for a given site, it can usually be determined by an economic analysis and environmental considerations.

From the brief discussion presented in section 1.2, a main conclusion is that substructures and foundations for movable bridges must be carefully selected and designed to preclude any settlement, movement, and displacement that may render the structure inoperable because of the particular structural-mechanical interaction on which bridge performance is based.

Loads and load combinations. The live load on movable bridges is as specified in the current AASHTO specifications. However, it may be applied either continuously or in separate parts and in such a manner as to produce maximum effects.

Impact, as a function of the span length, is computed as stipulated for conventional bridge types. Dead load stresses in structural parts where the stress varies with span movement and position or in parts that move or support moving parts should be increased 20 percent for impact or vibratory affects. This impact allowance should not be combined with live load stresses. Stresses induced by machinery or motive power should be increased 100 percent to reflect impact effects.

The stability of the span and its foundations should be analyzed for wind loads assuming the wind acts transversely, longitudinally, or diagonally at an angle of 45° with the bridge tangent. Exposed areas for transverse wind are as in the AASHTO specifications. Exposed areas for longitudinal wind should be taken as one-half of those for transverse wind, except for bascule spans when open when wind loads can also act on the floor. Detailed criteria for wind loads and stresses for various bridge positions are given by AASHTO.

Seismic loads are stipulated in the AASHTO specifications for seismic design. Movable bridges should be designed to resist these loads with the movable span in the open or closed position. However, when the movable span is in one position more than 90 percent of the time, only one-half of the seismic load may be considered for design of the other position.

Special features. Movable bridges have special features, such as counterweights, aligning and locking devices, traffic gates, houses for machinery and operations, and stairways, walks, and elevators. Of these, the counterweights are of concern because they become part of the structural system and must therefore be considered in the design of substructures and foundations.

Structural design provisions: swing spans. For swing spans continuous on three or four supports, the loads on the substructure may be checked for the following conditions (pivot pier):

Case I: Dead Load. The bridge may be open, or closed but with the end weight not driven. The pivot pier in this case must resist the entire load from the dead weight of the superstructure, plus wind loads and seismic forces.

Case II: Dead Load. The bridge may be closed, but with one end lifted to give positive end reaction. This may be equal to the reaction due to temperature plus 1.5 times the maximum negative reaction of the live load plus impact, or the force required to lift the span 1 inch, whichever is greater. All loads are in this case distributed to the pivot pier and the end support with full bearing contact.

Case III: Live Load plus Impact. The bridge is assumed again closed, with one arm loaded, and the other treated as cantilever.

Case IV: Live Load plus Impact. Loads and reactions on the pivot pier may be calculated treating the bridge as a continuous structure.

The maximum stresses should be calculated using the following load combinations:

- Case I alone, plus 20 percent more load
- Case I with Case III
- Case II with Case IV

Example of swing bridge. Figure 5–40 shows the double-leaf concrete swing bridge built across the Duwammish River in Seattle, Washington. Seismicity in the area is moderately active (SPC Zone C with a seismic acceleration coefficient $A = 0.25$).

The 480-foot dimension center-to-center of pivot piers was established to accommodate the channel width opening in the direction of flow. The ground at the site includes a hydraulic fill and recent alluvial sands and silts sitting on a heavily preconsolidated glacial till. Densification by vibrofloatation was specified to prevent liquefaction of the loose silts and hydraulic fill.

Static balance of each leaf about the pivot pier is achieved by thickening compo-

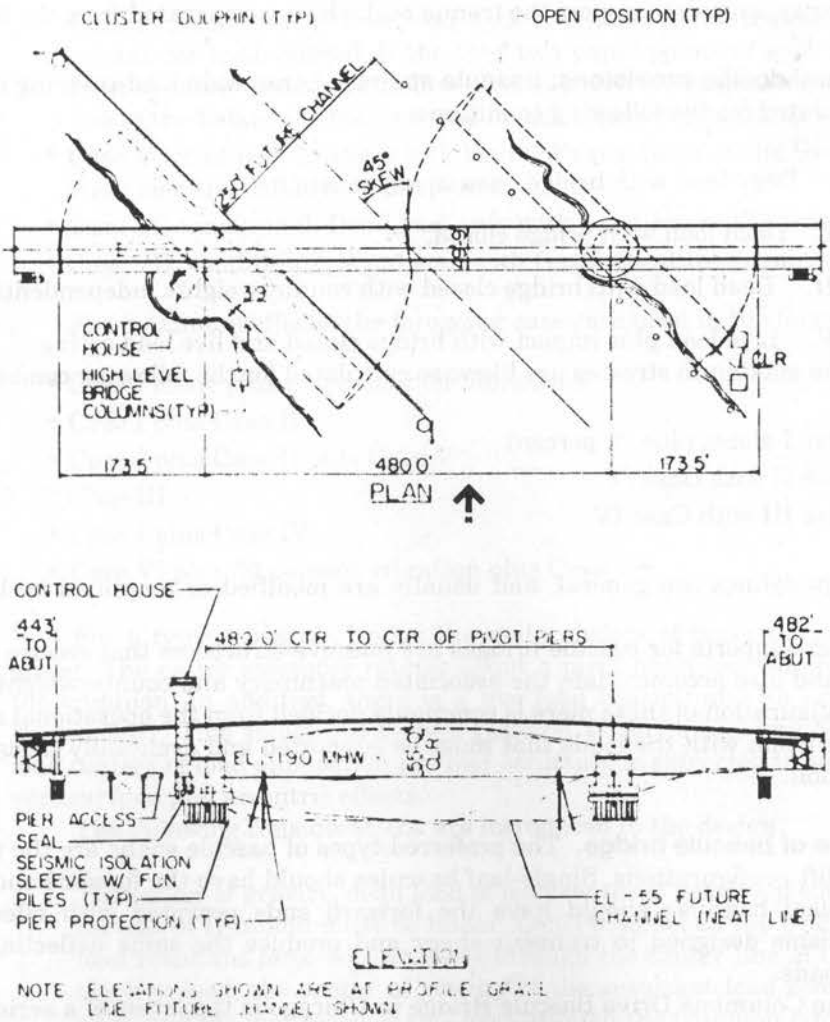

Figure 5–40 West Seattle Swing Bridge: plan and elevation.

nent section elements in the tail span and by adding ballast concrete so that the last 40 feet of the tail span is solid except for a 4-foot square access shaft (Kane, Mahoney, and Clark, 1990). Some precast ballast blocks are provided to adjust the static balance, if necessary.

The pier structure has a diameter of 42 feet, carries the superstructure loads to the foundation, and houses the drive machinery, emergency generators, and part of the control system. The walls of the pier are 32 inches thick and heavily reinforced.

The foundation consists of 48-inch diameter steel pipe sleeves around each foundation pile. the purpose of the sleeves is to control the elevation at which the piles begin to receive lateral support from the surrounding soil. Because the pier is located in the slope area of the channel excavation, without the sleeves the depth from the footing to the slope surface would vary from zero to 15 feet. Under these conditions, the lateral stiffness of the piles would vary, and significant torsional response to seismic excitation would result from the eccentricity between the center of mass and the center of stiffness. The sleeves serve to eliminate the variation in lateral stiffness and the associated eccentricity, and also support the tremie seal which is separated from the footing.

Structural design provisions: bascule spans. Stresses in load-carrying members may be calculated for the following conditions:

Case I. Dead load with bridge open in any position.

Case II. Dead load with bridge closed.

Case III. Dead load with bridge closed with counterweights independently supported.

Case IV. Live load plus impact with bridge closed and live load acting.

The maximum stresses are likewise calculated for the following combinations:

- Case I alone, plus 20 percent
- Case II with Case IV
- Case III with Case IV

These guidelines are general, and usually are modified or amplified by local building codes.

Pier supports for bascule bridges are massive structures that receive the trunnion girder and also accommodate the associated machinery and counterweights. The shape and configuration of these piers is commonly decided from the operational requirements in conjunction with the loads that must be supported and eventually transferred to the foundation.

Example of bascule bridge. The preferred types of bascule spans are the trunnion and rolling lift configurations. Single-leaf bascules should have the forward ends supported. Double-leaf bascules should have the forward ends provided with effective locking mechanisms designed to transmit shear and produce the same deflection under balanced loads.

The Columbus Drive Bascule Bridge in Chicago is the latest of a series of movable bridges built in downtown Chicago across the Chicago River and Sanitary and Ship Canal. It is a double leaf, trunnion-type bascule span with appreciable fixed bridges at the approaches. The superstructure consists of welded plate girders, designed by finite

element techniques (Xanthakos, 1973). The structural design complies with AASHTO criteria modified to reflect also City of Chicago specifications and design standards.

The stresses in main or counterweight members are calculated for the following conditions: (1) Condition 1, bridge closed; (2) condition 2, bridge open in any position that will produce maximum stresses in any member considered.

The following cases are considered (City of Chicago criteria):

- Case I, condition 1. Dead load only with reactions at the trunnion.
- Case II, condition 1. Live load reactions at the live load support on the river pier and at the anchor column, with no allowance for dead load relieved from the trunnion.
- Case III, condition 1. Dead load plus live load with reactions at the live load support on the river pier and at the anchor column with the dead load relieved from the trunnion. Members affected by this condition may be proportioned for a unit stress 25 percent higher.
- Case IV, condition 1. Live load with reactions at the trunnion and at the anchor column for loads placed at the first two panel points of each truss, which is sufficient to cause contact at the live load support. To these stresses is added the stress due to the balance of the live load on the bridge computed as specified in Case II.
- Case V, condition 1. Shear lock load with reactions at the live load support on the river pier and at the anchor column.
- Case VI, condition 2. Dead load only with reactions at the trunnion.
- Case VII, condition 2. Wind load with reactions at the trunnion and at the rack.

For maximum effects, the foregoing cases are used in the following combinations:

- Case I alone plus 20 percent for vibrations
- Case I plus Case II
- Case I plus Case II plus Case V
- Case III
- Case I plus Case IV
- Case VI plus 20 percent vibration plus Case VII

For a typical bascule bridge the main girders of trusses frame into the trunnion girder. The entire assembly rotates about a pivot point located along the center line of the trunnion. In addition, there is a live load bearing and an anchorage as shown in Figure 5–41. This structural system rests on a pier house, and because of the various load centers of load application the pier structure is subjected to several combinations of vertical load and eccentric effects.

The following considerations are introduced in the design:

1. The center of gravity, dead load of leaf, center of gravity of counterweight, and center line of trunnion must be linear. Otherwise, when the bridge is raised, the dead load resultant force will not pass through the center line of the trunnion. Without the live load, the center of gravity of the resultant load comes through the trunnion, and the pier receives this load through the trunnion girder.
2. With live load on the leaf, the center of gravity of the combined live load and dead load moves forward and away from the trunnion (see also Figure 5–41). The live

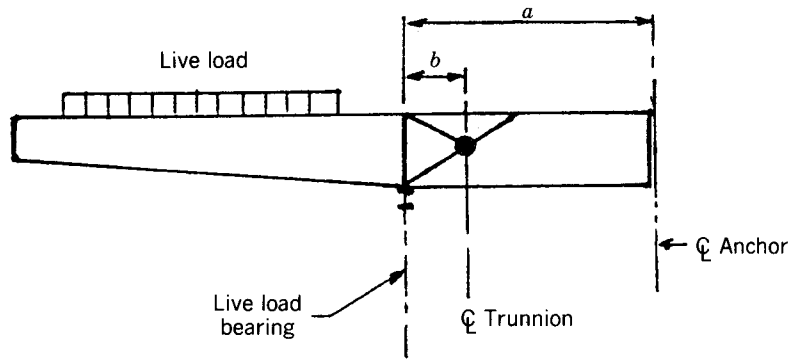

Figure 5–41 Girder and trunnion detail, bascule bridge.

load causes upward reactions at the live load bearing, and downward reactions at the trunnion, reducing the total load on the latter. For the orientation shown in Figure 5–41, the pier is subjected to a counterclockwise moment.

3. When the live load increases and becomes large enough to balance the structure over the forward support, the net load on the trunnion may approach zero. As more live load is added, the anchor column will become active, and the forward support (live load bearing) takes now the entire dead and live load plus a load equal to the negative reaction of the anchor. As the live load center of gravity moves away from the trunnion, the trunnion girder may deflect upward. The rise in the anchor bracket equals the trunnion upward deflection multiplied by the ratio a/b. At this stage the counterclockwise moment on the pier structure becomes a maximum.
4. It follows, therefore, that two cases are relevant to the design of the pier: (A) when the leaf is supported by the trunnion, and (B) when the leaf is supported on the live load bearing.
5. In determining the actual location of the center of gravity of the entire leaf, the design of the pier must consider an allowance for variations in the center of gravity of the counterweight mass by 5 to 6 percent of its vertical dimension.
6. The pier structure must have a spread base at the bottom of the anchor column to assist in engaging the desired amount of concrete as anchorage against uplift.
7. If dead load stresses vary as a result of change in position during operation, they may be increased by 20 percent to provide for the dynamic effect of the movement, but these increased stresses are not combined with live load stresses.

Guidelines for Layout of the Pier Structure.

1. The top of the pier concrete should be set at the live load bearing point. The top of the pit walls should be established with reference to the water elevation.
2. The layout of the top of the pit floor must ensure the following: (A) all parts of the movable leaf clear the top of the pit floor by at least 18 inches during opening; and (B) all parts of the movable leaf clear the inner faces of the pit walls by at least 18 inches during opening and provide enough clearance to allow erection of members for the system in the fully open position.
3. The base of anchor columns should be set at the same elevation as the top of the pit floor.

4. Channel clearance in both open and closed positions should correspond with applicable requirements.
5. Where trunnion columns are located over caissons, the bottom of the base should be at the same elevation as the bottom of the pit floor.
6. The counterweight should be sufficient to balance the bridge span with roadway and sidewalk floor and railing. However, the designer should also estimate the counterweight necessary to balance the bridge without roadway and sidewalk loads (initial lowering).
7. Foundation should preferably consist of drilled shafts supported on rock, or linear and prismatic elements.

Structural Design Provisions: Vertical Lift Spans. Piers for vertical lift spans have essentially the same design requirements as conventional piers in waterways. However, the following cases are distinguished:

Case I. Dead load, bridge open.

Case II. Dead load, bridge closed.

Case III. Dead load, bridge closed and counterweight independently supported.

Case IV. Bridge closed with live load acting.
For pier design, the following combinations of these cases may be considered:

- Case I alone plus 20 percent
- Case II plus Case III
- Case III plus Case IV

The towers and lift span, together with all lifting members except counterweight ropes, should be designed for dead load plus 20 percent. For towers supported partly or wholly by an adjacent fixed span, any live load without impact that can be placed on the supporting span beyond the warning gates should be included in the design of the supporting span.

Wind loads on the vertical lift span should be considered as in a simple fixed span.

5.6 SUPPORTS INTEGRAL WITH SUPERSTRUCTURE

In this category are (1) rigid frames with slant legs, (2) single-span rigid frame concrete bridges, and (3) delta-leg piers. These types are illustrated in Figure 1–6, and are briefly discussed in section 1.2.

Slant-Leg Bridges

As mentioned in section 1.2, the inclined frame bridge may fall within the definition of arches. The arch character in this case may be sustained by the ability of the supports to resist lateral as well as normal reaction components. The superstructure and substructure are treated as one unit with supporting legs, as shown in Figure 1–6(a). This type of construction eliminates the need for separate concrete piers while positioning the supports away from the lower roadway. The associated interaction of the inclined

legs and the superstructure girders induces indeterminancy to the third degree. The response of this system under a uniform dead load can be predicted by slope deflection or moment distribution. However, the case of movable loads requires the development of influence lines, necessitating complicated software programs and tedious solutions.

Heins and Wang (1976) have presented a study that evaluates the response of various inclined-leg bridges, and produced a series of influence line tables. These results may be utilized in the analysis of these structures.

Girder stiffness. The overall response of these bridges is particularly sensitive to the stiffness of the main superstructure girders. A study of typical girder properties by Heins and Wang (1976) resulted in the following expressions:

Bare steel:

$$\left.\begin{aligned} I_x &= \frac{(1.458L + 78.7)L^3}{1000} \\ A &= 0.01955 - 0.00028I_x + 0.0000011I^2{}_x \\ \text{Composite: } I_x &= -174450 + 9125L - 149.7L^2 + 1.08L^3 - 0.0025L^4 \end{aligned}\right\} \quad (5\text{–}59)$$

where L = end span (ft); I_x = moment of inertia (in^4); and A = cross-sectional area (in^2). Because the stiffness equations are functions of the girder spanlength L, for a given series of bridge dimensions the moment of inertia is readily established, and the corresponding area A is then calculated. These two properties determine the response to the effect of dead and live load, so that the envelopes of dead and live load moments can be obtained. Two sets of influence lines for moment, shear, and thrust (M, V, P) have been prepared and can be used directly in the analysis (Heins and Wang, 1976).

In developing the set of influence line tables, a specific range of parameters was selected. The end span L_1 is considered at intervals of 60, 80, 100, 120, and 140 feet. The interior span L_2 has corresponding lengths of 60 to 140 feet for each interval of L_1. The bridge height is set at 20 feet, which is the usual requirement for the normal vertical clearance in grade separations, with the inclined leg angle ϕ set equal to 45° and 60° for all length combinations. Table 5–7 gives a summary of these dimensions for the combinations considered in the study. In addition, a general computer program is available that develops force envelopes.

As an example, the influence line ordinate tables are arranged consistent with the point designation shown in Figure 5–42. The dimensions shown in this figure will accommodate a conventional grade separation with the lower roadway consisting of two lanes in each direction, with median and shoulders. The notation is, however, constant for all tabulated results. Spans $L_1$and L_2 are subdivided into ten divisions. The spacing between each point ID is therefore $L_1/10$ or $L_2/10$. The influence line tables are generated in the standard format so that unit loads are applied at points 2 through 10, B, 17 through 25, C, and 32 through 40. The resulting forces at the given joint locations are tabulated by Heins and Wang, 1976).

Single-Span Rigid Frame Concrete Bridges

Whether the end supports of rigid frames should be called abutments or piers is purely academic. Where reasonably unyielding foundations are easily obtainable, the rigid frame type may be an economical solution for one-span bridges. Although the design of

Table 5–7 Influence Line—Bridge Variables

L_1 (ft)	L_2 (ft)	H (ft)	ϕ (0)
60	60	20	45
60	60	20	60
60	80	20	45
60	80	20	60
80	80	20	45
80	80	20	60
60	100	20	45
60	100	20	60
80	100	20	45
80	100	20	60
100	100	20	45
100	100	20	60
60	120	20	45
60	120	20	60
80	120	20	45
80	120	20	60
100	120	20	45
100	120	20	60
120	120	20	45
120	120	20	60
60	140	20	45
60	140	20	60
80	140	20	45
80	140	20	60
100	140	20	45
100	140	20	60
120	140	20	45
120	140	20	60
140	140	20	45
140	140	20	60

a rigid frame is more complicated than that of a simply supported type, with the help of simple guidelines and sometimes computer programs a sufficiently simple and clear analysis can be carried out.

Characteristics. One-span rigid frames are structures consisting of horizontal members rigidly connected to the vertical supports. The vertical members at their lower ends must resist horizontal thrusts induced by the frame action. If the base of either vertical support is free to move horizontally, the frame becomes statically determinate.

Figure 1–6(b) shows versions of one-span rigid frames. These solutions may include configurations with articulated conditions such as (1) solid slab or rib frame with hinges at the lower ends of the supports, (2) one-span cantilever rigid frame with hinged supports, and (3) one-span rigid frame with cantilevers and fixed supports.

The structural deformation of a frame with hinged ends is shown in Figure 5–43(a). The end supports rest on footings that are free to rotate, producing the corresponding soil reactions H and V as shown.. The frame shown in Figure 5–43(b) has the base of the supports completely restrained, producing the structural determinations shown at the three reactions H, V, and M. The effect of rotation shown in Figure 5–43(c) means that the resultant V of the soil reactions becomes eccentric. If V is now applied at

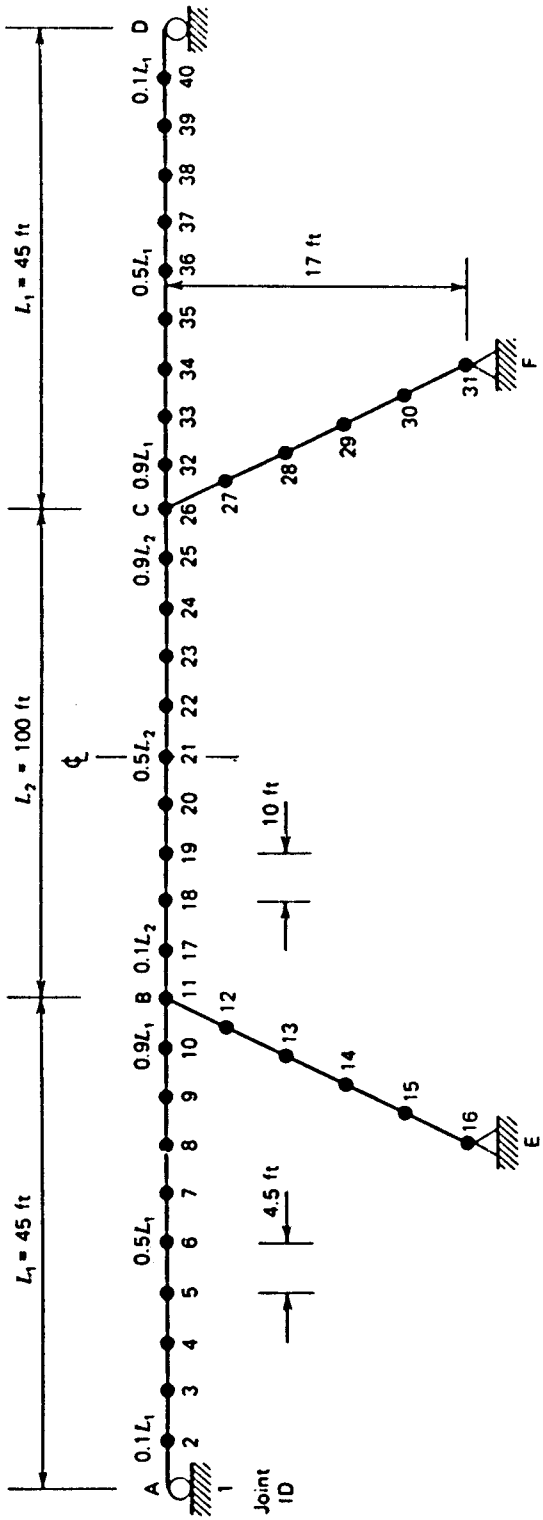

Figure 5–42 Bridge joint identifications—matrix model of bridge structure.

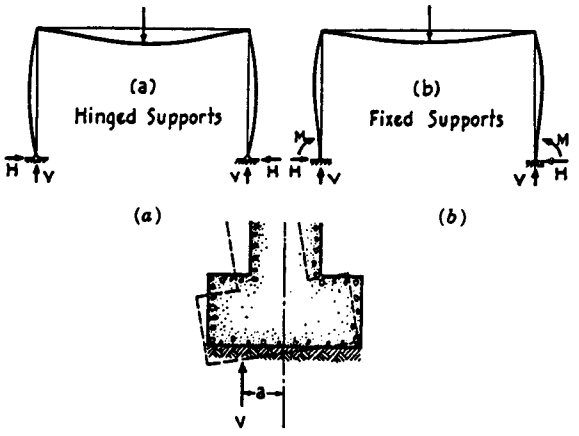

Figure 5–43 Rigid-frame bridges: (a) hinged supports; (b) fixed supports; (c) restraint offered by narrow footing.

a distance a from the midpoint as shown, the product Va is the moment that counteracts rotation and restraints the footing. However, if the soil can deflect, the footing is free to rotate and the moment at this point is zero. For most footing-soil interaction cases, the restraining moment Va is very small compared to the actual moment M corresponding to full fixity, so that the stresses in the support are only slightly affected by the restraining moment. From these comments, it follows that for ordinary frames with supports on comparatively narrow footings, the base may be assumed hinged.

Analysis. The distribution of moments, thrusts, and shears is largely controlled by the deflection of axes and the rotation of joints. A better conception and a more effective analysis is possible if we can understand the physical significance of the problem in relation to the mathematical treatment. Usually, this involves slope deflection or moment distribution methods normally covered in computer programs available in most computer libraries.

A complete analysis involves (1) correction for deck curvature, (2) frame dimensions and determination of axes and coefficients, (3) selection of frame constants that represent the end conditions, (4) earth pressure, (5) dead and live load analysis, (6) changes in length of deck and horizontal displacement, (7) dissymmetry and sidesway, and (8) estimation of moments and shears. Typically the end supports are analyzed as part of the total frame.

Hinged versus fixed ends. The design of a rigid frame with hinged ends is somewhat simpler because it has only one statically indeterminate value, namely, the horizontal thrust H in Figure 5–43(a). Conversely, a frame with fixed ends has three statically indeterminate parameters. The arrangement of vertical reinforcement in the supports of hinged frames is also simplified, whereas the effect of temperature changes, shrinkage, and uneven foundation settlement is less critical. The foundations for hinged frames are also simpler because they are not required to resist moments at the base of the supports. In some instances, it is easier to detail an effective hinge than to secure a full restraint at the ends to satisfy the condition of full fixity.

Conversely, there may be some uncertainty about the effectiveness of the bottom hinges (see also chapter 4), and fixed-end frames may in many cases be more economical. With fixed ends, there is no need for periodic inspection of the frame. Because the

degree of restraint is larger with fixed ends, it is possible to reduce the positive bending moments in both the span and the supports.

Simplified procedure. This section presents a simplified method of analysis for determining bending moments without reference to computer programs. The procedure applies to right-angle frames with hinged ends. The following two conditions are considered: (1) the moment of inertia in each member is constant, but the magnitude of the moment of inertia for the horizontal member is different from that of the vertical member; and (2) the moment of inertia in the horizontal member is variable, but constant in the two vertical members.

For rigid frames with fixed ends formulas are also given, but only for condition (1).

Experience shows that shallow haunches with lengths not exceeding 0.2 of the clear span do not materially affect the magnitude of the bending moments in the frame, so that the moment of inertia may be considered constant. Where the moment of inertia varies appreciably, the frame may be analyzed for condition (2). For straight and parabolic haunches, appropriate coefficients may be taken from tables (see also the following sections). For the vertical supports, the section properties are usually assumed the same, hence all formulas are based on constant moment of inertia.

The frame axes and theoretical length of members in frames with straight configurations and uniform member thickness coincide with straight lines drawn through the centers of gravity. Short haunches may be disregarded. When horizontal members are provided with haunches of appreciable length, the lines through the centers of gravity are composite lines that should be replaced by a straight axis so located that the areas below the axis comprised between the composite lines and the axis are about equal to the areas above the axis. The theoretical span length l of a horizontal member is measured between the center lines of the vertical supports. The theoretical height h of the vertical supports is measured from the horizontal axis to the top of the footing. When a thin footing is used, this height should be measured from the bottom of the footing. The clear height h' is the distance from the bottom of the support to the underside of the horizontal member. With haunches in the horizontal member, the underside of the member is taken at a point within the haunch where the cross section of the support has been appreciably increased by the intersection block. This adjustment is necessary because of the considerable effect of the intersection block on the vertical support.

A rigid frame bridge for typical highway intersections is usually subjected to vertical loads, temperature changes and shrinkage, and horizontal earth pressures. Where foundation conditions warrant, expected slight or differential movements of the base may also have to be provided for.

Dead loads may be considered as uniformly distributed along the span of the horizontal member. For this case, it is merely necessary to calculate the moments at the top and bottom of the vertical supports and then connect them with a straight line to obtain the bending moment diagram.

The relevant live load may consist of a lane load and concentrated loads. Bending moment diagrams for moving live loads will consist of two curves, one for positive bending moments and the other for negative bending moments. Special moment diagrams should be obtained for shrinkage and temperature changes, and for lateral earth pressures.

Position of Moving Live Load for Maximum Effects. The following guidelines may be used for positioning concentrated moving loads in one-span rigid frames to obtain maximum effects:

1. For maximum horizontal thrust and maximum negative moment at the end of the horizontal member (also top of the vertical support) the loads should be placed so that the position of the resultant coincides with the center of the span. In this respect the tandem load of Figure 2–3 may control the design for most cases.
2. For maximum positive bending moment, the loads should be placed on the span so that the position of the heavy load is on one side of the center of the span and the resultant on the other side. Also the distance of the heavy load from the center should be equal to $r(1 - 12C)/2(1 - 6C)$ where C is a frame constant as shown in subsequent sections, and r is the distance of the resultant from the nearest heavy load. This guideline is exact for frames with hinged ends, but approximate (although sufficiently accurate) for frames with fixed ends.

For a complete analysis it may be necessary to obtain maximum moments at intermediate points for moving loads, particularly for the horizontal member. In this case, for each point the most unfavorable position of loads should be selected, and this may involve time consuming and tedious effort. In lieu of this analysis, the following simplified procedure may be used: For positive moments find the maximum positive moment for the most unfavorable loading position. Then, plot this moment at the point under consideration, and draw a parabola between this point and the end of the span using the maximum moment as the maximum ordinate, as shown in Figure 5–44. For negative moment, plot at the supports above the axis the maximum value, and in the center of the span below the axis, plot one-third of the largest positive moment computed for the same position of loading. Draw a parabola between these three points. The section of this parabola above the axis may be considered as the envelope curve for the negative moments.

Hinged ends, vertical loads. Direct formulas are given for moments, shears, and thrust due to vertical loads for one-span right-angle rigid frames with hinged ends. The following notation is used:

l = theoretical span length of frame
h = theoretical height of frame
h' = clear height of frame as defined previously
y = distance of any point of vertical support above the hinge
I = constant moment of inertia of horizontal member, or minimum moment of inertia of member with variable moment of inertia
I_h = moment of inertia of vertical support
w = uniformly distributed vertical loading

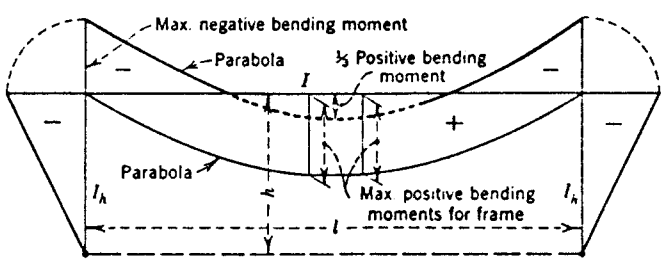

Figure 5–44 Diagrams of largest bending moments for live load.

P_1, P_2, P_3 = concentrated vertical loads (for example, HS truck)
a_1, a_2, a_3 = distances of concentrated loads from left center
H_1, H_2 = horizontal thrust at left and right hinge, respectively
H = horizontal thrust generated by vertical loading
M_{sx} = static moment at any point x
$M_{s(\max)}$ = maximum static moment
M_1 = maximum negative cantilever moment
C_1, C_2 = frame constants
α, β = constants for horizontal member with variable moment of inertia

The vertical reactions and shear diagrams for concentrated moving loads are the same as for simply supported spans.

Horizontal Thrust. This is the only statically indeterminate parameter for one-span frames with hinged ends. For vertical loads on the main span of the frame, the thrust at the left hinge acts from left to right and is negative. At the right hinge, it acts from right to left and is positive, or $H_1 = -H_2 = H$.

For uniformly distributed load (see also Figure 5–45a)

$$H = \pm\frac{l}{h}C_1 wl \tag{5–60}$$

For concentrated loads, the horizontal thrust H may be computed for single or for several loads (see also Figure 5–45b).

$$\text{Single load } P,\ H = \frac{l}{h}C_2\frac{a}{l}\left(1-\frac{a}{l}\right)P \tag{5–61}$$

$$\text{Several loads } P_i, \ldots\ldots,\ H = \frac{l}{h}C_2\Sigma\frac{a}{l}\left(1-\frac{a}{l}\right)P_i \tag{5–62}$$

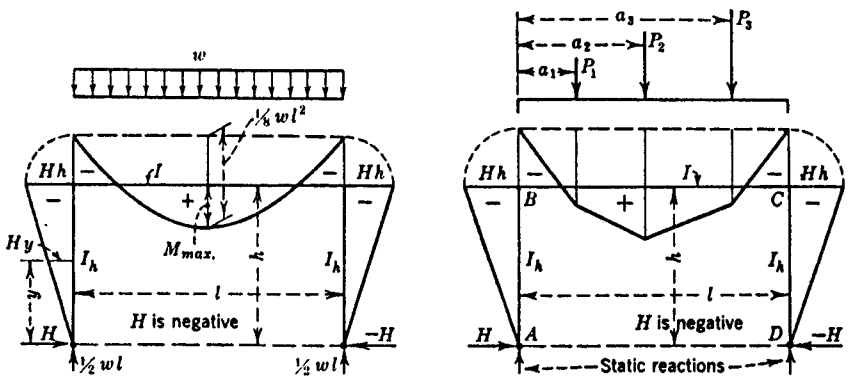

(a) *Uniformly Distributed Loading.* (b) *Concentrated Loading.*

Figure 5–45 Right-angle frame, hinged ends. Vertical loading.

Frame Constants C_1 and C_2. These are calculated for two cases: (1) moment of inertia of horizontal member constant, and (2) moment of inertia of horizontal member variable.

Case A, moment of inertia of horizontal member constant:

$$C_1 = \frac{1}{4\left[3 + 2\left(\frac{h'}{h}\right)^3\left(\frac{Ih}{I_h l}\right)\right]} \qquad C_2 = 6C_1 \tag{5–63}$$

Case B, moment of inertia of horizontal member variable:

$$C_1 = \frac{B}{4\left[2\alpha + \beta + 2\left(\frac{h^I}{h}\right)^3\left(\frac{Ih}{I_h l}\right)\right]} \qquad C_2 = 6C_1 \tag{5–64}$$

The constants α and β entering Equation (5–64) depend on the shape of the horizontal member, namely, the haunches, and on whether these are straight or parabolic. Other factors influencing the values of α and β are the ratio m of haunch to span, and the ratio of minimum to maximum moment of inertia of the horizontal span, I_c/I_s. Using the notation shown in Figure 5–46, the values of α and β may be obtained directly from Table 5–8 for straight or parabolic haunches, and different values of m and I_c/I_s. Note, however, that I_c is the minimum moment of inertia in the span, and I_s is the maximum moment of inertia at the vertical supports.

Moments for Vertical Loading. In the vertical members, the moments produced by the horizontal thrusts may be represented by a straight line as shown in Figure 5–45(a) and (b), because the moments at the hinges are zero. At any distance y, the corresponding moment is Hy, so that the maximum moment is at B, or

$$M_B = Hh. \tag{5–65}$$

For loads on the main span, the thrust H is negative (the legs of the frame tend to displace outward). Hence, it produces a negative moment at the corners of the frame, tending to reduce the positive moment in the span as shown.

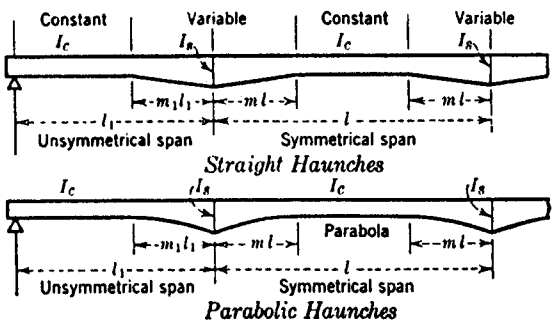

Figure 5–46 Girders with straight and parabolic haunches.

Table 5–8 Constants α and β for Spans with Symmetrical Haunches

Haunches	Constant	Ratio m	Values of $\frac{I_c}{I_s}$ 0.02	0.04	0.06	0.08	0.10	0.15	0.20	0.30	0.60	1.00
(a) Straight haunches (See Fig. 5–46 (a).)	$\alpha = \alpha'$	0.15	0.67	0.69	0.71	0.72	0.74	0.76	0.78	0.82	0.91	1.00
		0.2	0.58	0.61	0.63	0.64	0.66	0.69	0.72	0.77	0.88	1.00
		0.3	0.42	0.45	0.48	0.50	0.53	0.57	0.61	0.68	0.83	1.00
		0.4	0.27	0.32	0.35	0.38	0.41	0.46	0.51	0.59	0.79	1.00
		0.5	0.14	0.19	0.23	0.27	0.30	0.36	0.42	0.52	0.75	1.00
	β	0.15	0.91	0.92	0.92	0.93	0.93	0.94	0.95	0.96	0.98	1.00
		0.2	0.85	0.86	0.87	0.88	0.89	0.90	0.91	0.93	0.97	1.00
		0.3	0.68	0.71	0.73	0.74	0.76	0.79	0.81	0.85	0.93	1.00
		0.4	0.47	0.52	0.55	0.58	0.60	0.65	0.69	0.75	0.88	1.00
		0.5	0.23	0.30	0.35	0.39	0.42	0.49	0.55	0.64	0.84	1.00
(b) Parabolic haunches (See Fig. 5–46 (b).)	$\alpha = \alpha'$	0.15	0.74	0.76	0.78	0.79	0.80	0.82	0.84	0.87	0.94	1.00
		0.2	0.66	0.69	0.71	0.73	0.74	0.77	0.79	0.83	0.92	1.00
		0.3	0.52	0.56	0.59	0.62	0.63	0.68	0.71	0.76	0.88	1.00
		0.4	0.40	0.45	0.49	0.51	0.54	0.59	0.63	0.70	0.85	1.00
		0.5	0.29	0.35	0.39	0.42	0.45	0.51	0.56	0.64	0.82	1.00
	β	0.15	0.94	0.95	0.95	0.96	0.96	0.97	0.97	0.98	0.99	1.00
		0.2	0.90	0.91	0.92	0.93	0.93	0.94	0.95	0.96	0.98	1.00
		0.3	0.79	0.81	0.83	0.84	0.86	0.88	0.89	0.92	0.96	1.00
		0.4	0.64	0.69	0.72	0.74	0.76	0.79	0.82	0.86	0.93	1.00
		0.5	0.48	0.54	0.58	0.62	0.64	0.69	0.73	0.79	0.90	1.00

Hinged ends, horizontal pressure. The most common horizontal loads expected to act on a rigid frame bridge are braking forces, wind, and earth pressures represented by a rectangular or triangular diagram, as shown in Figure 5–47.

For horizontal forces caused by braking and wind, each hinge may be assumed to resist one-half. When earth pressures act alone, the horizontal thrusts at the hinges are again the only statically indeterminate values. For each frame, one thrust for each loading is statically indeterminate, where the thrust at the other hinge can be found from statics.

For one-sided horizontal pressures, the horizontal thrusts at both hinges act in the opposite direction with regard to the earth pressures, and their sum is the sum of all

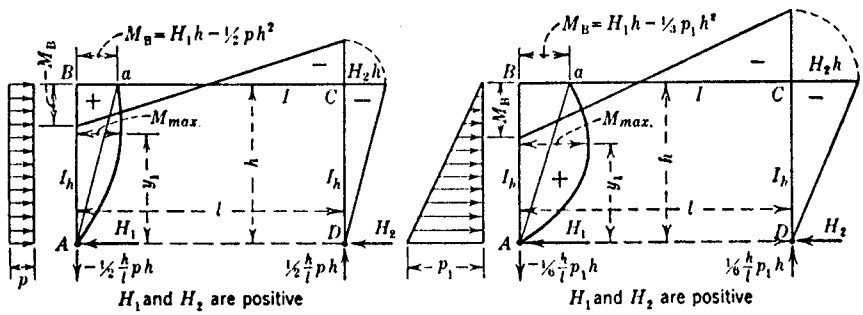

Figure 5–47 Right-angle frame; hinged ends; horizontal pressures.

horizontal pressures. For symmetrical horizontal pressures acting on both sides, the thrust at each hinge acts opposite to the direction of the pressure acting on the same leg of the frame. For these cases, three additional frame constants are introduced, denoted by C_3, C_4 and C_h.

Pressure on the Left Side of the Frame Only. Referring to Figure 5–47, when the pressure acts on one side only as shown, the horizontal thrusts are as follows:

Uniformly distributed pressure (Figure 5–47a)

$$H_1 = (1 - C_3)ph \qquad H_2 = C_3ph \tag{5–66}$$

Triangular pressure distribution (Figure 5–47b)

$$H_1 = (\frac{1}{2} - C_4)p_1h \qquad H_2 = C_4p_1h \tag{5–67}$$

Symmetrical Pressures Acting on Both Sides. Likewise, the horizontal thrusts H_1 and H_2 may be expressed in terms of the parameters C_3 and C_4

Uniformly distributed pressure

$$H_1 = -H_2 = (1 - 2C_3)ph \tag{5–68}$$

Triangular pressure distribution

$$H_1 = -H_2 = (\frac{1}{2} - 2C_4)p_1h \tag{5–69}$$

Frame Constants C_3 and C_4. As previously, these constants depend on the dimensions of the frame l and h, the moment of inertia of the frame member, and the ratio h'/h. When the depth of the intersection block is comparatively small, the ratio h'/h may be taken as 1.0.

For constant moment of inertia, and $h'/h = 1.0$,

$$C_3 = \frac{5\frac{Ih}{I_hl} + 6}{8\left(2\frac{Ih}{I_hl} + 3\right)} \qquad C_4 = \frac{0.225\frac{Ih}{I_hl} + 0.25}{2\frac{Ih}{I_hl} + 3} \tag{5–70}$$

For all other conditions

$$\left.\begin{aligned} C_3 &= \frac{1}{8}\left\{2 + \left[1 - 2\left(1 - \frac{h'}{h}\right)^2\right]\frac{C_h}{1 - C_h}\frac{1 - 8C_1}{1 - 4C_1}\right\} \\ C_4 &= \frac{1}{12}\left\{1 + 0.7\left[1 - \left(1 - \frac{h'}{h}\right)^2\right]\frac{C_h}{1 - C_h}\frac{1 - 8C_1}{1 - 4C_1}\right\} \end{aligned}\right\} \tag{5–71}$$

where C_1 is given by (5–63) for constant moment of inertia, and by (5–64) for variable moment of inertia; and

$$\frac{C_h}{1-C_h} = \frac{\left(\frac{h'}{h}\right)^2\left(3-2\frac{h'}{h}\right)}{2\left(\frac{h'}{h}\right)^3 + \frac{I_h l}{Ih}q} \tag{5–72}$$

where $q = \dfrac{2-12C_1}{1-4C_1}$ for constants moment of inertia (5–73)

$$q = \frac{2\alpha' - 4C_1(2a+\beta)}{1-4C_1} \text{ for variable moment of inertia} \tag{5–74}$$

Moments in the Vertical Supports. In the support or the frame not directly subjected to earth pressure, the moment varies as a straight line from zero at the hinge to a maximum at the top, as shown in Figure 5–47.

In the loaded leg, the bending moment diagram may be obtained as follows: Calculate the moment at the top of the loaded vertical member and plot it horizontally at the top. Then connect the point thus obtained with the bottom hinge, and consider this straight line as the closing line for the static moment diagram.

The moment at the top of the loaded leg is calculated as

$$M_B = H_1 h - \frac{1}{2}ph^2 \qquad \text{(uniform distributed pressure)} \tag{5–75}$$

$$M_B = H_1 h - \frac{1}{3}p_1 h^2 \qquad \text{(triangular distribution)} \tag{5–76}$$

The maximum positive moment in the loaded leg may be computed as follows:

Uniformly distributed pressure

$$M_{max} = \frac{1}{2}H_1 y_1 \text{ where } y_1 = H_1 / p \tag{5–77}$$

Triangular pressure distribution

$$M_{max} = H_1 y_1 - \frac{1}{2}\left(1 - \frac{1}{3}\frac{y_1}{h}\right)p_1 y_1^2 \tag{5–78}$$

where $y_1 = \left(1 - 1.41\sqrt{C_4}\right)h$ for pressure on one side

$y_1 = \left(1 - 2\sqrt{C_4}\right)h$ for symmetrical pressure on both sides

Temperature Changes and Shrinkage. The effect of temperature is analyzed for continuous bridges on multipiers in chapter 4. Changes in temperature and shrinkage likewise produce moments throughout the frame. Rise of temperature produces neg-

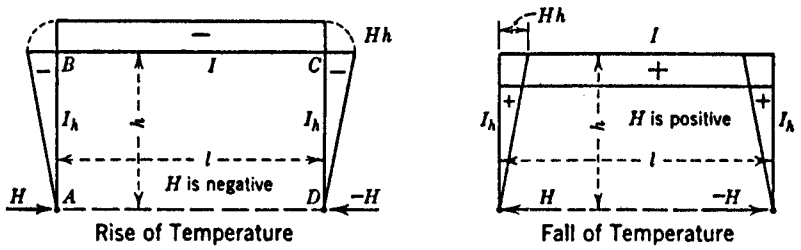

Figure 5–48 Right-angle frame, hinged ends; effect of temperature changes.

ative moments, whereas temperature fall and shrinkage cause positive moments. For practical purposes the effect of shrinkage may be assumed to be equivalent to a temperature fall of 15°F. The moment diagrams are as shown in Figure 5–48.

The only statically indeterminate value is the horizontal thrust which may be calculated as

$$H = -2C_2\alpha E t\frac{I}{h^2} \text{ (temperature rise)} \tag{5–79}$$

$$H = +2C_2\alpha E t\frac{I}{h^2} \text{ (temperature fall)} \tag{5–80}$$

where α= coefficient of thermal expansion, t = temperature change, and E = modulus of elasticity of concrete.

REFERENCES

AASTHTO, 1989: Guide Specifications for Design and Construction of Segmental Concrete Bridges.

AASHTO, 1994: AASHTO LRFD Bridge Design Specifications.

ASCE, 1977: "Tentative Recommendations for Cable-Stayed Bridge Structures," *ASCE Task Committee on Cable-Suspended Structures, J. Struct. Div.*, ASCE vol. 103, No. ST5, May.

ASCE, 1988: "Bibliography and Data on Cable-Stayed Bridges," *ASCE Committee on Long-Span Steel Bridges, J. Struct. Div., ASCE*, vol. 103, No. ST10, October.

ASCE, 1991: "Guidelines for Design of Cable-Stayed Bridges," *ASCE Committee on Cable-Suspended Bridges*, ASCE, New York.

FELGE, A., 1966: "Evaluation of German Cable-Stayed Bridges," Acier-Stahl-Steel, vol. 31, No. 12, December, pp. 523–532.

HASELER, E., 1900: Eiserne Brucken, Vieweg Publ.

HEINS, C. P., and R. Wang, 1976: "Influence Lines for Slant Legged Rigid Frame Highway Bridges," *Civ. Eng. Report*, Univ. of Maryland, College Park, Maryland, June.

KANE, T. A., T. F. MAHONEY, and J. H. CLARK, 1990: "West Seattle Swing Bridge," *Trans. Research Record 1275*, TRB National Research Council, Washington, D.C., pp. 62–66.

KAVANAGH, T. C., 1973: "Historical Development of Cable-Stayed Bridges," *ASCE Struct. Journ.*, ASCE vol. 99, No. ST7, July, pp. 1669–1672.

KAVANAGH, T. C., 1972: "Cable Supported Bridges," *Structural Steel Designers' Handbook*, F.S. Merritt, ed., McGraw-Hill Book Co., New York, Section 14.

KINNIER, H. L., and F. W. BARTON, 1975: "A Study of a Rigid Frame Highway Bridge in Virginia," *Virginia Highway and Transportation Research Council,* Dept. of Highways, Charlottesville, Virginia, April, VHTRC 75-R47.

LEONHARDT, F., and W. ZELLNER, 1972: "Comparative Investigations Between Suspension Bridges and Cable-Stayed Bridges for Spans Exceeding 600 m," (in German). Publications, *International Association for Bridge and Structural Engineering,* vol. 32-1, pp. 127–165.

MATHIVAT, J., 1966: "Reconstruction du pont de Choisy-le-Roi," Travaux, Janvier, No. 372.

MATHIVAT, J., 1974: "Structures de piles adaptees a la construction par encorbellement," Problems speciaux d'etude et d'execution des overages, Journees A.F.P.C., Avril 22–23.

PODOLNY, W., and J. M. MULLER, 1982: *Construction and Design of Prestressed Concrete Segmental Bridges*, Wiley, New York.

MEHRTENS, G. C., Eisenbruckenbau, Engelmann Publ., 3 vols., 1908.

"Moses Advocates Bridge Over Long Island Sound," *Civ. Eng.*, ASCE, vol. 35, No. 4, April, 1965, p. 95.

PODOLNY, W. and J. B. SCALZI, 1986: *Construction and Design of Cable-Stayed Bridges,* Wiley, New York.

SMITH, B. S., 1967: "The Single Plane Cable-Stayed Girder Bridges: A Method of Analysis Suitable for Computer Use," *Institution Civ. Eng.,* London, Paper No. 7011, November.

SMITH, B. S., 1968: "A Linear Method for Analysis for Double-Plane Cable-Stayed Girder Bridges," *Proc. Inst. of Civ. Eng.* January.

TANG, M. C., 1976: "Buckling of Cable-Stayed Girder Bridges," *J. Struct. Div. ASCE*, vol. 102, No. ST9, September.

THUL, H., 1972: "Developments in German Cable-Stayed Bridges," (in German), Der Stablbau, vol. 41, No. 6, June, pp. 161-171; vol. 41, No. 7, July, pp. 204–215.

XANTHAKOS, P. P., 1973: "Columbus Drive Bascule Bridge, Chicago," *Struct. Design,* In House Report.

XANTHAKOS, P. P., 1994: *Theory and Design of Bridges,* Wiley, New York.

CHAPTER 6

Wall Systems

6.1 DIAPHRAGM WALLS IN TRAFFIC UNDERPASSES

Diaphragm (slurry) walls can be used in traffic underpasses as abutment walls to support the superstructure loads and transfer them to the soil, and as ground support systems at the approaches. These uses imply two possible configurations: as load bearing elements and as retention systems.

This subject is covered in three references by Xanthakos (1974; 1979; 1994b). The first two deal with processes, applications, and engineering fundamentals of the slurry wall technique. The last publication focuses on structural uses and design requirements for major classes of structures and load-bearing elements. Although this practice covers a long period of development, the early practical problems associated with the interaction of design and construction have not changed. The associated requirements suggest an explicit interdependence of the design and construction methods that is far greater than routinely assumed in most types of construction. Thus, several areas of uncertainty must be answered qualitatively and quantitatively in the design stage by adopting proper design criteria and quality controls, and by specifying the construction procedures.

Conventional Diaphragm Walls

A conventional diaphragm wall is the structural system shown in Figure 6–1. The factors dictating panel size and dimensions depend on site conditions. A desired panel length sometimes cannot be provided in the field because of restrictions on availability of construction space and time.

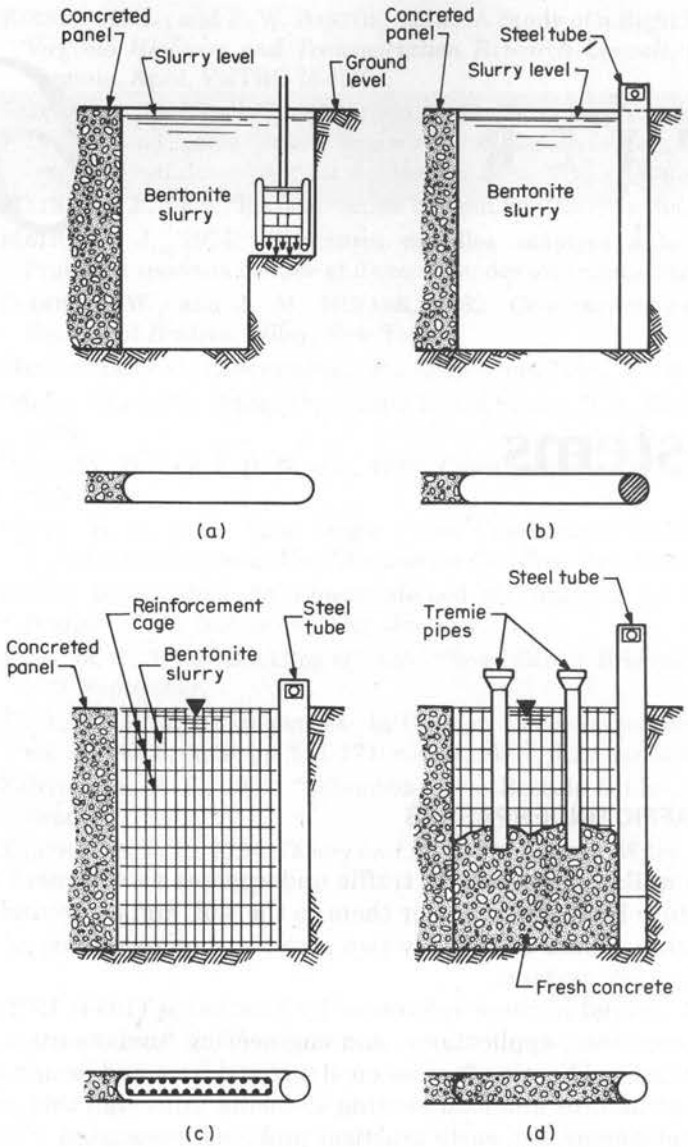

Figure 6–1 Typical construction sequence of a diaphragm wall, executed in four stages: (a) excavation, (b) insertion of steel tubing, (c) placement of reinforcement cage, (d) concrete placement.

Although it is advantageous to construct a wall in longer units, panel length is also governed by factors related to trench stability, concreting requirements, lifting and handling capability of available equipment, type and location of lateral bracing, and incidental factors such as delivery and supply of fresh concrete, storage facilities, and water supply.

The panel depth for conventional underpasses is determined solely by design and project requirements. A wall may be founded on rock or other firm material to transfer vertical load; it may be extended into an impervious layer to cut off underground water

flow; or it may be embedded below excavation level for lateral stability and control of movement.

The panel width (wall thickness) for the usual applications has a typical range from 18 to 30 inches (45 to 75 cm), and this will satisfy both the structural requirements and the excavation width of most types of equipment. The lower range (18 inches) is also considered a practical minimum width to allow the passage of tremie pipes within the reinforcing steel cage. A thinner wall produces materials savings, but is not necessarily the most economical design, especially if it must be heavily reinforced. The panel thickness should also be considered in relation to tolerances and protrusions in the finished wall, particularly for deeper than normal construction.

Panel sequence. For construction along streets, traffic may dictate the construction procedure. For continuous walls for an underpass, a suitable panel sequence is shown in Figure 6–2. This sequence will allow relatively free and the least restricted flow of traffic, while the work can proceed simultaneously on three successive panels as shown. As one panel is excavated, a second panel is prepared and a third is completed.

Anchored Walls

Anchored diaphragm walls in cuts for traffic underpasses can be used where the depth of the excavation exceeds the economic range of free cantilevers. In this case the anchors serve as permanent bracing, and hence one of the design requirements is protection against corrosion. Depending on anchor spacing, a usual anchor capacity range is between 45 and 200 kips (200 to 900 kN).

Anchors cannot be installed if major obstructions, such as utility lines and incidental underground structures, exist. In some instances there may be specific statutory re-

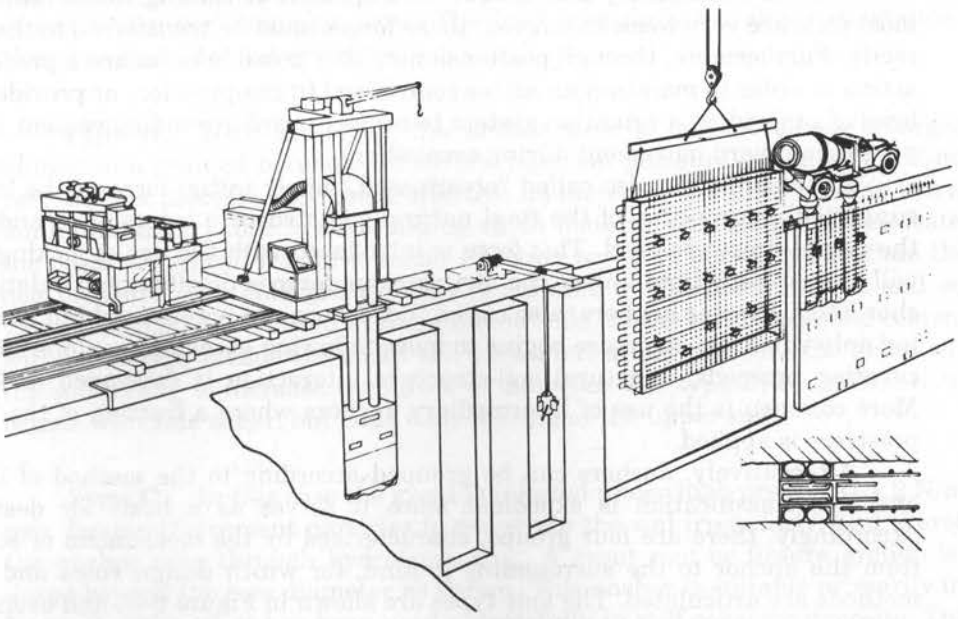

Figure 6–2 Typical panel installation and construction sequence.

quirements to be met, or the adjoining owner may have the right of support and refuse an easement. Since in most instances the installation will be permanent, it should be carried out under the implied guarantee that future activities will not impair, damage, or otherwise interfere with the system.

Compatibility with ground engineering problems. In terms of anchor response to loading, the method may be regarded as a special application of prestressing in foundation and ground work. Anchorages can thus be grouped into three main categories in terms of ground terminology and according to the geology and topography of the site: (1) soil anchors, covering 70 to 80 percent of the market; (2) rock anchors, representing 10 to 20 percent of applications; and (3) marine anchors, also installed in fluvial environments or aggressive water, accounting for about 10 percent of the market.

The clear predominance of soil anchors indicates the frequency of soil substratum in the majority of urban and industrial excavations, consisting mostly of alluvium, silty sand, and clay. Among the most common and frequent uses are as support retention systems in excavations, and as stabilizing systems for foundation slabs subjected to uplift caused by groundwater or heave.

AASHTO (1992 addition) includes anchored walls in the list of retaining walls for transportation structures for either temporary or permanent installations in either soil or rock, but does not give design guidelines. A complete and recent review of ground anchors and anchored structures is provided by Xanthakos (1991) and includes design methodologies, corrosion protection, and acceptance criteria.

Transfer of load. In a broad sense, anchors are used to mobilize the shear strength, and often the passive resistance of a soil. Anchors can thus receive earth loads acting on the structure—for example, a retaining wall—and transfer these loads back to the ground. Likewise, tensile forces can exist at the foundation of a modern structure as a result of the redundancy and unique arrangement of loading combinations, and since most soils are very weak in tension, these forces must be transferred to the ground indirectly. Furthermore, through posttensioning it is possible to induce a predetermined reaction in order to maintain an active zone of soil in compression, or provide the required level of preload on a retention system to cause inward ground movement that will compensate outward movement during excavation.

Active anchors, also called "prestressed," apply initial force to the structure thus supported, irrespective of the final natural soil-structure interaction, and according to the actual prestress level. This force is introduced with the use of jacking devices, and will persist with time unless the structure undergoes displacement relative to the anchor itself. Passive anchors, also called "dead," are not prestressed but respond to loading only when the structure begins to move following excavation on one side. As the excavation proceeds, a natural soil-structure interaction is developed and maintained. More common is the use of intermediary anchors where a fraction of the full potential prestress is applied.

Alternatively, anchors can be grouped according to the method of load transfer, and this classification is expedient since it serves as a basis for design methods. Accordingly, there are four groups, characterized by the mechanism of stress transfer from the anchor to the surrounding ground, for which design rules and construction methods are articulated. The four types are shown in Figure 6–3, and even though each type is more suitable under specific ground conditions, the choice is often dictated on a regional basis.

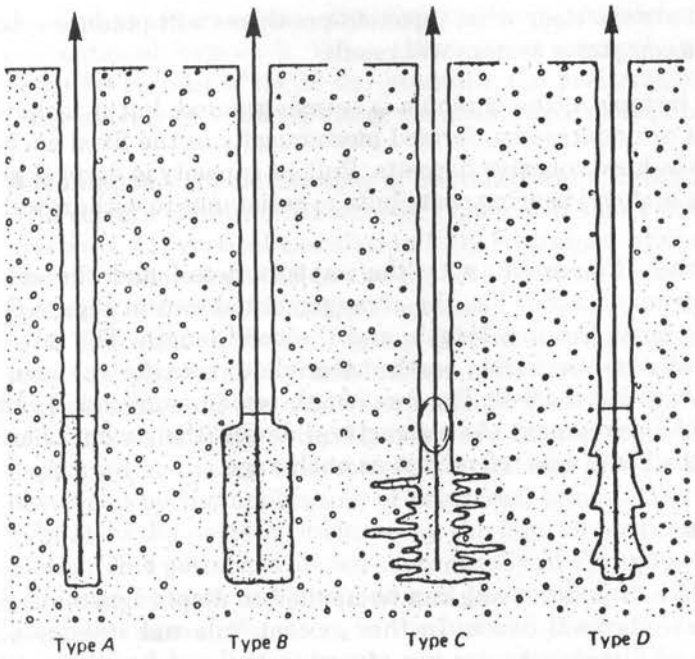

Figure 6–3 Anchor grouping according to the method of load transfer. Four types of fixed anchor zone for grout injection anchors.

Type A. This is characterized by a tremie-grouted straight shaft cylindrical hole of a uniform diameter, which may be lined or unlined according to the requirements of hole stability. This type is suitable in rock as well as in very stiff-to-hard cohesive layers where it is most commonly used. The load transfer is by shear resistance mobilized along the ground-grout interface.

Type B. With this type, the anchor zone is created as an enlarged cylinder formed in a grouted borehole under low injection pressure (usually < 1 N/mm^2 or 145 psi). In this process, the actual effective diameter of the fixed zone is increased with minimum disturbance to surrounding earth materials as the grout permeates through the pores or natural fractures under injection pressure normally less than the overburden pressure. The enlarged cylinder is suitable in soft fissured rock and coarse alluvium, but may also be used in fine-grained soils. In the latter case, the cement particles will not always invade the small soil pores, but under pressure the grout will compact the soil locally to increase the effective diameter. For type B, resistance to withdrawal begins with side shear, but ends with bearing at the upper end.

Type C. In this case the grout is injected under high pressure (> 2 N/mm^2 or 290 psi), forcing the cement particles to penetrate the soil irregularly, and thereby enlarge the anchor zone through hydrofracturing. A grout root or fissure system is thus produced beyond the core diameter as shown. This anchor is suitable primarily in cohesionless soil, although it has been used successfully in stiff cohesive deposits. The design is based on an assumed uniform shear along an appropriate diameter at the designated

fixed zone. It is not always clear what injection pressures will produce type B or C, and in many instances a composite system will result.

Type D. As in type A, the borehole is tremie-grouted, but it includes a series of enlargements (bells or underreams) formed mechanically in the fixed anchor zone. This type is used in stiff-to-hard cohesive deposits. Pullout capacity is derived primarily from side shear, but plug and end bearing contribute to resistance to withdrawal.

Anchor components. Consistent with the support detail and the method of load transfer, a typical ground anchor has the arrangement shown in Figure 6–4. The basic components are the head, the free length, and the bond length. The latter is the fixed zone interacting with the enveloping earth materials to transfer the load according to the four types shown in Figure 6–3. The free length remains unbonded and thus free to move within the soil environment. As a structural device, the anchor is attached to the ground support at the head, also referred to as anchorage.

Posttensioned Diaphragm Walls

The general principles of prestressing can be applied to diaphragm walls mainly to extend their effective (unbraced) depth. In this concept, internal stresses of a predetermined magnitude and distribution are introduced in the concrete that will partially or wholly counteract and balance the tensile stresses expected to occur in service from external loads (mainly the lateral earth pressures). From this principle the criterion of no tensile stresses in the concrete becomes relevant. This suggests that if there are no tensile stresses in the concrete, there can be no cracks, so that the concrete is no longer a brittle material but becomes an elastic support.

A common procedure is to posttension high-strength wire strands, properly located in the panel, after the concrete has cured. An associated advantage is the increase in the stiffness of the section and the subsequent decrease in elastic deflection, with a corresponding extension of the unbraced depth.

Construction and installation of posttensioned walls is reviewed by Xanthakos (1979, 1994b). When the diaphragm wall is completed, a separate capping beam that is

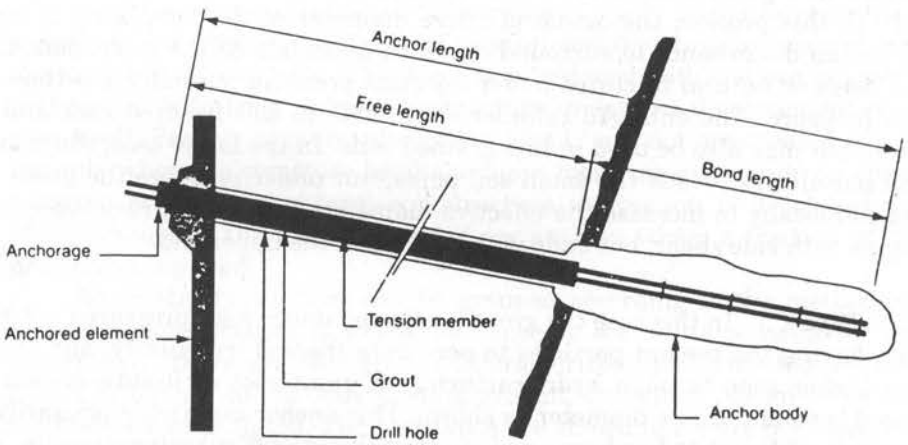

Figure 6–4 Schematic presentation of a ground anchor showing the three main components: anchorage (anchor head), free length, and fixed length (bond length).

detailed to accommodate the size and configuration of an abutment seat is placed in conventional formwork. When the concrete strength in the capping beam has reached about 80 percent of its 28-day strength, the posttensioning is introduced and continues progressively by working along the anchorages of each panel.

Advantages. The advantages of unbraced walls through posttensioning become obvious with certain classes of structures. Figure 6–5 shows two categories of walls suitable for prestress: (1) vertical cantilevers fully restrained at the base by sufficient embedment; and (2) walls supported at the top and bottom. These types are shown with the corresponding lateral earth stress diagrams.

The walls in the first group depend on an adequate embedment below excavation level to ensure stability and balance active and passive pressures, and also to limit lateral movement. Free cantilevers should therefore be used primarily in stiff or dense soil. The walls of the second group have the top braced, and are therefore beams simply supported at the top and bottom The pattern of wall deflection and stress distribution developed by the application of prestress, prior to any excavation, must be essentially similar to the pattern produced by the lateral earth pressure with the excavation completed. This pattern is shown conceptually in Figure 6–5 next to the walls, and may also take into account any preloading of the top bracing. Only the magnitude and at some point the sign of the curve in the moment diagram will change as the excavation progresses and bending moments are introduced by the action of the lateral earth pressures. The two conditions for which the wall must be analyzed are the initial phase of prestress with the wall fully embedded and the final stage with the full excavation completed. Walls that can provide this compatibility are, therefore, ideally suited to posttensioning.

Diaphragm walls in traffic underpasses conform to the requirements of posttensioned walls. At the bridge structure the walls are designed to function as integral abutments so that the superstructure supports the walls laterally at the top. At the bottom the walls are likewise laterally braced by embedment or by the roadway slab if sufficient stiffness is available. In the approach sections the wall height is usually within the optimum range of free cantilevers or walls anchored near the top.

Prefabricated Diaphragm Walls

Prefabricated concrete panels inserted in slurry trenches to form structural retaining systems were introduced in Europe in the early 1970s. The process can be visualized as the combined result of two foundation types: the prefabricated interlocking pile and the

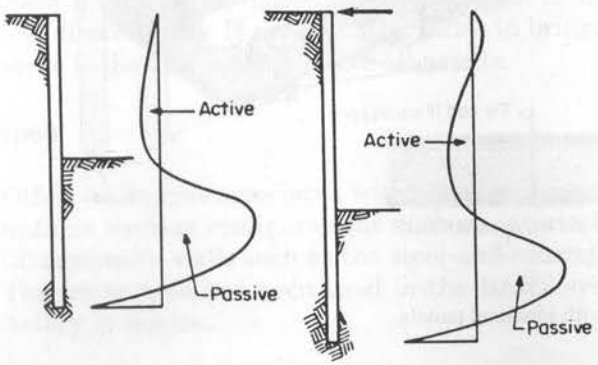

Figure 6–5 Walls suitable for posttensioning and patterns of lateral-earth-stress distribution.

sheet pile wall. The trench is likewise excavated under slurry, but the in situ tremie placement of concrete is replaced by the insertion of precast panels. Guide walls must be detailed according to the size and weight of the panels, since they must hold these sections until the wall becomes self-supported.

Grout systems must provide various functions in the initial slurry and in the final wall configuration. Thus the system must ensure trench stability, and also serve as an effective bonding and sealing agent between adjacent panels. Suitable systems include the single grout, and the so-called displacement grout (see Xanthakos, 1979; 1994b).

Panel type and configuration. Prefabricated panels are of conventional nonprestressed reinforced concrete. Conceivable variations are hollow panels or sections made with lightweight aggregate. Prestressing has been tried, but its practicality is yet to be established. Limitations on panel size are imposed by crane and hoisting capabilities, and a usual maximum weight for a single panel is 20 tons.

There has been a tendency to standardize panel size and configuration, prompted by economic motives, to ensure uniform installation details. Figure 6–6 shows typical panels that slot together. This interlocking ensures rigidity and produces a smooth wall. A second type, shown in Figure 6–7, has alternate beam and slab sections, with the beam usually twice as thick as the slab. Walls with identical panels are more suitable for grade separation structures because of the combinations of vertical and lateral loads.

Installation. For conventional traffic underpasses, the required panel length for lateral stability, geometry, and load transfer is well within the practical range. Standard details include fitting and lifting hooks for handling and positioning. The exposed face is

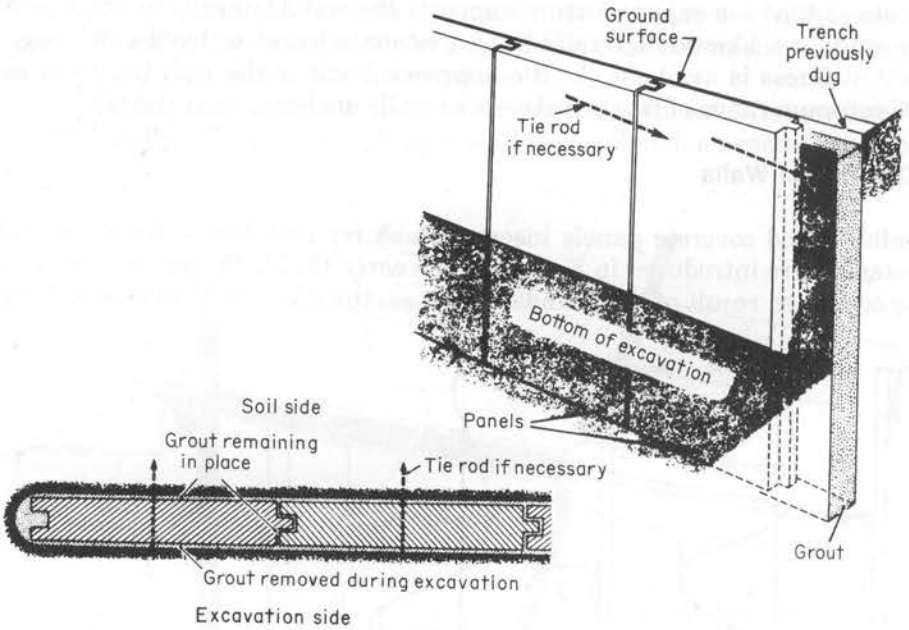

Figure 6–6 Prefabricated wall with identical panels.

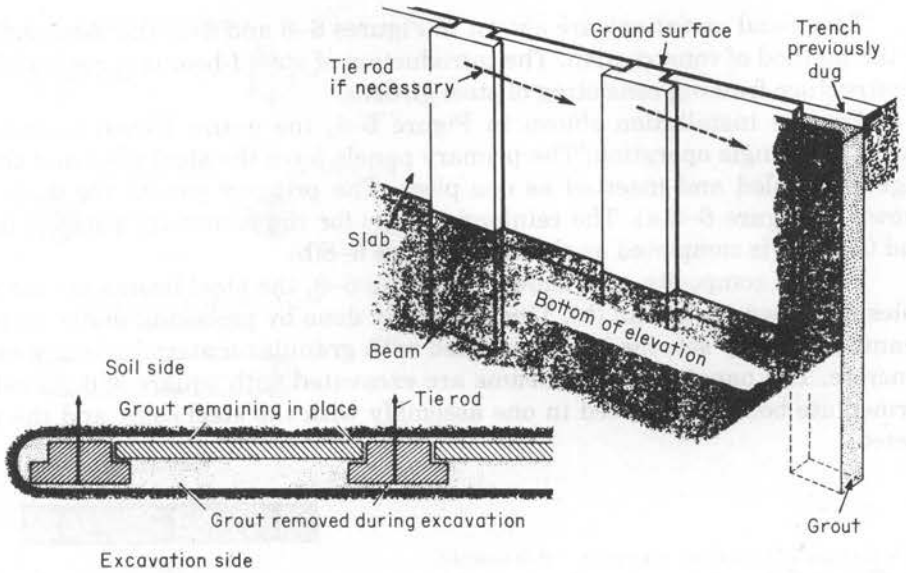

Figure 6–7 Prefabricated wall with beam-and-slab panels.

coated with a special compound to facilitate removal of any grout that may adhere to the concrete.

A casting yard usually must be provided at or near the construction site to accommodate at least the number of panels expected to be installed per day. For average job sites, a usual practice is to schedule the installation of three panels per day using one excavating machine and one crane.

The panels are lifted and held vertically, and then they are slowly inserted into the trench, normally excavated wider. This overwidth allows the grout to surround the precast sections completely. The sections are checked for alignment, disengaged from the crane, and held in position by special devices bearing on guide walls. This support is maintained until the grout has hardened enough to be integrated with the panels.

Advantages and disadvantages. Prefabricated walls have all the advantages inherent in precasting. The exposed wall has satisfactory appearance and smooth face, and is thus ideal for applications where exposure to public view is a construction feature.

However, the installation procedures must provide for the careful planning and strict adherence to schedule; the minimum job size necessary to offset certain fixed costs inherent in precasting; and the lack of horizontal continuity across panels. The last disadvantage is not a serious factor in bridge underpasses since a capping beam can serve to distribute the loads to all panels.

Other Wall Types

Other wall types associated with the slurry method are (1) bored pile walls, that can be built in various configurations such as interlocking, contiguous, and intermittent; and (2) composite walls such as the steel-and-concrete panels also referred to as SPTC walls. The latter type has been used in the BART system, and is considered for the Central Artery in Boston.

Two usual variations are shown in Figures 6–8 and 6–9, the main difference being in the method of construction. The introduction of steel I-beams is compatible with a superstructure framing consisting of steel girders.

For the installation shown in Figure 6–8, the entire trench is excavated under slurry in a single operation. The primary panels have the steel piles and the reinforcing cage assembled and inserted as one piece. The primary panels are then concreted as shown in Figure 6–8(a). The reinforcing cage for the secondary panel is inserted next, and the wall is completed as shown in Figure 6–8(b).

For the composite wall shown in Figure 6–9, the steel beams are set in predrilled holes as shown in (a) and (b). This is usually done by preboring under slurry. After the beams are firmly set, the holes are filled with granular material to block escaping fresh concrete. The panels between beams are excavated with square-end clamshells, the intermediate beam is inserted in one assembly with the steel cage, and the panel is concreted.

Applications

Traffic underpasses and underground motorways are usually constructed in congested metropolitan areas where a main problem is competition for construction space where space hardly exists. The scarcity of space excludes the opportunity to expand the public right-of-way, and this complicates construction further particularly with the presence of streets and utilities above and below grade.

However, motorways have the advantage of regular configuration and section geometry, and usually are depressed at congested intersections or at grade separations with minimum clearance to accommodate design requirements. The use of diaphragm walls results in several benefits, summarized as follows: (1) reduced disruption of surface activities including traffic during construction; (2) integration of the temporary and permanent ground support; and (3) the use of diaphragm walls as both substructure and foundation elements.

Construction with cast-in-place walls. The four-lane roadway with safety walls has been adopted in most regions of the United States and is also popular abroad. It may require from 50 to 60 feet (15 to 18 m) face-to-face of walls. For the usual vertical clear-

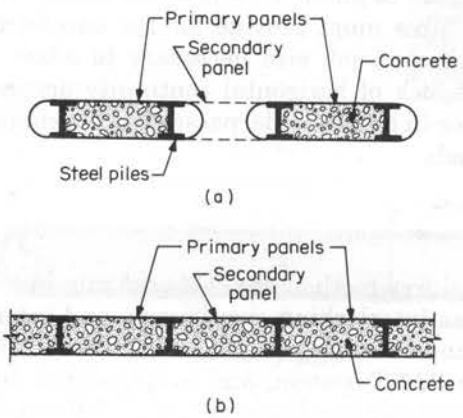

Figure 6–8 Typical composite wall: (a) outline of excavated panels; (b) finished wall.

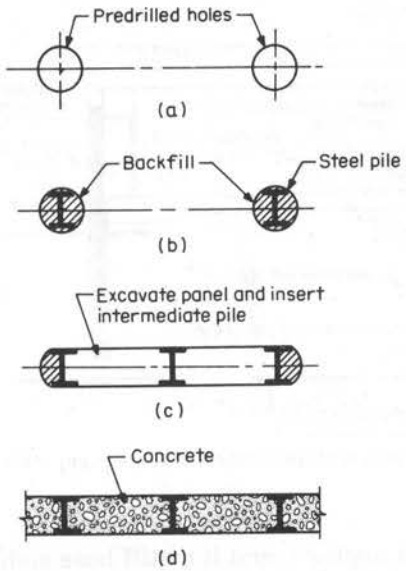

Figure 6–9 Alternate construction method of composite wall.

ance, the depth of excavation from street level to the underside of the base slab is of the order of 19 to 20 feet.

In the covered (bridge) portion the superstructure deck can brace the walls laterally at the top, as shown in Figure 6–10(a). This deck is normally constructed before general excavation so that all earth moving is done while the street is open to traffic. Since thermal movement is restrained by the wall, although not stopped, the design must accommodate internal stresses for both the superstructure and the walls. At the bottom, the walls are laterally braced by sufficient embedment or by the base slab if the latter is rigid.

In the open segment the walls must be checked for probable movement regardless of embedment. This movement can be partly stopped and controlled if some bracing is

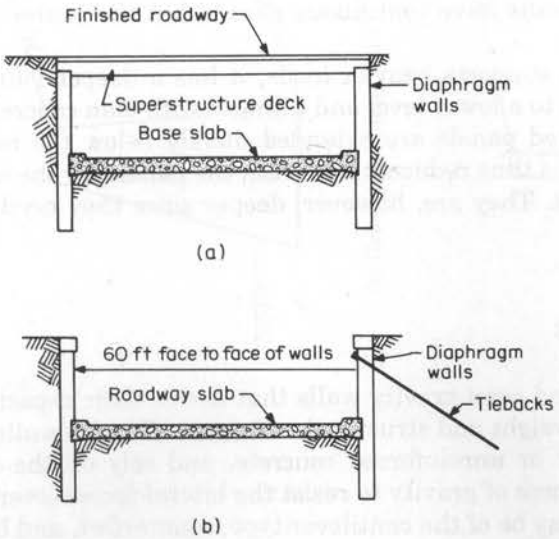

Figure 6–10 Diaphragm walls for traffic underpass: (a) Covered section. (b) Uncovered section for approach roadway.

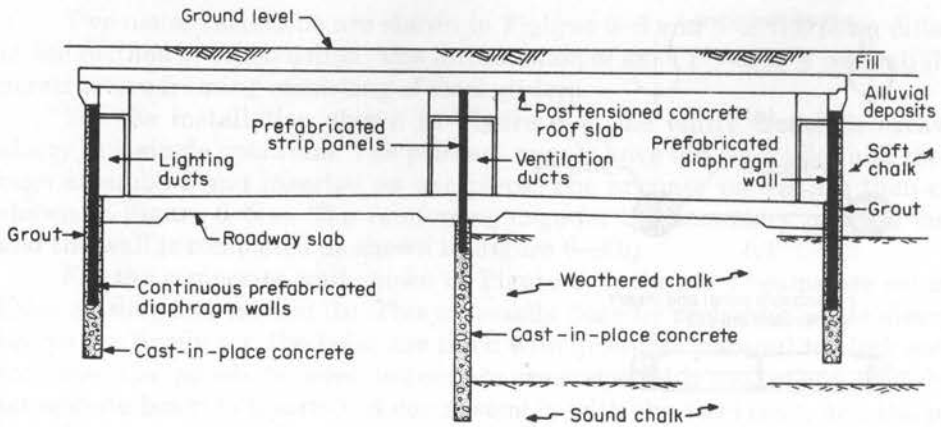

Figure 6–11 Cross section of a covered motorway built with prefabricated diaphragm walls *(from Leonard, 1974.)*

provided near the top, usually with ground anchors, and if a stiff base slab is placed as soon as the excavation reaches the intended depth, as shown in Figure 6–10.

Since the walls are exposed to public view, face treatment is mandatory. The choice includes precast panels, brick facing, or a separate concrete wall. Complete joint waterproofing at panel connection is often debated, the alternative being to provide drainage channels conveying seeping water to a sump.

A center wall can be considered for very wide roadways. This wall may be continuous or intermittent, and is usually built from ground level. Because it receives more loads than the outside (end) walls, it may have to be deeper for adequate bearing. If the bridge is designed as an integral structure, the center wall will be subjected to smaller longitudinal loads. Strip panels capped with a continuous beam will satisfy these requirements.

Construction with prefabricated panels. As mentioned, the advantages of precast walls are applicable to traffic underpasses. Figure 6–11 shows a typical section for a depressed motorway. The end walls have continuous panels, but the center support consists of strip sections.

Because the center wall supports heavier loads, it has a deeper foundation, provided by extending the trench to a lower level and filling it with lean concrete. With this configuration, the prefabricated panels are extended merely below the roadway slab, and their total length (depth) is thus reduced. Likewise, the panels for the end walls are set in lean concrete and grout. They are, however, deeper since they need embedment for lateral stability.

6.2 GRAVITY AND SEMI-GRAVITY WALLS

This group includes gravity and semi-gravity walls that derive their capacity from successful combinations of dead weight and structural resistance. Gravity walls are usually constructed of stone masonry or unreinforced concrete, and rely on the mass of the structure combined with the force of gravity to resist the lateral forces (overturning and sliding). Semi-gravity walls may be of the cantilever type, counterfort, and buttress con-

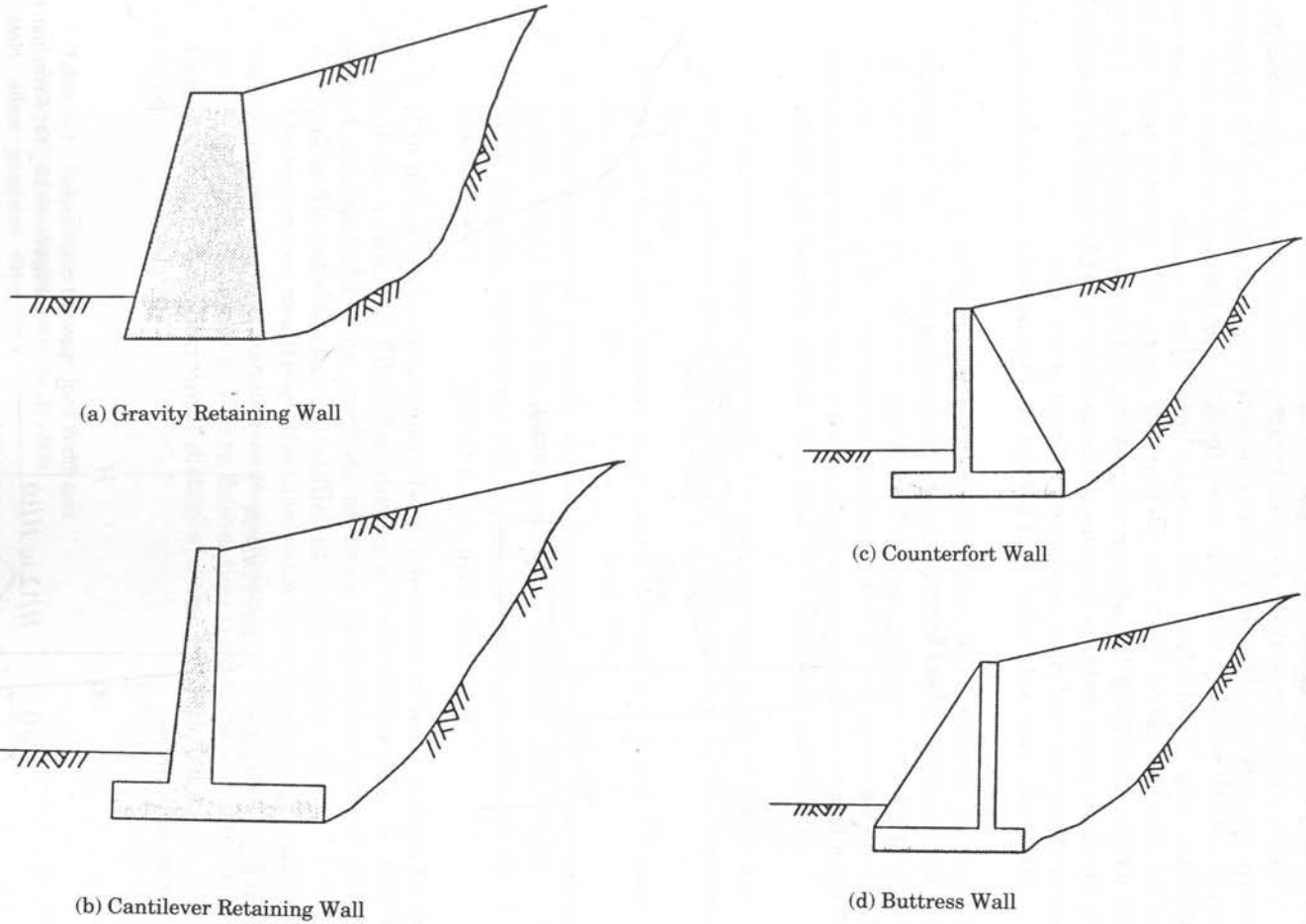

(a) Gravity Retaining Wall

(b) Cantilever Retaining Wall

(c) Counterfort Wall

(d) Buttress Wall

Figure 6–12 Typical gravity and semi-gravity walls; (a) gravity wall; (b) semi-gravity retaining wall; (c) semi-gravity counterfort wall; (d) semi-gravity buttress wall.

figuration, normally constructed of reinforced concrete. These walls resist the lateral forces by structural action such as flexural, compressive, and shear strength. Several wall configurations are shown in Figure 6–12.

These wall types may be used for bridge substructures or grade separations in permanent applications. The counterfort and buttress walls are used for high cantilevers to provide overall stability while the stem thickness is reduced without excessive outward deflection. The counterfort wall accepts more dead weight, but the resultant has a smaller distance (arm) from the overturning point. The buttress wall has less overall dead weight balancing the overturning moment, but its arm is larger. The counterfort wall provides more stability because of the greater weight. The final choice will also depend on geometry and final conditions in front of the wall.

The cantilever retaining wall shown in Figure 6–13 is also a semi-gravity type.

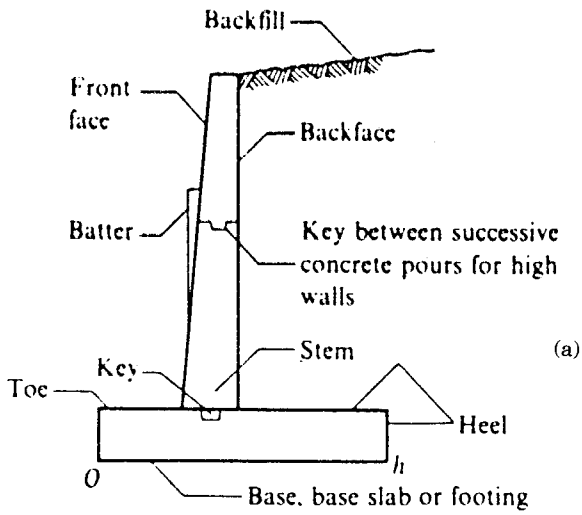

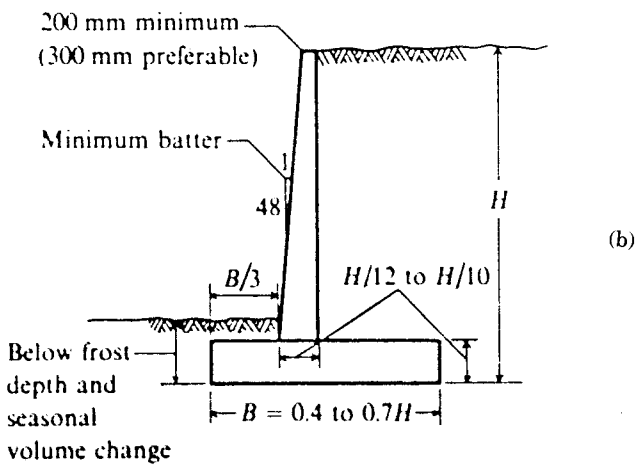

Figure 6–13 (a) Principal terms used with retaining walls. Note that "toe" refers to both point *O* and the distance from front face of stem; similarly "heel" is point *h* or distance from backface of stem to *h*. (b) Tentative design dimensions for a cantilever retaining wall. Batter is optional.

This wall has principal uses at present, particularly for low walls of fairly short length, and where the backfill zone is limited and it is necessary to use existing soil as backfill. Figure 6–13(a) identifies the components and terms used in wall design, and Figure 6–13(b) suggests common dimensions of a cantilever wall to be used for preliminary designs as first trial. These guidelines are based mainly on experience and refer to walls designed using the Rankine criteria.

6.3 MECHANICALLY STABILIZED EARTH WALLS AND PREFABRICATED MODULAR WALLS

Mechanically Stabilized Earth Walls

Mechanically stabilized earth walls (MSE) may be considered where conventional gravity, cantilever, or counterforted walls are structurally feasible, but substantial total and differential settlements are anticipated. These systems, usually proprietary, employ either metallic or polymeric tensile reinforcement in the soil mass, and a discrete modular precast concrete facing that is vertical or near vertical (see also Figure 1–13).

MSE walls should not be used under the following conditions:

1. Where two intersecting walls form an enclosed angle of 70° or less.
2. Where utilities other than highway drainage must be constructed within the reinforced zone.
3. Where flood plain erosion may undermine the reinforced fill zone, or any supporting footing.
4. When galvanized metallic reinforcement is exposed to surface or ground water contaminated by acid mine drainage or other industrial pollutants.
5. With metallic reinforcements subject to stray ground currents within 200 feet of the structure.

The potential for catastrophic failure because of scour is high for MSE walls, especially if the reinforced fill is lost during a scour occurrence. In this case, the design should consider alternate methods of scour protection such as sheet pile walls and riprap of sufficient size placed to sufficient depth to deter scour.

Under service conditions, the maximum slope (limiting tolerable differential settlement) for systems with panels less than 30 feet and with a minimum joint width 1/4–3/4 inch is given in Table 6–1. Where foundation conditions indicate large differential settlement over a short horizontal distance, a vertical full-height slip joint should be provided.

Table 6–1 Relationship between Joint Width and Limiting Differential Settlement for MSE Walls

Joint Width	Limiting Differential Settlement
3/4 inch	1/100
1/2 inch	1/200
1/4 inch	1/300

The intent of these criteria is to limit the allowable settlement of MSE walls to the longitudinal deformability of the facing in conjunction with the ultimate function of the structure. Inherently, MSE walls are flexible composite systems of granular soil and tensile inclusions that behave essentially as earth walls with vertical or near vertical faces. Thus, they exhibit considerable freedom to deform without structural distress, and hence bearing resistance (rather than settlement) usually controls the design.

Prefabricated Modular Walls

Prefabricated modular walls are also considered where conventional gravity, cantilever, or counterforted walls are used. They may consist of interlocking soil-filled reinforced concrete or steel modules or bins, resisting earth pressures as gravity walls (see also Figure 1–13).

Prefabricated modular systems should not be used under certain conditions (see also section 1.4).

6.4 GROUND MOVEMENT IN EXCAVATIONS

Ground response during and after an excavation is essential for the analysis and design of diaphragm walls in traffic underpasses and depressed roadways. Although the range of ground support systems in the last twenty-five years has been extended to include (besides sheet pile and soldier pile walls) secant and tangent pile walls, soil nail supports, chemically grouted walls, shotcrete and anchor bolt walls, lime columns, root pile walls, and soil cement walls, the focus of this brief review is on the performance of diaphragm walls in urban excavations. A comparative review of construction induced movement of in situ walls is given by Clough and O'Rourke (1990), and articulates the effects of the basic excavation and support process on a comparative basis.

As a practical approach for estimating movement, we refer to the method proposed by Peck (1969), presented in Figure 6–14. These data were compiled on settlements of the ground adjacent to temporary braced sheet pile and soldier pile walls. The charts give the settlement divided by the excavation depth, plotted against the distance from the wall also divided by the excavation depth. Three patterns of ground response are defined, with the smallest movements indicated for sands, stiff clays, and soft clays of small thickness (Category I). The maximum movement in Category I near the wall is 1 percent of the excavation depth. For well-designed and constructed walls (Grant, 1985), this performance has been considerably improved. An example is the Columbia Center in Seattle, Washington, where the maximum movement of a 36-meter excavation in stiff clay was 0.1 percent of the height.

Patterns of Movement

Diaphragm walls in traffic underpasses are built from ground level prior to any general excavation. In the final configuration the walls may be braced by: (1) the permanent superstructure at the top; (2) ground anchors near the top; and (3) embedment below excavation level.

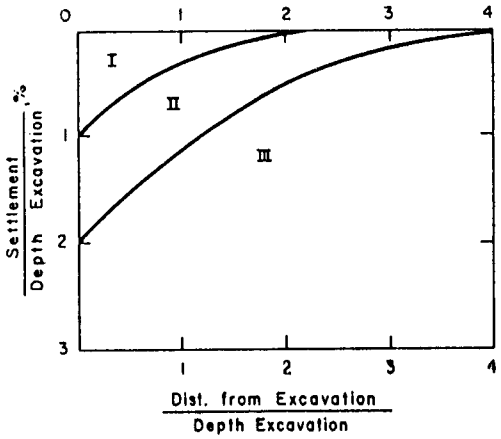

I - Sand and Soft to Hard Clay, Avg. Workmanship

II - Very Soft to Soft Clay
1. Limited Depth of Clay Below Bott. Exc.
2. Significant Depth of Clay Below Bott. Exc., But $N_b < N_{cb}$*

III - Very Soft to Soft Clay to a Significant Depth Below Exc. Bott. and $N_b > N_{cb}$

* N_b = Stability No. Using C "Below Base Level" = $\frac{\gamma H}{C_b}$
N_{cb} = Critical Stab No. for Basal Heave

Figure 6–14 Summary of soil settlements behind insitu walls.

Walls braced with permanent structure. This bracing provides maximum control of movement, particularly where the bracing systems can be installed prior to any general excavation. In this case composite wall movement will be associated with elastic shortening of the bracing system (top slab and possibly the bottom slab) and elastic deformation of the wall between supports.

Bracing by embedment. For walls braced with multilevel bracing, embedment below final excavation level for either static equilibrium or for control of movement is not warranted. Wall embedment, however, may be selected explicitly as bottom bracing, especially where dense and stiff ground is available or where rock exists at shallow depth. In this case, two considerations must be emphasized.

1. In sands considerable movement (sometimes 3 to 5 percent the wall height) is necessary to mobilize full passive resistance depending on the sand density. This movement is unrealistic and clearly intolerable. As a result, it has been suggested to reduce passive earth pressure coefficients by as much as 50 percent in the worst case, which corresponds to a design condition of loose sand with a high angle of wall friction. The development of passive pressure is also much dependent on vertical motion of the wall. The same problem in cohesive soils, particularly with reference to effective stresses, does not appear to have attracted the same attention, probably because these effects are likely to be of lesser importance than in the case of high internal soil friction.
2. Where embedment is extended to limit wall movement, the method of analysis and design must be correlated with the actual conditions. For example, in the case of a cantilever wall, or a wall braced at the top artificially and at the bottom by embed-

ment, working bending moments are deduced from a wall penetration corresponding to a factor of safety for rotational stability equal to unity. In order to ensure stability, either the active pressure is increased or the passive pressure is reduced by a factor of safety, and from these revised pressures a new wall penetration is determined by equilibrium. Thus the working bending moments do not correspond to the actual installed depth, and occasionally unrealistic features, such as higher shear forces, become apparent.

Bracing with ground anchors. Limiting conditions for a wall supported at the top by ground anchors and at the bottom by embedment are shown in Figure 6–15. In part (a) the wall is overloaded beyond its structural capacity, but this condition is unlikely with stiff diaphragm walls.

The combination of insufficient anchor length beyond the slip plane and insufficient wall embedment prompts the system to rotate as shown in Figure 6–15(b). Below excavation level, passive resistance is developed in connection with the slip plane and is perceived through measurement of wall displacement. In part (c) the wall has sufficient embedment and is stable below excavation level, but it tilts forward because the anchor is too short and is fixed within a zone that slips. Stability is restored when the fixed anchor zone is moved beyond the potential slip plane.

The condition shown in (d) involves slipping of the ground mass as a whole in a rotational pattern. Deformation measurements can serve to monitor this condition and as indication of pending failure. The wall shown in Figure 6–15(e) represents a stable structure-anchor-soil interaction, but large ground movement results in unstable foundation conditions for the existing building. This problem relates, therefore, to appropriate serviceability criteria.

It appears from these brief comments that the behavior of anchored walls is a complex matter since the ground, wall, and anchors must interact and work together in order to resist earth loads and restrict movement.

The conceptual presentation of wall and ground movement in Figure 6–15 does not solve practical problems, unless this process is quantified. The most serious problem

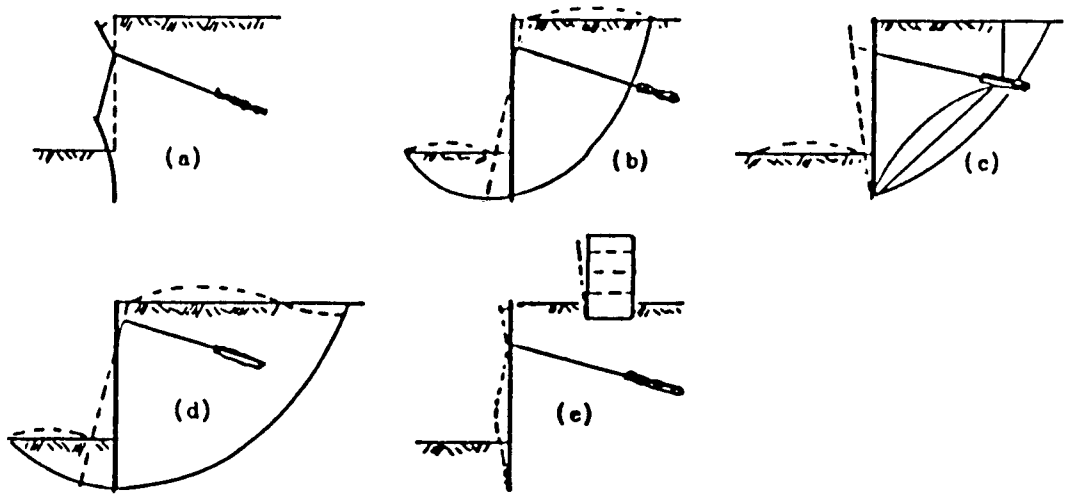

Figure 6–15 Limiting condition for anchored walls as they relate to fixed anchor location.

concerning movement occurring during excavation generally is with clays. As a braced cut in clay is deepened, ground movement around the cut tends to increase, the primary cause being increase in shear stresses applied to the soil as the factor of safety against base heave diminishes.

Comments on Control of Movement

The most important single parameters influencing the magnitude and pattern of movement are the soil stiffness or density and the stiffness of the support. Time effects are important for excavation in clay. In addition, the stiffness of the bracing influences movement of the system. The effective stiffness of the supports is influenced by the horizontal and vertical spacing, the structural section properties, and the type and execution of connections. These may be combined into a general stiffness parameter defined as EI/h^4 where EI is the flexural wall stiffness and h is the vertical spacing of the supports. Other factors affecting movement are discussed in the following sections.

Preloading. Preloading, already common for struts, has become a routine practice for ground anchors. Preloading may be estimated from a Rankine active state (triangular), according to apparent pressure diagrams, from a condition corresponding to the at rest pressure, or it can be applied until 1 inch of onward movement is observed.

Clough (1979) presents the diagrams shown in Figures 6–16 and 6–17, for sands and stiff clays, respectively. Results from field data and model tests were used to develop these plots. The preload has a strong effect on system movement. There is, however, a limit beyond which further increase in preload does not produce appreciable reduction in movement, and thus very large prestress loads are not indicated.

Optimal distributions of design preload diagrams can be trapezoidal, rectangular, or triangular. Trapezoidal and rectangular diagrams result in higher preloads for the uppermost supports and would normally be used where large movement is expected in

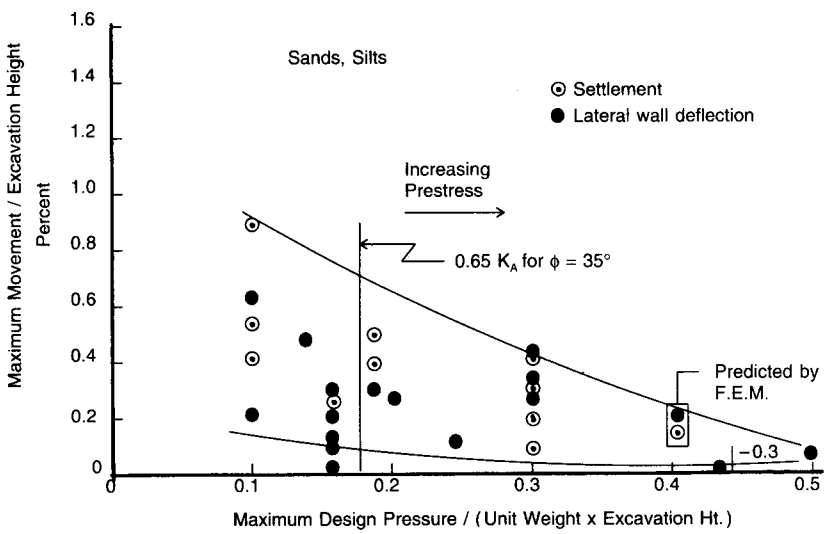

Figure 6–16 Effect of prestress load on movements of wall systems in sands *(from Clough, 1979).*

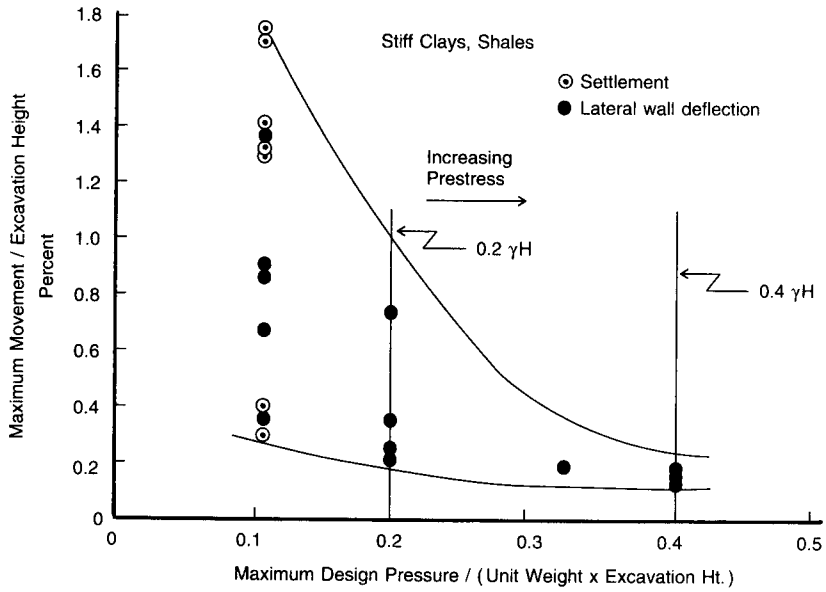

Figure 6–17 Effect of prestress load on movements of wall systems in stiff clays *(from Clough, 1979).*

the initial excavation stage. Triangular distributions result in higher preload forces for the lowest supports. Theoretically, they should be effective where a large component of displacement is movement below excavation level. This, however, may be academic since in most cases large movement will occur before the lowest support is in place.

Applying preloads to recreate at rest pressures is compatible with the design, but should not be expected to eliminate system movement. When applying at rest preloads, only the lateral component of stress relief is compensated for, but not the vertical stress relief across the base of excavation. Interestingly, the pattern and level of preload will determine the lateral stresses behind the wall.

Supports below excavation level. Movement in clay develops below excavation level after the initial excavation stage. If the bottom can be braced with the roadway slab and cross beams or by rock sockets, the result would be an effective control of time-dependent movement. Wall embedment below excavation level can be almost as effective, particularly in stiff clays, and examples are excavations in London clay (Xanthakos, 1994b).

Ground anchors. The position of the top row of anchors is usually dictated by the balance between the initial cantilever and the final moment, and by limitations on wall movement. A suggested depth is 1.5 meters (5 ft) provided local ground failure behind the wall does not occur while the anchor is prestressed.

The time-dependent movement observed for excavations in clay will indicate a transition from elastic to plastic behavior. There have been examples where a wall continued to move for eighteen months following the excavation, and this movement was nearly 10 percent the movement recorded at the end of excavation. In some instances, it may indicate consolidation of the soil around the fixed anchor zone.

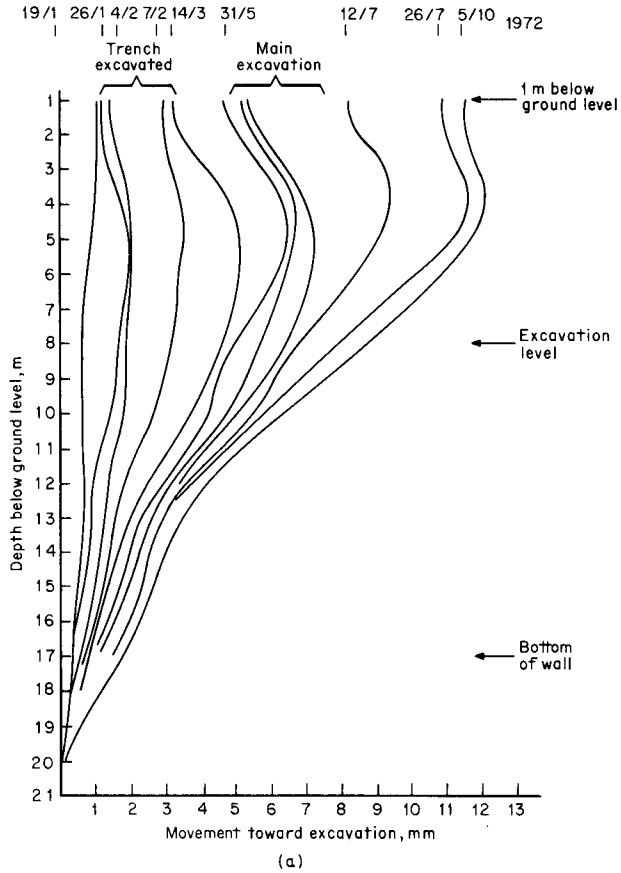

Figure 6–18 (a) Lateral movement of the cantilever diaphragm wall for the Reading bypass in London; (b) horizontal and vertical ground movement *(from St. John, 1975).*

Free cantilevers. Cantilever diaphragm walls (without bracing other than embedment below excavation level) are seldom used in urban excavations, but they are feasible in relatively shallow excavations, such as the upper sections of an approach to a traffic underpass, provided the resulting movement can be tolerated.

An example of a free cantilever is presented in Figure 6–18, showing the lateral movement of the walls for the Reading bypass in London. The total wall height is 17 meters (56 ft), and 9 meters is used as embedment below excavation. The ground consists of London clay in the upper crust, with the toe of the wall keyed into the much stronger Woolwich and Reading beds. Figure 6–18(b) shows the distribution of surface movement.

6.5 DESIGN PRINCIPLES OF DIAPHRAGM WALLS

Design Methodologies

Two design philosophies may be used to proportion diaphragm walls and check overall stability: (1) load service method, also referred to as working stress or allowable stress design (ASD); and (2) limit states design, also referred to as strength design method based on load and resistance factors. Certain basic principles of these methods have been discussed in previous sections.

A wall may reach a strength limit state and experience distress and structural damage, either local or global. Various failure modes may also develop in the soil that supports the wall such as bearing capacity failure, sliding, overturning, and overall instability.

Alternatively, a wall will have reached a serviceability limit state when it fails to perform its intended design function, partly because of excessive deformation or movement, or because of deterioration (i.e., excessive leakage). Serviceability limit states include excessive overall or differential movement, fatigue, vibration, and cracking.

Loads and resistance factors. The design loads are determined by multiplying the normally expected values, called "nominal" loads, by load factors. The summation of factored loads is the required strength, $\Sigma\gamma_i Q_i$. The design strength, or resistance, is found by multiplying the nominal strength by the resistance factor ϕR_n. Evidently the design is satisfied if $\phi R_n \; \Sigma\gamma_i Q_i$, which is Equation (3-11).

The load groups and types of loads are summarized in Table 2–17, which is AASHTO Table 3.22.1A. Among the loads that are essential to this discussion are the following:

Permanent loads: DD = Downdrag
DC = Dead load
EA = Earth pressure
EW = Water pressure
ES = Earth surcharge load

Transient Loads: LL = Live load, T = Temperature
WL = Wind load, S = Shrinkage
EQ = Earthquake, SE = Settlement

The primary function of diaphragm walls is to resist lateral pressures and also carry certain vertical loads. A relevant load group for ultimate and serviceability limit states may be a condensed form of AASHTO Equation (3–10), expressed in the following format:

$$\text{Group N} = \gamma(\beta_{DC}\,DC + \beta_L\,LL + \beta_E\,EA + \beta_{ES}\,ES + \beta_W\,EW + \beta_{EQ}\,EQ + \beta_{DD}\,DD) \quad (6\text{–}1)$$

where γ = overall load factor; β = load coefficient, and the load designation and subscripts are somewhat different from Table 2–17 to conform to the nomenclature of the section.

In some instances the inclusion of certain loads (for example dead, live load, and downdrag) may tend to decrease overall load effects and thus underestimate the design requirements. This can be true where bending stresses control the design, and extra wall thickness (normally available with diaphragm walls) relegates concrete compressive stress to secondary importance. In these instances, some of these loads may be omitted. A further point of interest is that vertical loads may tend to dissipate as they are absorbed by shear resistance at the interface so that the section for maximum moment does not coincide with the section of maximum axial load.

Load Factors. In order to fit strength design methods in diaphragm walls, the following conditions must be recognized: (1) several different types of loads may act on the wall; (2) the actual values of permanent loads may be less than or exceed the specified nominal values; (3) although limited data are available on the variability of permanent loads, their negative variability is less than the positive; (4) load combinations that have the greater number of loads appearing in Equation (6–1) should have the smallest value of γ, particularly where the load effects relate to very high dead load to transient load ratios; (5) where the number of types of loads to be considered is reduced (for example, approaches 2 or 1), load factor analysis approaches ASD merely by calibrating load and resistance factors to be compatible with safety factors; and (6) load factors for lateral earth stresses should relate to the fact that the earth behind the wall is not selected backfill but the original soil subject to changes during construction.

The inclusion of earthquake forces in Equation (6–1) yields AASHTO Group VII. Load coefficients β, shown in Table 6–2, agree in general with AASHTO Table 3.22.1A except as follows: (1) a coefficient has been included for downdrag forces; (2) the coefficient for dead load may be taken as 0.75 when checking members for minimum axial load and maximum moment; (3) a coefficient has been added for earth surcharge loads; and (4) the coefficient for lateral earth pressure covers a wider range (from 1.20 to 1.70) to account for the greater variability of natural soils behind walls.

Table 6–2 Load Coefficient β, Limit States

Type of Load	Coefficient β
DC = Dead Load of Structural Components	1.00
DD = Downdrag	1.80
EA = Earth Pressure, Lateral	1.20–1.70
Vertical	1.00
ES = Earth Surcharges	1.20–1.70
EW = Water Pressure	1.00
LL = Live Load	1.70
EQ = Earthquake	1.00

The load factor γ for each load group should be taken as shown in AASHTO Table 3–22.1A.

Performance (Strength Reduction) Factors. Performance factors are stipulated for three basic system components, namely the wall, anchorages, and the portion of the soil mobilizing passive resistance.

Code ϕ factors for concrete are applied to the nominal strength to obtain a reasonably dependable strength. These are factors taken from AASHTO for strength design and are shown in Table 3–3.

Performance factors for ground anchors must recognize the three basic failure mechanisms: (1) excessive yielding or fracture of the tendon; (2) failure of the ground-tendon bond; and (3) failure of the ground-grout bond (Xanthakos, 1991). These mechanisms are reviewed in some detail in subsequent sections. Resistance factors for ground anchors are stipulated as follows (failure occurring at the ground-grout interface as pullout failure):

Sand, based on soil data	$\phi = 0.60$
based on pullout tests	0.65
Clay, correlation with unconfined compressive strength	0.60
using shear stress from pullout field tests	0.65
Rock, presumptive value	0.50
laboratory rock-grout bond tests	0.70–0.75
pullout tests	0.80

These ϕ values are somewhat less than the values suggested by the LRFD specifications since it is felt that at this time the available statistical data are not sufficient to warrant reliability analysis.

Performance factors for the tensile resistance of ground anchors are suggested as follows:

Permanent:	Yielding of the gross section	$\phi = 0.90$
	Fracture of the net section	0.75

These factors are the same as in the LRFD specifications except that for temporary anchors load factor design is not recommended.

Performance factors for passive resistance are necessary for strength design and for serviceability limit states. In conjunction with Equation (3–11), active earth pressure is considered a load and is factored according to a load coefficient >1. Conversely, passive pressure is a resistance effect and is placed on the resistance side of the equation. Thus, when checking the overall equilibrium of the system, a performance factor must be applied to the passive resistance.

Performance factors for passive resistance are stipulated as follows:

Sand, semiempirical procedure using SPT data	$\phi = 0.45$
semiempirical procedure using CPT data	0.55
rational method, using ϕ (friction angle) from SPT data	0.35

rational method, using ϕ (friction angle) from CPT data	0.45
Clay, semiempirical procedure using CPT data	0.50
rational method	0.50–0.60
Rock , semiempirical procedure	0.60
Plate load test	0.55

where SPT = standard penetration test, and CPT = cone penetration test. These values are suggested on an interim basis, and may be revised as new information becomes available.

Commentary. The load factor method is applied to the combined system of soil and structure. Using the same methodologies, failure is explicitly examined in the structure (in this case load effects are moments, shears, and so on), and also in the soil/structure system (anchor-ground interaction, wall-soil interaction in passive zone). In the same context, serviceability states are not considered since this is primarily a strength condition.

For normal functions where the wall serves essentially as ground support to retain earth masses, the loads included in Equation (6–1) will cover all possible combinations and load groups. As the function of the wall is expanded, the typical load group N must be amplified to include other types of loads. For example, where walls serve as piers and abutments other loads will include wind, longitudinal forces, braking forces, and so on.

Design Principles of Anchored Walls and Anchorages

The transfer of load and modes of failure. From the theoretical and practical standpoint, the mechanism of load transfer is essential for the design of an anchorage that is safe and economical. Anchor load transfer theories often are based on idealized assumptions, and where conditions are different results can be misleading, particularly when theory is applied to nonhomogeneous ground conditions. A different approach is to infer the transfer of load from the wide variety of design rules available, all claiming origin from full-scale tests and general field experience. Since no empirical procedure can claim general applicability, routine reference to these rules can likewise lead to crude approximations.

Several topics remain incompletely understood, for example, load transfer mechanisms in nonidealized media, grout pressure limits beyond which beneficial effects begin to diminish, fixed anchor head-displacement relationships, and serviceability safety factors consistent with tests and actual loads. Construction procedures and workmanship have obvious effects on anchor pullout capacity and inhibit efforts to make accurate predictions. Thus, typically the work is supplemented by a testing program to confirm anchor capacity used in design.

Anchors can fail or become inoperable in one of the following ways:

1. By structural failure (rupture or sectioning) of the steel tendon and its component parts
2. By bond failure (slippage) at the tendon-grout interface
3. By shear failure along the contact surface of grout and ground

4. By failure within soil or rock supporting the anchorage
5. By crushing or bursting of the grout column around the tendon
6. By displacement or excessive slippage of the anchor head
7. By gradual long term deterioration (corrosion effects, etc.)

These mechanisms, and the concept of anchor design, are reviewed in detail by Xanthakos (1991). Hence, this section will discuss certain fundamental points relating mainly to anchor structural capacity and pullout resistance.

Failure of Tendon in Tension. Allowable working load in the steel tendon or factored resistance is determined from the characteristic strength f_{pu} by applying a safety factor or a performance factor. Some allowance may also be made for reduction in the structural capacity at the head, end block, and connection points (couplings) because of some yielding at these locations. Smaller working loads or strength factors may also be introduced if severe conditions are anticipated, and may lead to a reduction in the effective cross-sectional area of the tendon.

For working stress (service load) design, the maximum allowable stress F_t in the steel tendon is

$$F_t = 0.5 f_{pu} \tag{6–2}$$

for a factor of safety of 2. For load factor analysis the design strength of the tendon is

$$F_u = \phi f_{pu} \tag{6–3}$$

where ø is the strength reduction factor stipulated in the foregoing sections. These relations are for permanent installations. For temporary anchors the design should consider only working stresses under a reduced factor of safety. In this case

$$F_t = 0.625 f_{pu} \tag{6–4}$$

All symbols may indicate either stresses or forces in the tendon.

Failure of Grout-Tendon Bond. In anchor work, the development of grout-tendon bond is often considered adequate, and emphasis is placed on the ground-grout interface. However, the failure mode of a tendon bonded into grout is markedly different from the bond failure in pullout tests for conventional concrete. In ground anchors the grout is in tension, as is the steel, and the bond mechanism depends on the respective elastic properties of the steel and grout.

Guidelines and standards for permissible grout-tendon bond may be based on experimental data. For preliminary analyses and rule of thumb estimates, recommended bond stresses (allowable) under proof load should not exceed the following (based on grout strength 30 N/mm^2, or 4350 lb/in^2).

1.0 N/mm^2 (145 psi) for clean plain wire or plain bar tendon
1.5 N/mm^2 (220 psi) for clean crimped wire tendon
2.0 N/mm^2 (290 psi) for clean strand or deformed bar

For cement grout anchors, the minimum tendon embedment length for bond development recommended by a majority of codes is:

1. For tendons homed and bonded in situ, bond length = 3 meters (10 ft).
2. For tendons bonded under factory-controlled conditions, bond length = 2 meters (6.5 ft).

For a more detailed analysis of bond, including debonding conditions, reference is made to Xanthakos (1991).

Failure of ground-grout bond. Experimental and theoretical work has shown that shear resistance between ground and grout column is more complex than a simple model where uniform shear is assumed along the fixed anchor length. This complexity gives rise to essentially nonuniform bond distribution. In many instances the design is, therefore, grossly inaccurate if it is based on the simple model, yet tests show that where sections of the fixed length are overloaded and shear failure is imminent, other sections begin to receive and resist load so that equilibrium is reestablished.

Bond resistance is known to depend on the soil properties. An increase in the relative density of sand generally increases the angle of internal friction, which in turn increases the frictional resistance at the interface. For cohesive soils, increase in stiffness usually implies higher shear strength that improves bond capacity.

For a straight shaft, a simple theoretical expression for the average (uniform) shear stress τ along the ground-grout interface is related to the load P by

$$P = \pi DL\tau \tag{6–5}$$

where D is the effective grout column diameter and L is the fixed anchor length. This expression is valid under the following assumptions:

1. The transfer of load occurs uniformly over the fixed length.
2. The borehole and the fixed length have the same diameter.
3. Failure occurs by sliding at the interface for a smooth borehole, or by shearing along a zone adjacent to the interface for a rough borehole.
4. Debonding does not occur.
5. There are no discontinuities or weak planes that can alter the process of failure.

The shear resistance or bond, τ, is the summation of two components: adhesion and friction. This is expressed as

$$\tau = c_a + \sigma_n \tan \delta \tag{6–6}$$

where c_a = adhesion between ground and grout; σ_n = normal effective stress on the anchor zone; and δ = friction angle between the soil and the grout.

Where shear strength tests are carried out, all the factors in Equation (6–6) are lumped into a single parameter. In this case an allowable bond stress is computed from the shear strength test values with an appropriate factor of safety, usually 2 for working stress design. For load factor analysis, the performance factors mentioned in the foregoing sections are applied to the shear strength to obtain the design shear.

Anchors in Rock, Straight Shaft. The straight-shaft tremie-grouted type A shown in Figure 6–3 is considered the most suitable and applicable to rock. For preliminary estimates of anchorages in rock, the bond length can be established from direct

pullout tests. This procedure is simple, and consists of placing a cone sample vertical in the center of a steel form, filling the angular space with cement grout, and allowing it to cure. The sample is then pressed out and the bond strength is estimated from the pull-out force over the contact area. Ultimate bond strength values from various sources are available for normal conditions of loading and various types of rock. Table 6–3 gives a summary with typical ranges for the rock types indicated. Interestingly, if a 4-inch diameter is considered representative of small-diameter holes, and the ultimate bond strength values shown in Table 6–3 are averaged, the resulting load transfer capacity is essentially the values shown in AASHTO Table 5.7.6.2B. For example, a 4-inch diameter hole has a total interface area about 155 in^2 per foot of length. Using an average ultimate bond strength 250 psi from Table 6–3 for dolomite limestone, the load transfer capacity is 155 × 250 = 39 kips/lin. ft ≈ 40 which is the ultimate resistance per AASHTO Table.

Results from theoretical studies show a clear dependence of the shear (bond) stress distribution on the ratio of the elastic moduli of the anchor material E_a and the rock E_r. The smaller this ratio (meaning stronger rock and weaker grout) the larger the stress concentration at the proximal end, whereas higher ratios (meaning softer rock and stronger grout) result in bond that it is more evenly distributed. For E_a/E_r close to 10 (meaning soft rock), the bond distribution is essentially uniform. This behavior is shown in Figure 6–19 (Coates and Yu, 1970).

Noting that average E_a values for grout are about 1.5×10^4 N/mm^2 (about 2,200,000 lb/in^2) , it follows that the rock must have E_r values below 0.15×10^4 N/mm^2 (about 220,000 lb/in) before uniform bond distribution can be assumed. Relating rock compressive strength as proposed by Judd and Huber (1961), whereby UCS = $E_r/350$, it follows that the rock strength should be about 630 lb/in^2 (or 4.3 N/mm^2), and this excludes the majority of anchors installed in rock.

It appears that the mechanics of anchors in strong rock are yet to be fully explained, but their construction and performance becomes less of a problem because of the adequacy of installation procedures. This topic deserves, therefore, more attention with high-capacity anchors that may be subjected to debonding. More data on this subject are given by Xanthakos (1991).

Anchors in Sand. Experience demonstrates that the ultimate load of anchors in sand depends on the following: (1) relative density and degree of uniformity of the soil; (2) fixed anchor geometry and dimensions (mainly the length and to a lesser degree the

Table 6–3 Ultimate Bond Strength Values for Various Types of Rock

Rock Type	Ultimate Bond Strength (psi)	Ultimate Bond Strength (N/mm^2)
Granite and basalt	250–450	1.72–3.10
Dolomite limestone	200–300	1.38–2.07
Soft limestone	150–200	1.03–1.38
Slates and hard shales	120–200	0.83–1.38
Soft shales	30–120	0.21–0.83
Sandstone	120–150	0.83–1.03
Weathered marl	25–36	0.17–0.25

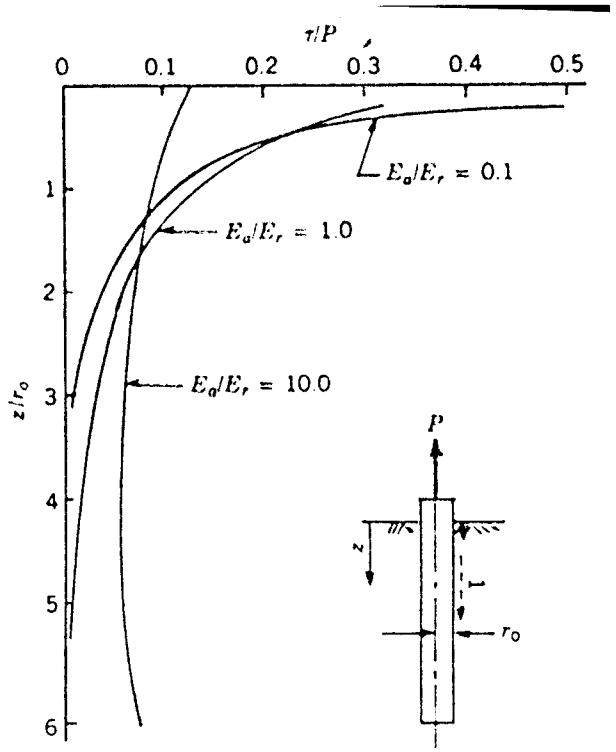

Figure 6–19 Variation of shear stress with depth along rock-grout interface; model study *(from Coates and Yu, 1970).*

diameter); (3) method of grout injection and grout pressure used; (4) dilatancy in the soil; and (5) to a lesser degree, the drilling method and equipment.

Anchors in sand can have a fixed length configuration of type A, B, or C in Figure 6–3. The end result will depend mainly on the soil density, type (whether fine or coarse), uniformity, and grout injection pressure.

For the low-pressure grouted type B anchors with enlarged cylinder, field trials have provided the following empirical rules for estimating ultimate capacity

$$T_n = LN'\tan\phi \tag{6–7}$$

where T_n = ultimate load capacity (nominal resistance) in kN; L = fixed anchor length (m); N' = a constant; and ϕ= angle of internal friction of sand.

Where the fixed anchor length is in meters, N' values range from 400 to 600 kN/m. If the fixed anchor length is in feet, N' values range from 27 to 41 kips/ft. Equation (6–7) takes into account soil permeability from 10^{-1} to 10^{-2} cm/s, overburden depth to the top of the fixed anchor of 20 to 45 feet, effective average diameter of the enlarged zone in the fixed anchorage of 15 to 24 inches, and range of anchor lengths within normal limits.

For straight shafts Type A anchors, Equation (6–7) is still valid, but the N' values are modified (Xanthakos, 1991). In this case N' values range from 130 to 165 kN/m if the fixed length is quoted in meters, and from 9 to 12 kips/ft if this length is given in feet. Likewise, Equation (6–7) is valid for overburden depth to the top of the fixed zone 18–30 ft (5.5–9 m), and effective average shaft diameter 7–8 in (280–310 mm). Where pressure grouting is used, the effect is a considerable increase in the nominal resistance. An empirical formula derived from field tests relates ultimate capacity T_n to grout pressure p' as follows

$$T_n = p'\pi DL \tan \phi \tag{6–8}$$

where D and L are effective anchor diameter and length in the fixed zone, respectively. The value of p' is taken as 2 psi (0.014 N/mm^2) for every foot of overburden above the top of the fixed zone, and is used as average over the fixed length.

Equation (6–7) provides simple but crude estimate of fixed anchor lengths and load capacity with probable upper and lower limits, but tends to be conservative since it does not consider important ground parameters. Deviation between estimated and actual ultimate capacity is more significant if this rule is applied to dense overconsolidated alluvium where N' values were initially established in normally consolidated material. The use of Equation (6–8) is recommended if used in conjunction with actual grout pressure.

For type C anchors in sand, theoretical predictions of load capacity are not reliable. Ultimate load estimates usually are based on design curves derived from field tests for a particular range of soil and parameters. In alluvium, some data are available from tests in medium sand and also in variable deposits of sand and gravel, for effective bore hole diameters of 100 to 150 mm. Probable ultimate capacity in the fixed zone is 90 to 130 kN/m for injection pressure 1 N/mm^2, and 190 to 240 kN/m for injection pressure 2.5 N/mm^2.

A complete review of procedures for estimating ultimate capacity based on theoretical and empirical data is given by Xanthakos (1991).

Anchors in Clay. Load capacity of anchors in clay generally is low, unless it can be improved by special procedures, because it depends on adhesion. Improvement may be achieved by (1) injecting irregular gravel into the augered hole over the fixed anchor length together with cement grout; (2) using bells or underreams; and (3) using high-pressure grouting.

As a first approximation, pullout capacity for tremie-grouted straight shaft may be derived theoretically as

$$T_n = \pi DLas_u \tag{6–9}$$

where s_u = averaged undrained shear strength over fixed length, and a = adhesion factor. Postgrouting appears to increase load resistance by causing hydraulic fracture in the clay locally, but these pressures should be well below the values causing bursting of the grout.

The foregoing review highlights the complexities of load transfer at the ground-grout interface and articulates the influence of many variables. For a complete design, reference to more detailed methodologies is therefore recommended (Xanthakos, 1991). If allowable stress design is used, the minimum factor of safety should be 2.5, and preferably close to 3.0. With strength design, the range of load and performance factors given in the preceding sections should be carefully assessed, and modified if necessary. Structural consistency will be provided if the load and resistance factors are calibrated to give compatibility with the safety factor used in ASD. For example, for a performance factor 0.6 and a load factor 1.7 applied on a global basis, an equivalent safety factor is 1.7/0.6 = 2.8.

Guidelines for anchor design. The load transfer requires the presence of suitable ground formations at reasonable depth. Ground types considered suitable for fixed anchor zones include nonplastic soils or dense soils with low plasticity, and granular materials such as silty sand or coarse sand and gravel. The fixed anchor zone should be located well beyond the ground mass expected to interact with the wall system.

Anchor Spacing and Inclination. For diaphragm walls supporting excavations for traffic underpasses, optimum anchor spacing usually is obtained from a structural analysis of loads, and potential capacity available in the fixed zone. Anchor spacing may also be influenced by structure geometry, panel size, and modular configuration.

Most anchors are inclined to facilitate anchor hole drilling, and grouting. Furthermore, anchors must be inclined to avoid adjacent foundations, or to reach a suitable anchorage layer. An angle of 15° with the horizontal is considered the minimum practical inclination that can accommodate proper grouting procedures. Within the range of moderate depths most soil anchors are installed at an angle of 15° to 30°. Where a suitable anchorage zone is relatively deep, a steeper angle (usually 45°) may be selected. Steeper anchor inclination also means increased vertical load, part of which must be resisted at the base of the wall.

Anchor Hole Diameter. This depends mainly on anchor size and type, corrosion protection requirements, drilling procedures, and ground conditions. Typical hole sizes are shown in Table 6–4 for anchors in rock using percussive methods. The effect of corrosion protection on drilled hole diameters is obvious.

Since the vast majority of soil anchors are drilled in a cased hole, the weight of the casing and its handling appear to impose an upper limit in hole size. Thus, at present the 6-inch hole is common and practical in this respect.

Suggested Design Procedure. Typical objectives are: (1) determination of working loads (ASD); (2) estimation of fixed and overall anchor length; (3) selection of tendon type; and (4) selection of stressing load. The latter is mandatory and confirms the design load. A detailed procedure is given by Xanthakos (1991).

Corrosion Protection. The protection of permanent anchors is an important task, and a mandatory requirement. Under a growing need to establish standards of protection and articulate protective systems, the anchor industry now distinguishes between single and double protection. By definition "single protection" constitutes one physical barrier between the steel tendon and the corrosive front. "Double protection" means that two such barriers are provided, and the main purpose of the outer barrier is to protect the inner barrier against damage during tendon handling and homing. In this context, the outer barrier may be considered sacrificial and redundant. Double protection has evolved as standard anchorage requirement in most European countries and North America, but is not universally accepted as necessary. Protective systems are reviewed in detail by Xanthakos (1991).

Lateral Earth Stresses

Changes in the state of stress of a soil are caused by (1) trench excavation under slurry whereby the slurry hydrostatic pressure replaces the initial at rest condition, (2) replacement of the slurry by fresh concrete, and (3) the general excavation and bracing sequence when more changes in the stress conditions occur.

Table 6–4 Typical Anchor Hole Diameter, 1/2″ dia. 270 KSI Strands

Type	Max. No. of Strands	4	7	9	11	13	17	21	27	31	52
Single Protection	Drill Hole Dia. In	2.5	3.0	3.5	4.0	4.5	5.0	5.5	6.0	6.5	9.0
Double Protection	Drill Hole Dia. In	4.5	5.0	5.5	6.0	6.5	7.0	7.5	8.0	8.5	11.0

The formulation of the problem of predicting lateral earth pressures on diaphragm walls is essentially a definition of appropriate boundary conditions, combined with the constitutive relations for the soil. However, with time the wall-soil system will return to the initial equilibrium so that the long-term lateral earth pressures will approach the initial condition at rest. In this case the walls should be designed using a coefficient of pressure at rest, K_o, computed from Equation (2–1) or (2–3).

During excavation, the walls may be temporarily braced with rakers, ground anchors, slopes and berms, wall embedment, and in some cases by the permanent structure. Restraining effects are caused by the system stiffness and wall fixity against rotation or translation. Four idealized forms of wall behavior are shown in Figure 6–20. The cantilever wall shown in (a) depends entirely on embedment for stability. The assumed linear stress distribution is consistent with wall movement and approaches the active state. The wall in (b) is supported elastically at the top and embedded in the lower end. Its deformation resembles the pattern of a simple beam, and there may be a point that does not displace laterally. The wall in (c) has a smaller embedment allowing some lateral movement, so that a stress redistribution will occur as shown. The multibraced or multianchored walls shown in (d) would be expected to move essentially in translation, so that with some preloading the earth pressures will approach a rectangular pattern.

For the walls shown in Figure 6–20(a) and (b), an analysis based on active pressures is consistent with system behavior, as long as the expected movement warrants this condition. For the walls shown in (c) and (d), the magnitude and distribution of earth pressures will depend on several factors, such as the application and level of preload or prestressing, degree or fixity or restraint, system stiffness, and construction procedure. Probable distribution patterns may have their origin in apparent pressure diagrams, and constitute therefore a semiempirical design. The application of this procedure to diaphragm walls must, however, recognize the explicit effect of the embed-

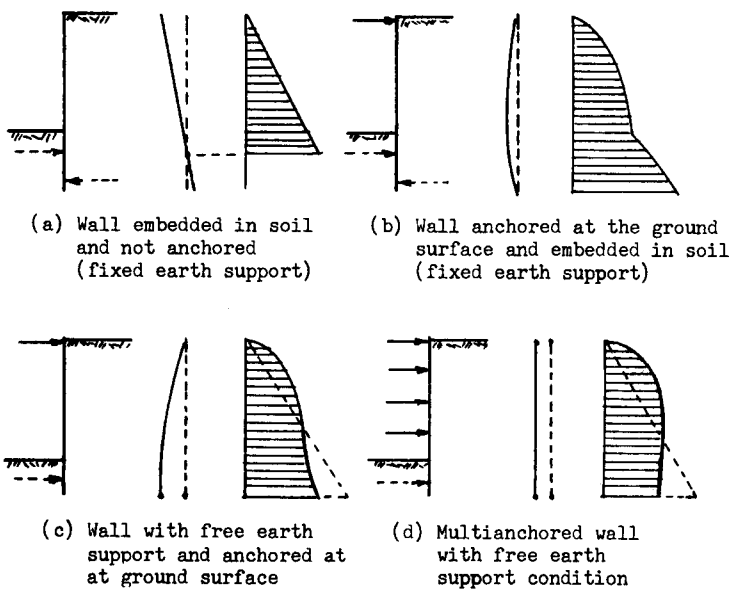

Figure 6–20 Basic types of wall supporting excavations; various restraints against rotation and translation.

ded portion, the considerable wall stiffness, the probable wall behavior according to flexular beam theories, and construction imperfections that may cause variations in strut loads. Thus, these diagrams are modified as suggested by Xanthakos (1994b).

Base Restraint and Passive Resistance

Statical analogy. The statical analogy of a braced wall is similar to a beam restrained against movement at the support points and acted upon by earth and water pressures. Concentrated forces or moments may act along the wall height. The top of the wall may be assumed to be free, pinned, or fixed against rotation and lateral displacement. The condition of the bottom support may be assumed as one of the following: (1) bottom supported by an elastic spring, or (2) bottom restrained according to Blum's theory. Beneath the point of zero pressure, a triangular counterpressure is assumed.

The method of fixed earth support. A diaphragm wall with free top and fixed bottom is shown in Figure 6–21 with the corresponding earth pressure diagrams. Passive resistance is developed on the left and right side of the wall, and the embedment is sufficient to yield a fixed bottom condition. The two components E_{pl} and E_{pr} can be calculated if the transition from e_{pl} to e_{pr} is known. An exact analysis, therefore, is not available, but an approximate analysis can be carried out using graphical procedures (Otta, Pantucek and Goughnour, 1981).

Equivalent Beam Method. This is a simplified form of the more complex graphical solution. Since the moment distribution shows a zero point below the base, the wall can be replaced by two beams hinged together at the point of zero moment. The upper part is considered as a simply supported beam, and the lower part a beam pinned at one end and fixed at the other. Since the design is governed by the maximum moment, it is sufficient to design the upper beam as shown in Figure 6–22. The point of zero moment B_0 (the lower end of the beam) is assumed to coincide with the point of zero loading. The beam shown in Figure 6–22 is then statically determinate with the assumed loading and end conditions.

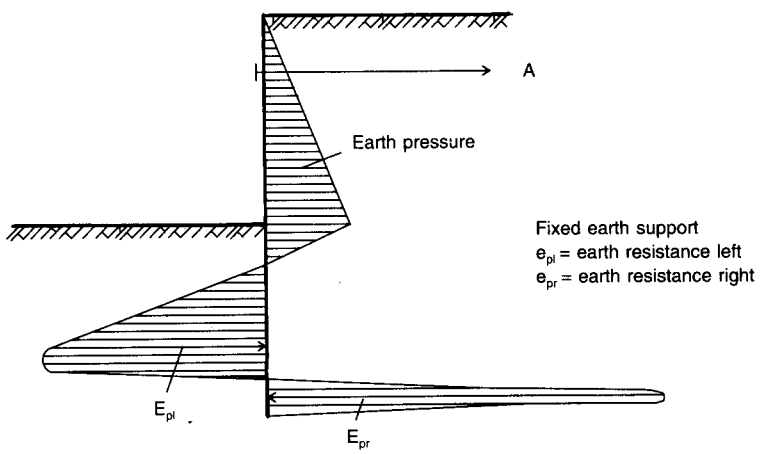

Figure 6–21 Distribution of active earth pressure and passive resistance; wall restrained at anchor level only, and bottom fixed.

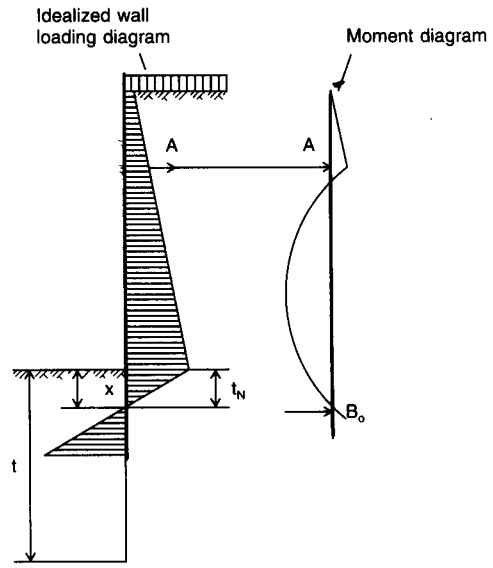

Figure 6–22 Blum's equivalent beam method, fixed-earth support.

The theoretical embedment t_o can be calculated from the equilibrium conditions shown in Figure 6–23. The moment M at distance z below point B_o is given by

$$M = B_o z - \gamma(K_{ph} - K_{ah})\frac{z^3}{6} \tag{6–10}$$

where the K factors denote passive and active pressure, and B_o is the reaction from the upper beam diagram. (Note: the point of application of B_o is obtained as the point of zero load). Setting $M = 0$ we obtain

$$z_o = \sqrt{\frac{6B_o}{\gamma(K_{ph} - K_{ah})}} \tag{6–11}$$

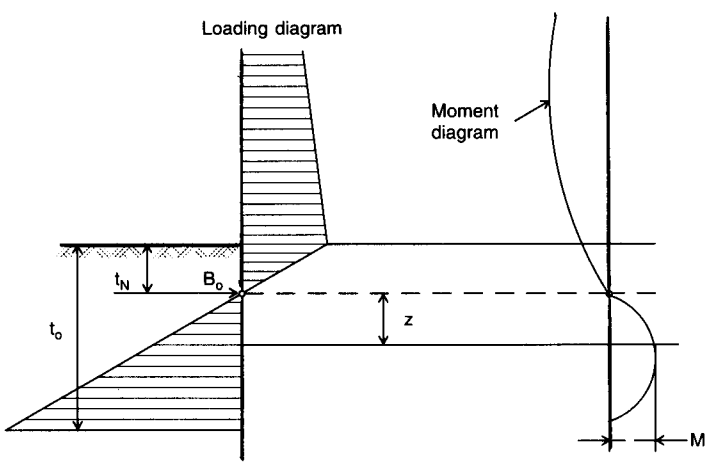

Figure 6–23 Loading and moment distribution, fixed-earth support.

and total embedment $t = T_N + z_o$ (6–12)

For a factor of safety n, the wall embedment is

$$t = t_N + n\sqrt{\frac{6B_o}{\gamma(K_{ph} - K_{ah})}} \tag{6–13}$$

The method of free earth support. This method assumes that the wall is rigid and may rotate about the bracing level. In this process passive pressure develops in the soil in front of the wall, and active pressure develops behind the wall. After the theoretical embedment is computed, its value may be increased 30 to 40 percent, or K_p may be divided by an appropriate factor of safety (not less than 2). For strength design, appropriate load and resistance factors are applied to the active and passive pressure.

For the limiting case, the passive resistance E_p shown in Figure 6–24 is just sufficient to balance the active force E_a. The condition $\Sigma M = 0$ at the brace level gives directly the necessary embedment t, while the condition $\Sigma H = 0$ gives the brace reaction. The maximum moment occurs at $Q = 0$.

Comparison with Fixed Earth Support. Without fixity at the bottom end of the wall, the maximum bending moment will be greater. Likewise, the embedment for a free-earth condition is less than for a wall with fixed end support. The choice must consider the actual soil conditions. A wall freely supported at the bottom may be assumed in firm soil conditions.

Analytical Solutions. A wall with free earth support conditions can be considered analytically, based on the diagram of Figure 6–25. The two different schemes reflect granular and cohesive soil. The analysis is carried out by satisfying static equilibrium. For an exact solution reference is made to Bowles (1988).

Measured Lateral Earth Stresses on Diaphragm Walls

Considerable data have been obtained from field observations and earth pressure measurements in diaphragm walls. Among the various configurations and conditions, this record covers: (1) pressures exerted on the walls of the trench by the fresh concrete; (2) walls braced by embedment into rock and by permanent slabs; (3) walls braced at the top and bottom prior to general excavation; (4) walls braced with struts; (5) anchored wall; and (6) free-cantilever walls (Xanthakos, 1994b).

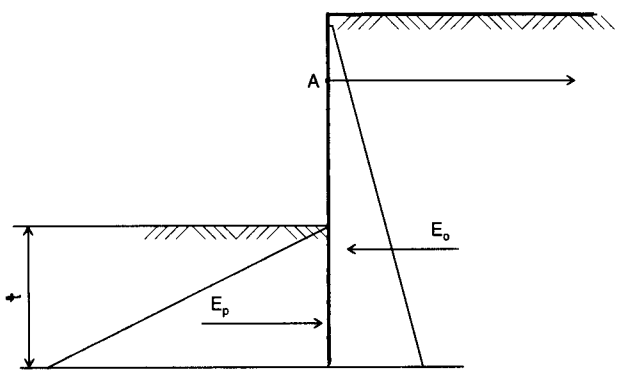

Figure 6–24 Active force and passive resistance in wall with free-earth support.

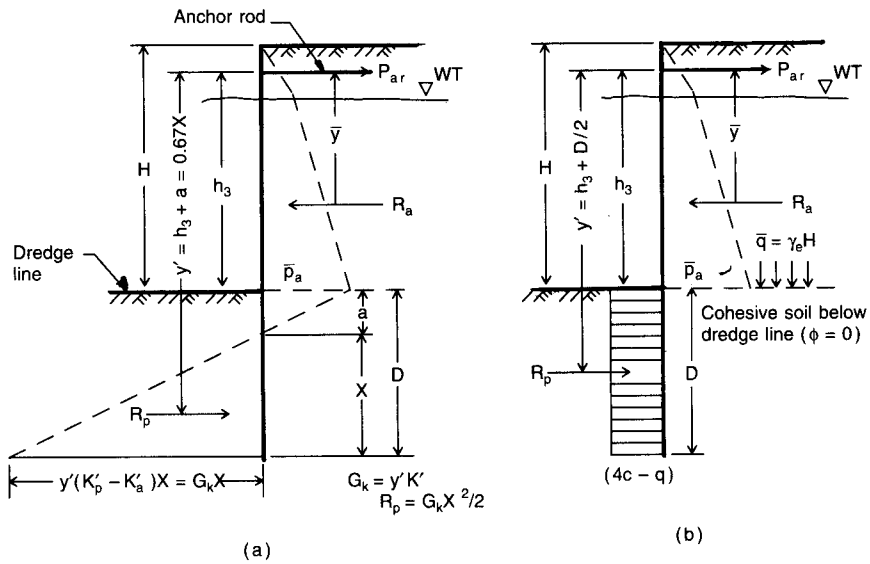

Figure 6–25 Anchored wall free-earth method; (a) All granular soil; (b) cohesive soil below dredge line wiht granular-soil backfill.

It appears, however, that although direct field measurements can supplement the methods of analysis, they also tend to inhibit a complete problem formulation. This is particularly important where lateral earth stresses must be correlated with predicted deformations. For example, limiting equilibrium analysis is simple in predicting collapse loads, but it does not predict deformations associated with limit loads, and provides no information for conditions other than those at the limit. Where this information is of particular value in the design, finite element analyses should be considered.

6.6 DESIGN PRINCIPLES OF GRAVITY AND SEMI-GRAVITY WALLS

Design Pressures

Earth pressures. Gravity and semi-gravity walls were briefly discussed in section 6.2, and typical wall configurations are shown in Figure 6–12. Earth pressures on these walls depend on the type and condition of the backfill, the slope of ground surface behind the wall, and freedom of the wall to rotate or translate to develop limiting conditions. AASHTO defines yielding walls as systems free to translate or rotate about their base. Conversely, restrained walls are fixed or partially inhibited to translate or rotate.

Yielding walls generally should be designed for active stress conditions and a wedge theory according to the Coulomb approach. The rotational movement necessary to yield active pressure conditions may be inferred from Table 2–2, or reference may be made to AASHTO Table 5.5.2A. These specifications also give procedures for determining the magnitude and location of the resultant earth pressure as a function of the slope of ground surface behind the wall.

For restrained walls, or for yielding walls where the tilting or deflection necessary to develop active pressure is not tolerable, lateral earth pressures should be computed assuming at-rest conditions, that is, using Equations (2–1) and (2–3). AASHTO includes also stipulations for the effect of traffic that can come within a horizontal distance from

the top of the wall as equal to one-half the wall height, as well as provisions for other surcharge loads.

Earth Pressure due to Compaction. As mentioned in section 2.2, compaction affects the lateral earth pressure, and this effect is demonstrated in Figure 2–2. When heavy static or dynamic equipment is used within a distance of about one-half its height behind the wall, the effect of additional earth pressure caused by compaction should be considered. Detailed methods for estimating this effect are given by Clough and Duncan (1971).

Water pressure and drainage. A usual problem with retaining walls is unsatisfactory drainage and improperly constructed drainage systems. The main function of drainage is to inhibit the formation of excessive water head behind the wall. In general, an inclined drainage system is more effective than a vertical system located at the back of the wall. The influence of the presence of drain and its location on excess hydrostatic pressure on a potential failure plane is shown in Figure 6–26 for three states and drain conditions.

Passive pressure. For the walls shown in Figure 6–12, the passive resistance in front of the structure should be neglected unless the wall is extended well below the frost penetration depth, scour, or other possible types of future disturbance and construction. Where passive earth pressure in front of a wall can be considered, AASHTO recommends the computation procedures developed by Caquot and Kerisel (1948) and shown in graphical form in AASHTO Figs. 5.5.2D and 5.5.2E. These aids are for sloping walls with horizontal or sloping backfill and friction at the wall-soil interface. Likewise the movement necessary to mobilize passive resistance may be taken from Table 2–2 or from AASHTO Table 5.5.2A.

Overall Stability

Gravity and semi-gravity walls should be proportioned to ensure stability against sliding, overturning, and bearing capacity failure. For allowable stress design, AASHTO gives the following factors of safety:

Sliding: $FS \geq 1.5$

Overturning: $FS \geq 2.0$ for footings on soil

$FS \geq 1.5$ for footings on rock

Bearing Capacity: See chapter 8

For ASD, unfactored dead and live loads should be used to determine the factor of safety against sliding and overturning. The effect of passive resistance in front of the wall should be considered only where competent soil or rock exists, and according to the foregoing section.

Stability at the strength limit state. For stability analysis purposes, walls can be grouped as follows: (1) walls with clayey soils in the backfill or foundation; (2) walls with granular backfills and foundations on sand and gravel; and (3) walls with granular backfills and foundations on rock (Duncan, Clough, and Ebeling, 1990).

For each group, stability criteria are summarized for ASD method and LFD (load factor design) in Figures 6–27 through 6–29. The uniform pressure distributions shown

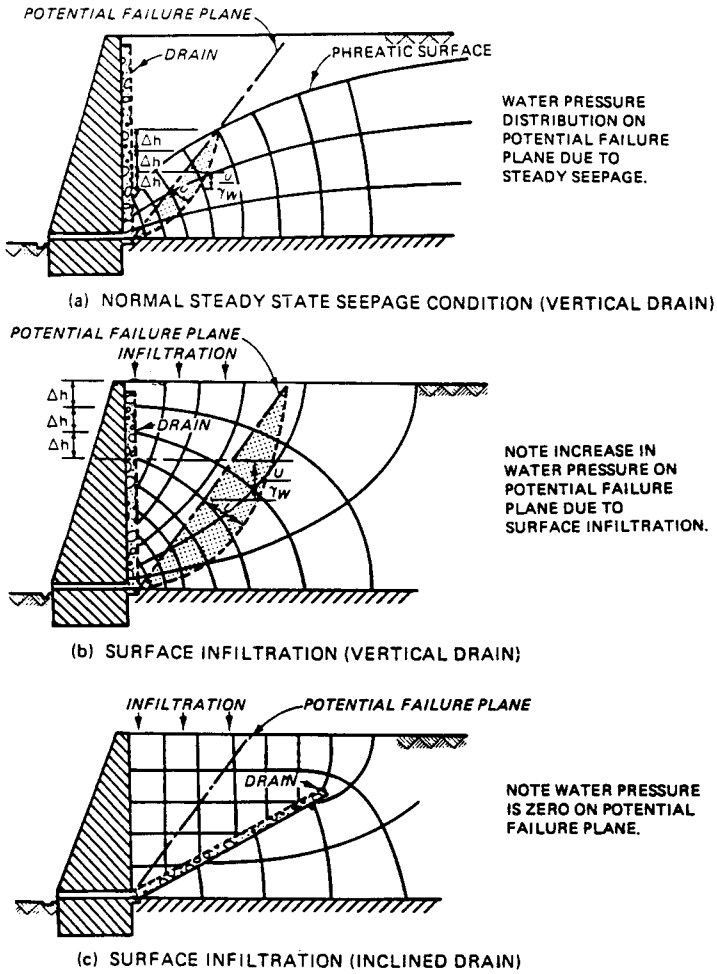

Figure 6–26 Effect of drain location on excess hydrostatic pressures on the failure plane *(from Geotechnical Control Office, 1982).*

in the figures are based on the approach introduced by Meyerhof (1953). Although gravity walls are shown, the same criteria are applicable for semigravity walls that develop similar foundation pressures under the effect of lateral loads.

Design Procedure

For either ASD and LFD, the design is carried out according to the following steps:

1. Select initial proportions and dimensions.
2. Determine loads and earth pressures.
3. Compute reaction on the base.
4. Check overall stability and safety criteria with regard to (a) overturning, (b) safety against sliding, and (c) acceptable bearing pressure.
5. Revise initial design and wall dimensions, and repeat steps 1 through 4, if necessary.
6. Consider foundation alternatives and provide cost comparison.

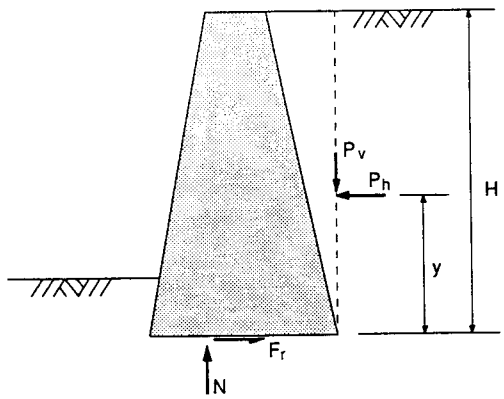

Earth Loads:

P_v and P_h based on experience, with allowance for creep
$y = 0.4\,H$

Stability Criteria:

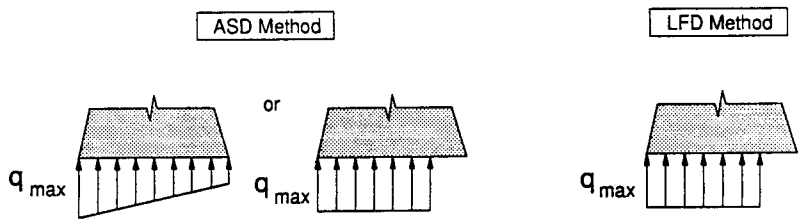

(1) N within middle third of base

(2) $R_I q_{ult} / FS \geq q_{max\ (unfactored)}$

(3) Safe against sliding:

$F_r / FS \geq P_{h\ (unfactored)}$

(4) Settlement within tolerable limits

(5) Safe against deep-seated foundation failure.

(1) N within middle half of base

(2) $\phi R_I q_{ult} \geq q_{u\,max}$

(3) Safe against sliding:

$\phi_s F_r \geq \Sigma r_i P_{hi}$

(4) Settlement within tolerable limits

(5) Safe against deep-seated foundation failure.

Figure 6–27 Earth loads and stability criteria for walls with clayey soils in the backfill or foundation *(from Duncan et al., 1990)*.

Figure 6–30 shows commonly used dimensions for a rigid gravity wall. These proportions can be selected for a first trial at sites where scour is not a problem. Similar proportions and dimensions for a cantilever semi-gravity wall are shown in Figure 6–13.

Reactions on base. A typical cantilever semi-gravity wall subjected to various loads is shown in Figure 6–31. The corresponding reactions are a force N normal to the base, and a tangent force F_r along the base. These reactions are determined from simple statics for each loading group under consideration.

Stability considerations. The location of the resultant along the base is determined by taking moments about the toe 0 of the wall. The stability criterion for ASD is that the resultant must lie within the middle-third (no tension at the interface permitted). For

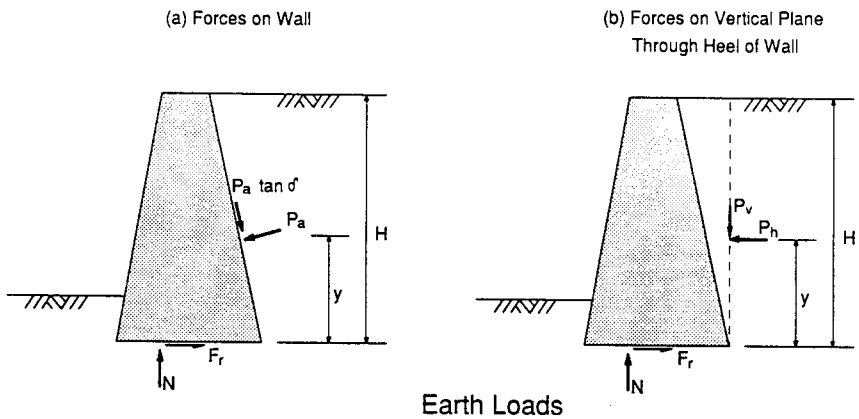

Earth Loads

P_a and P_h calculated using Coulomb active earth pressure theory δ' or P_a estimated using judgement, with allowance for movement of backfill relative to wall.
$y = 0.4\ H$

Stability Criteria

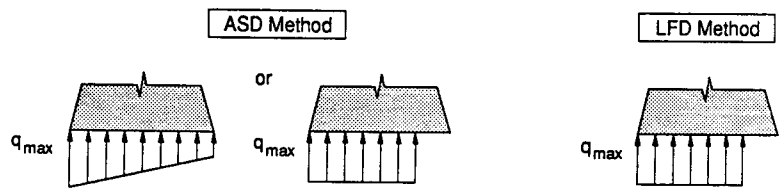

ASD Method	LFD Method
(1) N within middle third of base	(1) N within middle half of base
(2) $R_I q_{ult} / FS \geq q_{max\ (unfactored)}$	(2) $\phi R_I q_{ult} \geq q_{u\ max}$
(3) Safe against sliding: $F_r / FS \geq P_{h\ (unfactored)}$	(3) Safe against sliding: $\phi_s F_r \geq \Sigma r_i P_{h_i}$
(4) Settlement within tolerable limits	(4) Settlement within tolerable limits

Figure 6–28 Earth loads and stability criteria for wall with granular backfills and foundations on sand or gravel *(from Duncan et al., 1990).*

LFD, the criterion is that the resultant must lie in the middle-half, and this criterion replaces the check on the ratio of the stabilizing-to-overturning moment. For walls founded on rock, the acceptable location of the resultant has a greater range than for a wall on soil (see also Figure 6–29).

Referring to Figure 6–31, the dimension X_o giving the location of the resultant is obtained as

$$X_o = \frac{\Sigma M_o}{N} \tag{6–14}$$

where ΣM_o = summation of moments about point 0, and N = vertical resultant force. The eccentricity of the resultant, e, with respect to the mid point is

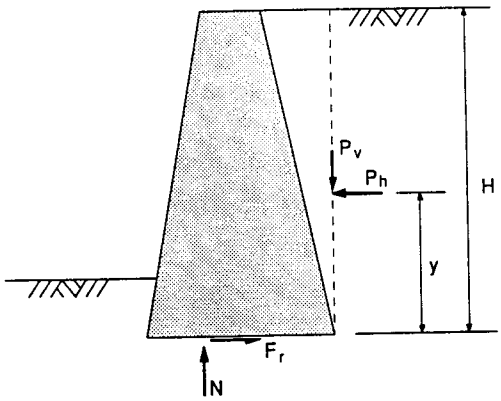

Earth Loads

P_h based on at-rest pressure
K_o : refer to Table 4.6
P_v estimated using judgement
y = 0.4 H

Stability Criteria

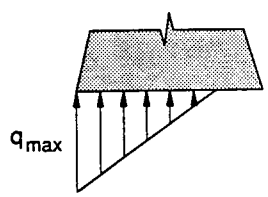

(1) N within middle half of base

(2) $R_I\, q_{ult} / FS \geq q_{max\ (unfactored)}$

(3) Safe against sliding

$F_r / FS \geq P_{h\ (unfactored)}$

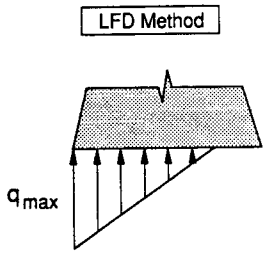

(1) N within middle three quarters of base

(2) $\phi R_I\, q_{ult} \geq q_{u\,max}$

(3) Safe against sliding

$\phi_s F_r \geq \Sigma \gamma_i P_{h_i}$

Figure 6–29 Earth loads and stability criteria for walls with granular backfills and foundations on rock *(from Duncan et al., 1990)*.

$$e = (B/2) - X_o \tag{6–15}$$

where B = base width.

Bearing failure criteria. Protection against bearing failure is ensured by applying a safety factor to the ultimate bearing capacity for ASD, and a performance factor for LRFD. The ultimate bearing capacity may be obtained from in situ tests or it may have its basis on semiempirical procedures (see also subsequent sections).

Thus, safety against bearing failure is checked as follows:

$$ASD \quad R_1 q_{ult} / FS \geq q_{\max} \tag{6–16}$$

$$LRFD \quad \phi R_1 q_{ult} \geq q_{u(\max)} \tag{6–17}$$

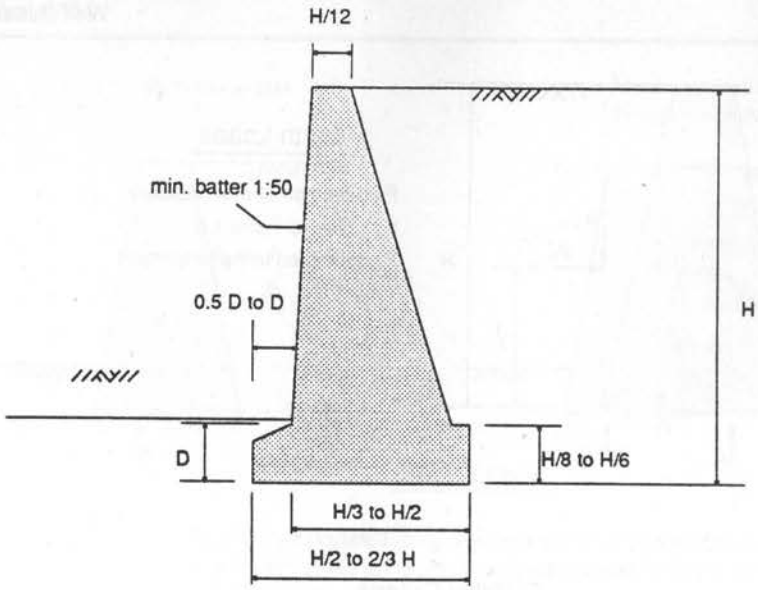

Figure 6–30 Preliminary dimensions for gravity walls.

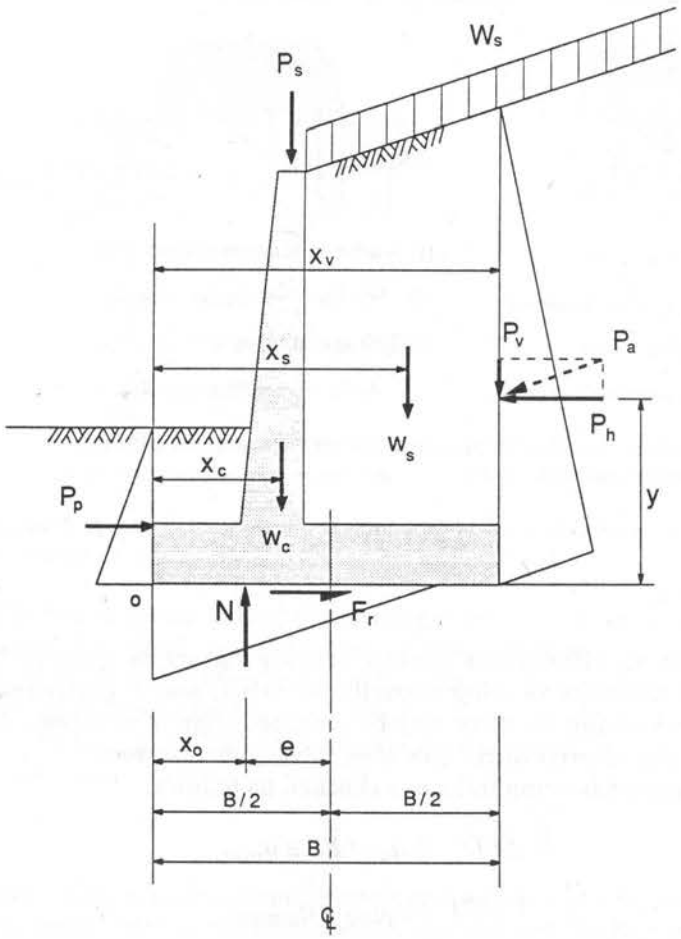

Figure 6–31 Forces on a typical retaining wall or abutment.

where q_{ult} = ultimate bearing capacity; R_1 = a reduction factor due to inclined loads; FS = factor of safety; ϕ = performance (strength reduction) factor; q_{max} = maximum bearing pressure due to unfactored loads (ASD); and $q_{u(max)}$ = maximum bearing pressure due to factored loads (LRFD).

Bearing Pressure Distribution. The bearing pressure distribution diagram for soils may be treated as a triangle, a trapezoid, and rectangle. For rock foundations, the diagram can be a triangle or a trapezoid (see also Figures 6–27 through 6–29). Therefore, the resultant will pass through the centroid of a triangular or trapezoidal distribution diagram, or the middle of a uniform stress block, as shown in Figure 6–32.

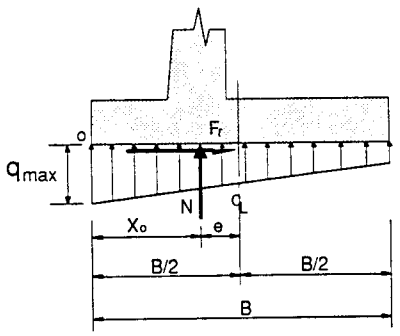

(a) Trapezoidal Distribution

$$q_{max} = \frac{N}{B} + \frac{6Ne}{B^2}$$

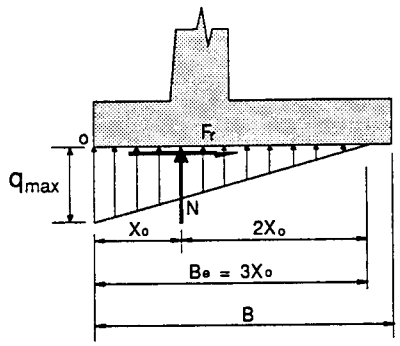

(b) Triangular Distribution

$$q_{max} = \frac{2N}{3X_o}$$

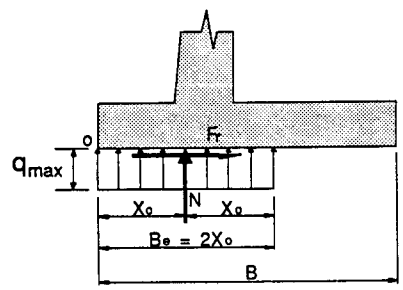

(c) Rectangular Distribution

$$q_{max} = \frac{N}{2X_o}$$

Figure 6–32 Various shapes of stress distributions and maximum bearing pressures.

Maximum Bearing Pressure. The maximum bearing pressures from the diagrams of Figure 6–32 are computed as shown next to the appropriate pressure distribution. Note that q_{max} may also be $q_{u(max)}$, and N may be the unfactored or factored loads.

Stability against sliding. For ASD, stability against sliding is satisfied if

$$\frac{Fr}{FS} \geq P_h \tag{6–18}$$

where FS = 1.5 (according to AASHTO); F_r = frictional resistance and P_h = horizontal force (earth pressure causing sliding). Some investigators recommend a value of FS = 2.0 for clays whose shear strength is less than 0.5 times the normal pressure. The frictional resistance F_r may be computed from

$$F_r = N \tan \delta_b + c_a B_e \tag{6–19}$$

where δ_b = friction angle between base and soil; c_a = adhesion (may be taken as the cohesion of the base soil); and B_e = effective width of base in compression as shown in Figure 6–32.

When sliding stability is checked according to LRFD, the criterion that must be satisfied is

$$\phi_s F_{ru} \geq \Sigma \gamma_i P_{hi} \tag{6–20}$$

Note that F_{ru} is the ultimate force resisting sliding, computed now from

$$F_{ru} = N_u \tan\delta_b + c_a B_e \tag{6–21}$$

where N_u = factored vertical resultant; ϕ_s = performance factor for sliding (values given in Table 6–5); γ_i = load factor for force component i; and P_{hi} = horizontal earth pressure force i causing sliding. Note that discretion is necessary in computing the factored vertical resultant N_u. In some instances the smaller load factors may be appropriate in factoring the load N since this will yield a more conservative requirement.

The inclusion of passive pressure in front of the wall is subject to the criteria discussed in the foregoing sections. When this is included, a factor of safety of 2.0 is recommended for ASD. Conversely, sliding failure may be initiated before the passive earth pressure in front of the wall is fully mobilized, hence in most cases its effect should be ignored.

Values of friction tanδ and adhesion c_a should be taken from AASHTO Table 5.5.5B.

Structural design. The heel section of the base footing or slab should be designed to support the entire weight of superimposed materials. For cantilever walls, the base slabs of counterforted or buttressed walls may be designed as beams (fixed or continuous) spanning between counterforts or buttresses. Note that the critical section for shear in footings is taken as indicated by ACI 318 (at distance d from the face of the stem for the toe section). Some authors suggest, however, to take the shear at the stem face for both toe and heel sections since it is more conservative and requires only a small amount of extra concrete.

Table 6–5 Performance Factors and Safety Factors for Shallow Foundations

Type of Limit State	Performance Factor
1. Bearing Capacity	
a. Sand	
Semi-empirical Procedure (SPT)	0.45
Semi-empirical Procedure (CPT)	0.55
Rational Method:	
using ϕ_f estimated from SPT	0.35
using ϕ_f estimated from CPT	0.45
b. Clay	
Semi-empirical Procedure (CPT)	0.50
Rational Method:	
using shear strength in lab tests	0.60
using shear strength from field vane tests	0.60
using shear strength estimated from CPT data	0.50
c. Rock	
Semi-empirical procedure	0.60
2. Sliding	
a. Precast concrete placed on sand:	
using ϕ_f estimated from SPT	0.90
using ϕ_f estimated from CPT	0.90
b. Concrete Cast in place on sand:	
using ϕ_f estimated from SPT	0.80
using ϕ_f estimated from CPT	0.80
c. Clay (where shear strength is less than 0.5 times normal pressure):	
using shear strength in lab	0.85
using shear strength from field vane test	0.85
using shear strength estimated from CPT data	0.80
d. Clay (where the strength is greater than 0.5 times normal pressure)	0.85

(From Tan, Duncan, Barker, and Rojiani, 1991)

Additional requirements. These relate to tolerable settlement and overall rotational stability. Settlement should be checked for walls placed on compressible soils. The actual (expected) settlement may be predicted using the same methods as for shallow foundations, discussed in other sections. Allowable settlement may be estimated as suggested in section 3.12.

6.7 COMMENTARY ON MECHANICALLY STABILIZED EARTH WALLS

Both AASHTO and the LRFD specifications contain extensive provisions, essentially similar in content and scope, for external stability and sliding, overturning, and bearing capacity and foundation stability.

Safety against structural failure. A preliminary estimate of the structural size of the stabilized soil mass may be obtained considering the reinforcement pullout. For designs according to the LRFD approach, the resistance factors shown in Table 11.5.6-1 (LRFD) have been reduced relative to those for strip reinforcement in view of theoretical and measured uneven stresses in longitudinal members of grids.

Polymeric Reinforcement. The methodology for determining tensile strength (AASHTO Art. 5.8.7.2) has been adopted from the recommended practice proposed by Task Force 27 of AASHTO-AGC-ARTBA. Where polymeric reinforcements are expected to resist tensile loads on a permanent basis, creep-derived tensile strength will govern the determination of usable tensile stresses. Laboratory creep tests may be conducted according to procedures outlined by McGowan and Andrews (1986), which represent modifications to creep test procedures for determining pressure ratings on thermoplastic pipe (ASTM, 1989).

If data from 10,000-hour duration creep tests are not available, creep reduction factors to the tensile strength may be obtained from Mitchell and Villet (1987), and Christopher and Holtz (1985). The resistance factors for tensile strength of polymeric reinforcement reflect the creep reduction factors, as well as the effect of aging, environmental losses, and probable construction damage. The resistance factors for limit state strength introduced by the LRFD specifications include a multiplier of 0.33 for the effects of construction damage, and a multiplier of 0.5 for the effects of postconstruction environmental and aging strength losses. There has been little testing performed to assess the effects of construction damage on polymeric reinforcements. Available test results indicate a minimum reduction factor to tensile strength of 20 percent if the backfill consists of sand, and as much as 70 percent if the backfill consists of gravels or crushed stone.

Minimum Length of Soil Reinforcement. The specified minimum uniform reinforcement length of 70 percent of the structure height has no theoretical basis, but has been used in many successful designs. Parametric studies based on minimum acceptable soil strengths have shown that structure dimensions that satisfy all stability requirements result in length-to-height ratios from 0.8H for low structures (i.e., 10 ft) to 0.63H for high structures (i.e., 40 ft).

Considerable shortening of the reinforcing elements from the minimum specified length of 0.7H may be possible only when accurate, site-specific data on strength of the unreinforced fill and foundation soil are available. There is evidence (Christopher, Gill, Giroud, Juran, Mitchell, Schlosser, and Dunnicliff, 1990), that suggests that shorter reinforcing lengths (i.e., 0.5 to 0.6H) substantially increase horizontal deformations. Where conditions include marginal stability, consideration should be given to ground improvement to enhance foundation stability.

Minimum Front Face Embedment. The minimum embedment requirements have been introduced to preclude local bearing resistance failure under the leveling pad or footing because of higher vertical stresses transmitted by the facing.

Internal stability. MSE walls may be subjected to internal failure by slippage (pullout) or rupture of the reinforcements.

Inextensible Reinforcements. In the analysis of structures stabilized with metallic strip or grid reinforcement, the in situ reinforced zone is assumed to be divided into two regions: the active and resistant zones. The failure surface is assumed to be as shown in Figure 6–33. This distribution is applicable to MSE walls with inextensible reinforcement regardless of the geometry of the reinforcement. The assumed pressure distribution is consistent with theories associated with retaining structures undergoing ro-

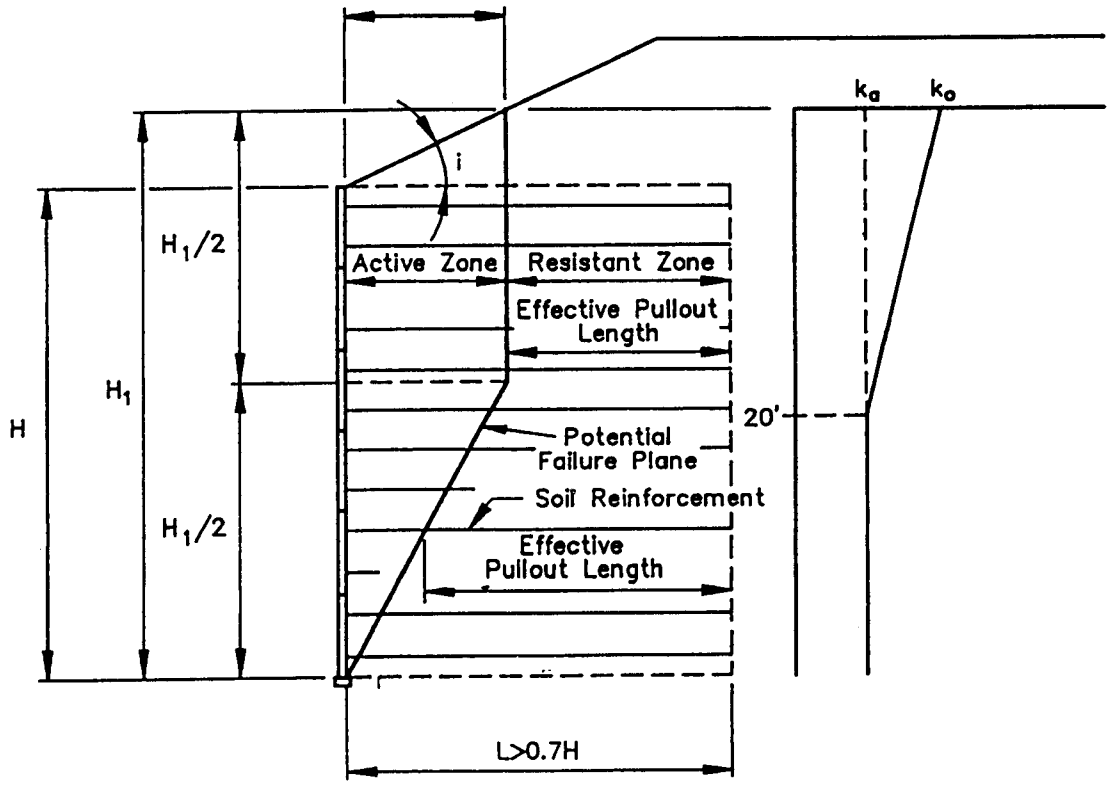

$$H_1 = H + \frac{\tan i \times .3H}{(1-.3 \tan i)}$$

Figure 6–33 Determination of failure plane and earth pressure coefficients MSE wall with inextensible reinforcements.

tation about the top. The earth pressure at the top is taken as the K_o condition, and decreases to the K_a values approximately at the 20-foot depth as shown.

For LRFD design, the factored horizontal stress σ_n at each reinforcement level should be

$$\sigma_h = \gamma_p \sigma_v K \tag{6–22}$$

where γ_p = load factor for each pressure (within the range shown in Table 6–2); K = horizontal pressure coefficient (K_o or K_a); σ_v = pressure due to vertical forces at reinforcement levels being evaluated (LRFD Article 11.9.5.2). The earth pressure coefficients K_o and K_a should be computed as specified in section 2.2.

Extensible Reinforcements. Internal stability must be checked also for wedge failure. In this case the failure plane is defined by a straight line passing through the wall toe and inclined at an angle of 45° + $\phi/2$ from the horizontal. Applicability of this theory to the design of MSE walls with extensible reinforcements has been documented by Bonaparte, Holts, and Giroud (1986), and Christopher et al. (1990).

Pullout design parameters. Both AASHTO and the LRFD specifications give the ultimate pullout capacity of ribbed or smooth steel reinforcing strips as a function of relevant parameters. AASHTO stipulates a maximum apparent coefficient of friction of 1.5 to be used at ground level, as opposed to a maximum value of 2.0 suggested by the LRFD specifications. This coefficient decreases linearly to $\tan\phi$ at the depth of 20 ft, where ϕ is the friction angle of the backfill. This variation of f^* is for ribbed reinforcing strips.

For smooth steel reinforcing strips, the apparent coefficient of friction should be constant at any depth and taken as $f^* = \tan\psi \leq 0.4$, where ψ = soil-reinforcement angle of friction.

Pullout resistance factors are determined from laboratory and field pullout tests, and are based on the capacity attained at a maximum displacement of 1/2 inch or at residual strength, whichever is less. The maximum apparent coefficient for ribbed reinforcing strips is applicable where the uniformity coefficient of the backfill granular fill is greater than about 4, and the backfill meets certain placement requirements.

For grid reinforcing systems, the pullout capacity is given for two cases: transverse bar spacing < 6 inches, and transverse bar spacing > 6 inches. With widely spaced transverse bars, the major portion of the resistance (almost 90 percent) is provided by passive soil action or bearing capacity on the transverse elements. An upper theoretical limit is placed on the passive resistance factor as a conservative approach. Any potential beneficial effects from friction are ignored because of possible strain incompatibility between frictional behavior and passive resistance when peak soil strength is mobilized. Conversely, at a transverse spacing, 6 inches or less pullout resistance is provided mainly by friction developed over the area enclosed by the reinforcement, but relatively limited data are available for closely spaced grids.

A review of theory and experimental record regarding pullout resistance is given by Mitchell and Villet (1987).

6.8 COMMENTARY ON PREFABRICATED MODULAR WALLS

External stability. In general, stability analysis can be carried out assuming that the system acts as a rigid body. Both AASHTO and the LRFD specifications introduce lateral earth pressure diagrams for various wall configurations. Since the wall friction angle δ influences the coefficient of active earth pressure, AASHTO gives values of δ for three main cases:

1. When significant vibrations of backfill are expected, or when the wall settles more than the backfill, $\delta = 0$.
2. When continuous pressure surfaces of precast concrete are provided (uniform width modules), $\delta = 1/2\,\phi$.
3. When averaged pressure surfaces are provided (stepped modules), $\delta = 3/4\,\phi$

These criteria reflect the fact that the wall friction angle δ is not a material property, but is a function of both the direction and magnitude of possible movements. When the

structure settles more than the backfill, δ is negative. Computations for stability should be made at each module level.

Sliding. Computations for stability against sliding may be based on the assumption that the entire soil-fill weight inside the module will be effective in resisting sliding. The coefficient of sliding friction at the wall base should be the lesser of the coefficients of either the backfill or the foundation soil.

Overturning. A maximum of 80 percent of the soil-fill weight inside the module should be considered in resisting overturning effects. The entire mass of soil within the module cannot be relied on in resisting overturning, since some soil will not arch. However, if a structural bottom is provided to retain the soil within the module, the entire soil weight may be included in computing resistance to overturning.

Passive resistance in front of the wall should be neglected in stability computations unless the wall is extended below the anticipated depth of disturbance (scour, freeze-thaw).

Bearing resistance and foundation adequacy. Both AASHTO and the LRFD specifications stipulate that bearing resistance should be computed assuming that dead loads and earth pressures are resisted by point supports per unit length at the rear and front of the modules or at the location of the bottom legs.

For ASD, the allowable bearing capacity for concrete modular units should be computed with a minimum factor of safety of 3 for Group I loading applied to the ultimate bearing capacity. For this computation, a minimum of 80 percent of the soil weight inside the modules should be considered effective. If foundation conditions require a footing under the entire area of the modules, 100 percent of the soil weight inside the modules should be included. Since concrete modular systems are relatively rigid and subject to structural damage under differential settlements, especially in the longitudinal direction, the design should provide a bearing capacity consistent with this behavior.

Structural capacity. In ASD, prefabricated modular units should be designed for developed unfactored earth pressures behind the wall and inside the modules. The rear face should be designed for the difference of these pressures.

Inside pressures (bin) are the same for each module and may be computed as

$$P_i = \gamma_s b \tag{6–23}$$

where P_i = pressure inside bin module; γ_s = unit weight of soil; and b = width of bin module.

For LRFD analysis, bin pressure

$$P_i = \gamma_p \gamma_s b \tag{6–24}$$

where γ_p = load factor for earth pressure. The recommended bin pressure relationships are based on data obtained for long trench geometry, and are generally conservative.

Concrete modules should be designed for bending in both vertical and horizontal directions between the supports. Steel reinforcing should be arranged symmetrically on both faces unless positive identification can be provided to preclude reversal of units.

6.9 DESIGN EXAMPLE 6–1, TRAFFIC UNDERPASS

Loads and forces. A traffic underpass carries an eight-lane roadway with median and safety walks, and has an opening 135 feet face-to-face of supports. The design has considered construction with diaphragm walls as end (abutment) supports, and intermittent panels for the center pier. The superstructure consists of precast box beams with a 4-inch concrete overlay. The bridge will be designed as an integral structure, that is, there are no provisions for expansion devices. Hence, the system must accommodate thermal movement and stresses associated with expansion and contraction.

From superstructure analysis, we select 27″ × 36″ precast box beams, structurally adequate to carry HS 20 loading and 50 lb/ft^2 concrete overlay. The beams weigh 565 lb/lin ft. A 16-foot vertical clearance is specified to accommodate special vehicles. The resulting cross section and final dimensions are shown in Figure 6–34.

The wall is assumed to have a pinned connection with the superstructure (no moment transfer). The base may be detailed as pinned, partially restrained, or fully restrained (fixed). The wall is laterally supported at the bottom by a stiff roadway slab, so that the base condition is essentially a pin support. The wall is therefore a vertical beam simply supported at the top and the bottom. The superstructure accommodates a 30-foot roadway with 3-foot walks on either side, giving a total bridge width 36 feet, or 12 precast box sections. Design criteria are according to AASHTO standard specifications.

Since the walls are not built integrally with the slabs, the span length (height) is the clear span plus the depth (width) of the wall, but need not exceed the distance between centers of supports. The span length is, therefore, 18.5 feet.

Loads from Superstructure. The superstructure is designed and built as two simple spans. The loads are as follows:

- Dead Load. Weight of beams plus overlay (per foot width of deck) is

  (565/3) + 50 = 240 lb, D.L. Reaction = 240 × 34 = 8160 lb = 8.16 kips

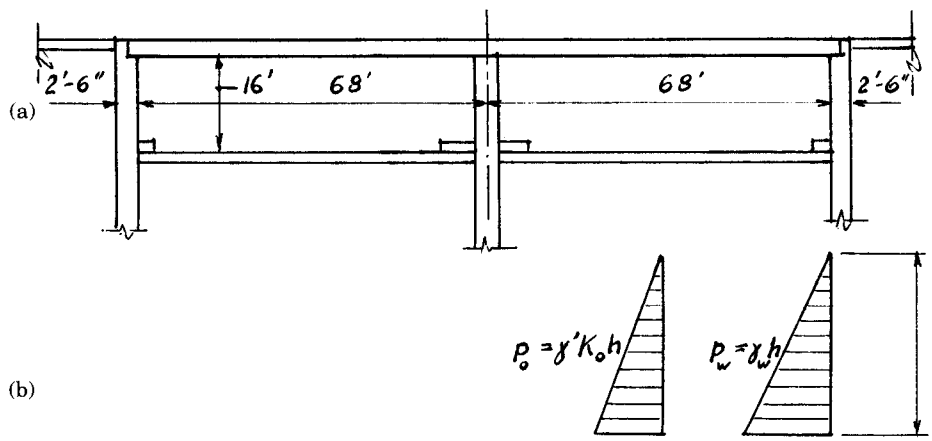

Figure 6–34 (a) Cross-sectional elevation, design example; (b) lateral pressures (earth and water).

- Live Load. For standard truck loading the end reaction (per lane) is 62 kips, or L.L. Reaction = 62 × 2/36 = 3.44 kips, per foot of wall length. This load is assumed to be distributed uniformly along the entire length of the wall. An allowance for impact is based on the standard impact formula, and is I = 26 percent. Impact will be applied to the diaphragm walls as a compressive force but not in the design for lateral earth pressures.
- Surcharge Load. Alternatively, the live load may be considered on the approach roadway and thus generate a corresponding lateral effect. Unlike the complex elastic distributions available to estimate this effect, a uniform surcharge loading is obtained by taking the tributary area of two HS trucks with dimensions 28 ft × 24 ft (axle length × roadway width at the approach), or 144/672 = 0.21 kips/ft^2. The design will also consider a uniform surcharge load from the weight of the approach slab, or 0.15 kips/ft^2. These surcharges are converted to a lateral pressure by multiplying by the appropriate earth pressure coefficient.
- Longitudinal Forces. For one lane occupying the entire bridge length, the longitudinal force is (0.05)(0.64 × 137 + 18) = 5.3 kips.
- Wind Load. May be disregarded since it is unlikely to control.
- Thermal Forces. Assume that the ground conditions and soil stiffness at both ends of the structure are compatible, and that the geometry of the structure justifies the assumption of zero point movement at the center pier. For a cold climate with a temperature range of 80°, the expansion to be accommodated at each end is therefore

$$69 \times 12 \times 80 \times 6 \times 10^{-6} = 0.40 \text{ in}$$

- Earthquake Forces. The bridge site is in a region of moderate seismic activity, so that Group VII in load factor design is unlikely to control.

Lateral Earth Forces. The soil profile consists of a thick layer of medium dense sand with $\phi' = 37°$, $K_0 = 1 - \sin \phi' = 0.40$, and $K_a = 0.25$. The sand layer extends about 35 feet below ground surface, and is underlain by a thick layer of silty clay with s_u = 3.0 kips/ft^2. The water table fluctuates within narrow limits, with a high water level almost 2 feet from ground surface (near the underside of the approach slab), and a normal water level 5 ft below this elevation. Since drainage behind the walls cannot be assured at all times, the walls will be designed for full water pressure and soil pressure for the K_0 condition. Because the sand extends to considerable depth below the excavation level, the structure must also be designed to resist uplift. The pressure diagrams are shown in Figure 6–34(b) for an effective wall height 18.5 ft. Taking γ = 122 lb/ft^3, the effective weight is γ' = 60 lb/ft^3. The corresponding pressures at the base are

$$P_o = (60)(0.40)(18.5) = 440 \text{ lb/ft}, \qquad P_w = (62.5)(18.5) = 1160 \text{ lb/ft}$$

Design of walls. For load factor design, the following groups are considered (load designation corresponds to Table 2–1).

$$\textit{Group I} = \gamma[\beta_D\,(DC) + 1.67\,(LL + I) + \beta_E\,(EA) + \beta_W\,(EW)]$$

where γ = 1.3; β_D = 1.0; DC = dead load from structure; $LL + I$ = live load plus impact from vehicles moving on superstructure; β_E = 1.3 (from Table 6–2, and based on data

from the in situ variability of soil properties); EA = earth pressure for K_o state; $\beta_W = 1.0$; and EW = water pressure.

$$Group\ I\ alternate = \gamma[\beta_D\ (DC) + \beta_{ES}\ (ES) + \beta_E\ (EA) + \beta_W\ (EW)]$$

where ES is the lateral load due to surcharge from approach slab for both dead and live load, and $\beta_{ES} = 1.50$ (from Table 6–2). Group I gives less moment and more axial load, whereas Group I alternate produces more moment and less axial load.

$$Group\ IV = \gamma[\beta_D\ (DC) + (LL + I) + \beta_E\ (EA) + \beta_W\ (EW) + \beta_T\ (T)]$$

$$Group\ IV \text{ alternate} = \gamma[\beta_D\ (DC) + \beta_{ES}\ (ES) + \beta_E\ (EA) + \beta_W\ (EW) + \beta_T\ (T)]$$

where $\gamma = 1.3$; $\beta_{ES} = 1.0$ (the same as the load coefficient for live load in Group IV); $\beta_E = 1.3$; $\beta_W = 1.0$; and β_T and T is the load coeffficient and the force due to temperature, respectively.

The value of T is the additional earth pressure mobilized as the wall moves towards the soil to accommodate the thermal expansion of the deck. Recall that thermal expansion is 0.40 inch at each end. For a wall height 18.5 feet, the ratio Δ/H is $0.40/(18.5 \times 12) = 0.0018$. The coefficient K denoting passive resistance mobilized by this movement is obtained graphically from Figure 2–1 for $\phi' = 37°$ and $\Delta/H = 0.0018$ as about 1.45. Note that the walls in the example satisfy either pattern of movement associated with these graphs, shown in Figure 2–2. The earth pressure representing T is, therefore, the difference between $K = 1.45$ and $K = 0.4$.

Since T is not considered a resistance but an active force, we will apply a load coefficient $\beta_T = \beta_E = 1.3$, so that in Group IV and alternate the sum $(EA + T)$ is consolidated into one calculation using an earth pressure coefficient $K = 1.4$. Note also that for Group IV alternate, ES will be computed for a uniform surcharge $0.21 + 0.15 = 0.36$ k/ft^2 multiplied by $K = 1.45$.

Analysis for Group IV Alternate. The problem is reduced to the following: (1) an axial load $P = (8.16 + 0.38\ h)$ kips where h = height from wall top, and P = load per linear foot of wall; (2) a uniform pressure $0.36 \times 1.45 = 0.52$ kips/ft along the entire wall height; (3) an earth pressure $P_e = (60)(1.45)(h)$; and (4) hydrostatic pressure $P_W = (62.5)(h)$.

The corresponding lateral pressure diagrams are shown in Figure 6–35.

From Figure 6–35(a) we calculate $R_A = R_B = 4.81$ kips

From Figure 6–35(b) we calculate

$R_A = 14.89 \times 1/3 = 4.96$ kips $\qquad R_B = 9.93$ kips

From Figure 6–35(c) we calculate

$R_A = 10.73 \times 1/3 = 3.57$ kips $\qquad R_B = 7.16$ kips

The maximum moments are computed as follows:

$M_{ES} = (0.125)(0.52)(18.5)^2 \qquad = 22.3$ ft-kips

$M_{EA} = (0.1283)(14.89)(18.5) \qquad = 35.3$ ft-kips

$M_W = (0.1283)(10.73)(18.5) \qquad = 25.5$ ft-kips

and $M_u = 1.3(22.3 + 1.3 \times 35.3 + 25.5) = 121.8$ ft-kips

Note that the design is controlled by minimum axial load and maximum moment. Thus the axial load P may be reduced to 75 percent, or may be omitted assuming that it may dissipate by shear resistance along the wall-soil interface.

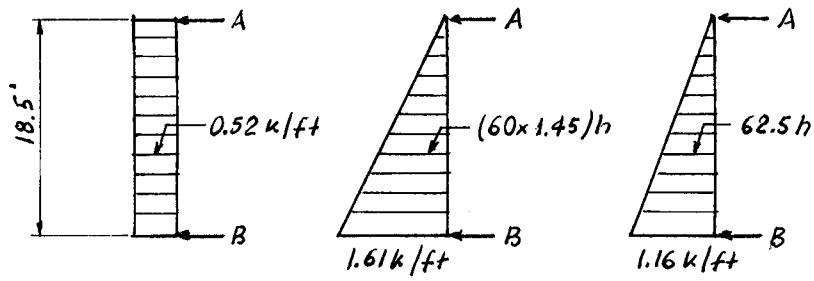

Figure 6–35 Pressure diagrams, analysis for Group IV alternate; (a) surcharge; (b) earth pressure; (c) water pressure. Design example 1.

Omitting P yields a member subject to flexure. For a wall 30-inch thick, we estimate d = 26 inches. Also f_y = 40,000 lb/in^2, and f'_c = 3500 lb/in^2. Next we select A_s = 1.71 in^2 provided by #9 @ 7 in. From AASHTO Equation (8–17) we compute

$$a = A_s f_y / 0.85 f'_c b = (1.71)(40{,}000)/(0.85 \times 3500 \times 12) = 1.9 \text{ in}$$

The nominal moment capacity is computed from AASHTO Equation (8–16) as

$$M_n = A_s f_y \left(d - \frac{a}{2} \right) = (1.71)(40)(2.08) = 142 \text{ ft-kips}$$

or $\phi M_n = 0.9 \times 142 = 127.8$ ft-kips > 121.8 ft-kips, OK.

The reinforcement ratio is $1.71/(12 \times 26) = 0.0055$, OK.

Uplift. Taking the water table at the underside of the approach slab gives an extreme condition. With ASD the usual practice is to provide a safety factor of 1.5 to 2.0 in resisting uplift. If this effect is resisted solely by dead weight (dead load from structure, overlying soil, etc.), the load factor design method simply reverts to ASD since it examines loads and resistances of nominal variability (dead load, water pressure). If dead load is not the only means for resisting uplift, the problem may be analyzed by the load factor approach where the standard calibration process provides a safety index that compares favorably with the intent of ASD. This is demonstrated as follows:

First compute the dead load from Figure 6–34 where member sizes and dimensions are selected to provide the required structural capacity excluding uplift effects.

- D.L. weight of superstructure = $8.16 \times 4 = 32.6$ kips
- D.L. diaphragm walls (plus center wall). Assume walls to extend 3 ft below underside of base slab:

  Weight = $3 \times 24 \times 0.37$ = 26.6 kips
- D.L. bottom slab = 0.30×136 = 40.8 kips

  Total D.L. 100.0 kips

The uplift caused by a water head of 20 feet is $20 \times 62.5 = 1.25$ kips/ft^2, or total uplift = $136 \times 1.25 = 170$ kips/ft of structure.

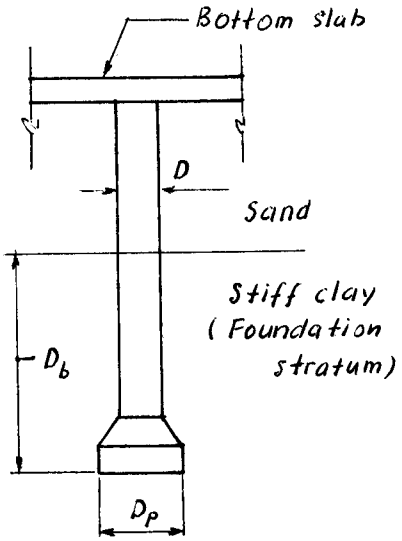

Figure 6–36 Uplift of underreamed shaft. Design example 1.

For a safety factor of 1.5 ASD, the dead load resists 100/1.5 = 67 kips of uplift forces, corresponding to a load reduction factor 0.67 (An alternative is to apply a factor of 0.75 to the dead load). The remaining uplift force 170 − 67 = 103 kips must be resisted by a deep foundation, such as drilled shafts, designed to resist pullout and proportioned to also resist tensile stresses. The assumption is made that there is no swell potential associated with expansive soils.

For underreamed shafts, the uplift resistance is estimated neglecting the side resistance above the bell, and assuming that the bell behaves as an anchor. Referring to Figure 6–36, the factored uplift capacity of the belled shaft is

$$Q_r = \phi Q_n = \phi Q_{s(bell)} \tag{6–25}$$

where

$$\phi Q_{s(bell)} = q_{s(bell)} Au \tag{6–26}$$

Also $q_{s(bell)} = N_u s_w A_u = \pi(D_p^2 - D^2)/4$, N_u = uplift resistance factor; D_p = diameter of bell; D = diameter of shaft; D_b = depth of embedment in the founding layer. Recall that s_u = 3.0 kips/ft^2. The factor ϕ is taken as 0.55 (this will correspond to a factor of safety of 1.8 in ASD). A lower factor is justified since drilled shafts in tension tend to unload the soil, which reduces the overburden stresses and hence the uplift resistance.

From the foregoing data we compute

$$A_u = 3.14(6^2 - 3^2)/4 = 21.2\text{ft}^2$$
$$q_{s(bell)} = 8.0 \times 3.0 = 24$$
$$Q_{s(bell)} = 24 \times 21.2 = 509 \text{ kips}$$

and

$$Q_R = 0.55 \times 509 = 280 \text{ kips/shaft}$$

The structure directly under the bridge is 36 feet long, and is subjected to a total uplift (remaining) 103 × 36 = 3708 kips. The required number of shafts is therefore 3708/280 = 13.2, say 14, shafts. These should be arranged along the bottom slab so that each shaft receives the same uplift reaction.

Resistance to uplift may also be considered in the form of additional weight of the

bottom slab. For the permanent condition, uplift may be eliminated if the walls are extended into the clay layer but the solution is not always possible, especially if the direction and source of groundwater flow are not exactly known. A final solution should be based on economic analysis of feasible options.

6.10 DESIGN EXAMPLE 6–2, ANCHORED DIAPHRAGM WALL

Figure 6–37 shows a diaphragm wall braced at two levels by ground anchors. With little or no prestressing, the loads developed in the anchors will correspond to the active state, if sufficient movement occurs to yield this condition, or to partially at rest pressures if movement is restrained. In any other case, lateral earth stresses behind the wall will be manifested by the level and sequence of prestressing.

In practice, prestressing is introduced to a level that is quite variable and often arbitrary. It may be related to ultimate or allowable anchor capacity, or it may have a theoretical basis. The variance of the methods is demonstrated in Table 6–6 (Xanthakos, 1991), and evidently these methods cover limiting equilibrium and apparent pressure theories.

The choice of an appropriate earth pressure diagram for estimating anchor prestress loads first depends on the tolerable wall and soil movement. If important adjacent structures are sensitive to settlement, increased prestressed levels provide a good choice in restricting excessive movement. These levels may be based on apparent pressure diagrams, earth pressure at rest, or active pressure increased by a factor 1.5 to 2.0. Field monitoring of walls shows that these higher pressures are likely to remain unless a major stability problem arises. If the surroundings can tolerate some movement, the prestress may be reduced to smaller values, for example, 75 percent the Terzaghi Peck apparent pressure or 1.25 times the active pressure.

For overall stability, we assume the failure plane to be as shown. The soil is dense sandy silt with $\phi = 30^\circ$ and $\gamma = 110$ lb/ft^3. We estimate $K_o = 0.5$ and $K_a = 1/3$.

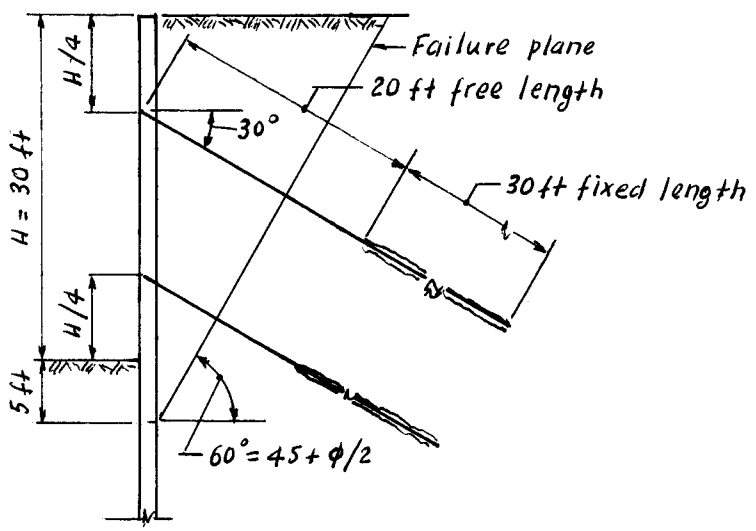

Figure 6–37 Wall section and anchor layout.

Table 6–6 Summary of Methods Used to Estimate Prestress Load on Anchors

Reference	Method
Kapp	Percentage of allowable tie-rod load (20–60%)
Mansur and Alizadeh	At-rest pressures
Rizzo, et al.	Active to at-rest
Shannon and Strazer	50% anchor yield load
Clough, et al.	Terzaghi–Peck rules ($0.4\gamma H$)
Liu and Dugan	15 × height wall (in psf)
Hanna and Matallana	Pressures halfway between active and at-rest
Oosterbanna and Gifford	Active pressures
Larsen, et al.	Pressures between active and at-rest

The horizontal earth thrust is computed for the K_o condition as follows:

$$P_e = 1/2\ \gamma K_o H^2 = 1/2\ (110 \times 0.5)(30)^2 = 24{,}750 \text{ lb/ft of wall (say 25,000 lb/ft).}$$

With these data the design is completed according to the following steps:

Step 1. Select anchor vertical spacing. We specify two rows of anchors, each row located at the one-quarter point from the top and bottom.

Step 2. Anchor horizontal force. The triangular pressure distribution is converted into a rectangular diagram of the same total magnitude. Each anchor is then assumed to take a load component from the top or bottom of the wall to the midheight, or 12,500 lb/ft. This load provides the basis for determining the prestress force, and is therefore an apparent load.

Step 3. Anchor inclination. The anchors are to be installed in dense sandy silt so that suitable anchoring strata are close to the ground and a steep angle is not necessary. Considering possible influence from adjacent utilities, foundations, and wall drawdown induced by anchor vertical component, we select an angle of 30° with the horizontal.

Step 4. Determine anchor load. For anchor inclinations of 30°, the anchor load is 12.5/cos 30° = 14.4 kips/ft for both upper and lower rows. For a horizontal anchor spacing of 10 feet, the design anchor load is 14.4 × 10 = 144 kips. For final design, the 10-foot spacing must be checked for compatibility with optimum wall panel length. An anchor load of 144 kips has a vertical component 144 × sin 30° = 77 kips. The design must, therefore, ensure that this load can be transferred to the ground by base bearing or side shear.

Step 5. Determine fixed anchor length. Since the sand is fine-grained but dense, cement grout injected under pressure will produce type B anchor zone (see also Figure 6–3) with essentially nonuniform diameter. From this consideration, we assume an effective hole diameter of 9 inches, which is consistent for a borehole diameter 4 to 6 inches. Assuming a height of overburden of 25 feet above the top of the fixed zone, we estimate $p' = 2 \times 25 = 50$ psi. For ASD and a factor of safety of 2, the fixed anchor length is obtained from Equation (6–8) as

$$L = \frac{2 \times 144{,}000}{50 \times 3.14 \times 9 \times \tan 30°} = 353 \text{ in} = 29.4 \text{ ft; Use 30 feet.}$$

Step 6. Determine failure plane and anchor free length. Using $\phi = 30°$, the failure plane is assumed to begin 5 feet below excavation level. The length from upper anchor

entry point to failure plane is 25.75 × sin 30° = 12.9 feet. Allowing 5 feet of penetration beyond the failure zone, the free length for the upper row is about 18 feet, say 20 feet. The same length is used for the lower row to provide the minimum stressing length.

Step 7. Select tendon steel for design load 144 kips. We select 0.6-in-dia 270-ksi strand, and an anchor tendon consisting of 5 strands. For a factor of safety of 2, the required steel area is 2 × 144,000/270,000 = 1.07 in^2. Each strand has a cross-sectional area 0.215 in^2, or total steel area provided = 5 × 0.215 = 1.07 in^2.

Anchor load capacity should be verified by field tests (Xanthakos, 1991).

6.11 DESIGN EXAMPLE 6.3, STABILITY OF GROUND-ANCHORED WALL SYSTEM

In the foregoing example, the slip failure is assumed to have a planar configuration. The forces acting in this manner are compared with the resisting force developed along the slip plane, and a factor of safety is thus established. Deformations are not computed, but lumped into the factor of safety. In the simplest form, the plane failure surface begins at the base of excavation and extends at an assumed angle (usually based on the Coulomb theory). Alternatively, the failure plane may be assumed to begin at the base of the wall, or at some distance below excavation level, as in Figure 6–37. The latter approach gives more conservative results. Probably a more realistic assumption of limit equilibrium analysis is a failure along a circular slip surface, often preferred by designers, based on the Fellenious slip circle, supplemented by Huder (1965), Locher (1969), and Malijain and Van Beveren (1974).

The sliding block method (Kranz, 1953) was essentially formulated with the intent to simplify the analysis by replacing the actual experimental failure shown in Figure 6–38(a) by the composite surface shown in (b) and (c). The failure prisms (*dce*) in active pressure as well as in passive (*bhg*) are replaced by equivalent forces P_a and P_p as shown in (c). With this simplification, the analysis shifts from the complex system wall-ground-anchors to the soil mass M represented by block *ecbf*. The wall and the anchors are replaced by their reactions on the mass, $-P_A$ for the wall and A for the tension in the anchor. The analysis is then carried out for a unit length of excavation.

Example with one row of anchors. Figure 1–14(b) shows a diaphragm wall in the uncovered section for approach roadway. If the base roadway is essentially a flexible pavement, the wall-ground-anchor system derives its stability by the anchorage at the top and wall embedment at the bottom. The analysis of this problem will be considered according to the Kranz method.

Referring to Figure 6–38, the soil mass M is defined by planes *bf* and *ce* and by a curved failure line *bc,* where *b* is the point of zero shear in the wall. Point *c* is located on the anchor axis at either of the following distances from the end.

- Half the fixed anchor length L_s if the spacing B between two adjacent anchors of the same row is less than or equal to $L_s/2$.
- Equal to B where $B > L_s/2$.

The failure curve *bc* represents a circle whose tangent at point *b* has an angle $(\pi/4 - \phi/2)$ with the wall as shown. This assumption is as close to reality as possible, since a

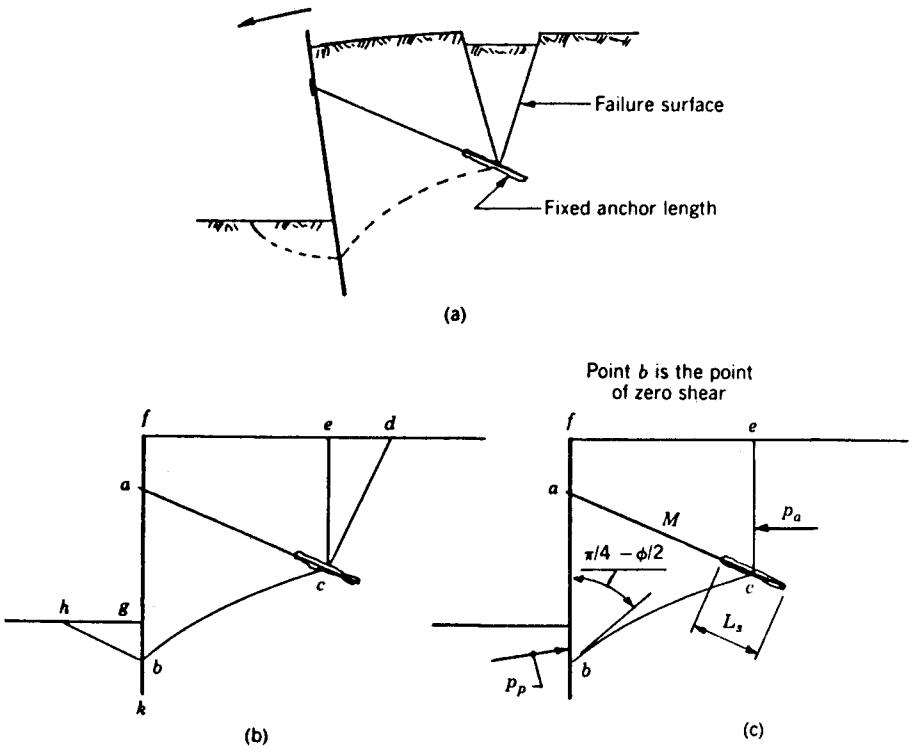

Figure 6–38 Failure of an anchored wall-ground system; (a) actual mode of failure; (b,c) simplification of the wall anchor system for stability analysis, using the sliding block method.

straight line between points *b* and *c* may yield conflicting results. The forces included in the equilibrium of the block are shown in Fig. 6–39, and are as follows:

1. Known Forces. These are W = weight of soil mass M; $-P_A$ = wall reaction equal to active pressure on height *bf;* and P_a = active pressure on plane *ec.* These three forces are calculated using effective stress since water pressure, if any, cannot stabilize the soil mass M, and hence should not be considered. Water pressure, however, may have to be introduced as horizontal component in P_a and vertical component in W. The force A is the tension in the anchor, and the force F_e is the resultant of exterior forces applied to the soil mass but having no stabilizing effects.
2. Unknown Forces. These are the two components due to friction and cohesion c of the reaction along surface *bc.* The cohesion component Q_c is parallel to *bc* and has a magnitude $2cR_o\sin\theta_o$ at distance $d = R_o\,\theta_o/\sin\theta_o$ from center O. The friction component Q_f is tangent to a circle with radius $R_o\sin\phi$. The forces Q_c and Q_f are limit values corresponding to the failure condition.

Computational Approach. As a first step we determine the direction and magnitude of the resultant R of forces $W, -P_A, P_a, A$ and F_e. On the main diagram of Figure 6–39, we establish the intersection point t of the resultant R with the Q_c axis. Initially the polygon is drawn for the forces A, P_a, W and $-P_A$ as shown in Figure 6–39, terminating at point u. A factor of safety is then selected and the polygon is completed from

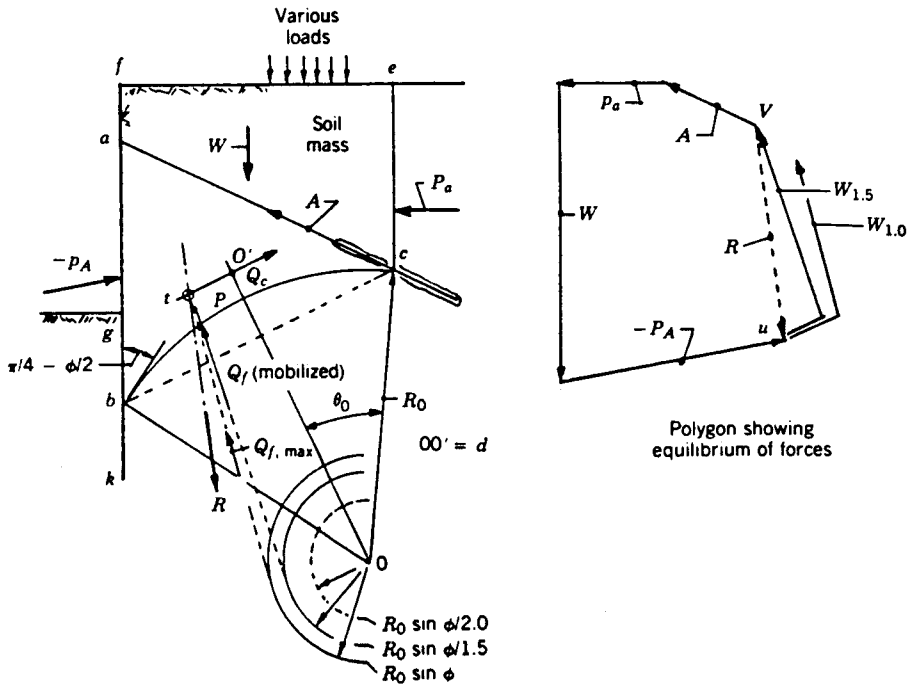

Figure 6–39 Assumed condition, forces and equilibrium diagrams for a sliding block necessary for stability analysis.

point u by adding two vectors as follows: (1) a vector equal to Q_c/F_s, and (2) a vector parallel to the tangent drawn from point t to the circle with radius $R_0 \sin\phi/F_s$, centered at O. The actual value of the factor of safety F_s is determined by trial-and-error procedure until the polygon of forces is closed exactly at point V. This factor is preselected by the designer.

The analysis is considered satisfactory if (1) the factor of safety F_s is at least 1.5; (2) point P where the Q_f line intersects circular surface bc is located in the central area of bc; and (3) the average stress along bc is the allowable (ASD) obtained from the failure stress with a factor of safety of 3.

6.12 DESIGN EXAMPLE 6–4, POSTTENSIONED DIAPHRAGM WALL

Basic concepts. Posttensioned diaphragm walls were discussed briefly in section 6.1. Typical wall configurations suitable for prestressing are shown in Figure 6–5. A consideration relevant to the design is the plurality of stages of loading corresponding to the excavation stages. For cast-in-place walls, the posttensioned concrete is designed for two stages: the initial stage with the wall fully embedded, and the final stage with full excavation completed. In some cases intermediate excavation stages may have to be considered.

Under allowable stress design, the permissible stresses are as follows:

Steel Stresses. Both the ACI Code and AASHTO specifications allow a stress in the prestressing steel of posttensioned members 0.70 f'_s where f'_s is the ultimate strength.

Concrete Stresses. A distinction is made for temporary stresses and of service loads after losses have occurred.

1. Immediately after transfer of prestress, extreme fiber stress
   Compression = $0.60 f'_{ci}$ (ACI) or $0.55 f'_{ci}$ (AASHTO)
   Tension = $3\sqrt{f'_{ci}}$
2. At service load after allowance for all prestress losses
   Compression = $0.45 f'_c$ (ACI), or $0.40 f'_c$ (AASHTO)
   Tension = $6\sqrt{f'_{ci}}$ (for members with bonded reinforcement)

where f'_{ci} = compressive strength of concrete at time of initial prestress, and f'_c = compressive strength of concrete at 28 days.

Resistance Factors. The computed strength capacity should not be less than the factored load effects. Strength (resistance) capacity factors ϕ should be applied to the nominal strength as follows:

- For flexure $\phi = 0.90$ (ACI), or 0.95 (AASHTO)
- For shear $\phi = 0.85$ (ACI), or 0.90 (AASHTO)

The design of prestressed concrete members ordinarily is based on $f'_c = 5000$ lb/in^2, with provisions for increase to 6000 lb/in^2. Since controls over materials and construction procedures of diaphragm walls cannot be instituted to the desired level, the strength range recommended by this author should be followed.

Final Design. This should include an accurate determination of stresses (and deformations) at the critical stages of loading. The following basic procedure is suggested:

1. Select appropriate load factors and loading groups that may govern.
2. Investigate compressive and tensile stresses in the concrete at transfer, generally using elastic theory.
3. Check factored resistance for final load stage based on an effective lever arm for the internal resisting couple.
4. Perform checks for excessive deflections and overstress. Where computer programs are available and reliable values of the horizontal subgrade reaction are obtainable, the analysis may consider the restraining effect of soil stiffness when the prestress is applied. If data are not available, this effect may be approximated if the wall is in stiff or dense ground, and ignored if the wall is cast in soft or loose ground.

Example. A 30-foot wide underpass has two diaphragm walls as end supports. The walls are braced laterally at the bottom by embedment into rock, and at the top by the deck of the structure. The unsupported wall height is 25 feet, and this is also the design span. The rock is overlain by loose sand with $\phi' = 28°$, and it is conceivable that the groundwater level may at times rise close to the street level. The wall must also resist a uniform lateral pressure 250 lb/ft^2 resulting from live load surcharge. The loads in the final position are, therefore: dead load from the deck, live load surcharge, water pressure, and lateral earth pressure.

The construction sequence will be as follows: (1) construct the diaphragm wall; (2)

introduce the prestressing at an appropriate time; (3) construct the deck supported on the walls, and bracing them at the top; and (4) excavate under roof and construct the underpass.

Step 1. Establish lateral pressure diagrams and appropriate design parameters. The coefficient of at rest pressure is $K_o = 0.53$. For $\gamma = 120$ lb/ft^3, $\gamma' = 57.5$ lb/ft^3. Lateral pressures at the base of the wall are as follows:

Effective earth pressure	= (57.50)(0.53)(25)	= 762 lb/ft
Pore pressure	= (62.5)(25)	= 1,562 lb/ft
Surcharge pressure	= 200 lb/ft	

The total resultant pressures are, therefore

Earth pressure	= (0.76)(25)/2	= 9.50 kips
Pore pressure	= (1.56)(25)/2	= 19.50 kips
Live load surcharge	= (0.20)(25)	= 5.0 kips

Wall section and pressure diagrams are shown in Figure 6–40. The wall is socketed into rock and is restrained against any translation at this point. Hence, passive resistance in front of the wall is unlikely below excavation level, and any pressure in this region is thus neglected in the computations.

Step 2. Compute maximum moments. From beam formulas we obtain

Earth pressure	M_e	= (0.1283)(9.50)(25) = 30.4 ft-kips
Pore pressure	M_W	= (0.1283)(19.50)(25) = 62.6 ft-kips

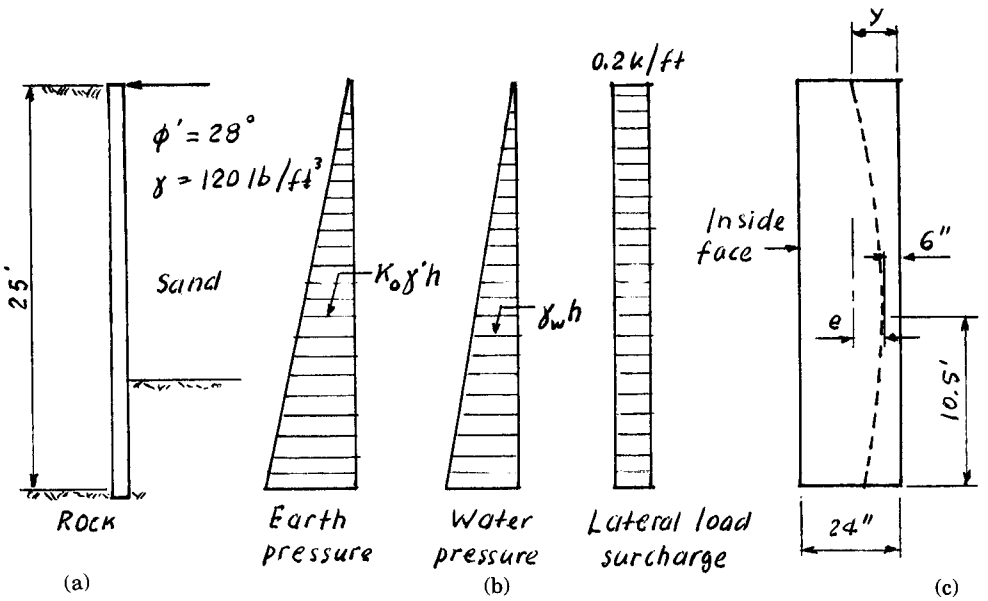

Figure 6–40 Wall of Design Example 4. (a) Wall section; (b) pressure diagrams; (c) tendon profile and details.

Live load surcharge $M_L = (0.125)(0.20)(25^2) = 15.6$ ft-kips

Total maximum moment at service loads $M_s = 108.6$ ft-kips

(Note: the maximum moment $M_s = 108.6$ ft-kips is approximate but conservative since the point of maximum moment for triangular diagrams is actually $0.577h$ from the top).

For strength design, the moments are factored accordingly. For this example we select a coefficient $\beta = 1.7$ for the earth pressure and the live load surcharge, and $\beta = 1.0$ for the water pressure. The factor γ is 1.30.

$$M_u = 1.30(46.0 \times 1.7 + 62.6) = 183 \text{ ft-kips}$$

Step 3. Select wall thickness and area of prestressing steel. Also $f'_c = 4000$ lb/in^2. A wall thickness of 24 inches is initially considered adequate, and is also the practical minimum for posttensioned diaphragm walls. We also select an area of prestressing steel $A_s^* = 0.60$ in^2/per foot of length of wall. At the point of maximum moment, the prestressing steel is located 6 inches from the outside (tension) face of the wall. The strands are arranged according to a parabolic profile, whose geometry is established by the design. The details are shown in Figure 6–40(c). At the section of maximum moment the eccentricity is $e = 6$ inches.

Step 4. Check stresses at transfer. We assume that the prestressing is applied when $f'_{ci} = f'_c = 4000$ lb/in^2, and that the restraining effect of the soil stiffness is disregarded in the initial computations.

The section properties of the wall are

$$A = 12 \times 24 = 288 \text{ in}^2$$

$$I = 12 \times 24^3 / 12 = 13824 \text{ in}^4$$

At the section of maximum eccentricity (also maximum moment) we compute the following:

For $A_s^* = 0.60$ in^2, and assuming 15 percent prestress losses, $f_{se} = 270 \times 0.65 \times 0.70 = 160$ ksi, giving a prestressing force $F = 0.60 \times 160 = 96$ kips/ft of wall. Hence

$$F/A = 96{,}000/288 = 333 \text{ lb/in}^2$$

$$Fey/I = (96{,}000)(6)(12)/13824 = 500 \text{ lb/in}^2$$

At transfer the stresses in the concrete are

compression $f_c = 333 + 500 = 833$ lb/in^2

tension $f_t = 333 - 500 = -167$ lb/in$^2 < 3\sqrt{f'_c} = 190$ lb/in^2, OK

Step 5. Check stresses for service conditions with excavation completed. $M_s = 108.6$ ft-kips. Compute

$$M_s y/I = (108{,}600)(12)(12)/13824 = 1132 \text{ lb/in}^2$$

The stresses in the concrete are now

compression $= 1132 - 167 = 965$ lb/in$^2 < 0.40 f'_c = 1600$ lb/in^2

tension $= -(1132 - 833) = -299$ lb/in$^2 < 6\sqrt{f'_c} = 380$ lb/in^2

Step 6. Check section for factored moments and strength design.
First we compute the steel ratio

$$P_p^* = \frac{0.60}{12 \times 18} = 0.0028$$

Next, we calculate the stress f_{su}^* (average stress in prestressing steel at ultimate load) for bonded members (AASHTO Eq. 9–17). Note that $\gamma^* = 0.40$ (stress-relieved steel) and $\beta_1 = 0.85$.

$$f_{su}^* = (270{,}000)\left[1 - (0.47)(0.0028)\frac{270{,}000}{4000}\right] = 245{,}700 \text{ lb/in}^2$$

The prestressing force is now $T' = (0.60)(245.7) = 147.4$ kips $= C'$.
Next we compute $a = (147.4)/(0.85 \times 4 \times 12) = 3.6$ inches.
The nominal moment M_n may be computed from

$$M_n = T'\left(d - \frac{a}{2}\right) = (147.4)\left(\frac{18 - 1.8}{12}\right) = 199 \text{ ft-kips}$$

or $\phi M_n = (0.90)(199) = 180$ ft-kips $\approx$183 ft-kips, OK. The conclusions from the foregoing analysis are:

1. The compressive strength of concrete is unlikely to govern the design because of the normally adequate wall thickness;
2. the live load should be placed on the outside of the bridge to induce lateral affects rather than vertical load;
3. the restraining effect of the soil stiffness is only a temporary benefit since it does not enter into the final analysis;
4. the prestressing force level is nominal and within the generally accepted practice; and
5. some tension may be allowed since all the loads are not sustained loads.

6.13 SEISMIC DESIGN REQUIREMENTS OF WALL SYSTEMS

General Principles

The principal functions of the wall systems discussed thus far are as retaining walls and as abutment supports at the ends of underpasses. Seismic effects on these structures generally depend on the relative stiffness of the support and the associated soil mass. Two main categories of soil-structure interaction are articulated: (a) flexible walls which move away from the soil sufficiently to minimize the soil pressure; and (b) rigid structures such as the walls discussed in this chapter.

Other articulations may refer to the class of structure and the functional requirements. For example, diaphragm walls for deep building basements typically are built to finish grade (usually street level), and are extended to a depth dicated by the basement enclosure or for the load transfer. Likewise, walls for subway construction are usually terminated at the top slab of the section, and may be extended below the base slab level for initial stability requirements. Unlike these systems, walls for bridges and highway

construction function as retention systems or as end supports to carry superstructure loads.

As mentioned in the foregoing sections, in the present state of knowledge, the recommended method of obtaining seismic earth forces is based on the use of equivalent static coefficients. Dynamic analyses using finite element techniques may be warranted for exceptional structures and conditions. In the equivalent static method a horizontal earthquake force equal to the weight of the soil wedge multiplied by a seismic coefficient is assumed to act at the center of gravity of the soil mass. This earthquake force is added to the static forces on the wall.

In the general case, the total earth pressure on a wall during an earthquake event is the composite effect of three possible contributions:

1. Static pressure due to gravity loads
2. Dynamic pressure due to the earthquake
3. Pressure due to the wall being displaced into the backfill by an external force, such as the horizontal sway of a bridge deck at a monolithic abutment (Matthewson, Ward, and Berrill, 1980).

We should note that it is not necessary or appropriate to design all earth-retaining structures for earthquake soil pressures. In several countries, for example, external retaining walls of modest height and without significant consequence of failure are generally not designed for earthquakes. It can be readily seen that an effective ground acceleration of about 0.3 g is required to produce an earthquake force increment equal to the static earth pressure for cohesionless soils. This means that a safety factor of 2.0 in a non-seismic design should allow walls to survive moderate earthquakes with acceptable displacements and tolerable damage. This rationale is applied to bridge design in New Zealand based on the premise that higher risks should be accepted for lesser structures by designing the walls for earthquakes of lower return period.

The earth pressure generated during an earthquake event may be computed by elastic theory, by approximate plasticity theory (Coulomb or Mononobe-Okabe), or by numerical methods modelling the soil as Winkler Springs or as finite elements (See also Section 7.9).

Where soil is retained by a completely rigid wall, the total pressure during an earthquake may be taken as the sum of the static and dynamic pressures, or

$$P_E = P_o + P_{oE} = \frac{1}{2} K_o \gamma H^2 + \alpha_h \gamma H^2 \tag{6–27}$$

where K_o = coefficient of at-rest pressure
α_h = seismic coefficient = 1/g (horizontal ground acceleration)
and other symbols are as previously.

Equation (6–27) should not be applied to saturated sands. For a vertical wall and horizontal ground surface, $K_o = 1 - \sin \phi'$ For other wall angles and ground slopes K_o may be assumed to vary proportionally to K_A. The at-rest pressure P_o may be taken to act at a height $H/3$, while the dynamic pressure $P_{oE} = \alpha_h \gamma H^2$ may be assumed to act at a height of 0.58 H. The walls should be non-yielding, i.e., the wall shown in Figure 6–34.

Gravity and Semi-Gravity Walls

According to the LRFD specifications, the pseudo-static approach introduced by the Mononobe-Okabe procedure may be used to estimate the equivalent static forces for seismic effects for gravity and semi-gravity retaining walls. Wall inertia forces should be accounted for, but for flexible cantilever walls forces resulting from wall inertia effects may be ignored in estimating the seismic lateral earth pressure. Where the wall supports a superstructure, the design should also include seismic forces transferred from the bridge bearing devices that do not slide freely (See also Section 7.9).

Anchored Walls

Likewise, the LRFD specifications recommend the Mononobe-Okabe theory in estimating the equivalent static forces on anchored walls provided that the maximum lateral earth pressure is computed using a seismic coefficient $k = 1.5A$. Forces resulting from wall inertia effects may be ignored in computing the seismic lateral earth pressure.

Mechanically Stabilized Earth Walls

External stability. According to the LRFD specifications, external stability should be analyzed considering (a) static forces, (b) the horizontal inertial force P_{IR} and (c) 50% of the dynamic horizontal thrust P_{AE}. The dynamic horizontal thrust P_{AE} should be estimated from the Mononobe-Okabe method and applied to the back of the reinforced fill at a height of 0.6 H from the base. The horizontal inertial force P_{IR} may be applied at the midheight of the structure.

Values of P_{AE} and P_{IR} may be computed from the following:

$$P_{AE} = 0.375 A_m \gamma_s H^2 \tag{6–28}$$

where

$$A_m = (1.45 - A)A \tag{6–29}$$

and

$$P_{IR} = 0.5\, A_m \gamma_s H^2 \tag{6–30}$$

where A = maximum earthquake acceleration
A_m = maximum wall acceleration coefficient at the centroid
γ_s = soil unit weight (kips/ft^3)
H = wall height (ft)

For structures with sloping backfill, the inertial force P_{IR} may be based on an effective mass having a height H_2 and a base width equal to 0.5 H_2 determined as follows:

$$H_2 = H + \frac{0.5H \tan(i)}{1 - 0.5 \tan(i)} \tag{6–31}$$

where i = slope angle of the backfill

The inertial force P_{IR} should be taken to act simultaneously with one-half the dy-

namic horizontal thrust P_{AE} computed from the Mononobe-Okabe method, and applied at 0.6 H_2 above the base of the back surface of the effective earth mass.

Internal stability. In general, reinforcements should be designed to withstand horizontal forces induced by the internal inertia force P_{ls} and the static forces. The total inertia force P_{ls} per unit length of structure may be taken equal to the mass of the active zone times the maximum wall acceleration coefficient A_m. This inertial force should be distributed to the reinforcements in proportion to their resistant areas as follows:

$$H_m = P_{ls}\left(\frac{A_R(eff)}{\Sigma A_R(eff)}\right) \tag{6–32}$$

where $$A_{R(eff)} = (b'_i L_{ei})/S_{Hi} \tag{6–33}$$

where H_m = incremental dynamic inertia force at level i (kips/ft of structure)
P_{ls} = internal inertia force (kips/ft)
b'_i = reinforcement width for layer i (ft)
L_{ei} = effective reinforcement length for layer i (ft)
S_{Hi} = horizontal reinforcement spacing for layer i (ft)

For seismic loading conditions, the specifications recommend reduction to 80% for the values of resistance factors applied to f^* (apparent coefficient of friction at each reinforcement level), N_p (a relevant passive resistance factor), and f_d (coefficient of resistance to direct sliding of the reinforcement).

REFERENCES

AASHTO, 1994: AASHTO LRFD Bridge Design Specifications.

AMERICAN SOCIETY FOR TESTING AND MATERIALS (ASTM), 1989: *Annual Book of ASTM Standards,* Vol. 04.08 Soil and Rock, Building Stones; Geotextiles, ASTM, Philadelphia, PA, p. 953.

BECKER, J. M., 1990: "Up/Down Construction-Decision Making and Performance," *Design and Performance of Earth Retaining Structures, Proc. of ASCE Specialty Conf.,* Ithaca, New York, June, pp. 170–189.

BONAPARTE, R., R. D. HOLTS, and J. P. GIROUD, 1986: "Soil Reinforcement Design Using Geotextiles and Geogrids", *Geotextile Testing and the Design Engineer,* ASTM STP 952, J. E. Fluet, Jr., ed., Philadelpha, PA, pp. 69–116.

BOWLES, J. E., 1988: *Foundation Analysis and Design,* McGraw-Hill, New York.

CAQUOT, A., and J. KERISEL, 1948: "Tables for the Calculation of Passive Pressure, Active Pressure and Bearing Capacity of Foundations," Gauthier-Villars, Imprimeur-Libraire, Libraire du Bureau des Longitudes, de L'Ecole Polytechnique, Paris, p. 120.

CHRISTIAN, J. T., 1989: "Design of Lateral Support Systems," *Design, Construction and Performance of Deep Excavations in Urban Areas, Proc. of BSCES/ASCE Seminar,* Boston, Mass., pp. 1–26.

CHRISTOPHER, B. R., and R. D. HOLTZ, 1985: *Geotextile Engineering Manual,* FHWA, Federal Highway Administration, U.S. Dept. of Transportation, Washington, D.C., p. 917.

CHRISTOPHER, B. R., S. A. GILL, J. GIROUD, I. JURAN, J. K. MITCHELL, F. SCHLOSSER, and J. DUNNICLIFF, 1990: "Reinforced Soil Structures, Vol. I, Design and Construction Guidelines," FHWA RD-89-043, *Federal Highway Administration, U.S. Dept. of Transportation,* U.S. Goverment Printing Office, Washington, D.C., p. 301.

CLOUGH, G. W., 1979: "Deformations and Earth Pressures-Excavating Wall Systems," *Proc. Slurry Walls for Underground Transp. Systems,* FHWA, Cambridge, Aug. 30–31, pp. 114–136.

CLOUGH, G. W. and J. M. DUNCAN, 1971: "Finite Element Analyses of Retaining Wall Behavior," *Journ. of Soil Mech. and Found. Div.,* ASCE, vol. 97, SM12, Dec., pp. 1657–1673.

CLOUGH, G. W., L. A. HANSEN, and A. I. MANA, 1980: "Prediction of Behavior of Supported Excavations under Marginal Stability Conditions," vol. IV, *Proc. 3d Intenr. Conf. Numerical Methods in Geomechanics,* pp. 1485–1502.

CLOUGH, G. W. and T. D. O'ROURKE, 1990: "Construction Induced Movement of in situ Walls," Design and Performance of Earth Retaining Structures, Proc. ASCE Spec. Conf., Ithaca, N.Y., pp. 439–470.

COATES, D. F. and Y. S. YU, 1970: "Three Dimensional Stress Distribution Around a Cylindrical Hole and Anchor," *Proc. 2nd Int. Conf. on Rock Mech.*, Belgrade, pp. 175–182.

DUNCAN, J. M., G. W. CLOUGH, and R. M. EBELING, 1990: "Behavior and Design of Gravity Earth Retaining Structures," *Proc. of Conf. on Design and Performance of Earth Retainig Structures,* ASCE, Cornell Univ., Ithaca, New York, June, pp. 251–277.

GEOTECHNICAL CONTROL OFFICE, 1982: "Guide to Retaining Wall Design," Geoguide 1, Engineering Development Dept., Hong Kong, Available from: *U.S. Army Engineer Waterways Experiment Station,* Vicksburg, MS.

GRANT, W. P., 1985: *Performance of Columbia Center Shoring Wall,* Proc. 11th Int. Conf. on Soil Mech. and Found. Engineering, vol. 4, San Francisco, CA, pp. 2079–2082.

HUDER, J., 1965: "The "Calculation of Ground Anchors and How They Operate," *Proc. Conf. Swiss Soc. of Soil Mech.,* May.

JUDD, W. R., and C. HUBER, 1961: "Correlation of Rock Properties by Statistical Methods," *Int. Symp. on Mining Research.*

KRANZ, E., 1953: "Uber die Verankerung von Spundwanden, 2 Auflage, Mitteilungen aus dem Gebiete des Wasserbaues und der Baugrundforschung, vol. 11, Ernst & Sohn, Berlin.

LEONARD, M., 1974: "Precast Diaphragm Walls Used for the A13 Motorway," Paris, *Proc. Diaphragm Walls Anchorages,* Inst. Civ. Eng., London.

LOCHNER, H. G., 1969: *Anchored Retaining Walls and Cut-Off Walls,* Losinger and Co., Bern, pp. 1–23.

MALIJAIN, P. A., and J. L. VAN BEVEREN, 1974: "Tied-back Excavations in Los Angeles Area," Proc. ASCE, 100, (CO3), pp. 337–356.

MATTHEWSON, M. B., J. H. WOOD, and J. B. BERRILL, 1980: "Earth retaining structures," *Bull. NZ Nat. Soc. for Earthq. Eng.,* 13, No. 3, pp. 280–293.

MCGOWAN, A., and K. Z. ANDREWS, 1986: "The Load-Strain-Time-Temperature Behavior of Geotextiles and Geogrids," *3rd Int. Conf. on Geotextiles,* Vienna, Austria.

MEYERHOF, G.G., 1953: "The Ultimate Bearing Capacity of Foundations under Eccentric and Inclined Loads," *Proc. 3rd Int. Conf. on Soil Mech. and Found. Engineering,* Zurich, vol. 1, pp. 440–445.

MITCHELL, J. K., and W. C. B VILLET, 1987: *Reinforcement of Earth Slopes and Embankments.* NCHRP Report 290, Transp. Research Board, National Research Council, Washington, D.C., p. 323.

MODJESKI and MASTERS, 1992: "Development of Comprehensive Bridge Specifications, *LRFD,*" NCHRP 12-33, TRB, Washington, D.C., April.

OTTA, L., M. PANTUCEK, and P. R. GOUGHNOUR, 1981: *Permanent Ground Anchors,* Stump Design Criteria, FHWA, Report PB83-165985, Sept., Washington, D.C.

PECK, R. B., W. E. HANSON, and T. H. THORNBURN, 1974: *Foundations Engineering,* 2nd ed., Wiley, New York.

PECK, R. B., 1969: *Deep Excavations and Tunneling in Soft Ground,* State-of-the-Art Report, 7th Int. Conf. on Soil Mech. and Found. Engineering, Mexico City, State-of-the-Art Volume, pp. 225–290.

ST. JOHN, H. D., 1975: *Recent Ressearch into the Movement of Ground around Deep Excavations,* Build. Res. Establish Bull. D2/F/1.

TAN, C. K., DUNCAN, J. M., BARKER, R.M., and K. ROJIANI, 1991: "An Engineering Manual for Shallow Foundations," Prel. Draft for NCHRP 24-4, VPI & SU, May.

XANTHAKOS, P. P., 1974: "Underground Construction in Fluid Trenches," *Colleges of Engineering,* Univ. of Illinois, Chicago.

XANTHAKOS, P. P., 1979: *Slurry Walls,* McGraw-Hill, New York, p. 622.

XANTHAKOS, P.P., 1994a: *Theory and Design of Bridges,* Wiley, New York, p. 1445.

XANTHAKOS, P. P., 1994b: *Slurry Walls as Structural Systems,* McGraw-Hill, New York, p. 855.

XANTHAKOS, P. P., 1991: *Ground Anchors and Anchored Structures,* Wiley, New York, p. 690.

XANTHAKOS, P. P., ABRAMSON, L. W., and D. A. BRUCE, 1994: *Ground Control and Improvement,* Wiley, New York, p. 910.

CHAPTER 7

Abutments

7.1 TOP OF ABUTMENT DETAILS AND TREATMENT

Various types of abutments are discussed in section 1.3, and are illustrated in Figures 1–7 through 1–10. Abutment configurations and details for integral and semi-integral construction are shown in Figures 1–11 and 1–12, and are discussed further in subsequent sections.

Top of abutment details are influenced by the conditions of the approach pavement, the type of superstructure, and the expansion length, including the type of bearings used at this location. The top of the abutment backwall that supports the approach slab may be constructed level, unless excessive skew and superelevated roadway make this impracticable. A standard 20 foot long approach pavement 14½ inches thick will induce a dead load reaction of approximately 3 kips per foot of width. This reaction should not be included in the design if its effect is to reduce the load on the piles.

Figure 7–1 shows section through top of abutment. This detail may be used when the approach roadway is a nonrigid type, such as gravel, crushed stone, or low type bituminous mix, and the expansion length is less than about 150 feet. The one-half-inch premoulded joint filler allows free movement of the superstructure, and allows end rotation as the structure is deflected under load. A sealed joint also excludes deck drainage through the opening.

When the approach surface is a rigid type (concrete slab), the end-of-slab treatment at an expansion abutment may be as shown in Figure 7–2, which shows abutment details for superstructures of steel framing with concrete slab. For all concrete superstructures or precast prestressed decks, the abutment configuration at the top is as shown in detail *A*.

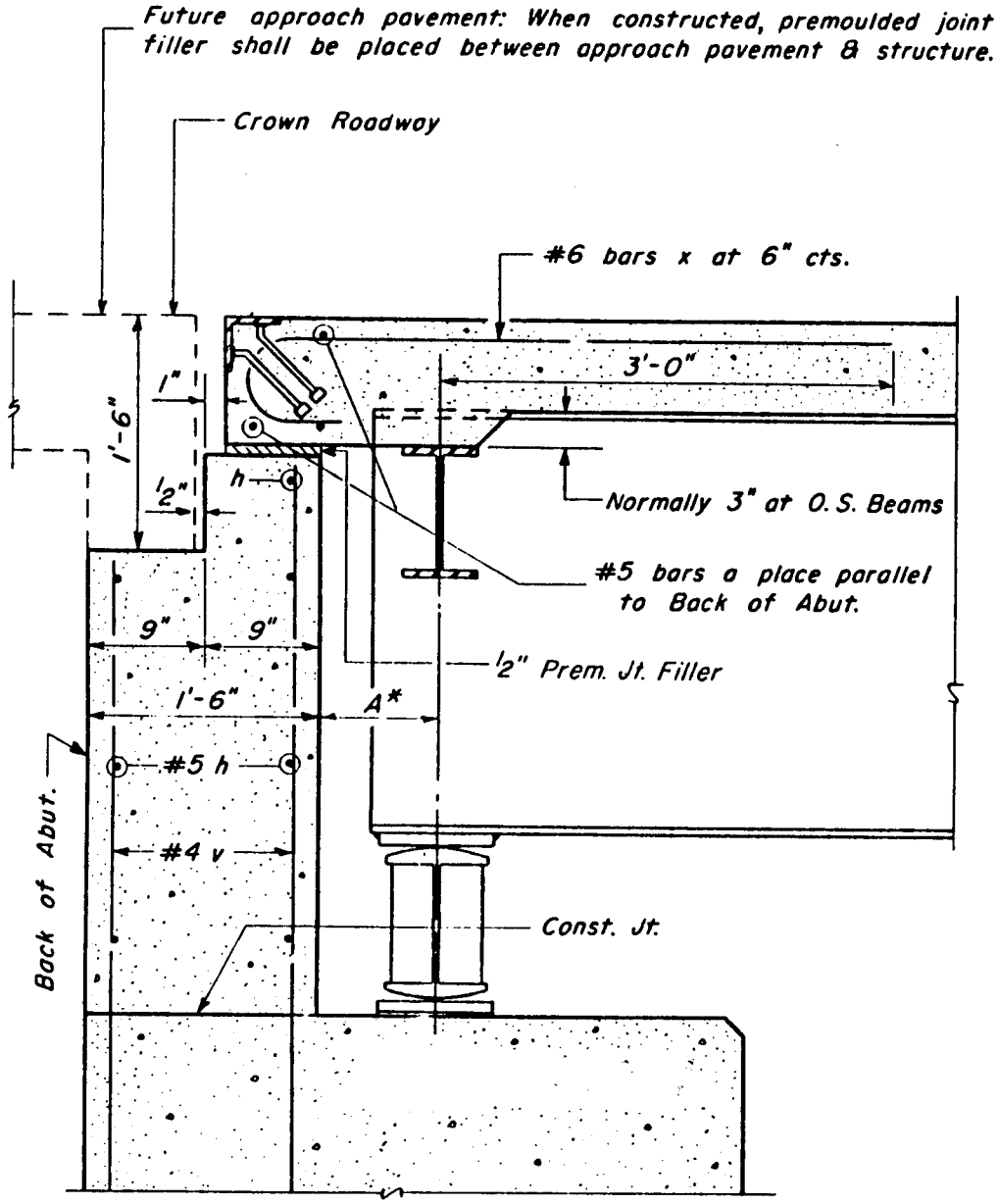

Figure 7–1 Details of abutment top, nonrigid approach roadway *(Illinois DOT).*

As shown in Figure 7–2, a preformed joint seal is usually inserted between the two expansion angles to seal the joint and inhibit drainage through the opening. The limitations and practical range of open joints formed with steel angles are dictated by the expansion length and the skew angle of the bridge. Where these criteria are exceeded, the joint may be formed with a sliding plate or a finger plate. State standards usually cover these aspects in detail.

When a neoprene expansion joint is placed at the opening formed by the steel angles, an anchorage load will be exerted against the abutment. This thrust is induced as

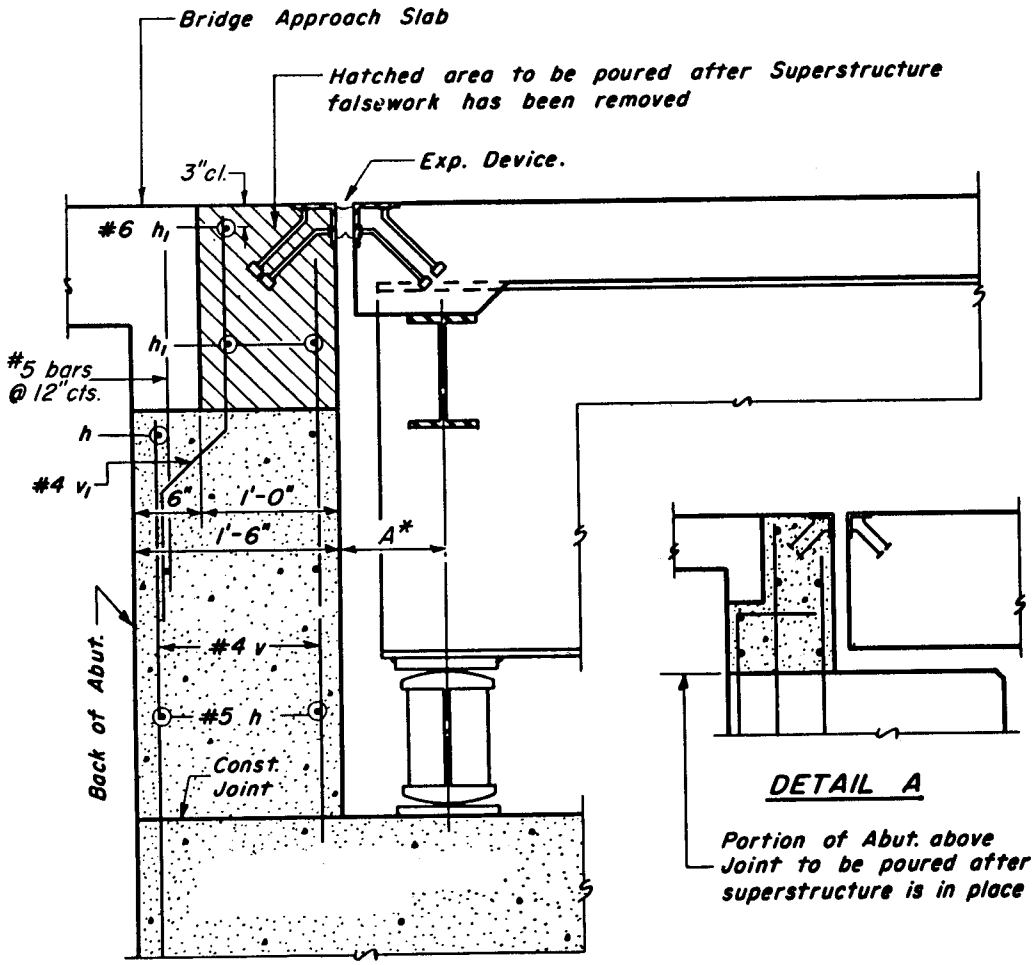

Figure 7–2 Details of abutment top, rigid approach roadway *(Illinois DOT)*.

the bridge expands, and should be applied at the point of connection to the abutment wall. The manner in which this lateral force is resisted is open to conjecture, and consideration should be given to the type of approach pavement as well as to the type of expansion bearing. The most logical theory is that this force is created as the neoprene seal is squeezed between the two steel angles when the bridge expands. It may be resisted by friction between the approach slab and the soil underneath, but until this assumption is warranted it may continue to act against the abutment wall. The following guideline is provided for the magnitude of this force:

Size of neoprene joint:	Force (kips/ft) =
2 to 4 inches	1.3
6½ inches	1.8

When a neoprene expansion joint is specified at one abutment or at one end of the superstructure unit, it should also be specified at the other abutment or end of the same unit, in order to balance the thermal forces acting on the fixed pier. If this arrangement is not provided, the thermal forces specified above should be applied to the fixed bearing.

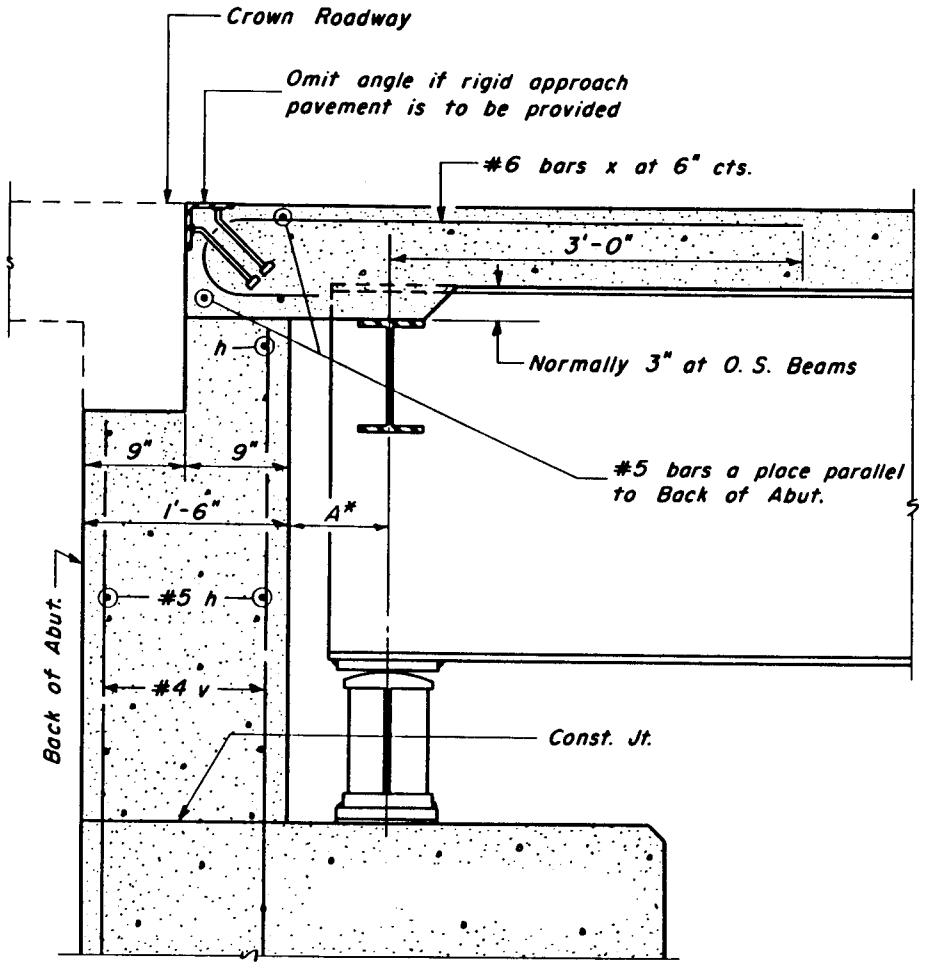

Figure 7–3 Detail of abutment top, fixed bearing *(Illinois DOT).*

With fixed bearings at the abutment, expansion joints in the deck are not necessary. In this case the top of the abutment can be detailed as shown in Figure 7–3. This detail is suitable with all types of approach surfaces, but it should be noted that it does not constitute an integral abutment.

The dimension *A* depends mainly on the skew angle and the width of the bottom flange plate, which also determines the width of the bearing plate. An edge distance of 4 inches between the corner point of the steel beam flange and the front face of the abutment wall usually is specified and provides the additional criterion. These considerations determine the bridge seat width, hence the dimensions of the abutment.

7.2 PILE BENT (STUB) ABUTMENTS, DESIGN CONSIDERATIONS

A typical pile bent abutment is shown in Figure 1–8. The dimensions of the height and width are minimum and may be increased to satisfy the layout criteria. A berm is provided in front of the bent, with a minimum clearance 1.75 feet below the underside of

the superstructure. Note that this layout will accommodate bearing devices 13 to 14 inches high, usually of the rocker or roller type.

Pile spacing. As a rule of thumb, and for preliminary estimates, the design may select n piles in the front row (R_2) and $n+1$ piles in the back row (R_1) at 8-foot maximum alternate centers. The dimensions B and C are established after the overall bent width is known, and are proportioned so that the pile loads between the back and front row are as equal as possible.

Design loads. The following loads should be applied to produce maximum effects.

1. Dead load of pile bent.
2. Dead load reaction from superstructure.
3. Dead load of approach slab (if an approach slab is to be provided).
4. Earth pressure on the back of the pile bent. This should have a pattern and magnitude compatible with the expected movement, or it may be stipulated by applicable standards as an equivalent fluid pressure. This pressure should be used with all combinations of loading.
5. Live load (HS truck or lane loading). This may be placed either on the bridge (reaction transmitted through the bearing) or on the approach slab (reaction transmitted through the backwall).
6. Live load surcharge, to be added on the lateral earth pressure if an approach slab is not provided, and coincident with live load reaction from the superstructure. Usually local standards stipulate a surcharge of 2 feet (about 230 lb/ft^2), which is substantially close to the surcharge of 0.21 kips/ft^2 used in the design example of section 6.9 by taking the tributary area of a truck load.
7. Thermal forces. These may be as specified in other sections where applicable. There may also be a temperature force applied as rolling friction at the expansion bearing, but may be neglected since it will act opposite to the earth pressure.

Referring to Figure 1–8, the total load carried by each row of piles may be assumed to be the static reactions R_1 and R_2 acting on the bottom of the cap. Hence, the load on piles is

$$\text{Back Row Pile Load} = \frac{R_{1(\max)}}{n+1} \tag{7–1}$$

$$\text{Front Row Pile Load} = \frac{R_{2(\max)}}{n} \tag{7–2}$$

Deflections or lateral movement of pile bents may be critical if joints can close, causing unwarranted forces to be induced in the superstructure and eventually transferred to the end bent as additional passive resistance. Although the pile bent shown in Figure 1–8 does not have a high degree of stiffness, resistance to deflection or translation is helped by the end wing walls and the battered piles. Pile bents with fixed bearings should also be designed for longitudinal forces.

7.3 CLOSED (FULL) ABUTMENTS, DESIGN CONSIDERATIONS

A typical section of a closed abutment is shown in Figure 1–9. Reinforcement details and design pressures represent applicable local standards. For this condition, the superstructure is anchored as shown. By placing the top dowels near the front face of the abutment, the end restraint is essentially removed and the superstructure can rotate at the ends with minimum resistance. The abutment wall is therefore assumed to have pinned top. The base of the abutment wall may be designed as pinned, partially fixed, or fixed. The two most usual conditions are shown in Figure 7–4(a) and (b) for free and fixed bottom, respectively. The main wall is subjected to the same forces as the pile bent, discussed in the foregoing section. Note that lateral earth pressure and surcharge load pressure are combined into one diagram.

If p and p_1 is the unit earth pressure at the top and bottom of the wall, respectively, and h is the wall height as shown, bending moment equations may be derived for the free and the fixed bottom condition.

Both Ends Free. From Figure 7–4 (a), the reactions are obtained as

$$R_u = \frac{1}{6}(p_1 + 2p)h \qquad \text{and} \qquad R_1 \frac{1}{6}(2p_1 + p)h \tag{7–3}$$

The point of zero shear is also the point of maximum moment, and is located at distance x_1 from the top given by

$$x_1 = \frac{p}{p_1 - p}\left[-1 + \sqrt{1 + \frac{1}{3}\left(\frac{p_1}{p} + 2\right)\left(\frac{p_1}{p} - 1\right)}\right]h \tag{7–4}$$

The maximum bending moment at distance x_1 is

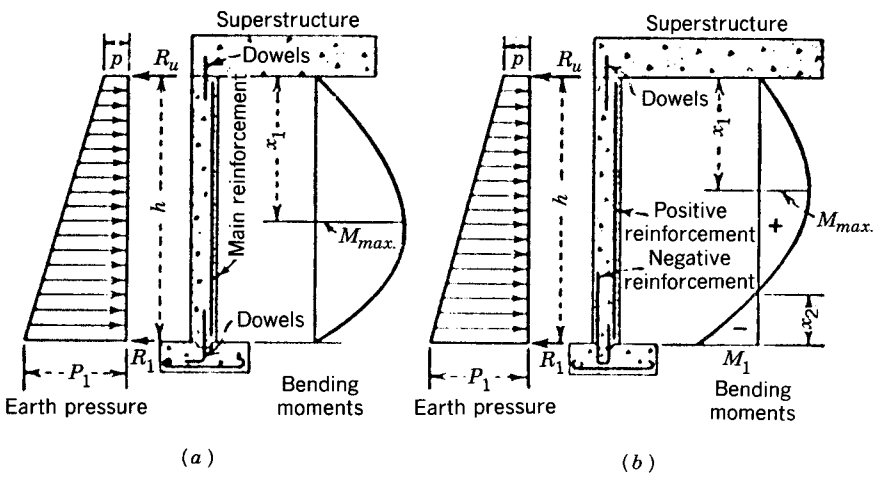

Figure 7–4 Abutment wall supported at top; (a) wall freely supported at bottom; (b) wall fixed at bottom.

$$M_{\max} = \frac{1}{18} \frac{\frac{x_1}{h}\left(3\frac{p}{p_1 - p} + 2\frac{x_1}{h}\right)}{2\frac{p}{p_1 - p} + \frac{x_1}{h}}(p_1 + 2p)h^2 \tag{7–5}$$

Both Ends Fixed. Referring to Figure 7–4(b), the reactions are computed as

$$R_u = \frac{1}{40}(4p_1 + 11p)h \qquad \text{and} \qquad R_1 = \frac{1}{40}(16p_1 + 9p)h \tag{7–6}$$

Likewise, the point of zero shear is the point of maximum (positive) moment, and is located at distance x_1 from the top given by

$$x_1 = \frac{p}{p_1 - p}\left[-1 + \sqrt{1 + \frac{1}{20}\left(11 + 4\frac{p_1}{p}\right)\left(\frac{p_1}{p} - 1\right)}\right]h \tag{7–7}$$

The maximum positive moment at distance x_1 is

$$M_{\max} = \frac{1}{120} \frac{\frac{x_1}{h}\left(3\frac{p}{p_1 - p} + 2\frac{x_1}{h}\right)}{2\frac{p}{p_1 - p} + \frac{x_1}{h}}(11p + 4p_1)h^2 \tag{7–8}$$

The negative moment at the bottom (fixed end) may be computed from

$$M_1 = -\frac{1}{120}(7p + 8p_1)h^2 \tag{7–9}$$

and the point of contraflexure is at distance x_2 from the bottom, given by

$$x_2 = \frac{p}{p_1 - p}\left[\left(5 + \frac{p_1}{p}\right) - 6\sqrt{1 + \frac{1}{240}\left(11 + 4\frac{p_1}{p}\right)\left(\frac{p_1}{p} - 1\right)}\right]h \tag{7–10}$$

Wall footing. For the abutment wall supported freely at the bottom, the footing is subject to vertical reactions from the superstructure, the weight of the structure and its footing, and the weight of fill placed on the interior part of the footing. The horizontal reaction due to lateral loads at the bottom is resisted by friction at the footing-soil interface and by a partial passive pressure, if certain conditions are satisfied (see also foregoing sections).

When the wall is fixed at the bottom, in addition to the loads and forces mentioned above, the footing is subjected to a moment M_1 transferred to it by the fixity of the abutment wall. Since overturning is not a design condition for either case (a) or (b) of Figure 7–4, the footing dimensions and projection beyond the wall face are determined to best balance the resulting soil pressure.

Earth pressure. Simple spans supported on closed abutments may be fixed at both supports when the back-to-back of abutment dimension does not exceed 45 feet. With both supports fixed, the abutments should be designed as restrained top and bottom. This implies that both top and bottom are restrained against movement either into or away from the backfill. Therefore, the at-rest pressure is the type suitable for this condition. For a well-compacted backfill of granular material it is reasonable to use K_o = 0.5, and unit weight γ = 120 lb/ft^3. The pressure p at the top of the wall, shown in Figure 7–4, is the result of a surcharge (usually 2 feet) with the live load placed on the approach pavement. Friction and cohesion behind the wall may be disregarded for simplicity. The foregoing assumptions result in an equivalent fluid pressure 0.5 × 120 = 60 lb. The reinforcement requirements shown in Figure 1–9 are based on a wall with both ends free (simple span) and an equivalent 50 lb fluid pressure.

An adequate drainage system should be provided behind the abutment wall, its function being to prevent water pressures from developing behind the wall.

7.4 GRAVITY AND THE SEMI-GRAVITY ABUTMENTS, DESIGN CONSIDERATIONS

When the bridge length exceeds the span for which expansion provisions are not needed (usually 40 to 45 ft), the abutments may have a fixed bearing at one end and an expansion bearing at the other. For this situation, both closed abutments must be designed as free cantilevers.

The design requirements of full abutments with unrestrained tops are essentially the same as for gravity and semi-gravity walls, discussed in detail in section 6.6. The abutment structure must be designed to resist overturning (FS ≥ 2.0), and sliding (FS ≥ 1.5). Dead and live loads are assumed uniformly distributed over the length of the abutment between expansion joints.

Except for gravity abutments, at least 1/8-inch of horizontal reinforcement per foot of height should be provided near exposed surfaces not otherwise reinforced to resist the formation of temperature and shrinkage cracks.

Drainage and backfilling. The backfill materials behind abutments should be free draining, nonexpansive soil, properly drained by a suitable system. Cohesive backfills are difficult to compact. Walls backfilled with cohesive soils should not be designed for active earth pressures, even if large movements are tolerable, because cohesive soils tend to creep. Thus, walls with cohesive backfills designed for active earth pressure will continue to move gradually and indefinitely, especially when the backfill is soaked by rain or by rising groundwater. In this case, the abutments must be designed for pressures between active and at rest.

In addition to the loads mentioned for gravity walls, abutments must be designed to withstand wind, longitudinal forces, centrifugal forces, and earthquake loads according to AASHTO Art. 3.2.1 or to LRFD Article 11.6.

7.5 ABUTMENTS ON MECHANICALLY STABILIZED EARTH WALLS

Abutment footings are proportioned to meet sliding and overturning criteria discussed in the foregoing sections. These members should also be designed to satisfy the maximum uniform bearing pressures using an effective width of foundation ($B - 2e$) where

B = width of retaining wall foundation, and e = electricity of load from center line of foundation (see also Figure 7–5).

Below the abutment footing, the MSE wall must be designed for any additional loads imposed by the footing pressure and supplemental earth pressure resulting from lateral loads applied at the bridge seat and from the backwall. The footing load may be assumed to be uniformly distributed over the effective foundation width ($L - 2e$) at the base of the footing, and to be distributed with depth using a slope 2:1 with the vertical. The supplemental loads may applied as shears along the bottom of the footing, diminishing uniformly with depth to a point on the face of the wall equal to twice the effective width of the abutment footing.

Horizontal stresses in abutment reinforced zones may be computed by superposition as follows (see also Figure 7–5):

$$\sigma_{H(\max)} = \gamma_p(\sigma_{v1}K + \sigma_{v2}K_a + \sigma_H) \tag{7–11}$$

where σ_H = lateral pressure due to surcharge; σ_{v1} = vertical (overburden) soil stress; σ_{v2} = vertical soil stress due to footing load; K = earth pressure coefficient; K_a = active earth pressure coefficient; and γ_p = load factor for earth pressure.

The factored horizontal force P_i acting on the reinforcement at any reinforcement level may be computed as

$$P_i = \sigma_{H(\max)}h_1 \tag{7–11a}$$

where $\sigma_{H(\max)}$ = factored horizontal stress as determined from Eq. (7–11)

h_1 = height of reinforced soil zone contributing horizontal load to the reinforcement, computed as the vertical distance from the midpoint between the layer under consideration and the next overlying layer to the mid-point between the layer under consideration and the next underlying layer.

The effective length used for analyzing internal stability under the abutment footing should be the greater of either the length beyond the end of the footing or a distance from the facing equal to 30 percent of the wall height.

Abutments should not be constructed on mechanically stabilized embankments if the anticipated differential settlement between abutments or between piers and abutments is greater than about one-half the limiting differential angular distortion discussed in section 3.12. This criterion is a general guideline, and where conditions warrant, a more detailed analysis will be required to assess the effects of differential settlement.

Where abutments are supported by piles, the horizontal force transmitted to the piles may be assumed to be resisted by the lateral capacity of the piles, or by the horizontal component of the batter piles. If necessary, additional reinforcement may be placed in the upper portion of the structure.

The mass equilibrium of the system should be checked at each level of reinforcement below the bridge seat. Moments should be taken at each level under consideration about the center line of the reinforced mass to determine the eccentricity of load at each level. A uniform vertical stress is then computed using a fictitious width ($B - 2e$), and the corresponding horizontal stress is determined by multiplying by the appropriate earth pressure coefficient.

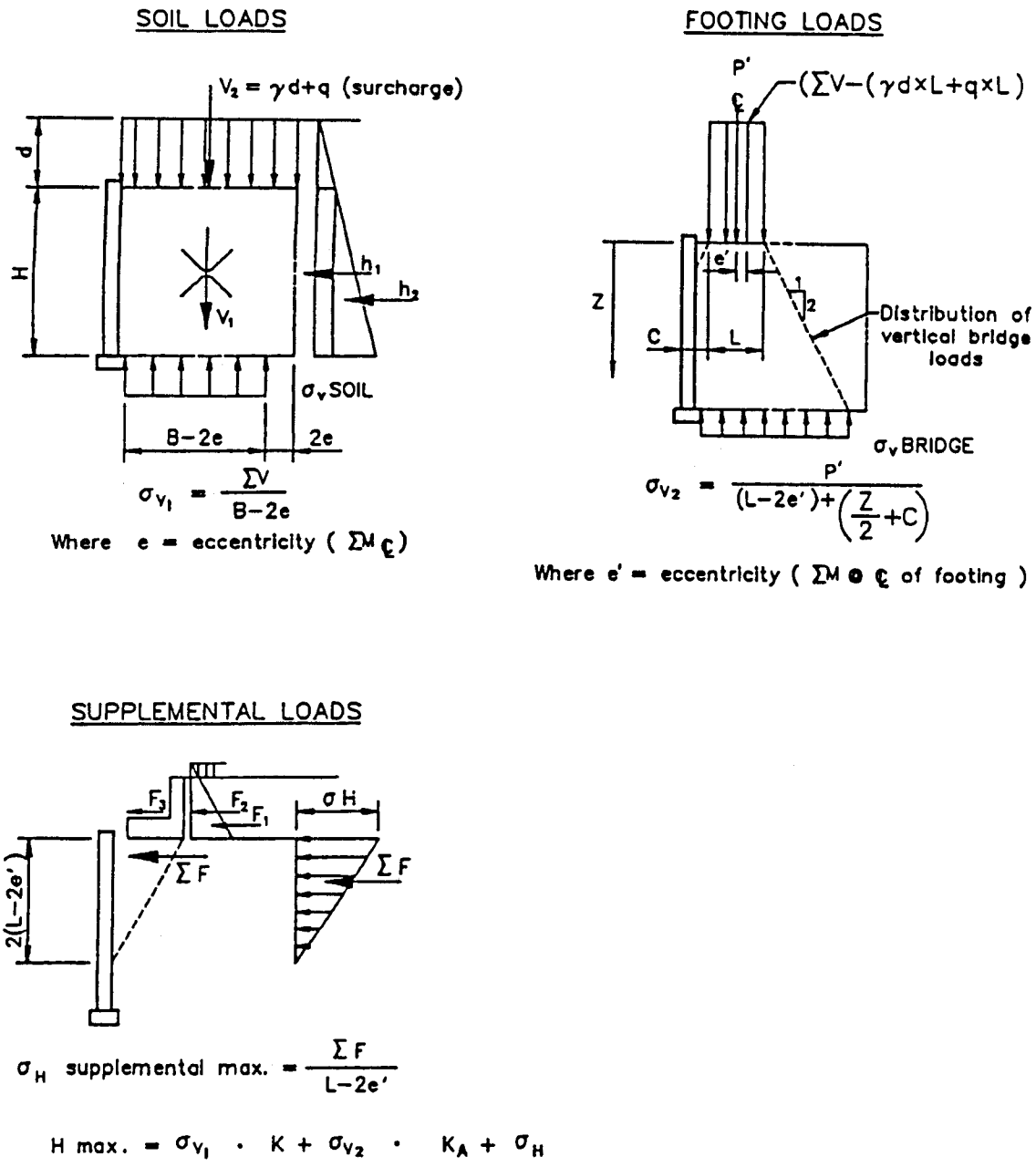

Figure 7–5 Horizontal stresses in abutments.

7.6 ABUTMENTS ON MODULAR SYSTEMS

Abutment seats may be constructed on modular units. In this case they must be designed for earth pressures and supplemental horizontal pressures from the abutment seat beam and earth pressure on the backwall. The top module should be checked for stability under the combined action of normal and supplemental earth pressures.

AASHTO stipulates minimum top module width as 6 feet. The center line of bearing should be at least 2 feet from the outside face of the top module, and the abutment beam seat should be supported and cast integrally to the top module.

The front face thickness of the top module must be designed for bending action developed by supplemental earth pressures. The loads on the abutment beam seat should be carried to the foundation level and considered acting on the footing. Differential settlement provisions should be considered.

7.7 WING WALLS

Wing walls may be placed parallel to the roadway, at some angle, or placed on the same alignment as the abutment wall. Possible configurations and structural solutions for wing walls of closed abutments are discussed in section 1.3.

Certain standards require the wing walls to be separated from the abutment wall with an open joint. AASHTO, however, allows the wing walls to be built as monolithic structures with the main abutment. In the latter case, reinforcing bars should be spaced across the junction between wing walls and abutment wall to tie them together. These bars should extend into the concrete on each side of the joint far enough to develop the strength of the bar, and should be varied in length in order to avoid planes of weakness.

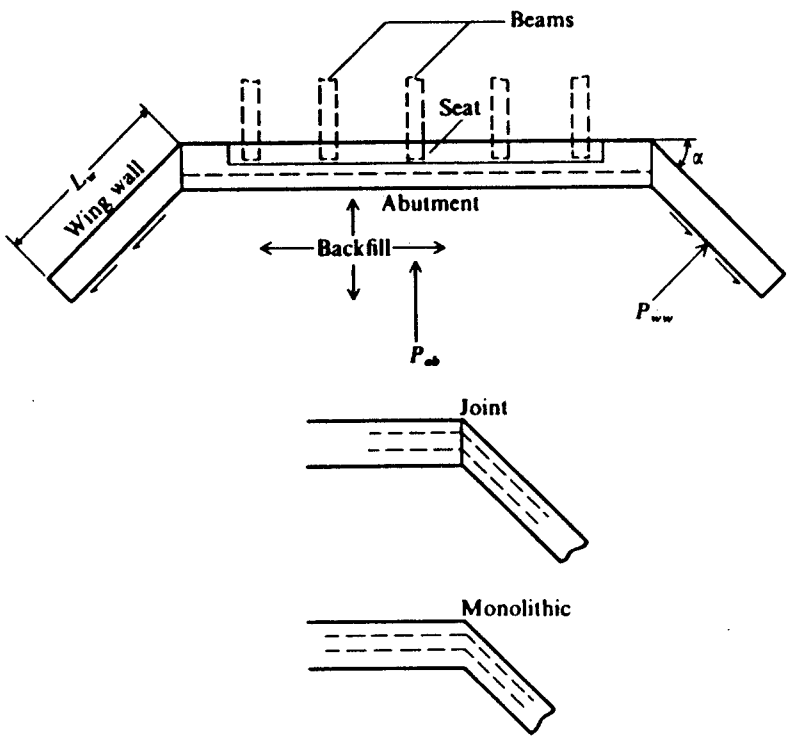

Figure 7–6 Bridge abutment and wing wall earth pressure and methods of construction. As abutment tilts forward, friction develops on wing walls as shown if wall is rigidly attached.

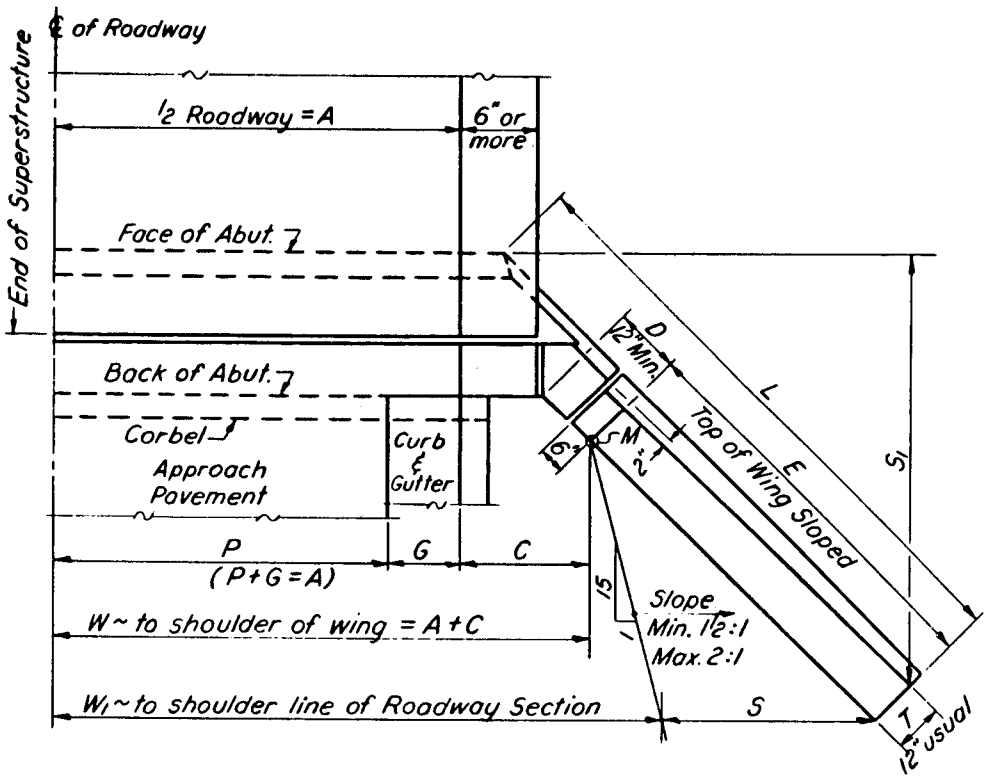

Figure 7–7 Layout of wing walls, closed abutment.

There appears to be some question as to how much design force (shear, tension, and moment) is produced at the junction of the abutment and the wing wall. Referring to Figure 7–6, it may appear that if the abutment wall carries the forces P_{ab} and P_{WW}, there is little left for the junction to carry, and in this case shrinkage and temperature reinforcement is all that is needed. However, it is more likely that wing walls respond as horizontal cantilevers near the top and close to the junction with the abutment, and as vertical cantilevers if they rest on spread footing and near the end.

Figure 7–7 shows a simple procedure to be followed for the dimensional layout of wing walls for a closed abutment. The wing wall makes an angle of 45° with the abutment wall. The following steps are necessary.

1. Select dimension W to an even 6-inch dimension so that D (the level portion of the wing wall) is 12 inches or more.
2. Establish wing wall length L as follows: (a) if the approach roadway slopes are 1½:1, calculate L to the nearest 6 inches to allow a slope 1½:1 along $S + T + S_1$ from actual shoulder elevation to toe of slope; (b) if the roadway slopes are 2:1 or flatter, calculate wing lengths for 2:1 slope along $S + T + S_1$.
3. Establish wing height and drop: (a) top of wing to be at top of curb or sidewalk along distance D to M; (b) calculate drop to nearest 3 inches so that inside face at the end is the same distance above earth slope as M is exposed above the ground.

7.8 ABUTMENTS FOR SEGMENTAL BRIDGES

Abutments for segmental bridges should conform to the general design requirements and loading conditions stipulated in AASHTO Art. 7.5.2. In addition, consideration must be given to erection loads, moments, and shears imposed by the construction methods. Besides the normal loads, there may be random and accidental loads that have their origin in unusual natural events and construction incidents. In most cases, the abutment types discussed in the foregoing sections will be found suitable and structurally adequate. Hence, this section reviews abutment configurations for special conditions.

Abutment types. Figure 7–8 shows an abutment for a nominal-height segmental bridge, classified as Type I. This abutment may be considered where poor quality of the soil makes it difficult to resist the horizontal thrusts due to earth pressures combined with braking and thermal forces. The abutment is essentially a gravity system founded on vertical piles or drilled shafts. At the base, the entire horizontal loads are resisted by embedded prestressed concrete ties anchored in the back into a continuous dead-man structure as shown. This arrangement ensures stability against sliding. Resistance to overturning is still provided by a resisting couple of forces in the front and back row of piles.

Separate End Support and Retaining Wall. In this case, the two main functions of superstructure support and retaining wall are articulated in two separate structures. A front wall supported on spread footing or piles provides the superstructure end

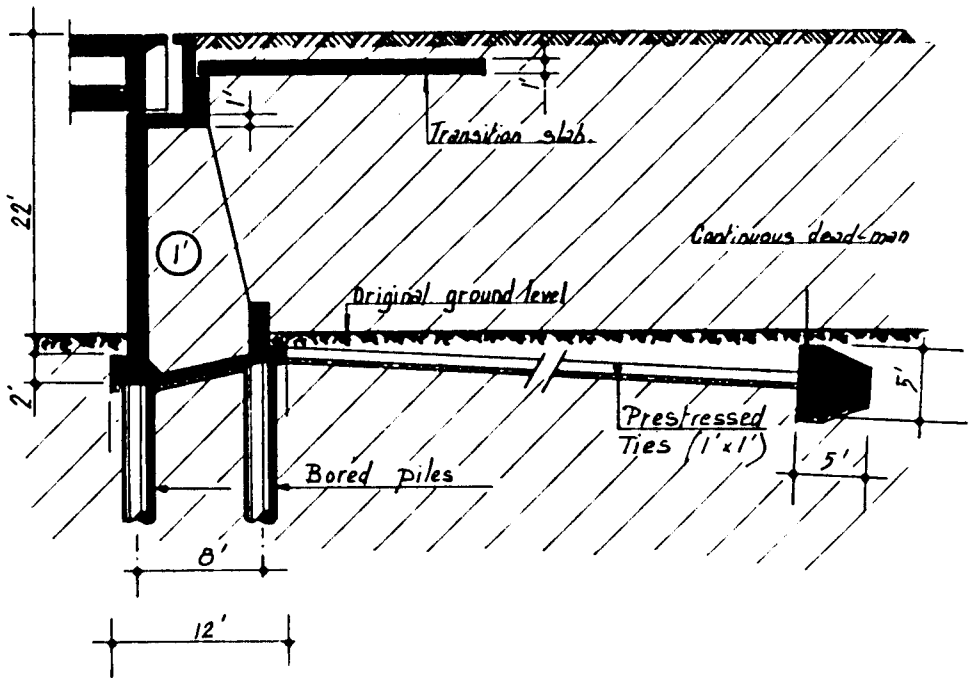

Figure 7–8 Abutment Type I, segmental bridges.

bearing. Behind this wall a separate MSE wall contains the approach fill. This scheme is designated as Type II.

Hollow Box Abutment. With relatively high bridges generating high levels of earth pressure behind the abutment wall, and where it is not possible or expedient to extend the approach fill under the deck, a suitable solution is an abutment built as a box, as shown in Figure 7–9, designated as Type III. A box with a front wall supports the superstructure and the approach roadway slab between the deck and the adjacent pavement. This structure may also be founded on piles or on spread footing. A hollow box abutment is essentially a derivative of the vaulted type shown in Figure 1–10.

Abutments Designed for Uplift. An example of segmental bridge with end uplift is the Tricastin Bridge over the Rhone River, France (Podolny and Muller, 1982). Piers were not desired in the waterway area, and this dictated a three-span structure

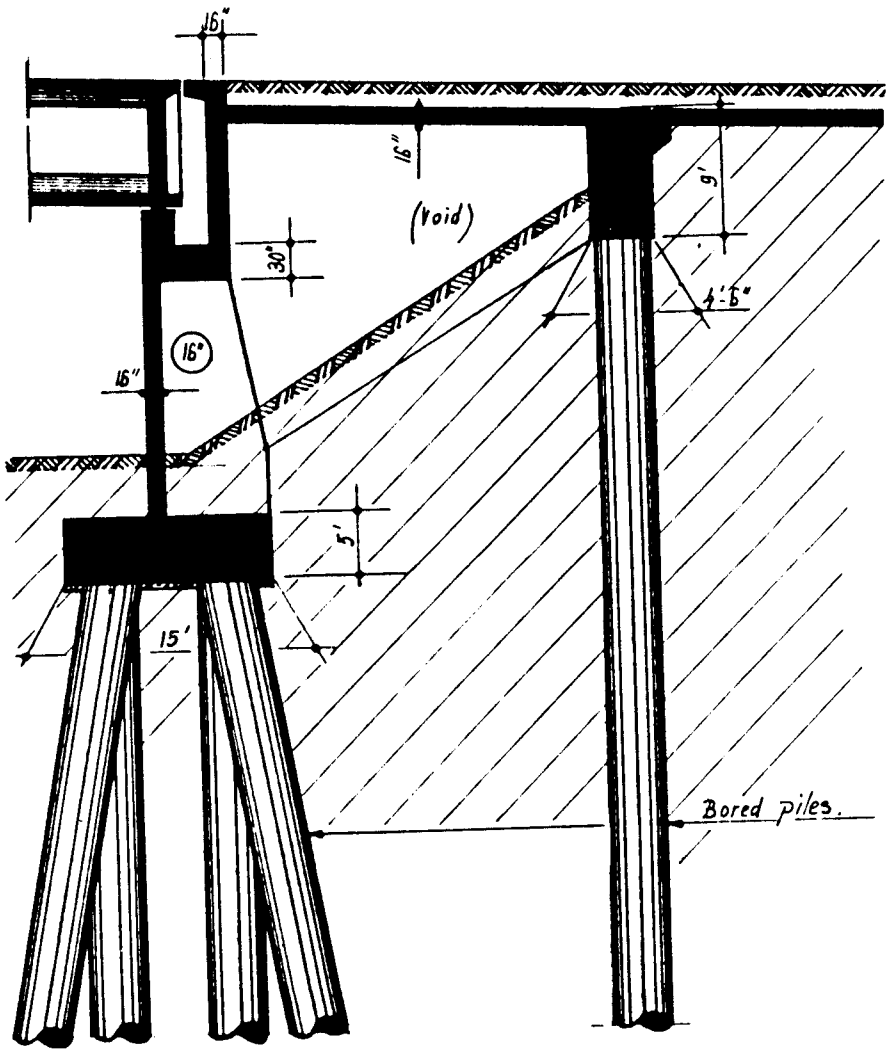

Figure 7–9 Hollow box abutment Type III, segmental bridges.

with a main span 467 feet and two short spans 83 feet each. The uplift is in this case transferred to the abutments.

An abutment designed and built to resist uplift is shown in Figure 7–10, designated as Type IV. A large caisson is open-dredged and filled with tremie concrete after completion of the excavation to the required foundation level to provide a total weight sufficient to balance the uplift reaction from the deck.

The abutment types shown in Figures 7–8 through 7–10 are not necessarily unique to segmental construction. The same or similar structures may be designed and built for medium-range bridges with truss and steel-box girder superstructures.

Commentary on abutment movement. A consideration relevant to the amount of horizontal movement that bridges in general can tolerate is the movement of abutments necessary to reduce the earth pressures to the design value. If an abutment, irrespective of its type, does not move, the earth pressure acting behind the structure is close to the at-rest value. If the abutment moves away from the backfill, the earth pressure will be reduced below the at-rest value. If this movement is large enough the earth pressure may be reduced to the active level.

If the backfill is a clean mix of sand and gravel, the earth pressure may be assumed to reduce to active values, if the horizontal movement of the abutment away from the backfill is about 0.004 times the height of the abutment wall. This criterion translates to 0.5-inch movement for a 10-foot high wall, 1.0 inch for a 20-foot wall, and 1.5 inches for a 30-foot high wall. These values may be used as a general guideline for sand and gravel backfill in a loose condition. In dense sand and gravel, the movement

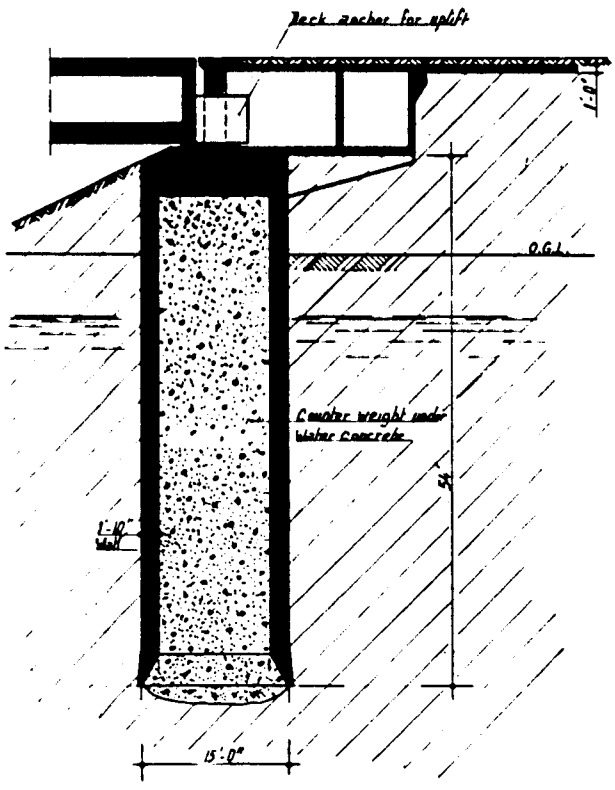

Figure 7–10 Abutment Type IV to resist uplift, segmental bridges.

necessary to reduce the earth pressure to active values is smaller than 0.004 times the wall height.

If the backfill consists of clay, or if it contains enough clay or plastic silt to impart cohesion and plasticity to the system, the movement necessary to bring the earth pressure to the active condition is much larger than for sand and gravel. Furthermore, cohesive soils have creep characteristics. Even though the wall may move enough to reduce the earth pressure to the active value, the pressure will begin to increase again as creep takes effect. Continuous movement has been demonstrated where active pressures were used to design walls backfilled with cohesive soils. Hence, where these materials provide the backfill, it is essential and structurally consistent to select pressures at rest.

It is apparent that the selection of earth pressures for the design of abutments will have certain implications regarding wall movement. If active pressures are introduced, the design should check how much movement will be necessary to develop these pressures. These considerations should be included in the design of expansion joints that will allow for temperature expansion and abutment movement.

Frost Effects

Water in soil expands when it freezes so that ice lenses may form, resulting in frost heave in the frozen soil. Foundation for closed abutments should be built below the frost line to prevent frost damage. This problem is less severe with pile bents built in embankments, unless the water level can rise to unexpected levels.

The maximum frost depth is usually available from local experience, or may be determined from frost-depth contour maps. The data shown in Figure 7–11 give an alternate procedure for estimating frost depth using a freezing index proposed by the U.S. Corps of Engineers (1949) and Brown (1964). According to this,

$$\text{Freezing Index} = N_{32°\text{F}} \times (32°\text{F} - T) \tag{7–12}$$

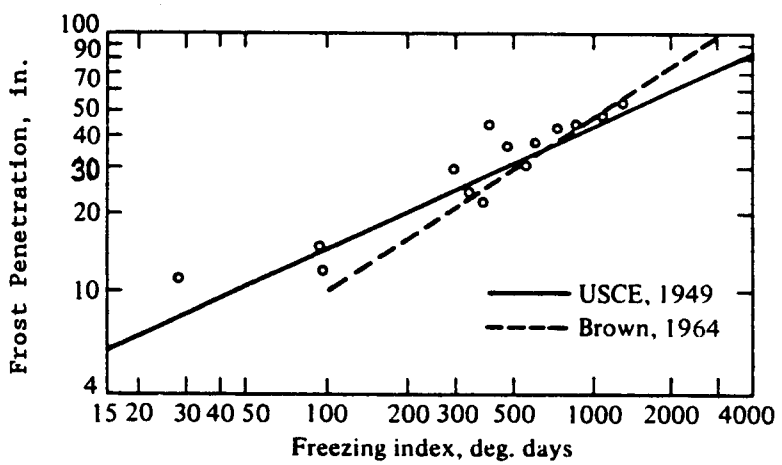

Figure 7–11 Design curves for maximum frost penetration based on the freezing index *(from U.S. Corps of Engineers, 1949; and Brown 1964).*

where $N_{32°F}$ = number of days below 32°F, and T = average daily temperature. For example, if $N_{32°F}$ = 25 days, and T = 22°F for a particular site, the freezing index is (25)(32–22) = 250. From the graph of Figure 7–11 the corresponding frost depth is obtained as about 20 inches.

7.9 SEISMIC DESIGN OF ABUTMENTS

General Principles

Certain basic principles are discussed in section 3.10 in conjunction with the two approaches used to formulate the current AASHTO philosophy in seismic design. The relative displacement effects are of particular importance. As mentioned, these may arise from out-of-phase motion of different parts of the bridge, from lateral displacement or rotation of the foundations, and differential displacement of abutments. This makes it necessary to stipulate minimum support lengths.

Numerous case histories of damage or failure of bridges attributed to abutment failure or displacement during earthquakes have demonstrated the need to address the seismic factor in abutment design. Damage may be associated with excessive settlement or slumping of the backfill, excessive displacement caused by high seismically induced lateral earth pressure, or the transfer of large longitudinal or transverse inertia forces from the bridge superstructure. Settlement of abutment backfill, and abutment or deck damage resulting from abutment movement may lead to loss of bridge access, and hence abutments must be regarded as an important parameter in the overall seismic design process.

The pattern of abutment movement or damage during past earthquakes has been documented in case histories. Evans (1971) has examined the abutments of 39 bridges within 30 miles of the 1968 M7 Inangahus earthquake in New Zealand. Of these, 23 showed measurable movement and 15 suffered some form of damage. Movement of free-standing abutments followed the general pattern of outward motion and rotation about the top after contact with the superstructure induced a corresponding restraint. Fill settlement was observed to be 10 to 15 percent of the fill height. Similar damage effects were documented on bridge abutments in the M7.1 Madang earthquake in New Guinea (Ellison, 1971); abutment movement was as much as 20 inches. Damage to abutments in the 1971 San Fernando earthquake is reported by Fung, LeBeau, Klein, Belvedere, and Goldschmidt (1971). Numerous instances of abutment displacement and associated damage have been reported on the Niigata and Alaska earthquakes, but these failures were primarily related to soil liquefaction.

As is evident from sections 7.1 through 7.8, abutment types vary and their main features are influenced by the characteristics of the bridge site, foundation conditions, bridge geometry, and loads from superstructure. For the wide variety of abutments discussed in the foregoing sections, the foundation may consist of spread footings, vertical or battered piles, and drilled shafts. Connection details to the superstructure may be structural joints, roller supports, or elastomeric bearings. Given the large number of design variables and relevant parameters combined with the complex abutment-superstructure-soil interaction, the analysis of abutment response during earthquakes is a complex problem.

Seismic Earth Pressures

Free-standing abutment walls. In this category are gravity or cantilever-type abutments that can yield laterally during an earthquake (i.e., by supporting superstructures through bearings that are free to rotate or slide). For these abutments, the earth pressures induced during an earthquake can be computed using the Mononobe-Okabe pseudo-static approach.

In highly seismic areas, the design of these abutments to provide zero displacement under peak ground acceleration is grossly unrealistic, and should be replaced by an approach where a small lateral displacement is acceptable. A method recently developed to estimate the magnitude of relative wall displacement during a seismic incident is included in this section. Based on a simplified approach, suggested guidelines are introduced for selecting a pseudo-static seismic coefficient and the corresponding displacement level for a given peak ground acceleration.

Mononobe-Okabe theory. This is essentially a static approach developed by Mononobe (1929) and Okabe (1926). Essentially the analysis is an extension of the Coulomb sliding wedge theory considering horizontal and vertical inertia forces acting on the soil. Complete details of the associated methodologies are given by Seed and Whitman (1970), and Richards and Elms (1979). The following assumptions are made:

1. The abutment is free to yield sufficiently to mobilize the soil strength and active pressure conditions. If the abutment is rigidly fixed and thus unable to move, the soil forces will be much greater than those predicted by this analysis.
2. The backfill is cohesionless material, with a definite friction angle ϕ.
3. The backfill is unsaturated so that liquefaction does not occur.

Equilibrium conditions of the active soil wedge behind the abutment are shown in Figure 7–12. These considerations lead to a value E_{AE} of the active force imposed on the soil mass by the abutment (and vice versa) when the latter is at the point of failure. The following expression gives E_{AE}

$$E_{AE} = \frac{1}{2}\gamma H^2(1-k_v)K_{AE} \tag{7–13}$$

where the seismic active pressure coefficient K_{AE} is given by

$$K_{AE} = \frac{\cos^2(\phi-\theta-\beta)}{\cos\theta\cos^2\beta\cos(\delta+\beta+\theta)} \times \left[1+\sqrt{\frac{\sin(\phi+\delta)\sin(\phi-\theta-i)}{\cos(\delta+\beta+\theta)\cos(i-\beta)}}\right]^2 \tag{7–14}$$

and where γ = unit weight of soil; H = height of soil face (as shown in Figure 7–12); ϕ = angle of friction of soil; θ = arc tan $[k_h/(1 - k_v)]$; δ = wall friction angle; k_h = horizontal acceleration coefficient; k_v = vertical acceleration coefficient; i = backfill slope angle; and β = slope of soil face.

If the abutment is moved towards the backfill, the equivalent expression for the passive force is

$$E_{PE} = \frac{1}{2}\gamma H^2(1-k_v)K_{PE} \tag{7–15}$$

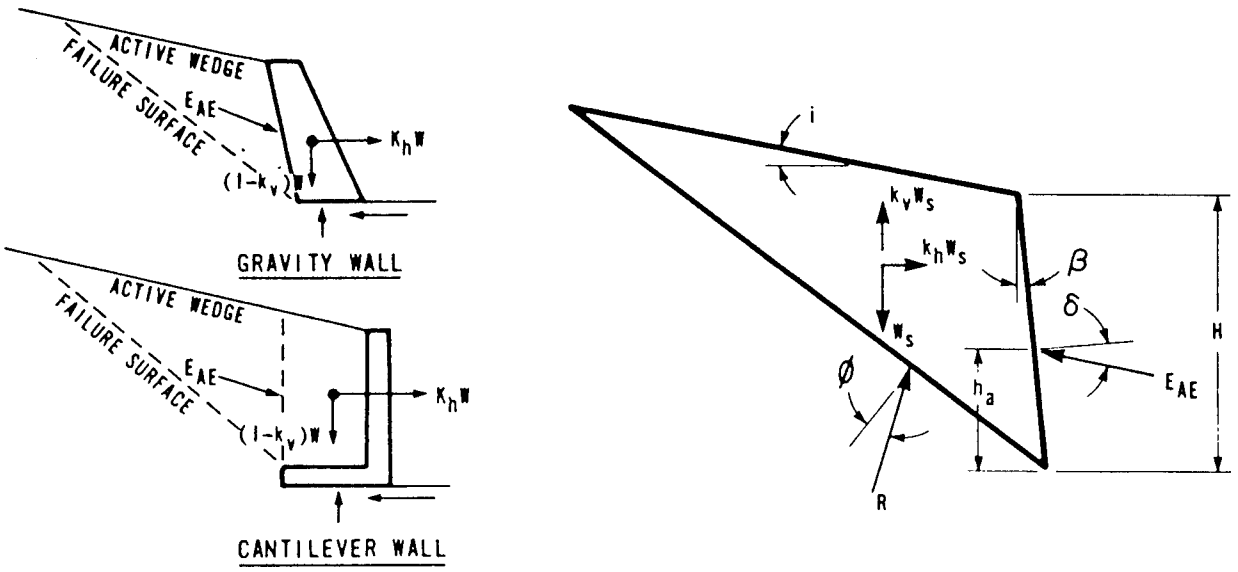

Figure 7–12 Active wedge force diagram.

where the seismic passive pressure coefficient K_{PE} is given by

$$K_{PE} = \frac{\cos^2(\phi - \theta + \beta)}{\cos\theta \cos^2\beta \cos(\delta - \beta + \theta)} \times \left[1 - \sqrt{\frac{\sin(\phi - \delta)\sin(\phi - \theta + i)}{\cos(\delta - \beta + \theta)\cos(i - \beta)}}\right]^2 \tag{7–16}$$

As the seismic inertia angle θ increases, the values of K_{AE} and K_{PE} approach each other, and for a vertical backfill they become equal when $\theta = \phi$.

This approach has a relative simplicity. Its accuracy, however, has been confirmed by model tests (Franklin and Chang, 1977) and by back calculations from observed failures of flood channel walls (Elms and Martin, 1979). In the latter case, however, the displacements were larger, and this could modify the effective value of k_h at which failure occurs.

The arm h_a that defines the point of application of the resultant soil pressure is usually taken as $H/3$ for the static conditions without earthquake effects. This arm becomes greater, however, when earthquake effects are present. This has been shown theoretically by Wood (1973), who determined that the resultant of the dynamic pressure is located approximately at the midheight, and confirmed by tests. Seed and Whitman (1970) have suggested that the static component of the soil force (computed from Eq. 7–13 with $\theta = k_v = 0$) acts at a height $H/3$, but the additional dynamic effect should be taken at height $0.6\,H$ (see also section 6.13). For simplicity, most engineers will assume $h = H/2$ for the composite effect, with a uniformly distributed pressure. Taking the location of the total resultant at midheight is also suggested by AASHTO (Elms and Martin, 1979).

The Mononobe-Okabe expression for active thrust is readily estimated for a given geometry and friction angle. The significance and the effects of the various parameters are not, however, directly obvious. Very useful data on these effects are included in AASHTO commentary on seismic design.

The effects of abutment inertia are not taken into consideration in the foregoing analysis. One approach is to neglect the inertia forces due to the mass of the abutment, but this is not a conservative assumption, and where the design must rely on the mass of the abutment for stability it is also an unreasonable assumption.

Design for displacement. If peak ground accelerations are used in the Mononobe-Okabe analysis, the size of gravity structures will often be too excessive. Alternatively, a more economical structure may be provided if the design accepts a small tolerable displacement rather than no displacement at all.

Test show that a gravity retaining wall will fail incrementally in an earthquake. For a given earthquake ground motion, the total relative displacement may be computed using the sliding block method proposed by Newmark (1965). A displacement pattern is assumed similar to that of a block resting on a plane rough horizontal surface subjected to an earthquake, with the block being free to move against frictional resistance in one direction only. Figure 7–13 shows relationship of the relative displacement to the acceleration and velocity time histories of soil and wall. At a critical value of k_h the wall is assumed to begin sliding; relative motion will continue until wall and soil velocities are equal.

Newmark computed the maximum displacement response for four earthquake records, and the results were plotted after scaling the earthquakes to a common maximum acceleration and velocity. Franklin and Chang (1977) repeated the analysis for a large number of both natural and synthetic records and added the results to the same plot. Upper bound envelopes are shown in Figure 7–14. All records are scaled to a maximum acceleration coefficient 0.5 and a maximum velocity V = 30 in/sec. The maximum

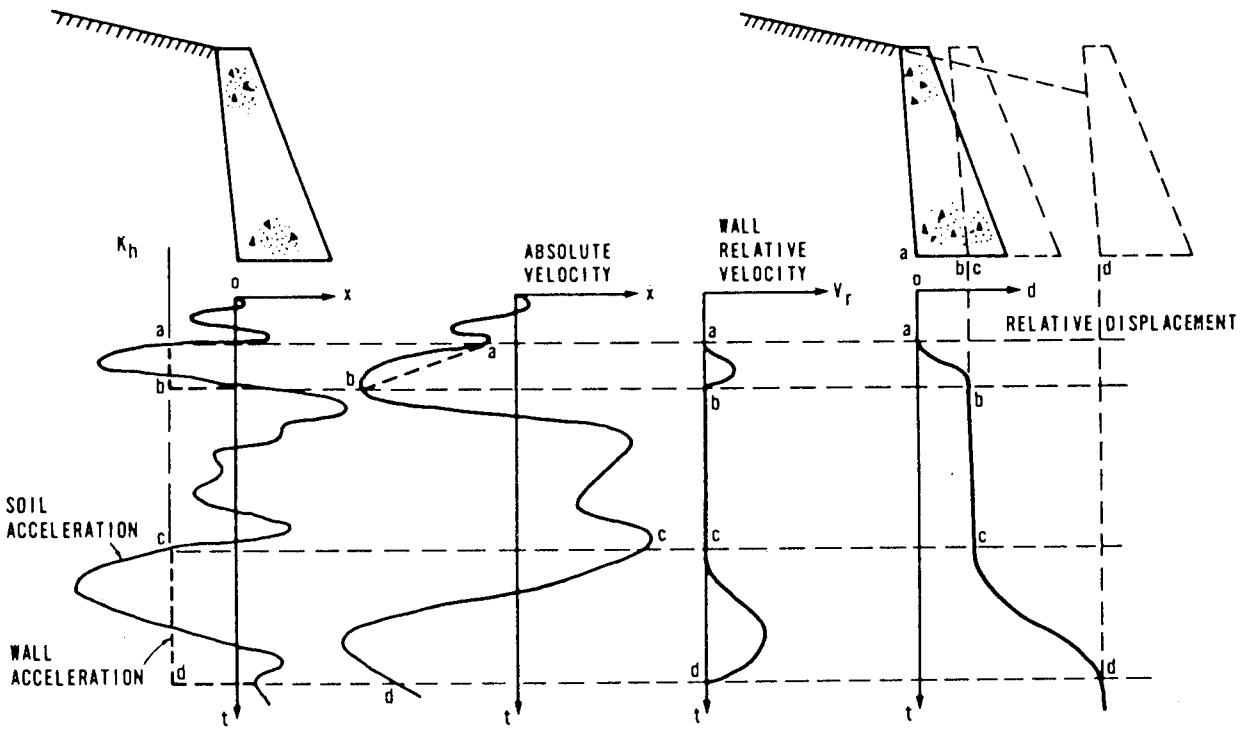

Figure 7–13 Relation between relative displacement and acceleration and velocity time histories of soil and wall.

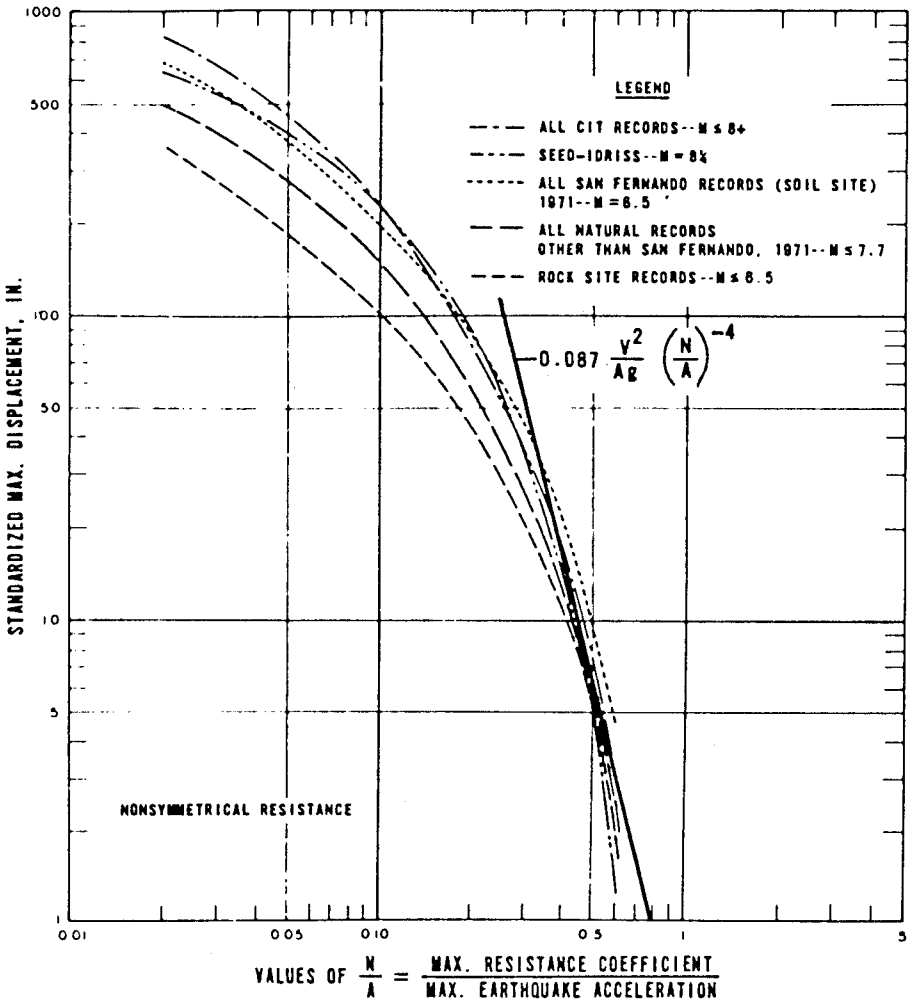

Figure 7–14 Upper bound envelope curves of permanent displacements for all natural and synthetic records analyzed by Franklin and Chang (1 inch = 25.4 mm).

resistance of coefficient N is the maximum acceleration coefficient sustainable by a sliding block before it slides. For a wall designed using the M-O method, the maximum coefficient is k_h.

Figure 7–14 shows that the displacement envelopes for all the scaled records have the same basic shape. For relatively low displacements, an approximation to the curves gives the following relation:

$$d = 0.087 \frac{V^2}{Ag}\left(\frac{N}{A}\right)^{-4} \tag{7–17}$$

where V = maximum velocity; A = acceleration coefficient; and g = acceleration of gravity = 32.2 ft/sec^2. The parameter d is the total relative displacement of a wall subjected to the ground motion. On Figure 7–14 a straight line is fitted, and since Equation (7–17) is derived from envelope curves it will tend to overestimate d for most earthquakes.

A suggested design approach is to choose a desired value for the maximum wall

displacement d together with appropriate earthquake parameters, and then use Equation (7–17) to determine the seismic acceleration coefficient for which the wall should be designed. The superstructure connections should be detailed to accommodate this displacement.

Elms and Martin (1979) applied this procedure to several examples and concluded that a value of $k_n = A/2$ should be adequate for most design purposes, provided that allowance is made for an outward displacement of the abutment of up to $10A$ inches.

For bridges with SPC C and D, more detailed analysis is necessary to articulate the transfer of structural inertia forces though bearings to free-standing abutments, particularly for category D, because of the continued bridge accessibility required after a major earthquake.

Figure 7–15 shows force diagrams for sliding steel bearings or pot bearings, describing limiting equilibrium conditions for a simple abutment. Where the bearings consist of unconfined elastomeric pads, the forces transferred to the abutment become more complex because these bearings are capable of transmitting significant force. This force initially depends on the relative movement between superstructure and abutment and can become quite large before slip occurs.

For bridges with SPC D classification, provisions should be made to connect superstructure and abutment using bolts and buffers, such as the detail shown in Figure 7–16. Linkage bolts are used to prevent spans dropping off supports. The rubber rings act as buffers to prevent damage due to impact. The knock-off section of the backwall will accommodate differential displacement between superstructure and abutment beyond the scope of the expansion device and will thus minimize impact damage. A typical detail provision used in the United States is to seal the gap between superstructure and abutment with bituminous material. Irrespective of these measures, some form of damage with possible abutment rotation should be expected in strong earthquakes.

The same guidelines suggest also the use of a settlement approach slab tied to the abutment. This will provide bridge access in the event of backfill settlement as well as additional abutment friction anchorage against lateral movement.

Non-yielding abutments. The M-O analysis assumes that the abutment is free to yield laterally enough to mobilize peak soil strength in the backfill. For granular backfills, the criteria of movement discussed in the foregoing sections translate into a deflection at the top of about 0.5 percent of the height. If an abutment is restrained against lateral movement (i.e., by ground anchors, batter piles, etc.), the lateral pressures will be greater than those computed from the M-O analysis (Wood, 1973). Where doubt exists, a factor of 1.5 should be applied to the peak ground acceleration to account for the lateral restraint of the abutment.

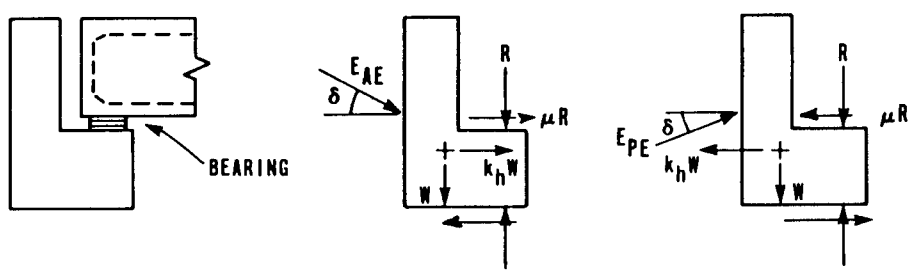

Figure 7–15 Force diagrams including bearing friction.

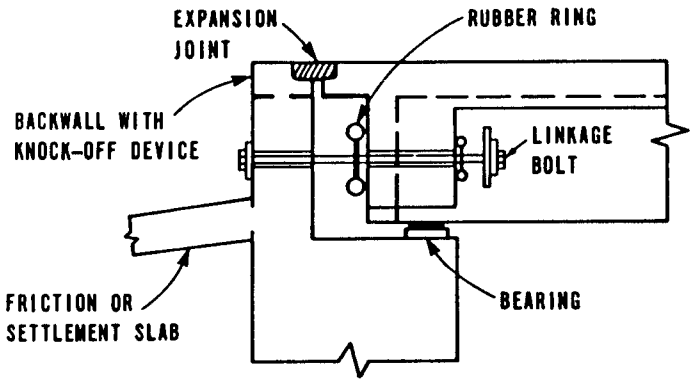

Figure 7–16 Abutment support detail.

Monolithic abutments. Figure 7–17 shows a monolithic or end diaphragm abutment commonly used for single and for two-span bridges in California. The end diaphragm is cast monolithically with the superstructure and may be supported directly on piles. The diaphragm acts as a retaining wall while the superstructure functions as a prop between abutments.

Monolithic abutments of this type have performed well during earthquakes, since they avoid problems related to backwall and bearing damage as the abutment yields; they also reduce the lateral load carried by columns or piers. On the other hand, the di-

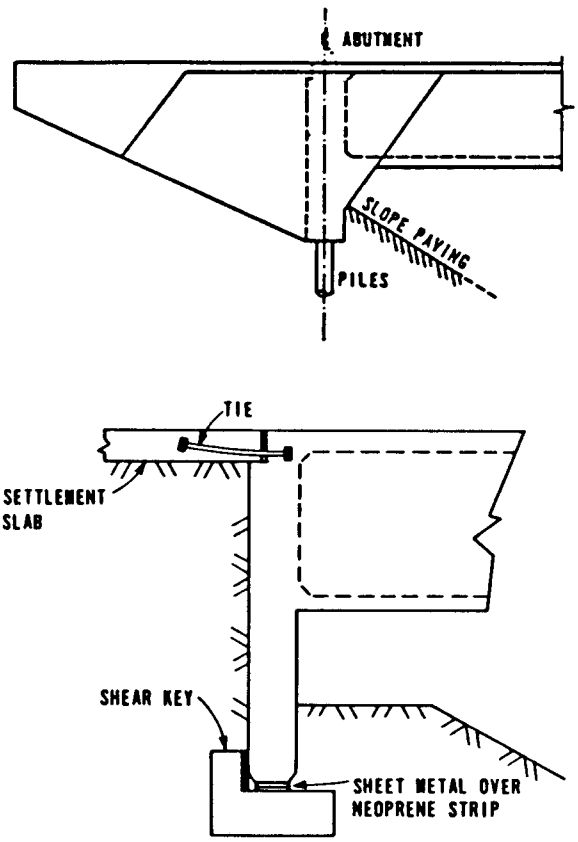

Figure 7–17 Typical monolithic abutments.

rect connection with the superstructure implies that higher longitudinal and transverse inertia forces are transmitted directly into the backfill, and provisions must be made for adequate passive resistance.

Free-standing or seat-type abutments are more compatible with the development of soil forces and with better control. However, the added joint introduces a potential collapse mechanism into the entire structure. Thus, monolithic abutments are viable alternatives and particularly suitable for bridges in SPC D. The response in this case may be heavier damage than for the free-standing abutment because of the higher forces transferred to the backfill, but the bridge as a whole has a lower collapse potential. When making estimates of monolithic abutment stiffness and associated longitudinal displacements during transfer of peak earthquake forces from the structure, a recommendation is to have the abutments proportioned to restrict displacements to 0.3 feet (9.1 cm) or less in order to minimize damage.

AASHTO Requirements

The foregoing criteria form the basis for the requirements of seismic design stipulated in the current AASHTO standard specifications.

Seismic performance category B. For free-standing abutments or retaining walls that can displace horizontally without major restraint, the M-O method of analysis is recommended, using $k_h = A/2$ and ignoring the effect of vertical acceleration. Abutments should be proportioned to slide rather than tilt, and thus they should be designed to accommodate displacements up to $10A$ inches. The seismic design should consider forces due to seismically induced lateral earth pressures, additional forces arising from wall inertia effects, and the transfer of seismic forces from the superstructure where bearing supports are not free to slide. For free-standing abutments restrained against horizontal movement by anchors or batter piles, the maximum lateral earth pressure may be computed using $k_h = 1.5A$ in conjunction with the M-O analysis.

For monolithic abutments (integrally formed with the superstructure), maximum earth pressures acting on the abutment may be assumed to be the maximum longitudinal earthquake force transferred from the superstructure. To minimize abutment damage, the abutment should be designed to resist the passive pressure that can be mobilized by the abutment backfill, which should be greater than the maximum computed longitudinal earthquake force transferred to the abutment. However, it may be assumed that the lateral active earth pressure during an earthquake is less than the superstructure earthquake load. When longitudinal seismic forces are also resisted by piers, the portion of earthquake load transferred to the abutment should be proportioned to each substructure stiffness.

Seismic performance category C. In addition to the foregoing provisions, the design should consider the mechanism of transfer of superstructure transverse inertial forces. Adequate resistance to lateral pressure should be provided by wing walls or abutment keys to minimize lateral displacement of the abutment.

Seismic performance category D. In addition to the requirements for Categories B and C, the design should consider the transfer mechanism of superstructure longitudinal and transverse inertia forces to the abutments as well as the associated abutment-soil interaction. In order to prevent the potential loss of bridge access due to abutment

damage, monolithic and end diaphragm construction is strongly recommended for short span bridges. Settlement or approach slabs linked to abutments by flexible ties should be mandatory.

7.10 DESIGN EXAMPLE 7–1, PILE BENT ABUTMENTS, ASD METHOD

Figure 7–18 shows the elevation and span lengths for a 7-span bridge with simple and continuous units as shown. Hinges are located in spans 1, 4, and 7, and the resulting superstructure configuration is three simple spans, and two-span continuous units with cantilever over the end supports. Both end bents are provided with fixed bearings. Because of severe geometric restrictions, the bridge is placed on a rather unusual skew angle, where all substructure elements form an angle of 65° with the vertical to the bridge axis.

The superstructure consists of a concrete deck on steel plate girders (72-inch web plate). There are 6 steel girders spaced at 7 feet 4 inches. The concrete slab is 8 inches thick, and the deck accommodates three lanes in the same direction. The bridge site is in a region of low seismic activity (Category A), and hence earthquake requirements do not apply. Referring to Figure 7–18, span 1 is 106 feet long, but because of the hinge, the actual design span is 95 feet. The severe skew angle of the bridge results in abutment lengths of about 100 ft. We will design End Bent 1 (fixed bearing) using ASD method.

A typical (initial) section of the bent is shown in Figure 7–19, together with the pile layout and spacing. Design lateral earth pressures have been established by the supervising authority, and are articulated as 35 lb equivalent fluid pressure. Since a structural approach slab is provided and supported on the back wall, live load surcharge from the fill is omitted.

Group I. This includes dead load, live load, and earth pressure.

1. Dead load from superstructure.

   From Superstructure design $DL_s = 418$ kips

2. Dead load, weight on bent.

   Referring to Figure 7–19(a), we calculate the following

   Section ① = (5.00)(5.00)(100)(0.15) = 375 kips

   ② = (9.00)(1.50)(100)(0.15) = 203 kips

   ③ = (2.50)(1.67)(100)(0.15) = 63 kips

   Total $DL_b = 641$ kips

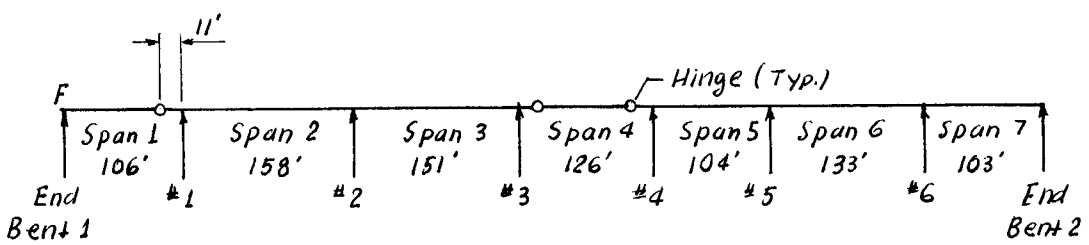

Figure 7–18 Bridge elevation, Design Example 7.1.

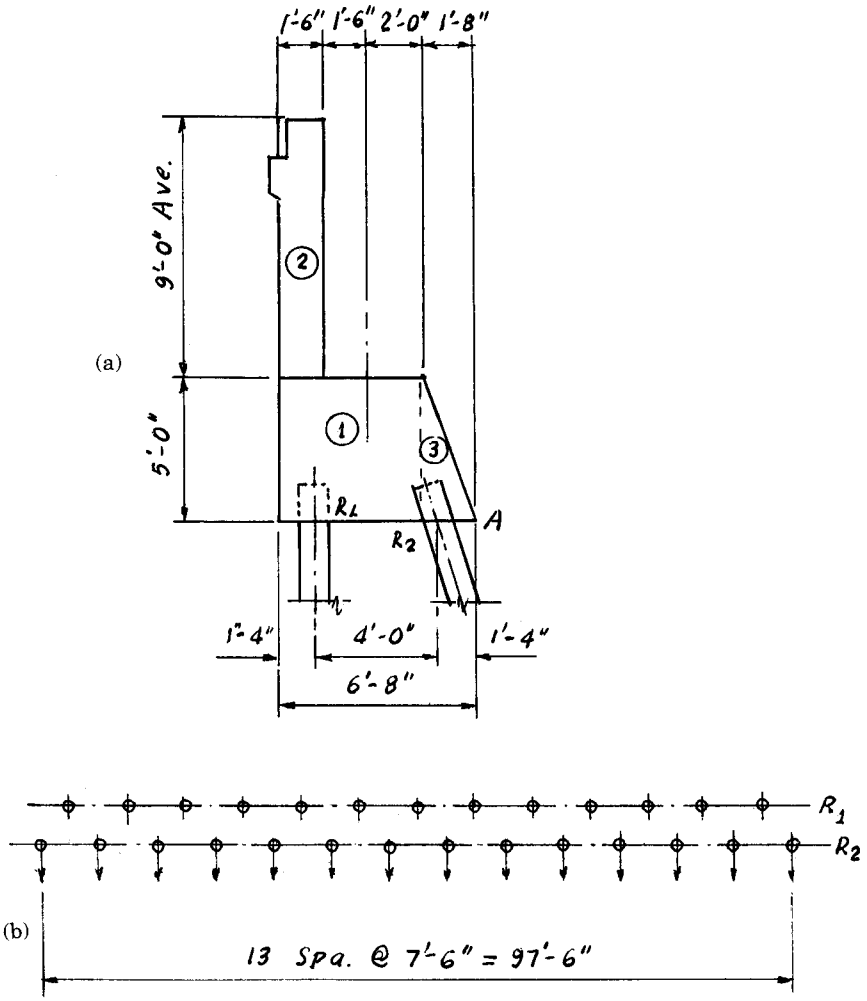

Figure 7–19 Bent of Design Example 7.1 (a) Preliminary section; (b) pile layout.

3. Dead load, weight of approach slab (24 feet wide)
   This is computed as (36)(1.875), or DL_{as} = 68 kips
4. Live load from bridge (HS 20 without impact)
   3 lanes load $LL = (3)(0.9)(64.9)$ or LL = 175 kips
5. Lateral earth pressure (lin. ft).
   For a height h = 14′, $P_e = (0.035)(\frac{14^2}{2})$ = 3.43 kips/lin. ft

Case A. Dead load plus earth pressure (check conditions necessary to balance lateral loads). Referring to Figure 7–19(a), we take moments about point A.

$$M_{DL_s} = 418 \times 3.67 = 1534 \text{ ft-kips}$$
$$M_b = 375 \times 4.17 = 1564 \text{ ft-kips}$$
$$203 \times 5.92 = 1202 \text{ ft-kips}$$
$$63 \times 1.11 = 70 \text{ ft-kips}$$

M_{as} = 68 × 6.17 = 420 ft-kips ↶

Earth pressure, total force = (3.43)(96) = 329 kips

M_e = (329)(4.67) = − 1536 ft-kips ↷

Total 1127 kips 3254 ft-kips ↶

From point A to resultant = x = 3254/1127 = 2.88 ft. Referring to Figure 7–20 the dimension e is computed as the difference 5.33 − 2.88 = 2.45 ft.

The total load of 1127 kips is distributed to the front and back rows as follows:

R_1 = (1127)(1.55)/4.00 = 436 kips

R_2 = 691 kips

Horizontal component of front row = 691/3 = 230 kips.

Unbalanced horizontal force = 329 − 230 = 99 kips.

This would give a lateral force of 99/27 = 3.7 kips per pile, which is excessive. An allowable horizontal force per pile is for this case 2 kips. The initial bent design must, therefore, be revised.

Figure 7–21 shows the revised (final) cross section of the bent. The intent of this revision is to increase the overall dead load, and further increase the load transferred to the front row by moving the bearing line closer to this row, and by placing the back row further away from the front row. The new loads are as follows.

1. Dead load from superstructure DL_s = 418 kips
2. Dead load, weight of bent
   - Section ① = (3.50)(4.50)(100)(0.15) = 236 kips
   - ② = 203 kips
   - ③ = (8.00)(2.50)(100)(0.15) = 300 kips
   - Total DL_b = 739 kips
3. Dead load, approach slab DL_{as} = 68 kips
4. Live load from bridge = same as before
5. Lateral earth pressure (lin. ft)

   For $p_e = (0.035)\left(\frac{15^2}{2}\right) = 3.94$ kips/lin. ft
6. Dead load, weight of earth
   - ⑦ = (12.50)(2)(100)(0.12) = 300 kips
   - ⑧ = (1.50)(2.00)(100)(0.12) = 36 kips

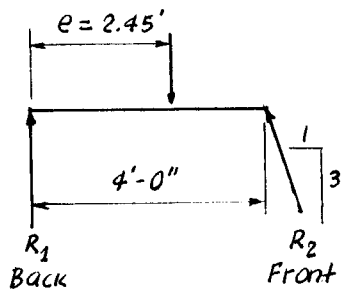

Figure 7–20 Pile details and batter.

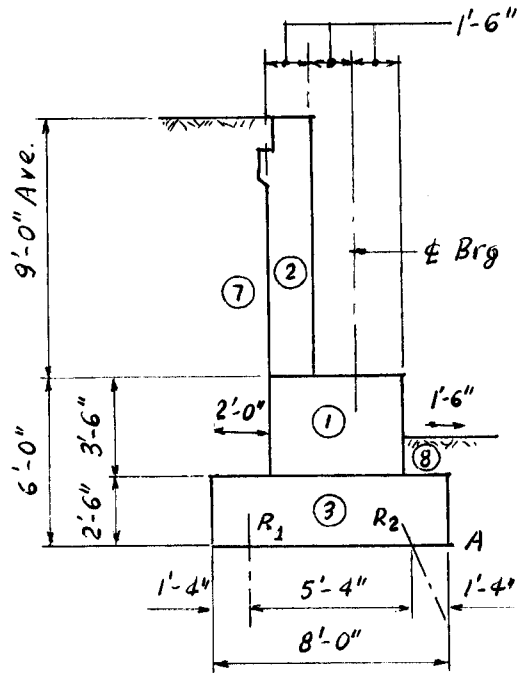

Figure 7–21 Final bent section, Design Example 7.1.

Case A (Revised). Dead load plus earth pressure. Taking moments about point *A* in Figure 7–21, we obtain

M_{DL_s}	418×3.00	=	1254 ft-kips	↶
M_b	236×3.75	=	885 ft-kips	↶
	300×4.00	=	1200 ft-kips	↶
	203×5.25	=	1066 ft-kips	↶
M_{as}	68×6.00	=	408 ft-kips	↶
M_7	300×7.00	=	2100 ft-kips	↶
M_8	36×0.75	=	27 ft-kips	↶
M_e	378×5	=	−1890 ft-kips	↷
Total	1561 kips		5050 ft-kips	↶

Distance from point *A* to resultant = 5050/1561 = 3.23 ft, giving $e = 6.67 - 3.23 = 3.44$ ft (see Figure 7–22). Therefore

$$R_1 = (1561)(1.89)/5.33 = 554 \text{ kips}$$
$$R_2 = 1007 \text{ kips}$$

Horizontal component of front row = 1007/3 = 336 kips

Unbalanced horizontal force = 378 − 336 = 42 kips, giving a horizontal force per pile = 42/27 = 1.6 kips, OK.

The stability against overturning about the front row of piles is checked next. The resultant of vertical loads gives a moment about point *A* = 6940 ft-kips, for a moment arm 6940/1561 = 4.45 ft, or 4.45 − 1.33 = 3.12 ft from R_2. The balancing moment is

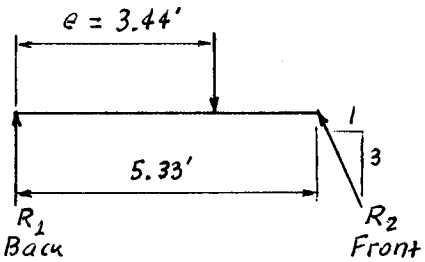

Figure 7–22 Pile details and batter.

therefore $M_b = (1561)(3.12) = 4870$ ft-kips, giving a factor of safety against overturning 4870/1890 = 2.58, or adequate.

Note: The analysis of piles subjected to lateral load involves certain assumptions. Methods for calculating lateral resistance are broadly divided into two categories: (1) initially calculate ultimate lateral resistance, and then obtain a working lateral load by applying a factor of safety; and (2) determine acceptable deflections at working lateral load (the allowable lateral load corresponds to an acceptable lateral deflection). The lateral load in either case is also a function of the top pile condition, free-head or fixed head. For a complete review of this subject, reference is made to Prakash and Sharma (1990), and to chapter 9.

Case B. (Case A plus live load on bridge)
Live load moment about point A,

$$M_{LL} = \underline{(175)(3.00)} = \underline{525} \text{ ft-kips}$$
$$\text{Total} = 1736 \text{ kips} \quad 5575 \text{ ft-kips}$$

Distance of resultant from point A, = (5575)/1736 = 3.21 ft.
Eccentricity $e = 6.67 - 3.21 = 3.46$ ft. Therefore

$$R_1 = (1736)(1.87)/5.33 = 609 \text{ kips}$$
$$R_2 = 1736 - 609 = 1127 \text{ kips}$$

Horizontal component of front row = 1127/3 = 376 kips
Unbalanced force = 378 – 376 = 2 kips, OK.

Case C. (Case A plus live load on approach slab)
For a 22-foot long approach slab, the live load reaction per lane is 43.6 kips.
Total reaction (3 lanes) = $43.6 \times 3 \times 0.9 = 118$ kips
Moment = $118 \times 6.00 = 702$ ft-kips
Total vertical load = 1561 + 118 = 1679 kips
Total moment = 5050 + 702 = 5752 ft-kips
Distance of resultant from point A = 5752/1679 = 3.43 ft
Eccentricity $e = 6.67 - 3.43 = 3.24$ ft. Therefore

$$R_1 = (1679)(2.09)/5.33 = 658 \text{ kips}$$
$$R_2 = 1679 - 658 = 1021 \text{ kips}$$

Horizontal component of front row = 1021/3 = 340 kips
Unbalanced force = 378 – 340 = 38 kips, per pile = 38/27 = 1.41 kips, OK.

Pile Load. From Case B, $R_2 = 1127$ kips, or per pile

$$R_2 = 1127/14 = 80.5 \text{ kips}$$

Horizontal component = 80.5/3 = 26.8 kips

Resultant axial load per pile $R = \sqrt{80.5^2 + 26.8^2} = 85$ kips

Use 45-ton piles

Load factor (strength design) method. The lateral load capacity of a pile under strength design approach would involve an estimation of the ultimate resistance. Since the most severe condition occurs under Case A (dead load and earth pressure), the comparison of factored effects and factored resistance reduces to these two loads. Because the dead load provides the resisting force, it should be factored by applying a load factor less than 1. Since the earth pressure represents the load effects, it should be factored by applying a load factor greater than 1. The two methods, load factor approach and ASD, become compatible and equivalent in this case merely by calibrating load and resistance factors to correspond to the factor of safety used in ASD.

Group II. This includes dead load, earth pressure, and wind on superstructure, and the design may consider an allowable stress 125 percent. Referring to Figure 7–23, the wind direction (lateral and longitudinal) is taken as shown, so that the component N normal to the abutment acts in the same direction as the lateral earth pressure.

The exposed depth of superstructure is computed as 11.66 feet, and includes parapet, concrete floor depth, plate girder, and superelevation. The span length exposed to wind is 96 feet. One-half of the lateral wind force is applied to the abutment, but the entire longitudinal wind must be resisted at this location. For wind computations, we use the simplified loading suggested in AASHTO Art. 3.15.2.1.3.

Lateral wind = (0.5)(96)(11.66)(0.05) = 28 kips $N = 25.5$ kips

Longitudinal wind = (96)(11.66)(0.012) = 13.4 kips $N = 5.6$ kips

Total $N = 31.1$ kips normal to the bent

This force acts about 7.5 feet above bridge seat, or 13.5 feet above bottom of footing.

Moment due to N, $M_N = (31.1)(13.5) = -420$ ft-kips

Total moment $M = 5050 - 420 = 4630$ ft-kips

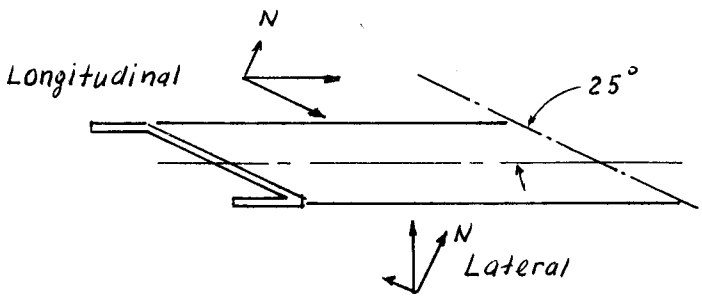

Figure 7–23 Wind forces, longitudinal and lateral.

Distance from point A to resultant = 4630/1561 = 2.97 ft, giving e = 6.67 – 2.97 = 3.70 ft. Therefore

$$R_1 = (1561)(1.63)/5.33 = 478 \text{ kips}$$
$$R_2 = 1561 - 478 = 1083 \text{ kips}$$

Horizontal component of front row = 1083/3 = 361 kips

Unbalanced horizontal force = (378 + 31) – 361 = 48 kips

Per pile, horizontal force = 48/27 = 1.78 kips, or for 125 percent stress 1.78/1.25 = 1.42 kips, OK.

Summary and conclusions. The foregoing analysis shows that a basic problem in designing pile bents supporting deep plate-girder superstructures is how to balance the lateral earth pressures behind the abutment wall. The earth pressure of 35 lb equivalent fluid should be the minimum to be used, and is warranted if clean sand is used as backfill and the bent is allowed to move to mobilize the active state. For this example, the movement is 15 × 0.004 × 12 = 0.72 inch, say 3/4 inch.

Because the capacity of batter piles to resist horizontal loads depends on the presence of dead weight (sustained load), the superstructure should be constructed before lateral earth forces are applied behind the abutment. A suggested construction procedure for embankment cones on bridge approaches provides for an active wedge behind the abutment to be left unfilled until the superstructure is in place. Beginning at the back of the abutment at the berm level, the embankment is sloped at 2:1, thus creating a triangular wedge to be filled and compacted by the bridge contractor. With heavy static or dynamic compaction used to minimize settlement, the increase in the lateral earth forces should be considered. Passive resistance in the berm in front of the bent should be ignored. If a predetermined abutment movement is to be induced, it may be superimposed on the requirements of the expansion device.

7.11 DESIGN EXAMPLE 7–2, FULL ABUTMENT

Figure 7–24 shows a full abutment cross section supporting a bridge across a waterway. The abutment has spread footing on sandy gravel with index properties as shown. The value of K = 0.40 approaches the at rest condition, and the ultimate bearing capacity of the foundation soil is estimated as 30.0 kips/ft^2. The friction angle δ between the footing and the soil has been determined to be 29°. The stability of the abutment will be checked using ASD and load factor (strength design) method.

The passive pressure in front of the abutment is neglected. A live load surcharge of 2 feet is placed on the backfill, and the weight of the approach slab is also a surcharge load. If the approach slab is supported on the abutment wall at one end and spans across the backfill, both surcharges should be omitted and the live load applied on the backwall as in Design Example 7.1. An equivalent fluid pressure is obtained as 0.40 × 120 = 48, use 50 lb/ft.

For conformity, we will use AASHTO designation of loads and load factors (AASHTO Table 3–22.1A), with the general group N expressed by AASHTO Equation (3–10). The application of these loads is shown in Figure 7–25. Note that this abutment provides the expansion bearing in a simple bridge span, with the other abutment fixed.

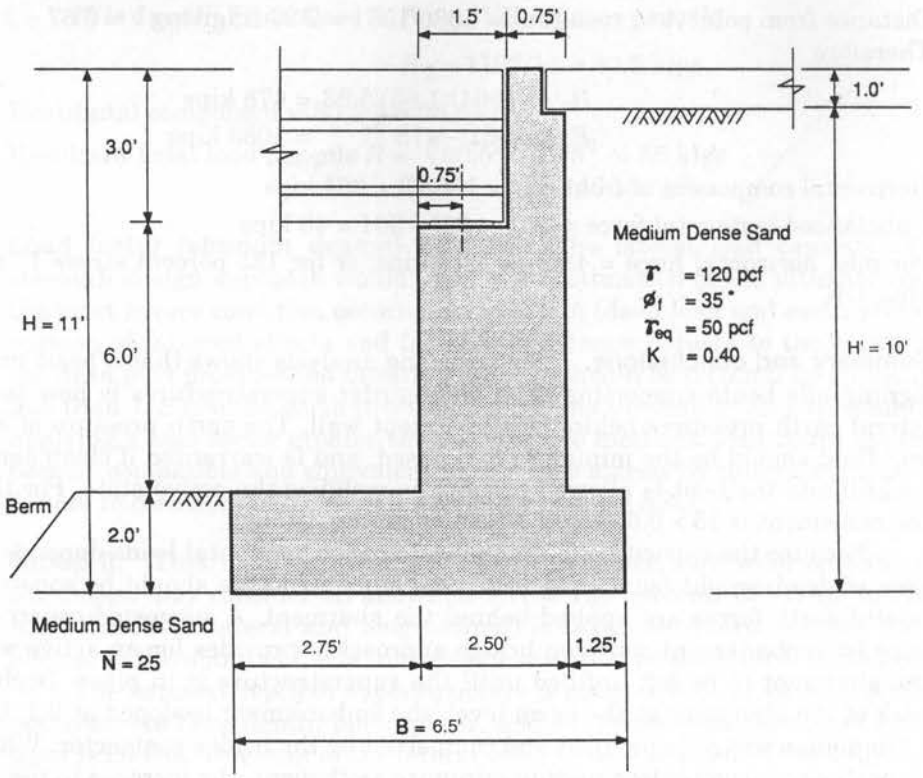

where $\overline{N}$ = average standard penetration test blow count
γ = unit weight of soil
ϕ_f = internal friction angle
γ_{eq} = equivalent fluid pressure
K = horizontal earth pressure coefficient

Figure 7–24 Bridge abutment of Design Example 7–2; configuration and dimensions.

The design philosophy is to apply one-half of the longitudinal forces acting on the bridge to the expansion bearing, provided that this force does not exceed the frictional resistance of the bearing, estimated as 10 percent of the dead load. Alternatively, many designers will also check the fixed abutment using 100 percent of the longitudinal forces assuming that the expansion bearings may become frictionless at some point during the service life of the bridge. Under these assumptions, loads and forces are computed as follows (reference to Figure 7–25).

- Dead load DL = 7.50 kips/ft (dead load from superstructure)
- Live load LL = 6.50 kips/ft (live load from superstructure)
- Wind W = 0.25 kips/ft (wind load on structure)
- WL = 0.05 kips/ft (wind load on live load)
- LF = 0.25 kips/ft (braking force)

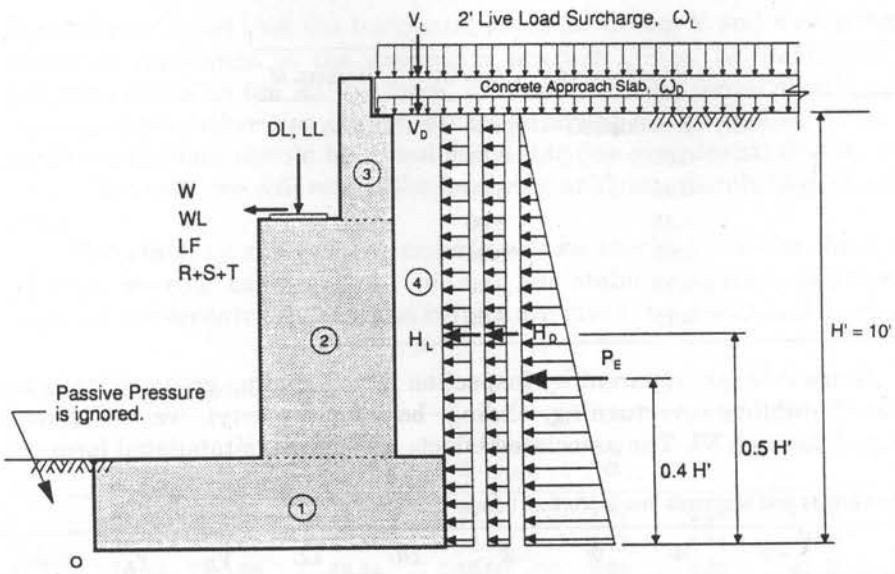

Figure 7–25 Abutment of Design Example 7–2; loads and forces.

- $R+S+T$ = 10% of DL (mainly shrinkage and temperature forces)
- Surcharge LL $W_L = (2)(120) = 0.24$ kips/ft^2

$W_D = (1)(150) = 0.15$ kips/ft^2

$P_E = (\frac{1}{2})(50)(10) = 2.50$ kips/ft

$H_L = (0.40)(0.24)(10) = 0.96$ kips/ft

$H_D = (0.40)(0.15)(10) = 0.60$ kips/ft

$V_L = (0.24)(1.25) = 0.30$ kips/ft

$V_D = (0.15)(1.25) = 0.19$ kips/ft

ASD method. For ASD analysis, the foregoing unfactored loads are used to compute moments about point 0. These effects are shown in a tabulated form as follows (see also Figure 7–25)

Vertical Loads

Item	V (unfactored)	Arm (ft)	Moment M_o
① (6.5)(2.0)(0.15)	1.95 (kips/ft)	3.25	6.34
② (6.0)(2.50)(0.15)	2.25	4.00	9.00
③ (0.75)(3.0)(0.15)	0.34	4.88	1.66
④ (1.25)(8.0)(0.12)	1.20	5.88	7.06
DL	7.50	3.50	26.25
LL	6.50	3.50	22.75
V_D	0.19	5.88	1.12
V_L	0.30	5.88	1.76

Horizontal Loads

Item	H (unfactored)	Arm (ft)	Moment M_o
P_E	2.50 (kips/ft)	4.00	10.00
H_D	0.60	5.00	3.00
H_L	0.96	5.00	4.80
W	0.25	8.00	2.00
WL	0.05	8.00	0.40
LF	0.25	8.00	2.00
$R+S+T$	0.75	8.00	6.00

Since it is not apparent by inspection which loading group controls the various aspects of stability (overturning, sliding, bearing capacity), we will consider AASHTO groups I through VI. The associated effects are shown in tabulated form.

Vertical Loads and Moments due to Vertical Loads

Item	①	②	③	④	DL	LL	V_D	V_L	Sum	%	Sum%
V (unfact.)	1.95	2.25	0.34	1.20	7.50	6.50	0.19	0.30			
I	1.95	2.25	0.34	1.20	7.50	6.50	0.19	0	19.93	100	19.93
II	1.95	2.25	0.34	1.20	7.50	0	0.19	0	13.43	125	10.74
III	1.95	2.25	0.34	1.20	7.50	6.50	0.19	0	19.93	125	15.94
IV	1.95	2.25	0.34	1.20	7.50	6.50	0.19	0	19.93	125	15.94
V	1.95	2.25	0.34	1.20	7.50	0	0.19	0	13.43	140	9.59
VI	1.95	2.25	0.34	1.20	7.50	6.50	0.19	0	19.93	140	14.24
M_v (unfact.)	6.34	9.00	1.66	7.06	26.25	22.75	1.12	1.76	Sum	%	Sum%
I	6.34	9.00	1.66	7.06	26.25	22.75	1.12	0	74.18	100	74.18
II	6.34	9.00	1.66	7.06	16.25	0	1.12	0	51.43	125	41.14
III	6.34	9.00	1.66	7.06	26.25	22.75	1.12	0	74.18	125	59.34
IV	6.34	9.00	1.66	7.06	26.25	22.75	1.12	0	74.18	125	59.34
V	6.34	9.00	1.66	7.06	26.25	0	1.12	0	51.43	140	36.74
VI	6.34	9.00	1.66	7.06	26.25	22.75	1.12	0	74.18	140	52.99

Horizontal Forces and Moments due to Horizontal Loads

Item	P_E	H_D	H_L	W	WL	LF	$R+S+T$	Sum	%	Sum%
H (unfact.)	2.50	0.60	0.96	0.25	0.05	0.25	0.75			
I	2.50	0.60	0	0	0			3.10	100	3.10
II	2.50	0.60	0	0.25	0			3.35	125	2.68
III	2.50	0.60	0	0.075	0.05	0.25	0	3.47	125	2.78
IV	2.50	0.60	0	0	0	0	0.75	3.85	125	3.08
V	2.50	0.60	0	0.25	0	0	0.75	4.10	140	2.93
VI	2.50	0.60	0	0.07	0.05	0.25	0.75	4.22	140	3.01
M_H (unfact.)	10.00	3.00	4.80	2.00	0.40	2.00	6.00	Sum	%	Sum%
I	10.00	3.00	0	0	0	0	0	13.00	100	13.00
II	10.00	3.00	0	2.00	0	0	0	15.00	125	12.00
III	10.00	3.00	0	0.60	0.40	2.00	0	16.00	125	12.80
IV	10.00	3.00	0	0	0	0	6.00	19.00	125	15.20
V	10.00	3.00	0	2.00	0	0	6.00	21.00	140	15.00
VI	10.00	3.00	0	0.60	0.40	2.00	6.00	22.00	140	15.71

It should be noted that the horizontal loads for Group V and VI should not exceed the frictional resistance of the expansion bearing. Since, by definition, this resistance has been taken as the R+S+T force, wind and braking forces should not be included in these groups. Otherwise stated, all longitudinal forces applied to an expansion substructure element should be consolidated into one component, that is, a frictional resistance. However, we will retain the foregoing analysis, merely to demonstrate the design steps.

The stability and bearing criteria will be checked now for three conditions: overturning, bearing capacity, and sliding. For stability against overturning, a check is made on the eccentricity, and the results are given in a tabulated form.

Eccentricity Check (Overturning)

Item	V (kips)	H (kips)	M_V (ft-kips)	M_H (ft-kips)	x_o ft	e ft	e_{max}	q_t (ksf)	$q_{(unit)}$ (ksf)
I	19.93	3.10	74.18	13.00	3.07	0.18	<1.08	3.58	3.24
II	10.74	2.68	41.14	12.00	2.71	0.54	<1.08	2.47	1.98
III	15.94	2.78	59.34	12.80	2.92	0.33	<1.08	3.20	2.73
IV	15.94	3.08	59.34	15.20	2.78	0.47	<1.08	3.51	2.87
V	9.59	2.93	36.74	15.00	2.27	0.98	<1.08	2.81	2.11
VI	14.24	3.01	52.99	15.71	2.62	0.63	<1.08	3.46	2.72

where x_o = location of resultant from point 0 = $(M_V - M_H)/V$
e = eccentricity of resultant = $(B/2) - x_o$
e_{max} = B/6 = 6.5/6.00 = 1.08 ft
q_t = trapezoidal bearing pressure at toe (see Figure 6–32a), kips/ft^2
q_{unit} = uniformly distributed bearing pressure at toe (see Figure 6–32c), kips/ft^2

Bearing Capacity Assessment

Item	V	H	H/V	D_f/B_e	R_1	q^v_{ult}	q^i_{ult}	q^i_{ult}/FS	q_{max}
I	19.83	3.10	0.16	0.33	0.58	30.00	17.40	4.35	>3.24
II	10.74	2.68	0.25	0.37	0.43	30.00	12.90	3.22	>1.98
III	15.94	2.78	0.17	0.34	0.59	30.00	17.70	4.42	>2.73
IV	15.94	3.08	0.19	0.36	0.53	30.00	15.90	3.97	>2.87
V	9.59	2.93	0.31	0.44	0.37	30.00	11.10	2.77	>2.11
VI	14.24	3.01	0.21	0.38	0.52	30.00	15.60	3.90	>2.72

where D_f = depth from ground surface to bottom of footing = 2.0 ft
B_e = effective base width = $2x_o$
R_1 = reduction factor due to inclined load
q^v_{ult} = vertical (ultimate) bearing capacity (kips/ft^2)
q^i_{ult} = inclined ultimate bearing capacity = $R_1\, q^v_{ult}$ (kips/ft^2)
FS = factor of safety for SPT method = 4.0
q_{max} = maximum bearing pressure = q_{unif}
(Note: the reduction factor R_1 for inclined loading is discussed in detail in chapter 8).

Resistance to sliding. Since the pressures are assumed to be uniformly distributed (Figure 6–32 c), the effective base width B_e for calculating resistance to sliding will be taken as $2x_o$. The results of the analysis are tabulated as follows:

Item	V (kips)	tanδ	F_r (kips)	FS	F_r/FS	H
I	19.83	0.554	10.99	1.5	7.33	> 3.10
II	10.74	0.554	5.95	1.5	3.97	> 2.68
III	15.94	0.554	8.83	1.5	5.55	> 2.78
IV	15.94	0.554	8.83	1.5	5.55	> 3.08
V	9.59	0.554	5.31	1.5	3.54	> 2.93
VI	14.24	0.554	7.89	1.5	5.26	> 3.01

where $F_r = V\tan\delta$

Summary. For ASD analysis, Group V gives most severe results with respect to eccentricity criteria. Group I results in the largest bearing pressure. Groups I and IV give about the least (almost the same) margin of safety in the bearing capacity pressure. These conclusions, however, cannot be generalized.

Strength design method. For this analysis, we will consider Groups I, II, and IV. The load factors γ and load coefficients β_i will be taken from AASHTO Table 3.22.1A, so that for each load type the two parameters are lumped into a single load factor $\gamma\beta_i$. This factor is as follows: DL = 1.3; LL = 2.17; E_v = 1.3; E_h = 1.69; E_{hd} = 1.69; E_{hL} = 2.17; W = 1.3; WL = 1.3; LF = 1.3 or 1.25; and R+S+T = 1.30 or 1.25. Using these factors we tabulate factored loads and moments due to factored loads.

Factored Vertical Loads V

Item	① D	② D	③ D	④	DL D	LL L	V_D D	V_L L	V_u Total
(unf.)	1.95	2.25	0.34	1.20	7.50	6.50	0.19	0	19.93
I	2.54	2.93	0.44	1.56	9.75	14.11	0.24	0	31.57
II	2.54	2.93	0.44	1.56	9.75	0	0.24	0	17.46
IV	2.54	2.93	0.44	1.56	9.75	8.45	0.24	0	25.91

Factored Moments M_v

Item	① D	② D	③ D	④ Ev	DL D	LL L	V_D D	V_L L	$M\mu_u$
M_v (unf.)	6.34	9.00	1.66	7.06	26.25	22.75	1.12	0	Total
I	8.24	11.70	2.16	9.18	34.13	49.37	1.46	0	116.24
II	8.24	11.70	2.16	9.18	34.13	0	1.46	0	66.87
IV	8.24	11.70	2.16	9.18	34.13	29.58	1.46	0	96.45

Horizontal Forces H

Item	P_E E_h	H_D E_{hD}	H_L E_{hL}	W	WL	LF	$R+S+T$	H_u
H(unf.)	2.50	0.60	0.96	0.25	0.05	0.25	0.75	Total
I	4.23	1.01	0	0	0	0	0	5.24
II	4.23	1.01	0	0.33	0	0	0	5.57
IV	4.23	1.01	0	0	0	0	0.98	6.22

Factored Moments due to Horizontal Forces, M_H

Item	P_E E_h	H_D E_{hD}	H_L E_{hL}	W	WL	LF	$R+S+T$	M_{Hu}
M (unf.)	10.00	3.00	4.80	2.00	0.40	2.00	6.00	Total
I	16.90	5.07	0	0	0	0	0	21.97
II	16.90	5.07	0	2.60	0	0	0	24.57
IV	16.90	5.07	0	0	0	0	7.80	29.77

Stability Against Overturning (Eccentricity Check)

Item	V_u (kips)	H_u (kips)	M_{Vu} (ft-kips)	M_{hL} (ft-kips)	x_o ft	e ft	e_{max} ft	q_t (ksf)	$q_{(unif)}$ (ksf)
I	31.57	5.24	116.24	21.97	2.99	0.26	<1.62	6.03	5.37
II	17.46	5.57	66.87	24.57	2.42	0.83	<1.62	4.75	3.61
III	25.91	6.22	96.45	29.77	2.60	0.65	<1.62	6.32	4.93

where x_o = location of resultant (distance from 0) = $(M_{vu} - M_{HL})/V_u$
e = eccentricity = $B/2 - x_o$
e_{max} = $B/4$ = 6.50/4 = 1.62 ft
$q_{(unif)}$ = uniformly distributed bearing pressure at toe (Figure 6–32c)
q_t = triangular or trapezoidal bearing pressure at toe (Figure 6–32)

(In this case, the resultant is in the middle third, and hence the trapezoidal diagram applies).

Bearing Capacity Check

Item	R_1	q^u_{ult} (ksf)	q^i_{ult} (ksf)	ϕq^i_{ult} (ksf)	q_{max} (ksf)
I	0.58	30.0	17.40	7.83	> 5.37
II	0.48	30.0	14.40	6.48	> 3.61
IV	0.53	30.0	15.90	7.16	> 4.93

where R_1 = reduction factor (the same as in ASD)
B_e = $2x_o$
q^i_{ult} = inclined bearing capacity = $R_1 q^v_{ult}$
ϕq^i_{ult} = factored bearing capacity
ϕ = performance factor = 0.45
q_{max} = maximum bearing pressure = q_{unif}

Resistance to Sliding. Since the uniformly distributed pressures are used, the effective width for calculating resistance to sliding is taken as $2x_o$, as in ASD analysis.

Item	V_u(kips)	tanδ	F_{ru}(kips)	ϕ_s	$\phi_s F_{ru}$	H_u
I	31.57	0.554	17.49	0.80	13.99	> 5.24
II	17.46	0.554	9.67	0.80	7.74	> 5.57
IV	25.91	0.554	14.18	0.80	11.34	> 6.22

where $F_{ru} = V_u \tan\delta$; and ϕ_s = sliding performance factor for SPT data.

Serviceability limit state criteria. Procedures for estimating the settlement of abutments under service conditions are discussed in subsequent sections. Tolerable movement criteria are discussed in section 8.9. The minimum average SPT blow count N within the range of depth from the footing base to depth B below that level is taken as 25.

Calculation of Settlement. For Group I (producing the largest bearing pressures), the effective base width is $B_e = 2x_o = 2 \times 3.07 = 6.14$ ft, and the uniform pressure is 3.24 kips/ft^2.

According to the Terzaghi and Peck (1967) method, reference is made to Figure 8–12 giving bearing pressures for one-inch of settlement of footings in sand. Using N = 25 and B_e = 6.14 ft, the bearing pressure corresponding to 1-inch settlement is interpolated from the graphs as 2.7 tons/ft^2 = 5.4 kips/ft^2. If the water table below the abutment foundation is assumed at least $2B$ precluding any effects on the bearing capacity, the calculated settlement of the footing is

$$\Delta = 3.24 / 5.40 = 0.60 \text{ inch}$$

From Table 5–9, the adjusted settlement using 90 percent reliability is

$$\Delta' = (1.05)(0.60) = 0.63 \text{ inch}$$

This settlement satisfies the tolerable movement criteria discussed in section 8.9.

Design of footing, ASD method. Since this is a conventional reinforced concrete substructure, the specified concrete strength is 3000 lb/in^2, and the reinforcing steel is Grade 40. Hence, f_c = (0.40)(3000) = 1200 lb/in^2, and f_s = 20,000 lb/in^2. The maximum bending moment for the toe section of the footing is taken at the face of the abutment wall, and is computed for a maximum uniform bearing pressure for Group I, q_{unif} = 3.24 kips/ft^2. Thus M = (3.24 − 0.30)(2.75)^2/2 = 11.11 ft-kips. Using n = 9, compute k = 1/(1+20/9 × 1.2) = 0.35, j = 1 − k/3 = 0.88, and a = (20,000)(0.88)/12,000 = 1.46.

For a 3-inch cover, d = 20.5 in, and

$$A_s = \frac{11.11}{(1.46)(20.5)} = 0.37 \text{ in}^2/\text{ft}, \text{Use } \#5@10 \text{ in} = 0.37 \text{ in}^2/\text{ft}$$

For maximum shear, we will take the critical section also at the wall face. Shear V = (2.94)(2.75) = 8.08 kips

$$v = (8.08) / 20.5x12) = 32 \text{ lb/in}^2 < 0.9\sqrt{f_c'} = 49 \text{ lb/in}^2$$

7.12 DESIGN EXAMPLE 7–3, SPILL-THROUGH ABUTMENT

Spill-through abutments may be selected where shallow foundations are feasible and economical. As shown in Figure 1–7, they have three main components: the footing, tapered columns, and the bridge seat. A spill-through abutment for this design example is shown in Figure 7–26 that includes a partial longitudinal elevation (transverse section) and the abutment seat. The configuration of this structure accommodates a two-lane

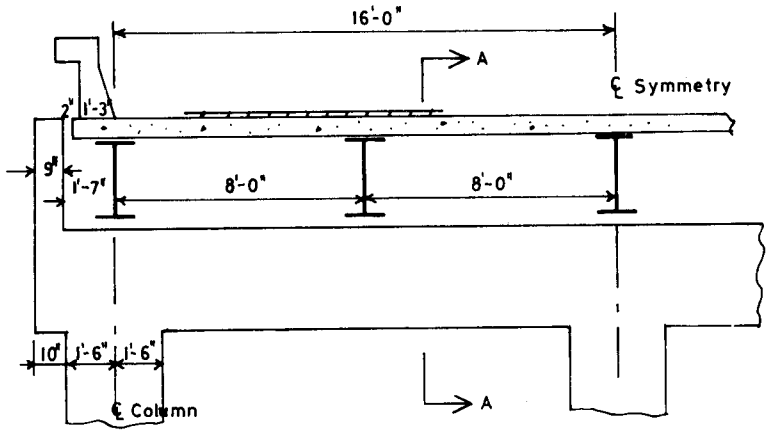

(a) Transverse section

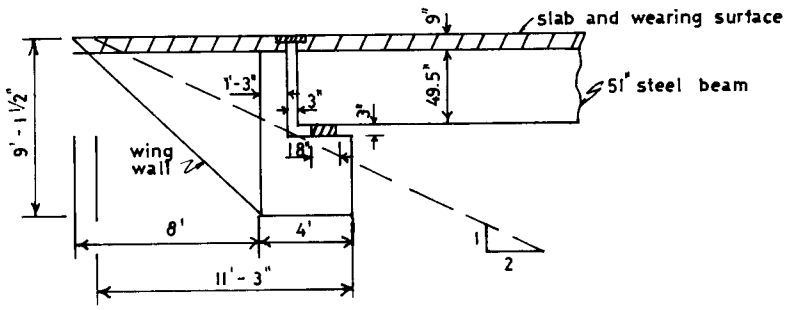

(b) Section A-A

Figure 7–26 Spill-through abutment; (a) partial longitudinal elevation; (b) abutment cross section A-A.

bridge deck supported on steel beams. The bridge has two simple equal spans, each 85 feet long. Three columns are used to support the beam seat and transfer the loads to the common footing. Three of the steel beams are set directly on the columns, and the other two between columns producing bending moments in the bridge seat.

Loads and Forces.

The abutment receives loads from the superstructure as well as loads and forces applied directly to it.

Dead load from superstructure. These are as follows:

Interior Beams	R_{DL} = 46.8 kips/beam
Exterior Beams	R_{DL} = 50.2 kips/beam

Live load from superstructure. For maximum moment in the beam seat the live load (HS 20) is placed as shown in Figure 7–27, centered over the interior beams. However, the trucks can be placed in different positions across the roadway to give maximum load effects on the abutment elements. For maximum live load reaction, one rear axle is placed directly over the bearing line, giving a reaction

$$P = 16(1 + 71/85) + 4(57/85) = 32.1 \text{ kips (conservative).}$$

Dead load, weight of abutment. An end view of the abutment is shown in Figure 7–28. The dead load is computed as follows:

Beam Seat	= 2.4 kips/ft
Back Wall	= 0.82 kips/ft
Wing Wall (each)	= 10.2 kips
Column (each)	= 21.6 kips
Footing	= 40.5 kips (each)

Longitudinal forces. These are taken as 5 percent of two lanes of live load, or F_L = $2(0.64 \times 85 + 18)(0.05) = 7.3$ kips, say 8 kips.

Friction. This is mobilized by temperature expansion and contraction. The abutment has teflon sliding bearings with a coefficient of friction taken as 0.06. Since the longitudinal forces due to expansion oppose each other at the fixed pier, they are transferred through the beams to the abutment bearings. Total friction

$$F_f = (46.8 \times 3 + 50.2 \times 2)(0.06) = 14.5 \text{ kips.}$$

Earth pressures. For a spill-through abutment pressures act on the beam seat and behind the columns, but they are partially offset by the earth pressure in front of the abutment. For simplicity, the earth pressure is assumed as 35-lb equivalent fluid, and since there is an approach slab a live load surcharge is not considered. The lateral pressure diagram is shown in Figure 7–29.

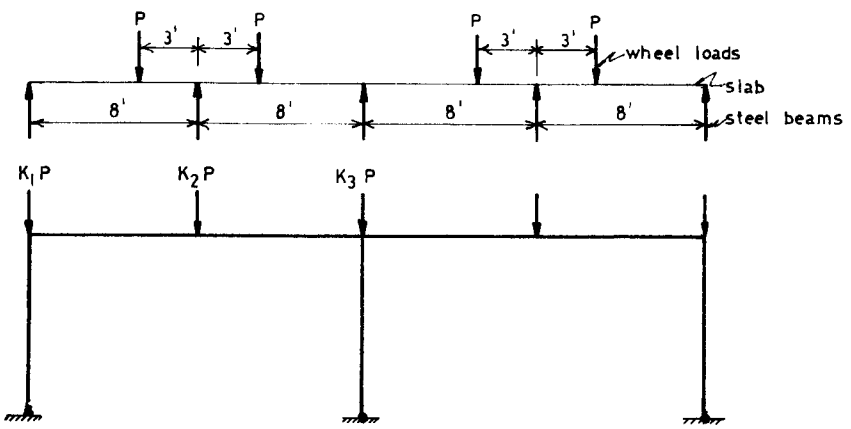

Figure 7–27 Live load arrangement, abutment of Figure 7–26.

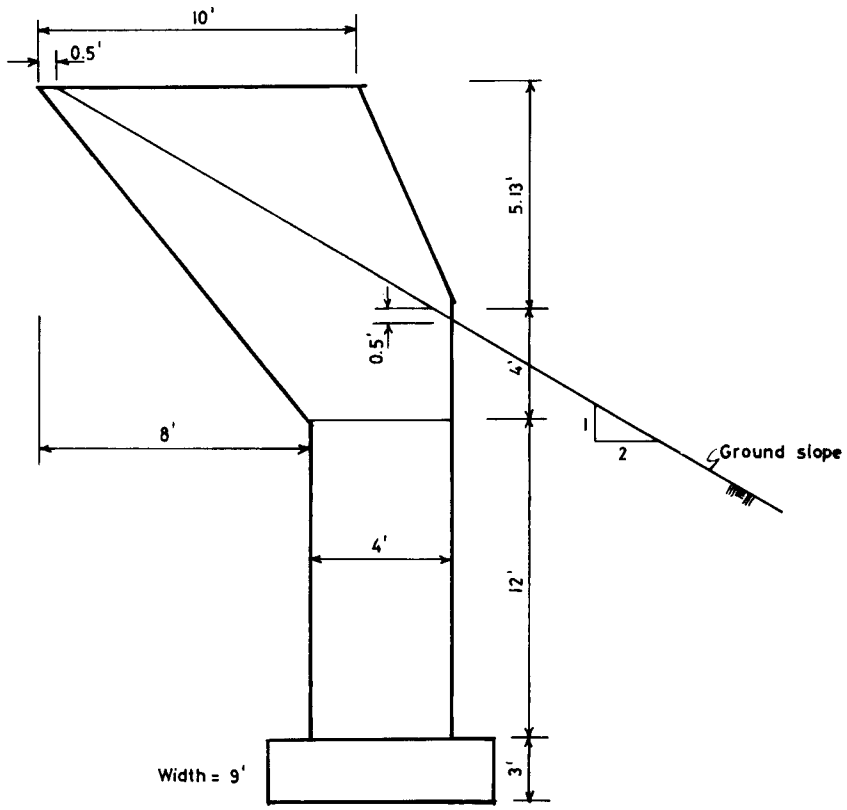

Figure 7–28 End view, abutment of Figure 7–26.

Base Stability

The abutment must be stable against sliding and overturning. The total dead load (superstructure plus abutment) and the lateral earth pressures are tabulated in Table 7–1. Also shown in this table are the longitudinal and transverse forces.

The longitudinal force 84.8 kips must be resisted by friction at the footing-soil interface. The coefficient of friction tan δ varies widely in the range 0.25 – 0.55 (in design example 2, tan δ = 0.55). For this example, we will use tan δ = 0.35. Then the factor of safety against sliding is

$$FS = \frac{(0.35)(560.7)}{84.8} = 2.3 > 1.5$$

The factor of safety against overturning is

$$FS = 2776/1149 = 2.4 > 2 \text{ (AASHTO Article 5.5.5)}$$

Footing and Bearing Pressure

The longitudinal overturning moment about the three footings is the total overturning moment given in Table 7–1 adjusted by the moment caused by the weight of the wing wall and back wall, and the heavy reactions. The resulting moment is

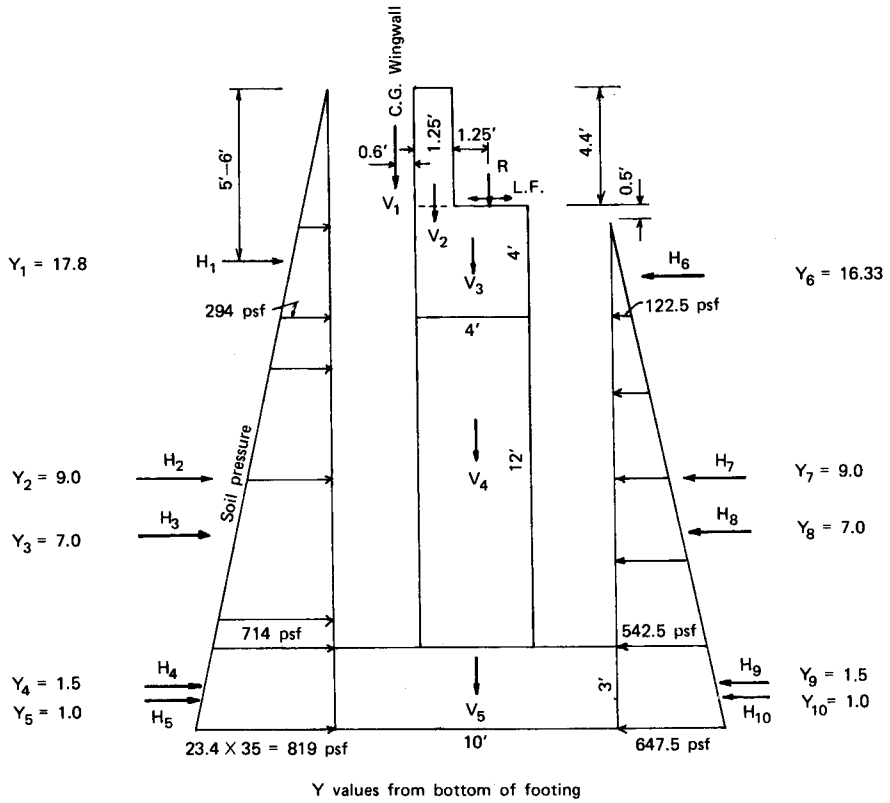

Figure 7–29 Loads on forces acting on abutment, example of Figure 7–26.

$$M_L = -1149 - 20.4(2.6) - 28.8(1.37) + 241(0.5) = 1175 \text{ ft-kips}$$

The overturning moment for one footing is, therefore

$$M_L = 1175/3 = 392 \text{ ft-kips}$$

Referring to Figure 7–27, the reactions at each column are calculated for $P = 32.1$ kips treating the beam seat as a continuous beam on rigid supports. The coefficients k_1, k_2 and k_3 are calculated as follows:

$$k_1 = 0.24 \qquad k_2 = 1.50 \qquad k_3 = 0.52$$

giving $k_1P = 7.8$ kips, $k_2P = 48.8$ kips, and $k_3P = 16.9$ kips.

The vertical loads and transverse moments on footings caused by frame action are obtained from frame analysis and are as follows:

Outside Columns =	$P = 200.3$ kips	$M_T = 40$ ft-kips
Inside Columns =	$P = 290.0$ kips	$M_T = 0$

The soil pressure is calculated from the relationship

$$p = \frac{p}{A} \pm \frac{M_L}{S_L} \pm \frac{M_T}{S_T}$$

Table 7–1 Vertical Loads, Lateral Forces, and Moments about Toe of Footing, Design Example of Figure 7–26

Type of Force	Magnitude	(k)	Arm (ft)	Moment (ft-k)
H_1: back soil pressure	$\frac{0.294}{2}(36.67)(8.4)$	45.3	17.8	+ 806
H_2: back soil pressure	0.294(3×3)(12)	31.8	9.0	+ 286
H_3: back soil pressure	$(0.714–0.294)(\frac{9}{2})(12)$	22.7	7.0	+ 159
H_4: back soil pressure	0.714(3)(3 × 9)	57.8	1.5	+ 87
H_5: back soil pressure	$(0.819–0.714)(\frac{3}{2})(27)$	4.3	1.0	+ 4
H_6: front soil pressure	$0.1225\left(\frac{3.5}{2}\right)(36.67)$	– 7.9	16.33	– 128
H_7: front soil pressure	0.1225(3 × 3)(12)	– 13.2	9.0	– 119
H_8: front soil pressure	$(0.5425–0.1225)(\frac{9}{2})(12)$	– 22.7	7.0	– 159
H_9: front soil pressure	0.5425(3)(3 × 9)	– 43.9	1.5	– 66
H_{10}: front soil pressure	$(0.6475–0.5425)(\frac{3}{2})(27)$	– 4.2	1.0	– 4
Longitudinal force		+ 14.9	19.0	+ 283
Total longitudinal force		84.8		
Total overturning moment				1149
V_1: weight of wing-walls	2(10.2)	– 20.4	7.6	– 155
V_2: weight of back wall	0.82(35.17)	– 28.8	6.4	– 184
V_3: weight of beam seat	2.4(35.17)	– 84.4	5.0	– 422
V_4: weight of columns	21.6 × 3	– 64.8	5.0	– 324
V_5: weight of footings	40.5 × 3	–121.5	5.0	– 607
R: dead-load reaction	3 × 46.8 + 2 × 50.2	–240.8	4.5	–1084
Total vertical force		–560.7		
Total righting moment				–2776

where the subscripts denote longitudinal and transverse directions. The section properties are calculated as follows

$$A = 9 \times 10 = 90 \text{ ft}^2, \quad S_L = 9 \times 10^2/6 = 150 \text{ ft}^3, \quad S_T = 10 \times 9^2/6 = 135 \text{ ft}^3$$

For outside columns

$$p = \frac{200.3}{90} \pm \frac{392}{150} \pm \frac{40}{135} = 2.22 \pm 2.61 \pm 0.30 = 5.13 \text{ or } -0.69 \text{ kips/ft}^2$$

For inside columns

$$p = \frac{290}{90} \pm \frac{392}{150} = 3.22 \pm 2.61 = 5.83 \text{ or } 0.61 \text{ kips/ft}^2$$

Since there can be no uplift pressure underneath the footing, the outside footings may be reanalyzed ignoring tension, or some soil weight above the footing may be included in the calculations. The maximum soil pressure 5.83 kips/ft^2 is within the allowable.

Whether the longitudinal moment should be resisted equally by three columns and their footings depends mainly on the stiffness of the superstructure and the rigidity of the abutment. For this example, this assumption is valid. Other possible load conditions to be investigated include live load in one lane only. This would increase the lateral bending moment at the bottom of the outside column by about 50 percent, and would induce a lateral moment at the bottom of the inside column close to 20 ft-kips. The total

vertical load on the outside column would be somewhat increased, but the load on the inside column would be slightly decreased. The new soil pressure would change but not enough to warrant a larger footing.

Other Members

The design of the abutment is completed by calculating shears and moments in the beam seat, back wall, columns, and footings, and then estimating the amount of reinforcement to resist moments and shears in each member.

7.13 DESIGN EXAMPLE 7–4, ABUTMENT FOR A SIMPLE SPAN DECK TRUSS BRIDGE

A simple span highway deck truss bridge is 160 feet long and carries a two-lane deck. The design of the superstructure and the two abutments is based on the 1961 AASHTO Specifications and California Bridge Standards.

A typical end and front view of the abutment is shown in Figure 7–30(a) and (b) , respectively. Special abutment features are a high back wall resulting from the superstructure depth, a long wing wall separated from the main abutment by means of an open joint and stepped up as shown, and a low beam seat.

Loads and forces. These are (1) dead load from the superstructure and the weight of abutment; (2) live load; (3) wind on structure and live load, (4) braking (longitudinal) forces; (5) seismic forces; and (6) special loads that may be specified by the supervising authority.

Design considerations. Apparently, the 160-foot long span designed as a truss is in reality too short to be economically desirable. It is used, however, to demonstrate the design principles and effects on the selection and design of the superstructures. A Warren-type truss is selected with eight 20-foot panels, and the trusses are spaced at 19-foot centers. The stringers in the deck are designed to span the 20-foot floor beams, which are placed at each upper panel point. The allowable foundation pressure is 8 kips/ft^2.

Horizontal forces acting normal to the structure do not ordinarily act in the same horizontal plane as the main truss supports, and thus produce a torsion or overturning effect. These forces will be transferred from the point of application to the supports through members that are the most stiff rather than members arbitrarily added or designated for this purpose. Therefore, judgment is needed to determine the method of analysis to be used for each particular case.

One method of dealing with the overturning effect is to make the deck continuous and stiff to carry the transverse forces to the ends, where they are transmitted to the main truss supports by means of end sway bracing. Another method is to make the deck discontinuous (expansion joints at each panel). In this way, the horizontal forces acting on the upper portion of the bridge are transferred to the lower chords by means of the bracing at each panel. In the latter case, relative mass and stiffness of members should be considered in conjunction with the character of forces involved.

Design of abutment wall. Referring to Figure 7–30, the critical section for bending is 21 feet below the top of the wall.

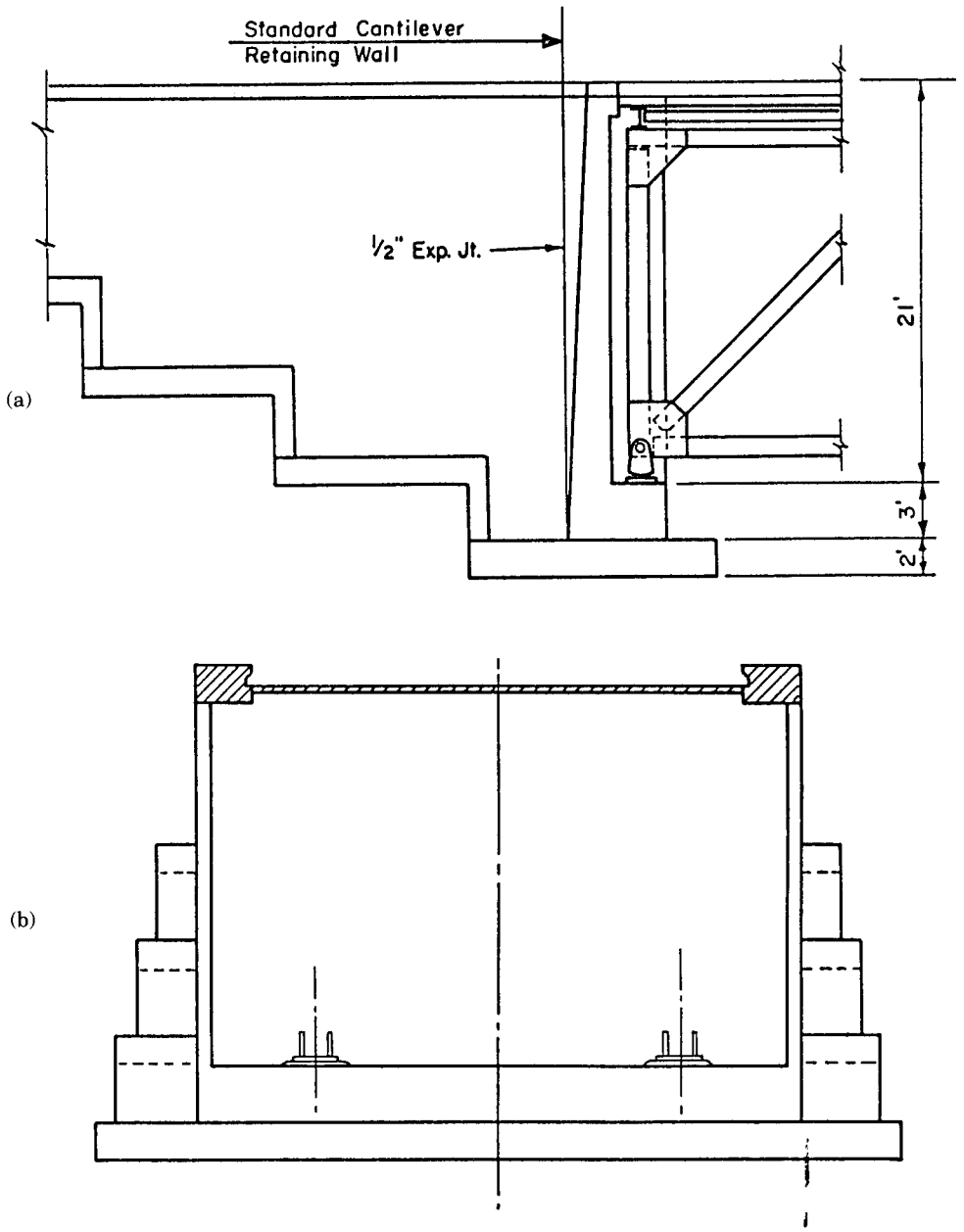

Figure 7–30 End and front view of abutment for truss bridge; Design Example 7–4.

Design stresses are: f_s = 20,000 lb/in^2; f_c = 1200 lb/in^2; and design lateral earth pressure = 36 lb equivalent fluid, plus 2 foot surcharge. Using a wall width at the top 12-inch minimum and a batter 5/8 in/ft, the wall thickness at the bottom is about 25 1/8 inches, giving d = 22.5 inches.

The moment at the base is computed as 71.4 ft-kips, hence

$$A_s = \frac{71.4}{1.46 \times 22.5} = 2.17 \text{ in}^2/\text{ft}, \text{Use } \#11@\ 8\tfrac{1}{2} \text{ in} = 2.20 \text{ in}^2/\text{ft}$$

However, for a complete analysis the moments are calculated at various wall heights and A_s is computed accordingly. The results are shown in Figure 7–31 in graphical form. It can be seen that at about H = 15.5 feet the bar spacing can be doubled, that is, alternate #11 bars are omitted.

Stability analysis and bearing pressure. Because the abutment configuration is not uniform, the analysis will consider loads and forces acting on the entire structure, rather than on a foot length of the abutment. Referring to Figure 7–32, loads are computed in this manner, and moments are calculated about point 0, the back of the footing. The results are tabulated as follows.

Item			Weight	Arm x	M_o
Surcharge	$2 \times 6.25 \times 0.12 \times 32$	=	48	3.12	150
Backfill A	$5 \times 24 \times 0.12 \times 32$	=	460	2.50	1,150
Backfill B	$1/2 \times 1.25 \times 24 \times 0.12 \times 32$	=	58	5.42	310
Stem C	$1/2 \times 1.25 \times 24 \times 0.15 \times 32$	=	72	5.84	420
Stem D	$1 \times 24 \times 0.15 \times 32$	=	115	6.75	780
Truss Seat	$3 \times 3 \times 0.15 \times 32$	=	43	8.75	380
Curtain Walls	$2 \times 21 \times 3 \times 0.15 \times 1$	=	19	8.75	170
Footing	$13 \times 2 \times 0.15 \times 42$	=	164	6.50	1,060
Fill on toe	$3 \times 2.75 \times 0.12 \times 32$	=	32	11.62	370
Fill on ends of Footing	$3 \times 13 \times 0.12 \times 10$	=	47	6.50	300
	$+ 1/2 \times 8.67 \times 13 \times 0.12 \times 10$	=	68	4.33	290
	Total		1,126 kips		5,380 ft-kips

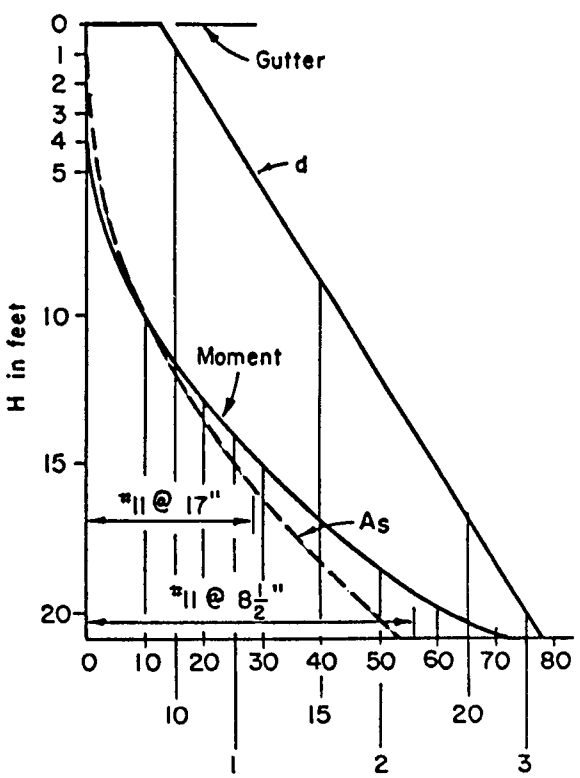

Figure 7–31 Moment and A_s diagram as a function of wall height; abutment of Figure 7–30.

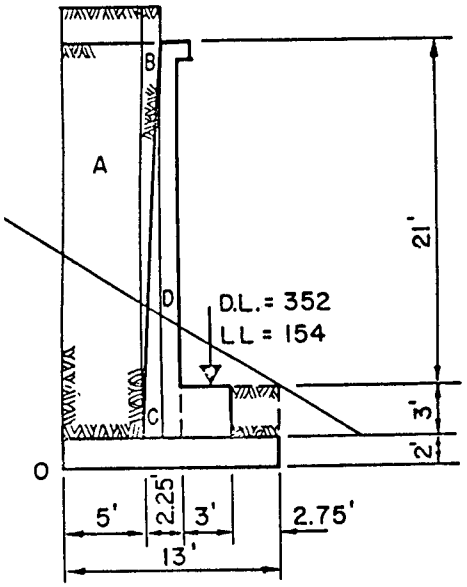

Figure 7–32 Abutment cross section showing dimensions and loads; Design Example of Figure 7–30.

Earth pressure with 2-foot surcharge (36 lb equivalent fluid) = 129.8 ft-kips per foot of abutment wall, or the entire abutment

	$M_{eo} = 129.8 \times 26.75$	= 3,470 ft-kips
DL Superstructure	$= 352 \times 8.75$	= 3,080 ft-kips
LL Superstructure	$= 154 \times 8.75$	= 1,350 ft-kips
Total = Vertical load	$V = 1632$ kips	M_o = 13,280 ft-kips

Distance x of resultant from point 0 = 13280/1632 = 8.13 feet
For a footing 13 feet wide $\times$ 42 feet long, the section properties are

$$A = 13 \times 42 = 546 \text{ ft}, \qquad I = 42 \times 13^3/12 = 7{,}700 \text{ ft}^4$$

Also, eccentricity $e = 8.13 - 6.50 = 1.63$ feet.

The footing pressure is obtained as

$$p = \frac{1632}{546} \pm \frac{1632 \times 1.63 \times 6.5}{7700} = 3.00 \pm 2.25$$

or

$$p_{max} = 5.25 \text{ kips/ft}^2, \; p_{min} = 0.75 \text{ kips/ft}^2$$

For stability against overturning we consider dead loads and earth pressures.

DL moment about point 0 = 5380 + 3080 = 8460 ft-kips
DL reaction = 1126 + 352 = 1478 kips
Distance of resultant from point 0 = 8460/1478 = 5.72 ft, or
distance from toe = 13.00 – 5.72 = 7.28 ft
Balancing moment = 1478 $\times$ 7.28 = 10759 ft-kips,
and stability against overturning = 10759/3470 = 3.10, OK

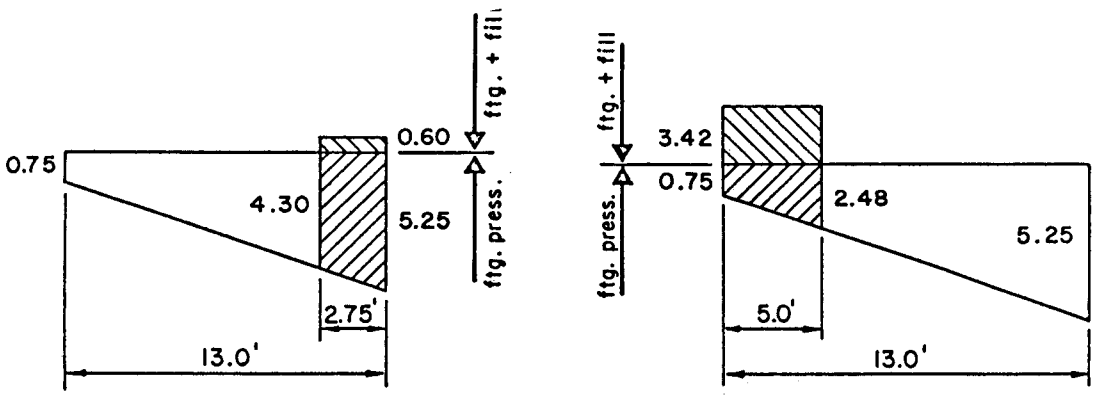

Figure 7–33 Pressure diagram, footing of Design Example 7–4.

For stability against sliding, the total lateral earth pressure is

$$10.66 \times 26.75 = 285 \text{ kips}$$

Using a coefficient of friction tan $\delta = 0.35$, the force resisting sliding is $1478 \times 0.35 = 517$ kips, giving a factor of safety against sliding = 517/285 = 1.8, OK.

Design of footing. For a 2-foot thick footing, $d = 20\frac{1}{2} \times$ inches

Toe design. Footing weight = 0.30 kips/ft
Toe fill = 0.36 kips/ft
Total 0.66 kips/ft

Moment at the face of the seat

$$M = (4.30 - 0.66)(2.75^2)/2 + (5.25 - 4.30)(2.75^2)/3 = 13.7 + 2.4 = 16.1 \text{ ft-kips}$$

$$A_s = \frac{16.1}{1.46 \times 20.5} = 0.54 \text{ in}^2$$

Extending alternate bars from the stem will be OK.

Heel design. Available $d = 21.5$ inches
Footing weight = $2 \times 0.15 = 0.30$
Fill on heel = $26 \times 0.12 = 3.12$
Total = 3.42 kips/ft

Moment at the face of the wall

$$M = (3.42 - 0.75)(5^2)2 - (2.48 - 0.75)(5^2)6 = 33.3 - 7.2 = 26.1 \text{ ft-kips}$$

$$A_s = \frac{26.1}{1.46 \times 21.5} 0.83 \text{ in}^2/\text{ft}, \text{ Use \#7 @ } 8\frac{1}{2} = 0.85 \text{ in}^2/\text{ft}$$

7.14 ABUTMENTS FOR ARCH BRIDGES

Arch bridges are structures shaped and supported in such a manner that intermediate transverse loads are transmitted to the supports primarily by axial compressive thrusts. Thus, the end supports (abutments) must be capable of developing lateral as well as normal reaction components.

An important decision in the design stage is the choice between abutments that are capable of providing the necessary horizontal reaction components and the use of a tied arch where the horizontal thrust is resisted by a tension bowstring (see also section 5.1).

Factors favoring the use of an elastic arch with spandrel columns and strong abutments are, in the sequence of importance: (1) strong foundation materials (such as competent rock) to withstand compression at or near the surface; (2) a high roadway alignment; and (3) site conditions allowing encroachment of the arch rib on the space between abutments. If the site is favorable, this choice is more economical because the ground strength is utilized to replace structural materials.

Typical arch forms. Early arches were of the voussoir or arch block, types. The early voussoir arch bridges consisted of a series of block usually with mortar joints. The individual arch blocks were held in equilibrium under the action of the lateral crown thrust T as shown in Figure 7–34. Once this crown thrust was determined, it could be combined with the various active external forces (dead or live) to form a line of axial pressure as shown. In these cases the abutment or end support was merely the end block of the system, and its function was to transmit the axial thrust and vertical load to the underlying foundation materials.

Modern arch bridges are monolithic or elastic structures. The term "elastic" refers to relevant elastic theories whereby the analysis takes into account the deflection or elastic distortion of the truss members under load. An example of an arch proper for concrete bridges is shown in Figure 7–35. Usually, this consists of a series of independent solid ribs or a single solid barrel. The stress distribution articulates two distinct structural forms: fixed arches and hinged arches, as shown in Figure 7–36. The latter

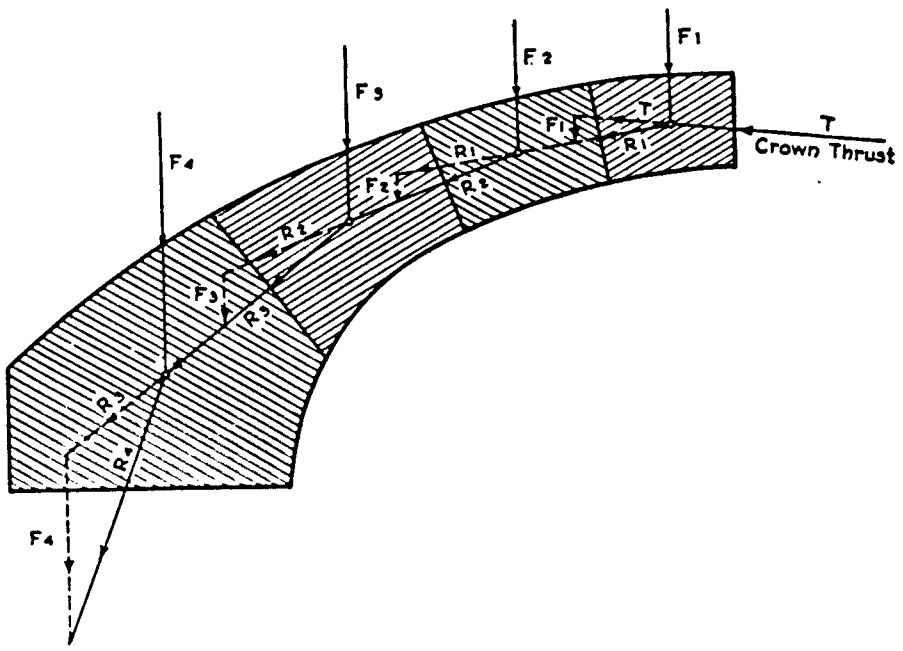

Figure 7–34 Early Arch (Voussoir type).

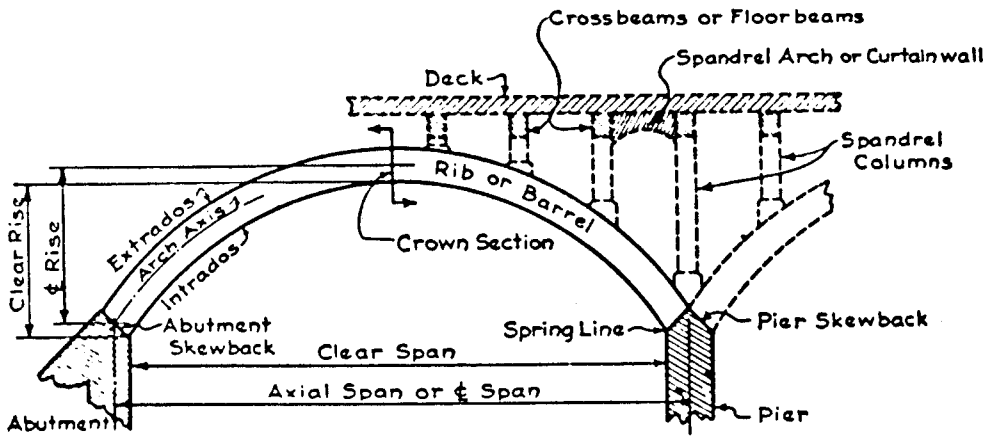

Figure 7–35 Structural arrangement of arch proper.

may be arranged as a single-hinge, two-hinge, or three-hinge type. The hingeless or fixed arch is by far the most common type in concrete bridges, although the other types are also utilized to some extent. For steel construction both fixed and hinged types are common.

The fixed arch, the two-hinged arch, and the single-hinged arch are subjected to stresses because of changes in temperature, differential settlement, or displacement of supports, or because of any compression, shrinkage and long-term creep in the material. The three-hinged arch is a statically determinate structure, hence free from these stresses.

Various configurations of abutments are shown in Figures 7–35 and 7–36. Essentially, these are massive structures shaped to receive the load primarily in com-

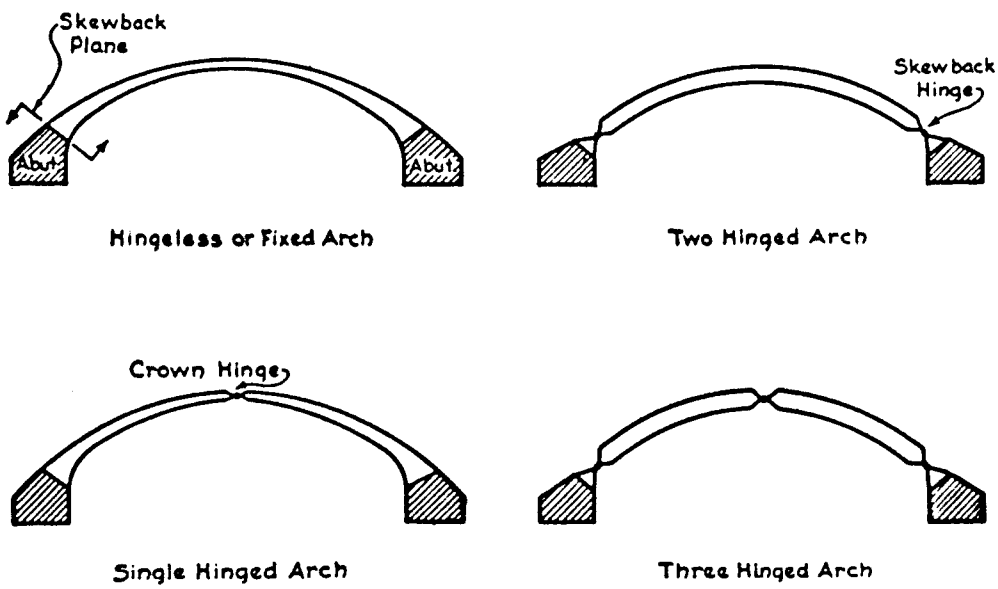

Figure 7–36 Stress distribution in arch proper, fixed and hinged arches.

pression and transfer this load (axial or lateral) to underlying rock or other firm material. Where solid rock is not available, the abutment may be designed and detailed to transfer the loads to piles or other suitable foundation elements. Hence, abutment configurations for arch bridges are not standardized, but are shaped according to the arch form, applied loads, and foundation materials.

Effect of support displacement. If the end supports can be assumed as fixed and unyielding , the end reactions perform zero work, and the first order analysis need not be modified. Where the abutments are expected to yield under load, a portion of the external energy will be used up in displacing them, so that the amount of energy absorbed by the frame will be reduced by the same amount. The effect of support displacement may be evaluated by introducing between the true structure and its supports an "ideal" section whose unit distortion is such as to completely reproduce the effect of the support. This ideal section is assumed in turn to rest on a rigid support, so that the original method of analysis can be carried out. Support movements are thus handled in the context of the analysis, either if they are known in absolute terms or if they are functions of the reactive forces.

For the example shown in Figure 7–37(a), the left abutment is not truly fixed at the skewback section *a-a*, but distorts under load to some position such as section *b-b*.

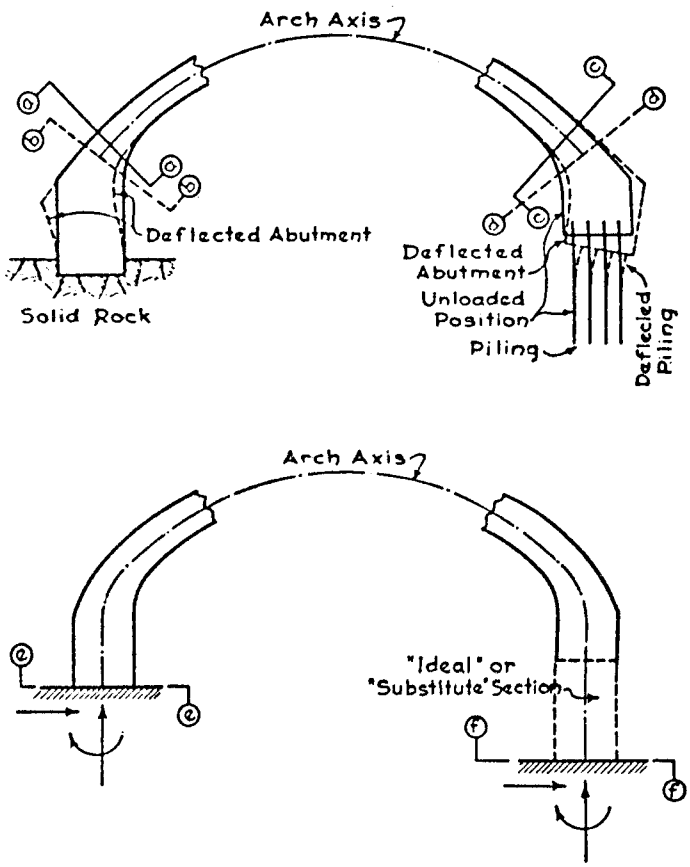

Figure 7–37 Example of yielding supports.

The base of the abutment rests, however, on solid rock so that the analysis can be completed without significant error if we assume the rock extends clear around to the rock base. This means that we consider section *e-e* in Figure 7–37(b) as the skewback section.

For the condition shown at the right support, the solution is not simple. However, if we can estimate the displacement that the pile footing will undergo under load, we may replace this footing by an "ideal" or "substitute" section of the same basic material as the arch rib proper, having dimensions that will make it deflect or distort under load exactly the same amount as the original footing. Figure 7–37(b) shows a condition where this substitution has been made. Thus, the "equivalent" frame has the skewback sections at *e-e* on the left support and *f-f* on the right. This structure may be analyzed as a fixed arch (Xanthakos, 1994).

7.15 ABUTMENTS FOR SUSPENSION BRIDGES

The cables of suspension bridges have a profile that is the reversed shape of an arch, and must resist tension forces. The abutments must therefore carry these forces and transfer them to the ground.

In rare cases it is possible to anchor the cables in natural rock. The shaft or tunnel that is to contain the anchor chain must then be driven to such depth and to reach and penetrate rock that is perfectly sound, proof against weathering, and of sufficient thickness to accommodate the anchorage.

Masonry anchorages and concrete blocks may be embedded below ground level, with backstays connecting them to the nearest towers, or they may constitute the end abutments of the side spans. The latter arrangement generally requires bending or curving the line of the cable or chain from its initial inclination to a more vertical direction in order to secure the necessary depth of anchor plate without excessive length of anchorage. In either scheme, the tensile forces transmitted to the masonry construction or end abutments must be resisted by friction at the base and by resisting pressure of the abutting earth. In addition to stability against sliding, these structures must also be designed for stability against tilting or overturning. The extreme pressures on the base should also be checked to ensure that they do not exceed the allowable stresses on the foundation materials.

Foundations on piles should be avoided where possible because they may give insufficient security against displacement of the anchorage. If such foundations are unavoidable, an ample proportion of bottom piles should be provided.

Special example. An unusual abutment is the foundation anchorage for the Humber suspension bridge in England, currently the longest suspension span in the world. The 36,000 ton (metric) pull from the suspension cables is eventually transferred into a clay formation at the Barton site by an anchorage scheme of composite construction. The initial high stress concentration is dissipated by terminating the steel cables in the upper half of the anchorage block. The lower part of the structure consists of five sections 24.5 meters (80 ft) deep excavated between diaphragm walls, as shown in Figure 7–38. The composite construction is over 70 meters (240 ft) long and has an average width of 40 meters (131 ft).

The main purpose of the composite construction was to penetrate the underlying clay in a controlled manner in order to prevent flooding of the excavation that might soften the clay formation and cause anchorage problems. The possibility of long-term effects was also considered, and the decision was to accelerate the construction program

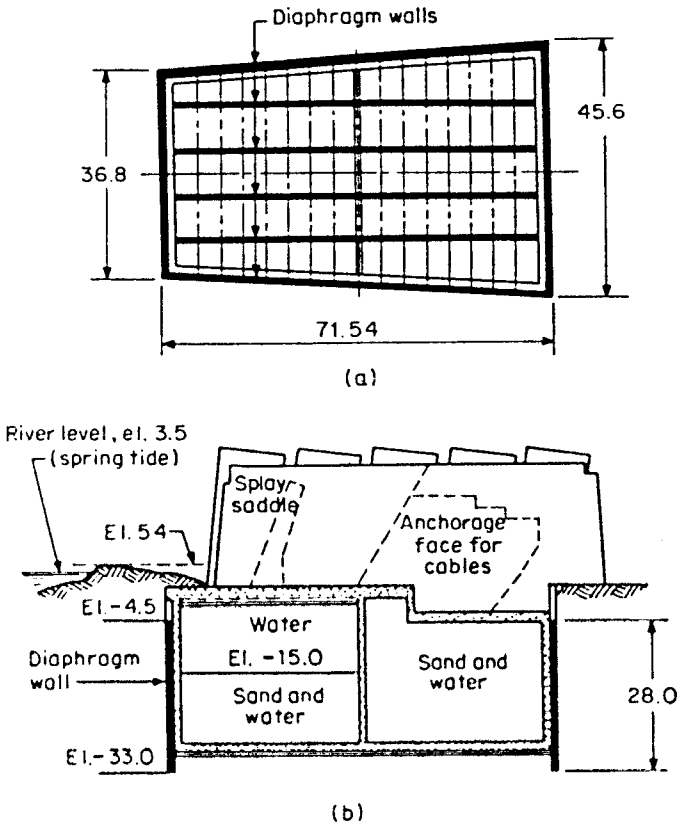

Figure 7–38 Foundation anchorage for the Humber suspension bridge at the Barton site: (a) plan showing diaphragm wall block and anchorage; (b) longitudinal section. All dimensions and elevations in meters.

to avoid these effects. However, simultaneous excavation of two adjoining cells between diaphragm walls was avoided. The bottom concrete in the cells was placed immediately following the removal of the overburden. By reducing the time the excavation was open, it was possible to control swelling and bottom softening that might result in a loss of strength.

The dead weight of the cell structure of the anchorage was increased considerably by pumping sand and water inside. The load from this operation was introduced progressively in order to control and check the response of the foundation.

The horizontal bracing of diaphragm walls across the five sections was provided by precast concrete struts placed in sets of two. This type of bracing on a project of this magnitude may well be regarded as the progenitor of the adaptation of precast members in large underground works.

A partial view of the two massive blocks is shown in Figure 7–39. The prefabricated struts have been left as permanent bracing. Although the entire construction is hardly a derivative of the classical abutment type, it is consistent with general definition of the end supports of the bridge, that is, the massive blocks receive the enormous tensile forces from the superstructure and transmit these forces to the foundation strata.

Vehicle loading. Section 2.3 provided a brief commentary on the rational design of long-span bridges and the associated vehicle loading. In general, the lack of an explicit design code inhibits the design approach, and very often the live load is established by the design consultant. Certain types of long-span bridges may become sensitive to er-

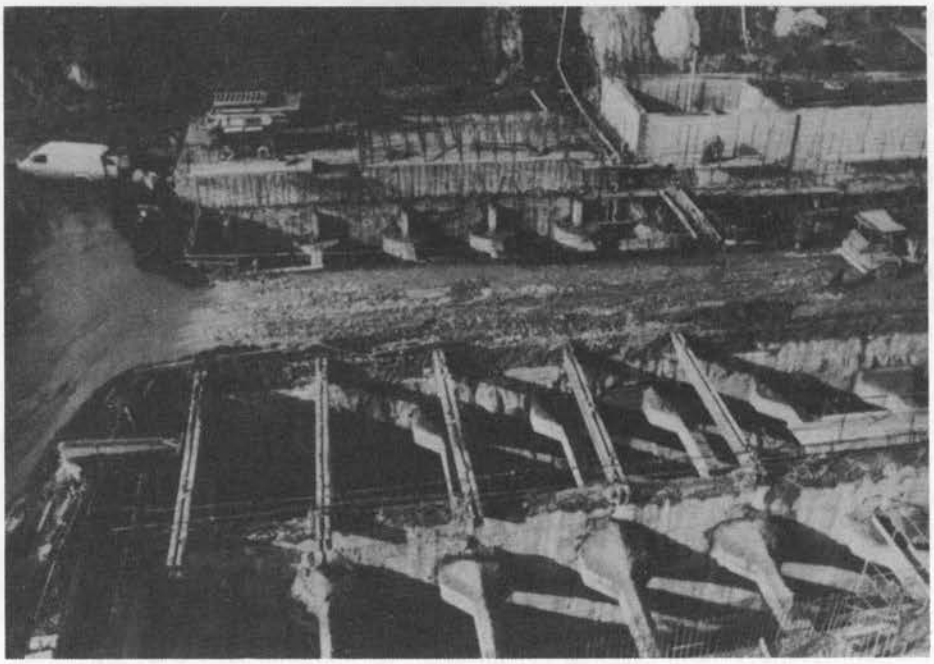

Figure 7–39 Part of the Humber bridge-foundation anchorage showing one of the five cells during excavation. Note the sets of precast-concrete struts *(ICOS)*.

rors or to changes in the live load model and distribution. Cable-stayed and suspension bridges may be considered typical cases that usually would fall outside the range of most codes normally appropriate for a shorter bridge under the same conditions.

Whereas the credible load occurring on a short-span bridge is the heaviest truck or trucks that can travel on the bridge deck, this is not necessarily the case for a long-span bridge, because the structure will not be entirely covered by the heaviest possible vehicles. For example, maximum loading on suspension bridges is known to occur when the traffic is stationary and bumper-to-bumper. When traffic begins to move, vehicle distance increases and load intensity decreases. For the maximum loading, therefore, the traffic is stationary and allowance should not be made for full impact.

Based on the foregoing criteria the ASCE Committee on Loads and Forces for Bridges (1981) provided recommendations for a basic lane load consisting of a uniformly distributed load U, and a single concentrated load P (Xanthakos, 1994). If more than one span is loaded, only one concentrated load P will be used per lane. No allowance is made for impact. As an example, for a loaded length of 6400 feet (1950 m), the concentrated load is 168 kips and the lane load is 400 lb/ft of lane.

The rate of dead to live load becomes quite relevant to the method of analysis. With the working stress method, the ultimate strength state is automatically exceeded when the allowable stress (usually 40 to 50 percent the ultimate strength) is exceeded, and this applies to both the structure and the soil. With strength design (load factor), the required strength is merely the sum of the factored loads. If the dead load D is the predominant load, the resulting required strength is merely $1.3D$. Considering the variability of resistance, engineers may be tempted to use strength design indiscriminately because it will give a more "economical" design, although the level of safety may not correspond to allowable stress design.

7.16 INTEGRAL ABUTMENTS

Fully integrated continuous construction was briefly discussed in section 1.3, and abutment details for integral bridges are shown in Figure 1–11(a) through (c) for three states, namely Illinois, Tennessee, and Ohio.

The routine use of continuous construction in the United States and Canada and the increase in the number of transportation departments that have adopted this design is shown in Figure 7–40. As of 1990, about 87 percent of responding departments used continuous construction with integral abutments for short- and medium-span bridges.

Many bridges built with deck joints at the abutments have been severely damaged because of the growth and pressure generated by jointed rigid pavements. After the deck joints are closed, the bridge deck is squeezed by the generation of pavement pressures that can easily exceed 1000 lb/in^2. Cumulatively, the total force generated by these pressures can reach 650 tons per lane of approach pavement (Burke, 1987). When the design of abutments for nonintegral bridges is finalized, these forces are not accounted for. In longer bridges with intermediate deck joints, piers have been cracked and in some instances fractured.

Stress considerations in integral bridges. The usual response to integral bridges is concern for potentially higher stresses that may develop in longer bridges, since integral construction is essentially equivalent to bridges with deck joints that closed. Although the majority of bridges with integral abutments have performed satisfactorily, many of them have demonstrated high stress levels. For example, an abutment supported on a single row of piles (see also section 1.3) may be considered flexible enough to accommodate longitudinal thermal cycling of the superstructure and dynamic end rotations induced by moving vehicles. However, the piles are routinely subjected to axial and flexural stresses that may approach, equal, or exceed the yield stress (Wolde-Tinsae, Greimann, and Yang, 1982; Jorgenson, 1983). Gamble (1984) has emphasized the effect of restraint stresses and the cracking that has occurred in continuous concrete frame bridges. In some instances, concrete strength below the specified and absence of shear reinforcement contributed to the overstress problem, although the failure of the structure was caused mainly by its stiffness and resistance to shrinkage and contraction of

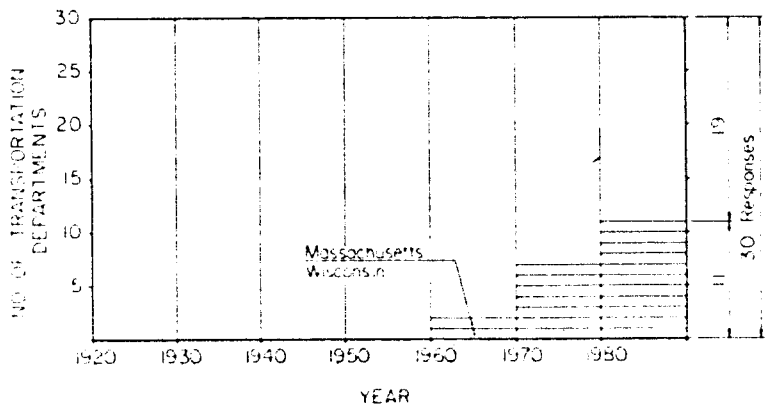

Figure 7–40 Design trends for continuous bridges: early conversion of simple spans to continuous spans.

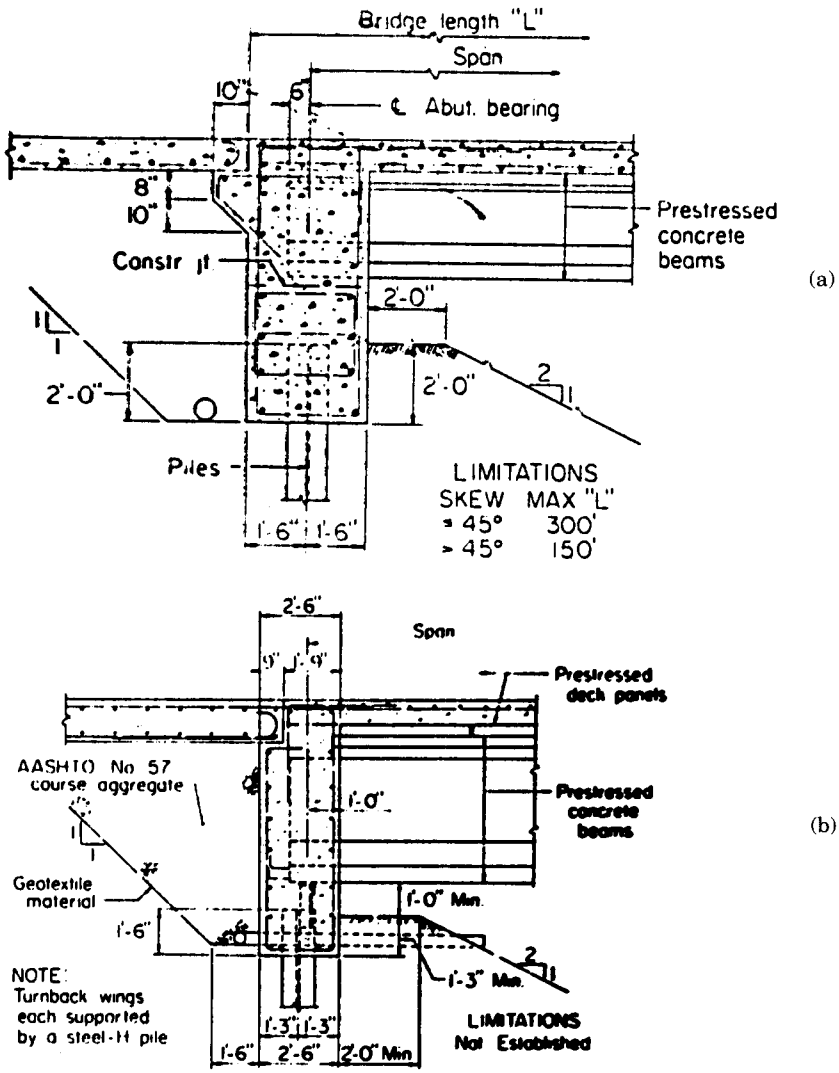

Figure 4–41 Integral abutment details; (a) Iowa; (b) Pennsylvania; (c) North Dakota; (d) semi-integral abutment, Ohio.

the bridge deck. These modes of failure demonstrate the need to provide flexibility in substructure design with appropriate reinforcement to withstand secondary stresses induced by foundation restraint and superstructure shortening.

Design of integral abutments. Figure 7–41(a) through (d) shows details of integral and semi-integral abutments. These supplement the abutment configurations shown in Figure 1–11(a) through (c). The obvious similarity between these abutments reflects the experience gained from early successful designs. Interestingly, the attributes of integral bridges are not always achieved without cost. Certain sections may operate at very high stresses that cannot be easily quantified and often are above the permitted levels. It may appear that the choice to build integral bridges and tolerate the higher

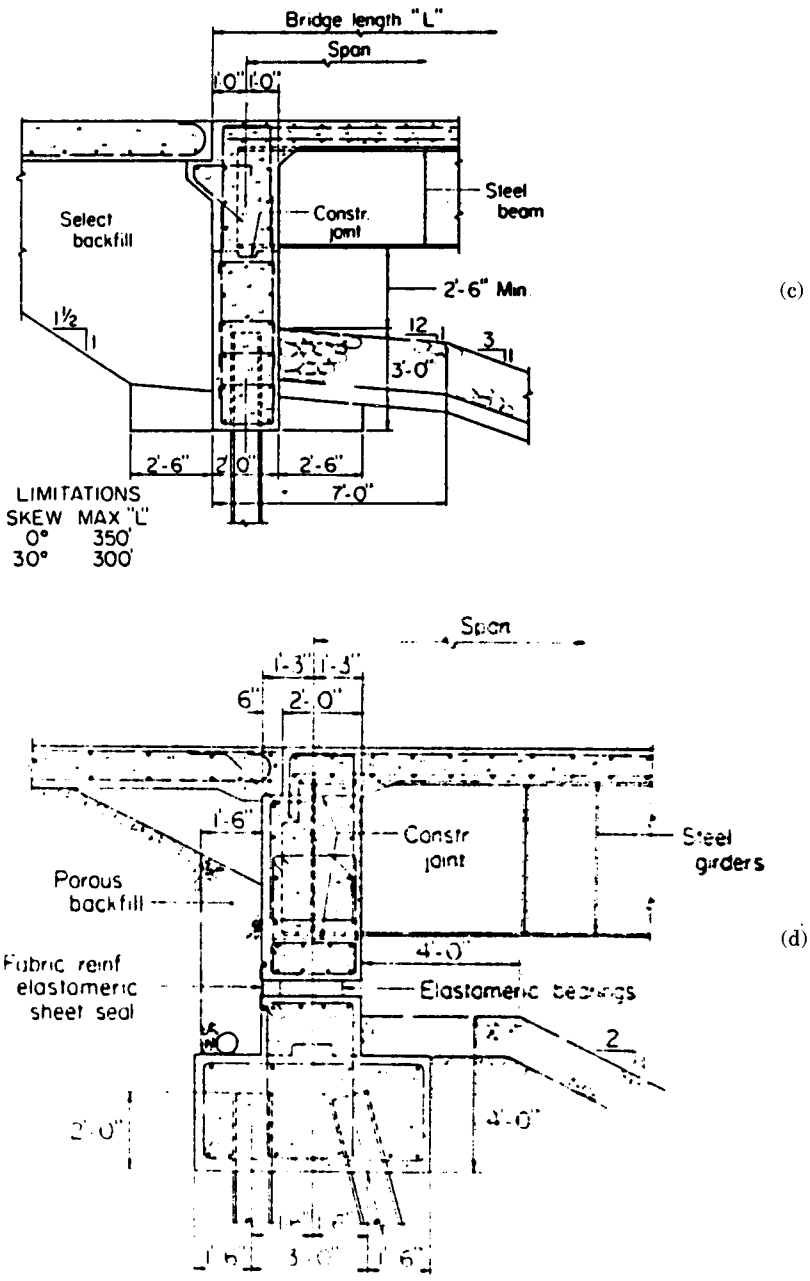

Figure 7–41 *(continued)*

stresses must be judged in terms of the more expensive jointed bridges with the associated vulnerability to destructive pavement pressures.

These details do not reflect other important design aspects such as skew and construction procedures that should be considered for specific bridges. For abutment design, the main factors that have a marked effect on performance, integrity, and durability are the passive pressure behind the abutment wall, and pile distress caused by lateral abutment movement.

Solutions that have been used to minimize or inhibit the development of passive pressure in abutment backfills as the bridge expands were mentioned in section 1.3, and include the use of selected backfill placed in a loose state, approach slabs supported on the abutment backwall there by preventing live load surcharge loads, and semi-integral abutments as shown in Figure 7–41(d).

Pile distress under axial load and lateral movement may be controlled by the use of a single row of slender piles and by the use of an abutment hinge (see also section 1.3).

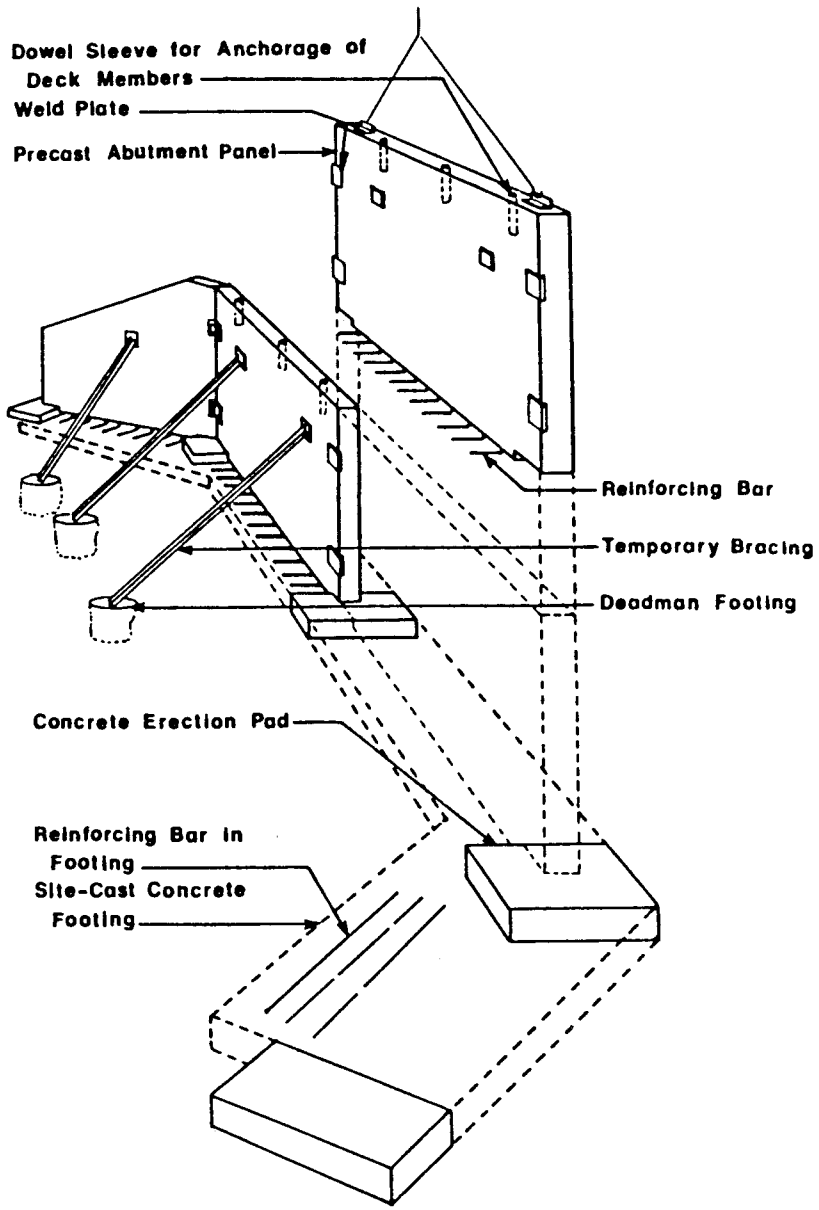

Figure 7–42 Precast abutment and wing walls.

AASHTO requirements. AASHTO recommends to design integral abutments to resist the forces generated by the thermal movement of the superstructure. Integral abutments should not be founded or keyed into rock. The movement should include the combined effect of temperature, creep, and long-term prestress shortening.

Maximum span lengths and design considerations should comply with recommendations outlined in FHWA Technical Advisory T5140.13 (1980) except where regional experience indicates otherwise. Appropriate drainage provisions should be made for any entrapped water behind the abutment.

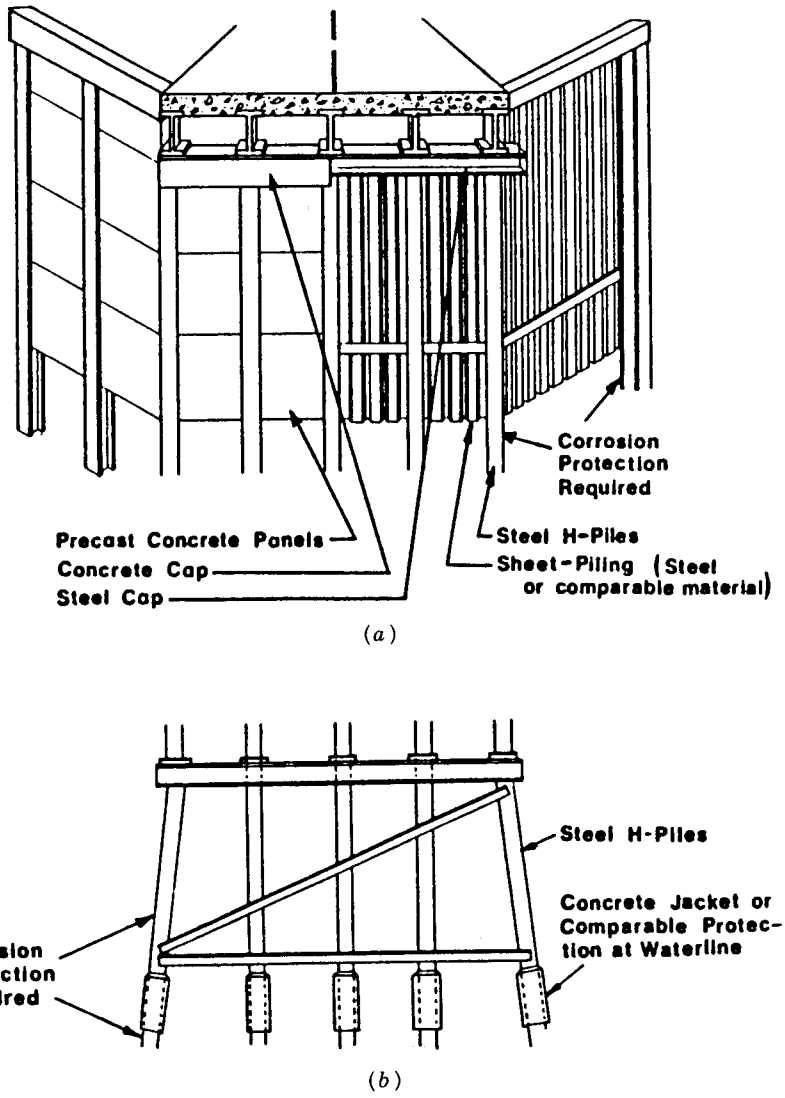

Figure 7–43 (a) Pile substructure and abutment details; (b) pile substructure and pier details.

7.17 PREFABRICATED CONCRETE SECTIONS

The substructure (piers and abutments) often requires 60 to 70 percent of the time required to construct a bridge (Sprinkel, 1978). Significant time savings can thus be realized if the time for substructure construction can be reduced through the use of prefabricated elements and innovative techniques. In many instances construction schedules can be telescoped by prefabricating and stockpiling the substructure members.

Figures 7–42 and 7–43 illustrate the use of precast concrete abutments and wing walls, and prefabricated piling, piers, and caps. Prominent features of the precast abutment shown in Figure 7–42 are the modular panels, conveniently prefabricated in various shapes and sizes to accommodate the abutment configuration and roadway width. The panels are set on cast-in-place concrete pads, temporarily supported, and then connected with weld plates and cast-in-place concrete footing (see also section 7.6). Other systems and configurations based on modular precast units may be combined to obtain a comparable abutment.

The pile substructure schemes shown in Figure 7–43 consist of prestressed concrete or steel H-piles with a concrete or steel cap. The piles are driven to the required depth and cut to the required height. Then they are capped with cast-in-place or precast concrete. For abutments, the piling may be backed with a precast concrete plank, a steel bridge plank, or a suitable cribing to retain the soil.

Practical considerations for the use of prefabricated substructure elements are summarized by GangaRao (1978), but with a limited applicability because of the many physical differences between bridge sites. The use of standardized elements is further inhibited by variable soil characteristics, bedrock location, and depth at which ample bearing is available. Almost all concepts for substructure applications require the use of either portland cement grout, mortar, concrete, or posttensioning to tie the elements together.

REFERENCES

AASHTO, 1994: AASHTO LRFD Bridge Design Specifications.

BROWN, W. G., 1964: "Difficulties Associated with Predicting Depth of Freeze or Thaw," *Canadian Geotech, Journ.*, vol. 1, No. 4, pp. 215–226.

BURKE, M. P., Jr., 1987: *Bridge Approach Pavements, Integral Bridges and Cycle Control Joints.* In Transportation Research Record 1113, TRB, National Research Council, Washington, D.C.

California Division of Highways, 1976: "Damage in the San Fernando Earthquake," *Prelim. Report, State of California Business and Transportation Agency, Dept. of Public Works,* Div. of Highways, Bridge Dept.

CLOUGH, G. W., and R. F. FRAGASZY, 1977: "A Study of Earth Loadings on Floodway Retaining Structures in the 1971 San Fernando Valley Earthquake," *Proc. 6th World Conf. on Earthquake Engineering,* New Delhi, pp. 7–37 to 7–42.

D'APPOLONIA, D. J., E. D'APPOLONIA and R. F. BRISSETTE, 1970: "Settlement of Spread Footings on Sand," (closure), *Proc. Journ. of Soil Mech. and Found. Div.*, ASCE, vol. 96, No. SM2, pp. 754–761.

ELLISON, B., 1971: "Earthquake Damage to Roads and Bridges, Madang, R.P.N.G., Nove. 1970," *Bull. New Zealand Society of Earthquake Engineering*, vol. 4, pp. 243–257.

ELMS, D. A. and G. R. MARTIN, 1979: "Factors Involved in the Seismic Design of Bridge

Abutments, "*Proc. Workshops on Seismic Problems Related to Bridges*, Applied Technology Council, Berkeley.

EVANS, G. L., 1971: "The Behavior of Bridges Under Earthquakes," *Proc. New Zealand Roading Symp.*, Victoria University, vol. 2, pp. 664–684.

FRANKLIN, A. G. and F. K. CHANG, 1977: "Earthquake Resistance of Earth and Rockfill Dams: Report 5: Permanent Displacements of Earth Embankments by Newmark Sliding Block Analysis," Misc. Paper S-71-17, *Soils and Pavements Lab., U.S. Army Engineer Waterways Experiment Station*, Vicksburg, Miss.

FUNG, G. G., R. F. LEBEAU, E. D. KLEIN, J. BELVEDERE, and A. G. GOLDSCHMIDT, 1971: "Field Investigation of Bridge Damage in the San Fernando Earthquake," *Prelim. Report, State of California Business and Transportation Agency, Dept. of Public Works.*

GAMBLE, W. L., 1984: *Bridge Evaluation Yields Valuable Lesson.* Concrete International, June, pp. 68–74.

GANGARAO, H. V. S., 1978: "Conceptual Substructure Systems for Short-Span Bridges," *Transportation Engineering Journ.*, ASCE, New York, Jan.

JORGENSON, J. L., 1983: *Behavior of Abutment Piles in an Integral Abutment Bridge.* In Transportation Research Record 903, TRB, National Research Council, Washington, D.C.

MONONOBE, N., 1929: "Earthquake-Proof Construction of Masonry Dams," *Proc. World Eng. Conf.*, vol. 9, p. 275.

NEWMARK, N. M., 1965: "Effects of Earthquakes on Dams and Embankments," *Geotechnique*, vol. 14, No. 2, pp. 139–160.

OKABE, S., 1926: "General Theory of Earth Pressure," *Journ. Japanese Soc. of Civ. Engineers,* vol. 12, No. 1.

PODOLNY, W., JR., and J. M. MULLER, 1982: *Construction and Design of Prestressed Concrete Segmental Bridges*, Wiley, New York, pp. 561.

PRAKASH, S., and H. D. SHARMA, 1990: *Pile Foundations in Engineering Practice*, Wiley, New York, p. 735.

RICHARDS, R. and D. G. ELMS, 1979: "Seismic Behavior of Gravity Retaining Walls," *Journ. of the Geotech. Engineering Div.*, ASCE, vol. 105, No. GT4.

SEED, H. B. and R. V. WHITMAN, 1970: "Design of Earth Retaining Structures for Dynamic Loads," *ASCE Specialty Conference-Lateral Stresses in the Ground and Design of Earth Retaining Structures*, ASCE.

SPRINKEL, M. M., 1978: "Systems Construction Techniques for Short Span Concrete Bridges," *Transportation Research Record 665: Bridge Engineering*, vol. 2, Transportation Research Board, National Research Council, Washington, pp. 226-227.

TERZAGHI, K., and R. B. PECK, 1967: *Soil Mechanics in Engineering Practice*, 2nd ed., Wiley, New York, pp. 729.

U. S. Army Corps of Engineers, 1949: "Report of Frost Penetration," Addendum No. 1, 1945-47, *Corps of Engineers, U.S. Army*, New England Division, Boston.

Virginia Prestressed Concrete Association, 1973: "New Approaches in Prestressed, Precast Concrete for Bridge Superstructure Construction in Virginia," Aug., pp. 4, 6, 10, 14, 17, 19, 25.

WOLDE-TINSAE, A. M., L. F. GREIMANN, and P. S. YANG, 1982: *Nonlinear Pile Behavior in Integral Abutment Bridges*, Iowa State Univ., Ames.

WOOD, J. H., 1973: "Earthquake-Induced Soil Pressures on Structures," Report No. EERL 73-05, *Earthquake Engineering Research Lab.*, Calif. Inst. of Technology, Pasadena.

XANTHAKOS, P. P., 1994: *Theory and Design of Bridges*, Wiley, New York, p. 1445.

CHAPTER 8

Footings

8.1 FACTORS AFFECTING SELECTION OF FOUNDATION TYPE

As mentioned in section 1.5, the main factors to be considered in selecting spread footings relate to suitable depth, groundwater effects, potential uplift, and influence of adjacent structures. In general, the selection process should consider the magnitude, type, and application of loads, proximity to suitable bearing layers, previous groundwater history, potential for liquefaction, undermining or scour, swelling potential, frost depth penetration, and cost considerations.

Probable Depth of Scour

Scour is the process of displacing stream bed materials as a result of the erosive action of flowing water. This action undercuts the soil, and may occur naturally or following channel restrictions and changes in flow pattern. For the usual conditions, the greatest scour should be expected to occur during the largest flood.

Scour rates vary according to the type of material. Loose granular soils are very susceptible to scour, whereas soils with cohesion or with some cementation are less prone to this process. AASHTO (1970) articulates typical scour rates for stream bed materials, expressed in terms of the time necessary to reach the maximum scour depth (Table 8–1).

For bridges located at stream crossings, the potential for scour should be investigated considering the worst conditions resulting from the 100-year flood. This usually involves designing the foundation for conditions after scour (see also chapter 3). This analysis is based on the assumption that all the stream bed materials within the scour

Table 8–1 Typical Scour Data.

Material	Time for Maximum Scour
Sands & gravels	hours
Cohesive soils	days
Glacial tills, sandstones & shale	months
Limestones	years
Dense granites	centuries

prism have been wasted away, and thus a reduced area is available for bearing or lateral support.

The scour depth will depend on the geological history of the site (depth of prior erosion to bedrock and subsequent redeposition of sediments, stream velocity, and area runoff), the hydraulics of flow, and the properties of the stream bed materials. Where the redeposition of sediments in the stream bed is of the order of 100 to 150 feet, careful analysis of borings is necessary to predict the depth of maximum scour. A detailed discussion on these topics is given by FHWA (1988), AASHTO (1970), and Copp and Johnson (1987).

Predictions on scour interact with several engineering principles such as hydraulics and hydrology, boring records, past experience with the performance of a given stream, and judgment. If careful records of driving resistance are available, the scour depth may be predicted as being where the penetration (SPT or CPT) resistance increases substantially (Kuhn and Williams, 1961). The AASHTO (1970) report lists several procedures for predicting scour, but concludes that engineering judgment is used more than any other method to estimate scour depth. Scour is accelerated if the foundation creates channel obstructions. These effects are the principal cause of differences resulting from theoretical predictions.

A normal approach to the scour problem should involve the following steps:

1. Select a suitable foundation type;
2. estimate the scour potential and effects such as depth, etc.;
3. estimate the cost of foundation for normal conditions and various scour scenarios; and
4. analyze cost versus risk, and assess the initial design accordingly.

In the absence of a detailed investigation, Terzaghi and Peck (1967) recommend placing the foundation at a depth not less than the elevation of the bottom of low-water channel plus four times the greatest rise of the river level (see also section 3.15).

Frost Effects

Frost effects were discussed briefly in section 7.8 (see also Figure 7–11). In general, footings should be placed below the frost line, because alternate freezing and thawing of the soil tends to maintain it in an unconsolidated (loose) state. Figure 8–1 shows approximately maximum frost depths for regions of the United States (Bowles, 1988); however, local codes should be consulted since they may provide data based on local experience. Recent weather extremes may also be consulted from weather records to confirm the possible effect of cold-weather cycles on frost depth.

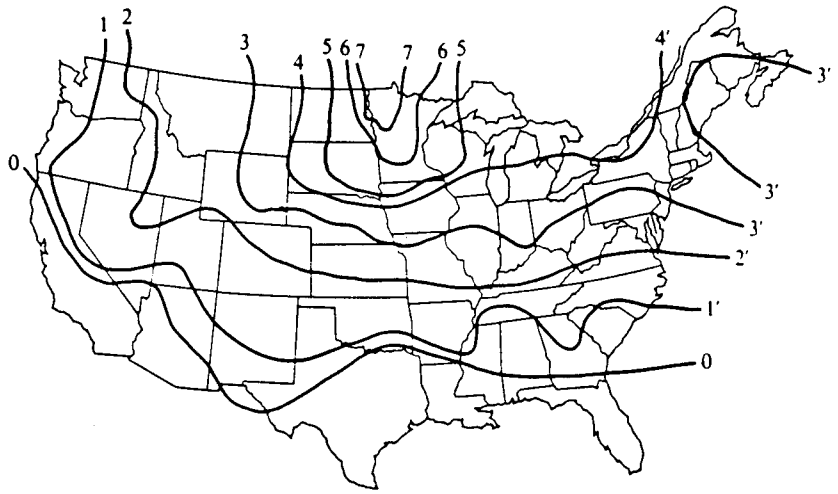

Figure 8–1 Approximate frost-depth contours for the United States, based on a survey of a selected group of cities.

Where frost protection is marginal or deficient, the design may consider the use of insulation to improve frost conditions.

Groundwater and Moisture Fluctuations

Groundwater. Seepage forces and hydraulic gradients should be evaluated where foundation excavations are to be extended below the groundwater table. Upward seepage forces in the bottom of an excavation can lead to piping in dense granular soil or heaving in loose granular soil with subsequent bottom instability. These problems can be controlled by adequate dewatering, usually using wells or well points.

The influence of groundwater table on bearing capacity of soils and rocks has been demonstrated in practical applications. Associated settlements should be considered, and where seepage forces are present they should be included in the analysis. An example of the effect of lowering the groundwater table on the bearing capacity of soils is given in section 3.13.

Moisture fluctuations. Clayey soils tend to shrink on drying and expand when wet. The lower the shrinkage limit and the wider the range of plasticity index, the more likely volume change is to occur and the greater its extent. These volumetric changes can follow the drying of the soil after it is depleted of natural moisture.

On a regional basis, volume changes are particularly troublesome in areas of the southwestern United States subjected to long dry periods and occasional heavy rains of short duration. The dry periods tend to desiccate the soil, while the rain causes swelling. Because the rainfall is not enough to leach and weather the clay minerals, they remain unchanged near the ground surface and are rapidly wetted during the rainy periods. Soils in these areas are difficult to use as foundation soils, since water vapor migrating from the water table condenses on the bottom sides of mat foundations and footings.

Nearby Structures

Occasionally foundations must be placed close or adjacent to existing structures. In this case the mutual influence on the behavior of the new and existing foundations should be investigated.

Figure 8–2 demonstrates potential problems that may arise when placing new footings adjacent to existing. The line from the base of the new footing to the edge of the existing footing should be at 45° or less with the horizontal. From this it follows that the distance m should be greater than the difference in elevation z_f. This criterion should produce conservative pressures in the common zone with contributions from more than one footing.

In Figure 8–2(b) a different situation prevails. If the new footing is lower than the existing, the possibility will exist that soil may flow laterally from beneath the existing footing. This may result in a corresponding settlement. As a first approximation, the problem may be analyzed by referring to Mohr's failure stress circle for triaxial compression.

Figure 8–3 shows the effects of excavation too close to an existing footing. In this case the qN_q term (see also subsequent sections) of the bearing capacity equation is lost. Problems of this nature may be avoided if a ground support system is placed to retain the soil in the K_o state, or if some form of ground improvement precedes the excavation.

Expansive and Collapsible Soils

The soils discussed at the beginning of this section (undergoing volume changes upon wetting and drying) are termed expansive soils. When such soils are encountered, the following solutions may be tried: (1) alter the soil by adding lime, cement or other admixtures, and institute compaction to low densities of water contents on the wet side of optimum; (2) control the direction of expansion, by allowing the soil to expand into cavities built in the foundation; (3) provide water control, so that the soil may be excavated to a depth where the weight of soil will control heave; (4) place the footing at a sufficient depth and/or leave an expansion zone between the ground surface and the foundation so that swell can take place without causing detrimental movement; and (5) load the soil to sufficient pressure (artificial) to balance swell pressure.

Collapsible or metastable soils are by definition unsaturated soils undergoing a

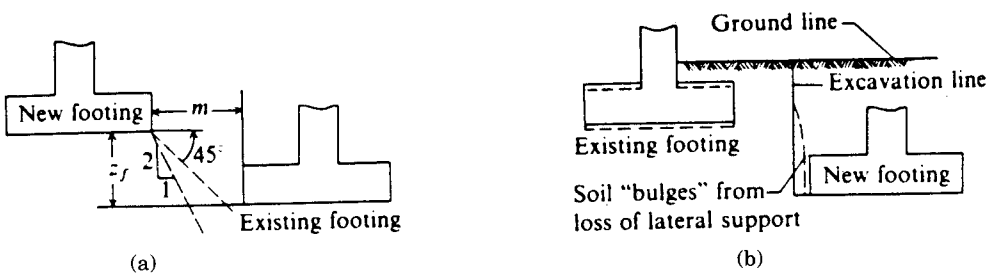

Figure 8–2 Location considerations for spread footings. (a) An approximation for spacing footings to avoid interference between old and new footings. If "new" footing is in relative position of "existing" footing, interchange words "existing" and "new". Make $m > z_f$. (b) Possible settlement of "existing" footing because of loss of lateral support of soil wedge beneath existing footing.

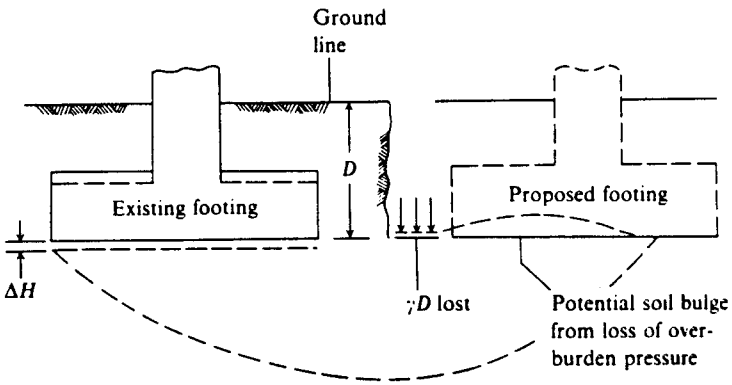

Figure 8–3 Potential settlement from loss of overburden pressure.

radical particle rearrangement and considerable volume loss upon wetting with or without additional loading (Clemence and Finbarr, 1981). Difficulties associated with the use of these soils as foundation support have long been recognized, but until recently concern was limited because such soils are located in arid regions with modest economic development potential. With recent advances in irrigation these regions have become available for development and associated construction, and collapsible soils are becoming relevant to the analysis and design of foundations.

Comprehensive reviews on the subject are given by Clemence and Finbarr (1981), Northen (1969), Sultan (1969), and Dudley (1970). Since 1970, major effort has focused on determining the mechanics of collapse, on predictive techniques and treatment methods, and on evaluating case histories.

8.2 FOOTING TYPES

Several footing types common in bridge foundations are shown in Figure 8–4. Footings generally can be divided into column and wall footings. A wall footing shown in Figure 8–4(e) is simply a strip of reinforced concrete, wider than the wall, used to distribute the load to the foundation soil. Strip footings are typically used with solid pier walls. Single column footings, shown in Figure 8–4(a) and (b), are usually square and some-

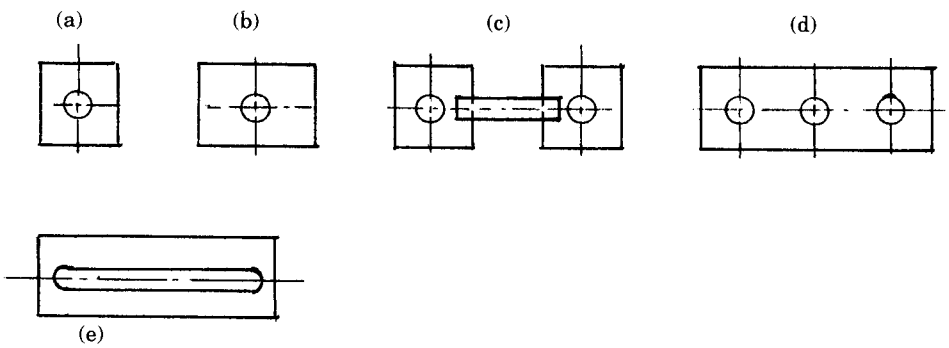

Figure 8–4 Footing types common in bridge foundations.

times rectangular. The choice depends on the variation of the transverse moments in the two principal directions. Unlike strip footings that display essentially one-dimensional action, single column footings (also referred to as spread footings) distribute the loads in two directions.

The combined footings under two or more columns shown in Figure 8–4(d) may be used under closely spaced or heavily loaded columns where single footings might completely or nearly merge. The footing shown in Figure 8–4(c) merely has a connecting beam that increases the stability of the foundation against overturning and against lateral forces.

Wall or column individual and combined footings are the most frequent types of spread foundations on soils of reasonable bearing capacity. If the soil at relatively shallow depth is weak, or if the column loads are great, the required footing area may become so large as to be uneconomical. In this case a deep foundation may be considered.

Occasionally spread footings may have pedestals, or they may be stepped or tapered to save materials. Strip, spread, and combined footings are considered in this chapter since they are the most basic and common types in bridge foundations.

8.3 BEARING CAPACITY THEORIES

General Principles

Currently there is no method for obtaining the ultimate bearing capacity of a foundation other than as an estimate. At least ten and probably fifteen theoretical solutions have been formulated since 1940. Little experimental verification has been provided except by using model footings. Using models with B = 25 to 75 mm and L = 25 to 200 mm (widths and lengths, respectively) appear to be popular because the ultimate bearing can be induced in the laboratory on a small prepared box of soil. Full size footings with dimensions 1 m × 1 m (3.3 × 3.3 ft) can develop ultimate loads 600 to 1000 kips, but require a rather expensive preparation and equipment to induce and measure loads of this magnitude.

Models, especially in sand, do not always give reliable test results compared to full-scale prototypes. This is because of scale effects where the model reaction engages only a small quantity of soil grains. Sand also requires confinement to develop resistance, and this is more feasible with very small models. In spite of these shortcomings, the use of models has gained popularity.

Bearing Capacity Equations

The Terzaghi Bearing Capacity Equation. This is one of the early theories proposed by Terzaghi (1943). The equation has the following form (general shear failure)

$$q_{ult} = cN_c s_c + 0.5\,\gamma B N_\gamma\, s_\gamma + qN_q \tag{8–1}$$

where q_{ult} = ultimate bearing capacity for uniform bearing pressure (ksf); c = soil cohesion (ksf) = s_u = undrained shear strength; γ = total unit weight of soil (kcf); q = effective overburden pressure at base of footing (ksf); N_c, N_γ, N_q = bearing capacity factors based on the value of internal friction of the foundation soil.

The coefficients s_c and s_γ are as follows

s_c = 1.0 (strip), 1.3 (round), 1.3 (square)
s_γ = 1.0 (strip), 0.6 (round), 0.8 (square)

For a continuous footing ($L > 5B$), $s_c = s_\gamma = 1.0$, hence

$$q_{ult} = cN_c + 0.5_\gamma BN_\gamma + qNq \tag{8–2}$$

which is AASHTO Eq. (4.4.7.1–1). All notations refer to Figure 8–5.

The values of N_c, N_γ and N_q may be obtained directly from AASHTO Table 4.4.7.1A.

Equation (8–1) introduces shape factors to extend the applicability of the bearing capacity theory. Terzaghi's criterion was produced from a slightly modified bearing-capacity theory developed by Prandl (1920), who used the theory of plasticity to analyze the punching of a rigid base into a softer (soil) material. This bearing-capacity equation is intended for shallow foundations where

$$D_f \leq B \tag{8–3}$$

so that the shear resistance along the edge of the soil mass engaged in the interaction can be neglected. The dimensionless factor N_γ is a function of the coefficient $K_{p\gamma}$. Since

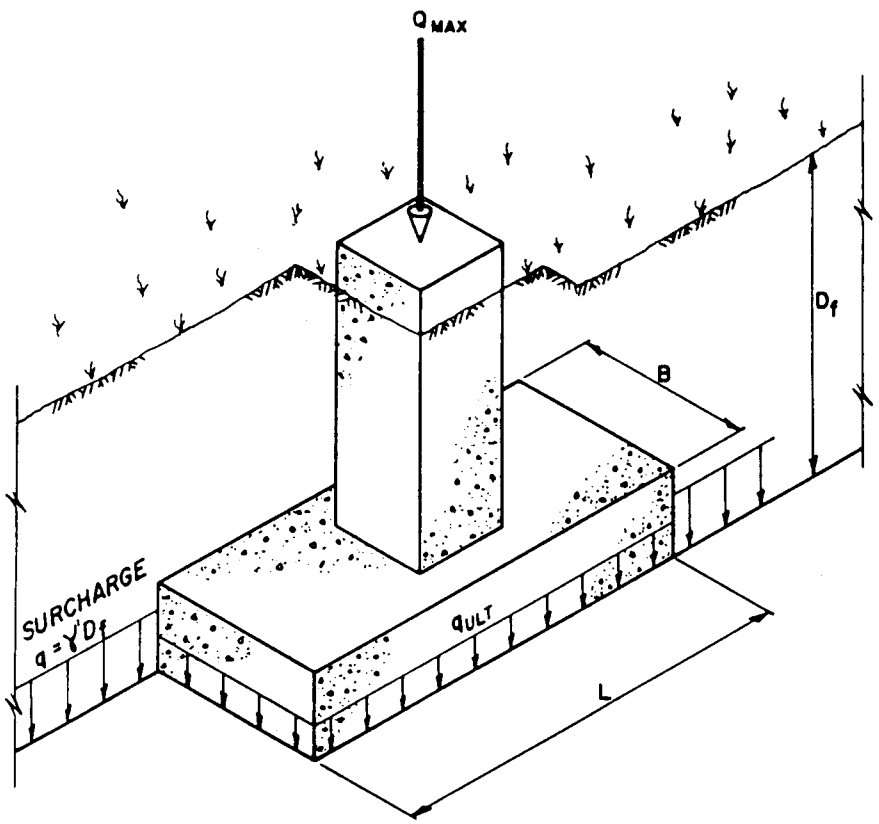

Figure 8–5 Design terminology for spread footing foundations.

Terzaghi did not explain how values of $K_{p\gamma}$ were obtained to compute N_γ (other than a $\phi - N_\gamma$ curve with three specific values), several investigations have arrived at approximate values of N_γ from back analysis and other theoretical considerations (Meyerhof, 1951, 1963; Vesic, 1973).

Meyerhof's bearing capacity equation. Meyerhof (1951, 1963) introduced a bearing capacity equation essentially similar to Equation (8–1), but including a shape factor s_q for the depth term Nq. He also included depth factors d_i and inclination factors i_i to deal with cases where the footing load is inclined from the vertical. Meyerhof (1963) modified somewhat his 1951 values for the shape, depth, and inclination factors. This theory has been used as a basis to produce a modified form of the general bearing capacity equation to account for these effects, and has produced AASHTO Eq. (4.4.7.1.1–1).

Hansen's bearing capacity method. Hansen (1970) proposed a general bearing capacity equation, which is essentially a further extension of Meyerhof's work. Hansen's shape, depth, and other factors contributing to the general equation are given in Table 8–2, and they represent revisions and extensions from earlier proposals. These extensions include a factor for a footing tilted from the horizontal b_i and for the possibility of the footing being on a slope g_i.

Referring to the notation of Table 8–2, the Hansen theory is valid for any D/B ratio and thus can be used for shallow (footings) and deep (piles, drilled shafts) foundations.

Commentary. Among the many bearing capacity theories, some of which were briefly mentioned, the Terzaghi equations were the first proposed and have been widely used. They are still popular, especially where it is not necessary to compute shape, depth, and other factors. They are, however, suitable for a concentrically loaded horizontal footing, which is most often the case with bridge foundations.

Some opinion has been expressed that the Terzaghi equations sometimes are unduly conservative, and probably should be applied to soils with little cohesion and with D_f probably in the range $B/2$ to $2B$ (Figure 8–5). Both the Meyerhof and Hansen methods are substantially used, especially where depth, shape, and inclination factors must be considered.

In developing the bearing capacity equation, Terzaghi considered a general shear failure in dense soil and a local shear failure for a loose soil. Thus, if local or punching shear is possible, the value of q_{ult} in Equation (8–2) should be computed using reduced shear strength parameters c^* and ϕ^* as follows:

$$\left.\begin{aligned} c^* &= 0.67c \\ \phi^* &= \tan^{-1}(0.67\tan\phi) \end{aligned}\right\} \qquad (8\text{–}4)$$

which are AASHTO Eqs. (4.4.7.1–3 and 4).

The following comments about the bearing capacity equations can be made:

1. The cohesion term predominates in cohesive soils.
2. The depth term qN_q is the main contributing factors in granular soils without cohesion. A small increase in D_f can increase q_{ult} considerably.
3. The footing-width term $0.5\gamma BN_\gamma$ increases the bearing capacity in both cohesive and cohesionless soils. However, this effect becomes less important as the footing width B decreases.

Table 8–2 Shape, Depth, Inclination, Ground and Base Factors for Use in either the Hansen (1970) or Vesic (1973) Bearing-Capacity Equations, (Factors apply to either method unless subscripted with (*H*) or (*V*). Use primed factors when $\phi = 0$)

Shape Factors	Depth Factors	Inclination Factors	Ground Factors (base on slope)
$s'_c = 0.2 \cdot \frac{B}{L}$ $s_c = 1 + \frac{N_q}{N_c} \cdot \frac{B}{L}$ $s_c = 1$ for strip	$d'_c = 0.4k$ $d_c = 1 + 0.4k$	$i'_{c(H)} = 0.5 - 0.5\sqrt{1 - \frac{H}{A_f c_a}}$ $i'_{c(V)} = 1 - \frac{mH}{A_f c_a N_c}$ $i_c = i_q - \frac{1 - i_q}{N_q - 1}$ (Hansen and Vesic)	$g'_c = \frac{\beta^\circ}{147^\circ}$ for Vesic use $N_\gamma = -2 \sin \beta$ for $\phi = 0$ $g_c = 1 - \frac{\beta^\circ}{147^\circ}$
$s_q = 1 + \frac{B}{L} \tan \phi$	$d_q = 1 + 2 \tan \phi (1 - \sin \phi)^2 k$		$g_{q(H)} = g_{\gamma(H)} = (1 - 0.5 \tan \beta)^5$
	$d_\gamma = 1.00$ for all ϕ	$i_{q(H)} = \left(1 - \frac{0.5H}{V + A_f c_a \cot \phi}\right)^5$	$g_{q(V)} = g_{\gamma(V)} = (1 - \tan \beta)^2$
$s_\gamma = 1 - 0.4 \cdot \frac{B}{L}$	$k = \frac{D}{B}$ for $\frac{D}{B} \le 1$ $k = \tan^{-1} \frac{D}{B}$ for $\frac{D}{B} > 1$ (rad)	$i_{q(V)} = \left(1 - \frac{H}{V + A_f c_a \cot \phi}\right)^m$	**Base factors (tilted base)** $b'_c = \frac{\eta^\circ}{147^\circ}$ $b_c = 1 - \frac{\eta^\circ}{147^\circ}$
where A_f = effective footing area $B' \times L'$ (see Fig. 8–6) c_a = adhesion to base = cohesion or a reduced value D = depth of footing in ground (used with B and not B') e_B, e_L = eccentricity of load with respect to center of footing area H = horizontal component of footing load with $H \le V \tan \delta + c_a A_f$ V = total vertical load on footing β = slope of ground away from base with downward = (+) δ = friction angle between base and soil—usually $\delta = \phi$ for concrete on soil η = tilt angle of base from horizontal with (+) upward as usual case *General:* 1. Do not use s_i in combination with i_i. 2. Can use s_i in combination with d_i, g_i, and b_i. 3. For $L/B \le 2$ use ϕ_{tr} For $L/B > 2$ use $\phi_{ps} = 1.5\phi_{tr} - 17$ For $\phi \le 34$ use $\phi_{ps} = \phi_{tr}$		$i_{\gamma(H)} = \left(1 - \frac{0.7H}{V + A_f c_a \cot \phi}\right)^5$ ($\eta = 0$) $i_{\gamma(H)} = \left(1 - \frac{(0.7 - \eta^\circ/450)H}{V + A_f c_a \cot \phi}\right)^5$ ($\eta > 0$) $i_{\gamma(V)} = \left(1 - \frac{H}{V + A_f c_a \cot \phi}\right)^{m+1}$ $m = m_B = \frac{2 + B/L}{1 + B/L} H$ parallel to B $m = m_L = \frac{2 + L/B}{1 + L/B} H$ parallel to L *Note:* i_q, $i_\gamma > 0$	$b_{q(H)} = \exp(-2\eta \tan \phi)$ $b_{\gamma(H)} = \exp(-2.7\eta \tan \phi)$ $b_{q(V)} = b_{\gamma(V)} = (1 - \eta \tan \phi)^2$ Notes: $\beta + \eta \le 90^\circ$ $\beta \le \phi$

(From Hansen, 1970)

4. When the soil beneath a footing is nonhomogeneous or stratified, some judgment is necessary in determining the bearing capacity, since there can be a number of interpretations.
5. The Terzaghi equation is simpler and easier to use. For example, it can be applied to a particular footing load without an iterative procedure.

Effect of eccentric loading. Eccentricity in pier footings is introduced with an axial load and moments about one or both principal directions of the footing. Referring to Figure 8–6, the effective (reduced) footing dimensions can be obtained as (Meyerhof, 1953; Hanson, 1970)

$$L' = L - 2e_x,\ B' = B - 2e_y \tag{8–5}$$

so that the effective footing area is now

$$A' = B'L' \tag{8–6}$$

Note that the last two equations are AASHTO Eqs. (4.4.7.1.1.1–1 and 2) and (4.4.7.1.1.1–3).

The value of q_{ult} obtained using the reduced footing dimensions B' and L' represents an equivalent uniform bearing pressure and *not* the actual contact pressure distribution beneath the footing. This equivalent pressure may be multiplied by the reduced area A' to calculate the ultimate load Q_{ult} from the standpoint of bearing capacity, or

$$Q_{ult} = q_{ult}(B'L') \tag{8–7}$$

where q_{ult} is computed from Equation (8–2) using B' in the γBN_γ term. The actual contact pressure distribution (usually trapezoidal) should be used in computing the reinforcement requirements (moments, shears, etc.).

The actual distribution of contact pressure for a rigid footing with eccentric loads

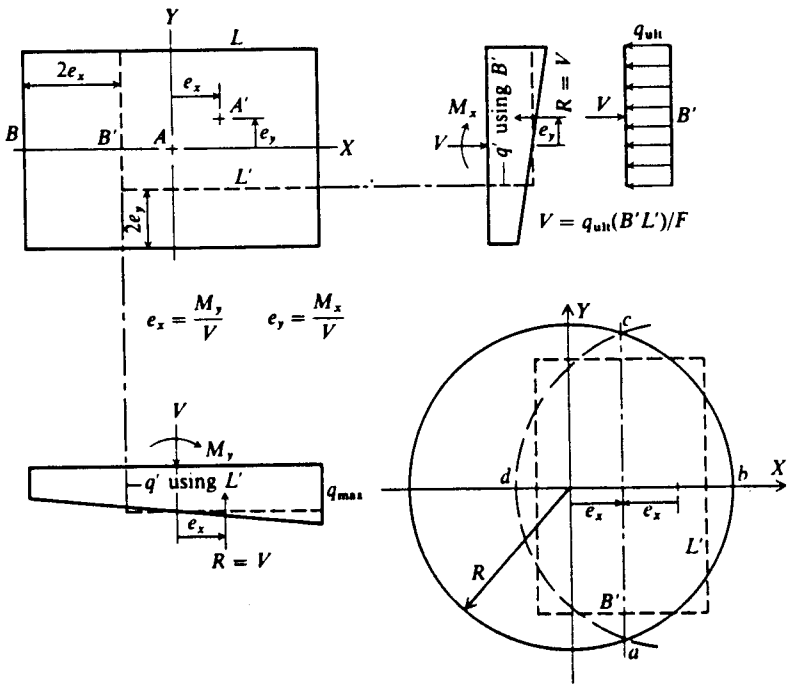

Figure 8–6 Method of computing effective footing dimensions when footing is eccentrically loaded for both rectangular and round bases.

may be computed from statics and flexural theory. Referring to Figure 8–7, if the resultant Q lies in the middle third ($e_L < L/6$)

$$\left.\begin{aligned} q_{max} &= Q[1+(6e_L/L)]/BL \\ q_{min} &= Q[1-(6e_L/L)]/BL \end{aligned}\right\} \tag{8–8}$$

For $L/6 < e_L < L/2$

$$\left.\begin{aligned} q_{max} &= 2Q/(3B[(L/2)-e_L]) \\ q_{min} &= 0 \end{aligned}\right\} \tag{8–9}$$

For an eccentricity in both directions, reference is made to AASHTO (1992).

Effect of groundwater table. In the foregoing equations q is based on the effective weight of the soil (see also Figure 8–5). The water table, however, is seldom above the base of the footing, since this would cause construction problems.

Ultimate bearing capacity should be computed on the basis of the highest anticipated groundwater level at the footing location. Where this effect must be considered, the q term may require adjustment. If the water table is at ground surface, the effective soil weight is approximately one-half, giving a q term about one-half the value with the water table below the footing level.

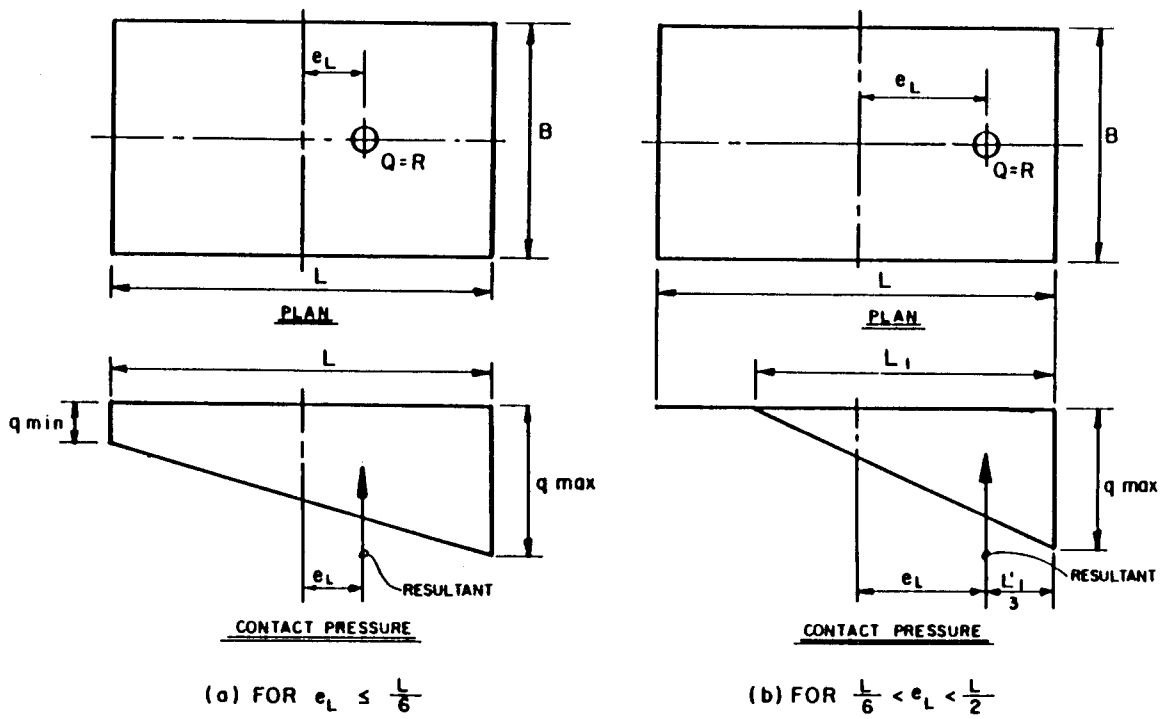

Figure 8–7 Contact pressure for footing loaded eccentrically about one axis.

When the groundwater level is below the wedge zone approximated depth of $0.5B\tan(45 + \phi/2)$, the groundwater effects can be ignored for bearing capacity. When the water table lies within the wedge zone, the effects should be considered.

Referring to Figure 8–8, the effect of groundwater table on the ultimate bearing capacity may be considered by using the weighted average soil unit weight in Equation (8–2). If $\phi < 37°$, the weighted average unit weight may be computed from

$$\begin{aligned} &\text{For } z_w \geq B \quad \gamma = \gamma_m \quad \text{(no effect)} \\ &\text{For } z_w < B \quad \gamma = \gamma' + (z_w / B)(\gamma_m - \gamma') \\ &\text{For } z_w < O \quad \gamma = \gamma' \end{aligned} \tag{8–10}$$

where γ = total unit weight; γ' = submerged (effective) unit weight; and γ_m = moist unit weight of soil.

Layered soils. In general, if the soil profile shows stratified deposits, the bearing-capacity equations should be modified to account for differences in failure mode between the homogeneous and the layered soil. Three general cases may be identified as follows:

1. The footing is on layered clays ($\phi = 0$) with two possible conditions: (A) the top layer is weaker than the lower layer; and (B) the top layer is stronger than the lower layer.
2. The footing is on layered soil with friction and cohesion, and with two conditions as in case 1.

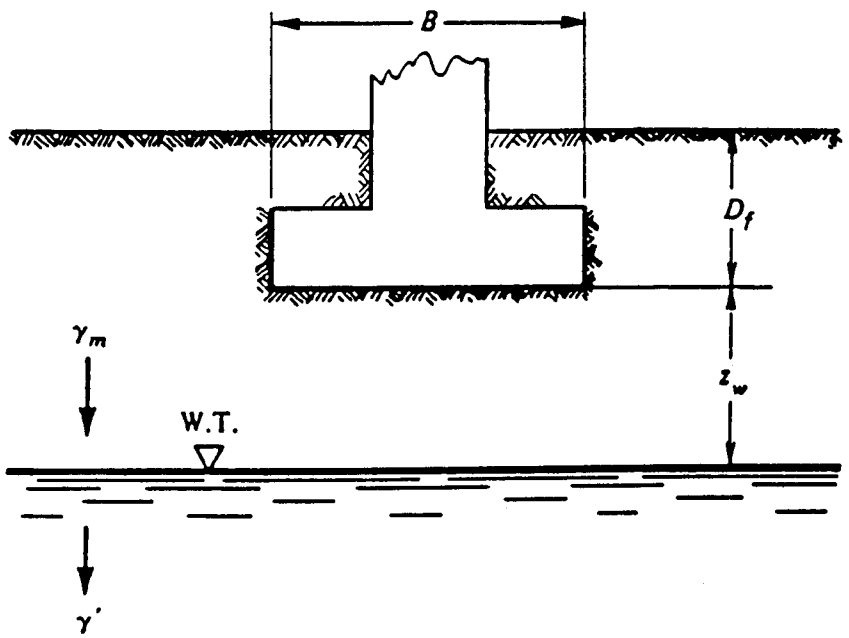

Figure 8–8 Definition sketch for influence of ground water table on bearing capacity.

3. The footing is on layered sand and clay soils with two possible conditions: (A) sand overlying clay; and (B) clay overlying sand.

Most of the experimental work carried out to provide criteria for q_{ult} has been confined to small models. Several analytical procedures have been introduced, and among those is the work by Button (1953), who used a circular arc as failure criterion, and established an approximate minimum $N_c = 5.5 < 2\pi$. Other work on this subject has been carried out by Meyerhof and Brown (1967), and Purushothamaraj et al. (1974).

Other conditions. Theories have been formulated to calculate the bearing capacities for foundations on slopes or adjacent to slopes (Meyerhof, 1953), and for foundations with inclined base (Kulhawy, Trautmann, Beech, O'Rourke, and McGuire, 1983).

Table 8–3 Presumptive Allowable Bearing Pressures for Spread Footing Foundations under Service Loads

Type of Bearing Material	Consistency in Place	Bearing Pressure (TSF)	
		Ordinary Range	*Recommended Value of Use*
Massive crystalline igneous and metamophic rock: graphite, diorite, basalt, gneiss, thoroughly cemented conglomerate (sound condition allows minor cracks)	Very hard, sound rock	60 to 100	80
Foliated metamorphic rock: slate, schist (sound condition allows minor cracks)	Hard sound rock	30 to 40	35
Sedimentary rock: hard cemented shales, siltstone, sandstone, limestone without cavities	Hard sound rock	15 to 25	20
Weathered or broken bedrock of any kind, except highly argillaceous rock (shale)	Medium hard rock	8 to 12	10
Compaction shale or other highly argillaceous rock in sound condition	Medium hard rock	8 to 12	10
Well-graded mixture of fine- and coarse-grained soil: glacial till, hardpan, boulder clay (GW-GC, GC, SC)	Very dense	8 to 12	10
Gravel, gravel-sand mixture, boulder-gravel mixtures (GW, GP, SW, SP)	Very dense	6 to 10	7
	Medium dense to dense	4 to 7	5
	Loose	2 to 6	3
Coarse to medium sand, and with little gravel (SW, SP)	Very dense	4 to 6	4
	Medium dense to dense	2 to 4	3
	Loose	1 to 3	1.5
Fine to medium sand, silty or clayey medium to coarse sand (SW, SM, SC)	Very dense	3 to 5	3
	Medium dense to dense	2 to 4	2.5
	Loose	1 to 2	1.5
Fine sand, silty or clayey medium to fine sand (SP, SM, SC)	Very dense	3 to 5	3
	Medium dense to dense	2 to 4	2.5
	Loose	1 to 2	1.5
Homogeneous inorganic clay, sandy or silty clay (CL, CH)	Very stiff to hard	3 to 6	4
	Medium stiff to stiff	1 to 3	2
	Soft	0.5 to 1	0.5
Inorganic silt, sandy or clayey silt, varved silt-clay-fine sand (ML, MH)	Very stiff to hard	2 to 4	3
	Medium stiff to stiff	1 to 3	1.5
	Soft	0.5 to 1	0.5

(Modified after U.S. Department of the Navy, 1982)

8.4 PRESUMPTIVE BEARING PRESSURES

Where presumptive values must be used, they should be based on a reasonable knowledge of geological conditions at or near the site. Presumptive bearing pressures provide a quick (but least accurate) method of determining allowable bearing loads for foundations. This easy reference relates the allowable pressure to the soil type and to a qualitative description of its condition, termed consistency in place. Unless more accurate or appropriate regional data are available, the presumptive values given in Table 8–3 may be used. These are allowable bearing pressures and apply only at service limit states.

The procedure in this case is direct and simple. With the allowable bearing pressure determined by reference to data such as Table 8–3, the required footing size may be obtained merely by dividing the load by the bearing pressure. Although the procedure is quick and correlates footing size with actual load and an allowable pressure, in most cases it may essentially give inaccurate predictions. It is seldom expedient in engineering terms to make estimates of allowable bearing pressure based on the soil type and a qualitative description of its consistency. In this context, presumptive bearing values may sometimes yield overconservative designs or results that are unsafe. Reference to these values is convenient for preliminary estimates and rule-of-thumb designs.

8.5 BEARING PRESSURES FROM TESTS

The bearing resistance of foundation soils may be estimated from the results of in situ tests or by observing foundations on similar soils. If in situ tests are contemplated, interpretation of results should take local experience into consideration. There are two types of tests: standard penetration tests (SPT), and cone pressuremeter tests (CPT).

Standard Penetration Tests (SPT)

SPT blow counts are commonly used to estimate soil properties such as the undrained shear strength s_u of clays and the angle of friction ϕ of sands. These provide index parameters that may be introduced in the bearing-capacity equations to compute the ultimate bearing resistance. SPT blow counts may also be used to estimate bearing pressure directly. This involves the use of semi-empirical procedures. Meyerhof (1956) proposed the following equation

$$q_{ult} = \frac{\overline{N}B}{10}\left(C_{W1} + C_{W2}\frac{D_f}{B}\right)R_1 \tag{8–11}$$

where $\overline{N}$ = average value of corrected SPT blow count within the range of depth from footing base to 1.5 B below the footing; C_{W1}, C_{W2} = dimensionless correction factors for ground water effect, as specified in Table 8–4; R_1 = dimensionless reduction factor accounting for the effect of load inclination, as shown in Table 8–5; and the rest of the symbols correspond to the notation of Figure 8–5.

The value of $\overline{N}$ is determined in two steps. First, in saturated very fine sand the measured SPT blow count is corrected for submergence effects as follows:

$$N = 15 + 1/2\,(N' - 15) \quad \text{for} \quad N' > 15 \tag{8–12}$$

Table 8–4 Coefficients C_{W1} and C_{W2} for Various Ground Water Depths

D_W	C_{W1}	C_{W2}
$>1.5B + D_f$	1.0	1.0
D_f	0.5	1.5
0.0	0.5	0.5

where N' = measured SPT blow count.

The average value of N determined as explained is used in Equation (8–11) to obtain q_{ult}, and also in analyses of footing settlement.

Cone Penetration Tests (CPT)

This procedure has gained broad acceptance in the United States, probably because it provides a continuous record of resistance to penetration. A 10-cm^2 penetrometer is used and may be combined with conventional methods for drilling and sampling. Cone penetration resistance is the tip bearing pressure necessary to cause continuous penetration of the cone through the soil at a speed of 2 cm/sec. The tip resistance q_c is usually reported in kg/cm^2, which is the same value when converted to tons/ft^2.

Values of q_c are used to estimate soil properties such as s_u and ϕ to be subsequently entered into the bearing capacity equations. Alternatively, cone penetration resistance can be used directly to estimate ultimate bearing capacity through empirical correlations. A relationship between ultimate bearing capacity in sand and cone penetration resistance is given as (Meyerhof, 1956)

$$q_{ult} = \frac{q_c B}{40}\left(C_{W1} + C_{W2}\frac{D_f}{B}\right)R_1 \tag{8–13}$$

where q_c = average value of cone penetration resistance*; and the factors C_{W1}, C_{W2}, and R_1 are taken from Tables 8–4 and 8–5 to represent the effect of water table and inclination as before.

Awkati has correlated values of ultimate bearing capacity to cone penetration resistance in clays (Schmertmann, 1977). Recommended values are summarized in Table 8–6 for strip and square footing.

The data shown in Table 8–6 can be used for footings that are below the ground surface. For footings in clay, it is not necessary to make corrections for the position of the groundwater table.

Pressuremeter Tests (PMT)

This procedure is carried out by inflating a membrane within a drilled hole and then measuring the volume of expansion in terms of the applied pressure. This test is common and popular abroad, and appears to be gaining broader acceptance in the United States. It requires specialty contractors who also provide recommendations about the interpretation of the test results. Useful data on this subject are given by Briaud (1990).

*Measured within the range of depth from footing base to 1.5 B below the footing.

Table 8–5 Load Inclination Factor, R_1

(i) For Square Footings

	Load Inclination Factor, R_1		
H/V	$D_f/B = 0$	$D_f/B = 1$	$D_f/B = 5$
0.10	0.75	0.80	0.85
0.15	0.65	0.75	0.80
0.20	0.55	0.65	0.70
0.25	0.50	0.55	0.65
0.30	0.40	0.50	0.55
0.35	0.35	0.45	0.50
0.40	0.30	0.35	0.45
0.45	0.25	0.30	0.40
0.50	0.20	0.25	0.30
0.55	0.15	0.20	0.25
0.60	0.10	0.15	0.20

(ii) For Rectangular Footings

	Load Inclination Factor, R_1		
	Load Inclined in Width Direction		
H/V	$D_f/B = 0$	$D_f/B = 1$	$D_f/B = 5$
0.10	0.70	0.75	0.80
0.15	0.60	0.65	0.70
0.20	0.50	0.60	0.65
0.25	0.40	0.50	0.55
0.30	0.35	0.40	0.50
0.35	0.30	0.35	0.40
0.40	0.25	0.30	0.35
0.45	0.20	0.25	0.30
0.50	0.15	0.20	0.25
0.55	0.10	0.15	0.20
0.60	0.05	0.10	0.15

(iii) For Rectangular Footings

	Load Inclination Factor, R_1		
	Load Inclined in Length Direction		
H/V	$D_f/B = 0$	$D_f/B = 1$	$D_f/B = 5$
0.10	0.80	0.85	0.90
0.15	0.70	0.80	0.85
0.20	0.65	0.70	0.75
0.25	0.55	0.65	0.70
0.30	0.50	0.60	0.65
0.35	0.40	0.55	0.60
0.40	0.35	0.50	0.55
0.45	0.30	0.45	0.50
0.50	0.25	0.35	0.45
0.55	0.20	0.30	0.40
0.60	0.15	0.25	0.35

(From Meyerhof, 1956)

Table 8–6 Correlation between Cone Penetration Resistance and Ultimate Bearing Capacity in Clays

	Value of q_{ult} (t/ft^2)	
q_c (*kg/cm^2 or t/ft^2*)	*Strip Footing*	*Square Footing*
10	5	9
20	8	12
30	11	16
40	13	19
50	15	22

(From Awkati).

The bearing resistance of foundation soils may be determined from results of pressuremeter tests as

$$q_{ult} = r_o + \kappa(P_l - P_o) \tag{8–14}$$

where r_o = initial total vertical pressure at foundation level; κ = empirical bearing capacity coefficient, taken from Figure 8–9; P_l = limit pressure measured in the pressuremeter test; and P_o = total horizontal pressure at depth where the test is performed. Equation (8–14) is an empirical relationship suggested by Menard (1965), Baguelin, Jazequel, and Shields (1978), and Briaud (1990).

Any consistent pressure units can be used in the calculations. An average value of limit pressure is taken over the range of depth from $1.5B$ above to $1.5B$ below the foundation level. Where the values of P_l vary considerably within a depth B above or below the foundation level, special averaging procedures are recommended (Baguelin et al., 1978).

8.6 BEARING RESISTANCE OF ROCK

Geotechnical Considerations

The bearing capacity and settlement of footings on rock is influenced by the presence, orientation, and condition of discontinuities, weathering profiles and other similar profiles as they apply at a given site, and the degree to which they must be considered in the analysis.

For footings placed on competent rock, reliance may be based on simple and direct analyses that have their origin in the uniaxial compressive strength and rock quality designation (RQD). Competent rock may be defined as a rock mass with tight discontinuities or with openings not wider than 1/8 in. For footings on less competent rock, more extensive investigations are necessary to assess the effects of weathering, and the presence and condition of discontinuities.

Bearing Capacity

Competent rock. The allowable bearing (contact) pressure for footings on level surfaces of competent rock may be determined as proposed by Peck, Hanson, and Thornburn (1974), shown in Figure 8–10. The RQD used in these data should be the av-

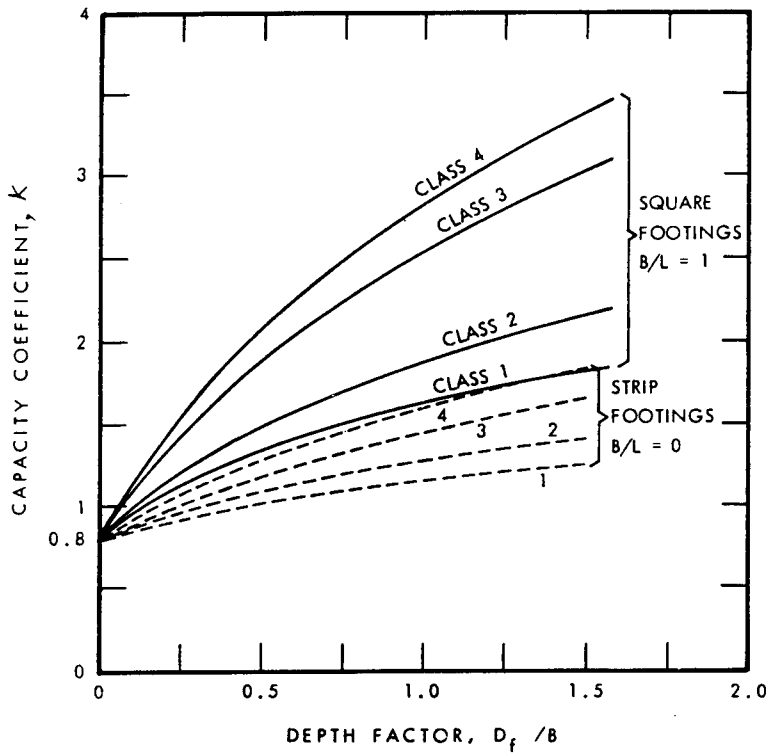

Soil Type	Consistency or Density	$(P_\ell - P_o)(t/ft^2)$	Class
Clay	Soft to Very Firm	< 12	1
	Stiff	8-40	2
Sand and Gravel	Loose	4-8	2
	Very Dense	30-60	4
Silt	Loose to Medium	< 7	1
	Dense	12-30	2
Rock	Very Low Strength	10-30	2
	Low Strength	30-60	3
	Medium to High Strength	60-100	4

Figure 8–9 Values of empirical capacity coefficient, κ *(from Canadian Foundation Engineering Manual, 1985).*

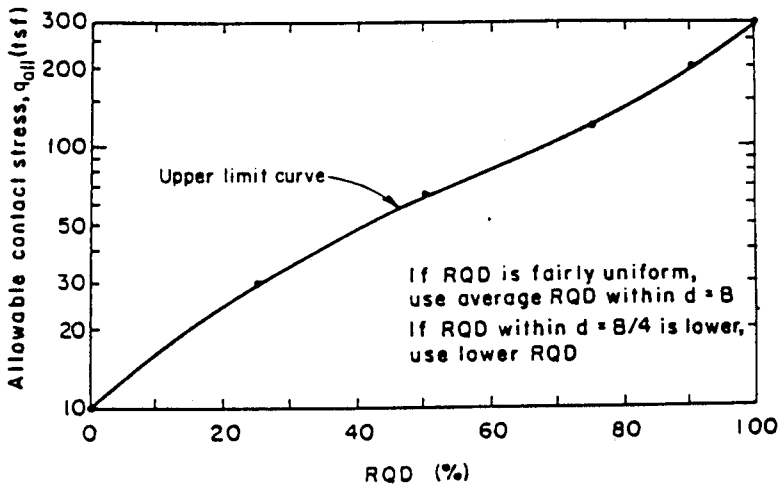

Note:
q_{all} shall not exceed the unconfined compressive strength of the rock or 0.595 $f'c$ of the concrete.

Figure 8–10 Allowable contact stress for footings on rock with tight discontinuities *(from Peck et al., 1974).*

erage RQD for the rock within a depth of B below the footing level, if the RQD values are essentially uniform within that depth. If rock within a depth of $0.5B$ below the base of footing has a lower quality, the RQD of the less competent rock should be used in the analysis. The maximum allowable contact pressure should not exceed the allowable bearing stress in the concrete.

Broken or jointed rock. For footings on broken or jointed rock, the bearing resistance may be determined from empirical correlations with the Geomechanics Rock Mass Rating (RMR) proposed by the Norwegian Geotechnical Institute, Rock Mass Classification System (Barton, Lein, and Linde, 1974), and as developed by Carter and Kulhawy (1988) and modified by Hoek (1983). The procedure is based on the unconfined compressive strength of the intact rock core sample. Depending on rock mass quality, measured in terms of RMR or NGI systems, ultimate bearing capacity varies from a small fraction to six times the unconfined compressive strength of intact rock core samples.

Analytically, the ultimate bearing capacity of footing on broken or jointed rock may be estimated from the relationship

$$q_{ult} = N_{ms} C_o \tag{8–15}$$

where N_{ms} = a coefficient, and C_o = uniaxial compressive strength of intact rock. Values of N_{ms} are given in AASHTO Table 4.4.8.1.2A. Values of C_o should be determined from results of laboratory tests of rock core samples obtained within $2B$ of the base of footing. Where the rock strength within this depth zone varies, the rock with the lowest capacity should be used. Alternatively, AASHTO Table 4.4.8.1.2B may be used to determine C_o. If the rock is of poor quality, the value of q_{ult} should be determined as the value of q_{ult} of an equivalent soil mass.

8.7 FAILURE BY SLIDING

Failure of footings by sliding is essentially subject to the same considerations as the stability of walls against sliding discussed in section 6.6. For foundations in clay, the possible presence of a shrinkage gap between the soil and the foundation should be considered. If passive resistance is included as part of the solution to resist sliding, consideration should be given to possible future removal of the soil in front of the foundation. For footings on cohesionless soils, sliding resistance is influenced by the roughness of the interface between the foundation and the soil. Sliding will occur if the shear strength at any point of the assumed slip surface (commonly taken as the foundation-soil interface) is less than the shear stress applied on the same slip surface under service loads.

For footing on soils with $\phi - c$ characteristics, the sliding resistance is expressed in Equation (6–19) in section 6.6, and is rewritten here in a different form as

$$Q_R = Q \tan \delta + c_a B \tag{8–16}$$

where Q_R = resistance to sliding of the footing, and Q, δ, c_a, and B are as before. If the soil beneath the foundation is sand and the base of the footing is rough (this is the usual case for concrete placed directly on soil), the full shear resistance of the soil will be mobilized so that $\tan \delta = \tan \phi$. For precast concrete footings, the coefficient of friction may be taken as $\tan \delta = 0.8 \tan \phi$, since in this case the footing will be relatively smooth.

If the foundation soil is clay, consideration should be given to the possibility of sliding by shear within a zone of clay beneath the footing, if this is a weaker plane. The sliding resistance in this case may be taken as the lesser of (1) the cohesion of the clay, or (2) one-half the normal stress on the interface between footing and soil. If the concrete is wet, the cohesion of the clay may be reduced to 0.5 + 0.7 times the undrained shear strength.

8.8 AASHTO AND LRFD REQUIREMENTS

AASHTO Requirements (Standard Specifications)

Footing excavations. In granular soils with relatively high permeability, footing excavations below the groundwater table should be made such that the hydraulic gradient in the excavation bottom is not increased to a level that could cause loosening or softening of the soil because of upward water flow. Furthermore, the excavations should be made such that hydraulic gradients and the removal of material has no adverse effect on adjacent structures.

Footing excavations in nonresistant, weathered moisture-sensitive rocks should be protected immediately after excavation with a lean concrete mix or other suitable materials.

Anchorages. Where footings are placed on inclined smooth rock surfaces that are not restrained by an overburden of resistant material, they should be anchored using rock anchors, bolts, dowels, keys, benching, or other suitable means. Shallow keys or benching of large footing areas should not be provided where rock removal may require blasting.

Eccentricity. In order to keep the footing pressure as uniform as possible, AASHTO stipulates that the location of resultant of pressure R on the base of the footing should be maintained preferably within $x/6$ of the footing dimension x in any direction. This criterion does not relate to the bearing capacity of the soil, but is rather intended to ensure as uniform a settlement as possible.

Factors of safety. Spread footings on soil should be designed for Group I (ASD) loading with a minimum factor of safety of 3.0 against a bearing capacity failure. The same criterion applies for spread footing on rock.

Dynamic ground stability. AASHTO articulates the requirements of design for dynamic ground stability by referring to the specifications for seismic analysis.

Footings on rock. Spread footings on rock should be designed to support the design loads with adequate bearing and tolerable settlement. The location of the resultant pressure R on the base of the footing should preferably be within $B/4$ of the center of the footing.

LRFD Specifications

Service limit states. Service limit states for foundation design include (a) settlements, (b) lateral displacements, and (c) bearing resistance estimates from presumptive bearing pressures. The limit state for settlement should be based on ridability and economy, where the cost of limiting foundation movement is compared to the cost of designing the superstructure so that it can tolerate larger movement, or to the cost of correcting the consequences of movement through maintenance.

Strength limit states. These include (1) bearing resistance failure, (2) excessive loss of contact, (3) sliding at the base of footing, (4) loss of overall stability, (5) structural capacity, and (6) loss of lateral support.

Foundations should be proportioned such that the factored resistance is not less than the effects of factored loads specified in other sections (see also Tables 2–18 and 2–19). For expediency, we repeat the design equation for LRFD as follows:

$$\phi R_n \geq \Sigma_{\gamma i} Q i \tag{8–17}$$

It should be noted that the tables for load factors do not list recommended values for γ or β for water pressure. If the water pressure is evaluated for the worst possible water level, it seems reasonable to use unfactored water calculations in LRFD analyses.

At present, load factor (strength design) methods for foundation analysis and design are not provided for in the standard AASHTO specifications. Although this excludes direct correlation between the two documents, the LRFD load and resistance factor approach may be used in conjunction with AASHTO loads and loading groups.

Resistance factors. Resistance factors for shallow foundations (footings) at both strength and service limit states are given in Table 8–7. Where statistical information was available, reliability theory combined with judgment was used to derive these values. In cases where there was insufficient information for calibration using reliability theory, values of resistance factors were chosen based on judgment so that design based on LRFD can be consistent with ASD procedures.

Table 8–7 Resistance Factors for Strength Limit State for Shallow Foundations, LRFD Specifications

	Method/Soil/Condition	Resistance Factor
Bearing Capacity and Passive Pressure	Sand	
	– Semi-empirical procedure using SPT data	0.45
	– Semi-empirical procedure using CPT data	0.55
	– Rational Method—	
	using ϕ_f estimated from SPT data	0.35
	using ϕ_f estimated from CPT data	0.45
	Clay	
	– Semi-empirical procedure using CPT data	0.50
	– Rational Method	
	using shear resistance measured in lab tests	0.60
	using shear resistance measured in field vane tests	0.60
	using shear resistance estimated from CPT data	0.50
	Rock	
	– Semi-empirical procedure, Carter and Kulhawy (1988)	0.60
	Plate Load Test	0.55
Sliding	Precast concrete placed on sand	
	using ϕ_f estimated from SPT data	0.90
	using ϕ_f estimated from CPT data	0.90
	Concrete cast-in-place on sand	
	using ϕ_f estimated from SPT data	0.80
	using ϕ_f estimated from CPT data	0.80
	Sliding on clay is controlled by the strength of the clay when the clay shear is less than 0.5 times the normal stress, and is controlled by the normal stress when the clay shear strength is greater than 0.5 times the normal stress (see Figure 1, which is developed for the case in which there is at least 6.0 IN of compacted granular material below the footing).	
	Clay (where shear resistance is less than 0.5 times normal pressure)	0.85
	using shear resistance measured in lab tests	0.85
	using shear resistance measured in field tests	0.80
	using shear resistance estimated from CPT data	0.85
	Clay (where the resistance is greater than 0.5 times normal pressure)	
	Soil on soil	1.0
	Passive earth pressure component of sliding resistance	0.50
Overall Stability	Where soil or rock properties and groundwater levels are based on laboratory or in-situ testing, shallow foundations on or near a slope evaluated for overall stability and resistance to a deep-seated failure mode	0.85

8.9 SETTLEMENT OF FOOTINGS IN SOIL, METHODS OF ANALYSIS

The Settlement Problem

The settlement of bridge foundations is particularly relevant since it will affect function and ridability as well as structural performance. The design of footings must, therefore, address two issues: (1) estimate the amount of settlement that the structure can tolerate, and (2) predict the amount of settlement that the footing will undergo as a result of loading the soil.

Soil settlement computations are, with the exception of occasional successful predictions, only best estimates of deformation expected to occur when the loads are applied. During the settlement process, the soil undergoes a transition from its initial body to a new state of stress under the additional load. The stress increment Δq produces a time-dependent accumulation of particle rolling, sliding, crushing, and elastic distortions in the soil system within a limited influence zone beneath the loaded area.

The principal components of the vertical movement are particle rolling and sliding producing a change in the void ratio, crushing that alters the material, and elastic deformation (usually a small fraction). As a result, if the applied stress is removed, only a little portion of the settlement will be recovered as elastic rebound. It is however, convenient to treat the soil as a pseudoelastic material to estimate settlements, an approach that appears reasonable since larger stress changes produce larger settlements.

Settlements may be classified as (1) immediate, or those that take place as the load is applied or shortly thereafter; and (2) consolidation, that occurs as time dependent over a period of months or years. Alternatively, and for the purpose of analysis, the total settlement may be considered as the sum of elastic, consolidation, and secondary components, and may be determined from

$$S_t = S_e + S_c + S_s \tag{8–18}$$

where S denotes settlement and the subscripts t, e, c, and s denote total, elastic, consolidation and secondary, respectively. Note the Equation (8–18) is also AASHTO Eq. (4.4.7.2–1).

Elastic settlement should be determined using the unfactored dead load plus the unfactored live and impact load assumed to extend to the footing level. Consolidation and secondary settlement may be estimated using the unfactored dead load only.

Approximate stress distribution in soil mass. Figure 8–11 shows an assumed pressure distribution due to the load Q introduced by a footing. The notation corresponds to the same symbols shown in Figure 8–5. There are several methods currently used to estimate the increased pressure at some depth below the loaded area, and a simple procedure is to assume the 2:1 slope as shown in Figure 8–11. If the stress zone is defined in this manner the pressure increase $q_u = \Delta q$ at depth z due to load Q is

$$q_u = \frac{Q}{(B+z)(L+z)} \tag{8–19}$$

which for a square footing is reduced to

$$q_u = \frac{Q}{(B+z)^2} \tag{8–20}$$

This approximation will give satisfactory comparisons with theoretical predictions from $z = B$ to about $4B$, but should not be used in the depth zone $z = 0$ to B.

Settlement of Footings in Sand from Standard Penetration Tests

Terzaghi and Peck procedure. This method, developed by Terzaghi and Peck (1967) has been widely used but is considered conservative in the sense that it often overestimates settlement. Recent studies by Tan and Duncan (1991) show that in many instances settlements estimated using the Terzaghi-Peck method are larger than the ac-

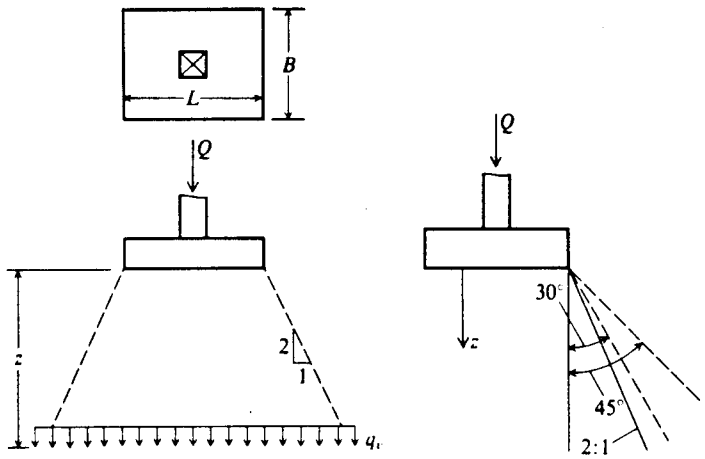

Figure 8–11 Approximate methods of obtaining the stress increase q_r in the soil at a depth z beneath the footing.

tual settlements. It appears that this method is reliable in the sense that it seldom underestimates settlement, but at the same time the results are not highly accurate. Since settlements of footing in sand are usually erratic, it follows that procedures that seldom underestimate settlements will tend to give overestimations. This approach, however, is often taken as a convenient compromise between accuracy and reliability.

The Terzaghi-Peck method may be used in the graphical form shown in Figure 8–12. The graphs are derived from the assumption of 1-in tolerable settlement. For a given width of footing and SPT blow count, the bearing pressure is obtained directly from the charts, and corresponds to 1-in settlement. If settlements other than 1-in provide the design criterion, the corresponding bearing pressures can be estimated by noting that settlements are very nearly proportioned to bearing pressures.

The value of N used in estimating the bearing pressure from these graphs should be the average value measured in all borings, within the range of depth from the footing base equal to B = footing width. Figure 8–12 can be used directly when the groundwater table is at a depth below the bottom of footing at least $2B$. For higher groundwater levels, the bearing pressure obtained from Figure 8–12 should be reduced as follows: (1) for shallow foundations with $D_f/B < \frac{1}{2}$, the pressures should be reduced by 50 percent; (2) for deeper foundations with $D_f/B = 1$, the pressures should be reduced by 30 percent.

If the groundwater level is between a depth $2B$ and the ground surface, the bearing pressure should be reduced by an amount between zero and 50 percent for shallow footings ($D_f/B < \frac{1}{2}$); for deeper foundations ($D_f/B \approx 1$) the bearing pressure should be reduced by an amount between zero and 30 percent.

According to Bazaraa (1967), the relationship between bearing pressure p_q footing width B and N values may be expressed analytically as

$$p_q = p_s \frac{N}{3}\left(\frac{B+1}{2B}\right)^2 \tag{8–21}$$

where p_q = bearing pressure corresponding to a given magnitude of settlement; p_s = settlement (in), and B = footing width (ft). Pressures calculated from Equation (8–21) should likewise be reduced for groundwater effects.

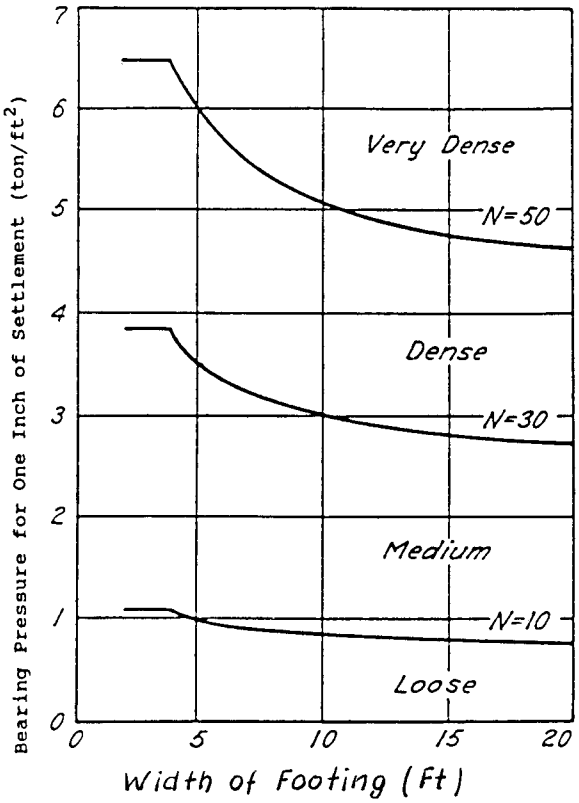

Figure 8–12 Bearing pressure for one inch of settlement of footings on sands *(from Terzaghi and Peck, 1967).*

Example. The minimum average N at a bridge site is 12. For a column footing with B = 11 feet, the bearing pressure corresponding to one-inch settlement is found graphically from Figure 8–12 as 1.0 ton/ft^2 if groundwater effects are absent. If the groundwater table can rise to the ground surface and the footing is shallow (D_f < 5.5 ft), the bearing pressure corresponding to one-inch settlement is 50 percent less, or 0.5 ton/ft^2. The bearing pressure causing a three-inch settlement should be about 2.0 tons/ft^2 if groundwater effects are not present, and about 1.0 ton/ft^2 with the water table at the surface.

D'Appolonia method. This method (D'Appolonia, D'Appolonia, and Brisette, 1970) uses the SPT blow count, but it is also based on elastic theory. The N values are used to estimate in situ soil compressibility. For footings on sand, the settlement is found from

$$p_s = \mu_0 \mu_1 \frac{p_a B}{M} \tag{8–22}$$

where p_s = settlement of footing (same length units as B); μ_0, μ_1 = settlement influence factors that depend on footing geometry, embedment depth, and depth to the relatively incompressible layer (dimensionless); p_a = average applied pressure under service loads; B = footing width; and M = modulus of compressibility.

Values of μ_0 and μ_1 are given in Figure 8–13. The modulus of compressibility M and the average SPT blow count may be correlated by referring to Figure 8–14. The value of SPT blow count used to estimate M is the average value within the range of

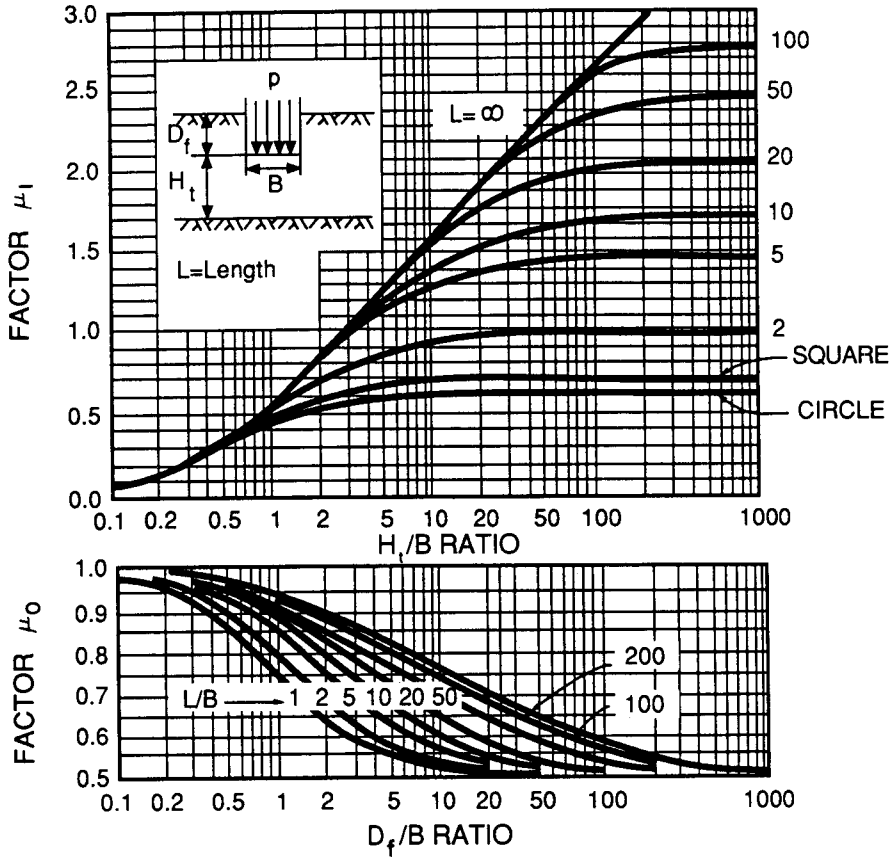

Figure 8–13 Settlement influence factors μ_0 and μ_1 for the D'Appolonia procedure *(from D'Appolonia et al., 1970).*

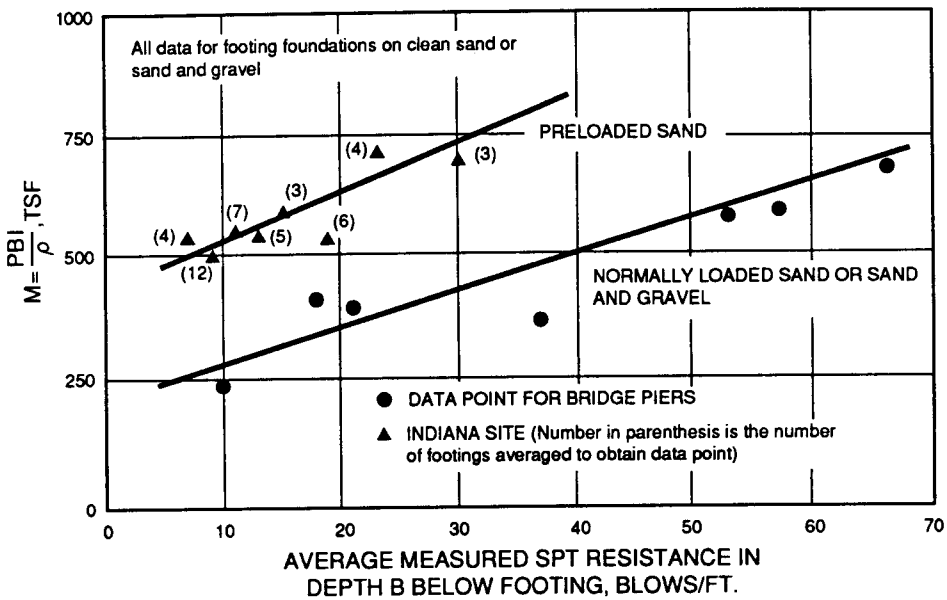

Figure 8–14 Correlation between modulus of compressibility and average value SPT blow count *(from D'Appolonia et al., 1970).*

depth from the footing level to depth B below that level. These investigators tend to agree with Meyerhof (1953, 1956, 1957) that the effect groundwater presence on soil modulus is reflected in the measured SPT blow count, hence no correction for groundwater effect is necessary.

Equation (8–22) can be rearranged to give the bearing pressure p_a in terms of a given settlement p_s, or

$$p_a = \frac{1}{\mu_0 \mu_1} \frac{p_s M}{B} \tag{8–23}$$

where all symbols are as previously.

The validity of the D'Appolonia method appears to be confirmed in studies reported by Tan and Duncan (1991), particularly with respect to the level of accuracy provided. More explicitly, the average settlements estimated using this method were about equal to the average values of actual settlements observed for a large number of footings.

Settlement of Footings in Sand from Cone Penetration Tests

Estimates of settlements of footings in sand using cone penetration test results may be made as proposed by Schmertmann (1970, 1977) who has also developed methods for computing elastic settlements. The CPT method has a rational basis, and uses the cone penetration resistance q_c as a measure of in situ soil compressibility.

The expression for calculating settlement of footings in sand is

$$p_s = C_p C_t \Delta p \Sigma \left(\frac{I_z}{E_s} \Delta Z \right) \tag{8–24}$$

where p_s = settlement; C_p = pressure change correction factor for initial overburden pressure (Table 8–8); C_t = time rate factor (or creep correlation factor), from Table 8–9; Δp = net increase in bearing pressure at foundation level; I_z = settlement influence factor that varies with depth and L/B ratio (from Figure 8–15 and Table 8–10); E_s = in situ soil modulus; and ΔZ = thickness of sublayer. The in situ modulus can be correlated with the value of cone resistance q_c.

Figure 8–15 shows the variation of settlement influence factor I_z with depth. The

Table 8–8 Pressure Change Correction Factor, C_p

$\frac{\sigma_{vo}'}{\Delta p}$	C_p
0.0	1.0
0.2	0.9
0.4	0.8
0.6	0.7
0.8	0.6
≥1.0	0.5

Note: σ_{vo}' = initial vertical pressure at level of bottom of footing (in pressure units)
Δp = average net bearing pressure at foundation level (same pressure units as σ_{vo}')

Table 8–9 Time Rate Factor, C_t for Settlements of Cohesionless Soils

Time	c_t
1 month	1.0
4 months	1.1
1 year	1.2
3 years	1.3
10 years	1.4
30 years	1.5

values of the parameters that define the dimensions of the settlement influence diagrams are given in Table 8–10.

For square footings, the in situ soil modulus E_s may be estimated from the expression

$$E_s = 2.5\, q_c \tag{8–25}$$

where q_c = cone penetrating resistance

For footings with $L/B \geq 10$ the soil deforms in a condition closer to plane strain, and the soil is stiffer because of the increased confinement. For these long footings the expression for estimating E_s is

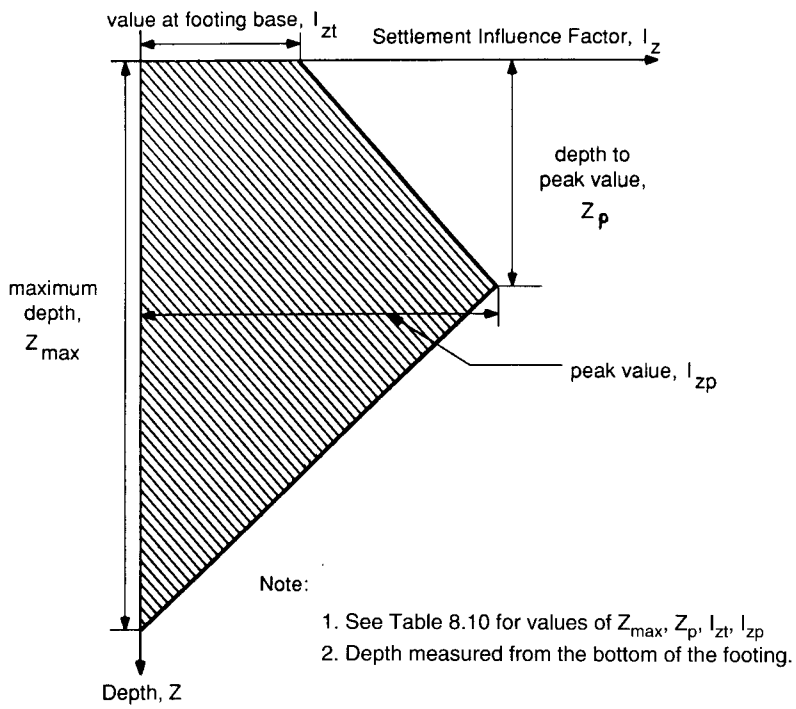

Figure 8–15 Variation of Schmertmann's improved settlement influence factors with depth *(from Schmertmann et al., 1977).*

Table 8–10 Coefficients to Define the Dimensions of Schmertmann's Improved Settlement Influence Factor Diagram in Figure 8–15

L/B	Max. Depth of Influence Z_{max}/B	Depth to Peak Value Z_p/B	Value of I_Z at top I_{Zt}	Peak Value of Stress Influence Factor I_{Zp}			
				$\frac{\Delta p}{\sigma_{vp}'} = 1$	$\frac{\Delta p}{\sigma_{vp}'} = 2$	$\frac{\Delta p}{\sigma_{vp}'} = 4$	$\frac{\Delta p}{\sigma_{vp}'} = 10$
1	2.00	0.50	0.10	0.60	0.64	0.70	0.82
2	2.20	0.55	0.11	0.60	0.64	0.70	0.82
4	2.65	0.65	0.13	0.60	0.64	0.70	0.82
8	3.55	0.90	0.18	0.60	0.64	0.70	0.82
≥ 10	4.00	1.00	0.20	0.60	0.64	0.70	0.82

Note: B = footing width
L = footing length
$\Delta p = \sigma_{vf}' - \sigma_{vo}'$ = net bearing pressure
σ_{vf}' = final vertical pressure at level of bottom of footing
σ_{vo}' = initial vertical pressure at level of bottom of footing
σ_{vp}' = initial vertical pressure at depth of peak influence

(From Schmertmann, et al., 1977).

$$E_s = 3.5\, q_c \tag{8–26}$$

For footings with L/B ratios between 1 and 10, the $E_s - q_c$ relationship may be estimated by interpolation.

The foregoing method can account for the variation in sand density and compressibility with depth. If the ground stratigraphy is heavily layered, the soil beneath the foundation level is divided into several sublayers, chosen so that the values of cone resistance within each sublayer are essentially constant. The value of the settlement influence factor for each sublayer is evaluated at midheight of the sublayer. Since the value of settlement influences factor peaks at some depth below the foundation level Z_p, it is necessary that a sublayer boundary occurs at Z_p.

The computational procedure is rather lengthy and warranted only when the site is characterized by extensive layering. If the soil profile shows sand layers of limited thickness overlying firm soil or rock, the influence diagram is terminated at the top of the firm layer. For homogeneous soil, the process is simplified since it is not necessary to divide the soil profile into sublayers. For homogeneous conditions, the settlement may be computed as follows

$$p_s = I' C_p C_t \left(\frac{\Delta_p}{q_c}\right) B \tag{8–27}$$

where I' = equivalent settlement influence factor from Table 8–11, and other terms are as previously.

By rearranging Equation (8–27), we can obtain an expression for estimating the pressure required to cause a given settlement, or

$$\Delta p = p_s \frac{q_c}{BI'} \frac{1}{C_p C_t} \tag{8–28}$$

This expression is convenient if the tolerable settlement is known and it is necessary to estimate the corresponding bearing pressure.

Table 8–11 Values of Equivalent Settlement Influence Factor

	Equivalent Settlement Influence Factor, I′			
L/B	$\frac{\Delta p}{\sigma_{vp}'} = 1$	$\frac{\Delta p}{\sigma_{vp}'} = 2$	$\frac{\Delta p}{\sigma_{vp}'} = 4$	$\frac{\Delta p}{\sigma_{vp}'} = 10$
1	0.25	0.27	0.29	0.34
2	0.27	0.28	0.31	0.36
4	0.30	0.32	0.35	0.40
8	0.35	0.37	0.40	0.46
≥ 10	0.37			

The Tangent Modulus (Janbu) Method for Settlement of Footings in Sand, Silt, and Clay

Janbu (1963, 1967) has developed an approach for estimating settlement of footings in soils using tangent modulus values to articulate soil compressibility. The soil beneath the footing is divided into a number of sublayers, each characterized by a value of constraint tangent modulus M_t. The settlement is estimated as the sum of reductions in thickness of each of the sublayers, and is expressed as

$$p_s = \Sigma\left(\frac{\Delta\sigma' v}{M_t} \cdot \Delta Z\right) \tag{8–29}$$

where p_s = settlement; $\Delta\sigma_v'$ = increase in effective stress with the sublayer due to footing load; M_t = tangent value of constrained modulus of the soil; and ΔZ = sublayer thickness.

The constrained tangent modulus will vary with the soil type, its density, whether it is normally consolidated or overconsolidated, and the stress history before and after the load is applied. Values of M_t can be obtained in conventional laboratory tests (Tan and Duncan, 1991). The pressures used in these tests should cover the range from the initial pressure (before the load is applied) to the final pressure (with the load applied). The parameter M_t is determined by dividing the stress increment in the sublayer, $\Delta\sigma_v' = \sigma_{vf}' - \sigma_{vo}'$, by the corresponding strain $\Delta\epsilon_v$, as shown in Figure 8–16. When laboratory tests are not contemplated for estimating M_t, good values may be obtained from Table 8–12 in conjunction with the following expressions:

For sands and silts, values of M_t may be estimated from

$$M_t = mp_{at}\left(\frac{\sigma_{va}'}{p_{at}}\right)^{0.5} \tag{8–30}$$

where m = dimensionless modulus number shown in Table 8–12; σ_{va}' = average vertical stress = $1/2(\sigma_{vo}' + \sigma_{vf}')$; and p_{at} = atmospheric pressure.

For normally consolidated clays, values of M_t may be estimated from

$$M_t = m\sigma_{va}' \tag{8–30a}$$

where m = dimensionless modulus number shown in Table 8–12, and σ_{va}' = average vertical stress as previously.

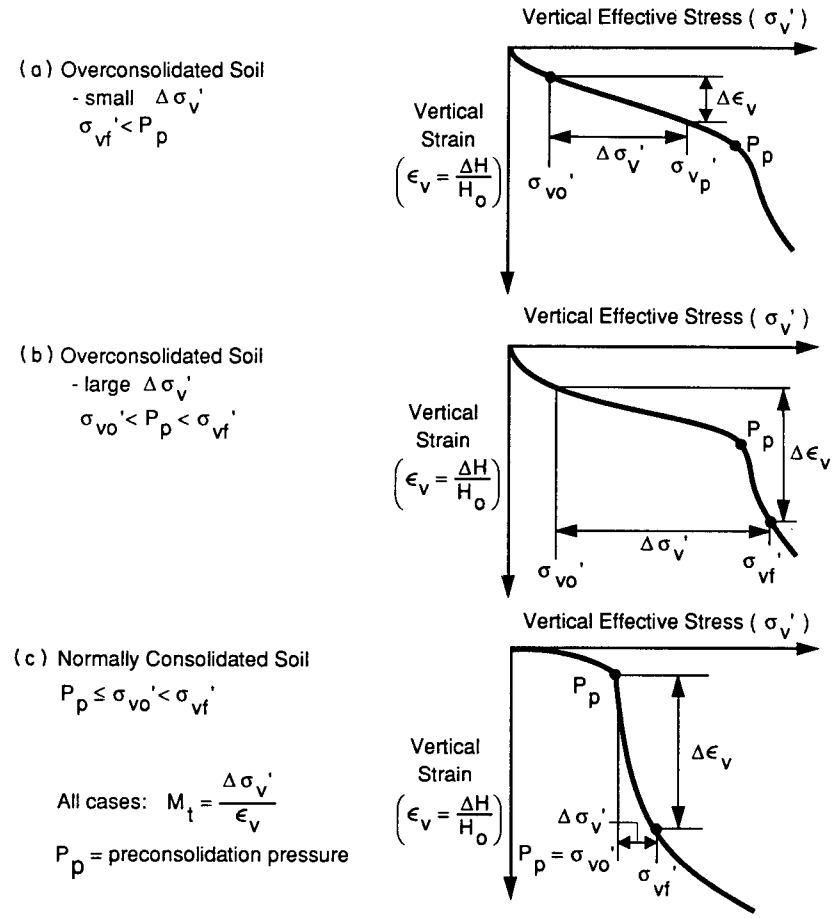

Figure 8–16 Determination of M_t from results of laboratory consolidation tests.

From Figure 8–16 and Table 8–12 it is apparent that values of M_t are higher for overconsolidated soils ($p_p > \sigma'_{vo}$). When the final pressures do not exceed the preconsolidation pressure ($\sigma'_{vf} < p_p$), the soil is being reloaded and the value of M_t is higher than where $\sigma'_{vf} < p_p$.

Settlement of Footings in Soil By Elastic Methods

Since the elastic settlement is essentially

$$\Delta H = \int_o^H \epsilon\,(dh) = \sum_{i=1}^{n} \epsilon_i H_i \tag{8–31a}$$

where ϵ_i = strain at layer H_i, any method that gives the strain in the appropriate sublayer may be used to estimate settlement.

Steinbrenner (1934) and Giroud (1972) have proposed the following equation for estimating settlement

Table 8–12 Values of Modulus Number, m, for Sands, Silts, and Clays

Sand	Relative Density (Dr)	$\sigma_{vo}' = p_p$	Value of m $\sigma_{vo}' < p_p < \sigma_{vf}'$	$\sigma_{vf}' < p_p$
	30% (Loose)	80–160	120–300	240–500
	50% (Medium)	120–240	200–400	350–700
	70% (Dense)	200–400	300–700	600–1200
Silt	**Porosity (N)**	$\sigma_{vo}' = p_p$	Values of m $\sigma_{vo}' < p_p < \sigma_{vf}'$	$\sigma_{vf}' < p_p$
	50%	25–50	40–200	120–240
	40%	60–120	80–400	300–600
	30%	100–200	150–700	500–1000
Clay	**In Situ Water Content**	$\sigma_{vo}' = p_p$	Value of m $\sigma_{vo}' < p_p < \sigma_{vf}'$	$\sigma_{vf}' < p_p$
	70%	6–12	10–80	60–120
	50%	9–18	15–120	90–180
	30%	15–35	25–200	150–350

Pp = preconsolidation pressure = highest pressure to which the soil has been subjected in the past.

(From Janbu, 1985).

$$p_f = \frac{p_b B}{E_s} I_p \tag{8–32}$$

where p_f = final (elastic) settlement; p_b = average bearing pressure; E_s = in situ soil modulus; I_p = dimensionless settlement influence factor depending on footing geometry, thickness of compressible layer, and Poisson's ratio; and B = width of footing. For estimating settlement of footings in sand and clay for drained conditions, Poisson's ratio ν may be taken as 0.3. In this case values of I_p for $\nu = 0.3$ may be taken from the graphs of Figure 8–17. The accuracy of this method depends on the accuracy with which the soil modulus is estimated. If settlement observations on similar soils are available, the soil modulus can be back-calculated from these data.

Another method is proposed by Schmertmann (1970) where the change in the Boussinesq pressure bulb (see AASHTO Fig. 4.4.7.2.1A) is interpreted as related to strain. Since the pressure bulb changes more rapidly from about 0.4 to 0.6B, this depth range is interpreted to have the largest strains. The same investigator also proposed using a triangular relative-strain diagram to model this strain distribution with ordinates 0.06 and 0 at B, 0.5B, and 2B. The area of the diagram is correlated with the settlement, and for constant E_s the settlement may be computed directly as the area of the triangle times the strain, or

$$\Delta H = 0.6B \frac{\Delta_q}{E_s} = 0.6B \in \tag{8–33}$$

where all symbols correspond to the notation of Equation (8–31). Schmertmann also incorporated two correction factors for embedment depth and time.

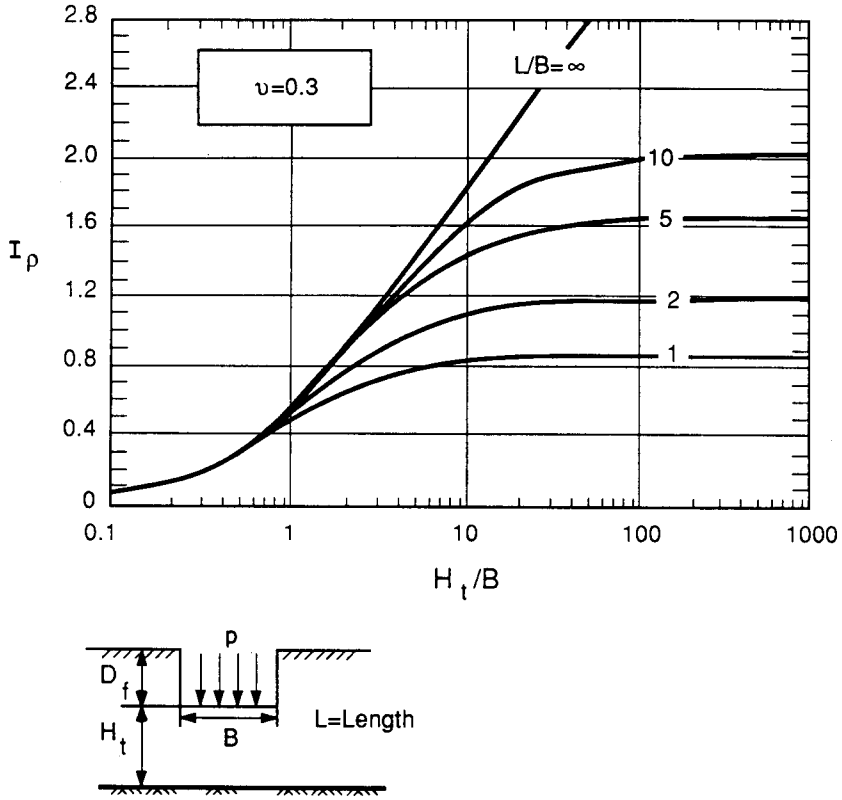

Figure 8–17 Settlement influence factor from Steinbrenner's approximation for $\nu = 0.3$ *(from Taylor and Matyas, 1983).*

Consolidation Settlement

Clays. Settlements resulting from consolidation of normally consolidated and lightly overconsolidated clays can be considerable. For fine-grained, saturated cohesive soils the settlement is time dependent; where such soils are loaded by fills, settlements as large as several feet may occur. Highly compressible clays are rarely suitable for bridge foundations since the tolerable settlement is usually limited to a small fraction of the anticipated settlement.

When consolidation theory is used to estimate settlement in clays, the following factors must be considered: (1) whether the clay is normally consolidated or preconsolidated (OCR > 1); (2) obtaining the in situ void ratio e_o and sufficient compression indices to profile the clay layers; and (3) estimating the average stress increase Δq in a layer of thickness H. These considerations are refined in the current AASHTO procedures for estimating settlement of footings on saturated or nearly saturated cohesive soils, and address initially overconsolidated soils, or initially normally consolidated soils. A distinction is also made between laboratory test results expressed in terms of the void ratio, or in terms of vertical strain.

Time dependent settlement in sand. Footings in sand continue to settle but at a slow and decreasing rate. The time rate factor is included in Schmertmann's method, and is

identified in Equations (8–24) and (8–27). A similar allowance for increased settlement with time may be used with other methods. A general expression in this case is

$$p_{st} = p_{si}C_t \tag{8–34}$$

where p_{st} = settlement at time t; p_{si} = settlement initially computed; and C_t = time rate factor obtained from Table 8–9.

Secondary Settlement

Footings in clay continue to settle at a slow and decreasing rate after the clay undergoes its initial compression. This process is termed secondary compression, and the associated settlement may be computed from

$$p_{sc} = C_a H_t \log \frac{t_{sc}}{t_p} \tag{8–35}$$

where p_{sc} = settlement due to secondary compression; C_a = coefficient of secondary compression (obtained from Table 8–13); H_t = total thickness of layer undergoing secondary compression; t_{sc} = time for which secondary compression is calculated; and t_p = time for primary compression (not less than one year). Equation (8–35) is essentially the same as AASHTO Eq. (4.4.7.2.4–1) but with a different notation.

Reliability of Settlement Analysis

The methods presented for estimating immediate (elastic) settlement of footings in soil may be used independently or as an adjunct to the procedures recommended by AASHTO. Factors that may influence settlement are embankment loading, lateral or eccentric loading, vibration loading from dynamic live loads or earthquakes, and so on.

For design purposes, consideration should be given to the total settlement expressed in Equation (8–18), and made up of elastic (immediate), consolidation, and secondary compression components. In cohesionless soils and unsaturated clays the immediate settlement predominates with perhaps some creep (secondary compression). Results of computations of immediate settlement may vary, but with some judgment these can converge to reasonably satisfactory predictions. Consolidation theory tends to predict settlement rather well, provided that representative soil samples are obtainable. However, the time rate for consolidation settlement is not well predicted, and this is because the coefficient of permeability is a significant factor.

Studies by Tan and Duncan (1991) have compared measured settlement with settlement calculated using the various procedures reviewed in the foregoing sections. These show that methods that result in settlements close to the average of measured

Table 8–13 Values of C_a for Clays

Natural Water Content of Clay	Value of C_a	
	For OCR = 1	*For OCR ≥ 5*
10%	0.001	0.0003 to 0.0005
20%	0.002	0.0006 to 0.0010
40%	0.004	0.0012 to 0.0020
80%	0.008	0.0025 to 0.0040

Table 8–14 Values of Adjustment Factor for 50 Percent and 90 Percent Reliability in Displacement Estimates

Method	Soil Type	Adjustment Factor	
		For 50% Reliability	*For 90% Reliability*
Terzaghi and Peck	Sand	0.45	1.05
Schmertmann	Sand	0.60	1.25
D'Appolonia, et al.	Sand	1.00	2.00

(From Tan and Duncan, 1991).

values tend to underestimate settlements half the time and overestimate them half the time. Methods that are more conservative (namely the Terzaghi and Peck method) tend to overestimate settlements more than half the time and to underestimate them rather infrequently.

A relatively accurate method may be considered as one that results in estimated settlement about equal to the average settlement for a group of footings. A reliable method is one that predicts settlements that are greater than or equal to the actual settlement most of the time (Tan and Duncan, 1991). An analysis shows that any method for estimating settlements of footings on sand can be modified by applying an adjustment factor to yield about the same combination of accuracy and reliability as any other method.

Adjustment factors for 50 percent and 90 percent reliability in calculated values of settlement are given in Table 8–14 for the three methods reviewed in the foregoing sections. As an example, to ensure that the D'Appolonia method (that predicts settlements about equal to the average value of actual settlements and underestimating settlements half the time) gives values that are equal or exceed the measured settlement about 90 percent of the time, the computed settlements should be multiplied by a factor of 2. This adjustment would increase the reliability from about 50 percent to 90 percent.

8.10 SETTLEMENT OF FOOTINGS IN ROCK

Competent rock. If footings are founded on competent rock, the settlement would not be large enough to cause problems, generally of the order of one-half inch or less. Where elastic settlements of this magnitude cannot be tolerated, or where very large loads are to be applied, such as at abutments for arch bridges or very tall piers, an analysis of settlement considering the rock characteristics is indicated. For rock masses with time-dependent settlement behavior, the procedures used for footings in soil may be used.

Broken or jointed rock. In rock masses with seams or soft material, consolidation and secondary settlements may occur. For most other rock masses, the settlement will occur immediately, and its magnitude may be estimated from elastic theory. A general expression of the elastic settlement of footing on broken or jointed rock is

$$p_m = \frac{P(1-\nu_m^2)}{\beta_2 E_m A^{0.5}} \tag{8–36}$$

where p_m = settlement of rock mass; P = applied load; ν_m = Poisson's ratio for rock

mass; β_2 = shape and rigidity factor; E_m = Young's modulus for rock mass; and A = footing area. Using typical values of ν_m and β_2, Kulhawy (1978) proposed that for circular, square, and rectangular footings ($L/B \leq 3$), Equation (8–36) may be modified as follows:

$$p_m = \frac{0.9P}{E_m A^{0.5}} \tag{8–37}$$

When $L/B \geq 10$, Equation (8–36) becomes approximately

$$p_m = \frac{0.7P}{E_m A^{0.5}} \tag{8–38}$$

If P is expressed in terms of q_o and A ($P = q_o A = q_o BL$) and $A = BL$, Equation (8–36) is reduced to AASHTO Eq. (4.4.8.2.2–2). For rectangular footings with $3 \leq L/B \leq 10$, the settlement may be estimated by interpolation.

The accuracy of settlement predictions using elastic theory depends on the accuracy with which the parameter E_m is obtained. For unusual or poor rock conditions, it may be necessary to determine the modulus from in situ tests, such as plate loading and pressuremeter tests. The presence of rock fractures tends to give a smaller rock mass modulus than for intact rock. This difference is associated with the discontinuity spacing, which in turn can be correlated with RQD, as shown in Table 8–15. In order to use these data, the values of E_r (Young modulus of rock core sample) and K_n (normal stiffness of discontinuities) are determined from laboratory tests. Typical values of E_r/K_n ranging from 0.2 to 4.2 meters, with an average of 1.2 meters, may be used for preliminary purposes.

Special problems. Special problems may arise in conditions such as weathering of rock, solution cavities, swelling of rock, creep, and mining subsidence. These problems call for special design considerations or foundation treatment. In some instances, the

Table 8–15 Values of Modulus Reduction Factor, $a_E = E_m/E_r$

	Value of a_E for E_r/K_n*		
RQD (%)	*0.1m*	*0.5m*	*1.0m*
<10	0.22	0.06	0.03
20	0.35	0.10	0.05
30	0.40	0.13	0.06
40	0.44	0.15	0.08
50	0.46	0.16	0.09
60	0.50	0.18	0.11
70	0.53	0.20	0.12
80	0.56	0.22	0.14
90	0.70	0.30	0.18
100	0.92	0.75	0.60

*Note: E_r/K_n is in meters; and
- E_r = Young's modulus for rock core sample
- K_n = Normal stiffness for discontinuities
- E_m = Young's modulus for rock mass
- For $Er/Kn \geq 10$, use equivalent soil modulus for analysis.

(From Kulhawy, 1978).

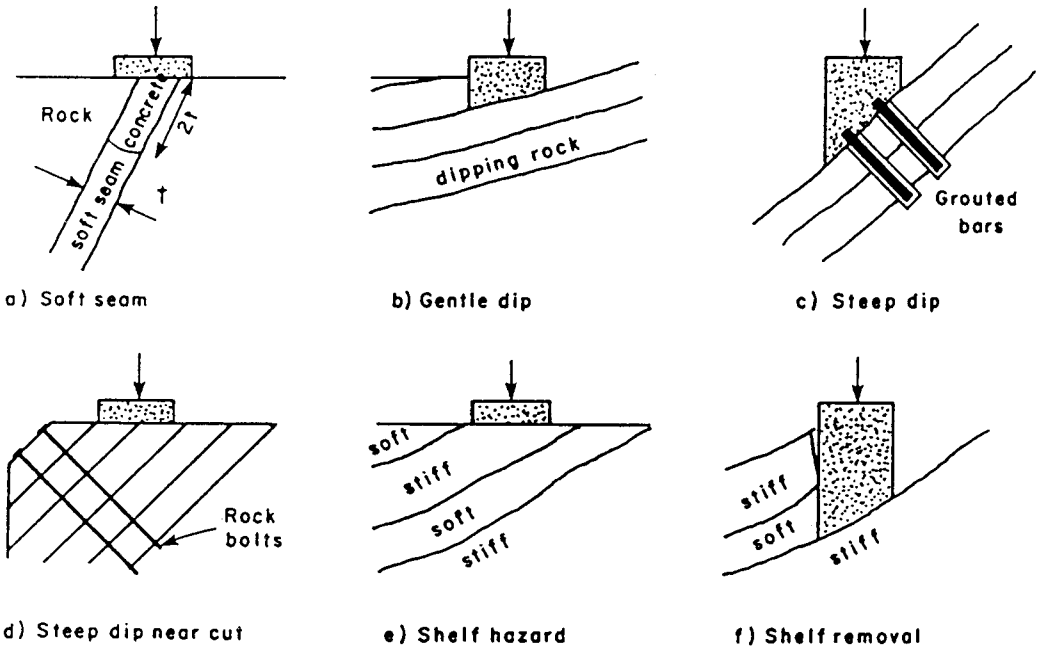

Figure 8–18 Rock foundation contact problems *(from Sowers, 1979).*

presence of sink holes in limestone make footing foundations impractical. A comprehensive review of these problems is given by Peck (1976).

Practical concerns relating to construction of footings in rock are:

1. Good contact between rock mass and foundation. If local defects are present, they may create special problems that will require special treatment. Typical contact problems with suggested solutions are shown in Figure 8–18. They include filling a narrow soft seam with dental concrete, anchoring footing on dipping rock surfaces with anchors or bolts, and avoiding obvious structural hazards by placing the foundation on the stiffer rock layer.
2. Effect of excavation on rock quality. Blasting often results in overbreak and fractures or opening of joints in the rock mass. Potential settlement problems can be avoided if the rock surface is properly cleaned, and fractured rock below the foundation is replaced with lean concrete or well-compacted gravel.

8.11 STRUCTURAL ACTION OF FOOTINGS

Gross and Net Soil Pressure

Figure 8–5 shows the design terminology for footing foundations, and the loads acting on the footing. If the footing thickness is t, the weight of soil above the footing is $\gamma(D_f - t)$ per unit area. With no column load, the only downward load is the weight of soil above the footing and the weight of the footing. This causes a soil pressure balanced by an equal and opposite upward reaction pressure of the same intensity. As a result,

the net effect on the concrete footing is zero. There are no moments or shears in the footing at this loading stage.

When a column load Q is added, the pressure under the footing increases by $q_n = Q/LB$. The total pressure now is the initial plus q_n. For calculating moments and shears in the footing, the initial pressure and its reactions are canceled out, leaving only the net pressure q_n to cause internal force effects in the footing.

Structural Requirements, Spread Footings

The design of a footing usually must consider bending, shear, development of reinforcement, and the transfer of load from a column or wall to the footing.

Flexure. Consider the square footing supporting a single given column shown in Figure 8–19. External moment on section A-A, taken at the face of the column, is caused by the net pressure q_n acting on an area bf. This is also the critical section for bending. If the column is now square or rectangular, the critical section should be taken at the face of the concentric square of equivalent area. If the footing is under a metallic column base, the critical section should be taken halfway between the column base and the edge of metallic plate.

Referring to Figure 8–19(a), the entire moment acting along section A-A is

$$M = (q_n bf)\frac{f}{2} \tag{8–39}$$

where $q_n bf$ is the resultant of the soil pressure on the hatched area and $f/2$ is the moment arm. This moment must be resisted by reinforcement placed at the bottom of the footing as shown in Figure 8–19(b).

In a similar manner, the soil pressure under the portion perpendicular to the direction A-A will cause a critical moment at the face of the column. This must be resisted by flexural reinforcement placed in a perpendicular direction at the bottom of the footing, resulting in two layers of steel, one each way. This reinforcement is distributed uniformly across the entire width of footing.

Consider now the rectangular footing shown in Figure 8–20 with dimensions b and l supporting a rectangular column as shown. The footing is under the action of a uniform net soil pressure q_n. In the long direction l, the moment due to q_n is taken along section B-B. This moment is

$$M_B = (q_n bf_b)\frac{f_b}{2} \tag{8–40}$$

The reinforcement in the bottom of the footing necessary to resist M_B is distributed uniformly across the entire width b. In the short direction b, the moment is taken along section A-A, and is

$$M_A = (q_n lf_a)\frac{f_a}{2} \tag{8–41}$$

The total reinforcement A_{st} required to resist M_A is distributed along the length l as follows:

Over a band width, centered on the center line of the column, equal to the length of the short side of the footing (width b), the portion of the reinforcement is

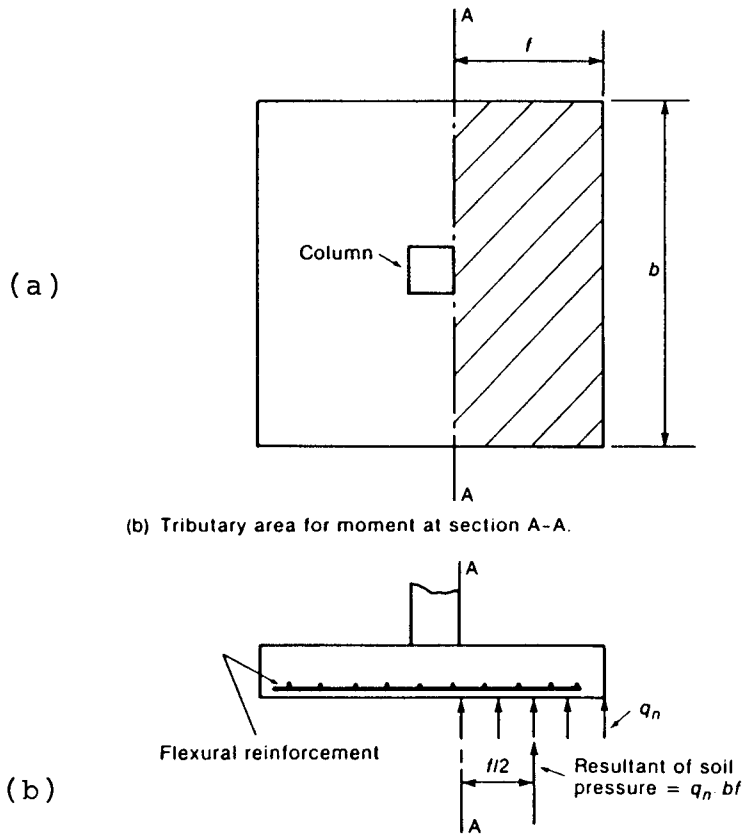

Figure 8–19 Flexural action of a spread footing. (a) Tributary area for moment at section A-A; (b) moment about section A-A.

$$A_1 = \frac{2A_{st}}{(B+1)} \tag{8–42}$$

where B = ratio l/b. The remainder of reinforcement $(A_{st} - A_1)$ required in the short direction is distributed uniformly outside the center band width of the footing.

Two-way shear. Referring to Figures 8–19 and 8–20, the footing is subjected to two-way or punching shear. The footing in this case may undergo shear failure, occurring suddenly with little, if any, warning. Once such a failure has taken place, the column may slide down the footing, with the reinforcing steel ripping out of its place, leaving no physical connection between the footing and the column. Thus, while a two-way footing possesses great ductility if it fails in flexure, it has no extra defense if it fails in shear. Quite frequently shear controls the footing thickness in bridge foundations.

Based on extensive tests, Moe (1961) concluded that the critical section for two-way shear is at the surface of the column. The ACI accepted this conclusion, but showed that a much simpler design equation could be derived by considering the critical section to be located at $d/2$ from the face of the column, where d is the effective depth. This simplification has been incorporated in the ACI Code and in the AASHTO specifications.

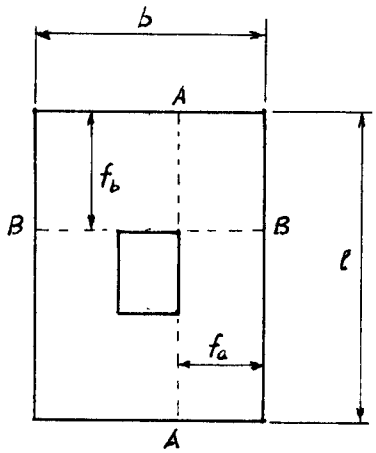

Figure 8–20 Flexural action in rectangular footing.

Thus, for the footings of Figures 8–19 and 8–20, the shear capacity is governed by two-way action, with a critical section located so that the perimeter b_o is a minimum, but not closer than $d/2$ to the perimeter of the concentrated load (i.e., face of column). This procedure is illustrated in Figure 8–21.

Design Shear Stress, Allowable Stress Design. The design shear stress may be computed from

$$v = \frac{v}{b_o d} \tag{8–43}$$

where v is the shear at the critical perimeter b_o, resulting from the net soil pressure on the portion shaded in Figure 8–22(a). The design shear stress v computed from Equation (8–43) should not exceed v_c given by

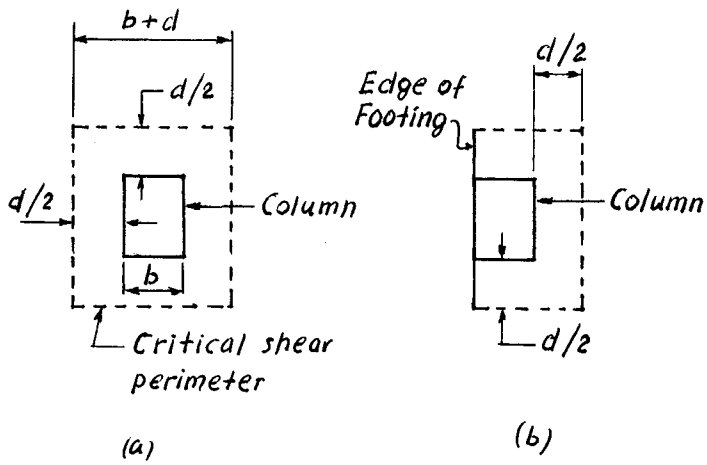

Figure 8–21 Location of critical shear perimeter; (a) interior column; (b) exterior column.

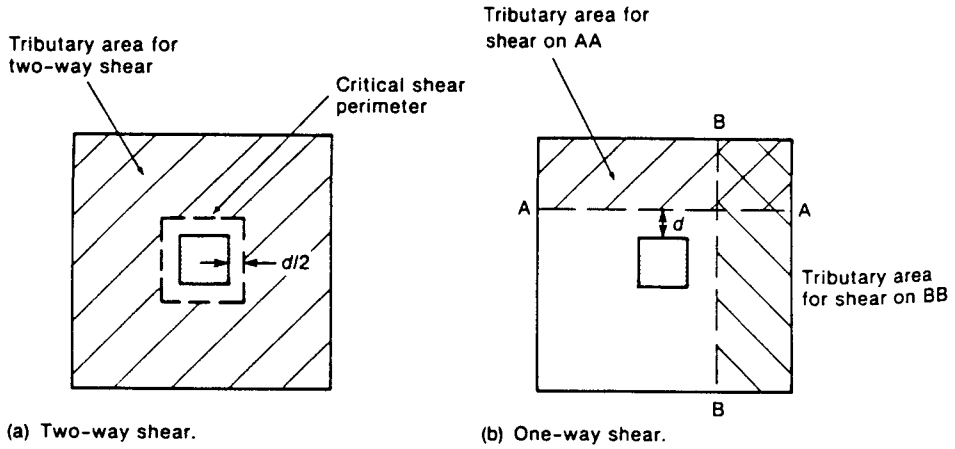

Figure 8–22 Critical sections and tributary areas for shear in footings.

$$v_c = \left(0.8 + \frac{2}{B_c}\right)\sqrt{f'_c} \le 1.8\sqrt{f'_c} \tag{8–44}$$

unless shear reinforcement is provided, where B_c = ratio of long side to short side of concentrated load area (AASHTO Article 8.15.5.6).

Strength Design Method. Design of the footing for two-way action is based on the following equation

$$V_u \le \phi V_n \tag{8–45}$$

where V_u = factored shear force in section; V_n = nominal shear strength; and ϕ = strength reduction factor = 0.85. In this case V_n should not be taken less than V_c, unless shear reinforcement is provided, where

$$V_c = \left(2 + \frac{4}{B_c}\right)\sqrt{f'_c} b_o d \le 4\sqrt{f'_c} b_o d \tag{8–46}$$

where all symbols are as previously (AASHTO standard specifications).

One-way shear. In the case of a uniformly loaded footing, the critical section for one-way shear should extend in a plane across the entire width and located at a distance d from the face of the column. Figure 8–22(b) shows two critical sections for one-way shear in a footing, and the tributary areas in checking one-way shear on these sections.

Design Shear Stress, Allowable Stress Design. The design shear stress v may be computed from

$$v = \frac{V}{bd} \tag{8–47}$$

where b is the footing dimension along which the shear is computed. The design shear stress computed from Equation (8–47) should not exceed v_c, taken as

$$v_c = 0.95\sqrt{f'c} \tag{8–48}$$

A more detailed calculation of the allowable shear stress can be made using AASHTO Equation (8–4). Where design shear stress v exceeds the shear stress carried by the concrete v_c, shear reinforcement should be provided.

Strength Design Method. Design of the footing is likewise based on Equation (8–45). The nominal shear strength V_n should not be less than V_c, unless shear reinforcement is provided, where

$$V_c = 2\sqrt{f'_c}bd \tag{8–49}$$

Since web reinforcement is rarely used in a footing, $V_u \leq \phi V_c$.

LRFD specifications. The strength design method for either two-way or one-way shear discussed thus far is based on the standard AASHTO specifications. The LRFD specifications retain the general expression for punching shear. If shear perimeters for individual loads overlap or project beyond the edge of the member, the critical perimeter b_o should be taken as that portion of the smallest envelope of individual shear perimeter which will actually resist the critical shear for the group under consideration.

For two-way action for footings without transverse reinforcement, the nominal shear resistance V_n may be computed as

$$V_n = \left(0.063 + \frac{0.126}{B_c}\right)\sqrt{f'_c}b_o d \leq 0.126\sqrt{f'_c}b_o d \tag{8–46b}$$

where all parameters are as previously. It should be noted, however, that f'_c in Eq. (8–46b) is given in kips/in^2, whereas the same parameter in Eq. (8–46) is expressed in lb/in^2. When appropriate conversions are made, these two equations become equivalent. For example

$$0.126\sqrt{4} = 0.252 \text{ kips/in}^2 = 4\sqrt{4000} = 4 \times 62.3 = 252 \text{ lb/in}^2$$

The LRFD specifications stipulate a resistance factor 0.90 for shear.

Development of reinforcement. The footing reinforcement is chosen assuming that the reinforcement stress reaches f_y along the maximum moment section at the face of the column, that is, the critical sections for development of reinforcement are assumed at the same locations as the critical sections for moments.

The reinforcement must extend far enough on each side of the point of maximum bar stress to develop this stress. This means that the bar must extend l_d (development length) from these points.

Transfer of load from column to footing. This involves the transfer of all forces (vertical and lateral) and moments.

Vertical loads are transferred by bearing stresses in the concrete and by stresses in the dowel bars that cross the joint. The area of the dowels can be less than that of the bars in the column, but not less than 0.005 times the gross column area. Additional reinforcement, however, must be provided where the forces exceed the concrete bearing strength.

The transfer of load by bearing and dowel bars will be illustrated in the following examples. Consider a column 33 in × 24 in supported on a spread footing. The column is provided with 10 #8 bars and 8 #7 bars as dowels. In the regular section the column has a gross area $A_g = 33 \times 24 = 792$ in^2, so that $A_c = 792 - 8 = 784$ in^2 and $A_s = 8$ in^2. The total axial capacity of the column is, using $f'_c = 3000$ lb/in^2 and Grade 40 steel, $\phi P_o = 0.70[0.85 \times 3000 \times 784 + 8 \times 40] = 1624$ kips, of which 1400 kips are carried by the concrete, and 224 kips are resisted by the steel. At the joint, the area of the dowels is $A_{sd} = 8 \times 0.6 = 4.80$ in^2, or less than the area of the column bars. The force transmitted by A_{sd} is $\phi A_{sd} f_y$, where ϕ is the strength reduction factor for the column. As a result, at the joint the load carried by the concrete is increased.

This joint may fail (limit states) by (1) crushing of the concrete at the bottom of the column, (2) crushing of the concrete in the footing under the column, (3) bond failure of the dowels in the footing, and (4) failure of the lap splice between the column dowels and the column bars.

Referring to Figure 8–23, where the supporting surface A_2 is wider than the contact area A_1, the maximum load carried by the concrete in bearing may be taken as

$$\phi P_o = \phi(0.85 f'_c A_1)\sqrt{\frac{A_2}{A_1}} \le \phi(1.7 f'_c A_1) \qquad (8\text{–}49b)$$

where A_2 is the area of the lower base of a cone sloping as shown, and defined by the first intersection with an edge (point B).

Evidently two cases must be considered: joints that do not transmit moments to

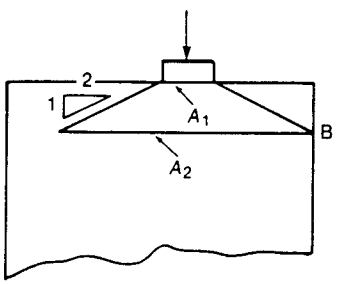

(a) Side view.

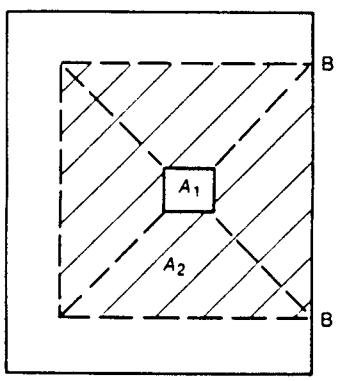

(b) Plan.

Figure 8–23 Definition of A_1 and A_2.

the footing, and joints that do. If no moments are transmitted, or if the eccentricity is within the middle third, the entire section will be in compression. The total force transfer by bearing is computed as $(A_g - A_{sd})$ times the bearing stress allowed on either member. If moments are transmitted by the column to the footing, compressive stresses may exist over part of the contact area. In this case, the area of dowels necessary to ensure the transfer may be found by treating the joint as an eccentrically loaded column with the maximum concrete stress not exceeding the smaller bearing stress. Usually, the final requirement is that all the column reinforcement should cross the interface.

Practical considerations. The minimum cover to the reinforcement in footings cast against and permanently exposed to earth is 3 inches. Sometimes the bottom of the excavation for footings is covered with a lean concrete mix as a seal to prevent the bottom from becoming uneven and to give a level surface for placing the reinforcement.

Most states have general guidelines or specific standards and criteria for the configurations and dimensions of footings. For example, the minimum thickness of any spread footing under a pier may be 2 feet, and unless design considerations indicate that a greater thickness is required, the minimum dimensions should be followed.

Under most bridges the footing for a fixed pier will not be the same as the footing for an expansion pier, and where the design indicates a reasonable variance, it should be reflected on the plans. The minimum width of a spread footing under an expansion pier should be about one-fourth the distance from the pier top to the base of the footing. If the footing is founded on rock, the footing width may be reduced to one-fifth of the pier height.

Any construction joints incorporated in a footing should be bonded with continuous reinforcement.

Strip or Wall Footings

Multiple-column piers in conventional grade separation structures have a pier wall above the footing, extending some distance above the ground. This wall serves to stiffen the foundation and also provides a crash wall at grade level (see also chapter 4).

A wall footing (or strip) cantilevers out on both sides of the wall. The soil pressure induces bending effects on either side, and as a result transverse reinforcement is required at the bottom to resist the cantilever moments. The critical section for design for flexure and anchorage are at the face of the wall. One-way shear is critical at a section at distance d from the face of the wall. Solid pier walls have similar design requirements.

Combined Footings

Combined footings, shown in Figure 8–4(c) and (d), may be used when the bearing areas under single footings tend to merge, and where a structural connection between adjacent column footing can improve overall stability. At best, the shape of the footing is chosen so that the centroid of the area in contact with the soil coincides with the resultant of the column loads for the prevailing loading group.

Sometimes a combined footing will be designed as two isolated footing pads joined by a strap or stiff beam as shown in Figure 8–4(c). The strap is part of the foundation and is designed as a beam with flexural and shear reinforcement.

Rectangular combined footing. Where combined footings are used for bridge piers, they are designed to provide a very rigid configuration. In this case, it is reasonable to assume that the resulting soil pressure varies linearly. This pressure will be uniform if the location of the resultant load (including the effects of eccentricity) coincides with the centroid of the footing area. The so-called rigid method is conservative and may result in overdesigns. Where conditions warrant, the analysis may be modified by considering beam-on-elastic-foundations principles. This procedure produces smaller design moments compared to those obtained from a rigid-method analysis.

The first step in the design of rectangular combined footings is to determine the location of the center of footing area. Next, the length and width are found. With the footing configuration known, the footing is treated as a beam supported on two or more columns and acted upon by the soil pressure. The shear and moment diagrams are drawn accordingly. The depth may be governed by the more critical two-way shear action or wide-beam shear. Critical sections are the same as for spread footing, that is, at distances $d/2$ and d from the column face. The common practice is not to use shear reinforcement for economy and to increase rigidity.

In the long direction, the total reinforcement should be uniformly distributed across the entire width of the footing. In the transverse (short) direction, computing the moments as for rectangular spread footing may be unrealistic and in considerable error. This is because the soil pressure is larger near the columns and smaller in the zone between columns. The zone closest to and at the column is most effective and should be provided with more reinforcement. From finite element analyses, Bowles (1988) has proposed an effective zone as shown in Figure 8–24. It should be noted that as the width of this zone decreases, its rigidity increases from the additional bars that are required. The increased rigidity will tend to attract moment from the zone between columns, but

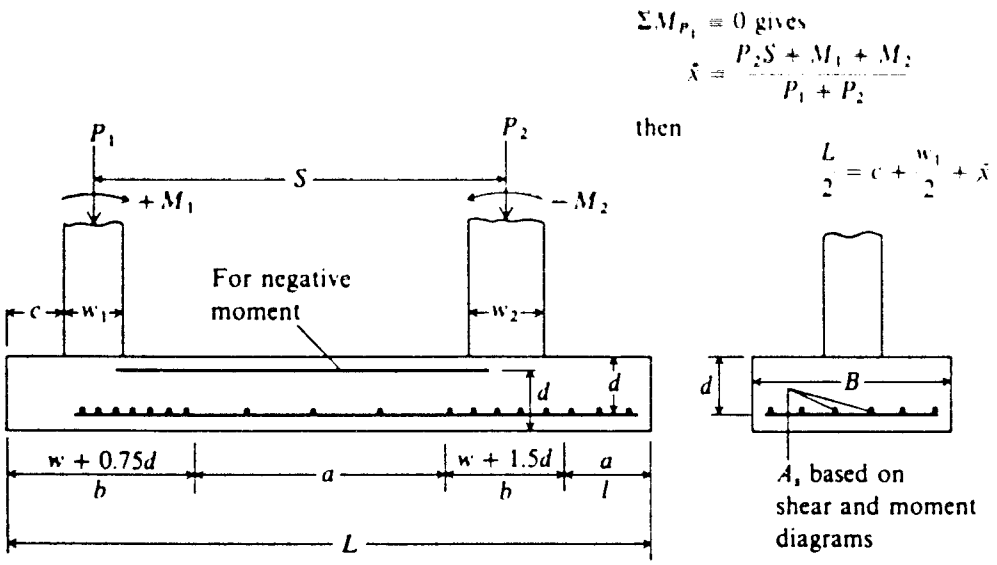

Figure 8–24 Steel for rectangular combined footing. Note the several values of d. Steel in zone a should satisfy minimum code requirements; in b should satisfy both bending and minimum code requirements.

would be difficult to predict. Making the effective zone reasonably narrower should ensure sufficient steel to accommodate the additional moment.

For computation purposes and shears or moment diagrams, the column supports should be considered as point supports. This simplifies the diagrams and computations, while the values at critical locations are the same. It should also be noted that combined footings are statically determinate for any number of columns as can be seen from statics. The column loads are initially known and will not be changed. For a rigid footing, the resulting soil pressure is $q = \Sigma P/A$. This condition is equivalent to a uniformly loaded continuous beam with the reactions (column loads) known. Any discrepancies must be rectified in the process of analysis.

Trapezoid-shaped combined footings. Trapezoidal footings are intended to accommodate columns with unbalanced loads under space limitations. A typical footing geometry necessary for a combined trapezoidal shape is shown in Figure 8–25. The following relationships are easily obtained.

Footing Area

$$A = \frac{a+b}{2} L \tag{8–49c}$$

$$x' = \frac{L}{3}\left(\frac{2a+b}{a+b}\right) \tag{8–49d}$$

where L = length of combined footing, and x' = distance from centroid to edge b. If $a = 0$, $x' = L/3$ (the shape is a triangle); if $a = b$, $x' = L/2$ (the shape is a rectangle). For a trapezoidal shape, therefore,

$$\frac{L}{3} < x' < \frac{L}{2}$$

A trapezoidal footing will in most cases be used for two columns. The reinforcement pattern is not regular, but not unusual for bridges.

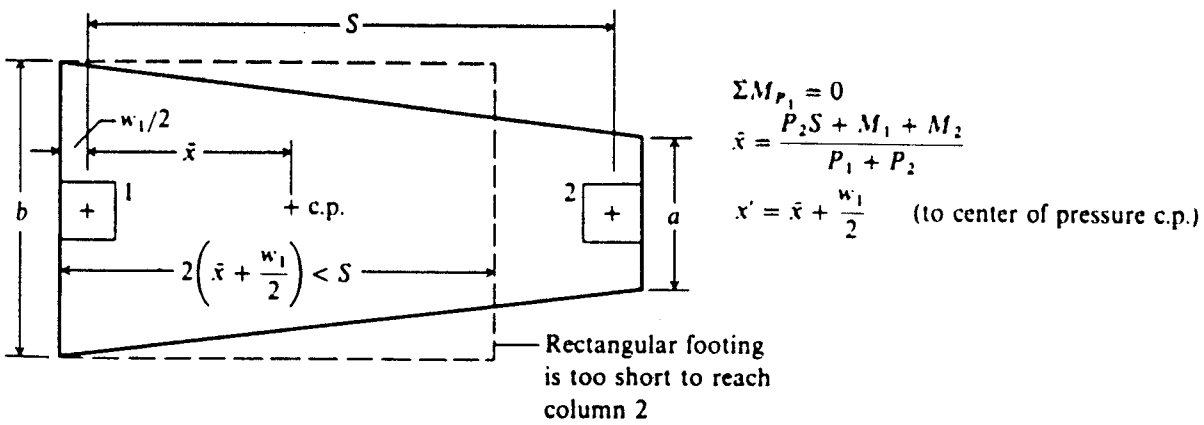

Figure 8–25 A trapezoidal footing is required in this case unless the distance S is so great that a cantilever (or strap) footing would be more economical.

With x' defined, the dimensions a and b are found solving Equations (8–49c) and (8–49d). The dimension L is known from the location and size of the columns, and is determined from the required bearing area.

With all dimensions established and the soil pressure and column loads known, the footing is treated as the rectangular footing, except that the soil pressure diagram will vary linearly from edge a to edge b. The resulting shear diagram is a second-degree curve, and the moment diagram a third-degree curve.

Strap footings. A strap connecting two column footings ensures better stability against lateral action, and may also be used to transfer moment caused by eccentricity to the adjacent column footing to induce a nearly uniform soil pressure. The strap has greater fixity in the vertical direction but provides less bearing area compared to a combined spread footing. However, the resultant soil pressure should preferably be at the footing centroid to induce a uniform pressure diagram.

In general, strap footings must satisfy certain requirements as follows:

1. They must be rigid to control rotation of the footings.
2. Footings should be proportioned for approximately equal and uniform pressures.
3. The strap may be constructed to be out of contact with the soil so that there is no soil pressure to interfere with the design assumptions.

The latter criterion is demonstrated in Figure 8–26, where a strap is used to cause the two-footing system to act as a beam. The resultant soil pressure R_1 on the left footing is estimated by taking moments about the line of P_2, or $R_1S' = P_1S$. The resultant soil pressure R_2 is computed from the summation of the vertical forces.

The equation shown in Figure 8–26 may be used to proportion the combined footing. The total length is dependent on the value of e, selected arbitrarily, so that the solution is not unique.

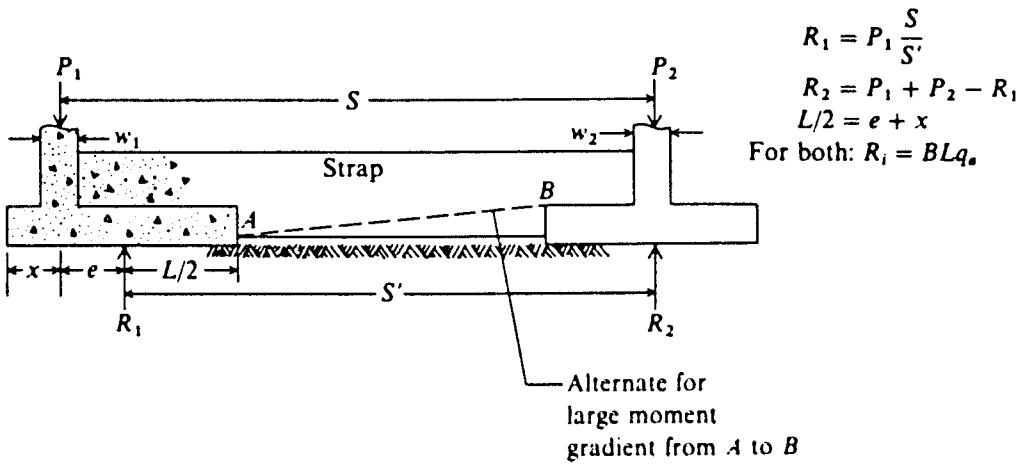

Figure 8–26 Assumed loading and reactions for a strap-footing design. Make strap width about same as smallest column w.

8.12 FLEXURAL STRENGTH OF MODIFIED SQUARE FOOTING, CASE STUDY

The strength of a spread footing under a single column load was shown to be governed by the shear capacity (punching or two-way shear), although the extent of flexure-shear interaction may be considerable. In the foregoing sections, the structural requirements of these footings are derived from the assumed behavior in punching shear and flexural action treating them as beams. Thus, the conventional method is to assume that the footing is rigid, and in practice this amounts to designing a rather thick system.

Conversely, treating the footing as a flexible member is conceptually admissible, but attempts at rigorous elastic solutions can encounter unique difficulties because of the complexity of boundary and loading conditions. As footings are essentially reinforced concrete slabs, yield line theories have been used in their analysis. Since flexural failures are preferred to shear failures, to ensure protection of a structure against punching shear (by inducing an earlier flexural failure), it is essential to have a resistance factor in shear smaller than that in flexure.

Based on the premise that beam-slab construction allows flexibility in redistributing structural materials to ensure economy, Nathan and Ranganatham (1978) conducted case studies of alternate structural forms as improved versions of footings that can resist punching shear failure and improve efficiency in terms of proper display of materials. These include (1) tapered footings, (2) slab with axis beams and fillets, and (3) slab with diagonal beam and fillets.

Contact pressure distribution. Since yield line analysis is the methodology of this study, with rigid plastic behavior assumed for the structure, the relevant deformation to correlate the contact pressure is the displacement of the rigid regions by the rotation of the yield lines. In accordance with this behavior, the contact pressure is assumed to have a parabolic distribution with the following form

$$q_i = nq_o + (1-n)q_o K_i^2 \cos^2\theta \tag{8–49e}$$

where q_o = pressure at a reference point; n = ratio of the soil pressure under the load to that at the reference point; and K_i = rotation of rigid region i.

Different failure modes are shown in Figure 8–27, resulting in different patterns of pressure distribution. The three modes of failure of tapered square footings are axis mode, radial mode, and diagonal mode.

Tapered footings. If M denotes the moment capacity of the footing at the face of the column, and κ is the ratio of M to the moment at the edge of the footing, the moment capacity at any distance r on the yield line is

$$M_r = \kappa M + (1-\kappa)M\left[1 - \frac{r\cos\phi}{a(1-a)}\right] \tag{8–49f}$$

Axis Mode. The failure mechanism shown in Figure 8–27(a) has eight yield lines, two emanating from each corner of the square column at an angle ϕ to the axis of the footing.

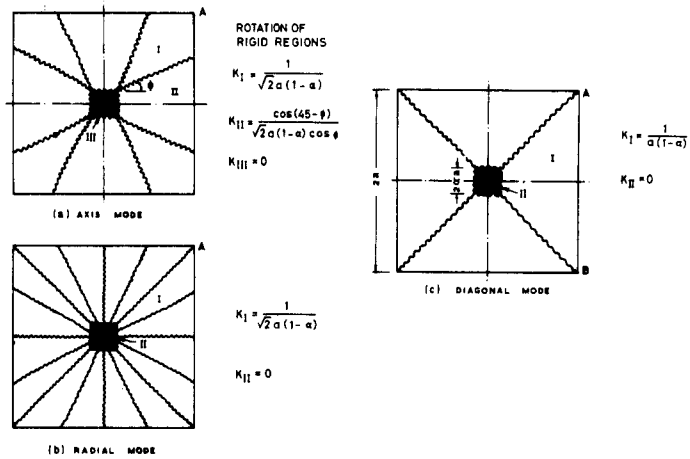

Figure 8–27 Failure modes in square footings.

Radial Mode. Any structural change made in a slab structure with a known critical failure mechanism must be followed by a search for possible changes in the collapse mechanism. In the tests of tapered footings, conical structural deflection has been observed with the formation of radial yield lines.

Diagonal Mode. For square individual footings, although the critical collapse mode (corresponding to the lowest collapse load) is the axis mode, the recording of a higher collapse load with radial collapse mode introduces the possibility of coaxing the structure to yield even higher returns by appropriate redistribution of materials. Such a possibility exists with the diagonal mode shown in Figure 8–27(b).

Beam-slab footings. Depending on the relative rigidity of the beam and slab, two different types of collapse modes are possible. If the beams are very strong and act as line supports, only the slab should be expected to fail, as shown in Figures 8–28(a) and 8–29(a). When the beams are not sufficiently strong, a combined failure is possible (composite mode), whereby beam failure follows the failure of the slab (yield lines) as shown in Figure 8–28(b) and 8–29(b).

Tests on footings. Nathan and Ranganatham (1978) report results of tests on footings in sand, with limiting ϕ values from a maximum of 44° for the dense state to a minimum of 27° for the loose state. As compacted in the test tank, the sand had a dry den-

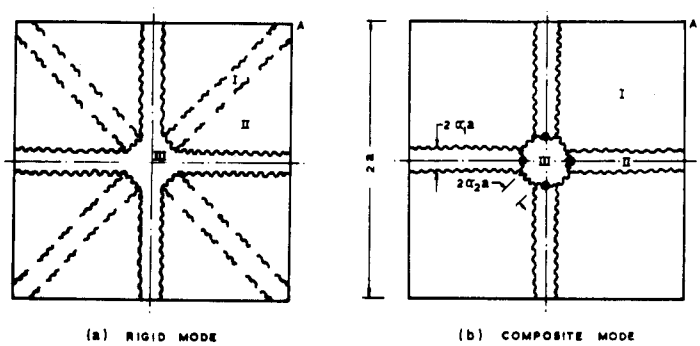

Figure 8–28 Failure modes in axis beam-slab footings.

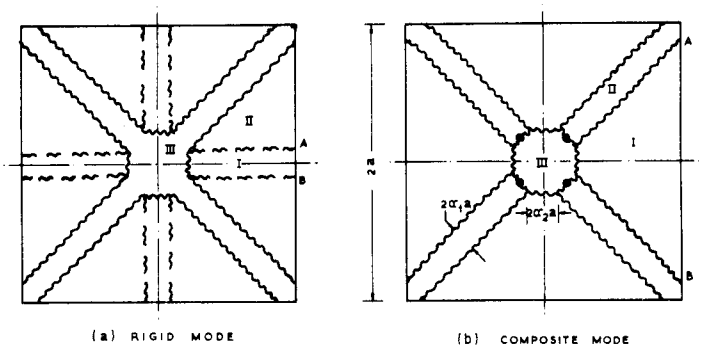

Figure 8–29 Failure modes in diagonal beam-slab footings.

sity 107 lb/ft^3, and a corresponding friction angle 42°. The tests involved reinforced concrete footing 3 feet square, with mild steel reinforcement.

Tapered Footings. The presence of circular action with formation of radial yield lines in tapered footings indicates the possible treatment of square footings similar to circular footings. The formation of radial lines means that circumferential strains predominate with negligible radial strain. The efficiency of such structural behavior with circumferential reinforcement has been verified experimentally with three spacings of ring reinforcement.

Analytical studies suggest that failure by diagonal collapse mode results in higher collapse load, and since it is not critical, it could not occur with a uniform resistive moment field (isotropic reinforcement mesh). One way to manifest this mode is by reducing the resistive moment capacity of the slab along the diagonal. This can be achieved by providing reinforcement in square loops at right angles along the diagonal. For this pattern, if the moment capacity per unit length along the axis is M, along the diagonal it is 0.706 M (M cos 45°).

Beam-Slab Footings. The structural behavior of beam-slab footings was studied with reference to a plane slab footing reinforced with isotropic mesh.

Results of tests and analysis. Tapered and beam-slab footings were studied experimentally and analytically. The results are summarized as follows:

Tapered Footings. The effect of taper κ on the flexural strength of tapered footings for the three collapse modes of Figure 8–27 is shown in Figure 8–30(a). A comparison is made for footings of the same thickness at the column face. The bottom line of each mode is for the case of uniform pressure ($n = 1$), whereas the top line is for the case of zero edge pressure ($n = \infty$). For footings with constant depth at the column face, an increase in taper means a corresponding reduction in concrete volume. The variation in the volume of concrete of a tapered footing and its collapse load W for diagonal mode with zero edge pressure is also shown in the inset diagram, expressed as a percentage of the reference plane slab footing with respect to taper. Apparently, the reduction in collapse load is not as great as the reduction in the quantity of concrete. Another way of interpreting this result is to compare collapse loads at constant footing volume by normalizing the collapse load with a factor defined as the ratio of tapered footing volume to the reference plane slab footing R_v. The results of Figure 8–30(a) so modified are shown in

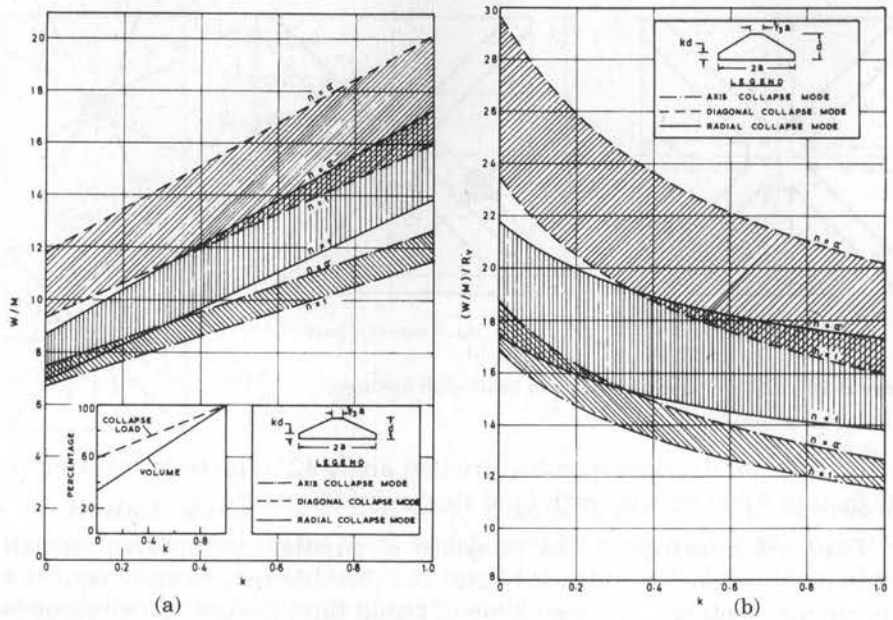

Figure 8–30 Theoretical collapse load of tapered footings.

Figure 8–30(b), showing that at constant footing volume, the collapse load increases with increase in taper (i.e., decrease in κ).

The effect of a change in contact pressure distribution is more pronounced in the diagonal mode because of the favorable distribution with a tendency to attract more concentration of contact pressure towards the column.

Beam-Slab Footings. Results of the yield line analysis are shown in Figure 8–31 for diagonal beam-slab footings. Part (b) shows the effect of $\overline{m}$, ratio of beam strength to slab strength, on the collapse load, for various ratios of negative moment capacity to positive moment capacity, i. The sloping line is governed by the composite fail-

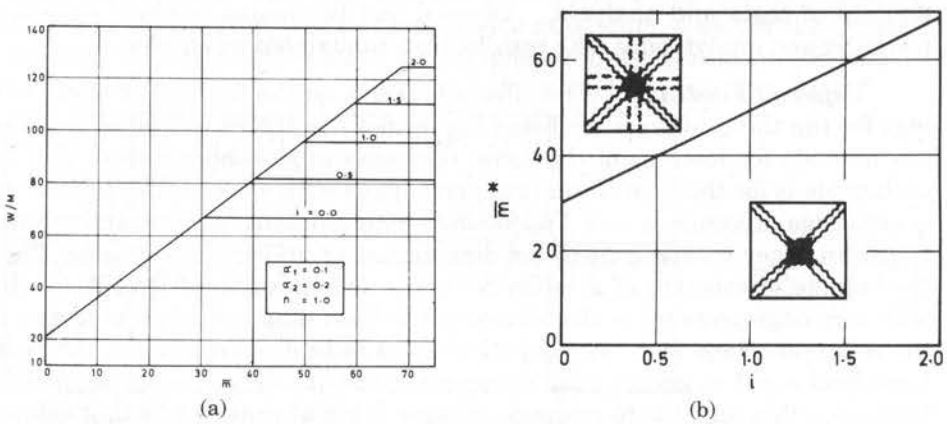

Figure 8–31 (a) Collapse load of diagonal beam-slab footings; (b) optimum beam moment capacity of diagonal beam-slab footing.

ure, indicating an increase in collapse load for an increase in $\overline{m}$ up to a particular value at which the beam becomes rigid enough to act as line support, resulting in the rigid mode. This value of $\overline{m}$, denoting the point of transition with the possibility of both modes, is termed the optimum and is denoted by $\overline{m}^*$. The variation of $\overline{m}^*$ is shown in Figure 8–31(b). A relevant observation is that an increase in the structural rigidity (by increasing the negative reinforcement, the beam size or the fillet size), results in a corresponding increase in the collapse load relative to the positive moment capacity of the footing.

8.13 STRUT-AND-TIE MODEL (LRFD SPECIFICATIONS)

General Principles

Strut-and-tie models may be used to design concrete sections and proportion reinforcement near supports and concentrated loads at strength and extreme limit states. Where nonlinear strain distribution must be considered, the conventional methods of analysis are not adequate. In this case, strut-and-tie models can provide a convenient way of approximating load paths and force effects.

The strut-and-tie model should be considered in deep footings and pile caps where the distance between the applied load and the supporting reactions is less than about twice the member thickness. The concept is fairly recent, and for more details reference is made to Collins and Mitchell (1991), and Schlaich, Schafer, and Jennewein (1987).

In traditional design, typical assumptions are that the shear flow remains constant and that the longitudinal strains vary linearly over the beam depth. For deep beams such as the member shown in Figure 8–32, these assumption are not valid. The shear stresses on a section just to the right of support A will be concentrated near the bottom face. The associated behavior can be predicted more realistically if the flow of forces through the complete member is studied. Thus, rather than determining V_u and M_u at different "critical" sections along the beam, the flow of compressive stresses from load P to the supports A and B and the required tension forces between A and B may be considered.

Structural Idealization

A member or a region thereof may be considered as an assembly of steel tension ties and concrete compressive struts interconnected at nodes to form a truss. The required dimensions of compressive struts and tension ties are parameters that must be considered in establishing the truss geometry. This principle is derived from the fact that cracked reinforced concrete resists the loads by compression in the concrete and tension in the steel. After significant cracking has occurred, the principal stress trajectories in the concrete tend to approach straight lines, and hence can be approximated by straight compressive struts. Tension ties represent the principal reinforcement.

A strut-and-tie truss model is shown in Figure 8–32. There are zones of high unidirectional compressive concrete stresses, represented by compressive struts. Regions subjected to multidirectional stresses, where the struts meet the ties at the truss joints, are represented by nodal zones. Because of the significant transverse dimensions of the struts and ties, a truss joint becomes a nodal zone with finite dimensions. The truss

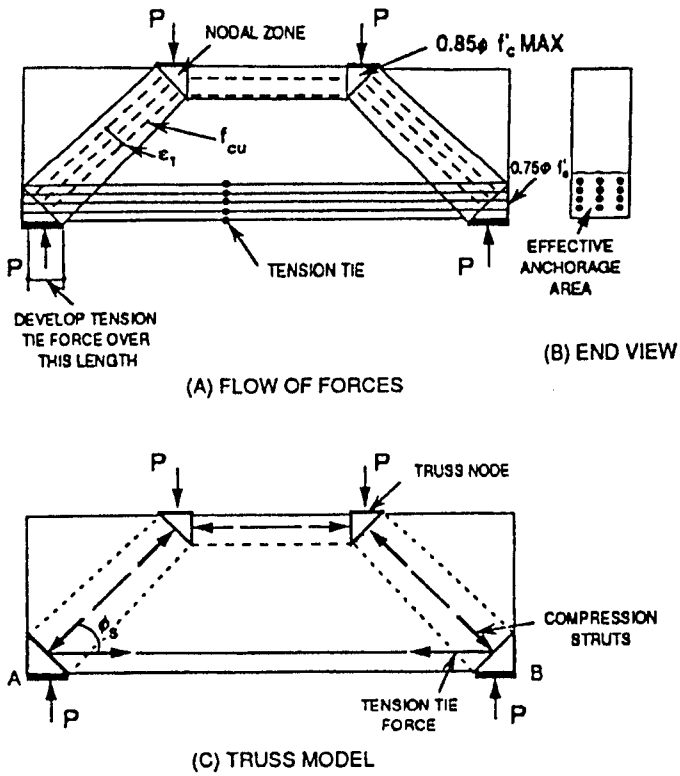

Figure 8–32 Strut-and-tie truss model for a deep beam.

geometry usually is established by trial and error where member sizes are first assumed, truss geometry is determined, and member forces are calculated and used to verify member sizes.

Proportioning of compressive struts. The nominal resistance of an unreinforced compressive strut, $P_{n,}$ may be taken as

$$P_n = f_{cu} A_{cs} \tag{8–50}$$

where P_n = nominal resistance; f_{cu} = limiting compressive stress; and A_{cs} = effective area of strut.

Effective Cross-Sectional Area of Strut. The value of A_{cs} may be determined from the available concrete area and the anchorage conditions at the ends of the strut as shown in Figure 8–33. When the strut is anchored by reinforcement, the effective concrete area may be considered to extend a distance up to six bar dimensions from the anchored bar, as shown in Figure 8–33(a).

Limiting Compressive Stress in Strut. The compressive stress f_{cu} is obtained from

$$f_{cu} = \frac{f'c}{0.8 + 170\,\epsilon_1} \leq 0.85 f'_c \tag{8–51}$$

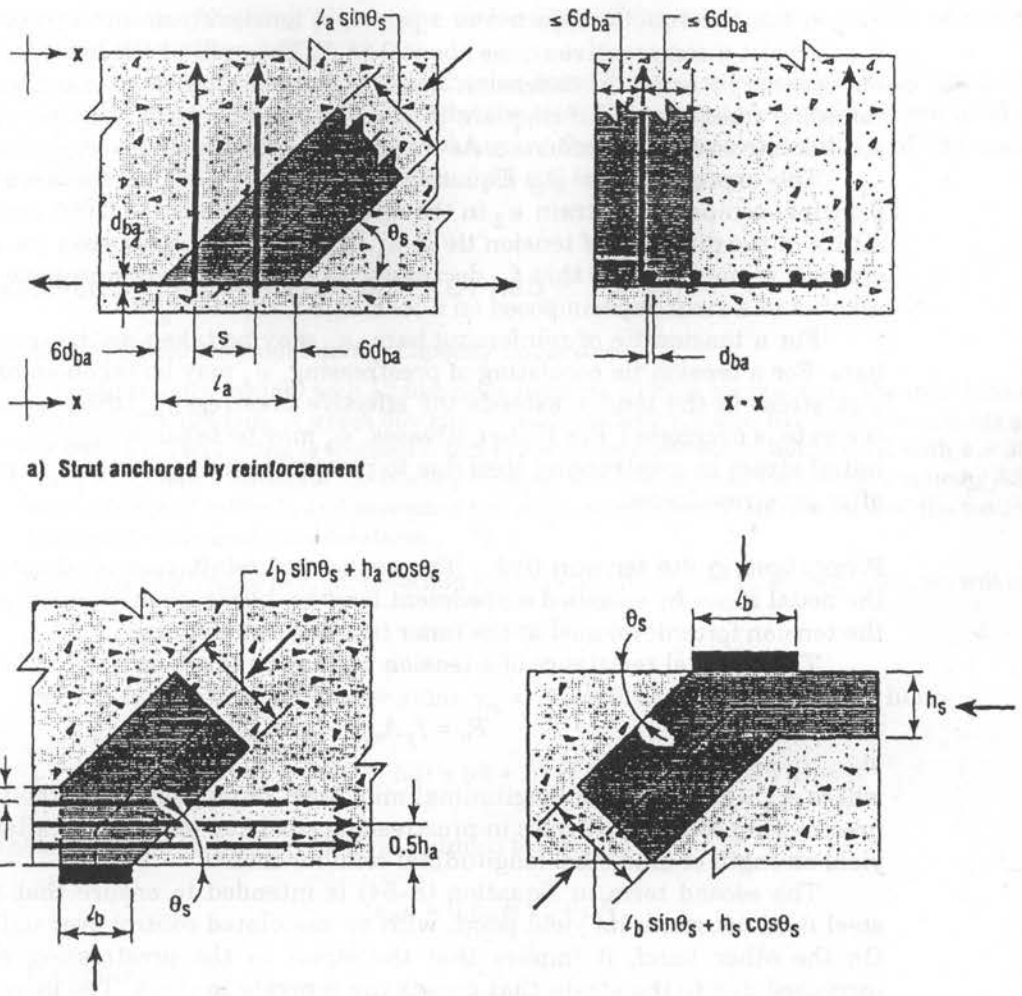

Figure 8–33 Influence of anchorage conditions on effective cross-sectional area of strut.

where
$$\epsilon_1 = (\epsilon_s + 0.002)cot^2 a_s \tag{8–52}$$

and a_s = smallest angle between the compressive strut and adjoining tension ties; ϵ_s = tensile strain in the concrete in the direction of the tension tie; and f'_c = specified compressive strength of concrete.

Reinforced Strut. If the strut contains reinforcement parallel to its axis, and has been detailed to develop its yield stress in compression, the nominal strut resistance is

$$P_n = f_{cu}A_{cs} + f_y A_{ss} \tag{8–53}$$

where A_{ss} = area of reinforcement in the strut.

If the concrete is subjected to a principal tensile strain not exceeding about 0.002, it can resist a compressive stress about $0.85 f'_c$. This will be the limit for regions that are not crossed by or joined to tension ties. The bars of a tension tie are bonded to the surrounding concrete, and if they are to yield in tension, there must be significant tensile strains imposed on the concrete. As these tensile strains increase, f_{cu} decreases.

The expression for ϵ_1, Equation (8–52), is derived on the assumption that the principal compressive strain ϵ_2 in the direction of the strut is 0.002 and that the tensile strain in the direction of tension tie is ϵ_s. When the angle between the strut and tie decreases, ϵ_1 increases so that f_{cu} decreases. At the limit, no compressive stress should be allowed in a strut superimposed on a tension tie, that is, $a_s = 0$.

For a tension tie of reinforcing bars, ϵ_s may be taken as the tensile strain in the bars. For a tension tie consisting of prestressing, ϵ_s may be taken as zero until the tension stress in the tendon exceeds the effective prestress f_{ps} (the precompression of the concrete is overcome). For higher stresses, ϵ_s may be taken as $(f_{ps} - f_{pe})/E_p$, where f_{ps} = initial stress in prestressing steel due to prestress, and f_{pe} = stress in prestressing steel after prestress losses.

Proportioning the tension ties. The tension tie reinforcement should be anchored to the nodal zones by specified embedment lengths, hooks, or mechanical anchorages, with the tension force developed at the inner face of the nodal zone.

The nominal resistance of a tension tie may be taken as

$$P_n = f_y A_{st} + A_{ps}(f_{pe} + f_y) \tag{8–54}$$

where A_{st} = total area of longitudinal mild steel reinforcement in the tie; A_{ps} = area of prestressing steel; f_{pe} = stress in prestressing steel due to prestress after losses; and f_y = yield strength of mild steel longitudinal reinforcement.

The second term in Equation (8–54) is intended to ensure that the prestressing steel does not reach its yield point, with an associated control over unlimited cracking. On the other hand, it implies that the stress in the prestressing elements will be increased due to the strain that causes the concrete to crack. The increase in stress associated with this action is arbitrarily limited to the same increase in stress that the mild steel will undergo. If there is no mild steel, f_y may be taken as 60,000 lb/in^2.

The tension tie reinforcement should be anchored to transfer the tension force to the node regions of the truss, using the same criteria applied to the development and splices of reinforcement in conventional reinforced concrete.

Proportioning of node regions. Node regions must satisfy strength criteria for compression struts and tension ties, and in addition they must be designed to conform to the stress limits specified in the foregoing section. Unless confining reinforcement is provided, the concrete compressive stress in the nodal regions should not exceed:

1. For node regions bounded by compressive struts and bearing areas = $0.85 \phi f'_c$.
2. For node regions anchoring a one-direction tension tie = $0.75 \phi f'_c$.
3. For node regions anchoring tension ties in more than one direction = $0.65 \phi f'_c$.

where ϕ = resistance factor for bearing on concrete. These limits in concrete compressive stresses in nodal zones are related to the level of confinement provided by the concrete in compression. Where necessary, the stresses in the nodal zones can be reduced by in-

creasing the size of bearing plates, the dimensions of the compressive struts, or the dimensions of the tension ties.

The reduced stresses on nodes anchoring tension ties are necessitated by the detrimental effects of tensile strains caused by the ties. If posttensioned tendons are used as ties and the stress does not need to be higher than f_{pc}, tensile straining of the nodal zone is not required, and in this case the $0.85\,\phi f'_c$ limit is appropriate.

8.14 DESIGN EXAMPLE 8–1, BEARING CAPACITY BY ASD

Example 8–1A, Solution from Bearing Capacity Equations

A spread (square footing) with 12-foot sides supports a single pier column. The total load on the footing is 725 kips, of which 555 kips is dead load and 170 kips live load. These loads are for Group I. The footing is founded 5 feet below ground surface in dense sand with $\phi = 35°$, and $\gamma = 115$ lb/ft^3. Estimate the bearing capacity and adequacy of the foundation using ASD with a factor of safety 3, and assuming the water table 3 feet below the base of the footing. Disregard settlement considerations.

Solution Referring to Figure 8–8 and Equation (8–10), $z_w = 3$ ft. Since $\phi < 37°$, we will use

$$\gamma = \gamma' + (z_w/B)(\gamma_m - \gamma')$$

For a void ratio 0.40 for dense sand, $\gamma_m = 115 + 0.40 \times 62 = 140$ lb/ft^3, hence

$$\gamma = 53 + \left(\frac{3}{12}\right)(140 - 53) = 53 + 22 = 75 \text{ lb/ft}^3 = 0.075 \text{ kips/ft}^3.$$

Without cohesion, Equation (8–2) is reduced to

$$q_{ult} = 0.5\gamma B N_\gamma + qN_q$$

Compute

$$q = \gamma D_f \quad \text{(Figure 8-5), or} \quad q = 53 \times 5 = 265 \text{ lb/ft}^2 = 0.265 \text{ kips/ft}^2$$

From Table 8–16, values of N_γ and N_q are interpolated for $\phi = 35°$, or

$$N_\gamma = \frac{41+56}{2} = 48 \qquad N_q = \frac{29+38}{2} = 33$$

Or, $q_{ult} = (0.5)(0.075)(12)(48) + (0.265)(33) = 21.6 + 8.8 = 30.4$ kips/ft^2, giving an allowable soil pressure = 30.4/3 = 10.1 kips/ft^2; or for Group I, total load capacity = 10.1 × 144 = 1450 kips.

Referring to Figure 8–34, the footing will now be checked for Group II and III loading. From a previous analysis, the following are computed:

Group II, $P = 555$ kips, $M_{x-x} = 420$ ft-kips, $M_{y-y} = 215$ ft-kips

Group III, $P = 725$ kips, $M_{x-x} = 795$ ft-kips, $M_{y-y} = 345$ ft-kips

and evidently, among the two groups, Group III controls.

Compute $e_x = 795/725 = 1.10$ ft, $e_y = 345/725 = 0.48$ ft. For a trapezoidal pressure distribution (see Figure 8–34a)

Table 8–16 Bearing Capacity Factors $N\gamma$ and N_q for Sands and Gravels.

Friction Angle, ϕ (degree)	N_7	N_q
28	17	15
30	22	18
32	30	23
34	41	29
36	56	38
38	78	49
40	110	64
42	155	85
44	225	115
46	330	160
48	495	220
50	760	320

(From Vesic, 1973).

$$q = \left(\frac{725}{144}\right)\left[1 \pm \frac{6(1.10+0.48)}{12}\right] = (5.04)(1 \pm 0.79) = 9.02 \text{ kips/ft}^2$$

$$= 1.06 \text{ kips/ft}^e$$

Alternatively, the bearing capacity of the footing subject to the eccentric loading resulting from Groups II and III may be computed from a reduced effective area assuming a uniform pressure distribution. This procedure is demonstrated in Figure 8–34(b), which is based on Equations (8–5) and (8–6). According to this procedure we calculate

$$y = 6.00 - 0.48 = 5.52 \text{ ft}, \quad \text{and} \quad x = 6.00 - 1.10 = 4.90 \text{ ft},$$

so that an effective (reduced) footing size is $11.04 \times 9.80 = 108$ ft^2.

For Group III loading, the equivalent (uniform) contact soil pressure is now $725/108 = 6.71$ kips/ft^2.

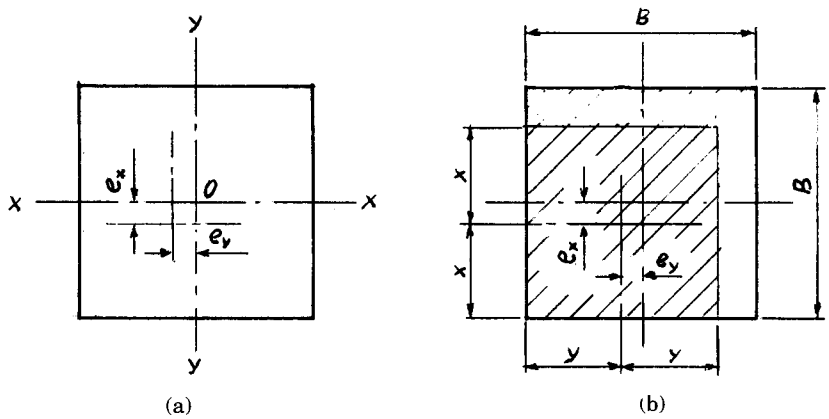

Figure 8–34 Footing of Design Example 8.1A.

Example 8–1B, Solution from SPT Data

A square footing 12 ft × 12 ft is founded in sand with $\gamma = 115$ lb/ft^3. Results from standard penetration tests are shown in Table 8–17. The footing will be 5 feet below ground surface. A firm stratum is located about 45 feet below the bottom of footing. Estimate the bearing capacity of the footing. Disregard settlement considerations.

Solution The capacity of the footing will be estimated from Equation (8–11).

First, the minimum average value $\overline{N}$ of SPT blow count within a depth of $1.5B$, or 18 feet below the bottom of footing, is estimated. This step is tabulated in Table 8–18. Note that $N' = N$ since corrected values for submergence effect are applicable only to silty sands below the water table. From Table 8–18, $\overline{N} = 11$.

The higher groundwater elevation shown in Table 8–17 indicates the critical water level is about 20 feet below the ground surface, or $D_W = 20$ feet. For this condition, the values of C_{W1} and C_{W2} in Equation (8–11) will be computed from Table 8–4 by interpolation, or

$$C_{W1} = 0.50 + (15/18)(0.5) = 0.91$$

$$C_{W2} = 1.00$$

Hence,
$$q_{ult} = \frac{11 \times 2}{10}\left(0.91 + 1 \times \frac{5}{12}\right) = 17.6 \text{ tons/ft}^2$$

For allowable stress design, the factor of safety is 3, so that

Table 8–17 Standard Penetration Test Data for Design Example 8–1B

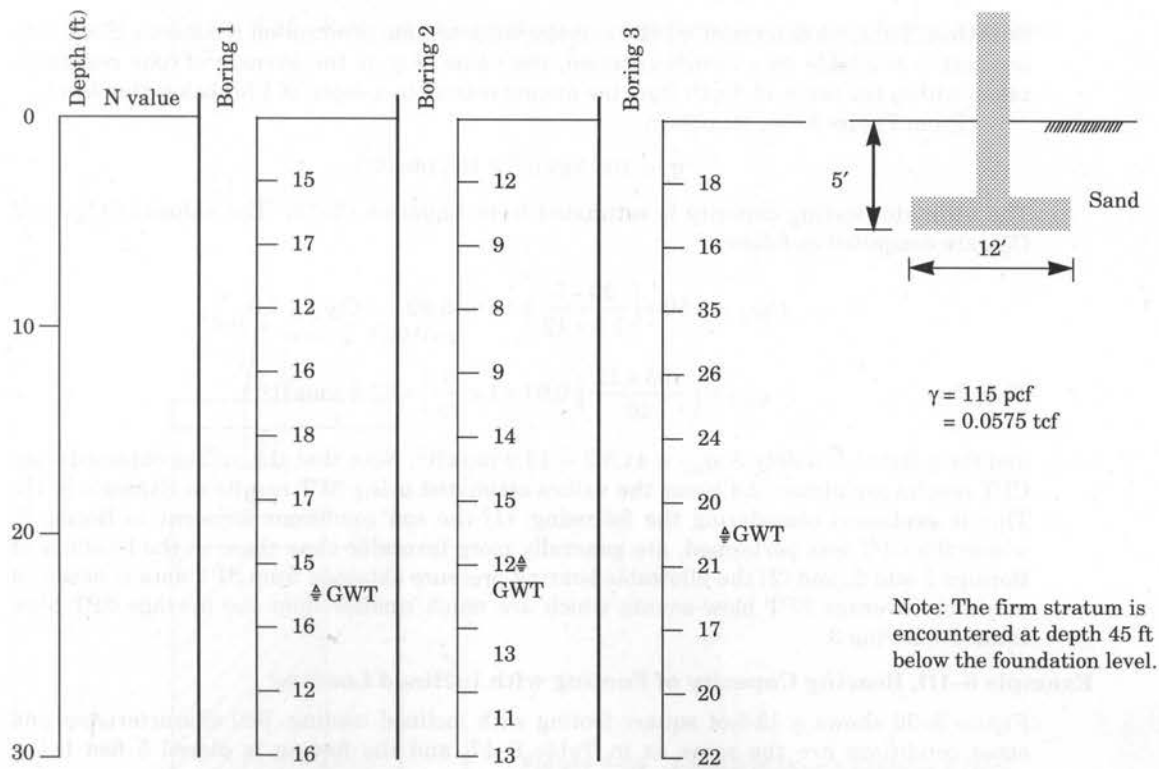

Table 8–18 Data for Estimating Bearing Capacity of Footing Using Results from Standard Penetration Test for Design Example 8–1B

Depth (ft)	Boring 1			Boring 2			Boring 3		
	N	N'	$\overline{N}$	N	N'	$\overline{N}$	N	N'	$\overline{N}$
6	17	17	17	9	9	9	16	16	16
9	12	12	15	8	8	9	35	35	26
12	16	16	15	9	9	9	26	26	26
15	18	18	16	14	14	10	24	24	25
18	17	17	16	15	15	11	20	20	24
21	15	15	16	12	12	11	21	21	24
24	16	16	16	13	13	11	17	17	23

N′ = Corrected N values for submergence effect; appplicable only to silty sands encountered below the water table. Thus N = 11 (the minimum average value)

$$q_{all} = 17.6/3 = 5.9 \text{ tons/ft}^2$$

If the groundwater table could rise to the footing level, $D_W = D_f$, then $C_{W1} = 0.5$. Then $q_{ult} = \dfrac{11 \times 12}{10}\left(0.50 + \dfrac{5}{12}\right) = 12.1$ tons/ft^2, and $q_{all} = 12.1/3 = 4.0$ tons/ft^2

Example 8–1C, Solution from CPT Data

Figure 8–35 shows results of a cone penetration test performed in the vicinity of Boring 3 of Example 8–1B. Based on these results, estimate the bearing capacity of the 12-foot square footing. Assume other conditions the same as in Example 8–1B.

Solution First, we determine q_c, the average value of cone penetration resistance. Since only one test is available as a design criterion, the value of q_c is the average of cone resistance taken within the range of depth from the footing bottom to a depth of $1.5B$ below that level.

From Figure 8–35, we obtain

$$q_c = 105 \text{ kg/cm}^2 = 105 \text{ tons/ft}^2$$

The ultimate bearing capacity is estimated from Equation (8–13). The values of C_{W1} and C_{W2} are computed as follows

$$C_{W1} = 0.50 + \left(\frac{20 - 5}{1.5 \times 12}\right)(0.5) = 0.92 \qquad C_{W2} = 1.0$$

Therefore $$q_{ult} = \left(\frac{105 \times 12}{40}\right)\left(0.91 + 1 \times \frac{5}{12}\right) = 41.8 \text{ tons/ft}^2$$

and for a factor of safety 3, $q_{all} = 41.8/3 = 13.9$ tons/ft^2. Note that the values obtained from CPT results are almost 2.4 times the values estimated using SPT results in Example 8–1B. This is explained considering the following: (1) the soil conditions adjacent to Boring 3, where the CPT was performed, are generally more favorable than those in the locations of Borings 1 and 2; and (2) the allowable bearing pressure obtained from SPT data is based on minimum average SPT blow counts which are much smaller than the average SPT blow count for Boring 3.

Example 8–1D, Bearing Capacity of Footing with Inclined Loading

Figure 8–36 shows a 12-foot square footing with inclined loading. Soil characteristics and other conditions are the same as in Table 8–17, and the footing is placed 5 feet below

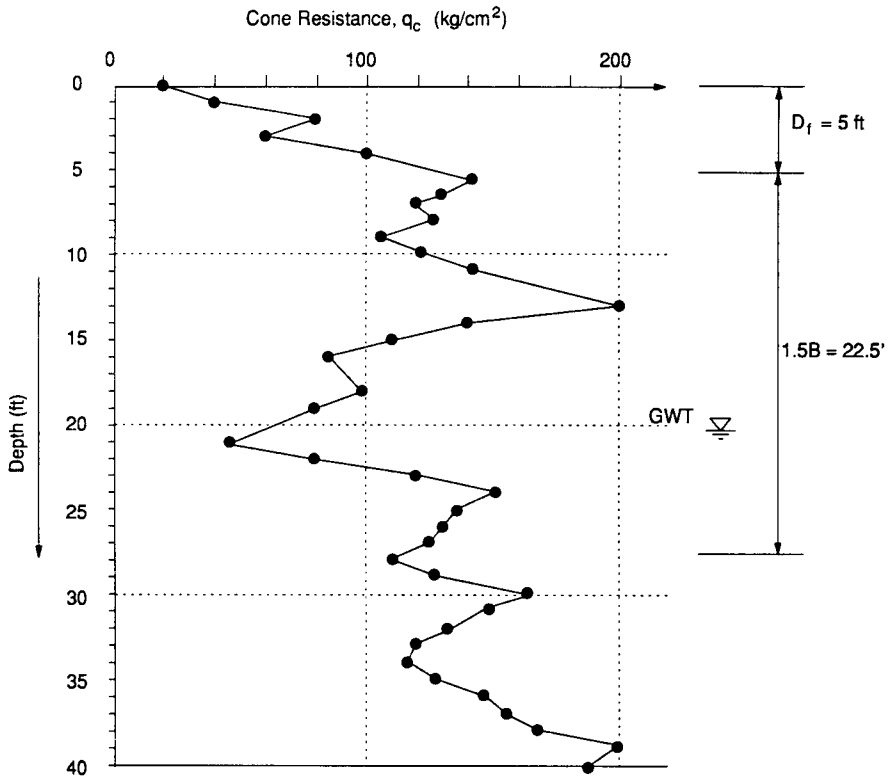

Figure 8–35 Result of cone penetration test performed adjacent to Boring 3 of Table 8–17.

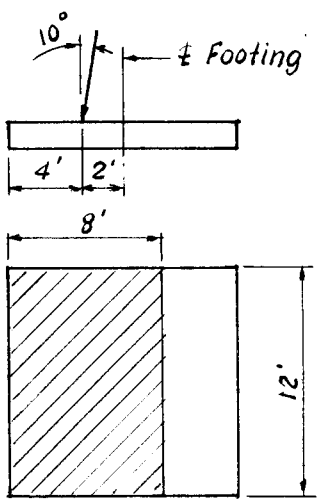

Figure 8–36 Footing of Design Example 8.1D.

ground surface. Estimate the bearing capacity of the footing using Equation (8–11) adjusted for inclined loading.

Solution First, we calculate the effective dimensions of the footing. Referring to Figure 8–36, $B' = 4 \times 2 = 8$ ft, $L' = 12$ ft.

From the angle of inclination 10°, $H/V = \tan 10° = 0.18$, where H and V are the horizontal and vertical components of the load, respectively. Recall from Example 8–1B that $\overline{N} = 11$ Also note that the groundwater table is at depth greater than 1.5 B' ($1.5 \times 8 = 12$) below the base of the adjusted (effective) footing, and hence $C_{W1} = C_{W2} = 1.0$.

The vertical component of the ultimate bearing capacity is computed from Equation (8–11) as

$$(q_{ult})_{vert} = \left(\frac{11 \times 8}{10}\right)\left(1 + 1 \times \frac{5}{8}\right) = 14.3 \text{ tons/ft}^2$$

This must be adjusted by multiplying by the reduction factor R_1, accounting for the effect of load inclination. From Table 8–5 we extract the following data

H/V	$D_f/B' = 0.00$	$D_f/B' = 1.00$
0.15	$R_1 = 0.65$	$R_1 = 0.75$
0.20	0.55	0.65

Actual $H/V = 0.18$, $D_f/B' = 5/8 = 0.62$, so that the value of R_1 is found by interpolation as

$$R_1 = (0.55)(1 + 0.04)(1 + 0.06) = 0.60$$

or

$$q_{ult} = (14.3)(0.60) = 8.6 \text{ tons/ft}^2 = 17.2 \text{ kips/ft}^2$$

For a factor of safety of 3, $q_{all} = 17.2/3 = 5.7$ kips/ft^2. The allowable vertical load is now

$$Q_{all} = (5.7)(8)(12) = 547 \text{ kips}$$

Factor of Safety against Sliding. The horizontal component of the resultant load is

$$H = 0.18V = (0.18)(547) = 98.5 \text{ kips.}$$

Using a moderate coefficient of friction $\tan \delta = 0.55$ (corresponding to $\delta = 29°$), the sliding resistance is

$$Q_f = (547)(0.55) = 300 \text{ kips, giving a factor of}$$
$$\text{safety against sliding } FS = 300/98.5 = 3.0 > 1.5, \text{ OK.}$$

8.15 DESIGN EXAMPLE 8–2, SETTLEMENT OF FOOTINGS

Example 8–2A

The footing of Example 8–1B, section 8.14, supports a service dead load 555 kips and a live load 170 kips. The footing is placed 5 feet below the ground surface. Using the data shown in Table 8–17, estimate the settlement on the footing using the Terzaghi-Peck procedure.

Solution According to this approach, the value of $\overline{N}$ used in estimating bearing pressure from the graphs of Figure 8–12 is the average value in all borings, within the depth range from the base of footing equal to B. From the data of Table 8–17, we obtain the following:

From Boring 1, $\overline{N} = 16$
From Boring 2, $\overline{N} = 11$
From Boring 3, $\overline{N} = 23$

Use $\overline{N} = 16$ for settlement calculations. From Figure 8–12 the bearing pressure corresponding to one-inch settlement is (obtained graphically)

$$q_1 = 1.7 \text{ tons/ft}^2, \text{ for } B = 12 \text{ ft and } \overline{N} = 16$$

The water table for this example is (Table 8–17) 20 feet below ground surface, and for settlement computation it will be taken at a depth approximately B below the footing level.

$$\text{Reduction} = 0.5 + \left(\frac{20-5}{2\times 12}\right)(1.0 - 0.5) = 0.81$$

Adjusted $q_1 = (0.81)((1.7) = 1.4 \text{ tons/ft}^2$

Total load = 555 + 170 = 725 kips = 362 tons, giving actual pressure $p = \dfrac{362}{144} = 2.5 \text{ tons/ft}^2$

The settlement corresponding to this pressure is 2.5/1.4 = 1.8 inches.

Note that q_1 may also be estimated from Equation (8–21), by using $P_s = 1$, $N = 16$, and $B = 12$. The resulting pressures will be given in tons/ft^2.

Therefore, $q_1 = \left(\dfrac{16}{3}\right)\left(\dfrac{13}{24}\right)^2 = 1.6$ tons/ft^2, which is in fairly good agreement with the value of q_1 obtained graphically.

Example 8–2B

For the footing of Example 8–2A, estimate the settlement using D'Appolonia et al. procedure. Assume that the sand is normally consolidated and that a firm stratum is at a depth of 40 feet below the footing elevation.

Solution Recall that from Borings 1, 2, and 3, the values of $\overline{N}$ are 16, 11, and 23. We will use again $\overline{N} = 16$ for settlement calculations.

From Figure 8–14, and using $\overline{N} = 16$ and normally loaded sand, we determine the modulus of compressibility as $M = 265$ tons/ft^2.

Next we determine the settlement influence factors μ_0 and μ_1 from Figure 8–13 using $D_f/B = 5/12 = 0.42$, and $H_t/B = 40/12 = 3.33$. Entering the graphs of Figure 8–13 with these values, we determine $\mu_0 = 0.87$ and $\mu_1 = 0.65$. The settlement of the footing is now estimated from Equation (8–22) as

$$P_s = (0.87)(0.65)\frac{(2.5)(12)}{265} = 0.064 \text{ ft} = 0.77 \text{ in}$$

or less than one-half the settlement computed by the Terzaghi-Peck method.

Example 8–2C

For the footing of Examples 8–2A and 8–2B, estimate the settlement using the elastic procedure stipulated by AASHTO.

Solution Recall that the elastic settlement of footings on cohesionless soils and stiff cohesive soils may be estimated from

$$S_e = [q_0(1-\nu^2)\sqrt{A}]/E_s\beta_z \qquad (8\text{–}55)$$

where q_0 = vertical pressure at base of loaded area (kips//ft^2); ν = Poisson's ratio; A = contact area of footing (ft^2); E_s = soil modulus (kips/ft^2); and β_z = factor accounting for footing shape and rigidity.

Recall that total load = 725 kips, or $q_o = 725/144 = 5.03$ kips/ft^2; also $A = 144$ ft^2. The soil modulus E_s is taken from AASHTO Table 4.4.7.2.2A for dense sand, or $E_s = 1000$

kips/ft^2; Likewise Poisson's ratio $\nu = 0.35$. The factor β_z is taken from AASHTO Table 4.4.7.2.2B for $L/B = 1$ and rigid footing, or $\beta_z = 1.08$.

The elastic settlement is computed as

$$S_e = [5.031(1 - 0.35^2))\sqrt{144}]/(1000)(1.08) = 0.050 \text{ ft} = 0.60 \text{ in.}$$

Example 8–2D

A 15-foot square footing supports a working load of 600 kips, of which 500 kips is dead load and 100 kips is live load. The footing is placed 5 feet below ground surface. Soil data are available from results of cone penetration tests shown in Figure 8–35. Estimate the settlement of the footing using Schmertmann's method (Barker, Duncan, Rojiani, Ooi, Tan, and Kim, 1991).

Solution First, we determine the dimension of the settlement influence diagram.

For a square footing $L/B = 1.0$

From Table 8–10, $Z_{max}/B = 2.00$, $Z_p/B = 0.50$, and $I_{zt} = 0.10$.

Assuming that the footing weight is about the same as the weight of excavated soil,

$$\Delta_p = (300)(15 \times 15) = 1.33 \text{ tons/ft}^2$$

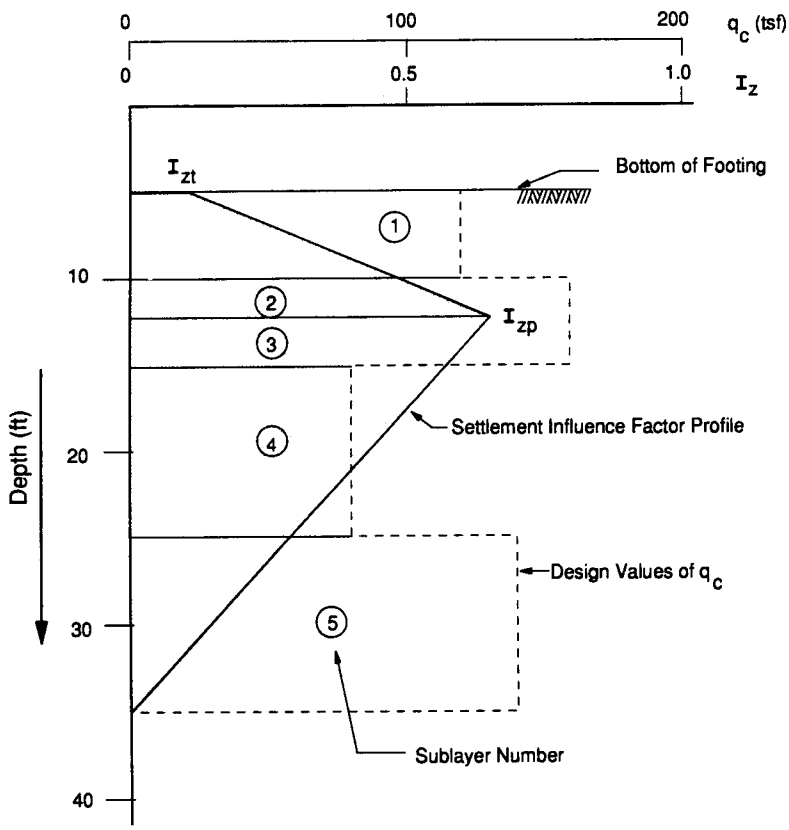

Figure 8–37 Settlement influence diagram and design values of cone resistance for the 15-foot square footing. Design Example 8.2D.

Table 8–19 Soil Layers and Parameters for Design Problem 8–2D

Sublayer Number	Depth (ft)	Thickness Δz (ft)	Average qc (tsf)	I_z	E_s=2.5 qc (tsf)	$\frac{I_z \Delta z}{E_s}$ (ft^3/t)
1	5–10	5.0	120	0.28	300	0.0047
2	10–12.5	2.5	160	0.55	400	0.0034
3	12.5–15	2.5	160	0.60	400	0.0038
4	15–25	10.0	80	0.42	200	0.0210
5	25–35	10.0	140	0.14	350	0.0040
					Σ	0.0369

The effective overburden pressure at Z_p is

$$\sigma'_{vp} = (0.0575)(5 + 0.5 \times 15) = 0.72 \text{ tons/ft}^2$$

and $$\Delta_p/\sigma'_{vp} = 1.33/0.72 = 1.85$$

The value of I_{zp} is interpolated from Table 8–10, as

$$I_{zp} = 0.60 + \frac{(0.64 - 0.60)}{2 - 1}(1.85 - 1) = 0.63$$

Using the computed values of z_{max}, I_{zt} and I_{zp}, we draw the settlement influence diagram as shown in Figure 8–37.

Using the data from Figure 8–35, the design value of q_c is determined as shown in Figure 8–37. For settlement purposes, the soil beneath the footing is divided into five layers as shown in Table 8–19.

The initial effective overburden pressure at footing level is

$$\sigma'_{vo} = (0.0575)(5) = 0.29 \text{ tons/ft}^2$$

hence, $$\sigma'_{vo}/\Delta_p = 0.29/1.33 = 0.22$$

From Table 8–8 and using $\sigma'_{vo}/\Delta_p = 0.22$, $C_p = 0.89$ (by interpolation)

The immediate settlement in the footing, P_i, may be computed from Equation (8–24) as

$$P_i = (0.89)(1.0)(1.33)(0.0369) = 0.044 \text{ ft or } 0.52 \text{ in.}$$

The settlement for any number of years following the immediate settlement may be estimated from P_i by applying a factor C_t, according to Equation (8–34) and Table 8–9. For example, for 3 years, $C_t = 1.3$, so that

$$P_t = (1.3)(0.52) = 0.68 \text{ in.}$$

8.16 DESIGN EXAMPLE 8–3, FOOTING IN ROCK

Figure 8–38 shows geotechnical data and site conditions for a bridge abutment near the Pennsylvania Turnpike (Lehigh County). The footing dimensions are 29.75 ft × 14 ft, and the footing base is at an elevation 380.00. From these data estimate the allowable bearing pressure for the footing.

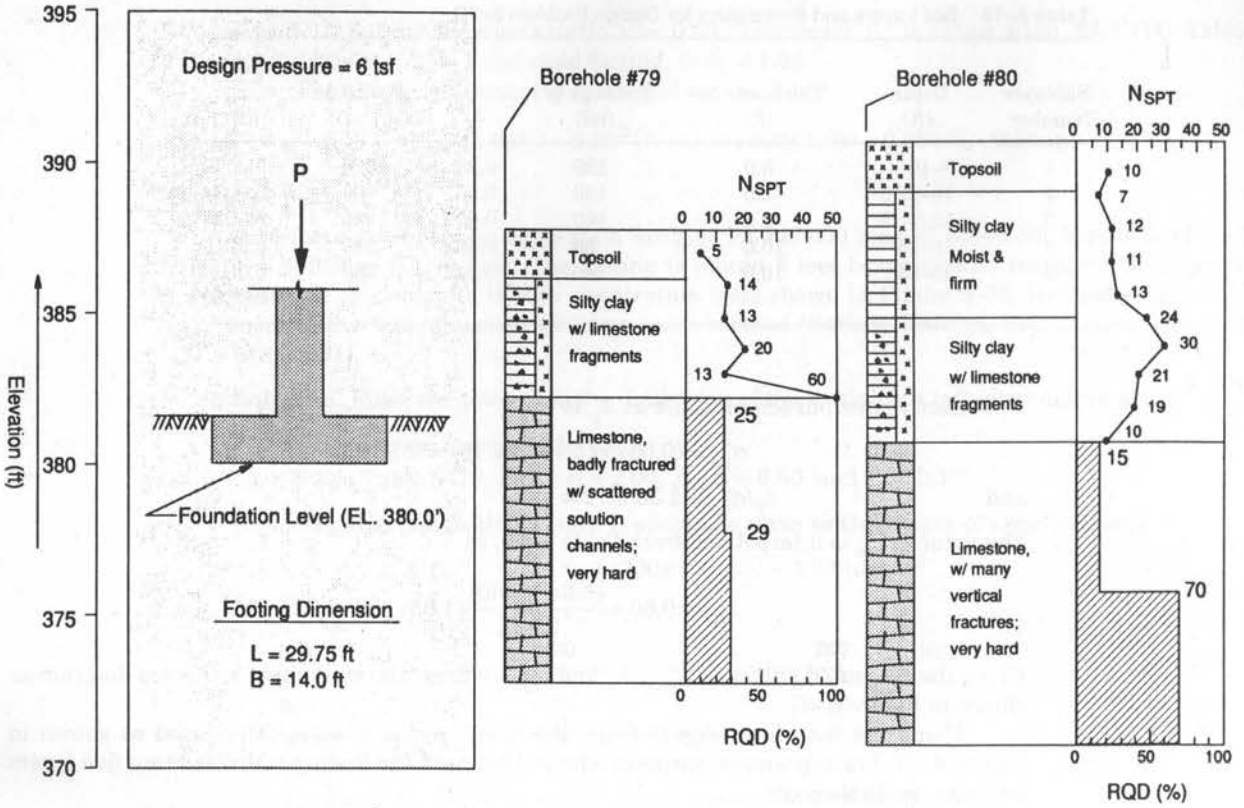

Figure 8–38 Geological conditions for a bridge abutment footing near Pennsylvania Turnpike (Lehigh County).

Solution The rock is badly fractured, hence the design should consider procedures specified for broken or jointed rock. The bearing resistance is correlated with RQD.

From Borehole #7

Core Run 1 (El. 377.50 → El. 382.50): RQD = 25%

Core Run 2 (El. 372.50 → 377.50) : RQD = 29%

From Borehole #8

Core Run 1 (El. 375.60 → 380.60) : RQD = 15%

Core Run 2 (El. 370.60 → 375.60) : RQD = 70%

For design purposes, we will use the lowest RQD, or 15%.

The allowable bearing pressure is correlated with RQD by reference to Table 8–20. By interpolation we obtain

$$q_{all} = 10 + \left(\frac{15-0}{25}\right)(30-10) = 22 \text{ tons/ft}^2$$

The allowable bearing resistance should not exceed the unconfined compressive strength of the rock, or $0.595\, f'_c$ of the concrete.

Alternatively, the bearing capacity may be checked analytically by the use of Equation (8–15). Referring to AASHTO Table 4.4.8.1.2A, and since more data are not available, RQD

Table 8–20 Allowable Bearing Pressures of Jointed Rock

RQD	Allowable Bearing Pressure* (tsf)
100	300
90	200
75	120
50	65
25	30
0	10

*Note: If the recommended value of allowable bearing pressure exceeds the unconfined compressive strength of the rock or allowable stress of concrete, the allowable bearing pressure should be taken as the unconfined compressive strength, or the allowable stress of concrete, whichever is less.

(From Peck, Hanson, and Thornburn, 1974).

values < 25 would indicate a rock of very poor quality whose q_{ult} should be the value for an equivalent soil mass. However, for comparison purposes we will use RQD 25-50 (an average value from all four core runs). Since limestone is rock type A in AASHTO Table 4.4.8.1.2A, the value of N_{ms} is 0.015.

The uniaxial compressive strength C_o may be extrapolated from AASHTO Table 4.4.8.1.2B for rock category A and limestone type. Considering the range 500–6000 kips/ft^2, we interpolate a reasonable value of C_o as 3000 kips/ft^2. Then

$$q_{ult} = (30.00)(0.015) = 45 \text{ kips/ft}^2 = 22.5 \text{ tons/ft}^2$$

Note that there is an obvious discrepancy between the two methods. Since Table 8–20 and Figure 8–10 (AASHTO Fig. 4.4.8.1.1A) are developed from the same reference (Peck, Hanson, and Thornburn, 1974), the analysis using either Table 8–20 or Figure 8–10 is warranted only if the rock is competent according to AASHTO criteria. Since the borehole data identify the rock as badly fractured, the bearing capacity must be determined from Equation (8–15), giving q_{ult} = 22.5 tons/ft^2. Thus, the design pressure for this example is 6 tons/ft^2 (F.S. = 22.5/6 = 3.75, OK).

Settlement The settlement will now be computed using a design (unfactored) footing pressure 6 tons/ft^2. The elastic modulus of rock (intact) is estimated as $E_o = 40 \times 10^3$ tons/ft^2.

In general, determination of the rock mass modulus should be based on results of in situ and laboratory tests. Since in this example the intact rock modulus E_o is known, the value of E_m in Equation (8–37) may be obtained by applying a reduction factor α_E to E_o, which accounts for discontinuities in the rock quality designation.

From Table 8–15, for RQD = 15%, the modulus reduction factor is

$$\alpha_E = 0.08, \text{ hence}$$

$$E_m = (0.08)(40 \times 10^3) = 3.2 \times 10^3 \text{ tons/ft}^2$$

Since L/B = 29.75/14 = 2.12 < 3, the settlement will be estimated from Equation (8–37), or

$$P_m = \frac{(0.9)(2500)}{(3.2)(10^3)(29.75 \times 14)^{0.5}} = 0.034 \text{ ft} = 0.41 \text{ in.}$$

8.17 DESIGN EXAMPLE 8–4, BEARING CAPACITY BY STRENGTH DESIGN

Example 8–4A, Footing in Sand

Using load and resistance factor approach, estimate the capacity of the footing of Example 8–1A for the same soil conditions.

Solution Recall that the ultimate bearing capacity for the footing has been computed using Equation (8–10) and $\phi = 35°$, or

$$q_{ult} = 30.4 \text{ kips/ft}^2$$

Recall that dead load = 555 kips; live load = 170 kips, also $\gamma = 1.3$, $\beta_D = 1.00$, $\beta_{LL} = 1.67$. Factored load = $1.30(555 + 1.67 \times 170) = 1089$ kips.

We assume that the friction angle ϕ has been estimated from SPT data. By reference to Table 8–2, the resistance factor ϕ is 0.35.

Therefore, the factored resistance of the footing is

$$\phi Q_n = (144)(0.35)(30.4) = 1532 \text{ kips} > 1089$$

Example 8–4B, Footing in Rock

Using load and resistance factor approach, estimate the bearing capacity of the footing of Example 8–3. The contact area of this footing is $29.75 \times 14 = 416$ ft^2. A design pressure of 6 tons/ft^2 was quoted in Example 8–3, hence the unfactored (service load) is $416 \times 12 = 4992$ kips, say 5000 kips. We will assume that 75 percent of this load, or 3750 kips, is dead load, and 1250 kips is live load.

Total factored load = $(1.3)(3750) + (2.17)(1250) = 4875 + 2712 = 7587$ kips. Recall that

$$q_{ult} = 22.5 \text{ tons/ft}^2 = 45 \text{ kips/ft}^2$$

Because the value of q_{ult} has been estimated using semiempirical procedures, the resistance factor will be taken as 0.6. Then

$$\phi Q_n = (0.6)(45)(416) = 11230 \text{ kips} > 7587$$

Example 8–4C, Resistance against Sliding

For the footing of Example 8–1D, determine the resistance against sliding under an inclined load of 547 kips. Use load and resistance factor approach. Recall that $V = 547$ kips (unfactored vertical load), and $H = 98.5$ kips (unfactored horizontal load). Note that H is a function of V, or $H = V \tan 10°$. Note also that the sliding resistance Q_r is likewise a function of V, or $Q_r = V \tan \delta$, where δ was assumed as 29°. It follows, therefore, that a meaningful application of the load-resistance concept is not possible because the same load that tends to cause sliding will also tend to resist sliding, hence both these effects might have conflicting load factors.

If H is assumed to be independent of V, such as the case of a vertical load combined with lateral forces, then a rational approach to the load-resistance concept would be possible. In this case the load V would be initially factored by a load factor less than 1.0, and then would be multiplied by a resistance factor, say 0.80, to account for the variability in the sliding resistance. Conversely, the horizontal force H, tending to cause sliding, would be factored by a load factor normally greater than 1.0, depending on the type of load that causes this force.

8.18 DESIGN EXAMPLE 8–5, LOAD FACTOR DESIGN

Example 8–5A, Square Footing

The footing of Example 8–1A is placed 5 feet below ground surface. Check the structural adequacy of the footing in moment and shear, and select the reinforcement using strength de-

sign approach. Assume a round column 3 feet 6 inches in diameter; f'_c = 3000 lb/in^2, and Grade 40 steel.

Group I Recall that total DL = 555 kips, and LL = 170 kips. The total dead load includes the weight of footing and the weight of earth above the footing.
Assuming a footing thickness 33 inches, the weight of footing is

$$12 \times 12 \times 2.75 \times 0.15 = 60 \text{ kips}$$

The weight of earth is 12 × 12 × 2.25 × 0.12 = 39 kips; the net dead loss is 555 − (60 + 39) = 456 kips. The equivalent square column has a side b such that $b^2 = (3.14)(3.5^2)/4$ or b = 3.1, say 3 feet.

Factored load effects in the footing may be obtained directly from the factored net soil pressure q_{un}, or

$$q_{un} = \frac{1.33 \times 456 + 2.17 \times 170}{144} = 6.68 \text{ kips/ft}^2$$

The footing thickness will be checked for two-way shear along a critical perimeter as shown in Figure 8–21(a), where b = 3 feet. For a 3-inch cover and with reinforcement in both directions, the average d is

$$d = 33 - 3 - (\text{one bar diameter}) = 29 \text{ inches}$$

The critical shear perimeter is shown in Figure 8–21(a), and the tributary area for two-way shear is shown in Figure 8–22(a). We compute $b + d$ = 3 + 2.42 = 5.42 ft, hence V_u = 6.68(144 − 5.42^2) = 768 kips (factored shear). Length of critical shear perimeter b_o = 4 × 5.42 = 21.67 feet = 260 inches.

Because β_c = 1.0,

$$V_c 4\sqrt{f'_c} b_o d = (4)(54.7)(260)(29) = 1650 \text{ kips}$$

or

$$\phi V_c = 0.85 \times 1650 = 1402 \text{ kips} > 768.$$

The critical section for moment is at the face of the column.

Referring to Figure 8–19(a), b = 12 feet, and f = 6 − 1.5 = 4.5 feet,

hence

$$M_u = 6.68\left(12.00 \times \frac{4.5^2}{2}\right) = 812 \text{ ft-kips}$$

Assuming that j = 0.9 the area of steel required is

$$A_s = \frac{812 \times 12000}{0.9 \times 40{,}000 \times 29} = 9.3 \text{ in}^2$$

Select 12 #8 bars each way, A_s = 9.48 in^2, and check for M_u.

Next, compute $a = \dfrac{9.48 \times 40{,}000}{0.85 \times 3000 \times 144} = 1.03$ inches

$$\phi M_n = \phi\left[A_s f_y\left(d - \frac{a}{2}\right)\right] = (0.90)(9.48)(40)(2.37) = 808 \text{ ft- kips} \approx 812$$

The balanced reinforcement ratio p_b is computed as

$$P_b = \frac{(0.85)(0.85)(3000)}{40{,}000}\left(\frac{87{,}000}{87{,}000 + 40{,}000}\right) = 0.037$$

Actual $p = (9.48)/(144 \times 29) = 0.0023 < 0.75(0.037) = 0.028$.

Group III Recall from Example 8–1A that the following loads and moments are applied to the footing for Group III.

$$P = 725 \text{ kips}, M_{x-x} = 795 \text{ ft-kips}, M_{y-y} = 345 \text{ ft-kips}$$

The net load is 725 − 99 = 626 kips. However, this reduction will not be applied since the reduced effective area is not known yet.

All the β factors for Group III in load factor design are 1.0, except for wind on structure, which is 0.3. However, the moments due to wind forces have already been adjusted to include this factor. Hence, all factored loads and moments for Group III are obtained from the values for Group I by applying a load factor $\gamma = 1.3$. Thus

$$P_u = 725 \times 1.3 = 943 \text{ kips}, M_{u(x-x)} = 795 \times 1.3 = 1034 \text{ ft-kips},$$
$$M_{u(y-y)} = 345 \times 1.3 = 448 \text{ ft-kips}.$$

Because P, M_{x-x} and M_{y-y} are factored by the same load factor, e_x and e_y should be the same as in Example 8–1A, and referring to Figure 8–34(b), $e_x = 1.10$ feet and $e_y = 0.48$ feet. Likewise, we obtain $y = 5.52$ feet, and $x = 4.90$ feet for the same (reduced) effective footing area as in Example 8.1A, or $11.04 \times 9.80 = 108$ ft^2.

The net load acting on the soil will be adjusted as follows:

footing $= 2.75 \times 0.15 = 0.41$

earth $= 2.25 \times 0.12 = 0.27$, or total $= 0.68$ kips/ft^2

Net (adjusted) load $P_{un} = 943 - (108 \times 0.68 \times 1.3) = 848$ kips

giving $$q_{un} = 848/108 = 7.85 \text{ kips/ft}^2 \text{ (net)}$$

The design will also check the bearing capacity of the foundation for Group III. For $P_u = 943$ kips, $p_u = 943/108 = 8.73$ kips/ft^2. Recall now from Example 8–1A that $q_{ult} = 30.4$ kips/ft^2. Recall now from Example 8–1A that $q_{ult} = 30.4$ kips/ft^2. Since the friction angle used to compute q_{ult} is assumed to have been estimated from SPT data, the resistance factor ϕ will be taken as 0.35.

Hence, $\phi q_{ult} = 30.4 \times 0.35 = 10.6$ kips/ft$^2 > 8.73$.

The reinforcement will be checked for both axes. Referring to Figure 8–34(b), for $2y = 11.04$ feet

$$M_u = 7.85\left(11.04 \times \frac{4.5^2}{2}\right) = 878 \text{ ft-kips}$$

This group controls the design, and the reinforcement must be increased. Select 14 #8 bars $A_s = 11.06$ in^2.

Compute $$a = \frac{11.06 \times 40{,}000}{0.85 \times 3000 \times 132} = 1.3 \text{ inches}$$

$$\phi M_n = (0.90)(11.06)(40)(2.36) = 939 \text{ ft-kips} > 878$$

Use 14 #8 bars in both directions.

In order to complete the design, we should also check the development requirements, the transfer of load at the column-footing joint, two-way shear for Group III, one-way shear, and reinforcement requirements at the top of footing for Group III assuming a trapezoidal pressure distribution.

This example is based on the bridge analyzed in section 2.9. Referring to Figure 2–21, several combinations of the lateral components P and N may be obtained by varying the

wind direction. From the analysis of the pier in section 2.9, the *N–P* combination results in equivalent overturning moments in both principal axes of the footing; hence, a square footing was selected. Conversely, a rectangular spread footing should be considered where the design moments about the principal footing axes are markedly different.

8.19 DESIGN EXAMPLE 8–6, STRIP FOOTING

Limit state design. The strip footing shown in Figure 8–39 supports a substructure element for a bridge. Since this pier is considerably long and continuous, the loads are given for a unit length (m). The dead load and live load are shown as G_u and Q_u, respectively. The corresponding load factors γ_f are also shown, and represent values according to the limit states approach discussed in section 3.4.

For the shallow foundation of this example, we will use Equation (8–19). Material properties, most probable values, worst credible values, and units are tabulated as follows:

Material Property		Most Probable Value	Worst Credible Value	Unit
Concrete unit strength		24	γ_f = 1.15	kN/m^3
Concrete strength		30	γ_m = 1.50	N/mm^2
Steel strength		425	γ_m = 1.15	N/mm^2
Soil unit weight		20	17	kN/m^3
	c'	10	5	kPa
	ϕ'	25	21	degrees
	N_c	19	16	—
	N_q	12	7	—
	$N\gamma$	8	3	—
Water unit weight		10	10	kN/m^3

where γ_f and γ_m are load and material factors, respectively (specified by applicable codes and criteria).

Bearing Capacity (Ultimate Limit State) From the loads and the worst credible values, we calculate the worst credible load affect S as follows:

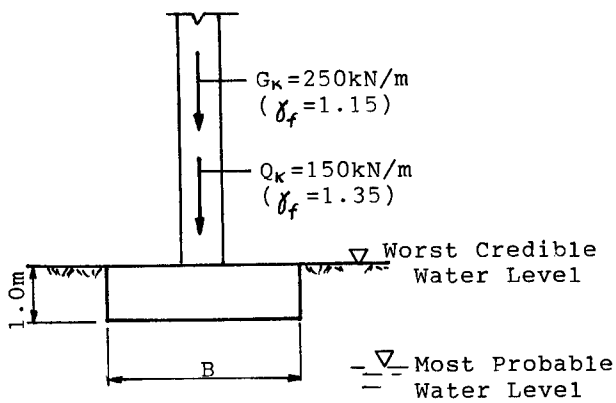

Figure 8–39 Strip footing of design example.

$$S = \left[\frac{(250 \times 1.15)}{B} + \frac{150 \times 1.35}{B}\right] + [(24 \times 1.15 \times 1.0) - (10 \times 1.0)]$$
$$= \frac{490}{B} + 17.6$$

Likewise, the design resistance is the worst credible resistance R, computed as

$$R = q_{ult} = [(5 \times 16) + \{0.5 \times (17 - 10) \times 3 \times B\} + (17 - 10) \times 1.0 \times 7] =$$
$$129 + 10.5B$$

For a structural performance factor γ_p = 1.2 (established from design criteria), Equation (3–12) gives

$$R \geq \gamma_p S, \text{ or } 129 + 10.5B = 1.2\left(\frac{490}{B} + 17.6\right).$$

When solved, this gives B = 3.9 m.

Allowable stress design. The loads are again: Dead load = 250 kN/m, live load = 150 kN/m, and the water table is taken at the ground surface. Material properties and soil strength parameters are taken with their most probable values from the foregoing table.

The contact soil pressure is now

$$q_p = \left(\frac{250 + 150)}{B}\right) + (24 - 10) \times 1.0 = \frac{400}{B} + 14$$

The ultimate bearing resistance is obtained from Equation (8–2), using the most probable values, and is divided by the factor of safety F to give an allowable soil pressure q_r, or

$$q_r = \frac{1}{F}[(10 \times 19) + \{0.5(20 - 10) \times B \times 8\} + (20 - 10)1.0 \times 12]$$
$$= \frac{1}{F}(310 + 40B)$$

Using F = 3, and setting $q_p = q_r$ gives

$$\frac{310 + 40B}{3} = \frac{400}{B} + 14$$

When solved, the foregoing equation gives B = 3.1 m.

8.20 SEISMIC DESIGN REQUIREMENTS

The 1992 AASHTO Specifications discuss the foundation design requirements in Division I-A, Section 6. Because the associated criteria are applicable to all three major seismic performance categories B, C and D and are extended to footings as well as to piles, this brief review maintains the same format.

Investigation Requirements

Slope instability, liquefaction, fill settlement, and increases in lateral earth pressure have been major factors contributing to bridge damage in past earthquakes. Because liquefaction in particular is credited for many bridge failures, it is essential to evaluate site liquefaction potential.

Seed (1979) suggested two basic approaches for assessing the cyclic liquefaction potential of a deposit of saturated sand subjected to earthquake shaking: (1) empirical methods based on field observations of the performance of sand deposits, and correlations between sites that have been not liquefied and SPT blowcounts; and (2) analytical methods based on laboratory studies of the liquefaction strength characteristics of soil samples, and the use of dynamic site response analysis to determine the magnitude and pattern of earthquake-induced shear stresses.

Once a liquefaction strength curve has been established, liquefaction potential may be evaluated from comparisons with estimated earthquake-induced shear stresses. The latter may be determined either from a simplified procedure (Seed and Idris, 1971), or by the use of a more detailed assessment of dynamic response such as the SHAKE program. Interestingly, a rough indication of the liquefaction potential may be obtained through the empirical correlation between the design earthquake and the epicentral distance to the most distant field manifestations of liquefaction, as suggested by Youd and Perkins (1977).

Footings

A usual practice for seismic design of foundations is to assume pseudo-static conditions where earthquake-induced foundation loads are determined from the reaction forces and moments necessary for structural equilibrium. When the analysis is based on bearing capacity theories involving a capacity reduction factor or an appropriate factor of safety, consideration should also be given to the factors associated with the dynamic nature of seismic loads.

Under cyclic loading at earthquake frequencies, the potential strength of many soils may exceed the static strength. For unsaturated cohesionless soils, the increase may be about 10 percent, but for cohesive soils it may reach 50 percent. However, for softer saturated clays and saturated sands there is a possibility of strength and stiffness degradation under repeated cyclic loading, particularly for bridges classified as SPC *C* and *D*.

Because earthquake loading is transient in nature, soil failure for a short time during a cycle may not be significant. Of greater concern is the magnitude of the cyclic foundation displacement or rotation associated with soil yield, as this may have a marked influence on the structural displacements or bending moments and shear distributions in columns. When the response of the structure is assumed to be elastic (this would be the result of a design decision), foundation systems may be considered in three groups.

Elastic Foundation Systems. When an elastic response procedure is appropriate, the foundation is expected to act in a similar manner. Usually, this may be the case in regions of low seismic activity.

Ductile Foundation Systems. When the potential strength of the superstructure is excessive with respect to the specified seismic forces, the foundation may be selected to limit the lateral forces that must be resisted. In this case the foundation ele-

ment, rather than the structure, may be chosen as the principal source of energy dissipation during the inelastic response. The requirements of ductile performance will be applicable to the foundation.

Rocking Structural Systems. In the design of earthquake-resisting pier walls and columns, a usual problem relates to the flexural capacity that can be absorbed by the foundation system without it becoming unstable (i.e., without overturning). In this case it may be better to chose rocking of parts or of the entire structure as the principal mechanism of earthquake resistance. Consequently, rocking parts of the structure and its foundation may be designed to remain elastic during the rocking motions.

Isolated column footings. Superstructure loads and earthquake-induced forces may be transmitted to the supporting soil by the footing as shown in Figure 8–40. The overturning moment capacity of this footing depends on the axial compression load acting simultaneously with the lateral force due to the earthquake, and on the footing dimensions.

The condition whereby a plastic hinge at the base of the column can develop with flexural overstrength while the footing remains elastic is shown in Figure 8–40(a). If the footing dimensions are not large enough, rocking or tipping may occur, as seen in Figure 8–40(b), while both the column and the footing remain elastic; at worst, permanent tilt due to plastic deformation in the soil will occur. When the footing is not protected by appropriate capacity design criteria, inelastic deformations may develop in the footing only, as shown in Figure 8–40(c). If these occur as a result of earthquake attack from the other direction also, the bearing capacity at the edges of the footing to sustain gravity loads may be lost, as seen in Figure 8–40(d).

It appears from these comments that (1) particular attention must be paid to the detailing of the column-footing connection (see also other sections), and (2) equivalent stiffness factors for the foundation system must be determined. Based on field and experimental data, engineers tend to agree that transient foundation uplift for rocking during earthquakes, resulting in separation of the foundation from the subsoil, is acceptable, provided appropriate design precautions are included (Taylor and Williams, 1979). These data also confirm that rotational yielding beneath rocking foundations can provide a useful form of energy dissipation. However, care must be taken to avoid unacceptable vertical deformations accompanying possible soil yielding during earthquake rocking, as well as excessive pier movement.

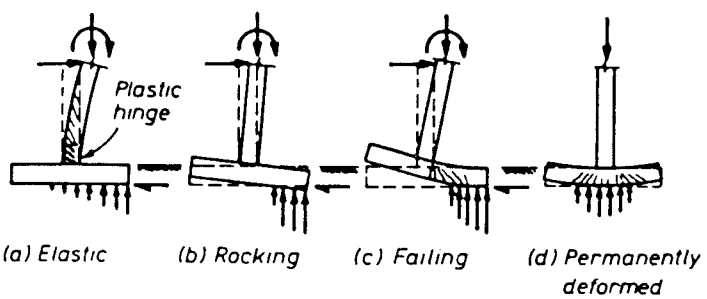

Figure 8–40 Response of isolated footings.

Pile Foundations

Mechanism of earthquake resistance. Pile foundations, discussed in detail in chapter 9, may be subjected to large concentrated forces as a result of overturning moments and shear forces developed during the seismic event. Three distinct situations are shown in Figure 8–41. Similar lateral force and gravity load intensities are assumed so that the lefthand pile or drilled shaft will be subjected to a considerable tensile reaction. The small arrows indicate the sections where the resulting horizontal and vertical forces from the surrounding soil may be applied to the pile.

The most desirable condition is shown in Figure 8–41(a). In this case the pier wall possesses ductility, and together with the piles and the pile cap, it is designed to resist the overstrength load input. However, a greater level of conservatism than that used in the capacity design of the superstructure may be necessary if the intent is to ensure that the piles will remain elastic at all times.

If an inelastic foundation system is chosen, it may be possible to assign energy dissipation to the piles while the structure above remains elastic. This intent may be implemented by yielding of the longitudinal reinforcement of the tension pile, as shown in Figure 8–41(b), or by the mobilization of friction along the soil-pile interface as shown in Figure 8–41(c). Neither alternative is, however, particularly desirable.

Effect of lateral loading on piles. The behavior of piles subjected to lateral forces and consequent bending moments and distortions is quite complex and discussed in some detail in sections 9.11 and 9.12. Most of the solutions for computing the lateral stiffness of vertical piles are based on assumptions of elastic behavior, utilizing the Winkler model, or the elastic continuum approach. The general features of this analysis are illustrated in chapter 9, and in the commentary of the AASHTO specifications.

A point of concern is that, within the soil, pile displacement will be affected by the earthquake response of the superstructure (dynamic effects), and in some cases also by movements of the superstructure (kinematic effects). The resulting pile-soil interaction can induce large local curvature in the piles, particularly when piles are installed in alternating hard and soft soil layers. In such cases, as shown in Figure 8–42, it may not be possible to avoid the development of plastic hinges, even if a conservative capacity design approach is used to protect the pile from damage during the inertial response of

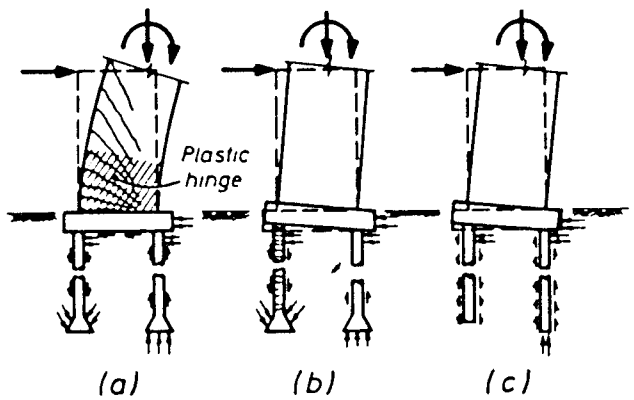

Figure 8–41 Pier walls supported on piles or caissons.

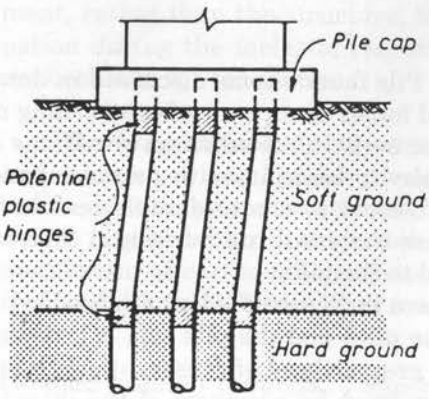

Figure 8–42 Locations of potential plastic hinges in embedded piles.

the superstructure. In this case, the evaluation of load effects and the associated intensities along the piles is rather uncertain, partly because of the variability of soil properties and partly because of the restraint available at the pile ends.

Special requirements and pile details. The uncertainties associated with the overall soil-structure response suggest a tolerant pile system. This will require toughness under induced curvature and shear; hence, suitable piles are steel H-sections and concrete-filled steel-cased piles. Nominal reinforcement should be provided and extended into the pile cap to tie the two elements together and facilitate the load transfer.

Experience from examples such as the one shown in Figure 8–42 has shown that reinforced concrete piles tend to hinge or shatter immediately below the pile cap. Thus, the tie or spiral spacing in this area should be reduced to provide better confinement. Clearly, it is desirable to implement the intent not to allow the piles to fail below the ground level, and to force the columns to undergo flexural yielding above the ground level. The additional design requirements specified by AASHTO for bridges classified as SPC C and D reflect a design philosophy consistent with the severity of seismic activity and the fact that structural damage below ground is not easily detectable following a major earthquake.

REFERENCES

AASHTO, 1992: Standard Specifications for Highway Bridges.

AASHTO, 1994: AASHTO LRFD Bridge Design Specifications.

ACI-ASCE Committee 426, 1974: "The Shear Strength of Reinforced Concrete Members," Chapter 5, "Shear Strength of Slabs," *Proc. ASCE, Journ. Struct. Div.*, vol. 100, No. ST8, Aug. pp. 1543–1591.

American Association of State Highway and Transportation Officials, 1970: NCHRP Synthesis of Highway Practice No. 5—Scour At Bridge Waterways, Highway Research Board, National Research Council, p. 37.

BAGUELIN, F., JAZEQUEL, J. F., and D. H. SHIELDS, 1978: *The Pressuremeter and Foundation Engineering,* Trans Tech Publications, Clausthal, p. 617.

BARKER, R. M., J. M. DUNCAN, K. B. ROJIANI, P. S. K. OOI, C. K. TAN, and S. G. KIM, 1991:

"Manuals for the Design of Bridge Foundations," TRB, National Research Council, Washington, December.

BARTON, N. R., R. LIEN, and J. LUNDE, 1974: "Engineering Classification of Rock Masses and Its Application in Tunnelling," Rock Mechanics, vol. 6, No. 4, pp. 189–236.

BAZARAA, A. R. S. S., 1967: "Use of Standard Penetration Test for Estimating Settlements of Shallow Foundations on Sand," *Ph.D. Dissertation Submitted to Dept. of Civ. Engineering,* Univ. of Ilinois, p. 380.

BOWLES, J. E., 1988: Foundation Analysis and Design, McGraw-Hill, New York, p. 1004.

BRIAUD, J. L., 1990: *The Pressuremeter,* The Netherlands, A. A. Balkeema, p. 314.

BUTTON, S. J., 1953: "The Bearing Capacity of Footings on a Two-Layer Cohesive Subsoil," 3d ICSMFE, vol. 1, pp. 332–335.

Canadian Geotechnical Society, 1985: "Canadian Foundation Engineering Manual," Second Edition, Bitech Publishers, Ltd., Vancouver, B.C., p. 460.

CARTER, J. P. and F. H. KULHAWY, 1988: "Analysis and Design of Foundations Socketed into Rock," Report No. EL-5918, Empire State Electric Engineering Research Corp. and Electric Power Research Institute, New York, p. 158.

CLEMENCE, S. P., and A. O. FINBARR, 1981: "Design Considerations in Collapsible Soils," *ASCE Geot. J.,* vol. 107, No. GT3, March, pp. 305–317.

COLLINS, M. P. and D. MITCHELL, 1991: "Prestressed Concrete Structures," Prentice-Hall, Englewood Cliffs, NJ.

COPP, H. D. and J. P. JOHNSON, 1987: Riverbed Scour At Bridge Piers, *U.S. Dept. of Transportation,* Federal Highway Administration, p. 73.

D'APPOLONIA, D. J., E. D'APPOLONIA, and R. F. BRISETTE, 1970: "Settlement of Spread Footings on Sand", (closure), *Proc. Journ. of Soil Mech. and Found. Div.,* ASCE, vol. 96, No. SM2, pp. 754–761.

DUDLEY, J. H., 1970: "Review of Collapsing Soils," *J. Soil Mech. Found. Div., ASCE,* vol. 96, No. SM3, Proc. Paper 7278, May, pp. 925–947.

Federal Highway Administration, 1988: "Technical Advisory-Interim Procedures for Evaluating Scour at Bridges," *U. S. Dept. of Transportation,* Office of Engineering, Bridge Div., p. 62.

HANSEN, J. B., 1970: "A Revised and Extended Formula for Bearing Capacity," Danish Geot. Institute, Bull. No. 28, Copenhagen, p. 21.

JANBU, N., 1963: "Soil Compressibility As Determined By Oedometer and Triaxial Tests," *Proc. European Conf. of Soil Mechanics and Found. Engineering,* vol. I, Wiesbaden.

JANBU, N., 1967: Settlement Calculations Based on Tangent Modulus Concept, Bull. No. 2, *Soil Mech. and Found. Engineering Series,* The Technical Univ. of Norway, Trondheim, p. 57.

JANBU, N., 1985: "Soil Models in Offshore Engineering," 25th Rankine Lecture, Geotechique, vol. 35, No. 3, p. 241.

KUHN, S. H. and A. B. WILLIAMS, 1961: "Scour Depth and Soil Profile Determination in River Beds," 5th ICSMFE, vol. 1, pp. 487–490.

KULHAWY, F. H., 1978: "Geomechanical Model for Rock Foundation Settlement," *Proc. Jour. of Geotech. Eng. Div.,* ASCE, vol. 104, No. GT2, pp. 211–227.

KULHAWY, F. H. and R. E. GOODMAN, 1987: "Foundations in Rock," Chapter 55 in *Ground Engineering Reference Manual,* Edited by F. G. Bell, Butterworths Publishing Co.

KULHAWY, F. H., C. H. TRAUTMANN, J. F. BEECH, T. D., O'ROURKE, and W. MCGUIRE, 1983: "Bearing Capacity of Shallow Foundations in Soil," Chapter 7 of *Transmission Line Structure Foundations for Uplift-Compression Loading,* EPRI Report EL-2870, Electric Power Research Institute, Palo Alto, California, p. 23.

MENARD, L., 1965: "Regle pour le calcul de la force portante et du tassement des fondations en

fonction des resultats pressiometriques," *Proc. 6th Intern. Conf. on Soil Mech. and Found.* Engineering, Montreal, vol. 2, pp. 295–299.

MEYERHOF, G. G., 1951: "The Ultimate Bearing Capacity of Foundations," Geotechnique, vol. 2, No. 4, pp. 301–331.

MEYERHOF, G. G., 1953: "The Ultimate Bearing Capacity of Foundations Under Eccentric and Inclined Loads," *Proc. 3rd Intern. Conf. on Soil Mech. and Found.* Engineering, Zurich, vol. 1, pp. 440–445.

MEYERHOF, G. G., 1956: "Penetration Tests and Bearing Capacity of Cohesionless Soils," *Proc. Journ. of Soil Mech. and Found. Engineering,* ASCE, vol. 82, No. SM1, pp. 1–11.

MEYERHOF, G. G., 1957: "The Ultimate Bearing Capacity of Foundations on Slopes," *Proc. 4th Intern. Conf. on Soil Mech. and Found. Engineering,* London, vol. 1, pp. 384–386.

MOE, J., 1961: *Shearing Strength of Reinforced Concrete Slabs and Footings Under Concentrated Loads,* Development Dept. Bull. D47, Portland Cement Assoc., Skokie, Ill., April.

MEYERHOF, G. G., 1963: "Some Recent Research on the Bearing Capacity of Foundations," CGJ. Ottawa, vol. 1, No. 1, Sept. pp. 16–26.

MEYERHOF, G. G. and J. D. BROWN, 1967: "Discussion: Bearing Capacity of Footings on Layered Clays," JSMFD, ASCE, vol. 93, SM5, Sept., pp. 361–363.

NATHAN, M. S. S. and B. V. RANGANATHAM, 1978: "Flexural Strength of Modified Square Footings," *ASCE Journ. Struct. Div.,* vol. 104, No. ST3, March, pp. 551–565.

NCHRP, 1970: Synthesis of Highway Practice 5.

NORTHEN, R. D., 1969: "Engineering Properties of Loess and Other Collapsible Soils," *Proc. 7th Intern. Conf. Soil Mech. Found. Eng.,* pp. 445–452.

PECK, R. B., 1976: "Rock Foundations for Structures," *Proc. Conf. on Rock Engineering for Foundations and Slopes,* Vol. II, Boulder, CO., p. 121.

PECK, R. B., W. E. HANSON, and T. H. THORNBURN, 1974: *Foundation Engineering,* 2nd ed., Wiley, N.Y. p. 514.

PURUSHOTHAMARAJ, P., et. al., 1974: "Bearing Capacity of Strip Footings in Two Layered Cohesive-Friction Soils," CGJ, Ottawa, vol. 11, No. 1, Feb., pp. 32–45.

SCHLAICH, J., K. SCHAFER, and M. JENNEWEIN, 1987: "Towards a Consistent Design of Structural Concrete," *PCI Journ.,* Vol. 32, No. 3, May–June, pp. 74–151.

SCHMERTMANN, J. H., 1970: "Static Cone to Compute Static Settlement Over Sand," *Proc. Journ. of Soil Mech. and Found. Engineering,* ASCE, vol. 96, No. 3, pp. 1011–1043.

SCHMERTMANN, J. H., 1977: Guidelines for Cone Penetration Test—Performance and Design, *U.S. Dept. of Transportation,* Federal Highway Administration, pp. 54–55.

SEED, H. B., 1979: "Soil Liquefaction and Cyclic Mobility Evaluation for Level Ground During Earthquakes," *Journ. of the Geotech. Eng. Div.,* ASCE, vol. 105, No. GT2.

SEED, H. B. and I. M. IDRISS, 1971: "A Simplified Procedure for Evaluating Soil Liquefaction Potential," *Journ. of the Soil Mech. and Found. Div.,* ASCE, vol. 97, No. SM9.

STEINBRENNER, W., 1934: "Tafeln zur Setzungberechnung," Die Strasse, pp. 121–124.

SULTAN, H. A., 1969: "Collapsing Soils, State-of-the-Art," *7th Intern. Conf. Soil Mech. Found. Eng.,* No. 5.

TAN, C. K. and J. M. DUNCAN, 1991: "Settlements of Footings on Sand—Accuracy and Reliability," published in the *Proc. Geotech. Engineering Congress,* Boulder, CO.

TAYLOR, P. W. and R. L. WILLIAMS, 1979: "Foundations for Capacity Designed Structures," Bull. of the New Zealand National Society for Earthquake Eng., vol. 12, No. 2.

TAYLOR, B. B., and E. L. MATYAS, 1983: "Influence Factor for Settlement Estimates of Footings on Finite Layers," Canadian Geotech. Journ., vol. 20, pp. 832–835.

TERZAGHI, K., 1943: *Theoretical Soil Mechanics,* Wiley, New York.

TERZAGHI, K., and R. B. PECK, 1967: Soil Mechanics in Engineering Practice, 2nd ed., Wiley, New York, p. 729.

U.S. Department of Navy, 1982: NAVFAC DM–7.1—Soil Mechanics, Naval Facilities Engineering Command, VA, p. 348.

VESIC, A. S., 1973: "Analysis of Ultimate Laods of Shallow Foundations," JSMFD, ASCE, vol. 99, SM1, Jan., pp. 45–73.

YOUD, T. L.and D. M. PERKINS, 1977: "Mapping Liquefaction-Induced Ground Failure Potential," *Journ. of the Geotech. Eng. Div.*, ASCE, Vol. 102, No. GT6.

CHAPTER 9

Driven Piles

9.1 SOIL-PILE INTERACTION

A brief review of the basic pile types was included in section 1.5, and characterized pile groups according to the main material. Piles can also be classified as deep foundations where the soil support is mobilized at some depth below the usable portion of the structure.

A basic condition that warrants the use of a deep foundation exists where soft soil is found near the ground surface and precludes a footing. A deep foundation is in this case used to transfer loads that cannot be adequately supported at shallow depths to a level where adequate support is available. Even though a deep foundation is a viable solution to the problem of soft soils, the most suitable and economical type is not always obvious unless a rational analysis is carried out. The ideal deep foundation type (driven piles, drilled shafts, and linear or prismatic panels) will depend on several factors, including the type of soft soil type of loads, depth of hard stratum, type of substructure, construction considerations' (available equipment, materials and so on), and overall costs.

Action of Soils around a Driven Pile

When driven piles pass through relatively soft material, and their tips penetrate a small distance into a stratum of ample bearing capacity, they are termed "bearing piles" (Figure 9–1a). When the piles develop their load-carrying capacity essentially by side shear, they are called "friction piles" (Figure 9–1b). In many instances, the capacity of a pile results from a combination of side shear and point resistance.

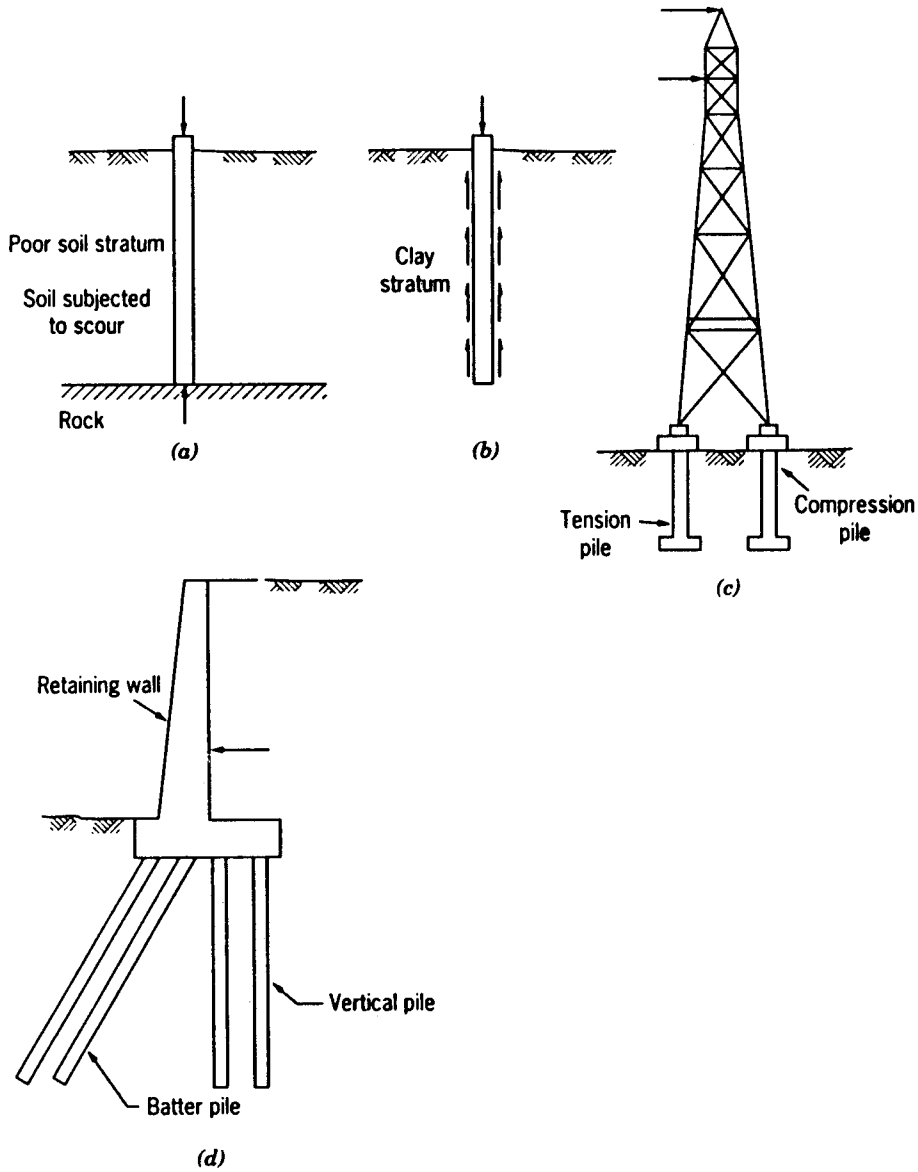

Figure 9–1 Different uses of piles: (a) bearing pile; (b) friction pile; (c) piles under uplift; (d) piles under lateral loads.

Substructures subjected to unusual lateral loads and overturning forces may have to maintain their stability through a combination of pile systems, as shown in Figure 9–1(c). In this case the overturning is resisted by a force couple. One of the pile rows is subjected to tension, and piles in this category are termed "tension piles." Other examples of tension piles are found in structures subjected to uplift and upward forces.

The retaining wall, or abutment, shown in Figure 9–1(d), derives its stability from the combined action of "batter piles" and "laterally loaded piles."

The method of installation may have a profound effect on the behavior of the pile under load, and thus its load-carrying capacity. During pile driving, the resistance to

penetration is a dynamic resistance, but when the pile is loaded by a structural weight, the result is a static resistance. Both dynamic and static resistance have a point bearing and shear component. Although dynamic and static resistance may not have the same magnitude, dynamic pile formulas and wave equations are often used to estimate the static load capacity of a pile.

Pile interaction with clays. The effects of pile driving in clays are (1) remolding or disturbance to the soil structure around the pile; (2) changes in the state of stress of the soil in the vicinity of the pile; (3) dissipation of the excess pore pressures developed around the pile; and (4) long-term increase in soil strength.

Typically, clays exhibit time effects, and these are the cause of the considerable difference in the pile capacity under dynamic and static loading. This behavior may be understood by reference to Figure 9–2, showing a pile of radius *ao*. Curve *A* represents the shear strength before the pile is driven; hence, it shows the undisturbed strength of the clay. Immediately after driving the pile, the shear strength is represented by curve *B*. The clay at point *a* before driving has moved to point *o*, and the clay originally at point *o* has moved to point *f*. The shear is now *oe*, and this is only a small fraction of the original shear *od*.

The clay of point *o* has been remolded, and a great portion of the intergranular pressure has disappeared. However, the total overburden pressure (intergranular pressure plus pore water) is essentially unchanged, thus loss of intergranular pressure means excess pore water pressure. Since the clay is less disturbed away from the pile, the pore pressure increase there is less. In addition, the lateral pressures adjacent to the pile increase considerably as the soil is displaced outwards during pile driving. The

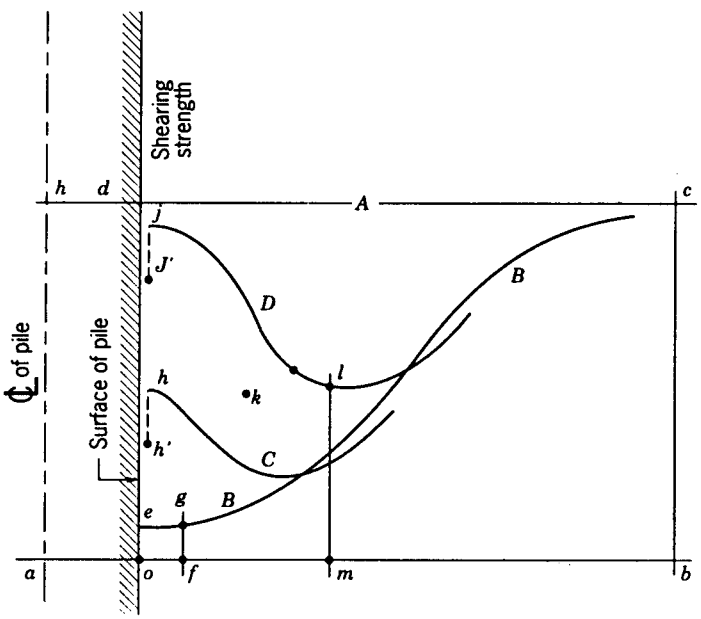

Figure 9–2 Shearing strengths in saturated clay before and after pile-driving operations *(from Prakash and Sharma, 1990).*

gradients resulting from these excess pressures generate seepage and start a process of consolidation. The direction of flow is radially away from the pile. The void ratio of the clay adjacent to the pile decreases, whereas the clay expands farther from the pile. Hence, after pile driving the clay regenerates shear friction at a faster rate.

The tip resistance during driving is generally large, because it equals the force required to cause the remolding. Any soil that may have a high undisturbed strength must be pushed away; the soil cannot be compressed because saturated soils are incompressible under quick loading (i.e., pile driving). Moreover, there is no convenient place for the soil to be displaced. Hence, a soil column extending to ground surface must be heaved up to allow the pile to continue its penetration. During pile driving, practically all the resistance in many clays is tip resistance. DeMello (1969) suggests that immediately after driving, the extent of remolding decreases from about 100 percent at the pile-soil interface to almost zero at about 1.5 to 2.0 pile diameters away from the pile. Orrie and Broms (1967) have shown that for concrete piles in sensitive clay, the undrained strength returns to the original value nine months later.

Pore pressure during driving. Measurements of excess pore pressures developed in a soil as a result of pile driving show that these pressures may become equal to or even exceed the effective overburden pressure (Lambe and Horn, 1965; Poulos and Davis, 1980; D'Appolonia and Lambe, 1971). In the immediate vicinity of the pile the excess pore pressure sometimes approaches 1.5 to 2.0 times the in situ vertical effective stress, and may even reach three to four times the vertical effective stress near the pile tip. However, this excess pore pressure dissipates rapidly away from this pile. If s denotes the radial distance from the pile, and r_o is the pile radius, beyond a distance s/r_o of about 4 for normal clays and about 8 for sensitive clays a rapid decrease in pore pressure occurs. The excess pore pressure is practically negligible beyond a distance of $s/r_o = 30$.

Sands. Vibrations resulting from pile driving in sands have two main effects: (1) densify the sand, and (2) increase the lateral in situ pressure around the pile. Results of penetration tests in sand prior to and after pile driving confirm that considerable densification of the sand occurs for a distance as large as eight diameters away from the pile. Increased density implies a greater friction angle. Likewise pile driving displaces the soil laterally and thus increases the lateral stress on the pile. The increase of the horizontal stress σ_h' acting on piles in sand is shown in tabulated form in Table 9–1 (Horn, 1966), and evidently it covers a wide range of values.

Negative Skin Friction

A pile driven in soft clay or in recently placed fill with its tip on dense stratum may exhibit a particular behavior when it is loaded. Consider, for example, the piles shown in Figure 9–3. During and immediately after driving, a portion of the load is resisted by adhesion at the soil-pile interface as shown in Figure 9–3(a). As consolidation of the soft clay begins, the load is transferred primarily at the pile tip.

If the pile is driven in a fill, the settlement of the latter may exceed the settlement of the pile. This condition occurs when the soil subsides relative to the piles. This differential settlement induces a downdrag force on the pile, also referred to as negative skin friction, as shown in Figure 9–3(b). The pile in this case must support the conventional

Table 9–1 Horizontal Stress on Pile Driven in Sand

Reference	Relationship	Basis of Relationship
Brinch, Hansen, and Lundgren (1960)	(a) $\sigma'_h = \cos^2\phi' \cdot \sigma'_v = 0.43\bar{\sigma}_v$ if $\phi' = 30°$ (b) $\sigma_h = 0.8\sigma'_v$	(a) Theory (b) Pile test
Henry (1956)	$\sigma'_h = K_p \cdot \sigma'_v = 3\sigma'_v$	Theory
Ireland (1957)	$\sigma'_h = K\sigma'_v = (1.75 \text{ to } 3)\,\sigma'_v$	Pulling tests
Meyerhof (1951)	$\sigma'_h = 0.5\sigma'_v$; loose sand $\sigma_h = 1.0\sigma'_v$; dense sand	Analysis of field data
Mansur and Kaufman (1958)	$\sigma'_h = K\sigma'_v$; $K = 0.3$ (compression) $K = 0.6$ (tension)	Analysis of field data

(From Horn, 1966)

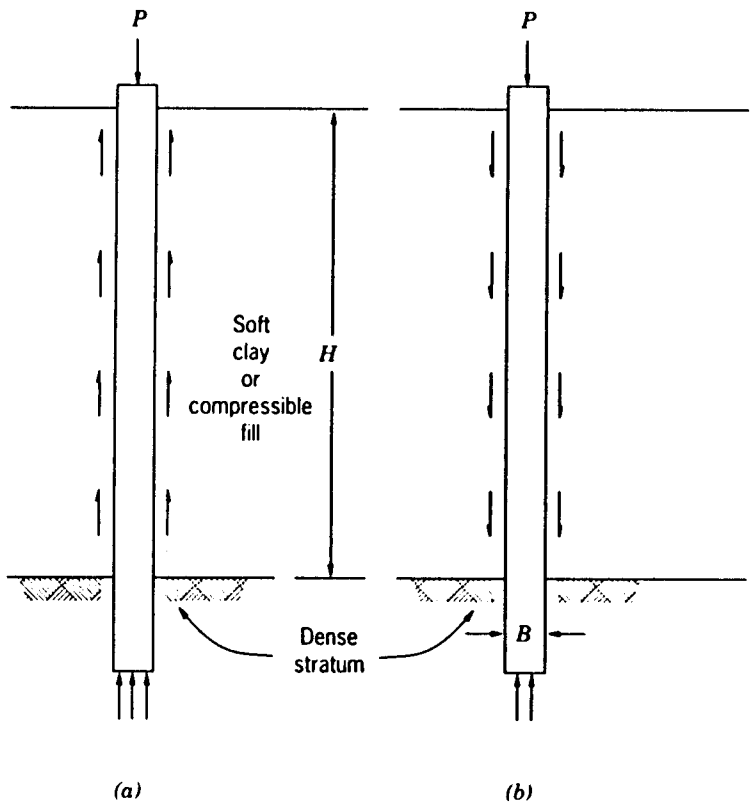

Figure 9–3 Piles in soft soil overlying dense strata: (a) skin friction immediately and during pile driving; (b) negative skin friction.

(normal) loads as well as the downdrag forces. Because the negative skin friction may often be as large as the positive values, it may lead to pile failure. Negative skin friction is discussed in more details in subsequent sections.

Fundamentals of Pile Group Action

The usual spacing of driven piles ranges from $3D$ to $4D$ where D is the diameter or side of the pile. The behavior of piles in a group may be markedly different from that of a single pile, especially if the piles transfer the load primarily by friction. The difference in behavior may not be as pronounced, however, in bearing piles.

Assumed failure patterns under pile foundations are shown in Figure 9–4 (Vesic, 1967), and evidently the effect of load is extended for some distance below the pile tip. Bearing piles typically penetrate a short distance into the hard stratum to develop their capacity, and they transfer the load to the stratum in a small pressure bulb below the pile tip, as shown in Figure 9–5(a). If the bearing stratum and any layers underneath have ample bearing capacity, each pile in the pile group will essentially carry the same load as that carried by individual piles acting alone. If the layers below the pile tip are compressible, the settlement of the pile group will be greater than the settlement of a single pile. This is explained by referring to Figure 9–5(b) showing overlapping zones of increased stress below the pile tips, so that the pile group is more likely to act as one unit. The total (resultant) stress shown by the heavy line may be several times greater than the component stress under a single pile. Likewise the effective width of a group of piles is several times greater than the effective width of a single pile. However, if the bearing stratum and the underlying layers are fairly incompressible, the settlement of a group of bearing piles will be essentially the same as the settlement of isolated piles under the same conditions.

The actions of closely spaced friction piles overlap, and this leads to a load distribution to the various piles which is not uniform. If, in a group of piles, the centrally loaded piles could settle more on loading than the exterior piles, it is possible that they might develop a somewhat greater friction than if all the piles settle equally. Because

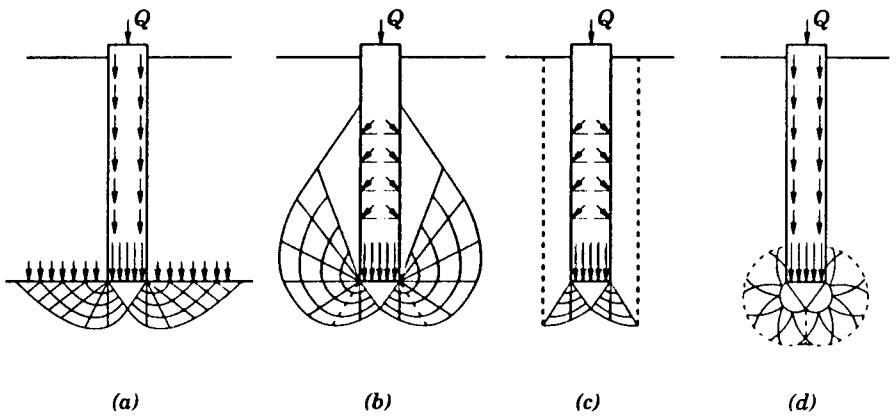

Figure 9–4 Assumed failure patterns under deep foundations (Vesic, 1967); (a) from Prandtl, Reissner, Caquot, Buisman, Terzaghi; (b) from DeBeer, Jaky, Meyerhof; (c) from Berezantsev and Yaroshenko; Vesic; (d) from Bishop, Hill and Mott; Skempton, Yassin, and Gibson.

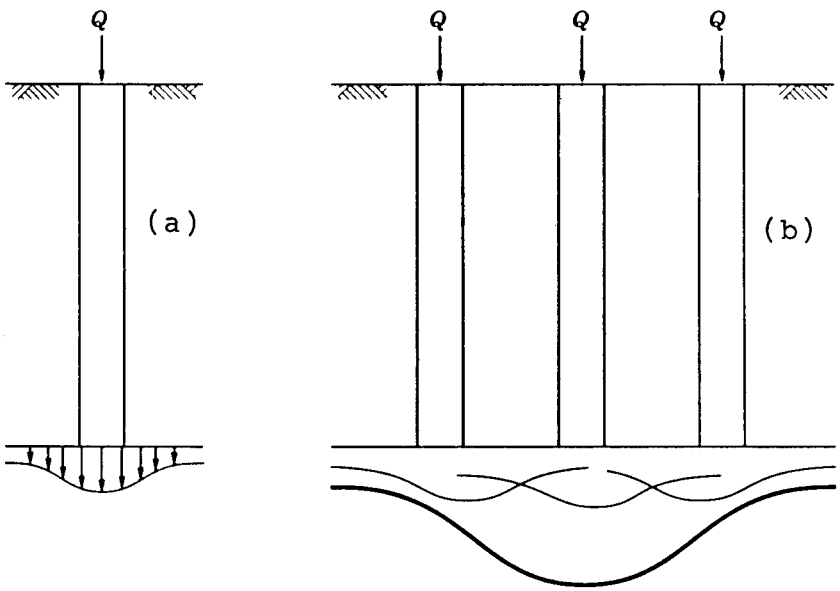

Figure 9–5 Stress conditions below tips of piles; (a) single pile; (b) group of piles.

all piles settle the same amount in a pile group, it follows that exterior piles carry a much greater load than the interior piles. Usually friction piles are arranged in groups with a spacing between $3D$ to $4D$.

A group of piles may fail under load per pile less than the failure load of a single pile. The load-carrying capacity of a group of piles may be determined by considering a failure surface along the perimeter of the group. These concepts are discussed in more detail in subsequent sections.

Settlement of Pile Groups

The settlement of a group of friction piles originates from three different sources:

1. Elastic shortening of the pile under compression and relative movement of the pile with respect to the immediately adjacent soil.
2. Settlement due to compression occurring in the soil between the piles.
3. Settlement associated with the compressibility of the soil layers below the tips of the piles.

The settlements in (2) and (3) above are usually much larger than the settlement in (1), although they are likely to occur at a slow rate because of consolidation and slow dissipation of pore pressure in saturated soil.

Because there is partial disturbance to the soil structure around the piles, accurate estimates of settlement (2) are not possible. We know, however, that this disturbance during pile driving may result in increased settlement after the service loads are applied. A remolded clay, when subjected to a given load, consolidates to a much smaller void ratio than achieved by the same load in the undisturbed clay state. Therefore, any structural disturbance tends to cause greater settlement.

Likewise, the settlement of a single pile is not representative of the settlement of the pile group. A test carried out to obtain the load-settlement behavior of the pile is more likely to give information on the failure load rather than settlements under service load conditions of a friction pile. The installation of piles usually alters the deformation and compressibility characteristics of the soil mass in different ways and to different degrees in comparison to a single pile. Predictions of pile group settlements may be made quantitatively, but actual settlements may in some cases be much larger.

Pile Pullout Resistance

In both sands and clays, piles under tension develop resistance to pullout without the bearing capacity. For piles of uniform diameter in sands, the ultimate uplift resistance is provided by shaft shear and the weight of the pile. The shaft friction in upward loading may not be the same as in the downward loading.

For clays, the ultimate resistance to pullout (adhesion) may be the same as under vertical downward loading. In soft clays, however, sliding failure may occur away from the pile-soil interface. In addition, negative pore pressures may develop in clays during pullout. The uplift capacity of a pile in clay under sustained loading may therefore be smaller than the short-term or undrained capacity. Clays tend to soften with time, and their strength is reduced due to dissipation of negative pore pressure.

Based on pullout tests of uniform diameter piles, Hegedus and Khosla (1984) present the following findings.

1. In overconsolidated clays, the undrained shear strength approach for ultimate pullout capacity predictions results in good agreement with the observed values when the effective pile surface is used in predictions.
2. In sands and nonplastic silts, the uplift capacity predicted on the basis of actual pile perimeter as the failure surface and the friction at this interface gives good results with the measured pullout load.

9.2 PILE TYPES AND SELECTION CRITERIA

In the foregoing sections, piles were classified according to the pile material, the amount of ground disturbance during installation, and the method of load transfer. This section will give a more detailed description of the five major categories of driven piles, namely timber, concrete, steel, composite, and special types.

Precast Concrete Piles

As the name suggests, these piles are cast, cured, and stored in a yard before they are installed in the field, usually by driving. They are available in various cross-sectional shapes, such as circular, octagonal, or square with chamfered corners, and may have central core holes to save weight. Precast concrete piles must be designed to withstand handling and driving stresses in addition to service loads. They can be designed to provide a wide range of load capacity (typically up to 300 tons or 2670 kN). These piles can carry fairly heavy loads through soft material to firm strata as end-bearing piles, but they are also suitable for use as friction piles when driven in sand, gravel, and clay.

Reinforced precast concrete piles are usually 40 to 50 feet (12 to 18 m) long, and have a usual maximum allowable stress of 33 percent of the 28-day concrete strength. These piles consist of internal cage reinforcement having four or more longitudinal bars. The lateral or tie reinforcement is provided by individual hoops or a spiral. In order to resist driving forces, tie reinforcement is closely spaced at the ends. Minor cracking with crack widths up to 0.01 inch (0.25 mm) would normally be considered acceptable, because cracking is almost impossible to eliminate. However, cracks may be the cause of pile deterioration under adverse environmental conditions.

AASHTO Article 4.5.16 gives criteria for size and shape, minimum area, driving points, reinforcement requirements, and handling stresses. Precast concrete piles may be either of uniform section or tapered. The latter should not be used for trestle construction except for the portion of the pile below the ground line. Tapered piles should not be used as columns in any location.

Cast-in-Place Concrete Piles

These piles are installed by placing concrete in a hole formed in the ground either by driving, boring, jetting, coring, or a combination of these methods. In the AASHTO context, cast-in-place concrete piles should be cast in metal shells that are to remain permanently in place. However, other types of cast-in-place piles, plain or reinforced, cased or uncased, may be used if the soil conditions are favorable and the method of placement is satisfactory. Compared to precast piles, cast-in-place piles have the following advantages:

1. They do not need casting and storage yards, and splices or cutting off points are not necessary. The piles are designed for service loads only because they are not subjected to driving and handling stresses.
2. Pile lengths can be adjusted to accommodate field conditions, and predetermination of pile length is not critical.

AASHTO Article 4.5.17 gives criteria for size and shape, minimum area, reinforcement requirements, and interaction with superstructure.

Steel H Piles

Steel piles can provide high strength, they are easy to handle, and are capable of carrying heavy loads to deep bearing strata. They can be used in almost any length because splicing is relatively easy, and they can be readily cut to any size.

Steel H piles (designated as HP) are suitable for penetrating rock as well as for driving through hard and resistant materials. The piles displace a minimum of soil mass during driving, and therefore they can be easily driven through dense materials without causing soil heave. These piles can carry loads in the range of 40 to 120 tons (356 to 1068 kN), and have a length range of about 60 to 100 feet (30 m). The maximum stress in the pile section usually is limited to 12,000 lb/in^2 (82.7 MPa).

Steel H piles are generally driven through soft soils to hard-bearing strata. A common problem with steel piles driven through loose materials to hard uneven rock is deviation from verticality and damage at the tip of the pile resulting in questionable end-bearing capacity. Where these problems are anticipated, the H piles should be protected by attaching hard steel points at their ends.

Pile points are generally considered desirable and economically justified. For a nominal additional cost, they afford to the pile an appreciable increase in bearing capacity while protecting also the pile from damage during driving. Pile points are highly recommended for all H piles designed to reach refusal through rocky material.

AASHTO Article 4.5.18 gives criteria for steel H piles. These cover metal thickness, lugs, and point attachments if pile penetration is through cobbles, boulders, debris, and other hard obstructions.

Unfilled Tubular Steel Piles

Steel pipe piles can be driven either open ended or close ended. Open-ended piles will experience less driving resistance and can be drilled through obstructions such as boulders and bedrock. The circular shape of these piles offers two main advantages: (1) the soil within the pile can be easily taken out, since there are no obstructions for cleaning out tools, and (2) the circular shape minimizes drag from waves and current forces in deep waters. Pipe piles can also be inspected for possible damage and deviation from plumb by lowering a light source within the hollow section. In areas of hard driving, pipe piles may be fitted with end caps.

AASHTO Article 4.5.19 provides criteria for metal thickness, splices, driving requirements, and analysis for column action.

Material deterioration and protection of steel piles. Deterioration of steel piles may be the result of damage during driving, or because of exposure to corrosive environments.

Corrosion is a complex phenomenon, and can be addressed here in a basic concept. Most metals are generally obtained by extraction from their oxides in a process requiring input of energy. In their final form, the refined metals are less stable than in their natural form, and under appropriate conditions they tend to revert to oxides; that is, corrosion is initiated. The severity of corrosion will depend on the nature of the environment in which the metal is placed. In general, swamps, peat bogs, and industrial and mine waste areas constitute corrosive environments.

From the foregoing brief discussion, it follows that when a steel pile is embedded in the ground it may corrode. The degree of corrosion will depend on the availability of moisture and oxygen and the composition of the surrounding soil. Corrosion protection alternatives will require one of the following measures:

1. Provide additional metal by increasing the pile section.
2. Isolate the pile from its environment by either surface coating or by encasement, and
3. Provide cathodic protection.

A summary of protection options is given in Table 9–2. Useful surveys on corrosion of piles are reported by Romanoff (1962) and by Manning and Morley (1981).

Prestressed Concrete Piles

Prestressed concrete piles are usually octagonal, square, or circular. The longitudinal steel is replaced by steel rods or wires under tension, enclosed in a conventional spiral. Pretensioned prestressed concrete piles are usually cast full length. Their length can be

Table 9–2 Corrosion Protection Guidelines

Pile Embedment Environment	Corrosion Potential	Recommended Protection
In impervious soils[a]	Very little	No protection required
In pervious soils[a]	To about 0.5 m below ground surface	Surface coating
Projecting into air	Atmospheric corrosion	Painting above ground
	Soil corrosion near ground	Concrete encasement or coal tar to 0.5 m above and below ground
Projecting into clean fresh water	No corrosion	No protection required
Projecting in sea water	Atmospheric corrosion above high tide	Painting
	Between high tide and mudline will corrode	Concrete encasement or coal tar

[a]Final recommendations will depend on the results of site-specific soil tests. If soils are corrosive one of the corrosion protection methods outlined in the text should be considered.

as much as 130 feet (40 m). Posttensionsed prestressed concrete piles are usually made in sections that can be assembled and prestressed in the plant or at the site. A typical pretensioned prestressed pile is shown in Figure 1–17. Section properties and allowable loads for prestressed concrete piles are shown in Figure 9–6.

Prestressed concrete piles are well suited to soil and water conditions that require high-capacity long piles. They are more durable than conventional reinforced concrete piles because the concrete is under continuous compression. The spalling during driving keeps hairline cracks closed so that aggressive chemicals cannot invade the concrete mass.

Raymond cylinder prestressed piles are an example of this type. These are made of a series of hollow-spun concrete sections reinforced with longitudinal and spiral steel. After curing, the sections are assembled, and high-strength steel wires are threaded through the holes, tensioned, and locked in place.

Prestressed concrete piles are covered in AASHTO Article 4.5.20. They may be solid or hollow, and must have a minimum compressive strength f'_c of 5000 lb/in^2. AASHTO requires an initial compressive stress not less than 700 lb/in^2 after losses mainly to prevent cracking during handling and installation. In addition, bending stresses should be investigated for all conditions during handling, with the tensile stress limited to $5\sqrt{f'_c}$.

Timber Piles

A typical timber pile is shown in Figure 9–7 with the applicable specifications. As mentioned, timber piles embedded below the permanent groundwater table may last for many years without treatment. Since the permanent water table can seldom, if ever, be ensured, treated timber piles are routinely specified in most cases.

Timber piles can either be round untrimmed logs or sawed square sections. The process of sawing can be detrimental to its durability because it removes the outer sapwood that absorbs preservatives. Round untrimmed logs provide the most economical form of timber piles.

Timber piles are mostly used as friction piles in granular soils. However, they cannot be driven against high resistance without damage, and hence they should be considered with caution in dense gravel or fill or as end-bearing piles in rock. Their usual length range is from 20 to 60 feet for diameters 6 to 16 inches. This size range will ac-

commodate design loads up to 50 tons, although the usual practice is to limit the design load to 30 tons as a protection against damage due to high driving.

Timber piles must conform to the requirements of AASHTO Article 4.5.21 regarding materials and treatment.

Special Types of Piles

Composite piles, shown in Figure 1–18, combine sections of dissimilar materials together so that the associated advantages of each component can be utilized. Other special types of piles are available for special uses and conditions, and include compacted piles with expanded base and thermal piles.

Expanded-base compacted (Franki) piles. This type, also called pressure-injected pile, was developed by using special equipment. A steel tube is first driven to the desired depth, and an enlarged base is then formed by feeding in small charges of zero-slump concrete. Each charge is driven out into the soil with hammer blows until the required base is formed. The pile shaft is then formed by depositing zero-slump concrete charges into the drive tube, and then compacting and ramming against the soil as the tube is withdrawn.

These piles are suitable for granular soils where bearing capacity is enhanced by the soil densification around the expanded base. Common pile lengths are from 20 to 60 feet (6 to 18 m), and pile shaft diameters range from 12 to 24 inches (300 to 600 mm). The piles have normal design loads of 60 to 120 tons (534 to 1068 kN).

Thermal piles. Piles in permafrost soil conditions normally transfer their loads to the ground according to two mechanisms:

1. The side support is provided by the development of the adfreeze bond between the soil or backfill and the pile surface.
2. The point or end-bearing support is provided in the conventional way by firm layers such as bedrock or dense thaw-stable sands.

The adfreeze bond between the pile surface and the surrounding soil decreases as the permafrost temperature increases. Thermal piles are therefore used to (1) ensure that long-term degradation of permafrost is prevented by removing heat from the ground, and (2) decrease the existing ground temperature around piles installed in warm-temperature permafrost. In this manner, thermal piles ensure the development of adequate adfreeze bond by keeping ground temperatures low and ensuring long-term thermal stability.

Selection Criteria and Comparison of Pile Types

The selection of a suitable pile type for bridge foundations is normally based on a consideration of soil and water conditions, availability of materials, construction schedule, substructure element to be supported, loads to be transferred, and overall economy. In addition, relevant characteristics of the various pile types should be taken into account since in many cases they may dictate the choice.

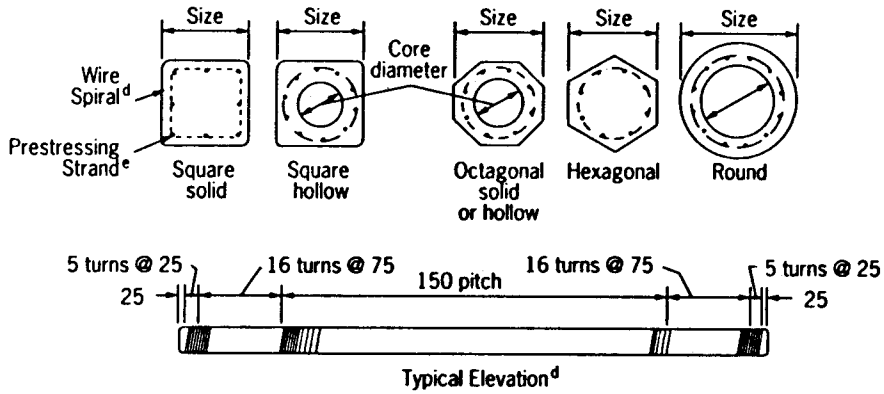

Size (mm)	Core Diameter (mm)	Section Properties[a] Area (mm^2)	Mass (kg/m)	Moment of Inertia ($10^6\ mm^4$)	Section Modulus ($10^3\ mm^3$)	Radius of Gyration (mm)	Perimeter (m)	Allowable Concentric Service Load[b,c] (kN) f'_c (MPa) 35	40	45	50	55
					Square Piles							
250	Solid	63,000	151	326	2,610	72	1.00	646	750	853	958	1,060
300	Solid	90,000	216	675	4,500	87	1.20	922	1,070	1,220	1,370	1,520
350	Solid	123,000	295	1,250	7,140	101	1.40	1,260	1,460	1,670	1,870	2,070
400	Solid	160,000	384	2,130	10,700	116	1.60	1,640	1,900	2,170	2,430	2,700
450	Solid	203,000	487	3,420	15,200	130	1.80	2,080	2,420	2,750	3,090	3,420
500	Solid	250,000	500	5,210	20,800	144	2.00	2,560	2,970	3,390	3,800	4,210
500	275	191,000	458	4,930	19,700	161	2.00	1,960	2,270	2,590	2,900	3,220
600	Solid	360,000	864	10,800	36,000	173	2.40	3,690	4,280	4,880	5,470	6,070
600	300	289,000	694	10,400	34,700	190	2.40	2,960	3,440	3,920	4,390	4,870
600	350	264,000	634	10,100	33,700	196	2.40	2,710	3,140	3,580	4,010	4,450
600	375	250,000	600	9,830	32,800	198	2.40	2,560	2,970	3,390	3,800	4,210

Octagonal Piles												
250	Solid	52,000	125	215	1,720	64	0.77	533	620	704	790	876
300	Solid	75,000	180	446	2,970	77	0.92	769	892	1,020	1,140	1,260
350	Solid	101,000	242	825	4,710	90	1.07	1,030	1,200	1,370	1,540	1,700
400	Solid	133,000	319	1,410	7,050	103	1.22	1,360	1,580	1,800	2,020	2,240
450	Solid	168,000	403	2,260	10,000	116	1.38	1,720	2,000	2,280	2,550	2,830
500	Solid	207,000	497	3,440	13,800	129	1.53	2,120	2,460	2,800	3,150	3,490
500	275	148,000	355	3,160	12,600	146	1.53	1,520	1,760	2,000	2,250	2,490
550	Solid	251,000	602	5,030	18,300	142	1.68	2,570	2,990	3,400	3,810	4,230
550	325	168,000	403	4,480	16,300	163	1.68	1,720	2,000	2,280	2,550	2,830
600	Solid	298,000	715	7,130	23,800	154	1.84	3,050	3,550	4,040	4,530	5,020
600	375	188,000	451	6,160	20,500	181	1.84	1,930	2,240	2,550	2,860	3,170
Round Piles												
900	650	304,000	730	23,400	52,000	277	2.83	3,120	3,620	4,120	4,620	5,120
1,200	950	422,000	1,010	61,800	103,000	383	3.77	4,320	5,020	5,720	6,410	7,110
1,350	1,100	481,000	1,150	91,200	135,000	435	4.24	4,930	5,720	6,520	7,310	8,100
Hexagonal Piles												
300	Solid	78,000	187	486	3,240	79	0.90	800	928	1,060	1,190	1,320
350	Solid	106,000	254	900	5,140	92	1.05	1,090	1,260	1,440	1,610	1,790
400	Solid	139,000	334	1,540	7,700	106	1.20	1,420	1,650	1,880	2,110	2,340

[a] Form dimensions may vary with producers, with corresponding variations in section properties.
[b] Allowable loads based on $N = (A/10^3)\,(0.33 f'_c - 0.27 f_{pc})$: $f_{pc} = 4.8$ MPa: Area in min^2.
[c] Allowable loads based on short column structural capacity only.

Figure 9–6 Section properties and allowable loads for prestressed concrete piles (CPCI, 1982).

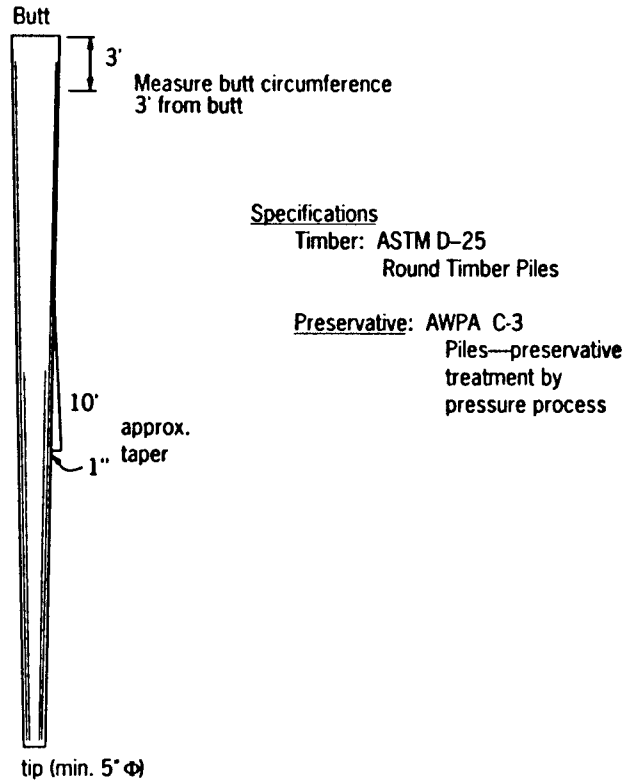

Figure 9–7 Typical timber pile *(from ASCE, Committee on Deep Foundations, 1984).*

Precast concrete piles. These are flexible in terms of length and load range. An important advantage is that they can be used either as end-bearing piles or where the load transfer must be attained by shaft friction. A main disadvantage is that they are difficult to handle without damage unless they are prestressed. They have a relatively high cost, and prestressed piles are difficult to splice.

Cast-in-place concrete piles. These have a lower initial cost, and tapered metal shells can be used to provide a higher bearing resistance in granular soils. They are therefore best suited as medium-load friction piles in these soils. Their main disadvantage is that they are difficult to splice after concreting, and their thin shells can be damaged during driving; redriving is not recommended.

Steel piles. Steel H piles have a usual length range of 60 to 100 feet, but longer lengths (>150 ft) can also be installed to suit ground conditions. Their main advantages are that they can be easily spliced, they have a broad size range, and they displace only a small amount of soil during driving. Disadvantages are potential damage when they are driven through obstructions, and their susceptibility to corrosion.

Concrete-filled steel pipe piles can be installed to almost any length, but the common length range is from 40 to 120 feet (12 to 36 m). Associated disadvantages are a high initial cost and soil displacement for closed-end pipe. Related advantages are better inspection and control during installation, higher load capacities, and easy splicing. These piles can also provide considerable bending resistance where the foundation must also resist lateral loads.

Timber piles. These are fairly inexpensive and suitable for the lower load range (usually 20 to 80 kips). They are easy to handle and resist decay below the water table. However, they are difficult to splice and vulnerable to damage during driving. Treatment to increase resistance to decay becomes mandatory because in most sites the groundwater table is subject to fluctuations.

9.3 DESIGN CONSIDERATIONS

General Requirements

Pile penetration. The required pile penetration is determined on the basis of the expected vertical and lateral loads and associated displacements of both the pile and the subsurface materials. Unless refusal is encountered, the design penetration for any pile should be not less than 10 feet into hard cohesive or dense granular material, and not less than 20 feet into soft cohesive or loose granular soil. Unless they are driven to refusal, piles for trestles or pile bents should penetrate a distance equal to at least one-third the unsupported pile length. Where piles penetrate soft or loose upper layers overlying a hard or firm stratum, they should have a sufficient penetration into the firm stratum to limit pile movement as well as to attain the required bearing capacity. These criteria are summarized in AASHTO Article 4.5.1.3.

Load capacity. Piles should be designed to have adequate bearing (load transfer) and structural capacity, and a tolerable settlement and lateral displacement. The load-bearing capacity of a pile is usually determined from a static analysis based on soil-structure interaction. This may be based on subsurface investigations, laboratory and in situ tests, analytical methods, pile load tests, and on a consideration of other available data. The design should also take into account: (1) the difference between the supporting capacity of a single pile and a group of piles; (2) the capacity of the soil strata to support the load of the pile group; (3) interaction effects with adjacent structures and foundations; (4) the transmission of forces from consolidating soil such as skin friction and downdrag forces; and (5) the potential of scour and its effects.

Effects of scour. There are three potential scour effects (FHWA, 1989) (see also other sections).

1. Aggradation and Degradation. The former is the deposition of bed materials eroded from other portions of a stream, whereas the latter is the removal of stream bed materials causing the bed elevation to be lower. The two processes are long-term effects associated with natural or man-made conditions.
2. General Scour and Contraction Scour. This is essentially the removal of stream bed material across the entire width of the stream as a result of increasing flow velocities. Flow velocities increase following contraction of the flow channel or a change in the downstream water elevation. An example of contraction scour is when the approach embedment of a bridge encroaches into the stream.
3. Local Scour. This occurs when bed material is removed from a small area of the width of the stream. Elements that obstruct flow, such as piers and abutments, cause an acceleration of the flow velocity with associated vortices which tend to wash away bed materials.

Settling ground and downdrag loads. Downdrag loads may be induced at sites underlain by compressible clays, silts, and peats, and especially where a fill has been recently placed, or where the groundwater level is markedly lowered. A downdrag effect should be treated as a load in investigating the bearing capacity and settlement of the pile foundation. Downdrag loads tend to reduce the usable pile capacity.

Downdrag forces should not be combined with transient loads because the latter cause downward movement of the pile foundation, causing a temporary reduction or elimination of the downdrag forces. Downdrag should be considered in pile capacity analysis in the case of a true end-bearing pile in hard soil or rock where the pile capacity is essentially controlled by its structural strength and pile settlement is not a design consideration. Where the pile capacity is controlled by a combined tip and shaft resistance, downdrag may be considered a settlement problem.

Protection against deterioration. From the foregoing sections, it appears that protection against deterioration must be considered, and often provided, for the three main pile types: steel, concrete, and timber.

The LRFD specifications identify the following conditions as indicative of a potential pile deterioration or corrosion situation:

- Resistivity less than 1000 ohm-cm
- pH less than 5.5
- pH between 5.5 and 8.5 in high organic content soils
- Sulfate concentrations greater than 0.10 percent
- Landfills and cinder fills
- Soils subject to mine or industrial drainage
- Areas with a mixture of high-resistivity soils and low-resistivity high alkaline soils
- Insects (wood piles)

In addition, the following water conditions should indicate a high potential of pile deterioration or corrosion situation:

- Chloride content greater than 500 ppm
- Sulfate concentration greater than 550 ppm
- Mine or industrial runoff
- High organic content
- pH less than 5.5
- Marine borers (wood piles)
- Piles exposed to wet/dry cycles

Corrosion of steel piles should be considered particularly in fill soils, soils with low pH, and in marine environments. Appropriate tests may be used to evaluate the corrosion potential. Sulfate, chloride, and acid attack is a potential problem in concrete pile foundations; decay from wetting and drying cycles or from insects and marine borers should be considered with timber piles.

Among the methods mentioned for the protection of steel piles, protective coatings, use of special steel alloys, or increased area are particularly recommended. Protection

coatings have been found to be resistant to abrasion and have a proven service record in the corrosive environment. Protective coatings should extend into noncorrosive soils several feet because the lower portion of the coating is usually more susceptible to abrasion loss during installation. Alternatively, the use of special steel alloys of nickel, copper, and potassium may enhance corrosion resistance in the atmosphere or splash zone of marine piling. Likewise, a sacrificial steel area may be considered for increased corrosion resistance. In the latter case, the steel section is oversized so that the available section area after corrosion meets the structural requirements.

Deterioration of concrete piles can be reduced by appropriate design procedures, such as the use of a dense impermeable concrete, sulfate resisting portland cement, increased steel cover, air entrainment, reduced chloride content in the concrete mix, cathodic protection, and epoxy coated reinforcement. Continuously submerged piles are less prone to deterioration. The ACI Code also provides maximum water-cement ratio requirements for special exposure conditions. For prestressed concrete, the code recommends a maximum water soluble chloride ion of 0.06 percent by weight of cement.

Cathodic protection of reinforcing and prestressing steel induces electronic flow from the anode to the cathodic pile. An external DC power source may be required to drive the current. However, cathodic protection requires electrical continuity between all steel that necessitates bonding the steel to electric connection. Epoxy coating of pile reinforcement have been found effective in many cases, but it is important to ensure that the coating is continuous.

Pile spacing, clearance, and embedment. AASHTO Article 4.5.15 specifies the minimum pile spacing as 2 feet 6 inches, or 2.5 pile diameters or widths. The distance from the side of any pile to the nearest footing edge should exceed 9 inches. The tops of piles should extend at least 12 inches into the concrete footing excluding any damaged pile material.

It should be noted, however, that this pile spacing is a minimum requirement and should be increased according to the anticipated pile group action.

Design Procedure for Pile Foundations

The usual steps in the design of a pile foundation include the following:

1. Develop a soil profile from the boring data available at the site, and identify favorable and unfavorable foundation zones.
2. Estimate the loads and moments for the ultimate and serviceability limit states. Articulate forces caused by negative skin friction.
3. For stream crossings, establish the water profile and include the best estimates of the expected depth of scour during floods.
4. Proceed with the selection of suitable pile types, and obtain preliminary pile lengths. Compare these alternatives for cost and expected performance.
5. Estimate the axial pile capacity in terms of load transfer and structural capacity. Determine the number of piles required, their spacing and location.
6. Investigate the soil-pile action in terms of (a) possible punching into a weak stratum in the pile profile; (b) tolerable settlement; and (c) uplift capacity of the pile group.

7. Check the structural adequacy of the piles under lateral load, and compare the calculated lateral displacement with tolerable value.
8. Establish the requirements for pile load tests to verify the design.

9.4 DESIGN APPROACH

AASHTO Criteria (Allowable Stress Design)

The design pile capacity is the maximum load that the pile can support without exceeding the tolerable movement. The pile capacity is determined from the ultimate load transfer capacity of the pile-soil system, or from the structural capacity of the pile section.

Ultimate load transfer capacity. The ultimate load transfer capacity under axial load is

$$Q_{ult} = Q_S + Q_T \tag{9–1}$$

where Q_{ult} = ultimate axial load transfer capacity; Q_S = ultimate shaft resistance; and Q_T = ultimate tip resistance.

The allowable or design axial capacity is

$$Q_{all} = Q_{ult}/FS \tag{9–2}$$

where FS is the factor of safety. In selecting the appropriate value of the factor of safety, the design should consider the reliability of the procedures used to estimate Q_{ult}, taking also into account the pile installation control. Suggested values of the factor of safety are given in Table 9–3.

The allowable capacity determined from Equation (9–2) should be checked for the corresponding settlement of the pile group. This should not exceed the tolerable differential movement discussed in other sections.

Structural capacity of pile sections. For portions of piles extending above the ground surface, or in soil that does not provide adequate lateral support to resist buckling, the structural capacity is governed by the criteria for compression members.

Table 9–3 Recommended Factor of Safety on Ultimate Geotechnical Capacity Based on Specified Construction Control (AASHTO)

	Increasing Construction Control				
Subsurface Exploration	X[1]	X	X	X	X
Static Calculation	X	X	X	X	X
Dynamic Formula	X				
Wave Eaquation		X	X	X	X
Dynamic Measurement and Analysis			X		X
Static Load Test				X	X
Factor of Safety	3.50	2.75	2.25	2.00[2]	1.90

[1]X = Construction Control Specified on Contract Plans

[2]For any combination of construction control that includes an approved static load test, a factor of safety of 2.0 may be used.

The maximum allowable stress on a pile section should not exceed the specified limits, and where damage or deterioration is anticipated, lower stresses are indicated.

Steel H Piles. The maximum allowable stress should not exceed 0.25 F_y, excluding the area of any tip reinforcement, where F_y is yield strength of steel. The maximum allowable stress may be increased to $0.33F_y$ if pile damage is unlikely. Static or dynamic load tests are indicated to confirm the design load when using an allowable stress of $0.33\,F_y$.

Unfilled Steel Pipe Piles. Likewise, the maximum allowable steel stress should not exceed 0.25 F_y over the minimum cross sectional area of the pile. This stress may be increased to $0.33\,F_y$ if pile damage is not anticipated, but in this case the design load should be confirmed by static or dynamic tests.

Concrete-Filled Steel Pipe Piles. The maximum allowable stress should not exceed $0.25F_y + 0.40\,f'_c$. The computed stress in this case is taken as the average over the total cross-sectional area of steel and concrete.

Precast Concrete Piles. The maximum allowable stress should not exceed $0.33f'_c$ on the gross cross-sectional area of the pile.

Prestressed Concrete Piles. For fully embedded piles where lateral support is provided, the maximum allowable stress should not exceed $0.33\,f'_c$–$0.27\,f_{pe}$ on the gross cross-sectional area of the pile, where f_{pe} is the concrete compression stress due to prestressing after losses.

Round Timber Piles. The maximum allowable stress is summarized in AASHTO Table 4.5.7.3A for the pile tip area.

For the usual terminology used in pile design reference is made to Figure 9–8.

Load Factor Approach

Service limit states. These include unacceptable settlements of pile groups, unacceptable deformations, or undesirable damage levels. A serviceability limit state corresponds to loss of function and utility, and occurs before collapse. It may be reached through excessive differential or total settlement, excessive lateral displacement, or structural deterioration of the piles.

The load coefficients γ and β and the percentage increase in allowable stresses for serviceability limit states are given in Table 2–17 under Service Load Groups.

Strength limit states. These include (1) bearing capacity failure of a single pile or a group of piles; (2) punching into lower weak strata; (3) loss of overall stability; (4) structural capacity and (5) uplift resistance. A summary of strength and service limit states is given in Table 9–4.

Pile foundations should be proportioned such that the factored resistance is not less than the factored loads. This leads essentially to Equation (8–17), where the β and γ factors may be taken from Table 2–17 for strength design limit states.

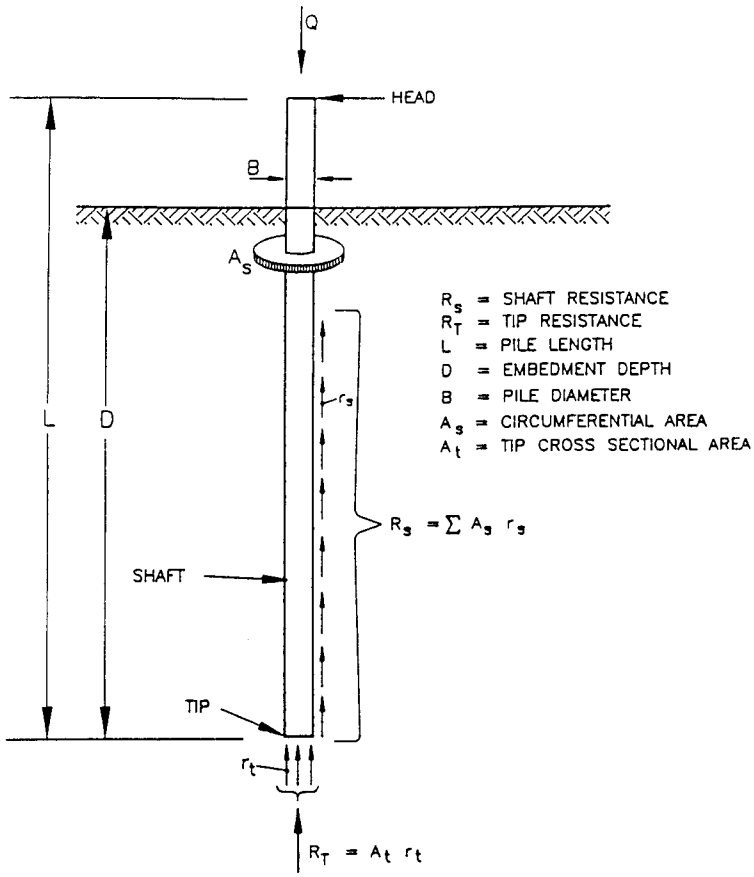

Figure 9–8 Design terminology for driven pile foundations *(from AASHTO)*.

Table 9–4 Summary of Ultimate and Serviceability Limit States that Must Be Considered in the Design of Pile Foundations.

Design Consideration	Ultimate Limit State	Serviceability Limit State
Structural capacity of single piles	X	
Bearing capacity of single piles	X	
Bearing capacity of pile groups	X	
Punching into lower weak stratus	X	
Settlement of pile groups		X
Tensile capacity of piles during uplift	X	
Uplift capacity of single piles	X	
Structural capacity of piles under lateral loading	X	
Lateral movement of pile groups when subjected to lateral loads		X

Table 9–5 Resistance Factors for Geotechnical Strength Limit States in Axially Loaded Piles. (LRFD Specifications)

	Method/Soil/Condition	Resistance Factor
Ultimate Bearing Resistance of Single Piles	Skin Friction: Clay	
	α-method (Tomlinson, 1987)	0.70
	β-method (Esrig & Kirby, 1979)	0.50
	λ-method (Vijayvergiya & Focht, 1972)	0.55
	End Bearing: Clay and Rock	
	Clay (Skempton, 1951)	0.70
	Rock (Canadian Geotech. Society, 1985)	0.50
	Skin Friction and End Bearing: Sand	
	SPT-method	0.45
	CPT-method	0.55
	Skin Friction and End Bearing: All Soils	
	Load Test	0.80
	Pile Driving Analyzer	0.70
Block Failure	Clay	0.65
Uplift Resistance of Single Piles	α-method	0.60
	β-method	0.40
	λ-method	0.45
	SPT-method	0.35
	CPT-method	0.45
	Load Test	0.80
Group Uplift Resistance	Sand	0.55
	Clay	0.55

Resistance factors. Resistance factors ϕ for pile foundations of strength limit states and axially loaded piles are given in Table 9–5. As in Table 8–7, statistical information was used in conjunction with reliability theory to derive these values, combined in some cases with judgment. Table 9–5 is taken from the LRFD specifications.

9.5 MOVEMENT AND BEARING RESISTANCE AT THE SERVICE LIMIT STATE

The General Settlement Problem of a Single Pile

Cohesionless soils. In general, settlement predictions of pile foundations are complex because of (1) disturbance and changes in the state of soil stress caused by the installation operations and (2) the uncertainty about the distribution and exact position of the load transfer. The disturbance and changes in the soil stress are discussed in section 9.1. The vertical displacement necessary to mobilize side shear (skin friction) usually does not exceed 0.2 inch, regardless of soil and pile types and dimensions, although some investigators report higher displacement values and close to 0.4 inch (Vesic, 1977; Sharma and Yoshi, 1988). However, the displacement necessary to mobilize point resistance is larger and depends on the soil type as well as on the pile type and size. In general, the ultimate skin friction is mobilized much sooner than the point bearing. The load transfer mechanism also depends on the pile length and the load level.

An example of load transfer is shown in Figure 9–9 where at loads up to 40 kips, the entire load is resisted by the shaft.

Cohesive soils. For piles in cohesive soils, the settlement consists primarily of two components: (1) short-term settlement occurring as the load is applied; and (2) long-term consolidation settlement occurring gradually as the excess pore pressure is dissipated.

In general, the short-term settlement results from elastic compression of cohesive soils. This component of settlement constitutes a significant portion of the total settlement for partially saturated soils and overconsolidated saturated cohesive soils.

In estimating the settlement of piles in clay, only unfactored permanent loads should be considered. However, when considering the settlement of piles in sand, unfactored live loads should be added to the permanent loads.

LRFD approach service limit state. For the purpose of estimating the settlement of pile groups, the loads are assumed to act on an equivalent footing located at two-thirds of the depth of embedment of the piles into the layer that provides support, as shown in Figure 9–10.

For piles in cohesionless soils, foundation settlement should be investigated using all applicable loads in the Service I load combination. For piles in cohesive soil, the Service I load combination is likewise used, but the transient loads may be omitted.

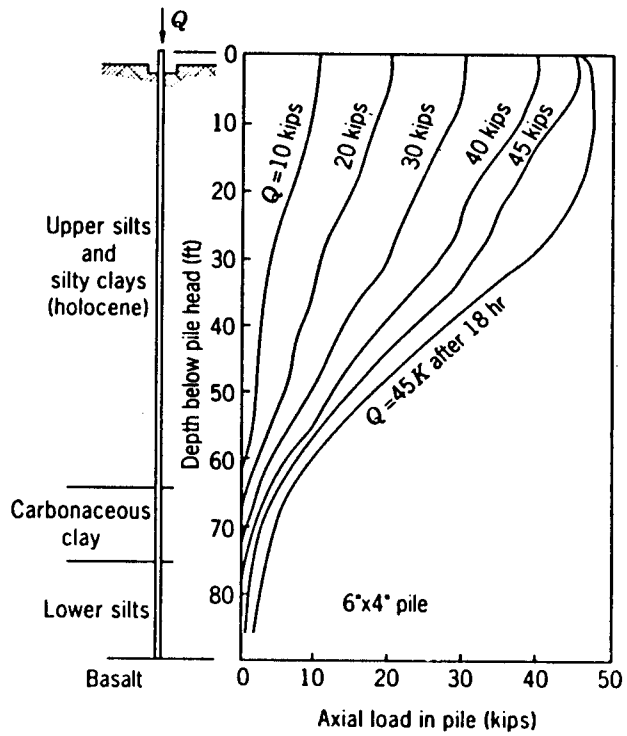

Figure 9–9 Load transfer from a steel pile driven through compressible silt to rock *(from Vesic, 1977).*

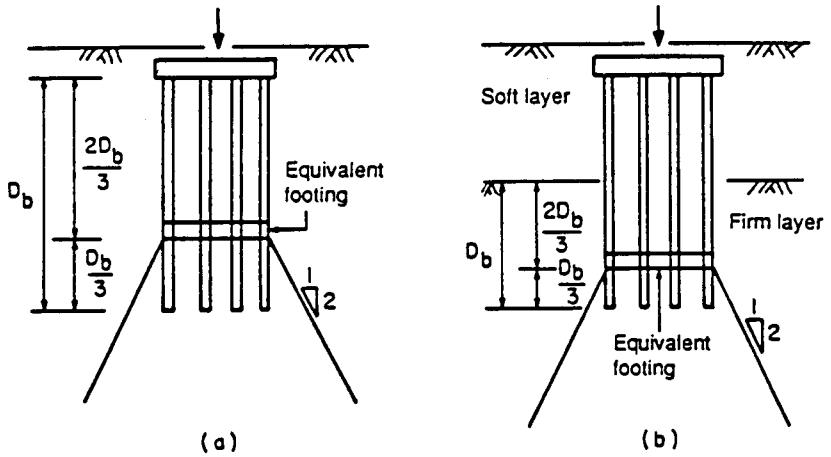

Figure 9–10 Location of equivalent footing *(from Duncan and Buchignani, 1976).*

Settlement of Piles in Cohesionless Soil

Single pile. Using a semiempirical method, the settlement of a single pile in sand can be broken down into three components as follows:

$$S_t = S_s + S_p + S_{ps} \tag{9–3}$$

where S_t = total settlement of the pile top; S_s = settlement due to the axial compression of the pile shaft; S_p = settlement at the base caused by the load transfer at the base; and S_{ps} = settlement of pile caused by the load transfer along the shaft.

These three components are computed separately and they are added together (Vesic, 1977). The elastic settlement S_s of the top is computed from

$$S_s = \left(Q_{pa} + \alpha_s Q_{fa}\right) L / A_p E_p \tag{9–4}$$

where Q_{pa} = actual load transmitted at the base for service dead and live loads; Q_{fa} = actual load transmitted as friction along the pile shaft at working loads; L = pile length; A_p = cross-sectional area of the pile; E_p = modulus of elasticity of the pile material; and α_s = a numerical factor depending on the distribution of friction along the pile shaft.

Vesic (1977) recommends taking $\alpha_s = 0.5$ for a uniform or parabolic skin friction along the pile shaft. However, the load-distribution pattern can be obtained by monitoring the load transfer during load tests such as the load transfer curves shown in Figure 9–9. The value of α_s is close to 0.67 for triangular skin friction distribution (zero at the pile head and maximum at the pile base).

The other two components of the total pile settlement may be computed from relationships correlating theoretical analyses and empirical data as follows (Vesic, 1977):

$$S_p = C_p Q_{pa} / (B q_p) \tag{9–5}$$

$$S_{ps} = C_s Q_{fa} / (D_f q_p) \tag{9–6}$$

Table 9–6 Typical Values of Coefficient C_p

Soil Type	Driven Piles	Bored Piles
Sand (dense to loose)	0.02–0.04	0.09–0.18
Clay (stiff to soft)	0.02–0.03	0.03–0.06
Silt (dense to loose)	0.03–0.05	0.09–0.12

(from Vesic, 1977).

where C_p = empirical coefficient (values given in Table 9–6); $C_s = 0.93 + 0.16\sqrt{D_f/B}(C_p)$; Q_{pa} = net point load under working conditions; Q_{fa} = net shaft load; q_p = ultimate end-bearing capacity of pile; B = pile diameter; and $D_f = L$ = embedded pile length.

In the foregoing estimates, the bearing capacity stratum is assumed to extend at least 10 pile diameters under the pile tip. Also, the soil below this stratum is assumed to be of comparable stiffness. The Vesic approach is recommended by AASHTO (Article 4.5.6.3).

Pile groups. The settlement of a pile group is normally greater than the settlement of a single pile under the same load and soil conditions because of the larger depth of influence of a group. No general theory to predict pile group settlements in cohesionless soil is available. Several empirical and semiempirical procedures with gross approximations are available, and should be used with caution.

The settlement of a pile group may be estimated as suggested by Meyerhof (1976). The settlement is related to the SPT blow count as follows:

$$p = \frac{2qI\sqrt{X}}{N_{corr}} \tag{9–7}$$

where q = net foundation pressure (including any negative skin friction per unit area) in tons/ft^2 applied at $2D_b/3$ (see also Figure 9–10); X = width or smallest dimension of pile group (ft); I = influence factor of the effective group embedment given by

$$I = 1 - D'/8X \geq 0.5 \tag{9–8}$$

D' = effective depth = $2D_b/3$; N_{corr} = average corrected penetration resistance within the seat of settlement (approximately one pile group width below the equivalent footing) as given in the following sections.

Alternatively, cone penetration tests (CPT) may be used to estimate settlement. Meyerhof (1976) relates the settlement p of a pile group to the average static cone penetration resistance as follows

$$p = \frac{qXI}{2q_c} \tag{9–9}$$

where q_c = average static cone resistance within the seat of settlement, and other parameters are as previously. This approach is followed by the LRFD specifications.

Settlement of Piles in Cohesive Soil

The settlement of pile groups in cohesive soil is complex. The long-term settlement may be calculated using the procedures suggested for estimating the settlement of shallow foundations (see also section 8.9). For this purpose, the load carried by a group of piles

in shaft resistance is assumed to be transferred to the soil through an equivalent footing located at two-thirds of the pile depth.

The components contributing to the total settlement are immediate (elastic) settlement, consolidation settlement, and secondary settlement.

9.6 DESIGN OF PILES FOR AXIAL LOAD, STRUCTURAL CAPACITY

The three limit states that may be reached in piles subjected to an axial load are (1) structural failure of the pile, (2) bearing capacity failure of the soil in the load transfer zone, and (3) excessive settlement rendering the foundation inoperable.

The structural capacity of piles for allowable stress design is discussed in section 9.4, and is essentially based on AASHTO Article 4.5.7. This section addresses, therefore, ultimate strength limit state and serviceability limit state.

Buckling Strength

Buckling considerations, fully embedded single piles. Earlier solutions for the elastic buckling loads of fully embedded piles were based on a subgrade modulus for the soil, assumed to be constant over the pile length. The governing differential equation in this case is

$$EI\frac{d^4y}{dx^4}+P\frac{d^2y}{dx^2}+ky=0 \tag{9–10}$$

where EI = flexural stiffness of the pile; P = axial load; and k = subgrade modulus. In solving Equation (9–10) these parameters were assumed to be constant. The boundary conditions for this problem are shown in Figure 9–11. The solutions of Equation (9–10) have been obtained in nondimensional form, letting

$$R=\sqrt[4]{\frac{EI}{k}} \quad \text{and} \quad Z=\frac{x}{R}, \quad Z_{\max}=\frac{L}{R} \tag{9–11}$$

where L = embedded length of the pile; R = relative stiffness factor; and Z = nondimensional depth coefficient. By combining with Equation (9–10) and rearranging, we obtain

$$\frac{d^4y}{dz^4}+\frac{PR^2}{EI}\bullet\frac{d^2y}{dz^2}+y=0 \tag{9–12}$$

If PR^2/EI denotes the axial load coefficient U, then

$$U_{cr}=\frac{P_{cr}R^2}{EI} \tag{9–13}$$

where the subscript cr represents the critical values of U and P. Combining Equations (9–12) and (9–13) yields

$$\frac{d^4y}{dz^4}+U\frac{d^2y}{dz^2}+y=0 \tag{9–14}$$

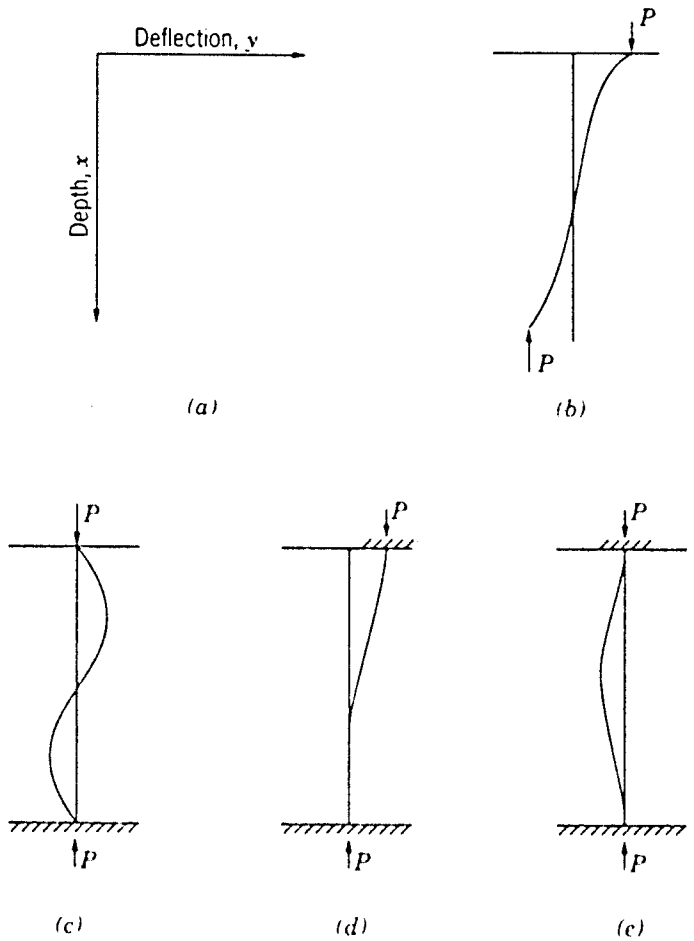

Figure 9–11 Pile boundary conditions (a) coordinate system (b) free (f), (c) pinned (*p*), (d) fixed translating (*Ft*), (e) fixed (*F*).

The critical values of the axial load coefficient U_{cr} are obtained by solving Equation (9–14) for U, considering the pile boundary conditions and the pile length Z_{max}. Referring to Figure 9–11, the boundary conditions are free (*f*), pinned (*p*), fixed-translating (*ft*), and fixed-non-translating (*F*). An analog computer is used to obtain these solutions (Davisson and Gill, 1963).

Buckling of partially embedded single piles. Column instability is usually a problem in the design of structures supported by piles that are partially free standing. In addition, piers subjected to vertical and lateral loads may have a pile foundation governed by flexural criteria. The analysis in this case is highly indeterminate and time consuming unless some simplifying assumptions are introduced. One of these assumptions is the depth below the ground surface at which the pile may be considered fixed. A procedure for estimating this depth has been proposed by Davisson and Robinson (1965), who present general solutions for buckling loads of partially embedded piles in terms of an equivalent free standing length.

The equivalent free standing length is the sum of the unsupported pile length above the ground, and an additional length to the depth of fixity below ground. The depth to fixity is a function of the flexural stiffness of the pile E_pI_p and the soil stiffness, the latter expressed in terms of the soil modulus E_s. The soil modulus is usually assumed constant with depth in clays, and is assumed to vary linearly with depth in sands.

For long piles, the equivalent free standing length is as follows:

Modulus constant with depth (cohesive soil)

$$L_{eq} = L_u + 1.4\,R \tag{9–15}$$

Modulus increasing linearly with depth (cohesionless soil)

$$L_{eq} = L_u + 1.8\,T \tag{9–16}$$

where L_u = unsupported length of pile extending above ground; $R = (E_pI_p/E_s)^{0.25}$; E_p = elastic pile modulus; I_p = moment of inertia of pile; E_s = soil modulus ($E_s = 67s_u$ for clays where s_u = undrained shear strength); $T = (E_pI_p/n_h)^{0.2}$; n_h = rate of increase of soil modulus with depth = E_s/z; and z = depth.

Note that the parameter R is the relative stiffness factor in Equation (9–11). This approach is recommended by the LRFD specifications.

The Davisson and Robinson procedure is applied to different boundary conditions at the top of the pile; the bottom boundary condition is assumed to be fixed against rotation and translation at the depth of fixity. Appropriate boundary conditions for the top of the pile may be defined considering the structure type, the fixity at bearings, and the number of rows of piles along the length and width of the pile group. Four possible boundary conditions at the top of the pile where it connects with the structure are shown in Figure 9–12, together with expressions of the critical pile load.

On the basis of lateral load tests of piles in sand, Alizadeh and Davisson (1970) have found that n_h is dependent on deflection when the lateral deflection is less than 3 percent of the pile width. At larger deflections, the value of n_h becomes essentially independent of the lateral deflection. Terzaghi (1955) recommends values of n_h that are appropriate for lateral deflections of about 5 percent of the pile width (see also Table 9–7). For analysis of pile buckling, values of n_h corresponding to smaller deflections (of the order of 0.5 percent of the pile width) appear to be appropriate. Evans and Duncan (1982) have shown that for lateral deflections of this magnitude, it is reasonable to use values of n_h about three times as high as the values recommended by Terzaghi. The last two columns of Table 9–7 give recommended values of n_h appropriate for lateral deflections of 0.5 percent of the pile width.

Effects of group action on buckling loads. These effects have been studied by Prakash and Sharma (1990). A main conclusion is that at pile spacing greater than eight times the pile diameter (width), neighboring piles have no effect on the soil modulus or buckling capacity. However, when the pile spacing is reduced to three times the pile width, the effective soil modulus is reduced to 25 percent of the value applicable to a single pile. For intermediate spacing, the modulus may be estimated by interpolation.

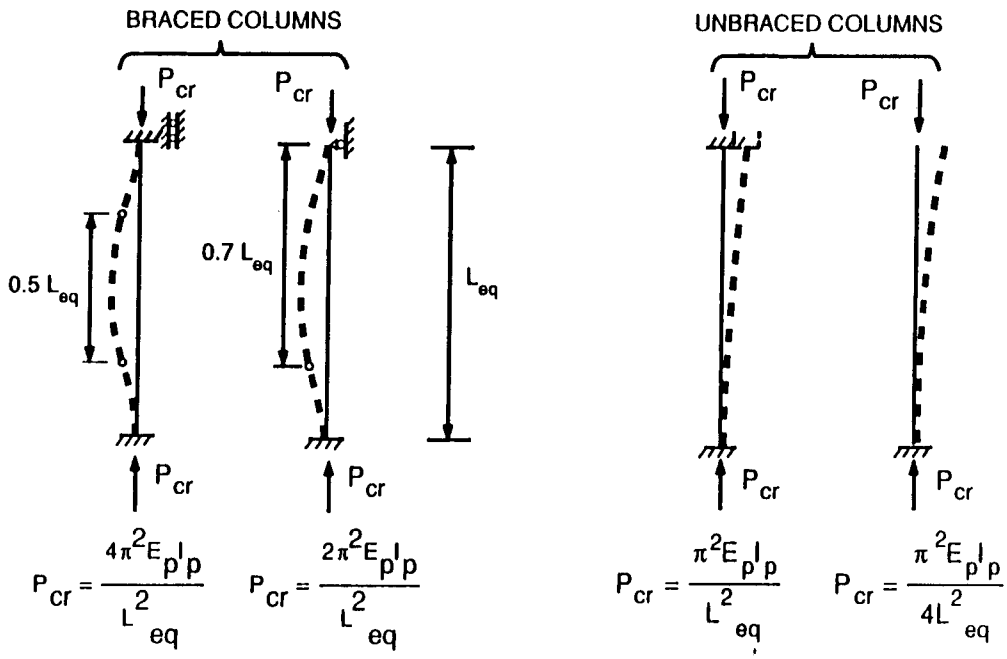

Figure 9–12 Critical buckling loads for centrally loaded columns with various end conditions.

Structural Capacity, Axial Compression, Single Pile

The design load in a pile should not exceed the factored axial capacity. This leads to the general requirement

$$\phi_a P_n \geq \Sigma \gamma_i P_i$$

where P_n = nominal structural capacity of the pile; ϕ_a = performance factor; P_i = axial load due to load i; and γ_i = load factor for load i.

The nominal axial structural capacity P_n of piles, excluding moment effects, may be taken as follows:

Prestressed concrete piles	$P_n = (0.85f'_c - 0.6f_{pre})A_c$
Precast concrete piles	$P_n = 0.85f'_c A_c + f_y A_y$
Steel H-piles	$P_n = f_y A_y$
Steel pipe piles	$P_n = f_y A_y$
Timber piles	$P_n = k_c S_c A_t$

Table 9–7 Coefficient of Horizontal Subgrade Reaction (η_h) in lb/in^3

	Terzaghi (1955)		Reese et al. (1974)	Recommended	
	Dry or Moist Sand	*Submerged Sand*	*Submerged Sand*	*Dry or Moist Sand*	*Submerged Sand*
Loose	8	5	20	30	15
Medium	24	16	60	80	40
Dense	65	39	125	200	100

Table 9–8 Performance Factors for the Nominal Axial Structural Capacity of Piles

Pile Type	Performance, Factor, ϕ_a	Eccentricity Factor, r
Prestressed Concrete Piles	0.75 for spiral columns 0.70 for tied columns	0.85 for spiral columns 0.80 for tied columns
Precast Concrete Piles	0.75 for spiral columns 0.70 for tied columns	0.85 for spiral columns 0.80 for tied columns
Steel-H Piles	0.85	0.78
Steel Pipe Piles	0.85	0.87
Timber Piles	1.20*	0.82

*Davisson et al. (1983) stated that the minimum factor of safety for the structural capacity of timber piles in compression in 1.25. The performance factor is greater than unity since the average load factor for vertical loads (dead and live loads) is greater than the factor of safety itself.

where f'_c = compressive concrete strength; f_y = yield stress of steel; f_{pre} = effective prestress in the concrete; A_c = cross-sectional area of concrete; A_y = cross-sectional area of steel; A_t = cross-sectional area of timber; S_c = 5 percent exclusion limit in compression parallel to grain; and k_c = factor to account for the treatment condition.

Values of the performance factor ϕ_a are given in Table 9–8.

If the axial load is applied eccentrically, the maximum load on each pile will not be uniform. There will be one pile in the group receiving the maximum load, as shown in Figure 9–13. The factored vertical load acting on the group of piles is P_g, and is applied at an eccentricity e_x and e_y from the principal axes as shown. The factored axial load $P_{x,y}$ on any pile is obtained from statics as

$$P_{x,y} = P_g\left(\frac{1}{N} \pm \frac{e_x x}{\Sigma x^2} \pm \frac{e_y y}{\Sigma y^2}\right) \tag{9–17}$$

where N is the number of piles in the group, and all other terms are self-explanatory.

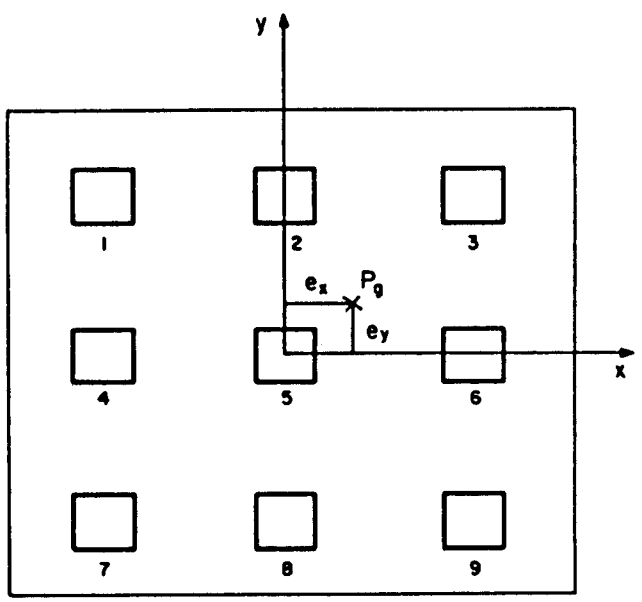

Figure 9–13 Eccentric loading on a pile group.

9.7 DESIGN OF PILES FOR AXIAL LOAD, GEOTECHNICAL CAPACITY OF SINGLE PILE

Presumptive Bearing Capacities of Soils and Rocks

Where sufficient soil data are not available for a rational estimate of pile bearing capacity, the design may consider presumptive bearing capacities. At best, estimates obtained in this manner should be used only as rough guides to actual capacity, and should be confirmed by pile load tests.

Presumptive bearing capacities that have been disseminated and introduced in design standards are allowable values intended in ASD.

Pile Bearing Capacities by Rational Methods

The ultimate bearing capacity of a pile is given by Equation (9–1) repeated here as

$$Q_{ult} = Q_S + Q_T \tag{9–18}$$

where Q_{ult} = ultimate bearing capacity (also referred to as geotechnical capacity); Q_S = ultimate shaft resistance; and Q_T = ultimate tip resistance.

Some designers prefer to subtract the weight of the pile from the second term of Equation (9–18), whereas others choose to include this weight with the actual load.

By extension, we define

$$Q_S = A_s q_s \qquad \text{and} \qquad Q_T = A_T q_T \tag{9–19}$$

where A_S = surface area of pile shaft; q_s = ultimate unit shaft resistance (friction or adhesion); A_T = area of pile tip; and q_T = ultimate unit tip resistance.

For load factor (strength design) the criterion may be expressed as in Equation (9–17) as

$$\phi_q Q_{ult} \geq \Sigma \gamma_i P_i \tag{9–20}$$

where ϕ_q is the performance factor for the ultimate bearing capacity of the pile, and all other terms are as previously.

AASHTO procedure for bearing capacity estimates. For cohesive soils, the ultimate bearing capacity of piles may be computed by total stress analysis (Tomlinson, 1987) for undrained loading conditions, or using effective stress methods (Meyerhof, 1976) for drained loading conditions. The axial capacity may also be calculated from in situ testing methods such as the cone penetration (Schmertmann, 1977) or pressuremeter tests (Baguelin, Jezequel, and Shields, 1978).

The ultimate bearing capacity in cohesionless soils may be calculated using an empirical effective stress method, or data from in situ tests and analysis such as the cone penetration (Schmertmann, 1977) or pressuremeter tests (Baguelin et al., 1978).

For piles driven to competent rock, the structural capacity will generally govern the ultimate bearing capacity. For piles driven to weak rocks, such as shale and mudstone, or poor quality weathered rocks, a static load test is recommended.

LRFD approach. The factored resistance may be written as

$$\phi_q Q_{ult} = \phi_{qs} Q_S + \phi_{qt} Q_T \tag{9–21}$$

where ϕ_{qs} = resistance factor for shaft resistance; ϕ_{qt} = resistance factor for tip resistance, and ϕ_q is as in Equation (9–20). Resistance (performance) factors for bearing capacity (geotechnical strength) are given in Table 9–5. Both ultimate shaft and tip resistance develop in response to foundation displacement. The maximum values of each are unlikely to occur at the same displacement. The shaft resistance is normally fully mobilized at displacements of about 0.1 to 0.4 inch. The tip bearing, however, is mobilized after the pile settles about 8 percent of its diameter.

Shaft Resistance

Adhesion. The pile interaction with clays mentioned in section 9.1 shows that the soil around the pile is markedly disturbed. In some instances, after a complete consolidation, the shear strength of the clay at the pile interface may be greater than the shear strength prior to driving. In sensitive clays or stiff overconsolidated clays, however, the final shear strength may be considerably less than that of the undisturbed soil (Meyerhof, 1976).

The so-called α method relates the adhesion at the pile-clay interface to the undrained shear strength of the soil. The ultimate unit shaft resistance q_s is given by

$$q_s = \alpha s_u \tag{9–22}$$

where s_u = mean undrained shear strength, and α = adhesion factor applied to s_u. The adhesion factor α may be assumed to vary with the value of undrained shear strength s_u as shown in Figure 9–14. There is considerable scatter of data around the curves (not shown in the figure) because factors such as the pile length, overconsolidation ratio, and lateral earth pressure coefficient are neglected (Tomlinson, 1987). Variation in the undrained shear strength may also contribute to the scatter.

Friction. The so-called β method is based on effective stress analysis for predicting the skin friction of piles in cohesionless soils. The ultimate unit skin friction q_s is related to the effective stresses as follows:

$$q_s = \sigma_h' \tan\delta = K \tan\delta \sigma_v' = \beta \sigma_v' \tag{9–23}$$

where σ_h' and σ_v' are the horizontal and vertical effective stresses, respectively; δ is the friction angle between the pile and the soil; and K is the coefficient of lateral earth pressure. From Equation (9–23), $\beta = K\tan\delta$. The coefficient K is a function of the initial in situ horizontal stress and the stress changes that occurred as a result of the construction (Kulhawy, Trautmann, Beech, O'Rourke, and McGuire, 1983). The excess pore pressure generated as the pile is driven results in a lower σ_v', giving a higher initial K value. As the pore pressure dissipates, K changes with time. Depending on the overconsolidation ratio (OCR), the values of K may be higher or lower than the at-rest pressure coefficient K_o. The relationship between β and OCR is shown in Figure 9–15 (Esrig and Kirby, 1979).

The β method is suggested for piles in normally consolidated and lightly overconsolidated clays. This procedure tends to overpredict skin friction of piles in heavily overconsolidated soils. For heavily overconsolidated clays, β should not exceed a value of 2.

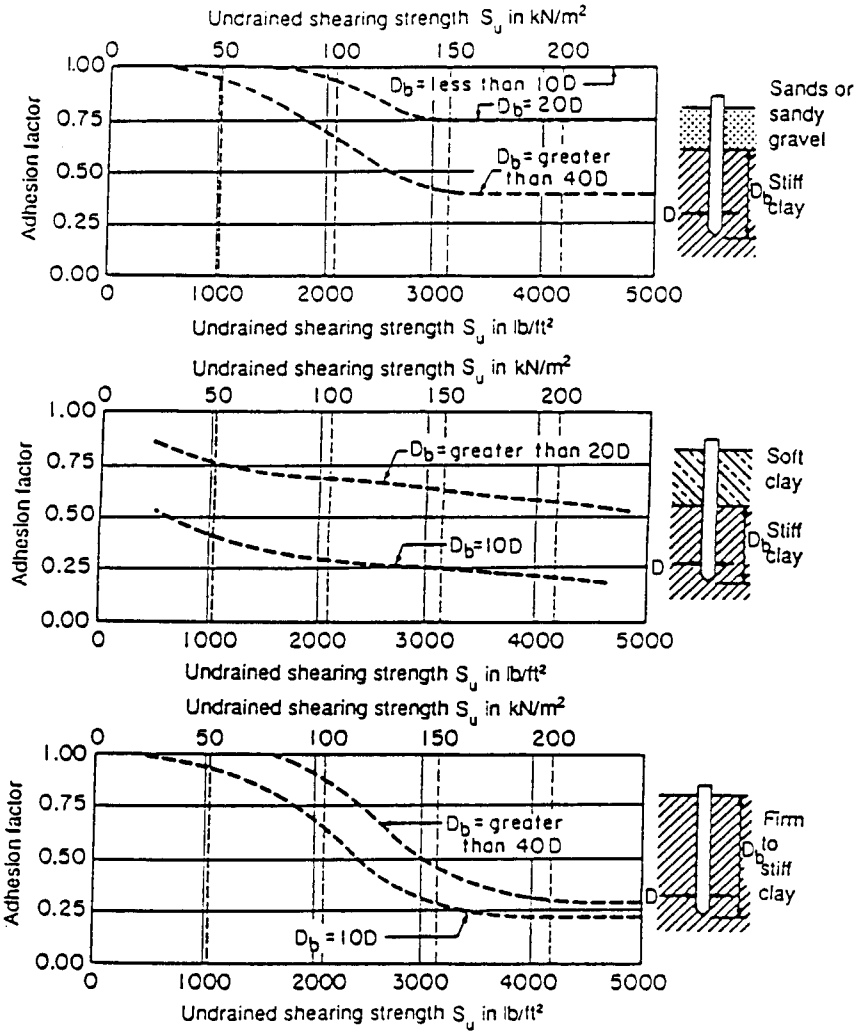

Figure 9–14 Design curves for adhesion factors for piles driven into clay soils *(from Tomlinson, 1987).*

The λ method. Vijayvergiya and Focht (1972) have concluded that the passive lateral earth pressure $\sigma_h' = \sigma_v' + 2s_u$ and the ultimate shear resistance of a pile are related. The proposed relationship is

$$q_s = \lambda\left(\sigma_v + 2s_u\right) \tag{9–24}$$

where λ is an empirical coefficient that can be taken from Figure 9–16. The value of λ decreases with pile length and was established empirically from an analysis of results of load tests on steel pipe piles. The foregoing procedure reflects the LRFD approach.

Tip Resistance

A general expression for estimating the bearing capacity associated with the tip resistance is derived on the basis of the theory of plasticity (Kulhawy et al., 1983), and is essentially similar to the expression for a strip footing. This leads to Equation (8–2),

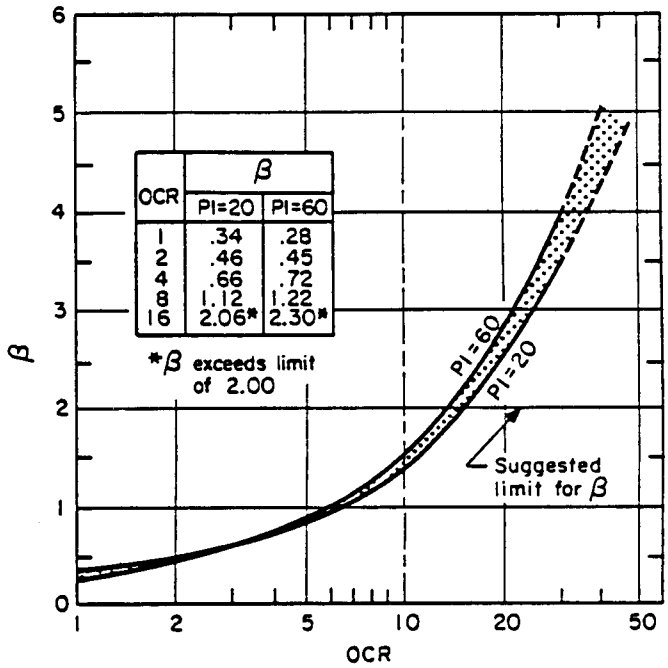

Figure 9–15 β versus OCR for full displacement piles *(from Esrig and Kirby, 1979).*

which can be modified to include the effect of depth and shape of the pile group and also the influence of the soil rigidity.

For piles in saturated clay with zero friction and $c = s_u$, the pile tip capacity is obtained as

$$q_p = 9s_u + \sigma_v \tag{9–25}$$

so that

$$Q_p = 9s_u A_p + \sigma_v A_p \tag{9–26}$$

where A_p = area of pile point. Noting that the term $\sigma_v A_p$ is the weight of the pile (approximately), this term may be disregarded. Hence, for saturated clays the ultimate tip resistance is

$$Q_p = 9s_u A_p \tag{9–27}$$

where s_u is the undrained shear strength of the clay near the pile base. This procedure is recommended by the LRFD specifications.

For cohesionless soils such as coarse-grained sands, $c = 0$. In this case, the friction angle can be correlated to the standard penetration test blow count and the cone penetration resistance as proposed by Kulhawy et al. (1983). For depth-to-width ratios between 4 and 5, the drained ultimate tip resistance may be approximated as

$$q_p = \sigma_v' N_q s_q d_q r_q \tag{9–28}$$

where $N_q s_q d_q r_q$ is a bearing capacity factor obtained from Figure 9–17. The rigidity index I_r, included as a parameter in these graphs, accounts for the deformability of the soil and the variation of the bearing capacity factor with depth. Vesic (1975) defines I_r as follows

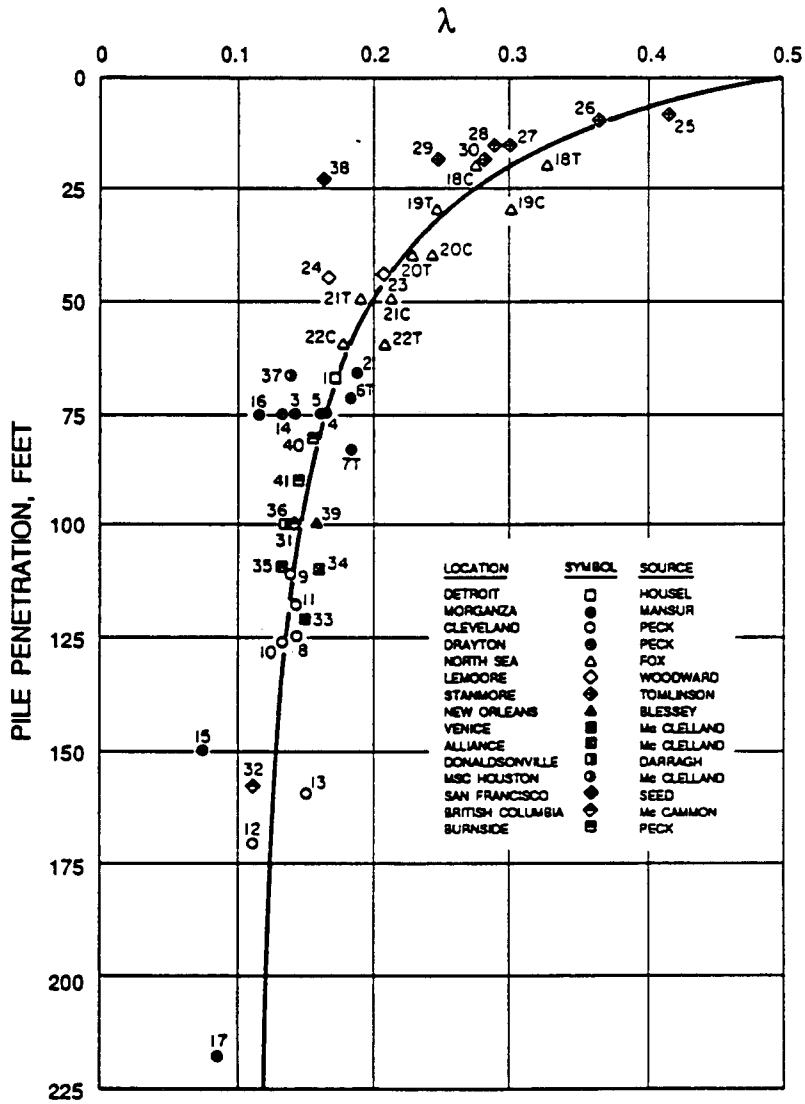

Figure 9–16 λ coefficient for driven pipe piles *(from Vijayvergiya and Focht, 1972).*

$$I_r = \frac{E_s}{2(1+\mu)\sigma_v' \tan\phi'} \tag{9–29}$$

where E_s is the soil modulus, μ is Poisson's ratio for the soil, and σ_v' is the vertical effective stress measured at a depth of $D/2$ below the base of the pile. The rigidity index for sands is approximated by Kulhawy et al. (1983) as follows:

For loose sand

$$I_r = \frac{30}{\left(\sigma_v'\right)^{0.5} \tan\phi'} \tag{9–30}$$

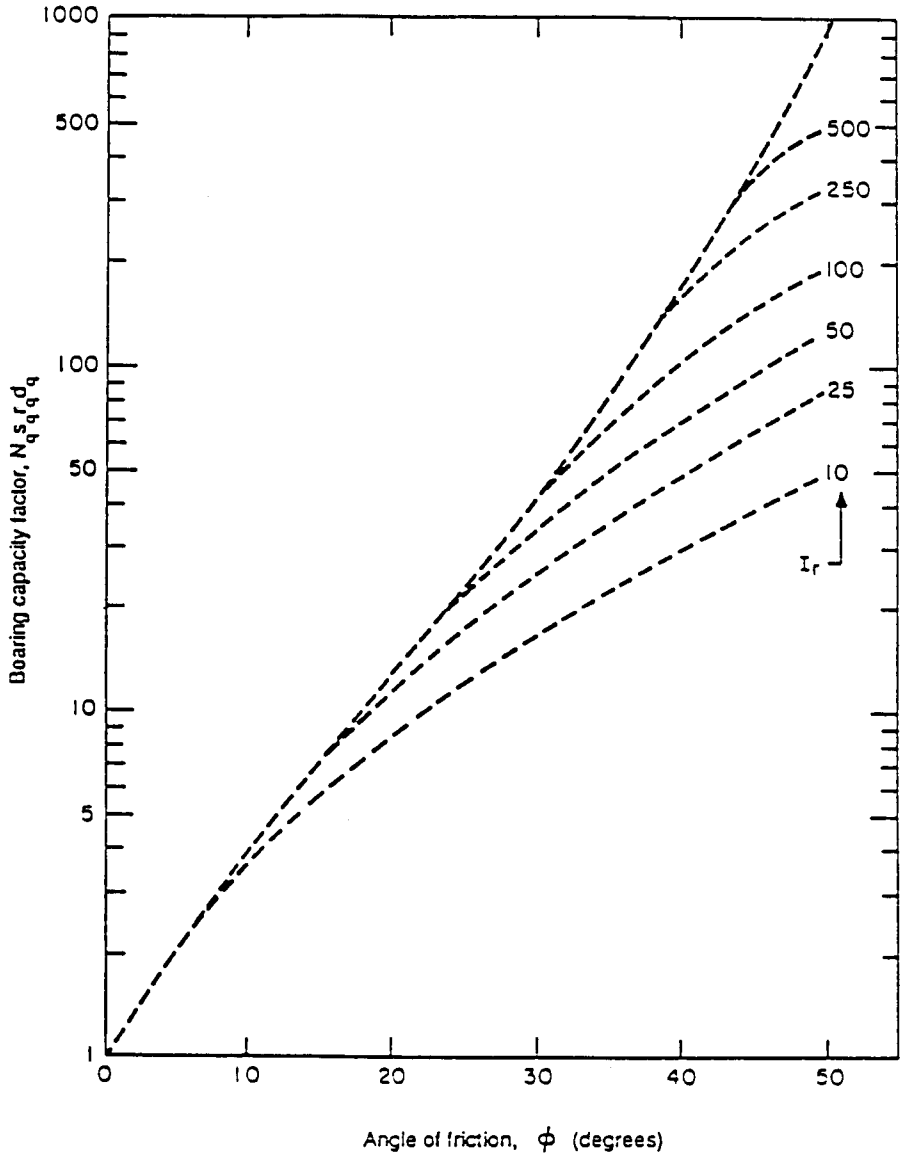

Figure 9–17 Modified *Nq* bearing capacity factor for deep foundations *(from Kulhawy et al., 1983).*

For dense sands

$$I_r = \frac{110}{\left(\sigma_v'\right)^{0.5} \tan\phi'} \tag{9–31}$$

where σ_v' is expressed in tons/ft^2.

Tip resistance of piles in rock. The ultimate unit tip resistance q_p of piles driven to rock may be estimated from the uniaxial compressive strength as follows (*Canadian Foundation Engineering Manual,* 1985)

$$q_p = 3\sigma_c K_{sp} d \tag{9–32}$$

where σ_c = average uniaxial compressive strength of the rock core, and K_{sp} = dimensionless bearing capacity coefficient.

The coefficient K_{sp} may be computed from

$$K_{sp} = \frac{3 + s_d / D}{10\left(1 + 300 t_d / s_d\right)^{0.5}} \tag{9–33}$$

where d = dimensionless factor = $1 + 0.4H_s/D_s \leq 3.4$; t_d = width of rock discontinuities, s_d = spacing of discontinuities; D = pile width (or diameter); H_s = embedment depth of pile socketed into rock = 0 for piles resting on top of the bedrock; and D_s = diameter of socket. The coefficient K_{sp} may be obtained directly from Figure 9–18.

The procedure is not applicable to soft stratified rocks such as shale or limestone. Furthermore, where the method is valid and can be applied, the rock would be expected to be sufficiently competent so that the structural capacity will govern (see also AASHTO comments in the foregoing sections). In general the method will apply only if $s_d > 1$ foot, $t_d < 0.25$ inch for unfilled discontinuities, or $t_d < 1$ inch for discontinuities filled with soil or rock debris, and $D > 1$ foot.

Pile Resistance Estimated from In Situ Tests

Owing to the difficulty of obtaining good quality samples of cohesionless soils for laboratory testing, in situ tests are widely used to obtain design parameters for estimating the tip and shaft resistance of piles. Two frequently used in situ test methods are the standard penetration test (SPT), and the cone penetration test (CPT).

SPT method. Applied only to sands and nonplastic silts, this method (Meyerhof, 1976) correlates the tip capacity and shaft resistance with the SPT blow count.

Tip Resistance. The ultimate unit tip resistance (tons/ft^2) of piles driven to a depth D_b into a cohesionless soil can be estimated as

$$q_p = \frac{0.4\, N_{corr} D_b}{D} \leq q_l \tag{9–34}$$

where

$$N_{corr} = \left[0.77 \log_{10}\left(\frac{20}{\sigma_v'}\right)\right] N \tag{9–35}$$

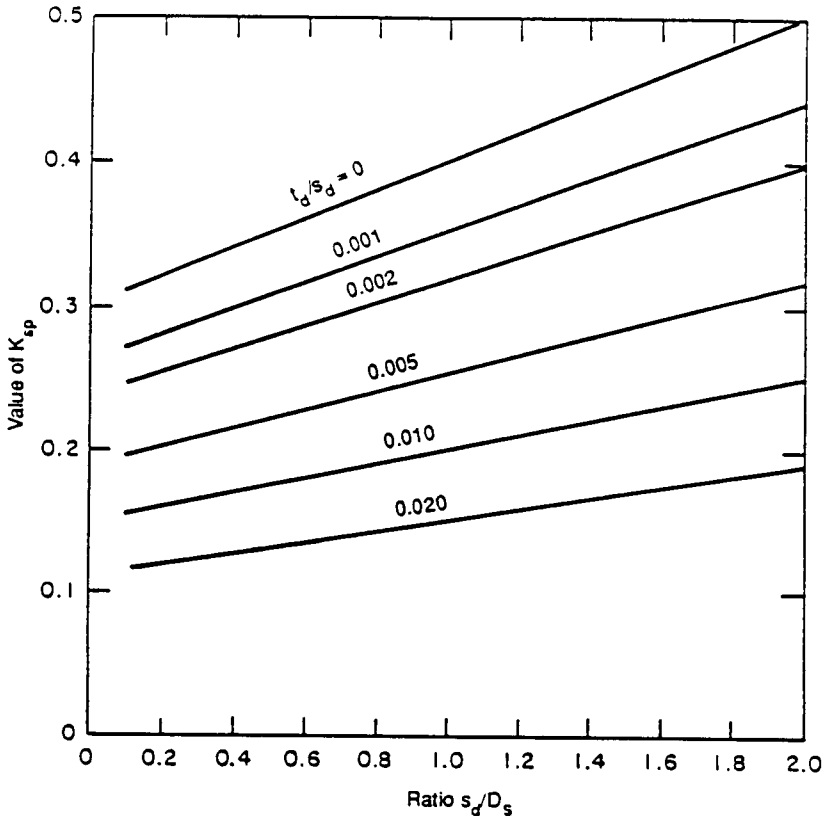

Figure 9–18 Bearing capacity coefficient K_{sp} *(from Canadian Foundation Engineering Manual, 1985).*

and N = measured SPT – N value; σ_v' = effective vertical stress at the pile tip (tons/ft^2); D = pile width or diameter (ft); and q_1 = limiting point resistance (tons/ft^2) determined as follows:

$$\left.\begin{aligned} q_1 &= 4N_{corr} \text{ for sands} \\ q_1 &= 3\,N_{corr} \text{ for nonplastic silt} \end{aligned}\right\} \tag{9–36}$$

The parameter N_{corr} is the representative SPT blow count near the pile tip corrected for overburden pressure σ_v'.

The implication of Equation (9–34) is that the ultimate unit tip capacity in a cohesionless layer increases linearly with the embedment ratio D_b/D up to a critical value of 10 for sands and 7.5 for silts. At higher ratios, the tip capacity remains constant at the limiting value q_1.

If the flow count shows an unusual variation, Meyerhof (1976) recommends that, if the distance H from the pile tip to the weak deposit is less than 10 pile diameters, the ultimate tip resistance can be computed as

$$q_p = q_o + \frac{(q_1 - q_0)H}{10D} \leq q_1 \tag{9–37}$$

where q_1 is the limiting unit tip resistance in the upper stratum and q_o is the limiting unit tip resistance in the lower stratum.

Skin Friction. The skin friction of piles driven in cohesionless soil may be estimated as follows:

For displacement piles $q_s = \overline{N}/50$ (9–38)

For nondisplacement piles $q_s = \overline{N}/100$ (9–39)

where q_s = unit skin friction (tons/ft^2), and $\overline{N}$ = average (uncorrected) SPT blow count along the pile shaft (blows/ft). Steel H piles are nondisplacement piles.

Displacement piles with solid or hollow sections having a closed end displace a relatively large volume of soil during driving. Nondisplacement, such as steel H piles and open-ended sections, usually have a small cross-sectional area. In the latter case, plugging occurs when the soil between the flanges in the H-pile or the soil in the cylinder of an open-ended pile adheres fully to the pile and moves down with the pile as it is driven.

CPT method. The cone penetration test may be used to determine (1) the cone penetration resistance q_c, which is related to the tip capacity; and (2) the sleeve friction f_s, which can be used to estimate the skin friction.

The resistance q_p may be determined as shown in Figure 9–19. The minimum average cone resistance between 0.7 and 4 pile diameters below the elevation of the pile tip should be obtained by a convergence procedure based on trial and error, using the minimum-path rule. The minimum-path rule should also be used to determine the value of cone resistance for the soil for a distance of eight pile diameters above the tip, and the two results should be averaged to give the design pile tip resistance.

The procedure outlined in Figure 9–19 was initially developed by Begemann, and later modified by Nottingham and Schmertmann (1975), who found that using a weighted average cone resistance gives a good estimation of end bearing capacity in piles for all soil types.

The procedure proposed by Nottingham and Schmertmann may be used to estimate the skin friction of piles. The skin friction resistance Q_s is

$$Q_s = K_{s,c}\left[\sum_{L_f=0}^{8D}\left(L_f/8D\right)f_s a_s + \sum_{L_f=8D}^{Z} f_s a_s\right] \tag{9–40}$$

where Q_s = skin friction resistance of the pile (tons); $K_{s,c}$ = correction factors K_c for clays and K_s for sands, obtained from Figure 9–20; L_f = depth to point considered (ft); f_s = unit local sleeve friction resistance from CPT at the point considered (tons/ft^2); a_s = pile perimeter (ft); and Z = total embedded pile length (ft).

This method has the following advantages: (1) it gives corrections for the type of cone penetrometer used (electrical vs. mechanical); (2) it accounts for the material of the pile; (3) it considers the soil type; and (4) it provides for correction for the depth of the pile embedment.

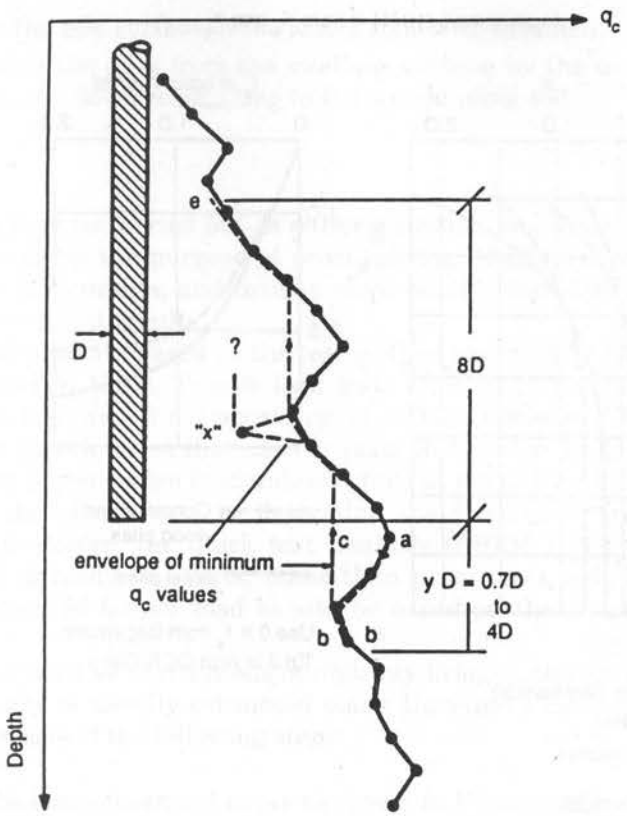

$$q_p = \frac{q_{c1} + q_{c2}}{2}$$

q_{c1} = Average of all values of q_c along path a-b-c over a distance of yD below the pile tip. Sum q_c values measured at each elevation in the downward path a-b. Sum q_c values at every elevation where a cone resistance reading is made, along the upward path b-c, but at each elevation take the minimum of (i) the q_c value at that elevation or (ii) the lowest q_c value between that elevation and the elevation of point b. This method of determining q_c is called the "minimum path" rule. Compute q_{c1} for y-values from 0.7 to 4.0 and use the minimum q_{c1} value obtained.

q_{c2} = Average q_c over a distance of 8D above the pile tip (path c-e). Use the minimum path rule as for path b-c in the q_{c1} computations. Ignore any very extreme peaks or depressions (such as "x" in the diagram above) if the soil is a sand, but include these in minimum path if the soil is a clay.

Figure 9–19 Pile end-bearing computation procedure after Begemann *(from Nottingham and Schmertmann, 1975).*

Piles in Swelling and Shrinking Soils

Soils containing substantial amounts of clay minerals tend to increase in volume when they are above the water table and come in contact with moisture. This swelling subsides when the moisture is removed by drying, and these soils undergo a high volume decrease (shrinkage). The extent of volume change depends on several factors, such as

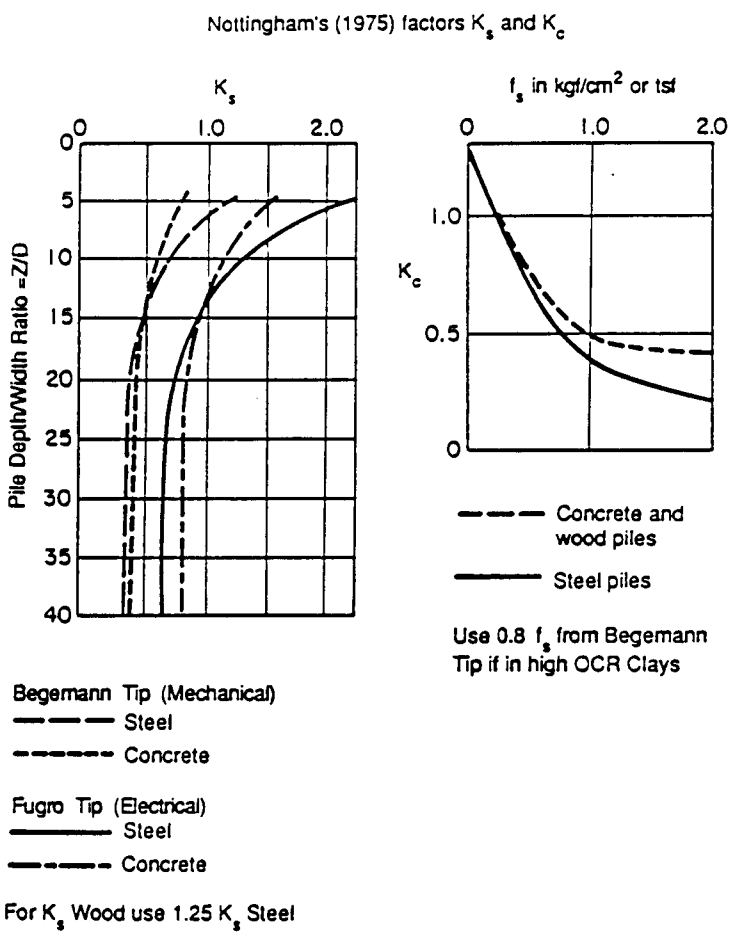

Figure 9–20 Shaft friction correction factors *(from Nottingham and Schmertmann, 1975).*

mineralogy, initial moisture content, and soil particle structure, and also on the new environmental conditions imposed on the soil. A procedure for classifying the swelling and shrinking potential of clay-rich soils is usually based on Atterberg limits and grain-size test data. Another method involves laboratory swelling tests.

These methods, however, may either become time consuming or lead to uncertain interpretation of test results. For practical purposes, soils with a plasticity index greater than 30 may be considered as having high swelling and shrinking potential.

Pile foundations are routinely selected in swelling and shrinking soils so that the load transfer is attained in stable ground conditions below the active zone. Piles installed in such soils will, however, be subjected to uplift forces in the zone where swelling occurs. Design considerations may involve one or a combination of the following procedures.

1. Coating the pile surface in the active zone with bitumen.
2. Separating the piles from the swelling medium by the use of floating sleeves that move up and down responding to the surrounding soil.

Pile Load Tests

Load testing may be carried out as either a routine procedure or a high-level load test. Routine tests serve the purpose of proof loading. High-level tests provide information useful in the final design, and involve more reliable test data combined with more detailed analysis of test results.

Pile load tests are based on the test method specified by ASTM D1143-90 (modified and reapproved in 1987). Tensile load tests conform to ASTM D3689-83. Lateral load tests on piles are carried out according to ASTM D3966-90. The slow maintained load test is a long duration test that usually lasts 70 hours or longer. The test pile is loaded to 200 percent of the design load unless it fails at a lower load level.

Where the objective is to determine the factored bearing resistance of a pile for limit state design, the quick test methods (ASTM D1143-81) are preferable over the slow test procedures. Tests, other than proof tests, should be carried to failure, and the designated failure load should be based on the shape of the load movement curve.

For piles used as foundations of highway bridges, the lower bound value for vertical pile capacity is usually estimated using Davisson's method (NAVFAC, 1982). This procedure consists of the following steps:

1. Draw the load-movement curve as shown in Figure 9–21.
2. Obtain the elastic movement $\Delta = Q_{va}L/AE$ of the pile, where Q_{va} is the applied load, L is the pile length, A is the pile cross-sectional area, and E is the elastic modulus of the pile material.
3. Draw a line OA based on the equation for elastic movement. Draw a line BC parallel to OA at a distance $x = 0.15 + D/120$ in (D = pile diameter in inches).
4. The failure load is at the intersection of BC with the load-movement curve—point C.

This procedure was originally recommended for driven piles. Its main advantage is that the limit line can be drawn before starting the test. Hence, it can be used as an acceptance criterion for proof tested contract pile.

In the design phase, the anticipated driving stress levels may be predicted by wave equation analysis. During pile installation, dynamic measurements of force and acceleration at the pile head may be used to measure driving stress levels. The wave equation solution requires computer programs (Hirsh, Carr, and Lowery, 1976; Goble and Rausche, 1987). These model the pile hammer, helmet and pile sections using a series of mass elements connected by weightless springs. The wave equation simulation allows the designer to confirm that the proposed pile section can be driven to the required capacity and penetration without damaging driving stress levels.

Dynamic monitoring consists of recording force and acceleration measurements at the pile head during initial pile installation or during restriking. Dynamic measure-

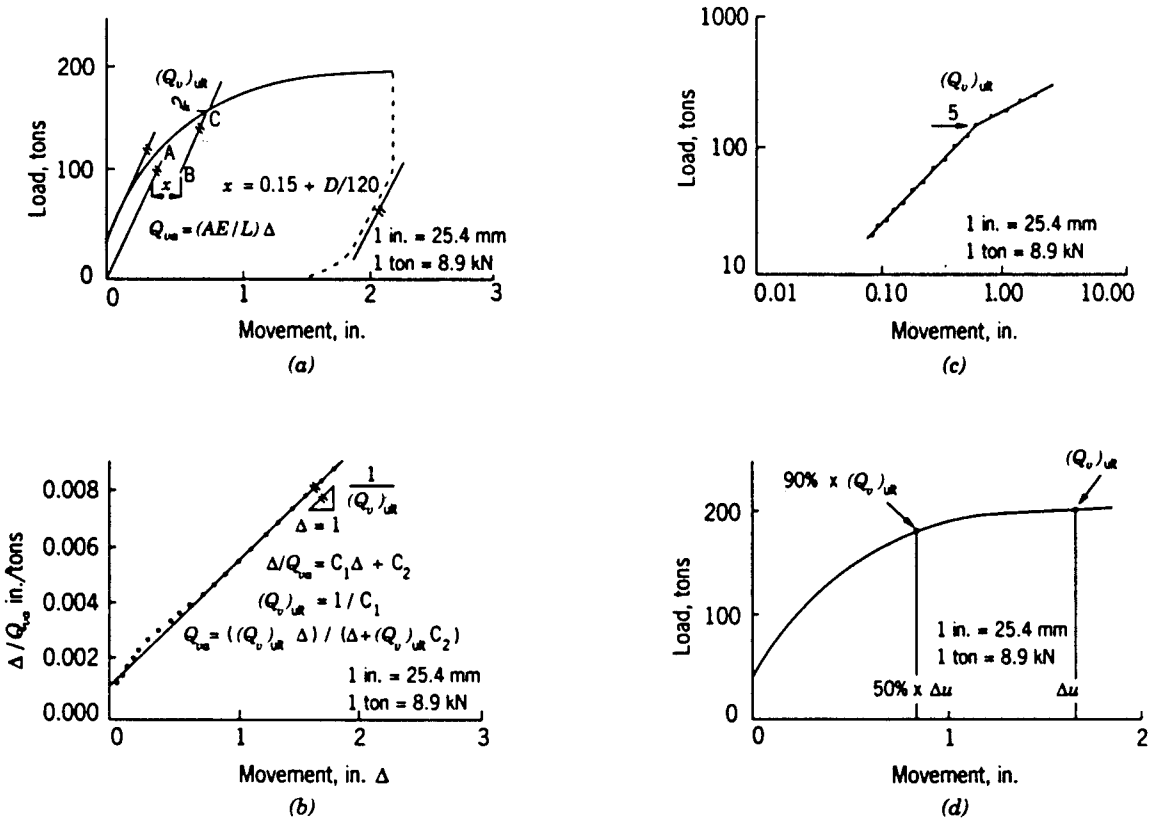

Figure 9–21 Load test interpretation methods by Davisson, Chin, De Beer, and Brinch Hansen's 90 percent criterion (Fellenius et al., 1989; Sharma and Yoshi, 1987); (a) Davisson's method; (b) Chin's method; (c) De Beer's method; (d) Brinch Hansen's 90 percent criterion.

ments of force and acceleration may also be used to estimate the pile capacity, resistance distribution, and soil quake and damping parameters (Rausche, Moses, and Goble, 1972).

Nondisplacement Piles

Steel H piles can fail in two ways. First, they can become plugged when the soil between the flanges adheres fully to the metal surface. Under this condition the effective area of the pile is the area of the resulting rectangle, and the skin friction is the sum of the soil adhesion at the flanges and the full soil-to-soil shear resistance along both sides of the soil plug. The point resistance is computed for the area of the enveloping rectangle.

Alternatively, steel H-piles can fail without plugging. In this case, the skin friction of the pile is estimated using adhesion on the entire perimeter of the section, whereas the tip resistance is based on the steel cross-sectional area only. Plugging may occur when the piles are driven in soft to medium clays and loose to dense sands. Piles normally should not plug in medium to very stiff clays and in very dense sands.

Likewise, open-ended piles may or may not plug. In a plugged pipe pile, the skin

friction may be computed assuming adhesion is developed on the outside surface only, whereas the gross area contributes to tip resistance.

If the pipe pile remains unplugged, the skin friction is calculated assuming that the soil adheres to both the inside and outside surfaces of the pile. The tip resistance may be predicted based on the cross-sectional area of the steel alone.

9.8 BEARING CAPACITY OF PILE GROUPS

Certain basic principles of pile group action were discussed in section 9.1. The interaction of piles in a group and the associated settlement patterns is shown in Figure 9–5, presenting the overlapping zones of increased stress below the pile tips prompting the group to act as one unit.

For strength design, the requirements for pile groups are essentially similar to those for single piles, or

$$\phi_g Q_g \geq \text{group load effect} \tag{9–41}$$

The ultimate bearing capacity of a pile group in sand is determined by summing the capacities of all piles in the group. The group efficiency, defined as the ratio of the ultimate load capacity of the pile group to the sum of the ultimate capacities of the individual piles, is suggested as unity. Evaluation of the group capacity of piles in sand is the same, irrespective of the contact between the pile cap and the ground.

For pile groups in cohesive soil, the presence and contact of the pile cap with the ground must be taken into account. With the cap in firm contact with the ground, the pile group consisting of the piles and the block of soil contained within the piles, may fail as a unit. In this case, the ultimate bearing capacity is the minimum of the following values: (1) the sum of individual pile capacities, and (2) the bearing capacity associated with block failure of the group.

For a pile block with dimensions X, Y and Z as shown in Figure 9–22, the bearing capacity is

$$Q_g = (2X + 2Y)Z\bar{s}_u + XYN_c s_u \tag{9–42}$$

where $\bar{s}_u$ = average undrained shear strength along the depth of penetration of the piles; s_u = undrained shear strength at the base of the group; and

$$N_c = 5(1 + 0.2X/Y)(1 + 0.2Z/X) \text{ for } Z/X \leq 2.5 \tag{9–43}$$

$$N_c = 7.5(1 + 0.2X/Y) \qquad \text{for } Z/X > 2.5 \tag{9–44}$$

If the pile cap is not in firm contact with the ground and the clay at the surface is soft, the individual pile capacity is modified by an efficiency factor n, where $n = 0.65$ for a pile spacing of $2.5D$ and $n = 1.0$ for a pile spacing of $6D$, with values of n interpolated in this range. The group capacity is obtained as the lesser of the individual pile capacities multiplied by n and the bearing capacity of the pile block. This procedure is recommended by the LRFD specifications.

If the clay is overconsolidated and insensitive, the pile group should be analyzed assuming contact of the pile cap with the ground. If a pile group contains batter piles, they may be treated as vertical piles. The performance factors for the group capacity ob-

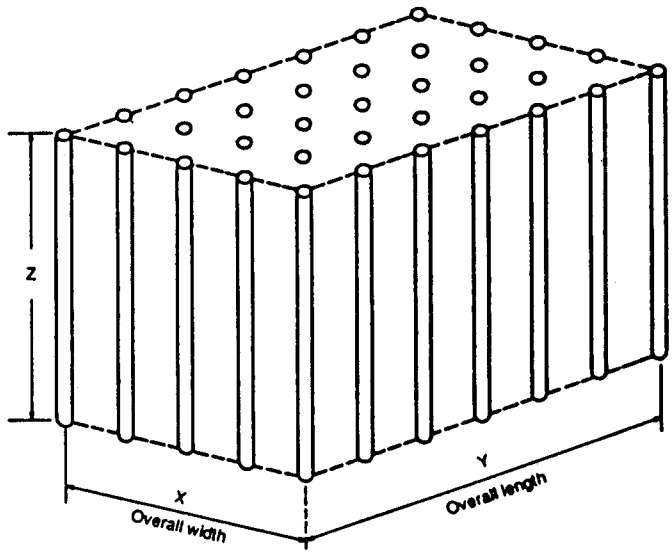

Figure 9–22 Pile group acting as block foundation.

tained using the sum of individual pile capacities are the same as those of a single pile (see Table 9–5). A separate performance factor should be used for the block failure.

9.9 UPLIFT CONSIDERATIONS

Uplift of a pile foundation may be caused by swelling, frost heave, buoyancy, lateral loads, and upward loads. Long piles should normally have adequate pullout resistance, but short piles bearing on bedrock should be checked for uplift loads. Where piles are subjected to uplift, they should be investigated for both resistance to pullout and structural capacity to resist tension.

Uplift capacity of single pile. Uplift capacity of a single pile may be considered on the basis of the principles discussed in section 9.1. For strength design, the ultimate uplift capacity is computed as for piles in compression, or

$$\phi_u Q_s \geq P_{x,y} \tag{9–45}$$

where Q_s = ultimate uplift capacities due to shaft resistance; $P_{x,y}$ = factored tensile load effect computed from Equation (9–17); and ϕ_u = performance factor for uplift capacity from Table 9–5.

As mentioned in section 9.1, the shaft friction in upward loading for piles in sand may not be the same as in downward loading. Furthermore, piles in tension unload the soil, and this reduces the overburden effective stress and the uplift skin friction resistance. Similar considerations influence the uplift resistance of piles in clay. Accordingly, the performance factors for axial compression and uplift are different.

Uplift capacity of pile group. The uplift resistance Q_{ug} of a pile group may be estimated as the lesser of (1) the sum of the individual pile uplift resistance, or (2) the uplift capacity of the pile group considered as a block. The mechanism of block failure is different for piles in clays and sands.

The shaft friction of pile groups in sands deteriorates with time if the foundation is subjected to vibratory and lateral loads. Tomlinson (1987) suggested that the weight of the block uplifted should be estimated using a spread of load of 1 to 4, as shown in Figure 9–23(a), from the base of the pile group. Effective unit weights should be used for soil below the groundwater level.

For piles in clay, the ultimate uplift resistance of the block under undrained shear conditions is, by reference to Figure 9–23(b)

$$Q_{ug} = (2XZ + 2YZ)\bar{s}_u + W_g \tag{9–46}$$

where $\bar{s}_u$ = average undrained shear strength along pile shaft, and W_g = weight of the block of soil, piles and pile cap.

Structural capacity. Ignoring the tensile strength of concrete, the tensile loads should be resisted by the steel reinforcement alone. The resulting requirement is

$$\phi_t f_y A_y \geq P_{x,y} \tag{9–47}$$

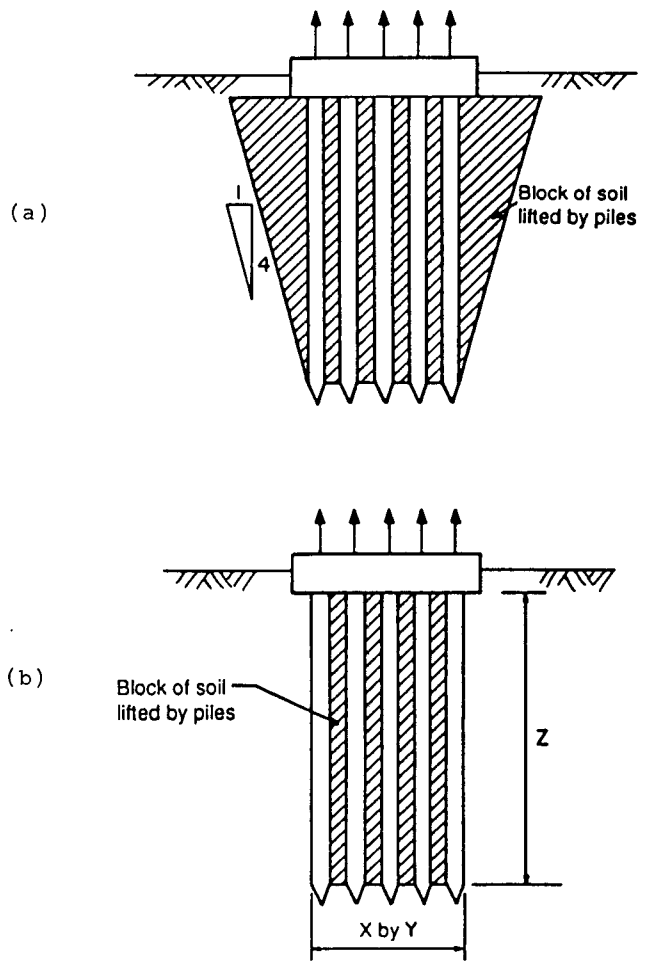

Figure 9–23 (a) Uplift of group of closely-spaced piles in cohesionless soil. (b) Uplift of group of piles in cohesive soils *(from Tomlinson, 1987).*

where f_y = yield strength of steel; A_y = cross sectional area of steel; and ϕ_t = performance factor for steel = 0.90 (the same for steel H and pipe piles, and steel reinforcement).

For timber piles, the parallel-to-grain tensile strength is higher than the compressive strength. Hence, the tensile capacity of the pile is not critical provided the uplift load does not exceed the compressive load.

9.10 NEGATIVE SKIN FRICTION

Negative skin friction is a downward force induced in a pile when the surrounding soil moves downward relative to the pile. Situations where this condition may conceivably arise where mentioned in section 9.1.

Negative skin friction or adhesion may be estimated using the rational methods presented in section 9.7 (namely the α, β and λ methods). For example, using the α method, the ultimate unit shaft resistance is, from Equation (9–22),

$$q_{sn} = \alpha s_u \tag{9–48}$$

The downdrag load is therefore

$$P_{sn} = q_{sn}\alpha_s D_n \tag{9–49}$$

where P_{sn} = downdrag load; α_s = pile perimeter; and D_n = length of pile embedded in settling soil.

Alternatively, the negative skin friction $Q_{f(neg.)}$ for both cohesionless and cohesive soils can be estimated as suggested by Vesic (1977)

$$Q_{f(neg.)} = \overline{N}_o \overline{p}_o A \tag{9–50}$$

where $\overline{N}o$ = nondimensional coefficient obtained from Table 9–9; $\overline{p}_o$ = mean normal effective stress; and A = area of shaft in the zone of settling soil ($A = \pi BL$ for a pile with diameter B and length L in the zone of settling soil).

In Table 9–9 uncoated and coated piles are mentioned. Uncoated piles are sections without surface treatment. Coated piles are sections treated with bitumen or bentonite, intended to reduce the adhesion between the soil and the pile surface.

Negative skin friction may also be estimated using the empirical relationship proposed by Garlanger (1973). Empirical values are obtained from Table 9–10.

Design requirements. In areas where there is a potential for the development of negative skin friction, batter piles should be avoided. This is mainly because (1) the magnitude of downdrag on the outer side of batter piles is markedly larger than the inner ver-

Table 9–9 Values of N_0 for Various Conditions[a]

Soil and Pile Condition	N_0
(a) Uncoated pile	
(i) In soft compressible layers of silt and clay	0.15–0.3
(ii) In loose sand	0.3–0.8
(b) Pile coated with bitumen or bentonite	0.01–0.05

[a]Values provided by Vesic (1977).

Table 9–10 Empirical Values of Negative Skin Friction

Soil Type	Negative Skin Friction
Sand	0.35 to 0.5 $\sigma'_v A$
Silt	0.25 to 0.35 $\sigma'_v A$
Clay	0.20 to 0.25 $\sigma'_v A$

Note: σ'_v = average effective vertical stress. A = area of shaft in the zone of settling soil. The units of σ'_v and A have to be consistent to yield a force unit for the negative skin friction.

tical piles, and (2) the settling soil tends to move away from the inner piles. These factors combined can induce excessive bending of the batter piles.

Although downdrag loads are unlikely to cause capacity problems, they may have undesired settlement effects. Thus, settlement of pile groups should be checked when downdrag (unfactored) loads act together with dead loads. Temporary live loads and downdrag loads do not produce additive effects. This is because the temporary live loads tend to compress the pile elastically and reduce or cancel the effect of the downdrag. When the live load is removed, the pile will rebound elastically and will restore the downdrag load.

If the downdrag load exceeds the live load, the structural or geotechnical capacity should be checked for dead loads plus downdrag. The load factor for the downdrag is the reciprocal of the performance factor for the ultimate skin resistance of the pile. This relationship is expressed as

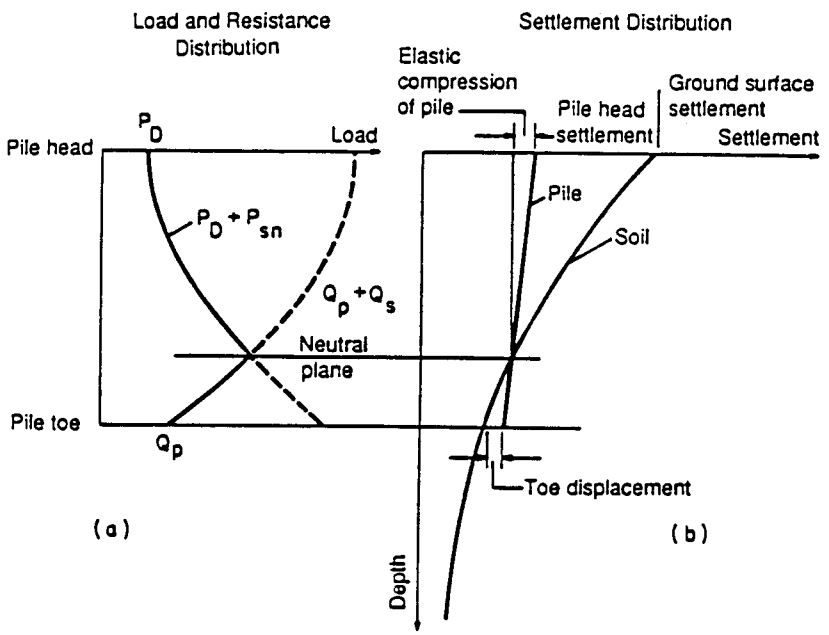

Figure 9–24 Calculation of the location of the neutral plane and the settlement of a pile or a pile group *(from Canadian Foundation Engineering Manual, 1985).*

$$\phi R \geq \gamma_d P_d + \frac{1}{\phi_{qs}} P_{sn} \tag{9–51}$$

where R = nominal resistance; ϕ = performance factor; P_{sn} = downdrag load; and ϕ_{qs} = performance factor for the ultimate skin pile resistance.

Neutral plane. This is defined as the elevation at which the settlement of the pile and the settlement of the soil are the same, as shown in Figure 9–24. Above the neutral plane, the soil loads the pile in negative skin friction, but below the neutral point the pile derives support from the soil. The load distribution and pile resistance are shown in Figure 9–24(a). A dead load P_d is applied at the top of the pile, and because of the negative skin friction, the total load ($P_d + P_{sn}$) acting on the pile increases with depth. The pile resistance is equal to the tip capacity Q_p at the toe, and increases upwards as the skin friction Q_s increases, represented by the curve ($Q_p + Q_s$). The two curves intersect at the neutral plane which is the location of the maximum load on the pile. For piles bearing on rock the neutral plane is located at the pile tip.

Figure 9–24(b) illustrates the procedure for estimating the settlement of the pile cap. This settlement is the sum of the settlement at the neutral plane and the elastic compression of the pile above the neutral plane. Unfactored loads should be used to estimate settlement.

9.11 PILE FOUNDATIONS UNDER LATERAL LOADS

General Considerations

Lateral loads on pile foundations commonly arise from wind, horizontal live loads, earth and water pressures, and earthquake effects. The two conditions of fixity of the pile head, free head and fixed head, may conceivably occur in practice in conjunction with pier and abutment configurations used in most cases. Isolated piles under single columns are usually considered as free-headed, whereas piles under a footing or stiff pile cap are usually analyzed with their tops assumed fixed. Fixity in this case is taken as restraint against rotation whereas the pile top is free to translate laterally, as shown in Figure 9–11(d).

Piles under lateral loads must, therefore, be designed to resist such combinations of forces first without failing (undergoing structural or bearing capacity failure), and then without deflecting excessively (a serviceability limit state). Under allowable stress design, an allowable lateral load is obtained by applying a factor of safety to the ultimate failure load, and then confirming that the corresponding lateral deflection does not exceed the allowable for the service conditions. Hence, methods for calculating the lateral resistance of vertical piles are broadly divided into two categories: (1) methods for calculating ultimate lateral resistance; and (2) methods for determining the lateral deflection of piles at working loads.

Batter Piles

When the lateral loads on a pile foundation are considerable, batter piles can be used effectively to receive and transmit these loads to the ground. Most states require the exterior rows of pile groups to be battered as a mandatory design criterion. The degree of

batter depends on the pile type and the relationship of the lateral loads to the vertical loads. Installation of batter piles by driving is feasible for batters as large as 1 horizontal to 2 vertical, although the practical batter is less steep. The greatest efficiency is achieved by using piles battered in opposite directions.

A simple graphical procedure for estimating the compressive and tensile forces in pile groups containing batter piles is described by Tomlinson (1987). This method assumes that (1) the batter piles are pinned at their point of intersection; (2) the vertical piles in the group do not carry lateral loads; and (3) batter piles carry only axial load. This procedure does not consider the soil-pile interaction, pile and soil stiffness, and pile head fixity, factors that can alter the mechanism of force distribution in the pile group. The method is, however, useful for obtaining preliminary pile layouts, and the results are reasonably accurate if the lateral load does not exceed 20 percent of the vertical load.

If the pile group has more than three rows of piles, Tomlinson's procedure is not applicable. In this case, more complex methods of linear elastic and nonlinear elastic soil response may be used for analyzing two-dimensional and three-dimensional pile groups, but they typically require computer usage. Procedures that may be used to estimate pile forces and displacements of pile groups include Hrennikoff's (1950) linear elastic analysis that can model the problem in two dimensions; the approach by Saul (1968) who expanded Hrennikoff's solution to three dimensions; the method of O'Neill, Ghazzaly, and Ha (1977); and the procedure developed by O'Neill and Tsai (1984) for the analysis of three-dimensional pile groups with nonlinear soil response and soil-pile interaction.

Vertical Piles, Criteria for Lateral Deflection

The condition that normally governs the design of laterally loaded vertical piles is the maximum tolerable deflection or the structural capacity of the pile. Reaching or approaching the ultimate lateral capacity of the soil requires considerable displacements that are either unattainable or unacceptable so that this condition is seldom a realistic possibility. Thus, in designing a group of vertical piles to resist lateral loads, the analysis should investigate the lateral deflections and the structural capacity of the piles.

Single pile deflection. The two generally used approaches for calculating lateral deflections are the subgrade reaction method, and the elastic continuum approach.

Subgrade Reaction Method. This method treats a laterally loaded pile as a beam on elastic foundation, as shown in Figure 9–25(c). The usual assumption is that the beam is supported by a Winkler soil model, where the elastic soil medium is replaced by a series of infinitely closely spaced independent elastic springs. The stiffness of these springs k_h (also called the modulus of horizontal subgrade reaction) is expressed as follows:

$$k_h = \frac{p}{y} \tag{9–52}$$

where p = soil reaction per unit length of pile, and y = corresponding pile deformation. In reality, the soil reaction-deflection relationship is nonlinear and the Winkler ideal model would require modification, using the p-y curves approach. The behavior of a pile

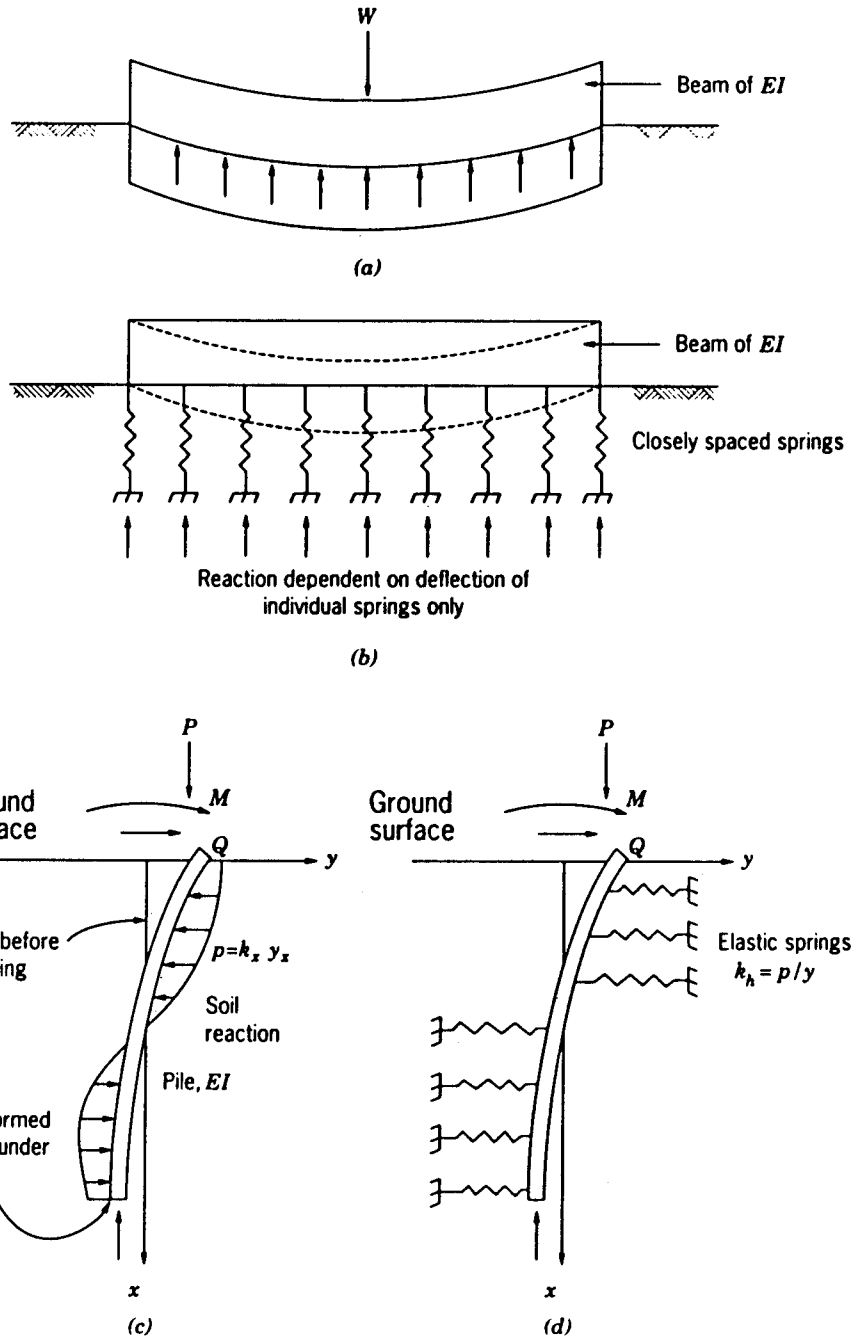

Figure 9–25 Behavior of laterally loaded pile; subgrade reaction approach; (a) beam on elastic foundation; (b) Winkler's idealization; (c) laterally loaded pile in soil; (d) laterally loaded pile on springs.

can thus be analyzed by using the equation of an elastic beam on elastic foundation, expressed by

$$\frac{d^4y}{dx^4} + \frac{k_h y}{EI} = 0 \tag{9–53}$$

Elastic Continuum Approach. The theory of subgrade reaction will give unsatisfactory results unless the continuity of the soil mass is taken into account. Treating the soil as an elastic continuum is theoretically more realistic, but a practical problem is the determination of the soil modulus E_s. In addition, this approach needs more field verification by applying the theoretical concept to practical problems.

Referring to Figure 9–26, the theoretical basis for the elastic continuum approach is derived from the following:

1. The pile is assumed to be a thin rectangular vertical strip of width B, length L, and constant flexibility EI. The pile is divided into $(n + 1)$ elements of equal length except those at the top and the tip of the pile, which are of length $\delta/2$.
2. To simplify the analysis, horizontal shear stresses that may possibly develop between the soil and the sides of the pile are not taken into account.
3. Each element is assumed to be acted on by a uniform horizontal force P assumed constant across the width of the pile.
4. The soil is considered an ideal, homogeneous, isotropic, semi-infinite elastic material, with its elastic modulus and Poisson's ratio unaffected by the presence of the pile.

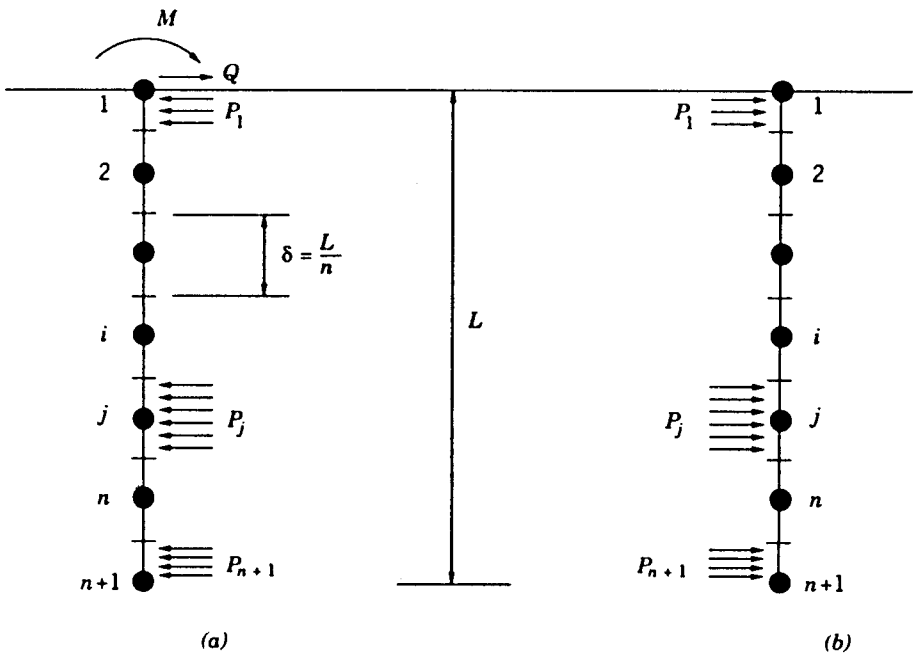

Figure 9–26 Stresses acting on (a) pile; (b) soil adjacent to pile *(from Poulos, 1971a).*

All three methods, elastic, subgrade reaction and *p-y* analysis, are described by Poulos and Davis (1980).

Evans and Duncan Procedure. This approach (Evans and Duncan, 1982) relates the lateral deflection to the lateral load using the so-called characteristic load P_c. This parameter characterizes the important properties of the pile (diameter, stiffness) and the soil (strength, stiffness) that determine the response of the soil-pile system to the lateral loads. The larger the value of P_c, the greater is the capacity of the pile to resist the imposed lateral load and the smaller is the lateral deflection.

Charts in dimensionless form have been developed for sand and clay, and are presented in Figures 9–27 and 9–28, respectively. The charts show the variation of P_{sp}/P_c with Y_{sp}/D, where P_{sp} is the unfactored lateral load, Y_{sp} is the pile displacement, and D is the pile width or diameter. The nonlinear soil behavior modeled in this case is the same as in the *p-y* method of analysis. The procedure demonstrated in Figures 9–27 and 9–28 involves the following steps:

1. Select a pile section of a given width or diameter D, modulus E_p, and moment of inertia I_p.

   For prestressed and precast concrete piles the value of E_p may be inferred from the compressive concrete strength as shown in Figure 9–29. The steel modulus can be taken as 29×10^6 lb/in^2. For timber piles of all species of Douglas fir and southern pine piles, E_p may be taken as 1.5×10^6 lb/in^2. Data on the sectional

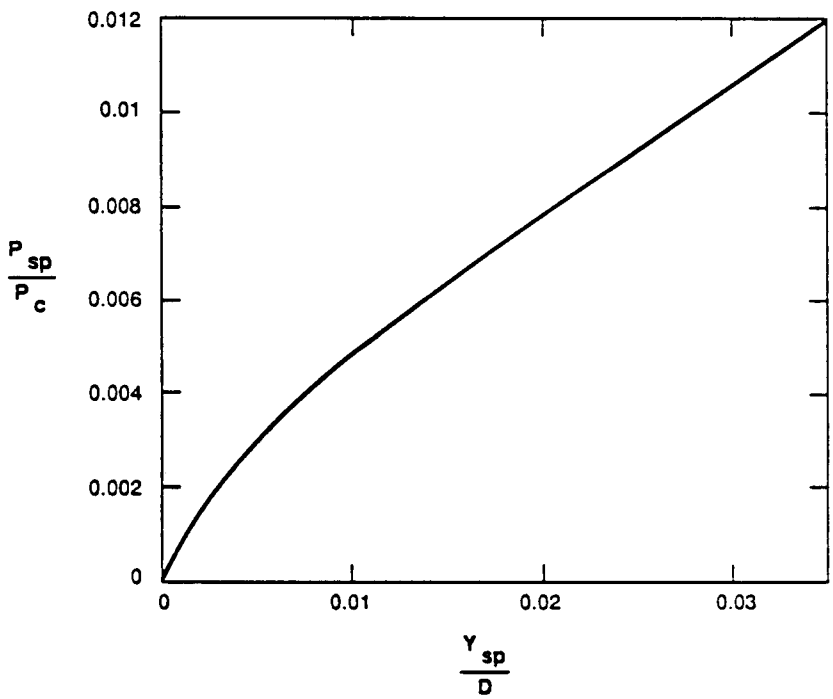

Figure 9–27 Lateral load versus deflection for fixed head piles in sand *(from Evans and Duncan, 1982).*

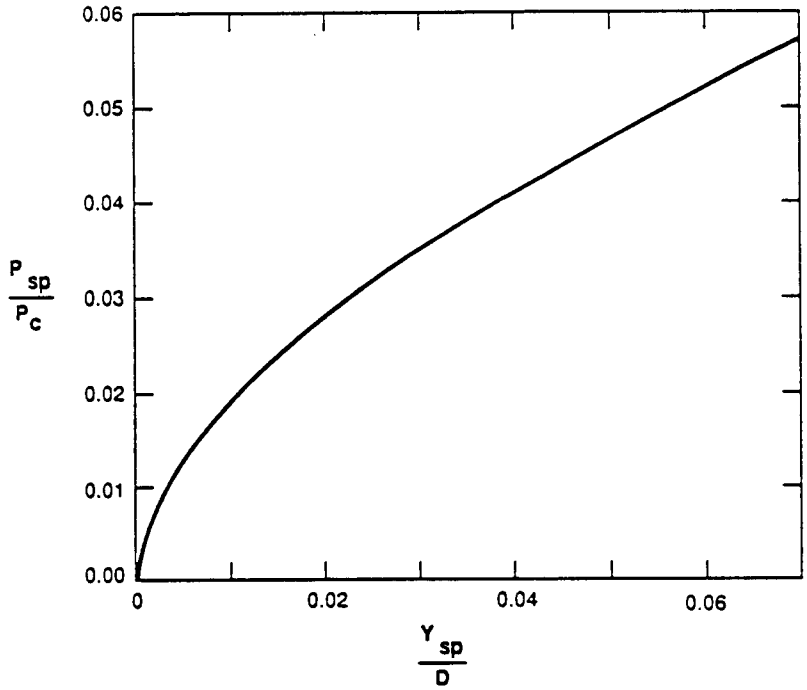

Figure 9–28 Lateral load versus deflection for fixed-head piles in clay *(from Evans and Duncan, 1982).*

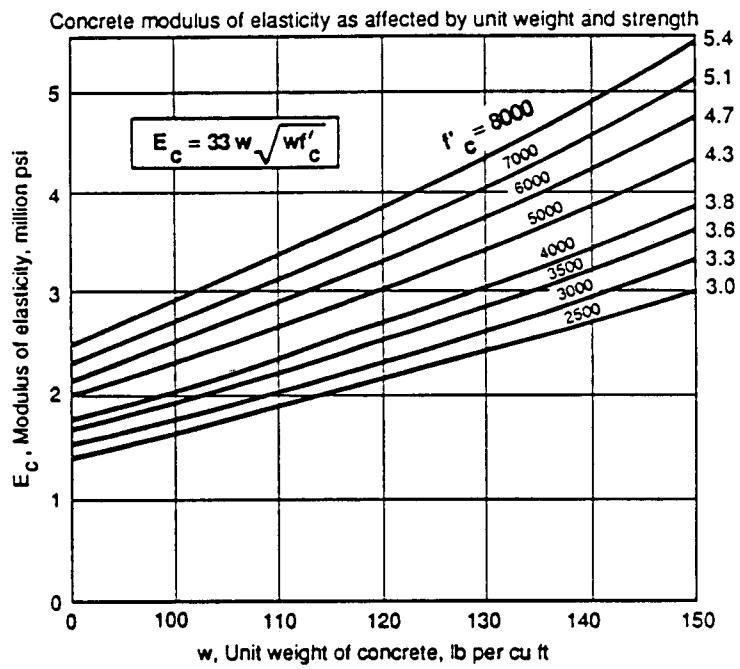

Figure 9–29 Modulus of elasticity of concrete *(from PCI, 1985).*

properties of prestressed concrete, steel H and pipe piles are usually obtained from manufacturers.

2. Estimate the average undrained shear strength for clays, or the average angle of internal friction for sands.

   The soil behavior close to the ground line is most relevant to pile response under lateral load. The properties of s_u and ϕ' should be averaged over a depth extending about eight pile diameters below the top of the pile. Effective unit weight should be used below the water table in sands.

3. Determine the characteristic load P_c from the following equations:

$$\text{For clay } P_c = 7.34D^2\left(E_pR_I\right)\left(s_u/E_pR_I\right)^{0.683} \tag{9–54}$$

$$\text{For sand } P_c = 1.57D^2\left(E_pR_I\right)\left(\gamma' D\phi' K_p/E_pR_I\right)^{0.57} \tag{9–55}$$

   where R_I = moment of inertia ratio = I_p/I_{SOLID}; $I_{solid} = \pi D^4/64$; K_p = passive earth pressure coefficient; and ϕ' = angle of internal friction, degrees.

4. Compute the ratio P_{sp}/P_c.
5. Refer to Figure 9–27 or 9–28 to determine the value of Y_{sp}/D.
6. Calculate Y_{sp} from $Y_{sp} = D(Y_{sp}/D)$, using the value of Y_{sp}/D obtained from step 5.

Appropriate load-deflection diagrams have been developed based on the foregoing analysis, shown in Figures 9–30 to 9–33. These charts are for prestressed concrete piles (10, 12, 14, 16, and 18 inches square), and steel H-piles (HP 10 × 42, HP 10 × 57, HP 12 × 53, HP 12 × 74, HP 14 × 73, and HP 14 × 89) in clay and sand. For the soil conditions shown and for a given pile type and size, the lateral deflection can be estimated directly from the graphs. For example, for a lateral load of 10 kips acting on a 12 × 12 in prestressed concrete pile driven in clay with undrained shear strength of 1 kip/ft^2, the corresponding lateral deflection is found directly from Figure 9–31 as 0.1 in.

For piles in sand, the diagrams were developed for friction angles of 30°, 35°, and 40°, since for smaller friction angles the sand is generally loose and piles would normally not be used to resist lateral loads. The water table was taken at or above the ground level. For intermediate friction angles, the deflection may be estimated by interpolation.

For clays, the diagrams were derived using undrained shear strengths of 1, 2, and 4 kips/ft^2. Deflections for intermediate shear strength may likewise be computed by interpolation.

Deflection of pile groups. In the foregoing analysis the piles are assumed to have fixed heads, that is, the tops are prevented from rotating. This is usually the case, since piles are mostly used in groups and are encased in rigid caps or concrete footings that are part of the substructure element.

In general, groups of piles behave as individual units if they are spaced at more than 6 to 8 diameters parallel to the direction of the lateral load application. In order to respond as individual units in a direction perpendicular to the lateral load their spacing

(text continues on page 647)

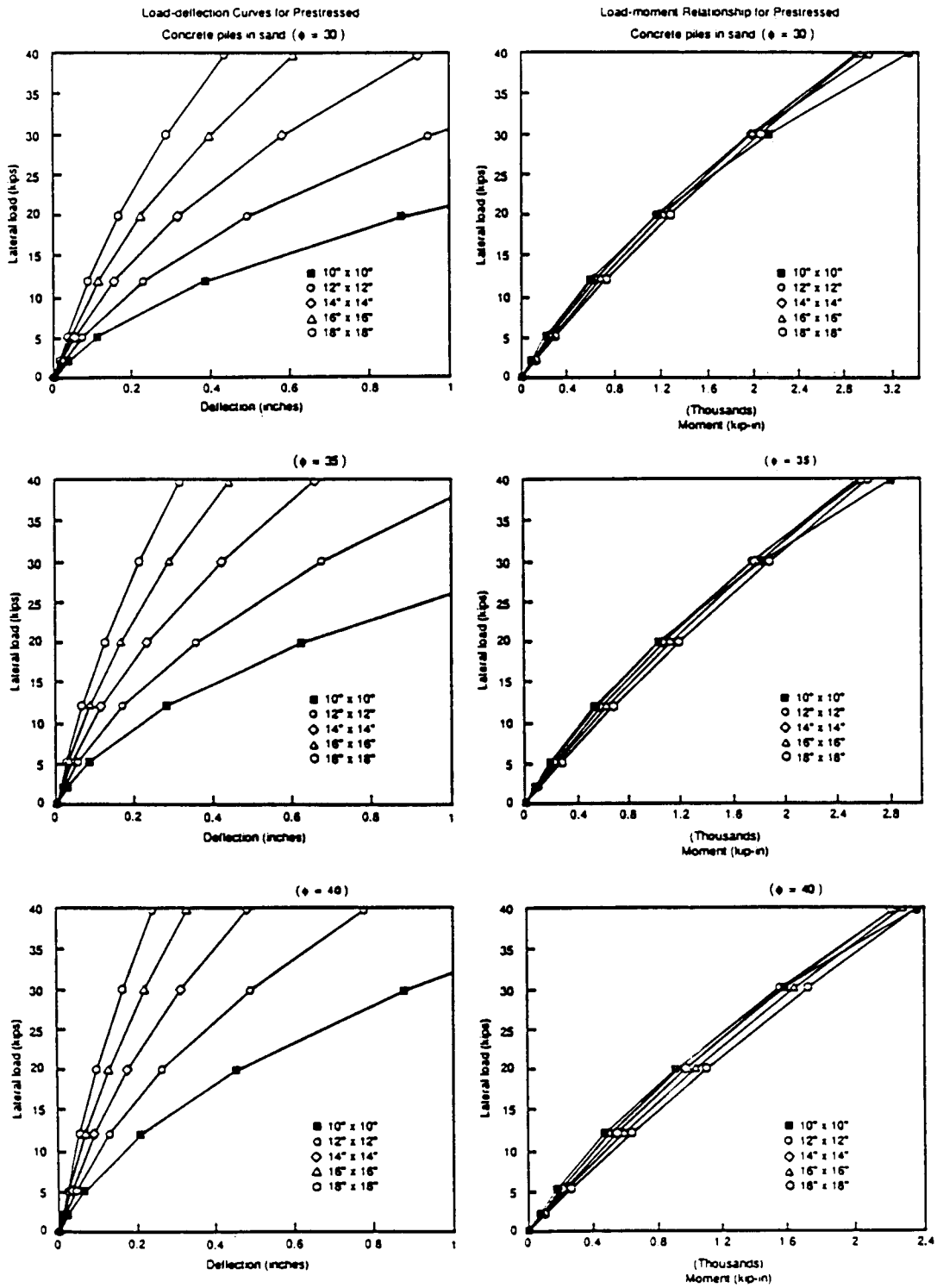

Figure 9–30 Load versus deflection and load versus moment for prestressed concrete piles in sand.

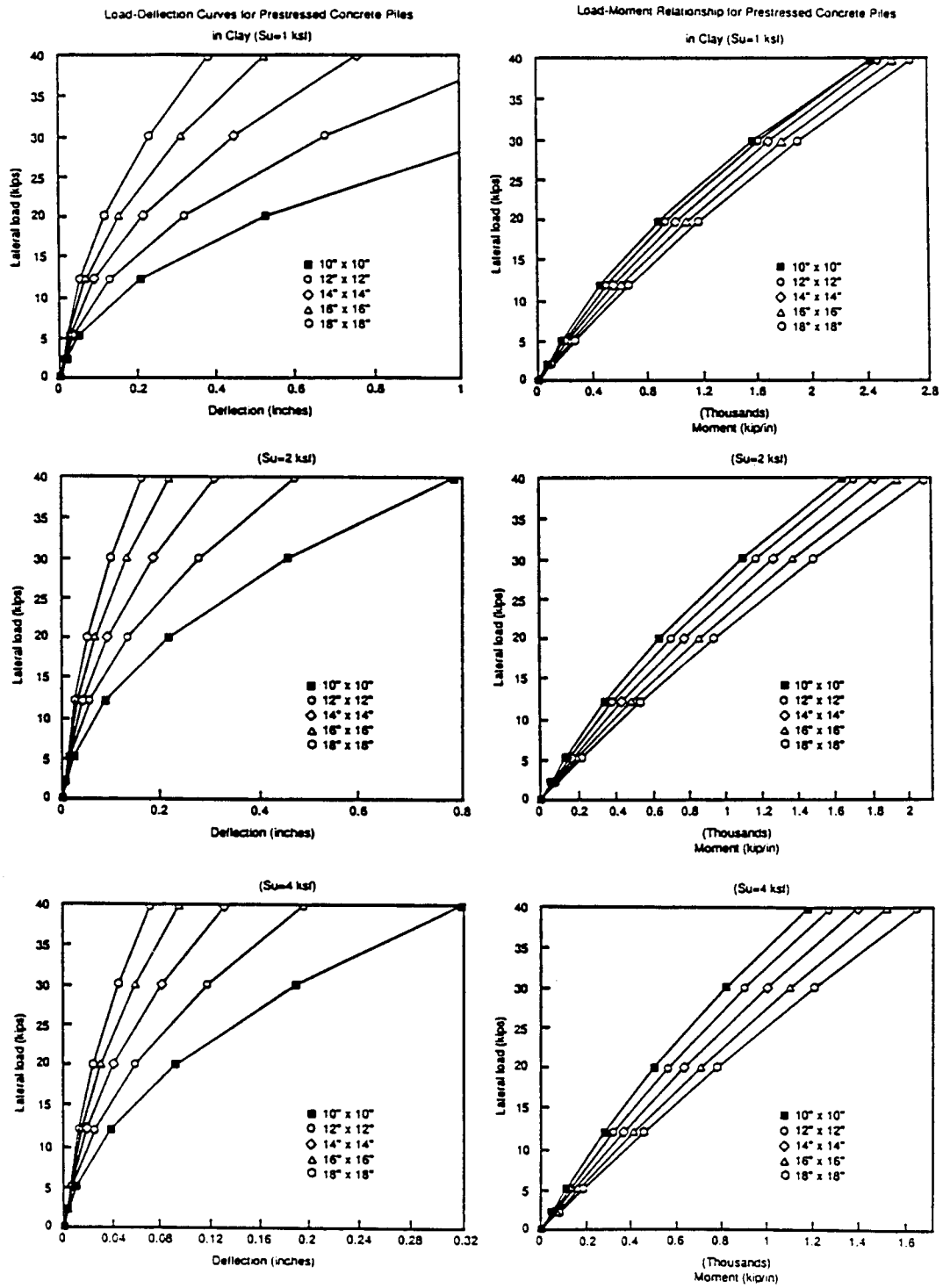

Figure 9–31 Load versus deflection and load versus moment for prestressed concrete piles in clay.

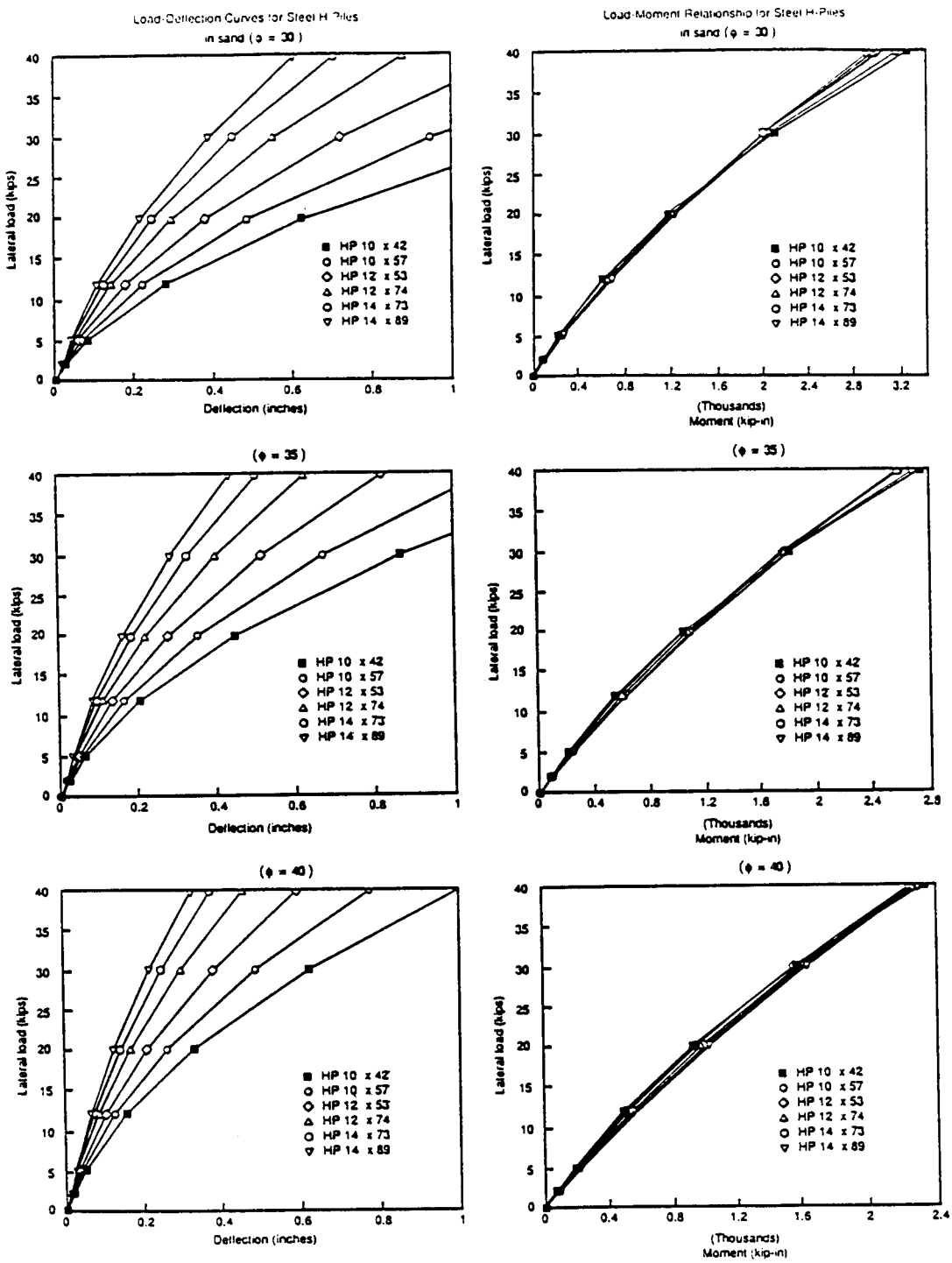

Figure 9–32 Load versus deflection and load versus moment for steel-H piles in sand.

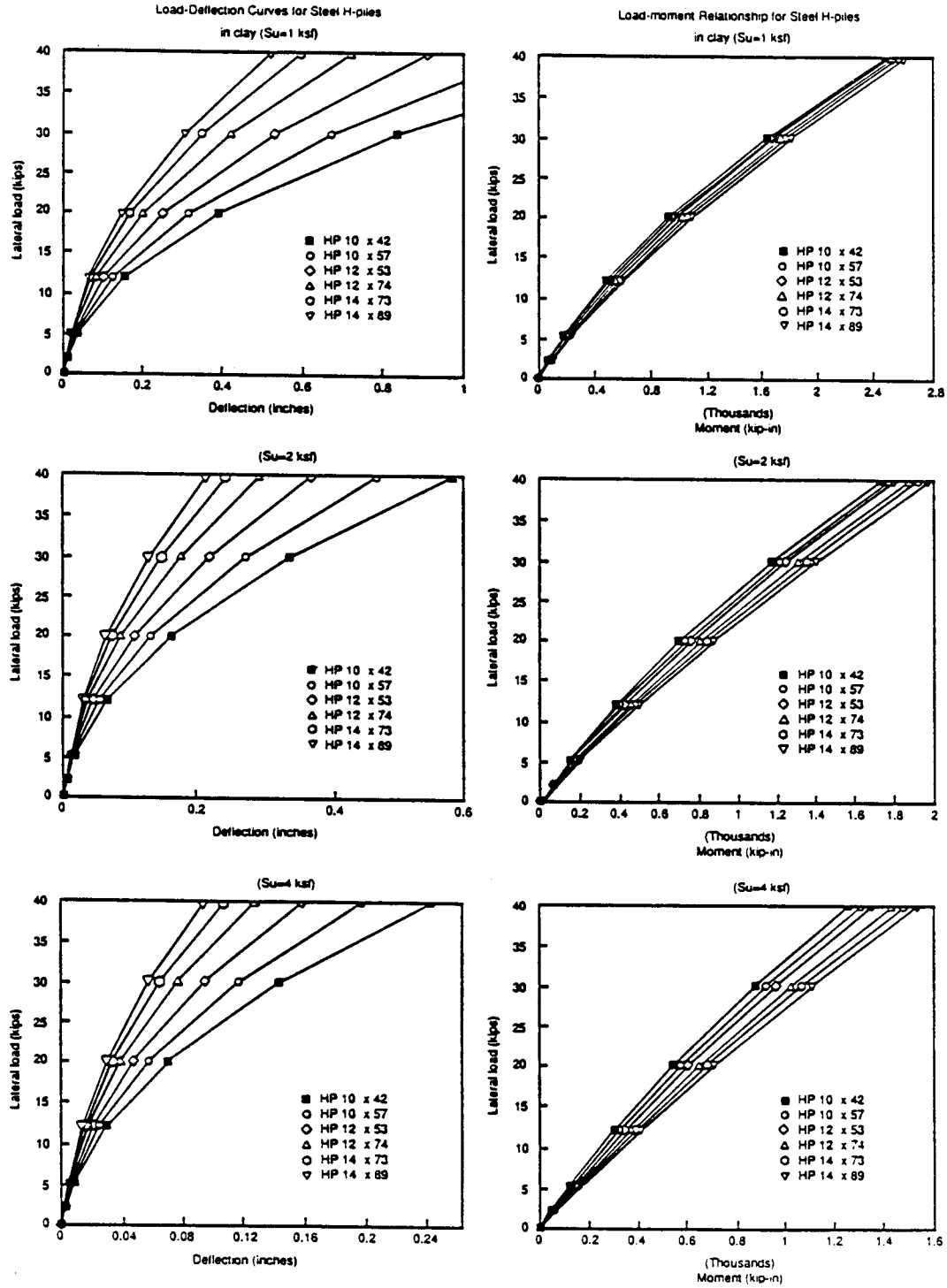

Figure 9–33 Load versus deflection and load versus moment for steel-H piles in clay.

should exceed 2.5 diameters. In estimating the lateral load capacity of the pile group a reduction in the coefficient of subgrade reaction should be made as shown in Table 9–11.

Alternatively, the lateral deflection of a group of piles may be estimated using the empirical expression

$$Y_g = \frac{A + N_{PILE}}{B\sqrt{\frac{S}{D} + \frac{P_{sp}}{CP_N}}} Y_{sp} \tag{9–56}$$

where Y_{sp} = lateral displacement of a single fixed-head pile subjected to a lateral load P_{sp}; N_{PILE} = number of piles in the group; S = average pile spacing; D = pile width or diameter; $P_{sp} = P_{yg}/N_{PILE}$ (P_{yg} = lateral load on pile group); and P_N is given by

$$\left.\begin{aligned} P_N &= K_p \gamma D^3 \text{ for sand} \\ P_N &= s_u D^2 \quad \text{for clay} \end{aligned}\right\} \tag{9–57}$$

where the parameters K_p, γ and s_u are as previously. The factors A, B and C in Equation (9–56) are empirical coefficients that can be taken as follows:

A = 16 for clay and 9 for sand
B = 5.5 for clay and 3 for sand
C = 3 for clay and 16 for sand

Equation (9–56) is the result of a parametric study of a large number of pile groups based on the theory proposed by Focht and Koch (1973). In this study the piles were uniformly spaced, but the analysis is valid for groups with nonuniform spacing using an average spacing in the calculations.

Alternatively, pile groups may be designed to resist lateral loads based on presumptive values, as in the example of section 7.10.

Table 9–11 Group Reduction Factor for the Coefficient of Subgrade Reaction[a]

Pile Spacing in the Direction of Loading	Group Reduction Factor for n_h or k^b
3*B*	0.25
4*B*	0.40
6*B*	0.70
8*B*	1.00

[a]Also adopted in *Canadian Foundation Engineering Manual,* 1985. *Foundation and Earth Structures, Design Manual 7.2,* NAVFAC, DM 7.2 (1982) also recommends these values.

[b]n_h is applicable for soil modulus linearly increasing with depth, and k is applicable for soil modulus constant with depth.

(From Davisson, 1970)

Piles under Axial Load and Bending Moment

Single pile. A simple procedure for calculating the maximum bending moment M_{sp} induced by a lateral load at the top of the pile is based on the use of design charts shown in Figures 9–34 and 9–35 for sand and clay, respectively. The pile is assumed to have fixed head. The graphs show the variation of M_{sp}/M_c with P_{sp}/P_c where M_{sp} = maximum moment in the single pile and M_c = characteristic moment. The parameters P_{sp} and P_c are as previously. The procedure involves the following steps (Evans and Duncan, 1982).

1. Select a pile section of a given width or diameter D, modulus E_p, and moment of inertia I_p.
2. Estimate the average undrained shear strength s_u for clays and the average friction angle ϕ' for sands. The behavior of the pile is likewise controlled by the soil characteristics close to the ground line. Below the water table, effective weights should be used.
3. Determine the characteristic load P_c from Equations (9–54) and (9–55).
4. Calculate the factored lateral load $\gamma_h P_{sp}$ and the ratio $\gamma_h P_{sp}/P_c$, where γ_h is the lateral load factor.
5. Refer to the graphs of Figure 9–34 or 9–35 to determine the ratio M_{sp}/M_c.

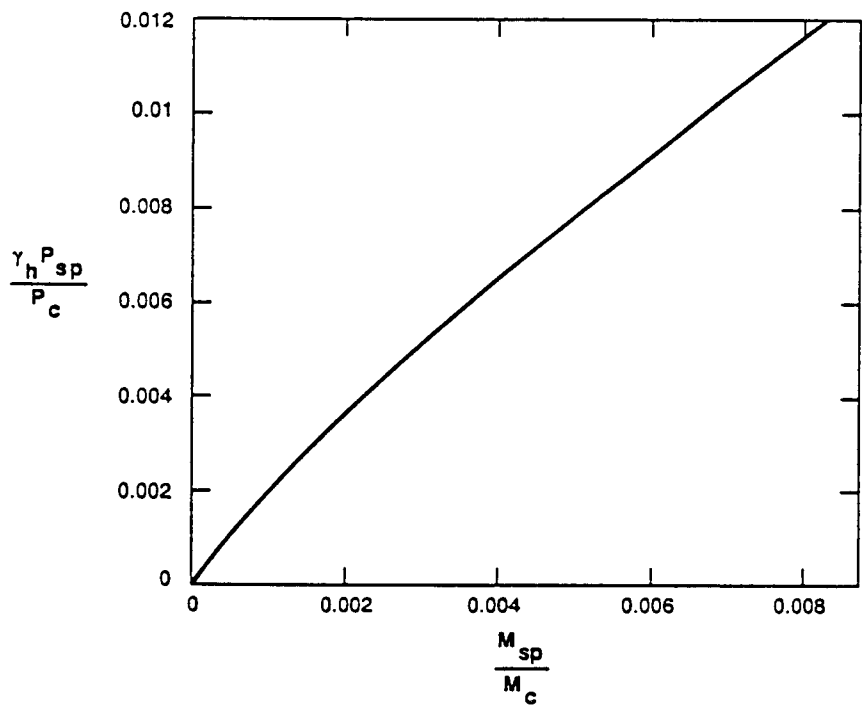

Figure 9–34 Lateral load versus moment for fixed-head piles in sand *(from Evans and Duncan, 1982).*

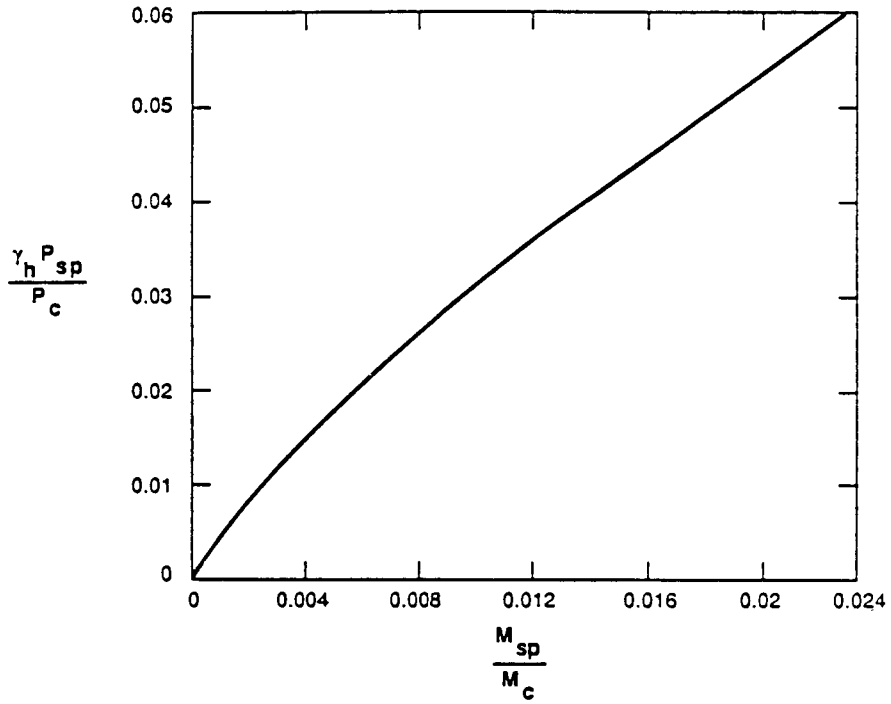

Figure 9–35 Lateral load versus moment for fixed-head piles in clay *(from Evans and Duncan, 1982).*

6. Calculate the characteristic moment M_c from the following:

$$\text{For clay } M_c = 3.86D^3(E_pR_1)(s_u/E_pR_1)^{0.46} \tag{9–58}$$

$$\text{For sand } M_c = 1.33D^3(E_pR_1)(\gamma' D\phi' K_p/E_pR_1)^{0.4} \tag{9–59}$$

7. With M_c and M_{sp}/M_c known, compute $M_{sp} = M_c(M_{sp}/M_c)$.

Appropriate lateral load-moment diagrams based on the foregoing procedure are likewise shown in Figure 9–30 to 9–33 for prestressed concrete and steel H-piles in clay and sand. For these conditions, the bending moments may be estimated directly from the charts. For the same example of the lateral load of 10 kips applied at the top of a 12 × 12 in prestressed concrete pile in clay with undrained shear strength 1 kip/ft^2, the resulting bending moment is 400 kip-in.

Bending moments in pile groups. From the preceding discussion, it becomes apparent that the deflection of any pile in a group causes deflection of the surrounding soil and adjacent piles, eventually leading to a greater deflection for the pile group than for a single pile subjected to the same load. Accordingly, the bending moment in a pile within a group will be larger than in a single pile under the same loading.

Brown, Reese, and O'Neill (1987, 1988) have determined that the maximum bending moment in a group of free-head piles occurs in the leading row (front) of piles, but current theories on lateral loading of pile groups cannot confirm this behavior. A semi-

empirical procedure that provides a reasonable estimation of load effects and moments in the leading row of a pile group has been developed based on the work by Focht and Koch (1973). Results thus obtained compare favorably with results from field tests. The moment increase because of group interaction has been studied for a representative number of cases first by estimating the pile group deflection according to the theory of Focht and Koch (1973) and then "softening" the soil (reducing s_u or ϕ') until the single pile deflection (calculated using the Evans and Duncan approach) matches the lateral deflection of the pile group. This investigation produced the following semiempirical relationships correlating the maximum bending moment of the most severely loaded piles in the group to the maximum bending moment in a single pile:

$$M_g = \left[Y_g / Y_{sp}\right]^n M_{sp} \tag{9–60}$$

where M_{sp} = maximum bending moment in a single fixed-head pile subjected to a lateral load P_{sp} estimated as suggested in the previous sections,

M_g = maximum bending moment in a single pile within a pile group
Y_{sp} = lateral deflection of a single fixed-head pile subjected to a lateral load P_{sp} estimated according to the foregoing procedure
Y_g = lateral group deflection from Equation (9–56)

Also

$$n = \frac{\gamma_h P_{sp}}{150 P_N} + 0.25 \quad \text{for clay} \tag{9–61}$$

$$n = \frac{\gamma_h P_{sp}}{300 P_N} + 0.30 \quad \text{for sand} \tag{9–62}$$

where P_N is obtained from Equation (9–57) and γ_h is the load factor for the lateral load.

Pile Behavior for Deflection and Moment beyond the Elastic Range

Application of p-y curves to cohesionless soil. This procedure, referred to briefly in the foregoing sections, allows the extension of pile analysis beyond the elastic range, that is, where the soil yields plastically (Matlock, 1970; Reese and Welch, 1975; Bhushan, Haley, and Fong, 1979). The analysis involves a step-by-step iterative process.

The theoretical basis is expressed by Equation (9–52). The resulting differential equation for a pile assumed to be a linearly elastic beam can be solved if the soil modulus k_h is expressed as a function of x and y, where x is the depth below the surface and y is the pile deflection. The numerical description of the soil modulus is best accomplished in this case by a family of curves showing the soil reaction p as a function of deflection y (Reese and Welch, 1975). In general, these curves are nonlinear and depend on several parameters such as depth, shear strength of soil, and number of load cycles (Reese, 1977).

An example of p-y curves is shown conceptually in Figure 9–36. These curves are assumed to have the following characteristics:

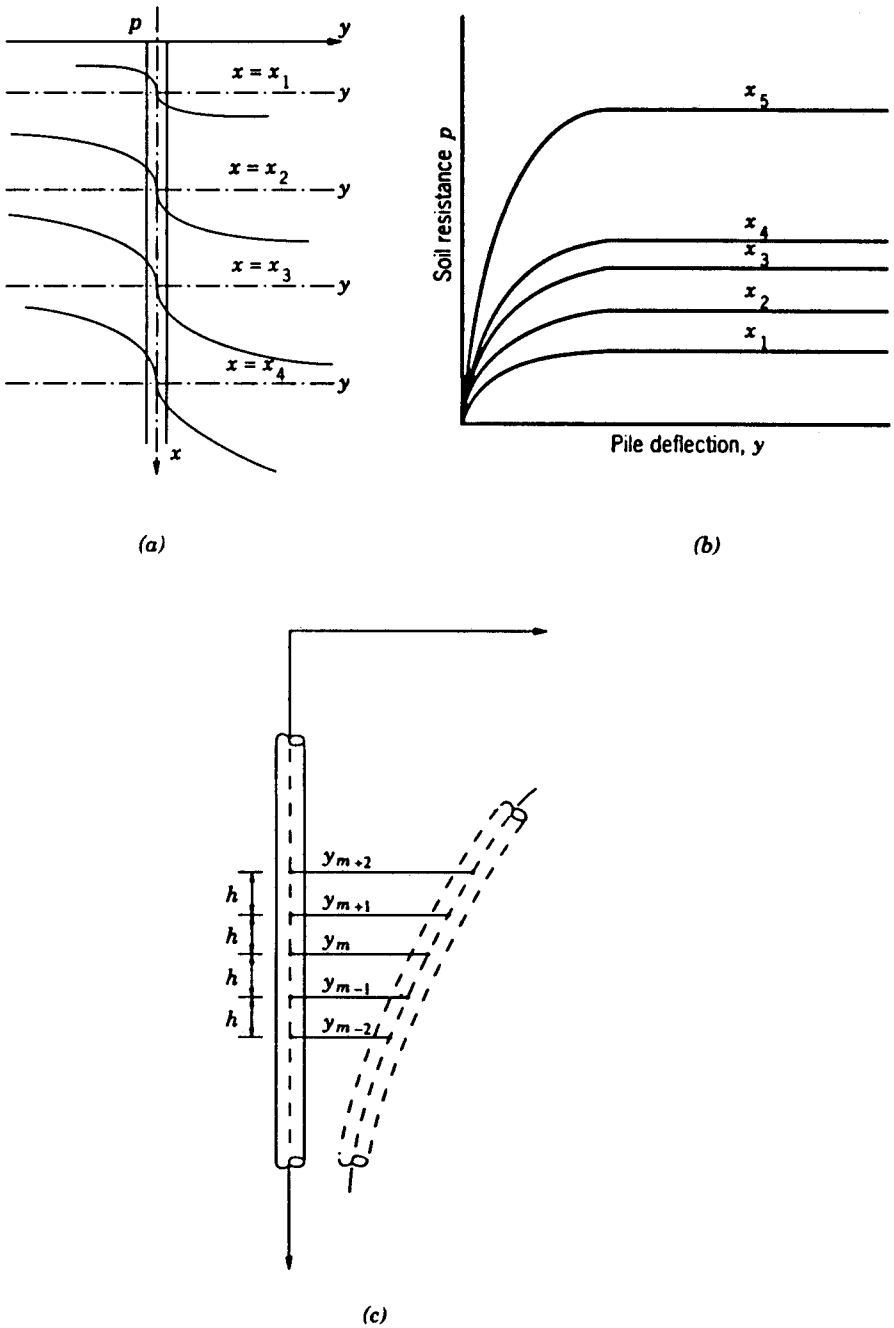

Figure 9–36 Set of p-y curves and representation of deflected pile; (a) shape of curves at various depths x below soil surface; (b) curves plotted on common axes; (c) representation of deflected pile.

1. Sets of p-y curves represent the lateral deformation of soil under a horizontally applied pressure on a discrete vertical pile section at some specific depth.
2. The curves are independent of the shape and stiffness of the pile element, and are not affected by loading above and below the discrete vertical area of soil at that depth.
3. Pile deflection at a depth is for practical purposes assumed to be dependent on the soil reaction at the same depth and hence the soil can be replaced by a mechanism represented by a set of discrete p-y characteristics as shown in Figure 9–36(b).

The p-y curves obtained from lateral load tests in the field on full-size piles have been critically analyzed and provided the basis for a procedure developed by Reese, Cox and Koop (1974) for constructing p-y curves in cohesionless soil. This approach involves the following steps:

Step 1. Carry out field or laboratory tests to estimate the angle of internal friction ϕ and the unit weight γ of the soil at the site.

Step 2. Calculate the factors $\alpha = 1/2\phi$, $\beta = 45 + \alpha$, $K_o = 0.4$ and $K_A = \tan^2(45 + \phi/2)$. Also two parameters p_{cr} and p_{cd}. The latter are functions of the soil properties and a critical depth x_r obtained graphically (Prakash and Sharma, 1990).

Step 3. Select a particular depth x at which the p-y curves can be drawn. Compare this depth with the critical depth x_r obtained in step 2 to determine if the values of p_{cr} and p_{cd} are applicable.

Step 4. Select appropriate values n_h for the soil. Also calculate the following parameters (n_h is the constant of horizontal subgrade reaction):

$$p_m = B_1 p_c \tag{9–63}$$

where B_1 is taken from Table 9–12 and p_c is computed as p_{cr} or p_{cd}.

Next, calculate

$$y_m = B/60 \tag{9–64}$$

where B is the pile width, and

$$p_u = A_1 p_c \tag{9–65}$$

where A_1 is likewise taken from Table 9–12. With the preceding parameters known, calculate

$$y_u = 3B/80 \tag{9–66}$$

$$M = (p_u - p_m)/(y_u - y_m) \tag{9–67}$$

$$n = p_m/my_m \tag{9–68}$$

$$C = p_m/(y_m)^{1/n} \tag{9–69}$$

$$y_k = (C/n_h x)^{n/(n\text{-}1)} \tag{9–70}$$

$$p = Cy^{1/n} \tag{9–71}$$

Step 5. Referring to Figure 9–37(b) locate y_u on the y axis. Enter with this value of y_u as y in Equation (9–71) to determine the corresponding p value which will define the k point. Connect point k with origin O thus establishing line Ok in Figure 9–37(b).

Table 9–12 Values for Coefficients A_1 and B_1

$\frac{x}{B}$	A_1		B_1	
	Static	*Cyclic*	*Static*	*Cyclic*
1	2	3	4	5
0	2.85	0.77	2.18	0.50
0.2	2.72	0.85	2.02	0.60
0.4	2.60	0.93	1.90	0.70
0.6	2.42	0.98	1.80	0.78
0.8	2.20	1.02	1.70	0.80
1.0	2.10	1.08	1.56	0.84
1.2	1.96	1.10	1.46	0.86
1.4	1.85	1.11	1.38	0.86
1.6	1.74	1.08	1.24	0.86
1.8	1.62	1.06	1.15	0.84
2.0	1.50	1.05	1.04	0.83
2.2	1.40	1.02	0.96	0.82
2.4	1.32	1.00	0.88	0.81
2.6	1.22	0.97	0.85	0.80
2.8	1.15	0.96	0.80	0.78
3.0	1.05	0.95	0.75	0.72
3.2	1.00	0.93	0.68	0.68
3.4	0.95	0.92	0.64	0.64
3.6	0.94	0.91	0.61	0.62
3.8	0.91	0.90	0.56	0.60
4.0	0.90	0.90	0.53	0.58
4.2	0.89	0.89	0.52	0.57
4.4 to 4.8	0.89	0.89	0.51	0.56
5 and more	0.88	0.88	0.50	0.55

[a]All these values have been obtained from the curves provided by Reese et al. (1974).

Next, locate point m making use of the values of y_m and p_m from Equations (9–64) and (9–63), respectively. Plot the parabolic curve between points k and m. Subsequently, locate point u from the values of y_u and p_u obtained from Equations (9–66) and (9–65), respectively, and connect points m and u with a straight line.

Step 6. Repeat the above procedure for various depths to obtain p-y curves at each depth below ground surface.

The parameters p_{cr} and p_{cd} mentioned in Step 3 may also be obtained directly from the following expressions:

$$p_{cr} = yx\left[\frac{K_o x\tan\phi\sin\beta}{\tan(\beta-\phi)\cos\alpha}+\frac{\tan\beta}{\tan(\beta-\phi)}(B+x\tan\beta\tan\alpha)\right.$$
$$\left.+K_o x\tan\beta(\tan\phi\sin\beta-\tan\alpha)-K_A B\right] \tag{9–72}$$

$$p_{cd} = K_A B\gamma x\left(\tan^8\beta-1\right)+K_o B\gamma x\tan\phi\tan^4\beta \tag{9–73}$$

where all the parameters are as before and B is the pile width.

With the p-y curve established as outlined in the preceding section, the calculation

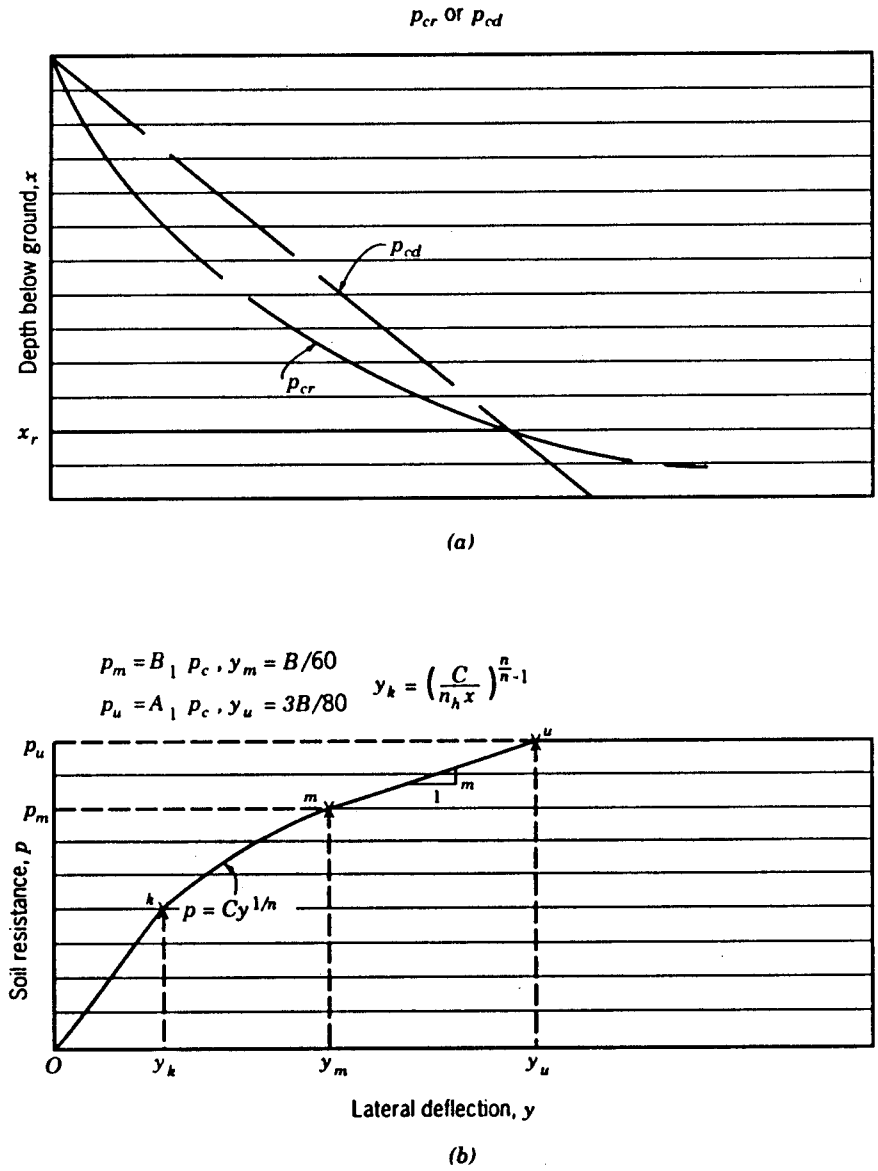

Figure 9–37 Obtaining the value of x_r, and establishing p-y curve; (a) obtaining the value of x_r, at the intersection of p_{cr} and p_{cd}; (b) establishing the p-y curve.

of deflection and moment beyond the elastic range may be carried out in the following sequence:

1. Establish the p-y curve using the foregoing procedure.
2. Determine the parameter n_h (constant of horizontal subgrade reaction), and calculate $T = (EI/n_h)^{1/5}$. Determine the deflection along the pile length for the given lateral load and moment. The T value calculated in this step will be the first trial value referred as $(T)_{trial}$ in the steps to follow.

3. For the deflections determined in step 2, obtain the corresponding pressure from the p-y curve established in step 1. Then, calculate the soil modulus $k = (p/y)$, where p is the soil reaction and y is the pile deflection. This will yield the first trial value for k, which is then plotted with depth.
4. From the value of k obtained in step 3, calculate new $n_h = (k/x)$ where x is the depth below ground. Then compute $T = (EI/n_h)^{1/5}$ and compare this value with $(T)_{trial}$ obtained in step 2. If these values do not match reasonably, proceed with a second trial.
5. With an assumed value of T closer to the value obtained from step 4, repeat steps 2, 3, and 4 to obtain a new T.
6. Plot the latest T value on the ordinate and the $(T)_{trial}$ on the abscissa and join the points. Draw a line at 45° from the origin. The intersection of this line with the trial line will give the actual T.
7. With the finally obtained T, calculate deflections y, soil reactions p, and moments M along the pile length using the subgrade reaction approach.

Interestingly, this procedure applies to a single pile. Similar methods are available for a pile in cohesive soil (Prakash and Sharma, 1990).

9.12 STRUCTURAL CAPACITY OF PILES SUBJECTED TO AXIAL LOAD AND BENDING

General Procedure

The structural capacity of a pile is influenced by both the bending moment and the axial load. An axial load-moment interaction diagram is usually produced as an envelope of several combinations of moment and axial load that could cause structural failure in the piles (see also previous sections). The problem is essentially similar to the analysis of columns subjected to moment and axial load, and thus the derivation of a computation method involves relationships based on strain compatibility and mechanics.

Normalized load-moment interaction diagrams for various pile types are shown in Figures 9–38 through 9–42. The factored axial load $\Sigma\gamma_i P_i$ has been normalized by dividing by the factored nominal axial capacity $\phi_a P_n$. The factored bending moment $\gamma_m M$ has likewise been normalized by dividing by the factored nominal capacity $\phi_m M_n$. As in previous presentations, the γ factors take into account uncertainties and variations in the loads and moments, whereas the ϕ factors reflect the uncertainties in the structural capacity.

The steps involved in checking the structural adequacy of piles by reference to the normalized load-moment interaction curves are summarized as follows:

1. Determine the axial load per pile and calculate the combined axial load effect $\Sigma\gamma_i P_i$.
2. Calculate the nominal structural capacity P_n of the pile (direct methods are presented in the following sections).
3. Select the performance factor ϕ_a from Table 9–13, and calculate the product $\phi_a P_n$.
4. Compute the factored design moment $\gamma_m M$.

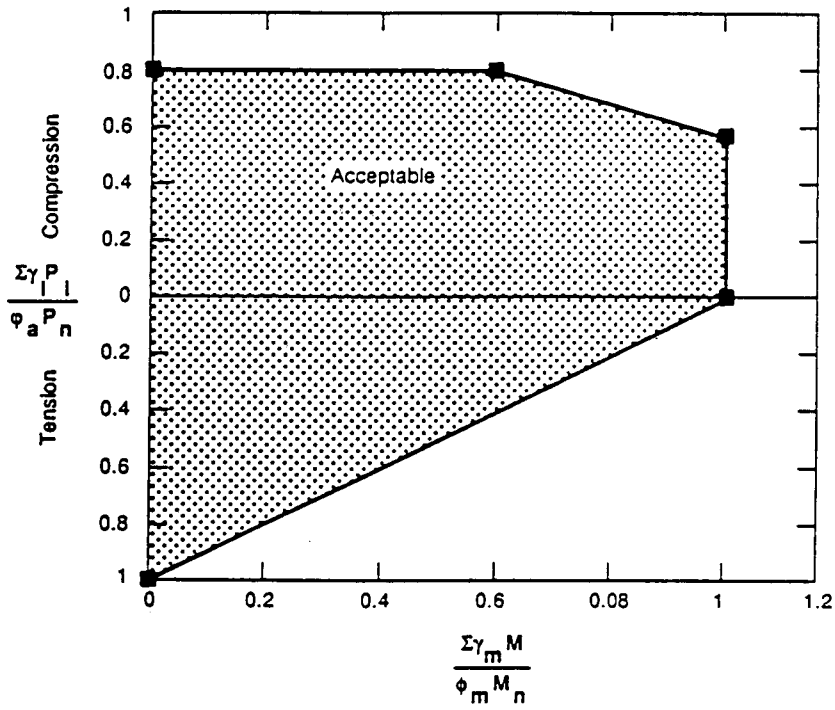

Figure 9–38 Normalized load-moment interaction curve for prestressed concrete piles.

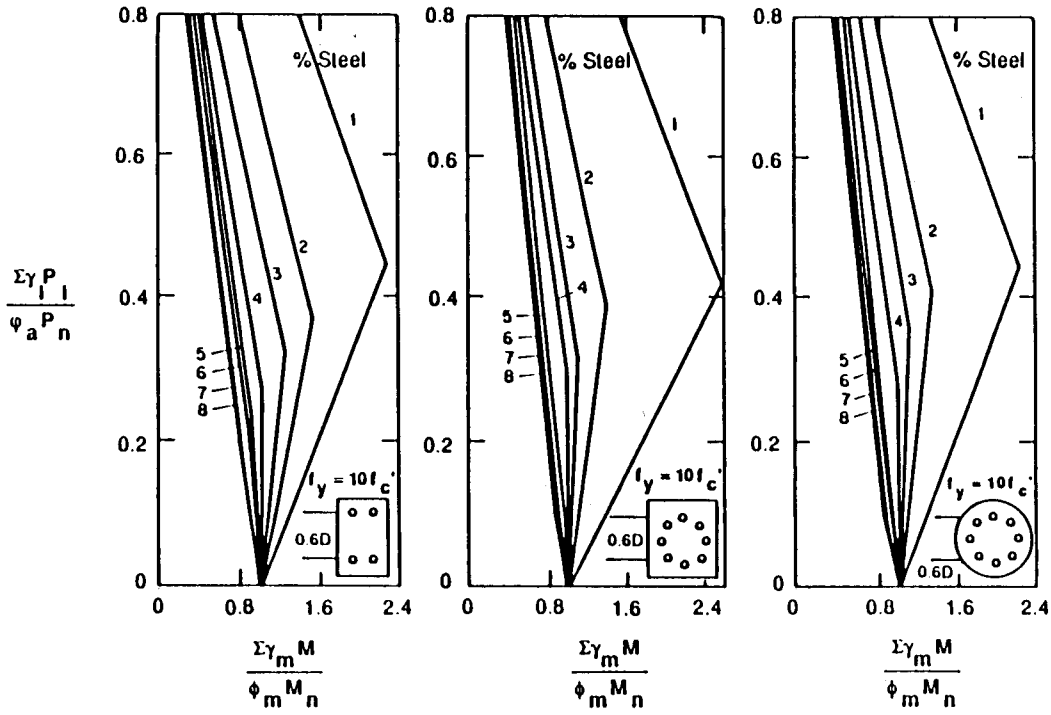

Figure 9–39 Normalized load-moment interaction curves for precast concrete piles.

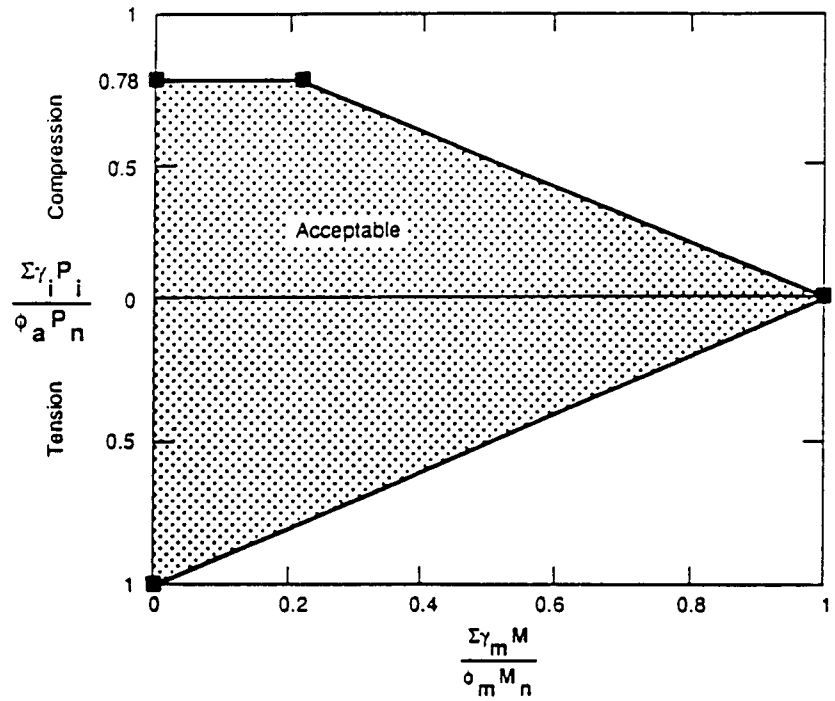

Figure 9–40 Normalized load-moment interaction curve for steel H-piles.

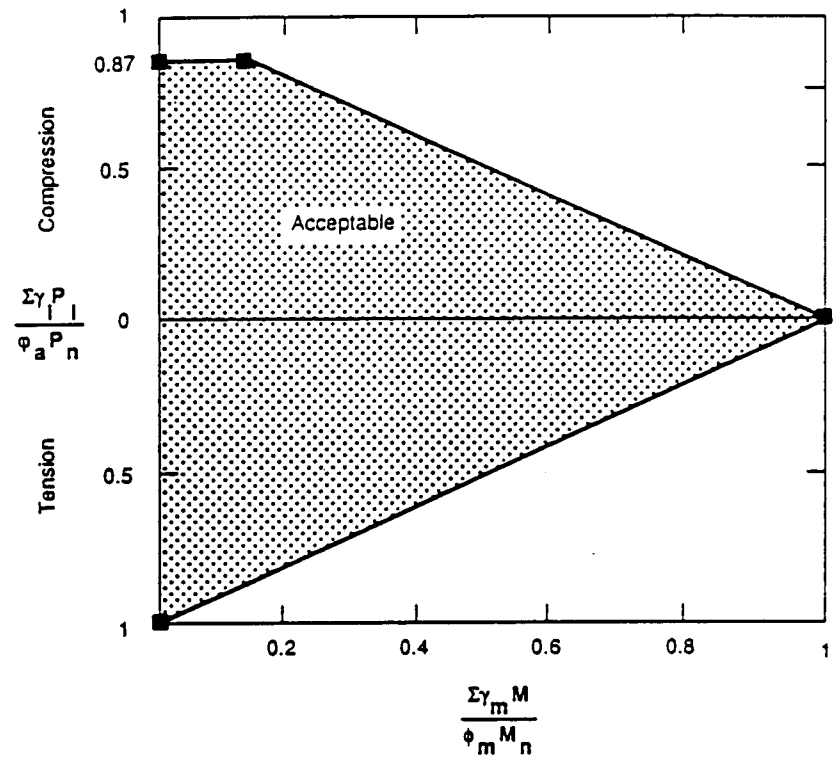

Figure 9–41 Normalized load-moment interaction curve for steel pipe piles.

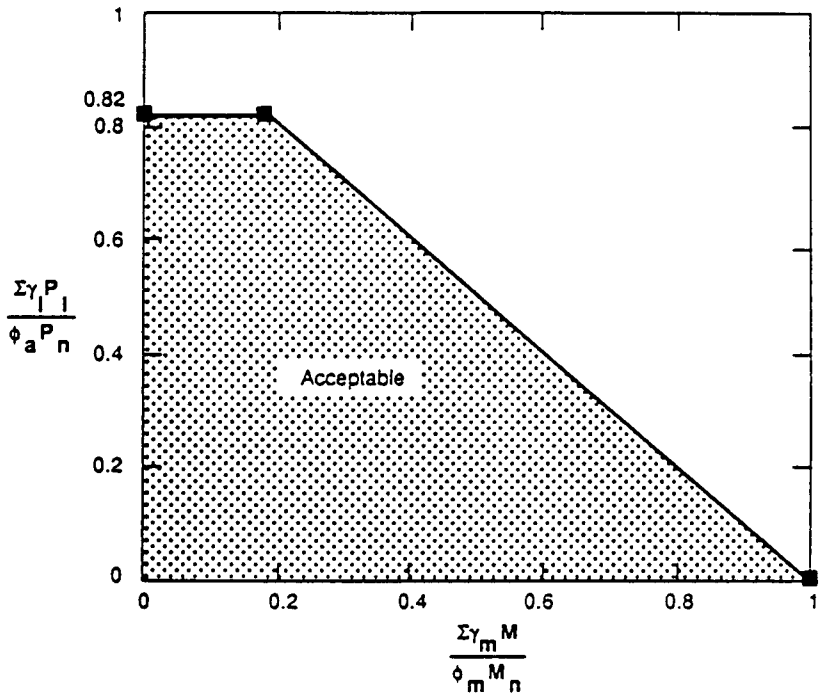

Figure 9–42 Normalized load-moment interaction curve for timber piles.

5. Estimate the nominal structural moment capacity M_n (direct procedures are presented in the following sections).
6. Select the performance factor ϕ_m from Table 9–14, and calculate $\phi_m M_n$.
7. Obtain the ratios $\Sigma\gamma_i P_i/\phi_a P_n$ and $\Sigma\gamma_m M/\phi_m M_n$, and use these data as ordinates to locate a point on the normalized load-moment interaction diagram. If the point thus located falls on or close to the interaction curve and inside the area enveloped by the interaction diagram and the two axes, the pile selected has sufficient structural capacity. If the point falls outside, a larger pile section should be considered

Table 9–13 Summary of Performance Factors for the Nominal Axial Structural Capacity of Piles

Pile Type	Performance Factor, ϕ_a
Prestressed Concrete Piles	0.75 for spiral columns 0.70 for tied columns
Precast Concrete Piles	0.75 for spiral columns 0.70 for tied columns
Steel H-Piles	0.85
Steel Pipe Piles	0.85
Timber Piles	1.20*

*Davisson et al. (1983) stated that the minimum factor of safety for the structural capacity of piles in axial compression is 1.25. The performance factor is greater than unity because the average load factor for vertical loads (dead and live loads) is greater than the factor of safety.

Table 9–14 Summary of Performance Factors for the Nominal Moment Capacity of Piles

Pile Type	Performance Factor, ϕ_m
Prestressed Concrete Piles	0.9
Precast Concrete Piles	0.9
Steel H-Piles	0.9
Steel Pipe Piles	0.9
Timber Piles	0.9*

*Davisson et al. (1983) stated that the minimum factor of safety for bending in timber piles is 1.40. The performance factor is obtained by dividing the load factor for lateral loads (= 1.3) by the factor of safety (= 1.4).

and the steps repeated until convergence is obtained. Similarly, if the point is inside the safe zone but far away from the interaction curve, it may indicate excess capacity, and in this case the process may be repeated using a smaller pile section.

Procedure for Estimating Axial and Moment Capacity

Axial compression. Section 9.6 gives a summary of the structural capacity P_n of various pile types under axial compression in terms of relevant material strengths. These cover prestressed concrete piles, steel piles, precast concrete piles, timber piles, and steel pipe piles.

Nominal moment capacity. The nominal moment capacity M_n normally varies depending on the section geometry and pile strength.

Prestressed Concrete Piles. The nominal moment capacity M_n depends on the section configuration, the concrete compressive strength, and the level of prestress. For pile lengths between 40 and 140 feet, the tendons are typically stressed between 700 and 1200 lb/in^2. Typical concrete compressive strength is in the range of 5000 and 8000 lb/in^2. The *PCI Design Handbook* (1985) gives expressions for the ultimate moment capacity based on an assumed prestressed level and concrete strength. Relevant data are tabulated in Table 9–15. A comparison of pile types in Table 9–16 shows that the maxi-

Table 9–15 Expressions for the Nominal Moment Capacity, M_n, of Piles in the Absence of Axial Loads

	M_n
Prestressed Concrete (after PCI Design Handbook, 1985)	$0.37DA_{ps}f_{pu}$—solid square piles $0.32DA_{ps}f_{pu}$—solid circular and octagonal piles $0.38DA_{ps}f_{pu}$—hollow square piles $0.34DA_{ps}f_{pu}$—hollow circular and octagonal piles
Precast Concrete	See Table A2–5 (PCI Design Handbook, 1985)
Steel H-Piles	$f_y z_p$
Steel Pipe Piles	$f_y z_p$
Timber Piles	$k_b s_b z_e$

Table 9–16 Maximum Difference between Calculated Moment Capacity and Value Provided by Manufacturer

	Calculated using PCI Equation in Table A2–4 with $\phi_m = 0.9$ (kip-ft)	From Santa Fe Pomeroy Charts (kip-ft)	% Difference
10 in square	34	29	17
12 in square	62	55	13
14 in square	96	87	10
16 in square	147	142	4
18 in square	206	198	4

mum difference between the ultimate moment capacity given by PCI and a pile manufacturer (Santa Fe Pomeroy) does not exceed about 20 percent for the section shown.

The prestressing tendons in this case consist of Grade 270 steel with a diameter of 7/16 inch or 1/2 inch (nominal area 0.115 in^2 and 0.153 in^2, respectively).

Precast Concrete Piles. The nominal moment capacity is a function of the shape of the cross section, the percentage of steel and its layout, the concrete compressive strength, and the pile dimensions. No general expression is available. For the usual

Table 9–17 Nominal Moment Capacity, [Mn], for Precast Concrete Piles.

Ratio of Area of Steel to Gross Cross-Sectional Area	$\frac{M_n}{f_c' D A_g}$		
	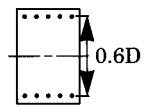	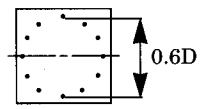	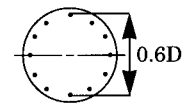
0.01	0.043	0.037	0.037
0.02	0.074	0.074	0.067
0.03	0.106	0.102	0.088
0.04	0.137	0.120	0.107
0.05	0.167	0.139	0.126
0.06	0.194	0.157	0.144
0.07	0.226	0.176	0.161
0.08	0.254	0.193	0.176

Chart applies to any value of f_c' and f_y provided $f_y = 10f_c'$.

f_c' = 28 day concrete cylinder strength
f_y = yield stress of steel
D = pile width or diameter
A_g = gross cross-sectional area of concrete
f_{pu} = ultimate strength of the tendons in prestressed concrete piles
f_y = yield stress of steel
S_b = 5% exclusion value for the modulus of rupture of timber piles (see Table A2–2)
D = pile width or diameter
A_{ps} = nominal area of prestressing tendons
Z_e = elastic section modulus of timber piles
Z_p = plastic section modulus of steel piles
k_b = factor to account for the treatment conditioning of the timber pile and where along the pile the ultimate moment capacity is required

Table 9–18 k_c Factor to Account for the Treatment Condition of Timber Piles when Calculating the Axial Compressive Strength Parallel to Grain

		Treatment Conditioning			
Location	*Pile Length*	*Untreated or Air-Seasoned*	*Kiln Dried*	*Boulton Process*	*Steamed*
Pile Butt	All Lengths	0.534	0.473	0.457	0.396
Pile Tips	≤50ft.	0.473	0.427	0.412	0.366
	>50ft.	0.442	0.396	0.366	0.335

(After Davisson et al., 1983)

steel ratios, the dimensionless ultimate moment capacity for various precast shapes may be taken from Table 9–17, which is applicable if the yield strength of the steel f_y is about ten times the compressive strength of the concrete f'_c.

Steel Piles. The data provided in this section are for H-piles and pipe piles without concrete fill. Open-ended piles are seldom used in bridge foundations. Pipe sections have distinct column characteristics and are advantageous when piles have free-standing portions. If these requirements do not apply, steel H-piles may be chosen because they are cost effective. Sectional properties may be readily found in AISC tables.

The nominal capacity may be estimated as the product of the yield strength of the steel and the plastic section modulus, or $M_n = f_y Z_p$.

Timber Piles. Expressions for the axial capacity are given in section 9.6. The factor k_c may be obtained from Table 9–18, and accounts for the treatment conditioning of the pile.

The nominal moment capacity of wood piles may be calculated as the product of the 5 percent exclusion limit for the modulus of rupture of green small clear wood specimens (S_b) shown in Table 9–19, the elastic section modulus of the pile Z_e, and a treatment conditioning factor k_b obtained from Table 9–20 (Davisson, Manuel, and Armstrong, 1983) or

$$M_n = k_b Z_e S_b \tag{9–74}$$

Table 9–19 5% Exclusion Values for Compression Parallel to Grain and Modulus of Rupture for Timber Piles

		Compression Parallel to Grain (psi) S_c	Modulus of Rupture (psi) S_b
Douglas Fir	Coast	2577	5499
	Interior West	2558	5538
	Interior North	2479	5525
	Interior South	2308	5290
Southern Pine	Loblolly	2504	5328
	Longleaf	3158	6391
	Shortleaf	2599	5515
	Slash	2923	6838

(After Davisson et al., 1983)

Table 9–20 k_b Factor to Account for the Treatment Condition of Timber Piles when Calculating the Nominal Moment Capacity

		Treatment Conditions			
Location	*Pile Length*	*Untreated or Air-Seasoned*	*Kiln Dried*	*Boulton Process*	*Steamed*
Pile Butt	All Lengths	0.490	0.448	0.420	0.364
Pile Tips	≤ 50ft	0.448	0.406	0.378	0.336
	> 50 ft	0.378	0.350	0.322	0.280

(After Davisson et al., 1983)

If the pile diameter exceeds 12 inches, the M_n value obtained from Equation (9–74) should be multiplied by $(12/D)^{1/9}$, where D is the pile diameter in inches.

9.13 DESIGN EXAMPLES

Design Example 9–1

This example presents the design procedure for estimating the buckling load for a partially embedded free standing pile. It involves the following steps.

1. Estimate the value of n_h (for sands) or E_s (for clays) and calculate the values of T (for sands) or R (for clays). These parameters are identified and described in section 9.6. For pile groups the soil modulus should be reduced to reflect the effect of neighboring piles on the group interaction.
2. Calculate the equivalent length of the pile from Equations (9–5) or (9–16) for cohesive and cohesionless soil, respectively.
3. Referring to Figure 9–12, select the appropriate configuration based on the support conditions and end restraint. Calculate the buckling load P_{cr} using one of the four expressions presented in Figure 9–12 for the appropriate boundary conditions.

   When the ideal buckling load has been determined, a safe design load can be obtained for the pile taking into account the effects of end moments and eccentricity of loading as in conventional columns.

Design Example 9–2

An HP 14x89 pile 30 feet long carries a dead load of 42 tons and a live load of 33 tons. Electric cone penetration tests (described in section 9.7) have been carried out and results are shown in Figure 9–43. Based on these data, determine the structural and bearing capacity of the pile.

From appropriate design aids, we obtain the section properties of the pile as follows: depth D = 13.83 inches; flange width b_f = 14.7 inches; cross sectional area A = 26.1 in^2; web and flange thickness $t_w = t_f$ = 0.615 inches.

The structural and geotechnical adequacy of the pile will be analyzed for two con-

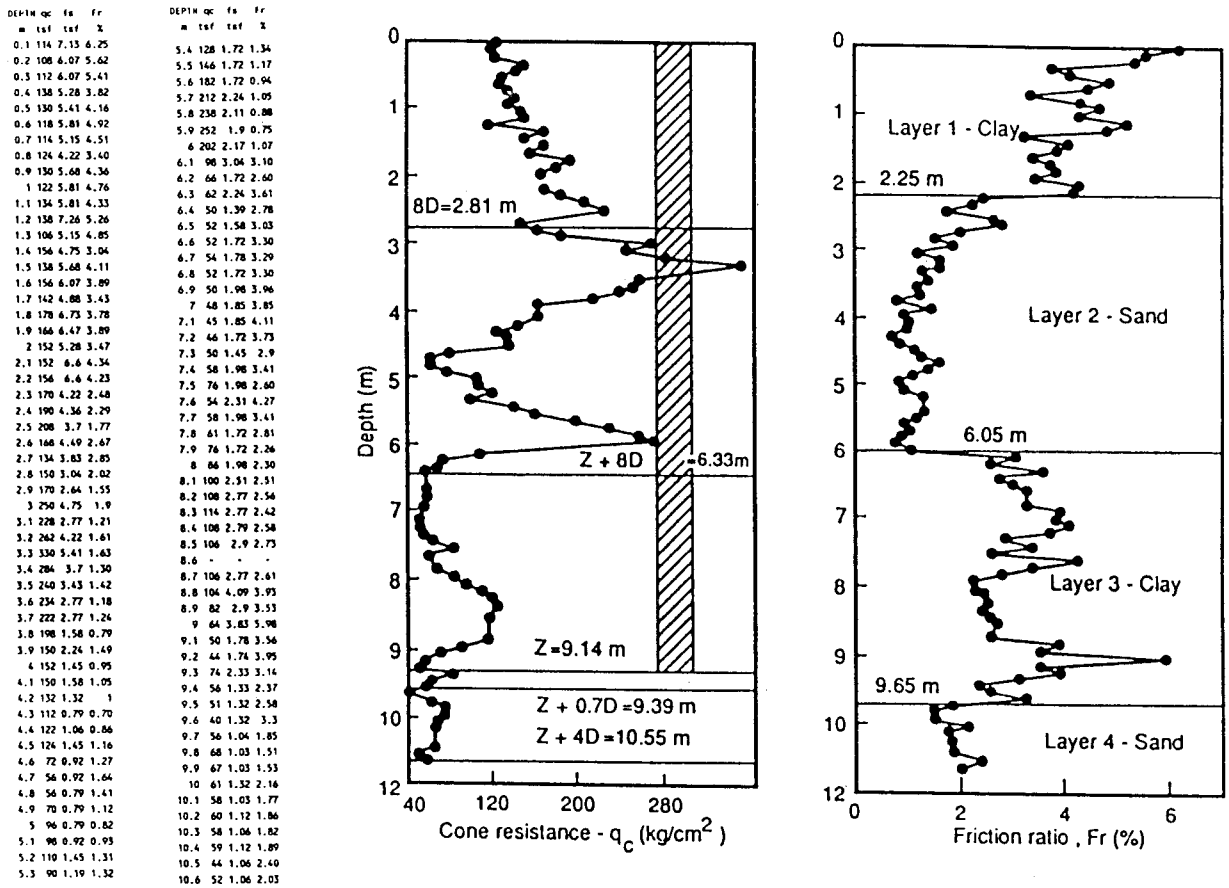

Figure 9–43 Cone penetration test data for Design Example 9.2.

ditions: (1) with the pile assumed plugged; and (2) with the pile assumed unplugged. The condition that yields the minimum capacity will be the basis for design.

Condition 1, pile unplugged. For Group I loading, the factored load is (AASHTO Load Factor)

$$\gamma P_u = 1.3P_D + 2.17P_L = (1.3)(42) + (2.17)(33) = 126 \text{ tons/pile}$$

From section 9.6, the nominal structural capacity P_n, excluding moment effects, is merely $f_y A_y$, or $P_n = (36)(26.1) = 940$ kips = 470 tons/pile. From Table 9–8 the performance factor ϕ_a is 0.85, giving a factored resistance

$$\phi_a P_n = (0.85)(0.78)(470) = 310 \text{ tons} > 126 \text{ tons, OK.}$$

Bearing Capacity. From Figure 9–43, it is evident that the pile will be installed through three different soil layers. The ultimate bearing capacity is therefore obtained as the sum of the skin friction in layer 1 (clay), 2 (sand), and 3(clay), and the tip resistance of the pile.

The tip resistance (end bearing) may be calculated using the minimum path rule mentioned in section 9.7 and shown in Figure 9–19. Values of q_{c1} and q_{c2} are obtained

following the procedure described in that figure. For q_{c1}, the process is tabulated as follows:

y	yD (m)	Z + yD (m)	q_{c1}
0.7	0.25	9.39	[44+2(74)+44]/4 = 59 tsf
1.0	0.35	9.49	[44+74+3(56)+44]/6 = 55 tsf
1.5	0.53	9.67	[44+74+56+51+6(40)]/10 = 46.5 tsf
2.0	0.70	9.84	[44+74+56+51+40+56+2(68)+56+5(40)]/14 = 50.9 tsf
2.5	0.88	10.02	[44+74+56+51+40+56+68+67+4(61)+56+5(40)]/18 = 53.1 tsf
3.0	1.05	10.19	[44+74+56+51+40+56+68+67+61+5(58)+56+5(40)]/20 = 53.2 tsf
3.5	1.23	10.37	[44+74+56+51+40+56+68+67+61+58+60+7(58)+56+5(40)]/24 = 54 tsf
4.0	1.41	10.55	[44+74+56+51+40+56+68+67+61+58+60+58+59+10(44)+5(40)]/28 = 49.7 tsf

The value of q_{c2} is taken as 40 tons/ft^2 because there is no value of q_c, for a diameter above the tip, which is less than the value of 40 tons/ft^2 at yD = 0.53 m below the pile tip. The value of q_p is the average of q_{c1} and q_{c2}, or q_p = (46.5 + 40)/2 = 43.3 tons/ft^2. For a pile assumed to be unplugged, the point resistance is provided by the cross-sectional area of the section, or $Q_p = q_p A_p$ = (43.3)(26.1)/144 = 7.9 tons.

Likewise, the ultimate skin resistance is obtained from Equation (9–40) for the *CPT* method. For an unplugged pile, the soil adheres to the entire perimeter of the H section. Accordingly,

Pile perimeter a_s = 2(14.7 + 13.83 + 14.7 – 0.615)/12 = 7.1 feet

• At Layer 1: L_f = depth to the point under consideration = 2.25 m = 7.4 feet. Also 8D = (8)(13.83)/12 = 9.2 feet, and $L_f/8D$ = 7.4/9.2 = 0.8. For the depth range from 0 to 2.25 meters (7.4 ft) the average f_s is 5.8 tons/ft^2 (from Figure 9–43). From Figure 9–20, the shaft friction correction factor K_c for piles in clay is 0.2. Hence Q_{s1} = (0.8)(0.2)(7.1)(7.4)(5.8) = 48.6 tons.

• At Layer 2: Initially, a depth of embedment correction must be made between the top of this layer (2.25 m or 7.4 ft) and depth of 8D (2.8 m or 9.2 ft).

At 7.4 feet, $L_f/8D$ = 7.38/9.22 = 0.8
At 9.2 feet, $L_f/8D$ = 1.0
Hence, $(L_f/8D)_{ave}$ = (0.8 + 1.0)/2 = 0.9

The pile penetration-to-diameter ratio is computed as follows:

$$Z/D = (30)(12)/13.83 = 26.0$$

From Figure 9–20, the shaft friction correction factor for piles in sand is K_s = 0.7. For the depth range from 2.25 meters (7.4 ft) to 2.8 meters (9.2 ft), the average f_s is 3.94 tons/ft^2. Hence,

$$Q_{s2a} = (0.9)(0.7)(7.1)(9.2 - 7.4)(3.94) = 32.4 \text{ tons}$$

For the depth range from 2.8 meters (9.2 ft) to 6.05 meters (19.85 ft), the average f_s is 2.04 tons/ft^2. Hence,

$$Q_{s2b} = (0.7)(7.1)(19.85 - 9.20)(2.04) = 108 \text{ tons}$$

• At Layer 3: For the depth range from 6.05 meters (19.85 ft) to 9.14 meters (30 ft), the average f_s is 2.23 tons/ft^2. From Figure 9–20, K_c = 0.2. Hence,

$$Q_{s3} = (0.2)(7.1)(30 - 19.85)(2.23) = 32.1 \text{ tons}$$

The total skin friction is now

$$Q_s = 48.6 + 32.4 + 108.0 + 32.1 = 221 \text{ tons}$$

For the *CPT* method the resistance factor is obtained from Table 9–5 as $\phi = 0.55$. Hence the factored resistance is the geotechnical capacity (7.9 + 221) multiplied by 0.55. Or,

$\phi Q_{ult} = (0.55)(229) = 126$ tons, the same as the required capacity, OK.

Condition 2, pile plugged. The tip resistance of a plugged pile is computed using the cross-sectional area of a rectangle with dimensions 13.83 inches × 14.7 inches, or

$$Q_p = (43.3)(13.83)(14.7)/144 = 61.1 \text{ tons}$$

Likewise, the ultimate skin friction is obtained as the sum of the adhesion at the flanges and the full soil-to-soil shear resistance along both sides of the soil plug.

Pile perimeter for flange adhesion = 2(14.7)/12 = 2.45 feet
Pile perimeter for soil shear resistance = 2(13.83)/12 = 2.31 feet.

• At Layer 1: Assume that the soil-to-soil shear resistance is 1.5 times the adhesion. Hence,

$$Q_{s1} = (0.8)(0.2)(2.45 + 1.5 \times 2.31)(7.38)(5.8) = 40.5 \text{ tons}$$

• At Layer 2: Assume that the soil-to-soil shear resistance is 1.5 times the soil-to-pile friction in sand.

For the depth range from 2.25 meters (7.4 ft) to 2.81 meters (9.22 ft),

$$Q_{s2a} = (0.9)(0.7)(2.45 + 1.5 \times 2.31)\,(9.22 - 7.38)(3.94) = 27.0 \text{ tons}$$

For the depth range from 2.81 meters (9.22 ft) to 6.05 meters (19.85 ft),

$$Q_{s2b} = (0.7)(2.45 + 1.5 \times 2.31)(19.85 - 9.22)(2.04) = 89.8 \text{ tons}$$

• At Layer 3: Assume that the soil-to-soil shear resistance is 1.5 times the adhesion.

For the depth range from 6.05 meters (19.85 ft) to 9.14 meters (30 ft),

$$Q_{s3} = (0.2)(2.45 + 1.5 \times 2.31)(30 - 19.85)(2.23) = 26.7 \text{ tons}$$

Total skin friction Q_s = 40.5 + 27.0 + 89.8 + 26.7 = 184 tons, or total ultimate pile capacity Q_{ult} = 184 + 61 = 245 tons > 229, OK.

Hence, the unplugged condition controls the design, with an estimated capacity of 229 tons.

Design Example 9–3

Figure 9–44 shows plan, cross section, and soil data for a shaft footing. The loads from the superstructure include 55 kips dead load, and 48 kips live load. Determine the adequacy of the foundation.

Loads acting on piles. Additional loads to be resisted are the weight of the pile cap and the weight of soil above the pile cap.

Weight of pile cap	$= (4)(7)(7)(150)/1000$	$= 29.4$ kips
Weight of soil	$= 6(7 \times 7 - 4 \times 2)(120)/1000$	$= 29.5$ kips
Total dead load	$= 55 + 29.4 + 29.5$	$= 114$ kips

The required capacity is, therefore,

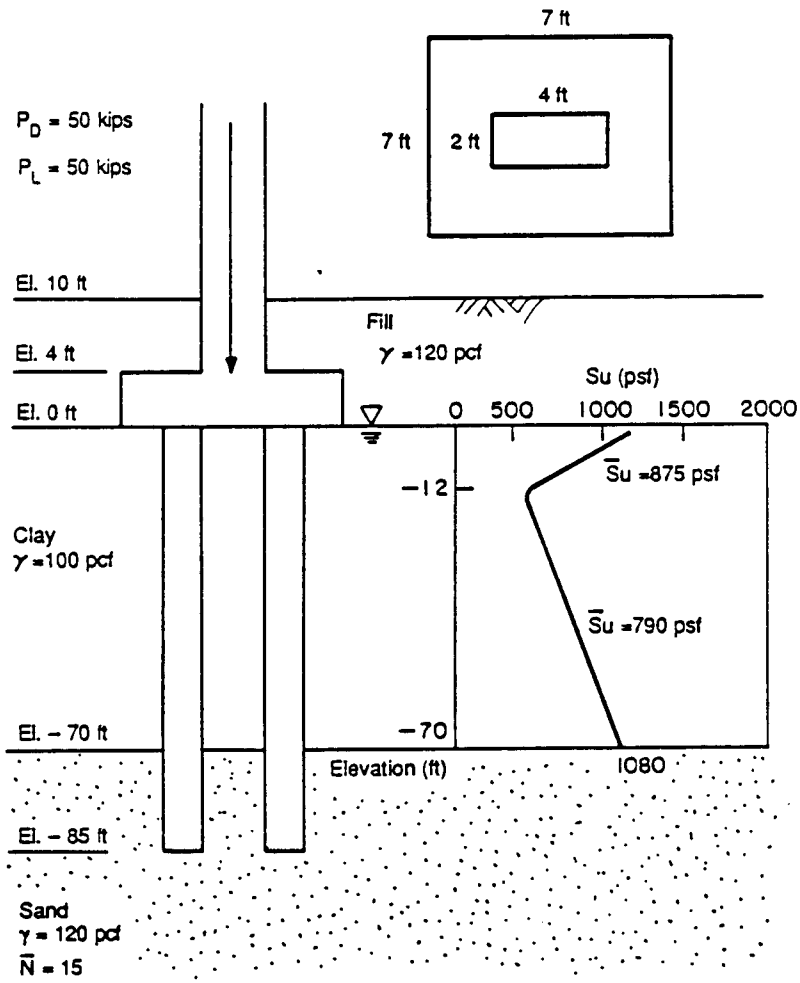

Figure 9–44 Figure for Design Example 9.3.

$$P_u = 1.3P_D + 2.17P_L = (1.3)(114) + (2.17)(48) = 252 \text{ kips}$$

For a first trial we select 12 inches × 12 inches prestressed concrete piles, with f'_c = 5000 lb/in^2 and six 7/16-inch grade 270 strand. The piles have an initial prestress of 700 lb/in^2 to inhibit cracking and structural damage during handling.

Axial capacity of single pile. This involves structural capacity and geotechnical strength.

Structural Capacity. From section 9.6, the structural capacity is

$$P_n = (0.85f'_c - 0.6f_{pre})A_c = (0.85 \times 5 - 0.6 \times 0.7)(144) = 552 \text{ kips/pile.}$$

From Table 9–8, the performance factor is $\phi_a = 0.70$, and the eccentricity factor is r = 0.80. Hence, the factored resistance is

$$\phi_a r P_n = (0.70)(0.80)(552) = 309 \text{ kips}$$

or, one pile is sufficient to carry the entire load of 252 kips.

Bearing Capacity. Referring to Figure 9–44, from elevation 0 to −12 feet, s_u = 0.875 kips/ft^2, and α = 0.8. From elevation −12 to −70 feet, s_u = 0.79 kips/ft^2, and α = 0.83. Assuming that the pile penetrates into the lower sand layer, the ultimate bearing capacity consists of skin friction and tip resistance.

The skin friction of the pile section in the clay is calculated from Equation (9–22), or

$$Q_s = (0.8)(0.875)(12)(4) + (0.83)(0.79)(58)(4) = 34 + 152 = 186 \text{ kips}$$

The skin friction for the pile section in sand is computed noting that from elevation −70 to −85 feet, N = 15. Then, from Equation (9–38)

$$Q_s = \frac{15}{50}(4)(15) = 18 \text{ tons} = 36 \text{ kips}$$

The tip resistance of pile in sand is computed from Equations (9–34) through (9–36). Note that at the pile tip $\sigma'_v = 70(100 - 62.4) + 15(120 - 62.4) = 3500$ lb/ft^2 = 1.75 tons/ft^2. From Equation (9–35) we obtain

$$N_{corr} = [0.77 \log_{10}(20/1.75)](15) = (0.815)(15) = 12$$

Since the pile penetrates 15 feet into the sand layer, we use $q_p = q_1$ where q_1 is estimated from Equation (9–36). Hence, Q_p = (48)(1) = 48 tons = 96 kips. From Table 9–5 the performance factor for the α method is 0.70. Likewise the performance factor for the *SPT* method is 0.45. Hence,

$$\phi_q Q_{ult} = (0.70)(186) + (0.45)(36 + 96) = 130 + 59 = 189 \text{ kips}$$

Number of piles required = 252/189 = 2 piles. However, use 4 piles minimum.

Capacity of pile groups. Because the pile group is in sand, its capacity is the number of piles times the factored capacity of a single pile, or 4 × 196 = 784 kips, OK.

Estimation of settlement. In the absence of more precise data, we assume that the tolerable settlement is 1½ inches. The expected settlement is computed as suggested by Meyerhof (1976), discussed in section 9.5, by making use of Equation (9–7).

We compute $X = Y = 3 + 1 = 4$ feet

$$I = 1 - (10)/(8)(4) = 0.688$$

$$P_D + P_L = 114 + 48 = 162 \text{ kips}$$

$$q = 162/4^2 = 10.12 \text{ kips/ft}^2 = 5.06 \text{ tons/ft}^2$$

The settlement is, therefore,

$$p = (2)(5.06)\sqrt{4}(0.688)/12 = 1.16 \text{ in} < 1.50 \text{ in, OK.}$$

Effect of downdrag. Because the piles are driven in soft-to-medium clay overlain by a fill layer and have their tips on a dense stratum, downdrag forces may develop and should be checked. Whereas downdrag loads are unlikely to cause capacity problems, they may increase the settlement. The problem may be analyzed as discussed in section 9.10, with the neutral plane determined as shown in Figure 9–24.

Calculation of the location of the neutral plane for this example shows that the neutral plane occurs at a depth of approximately 54 feet. The load due to downdrag at the neutral plane is computed as 172 kips/pile or 688 kips for the pile group, or much greater than the working load of 162 kips used in the settlement analysis. Thus, the settlement due to downdrag will exceed the tolerable, and the foundation is not adequate. Therefore, the foundation should be redesigned using more piles or longer piles.

Design Example 9–4

Figure 9–45 shows the foundation for a pier shaft along with relevant soil data and the loads from the superstructure. The structure is subjected to a lateral force of 40 kips associated with stream flow. Check the lateral deflection of the pile group and the structural adequacy of the system. Use the procedure developed by Evans and Duncan (1982) and expressed in Equations (9–56) and (9–57).

Lateral deflection. This involves the deflection of a single pile and the displacement of a group of piles.

Single Pile Deflection. The lateral load per pile is 40/4 = 10 kips. Referring to section 9.11, $Y_{sf}P_{sf} = 1 \times 10 = 10$ kips/pile for $Y_{sf} = 1$. Next, we compute the section properties of the pile, namely $E_p = 4300$ kips/in^2, $D = 12$ inches, $I_p = 1728$ in^4; $I_{SOLID} = \pi(12)^4/64 = 1018$ in^4, $R_I = 1728/1018 = 1.7$. The characteristic load P_c is calculated from Equation (9–54), or

$$P_c = \frac{(7.34)(12)^2(4300)(1.7)}{\left[144(4300)/(1.7)\right]^{0.688}} = 595 \text{ kips.}$$

Also $Y_{sf}P_{sf}/P_c = 10/595 = 0.017$ for $Y_{sf} = 1$ (unfactored). From Figure 9–28,

$$Y_{sp}/D = 0.008, \text{ or } Y_{sp} = 0.008 \times 12 = 0.1 \text{ inch}$$

Pile Group Deflection. In the absence of more specific data, the tolerable lateral deflection is assumed as 0.5 inch. From Equation (9–50),

$$P_n = s_u D^2 = (1)(12)^2/144 = 1 \text{ kip}$$

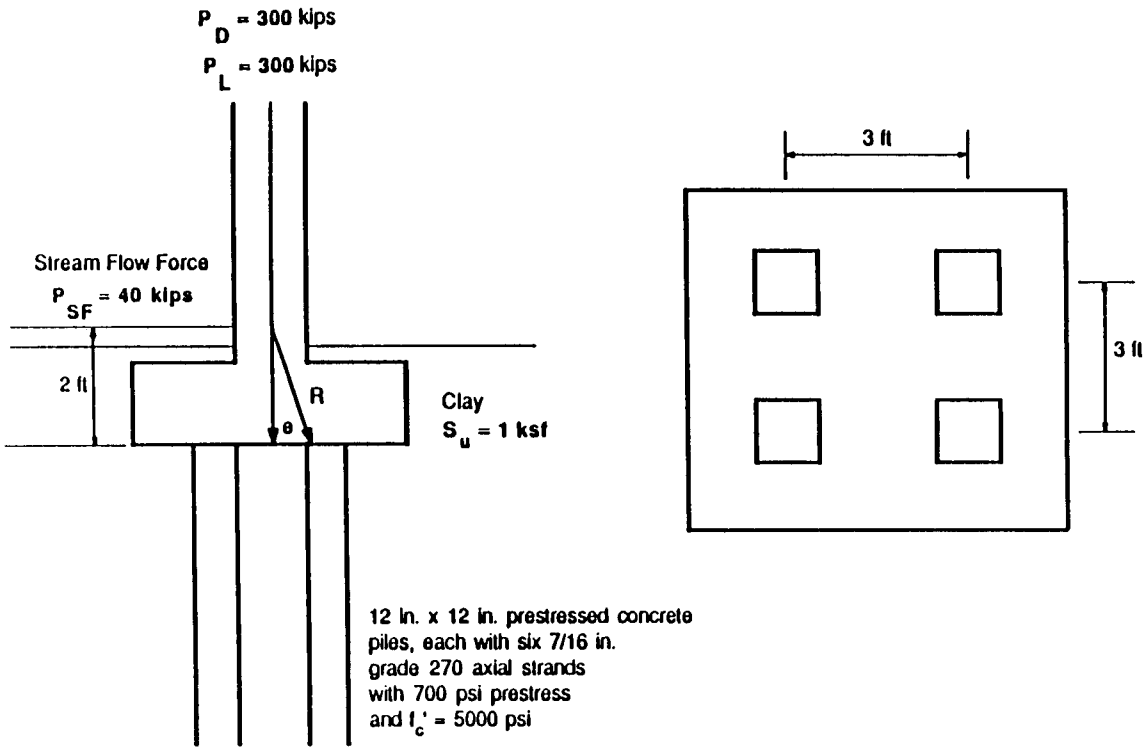

Figure 9–45 Figure for Design Example 9.4.

The group lateral deflection corresponding to a lateral load per pile of 10 kips is computed from Equation (9–56), or

$$Y_g = \left[\frac{16+4}{(5.5)\sqrt{\frac{36}{12}+\frac{10}{3x1}}}\right]^{(0.1)} = (1.445)(0.1) = 0.14 \text{ in} < 0.5 \text{ in, OK}$$

Structural capacity. The design bending moment M_{sp} for a single pile is computed as follows: Referring to Figure 9–35,

$$M_{sp}/M_c = 0.0048 \quad \text{for} \quad P_{sp}/P_c = 0.017.$$

The characteristic moment M_c is now obtained from Equation (9–58)

$$M_c = \frac{(3.86)(12)^3(4300)(1.7)}{[144(4300)/(1.7)]^{0.46}} = 82{,}760 \text{ in-kips}$$

$$\text{and } M_{sp} = (0.0048)(82{,}760) = 397 \text{ in-kips}$$

The design bending moment for the pile group is computed as follows:
From Equation (9–60), $Y_g/Y_{sp} = 0.14/0.10 = 1.4$. Also $Y_{sf}P_{sf} = (1.3)(10) = 13$ kips/pile for $Y_{sf} = 1.3$. From Equation (9–61),

$$n = (13)/(150)(1) + 0.25 = 0.337$$

$$M_g = (1.4)^{0.337}(397) = (1.13)(397) = 449 \text{ in-kips/pile.}$$

Next, the structural adequacy of the piles is checked for direct load and the effect of eccentricity. Group I AASHTO load includes dead load, live load and stream flow pressure, or

$$P_u = \gamma_D P_D + \gamma_L P_L = (1.3)(300) + (2.17)(300) = 1041 \text{ kips}$$

Likewise $\gamma_{sf} P_{sf} = (1.3)(40) = 52$ kips.

Referring to Figure 9–45, the eccentricity e at the base of the footing is

$$e = (52)(2)/1041 = 0.1 \text{ foot}$$

Also $$\Sigma x^2 = (4)(1.5)^2 = 9 \text{ ft}^2.$$

The load on the most heavily loaded pile is, therefore

$$P_{x,y} = (1041)[(1/4) + (0.1)(1.5)/9] = 260.3 + 17.4 = 278 \text{ kips/pile.}$$

The structural capacity (axial compression) is obtained from section 9.6, as

$$P_n = \left(0.85f_c' - 0.6f_{pre}\right)A_c = \left[(0.85)(5) - (0.6)(0.7)\right](144) = 552 \text{ kips/pile}$$

From Table 9–13, $\phi_a = 0.70$, or $\phi_a P_n = 552 \times 0.70 = 386$ kips/pile
Also, $P_{x,y}/Q_a P_n = 278/386 = 0.72$, and $\gamma_m M = 1 \times 449 = 449$ in-kips
Nominal area of 7/16 inch tendons $A_{ps} = 0.115$ in^2. From Table 9–15

$$M_n = 0.37 D A_{ps} f_{pu}, \text{ or}$$

$$M_n = (0.37)(12)(6)(0.115)(270) = 827 \text{ in-kips/pile}$$

For $$\phi_m = 0.9, \ \phi_m M_n = (0.9)(827) = 744 \text{ in-kips/pile,}$$

and $$\frac{\gamma_m M}{\phi_m M_n} = \frac{449}{744} = 0.60$$

The point (0.60, 0.72) plots inside the interaction diagram of Figure 9–39, and hence the structural capacity is adequate.

9.14 BRIDGE FOUNDATIONS WITHOUT PILES

The settlement considerations discussed in the foregoing sections may be addressed in two ways: (a) by designing foundations that can ensure that the actual settlement will be within tolerable or acceptable values; or (b) by designing bridges that can accommodate relatively large settlements but without exceeding the functional and operational limits of the structure.

Incompletely rigid substructure elements may be overstressed and cracked if they are not strong enough to equalize the settlement by bridging the crater, thus increasing

the pressure along its periphery and, at the same time, are not flexible enough to adjust to the settlement profile. From a simple bending analysis it can be shown that a flexible footing or foundation mat can be successfully used where a heavy reinforced concrete element has failed, suggesting that foundations with flexible bottom can undergo considerable differential settlements without failing.

Conversely, certain types of bridges can undergo considerable settlement without damage, and examples are statically determinate structures. Two extreme cases may be mentioned. A simply supported steel truss bridge was jacked up to keep it at the original profile while the masonry abutments and the approach fills were built up to accommodate foundation settlements approaching 19 ft. The soil profile in this case consists of three distinct layers. Layer 1 is mud, layer 2 is clay, and layer 3 is fine sand with many hollow shells, the disintegration of which accounted for much of the settlement.

The second example that may indicate the amount of settlement that can be sustained without damage by a statically determinate structure involves a three-hinged arch structure. This bridge was kept in service although it settled about 6.5 feet, with 5-foot differential settlement at the abutments. The foundation had been designed on the basis of a satisfactory driving record of individual piles but without tests to document the load transfer. Driving sheet piles on the river side was expected to arrest the settlement problem but did not slow down the rate of the continuously measured settlements. This provided a further indication that the vertical displacement was essentially the result of consolidation of the underlying soil layers, and was unrelated to lateral and upward flow. When part of the approach fill was removed and replaced by a light trestle, the rate of settlement was decreased appreciably. A statically indeterminate structure, such as a two-hinged arch or a rigid frame, would have failed inevitably at a fraction of the differential settlement that the three-hinged arch bridge was able to tolerate.

Bridge designs to accommodate settlement. The foregoing principles are reflected in the design policy introduced by Karasopoulos (1984) for the Maine DOT. Several bridge projects have been constructed with spread footings resting on relatively soft soils. Traditionally these structures would have been designed with pile foundations driven to bedrock or refusal. The design of these bridges anticipated and provided for settlements as large as 21 inches. The underlying philosophy in this case was that a more cost-effective structure could result by eliminating the cost of pile foundations and by accepting a larger settlement as long as the utility of the bridge was not sacrificed.

Thus, for the last 15 years the Maine DOT has constructed several single-span bridges on low traffic volume roads with foundations that allow for settlement. These structures have shallow abutments placed on riprap-protected slopes. Where stream velocities are low and scour of these slopes is not anticipated, the abutment foundations consist of spread footings. Where scour is predicted, pile foundations are provided. Preset pile lengths are specified to eliminate the cost of splices and cut-offs. In these applications the length of piles is determined mainly to protect the structure from scour effects. Typical settlements of 2 to 4 inches have occurred without detrimental effects on the structure.

The underlying premise is that by allowing some controlled settlement, piles do not have to be driven to refusal. The resulting cost savings have ranged from 5 to 15 percent of the total bridge cost.

The usual practice for multiple-span continuous bridges has been to provide pile foundations where the piles are driven to refusal. In the State of Maine this is usually

achieved with relatively short piles. Exceptions are noted, however, with bridges in marine clays where bearing piles up to 200 ft long may be required. In addition, many of these piles must be designed for downdrag forces (negative skin friction) combined with superstructure loads. The associated costs in this case are documented and may represent one-third of the total bridge cost.

Karasopoulos (1984) also reports that even with this appreciable additional expenditure to ensure a trouble-free structure, in the majority of cases problems have been experienced with abutments that tend to move and rotate backwards or away from the superstructure. Other problems are related to settlement of the roadway approaches that has been appreciable, causing bumps to develop at the junction with the superstructure. An immediate consequence is a reduced rideability level.

Case histories. Karasopoulos (1984) presents two interesting bridge projects constructed on major highways on relatively deep layers of soft soils without pile foundations.

Wells Bridge. This bridge is a single span structure 103 feet long and 42 feet wide, built on a 59° skew. The end supports are reinforced earth retaining walls about 250 feet long constructed parallel to the railroad tracks. Shallow reinforced concrete abutments are placed on top of the fills behind the retaining walls. The overall height of these abutments was kept as shallow as possible to inhibit rotational movement.

The project was built in two phases. In phase 1, the retaining walls and approach fills were constructed. Retaining wall options included metal bin-type walls and reinforced earth systems, with the latter selected because of a lower cost. The immediate approaches to the structure were surcharged for a period of one year before constructing the bridge abutments and the superstructure in phase 2.

Because of the large embankment loading and the presence of the thick compressible clay layer, settlement estimates were made for several locations around the bridge and the approach fill sections. The maximum settlement in the approach fills was computed as 30 inches. At the abutment location within the reinforced earth section, the total settlement was estimated as 25 inches. However, by constructing the retaining walls and surcharging the approach fills for about one year, the settlement analysis showed that one-third of the total settlement should occur before the structure was built.

Alternate bridge types and configurations considered in the analysis included the following structures (1979 dollars):

(a) 3-span structure supported on piles, estimated cost : $ 1,060,000
(b) 3-span structure on spread footing, estimated cost : $ 760,000
(c) 1-span structure on spread footing, estimated cost : $ 910,000

Adverse soil conditions combined with a severe skew (59°) suggested the possibility of major differential settlement between substructure units, with corresponding effects on the superstructure. The single span bridge was selected because of the least number of substructures (2) and the greater compatibility with a settlement problem. Because of the anticipated 21 inches of post-construction settlement of the structure and its immediate approaches, the design incorporated the following features.

1. A vertical, as built, clearance of 24′–6″ to the railroad tracks, so that after settlement no less than 22′–6″ would remain in place.

2. Relatively flexible reinforced earth retaining walls with very shallow concrete abutments that can conform to the pattern of movement without inducing distortion stresses.
3. Bridge bearings designed and installed so that additional shim plates can be inserted in the future to compensate for any undesirable differential settlement between abutments.
4. Rigid end diaphragms that can resist jacking forces in the event the bridge must be jacked up for bearing adjustments.
5. Abutment bridge seats wider than normal (3′–6″ wide) to facilitate jacking equipment for future bearing adjustments.
6. An additional construction joint near the abutment top, placed to facilitate the removal and reconstruction of the bridge joints if necessary.

   Reported (measured) settlement is as follows (as of 1984):

   (a) Embankment settlement of 15 inches as of May 1983, compared with the predicted 16.5 inches for the same period. Theoretically the embankment was expected to settle an additional 12 inches.
   (b) A differential settlement between 4 and 5.5 inches between wall panels. Structurally, the walls appear in satisfactory condition and have absorbed the effects of settlement successfully.
   (c) Measurements to check the separation between adjacent wall panels near the top. These show that essentially no relative lateral movement of the top of the wall panels has occurred.
   (d) A total settlement of 4.5 inches at the west end and 3.5 inches at the east end of the southerly abutment. This differential settlement is mainly due to the imbalance of embankment loading.
   (e) A settlement of 4.6 inches at the east end, and 3.2 inches at the west end of the northerly abutment.

The severe skew combined with the differential settlement at each abutment has caused some shifting at the bridge joints and bearings.

Saco, Interstate 195 Bridge. This project consists of twin structures carrying the Interstate 195 spur over the Maine Turnpike in the City of Saco. Construction of the bridge was completed by the end of 1982. Each bridge has two simple spans, each 118.5 feet long and 38 feet wide on 0° skew.

Adverse soil conditions exist at the site. A top layer 23 feet thick consists of medium dense sandy material. Beneath this layer there is a 135-ft thick marine deposit of very sensitive medium to stiff silty clay. Bedrock is found 170 to 180 feet below the existing ground.

Embankment settlements were anticipated to exceed 5 feet because of the compressibility of the silty clay under the effect of embankment loads, expected to occur over a period of several years. The intent of the design was to limit postconstruction settlements at the structure to about 1 foot. During a 30-year period sand drains were used and the site was surcharged for 17 months.

The substructure elements are built on spread footings with provisions allowing for future settlement of abutments and piers. An alternate scheme consisted of a similar two-span bridge with foundations supported on steel H piles driven to ledge. Pile length varied from 168 to 200 feet. The pile foundations produced an increase of $315,000 in the construction cost.

The 17-month surcharge and sand drain scheme was expected to induce a preconstruction settlement slightly in excess of 4 feet. The actual settlement for the preconstruction period ranged from 3.6 to 3.9 feet.

The settlement analysis indicates that the piers will undergo a settlement ranging from 3.5 to 9.5 inches. The abutments are expected to have a 1-inch short (elastic) settlement and from 1 to 3 inches long term (consolidation) settlement. The abutments are also expected to rotate about 4 inches away from the piers.

Likewise, the design features of the Wells Bridge were incorporated in the Saco project. In addition, steel plates were placed under the pier bearings. These plates may be removed when necessary to eliminate the differential settlement between abutment and adjoining pier. Special expansion devises have been installed at the abutments that can be adjusted as needed following abutment rotation.

Commentary. Both the Wells and the Saco bridges have design features articulated on an experimental basis. Thus far they have performed satisfactorily, although lack of previous experience with this type of work may tend to inhibit conclusions and predictions about their long term performance. It is likely that at some point and time corrective actions will become necessary. However, it is estimated that the cost of these remedies will be much less than the savings achieved in the original construction. Interestingly, under similar conditions, pile-supported substructure units should not be expected to be maintenance-free, and rotational movements may require time consuming and costly repairs.

REFERENCES

AASHTO, 1994: AASHTO LRFD Bridge Design Specifications.

ALIZADEH, M., and M. T. DAVISSON, 1970: "Lateral Load Test on Piles—Arkansas River Project", *ASCE JSMFED,* vol. 96, No. 9, pp. 1583–1604.

BAGUELIN, F., J. F. JEZEQUEL, and D. H. SHIELDS, 1978: *The Pressuremeter and Foundation Engineering*, Trans Tech Publications, Clausthal, p. 617.

BHUSHAN, K., S. C. HALEY, and P. T. FONG, 1979: "Lateral Load Tests on Drilled Piers in Stiff Clays," *J. Geotech. Eng. Div. ASCE,* vol. 105, No. GT8, August, pp. 969–985.

BROWN, D. A., L. C. REESE, and M. W. O'NEILL, 1987: "Cyclic Lateral Loading of a Large-Scale Pile Group," *ASCE Journal of Geot. Div.*, vol, 113, No. 11, Nov., pp. 1326–1343.

Canadian Geotechnical Society, 1985: "Canadian Foundation Engineering Manual," 2nd ed., Bitech Publishers Ltd., p. 460.

DAVISSON, M. T., 1963: "Estimating Buckling Loads for Piles," *Proc. 2nd Pan American Conf. on Soil Mech. and Found. Eng.*, Sao Paulo, vol. 1, pp. 351–371.

DAVISSON, M. T., and H. L. GILL, 1963: "Laterally Loaded Piles in a Layered Soil System," *J. Soil Mech. Found. Div.*, ASCE, vol. 89, No. SM3, pp. 63–94.

DAVISSON, M. T. and K. E. ROBINSON, 1965: "Bending and Buckling of Partially Embedded Piles," *Proc. 6th Intern. Conf. on Soil Mech. and Found. Eng.*, Montreal, Canada, vol. 2, pp. 243–246.

DAVISSON, M. T., F. S. MANUEL, and R. M. ARMSTRONG, 1983: "Allowable Stresses in Piles," FHWA Report No. RD-83/059, p. 191.

DAVISSON, M. T., 1989: "Foundations in Difficult Soils—State of the Practice Deep Foundations—

Driven Piles," *Seminar on Foundations in Difficult Soils,* Metropolitan Section, ASCE, New York, April.

DAVISSON, M. T., 1970: "Lateral Load Capacity of Pile Groups," HRR, no. 333, pp. 104–112.

D'APPOLONIA , D. J. and T. W. LAMBE, 1971: "Performance of Four Foundations on End Bearing Piles," *J. Soil Mech. & Found. Dn.*, ASCE, vol. 97, No. SM1, pp. 77–93.

DEMELLO, V. F. B., 1969: "Foundations of Buildings on Clay," State of the Art Report, *Proc. 7th Intern. Conf. of Soil Mech. and Found. Eng.*, Mexico City, vol. 2, pp. 49–136.

DUNCAN, J. M., and A. L. BUCHIGNANI, 1976: "An Engineering Manual for Settlement Studies," *Geotechnical Engineering Report*, Dep. of Civil Eng., University of California at Berkeley, p. 94.

ESRIG, M. E., and R. C. KIRBY, 1979: "Advances in General Effective Stress Method for the Prediction of Axial Capacity for Driven Piles in Clay," *11th Annual Offshore Technology Conf.*, Houston, TX, pp. 437–449.

EVANS, Jr., L. T., and J. M. DUNCAN, 1982: "Simplified Analysis of Laterally Loaded Piles," *UC Berkeley Rept. No. UCB/GT/82-04*, July, p. 245.

FELLENIUS, B. H., SAMSON, L. and F. TAVENAS, 1989: "Geotechnical Guidelines—Pile Design," *Public Works Canada*, Marine Works Sector, Ottawa Ontario K1A OM2, Canada, August.

FHWA, 1989: "Interim Procedures for Evaluating Scour at Bridges."

FOCHT, J. A., and K. J. KOCH, 1973: "Rational Analysis of the Lateral Performance of Offshore Pile Groups," *Proc. 5th Offshore Technology Conf.,* Houston, TX, vol. 2, Paper OTC 1896, pp. 701–708.

GARLANGER, J. E., 1973: "Prediction of the Downdrag Load at Culter Circle Bridge," *Symp. on Downdrag of Piles*, MIT, Cambridge.

GOBLE, G. G., and F. RAUSCHE, 1987: "Wave Equation Analysis of Pile Foundations-WEAP 87, User's Manual," FHWA Report No. IP-86-23, *U.S. Dept of Transportation,* Turner-Fairbanks Highway Research Center, McLean, VA.

HEGEDUS, E. and V. K. KHOSLA, 1984: "Pullout Resistance of H-Piles," J. Geotech. Eng., ASCE, vol. 110, No. 9, Sept. pp. 1274–1290.

HIRSCH, T. J., L. CARR, and L. L. LOWERY, 1976: "Pile Driving Analysis-Wave Equation User's Manual," *TTI Program*, vols. 1–4, FHWA Report No. IP-76-13, *U.S. Dept. of Transportation, Federal Highway Administration*, Turner-Fairbanks Highway Research Center, McLean, VA.

HORN, H. M., 1966: "Influence of Pile Driving and Pile Characteristics on Pile Foundations Performances," *Notes for Lecturers to New York Metropolitan Section*, ASCE, Soil Mech. and Foundation Group.

HRENNIKOFF, A., 1950: "Analysis of Pile Foundations with Batter Piles," *Transactions ASCE*, CXV.

KARASOPOULOS, T. H., 1984: "Bridge Foundations Without Piles", *Transp. Research Board*, 63rd Annual Meeting, Washington, D.C.

KULHAWY, F. H., C. H. TRAUTMANN, J. F. BEECH, T. D. O'ROURKE, and W. MCGUIRE, 1983: "Transmission Line Structure Foundations for Uplift-Compression Loading," *EPRI Rept. EL-2870*, Electric Power Research Institute.

LAMBE, T. W and H. M. HORN, 1965: "The Influence on an Adjacent Building of Pile Driving for the MIT Materials Center," *Proc. 6th Intern. Conf. of Soil Mech. and Found. Eng.,* Montreal, vol. 2, pp. 280–285.

MANNING, J. T. and J. MORLEY, 1981: "Corrosion of Steel Piles," Piles and Foundations, F. F. Young, ed., Tharm Telford Ud., *The Institution of Civ. Eng., London*, pp. 223–229.

MATLOCK, H., 1970: "Correlation for Design of Laterally Loaded Piles in Soft Clay," *Proc. Offshore Technology Conf.*, Houston, TX, Paper No. OTC 1204.

MEYERHOF, G. G., 1976: "Bearing Capacity and Settlement of Pile Foundations," *ASCE JGED*, vol. 102, No. GT3, March, pp. 196–228.

NAVFAC DM7.2, 1982: "Foundations and Earth Structures," *Dept. of the Navy, Naval Facilities Engineering Command*, May.

NOTTINGHAM, L., and J. SCHMERTMANN, 1975: "An Investigation of Pile Capacity Design Procedures," *Final Report D629 to Florida Dept. of Transportation from Dept. of Civ. Eng.*, Univ. of Florida, September, p. 159.

O'NEILL, M. W., GHAZZALY, O. I., and H. B. HA, 1977: "Analysis of Three-Dimensional Pile Groups with Non-Linear Soil Response and Pile-Soil-Pile Interaction," *9th Annual Offshore Technology Conf.*, Houston, May, pp. 245–256.

O'NEILL, M. W., and C. N. TSAI, 1984: "An Investigation of Soil Nonlinearity and Pile-Soil Pile Interaction in Pile Group Analysis," Research Rept. No. UHUC 84-9, *Dept. of Civil Eng.*, Univ. of Houston, November, prepared for U.S. Army Engineer Waterways Experiment Station, Vicksburg, Miss.

OOI, P. S. K., J. M. DUNCAN, K. B. ROJIANI, and R. M. BARKER, 1991: "Engineering Manual for Driven Piles," NCHRP 343, TRB, Washington.

ORRIE, O., and B. B. BROMS, 1967: "Effects of Pile Driving on Soil Properties," *J. Soil Mech. and Found. Dn.*, ASCE, vol. 93, No. SM5, pp. 59–73.

PECK, R. B., 1958: "A Study of the Comparative Behavior of Friction Piles," *Highway Research Board*, Special Report 36.

POULOS, H. G. and E. H. DAVIS, 1980: "Pile Foundation Design and Analysis," Wiley, New York, pp. 397.

POULOS, H. G. and E. H. DAVIS, 1979: *Pile Foundations Analysis and Design,* Wiley, New York.

PRAKASH, S. and H. D. SHARMA, 1990: "Pile Foundations in Engineering Practice," Wiley, New York, p. 734.

Prestressed Concrete Institute, 1985: "PCI Design Handbook—Precast and Prestressed Concrete," 3rd ed., *Prestressed Concrete Institute*, Chicago, Ill.

RAUSCHE, F., F. MOSES, and G. G. GOBLE, 1972: "Soil Resistance Predictions from Pile Dynamics," *J. Soil Mech. Found. Div.*, ASCE, vol. 98, No. SM9, pp. 917–937.

REESE, L. C., 1977: "Laterally Loaded Piles: Program Documentation," *J. Geotech. Eng. Div.*, ASCE, vol. 103, No. GT4, April, pp. 287–305,

REESE, L. C., W. R. COX, and F. D. KOOP, 1974: "Analysis of Laterally Loaded Piles in Sand," *Proc. Offshore Technology Conf.*, Houston, TX, Paper No. OTC 2080, pp. 473–483.

REESE, L. C., and R. C. WELCH, 1975: "Lateral Loading of Deep Foundations in Stiff Clay," *J. Geotech. Eng. Div.*, ASCE, vol. 101, No. GT7, July, pp. 633–649.

ROMANOFF, M., 1962: "Corrosion and Steel Piling in Soils," *Journ. Soil Mech. and Found. Div.*, ASCE, vol. 66, No. 3, Feb., pp. 1–22.

SAUL, W. E., 1968: "Static and Dynamic Analysis of Pile Foundations," *ASCE Journ., Struct. Div.*, vol. 94, No. ST5, May, pp. 1077–1100.

SCHMERTMANN, J. H., 1977: "Guidelines for Cone Penetration Test-Performance and Design," *U.S. Dept. of Transportation*, Federal Highway Administration, pp. 54–55.

SHARMA, H. D., and R. C. YOSHI, 1988: "Drilled Pile Behavior in Granular Deposits," *Can. Geotech. J.*, vol. 25, No. 2, May, pp. 222–232.

SODERBERG, L. O., 1962: "Consolidation Theory Applied to Foundation Pile Time Effects," *Geotechnique*, vol. XII, No. 3, pp. 217–225.

TAYLOR, D. W., 1948: *Fundamentals of Soil Mechanics*, Wiley, New York.

TERZAGHI, K., 1955: "Evaluation of Coefficient of Subgrade Reaction," *Geotechnique*, No. 5, pp. 297–326.

TOMLINSON, M. J., 1987: "Pile Design and Construction Practice," *Viewpoint Publication*, p. 415.

VESIC, A., 1967: "Ultimate Loads and Settlement of Deep Foundations in Sand," *Proc. Symp. on Bearing Capacity and Settlement of Foundations*, Duke Univ., Durham, NC, p. 53.

VESIC, A., 1975: "Bearing Capacity of Shallow Foundations," Chapter 3 in *Foundation Engineering Handbook,* ed. by H. Winterkorn and H. Y. Fang, Van Nostrand Reinhold Co., New York, pp. 121–147.

VESIC, A., 1977: "Design of Pile Foundations," *Transportation Research Board*, National Research Council, Washington, D.C.

Vijayvergiya, V. N. and J. A. Focht, Jr., 1972: "A New Way to Predict the Capacity of Piles in Clay," *4th Annual Offshore Technology Conf.*, Houston, vol. 2, pp. 865–874.

CHAPTER 10

Drilled Shaft Foundations

The fundamentals of drilled shafts were discussed in section 1.5. The same section presented a review of construction methods and discussed the factors to be considered in selecting drilled shafts for bridge foundations. In general, drilled shafts may be considered where suitable soil does not exist for spread footings. However, they should be compared for cost and feasibility with driven piles. In many instances, drilled piers provide a good choice, particularly when considerable lateral loads or uplift must be resisted and when deformations are limited by serviceability criteria.

10.1 ASSESSMENT OF CONSTRUCTION METHODS

A drilled pier is constructed by drilling a cylindrical hole using suitable equipment, inserting a reinforcing steel cage, and then filling the hole with concrete. The pier shaft may be straight for the entire depth, or it may have an enlarged base. Other convenient terminology is a drilled shaft, a drilled caisson (or simply caisson), and a bored pile. The term caisson may also be used to describe large prefabricated box type structures that can be sunk through soft ground or water to provide a dry working area. The same term may also be used as a regional preference such as the Chicago caisson.

The three basic construction methods mentioned in section 1.5 are (1) dry installation, (2) installation with casing, and (3) installation under slurry. Among the early construction methods are the Chicago and Gow methods shown in Figure 10–1. In the Chicago method, shown in Figure 10–1(a), a circular pit was excavated to a convenient depth and a cylindrical shell of vertical boards or staves was placed and held in place by an inside compression ring. A second tier was placed, to be followed by a third set, and so on, until the intended depth was reached. In the Gow method, stability was provided by a series of telescoping metal shells sequentially reducing the diameter of successive tiers as shown in Figure 10–1(b).

The shaft base could be enlarged by hand digging if additional bearing capacity

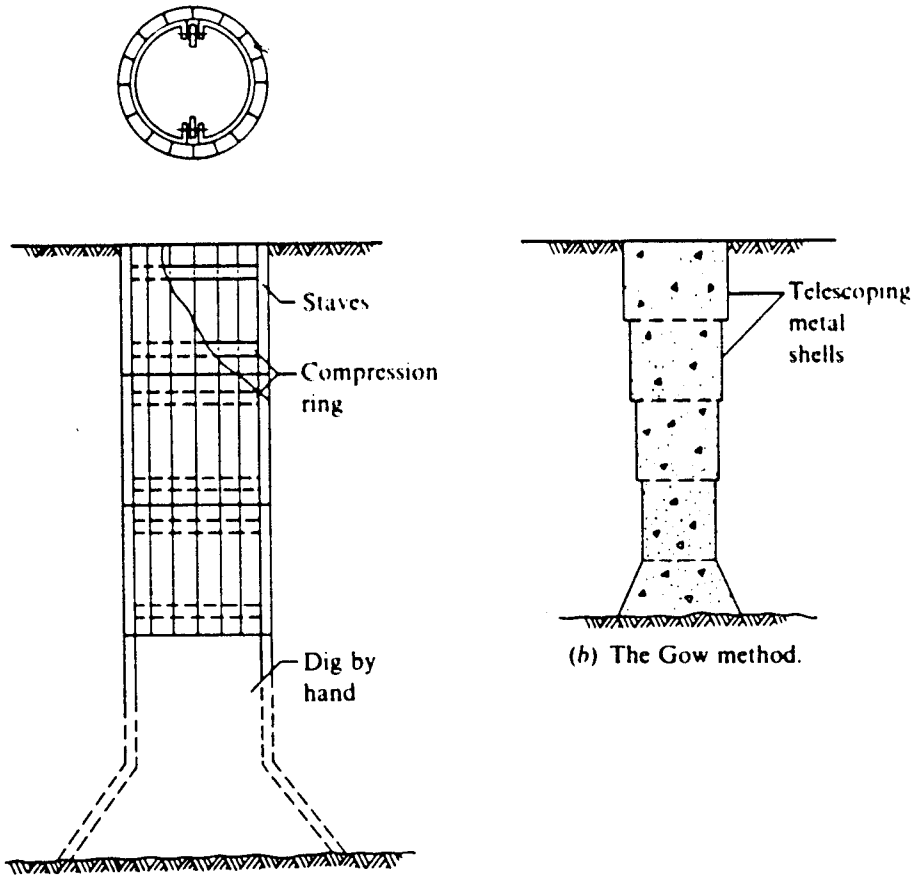

Figure 10–1 Early methods of caisson construction.

was necessary. A reinforcing cage was placed in the shaft and the hole was filled with concrete. The shaft supports for the Chicago and Gow methods were usually left in place, since the foundation pier was not designed to transfer the load by shaft resistance, and because they would not be easy to remove after the concrete had been poured.

Dry method. This method, shown in Figure 10–2, is feasible in stable soil above the water table. In most cases the shaft is partially filled with concrete as shown in Figure 10–2(b), the rebar cage is set, and the shaft is completed as shown.

Casing method. Typical installation procedures are shown in Figure 1–20 for a specific site and soil stratigraphy. The use of a casing implies that there is an impermeable layer below the casing zone into which the casing can be socketed. When the casing is seated, the initial slurry is bailed out and the shaft is extended to the required depth.

The casing may be left in place or pulled. As mentioned, early withdrawal may prevent the fresh concrete from displacing slurry trapped in the annular space. Thus, this phase must ensure (1) the concrete inside the casing is still in a fluid state (flow-

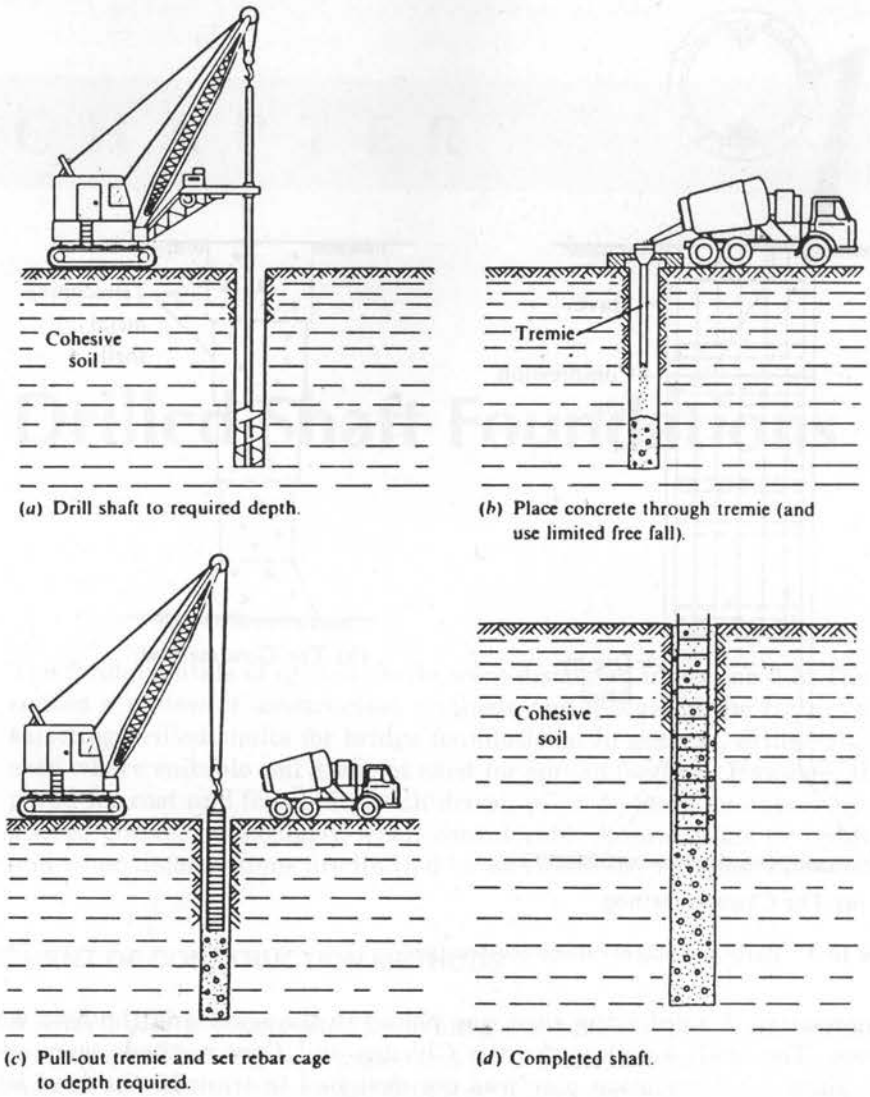

(*a*) Drill shaft to required depth.

(*b*) Place concrete through tremie (and use limited free fall).

(*c*) Pull-out tremie and set rebar cage to depth required.

(*d*) Completed shaft.

Figure 10–2 Dry method of drilled pier construction.

able), and (2) the concrete head is sufficient for the fresh mix to displace the slurry and not vice versa.

Pulling the casing may result in an oversize top shaft segment. This enlargement is inconsequential, but its exact size must be known in comparing the actual concrete volume to ensure that the finished foundation does not have accidental voids.

Slurry method. Excavation under slurry support is indicated in any situation requiring casing. In this case the slurry is used merely to help drill the hole and may be removed when the excavation is completed. Because the slurry functions are limited, the associated controls are somewhat simplified. Slurry-mixing facilities are not always necessary, and although a substantial part of bentonite is wasted, savings in time and equipment use offset this waste. Most contractors maintain quality control merely by visual observation, sometimes supplemented by in situ tests. If sodium bentonite is not

available, commercial sodium bentonite or local clays mixed with CMC can produce an acceptable slurry (Xanthakos, 1979).

Two methods are recommended to advance the hole, depending on the type of ground. In predominantly loose sands, the hole is advanced by stirring the soil with an earth auger, adding bentonite and water as the excavation becomes deeper. A surface casing is placed that extends below the unstable formation. Water and bentonite are continuously added and mixed as the bit is lifted and churned. If mixing facilities are not available at the site, the dry bentonite is merely dumped into the slurry in the hole. When the final depth is reached, the remaining casing is lowered and properly seated in the final bed by driving or rotating.

The second method is used in ground with silts and clays. In this case, the excavation is carried out with a drilling bucket under bentonite slurry. The latter may be either premixed or prepared by churning bentonite with water in the hole. Because it is not desirable to have stiff cohesive clays processed into a gelled slurry, the drilling bucket is moved up and down to discharge the clay in bulk as the hole is advanced. As they are encountered, boulders and heavy gravels are removed, broken up, or loosened by special tools.

Large-diameter piles designed as load bearing elements often have their base resting on rock or other firm formation (hardpan). In this case, the entire slurry may be bailed out of the hole, leaving the casing only. In these conditions it is possible to underream the hole, inspect and test the bottom visually, and place the concrete in the dry.

Concreting the hole under slurry. Unless the bottom of the hole is in impervious formation, the slurry should not be removed because of the danger of blow-in and base failure. Alternatively, certain codes require the hole to be drilled under slurry protection, implying that the fresh mix must be tremied while the slurry remains in the hole.

For the usual range of hole diameters (6 to 12 ft) one tremie pipe located at the center will ensure the flow of the mix and the complete displacement of bentonite. An optional method of placement involves the use of a concrete pump of the piston-displacement type coupled to a 3-inch flexible rubber hose of sufficient length, attached to a rigid pipe. After the pipe and the hose are inserted into the hole with the ends touching the bottom, a plastic plug is inserted in the line to separate the initial batch of concrete from the slurry, as is done in a tremie pipe. As the fresh mix is discharged and travels down the pipe, it pushes the plug toward the bottom and out of the pipe and begins to fill the hole. The plug is recovered by floating out.

10.2 PRACTICAL CONSIDERATIONS

Vertical alignment. The alignment of the hole may often be difficult to maintain, either in plan or in elevation, particularly when the elements are placed side by side to form a continuous wall, and the installation is under slurry. Other considerations relate to hole enlargement and slurry-mud communication between holes in the same vicinity when the excavation is in pervious ground.

When the shafts are to be used only as load bearing elements, the tolerable vertical misalignment is determined from the allowable eccentricity of the design axial load. Relevant criteria are as follows (for maximum misalignment):

- Category A: Unreinforced shafts installed in ground offering minimum lateral restraint; not to exceed 0.125 × diameter.
- Category B: The same as in A, but the soil is competent for lateral restraint; not more than 0.015 × shaft length.
- Category C: Reinforced concrete shaft, to be determined on a case-by-case basis by the designer.

Slurry disposal. Slurry disposal may be a problem, particularly in built-up areas. Contractors usually provide large storage tanks at the site where the slurry may be stored temporarily and reconditioned for reuse. If space is available, used slurry may be stored in a pit excavated for this purpose. Eventually, any unused slurry must be removed for disposal.

Quality control of concrete. For a specified concrete strength f_c' in the range of 3000 to 3500 lb/in^2, the required slump is between 7 and 9 inches. The higher slump is necessary for construction under slurry where extra mass mobility and flowability are necessary to displace the slurry completely. The use of suitable plasticizers and air entraining in this case may be beneficial and should be considered, but under competent technical advise.

In order to check and confirm the structural continuity of the shaft, its volume should be compared to the actual concrete volume placed. Test cylinders should be routinely obtained, and a record of concrete strength should be compiled.

Underreaming. Underreaming or belling (base enlargement) can be done in stable soils where an increased base is necessary for the transfer of load. Underreaming may not be necessary in rock where the bearing capacity is at least as large as the concrete strength.

Underreaming procedures were mentioned in other sections. In general, the process produces unconsolidated cuttings on the base soil. Some of these may be isolated into the reamer seat of the underream device, or a temporary casing can be installed to allow access to the base for visual inspection and manual removal of excavated materials.

Bells may produce a base that is up to four times the shaft diameter. An enlarged base is, however, seldom reinforced because of the obvious difficulties. When the maximum slope of the underream is about 45°, two-way action shear will govern so that punching effects should not be expected. Bending considerations similar to a footing action are unlikely to control because bending stresses due to upward pressures are absent.

Ground loss. A hole drilled in the dry causes the surrounding soil to squeeze into the excavated area, resulting in surface subsidence in the immediate vicinity. A hole in very soft or loose ground excavated under slurry may have a reverse effect, pushing the soil toward the ground, thus increasing the hole size and until passive resistance rectifies this movement. Lukas and Baker (1978) propose to investigate the stability of a dry hole from the squeeze ratio R_s given by

$$R_s = p_o' / s_u \tag{10–1}$$

where p_o' = effective overburden stress and s_u = undrained shear strength. If $R_s < 6$, some squeezing may occur, although slow enough to be inconsequential. If $R_s > 6$,

squeezing is most likely to take place, and if R_s approaches 8 or 9 it will occur as the hole is excavated.

This criterion is based on experience with Chicago clay so that the boundaries may be somewhat different at other locations. In general, ground loss may be controlled by (1) rapid excavation followed by prompt concrete placement, (2) the use of a shaft line, and (3) the use of slurry.

10.3 USUAL DEFECTS AND REPAIRS

Possible defects of a finished element and the conditions under which they occur can be summarized as follows:

1. Overstressing the soil beneath the base due to insufficient bearing (contact) area or because of unconsolidated materials at the bottom
2. Improperly placed concrete, resulting in voids and cavities within the set concrete
3. Structural discontinuities and deviations from the true vertical line causing local stress concentrations
4. Excessive mixing with bentonite mud affecting the development of concrete strength

Unlike belled subpiers where bearing capacity failure is improbable or exceptionally rare, insufficient load transfer at the base of straight shafts may be a possible cause of settlement during service, particularly where the transfer of load is mainly by direct bearing. Limited contact area or the presence of soft materials at the bottom are the main causes.

Methods for checking and repairing defective elements. For settlement-sensitive substructure and where heavy loads are to be carried, a postconstruction investigation may be specified to check the continuity and integrity of the foundation. Alternatively, this program may be confined to in situ tests to confirm the assumed load transfer, either by base bearing or by shaft resistance.

If there is indication that the set concrete is defective in one of the ways mentioned, a good check on its quality and soundness is by means of diamond coring (Baker and Khan, 1971). The larger the diameter of the core, the more reliable the results, but the more expensive the test. Diamond coring can be supplemented by other test procedures such as caliper logging, incinometer readings, seismic-wave and velocity measurements, and three-dimensional logging. The damaged areas are usually repaired by grouting, but even with the best techniques and materials available, the repairs are carried out on a speculative basis. Thus efforts to repair local defects can fail more often than they succeed. Grouting has been found effective where a clear void exists and is not filled with earth materials, provided enough pressure can be developed between two grout holes. For prismatic elements (discussed in chapter 11), these defects are likely to be less serious because of the larger cross sectional area usually available.

Load tests. These constitute the best procedure for confirming the design load capacity. Where the possibility of excessive settlement is disclosed, the usual remedy is to construct a second element adjacent to the first shaft and provide a rigid connection at the top.

Most problems associated with the transfer of load can be prevented if the final excavation stages are monitored. Particular emphasis should be on the rate of drilling and on the type of excavated materials in the last few feet of penetration. Bottom cleaning should be thorough, and unconsolidated soft materials should be removed completely. Hard clay, very dense sand, and other firm strata will slow drilling considerably and may thus indicate the presence of a suitable foundation level. In addition, a test subpier will disclose the foundation conditions and provide data for a semiempirical design.

10.4 AASHTO REQUIREMENTS

AASHTO Article 4–6 contains provisions for axially and laterally loaded shafts in soil or extended into rock. Suitable materials are cast-in-place concrete, deformed bar steel reinforcement, and structural steel sections. Permanent steel casings may be considered in the design.

The method of construction may be as discussed in section 10.1, and the shaft embedment should be determined according to the vertical and lateral load capacity of both the shaft and subsurface materials.

Shaft configuration. The design terminology for drilled shaft foundations is shown in Figure 10–3. For rock-socketed shafts that require casing through the overburden soils, the socket diameter should be at least 6 inches less than the inside diameter of the cas-

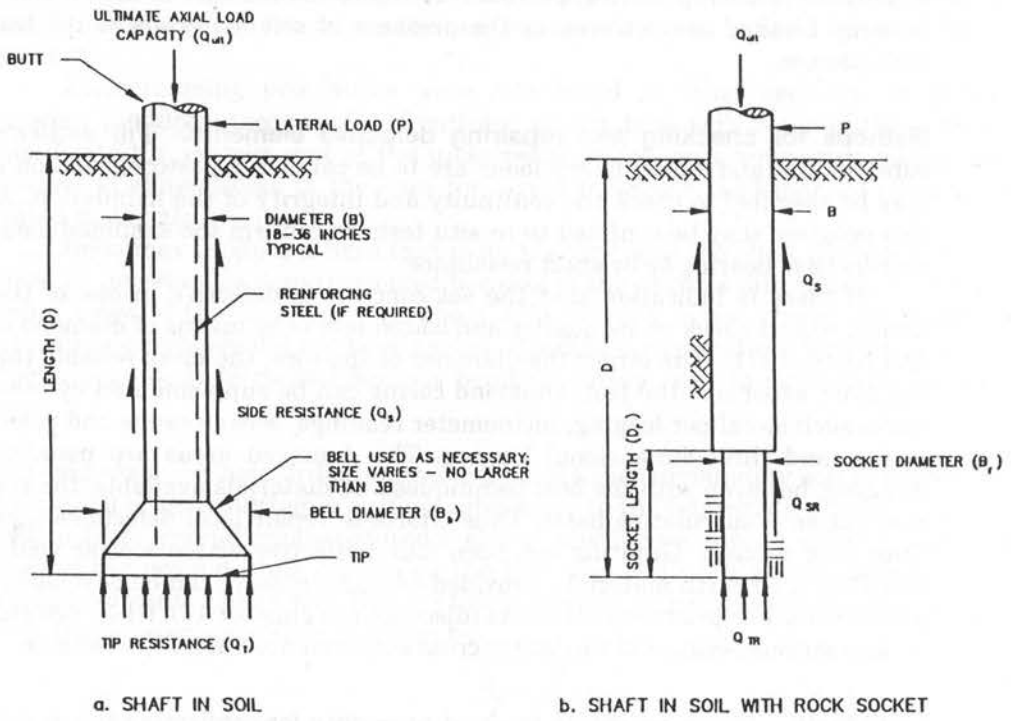

Figure 10–3 Design terminology for drilled shaft foundations.

ing to facilitate the insertion and removal of the drilling tool. Where casing is not required, the socket diameter may be the same as the shaft diameter throughout the soil.

The use of batter shafts to increase the lateral capacity of the foundation is not recommended because of the difficult construction and higher cost. In this case, consideration should be given to a larger shaft diameter to obtain the required lateral capacity.

Slurry. Specifications recommend the premixing of slurry with water, also allowing sufficient time for hydration prior to introduction into the shaft. Adequate desanding facilities may be used as necessary. Control tests are suggested at various stages to check the density, viscosity, and pH. An acceptable range of values is given in Table 10–1. These tests should be carried out during shaft excavation to establish a working pattern and the consistency of the operation. The slurry should be tested before the placement of concrete, and it should be recirculated to remove the solid fraction as provided for in the specifications.

Commentary. The control limits for the properties of slurries are essentially similar to the guidelines established in "Slurry Walls" (Xanthakos, 1979), and are shown in Table 10–2. These limits are quite general, but the range can be further narrowed down or refined when the scope of work is known more specifically. There is some question whether and when the apparent viscosity, Marsh cone viscosity, plastic viscosity, yield strength, and 10-min gel strength are relevant and must be used for the control of slurries.

Reference to the flow curves shows that the apparent viscosity depends on the rate of shear of the measuring system. Plastic viscosity measures resistance to flow for ideal slurries or for slurries of very low initial shear strength. For the usual conditions, the plastic viscosity must be combined with the 10-min gel strength to provide the flow behavior.

Although Marsh cone tests do not provide absolute viscosity measurements, they give useful data for routine site work, and are simple and practical in relating the slurry properties to the soil conditions on a comparative basis.

The Bingham yield stress is important when studying the flow curve and useful for a theoretical analysis of colloidal behavior. However, in practice it is seldom necessary to estimate this stress; furthermore, its correlation to the initial or the 10-min gel strength is difficult.

Interestingly, for a stratified soil profile, the slurry must be initially proportioned for the soil layer that has the highest permeability and is most vulnerable to sloughing and peel-off. This tendency for the face is shown in Table 10–3 for the most common soil

Table 10–1 Range of Values of Physical Properties of Slurries (68°F)

Property (Units)	Time of Slurry Introduction	Time of Concreting (In Hole)	Test Method
Density (pcf)	64.3 to 69.1	64.3 to 75.0	Density Balance
Viscosity (sec. per quart)	28 to 45	28 to 45	Marsh Cone
pH	8 to 11	8 to 11	pH paper or meter

Table 10–2 Control Limits for the Properties of Slurries*

	Property							
Function	*Average bentonite concentration,† %*	*Density, lb/ft³*	*sp gr*	*Plastic viscosity, cP*	*Marsh cone viscosity*	*10-min gel strength (Fann), lb/100 ft²*	*pH*	*Sand content, %*
Face support	>3–4	>64.3	>1.03	....	Limits	‡	....	>1§
Sealing process	>3–4	.....	.....	....	established	.....	....	1
Suspension of detritus	>3–4	.....	.....	....	by soil type	>12–15		
Displacement by concrete	<15	<78	<1.25	<20		.....	<12	<25
Separation of noncolloids	.....	.....	.....	....		.....	....	<30
Physical cleaning	<15	<78	<1.25	....		.....	....	<25
Pumping of slurry	.....	.....	.....	....		Variable		
Limits	>3–4	>64.3	>1.03	<20		>12–15	<12	>1
	<15	<78	<1.25	....		.....	....	<25

*Controls are not considered necessary for apparent viscosity and yield stress. Whereas fluid loss commonly is judged by standard filtration test and a maximum film thickness of 2 mm, better control limits are established by stagnation-gradient tests.

†Should be expected to vary widely because of different bentonite brands.

‡The shear strength of filter cake is more applicable to peel-off control (also the time required for its formation).

§Optional.

types. The entry "none" indicates a face that is stable but not indefinitely; "some" means that sloughing and peel-off do not occur for some time after the face is exposed; "appreciable" indicates that caving can occur at any time, whereas "high" and "very high" preclude excavation unless the face is protected. The tendencies characterized in Table 10–3 are for unsupported faces for either linear or circular excavations.

The most critical soil layer can be correlated with the viscosity requirements by means of Table 10–4. This correlation is based on practical experience, and although it is given in terms of the funnel viscosity, it provides satisfactory results. Thus, the proportioning of the slurry involves the following steps:

Table 10–3 Relation between Soil Grains and Tendency to Collapse

	Tendency to collapse	
Type of soil	*Dry soil**	*Soil with water**
Clay	None	None
Silt	Usually none	Some
Silty sand	Some	Appreciable
Fine sand (moist)	Appreciable	Appreciably higher
Coarse sand	Appreciably higher	High
Sandy gravel	High	Very high
Gravel	Very high	Very high

*See text for elaboration of meaning of these terms.

Table 10–4 Funnel Viscosity for Common Types of Soil

	Funnel viscosity, s/946 cm^3	
Type of soil	*Excavation in dry soil*	*Excavation with groundwater*
Clay	27–32	
Silty sand, sandy clay	29–35	
Sand, with silt	32–37	38–43
Fine to coarse	38–43	41–47
And gravel	42–47	55–65
Gravel	46–52	60–70

1. Determine the noncolloid fraction (from density requirements) necessary to maintain hole (or trench) stability. This may include some soil from the excavation, but excessive retention may spoil the slurry.
2. Select the funnel viscosity by reference to Table 10–4.
3. Establish the applicable control limits from Table 10–2, and refine this range for the particular conditions at the site.
4. Determine whether control agents are necessary (Xanthakos, 1979).
5. Proportion the constituent materials. This may have a technical basis of tests and flow curves, but may be supplemented with practical experience.

For a complete discussion of the technology, preparation, uses, and control of slurries, reference is made to Xanthakos, (1979).

10.5 DESIGN REQUIREMENTS

Effect of Construction Methods on Design

Invariably, design methods assume that the construction methods of drilled shafts is done under competent supervision and ample quality control, and that the finished foundation is durable and has structural integrity. Unless the specified procedures are followed in the field, the final shaft may have distinct defects, likely to influence its structural and bearing capacity. Typical examples are (1) a casing withdrawn prematurely and when the concrete has set, thereby allowing the slurry or soil to move into the gap created by this withdrawal; and (2) unconsolidated material left at the bottom. In both these cases, there may be a reduction in the bearing capacity of the foundation, excessive settlement, or both. Examples of construction deficiencies are shown in Figure 1–21, with potential solutions and remedies summarized in Table 1–2.

Design Approach

Drilled piers are deep foundations that must be capable of transferring the imposed loads to the soil without reaching a limit state. The loading conditions should include both axial and lateral loads, according to the specified load groups and combinations. The two basic design considerations are ultimate load capacity and settlement. The ultimate load capacity must be governed by the structural capacity of the shaft or by the bearing capacity of the soil (geotechnical strength). Where the foundation is also sub-

jected to lateral loads, it must be safe against the ultimate failure of the soil or the shaft, and excessive lateral deflection should not occur.

Structural Capacity

Drilled shafts are widely used in bridge foundations to carry compressive as well as tension loads. Axially loaded shafts may fail in compression or by buckling. Buckling is possible in long and slender members that extend above the ground line. Scour of the soil around the shaft will expose portions of the member, thus extending the unbraced length and making the shaft more prone to buckling.

A drilled shaft in soil is unlikely to undergo compression failure, because the bearing capacity will be reached before the structural strength is exceeded. Compression failure may occur, however, for an overloaded shaft founded in rock. Typically, all possible modes of failure must be investigated. Tension loads may exist, particularly with large overturning moments from unusual superstructure lateral loads or uplift.

Laterally loaded shafts may fail in flexure if the induced bending exceeds the moment resistance of the member. Thus, the structural capacity of a drilled shaft is largely dependent on both the induced moment and the axial load, and is typically checked using load-moment interaction diagrams (see also section 9.12).

Geotechnical Strength (Bearing Capacity)

The ultimate bearing capacity of a drilled shaft is the sum of the tip and shaft resistance. During failure, the shear stress at the shaft soil interface reaches a limiting value. This state may be reached under either compressive or upward load.

In saturated clays, drilled shafts are usually designed under total stress analysis ($\phi = 0$) using the undrained shear strength s_u. Long-term loads tend to consolidate the clay with time with a corresponding increase in the shear strength, and some settlement will follow this consolidation. Alternatively, negative pore pressures can develop along the sides of the shaft in heavily overconsolidated clays or shales, and cause softening of the soil with time. As a result, the total stress method becomes less conservative, and instead an analysis is recommended based on the undrained shear as measured on a triaxial or direct shear specimen previously allowed to imbibe water. This procedure is intended to approximate the long term softening behavior.

Movement

As in other types of foundations, horizontal movement may result from the application of wind loads, earth pressures, stream flow, braking forces, and earthquakes. The associated effects are discussed in other sections. In principle, it is mandatory to estimate the maximum anticipated settlement and lateral movement and compare them with the tolerable values. If both vertical and horizontal movement are predicted, the horizontal displacement of pier foundations should be limited to 1 inch. If vertical displacements are small, the horizontal displacement may be allowed to reach 1.5 inches. These guidelines must, however, be assessed in conjunction with the anticipated thermal expansion of the bridge, and the location and type of bearings.

Load tests on instrumented drilled shafts have shown that the movement required to mobilize the shaft resistance is smaller than the vertical displacement necessary to mobilize the base bearing. In general, the full shaft capacity is mobilized for a vertical displacement less than 1 percent of the shaft diameter. For the same shaft in clay, base

bearing is not mobilized until the shaft settles about 2 to 5 percent of its diameter. In sand, the shaft resistance is fully developed at settlements less than 1 percent of the shaft diameter. Much larger displacement is needed to mobilize the end bearing, and often exceeds the tolerable vertical movement. This consideration is important as a design criterion when the analysis is based on allowable stresses; it means a larger portion of shaft resistance beyond the safety factor (often all of it) must be developed before any load can be resisted at the tip of the element. For design purposes, an ultimate end-bearing capacity is usually established with reference to some specified settlement, usually 5 percent of the shaft diameter.

Shaft Spacing

Drilled shafts should be spaced far apart to facilitate extraction of the casing and exclude slurry mud communication between adjacent holes. Deficiencies associated with these operations are most likely to affect the transfer of load. The minimum spacing usually recommended between adjacent subpiers (edge-to-edge) is 3 feet. The minimum spacing specified should also include allowance for alignment deviations, accuracy in verticality, oversized hole, and other construction deviations. In the final configuration, optimum hole spacing should be a function of anticipated loads, size and diameter of shaft, and configuration of substructure elements to be supported.

Subsoil Conditions

Expansive or swelling soils have a tendency to undergo volume changes because of variations in their moisture content. A quantitative measure of this characteristic is the coefficient of linear expansivity "COLE" which gives an estimate of the potential vertical component of swelling in the soil. A definition of low, moderate, and high expansivity is given by Krohn and Slosson (1980) as follows:

- High: Generally observed in soils high in clay, made up of large percentage of montmorillonite minerals (found also in bentonite). These soils have a COLE value usually greater than 6 percent.
- Moderate: Generally exhibited in soils with moderate amounts of clays that also contain some montmorillonite minerals. For these soils the COLE value varies between 3 and 6 percent.
- Low: Usually observed in soils containing some clay. The clay, however, consists of the mineral kaolinite with low swelling characteristics and limited thixotropic behavior. These soils have COLE values less than 3 percent.

The Waterways Experiment Station (WES) classification method identifies the swell potential in terms of the Atterberg limits and the swell suction pressure measured in a soil suction test. The WES classification for low, marginal, and highly expansive soils is presented in Table 1–1.

The depth at which seasonal moisture changes occur can be identified following certain simple observations, namely: (1) The depth to which jointed, slickensided, and blocky soils are obtained in tube samples; (2) The depth to which there is a change in color; (3) The depth to which moisture content is erratic; and (4) The depth to which the liquidity index is erratic. The liquidity index usually approaches a constant value in layers of stable moisture.

Where the presence of expansive soils is suspected, remedies should include the following (Reese and O'Neill, 1988):

1. Identify the expansive soil
2. Estimate the probable depth of the expansive layers
3. Predict the probable amount of swell
4. Estimate the uplift force
5. Specify appropriate construction alternatives to counteract uplift loads

Recommended procedures to deal with expansive soils and the associated uplift are shown in Figure 10–4. The use of a permanent outside casing, shown in Figure 10–4(a), is intended to isolate the shaft from the soil environment. Whereas it eliminates uplift, it also deprives the element of useful shaft area necessary to resist vertical loads. The composite shaft shown in Figure 10–4(b) incorporates a steel H-pile placed in the area of the expansive layer. The steel section resists tension caused by uplift, and is coated with an asphaltic layer so that the uplift loads are not transmitted through the surrounding concrete. The scheme shown in Figure 10–4(c) relies on the use of tension reinforcement to resist upward forces caused by uplift loads.

Site Conditions

For bridge foundations in active waterways, scour may be the cause of a serious problem. In this case, the geotechnical strength should be estimated, assuming that the soil above the estimated scour is inactive or has been removed.

The three basic forms of scour (aggradation and degradation, general scour and contraction scour, local scour) are discussed in other sections, and are usually evaluated for a flood with a return period of 100 years. The FHWA (1989) recommends the following: (1) The top of the pier cap should be placed below the depth of contraction scour to reduce obstruction to flow and to minimize local scour, and (2) fewer but longer shafts should be used to reduce the associated interaction in the scour zone.

Deterioration of drilled shafts may occur because of attack by deleterious substances in the ground, such as organic materials, acids, sulphates, and salt. Abrasion of concrete is possible where the drilled shafts are exposed to soils being moved by current and waves, floating debris, and ice. High quality concrete and ample cover for the reinforcement are the best protection against abrasion and corrosion. Where the soil environment contains sulphates, sulphate-resisting cement should be used in the concrete mix.

10.6 GENERALIZED DESIGN APPROACH

The usual approach to the design of drilled shafts involves the following steps:

1. Based on the soil data, prepare a soil profile showing strength characteristics, compressibility parameters, stress history and soil geology. Identify favorable and unfavorable zones in the soil in the context of load transfer.
2. Determine the loads acting on the shafts for the ultimate and serviceability limit states, and include forces caused by uplift and negative shaft friction.

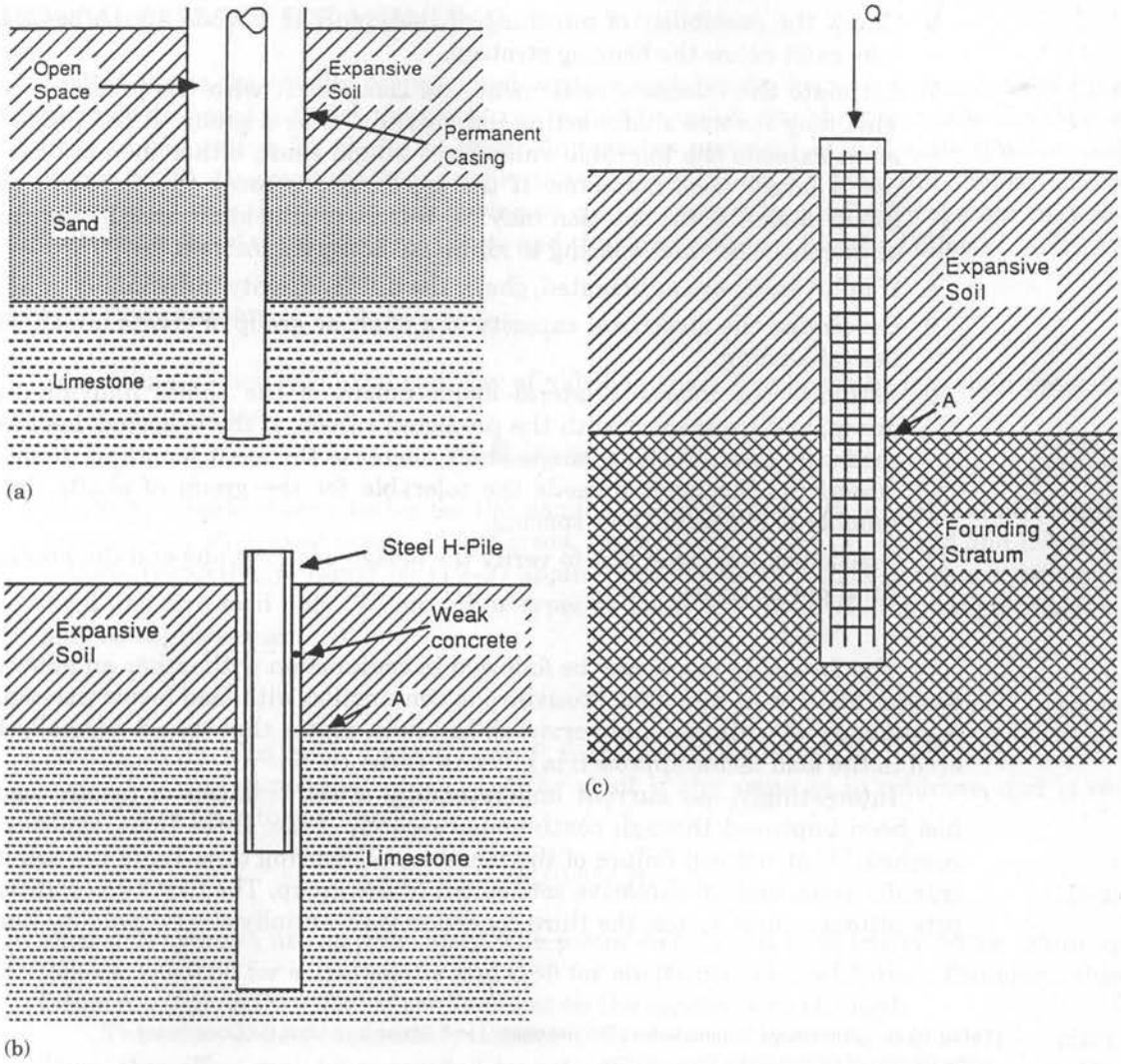

Figure 10–4 Use of permanent surface casing for design in expansive soils; (b) Raba method of design in expansive soil; (c) use of rebar cage for design in expansive soil *(from Reese and O'Neill, 1988)*.

3. Where the foundation is contemplated in waterways and stream crossings, develop the water profiles and estimate the depth of the design scour.
4. Select an optimum length based on the soil profile and the intended mode of load transfer, and estimate the axial capacity of individual shafts considering both the structural capacity and geotechnical strength.
5. Given the total load, estimate the required number of shafts and prepare a layout showing their location and dimensions. Check the capacity of a single shaft or the groups of shafts. If the capacity of a single shaft is not sufficient, an alternative is to increase the length or use a larger diameter. If the capacity of the group is not sufficient, an alternative is to use more shafts.

6. Check the possibility of punching of the group as a whole into a weak layer that may exist below the bearing stratum.
7. Estimate the tolerable settlement and compare it with the predicted settlement. This may involve shafts acting individually or as a group. If the predicted settlement exceeds the tolerable value for a single shaft, either increase the length or use a larger base diameter. If the settlement exceeds the tolerable value for a group of shafts, the solution may be to increase the shaft length, use more shafts, or increase the shaft spacing to minimize group interaction.
8. If uplift loads are anticipated, check the uplift capacity individually or as a group.
9. Determine the structural capacity of a shaft or group of shafts under the effect of lateral loading.
10. Estimate the tolerable lateral displacement of the shafts individually or as a group, and compare it with the predicted values. If the expected displacement exceeds the tolerable for a single shaft, increase the shaft length or diameter. If the lateral displacement exceeds the tolerable for the group of shafts, increase the number of shafts or their spacing.
11. Consider a field load test to verify the design assumptions and the predicted structural performance.

The foregoing steps may be followed in conjunction with either an allowable stress design (ASD) or as a routine procedure in conjunction with load factor (strength design). A summary of ultimate and serviceability limit states that would normally be considered in the load factor approach is given in Table 10–5.

Interestingly, our current understanding of the behavior of axially loaded shafts has been improved through continuous research. Thus, three limit conditions may be reached: (1) structural failure of the member, (2) bearing capacity of the soil in the load transfer zone, and (3) excessive settlement of the group. The first two conditions constitute ultimate limit states; the third condition is essentially a serviceability limit state.

Table 10–5 Summary of Ultimate and Serviceability Limit States that Must Be Considered in the Design of Drilled Shaft Foundations

Design Consideration	Ultimate Limit State	Serviceability Limit State
Structural capacity of single drilled shafts	X	
Bearing capacity of single drilled shafts	X	
Bearing capacity of groups of drilled shafts	X	
Punching into lower weak stratum	X	
Settlement of single drilled shafts		X
Settlement of groups of drilled shafts		X
Tensile capacity of drilled shafts during uplift	X	
Uplift capacity of single drilled shafts	X	
Structural capacity of drilled shafts under lateral loading	X	
Lateral movement of single drilled shafts when subjected to lateral loads		X
Lateral movement of groups of drilled shafts when subjected to lateral loads		X

10.7 STRUCTURAL CAPACITY FOR AXIAL LOAD

Drilled shafts are usually proportioned to carry compressive loads, but occasionally they must be designed to resist tension forces caused by uplift. Buckling normally should not be a consideration for shafts of usual dimensions installed in soft soils (Poulos and Davis, 1980). However, buckling analysis may be indicated for long and slender shafts extending above the ground and having no confinement. The possibility of scour may result in increased unconfined segments and thus may enhance buckling effects.

Shaft Capacity in Compression

The ultimate (factored) axial capacity of a drilled shaft should not be less than the sum of the factored axial loads, or

$$\phi_a P_n \geq \gamma_D P_D + \gamma_L P_L \tag{10–2}$$

where ϕ_a = performance factor for the nominal axial capacity; P_n = nominal structural capacity; P_D, P_L = axial dead and live loads, respectively; and γ_D, γ_L = dead and live load factors, respectively. Equation (10–2) applies essentially to a load group consisting of dead and live load only. Where other types of loads are involved, the design criterion may be expressed as

$$\phi_a P_n \geq \Sigma \gamma_i P_i \tag{10–3}$$

where γ_i is the load factor for load i and P_i is the axial load due to i.

The factored nominal capacity of the shaft is the same as in columns, and is repeated here for convenience. Thus

$$\phi_a P_n = r\phi_a (0.85 f'_c A_c + f_y A_y) \tag{10–4}$$

where all symbols are as previously. The parameter r is an eccentricity factor taken as follows: r = 0.85 for spiral shafts and 0.80 for shafts provided with ties. Therefore, this factor represents the effect of confinement on the compressive strength.

The effect of load eccentricity is essentially the same as for a group of driven piles. Thus, this effect may be quantified by referring to Figure 9–13 and Equation (9–17), where N is now the number of drilled shafts in the group, and other terms are self-explanatory.

Where compelling reasons exist for the use of unreinforced shafts, an allowable concrete stress may be taken as

$$f_c = 0.25 f'_c \tag{10–5}$$

As an example of eccentric load application, consider a group of drilled shafts as shown in Figure 9–13. In this case, P_g = 450 tons, e_x = 4 feet, e_y = 2 feet, and the shaft spacing is 6 feet in either direction. From these data, we compute $\Sigma x^2 = 6(6)^2 = 216$, and $\Sigma y^2 = 216$.

The most heavily loaded shaft is element 3 in the quantant shown, or

$$P_3 = 450[1/9 + 4(6)/216 + 2(6)/216] = 125 \text{ tons}$$

Likewise, we determine that shaft 7 must resist a tensile force

$$P_7 = 450[1/9 - 4(6)/216 - 2(6)/216] = -22.2 \text{ tons}$$

Specification Requirements

AASHTO. AASHTO (Section 4.6.6) stipulates a minimum shaft diameter of 18 inches, with shaft sizing in 6-inch increments. Where the potential for lateral loading is not significant, drilled shafts need to be reinforced for axial loads only. The design of longitudinal and spiral reinforcement should conform with the requirements of reinforced compression members.

The minimum clear distance between longitudinal (vertical) bars should not be less than three times the bar diameter or three times the maximum aggregate size. Where heavy reinforcement is contemplated, consideration may be given to an inner and outer reinforcing cage. Splices, when used, should develop the full capacity of the bar in tension and compression. This may be accomplished by lapping, welding, and special connectors.

Transverse reinforcement should be provided and designed to resist stresses caused by fresh concrete flowing from inside the cage to the side of the excavated hole. Transverse reinforcement may consist of hoops or spirals.

LRFD specifications. The LRFD requirements are essentially the same as in the standard AASHTO specifications. The shaft sizing in 6-inch increments is dictated by the availability of most drilling tools and casings used in the domestic market.

Those portions of drilled shafts that are not supported laterally should likewise be designed as reinforced concrete columns, with the reinforcement extending a minimum of 10 feet below the plane where the soil is assumed to provide full fixity. Sufficient reinforcement should also be provided at the junction of the shaft with the superstructure to make a suitable connection.

A distinction is made between shafts that normally are not stressed to levels where the allowable concrete stress is exceeded and shafts that represent exceptions. The former involve construction using generally accepted procedures and are subjected to conventional load effects. Among the latter are (1) shafts with sockets in hard rock, (2) shafts subjected to lateral loads, (3) shafts subjected to uplift loads from expansive soils or direct application of upward loads, and (4) shafts with unreinforced bells.

Buckling of Laterally Unsupported Shafts

In section 9.6 the buckling load of fully embedded piles was considered in terms of the subgrade reaction. For partially embedded single piles, the buckling load was analyzed as proposed by Davisson and Robinson (1965). The Davisson-Robinson approach may be extended to drilled shafts under similar conditions, namely: (1) The equivalent free-standing length is the sum of the unsupported length of the drilled shaft above the ground and an additional length to the point of full fixity below ground; (2) the depth to full fixity is a function of the flexural stiffness of the shaft, E_pI_p, and the soil stiffness; and (3) the soil modulus is considered to remain constant with depth for clays, and to vary linearly with depth in sands. Thus, for convenience, we repeat the governing expressions as follows:

Modulus constant with depth (clays)

$$L_{eq} = L_u + 1.4R \tag{10–6}$$

Modulus increasing linearly with depth (sands)

$$L_{eq} = L_u + 1.8T \tag{10–7}$$

where all terms are as in section 9.6 and all lengths apply to drilled shafts.

The Davisson-Robinson procedure applies likewise to different boundary conditions at the top of the drilled shaft, whereas the bottom boundary condition is assumed to be full fixity against rotation and translation at the depth of fixity. Possible boundary conditions at the top of the shaft are shown in Figure 9–12, together with expressions of the critical shaft load. The coefficient n_h (rate of increase of soil modulus with depth) may be found from Table 9–7.

Group effects. As in pile groups (section 9.6), the effect of shaft spacing on the soil modulus may be predicted as suggested by Prakash and Sharma (1990). When the shaft spacing is greater than eight times the shaft width, neighboring shafts have no effect on the soil modulus or buckling strength. At a shaft spacing three times the shaft width, the effective soil modulus is reduced to 25 percent of the value for a single shaft. For intermediate spacing, the modulus may be estimated by interpolation.

Suggested design approach. Buckling loads for partially embedded shafts may be estimated according to the following steps:

1. Calculate the value of n_h for sands or E_s for clays
2. Obtain the value of T for sands or R for clays (note that these steps should reflect any adjustment dictated by close geometry)
3. Calculate the equivalent length L_{eq} from Equation (10–6) or (10–7)
4. Based on the boundary conditions, use an appropriate expression from Figure 9–12 to obtain the buckling load.

With the buckling load estimated, the design load for the shaft may be predicted by normal procedures applied to beam-column behavior, considering the effect of end moments and load eccentricity.

10.8 GEOTECHNICAL STRENGTH (BEARING CAPACITY), AXIALLY LOADED SHAFTS

Presumptive Values

When sufficient soil data are not available to allow a quantitative analysis of shaft bearing capacity, the usual approach is to resort to presumptive values. These are essentially based on regional experience with similar foundation types, and are intended to give only a rough guide to probable capacities. When used in final design, presumptive values should be supplemented by load tests or by rational methods of analysis based on soil data from the site.

Presumptive bearing capacities may be found in published codes and are thus allowable values intended for use in service load design.

Shaft Bearing Capacity by Rational Methods

As in driven piles, the ultimate capacity of drilled shafts is the sum of the side and base resistance. This yields Equation (9–18), repeated here as

$$Q_{ult} = Q_s + Q_p \tag{10–8}$$

where the notation is slightly different. Q_s is the ultimate side resistance of the drilled shaft, and Q_p is the ultimate load resisted by the base. Evidently

$$Q_s = A_s q_s$$

and

$$Q_p = A_p q_p \tag{10–9}$$

where A_s = surface area of the sides of the shaft along its effective penetration depth; A_p = area of the base; and q_s, q_p are the ultimate shaft and base unit resistance, respectively.

For load factor design, the bearing capacity is

$$\phi_q Q_{ult} \geq \gamma_D P_D + \gamma_L P_L \tag{10–10}$$

where ϕ_q is the performance factor, and all other symbols are as before.

AASHTO approach. According to the standard AASHTO specifications, the ultimate axial capacity Q_{ult} of drilled shafts must be determined for compression and uplift loading as follows:

$$Q_{ult} = Q_s + Q_p - W \tag{10–11}$$

$$Q_{ult} \leq 0.7 Q_s + W \tag{10–12}$$

where W is the weight of the shaft and other terms are as before. The allowable or working load may be determined as

$$Q_{all} = Q_{ult} / FS \tag{10–13}$$

where FS is the factor of safety.

The usual design terminology adapted by AASHTO is shown in Figure 10–3, where all symbols correspond to the notation used in this text except that the subscript t is used to designate tip (base) resistance.

LRFD approach. The factored resistance of the strength limit state may likewise be expressed as for driven piles, that is, Equation (9–21) where the term "drilled shaft" substitutes "driven pile". However, the performance of drilled shafts can be greatly influenced by the method of construction, particularly side resistance. The design should consider the ground and groundwater conditions, and articulate the construction method to ensure the expected performance. Because shafts derive their geotechnical strength from side and tip resistance, the construction procedures should be consistent with the soil-structure interaction assumed in the design.

Shaft Resistance in Cohesive Soils

The ultimate geotechnical strength of drilled shafts in clay is usually governed by the conditions at the end of construction; hence, these members are designed following the total stress approach. In some instances, however, the strength of the soil may decrease with time—examples are installations in expansive clays that swell after construction. Changes in the shear strength of the soil with time can also occur where soil consolidation around the shaft results in downward movement relative to the shaft inducing negative skin friction at the interface. The corresponding increase of load can cause excessive settlement. In such cases, effective stress analysis is indicated.

Total stress analysis. According to the α method (see also section 9.7), the shaft resistance is expressed as a function of the undrained shear strength s_u of the clay as follows

$$q_s = \alpha s_u \tag{10–14}$$

where q_s is the ultimate unit shaft resistance and α is an adhesion factor. Integrating (10–14) along the entire effective length of the shaft yields AASHTO Equation (4.6.5.1.1–1). Reference to Figures 10–5 and 10–6 provides identification of portions of a drilled shaft that should not be considered in contributing to the shaft resistance. Recommended values of the adhesion factor α are given in Table 10–6 (Reese and O'Neill, 1988). These data are consolidated in AASHTO Table 4.6.5.1.1A.*

Effective stress analysis. According to this approach (also referred to as the β method in section 9.7) the ultimate unit shaft resistance under long-term sustained load may be estimated as follows:

$$q_s = \frac{K}{K_o}\left[\sigma'_v K_o \tan\left\{\phi'\left(\frac{\delta}{\phi'}\right)\right\} + c'\right] \tag{10–15}$$

where all symbols are as previously. Terms with prime indicate effective values, and δ is the angle of friction at the interface. Potyondy (1961) has determined that the values of δ/ϕ' may be taken as 0.50 for clay/steel interface, and 0.68 to 0.95 for clay/concrete interface. The ratio K/K_o depends on the method of installation, with typical values ranging between two-thirds and one.

Shaft Resistance in Cohesionless Soils

Procedures for determining the shaft resistance in sands are based on a limited number of field tests. The shear strength is expressed in terms of the angle ϕ', or it may be related to values of SPT blow count. These considerations lead to AASHTO Eq. (4.6.5.1.2–1). Several methods based on this approach are summarized in Table 10–7 (Barker, Duncan, Rojiani, Doi, Tan, and Kim, 1991). The LRFD specifications make reference to the same table. Quiros and Reese (1977), and Reese and O'Neill (1988), have found that the unit side resistance should be limited to 2 tons/ft^2, which is the maximum value measured in practice. This conclusion has prompted AASHTO to limit the ultimate unit load transfer in side resistance to 4 kips/ft^2.

*The same procedure is recommended by the LRFD specifications.

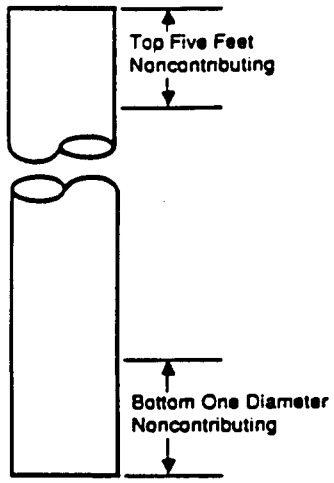

Figure 10–5 Nomenclature and articulation of portions of straight drilled shafts usually ignored in estimating side resistance in cohesive soil.

The AASHTO approach is based on the Reese and O'Neill (1988) procedure shown in the last line of Table 10–7, and is essentially an extension of the β method. Interestingly, this approach is different in that the shaft resistance is independent of the soil friction angle and the SPT blow count. The suggestion is that the friction angle approaches a common value for uncemented sands because of the high shear strains and stress relief that occur during drilling. In this context the unit shaft resistance is $q_s = \beta\sigma_v'$ as shown in Table 10–7.†

Base Bearing in Cohesive Soils

For shafts loaded under undrained conditions, the base bearing q_p is obtained from bearing capacity theories. Thus

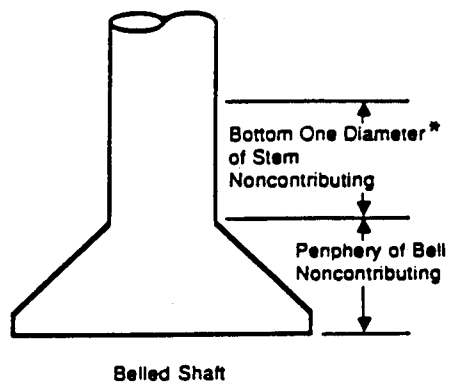

Figure 10–6 Nomenclature and articulation of portions of belled shafts usually ignored in estimating side resistance in cohesive soil.

†The friciton angle of sands may be correlated to the SPT blow count or cone resistance as specified in LRFD Table 10.8.3.4.2–2.

Table 10–6 Recommended values of α for drilled shafts in clay

Location Along Drilled Shaft	Undrained Shear Strength, S_u	Value of α
From ground surface to depth along drilled shaft of 5 ft	—	0
Bottom 1 diameter of the drilled shaft or 1 stem diameter above the top of the bell	—	0
All other points along the sides of the drilled shaft	< 2 tsf	0.55
	2–3 tsf	0.49
	3–4 tsf	0.42
	4–5 tsf	0.38
	5–6 tsf	0.35
	6–7 tsf	0.33
	7–8 tsf	0.32
	8–9 tsf	0.31
	>9 tsf	Treat as Rock

*The depth of 5 ft may be increased if the drilled shaft is installed in expansive clay, or if there is substantial groundline deflection from lateral loading.
(From Reese and O'Neill, 1988)

Table 10–7 Summary of Procedures for Estimating Side Resistance, q_s, *TSF*, in Sand. *TSF* = tons/ft^2

Reference	Description
Touma and Reese (1974)	$q_s = K\sigma_v' \tan\phi_f$ <2.5 TSF for which: $K = 0.7$ for $D_b \leq 25.0$ FT $K = 0.6$ for 25.0 FT < $D_b \leq 40.0$ FT $K = 0.5$ for $D_b > 40.0$ FT
Meyerhof (1976)	$q_s = \frac{N}{100}$
Quiros and Reese (1977)	$q_s = 0.026N < 2.0$ TSF
Reese and Wright (1977)	for N ≤ 53: $q_s = \frac{N}{34.0}$ for 53 < N ≤ 100: $q_s = \frac{N - 53}{450} + 1.6$
Reese and O'Neill (1988)	$q_s = \beta\sigma_v' \leq 2.0$ TSF for $0.25 \leq \beta \leq 1.2$ for which: $\beta = 1.5 - 0.135\sqrt{z}$

where N = uncorrected SPT blow count; σ_v' = vertical effective stress; ϕ_f = friction angle of sand; K = load transfer factor; D_b = embedment of drilled shaft in sand bearing layer, and β = load transfer coefficient.

$$q_p = N_c s_u < 40 \text{ tons/ft}^2 \tag{10–16}$$

where s_u = average undrained shear strength of clay over a depth of one to two diameters below the base, and $N = 6(1 + 0.2Z/D_p) \leq 9$. The parameter Z is the distance over which the shaft extends into the ground, and D_p is the base diameter (AASHTO and LRFD).

AASHTO specifies a limiting value of q_p of 40 tons/ft^2. This limit is not derived from theoretical considerations, but represents the largest value measured in the field. The bearing capacity factor N_c should be reduced to two-thirds of its value in soft clays to account for large displacements before bearing capacity failure occurs.

Reese and O'Neill (1988) have introduced criteria to be used if D_p exceeds 75 inches (6.25 ft), reflected in Article 4.6.5.1.3 of AASHTO.

For drained conditions, the ultimate unit base resistance may be approximated as proposed by Kulhawy, Trautmann, Beech, O'Rourke, and McGuire (1983), or

$$q_p = \sigma_v' N_q' \tag{10–17}$$

where σ_v' is the vertical effective stress and N_q' is a modified bearing capacity factor obtained from Figure 9–17 (see also section 9.7). The value of N_q' depends on the rigidity index I_r defined in Equation (9–29). For clays, however, the rigidity index may be approximated as

$$I_r = 320(1 - LI)s \tag{10–18}$$

where LI is the liquidity index of the clay and s is a stress correction factor. These parameters may be estimated as follows:

$$LI = (w_n - PL)/(LL - PL) \tag{10–19}$$

$$s = 2.2/(1.2 + \sigma_v)\sigma_{n1} \tag{10–20}$$

where w_n = natural water content of the clay; PL = plastic limit; LL = liquid limit; σ_v = original vertical in situ stress; and σ_{n1} = normalizing stress = 1 ton/ft^2. Equation (10–18) is valid for liquidity indices between 0 and 0.9.

Base Bearing in Cohesionless Soils

The large settlements necessary to mobilize base bearing in sand suggest that ultimate resistance should be based on tolerable displacements. This principle is reflected in the procedures summarized in Table 10–8. The unit values of the ultimate base bearing are based on a downward movement equal to either 1 inch or 5 percent of the base diameter. Reese and O'Neill (1988) have suggested that for base diameters greater than 50 inches, q_p should be reduced to q_{pr} as follows

$$q_{pr} = \frac{50}{D_p} q_p \tag{10–21}$$

where D_p is the base diameter in inches, and q_p is the ultimate base unit resistance calculated from Table 10–8. This criterion is incorporated in the AASHTO and LRFD specifications.

Table 10–8 Summary of Procedures for Estimating Base Resistance, q_p, of Drilled Shafts in Sand

Reference	Description		
Touma and Reese (1974)	Loose	q_p (tsf) = 0	k = 1 for $D_p < 1.67$ ft & k = $0.6D_p$ for $D_p \geq$ 1.67 ft.
	Medium Dense	q_p (tsf) = $\frac{16}{k}$	
	Very Dense	q_p (tsf) = $\frac{40}{k}$	Applicable only if $D_b > 10D$
Meyerhof (1976)	q_p (tsf) = $\frac{2N_{corr}D_b}{15D_p} < \frac{4}{3}N_{corr}$ for sand $< N_{corr}$ for nonplastic silts		
Quiros and Reese (1977)	Same as Touma and Resse (1974)		
Reese and Wright (1977)	q_p (tsf) = $\frac{2}{3}$N	for N ≤ 60	
	q_p (tsf) = 40	for N > 60	
Reese and O'Neill (1988)	q_p (tsf) = 0.6N	for N ≤ 75	
	q_p (tsf) = 45	for N > 75	

where N_{corr} = SPT blow count corrected for overburden pressure
= $[0.77\log_{10}(20/\sigma_v')]$N
N = uncorrected SPT blow count
D_p = base diameter of drilled shaft in ft
D_b = embedment of drilled shaft in sand bearing layer

Resistance (Performance) Factors

Performance factors for drilled shafts are shown in Table 10–9 taken from the LRFD specifications. Comparing the five methods of analysis shown in Table 10–8, it is evident that their application may result in widely divergent estimations of bearing capacity for the same conditions. Since data from field tests are limited, it is not possible to recommend values of performance for drilled shafts in sands and gravels. Hence, these values should be used with judgment so that the design may be consistent with results obtained from ASD procedures. The inherent greater variability of shaft capacity in sands suggests that resistance factors in this case should be smaller than for shafts in clay.

10.9 BEARING CAPACITY FROM LOAD TESTS

The foregoing analyses provide a rational basis for estimating the ultimate bearing capacity of drilled shafts as the sum of shaft and base resistance, but give no indication of the probable subdivision of this capacity between side resistance and base bearing. A main point is that shaft resistance is usually developed at much smaller vertical displacements than base bearing.

The load test (Reese and O'Neill, 1969) shown in Figure 10–7 illustrates the transfer of load and the development of resistance as a combination of two separate contributions. The drilled shaft has a diameter of 30 inches, and is 23 feet long. The load transfer curves suggest the following behavior:

Table 10–9 Resistance Factors for Geotechnical Strength Limit States in Axially Loaded Drilled Shafts, LRFD Specifications

	Method/Soil/Condition		Resistance Factor
Ultimate Bearing Resistance of Single Drilled Shafts	Side Resistance in Clay	α-method (Reese & O'Neill, 1988)	0.65
	Base Resistance in Clay	Total Stress (Reese & O'Neill, 1988)	0.55
	Side Resistance in Sand	1) Touma & Reese (1974) 2) Meyerhof (1976) 3) Quiros & Reese (1977) 4) Reese & Wright (1977) 5) Reese & O'Neill (1988)	See Discussion in Text
	Base Resistance in Sand	1) Touma & Reese (1974) 2) Meyerhof (1976) 3) Quiros & Reese (1977) 4) Reese & Wright (1977) 5) Reese & O'Neill (1988)	See Discussion in Text
	Side Resistance in Rock	Carter & Kulhawy (1988) Horvath and Kenney (1979)	0.55 0.65
	Base Resistance in Rock	Canadian Geotechnical Society (1985) Pressure Method (Canadian Geotechnical Society, 1985)	0.50 0.50
	Side Resistance and End Bearing	Load Test	0.80
Block Failure	Clay		0.65
Uplift Resistance of Single Drilled Shafts	Clay	α-method (Reese & O'Neill, 1988) Belled Shafts (Reese & O'Neill, 1988)	0.55 0.50
	Sand	1) Touma & Reese (1974) 2) Meyerhof (1976) 3) Quiros & Reese (1977) 4) Reese & Wright (1977) 5) Reese & O'Neill (1988)	See Discussion in Text
	Rock	Carter & Kulhawy (1988) Horvath & Kenney (1979) Load Test	0.45 0.55 0.80
Group Uplift Resistance		Sand Clay	0.55 0.55

1. Upon application of the first load increment (approximately 25 kips), shaft resistance (side shear) develops practically along the entire shaft length. The shaft resistance Q_{si} for any segment length ΔL_i may be obtained as the difference in shaft load between the top and the base of the element. The sum of these contributions is simply the load $P = 25$ kips.
2. When the second load increment is applied (approximately 64 kips), the load transfer is again accomplished by shaft resistance indicated by the non-parallel curves although a very small tip resistance is present.
3. The application of the third increment (approximately 170 kips) produces a limiting value in the shaft resistance, indicating that the ultimate shaft resistance has been reached and that additional load is now resisted by base bearing (approximately 15 kips).
4. The addition of the last load increment (approximately 280 kips) produces the load

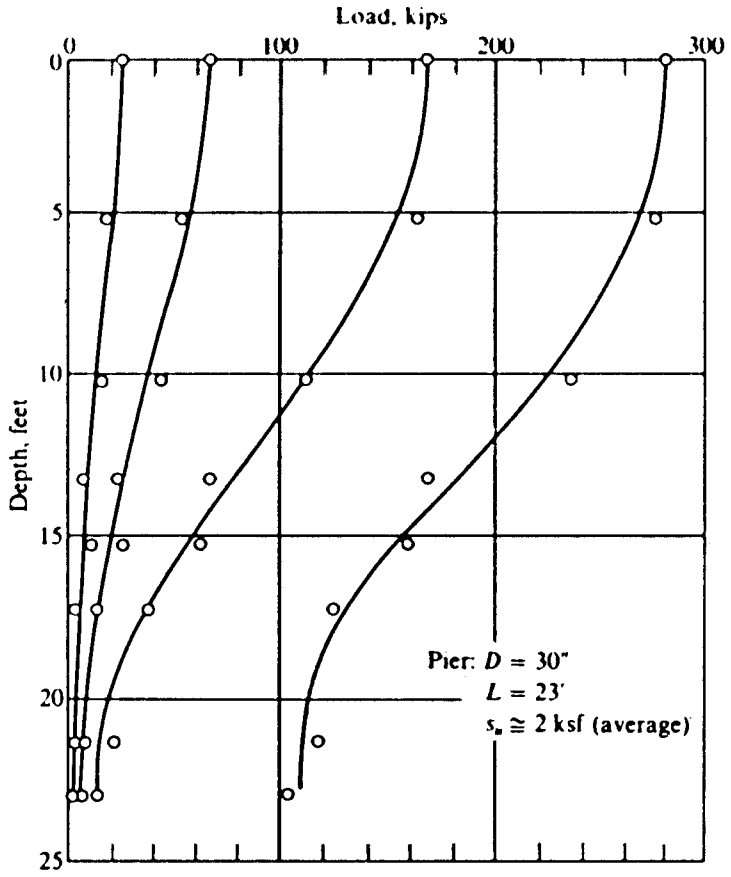

Figure 10–7 Load distribution for drilled pier *(from Reese and O'Neill, 1969).*

transfer curve shown at the extreme right. The side resistance remains practically unchanged as can be seen from the nearly parallel curves between the third and the fourth load increment, so that the additional load is now carried by base bearing.

Referring again to Figure 10–7 and considering the loading stages, the following comments are made:

1. For an ultimate load of 280 kips, the subdivision between shaft resistance and base bearing is as follows: shaft resistance Q_s = 170 kips, base bearing Q_p = 110 kips.
2. From the actual shaft resistance developed in this case, Q_s = 170 kips, and for the given value of s_u = 2 kips/ft, the adhesion factor α is calculated as

$$\alpha = \frac{Q_s}{\pi D L s_u} = \frac{170}{23 \times 3.14 \times 2.5 \times 2} = 0.47$$

which is in fairly good agreement with the values of α obtained directly from Table 10–6. If an effective length of 23–5 = 18 feet is used, α is calculated as 0.60, which is even closer to the value of 0.55 shown in Table 10–6.

3. It appears that, despite the simple format and straightforward formulas, the estimation of the ultimate bearing capacity of drilled shafts is not a simple problem, because it involves a complex load distribution process. In most cases the entire shaft resistance may have to be mobilized before any load can be transferred by base bearing.
4. Because maximum shaft resistance and base bearing are not developed simultaneously, some practitioners have chosen to use one or the other rather than a combination, although this is unduly conservative. Alternatively, designers may attempt to use an interaction to obtain the ultimate bearing capacity as a combination of shaft resistance and base bearing (see also subsequent sections).

10.10 AXIAL RESISTANCE IN ROCK

Drilled shafts may be socketed in rock to limit vertical displacement, increase the load-carrying capacity, or provide fixity for resistance against lateral loads. Typically, the side resistance from overlying soils are ignored. A recommendation is to provide a socket depth one to three times the shaft diameter (Canadian Geotechnical Society, 1985). The design procedures usually assume that (1) the socket is constructed in sound rock that is not expected to degrade when excavated and exposed to air-water effects, (2) the drilling fluid will not act as lubricant along the sides of the excavation, and (3) the bottom is thoroughly cleaned.

Where the rock socket capacity is derived primarily from side shear, the settlement within the socket will be small. When the load capacity is based primarily on base bearing, the associated settlement may be large and should be checked.

The design procedure assumes that the axial load is carried entirely by side resistance if the computed settlement is less than 0.4 inch. When the settlement exceeds this value, slip occurs between the concrete element and the rock. At this stage any additional load is resisted by base bearing, whereas the side resistance is assumed to reduce to zero. This approach may be overconservative, and alternate procedures are available for proportioning the ultimate load between side and tip resistance (Carter and Kulhawy, 1988).

The design procedure involves the following steps:

1. Estimate the settlement of the section socketed in rock. This consists of two components: (a) the elastic shortening P_e that is computed from elastic methods and (b) the settlement of the base which can be computed as

$$P_{base} = \frac{(\Sigma P_i) I_p}{D_s E_r} \tag{10–22}$$

where I_p = influence coefficient obtained from the graphs of Figure 10–8; D_s = diameter of the base of the socket (ft); and E_r = modulus of elasticity of the rock (tons/ft^2). The rock modulus E_r (in situ) may be estimated from

$$E_r = K_E E_i \tag{10–23}$$

where E_i = intact rock modulus found either by testing or estimated from Figure 10–9 (tons/ft^2); and K_E = modulus modification ratio related to RQD (rock quality designation) as shown in Figure 10–10.

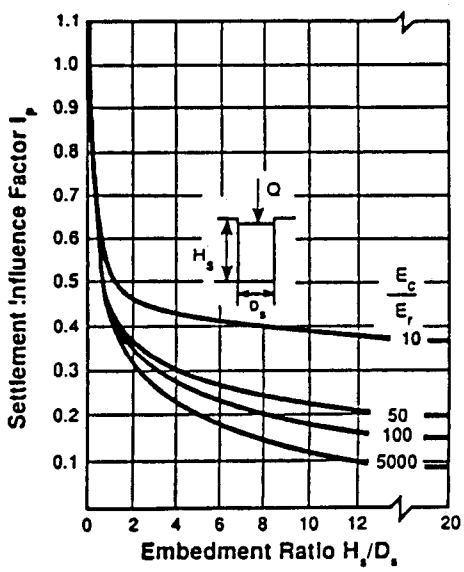

Figure 10–8 Elastic settlement influence factor as a function of embedment ratio and modular ratio *(from Reese and O'Neill, 1988).*

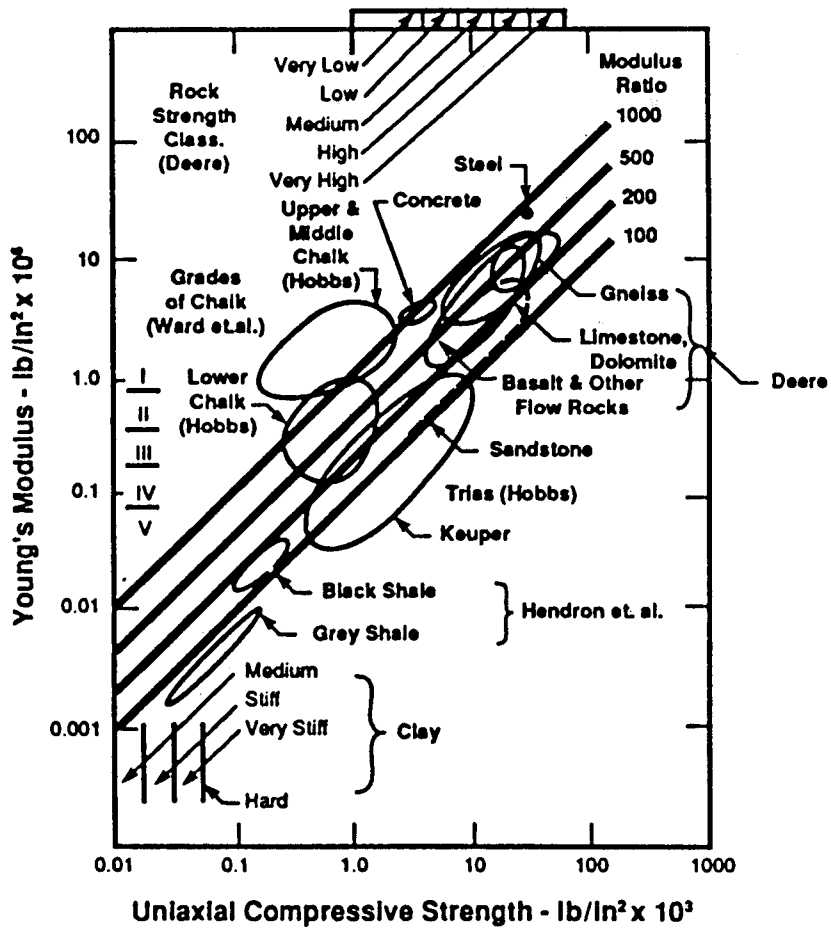

Figure 10–9 Engineering classification of intact rock *(from Reese and O'Neill, 1988).*

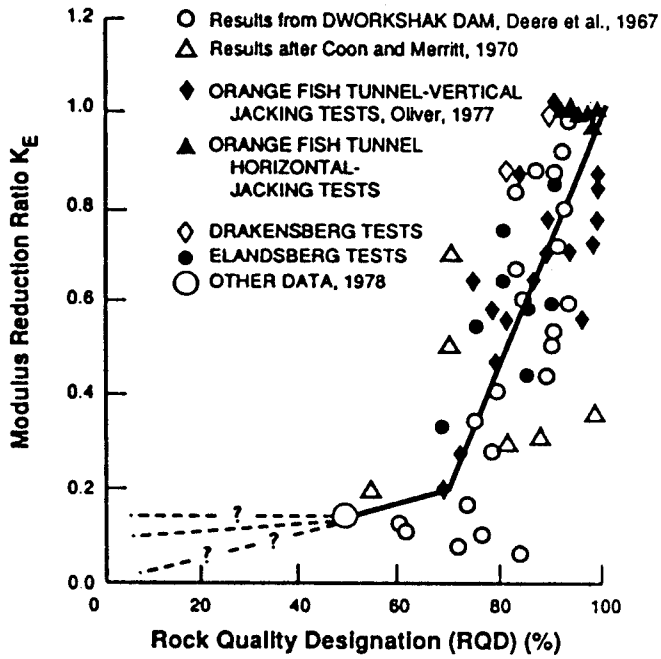

Figure 10–10 Modulus reduction ratio as a function of RQD *(from Reese and O'Neill, 1988).*

2. Calculate the sum $P_e + P_{base}$. If this is less than 0.4 inch, the bearing capacity is computed based on shaft resistance alone (step 3). If the sum is greater than 0.4 inch, the bearing capacity is computed based on base resistance alone (step 4).
3. Determine the side resistance as follows: If the uniaxial compressive strength of the rock q_u is less than or equal to 280 lb/in^2, the ultimate unit side resistance is (Carter and Kulhawy, 1988)

$$q_s = 0.15 q_u \tag{10–24}$$

If q_u exceeds 280 lb/in^2, the side resistance is given by Horvath and Kenney, (1979) as

$$q_s = 2.5\sqrt{q_u} \tag{10–24a}$$

where q_s and q_u are in lb/in^2.

4. Estimate the base resistance of the drilled shaft socket from the uniaxial compressive strength as follows (Canadian Geotechnical Society, 1985):

$$q_p = 3 q_u K_{sp} d \tag{10–25}$$

where q_u = average uniaxial compressive strength of the rock, and K_{sp} = dimensionless bearing capacity coefficient. The coefficient K_{sp} is given by

$$K_{sp} = \frac{3 + s_d / D_s}{10(1 + 300 t_d / s_d)^{0.5}} \tag{10–26}$$

where d = dimensionless depth factor = 1 + 0.4 $H_s/D_s \leq 3.4$; s_d = spacing of rock discontinuities; t_d = width or thickness of discontinuities; D_s = diameter of socket; and H_s = embedment of socket = 0 for drilled shafts resting on bedrock.

The foregoing method is not applicable to soft stratified rocks such as shale or limestone. Where the method is applicable, the rock strength is usually extremely sound, so that the design is governed by the structural capacity of the reinforced concrete member. The method is applicable only if $s_d > 1$ foot and $t_d < 0.25$ inch for unfilled discontinuities, or $t_d < 1$ inch for discontinuities that are filled with soil or rock debris, and $D_s > 1$ foot.

When pressuremeter tests are carried out, results can be used to estimate the base resistance (Canadian Geotechnical Society, 1985). In this case

$$q_p = K_b(p_1 - p_o) + \sigma_v \tag{10–27}$$

where p_1 = limit pressure estimated from the pressuremeter test averaged over a distance of two diameters above and below the base; p_o= at rest horizontal earth stress at the base level; σ_v = total vertical stress at the base level; and K_b = dimensionless coefficient depending on the socket diameter as shown in Table 10–10.

Alternatively, the coefficient K_{sp} may be obtained by reference to Figure 10–11, where all terms are self-explanatory.

Load tests. Where conditions warrant, full scale load tests should be carried out on drilled shafts to confirm the structural behavior and response to the applied loads. Load tests should be planned, devised, and conducted in the field according to prescribed standards and modified as necessary for the actual site conditions.

Full scale drilled shafts installed under the same construction procedures should be used as test elements and loaded in a manner that will disclose the structural response and provide data on the load capacity, load transfer characteristics, division of load between shaft resistance and base bearing, load-displacement mechanism, and will also allow an assessment of the validity of the design assumptions. A load-deformation response at the top of the shaft should, as a minimum, be obtained.

The test scope and range may include compression, uplift, lateral load, or their combinations. The test results should reflect the effect of the soil conditions, rock, groundwater, and construction procedures (for example, bottom cleaning, the use of casing, slurry, and so on).

In many instances it will be desirable to obtain a plunging failure. However, a test concluded in this manner may be economically or physically unwarranted or impractical because it may require exceptionally heavy test loads. In such cases, the load test should be continued until the base of the shaft undergoes a settlement equal to at least 5 percent of the base diameter.

10.11 GROUP ACTION

As is the case with pile groups (section 9.8), the behavior of groups of drilled shafts in cohesive soils is influenced by the top conditions, and largely depends on whether the cap is in contact with the ground. If this contact is maintained, a group of shafts, consisting of the shafts together with the block of soil contained within the block, may fail as a unit. The ultimate bearing capacity in this case may be taken as the minimum of the following two values: (1) the sum of the individual capacities, or (2) the bearing capacity for block failure of the group.

The analysis may be carried out as in section 9.8. Referring to Figure 9–22, the

Table 10–10 Coefficient H_b, LRFD Specifications

H_s/D_s	0	1	2	3	5	7
K_b	0.8	2.8	3.6	4.2	4.9	5.2

term "pile" is simply replaced by the notation "shaft." The bearing capacity for block failure is given by Equation (9–42), where the term N_c is computed from Equation (9–43) or (9–44).

If the cap is not in firm contact with the ground and the clay is normally consolidated, slightly overconsolidated, or sensitive, the individual shaft capacity should be multiplied by an efficiency factor n. This factor may be taken as 0.7 for a center-to-center spacing of $3D$, and 1.0 for a shaft spacing of $6D$ (Reese and O'Neill, 1988). The value of n may be interpolated for intermediate spacing.

If the cap is not in firm contact with the ground, and the clay is heavily overconsolidated and insensitive, the group capacity should be estimated as in the case where the cap is in contact with the ground.

The construction of drilled shafts in sand causes stress relief. The sand may also undergo a decrease in its density during construction. In this case the ultimate bearing capacity of the shaft group may be estimated by multiplying the sum of the ca-

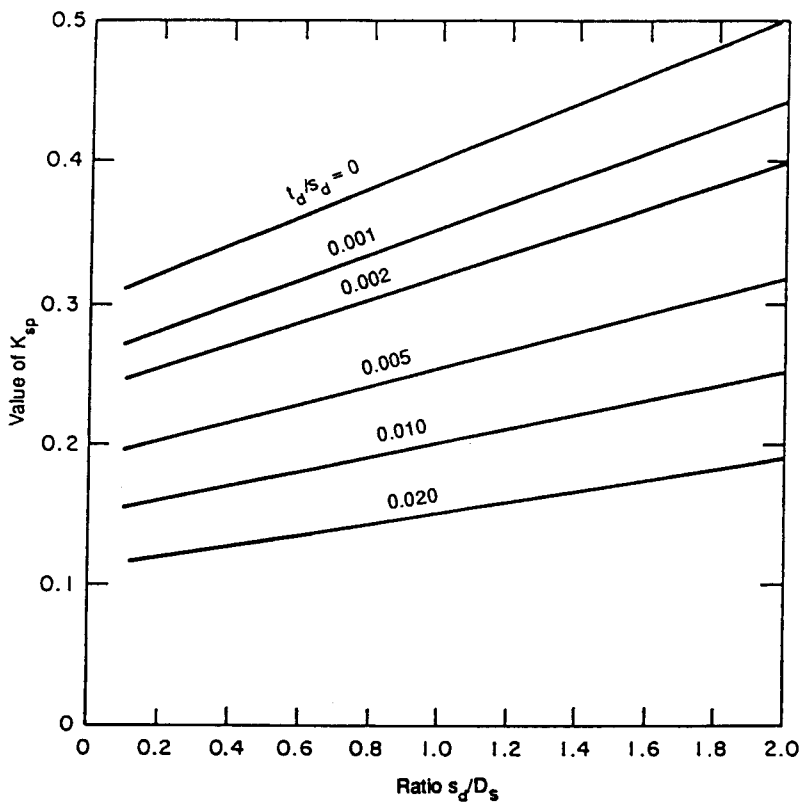

Figure 10–11 Bearing capacity coefficient, K_{sp} *(from Canadian Geotechnical Society, 1985).*

pacities of all the shafts in the group by an appropriate efficiency factor. This factor is defined as the ratio of the ultimate load capacity of the group to the sum of the individual capacities. According to Reese and O'Neill (1988), it can be taken as the factor n in clays.

Block failure is also likely when the base of a group of shafts overlies a layer of soft soil which is much weaker than the layer where the group is terminated. The bearing capacity may be computed now as

$$q_p = q_o + \frac{(q_1 - q_o)H}{10X} \leq q_1 \tag{10–28}$$

where q_o = bearing capacity of base if it were at the top of the lower (weak) soil; q_1 = bearing capacity of base in the upper soil with the softer lower soil absent; H = vertical distance from the base of the group shaft to the top of the weak layer; and X= width (least horizontal dimension) of the group.

The resistance factors for the group capacity calculated using the sum of individual capacities should be the same as for single shafts. However, a separate performance factor is suggested when block failure is investigated.

10.12 SAFETY FACTORS FOR ASD

For drilled shafts in soil or socketed in rock, AASHTO stipulates a minimum factor of safety of 2.0 against bearing-capacity failure (end bearing, side resistance, or combined) when the design is based on the results of load tests conducted at the site. Otherwise, shafts should be designed for a minimum factor of safety of 2.5. These values are based on a normal level of field quality controls. If this level cannot be assured, the factors of safety should be increased.

For the general case the working stress method involves a semiempirical prediction of the peak-load transfer, that is, the ultimate load discussed in the foregoing sections. A working load is then obtained by dividing the ultimate resistance by an appropriate factor of safety, and Equation (10–13) is derived.

Because the ultimate shaft and base resistance are reached at different vertical displacements, two different factors of safety must be introduced. Accordingly, the working load is obtained from Equation (10–8) as

$$P_W = \frac{Q_s}{F_s} + \frac{Q_p}{F_p} \tag{10–29}$$

where Q_s and Q_p are as previously, and F_s and F_p are the factors of safety for shaft and base resistance. If F is the factor of safety relating P_W and Q_{ult} ($P_W = Q_{ult}/F$), we can easily obtain

$$F = \frac{F_s F_p (1+R)}{F_s + F_p R} \tag{10–30}$$

where $R = Q_s/Q_p$.

For the usual problems F_p may be taken the same as F_s in which case they should be at least 2 and preferably 2.5. Where base bearing is rather uncertain compared with shaft resistance, or where the tip resistance constitutes the larger fraction of the total load capacity, a greater factor of safety is suggested, and close to 3. In this case the factor of safety for combined shaft and base load should be close to 2.5.

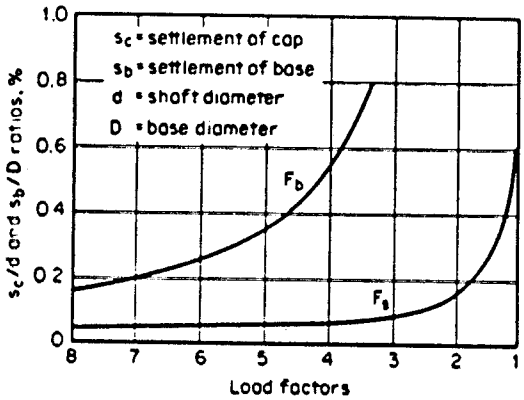

Figure 10–12 Examples of curves relating load factors with s_c/d and s_b/D for use in design *(from Whitaker and Cooke, 1965).*

A more rational approach to the safety factor problem is possible if the shaft and base deformation compatibility is known (Whitaker and Cooke, 1965). An example based on an experimentally derived relationship between shaft and base settlement is shown in Figure 10–12, where the notation is slightly different, with the subscript b denoting base. The mean curves of F_b and F_s are obtained from load-settlement curves and are plotted versus the percentage settlement s expressed in terms of shaft and base diameter. The two curves are far apart because ultimate shaft resistance is reached at much smaller displacements. For example, for s_c/d greater than 0.7 percent F_s is approaching unity indicating that shaft resistance is exceeded. This does not mean that the shaft resistance is now inoperative, but shows that further settlement under load is governed by the response of the base.

Similar curves may be developed for most practical problems. Estimates are first made of the ultimate shaft and base resistance. Assuming that the settlement of the cap (top) and the base (tip) are equal to the allowable settlement, a value of F_s and an approximate value of F_b can be found from the curves. Working values of shaft and base load are then estimated, the shaft compression is calculated, and the base settlement is recalculated, leading to a second value of F_b from the curve. By successive approximations a more accurate value of F_b is obtained, and allows estimation of the base working load.

Since the foregoing procedure requires an empirical relationship that applies to the test site only and reflects the actual duration of the test, it does not include long-term effects (consolidation and secondary settlement). Evidently, a displacement-compatibility determination of the working load results in a greater factor of safety for base resistance than for shaft resistance.

10.13 SETTLEMENT CONSIDERATIONS

Single Shafts

Drilled shafts respond to load much as driven piles. Thus, settlement of shafts installed in sand and rock are usually small and they occur fairly rapidly. However, shafts in clay respond slowly to load and may continue to settle over a longer period of time as consolidation takes place.

In estimating the settlement of drilled shafts in clay, only unfactored permanent

loads should be considered. Transient loads are omitted because they do not contribute to the settlement. However, unfactored live (transient) loads must be included with the permanent loads when estimating the settlement of drilled shafts in sand.

At service loads, the settlement of drilled shafts may be estimated using elastic methods of analysis. AASHTO recommends elastic approach provided the stress level is moderate relative to Q_{ult}. With high stress levels, however, consideration should be given to methods of load transfer.

A summary of load-settlement data for drilled shafts is given by Reese and O'Neill (1988). Figures 10–13 and 10–14 show load-settlement curves for side-resistance and base bearing versus settlement, respectively for shafts in clay. Likewise, Figures 10–15 and 10–16 show similar curves for shafts in sand.

The derivation of the load-settlement curves took into account the elastic shortening of the shaft. Long-term settlement in clay is not reflected in the data of Figures 10–13 and 10–14. Therefore, consolidation settlement should be added to the short-term displacement, but in heavily overconsolidated soils this settlement is usually small.

The settlement due to base load is different for shafts in cohesionless and cohesive soils. Drilled shafts in clay display a well-defined plunging load as is typically inferred from Figure 10–14. Conversely the tip load of shafts in sand continues to increase with

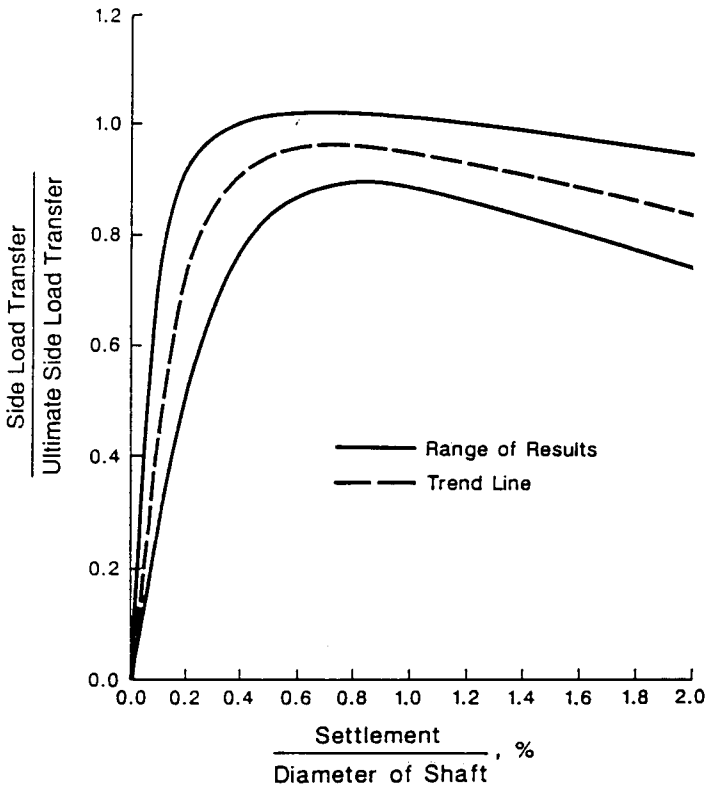

Figure 10–13 Normalized curves showing load transfer in side resistance versus settlement for drilled shafts in clay *(from Reese and O'Neill, 1988).*

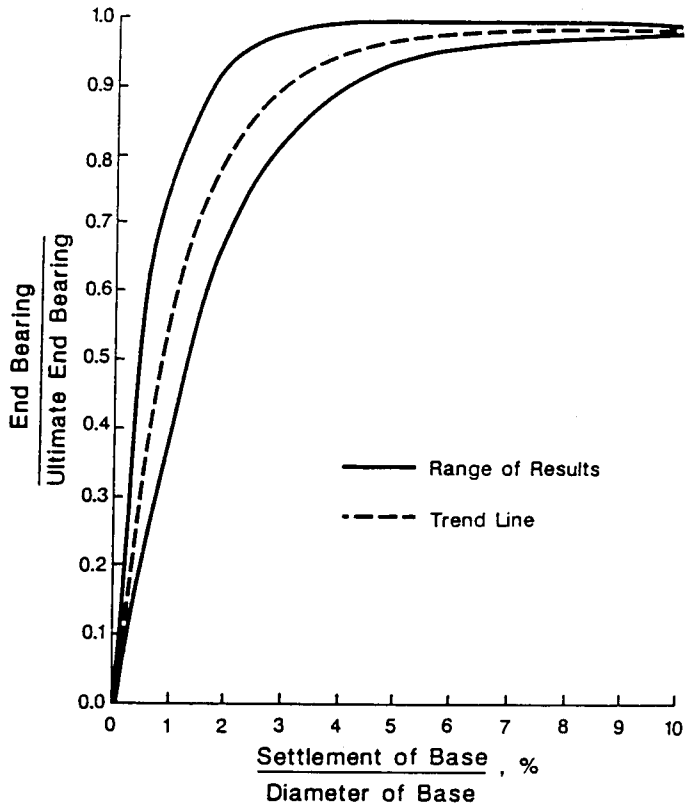

Figure 10–14 Normalized curves showing load transfer in end bearing versus settlement for drilled shafts in clay *(from Reese and O'Neill, 1988).*

increasing settlement beyond 5 percent of the base diameter. The base load Q_p is fully mobilized at displacements of 2 to 5 percent of the base diameter for shafts in clay. For shafts in sand, there is no well-defined failure load at any displacement, as shown in Figure 10–16. In this case, the ultimate unit end bearing is defined arbitrarily as the bearing pressure required to cause a specific settlement, of the order of 5 percent of the shaft diameter, but this does not necessarily correspond to the complete failure of the soil at or beneath the base.

The curves in Figures 10–13 and 10–15 also show the settlement at which the ultimate side resistance is mobilized. This occurs typically at displacements of 0.2 to 0.8 percent of the shaft diameter for shafts in cohesive soils, and at displacements of 0.1 to 1 percent for shafts in cohesionless soils.

For relatively long shafts (length > 100 ft) in either sand or clay, the effect of elastic shortening may be estimated as suggested by AASHTO Article 4.6.5.5. The elastic shortening p_e is computed as

$$p_e = PD / AE_c \tag{10–31}$$

where P = load acting on shaft; D = total shaft length; and A, E_c = cross-sectional area and elastic modulus, respectively. Equation (10–31), however, does not consider any

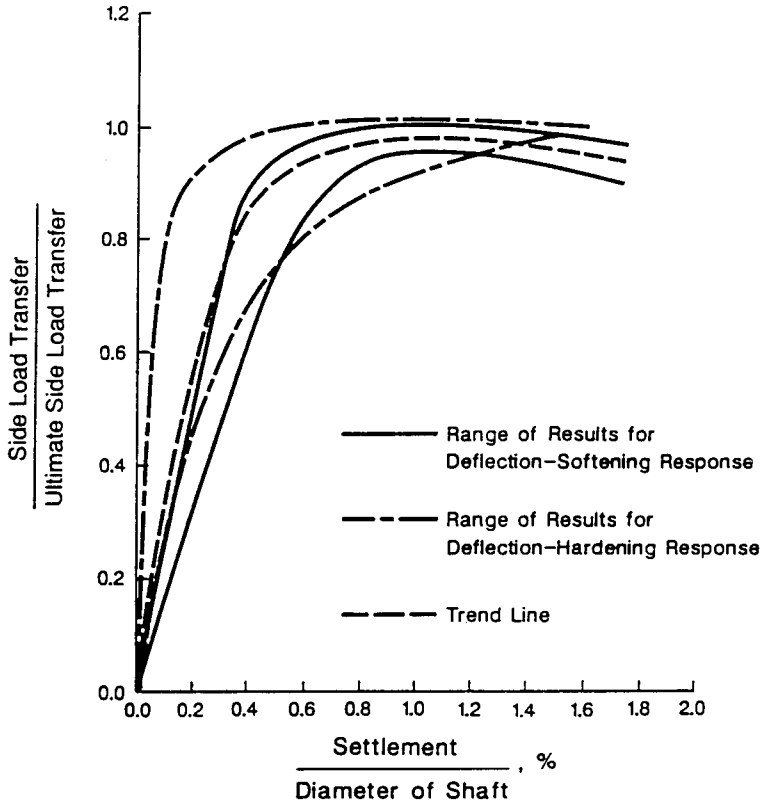

Figure 10–15 Normalized curves showing load transfer in side resistance versus settlement for drilled shafts in cohesionless soils *(from Reese and O'Neill, 1988).*

load absorbed by side resistance along the shaft length, and hence tends to overestimate the elastic shortening.

Group Settlement

The settlement analysis of a group of shafts is essentially similar to the settlement analysis of a pile group discussed in section 9.5. Thus the settlement of a group of shafts generally is larger than the settlement of an individual pile under the same load and soil conditions.

Cohesionless soil. The settlement can be related to the SPT blow count as suggested by Meyerhof (1976). This relationship is expressed by Equation (9–7) and need not be repeated here. The settlement of a group of drilled shafts in silty sand is estimated to be twice the value obtained using Equation (9–7).

Static cone penetration tests may also be used to predict the settlement of a group of drilled shafts. In this case the settlement may be computed from Equation (9–9).

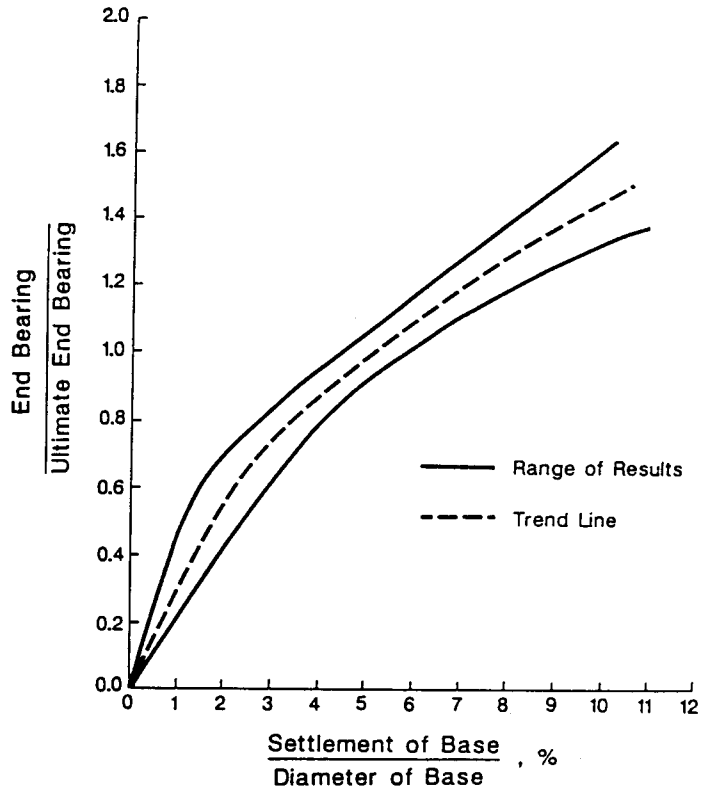

Figure 10–16 Normalized curves showing load transfer in end bearing versus settlement for drilled shafts in cohesionless soil *(from Reese and O'Neill, 1988)*.

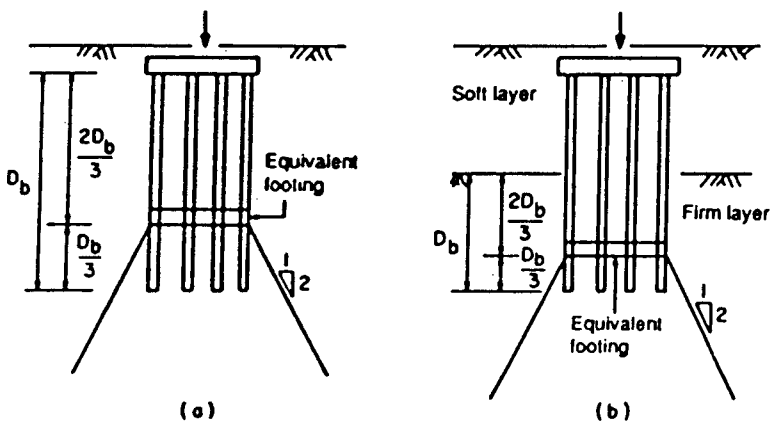

Figure 10–17 Location of equivalent footing *(from Duncan and Buchignani, 1976)*.

Cohesive soils. The settlement of a group of drilled shafts in clay will probably take place over a long period of time. The long-term effects may be estimated using the same procedures that apply to shallow foundations. The load on the group of shafts is assumed to be transferred to the soil through an equivalent footing located at two-thirds the depth of the shafts, as shown in Figure 10–17.

The total settlement of a group of shafts in clay is the total of three contributions, namely immediate settlement, consolidation settlement, and secondary compression. It can be estimated using the same procedures as in shallow foundations.

In practice, the adequacy of a drilled shaft foundation with regard to the tolerable settlement may be inferred from the estimated individual or group shaft settlement. If the predicted settlement for the individual shaft exceeds the tolerable, the usual remedy is to increase the length of the shaft or its base diameter and repeat the analysis. If the predicted settlement of the group exceeds the tolerable, the usual solution is to use more shafts, or increase their length and spacing.

10.14 NEGATIVE SKIN RESISTANCE (DOWNDRAG)

As mentioned in section 9.10, negative skin resistance is a downdrag force introduced when the surrounding soil moves downward relative to the shafts. This can occur because of the placement of fill, groundwater fluctuations, or it may have its origin from other sources.

Methods for estimating negative skin friction were discussed in section 9.10 for driven piles, and may be applied also to the analysis of drilled shafts. When using the α method, the top five feet and bottom one stem diameter should be deducted from the shaft length as noncontributing to the load transfer. An allowance should also be made for a possible increase in the undrained shear strength of the clay with time as the consolidation process continues. The use of the β method (effective stress analysis) is a viable alternative where the long-term conditions following consolidation must be considered. In this case, the unit negative skin friction q_{sn} is calculated as

$$q_{sn} = \beta\sigma'v \tag{10–32}$$

and the total downdrag force is

$$P_{sn} = q_{sn}a_s D_n \tag{10–33}$$

where P_{sn} = downdrag load; a_s = perimeter of drilled shaft; and D_n = shaft length assumed to be effective.

Whereas downdrag loads are unlikely to cause capacity problems, they may increase the settlement of the foundation. The settlement of drilled shafts should be checked for downdrag and dead loads acting together. Transient loads should not be considered with downdrag forces, because the former tend to compress the shaft elastically and counteract the effect of the latter. When the transient load is no longer applied, the drilled shaft will rebound elastically thus restoring the downdrag load.

If the downdrag load exceeds the live load, the structural and soil capacity should be checked for dead load plus downdrag. The procedure is similar to driven piles under the same conditions, and the stability criterion is expressed by Equation (9–51).

Neutral Plane

In section 9.10, the neutral plane was defined as the elevation at which the settlement of the member is the same as the settlement of the soil. This interrelationship is shown conceptually in Figure 9–24. For drilled shafts, the two curves likewise intersect at the neutral plane, and this defines the location of the maximum load on the member. The neutral plane of drilled shafts bearing on rock is located at their base.

10.15 UPLIFT RESISTANCE

Single Shaft

Soil capacity. Uplift resistance should be considered when drilled shafts are subjected to upward loads. The shafts in this case should be checked for structural strength and resistance to pullout.

The uplift resistance of a single shaft, straight sided, may be estimated as for a drilled shaft in compression. The uplift resistance of a belled shaft may be predicted neglecting the side resistance above the bell. In this case, the bell is assumed to behave as an anchor. The resistance factors for uplift are logically lower than those for axial compression because (1) the diameter contracts due to Poisson's effect, and (2) drilled shafts in tension unload the soil. These effects reduce the effective overburden stress and the lateral stress coefficient and hence the uplift side resistance.

The design requirement for uplift is expressed as follows:

$$\phi_u Q_s \geq P_{x,y} \tag{10–34}$$

where Q_s = ultimate uplift capacity due to shaft resistance; $P_{x,y}$ = factored tensile load acting on the drilled shaft, and ϕ_u = resistance factor for uplift.

For enlarged bases and neglecting side resistance, the uplift capacity may be computed as

$$Q_{s,bell} = q_{s,bell} A_u \tag{10–35}$$

The factor $q_{s,bell}$ is the unit uplift capacity of the belled shaft, computed as

$$q_{s,bell} = N_u s_u \tag{10–36}$$

where N_u is an uplift adhesion capacity factor, and s_u is the undrained shear strength over a distance of 2 D_p above the base. If the soil above the foundation level is expansive, s_u should be averaged over 2 D_p above the base, or over the depth of penetration D_b, whichever is less, where D_b and D_p are as shown in Figure 10–18. Also, A_u = $\pi (D_p^2 - D^2)/4$ where D = shaft diameter.

The value of N_u varies from 0 at D_b/D_p = 0.75 to 8 at D_b/D_p = 2.5 (Yazdanbod, Sheikh, and O'Neill, 1987). The top of the founding stratum D_b should be taken at the base of the zone of seasonal moisture change. The procedure ignores the uplift resistance contribution due to soil suction and the weight of the element, hence gives conservative results. This procedure is recommended by the LRFD specifications.

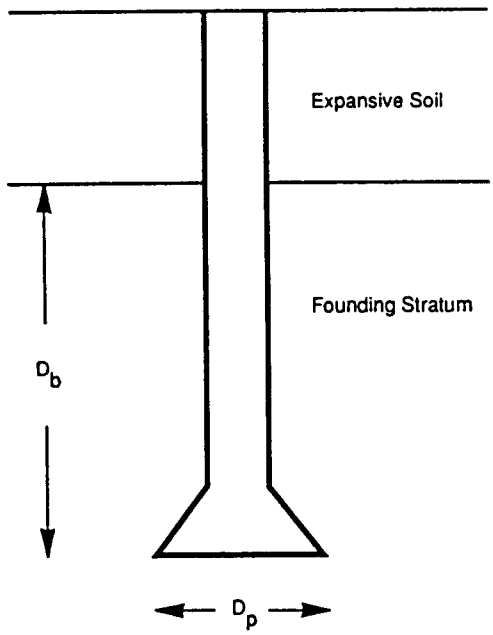

Figure 10–18 Uplift of an underreamed drilled shaft.

Structural capacity. The uplift structural capacity should ignore any tensile strength of the concrete, and should be estimated considering the tensile reinforcement. This yields

$$\phi_t f_y A_y \geq P_{x,y} \tag{10–37}$$

where f_y is the tensile strength of the reinforcing steel, and A_y is the total steel area. The performance factor ϕ_t is 0.9.

Group of Shafts

The ultimate uplift capacity of a group of drilled shafts may be taken as the lesser of two values: (1) the sum of the individual shaft uplift capacities, or (2) the uplift capacity of the group considered as a block. Essentially, the analysis is similar to the behavior of a group of piles discussed in section 9.9.

The shaft resistance of the group in sands should be expected to deteriorate under vibratory effects or where lateral loads are present. A suggested interaction between the group and surrounding soil is shown in Figure 9–23(a) and applies to both piles and drilled shafts. Likewise the uplift resistance of a group of shafts in clay may be inferred from Figure 9–23(b), and quantitatively it is expressed by Equation (9–46).

10.16 DRILLED SHAFTS UNDER LATERAL LOAD

Lateral loads on drilled shafts arise from wind, earthquake, water pressure, earth pressure, and live load traction. Where expansion bearings are provided, lateral loads are associated with friction.

In section 9.11, we discussed the design requirements of pile foundations subjected

to lateral load effects. A usual solution in this case is the use of batter piles to receive and transmit these loads to the ground. However, with drilled shafts, construction of batter elements is difficult and impractical; therefore, their use is discouraged.

As in pile foundations, the two controlling criteria of drilled shaft analysis for lateral load are the structural capacity and the maximum lateral displacement that can be tolerated. A quantitative assessment of tolerable lateral displacement cannot be standardized, because it must be consistent with the function and type of structure, restraint and fixity level of bearings, anticipated service life, and consequences of unacceptable displacement on the expected structural performance. AASHTO (Article 4.6.5.6.2) stipulates that lateral displacement analysis should be based on the results of in situ or laboratory tests to characterize the load/deformation behavior of the foundation elements. Whereas ultimate soil failure is unlikely to occur since it will require exceptionally large displacements, structural capacity and tolerable lateral deflection are the prime factors to be considered.

Short Rigid Shafts

For short rigid shafts, a usual assumption is that the member will rotate rigidly about a point designated as the center of rotation as shown in Figure 10–19 so that a resisting moment is developed on the base from the toe and heel pressure profiles qualitatively presented.

It may appear that if the correct interaction of a rigid pier-soil system is as shown, it will be very difficult to model in any computer program unless a load test is available to supplement the approach. Bowles (1988) suggests that, unless the shaft length/width ratio is less than about 2, this model is not likely to develop. Very short stub shafts with length/width ratio less than about 2 may be analyzed as footings with a passive pressure on the shaft approaching the response of a rigid laterally loaded pier.

Lateral load tests on drilled shafts of small length/width ratios tend to confirm that the base rotation shown in Figure 10–19 is inconsequential (Bhushan and Askari, 1984). Results of tests show no discernible difference in capacity for shafts with enlarged base and strength elements. Similar conclusions are reported by Davisson and Salley (1972) from four laterally loaded test shafts.

Based on the assumption that a rigid shaft remains underformed as it rotates about a rotation center as shown in Figure 10–19, several early methods were suggested (Matlock and Reese, 1961; Czerniak, 1957). Nondimensional curves were presented on the premise that the soil modulus varies linearly with depth.

Lateral Deflection, Single Shaft

Three methods are available to predict the deflection of a shaft under lateral load, as in driven piles. There are (1) elastic analysis, (2) subgrade reaction analysis, and (3) p-y analysis. The first two assume that the soil behaves linearly, whereas the p-y approach employs nonlinear models and thus requires computer use and considerable engineering effort.

The actual restraint of the top of a drilled shaft has a decisive influence on the magnitude and pattern of the lateral deflection under load. Shafts embedded in reinforced concrete caps and restrained from rotation are likely to deflect laterally without end rotation. With single connections to the substructure, a drilled shaft will probably translate and also rotate at the top. As a rule of thumb, a shaft with unrestrained top

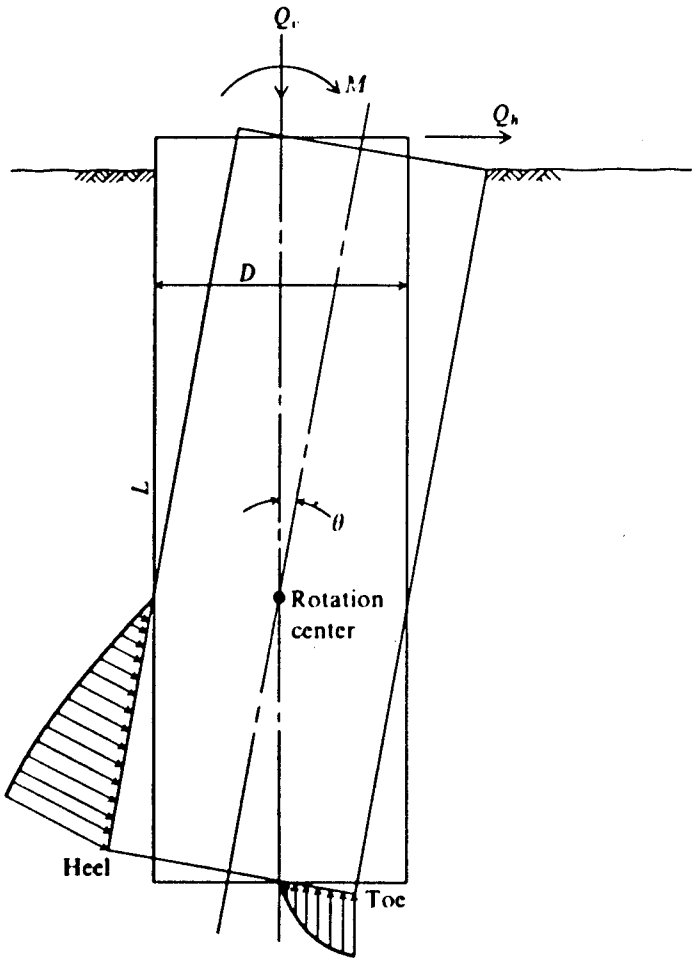

Figure 10–19 Idealization of rigid pier rotation with rotation angle θ greatly exaggerated. The toe and heel pressures will be highly indeterminate. While toe pressure is nearly vertical the heel pressure has both horizontal and vertical components giving the slope shown.

(free-head) has four times the lateral deflection of a fixed-head shaft subjected to the same lateral load.

Fixed head. Evans and Duncan (1982) relate lateral displacement to the lateral loads using the characteristic load P_c, which articulates the important parameters of the shaft (diameter, stiffness) and the soil (strength, stiffness). A large value of P_c indicates a greater capacity to resist lateral loads and a smaller lateral deflection. The procedure applies to drilled shafts with a length/diameter ratio of 10 or greater for shafts in firm soils and 15 or greater for shafts in soft soils.

The procedure is discussed in section 9.11 since it applies also to driven piles, with reference to Figures 9–27, 9–28, and 9–29. Because some of the steps are somewhat different, it is repeated here in the context of drilled shafts. The following steps are involved, based on fixed-head conditions: (P_{sp} is the unfactored lateral load)

1. Select the diameter D, the concrete modulus E_c and the steel reinforcement for the shaft. The parameters entering the analysis are the flexural stiffness of the shaft E_p/I_p, and the moment of inertia ratio R_I (shaft to a solid unreinforced concrete section). The moment of inertia of the shaft is calculated considering the separate contribution of the concrete and the steel, Young's modulus for the shaft E_p is the same as the concrete modulus E_c obtained from Figure 9–29.
2. Estimate the average undrained shear strength s_u for clay and the friction angle ϕ for sand. The same guidelines apply as in section 9.11.
3. Determine the characteristic load P_c making use of Equations (9–54) and (9–55) where R_I = moment of inertia ratio = I_p/I_{SOLID}; where $I_{SOLID} = \pi D^4/64$. Values of R_I may be obtained from Table 10–11.
4. Calculate the load ratio P_{sp}/P_c.
5. Referring to Figures 9–27 or 9–28 determine the value of Y_s/D.
6. Calculate $Y_s = D(Y_s/D)$.

Design aids have been developed based on the Evans-Duncan approach for some commonly used drilled shaft sections. Charts for drilled shafts of 18-, 24-, 30-, and 36-inch diameters for installations in sand are shown in Figure 10–20, and are self-explanatory. Deflections can be obtained by direct reference to the charts, developed for friction angles of 30°, 35°, and 40°. The water table is assumed to be at or above the ground surface. For soils with intermediate friction angles, the lateral deflection may be determined by linear interpolation. Similar charts are available for shafts in clay (Ooi, Rojiani, Duncan, and Barker, 1991) and for undrained shear strengths of 1, 2, and 4 kips/ft^2.

The use of these charts can be demonstrated by a simple example. Consider a lateral load of 30 kips acting on drilled shaft with a 24-inch diameter in sand with $\phi = 35°$. For the percent steel reinforcement, the lateral deflection is obtained from Figure 10–20(a) as 0.16 inch. For 2 percent steel reinforcement, the lateral deflection is found from Figure 10–20(b) as 0.15 inch. For 3 percent steel reinforcement, the lateral deflection is found from Figure 10–20(c) as 0.14 inch. These results are subject to scaling variations.

Free head. Free-head conditions exist where the top of the shaft is not interacted structurally with substructure members. Consider, for example, the drilled shaft shown in Figure 10–21, which is essentially an element extending above the ground and sub-

Table 10–11 R_I Values for Drilled Shafts with E_c = 3500 ksi, E_s = 29000 ksi, and c = 3 inches

	Diameter of Drilled Shaft			
A_s/A_g	*18 inches*	*24 inches*	*30 inches*	*36 inches*
0.01	1.06	1.07	1.09	1.09
0.02	1.11	1.14	1.16	1.18
0.04	1.21	1.27	1.31	1.34
0.08	1.38	1.50	1.58	1.63

where A_s = area of steel and A_g = gross cross-sectional area of drilled shaft

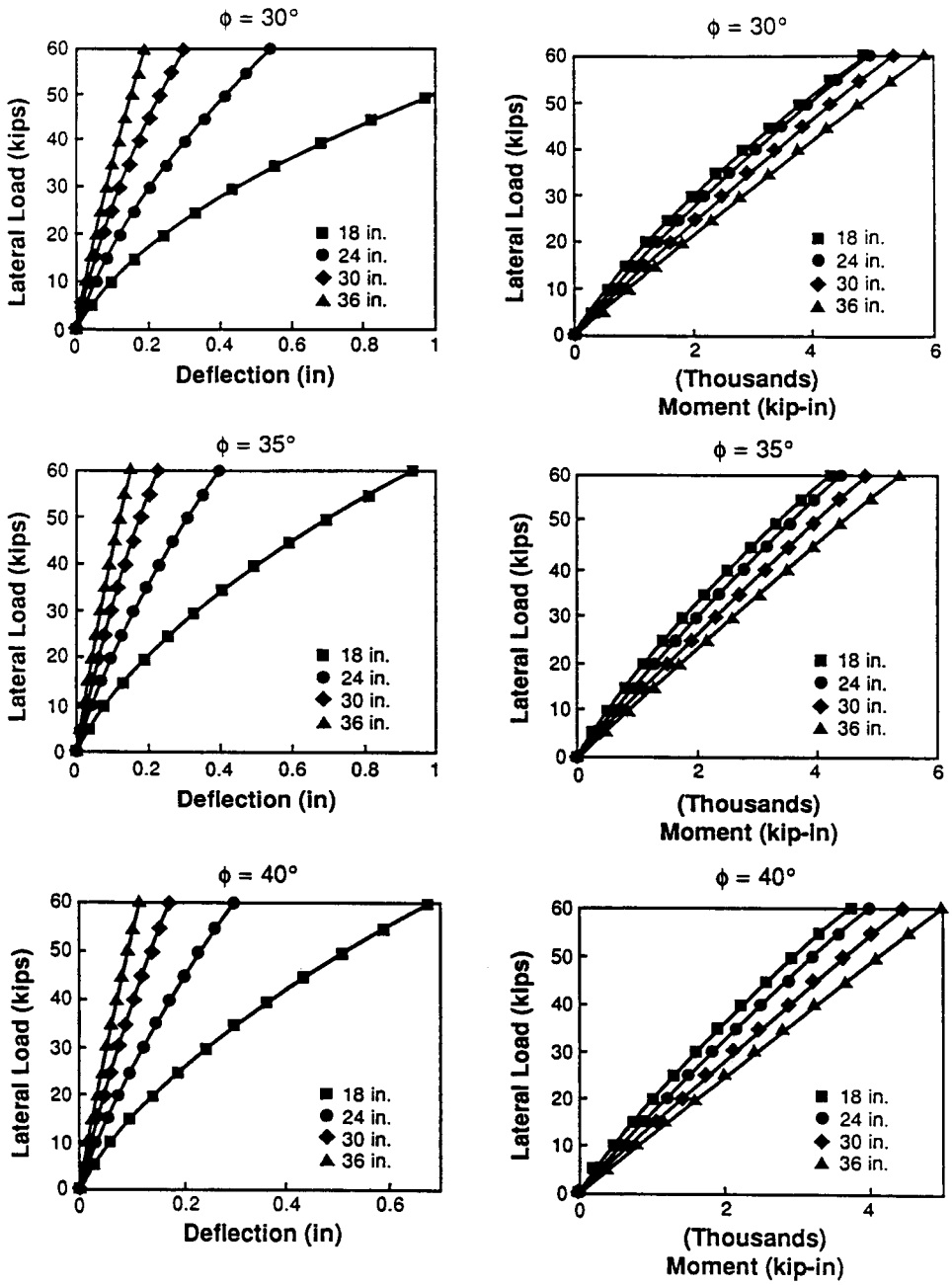

(a)

Figure 10–20 (a) Load versus deflection and load versus moment for drilled shafts (A_s/A_g= 1 percent) in sand; (b) load versus deflection and load versus moment for drilled shafts (A_s/A_g = 2 percent) in sand; (c) load versus deflection and load versus moment for drilled shafts (A_s/A_g = 4 percent) in sand.

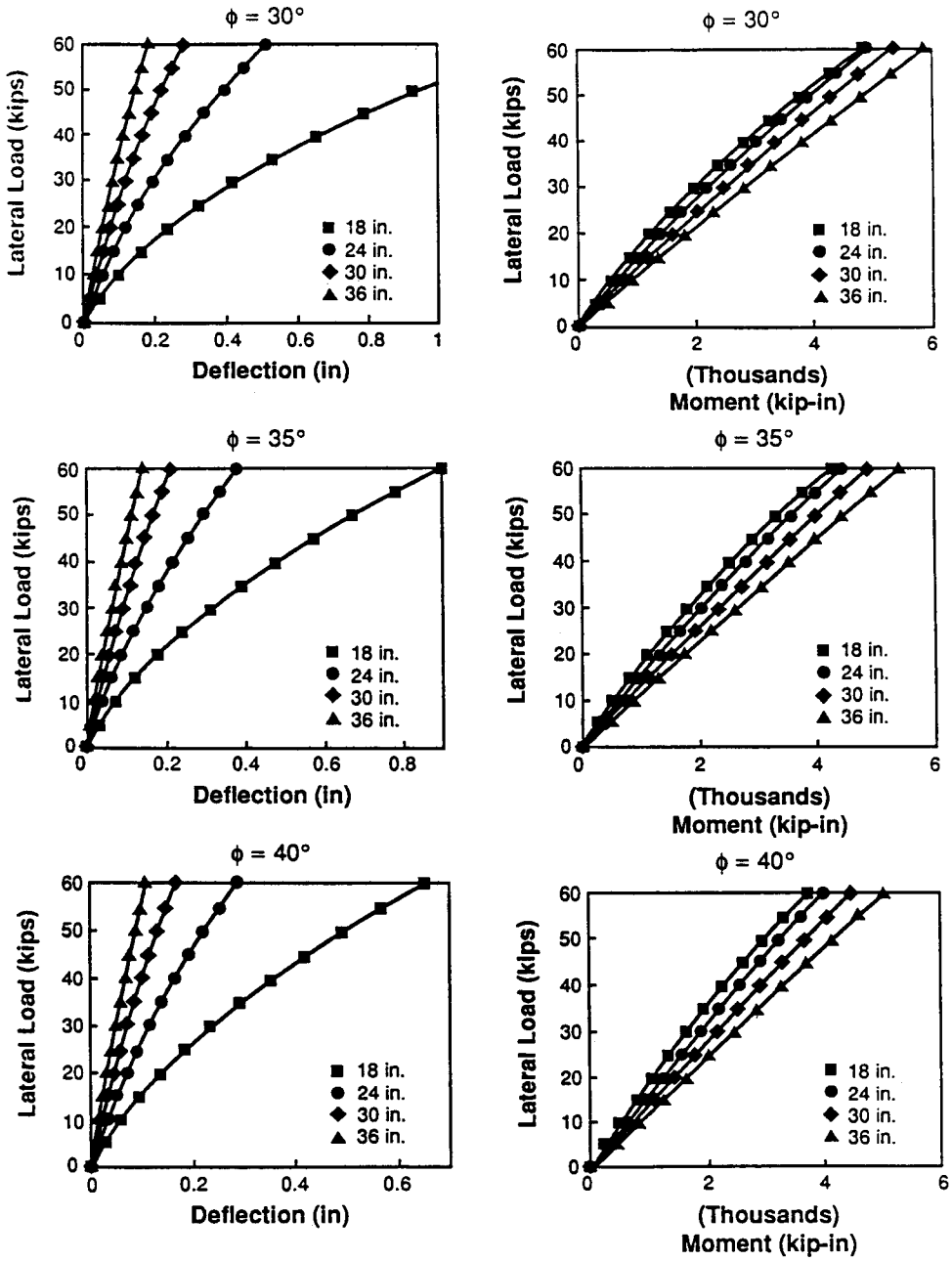

(b)

Figure 10–20 *(continued)*

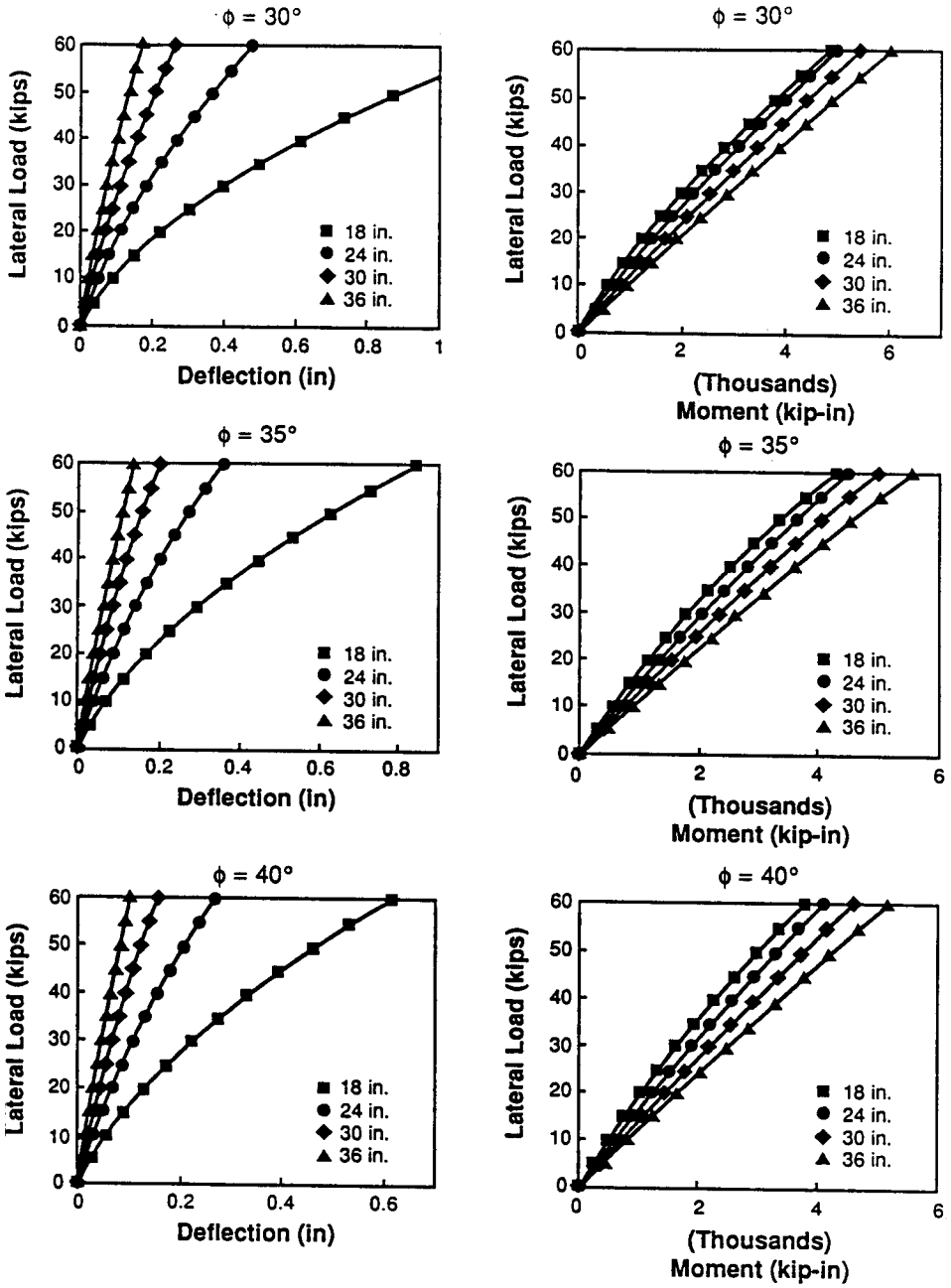

(c)

Figure 10–20 *(continued)*

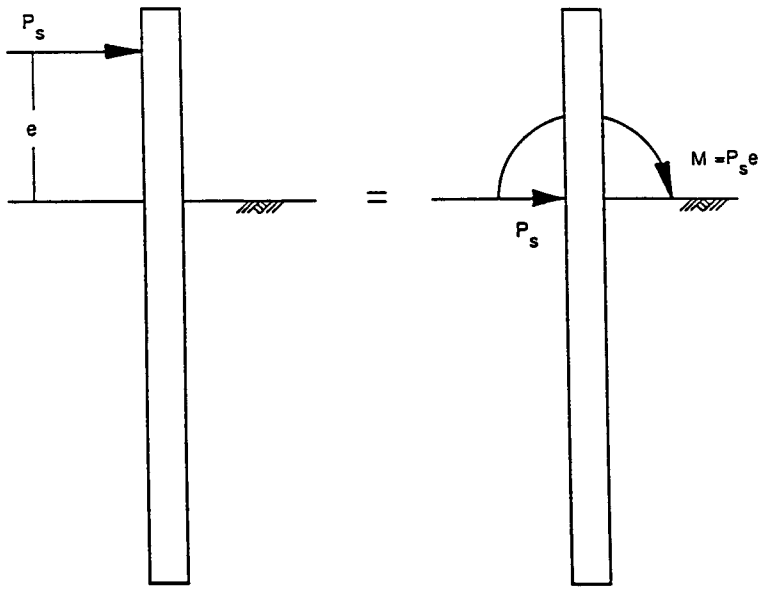

Figure 10–21 Resolution of eccentric load into a lateral load acting on the groundline and a moment.

jected to the effect of a lateral load applied at the top. This condition is resolved into the scheme shown at the right, consisting of a moment and a lateral load acting at ground line as shown. The lateral displacement of the shaft can now be estimated by a nonlinear superposition of the deflection Y_{sp} caused by the lateral load and the deflection Y_{sm} caused by the bending moment.

The component Y_{sp} caused by the groundline lateral load may be found from the graphs of Figures 10–22 and 10–23 for sand and clay, respectively, as in the foregoing procedure. The lateral deflection component Y_{sm} caused by the moment at the top may be estimated following the procedure described for piles (section 9.11). This involves the following steps:

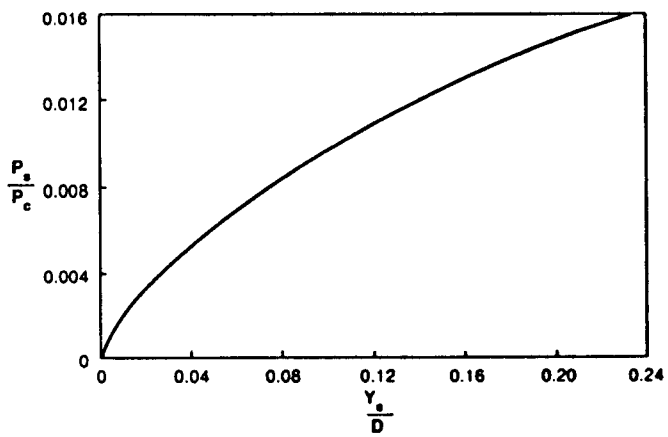

Figure 10–22 Load deformation curves for free-head drilled shafts in sand *(from Evans and Duncan, 1982).*

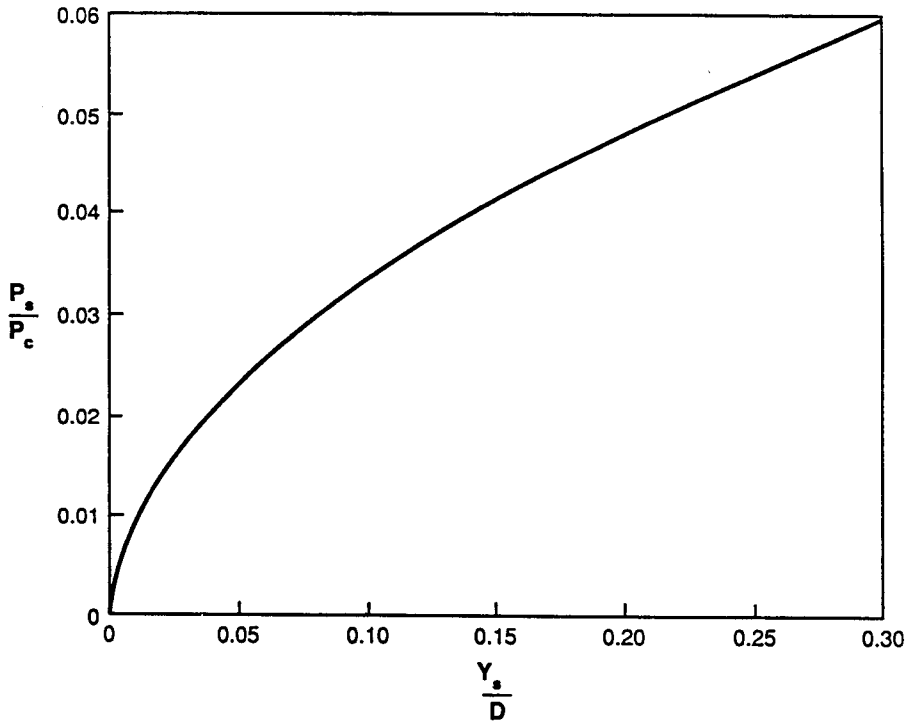

Figure 10–23 Load deformation curves for free-head drilled shafts in clay *(from Evans and Duncan, 1982).*

1. Compute the moment $M_e = P_s e$. (Figure 10–21).
2. Determine the characteristic moment M_c for clay and sand using Equations (9–58) and (9–59), respectively, where the notation is the same, and R_I, K_p, and ϕ' are as defined previously.
3. Calculate the ratio M_e/M_c.
4. With the ratio M_e/M_c known, refer to Figures 10–24 and 10–25 for sand and clay, respectively, to determine the ratio Y_{sm}/D.
5. Calculate $Y_{sm} = D(Y_{sm}/D)$.

With Y_{sp} and Y_{sm} known, the total lateral deflection of the free head shaft can be estimated as suggested by Evans and Duncan (1982) using nonlinear superposition. This involves the following steps:

1. With Y_{sm} and using Figure 10–22 or 10–23, calculate P_m as shown in Figure 10–26(b). P_m is the equivalent lateral load that would cause deflection Y_{sm}.
2. With Y_{sp} and using Figure 10–24 or 10–25, calculate M_p as shown in Figure 10–26(e). M_p is the equivalent moment that would cause deflection Y_{sp}.
3. Determine the deflection Y_{spm} caused by the lateral load $(P_s + P_m)$ as shown in Figure 10–26(c). Y_{spm} is the deflection caused by the sum of the real load plus the equivalent load.

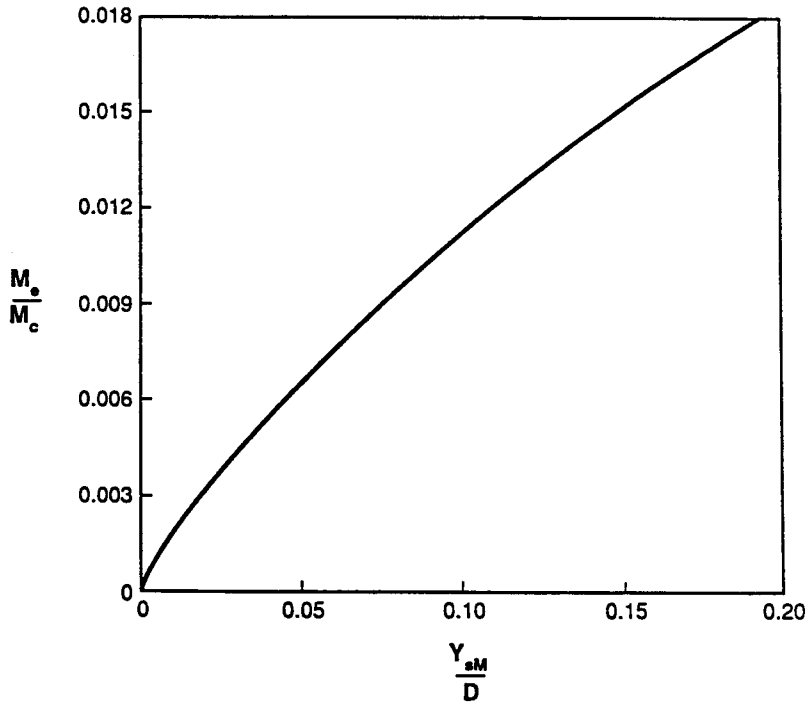

Figure 10–24 Moment deformation curves for free-head drilled shafts in sand *(from Evans and Duncan, 1982).*

4. Determine the deflection Y_{spm} caused by the moment $(M_s + M_p)$ as shown in Figure 10–26(f). Y_{spm} is the deflection caused by the real moment plus the equivalent moment.
5. Calculate the total deflection $Y_s = 0.5(Y_{spm} + Y_{smp})$ from steps 3 and 4.

Lateral Deflection, Groups of Shafts

As in a group of piles, the deflection of a group of shafts will in general be larger than that of a single element for the same load. This increase is probably caused by interaction effects, where the surrounding soil deflects with each individual shaft and thus increases the deflection of neighboring shafts. Investigators caution, however, that with a single row of shafts subjected to a load normal to their line, ground action may not be considered unless the shafts are placed closer than three diameters. Group action should be considered when the lateral load acts along the shaft line.

Fixed head. The analysis of a group of shafts is similar to a group of piles. Thus, the lateral deflection may be computed semi-empirically using Equation (9–56) repeated here for convenience as

$$Y_g = \frac{A + N_{ds}}{B\sqrt{\frac{S}{D} + \frac{P_s}{CP_N}}} Y_s \tag{10–38}$$

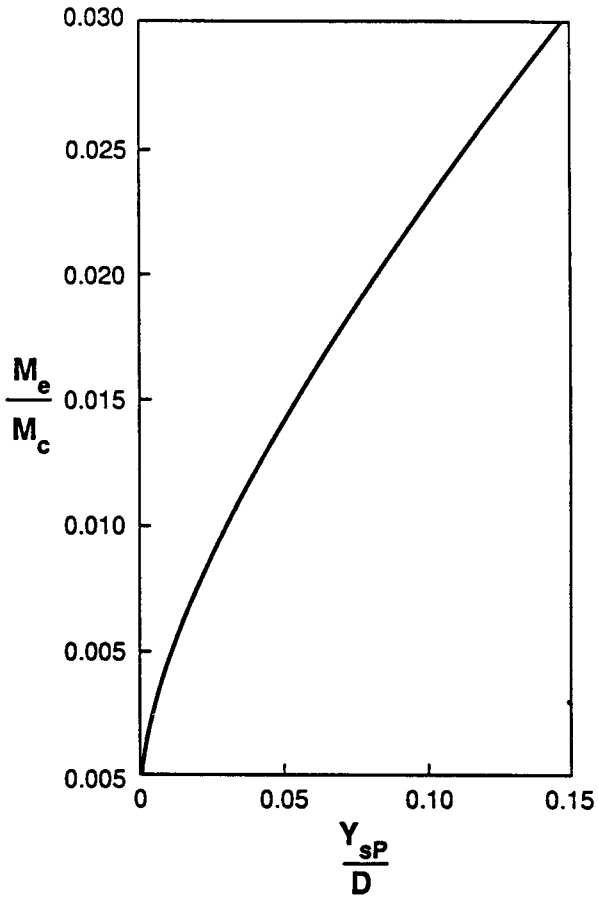

Figure 10–25 Moment deformation curves for free-head drilled shafts in clay *(from Evans and Duncan, 1982).*

where Y_s = lateral displacement of a single fixed-head shaft subjected to a lateral load P_s; N_{ds} = number of shafts in the group; S = average shaft spacing; D = shaft diameter; P_s = average lateral load per shaft = P_{yg}/N_{DS}; P_{yg} = lateral load on the group; and

$$\begin{aligned} P_N &= K_p \gamma D^3 \quad \text{for sand} \\ P_N &= s_u D^2 \quad \text{for clay} \end{aligned} \tag{10–39}$$

where K_p, γ, D, and s_u are as previously. The coefficients A, B, and C are the same as in pile groups, or

A = 16 for clay and 9 for sand
B = 5.5 for clay and 3 for sand
C = 3 for clay and 16 for sand

A computer program for estimating the lateral displacement of a group of shafts based on the foregoing theory (Focht and Koch, 1973) is available and may be used in parametric studies.

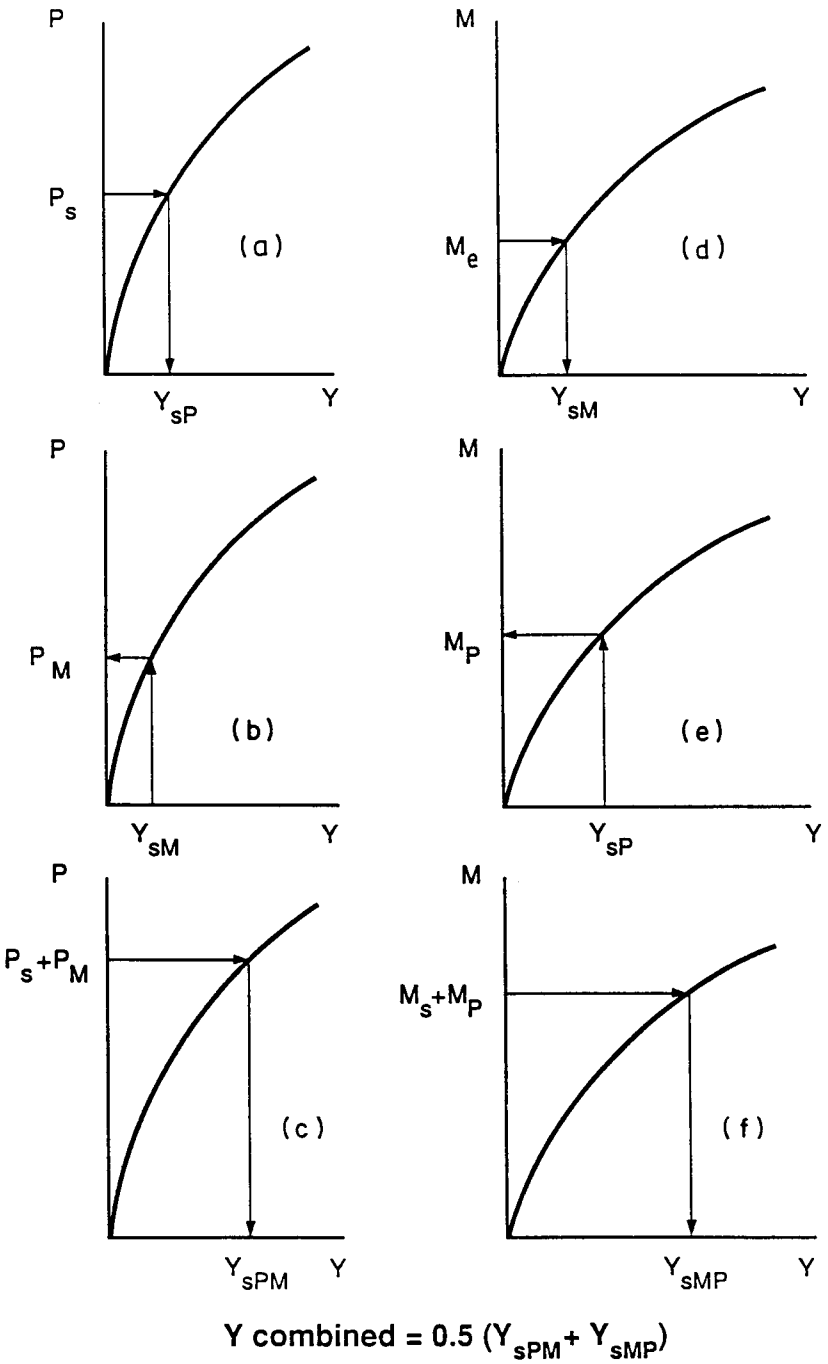

Figure 10–26 Nonlinear superposition *(from Evans and Duncan, 1982).*

Free head. As in a single free-head shaft, a load acting above the ground line will produce two components of lateral deflection: (1) a component caused by the lateral load at ground line, and (2) a component due to the movement at ground line. The composite lateral deflection of the shaft group is again estimated using the Focht and Koch (1973) procedure.

If the lateral displacement of a group of shafts exceeds the tolerable value, the problem may be rectified by increasing the shaft diameter, shaft spacing, or the number of shafts.

10.17 FLEXURAL ANALYSIS, LATERALLY LOADED SHAFTS

Bending Moment in a Single Shaft

Fixed head. A simple procedure for estimating the maximum bending moment induced in a single shaft by a lateral load (Figure 10–21) is suggested by Evans and Duncan (1982), and is essentially similar to the analysis of piles discussed in section 9.11. Reference is made to Figures 10–27 and 10–28 for shafts drilled in sand and clay, respectively, which are the same as Figures 9–34 and 9–35 except for a slight difference in the notation. These charts show the variation in M_s/M_c and P_s/P_c where M_s is the maximum moment in a single shaft and M_c is the characteristic moment.

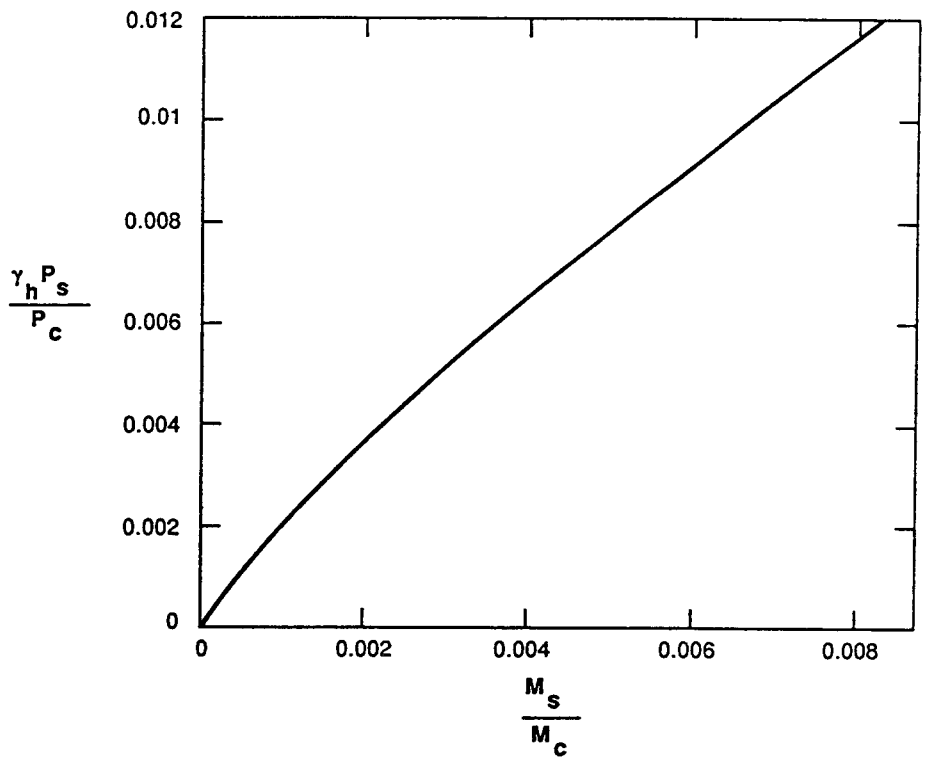

Figure 10–27 Lateral load versus moment for fixed-head drilled shafts in sand *(from Evans and Duncan, 1982).*

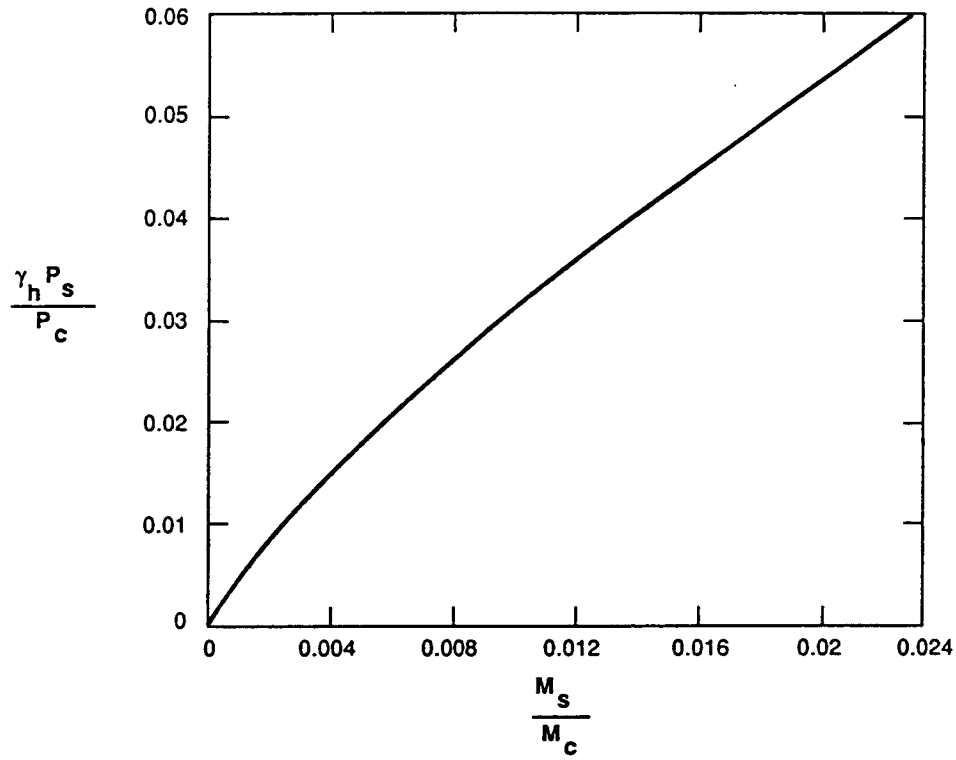

Figure 10–28 Lateral load versus moment for fixed-head drilled shafts in clay *(from Evans and Duncan, 1982).*

By making use of these charts, the bending moment is estimated as discussed in section 9.11 for driven piles. The procedure involves the following steps:

1. Select the shaft section (diameter D, elastic modulus E_p, and moment of inertia I_p).
2. Obtain the soil strength parameters s_u and ϕ', noting that shaft behavior is controlled mainly by the layer close to the ground surface. The soil parameters should therefore be averaged over a depth extending about eight shaft diameters from the top of the shaft.
3. Determine the characteristic load P_c as previously.
4. Compute the factored lateral load $\gamma_h P_s$, and the ratio $\gamma_h P_s / P_c$, where γ_h is the lateral load factor.
5. Referring to Figures 10–27 and 10–28 for sand and clay, respectively, obtain the value of M_s / M_c.
6. Obtain the characteristic moment M_c using Equations (9–58) and (9–59) for clay and sand, respectively.
7. The moment M_s is now calculated as $M_s = M_c(M_s / M_c)$.

Based on the foregoing procedure, appropriate charts have been developed as design aids for some commonly used shaft sizes, namely 24-, 30-, and 36-inch diameters, and for steel reinforcement ratios of 1, 2, and 4 percent. These charts are included in

Figure 10–20(a) through (c) for sand. For shafts in clay, similar charts are given by Ooi et al. (1991). It should be noted that whereas the effect of soil strength on the moment is considerable since it determines the lateral deflection and fixity of the shaft, the effect of the steel ratio is less significant.

Free head. For a free-head shaft, the maximum moment occurs at some depth below the ground surface. The behavior of a free-head shaft comes closer to the rigid element shown in Figure 10–19. The maximum moment is partly caused by the lateral load applied at ground level and partly by the moment at the same level. Both the maximum moment and the depth at which it occurs must be known for design purposes.

Procedures for determining these quantities have been developed by Evans and Duncan (1982), and by Matlock and Reese (1961) mentioned in section 10–16 for short rigid shafts. The latter may be applied based on the deflection at ground level calculated from the Evans-Duncan procedure. When the groundline deflection Y_s has been calculated, the maximum moment and the depth at which it occurs may be determined as follows:

1. Calculate the characteristic length T of the drilled shaft from the following expression by solving for T

$$Y_s = \frac{2.435P_s}{E_pI_p}T^3 + \frac{1.623M_e}{E_pI_p}T^2 \tag{10–40}$$

   where all terms are as previously defined.
2. Estimate the maximum bending moment along the shaft length from the expression

$$M = k_M M_e \tag{10–41}$$

   where M_e is the moment at the ground line ($M_e = P_s e$ in Figure 10–21), and k_m is a moment multiplier which is a function of T/e. This factor may be computed as

$$k_M = 1 + 0.756(T/e) \tag{10–42}$$

   where T is the characteristic length obtained from Equation (10–40). The approximate location of the maximum moment may be obtained from Table 10–12 as a function of the ratio T/e, and is expressed as a ratio z/T where z is the depth from ground line to the maximum moment level.

Bending Moment in a Group of Shafts

Because the deflection of a group of shafts is generally larger than for a single shaft for the same conditions of loading and soil strength, the bending moment in a drilled shaft within a group is also larger than in a single shaft.

Fixed head. Extending the analysis of pile groups (Brown, Reese, and O'Neill, 1987, 1988) to drilled shafts, we may conclude that the maximum bending moment in a group occurs in the leading row (front). However, current theories do not appear to confirm this behavior. A semi-empirical procedure that provides a reasonable approximation of the maximum moment in the leading row is proposed by Focht and Koch (1973) and is

Table 10–12 Approximate Location of the Occurrence of the Maximum Bending Moment in Free-Head Drilled Shafts

T/e	z/T
0.0	0.0
0.1	0.4
0.2	0.5
0.3	0.6
0.4	0.7
0.5	0.8
0.8	0.9
1.6	1.0
3.0	1.2
14.0	1.4

verified by results from field tests. This approach is also applied to pile groups and is discussed in section 9.11. The quantitative analysis of the maximum moment is given by Equations (9–60) through (9–62).

Free head. A group of free-head shafts under lateral load will develop the maximum bending moment in the leading row. Likewise, the procedure for softening the soil and matching the deflection of a single free-head shaft can be used to estimate the bending moment. Where the lateral load is applied above the ground line, the analysis must consider two contributions representing the moment and the lateral load acting at the ground line.

Structural Capacity under Bending and Axial Load

A typical analysis usually involves axial load-moment interaction diagrams produced as an envelope of several combinations of moment and loads that could result in structural failure (see also section 9–12).

Normalized load-moment interaction diagrams for drilled shafts are shown in Figures 10–29 and 10–30 for $f_y = 10\,f'_c$ and $f_y = 15f'_c$, respectively. The factored axial load $\Sigma\gamma_i P_i$ is normalized by dividing by the factored nominal axial capacity $\phi_a P_n$. The factored moment $\gamma_M M$ is similarly normalized by dividing by the factored nominal moment capacity $\phi_M M_n$. The factored axial capacity is estimated from Equation (10–4), which is the typical strength expression of axially compressive members. Normalized load-moment interaction diagrams may be developed for any ratios f_y/f'_c and cage diameters other than $0.6D$. The factor ϕ_a is as provided by AASHTO or LRFD, and is different for spiral and tied columns.

With interaction diagrams available, the structural capacity can be checked as follows:

1. Estimate the combined axial load on the group, $\Sigma\gamma_i P_i$.
2. Compute the factored nominal axial capacity $\phi_a P_n$, from Equation (10–43).

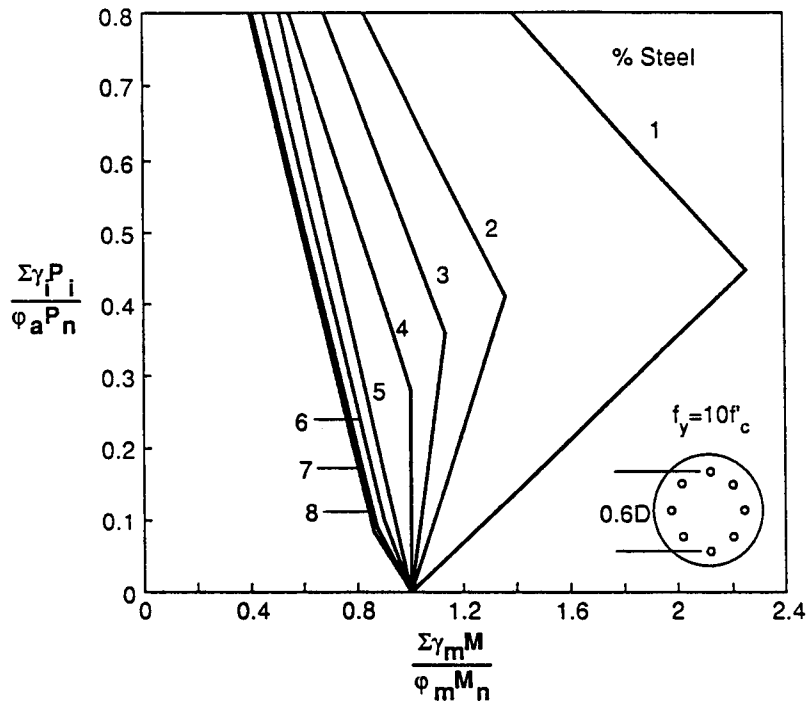

Figure 10–29 Normalized load-moment interaction curves for drilled shafts $f_y = 10 f'_c$.

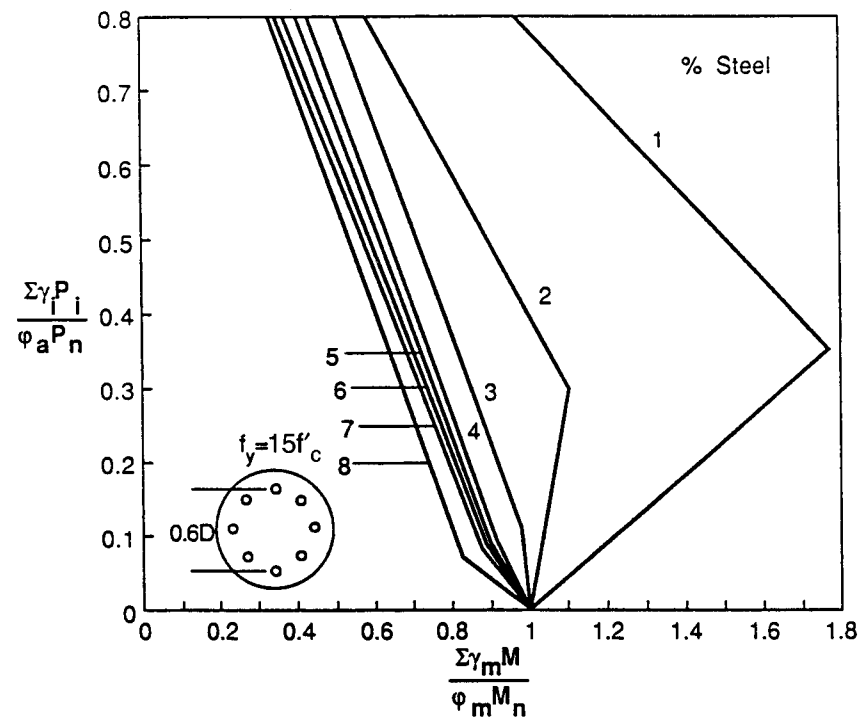

Figure 10–30 Normalized load-moment interaction curves for drilled shafts $f_y = 15 f'_c$.

Table 10–13 Nominal Moment Capacity, M_n, for Drilled Shafts

Ratio of Area of Steel to Gross Cross-Sectional Area	$\frac{M_n}{f_c' D A_g}$ 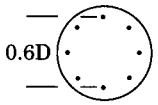 $f_y = 10f_c'$	$f_y = 15f_c'$
0.01	0.037	0.050
0.02	0.067	0.092
0.03	0.088	0.119
0.04	0.107	0.147
0.05	0.126	0.172
0.06	0.144	0.197
0.07	0.161	0.208
0.08	0.176	0.244

f_g' = 28 day concrete cylinder strength
f_y = yield stress of steel
D = diameter of drilled shaft
A_g = gross cross-sectional area of concrete

3. Estimate the factored (required) moment $\Sigma\gamma_m M$.
4. Estimate the nominal structural moment capacity M_n of the shaft. This may be based on a complete analysis, or it may be obtained from design aids such as Table 10–13.
5. From step 4, obtain the factored moment $\phi_m M_n$ where $\phi_m = 0.9$ for reinforced concrete.
6. Determine the ratios $\Sigma\gamma_i P_i / \phi_a P_n$ and $\Sigma\gamma_m M / \phi_m M_n$, and with these values locate an appropriate point on the diagram space. If the point falls inside the area defined by the interaction curve and is close to the curve, the shaft capacity is adequate. If this is not the case, the analysis should be repeated until the results converge.

10.18 DESIGN EXAMPLES

Design Example 10–1

A drilled shaft with diameter 36 inches supports a dead load of 110 tons and a live load of 32 tons. The shaft is 50 feet long. Check the structural and geotechnical adequacy of the foundation for the soil conditions shown.

1. Estimate the required capacity of the shaft. This is the sum of the factored loads.

$$\gamma_D P_B + \gamma_L P_L = 1.3(110) + 2.17(32) = 143 + 69 = 212 \text{ tons} = 424 \text{ kips}$$

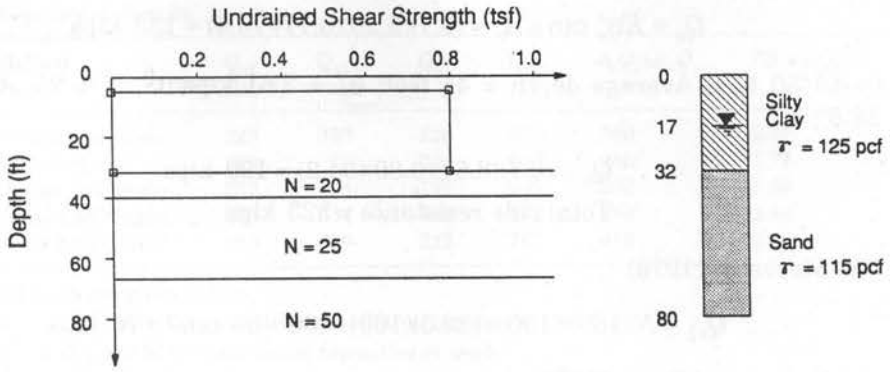

2. Estimate the structural capacity of the shaft (design strength) from Equation (10–4). Because the shaft is provided with ties, we use $r = 0.8$, and $\phi_a = 0.7$. Therefore,

$$\phi_a P_n = (0.8)(0.7)(0.85 f'_c A_c + f_y A_y)$$

Select concrete with $f'_c = 3500$ lb/in^2, Grade 60 reinforcement, and 20 #10 bars. Compute

$$A_y = (20)(1.27) = 25.4 \text{ in}^2, \quad A_g = (3.14)(36)^2/4 = 1017 \text{ in}^2$$
$$A_c = 1017 - 25 = 992 \text{ in}^2$$
$$\phi_a P_n = (0.8)(0.7)[(0.85)(3.5)(992) + (60)(25.4)]$$
$$= 2506 \text{ kips} > 424 \text{ OK}$$

Note that the required strength is only a small fraction of the design strength. However, we keep the 36-inch diameter, based on the fact that in the particular locality where this construction is contemplated, most of the available equipment handles 36-inch holes. The amount of steel provided is in the nominal range, or 2.5 percent.

3. Estimate the geotechnical capacity of the shaft. Note that the upper 32 feet are in clay, and the lower 18 feet are in sand. The top 5 feet of the shaft will be ignored. Effective length of the shaft in clay = 27 feet, $s_u = 0.8$ tons/ft^2 = 1.6 kips/ft^2. Compute $A_{s2} = (3.14)(36)(27)/12 = 254$ ft^2

- Side resistance of shaft in the clay, $Q_{s2} = \alpha s_u A_{s2} = (0.55)(1.6)(254) = 223$ kips

For the shaft portion in sand, the effective length is 18 feet.
From depth 32 to 40 feet, $N = 20$
From depth 40 to 50 feet, $N = 25$
Average $N = [(20)(8)+(25)(10)]/18 = 22.2$

- Side resistance of shaft in sand (Table 10–7)

(a) Touma and Reese (1974). For $D_b < 25$ ft, $K = 0.7$
Depth 32–40 feet, Average depth 36 feet; $\sigma'_v = 3.28$ kips/ft^2, $N = 20$, $A_s = 75.4$ ft^2, $\phi' = 37.5°$;

$$Q_s = K\sigma'_v \tan\phi' A_s = (0.7)(3.28)(0.77)(75.4) = 133 \text{ kips}$$

Depth 40–50 feet; Average depth = 45 feet; σ'_v = 3.61 kips/ft^2, N = 25, A_s = 94.2 ft^2, ϕ' = 38.8°;

$$Q_s = (0.7)(3.61)(0.80)(94.2) = 190 \text{ kips}$$

Total side resistance = 323 kips

(b) Meyerhof (1976)

$$Q_{s1} = N(169)/100 = (22.5)(169)/100 = 38 \text{ tons} = 76 \text{ kips}$$

(c) Quiros and Reese (1977)

$$Q_{s1} = (0.026)(22.5)(169) = 99 \text{ tons} = 198 \text{ kips}$$

(d) Reese and Wright (1977)

$$Q_{s1} = (23.5)(169)/34 = 117 \text{ tons} = 234 \text{ kips}$$

(e) Reese and O'Neill (1988)

$$\beta = 1.5 - 0.135\sqrt{50} = 0.55$$

$$\sigma'_v = [(125)(17) + (125 - 62.4)(15) + (115 - 62.4)(9)]/1000 = 3.54 \text{ kips/ft}^2$$

$$Q_{s1} = \beta\sigma'_v A_s = (0.55)(3.54)(169) = 330 \text{ kips}$$

- Base resistance of shaft (Table 10–8)

(a) Touma and Reese (1974)

$$Q_p = (16)A_g/0.6D = (16)(1017)/(0.6)(3) = 9040/144$$
$$= 63 \text{ tons} = 126 \text{ kips}$$

(b) Meyerhof (1976)

$$D_b = 18 \text{ ft}, \quad D_b/D_p = 18/3 = 6 < 10, \quad N_{corr} = 18$$

$$q_p = \frac{2N_{corr}D_b}{15D_p} = (2)(18)(18)/(15)(3) = 14.4 \text{ tons/ft}^2$$

$$Q_p = (7.07)(14.4) = 102 \text{ tons} = 204 \text{ kips}$$

(c) Quiros and Reese (1977)

The same as Touma and Reese, i.e., Q_p = 126 kips

(d) Reese and Wright (1977)

$$Q_p = (2/3)(25)(7.07) = 118 \text{ tons} = 236 \text{ kips}$$

(e) Reese and O'Neill (1988)

$$Q_p = (0.6)(25)(7.07) = 106 \text{ tons} = 212 \text{ kips}$$

Summary of Results

Method	Q_{s2} clay	Q_{s1} sand	Q_p	Q_{ult}	$\phi_s Q_s + q_p Q_p$	$FS = Q_{ult}/28$
Touma and Reese	223	323	126	672	369	2.37
Meyerhof	223	76	204	503	285	1.77
Quiros and Reese	223	198	126	547	307	1.93
Reese and Wright	223	234	236	693	380	2.44
Reese and O'Neill	223	330	212	765	416	2.69

All loads are given in kips.
ϕ_{qs} = 0.65 (from Table 10–9) for calculating capacity in clay
$\phi_{qs} = \phi_{qp}$ = 0.50 for calculating capacities in sand

This example demonstrates the wide disparity of results obtained by five different methods. For strength design, the Reese and O'Neill method appears to be the only method satisfactory for the assumed load and resistance factors. For allowable stress design, the three first methods give a factor of safety less than 2. Accordingly, either the shaft length must be increased or a larger diameter must be used.

The Touma and Reese method and the Quiros and Reese method provide solutions assuming a tolerable settlement of 1 inch. The Reese and Wright and Reese and O'Neill methods are based on a settlement of 5 percent of the base diameter, or 1.8 inches. This explains the higher base resistance (almost double) obtained by the last two methods.

4. Check settlement under working load.

The largest portion of the shaft capacity is derived from side resistance and base bearing in sand. Hence, the settlement may be analyzed from the curves of Figures 10–15 and 10–16.

The concrete modulus for the shaft is taken as 3.5×10^3 kips/in^2. Assuming that the average shear transfer (side resistance) is 60 percent of the total working load (first trial), the elastic shortening is estimated from Equation (10–31) as

$$p_e = \frac{(0.6)(142)(2000)(50)(12)}{(1017)\left(3.5x10^3\right)1000} = 0.029 \text{ in}$$

Making use of the trend lines in Figures 10–15 and 10–16, the following tabulation is obtained:

Trial Settlement (in)	Side Resistance			End Bearing			Total
	P/D	(%) Q/Qs	Q^*	P/D(%)	Q/Q_p	Q^{**}	Q_T
0.03	0.082	0.35	160	0.083	0.02	5	165
0.07	0.19	0.55	251	0.19	0.10	24	275***

* Side resistance is assumed to be obtained from the Reese-Wright method. Then Q_s = 223 + 234 = 457 kips
** Likewise base resistance is obtained from the Reese-Wright method, or Q_p = 236 kips
*** The total load Q_T is very close to the working load of 284 kips, hence convergence is assumed to have been reached for a settlement of 0.07 inch

The settlement at the top of the shaft is the settlement of the base plus the elastic compaction, or p_t = 0.03 + 0.07 = 0.1 inch. The following conclusions are appropriate:

1. The design is acceptable in terms of factors of safety stipulated by AASHTO for the working stress method.
2. For strength design, the shaft satisfies the load transfer requirements for the strength limit state and also complies with the serviceability limit state.
3. The statement made in previous sections is verified in terms of load transfer, that is, at working loads most of the load is resisted by side shear.

Design Example 10–2

The drilled shaft with an enlarged base shown in Figure 10–31 is subjected to a dead load of 250 kips and a live load of 80 kips. It is installed in stiff clay with uniform $s_u = 2$ kips/ft^2. The groundwater table is far below the base of the foundation and need not be considered. Check the adequacy of the member in structural and geotechnical capacity.

1. Estimate the required strength. This is the sum of the factored loads

$$\gamma_D P_D + \gamma_L P_L = (1.3)(250) + (2.17)(80) = 325 + 174 = 499 \text{ kips}$$

2. Estimate the structural capacity (design strength) from Equation (10–4). The concrete strength is again 3500 lb/in^2, and the steel is Grade 60. The gross area of the shaft is $A_g = 3.14 \times 15^2 = 707$ in^2. We select 16 #9 bars $A_y = (16)(1.0) = 16$ in^2, providing a steel ratio in excess of 2 percent. We compute $A_c = 707 - 16 = 691$ in^2. The factored nominal strength is now

$$\phi_n P_n = (0.8)(0.7)[(0.85)(3.5)(691) + (60)(16)] = 1688 \text{ kips, OK}$$

3. Check structural capacity of underream. The shape of the underream is shown in Figure 10–31. The underream angle is 60°. The maximum diameter of an underream should not exceed three times the shaft diameter. Typically the outside of the bell is left unreinforced. The maximum tensile stress will occur near the notch, if one is provided, because of stress concentration effects. Reese and O'Neill (1988) give guidelines for the maximum bearing stresses in an unreinforced underream with a bell diameter three times the shaft diameter, summarized in Table 10–14.

From Table 10–14, the maximum bearing pressure that will accommodate a 60° underream and $f'_c = 3500$ lb/in^2 is found by interpolation as 20.5 kips/ft^2. The structural capacity of the bell is, therefore,

$$(0.85)(20.5)(3.14)(3.5)^2 = 670 \text{ kips} > (499 - 281) = 218 \text{ kips where 281 is } Q_{s2}$$

4. Bearing capacity (geotechnical strength) is based on side resistance and base bearing. The effective shaft length is obtained from Figure 10–31 by omitting the top and bottom sections as noncontributing to the load transfer. This length is 40 – 5.0 – 2.5 = 32.5 feet. Shaft area

$$A_{s2} = (3.14)(2.5)(32.5) = 255 \text{ ft}^2$$

$$Q_{s2} = \alpha s_u A_{s2} = (0.55)(2)(255) = 281 \text{ kips}$$

In order to estimate the base bearing, we first consider $D_p = 7 \times 12 = 84$ inches > 75 inches, hence a reduced base resistance must be obtained. Referring to section 10.8 and AASHTO Article 4.6.5.13, we compute

$$a = 0.0071 + 0.0021\, Z/D_p$$

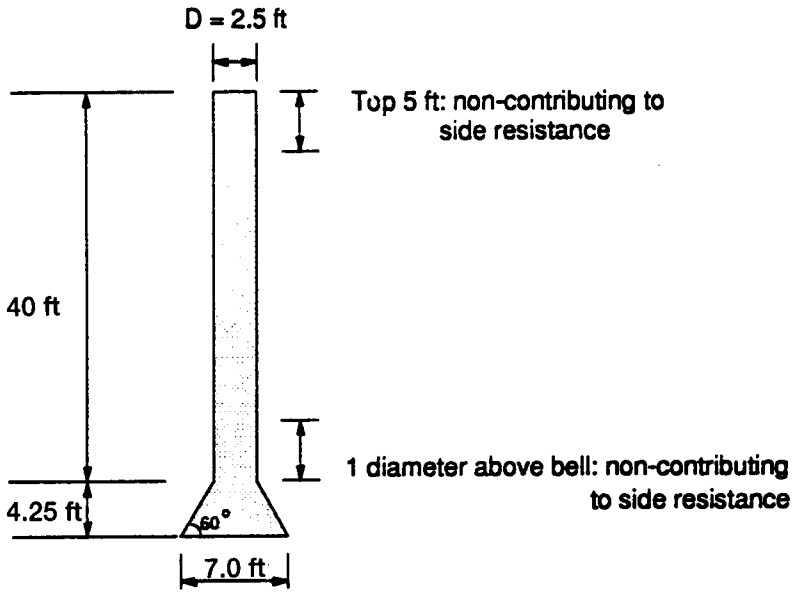

Figure 10–31 Drilled shaft of Design Example 10.2.

where Z is the total shaft length = 44.25, and D_p is the bell diameter.

$$a = 0.0071 + 0.0021\,(44.25/7.00) = 0.0204 \le 0.015$$

$b = 0.45\sqrt{s_u}$, where s_u is expressed in kips/ft^2, or $b = 0.45\sqrt{2} = 0.636$

Next, we compute

$$F_r = \frac{2.5}{aD_p + 2.5b} \text{ where } D_p \text{ is expressed in inches, or}$$

$$F_r = \frac{2.5}{(0.015)(7.0)(12) + (2.5)(0.636)} = 0.87$$

Also $q_{pr} = 0.87q_p$, where $q_p = N_c s_u \le 40$ tons/ft^2

$$N_c = 6[1 + 0.2Z/D_p] \le 9, \text{ or}$$

Table 10–14 Maximum net bearing pressure that can be sustained in underreams without cracking.

Underream Angle	f'_c*	
	3 ksi	4ksi
45*	8 ksf	15 ksf
60*	16 ksf	25 ksf

These values apply to bells with toe heights of 3 in. and a base diameter equal to three times the diameter of the shaft.

*f'_c = 28 day concrete compressive strength

(From Reese and O'Neill, 1988)

$$N_c = 6[1 + (0.2)(44.25)/7.0] = 13.6 > 9, \text{ use } N_c = 9$$

Then $q_p = (9)(1) = 9$ tons/ft^2 = 18 kips/ft^2, and $Q_p = (0.85)(18)(3.14)(3.5)^2 = 589$ kips. The factored ultimate bearing capacity is

$$\phi_{qs}Q_s + \phi_{qp}Q_p = (0.65)(281) + (0.55)(589) = 183 + 324 = 507 \text{ kips, OK}$$

5. Check settlement for working load conditions. From Figure 10–13, the maximum side shear is mobilized at a displacement of 0.6 percent of the shaft diameter, or (0.6)(30)/100 = 0.18 inch. When this settlement occurs, the full side resistance of 281 kips is assumed to be acting along the shaft. The remainder of the working load is 330 – 281 = 49 kips, and it is assumed to be carried by base bearing. For an ultimate bearing capacity of 589 kips, the percentage carried by the base under working load is therefore 49/589 = 0.08 or 8 percent.

From Figure 10–14, at a load (base) of 8 percent of the ultimate bearing, the corresponding settlement of the base is roughly 0.2 percent of the base (by scaling), or settlement of base = (0.2)(84)/100 = 0.17 inch, almost the same settlement at which full side resistance is mobilized. Thus, at working load the entire shaft resistance will be mobilized but only 8 percent of the base bearing. This trend was also verified in Design Example 10–1.

The elastic shortening of the shaft ignoring the bell section can be estimated as previously, that is, from Equation (10–31) where

$$P = \frac{P_D + P_L + \text{ load carried by base}}{2} = \frac{330 + 49}{2} = 190 \text{ kips}$$

or

$$P_c = \frac{(190)(1000)(40)(12)}{(707)\left(3.5 \times 10^6\right)} = 0.037 \text{ in}$$

Total settlement of the top = 0.18 + 0.04 = 0.22 in.

Design Example 10–3

A 36-inch diameter drilled shaft is socketed 10 feet into basalt to support a single column pier of a highway ramp. For Group I, the loads acting on the column are: dead load = 320 kips; live load = 125 kips. The compressive strength of the basalt is 1.0 kip/in^2 and the RQD is 70 percent. The shaft will be checked for structural and geotechnical capacity.

1. Calculate the required strength as the sum of the factored loads

$$\gamma_D P_D + \gamma_L P_L = (1.3)(320) + (2.17)(125) = 476 + 271 = 747 \text{ kips}$$

2. Estimate the structural capacity assuming $f'_c = 3500$ lb/in^2 and 18 #10 Grade 60 bars, $A_y = (18)(1.27) = 22.9$ in^2. Likewise $A_c = 1017 - 23 = 994$ in^2.

The factored nominal strength is obtained again from Equation (10–4) as

$$\phi_a P_n = (0.8)(0.7)[(0.85)(3.5)(994) + (60)(22.91)] = 2425 \text{ kips} > 747 \text{ kips.}$$

3. Estimate the bearing capacity (geotechnical strength). From Figure 10–9, the elastic modulus for intact basalt is 5×10^2, and the modulus ratio is 500. From Figure 10–10 the modulus of the in situ rock mass (RQD = 70 percent) is 20 percent of the in-

tact modulus. The in situ modulus of the rock is, therefore, $E_r = (0.2)(5 \times 10^2) = 100$ kips/in^2.

The bearing capacity of the rock socket may be derived from shaft resistance or from base bearing. This is determined if we calculate $p_e + p_{base}$. If this sum is less than 0.4 inch, the axial load is carried entirely by shaft resistance (see also section 10.10).

The elastic shortening (working loads) is computed as

$$p_e = \frac{(445)(1000)(10)(12)}{(1017)/(3.5 \times 10^6)} = 0.015 \text{ in}$$

Likewise, we compute

$$p_{base} = \frac{(\Sigma P_i) I_p}{D_s E_r},$$

where I_p is estimated from Figure 10–8. Note that $H_s/D_s = 10/3 = 3.33$, and $E_c/E_r = 3.5 \times 10^3/10^2 = 35$, giving $I_p = 0.35$.

Therefore,
$$p_{base} = \frac{(445)(1000)(0.35)}{(36)\left(100 \times 10^3\right)} = 0.043 \text{ in}$$

Total $p_e + p_{base} = 0.015 + 0.043 = 0.06$ inch < 0.4 inch, or the drilled shaft capacity is derived primarily from shaft resistance.

Since q_u exceeds 280 psi, the unit side resistance is estimated from Equation (10–24a), or $q_s = 2.5\sqrt{1000} = 79$ lb/in^2. The ultimate side resistance is now

$$Q_s = (79)(3.14)(36)(10)(12)/1000 = 1071 \text{ kips}$$

Factored capacity = (0.65)(1071) = 696 kips < 747 kips, not OK. The shaft must be checked using a larger diameter (say 42 inches) or increased socket length (say 11 feet). For the latter, $Q_s = (1071)(11)/10 = 1178$ kips, and $\phi_{qs} Q_s = (0.65)(1178) = 766$ kips > 747 kips, OK.

Interestingly, convergence is attained at this point, and the analysis need not be repeated, although $H_s/D_s = 11/3 = 3.67$ and the total deflection may change somewhat but still less than 0.4 inch.

Design Example 10–4

A drilled shaft is part of a lateral protection system installed in a waterway. The shaft has a diameter of 24 inches, and is constructed in silty clay with an undrained shear strength (average) of 2 kips/ft^2. The potential of loss of lateral capacity due to scour has been considered, so that the shaft will be checked for a lateral load of 25 kips, representing stream flow pressure acting about 9 feet above ground line. The shaft is reinforced with 10 #8 bars. Young's modulus for the concrete is taken again as 3.5×10^3 kips/in^2.

1. Calculate the steel percentage.

$$A_y = (10)(0.79) = 7.9 \text{ in}^2, \qquad A_g = (3.14)(12^2) = 452 \text{ in}^2$$

Steel ratio = 7.9/0.52 = 1.75 percent

2. Estimate the lateral deflection for a load of 25 kips assumed to act along the ground line. Form Table 10–11, and interpolating between a steel ratio of 0.01 and 0.02, we obtain $R_1 = 1.12$. Then

$$E_p R_1 = 3.5 \times 10^3 \times 1.12 = 3920 \text{ kips/in}^2$$

The characteristic load is obtained next from Equation (9–54) as

$$P_c = (7.34)(24)^2(3920)\left(\frac{2}{144}\frac{1}{3920}\right)^{0.683} = 3190 \text{ kips}$$

From Figure 10–23, and $P_s/P_c = 25/3190 = 0.0078$, we obtain graphically $Y_{sp}/D = 0.01$ (Note that this depends on the accuracy with which the graphs are read), and

$$Y_{sp} = (0.01)(24) = 0.25 \text{ in}$$

3. Estimate the lateral deflection due to a moment of $9 \times 25 = 255$ ft-kips applied at ground line. $M_e = (225)(12) = 2700$ in-kips. The characteristic moment M_c is computed as

$$M_c = (1.33)(24)^3(3920)\left(\frac{2}{144}\frac{1}{3920}\right)^{0.46} = 653{,}000 \text{ in-kips}$$

or

$$M_e/M_c = 2700/653{,}000 = 0.0041$$

Using $M_e/M_c = 0.0041$, from Figure 10–25, we obtain

$$Y_{sm}/D = 0.01, \text{ or } Y_{sm} = (0.01)(24) = 0.24 \text{ in}$$

4. With Y_{sp} and Y_{sm} calculated, the lateral deflection of the shaft is obtained by linear superposition.

From Figure 10–23 and $Y_{sp} = 0.01$, $P_m/P_c = 0.0095$, or $P_m = (0.0095)(3190) = 30.3$ kips

From Figure 10–25, and $Y_{sm}/D = 0.01$, $M_p/M_c = 0.005$, or $M_p = (0.005)(653{,}000) = 3265$ in-kips

$$P_s + P_m = 25 + 30.3 = 55.3 \text{ kips}$$

$$\frac{P_s + P_m}{P_c} = \frac{55.3}{3190} = 0.017$$

From Figure 10–23, $Y_{spm}/D = 0.03$, or

$$Y_{spm} = (0.03)(24) = 0.72 \text{ in}$$

$$M_e + M_p = (2700 + 3265) = 5965 \text{ in-kips}$$

$$\frac{M_e + M_p}{M_c} = \frac{5965}{653{,}000} 0.0091$$

From Figure 10–25, $Y_{smp}/D = 0.025$, or $Y_{smp} = (0.025)(24) = 0.60$ in

$$Y_s = 0.5(Y_{spm} + Y_{smp}) = 0.5(0.72 + 0.60) = 0.66 \text{ in}$$

5. Compute the maximum bending moment in the shaft.

$$\text{First, calculate } I_p = \frac{\pi D^2}{64} R_I = \frac{(3.14)(24)^2}{64}(1.12) = 18250 \text{ in}^4$$

A load factor of 1.3 is applied to the lateral stream force and moment component according to AASHTO. The characteristic length T is obtained from Equation (10–40), or

$$\frac{(2.435)(1.3)(25)}{(3.5)(10^3)(18250)} T^3 + \frac{(1.623)(1.3)(2700)}{(3.5)(10^3)(18250)} T^2 = 0.66$$

or

$$\frac{T^3}{806{,}500} + \frac{T^2}{11{,}210} - 0.66 = 0$$

This is solved by trial and error and gives T = 62 inches.

Next, we compute the ratio T/e = (62)/(9)(12) = 0.57

From Equation (10–42), we compute

$$k_M = 1 + (0.756)(0.57) = 1.43$$

The maximum bending moment is obtained from Equation (10–41) as

$$M = k_M M_e = (1.43)(2700) = 3860 \text{ in-kips}$$

6. Calculate the moment capacity of the shaft, using f'_c = 3500 lb/in^2 and f_y = 60,000 lb/in^2, or f_y/f'_c = 17.

From Table 10–13, the ratio $M_n/f'_c DA_g$ is obtained by linear interpolation for 1.75 percent steel ratio as 0.090, or

$$M_n = (0.090)(3.5)(24)(452) = 3415 \text{ in-kips}$$

$$\phi_m M_n = (0.9)(3415) = 3070 \text{ in-kips}$$

$$\gamma_m M/\phi_M M_n = 3860/3070 = 1.25 \text{ for } \gamma_m = 1.$$

This should be interacted with $\Sigma\gamma_i P_i/c_a P_n$, and the appropriate point located on the diagrams of Figure 10–3. It may appear that this point will plot inside the diagram for 1.75 percent reinforcement. If this is not the case, however, either the steel reinforcement or the shaft diameter may be increased.

Design Example 10–5

A group of fixed-head drilled shafts supports a hammerhead pier as shown in Figure 10–32. This group is subjected to a lateral wind load of 120 kips, acting 10 feet above the base as shown. The dead load and the live load are 550 kips and 200 kips, respectively. The shafts are reinforced with 9 #9 bars each giving a 2 percent steel reinforcement ratio. Check the structural and geotechnical adequacy of the system.

1. Compute $A_g = (3.14)(12^2) = 452$ in^2, $A_y = 9 \times 1 = 9$ in^2.

2. Calculate the lateral deflection of a single shaft. Load (lateral) per shaft = 120/6 = 20 kips. For N = 10, ϕ' = 35° (Meyerhof, 1956). The lateral deflection of a single pile

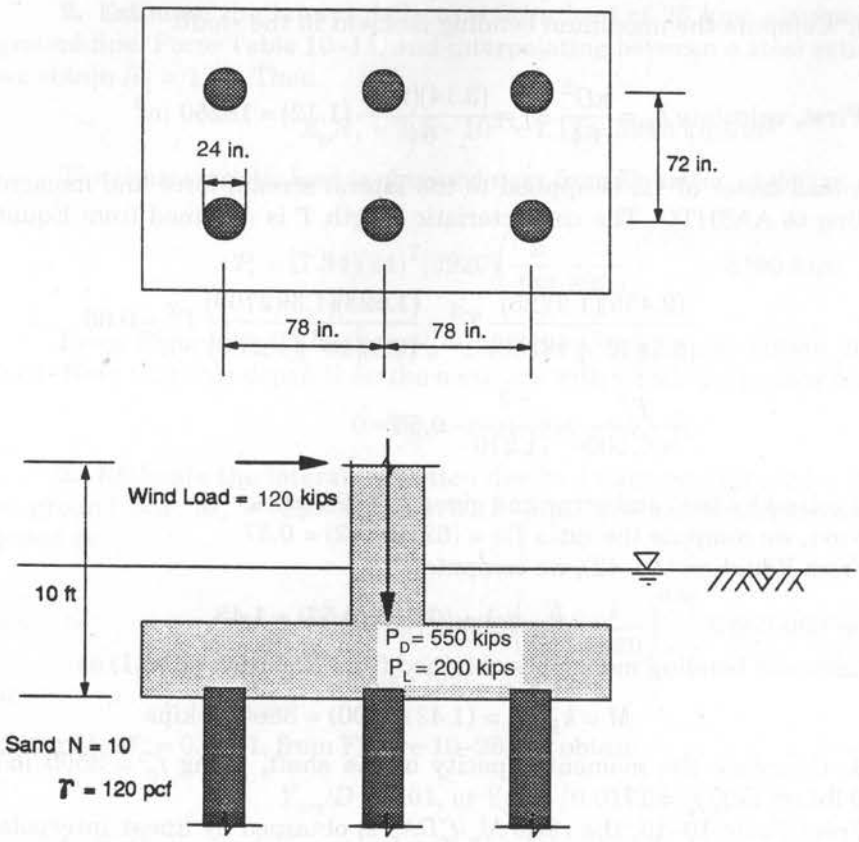

Figure 10–32 Layout and details of shaft group. Design Example 10–5.

may be predicted by reference to Figure 10–20 (b). For $\phi' = 35°$, $D = 24$ in, and $A_y/A_g = 2\%$, $Y_s = 0.1$ in (obtained graphically).

3. Predict the group deflection. This can be estimated from Equation (10–38) for fixed head. First, we compute

$$P_N = K_p \gamma D^3 = \left(\frac{1+0.574}{1-0.574}\right)\left(\frac{120}{(1000)(12^3)}\right)(24^3) = 3.55$$

$$Y_g = \frac{9+6}{3\sqrt{3.25+\dfrac{20}{(16)(3.55)}}}((0.10) = (265)(0.10)) = 0.27 \text{ in}$$

4. Establish the location of the resultant force on the cap. The sum of the factored loads is

$$\Sigma\gamma_i P_i = (1.3)(550) + (2.17)(200) = 715 + 434 = 1149 \text{ kips}$$

$$\gamma_w P_w = (1.3)(120) = 156 \text{ kips}$$

Eccentricity of the resultant is (156)(10)/1149 = 1.36 feet

5. Obtain the axial load in the most heavily loaded shaft. This requires use of Equation (9–17), where the term $e_y y$ is zero. Therefore,

$$P_{x,y} = (1149)\left[\frac{1}{6} + \frac{(1.36)(6.5)}{(4)(6.5^2)}\right] = (1149)(0.219) = 252 \text{ kips}$$

6. Estimate the maximum bending moment in a single shaft. By reference to Figure 10–20 (b), we obtain directly M_s = 1200 in-kips (scaled graphically).

7. Estimate the maximum bending moment of the most heavily loaded shaft, using Equation (9–60) where Y_{sp} and M_{sp} are for shafts.

First, we compute $n = \dfrac{\gamma_h P_s}{300 P_n} + 0.3 = \dfrac{(1.3)(20)}{(300)(3.55)} + 0.3 = 0.33$

$$M_g = \left(\frac{0.27}{0.10}\right)^{0.33} M_s = (2.70)^{0.33}(1200) = 1800 \text{ in-kips}$$

8. Check the structural adequacy of the shaft section using interaction diagrams. Excluding the eccentricity factor, the factored axial capacity is

$$\phi_a P_n = (0.7)[(0.85)(3.5)(443) + (60)(9)\,] = 1300 \text{ kips/shaft}$$

The moment capacity is obtained from Table 10–13 for f_y/f'_c = 17 and a steel ratio 0.02. Using linear interpolation, we obtain $M_n/f'_c DA_g$ = 0.102 or M_n = (0.102)(3.5)(24)(452) = 3873 in-kips.

The following ratios are computed now

$$\frac{P_{x,y}}{\phi_a P_n} = \frac{252}{1300} = 0.20 \qquad \frac{M_g}{\phi_M M_n} = \frac{1800}{(0.9)(3873)} = 0.52$$

Referring to Figure 10–30, the point (0.52, 0.20) plots well within the load-moment interaction diagram for a steel ratio of 2 percent. The structural capacity is more than adequate, and either size or the reinforcement ratio could be reduced.

Design Example 10–6

An 18-inch diameter drilled shaft is reinforced with 8 #5 bars. Compute the moment of inertia I_p, and the moment of inertia ratio R_I. Use E_c = 3500 kips/in^2, E_s = 29,000 kips/in^2, and cover c = 3 inches.

1. Moment of inertia of gross cross section

$$I_c = \frac{\pi D^4}{64} - 8\frac{\pi d_s^4}{64} - \left(2 + \frac{4}{(\sqrt{2})^2}\right)\frac{\pi d_s^2}{4}\left(\frac{D}{2} - c - \frac{ds}{2}\right)^2$$

or $$I_c = 5113 \text{ in}^4$$

2. Moment of inertia of steel

$$I_s = 8\frac{\pi d_s^4}{64} + \left(2 + \frac{4}{\left(\sqrt{2}\right)^2}\right)\frac{\pi d_s^2}{4}\left(\frac{D}{2} - c - \frac{d_s}{2}\right)^2$$

$$\text{or } I_s = 40 \text{ in}^4$$

3. $E_pI_p = E_cI_c + E_sI_s$, or

$$E_pI_p = (3500)(5113) + (29000)(40) = 1.91 \times 10^7 \text{ kips-in}^2$$

For the equivalent homogeneous section, we use $E_p = E_c$

$$\text{Hence, } I_p = \frac{E_cI_c + E_sI_s}{E_c} = \frac{1.91 \times 10^7}{3500} = 5444 \text{ in}^4$$

4. Moment of inertia ratio

$$R_I = \frac{I_p}{I_{SOLID}} = \frac{(5444)(64)}{\pi\left(18^4\right)}, \text{ or } R_I = 1.06 \text{ for } A_s / A_g = 0.01$$

Design Example 10–7

This example presents solutions to the problem of laterally loaded drilled shafts using the two methods briefly discussed in section 10.16 in connection with short rigid elements (Czerniak, 1957; Matlock and Reese, 1961). The drilled shafts are treated as rigid elements that remain undeformed as they rotate about a well-defined center, and the soil modulus is assumed to vary linearly with depth, that is, $E_s = kx$. This assumption gives greater consistency than the assumption of constant E_s, although it does not constitute a rational approach to a behavior essentially inelastic. Nondimensional curves included with the foregoing references are used to obtain bending moment diagrams.

For the soil conditions assumed in this example, a value of $k = 5$ is believed to suit the design approach. This parameter is essentially obtained from empirical data and may vary with actual lateral deflection, depth, shaft diameter, type of loading, and soil characteristics. However, the accuracy of k is not critical, and a 32 to 1 variation is necessary to produce a 2 to 1 variation in the moments.

For the Czerniak method, a soil pressure (passive) of 250 lb/ft is used. The results are compared for the two methods, and differences of convergence are explained.

Figure 10–33 (a) and (b) shows wall and drilled shaft layout of typical section, respectively, for the Design Example. The wall provides a retaining earth system for medium height embankments (10 to 15 feet). The wall beams are set on the outside half of the shafts and are laterally supported by the inside half extended above the top as shown. A foundation girder is provided as shown. The wall retains an earth height of 10.5 feet and a live load surcharge of 2 feet. Since sufficient lateral movement is assumed to occur, the wall is designed for the active condition using 40 lb equivalent fluid pressure.

From Figure 10–33 (b)

$$y = \frac{h^2 + 3hh'}{3(h + 2h')} = \frac{10.5^2 + 3(10.5)(2)}{3(10.5 + 2 \times 2)} = 3.98 \text{ ft}$$

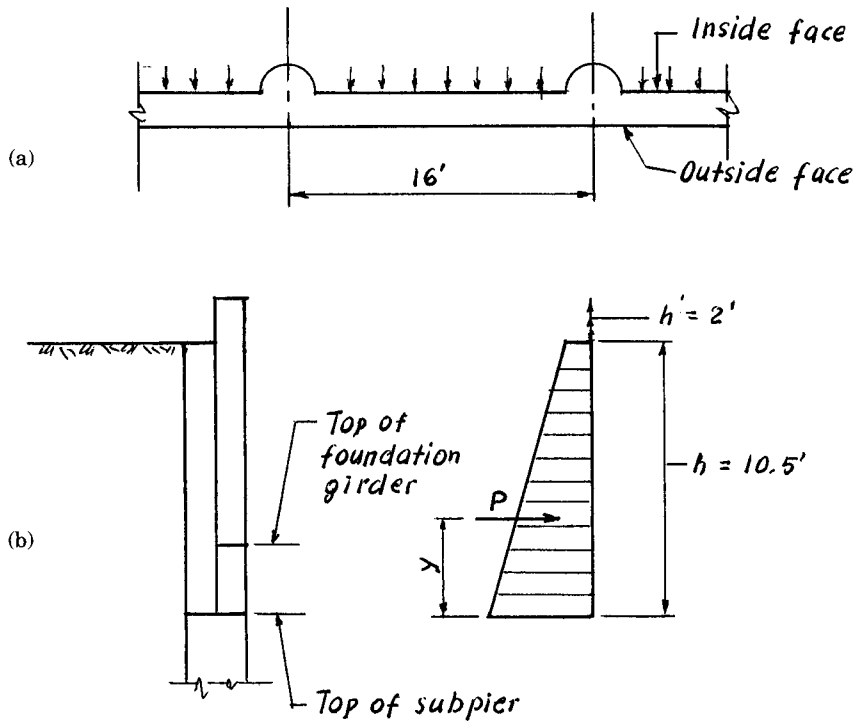

Figure 10–33 (a) Wall and drilled shaft layout; (b) Typical section. Michigan-Oak Underpass.

$$P = (0.5)(40)(10.5)(10.5 + 4) = 3.05 \text{ kips/ft of wall length}$$

For a shaft spacing of 16 feet, the total lateral load transmitted to each shaft is P_T = (16)(3.05) = 49 kips, and the moment at the top of the shaft is M_T = (49)(3.98) = 195 ft-kips.

For a wall thickness of 19 inches, the vertical load on each shaft is (16)(12.5)(1.58)(0.15) = 48 kips.

From a preliminary analysis the tip elevation of the shaft is –40, and a tentative shaft diameter is 3 feet 9 inches. This gives a total drilled shaft length of about 48 feet. For $E_c = 2.9 \times 10^6 \text{lb/in}^2$, the moment of inertia of the shaft is $I_s = (3.14)(3.75^4)(12^4)/64 = (20.1)(10^4)\text{ in}^4$, $EI = 58.3 \times 10^{10}$.

Method 1 (Matlock-Reese) Using $k = 5$, we compute

$$T = \left(\frac{58.3 \times 10^{10}}{5}\right)^{1/5} = 163 \text{ inches},$$

also $L = 48 \times 12 = 576$ inches; $Z_{max} = 576/163 = 3.53$. The loads and moments acting at the top of the shaft are shown in Figure 10–34.

For the maximum moment caused by the lateral load P_T, we select $A_M = 0.75$ from Figure 17 of the reference. Then $M_{T(max)} = (50)\left(\frac{163}{12}\right)(0.75) = 510$ ft-kips.

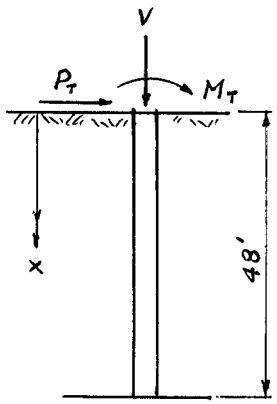

Depth (in)	Moment M_A, ft-kips, due to P_T	Moment M_B, ft-kips, due to M_T
0	0	195
100	360	187
200	502	148
300	421	94
400	210	48
500	68	14
550	14	0

Figure 10–34 Loads and moments, shaft of Design Example.

The moments at various depths x are now tabulated as follows:

Depth x (in)	$Z = \frac{x}{T}$	A_M	$M_A = P_T T A_M$ (ft-kips)
100	0.61	0.53	360
200	1.22	0.74	502
300	1.84	0.62	421
400	2.45	0.31	210
500	3.06	0.10	68
550	3.37	0.02	14

The maximum moment caused by M_T is obviously M_T = 195 ft-kips for $x = 0$. From Figure 20 of the reference, and using curve 4, we select appropriate values for B_M. The moments at various depths x are likewise tabulated as follows:

Depth x (in)	$Z = \frac{x}{T}$	B_M	$B_M = B_M T$ (ft-kips)
0	—	1.00	195
100	0.61	0.96	187
200	1.22	0.76	148
300	1.84	0.48	94
400	2.45	0.22	43
500	3.06	0.07	14
550	3.37	0	0

The total moment is the sum of $M_A + M_B$, tabulated as follows:

Depth (in)	0	100	200	300	400	500	550
$M = M_A + M_B$	195	547	650	515	253	82	14

These moments are plotted in Figure 10–35. The maximum moment occurs approximately at a depth of 16 feet, and has a value M_{max} = 660 ft-kips.

The horizontal displacement of the top of the shaft has two components: a displacement produced by P_T = 49 kips, and a displacement produced by M_T = 195 ft-kips. Using Figure 13 from the reference, A_y = 2.5 (curve 4). The displacement caused by P_T is

$$\Delta y_p = A_y \frac{P_T T^3}{EI} = (2.5)\frac{\left(50\times 10^3 \times 163^3\right)}{(58.3)\left(10^{10}\right)} = 1.0 \text{ inch.}$$

The displacement caused by M_T acting at the top is obtained by reference to Figure 18. We select B_y = 1.7. Then

$$\Delta y_m = B_y \frac{M_T T^2}{EI} = (1.7)\frac{(195)(12)\left(10^3\right)\left(163^2\right)}{(58.3)\left(10^{10}\right)} = 0.2 \text{ inch}$$

Total displacement y = 1.0 + 0.2 = 1.2 inches

Method 2 (Czerniak) We compute

$$E = \frac{M_T}{P_T} = \frac{195}{49} = 3.9 \text{ feet.}$$

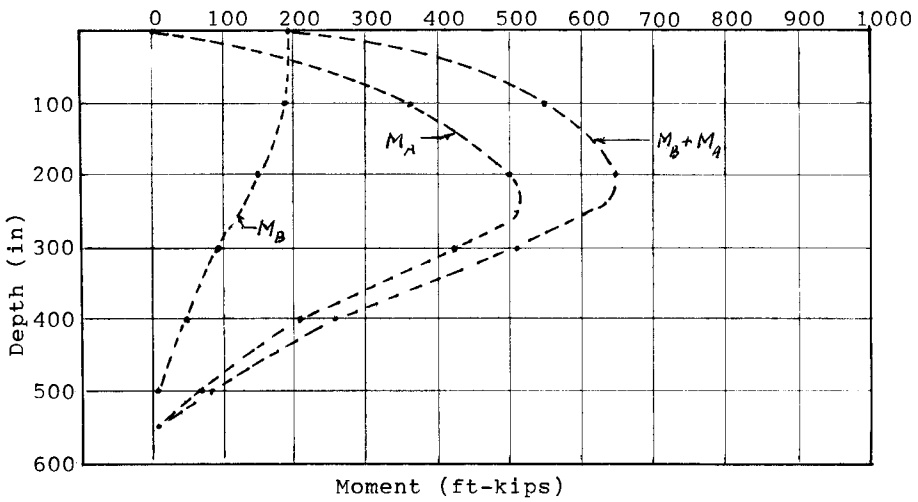

Figure 10–35 Moment diagrams, M_A, M_B, $(M_A + M_B)$.

Using $R = (0.25)(3.75) = 0.9375$ kips/ft/ft, we can write

$$L^3 - \frac{(14.14)(50)L}{0.9375} - \frac{(18.85)(195)}{0.9375} = 0,$$

or $L^3 - 755L - 3920 = 0$, which, solved, gives $L = 29.53$ ft, and $E/L = 3.9/29.53 = 0.132$. For M_{max}, $V = 0$, or $1 - 10.584K^2 + 9.584K^3 = 0$, where $K = x/L$, or $K^3 - 1.102K^2 + 0.1044 = 0$, which gives $K = 0.380$, 0.361, hence $x = LK = 11.2$ feet. $M_{max} = (50)(29.53)(0.132 + 0.380 - 0.201 + 0.050) = 533$ ft-kips.

The maximum moment obtained from method 2 is 80 percent of the maximum moment obtained from method 1. A more satisfactory agreement may be obtained if a better convergence between the lateral soil pressure and the coefficient k is possible. The soil pressure (250 lb/ft) for the site conditions is reasonable. However, the value of $k = 5$ used in method 1 may be unduly conservative.

These shafts, and the portion above their top, are reinforced with tension steel concentrated along the tension semiperimeter. This is possible because there is no reversal of the direction of the lateral loads, and gives considerable economy by increasing the structural capacity of the shaft for less reinforcement.

The foregoing design has been used by the author in highway projects in Chicago and other midwest locations. Considerable reduction in the shaft length is possible if the transfer of vertical load is assumed by side resistance and base bearing according to the current approach. Walls of this type may be compared with the wall systems discussed in chapter 6 for economy, constructibility, and performance.

REFERENCES

AASHTO, 1994: AASHTO LRFD Bridge Design Specifications.

BARKER, C. W. and F. KHAN, 1971: Caisson Construction Problems and Corrections in Chicago, J. ASCE Soil Mech. Found. Div., February, pp. 417–439.

BARKER, R. M., J. M. DUNCAN, K. R. ROJIANI, P. S. K. OOI, C. K. TAN, and S. G. KIM, 1991, *Manuals for the Design of Bridge Foundations*, NCHRP Report 343, TRB, Washington, D.C., p. 308.

BHUSHAN, K., 1982: "Discussion: New Design Correlations for Piles in Sands," JGED, ASCE, GT11, Nov., pp. 1508–1510.

BHUSHAN, K. and S. ASKARI, 1984: "Lateral-Load Tests on Drilled Pier Foundations for Solar Plant Heliostats," ASTM STP No. 835, pp. 140–156.

BOWLES, J. E., 1988: *Foundation Analysis and Design*, McGraw-Hill, New York, p. 1004.

BROWN, D. A., REESE, L. C., and M. W. O'NEILL, 1988: "Cyclic Lateral Loading of a Large Scale Pile Groups," *ASCE, JGED*, vol. 113, Np. 11, Nov., pp. 1326–1343.

Canadian Geotechnical Society, 1985: "Canadian Foundation Engineering Manual," 2nd ed., Bitech Publishers Ltd., p. 460.

CARTER, J. P. and F. H. KULHAWY, 1988: "Analysis and Design of Foundations Socketed into Rock," EPRI Report No. EL-5918, N.Y., p. 158.

CZERNIAK, E., 1957: "Resistance to Overturning of Single, Short Piles," *J. Struct. Div.*, ASCE, vol. 83, No. ST2, Proc. Paper 1188, March, pp. 1–25.

CUMMINGS, E. M., 1960: "Cellular Cofferdams and Docks," T*rans. ASCE*, vol. 125, pp. 13–45.

DAVISSON, M. T., and K. E. ROBINSON, 1965: "Bending and Buckling of Partially Embedded Piles," *Proc. 6th Int. Conf. Soil Mech. and Found. Eng.*, Montreal, Canada, pp. 243–246.

DAVISSON, M. T. and J. R. SALLEY, 1972: "Settlement Histories of Four Large Tanks on Sand," *5th PSC*, ASCE, vol. 1, part 2, pp. 981–996.

DUNCAN, J. M. and A. L. BUCHIGNANI, 1976: "An Engineering Manual for Settlement Studies," *Geotechnical Engineering Report*, Univ. of California, Berkeley, p. 94.

EVANS, Jr., L. T. and J. M. DUNCAN, 1982: "Simplified Analysis of Laterally Loaded Piles," UC Berkeley Rept. No. UCB/GT/82-04, July, p. 245.

FHWA, 1989: "Interim Procedures for Evaluating Scour at Bridges," p. 62.

FOCHT, J. A. and K. J. KOCH, 1973: "Rational Analysis of the Lateral Performance of Offshore Pile Groups," *Proc. 5th Offshore Technology Conf.*, Houston, TX, vol. 2, Paper OTC 1896, pp. 701–708.

HORVATH, R. G. and T. C. KENNEY, 1979: "Shaft Resistance of Rock Socketed Drilled Piers," *Proc. Symp. on Deep Foundations*, ASCE, Atlanta, Georgia, pp. 182–214.

KROHN, J. P. and J. E. SLOSSON, 1980: "Assessment of Expansive Soils in the United States," *Proc. 4th Intern. Conf. on Expansive Soils*, ASCE, vol. 1, Denver, CO., June, pp. 596–608.

KULHAWY, F. H., TRAUTMANN, C. H., BEECH, J. F., O'ROURKE, T. D., and W. MCGUIRE, 1983: "Transmission Line Structure Foundations for Uplift-Compression Loading," *EPRI Rept. EL-2870*, Electric Power Research Institute.

LUKAS, R. G. and C. N. BAKER, 1978: "Ground Movement Associated with Drilled Pier Installations," *ASCE Spring Convention*, Pittsburgh, Preprint No. 3266, p. 16.

MATLOCK H. and L. C. REESE, 1961: "Foundation Analysis of Offshore Pile Supported Structures," *Proc. 5th Intern. Conf. on Soil Mech. and Found. Eng.*, vol. 2, pp. 91–97.

MEYERHOF, G. G., 1976: "Bearing Capacity and Settlement of Pile Foundations," ASCE JGED, vol. 102, No. GT3, March, pp. 196–228.

OOI, P. S. K., K. B. ROJIANI, J. M. DUNCAN, and R. M. BARKER, 1991: "Engineering Manual for Drilled Shafts," NCHRP 343, TRB, Washington, D.C.

POTYONDY, J. G., 1961: "Skin Friction between Various Soils and Construction Materials," *Geotechnique*, vol. XI, No. 4, pp. 339—353.

POULOS, H. G. and E. H. DAVIS, 1980: *Pile Foundation Design and Analysis*, Wiley, New York, p. 397.

PRAKASH S. and H. D. SHARMA, 1990: "Pile Foundations in Engineering Practice, Wiley, New York, p. 734.

QUIROS, G. W. and L. C. REESE, 1977: "Design Procedures for Axially Loaded Drilled Shafts," Research Rept. 176-5F, Project 3-5-72-176, *Center for Highway Research,* Univ. of Texas, Austin, Dec., p. 156.

REESE, L. C. and M. W. O'NEILL, 1969: " Field Tests of Bored Piles in Beaumont Clay," *ASCE Annual Meeting,* Chicago, Preprint No. 1008, p. 39.

REESE, L. C. and M. W. O'NEILL, 1988: "Drilled Shafts: Construction Procedures and Design Methods," FHWA Publication No. FHWA-HI-88-042 or ADSC Publication No. ADSC-TL-4, Aug., p. 564.

REESE, L. C. and S. J. WRIGHT, 1977: "Drilled Shaft Manual-Construction Procedures and Design for Axial Loading," vol. 1, *U.S. Dept. of Transportation*, Implementation Div., HDV-22, Implementation Package 77-21, July, p. 140.

TERZAGHI, K., 1945: "Stability and Stiffness of Cellular Cofferdams," *Trans. ASCE*, vol. 110, pp. 1083–1202.

TOUMA, F. T. and L. C. REESE, 1974: "Behavior of Bored Piles in Sand," *ASCE JGED*, vol. 100, No. GT7, July, pp. 749–761.

WHITAKER, T. and R. W. COOKE, 1965: "Bored Piles with Enlarged Bases in London Clay," *Proc. 6th Int. Conf. Soil Mech. Found. Eng.*, Montreal.

XANTHAKOS, P. P., 1979: *Slurry Walls,* McGraw-Hill, New York, p. 622.

YAZDANBOD, A., SHEIKH, S. A., and M. W. O'NEILL, 1987: "Uplift of Shallow Underream in Jointed Clay," *Proc. ASCE, Foundations for Transmission Line Towers*, ed. by J. L. Briaud, Atlantic City, New Jersey, April, pp. 110–127.

CHAPTER 11

Prismatic and Linear Foundations

A brief discussion of linear and prismatic elements used in bridge foundations is included in section 1.5. In general, this type is indicated where it can replace a group of piles or shafts under conditions ensuring improved efficiency and structural performance. Two criteria are relevant to the optimum design and use: (1) The structural capacity is compatible with the geotechnical strength so that neither is wasted; and (2) there is no reduction in performance factors because of redundancy considerations.

11.1 SHAPES AND CONFIGURATIONS

The adaptation of special-shape foundation elements has resulted from the development of machines that could perform slot excavations, thus expanding the range of foundation options. Typical configurations are shown in Figure 11–1. Variations from the basic sections can be worked out for unusual substructures and special classes of bridges. Where a bridge project includes diaphragm walls, the use of prismatic foundations can be considered a logical choice, since it means the same equipment and construction procedures.

Linear or prismatic elements can replace a system of driven piles or drilled shafts. This substitution may be particularly advantageous where heavy loads require unusually large monolithic structures, where the foundation is exceptionally deep or in difficult ground, and where large thrusts and bending moments must be resisted ant the lateral displacement must be kept to a minimum. Prismatic panels exhibit unusual flexibility in size, shape, and plan, which makes them suitable for any combinations of loads.

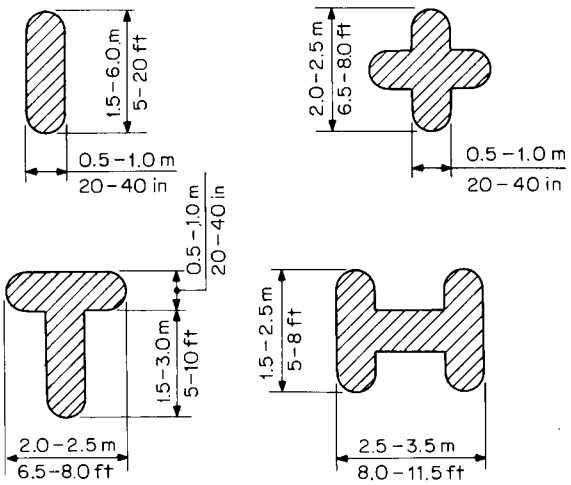

Figure 11–1 Cross sections of typical load-bearing elements.

Linear or prismatic diaphragm wall panels can replace an equivalent row of piles, giving a monolithic structure that is independent of fixed tolerances (for example, pile spacing). A T section acts as a T beam, and offers a compatible solution when the foundation is subjected to specific compression and tensile effects, but without stress reversal. Shapes of I and H configuration are suitable for resisting vertical and lateral loads that can change magnitude and direction. An element with an X section is indicated where vertical loads control the design.

An important advantage is the elimination of construction joints, round-end tubes, casings, and all the associated appurtenances (mandatory in wall construction). This makes scheduling and installation feasible on a more efficient basis. A single element may be excavated and cleaned on the same day, and reinforced and concreted the following day.

11.2 CONSTRUCTION CONSIDERATIONS

Certain construction considerations apply also to the walls discussed in section 6.1, including conventional diaphragm walls and derivative systems. This review, however, is intended to provide a summary of procedures as they relate to the installation of load bearing elements of linear and prismatic sections. A detailed review of construction fundamentals is given by Xanthakos (1994).

Effect of site conditions. The construction procedures stipulated in the contract documents should reflect a design that is closely related to relevant site conditions. These are:

1. Soil characteristics that may require control as they may affect trench stability and composition of slurry.
2. The presence of boulders and other underground obstacles, the removal of which may require special tools and equipment.
3. Site layout and space availability, since this may affect plant size, equipment, and daily operations.

4. Aggressiveness of groundwater to the extent that it may affect the slurry controls and steel protection.
5. Traffic closure or maintenance because of the obvious effects on construction scheduling and productivity.

In particular, attention is drawn to the presence of large boulders and other obstructions. Typically, these can slow down the excavation and may require conversion to percussive tools.

Excavating Systems

Although it is seldom necessary to identify the method of excavation and type of equipment in the design stage, expediency requires a fundamental knowledge of certain types of equipment and their optimum ranges. Engineers are cautioned, however, that the ideal endeavor for any contractor is to use a process and equipment that will complete the work in the shortest possible time and at the least possible cost. Any misconceptions with regard to these considerations can be resolved by a simple statement: For this type of work, only excavating systems developed for this purpose should be used.

Classification of excavating systems. Since only bearing elements are discussed here, we consider machines and equipment developed for this purpose.

Bucket and Grab Types. These machines have a high weight-to-volume ratio to overcome drag and flotation effects of gelled slurry. The grabs are usually round or egg-shaped to provide half-rounded ends. The excavation is carried out directly and the materials are discharged by the grab in a cyclic process. Examples are mechanical diggers, bucket excavators, shovels, and special grabs and clamshells.

Occasionally a kelly is used to which the main equipment is fixed. The kelly is guided above the ground and functions to position and control the equipment above the ground, guide the machine, and provide additional weight. Kelly bars are much heavier and suitable where restricted headroom and weight limitations do not exist.

Percussive Tools. These are extra heavy and rigid, and often of special design. They are used to break rock or loosen hard ground where other types of equipment become inoperative. The excavation is slower and has a higher cost. The cost factor should be analyzed when the foundation must be socketed into rock for extra bearing. This means that the excavating implement must be converted to percussive tools when the rock is reached.

Rotary Drilling. Equipment of this type performs slot excavation. The drilling bits loosen the soil through simultaneous action, helped by side cutters moving vertically to cut through soil not reached by the bits. The soil is consolidated into individual cuttings that are mixed with slurry and held in suspension, and then circulated upward through the drill stem and reverse circulation hose for separation in screens and cyclones. These machines are particularly suitable for excavating panels for linear and prismatic elements.

Factors affecting selection of equipment. Load-bearing elements are built in the configurations shown in Figure 11–1. The linear element is usually excavated in one equipment pass. The T-element usually requires two equipment passes, as does the

X-element. The I-element typically requires three equipment passes. The dimensions of these elements are dictated by design considerations, but must also be compatible with the excavating range of equipment locally available.

Consistent excavation rates, horizontal and vertical accuracy, and flexibility to deal with special site and soil conditions are the main factors that influence the choice of equipment. The selection must also be satisfactory in terms of cost and maintainability, that is, equipment is often chosen because it can do the job at the least total cost. However, load-bearing elements are built in trenches 24 to 48 inches wide. These require better excavation accuracy, coordination between excavation rates and materials handling, and operational flexibility with phases such as cage installation and concreting. This work may be better executed with more sophisticated equipment and better controls.

Deep foundations are commonly built in soils that vary from soft to hard, and often they encompass the entire range. Most clay and sand formations can be excavated with most machine types, but a serious drop in efficiency should be expected in hard formations, dense gravel, bouldery ground, and bedrock. Operating difficulties and efficiency, penetrating rates, and drilling output become often critical from the viewpoint of construction scheduling and also in terms of design consistency. Engineers are thus cautioned to request data from field performance in order to quantify the operation in terms of time. These data may be used as guidelines in the design stage and as criteria for detailing the project. For example, most excavating systems have depth limitations, or at some point efficiency decreases to a level at which the machine becomes inoperable.

Project specifications normally should dictate or define the final results, but occasionally it is necessary to identify certain processes to ensure a foundation consistent with the intended capacity and transfer of load. This may restrict the choice of equipment to those types that are provided with automatic control devices, comply with minimum excavation rates, and are commercially available. A review of excavation equipment is given by Xanthakos (1979, 1994).

Excavation under Slurry

Linear and prismatic panels are typically excavated under slurry protection. The slurry is introduced as soon as the excavation begins and remains until the excavation is completed, to be eventually replaced by the fresh concrete. Because it fulfills a multiple function, stability controls are essential regarding viscosity, pH, and density, and must be specified accordingly.

Preparing the base. If an element is intended for base bearing, the bottom of the excavation must be checked and cleaned before concrete placement. Because visual inspection is excluded, special care is necessary to ensure a clean bottom and thus provide a firm foundation. Although the design procedures are usually based on the assumption that the construction is completed under competent supervision and with adequate quality control, the condition of the final excavation should be verified by field checks.

The shape of the base depends largely on the equipment performing the excavation. The bottom may be nearly flat and level, or it may have one of the profiles shown in Figure 11–2. There has been no evidence to indicate that the shape of the bottom influences the load-bearing capacity, at least from the theoretical standpoint; hence there should be no objection to the use of machines that do not provide flat or square bottoms.

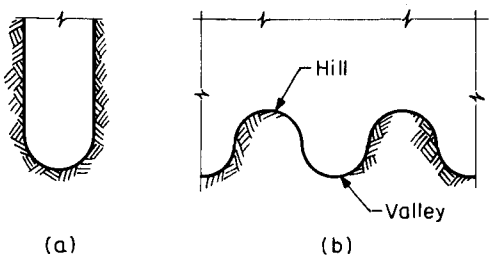

Figure 11–2 Different bottom shapes: (a) round cross section cut by a round-end clamshell; (b) irregular bottom excavated by a rotary long drill.

A smooth square base is, however, better cleaned at the end of excavation with a square-end clamshell or by shifting the drill to even the hills.

Soft materials tend to accumulate at the base, or they remain in suspension near the base where the viscosity of the slurry provides this capacity. Their presence may easily be detected by taking samples of bentonite near the bottom. If these have unusually high density, the slurry must be recycled or replaced by a fresh solution before concreting.

There should be no compromise in the matter of bottom cleanliness and condition. In most instances it is only necessary to pass an airlift in order to obtain a satisfactory base. A small amount of dry or plastic cuttings left at the bottom is unlikely to affect the bearing capacity, but if 1 inch (2.5 cm) or more of soft mud is accumulated at the bottom, it can have a marked effect on the load transfer. This mud is unlikely to be displaced by the fresh concrete, although it will be partially consolidated by its weight, and thus it may provide a zone of postconstruction settlement.

In some instances, bottom softening may be caused by seepage and soil impregnation by slurry of the zone just below excavation level. This penetration is stopped by rheological blocking, but may reoccur with the passage of tools to clean or level the base. Although it can raise the moisture level of the soil layer just below the base, it should not have a real influence on the compressibility and load carrying capacity.

Control limits. For the usual excavations slurries perform the following functions:

1. Support the face of the excavation and prevent sloughing and peeling off.
2. Seal the formation and form a filter cake, necessary to deter slurry loss to the ground.
3. Support detritus thereby preventing sludgy unconsolidated material from settling down at the bottom.
4. Carry the cuttings in the slurry volume thereby preventing sedimentation in the mud circuit.

Simultaneously, these functions must be compatible with certain operations, namely:

5. Ensure the flow of concrete from tremie pipes to allow complete displacement by fresh concrete.
6. Ensure free flow in the pipe circuit to facilitate materials handling.
7. Aid sedimentation in tanks and facilitate the separation of solids in screens and cyclones.
8. Facilitate disposal in dump areas.

Face Support. Stability of linear short panels is usually ensured by considering the arching effect (Xanthakos, 1979; 1994). If the analysis indicates a need for a heavier slurry, noncolloid materials (soil from the excavation) may be added to the slurry to increase its density. Stability, however, may have to be checked for T-, I-, and X-sections (Figure 11–1), especially along reentry corners where the failure surfaces may intersect. Experience, however, shows that stability problems with short linear and prismatic excavations have seldom been the case, and can be avoided if the element is excavated and concreted in the shortest possible time.

Suspension of Excavated Materials. For foundation elements, the ability of slurries to keep excavated materials in suspension is probably the most critical requirement. A shear strength of slurry of the order of 75 dyn/cm^2 (about 15 lb/100 ft^2) will support sand particles 1 mm in size, which is the average particle size of coarse sand. Some doubt exists whether this should be the initial or 10-min gel strength, but according to experience the latter gives good results. If a higher gel strength is found necessary, it can be provided with extra bentonite.

Displacement by Concrete. For these excavations, the concrete placement and subsequent displacement of slurry is carried out under more favorable conditions. Because the trenches are relatively short, plug flow (initial batch of concrete on top) is usually ensured if the density of the slurry at the time of concrete placement does not exceed 75 to 80 lb/ft^3, which is equivalent to a specific gravity of 1.25. The plastic viscosity of the slurry should not be greater than 20 cP during concrete placement.

Separation of Noncolloid Fraction. A more efficient collection of entrained sand is possible with a thinner slurry, but no controls should be established for the separation of clay cuttings since only well-preserved samples are susceptible to mechanical separation.

Pumping of Slurry. This is important in reverse circulation. For effective pumping, sand particles and clay cuttings should not be allowed to settle in the pipe circuit if flow is interrupted. Because of thixotropy, higher pumping pressures are required to restart flow than to maintain it. When the pump is restarted, the applied pressure must overcome the shear strength of slurry attained during shutdown.

The control limits associated with the foregoing functions and operations are summarized in Table 10–2, since they apply also to drilled shafts installed under slurry. The same comments made for shafts apply also to linear and prismatic excavations.

Effect of soil conditions. Potentially troublesome situations are excavations in very pervious ground with low groundwater table. This may result in a considerable loss of slurry before a seal is formed to stop slurry flow toward the ground. Excavation in very soft clay with low cohesion, intended to reach harder formations, may give rise to stability problems. More important, the clay cuttings may not be suspended, but dispersed in the slurry or settling to the bottom. In this instance, extra care is warranted to provide a clean base.

Concreting

Reinforcing cages are usually assembled in the shop, if practicable, or at the site. For very deep panels, the cages may reach formidable dimensions, and this can cause handling problems. During hoisting, the action of its own weight can result in severe distor-

tion of the cage. With the exception of linear panels and X sections, the cage is likely to have a center of gravity that does not coincide with the geometric center; hence it must be held in the right position before it is inserted in the panel.

The requirements of concrete placement are the same as in conventional diaphragm walls. However, the shape and configuration of the trench may dictate the location and number of tremie pipes. A T section of nominal dimensions can be filled with one tremie pipe placed at the junction of the stem and the flange. An I or square section will probably require one tremie pipe at each opposite corner. An X section can be concreted with one tremie pipe at its center.

Because there are no construction joints, the construction is simplified and allows more efficient scheduling. A single element can be excavated in one day, and reinforced and concreted the next day. If an airlift is contemplated, it should be done just before concreting to prevent recurrence of cavitation while the panel is open. Once the concrete pour has started, it should continue uninterrupted.

Construction Problems and Remedies

Essentially the same potential problems can arise as in drilled shafts, discussed in section 10.3. Because of the extra concrete area usually available with linear and prismatic elements, there is ample structural capacity so that deficiencies in this context are extremely rare. Because of the exceptionally large loads expected to act on these elements as a result of a philosophy intended to optimize the design, insufficient bearing capacity at the base may be a possible cause of settlement, particularly where the load transfer is primarily through direct bearing. In these cases, the design must ensure the compatibility between the structural and geotechnical capacity to satisfy the economic criteria of this application.

11.3 THE TRANSFER OF AXIAL LOAD: BASIC CONCEPTS

Base Bearing

The transfer of load by base bearing (tip resistance) is influenced by the depth and size of the element, the soil characteristics, disturbance of the base, and the contact between the concrete and the soil underneath.

Loosening of the base, sometimes occurring with shafts drilled by casing in saturated soils, is limited and unlikely in prismatic panels excavated under slurry. Where the base resistance has been found lower than predicted, this has been attributed to the presence of soft materials that remained in the bottom because of poor cleaning procedures. The general conclusion is, therefore, that for well-supervised and well-constructed projects, the method of excavation and concrete placement causes minor disturbance to the soil so that base resistance will develop as predicted.

Side Resistance

As in drilled shafts, in the usual range of working loads the transfer of load in linear and prismatic elements begins with skin friction or side adhesion and is completed by base bearing when sufficient vertical displacement has occurred. Even the best methods

of analysis are semi-empirical, relating side resistance to a friction factor for sands, and to the undrained shear strength for clays. When a panel is excavated under slurry, the presence of any bentonite at the interface (not displaced by the rising fresh concrete) can influence the development of shaft resistance in the soil-structure interaction. Two questions often raised are (1) when and how the bentonite mud is completely swept or absorbed by the rising fresh concrete, and (2) to what extent any bentonite left at the interface will inhibit the development of side shear.

Interestingly, these considerations would also apply to any excavations, linear or circular, under slurry. Some suspicion that slurries may adversely affect the shear resistance stems from their use as lubricants in caisson and tunnel construction. Field tests of piles cast in bentonite slurry have disclosed a stabilized layer of bentonite clay that caused a decrease in shaft shear. Other comments suggest that during concreting some cementitious material may diffuse into or mix with the filter cake, and this will produce a mix similar to a clay-cement grout with a shear strength depending on the type of clay and cement. If the cake is from residual native clay slurry, it will produce a weak mix. With a bentonite cake the mix should be much stronger. If the cement penetrates the cake, the shear resistance will depend on the shear strength of the mix, the soil, or their interface. If part of the thickness of the cake remains unaffected by cement penetration, its shear strength will probably control the shear resistance. With time the filter cake will tend to consolidate so that its strength should be predicted from tests at the appropriate overburden pressure. Results on two types of bentonite (English, converted sodium; Wyoming, natural sodium) produced undrained angles of shear resistance 15° and 6°, respectively. These results may suggest that the side friction for excavations under Wyoming bentonite may be a fraction of that under English bentonite.

It appears from these comments that the type, porosity, and permeability of the soil around the element will determine the associated interaction in the final position. In impervious clay, neither filtration nor soil impregnation will occur, and during the concrete placement all bentonite should be expected to be swept from the interface. Sand and gravel formations are prone to deep filtration and rheological blocking according to the void size and distribution, the hydraulic gradient, and the shear strength of the slurry. All free bentonite is swept by the rising concrete mix, but the sweeping action does not extend beyond this zone. Although some colloid matter may remain between the bulk of the vertical earth face and the hardened concrete, experience and field tests confirm that considerable friction is still available. This friction is further improved by the roughness of the interface, which is typical in sand-gravel excavations.

A hole in clay is thus equivalent to a cased hole, whereas a slurry panel in pervious soil promotes a slurry-soil interaction. The practical significance of these phenomena may be tested in actual panels, and results from these tests provide the basis for establishing design criteria.

11.4 DATA FROM LOAD TESTS

Field Tests on Linear Panels

UNO building in Vienna. Figure 11–3 shows load-settlement curves of test panels of circular and linear configuration for the UNO Building in Vienna (Kienberger, 1974). Panels I and II have the same depth, but a direct comparison of load transfer is not

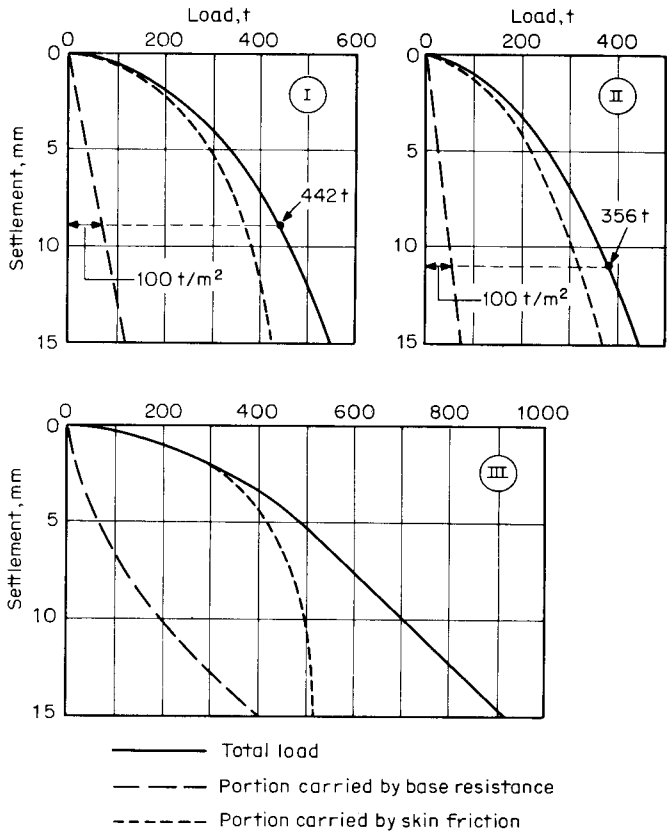

Figure 11–3 Load-settlement behavior of test elements for the UNO Building in Vienna *(from Kienberger, 1974).*

practical because of the difference in the shape and cross section. Relevant data are summarized in Table 11–1. The ground at the test site consists of gravel, silty clay, and fine sand, generally stiff or dense.

The load transfer characteristics of panels I and II can be correlated, however, noting that in both cases the ultimate base bearing q_p is about 10 kg/cm^2 (100 tons/m^2), or 20.6 kips/ft^2. The total load carried by the circular element is 356 tons, and of this load 293 tons are resisted by side shear and 63 tons are resisted by base bearing. The average shear stress (ultimate) q_s at the interface is 7.9 tons/m^2 or 1.63 kips/ft^2. For the linear panel I, the total load is 442 tons, and skin friction amounts to 372 tons, giving an average q_s at the interface 8.0 tons/m^2 (1.65 kips/ft^2), or the same as for the circular panel. The vertical displacement corresponding to these loads are 9 mm (0.36 in) and

Table 11–1 Test Elements for the UNO Building in Vienna

Element	Dimensions and shape	Test load, *t*	Depth, *m*
I	50- by 150-cm diaphragm-wall panel	500	13
II	90-cm-diameter pile	500	13
III	50- by 150-cm diaphragm-wall panel	1000	24

(From Kienberger, 1974)

11.4 mm (0.45 in) for the linear and circular panel, respectively. The small difference in settlement reflects differences in the methods of installation and bottom cleaning. For the linear panel, the bentonite was premixed and consistently controlled, but for the circular panel bentonite and water were mixed and added as the hole was advanced. The base of the hole was cleaned before concreting, but some loose material was left at the bottom.

Pullout tests showed the same side shear for both elements I and II at the same top displacement. For the two linear panels, a displacement of 15 mm (0.6 in) mobilized a shear resistance of 4.2 tons/m^2 (0.87 kips/ft^2) in the zone of silty clay and fine sand, but the shear resistance was rather uncertain in the gravel and fill layers.

Surface deformation between and around the panels was uniform. The three elements were placed sufficiently apart (15 m, or 50 ft) to exclude overlapping of their influence zones. The latter diminished, however, within a smaller cone that covered an area radially from the face about 1½ times the shaft diameter or the diameter of a corresponding circle for the linear panels. The two linear panels have the same zone of influence despite the difference in depth.

Tests in Boston clay. Goldberg (1979) reports results of tests of linear panels in clay, carried out in connection with the MBTA Red Line extension. The blue clay is highly sensitive (loss of strength upon disturbance). The tests involved two panels, 18 and 6.5 feet long, respectively, and 3 feet wide. Both panels were 60 feet deep, and the shorter unit was loaded to failure.

Results from these tests indicate that base bearing was negligible and might be ignored in design. The load-carrying capacity was essentially derived from shaft resistance. The ultimate side shear q_s was estimated as 1200 lb/ft^2. Based on these results a wall element 60 feet deep could accommodate a design load of 80 kips/ft of wall (linear) for a factor of safety of 1.8. This load would include, however, the dead weight of the wall, estimated at 27 kips/ft.

Test panels in London clay. Tests on diaphragm wall panels in London clay are reported by Corbett et al. (1974). The test panels measure 1.2 by 0.5 meters in plan, and are 14.4 meters deep. The excavation was completed with a cable-operated grab, and before placing the concrete, the slurry was replaced with a fresh solution. On completion of the pour, an overbreak of 8.5 percent was observed, indicating some cavitation and overexcavation in the granular layers. The soil profile is typical for London, and consists of successive layers of sandy clay (brick earth), sand and gravel, and stiff fissured clay.

Using an adhesion factor of 0.5 for clay (consistent with Table 10–6), a friction factor of 0.7 (Table 10–7) for sand, and a bearing-capacity factor of 9.0, Corbett et al. (1974) estimated an ultimate shaft resistance of 2190 kN (490 kips) and an ultimate base bearing of 740 kN (170 kips) giving a total ultimate capacity of 2930 kN (660 kips).

The panels were subjected to six cycles of loading, the first five being incremental and the sixth consisting of a constant-rate load application. For the last cycle, a maximum load of 4000 kN (900 kips) was sustained. At this load level, the shaft carried 3650 kN (820 kips), leaving only 350 kN (80 kips) for the base bearing, or about one-half the estimated base bearing.

The actual ultimate shaft resistance was about 65 percent higher than estimated. It is therefore conceivable that both the factor α for clay and K for sand (Touma and Reese, 1974) were underestimated and that favorable construction (overbreak and face

irregularities) contributed to increased shaft resistance in all three layers. An analysis of this foundation is included in the design examples. (Xanthakos, 1994).

Laboratory Tests

Using the apparatus shown in Figure 11–4, Farmer et al. (1971) have investigated the effect of bentonite on skin friciton and for concrete-sand interfaces. The sand samples have a bulk density of 1660 kg/m^3 (104 lb/ft^3) and a relatively low degree of saturation to allow the formation of a stable cylindrical opening. The slurry was introduced and remained until an interaction zone 5 mm thick (0.2 in) was formed at the interface. Then the slurry was replaced by fresh concrete (6-inch slump) through a tube intended to simulate the upward flow motion of tremie concrete. A relatively unscoured filter cake was observed when the interface was exposed.

After the concrete was allowed to set, a confining pressure was applied through the polythene membrane for 5 hours, inducing horizontal compression while constraining vertical compression against the top and bottom plates. The vertical displacement of the element was measured upon the application of incremental loads. The test was repeated at a confining pressure of 0.07, 0.14, 0.21, 0.28, and 0.35 N/mm^2 (10, 20, 30, 40, and 50 lb/in^2, respectively), and for each set the load application was continued until excessive displacement occurred.

Test results. The average friction-pressure ratio is plotted in Figure 11–5 versus the vertical displacement for concrete-sand and for concrete-sand-bentonite interfaces. For low displacements, the friction is somewhat higher when bentonite is present, but with

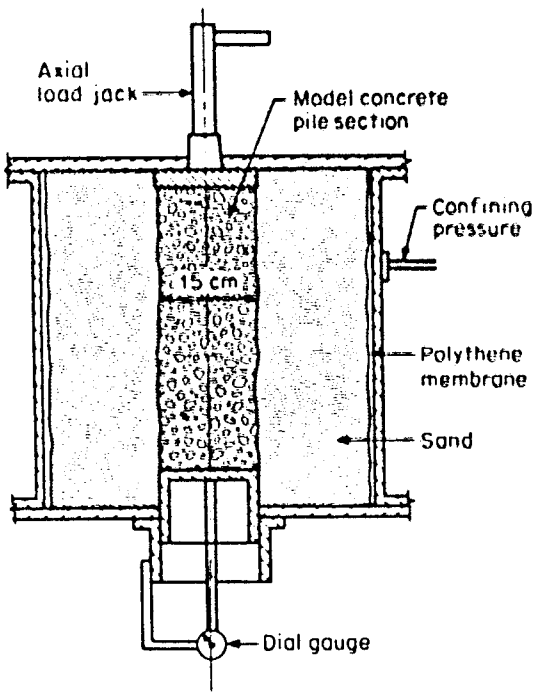

Figure 11–4 Triaxial shear apparatus used to investigate the effect of bentonite on skin friction *(from Farmer et al., 1971).*

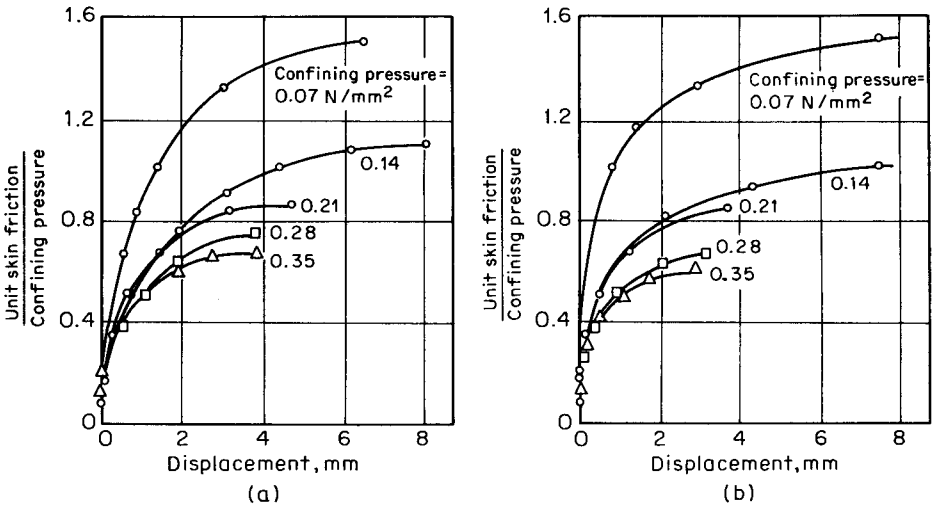

Figure 11–5 Friction-displacement characteristics of model pile; (a) concrete-sand interface. (b) concrete-bentonite-sand interface *(from Farmer et al., 1971).*

larger displacements the friction is greater without bentonite. The difference, however, is small and less than 10 percent.

The friction increases with increasing displacement and attains peak values (ultimate resistance) at displacements from 5 to 10 mm (0.2 to 0.4 in), which is in good agreement with results from field tests. The fully developed load transfer increases with confining pressure. This relationship is, however, nonlinear in the range of low confining pressures and tends to become linear in the range of higher confining pressures, as shown in Figure 11–6.

Field Tests on Drilled Shafts

Field tests on bored piles (diameter from 30 to 37 inches) have been carried out by Reese and Touma (1973). These tests and results thereof are also described by Xanthakos (1979, 1994), and will not be repeated here. They include load-distribution curves, load-settlement curves, and load-transfer curves. An important conclusion is the adverse effect of poor cleaning procedure on the development of base resistance. This effect is compounded by poor concrete placement methods.

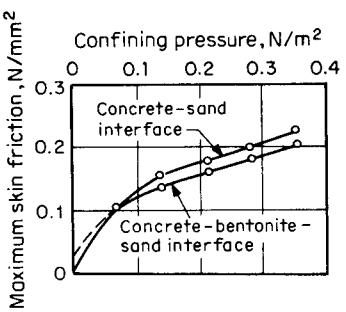

Figure 11–6 Skin friction vs. confining pressure; fully developed load transfer *(from Farmer et al., 1971).*

11.5 GUIDELINES FOR THE DESIGN OF LOAD BEARING LINEAR AND PRISMATIC ELEMENTS

Neither AASHTO, LRFD, or other domestic literature contains guidelines for the analysis of load bearing linear and prismatic elements, or for the distribution of load between side shear and tip resistance. Interestingly, linear and prismatic foundations have been used in Europe on a routine basis, and are becoming common practice in the United States in both building construction and bridge work.

This trend follows the experience with slurry walls that has demonstrated their capacity to function as foundation elements. It appears that very often advances in the field of foundation engineering evolve from the ability to devise new ways of construction and observe how the new systems behave under field conditions.

Effect of shape. The foundation shapes shown in Figure 11–7 demonstrate how the configurations and dimensions can influence the load transfer. The round element shown in Figure 11–7(a) will develop its full shear along the entire perimeter. This is also true for the elongated I-section shown in Figure 11–7(c). The short I-section shown in Figure 11–7(b) will most likely develop its shear along a modified "effective" perimeter as shown, representing the shortest path of the side resistance profile. In this case, the weight of the soil fillet between flanges should be added to the vertical load.

The length-to-width ratio can influence the division of load between side and base, but this is not as yet explicitly defined. This conclusion follows a theoretical investigation of shafts with enlarged bases showing that the latter may not offer appreciable advantages over straight-shaft elements of the same diameter and length when the length-to-diameter ratio exceeds about 25, unless the stratum at the base is much stiffer than the overlying layers. In general, a higher modulus of the base materials compared to the modulus of the shaft materials, and a smaller length-to-width ratio, would indicate that a greater portion is resisted by base bearing.

Likewise, the entire shaft length may not be considered effective in developing side resistance, and this guideline follows the experience with drilled shafts discussed in chapter 10.

Useful guidelines. It appears from these comments that linear and prismatic panels are viable options in bridge foundations as they are with other classes of structures. The unconventional shapes shown in Figure 11–1 offer possibilities beyond the range of drilled shafts. The cost for site installation and diaphragm wall construction may often be 85 to 90% of the cost of large shafts, and may even be less compared to the cost of long prestressed piles. The difference in the design of the substructure may reduce

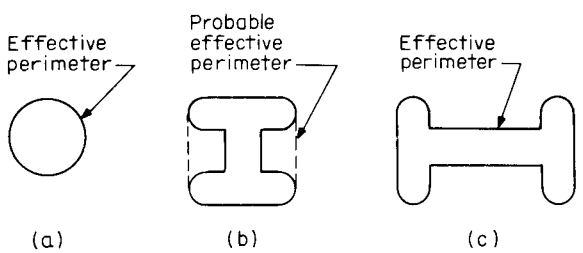

Figure 11–7 Influence of shape of load-bearing elements on effective perimeter.

these costs further; hence, it is essential to investigate the potential of these elements in bridge foundations.

The procedures outlined in the following sections reflect a combination of empirical data and theoretical concepts. They are also based on site conditions and construction methods assumed to be controllable in the context of design. Consideration should also be given to the large number of variables that cannot be isolated, and often are lumped into a single parameter. Thus, the design recommendations should not be used indiscriminately, but should be useful for most situations.

The following items should be placed on the construction agenda:

1. It is advantageous to excavate the panel, place the reinforcing cage, clean the bottom, and pour the concrete as soon as possible. The shorter the time a panel is open, the less the soil disturbance, cavitation, sloughing, bottom softening, and other related effects.
2. The method of excavation and bottom cleaning will affect the development of base bearing and side resistance. Soft base, roughness of the concrete-soil interface, moisture sensitivity of the earth materials, slurry displacement conditions, and changes in the in situ earth stresses are some of the factors that influence the load transfer. These are commonly expresses by a single performance parameter.
3. Excavating machines that produce a smooth face are no better than those that give a rough interface, but in practice it is difficult to express the difference quantitatively. Machines that remove excavated soil (for example, reverse circulation) should be preferred to excavators that do not.
4. The load transfer characteristics of slurry panels (linear or prismatic) are essentially the same as in drilled shafts and also as in dry construction. However, certain parameters are different.

Design Approach

The design philosophy of linear and prismatic panels is similar to the design of drilled shafts: The foundation must carry the imposed load safely, and must not undergo excessive movement. Hence, the two conditions for which the members must be checked are the ultimate strength state and the serviceability limit state. The usual steps involved in the analysis and design are essentially the same as in section 10.6, and need not be repeated here.

11.6 STRUCTURAL CAPACITY FOR AXIAL LOAD

Linear and prismatic elements are usually proportioned to carry compressive loads, and for this function the most suitable configurations are the simple linear panels and the X section. Occasionally, the members may have to resist uplift. If the latter is the primary type of load, consideration should be given to drilled shafts of circular shape where sufficient reinforcement (tensile) can be provided without excess cross-sectional area of the concrete. Buckling is very unlikely to control the design because of the small slenderness ratio.

The ultimate (factored) axial capacity should not be less than the sum of the factored axial load, expressed as

$$\phi_a P_n \geq \gamma_D P_D + \gamma_L P_L \tag{11–1}$$

which is Equation (10–2) repeated here for convenience, and the notation is the same as previously. Likewise, if several loads are involved, the design criterion is

$$\phi_a P_n \geq \Sigma \gamma_i P_i \tag{11–2}$$

The factored nominal capacity of the elements is

$$\phi_a P_n = r\phi_a \left(0.85 f_c' A_c + f_y A_y\right) \tag{11–3}$$

where A_c may be taken as the net cross-sectional area. The capacity reduction factor ϕ_a may be taken as 0.70 according to AASHTO. The parameter r is intended to represent the effect of a given eccentricity. For round elements, this factor is 0.85 with spiral reinforcement and 0.80 with ties. For linear or prismatic panels, unless the eccentricity of the applied load is severe, the factor r may be taken as 1.0.

Where the use of unreinforced elements is indicated with a low intensity of load and a minimum practicable size, under service conditions the allowable concrete stress may be taken as

$$f_c = 0.25 f_c' \tag{11–4}$$

There is some concern that the extreme concrete near the face may be intermixed with bentonite with an accompanying reduction in its integrity and strength. On the other hand, experience shows that overexcavation usually results in panels wider than the initial specified wall thickness. Hence, reduction in the effective wall thickness is not considered necessary.

11.7 GEOTECHNICAL CAPACITY: AXIAL LOAD IN COHESIVE SOILS

As in drilled shafts, the analysis is based on the total stress approach. However, caution must be exercised when strength reduction is possible after construction (for example, in expansive clays) or when consolidation of the soil around the element can result in a downward movement imposing downdrag forces. In these cases, effective stress analysis is appropriate.

Shaft Resistance

According to the α method, the shaft resistance may be expressed in terms of the undrained shear strength s_u, and thus Equation (10–14) is repeated here for convenience

$$q_s = \alpha s_u \tag{11–5}$$

Normally, values of α may be taken from Table 10–6, applied primarily to drilled shafts. Alternatively, this author recommends the following values for α.

1. In soft clays (q_u < 0.5 tons/ft^2), the factor α may be taken as 1, because failure should be expected to occur in the soil some distance away from the face, and q_s is therefore the same as s_u.

2. For stiff clays (q_u from 1.0 to 2.0 tons/ft^2), α can be expected to vary from 0.45 to about 0.60. The value of 0.45 is commonly taken for the stiff London clay and is close to the average shear strength obtained in triaxial tests. The value 0.6 is appropriate for the lower limit in this strength range and approaches the upper value of α in Table 10–6.
3. For hard clays (q_u > 4 tons/ft^2) the shaft resistance is roughly equivalent to the shear strength of a hard bentonite-clay coating at the interface. This can be taken as 2000 lb/ft^2 (96 kN/m^2).

It should be noted that the alternate approach in estimating the α values is more conservative for panels in very stiff to hard clays, and more realistic for panels in soft clays. An upper and a lower panel segment may be considered as noncontributing to the side shear as in drilled shafts. These values are suggested on an interim basis. A field test is recommended to confirm the design assumptions.

Base Bearing

For panels loaded under undrained conditions, the base resistance q_p is obtained from bearing capacity theories as in drilled shafts, or

$$q_p = N_c s_u \leq 40 \text{ tons/ft}^2 \tag{11–6}$$

Whitaker and Cooke (1965) recommend N_c values of the order of 6.5 when s_u is taken as the average shear strength from soil tests, and this is intended to compensate for sample disturbance and other incidental effects. N_c may be taken as 9 for the $\phi = 0$ condition. The value of 9 is also consistent with fairly undisturbed samples of nonfissured clays. According to Skempton (1951), $N = 6\ (1 + 0.2\ Z/D_p)$. The parameter Z is the embedment of the element in the ground, and D_p may be takes as the equivalent base diameter. The value of s_u should be averaged over a depth of one to two equivalent base diameters.

For drained conditions, both the side resistance and base bearing may be estimated as in drilled shafts.

11.8 GEOTECHNICAL CAPACITY: AXIAL LOAD IN COHESIONLESS SOILS

Side Resistance

On the continent, ultimate shaft resistance is expressed in terms of the effective overburden stress σ_v', the friction angle between concrete and sand, and the coefficient K (ratio of horizontal to vertical effective stress, usually taken as K_o).

For linear and prismatic panels, this author recommends the Touma-Reese (1974) procedure, described in Table 10–7, in some respects equivalent to the foregoing procedure. Then,

$$q_s = K\sigma_v' \tan\phi' < 2.5 \text{ tons/ft}^2 \tag{11–6a}$$

The factor K in Equation (11–6) is not the stress ratio but is as shown in Table 10–7. For convenience, the values of K are repeated here as follows:

$$K = 0.7 \text{ for } D_b \leq 25 \text{ ft}$$
$$K = 0.6 \text{ for } 25 \text{ ft} < D_b \leq 40 \text{ ft}$$
$$K = 0.5 \text{ for } D_b > 40 \text{ ft}$$

where D_b is the embedment in the sand layer. Smaller values of K with increasing depth are consistent with the results shown in Figure 11–6, confirming that the ratio of the maximum friciton to the confining pressure decreases nonlinearly with increasing confining pressure. In some instances the Touma-Reese method (based on a consideration of the friction angle) may be over-conservative (see also Design Example 10.1). In this case the Reese and O'Neill (1988) approach presented in Table 10–7 may be considered a viable option analysis for uncemented sands and where some stress relief can be assumed to occur during excavation. Reduction in the value of the coefficient K suggested with the Touma-Reese approach is also consistent with a smaller K_o associated with a greater friction angle as the depth increases.

Base Bearing

As in drilled shafts, all available procedures for estimating base bearing in sand are based on tolerable displacements. This approach may involve either 1 inch of downward movement or 5 percent of an equivalent base diameter, although the latter is rather different to correlate with the various configurations of Figure 11–1. The procedures summarized in Table 10–8 are applicable subject to the following comments:

1. The Touma and Reese (1974) approach is based on 1-inch settlement and correlates q_p with the base diameter, hence it is intended primarily for drilled shafts. Its application to linear and prismatic elements using the concept of an "equivalent" base diameter should be accepted with caution.
2. The Reese and O'Neill (1988) approach likewise correlates settlement to the base diameter, with 5 percent being the accepted (tolerable) value. Whether a linear or prismatic element and a shaft of an "equivalent" diameter will have the same settlement under the same load cannot be confirmed. Hence, judgment is likewise necessary in interpreting these criteria.

Performance Factors

The general consensus is that there is greater variability of the capacity of foundation elements excavated in sand than in clay, and this may suggest that the resistance factors for elements in sand should be smaller than for the same elements in clay, particularly for the base resistance. The same caution has been demonstrated for drilled shafts.

Performance factors are shown in Table 10–9, and evidently no specific values are indicated for elements in sand mainly because of the shortage of field data. Hence, the suggestion to use smaller values for sands and gravels should be followed using judgment and available experience with similar conditions. Strength analysis may also be correlated with ASD.

11.9 AXIAL RESISTANCE IN ROCK

A socket in rock can be formed in two ways, with the choice depending on the desired extent of penetration and the hardness of rock material. Shallow sockets in soft to medium-hard rock can be formed with lightweight chisels dropped from a clamshell or from a percussive rig. If deep sockets must be provided, or the rock material is medium-hard to hard, the most suitable tool usually is a rotary drill or a churn drill.

Linear or prismatic panels may be socketed in rock for increased load capacity, or to provide fixity necessary to resist lateral loads. For design purposes, the usual assumptions are as in drilled shafts, that is, (1) the socket is formed in sound rock not likely to be degraded as a result of the excavation; (2) the bentonite will not act as lubricant along the sides of the socket; and (3) the bottom can be thoroughly cleaned.

The usual design procedure is to assume that the axial load is carried only be side resistance along the socket depth when the computed settlement is less than 0.4 inch, and by base bearing alone when the computed settlement exceeds this value. The settlement in this case refers to the settlement of the section socketed in rock, and consists of (1) the elastic shortening computed from elastic methods, and (2) the settlement of the base.

The procedure is the same as in drilled shafts, discussed in section 10.10, and involves the steps proposed by Reese and O'Neill (1988). Since no allowance is made for loads to be carried by a combination of side resistance and base bearing, the design is conservative. Note that the parameter D_s appearing in the analysis of drilled shafts is the diameter of a circular socket. For linear and prismatic panels, an equivalent diameter should be computed.

11.10 GROUP ACTION

Consider the group of linear elements shown in Figure 11–8. There is no reason for the group to act any differently from the group of piles or drilled shafts shown in Figure 9–22. Hence, the six panels together may form and act as a block foundation with dimension Y and X as shown and depth Z, the same as the depth of individual panels.

If the group is constructed in sand, its combined capacity may be estimated by summing the individual capacities of the panels. The ratio of the ultimate load capacity of the panel group to the sum of the individual load capacity of the group is therefore taken as unity. The analysis is the same regardless of the contact of the panel cap with the ground.

For panel groups in clays, failure of the system as a group should be considered when the cap is in firm contact with the ground. In this case, the ultimate bearing ca-

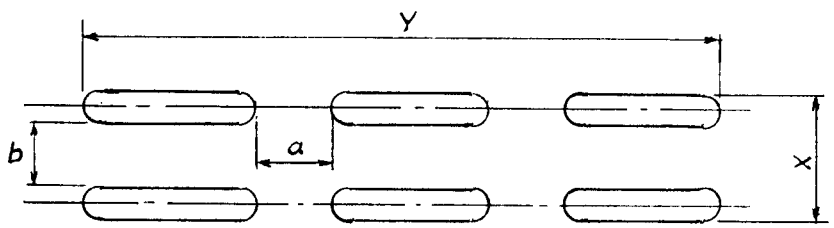

Figure 11–8 Group action of linear elements.

pacity is the lesser of the following: (1) the sum of individual panel capacities, and (2) the bearing capacity of the block as defined in Figure 11–8. In the latter case, the capacity is estimated from Equation (9–12). A separate performance factor must be used for the block mechanism (usually 0.65).

Interference between overlapping zones in a group of panels may be avoided if the dimensions a and b in Figure 11–8 are properly selected. The recommended minimum value of a is twice the thickness of the panel, and the recommended minimum value of b (distance face-to-face) is three times the thickness of the panel. These dimensions may be used for sand and clay.

Factors of Safety

The minimum factor of safety under allowable stress design should be 2.0 for bearing-capacity failure when the design is based on results of load tests at the site. Otherwise, the factor of safety should be increased to 2.5. Likewise, these are recommended values assuming a normal level of field quality controls, and should be increased when this level cannot be provided. Alternatively, the factor of safety may be introduced as in section 10.12.

11.11 SETTLEMENT CONSIDERATIONS

Single Panels

The loading conditions for settlement considerations will largely depend on the type of soil. If the soil is saturated cohesive material, unfactored permanent loads should be used since the settlement is a function of time. If the soil is in nonsaturated conditions, or it is granular , or it is a ϕ-c soil, the settlement will occur fairly rapidly, and unfactored transient loads must be included with the permanent loads. The settlement of a soil for which consolidation theory does not apply may be different. In this case, there may be a gradual buildup of dead load as the bridge is constructed, and this may result in more dense soil conditions when the live load is applied. Similar comments were made for drilled shafts.

The summary of load-settlement data shown in Figure 10–13 through 10–16 applies primarily to drilled shafts in sand and clay, and the settlement necessary to mobilize ultimate side shear or base bearing is expressed as a percentage of the shaft and base diameter, respectively. These results should not be extrapolated indiscriminately to linear and prismatic panels.

Field tests. Reese and Touma (1973) have reported results of tests on bored piles in stiff clay and water-bearing sand. Regardless of the method of installation and bottom cleaning, a relevant conclusion is that peak load transfer in side resistance is reached at a relative shaft movement (displacement of a point with respect to its original position) of 4 to 5 mm (0.16 to 0.2 inch) in clays. For sands, the relative displacement varies from 5 to 10 mm (0.2 to 0.4 inch). The results from Figure 11–5 show that maximum skin friction for concrete-sand-bentonite interface is attained at displacements of the order of 5 to 10 mm (0.2 to 0.4 inch), which is in good agreement with the results obtained by Reese and Touma (1973).

The test panels of Table 11–1 and Figure 11–3 were constructed in ground consisting of gravel, silty clay, and fine sand. The vertical displacement corresponding to the maximum side resistance is about 6 to 7 mm (0.24 to 0.28 inch).

Burland (1963) has reported tests on two diaphragm wall panels in London clay, 120 cm long, 50 cm wide, and 40 feet deep. Each panel was subjected to two load cycles. The first consisted of incremental loads (one-fourth the working load) until the rate of settlement was reduced to 0.002 inch per 30 minutes. The second test involved a maximum load applied for 24 hours, after which the panels were unloaded and the rebound was observed. The results of the incremental load test are shown in Figure 11–9; Figure 11–10 shows results from the second load cycle. For both tests, peak side shear is reached at an average vertical displacement of 0.2 inch (5 mm).

At present there is no evidence to suggest that the settlement of linear and prismatic panels necessary to mobilize full side resistance may be expressed in terms of the section geometry. Until more evidence is forthcoming, this author recommends the following:

- The displacement necessary to mobilize peak shaft resistance in clay may be taken as 0.2 inch (5 mm).
- The displacement necessary to mobilize peak side friction in sands may be taken as 0.2 to 0.4 meter (5 to 10 mm), depending on the confining stress. The lower this stress the greater the displacement necessary to mobilize full side friction.

The settlement due to base load can be correlated with the behavior of drilled shafts. Thus, the settlement should be different for panels in cohesionless and cohesive soils. The panels in clay shown in Figure 11–9 and 11–10 show a well-defined plunging load as is typically inferred from Figure 10–14. The panels of Figure 11–3, built in gravel and fine sand, show a tip load that continues to increase with settlement beyond the tolerable values, as is also inferred from Figure 10–16. Hence, for panels in sand, there is no well-defined failure load at any displacement. In this case, ultimate base re-

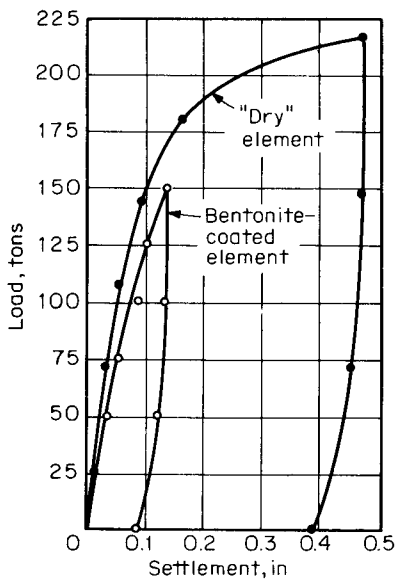

Figure 11–9 Load-settlement curves for incremental-load tests on diaphragm-wall panels *(from Burland, 1963).*

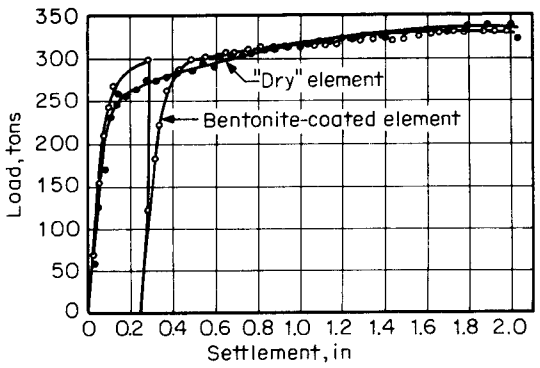

Figure 11–10 Load-settlement curves for constant-rate penetration tests on diaphragm-wall panels *(from Burland, 1963)*.

sistance must be defined in terms of a fixed settlement, or as a function of a displacement related to the section geometry. This criterion is reflected in the procedures suggested for estimating peak base capacity in sand.

Group Settlement

The settlement analysis of a group of panels is similar to the settlement of shaft groups. However, when the layout and clearance between adjacent panels is as shown in Figure 11–8, it is unlikely for the group to develop interference between the zone of individual panels. Thus, the group settlement may be inferred from the individual panel settlement.

11.12 DOWNDRAG AND UPLIFT

Downdrag Forces

Downdrag loads may develop around linear and prismatic panels, and may have their origin from the same sources discussed for drilled shafts. The α method (Equation 9–48) may be used to estimate negative side resistance in clays, and the β method is appropriate in sands, or where the long-term conditions following consolidation must be considered (Equation 10–32).

It is very unlikely that downdrag loads will cause capacity problems, although they may increase the settlement. The settlement should be checked for the same load combinations as in drilled shafts.

Uplift Resistance

Single or group panels may be subjected to uplift that has its origin from overturning moments, upward loads, and frame action. Since all panels are vertically straight, their uplift resistance may be estimated as for panels in compression.

Pullout resistance is usually adequate for long panels, but may have to be checked for shallow elements and where the load capacity is derived from bearing on rock. Alternatively, the models shown in Figure 11–11 may be used to check individual uplift capacity, or where there is no overlapping of the zones of influence. In the truncated cone model, the uplift force is resisted by the weight of the concrete and the soil in the

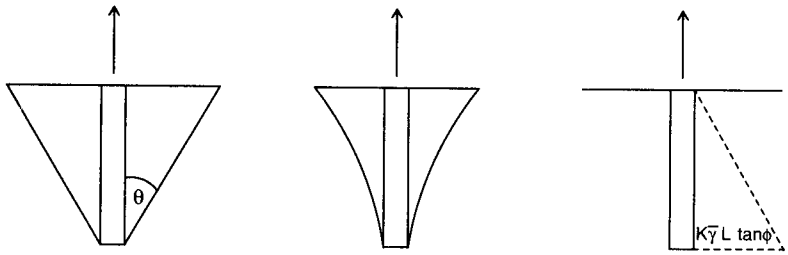

(a) Truncated cone (b) Curved surface (c) Cylindrical shear

Figure 11–11 Uplift capacity models: (a) Truncated cone; (b) curved surface; (c) cylindrical shear.

cone. In the curved surface model, the uplift must be balanced by the weight of concrete and soil above the curved surface, and by shear resistance along that surface. The final model assumes that shear failure occurs on a cylindrical surface along the shaft, so that uplift is resisted by the weight of concrete and the shear strength along the shaft.

11.13 EFFECTS OF LATERAL LOAD

Figure 11–12 shows two views of a linear panel embedded in the ground. Both cases involve a lateral load acting at the top as shown. The panel in Figure 11–12(a) will probably act as a semigravity wall. Without confinement in the ground, the tendency to overturn will be resisted by a balancing moment that is taken as the weight of the panel multiplied by the moment arm about point 0. With confinement in the ground, the panel will have to be extracted like a tooth before failure can occur. Hence, possible movement of the panel in this case is rotation about point 0 or lateral translation associated with tendency to slide along the base. Either movement will mobilize some passive resistance along the left end, but with rotation about point 0 passive resistance may develop along both ends.

The panel shown in Figure 11–12(b) may be considered rigid and assume to rotate about a pivot point 0 located as shown.

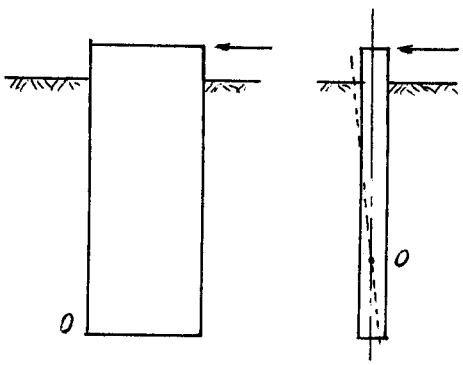

(a) (b)

Figure 11–12 Lateral load action on a linear element.

Ultimate lateral resistance. A suggested mechanism of mobilization of lateral resistance of a rigid element with free top is shown in Figure 11–13. Considering the equilibrium conditions and setting $\Sigma F_y = 0$, we obtain

$$Q_{ult} - \int_{x=0}^{x=x_r} p_{xu} B dx + \int_{x=x_r}^{x=L} p_{xu} B dx = 0 \tag{11–7}$$

Also setting $\Sigma(M) = 0$ yields

$$Q_{ult} e + \int_{x=0}^{x=x_r} p_{xu} B x dx - \int_{x=x_r}^{x=L} p_{xu} B x dx = 0 \tag{11–8}$$

where B = width of element, and x_r = depth point of variation. If the distribution of ultimate unit soil resistance p_{xu} with depth x is known, the value of x_r and Q_{ult} can be obtained from Equations (11–7) and (11–8). This basic concept has been used by Broms (1964a, b). The following simplifying assumptions are made:

1. The soil is purely cohesionless ($c = 0$) or purely cohesive ($\phi = 0$).
2. Short rigid and long flexible elements are considered separately. The criteria for short panels are $L/T \geq 2$ or $L/R \geq 2$, where

$$T = \left(\frac{EI}{n_h}\right)^{1/5} \qquad R = \left(\frac{EI}{k_h}\right)^{1/4} \tag{11–9}$$

E = elastic modulus of panel; I = moment of inertia of section; $k_h = n_h x$ for linearly increasing soil modulus k_h with depth x; n_h = constant modulus of subgrade reaction; and k = modulus value in cohesive soil that is constant with depth.

The criteria for long panels are $L/T \leq 4$ or $L/R \leq 3.5$.

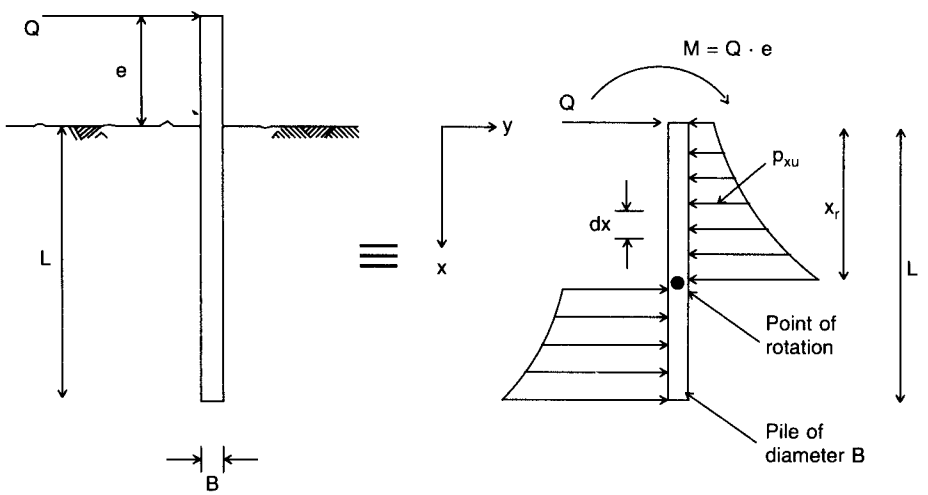

Figure 11–13 Mobilization of lateral resistance for a laterally loaded element with free top.

3. Free-head short panels are expected to rotate about a center of rotation, while fixed-head panels will move laterally in translation (see Figure 11–14a and b).
4. Distribution of ultimate soil resistance along the panel length for different end conditions is shown in Figure 11–14 for short members.

This discussion deals mainly with short panels since most of the linear and prismatic elements reviewed in this chapter fall within this category.

Panels in cohesionless soil. The active earth pressure on the back of the panel is neglected. The distribution of passive resistance along the front of the panel is at any depth as shown in Figure 11–14(e) and (f) for free and fixed head, respectively. In this case

$$p = 3B\sigma_v' K_p = 3\gamma' LBK_p \tag{11–10}$$

where p = unit soil pressure (resistance); σ_v' = effective overburden stress; γ' = effective unit weight of soil; L = embedded length of panel; B = width of panel normal to the direction of load; and K_p = coefficient of passive pressure.

This pressure is independent of shape of the element and applies to linear, I-, T-, and X-sections. Full lateral resistance is mobilized at the movement considered.

Short panels in cohesive soil. The passive resistance may be assumed zero at ground surface to a depth $1.5B$, and then as having a constant value $9\,c_u B$ below this depth, as shown in Figure 11–14(c) and (d) for free and fixed top, respectively. The parameter c_u is the soil cohesion or undrained shear strength.

The foregoing procedure is general and supplements the methods of analysis for laterally loaded piles and drilled shafts.

Acceptable lateral displacement. Under the effects of lateral loads, the controlling design criteria are the structural capacity and the maximum lateral displacement that can be tolerated. Ultimate soil failure under the effect of lateral loads is extremely rare because it will require larger displacements far exceeding the tolerable values.

The actual restraint at the top of the panel has a marked influence on the magnitude and pattern of the lateral deflection. Panels rigidly connected to heavy footings or caps are likely to deflect laterally without end rotation. Very often, however, linear panels have single connections with the substructure, and will probably translate and also rotate at the top. In this case the deflection may be three to four times the lateral deflection of a fixed-head panel under the same lateral load.

Among the procedures available for estimating the lateral deflection is the subgrade reaction approach (Reese and Matlock, 1956; Matlock and Reese, 1962), and the elastic continuum approach (Poulos, 1971a and b; Poulos and Davis, 1980).

The method suggested for drilled shafts in section 10.16 may be used to predict the lateral displacement of linear and prismatic elements under lateral load. The parameter D should be substituted by the width of the panel in the direction normal to the applied lateral load. The results should be valid because the actual flexural stiffness $E_p\, I_p$ will be entered where I_p is the moment of inertia of the member about the axis normal to the direction of the load.

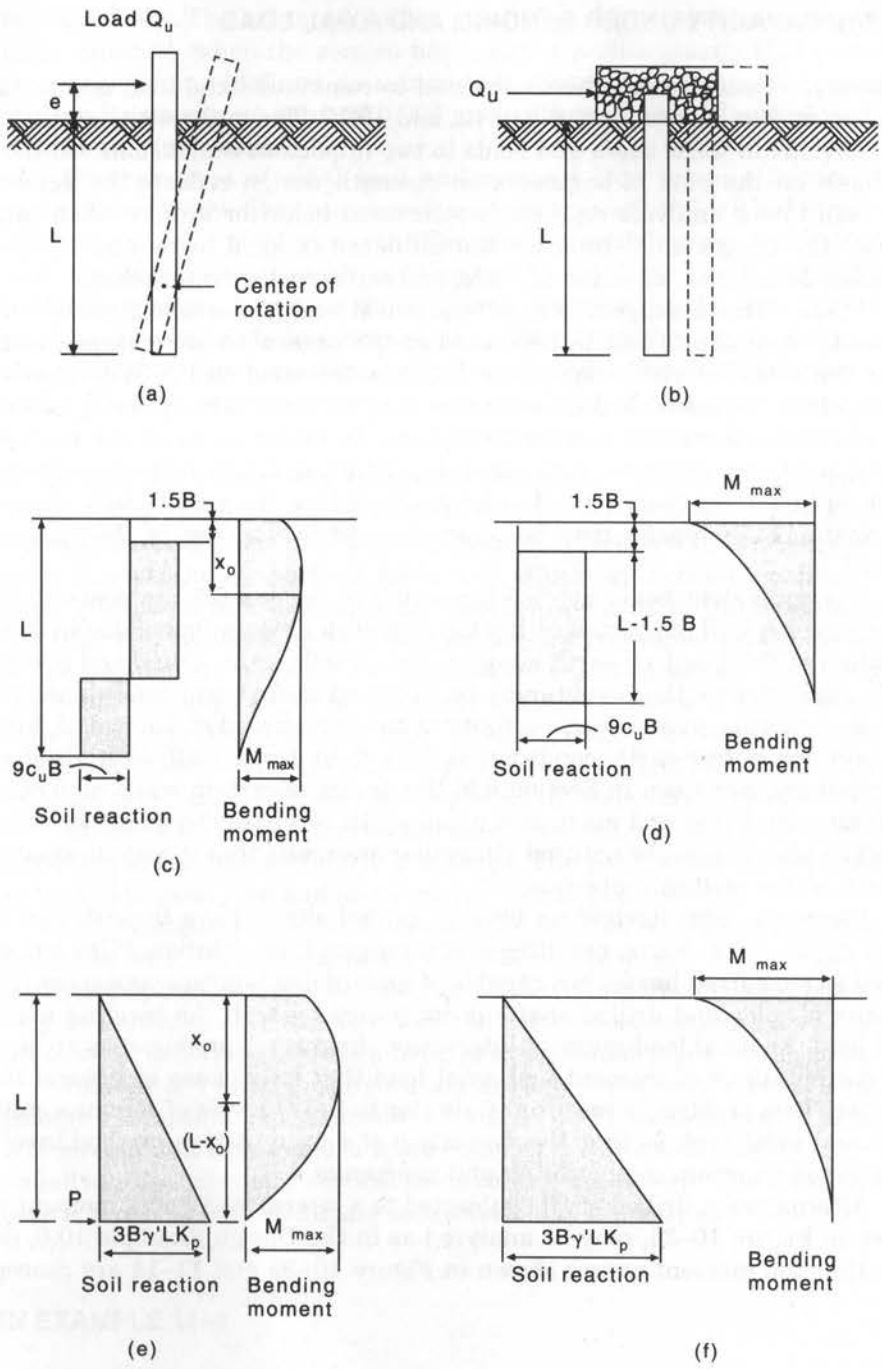

Figure 11–14 Rotational and translational movements and corresponding ultimate soil resistances for short shafts under lateral loads. Deformation modes: (a) free head; (b) fixed head. Soil reactions and bending moment in cohesive soils; (c) free head; (d) fixed head. Soil reactions and bending moments in cohesionless soils: (e) free head; (f) fixed head *(from Broms, 1964a and b)*.

11.14 STRUCTURAL CAPACITY UNDER BENDING AND AXIAL LOAD

Summary. Concrete members subjected to combined axial load and bending moment are discussed in Sections 4.6, 6.5, 9.12, and 10.17. The multiplicity of methods of analysis is obvious in these cases and leads to two important conclusions: (a) the documented emphasis on the part of engineers on strength design reflects the general conviction that load factor analysis represents structural behavior more realistically than ASD; and (b) the design must consider the influence of axial loads and moments, member stiffness, deflections, duration of loads, and soil-structure interaction.

These criteria suggest several structural and geotechnical models. For example, first-order load effects may be computed on the basis of elastic analysis where the stress below the specified yield strength is E_s times the steel strain. With regard to stiffness assumptions, an uncracked cross section may be assumed neglecting all reinforcement, or a transformed cracked section throughout. In most instances, the most correct representation of the ultimate state may be obtained using moment-curvature relationships. In lieu of an exact second-order analysis that can realistically represent member deformation, the results may be approximated by the use of the moment magnifier method.

The equivalent beam method presented in Section 6.5 can describe the structural behavior for a wall supported at the top and with its base embedded in the ground. The condition of fixed or free earth support should reflect the actual soil conditions. A wall freely supported at the bottom may be assumed in firm soil conditions. The maximum moment becomes greater without fixity at the bottom end of the wall. Likewise, the embedment for a free-earth condition is less than for a wall with fixed end support. Interestingly, as shown in Section 6.9, the design of certain walls may be controlled by minimum axial load and maximum moment. In this case the axial load may be reduced to 75%, and may even be omitted altogether assuming that it may dissipate by shear resistance at the wall-soil interface.

Elements characterized as piles or drilled shafts have their design based on the use of appropriate charts, resulting in a semi-graphical solution. Piles and shafts are assumed to have fixed heads, but capable of undergoing lateral translation. The structural capacity of piles and drilled shafts is controlled by both the bending moment and the axial load. An axial load-moment interaction diagram is produced as an envelope of several combinations of moment and axial load that may cause structural failure of the member. This problem is essentially similar to the analysis of columns subjected to moment and axial load, so that the derivation of a computation method involves relationships based on strain compatibility and mechanics.

Alternatively, drilled shafts subjected to a lateral load and a moment at the top, as shown in Figure 10–34, may be analyzed as in the Design Example 10.6, Section 10.18. Note that the moment curves shown in Figure 10–35 and 11–14 are conceptually similar.

Commentary. The ACI defines short columns as members where the length effect on secondary moments owing to the deflection response under load is very small and may be disregarded. The short column can be analyzed or designed from the strength of its cross section alone. The column interaction diagrams shown in the foregoing sections are plots of the member axial load against the moment capacity that can be carried si-

multaneously. The balanced failure point (P_{nb}, M_{nb}) represents the axial load and moment capacity when the section has a strain profile exactly that assumed for balanced strain conditions (defined as a condition where the extreme compression fiber strain reaches its maximum value of 0.003 just as the outermost layer of tensile reinforcement reaches its yield strain $e_y = f_y/E_s$).

Combinations of axial load and moment that produce failure for $P_n \geq P_{nb}$ will cause the extreme fiber compression strain to reach the critical strain 0.003 before the steel reaches the yield strength. Conversely, combinations producing $P_n < P_{nb}$ would have the tension steel reach yielding conditions first. The latter is the most desirable condition because it implies ductility and extension of the structural behavior into the plastic range before failure occurs. The strain condition that results in a force distribution such that the summation of the compression forces equals the summation of the tension forces results in a moment value associated with pure flexure.

Guidelines for linear and prismatic elements. Unlike diaphragm walls where the axial load is relatively small compared with the moment effects and thus unlikely to control the design, the load bearing elements discussed in this section are designed and built to carry heavy vertical loads and often considerable bending moments. In this case, the interaction diagrams are the key concepts for understanding cross-sectional behavior and should form the basis for the design procedure. On the other hand, failure of the member by allowing the concrete to reach its dangerous strain before the steel reaches its yield strength is extremely unlikely because of the generous cross-sectional area usually provided in this type of work. Hence, load bearing elements should normally have extra structural capacity, and their design should be controlled by the ultimate geotechnical strength or by displacement considerations at service loads.

Linear wall panels can replace an equivalent row of piles, and provide a monolithic structure independent of fixed tolerances. The panels may be designed as slab sections subjected to axial load and moments per foot of panel length.

A T configuration should normally be selected where the foundation is subjected to compression loads and moments but without reversal, for example, foundations supporting diaphragm walls functioning as end supports in underpasses. These sections may be analyzed as T beams where the entire cross-sectional area is subjected to compressive stresses and there is a neutral axis at some point in the stem.

Shapes of I and H configuration are selected where vertical and lateral loads can change magnitude and direction. Flexural theory combined with direct load principles will govern and may require more complex solutions. Elements with an X section are usually indicated where vertical loads control the design. The structural capacity in this case is most unlikely to dictate section size and dimensions.

11.15 DESIGN EXAMPLE 11–1

Figure 11–15 shows three different schemes for the pier foundation of an 18-span highway bridge. Piers 1 through 11 support a narrower roadway, whereas piers 12 though 17 are proportioned to support a wider structure. Scheme A consists of 3-foot diameter precast prestressed concrete piles and represents the conventional design. Scheme B is essentially similar to A except that the elements are caissons drilled under slurry pro-

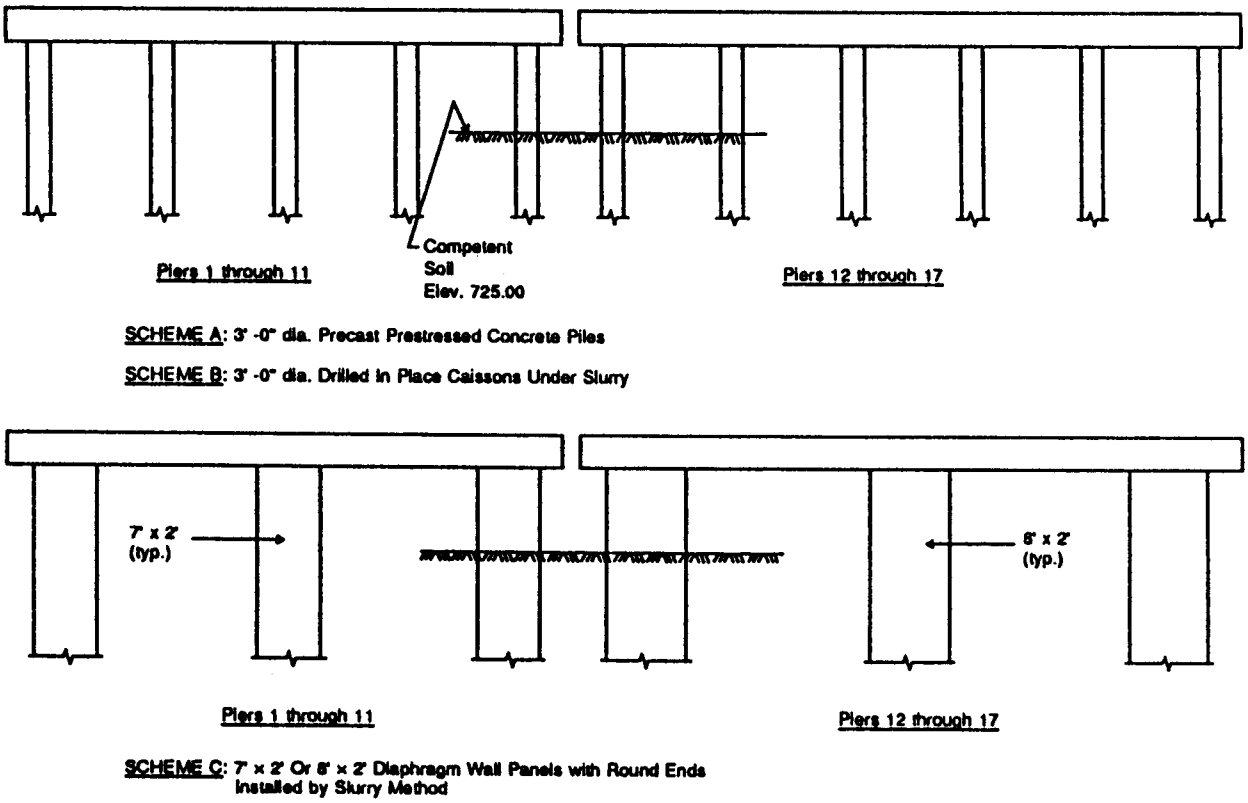

Figure 11–15 Elevation of substructure and foundation elements, bridge of design example.

tection. Scheme C is the alternate design and consists of 7 ft x 2 ft or 8 ft x 2 ft linear panels installed by the slurry method. Competent soil is found at elevation 725.00 for all schemes. Below this level the ground consists of stiff clay with $q_u = 2.50$ tons/ft^2.

Piers 1 through 11. The conventional design (scheme A) indicates bottom of pile elevation 658.00, and a working load of 240 tons per pile. From a back analysis, the design is traced as follows:

$$\text{Pile Embedment} = 725 - 658 = 67 \text{ ft}$$

$$\text{Effective perimeter} \quad S = 3.14 \times 3 = 9.42 \text{ ft}$$

$$\text{Area} \quad A_b = 3.14 \times 1.5^2 = 7.06 \text{ ft}^2$$

using $s_u = 1/2\, q_u = 2.5$ kips/ft^2, $\alpha = 0.5$, and $N_c = 9$, we compute the following

$$Q_s = 9.42 \times 67 \times 0.5 \times 2.5 = 789 \text{ kips}$$

$$Q_b = 7.06 \times 9 \times 2.5 = 159 \text{ kips}$$

$$Q_{ult} = 948 \text{ kips} = 474 \text{ tons}$$

Using a factor of safety of 2 for both side resistance and base bearing, the working load per pile is 474/2 = 237 tons, 249 tons OK.

Scheme C. For this scheme, five piles are replaced by three panels as shown in Figure 11–15. The design load per panel (working load) is therefore 240 × 15/3 = 400 tons.

Using the same parameters, we calculate the side resistance and base bearing

$$Q_s = 16.3 \times 67 \times 0.5 \times 2.5 = 1365 \text{ kips}$$

$$Q_b = 13.1 \times 9 \times 2.5 = 295 \text{ kips}$$

$$Q_{ult} = 1660 \text{ kips} = 830 \text{ tons}$$

Using again a factor of safety of 2 for both shaft resistance and base bearing, the working load on one element is 830.2 = 415 tons, use 400 tons OK.

Piers 12 through 17. As shown in Figure 11–15, three linear panels, each 8 ft x 2 ft, will replace six piles. Each panel must resist a working load of 480 tons. For scheme C, the following are computed:

$$\text{Effective perimeter } S = 12 + 6.28 = 18.3 \text{ ft}$$

$$\text{Area } A_b = 6 \times 2 + 3.14 \times 1 = 15.1 \text{ ft}^2$$

Using the same parameters, the side resistance and base bearing are

$$Q_s = 18.3 \times 67 \times 0.5 \times 2.50 = 1532 \text{ kips}$$

$$Q_b = 15.1 \times 9 \times 2.50 = 340 \text{ kips}$$

$$Q_{ult} = 1872 \text{ kips} = 936 \text{ tons}$$

For a factor of safety of 2 for both shaft resistance and base bearing, the working load per panel is 1872/2 = 936 kips = 468 ≈ 480 OK.

Summary of quantities. Piers 1 through 11

$$\text{Scheme A} = 5 \times 67 = 335 \text{ lin ft of piles}$$

$$\text{Scheme C} = 7 \times 3 \times 67 = 1407 \text{ ft}^2 \text{ of wall panels}$$

Piers 12 through 17

$$\text{Scheme A} = 6 \times 67 = 402 \text{ line ft of piles}$$

$$\text{Scheme C} = 8 \times 3 \times 67 = 1608 \text{ ft}^2 \text{ of wall panels}$$

These quantities are per pier. The foundation cost for each scheme can be obtained by applying relevant unit prices. It is conceivable that these prices will vary regionally.

REFERENCES

BROMS, B., 1964a: "The Lateral Resistance of Piles in Cohesive Soils," *J. Soil Mech. Found. Div.*, ASCE, vol. 90, No. SM2, March, pp. 27–63.

BROMS, B., 1964b: "The Lateral Resistance of Piles in Cohesionless Soils," *J. Soil Mech. Found. Div.*, ASCE, vol. 90, No. SM3, pp. 123–156.

BURLAND, J. B., 1963: Discussion, Session 4, *Symp. of Grouts and Drilling Muds,* in "Grouts and Drilling Muds in Engineering Practice," Butterworths, London.

CORBETT, B. O., et al., 1974: "A Load Bearing Wall at Kensington and Charles Town Hall," London, *Proc. Diaphragm Walls Anchorages*, Inst. Civ. Eng., London.

CZERNIAK, E., 1957: "Resistance to Overturning of Single, Short Piles," *J. Struct. Div.*, ASCE, vol. 83, No. ST2, Proc. Paper 1188, March, pp. 1–25.

FARMER, I. W., et al., 1971: "The Effect of Bentonite on the Skin Friction of Cast-in-Place Piles," *Proc. Behavior Piles*, Inst. Civ. Eng., London.

GOLDBERG, D. T., 1979: "Geotechnical Aspects of Slurry Walls," *Symp. Slurry Walls for Underground Transp. Systems*, U.S. DOT, FHWA, Cambridge, MA, Aug. 30–31.

KIENBERGER, H., 1974: "Diaphragm Walls as Load Bearing Foundations," *Proc. Diaphragm Walls Anchorages*, Inst. Civ. Eng., London.

MATLOCK, H., and L. C. REESE, 1962: "Generalized Solutions for Laterally Loaded Piles," *Transactions ASCE*, vol., 127, Part 1, pp. 1220–1247.

POULOS, H. G., 1971a: "Behavior of Laterally Loaded Piles, I-Single Piles," *J. Soil Mech. Found. Div.,* ASCE, vol. 97, No. SM5, pp. 711–731.

POULOS, H. G., 1971b: "Behavior of Laterally Loaded Piles, II-Pile Groups," J. Soil Mech. Found Div., ASCE, vol. 97, No. SM5, pp. 733–751.

POULOS, H. G. and E. H. DAVIS, 1980: *Pile Foundation Design and Analysis*, Wiley, New York, p. 397.

REESE, L. C. and H. MATLOCK, 1956: "Non-dimensional Solutions for Laterally Loaded Piles with Soil Modulus Assumed Proportional to Depth," *Proc. 8th Int. Texas Conf., Soil Mech. Found. Eng.*, Austin, Texas, pp. 1–41.

REESE, L. C. and F. T. TOUMA, 1973: "Bored Piles Installed by Slurry Displacement," *Proc. 8th Int. Conf. Soil Mech. Found.* Eng., Moskow.

REESE, L. C. and M. W. O' NEILL, 1988: "Drilled Shafts: Construction Procedures and Design Methods," FHWA Publication No. FHWA-HI-88-042 or ADSC Publication No. ADSC-TL-4, Aug., p. 564.

SKEMPTON, A. W., 1951: "The Bearing Capacity of Clays," *Proc. Building Research Congress,* London, vol. 1, pp. 180–189.

TOUMA, F. T. and L. C. REESE, 1974: "Behavior of Bored Piles in Sand," *ASCE JGED*, vol. 100, No. GT7, July, pp. 749–761.

WHITAKER, T. and R. W. COOKE, 1965: "Bored Piles with Enlarged Bases in London Clay, *Proc. 6th Int. Conf. Soil Mech. Found.* Eng., Montreal.

XANTHAKOS, P. P., 1979: *Slurry Walls*, McGraw-Hill, New York, p. 622.

XANTHAKOS, P. P., 1994: *Slurry Walls as Structural Systems*, McGraw-Hill, New York, p. 855.

CHAPTER 12

Strengthening and Rehabilitation

12.1 DESIGN OPTIONS TO REDUCE MAINTENANCE AND REPAIR

General Principles

The previous chapters show the complexity of bridge designs as more sophisticated bridge types are introduced. A complete bridge design should contain provisions for inspection and rating, and should incorporate details that reduce and facilitate maintenance and repair. Interestingly, however, maintainability criteria for bridges have not been formally stated or included in standard design specifications and manuals.

The required continued use of a bridge while rehabilitation is performed is documented through past experience. Details and configurations of bridge superstructures and substructures could be selected to provide compatibility with rational criteria expressing the requirements for accessibility, corrosion protection, ease of rehabilitation, and uninterrupted function while the structure is under repair.

Knowing where failures might occur can improve maintenance planning and scheduling. Many bridge failures have been attributed to poor maintenance. Whether the primary reason is lack of adequate funding and staffing is not an engineering concern. A relevant comment, however, is that deferral of maintenance leads to more costly reconstruction. Thus, designing bridges and their components for maintainability is a cost-effective approach that should result in safer structures and longer life.

Accessibility. Accessibility refers to bridge components expected to require regular inspection and maintenance work. With reference to substructure, pier caps should be sized to provide reasonable placement of jacks, and also designed to support jack loads.

This operation is necessary when bearings and hinges must be repaired or replaced and the load must be transferred to temporary supporting devices.

Where an elaborate drainage system is provided, access for cleaning and flushing the system is essential. Drainage systems often are attached to substructure elements and pier columns. Inability to access may result in some systems becoming inoperable, with subsequent deterioration of other bridge components. Inlet catch basins, pipes, and expansion devices are examples of mechanical devices whose limited performance can cause the acceleration of structural deterioration. For bridges where accessibility to portions of the structure for inspection and maintenance is difficult from the bridge deck or from beneath the deck, means of access to all components and parts should be provided in the form of walkways, platforms, and ladders. This should apply to routine maintenance, and occasional repair and rehabilitation.

Use of Materials

Concrete is typically used for substructures. One of the most important factors affecting concrete quality is the water-cement ratio. The durability of concrete is greatly increased by using a low water-cement ratio (Jackson, 1932). For bridge decks in Kansas, McCollon (1976) has found that increasing the concrete cover from 2 to 3 inches and decreasing the water-cement ratio from 0.44 to 0.34 would triple concrete deck life, although it should also induce the tendency for tension cracks.

Low-slump concrete has been found suitable in retarding salt contamination. On this basis, TRB-NCHRP (1979) has recommended a water-cement ratio of 0.4 or less for concrete exposed to salt intrusion—this would apply to pier caps and columns at locations of expansion joints. Concrete quality is further enhanced by the use of entrained air. Certain types of sealers can be used to protect concrete surfaces, and epoxy-coated steel bars are commonly used in concrete exposed to salt environment. Quality concrete is attained through the use of nonporous, durable aggregates, proper vibration to ensure placement without voids, and good curing techniques.

Specifications and quality assurance should ensure proper slump and consolidation during pouring and curing. AASHTO specifies the nominal and maximum slump for various types of work in Article 8.4.2. Experience also shows that quality control techniques are essential for underwater concrete construction, and some states use prestressed concrete piles manufactured under strict quality control to reduce concrete pile deterioration.

However, research shows that in a salt environment reinforced concrete is subject to deterioration from reinforcing steel corrosion. As long as chlorides are used for ice and snow removal, all concrete structures should be expected to deteriorate if the steel is left unprotected. Roadway drainage slots should be eliminated and drainage systems should be designed to eliminate drainage onto pier caps, columns, or piles. Among the various methods suggested to protect concrete reinforcing elements are cathodic protection, polymerized concrete, wax-bead impregnation, low-slump or latex-modified concrete overlays, waterproofing systems, sealers, metallic-coated bars, and epoxy-coated bars.

Foundations and Substructure Systems

Substructure and foundation costs represent a considerable percentage of the total bridge cost. In addition, when substructure construction is completed, a major portion is covered by earth or water. Rehabilitation and inspection below the waterline and

ground surface are difficult and costly (see also following sections), particularly where the substructure environment constitutes the most severe conditions to which bridge components are subjected. Examples are bridge foundations subjected to the action of moving water, and concrete elements under the effect of freeze-thaw attacks. Thus, a structure may become weak and even fail because of materials, deterioration, scour, overloading, floods and storms, and inadequate maintenance.

Hydraulic factors and conditions, in particular, may be a major cause of foundation problems (Csagoly and Dorton, 1978). From an international survey of major bridge failures, 66 of 143 failures were caused by scour. This suggests that bridge sites in waterways should be selected to minimize scouring action. In this context, straight stream alignment, right-angle bridge crossing, high-bank approaches, and narrow channels are desirable hydraulic features for bridge locations. Designers may prevent catastrophic scour by placing the bottom of foundations conservatively below the level of anticipated scour, and by protecting the foundations from scour in a meandering stream. Protective riprap, sheet piling, and training structures may be used where applicable (see also other sections).

Substructure problems may also occur in the splash zone and adjacent to the normal waterline or water table. Deterioration may be initiated in the wet-dry zone from rot, corrosion, and marine organisms. Vulnerable locations should therefore be identified and properly protected, recognizing that substructure and foundation systems are the most difficult and costly to repair and rehabilitate. Shanafelt (1985) gives the following guidelines when designing substructures and foundation systems:

1. Substructures should be supported on safe foundation systems designed from a thorough consideration of soil and hydraulic conditions. The factors of safety should be higher for soil-structure interaction and soil strength.
2. Structure configuration and alignment should be selected to minimize the likelihood of scour conditions, particularly with respect to the location and type of piers and footings.
3. Pile foundations should be considered when expansive and compressible soils extend for a considerable depth. The removal of unsuitable material beyond a depth of 10 feet (3 m) will in most instances be uneconomical, and where very deep compressible materials exist, it may be difficult to design a system that will inhibit excessive settlement. At the extreme cases, a viable jacking system should be incorporated in the design for future adjustments. When batter piles are used, pier cap width should be increased accordingly.
4. Sufficient time should be allowed for the settlement of fill and underlying soft layers before substructure construction to prevent settlement and the development of downdrag forces.
5. Steel piles should be specified with protective coatings. However, coatings will deteriorate and recoating is generally costly and difficult. Cathodic protection may be indicated for immersed steel. Weathering steel, however, performs no better than regular steels in immersed and splash zones and should not be used unprotected at these locations.
6. Concrete placed under water should have aggregates and cement that will remain inactive in water environment. Adequate concrete cover is essential and should be controlled during construction. The fresh concrete should not be placed in running water or allowed to fall through water. Aggregates should be free of fines that may

cause laitance. Underwater concrete should always be discharged into previously placed concrete in a continuous operation. New concrete should not be exposed to running water for a least four days. When concrete is placed in the dry, laitance and foreign materials should be removed from contact surfaces of previously placed concrete.

7. Concrete piles should have adequate cover over the reinforcement, and epoxy-coated bars should be specified in salt environments. Plastic sleeves may be effective in salt splash zones. Timber piles must be properly treated for the actual environment.
8. Void or hollow abutments should be provided with access openings.

Detailed directions and specific recommendations for bridge maintenance and repairs are provided by AASHTO (1995) *Manual for Maintenance Inspection of Bridges*. This document has been prepared to serve as a standard for implementing mainteneance programs and to provide a unified approach to the policy of identifying the physical condition and maintenance needs of bridges. This manual in the current edition contains revisions up to date.

12.2 PROCEDURES FOR DETECTING DEFECTS AND DETERIORATION

Structures above the Water Line

The need to detect defects and assess the deterioration level of bridges may be related to safety or to the compilation of an information base for a bridge management system. In this discussion, detecting defects is necessary for bridge repairs and rehabilitation.

Concrete is the most widely used material in bridge substructures and foundations, the main reason being that it is relatively inexpensive and durable. Various techniques have been used to detect defects and structural deterioration, ranging from striking the concrete surface to detect delamination to the radiography of posttensioned members. Some new applications of technology from other fields appear to be promising, and examples are infrared thermography and radar.

Steel is much stronger and more homogeneous than concrete and timber. The most common types of deterioration of steel are corrosion and fatigue cracking. Corrosion may be a frequent cause of problems in steel piles and steel reinforcement. Investigative tecniques include radiography and ultrasonics, better suited to detecting internal defects. With the development of suitable data processing techniques, acoustic emission measurement may prove useful for long term monitoring of steel members.

Timber is strongly anisotropic and has vastly different properties parallel and perpendicular to the grain. Material deterioration is caused by one or a combination of factors. In timber piles, this may include decay due to fungi, insect attack, marine borer attack, and mechanical wear. Decay of timber piles caused by the growth of fungi can be prevented if the timber can be kept either dry or permanently submerged, and this is because the growth of fungi needs moisture, air, and temperature. Insects like termites are destructive to timber piles, whereas beetles may damage them above the high water level. Also, no marine location is completely safe from marine borers causing serious damage to timber piles. As mentioned in other sections, the life of timber piles may be considerably extended by treatment with creosote, oil-borne preservatives, or salts.

Timber piles may also be subjected to mechanical wear such as abrasion.

Recommended methods of protection include fill placement around the damaged piles, armor placement to provide resistance to abrasion, and concrete encasement, used in conjunction with creosote treatement. Interestingly, highway bridges supported on timber piles are relatively few in number and are generally located on secondary highways.

Concrete Components

Concrete is the least homogeneous of the common construction materials. In this respect, the most important property of the cement paste is its porosity, because the hydration products of the portland cement never completely fill the space initially occupied by the cement particles and water in the concrete mix. The size and distribution of the pores within the paste influence many of the important properties of concrete such as strength and durability. Furthermore, whereas concrete itself is generally isotropic, the addition of reinforcement makes it anisotropic (i.e., its strength varies with the direction of loading).

Concrete is a poor conductor of electricity and heat. It is much more resistant to fire than steel or timber, but intense heat will damage concrete and cause spalling of the cover from the reinforcement. Concrete is typically treated as an elastic material under service loads. However, the strain at the proportional limit is small; sustained load results in creep. Because of its low tensile strength it is susceptible to cracking, and the width of cracks must be controlled by steel reinforcement. Relevant to concrete durability is the high internal humidity and the constant exchange of moisture between the concrete and its environment, resulting in large volume changes.

Common defects and modes of deterioration. The most common forms of defects and deterioration that occur in concrete substructures and foundations are summarized in the following sections.

Cracking. A crack is defined as an imcomplete separation into one or several parts, with or without space between them. The significance of cracking relates to the origin of cracks and subsequent magnification. Several causes of cracking may be summarized as follows.

- Plastic shrinkage cracks result from rapid drying of concrete in the plastic stage. These cracks are usually wide and shallow, often in a well-defined pattern or spaced at regular intervals.
- Drying shrinkage cracks follow the drying of restrained concrete that has hardened. They are usually finer and deeper than plastic shrinkage cracks and have random orientation.
- Settlement cracks may be of any orientation and width, attributed to foundation settlement.
- Structural cracks beyond the control of reinforcement, resulting from differences between assumed (predicted) and actual stress intensity. The width varies but the operation is often well defined.
- Map cracking (a closely spaced network of cracks) resulting from chemical reactions between the mineral aggregates and the cement paste. These cracks increase in number and width with time. Several chemical reactions are possible, but the predominant versions involve the alkalis from the cement and two constitutents of

some aggregates. The result may be serious damage of the concrete manifested as abnormal expansion, cracking, and loss of strength.

- Corrosion-induced cracking, usually associated with shallow cover, appearing directly above the reinforcement. These terminate at the reinforcement, and their width increases with continuing corrosion.

Scaling. Scaling is the flaking away of surface mortar of the concrete. During this process coarse aggregate is exposed and eventually becomes loose. Scaling results from repeated freezing of concrete saturated with water, and is aggravated by the presence of salts.

Scaling may also occur in a weak surface layer because of poor finish or curing, including construction in the rain, in which case it may progress no deeper. More commonly it is caused by insufficient air entrainment and may eventually lead to complete disintegration of the concrete.

Corrosion of Reinforcement. Corrosion occurs when oxygen and moisture are present and the passivity of the steel is destroyed by the carbonation of concrete or by the presence of more than the threshold concentration of chloride ions at the steel surface. As the steel reinforcement corrodes, it expands and causes the delamination of concrete at or near the level of reinforcement. With a continuing corrosion process, delaminations eventually become detached from the main concrete volume and result in a spall. Corrosion is normally intiated by the ingress of chloride ions, and is identified as a serious problem in highway structures subjected to salt applications.

Honeycombing and Air Pockets. These may be present in formed surfaces and originate at the time of construction. Air pockets are caused by inadequate consolidation, whereas honeycombing occurs when the mortar does not fill the spaces between the coarser aggregate.

Chemical Attack. The most common form of chemical attack is by sulfates. Attack by acids can be more serious where it occurs, but tends to be localized. Naturally occurring sulfates of sodium, potassium, calcium, or magnesium are sometimes found in soil or dissolved in groundwater adjacent to concrete substructures and foundations. When evaporation can take place from an exposed face, such as an abutment or retaining wall, the dissolved sulfates may accumulate at the face and increase the potential for deterioration.

The deterioration of concrete by acids is primarily the result of a reaction between chemicals and calcium hydroxide. In most cases this reaction results in the formation of water-soluble calcium compounds, which are leached away. Acid attack of concrete in bridges is uncommon, but it can occur as a result of bird or animal droppings. In this case structural deterioration occurs as a combination of acid attack with scaling and even corrosion of embedded reinforcement.

Wear. Excessive wear may appear on concrete surfaces exposed to traffic abrasion and is usually concentrated in the wheel tracks. It is noticed therefore on concrete decks, and seldom if ever in substructure elements.

Erosion. Ice movement, or abrasion by solid particles in rivers with high bedload, can cause serious erosion of the surface of piers and abutments built in river streams and lakes. Similar deterioration can occur in marine structures where erosion is combined with cavitation damage from wave action.

Field detection procedures. Several nondestructive techniques are available for assessing concrete damage and defects. Where the equipment and procedures have been standardized, the applicable test methods are listed in Table 12–1.

Visual Inspection. Deterioration is initially assessed by visual inspection, and the results are reported on standard forms, supplemented by photographs and sketches of significant sections.

In carrying out a visual inspection, it is customary to identify and describe cracks with respect to their location, orientation, and width. Depth is also important but can only be determined by coring. Crack widths should be estimated with sufficient accuracy using suitable formats. Ravelled edges or moisture associated with a crack may make the crack more visible and appear wider than it is. Conversely, narrow cracks are difficult to identify on surfaces that are rough or uniformly wet or dry.

Scaling should be reported with respect to location and extent. Corrosion of reinforcement is usually detected by the presence of rust stains on the concrete surface. However, some care is necessary to distinguish these effects from ferrous sulfide inclusions in the aggregate or the rusting of wires. Delaminations are not usually visible except where they are very shallow and are accompanied by a discoloration. Spalls are easily recognized, and the reinforcing steel is often exposed within the spalled area. Useful guidelines and standardized procedures will be found in the references at the end of this chapter.

Nonvisual Inspection. Inspection of closed cells and inaccessible areas may be supplemented by drilling holes to expose areas suspected of being defective. A small hole permits examination of the interior of closed voids using suitable instruments, especially in pretensioned and voided members. Larger holes made with a core drill enable observations with the help of light and a mirror or periscope.

Among the most sophisticated techniques used to assess the level of deterioration and structural damage not obvious by visual examination are (1) rebound and penetration methods, (2) stress wave methods, (3) magnetic methods, (4) electrical methods, (5) chemical methods, (6) nuclear methods, (7) thermography, (8) radar procedures, (9) ra-

Table 12–1 Standard ASTM and AASHTO Test Methods for Use in the Field

Designation*	Title
C 42 T 24	Method of Obtaining and Testing Drilled Cores and Sawed Beams of Concrete
C 597	Test Method for Pulse Velocity Through Concrete
C 803	Test Method for Penetration Resistance of Hardened Concrete
C 805	Test Method for Rebound Number of Hardened Concrete
C 823	Practice for Examination and Sampling of Hardened Concrete in Constructions
C 876	Test Method for Half Cell Potentials of Reinforcing Steel in Concrete
D 3633	Test Method for Electrical Resistivity of Membrane-Pavement Systems

*ASTM test methods are designated C or D.
AASHTO test methods are designated T.

diographic investigation, and (10) air permeability methods. Some of these methods were mentioned in section 10.3 in connection with defects and repairs of drilled shafts as a post-construction operation. A complete description is provided by Manning (1985).

Comparison of Test Methods. A comparative summary of test methods is presented in Table 12–2. This table suggests that a good visual survey supplemented by a judicious selection of techniques to investigate possible defects provides a good approach. The disadvantage of visual survey is the inability to detect hidden problems. Because the detection of corrosion of embedded reinforcement is rather difficult, other techniques are suggested, and include concrete cover, half-cell potential, and chloride-ion content tests. The nature of chemical attack and the quality of concrete that may be contributing to scaling, wear, or abrasion damage are better determined by taking cores for laboratory examination.

Laboratory procedures. Most of the test methods suggested for field investigations could also be used in the laboratory. Strength can be measured directly, and core samples can be taken from both sound and deteriorated sections of concrete members for laboratory testing.

The usual laboratory procedures include a petrographic analysis, physical tests, and chemical tests. A petrographic analysis is a detailed examination of the material, composition, and structure of the concrete, and may include identification of the mineral aggregates, the paste-aggregate interface, and assessment of the structural in-

Table 12–2 Capability of Investigating Techniques for Detecting Defects in Concrete Structures and Field Use

	Capability of Defect Detection[a]					
Technique	*Cracking*	*Scaling*	*Corrosion*	*Wear and Abrasion*	*Chemical Attack*	*Voids in Grout*
Visual	G	G	P	G	F	N
Hardness	N	N	P	N	P	N
Sonic	F	N	G	N	N	N
Ultrasonic	G	N	F	N	P	N
Magnetic	N	N	F	N	N	N
Electrical	N	N	G	N	N	N
Chemical	N	N	G	N	N	N
Nuclear	N	N	F	N	N	N
Thermography	N	G[b]	G	N	N	N
Radar	N	G[b]	G	N	N	N
Radiography	F	N	F	N	N	F
Air Permeability	N	N	F	N	N	F

[a]G = good; F = Fair; P = Poor; N = Not suitable

[b]Beneath bituminous surfacings.

tegrity of the paste itself. Physical test methods are used to assess the strength of concrete and include testing cores to failure in compression. Chemical test methods are particularly important for determining the carbonation and chloride ion content, but require careful interpretation of the results.

Steel and Timber Components

Field procedures for steel members, including steel piles, encompass a wide variety of techniques because steel is more homogeneous and isotropic than concrete, and therefore flaws and defects are generally easier to recognize. Many of these procedures can also be applied in the laboratory.

Visual inspection implies that the member is accessible or can be exposed. Rusted steel varies in color from dark red to dark brown. The parts of steel having trapped moisture, particularly in association with salt, are the most vulnerable to corrosion. Simple test procedures that can be applied in the field include x-ray and gamma-ray examination, ultrasonic testing, penetrating dyes, magnetic particles, eddy currents, electromagnetic induction, and acoustic emission. However, despite the relatively good defect detection capabilities shown by a variety of these examination techniques, it is often difficult to obtain good results in real structures under field conditions. In such cases combination systems may be used to verify test results.

Timber components are unlikely to be found in substructures, except in foundations in the form of timber piles. The most common defects have been discussed in the foregoing sections. In general, the state of the art in deteting defects and deterioration is not as advanced as for concrete and steel. The best method probably available is to expose the piles, if accessibility is not prohibited, and carry out a thorough visual inspection. Any probe such as a knife, ice pick, nail, or brace and bit, can be used to test for internal decay or infestation. The ease with which a member can be penetrated is a measure of its soundness. Other procedures that can be used in the field to supplement visual examinations include electrical methods, sonic and ultrasonic techniques, and specimens obtained from more detailed laboratory analyses. For a complete description, see Manning (1985).

12.3 ASSESSMENT OF DEFICIENCIES OF SUBSTRUCTURES BELOW THE WATER LINE

Basic Considerations

Deficiencies of bridges below the water line include scour and structural distress, damage, and deterioration that sometimes remain undetected or are endured until the potential for a major structural failure becomes apparent. In general inspection procedures are available, but their application is sometimes complicated by inaccessibility. Useful guidelines are provided by AASHTO's *Manual for Maintenance Inspection of Bridges* (1995) and in NCHRP *Synthesis of Highway Practice 88*, "Underwater Inspection and Repairs of Bridge Substructures." The objective of this section, therefore, is to present current methodologies for evaluating the effects of below-the-water-line deficiencies on the structural capacity of the substructure. A rating system for identifying the urgency of corrective action is also included.

Brief review of inspection techniques. Procedures for evaluating concrete, steel, and timber under water have been evaluated and disseminated in the references mentioned in this discussion.

The inspection of concrete under water normally includes visual assessment, measurement of physical dimensions, and soundings. Because of the associated expense, cores are usually taken under water only when other evidence is not conclusive. Cores are typically used to obtain compressive strength and chloride content and penetration, but they can also provide data from a wide variety of physical and chemical analyses.

Voltage potential readings of the reinforcing steel are sometimes taken under water. These indicate only whether or not corrosion is active and the extent of the concrete surface involved in the process. The most reliable results are obtained when the readings are used in conjunction with a chloride penetration analysis of a core sample.

Two additional services have been developed to evaluate concrete: (1) a polarization resistance device for measuring the rate of corrosion; and (2) a cat scanner for testing concrete piles under water.

The inspection of steel under water normally includes visual assessment, measurement of physical dimensions, and sounding bolts and rivets. Ultrasonic testing has been used, but has several drawbacks when applied under water.

The inspection of timber components under water likewise includes visual assessment, measurement of physical dimensions, soundings, pointed probe resistance testing, and use of an increment borer. Sonic pulse velocity testing is also available for underwater applications.

System rating of substructure. The Federal Highway Administration's *Guide for Structure Inventory and Appraisal* (1988 edition) item 60 is the rating system for substructure conditions. This item describes the physical condition of piers, abutments, piles, fenders, footings, and other components. The intent is to rate and code the condition according to generally described condition ratings.

All substructure elements should be inspected for visible signs of distress including evidence of cracking, section loss, settlement, misalignment, scour, collision damage, and corrosion. The rating given by item 113 (Scour-Critical Bridges) may have a significant effect on item 60 if scour has substantially affected the overall condition of the substructure. Any rating regarding the substructure condition should be made independent of the deck and superstructure evaluation.

Integral-abutment wing wallls to the first construction or expansion joint should be included in the evaluation. For nonintegral schemes, the substructure is considered as the portion below the bearings. Where the superstructure and substructure are integral, the substructure is the portion below the superstructure.

Commentary. The sufficiency rating formula introduced by the FHWA is a method for assessing the factors that indicate the sufficiency of a bridge to remain in service. This rating is used as input into the highway Bridge Replacement and Rehabilitation Program for prioritizing bridge replacement and rehabilitation plans under federal funding. The sufficiency rating is generated through the use of a complex formula that includes input from many factors.

The overall structure condition appraisal is a composite rating representing the average of several factors, including the substructure condition. There is some concern

(Rissel, Graber, Shoemaker, and Flournoy, 1982), however, that of the total items considered in establishing this appraisal, deficiencies below the water line are represented by a small contributing factor, whereas underwater deficiencies are clearly of a criticial nature and affect the load-carrying capacity. In this case, they can be the determining factor for the overall structure condition appraisal.

Proposed Guidelines

There appears to be a need to standardize and expand the guidelines with respect to the interpretation and application of the provisions related to item 60 (SI and A). Certain common views, for example, become apparent. Scour of piles, either in a bent or under an exposed footing, is of little concern to bridge offices with respect to structures in salt water. The exception is untreated timber piles that are in this case susceptible to borer damage. Some states consider scour of pile footings in fresh water critical because of the abrasive action of fast-flowing stream bed materials. Most states considered the exposure of spread footing (not on piles) a critical condition demanding immediate remedies. However, the loss of lateral support on a pier shaft was not considered critical unless the spread footing was exposed as well.

Section loss of a concrete pile is critical when reinforcing bars are completely exposed. Section loss of a timber pile (inside section) is critical and requires prompt replacement in warm salt water because of the action of marine borers.

Rissel et al. (1982) proposed certain guidelines used to arrive at a maintenance urgency index. Specific comments from states concerning these guidelines are summarized as follows.

Scour around Piles. Scour around piles raises concern about scour resistance of the stream bed and pile penetration. Light scour is not considered a major problem and requires no riprap because of the minimum pile length normally required by the specifications. Where greatest pile lengths are required, the opinion is that a substantial amount of scour may be accepted without endangering the structure. With particularly scourable beds, any scour should be a serious problem because of possible abrasion damage.

Undermining of Footing. For a pile footing, two relevant parameters are the type of water (salt or fresh) and type of pile (timber, steel, or concrete). In salt water, borers and corrosion are main concerns, but in fresh water, abrasion of piles due to granular soils is a factor. When scour exposes the pile, it should be rated separately. Scour of a spread footing is critical and should be repaired promptly.

Section Loss of Concrete Pile. The consensus of opinion suggests that if the main reinforcing bars are exposed, a lower rating should be applied, meaning that this deficiency will have structural consequences and reduction in structural capacity.

Section Loss of Steel Pile. Again, with some minor differences in the boundaries between ratings, states agreed with the proposed guidelines, but it was recommended to quantify the rating by estimating the extra stress induced in the member because of the section loss.

Section Loss of Timber Pile. A relevant factor is whether the decay is internal or external. Internal decay is more likely to be caused by borer activity in salt water. A suggestion in this case was to replace internally decayed piles, or closely monitor the process.

Settlement. There was relatively little agreement concerning settlement. Ridability and ability of the bearings to contract and expand were the prime factors, and in many instances there was more concern with regard to the ability of a bridge to function and carry traffic.

Whereas both AASHTO and the FHWA maintain the policy of revising and modifying the rating system as additional research and closer observation provide new input and result in new criteria, the administrative level at which the assessment modification is approved is not within the scope of this discussion and is not addressed here.

Structural Capacity Analysis

The history of the site is significant because it helps to determine whether conditions have remained the same or whether they are changing. This allows the inspection process to identify deficiencies requiring closer observation and monitoring. Defects resulting from settlement (for example, cracking) may be exacerbated if the structure is located in an active seismic zone.

One example that may suggest the level of inconsistency in assessing a deficiency is the case of exposed piles under a footing. The piles may function in completely different environments and conditions depending on geographical locations. In a coastal region, exposed timber piles could be subjected to the effects of marine borers, but this would be of no concern in assessing the pile deficiency in a freshwater area. On the other hand, the same pile in fresh water would be exposed to the action of abrasion and scour because of fast moving water, while in coastal regions scour pockets may merely fill back in during the next season.

Because of the need to rate bridges under the federally mandated bridge inspection program to ensure eligibility under federal funding, state agencies have attempted to standardize procedures for evaluating the consequences of deterioration, but thus far this involves engineering approaches largely judgmental in nature.

Analysis of substructure units is not always carried out. This becomes a requirement when it appears warranted by a deficiency, but in many instances the solution is to repair the deficiency without performing an analysis, either above or below the water line.

Current practice. Reduced stresses and cross-sectional areas are usually incorporated into commonly accepted analysis computations, but without the use of methods considered unique to measure the structural adequacy of concrete, steel, and timber. Very seldom is a substructure unit analyzed for the consequences of settlement when it occurs. Shimming is the usual corrective action because it is inexpensive and easy to apply. Yet, from the discussion of section 3.12, there are explicit criteria regarding tolerable settlement and angular deviation. If the effects of settlement indicate continuing structural distress, steps should be taken to determine the cause.

Only few states evaluate the overall stability of a bridge for scour of foundation

material beneath spread footings. The action most frequently taken is not to analyze the deficiency but rather to correct it. Because many bridge failures have been caused by scour, early intent to repair it is justified, but safety may be further enhanced if the cause and consequence of scour are analyzed.

Reduced frictional capacity of a pile because of scour action is calculated in some instances. Reduced lateral support of a pile deprived of earth resistance because of scour is rarely calculated. Likewise, these deficiencies are not analyzed but merely repaired.

Suggested practice. Rissel et al. (1982) proposed inspection combined with structural capacity analysis extended to substructure elements, the latter considered as critical and often less redundant than their superstructure counterparts. An example that compares redundancy is a bent supporting 10 beams, while the bent itself rests on three piles. In this instance, the failure of one pile may be more serious than the failure of one beam.

Three methods are suggested to assess the severity of deteriorations at the inspection level.

Method I. In this case, specific instances of borderline deterioration should be exemplified. Cases would be delineated, such as scour of spread footings and internal decay in salt water. These qualitative discussions can provide the inspection team with quick ability to assess the severity of a deficiency. This assessment should be verified later with a more exact structural analysis.

Method II. With this method, the intent is to develop mathematical relations that express the structural capacity, prior to inspection. These equations should include parameters that account for material strength reduction and section loss, and could be used to analyze any member below the water line, for example, a pile at any location. This design aid should be incorporated in the bridge inspection folder as reference material.

Given the complexity of substructure and foundation analysis and the available methodologies, this method would require field personnel with sufficient structural background, equipped with programable calculators. An alternative to this is a complete analysis in the office based on data obtained in the field.

Method III. A third method is to use generalized charts and graphs to determine the basic loads (generally live load and dead load) transmitted to the substructure and foundation. Properly trained personnel could make an intitial assessment of the structural capacity of the substructure at the bridge site, based on measurements and data obtained at the inspection. Where the results warrant, the initial assessment could be verified with a more exact office analysis.

Interestingly, the deterioration of a substructure unit supporting short spans can under certain circumstances become more critical than in a unit that supports long spans. This is mainly because the ratio live-to-dead load is much larger in the former and small in the latter. Substructures supporting long spans are also designed for additional considerable forces such as wind, braking, and temperature changes. These forces are included in the initial design but commonly ignored in the live load capacity analysis. The result is that for long spans, larger capacity is usually predicted than is neces-

sary to support dead and live load only, although in some instances the initial design may have been controlled by Group I.

12.4 REPAIR OF SCOUR DAMAGE

The General Scour Problem

Scour was discussed in sections 2.5, 3.15, and more extensively in connection with the stability of piers in waterways. In this section, scour is reviewed in connection with the associated damage and corrective measures. Bridge maintenance and replacement costs are often directly dependent on scour effects.

As mentioned in section 3.15, the potential for scour damage can be reduced and reasonably controlled by appropriate procedures in the design stage. However, even where this potential was properly considered, changes occurring subsequent to construction can lead to problems. For example, restrictions in the waterway due to aggredation or the accumulation of debris can enhance the capacity of a stream to transport sediment and result in localized scour. The characteristics of stream flow can also be changed by activities related to development and lead to unexpected scour problems.

The types of streambed materials and local geology and soil conditions are important factors directly related to the potential of scour. This potential also exists at sites subjected to medium or heavy flooding. Interestingly, some of the initial techniques used to counter scour may be applied to repair a bridge that has been damaged. NCHRP Report 243 (1981) gives the following summary of remedial measures.

1. Use dumped rock riprap around substructure units and at fills in embankments to repair scour damage and to provide future protection.
2. Where possible, leave in place sheet-pile cofferdams used during construction.
3. Remove objects from the channel likely to change the flow characteristics or likely to harbor debris.
4. Modify, if possible, the channel upstream and downstream to reduce scour potential at the bridge site (see also section 3.15). A sheet-pile cofferdam, for example, can be used to control degradation of a stream.
5. Construct a massive toe at the foot of the riprap slope protection to prevent undermining.
6. Construct spur dikes or jetties, where applicable, to provide partial diversion of the stream.
7. Repair substructure elements by injecting grout or by cast-in-place concrete.
8. Promote the growth of vegetation at channel/bank locations where its presence may counter tendency to scour.

Data review. The literature contains an impressive record on scour, although the matter of repair is not necessarily the main focus of this work. An excellent review of practice is provided by NCHRP Synthesis 5 (1970), which gives also formulas and charts for predicting scour depth. A statistical summary of the causes of bridge failures is given by Chang (1973). This work shows that bridge abutments are damaged most frequently,

followed by bridge piers and superstructures. Most of the failures presented are attributed to a deficiency in the flow path or to a vigorous change in flow.

In investigating scour around piers, Hopkins, Vance, and Kasraie (1980) conclude that three scouring actions are usually involved: (1) general scour occurring from natural changes in the stream, (2) contraction scour caused by narrowing of the waterway at the bridge site, and (3) local scour caused by flow disturbance introduced by the presence of the bridge pier.

Brice and Blodgett (1978) present case histories of a large number of bridges and give a comprehensive documentation of countermeasures for hydraulic problems. Performance ratings are given for flow control countermeasures such as spurs, dikes, spur dikes, check dams, and jack fields. Streams are classified into types with regard to the lateral stability and behavior correlated with the design of remedial work. It appears that local scour by itself would not be of sufficient extent to explain most failures, since it accounts for less than 20 percent of the total scour depth. It follows, therefore, that deficiencies in the flow path and vigorous changes in flow would result from natural changes in the stream and narrowing of the channel. The same investigators describe the various types of revetment and bed armor, and flow control structures. Revetment armor may be one of the following: riprap, rock and wire mattress, and gabion; concrete riprap; concrete-grouted riprap; and concrete-filled fabric mats and bulkheads.

Structures for controlling flow can be provided either within or outside a channel, and they act as a countermeasure by controlling the direction, velocity, and depth of flowing water. Figure 12–1 shows the various types of structures that can be constructed to help regulate stream flow, control corrosion, and protect the bridge crossing. Their application at a given site may be adapted to fit particular situations. Spurs, retards, dikes, and jack fields may be located either upstream or downstream from the bridge.

Flow control structures. The structures shown in Figure 12–1 have been tested in the field, and if properly designed and located, they can provide positive results.

A spur is a linear structure, either permeable or impermeable, built out in the stream from the bank. Its function is to alter the direction of flow, induce deposition, and reduce the flow velocity along the bank. Spurs are sometimes referred to as jetties, groins, dikes, deflections, and so on. They may protect the banks of the stream more effectively and at less cost than riprap revetments. In addition, they serve to stabilize the

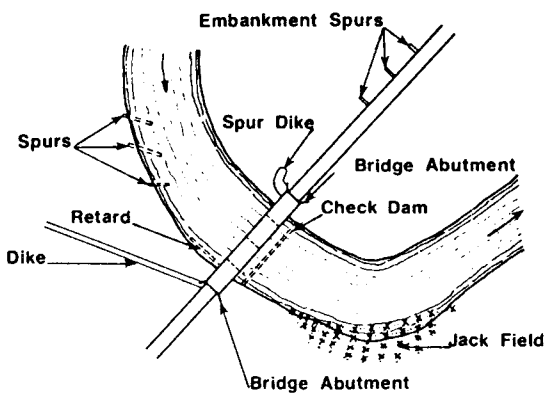

Figure 12–1 Typical placement of flow-control structures.

channel, control flow at a bent, and direct flow through the intended bridge opening. They can be constructed perpendicular to the stream bank or inclined upstream or downstream. An upstream-inclined spur is recommended if the area of flow water velocity is formed upstream from it, erosion of the upstream face is prevented, and the need for revetment (except on the spur nose) is eliminated. The length of spurs should be 50 feet minimum for bank protection on straight reaches, long radius bends, and braided channels. Shorter spurs may be more costly than riprap revetment along the bank. The recommended spacing between spurs is 1.5 to 6.0 times the length of the project upstream. Spurs may constructed of earth or rock, or using timber, sheet or steel piles.

A retard is a linear structure usually built parallel to the stream bank, and it can be either permeable or impermeable. Retards are more effective in maintaining the existing stream alignment than are spurs. A special type of retard is a line of concrete jacks. Each jack consists of three 16-foot concrete beams bolted together at right angles. Several lines of jacks can be used if necessary. Likewise, retards tend to reduce flow velocity, induce deposition, or maintain an existing flow alignment.

Dikes are used to control over-the-bank flow, mostly in areas of flood plains. They may be constructed on one or both sides of the bridge openings and function similarly to spur dikes. A spur dike is a straight and outward curving structure that turns upstream or downstream from the approach embankment. Its main purpose is to prevent erosion by eddy action at abutments and piers where flow moving along the upstream side of an approach fill enters the main flow at the bridge. Spur dikes are usually impervious, revetted earth embankments, but rock and concrete rubble may also be used. Spur dikes at highway stream crossings are used for three main reasons: (1) to move the point of high vortex action away from the abutments; (2) to cut off the path of low resistance along a cleared right-of-way and force water through vegetation on the flood plain; and (3) to streamline the flow through a bridge opening to reduce velocity concentrations.

A check dam, as shown in Figure 12–1, can be used to control the water velocity and degradation. Check dams have been constructed of rock, riprap, concrete, sheet pile, rock and wire mattress, gabions, or concrete-filled fabric mat. They have been found effective for reducing degradation in small streams. In alluvium streams, however, an unacceptable scour damage may occur from the check dam. Among the highly recomended references for the effectiveness and performance of the various types of countermeasures for the control of scour are Brice and Blodgett (1978), Rothwell and Bohan (1974), and Keefer et al. (1981).

Methods of Repairing Scour Damage

Figure 12–2 shows a typical repair that may be implemented where pier footings supported on piles have been undermined by scour. A concrete subfooting that envelopes the original foundation as shown provides protection to both the footing and the piles and restores the structural continuity with the soil system. This repair can be accomplished by constructing a cofferdam around the pier, pumping out the water, and forming for the subfooting. The stone riprap is normally placed after the cofferdam is removed, and is used to protect the new foundation. Where possible, riprap should not extend above the original stream bed because it could act as an obstruction to stream flow.

The stone used for the riprap can vary in size, but in a typical application it could weigh 500 to 1500 lb with at least 50 percent of the stone weighing more than 300 lb. For sizing riprap around piers, the following equation is useful:

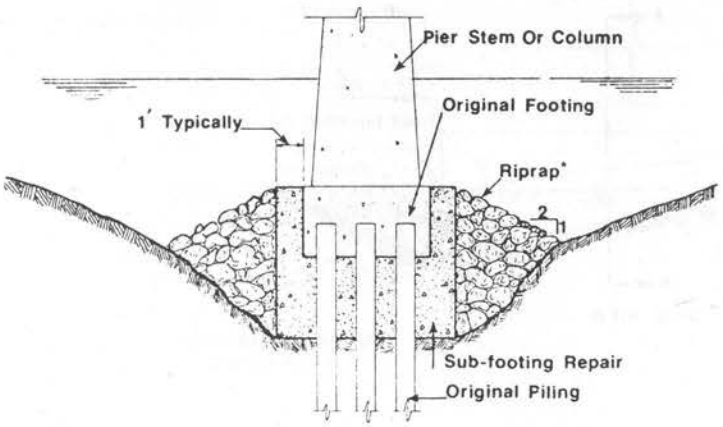

Figure 12–2 Section showing repair to scour-damaged pile footing using concrete jacketing and riprap.

$$\frac{d_{so}}{D} = 2.5\,F^3 \tag{12–1}$$

where d_{so} = average stone diameter, ft; D = depth of flow, ft; F = Froude number of flow = $V/\sqrt{gD}$; V = average velocity of flow (ft/s); and g = acceleration of gravity = 32.2 ft/sec^2.

Equation (12–1) may be applied to determine the minimum sized stone at the location of most severe attack, and smaller sized stone may be used at extremities where conditions are expected to be less severe.

For footings partially undermined by scour, the repair procedure may consist of a flexible nylon form shaped as a tube and filled with structural mortar. This configuration is cut to suitable lengths and joined together by using a high tensile strength nylon stitching. The fabric tube is then wrapped around the scour area and extended several feet beyond the zone affected.

Once the fabric tube is in proper position, mortar is pumped into it through suitable openings in the top layer of the material. Grout injection pipes to fill voids under the footing are placed as shown in Figure 12–3. After the fabric form has been filled, all voids between it and the foundation can be plugged by using a smaller fabric form as shown in section A-A. Subsequently, the void between footing and the stream bottom is filled by pumping mortar through the prepositioned injection pipes. Several escape pipes should be provided to allow water to flow out from the voids during the operation.

Other means that can be used to correct scour damage discussed previously are shown in Figure 12–4. According to this technique, concrete riprap in bags is placed around the damaged areas up to a height slightly below the existing footing. This provides a form for tremie concrete pumped into the damaged zone as shown in sections A-A and B-B of Figure 12–4. This method is intended to be applied completely under water.

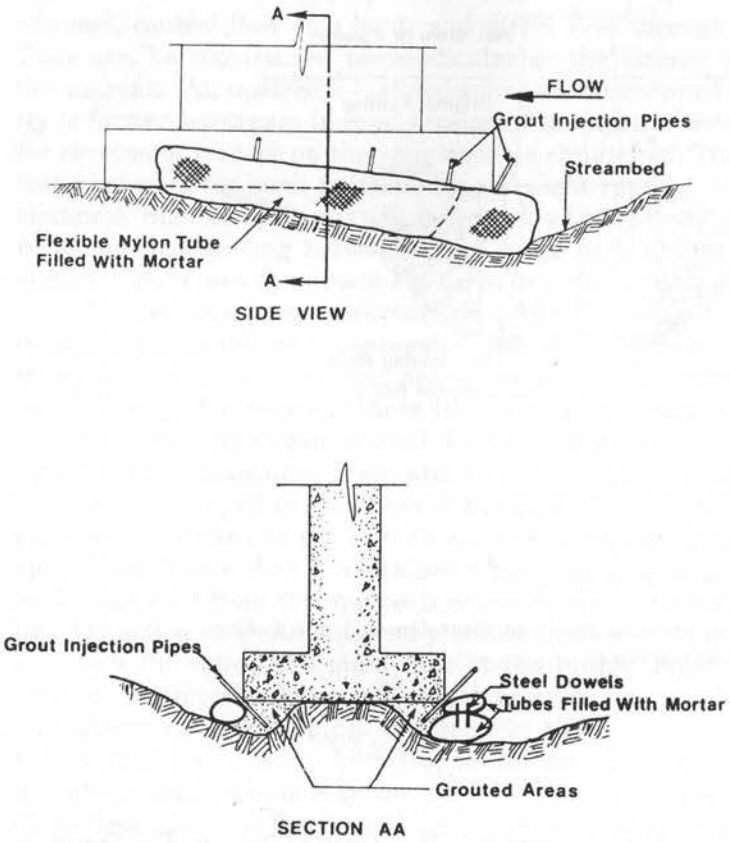

Figure 12–3 Repair of scour damage using a flexible nylon tube form filled with mortar.

On many occasions, the whole streambed may be affected by scour. This problem may arise from changes in streamflow characteristics due to man-made causes. For example, the relief of a downstream constriction in the stream channel can lead to increased velocities upstream, particularly during heavy rains, and this can cause the streambed erosion shown in Figure 12–5. Further damage in this case can be prevented by rebuilding the affected area with a crushed stone subbase topped with a heavier stone riprap. A combination of this method and the tube form technique could be used to repair footings where required.

Bridge abutments in waterway crossings are usually positioned at higher elevations, yet they often require repairs to correct damage due to scour. Figure 12–6 shows two repair cases for abutments on soil and piles, respectively. For the repair technique shown in Figure 12–6(a), machine bolts are driven into predrilled holes spaced about at 2-foot centers, with the intent to tie the original and the new structure together. A similar subfooting repair has been applied to the abutment supported on piles, shown in Figure 12–6(b). In this case, the piles provide the rigid connection between the old and the new concrete. Additional protection could be provided with the flow control structures discussed in the foregoing sections.

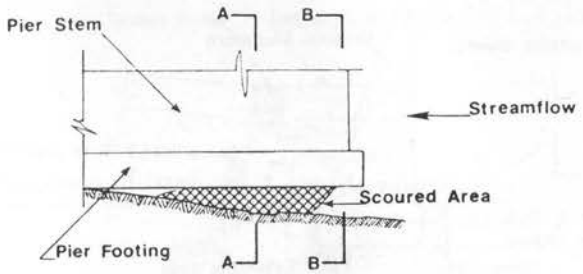

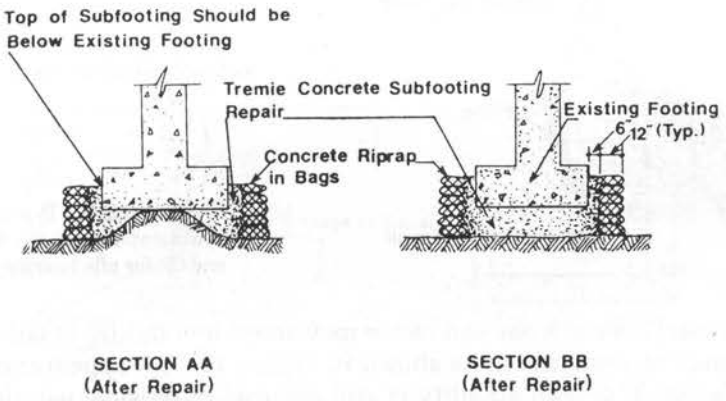

Figure 12–4 Repair of scour damage using concrete riprap in bags and tremie concrete subfooting.

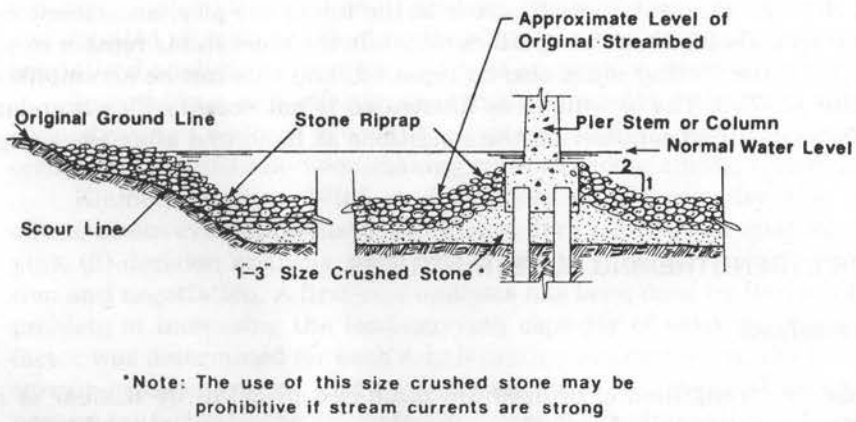

Figure 12–5 Section showing rebuilding of streambed that has been scoured out exposing pier footings and piling.

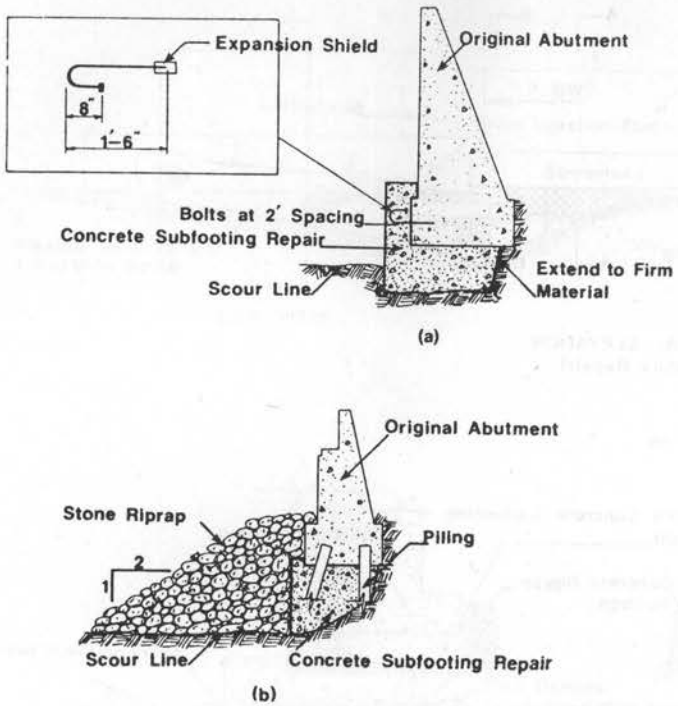

Figure 12–6 Typical sections of abutment repair; (a) for soil bearing and (b) for pile bearing.

In extreme cases, severe scour can cause movement and failure of substructure elements. Repairs may be undertaken as shown in Figure 12–7, if appearance is not considered a major factor. If overall stability is still ensured, a possible solution is to drill several holes through the deck and into the pier stem. Grout and steel dowels are inserted into the cavity thus formed to stop further tipping of the pier until the footing is repaired, as shown in Figure 12–7(a). A first-stage pier enlargement is constructed to an elevation above the water line. After this concrete has attained strength, it can be used as a seat to jack the superstructure back approximately to its original grade. Steel shims are used to support the deck while the second stage repair is made, as shown in Figure 12–7(b). For the placement of second-stage concrete, additional holes can be drilled through the deck to gain access to the top of the pier, and closed monolithically with the second-stage concrete placement while the steel shims remain in place. Prior to stem repair, the footing must also be repaired, and this can be accomplished as shown in Figure 12–7(a). The technique as illustrated is not necessarily a standard procedure and can be modified considering the conditions at hand and after assessing overall stability.

12.5 METHODS FOR STRENGTHENING SUBSTRUCTURES

Cost Effectiveness Analysis

Methods for strengthening bridges are discussed in detail by Klaiber et al. (1987) in connection with several other options, namely, maintenance, rehabilitation, repair, and stiffening. The term strengthening refers to the increase of the load-carrying capacity of an existing bridge to provide the structure with a service level higher than in the origi-

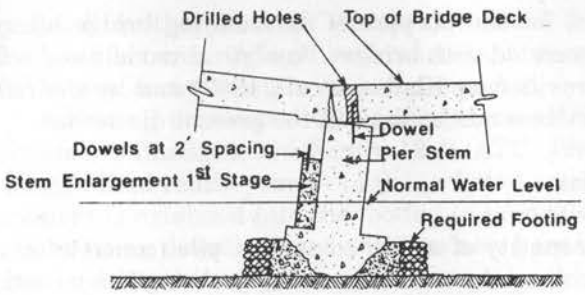

(a) Section Thru Pier Stem Showing First Stage of Repair

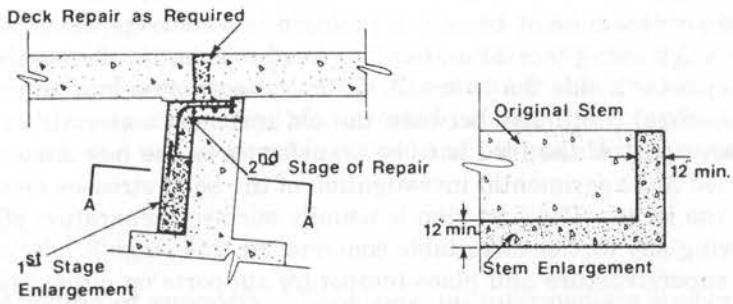

(b) Section Thru Stem Showing Second Stage of Repair

Note: This repair should be undertaken only if the stability of the pier and other attendant damages are judged to be acceptable and amenable to repair

Figure 12–7 Repair of a pier and deck that has moved or tilted as a result of scour.

nal design, also identified as upgrading. Strengthening procedures may be articulated and detailed to apply to the majority of bridges, excluding structures that require highly specialized analytical techniques such as suspension, curved, and cable-stayed bridges.

Invariably a cost effectiveness analysis cannot isolate the substructure from the superstructure, hence it is used as a systems analysis where the entire bridge is considered under specified decision-making rules to choose among alternatives.

Klaiber, Dunker, Wipf, and Sanders (1987) consider the following five cost-effectiveness evaluation methods: (1) standard benefit-cost analysis, (2) consumers' surplus, (3) decision analysis, (4) multi-attribute analysis, and (5) multi-objective evaluation and negotiation. A first-cost analysis has been used by Berger (1978) to address the problem of increasing the load-carrying capacity of existing bridges. An improvement factor was determined for each rehabilitation alternative on the basis of improved load-carrying characteristics, and a cost effectiveness factor was obtained by dividing the improvement factor by the estimated unit cost of the alternative.

Whereas these brief comments highlight the complexity of the decision-making process, they also demonstrate the difficulties of accurately assessing present and fu-

ture costs for most bridges for the purpose of determining bridge lift cycle costs and other economic aspects associated with bridges. Analytical models and a further discussion on these topics are provided by Klaiber et al. (1987) and by the references at the end of this chapter; they are beyond the scope of the present discussion.

Strengthening of Pier Columns and Piles

Improving the structural capacity of a pier column or pile (concrete or timber) can be achieved by encasing the column in concrete or steel jackets. The jacketing may be applied to the full length of the member or only to severely deteriorated sections. The intent of this process is to increase the cross-sectional area of the column and also reduce its slenderness ratio. Partial encasement may also be particularly effective when an unbalanced moment acts on the column. Figure 12–8 illustrates two such concepts for member addition, used in work for strengthening concrete structures (Westerberg, 1980).

The complete encasement of an existing column in a concrete jacket has been used frequently for strenghtening pier columns. The reinforcement is placed around the existing column perimeter inside the jacket. A difficulty most often encountered is the development of structural continuity between the old and new material, and this is the critical stage where part of the load is to be transferred to the new material. Soliman (1985) has included an experimental investigation of the bond stresses between the initial column and the jacket. The first step is usually surface preparation of the existing column by removing any dirt or unsuitable concrete. At this stage it may also be desirable to jack the superstructure and place temporary supports on either side of the column. This may be necessary because shrinkage can cause compressive stresses on the column that will be reduced if the existing column is unloaded. Supports will also be required if the column shows signs of deterioration. Finally, this procedure will allow the new material to share equally both dead and live loads after the supports are removed. Old reinforcing bars should be cleaned of any corrosion and treated with an epoxy coating. Additional longitudinal reinforcement and stirrups are placed around the column. Spiral reinforcement could be used to increase the structural capacity and ductility, as

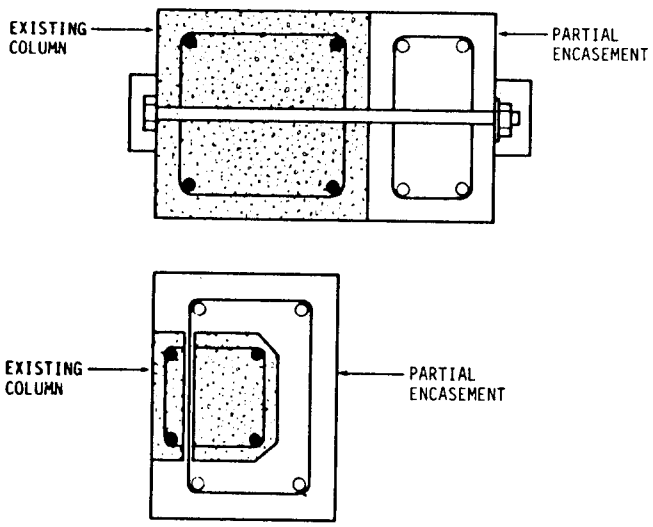

Figure 12–8 Partial jacketing of an existing column.

explained in other sections. An epoxy resin is then applied to the old concrete to promote bond between old and new concrete. Formwork is then placed to form the jacket, and the new concrete is placed and compacted.

Jacketing techniques that have been used for seismic retrofitting of existing pier columns are illustrated in Figure 12–9 (ATC, 1983). Figure 12–9(a) shows the addition of longitudinal reinforcement in the jacketed area around the existing column. The reinforcement is extended into the footing in predrilled holes to ensure the structural continuity by using dowels spliced with the new bars in the column. New ties are placed and bonded using gunite.

A procedure used to improve the lateral capacity of a column is shown in Figure 12–9(b). There are two methods for adding lateral reinforcement: by wrapping the existing column with tensioned prestressing wire, and by adding a series of No. 4 hoops with a turnbuckle included to pretension the two ends of the hoops together. Both methods should include the application of a protective layer of shotcrete or cast-in-place concrete.

The jacketing of concrete columns with steel shapes is essentially similar. Three versions are shown in Figure 12–10 and involve a primary load transfer between the steel and the column by shear friction. The column is first cleaned of dirt and old concrete, and any exposed bar is also cleaned and treated. The steel shapes are treated with an epoxy coating and erected around the column. These steel shapes form the jacket, and new concrete is poured and compacted in the annular space.

Additional Bridge Continuity

Addition of supports. Supplemental intermediate supports may be added, if geometric restrictions allow, to reduce span length and the associated moments and shears. By changing a single-span bridge to a continuous structure, the stresses are markedly al-

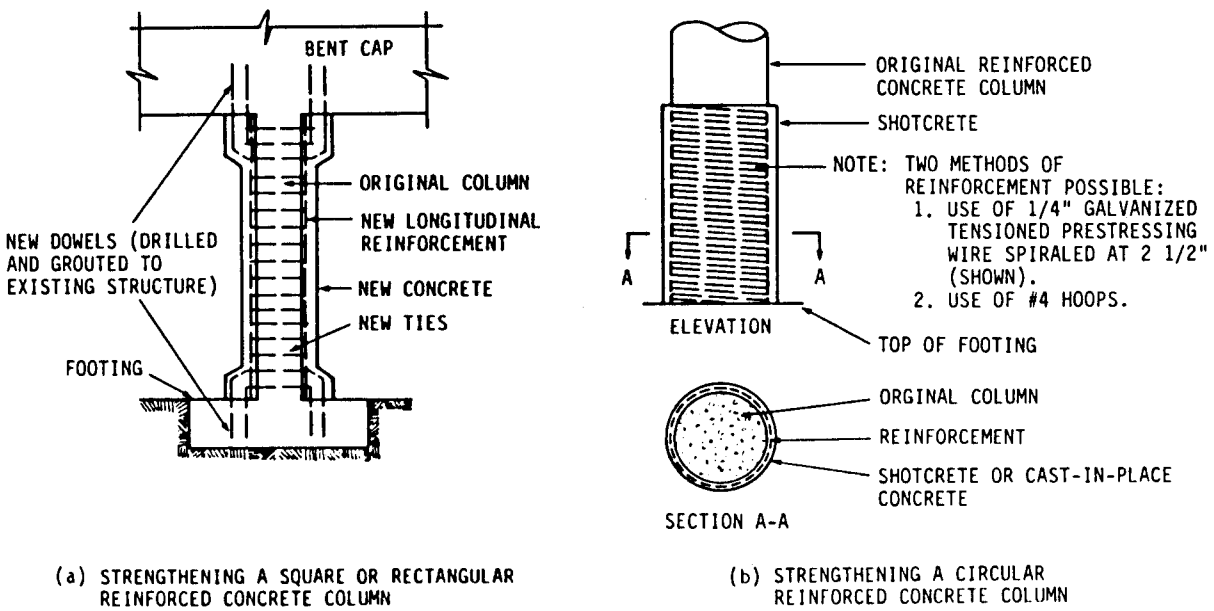

(a) STRENGTHENING A SQUARE OR RECTANGULAR REINFORCED CONCRETE COLUMN

(b) STRENGTHENING A CIRCULAR REINFORCED CONCRETE COLUMN

Figure 12–9 Examples of concrete jacketing techniques.

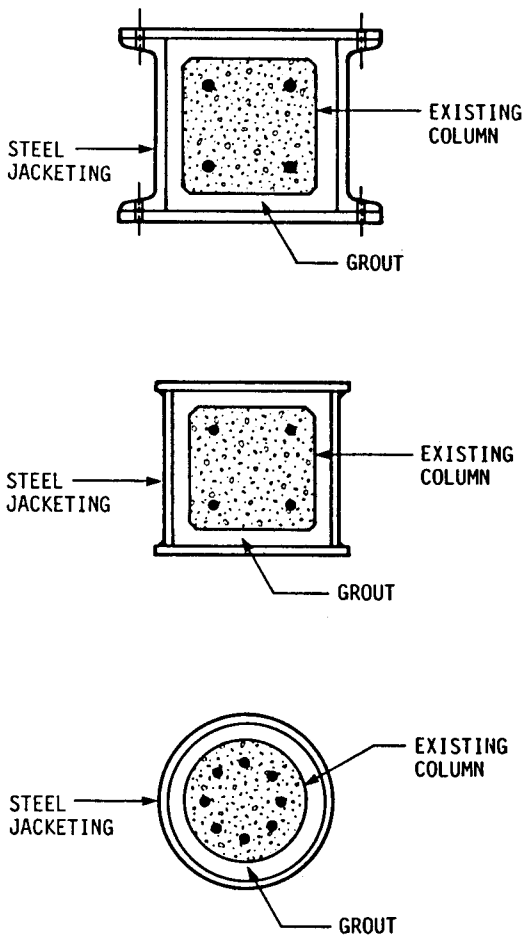

Figure 12–10 Cross-sectional view illustrating jacketing of concrete columns with steel shapes.

tered with a considerable increase in structural capacity. The method may be expensive because new supports are added, but it may be a viable solution in certain cases.

Applicability. The structural benefits resulting from the conversion are demonstrated in Figure 12–11, showing the maximum positive moment for simply supported single-span bridges of various lengths caused by HS 20 loading (truck or lane), and also the maximum moment (positive or negative) results when an intermediate support is added. Two different locations of the additional support are considered, corresponding to a span ratio $n = 1.0$ and 1.5.

These advantages, however, may not be realized if there is no suitable location for an additional pier, or where soil conditions or stream characteristics would require a foundation whose cost is unacceptable and prohibitive. In general, the conversion is feasible and cost-effective with medium-to-long span bridges. A thorough analysis is required for truss bridges because of the complex structural modification associated with the additional support, and also because in many cases the truss would have to be modified by adding new members in areas of moment and stress reversal.

Design Requirements. The design of an intermediate pier depends largely on the loads to be transferred, bridge dimensions, and soil conditions. Hence, the design must be carried out as in standard substructure and foundations discussed in other

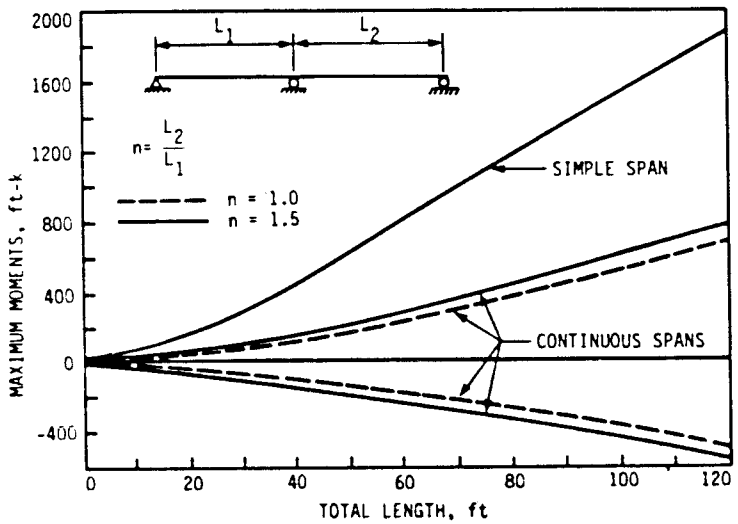

Figure 12–11 Maximum live-load moments for simple-span versus continuous two-span bridges.

chapters. If the bridge is in good to excellent condition, providing a new pier support is compatible with the life expectancy of the structure, and if the only problem is inadequacy of the superstructure to accommodate present loading, the solution is economically sound.

The pier type and method of installation will depend on the anticipated loads and soil conditions. A common pier system in this case is steel H-piles with a steel or timber beam used as a pier cap. A method reported by Roberts (1978) enables the piles to be installed with a minor modification to the existing bridge. Square holes 2 ft × 2 ft are cut through the deck above the point of application of the piles, allowing the piles to be driven into position through the deck. The piles are cut off so that a pile cap and rollers can be placed under the beams. Concrete pile bents, solid piers, or hammerhead piers should not be excluded, provided their higher cost is justified.

Another important consideration is the modified structural action of the superstructure system in the continuous scheme. If the initial design is noncomposite, areas of positive moment that now become zones of negative moment or stress reversal need only be checked for the new stresses. If the initial bridge deck acts compositely with the beams, the deck in the negative moment area should be removed and replaced with a slab properly reinforced. Likewise, composite beams with bottom cover plates or variable plate thickness will have to be checked and modified, if necessary, to handle the new stresses and stress pattern.

Modification of simple spans. In this case, adjacent simple spans that are simply supported are connected at piers with a moment and shear connector arrangement so that they become continuous beams. The overall deck modification is conversion to integral bridge, hence is governed by the design and functional requirements discussed in other sections.

If the intent of the new design is to shore the simple span temporarily so that the pier or piers under consideration accept no load during the modification of the beams, the new continuous system will act as such for all loads, inlcuding dead loads from the

superstructure, although the actual dead load moment diagram will also depend on the method of shoring and the number of shoring points. If the dead-load support condition is not altered during modification, the resulting arrangement will respond as a continuous beam with respect to live load only.

The conversion is more feasible for steel and timber stringers, although it may apply to reinforced concrete beams (single or prestressed) by making the deck slab part of the resisting system.

The effect of continuity versus simple action is illustrated in Figure 12–12, showing the maximum moments in a two-span continuous bridge for HS 20 loading (truck or lane), and also the maximum moments in the same bridge but with the intermediate support as simple span. Likewise two span ratios are used, 1.0 and 1.5. The same effect versus simple action is illustrated in Figure 12–13 for three adjacent spans converted into a continuous unit, for span ratios n = 1.0 and 1.5. As an example, if two adjacent 40-foot simple spans are made continuous for live load, the maximum positive moment is reduced from 450 ft-kips to 358 ft-kips. However, a negative moment of 267 ft-kips is induced at the interior support.

Interestingly, the conversion from simple to continuous spans also alters the shears and reactions of all supports. In general, continuity results in larger reactions at the interior supports, and the percentage increase is greater for a two-span unit. The new arrangement also introduces a new distribution of longitudinal and lateral forces, and if the intermediate pier has fixed bearings, it may require a heavier configuration with a corresponding increase in the foundation requirements.

Some concern may exist regarding the splice requirements to connect the adjacent beams at the pier, the contention being that this location becomes now the point of maximum live load moment (negative) and probably a point of considerable negative dead load moment. However, experience shows that the design criteria for a field splice at this location yield only modestly heavier parameters than when the splice is located at

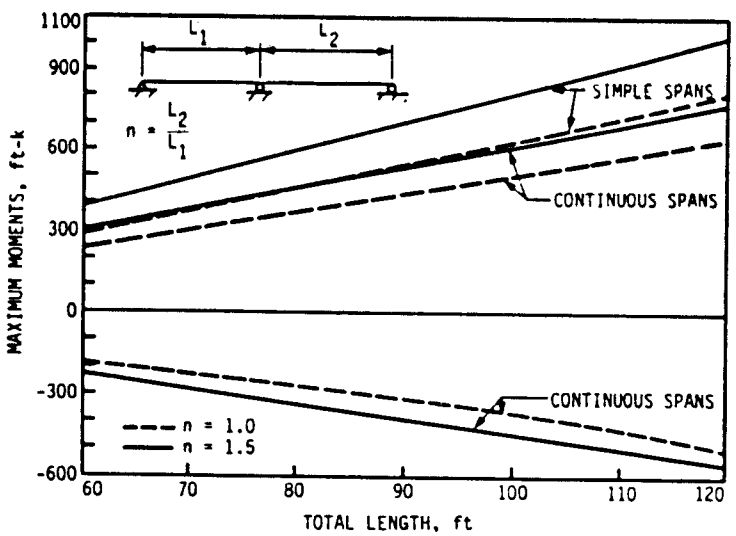

Figure 12–12 Maximum live-load moments for one continuous two-span bridge versus two adjacent simple-span bridges.

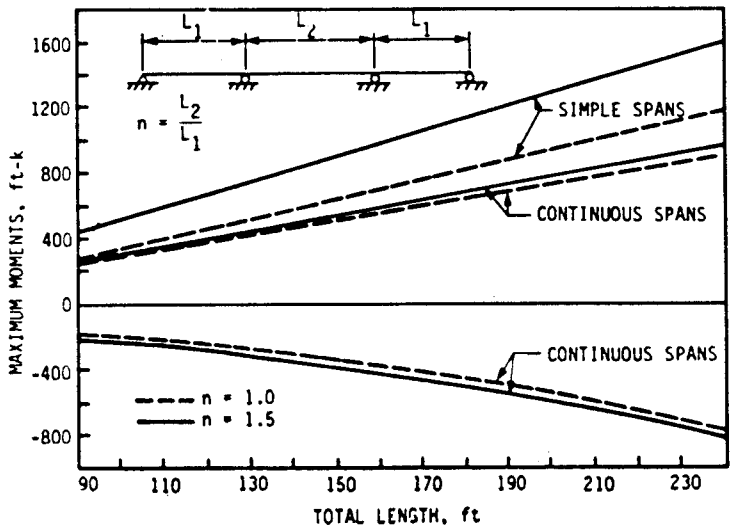

Figure 12–13 Maximum live-load moments for one continuous three-span bridge versus three adjacent simple-span bridges.

the point of dead load contraflexure. In fact, some states stipulate that the field splice for continuous beams in ordinary bridges be located at the piers to facilitate erection.

12.6 REPLACEMENT AND REPAIR METHODS

Replacement Systems

Replacement, as used herein, is not necessarily total replacement of the structure because of obsolesence or because of maturity in the effective lifespan. Rather, it means the replacement of certain members because of damage or accelerated deterioration, while the main structure remains functional and structurally safe. Thus, factors that must be considered in choosing this option are (1) cost and availability of materials, (2) cost and availability of forms and equipment for fabricating and handling the necessary bridge components, (3) quailified labor at the site, and (4) the functional and structural characteristics desired in the replacement system. The replacement systems for substructure and foundations presented here are intended to provide descriptive and practical data, useful in making decisions and preliminary choices.

Practical innovative concepts have appeared in the literature and some have been tried in the field. Hanson (1972) and GangaRao (1978) have presented concepts for the use of prefabricated substructure components, presented in Figures 12–14 and 12–15. The installation process is self-explanatory. However, such components may not have general use because of the many differences between bridge sites, such as soil-bearing characteristics, location of bedrock, and depth at which acceptable bearing is available, all tending to inhibit effort to standardize the precast members. In other instances, successful results have been obtained by prefabricating a part of the substructure. For example, a prefabricated abutment was used in a bridge in Virginia by first constructing a

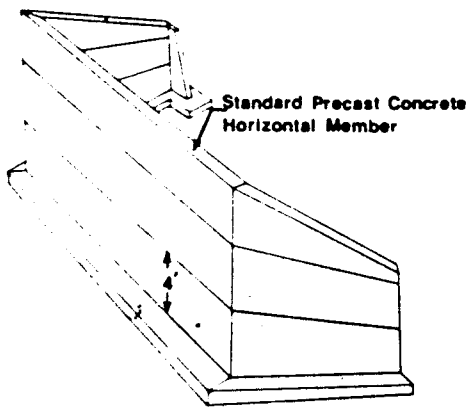

Figure 12–14 Abutment with precast concrete horizontal members.

level surface from which to work (cast-in-place footing), and then placing the prefabricated elements on top of this footing, as shown in Figure 12–16. Portland cement mortar was placed in the keyways between the segments, and two posttensioned strands were used to tie the segments together. Commonly, all concepts for using prefabricated concrete units in the substructure require the use of portland cement grout or posttensioning to integrate the units.

Other recommended replacement systems for abutments are the precast members shown in Figure 12–17, where the erection process and sequence are self-explanatory. These panels are modular and therefore easily precast in various lengths and widths to accommodate a range of abutment heights and roadway widths. The panels are set on cast-in-place concrete pads and temporarily supported, and then connected with weld plates and cast-in-place concrete footing, as shown in Figure 12–17. There is, therefore, an essential similarity with the replacement systems of Figure 12–16. Several other systems are available (both proprietary and nonpropietary) utilizing precast concrete units, and should be considered to arrive at a choice based on comparison.

Conceptually, these replacement systems are similar to the modular units for walls and abutments discussed in other sections.

For pile substructures and foundations, an example of replacement system is

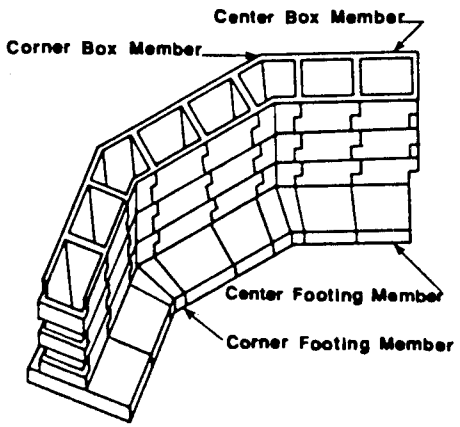

Figure 12–15 Abutment with precast concrete box members.

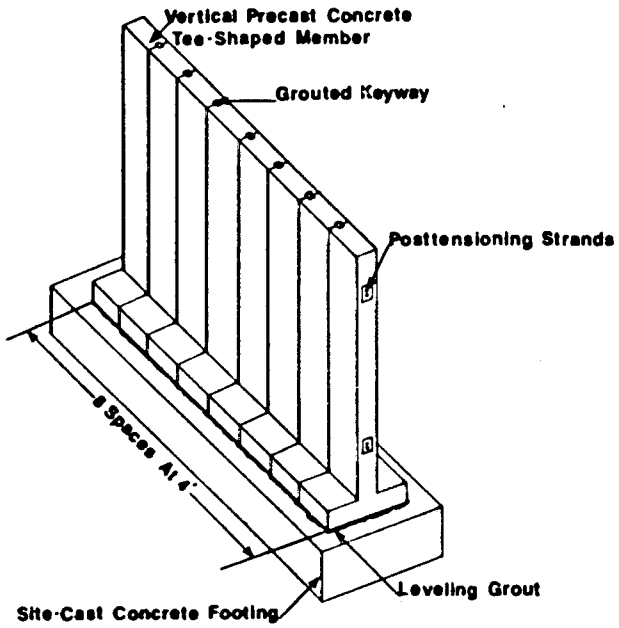

Figure 12–16 Abutment with precast concrete vertical tee-shaped members.

shown in Figure 12–18(a) and (b) for abutments and piers, respectively. Prestressed concrete or steel H-piles are driven to the required depth and cut to the required level. The piles are sometimes capped with a steel section. Connections between the pile cap and the piles are usually achieved with in-situ-cast concrete or welds, as shown in Figure 12–19. Steel angles are connected to the H-piles to stabilize the bent or pier. In water crossings, the H-piles are frequently jacketed in concrete or protected in an equivalent manner at the water line to inhibit corrosion. For abutments, the piling may be backed with precast concrete plank, or horizontally heavy timber planking. An alternative is to use concrete, steel, or timber cribing to retain the soil or riprap for slope protection.

Commentary. The systems presented in the foregoing section are merely conceptual, and should be analyzed for design and construction of a specific replacement. The market contains a fair share of proprietary designs. Inclusion of a proprietary system in this discussion is mainly for the purpose of comparison. The characteristics desired in the completed structure are usually the prime concern when choosing between alternatives. A system should be selected because it provides the best combination of first cost, maintenance cost, and service life, and this criterion may be used in lieu of a cost effectiveness analysis. Service life is generally a function of the traffic volume and the severity of conditions to which the structure is subjected. The lower the traffic volume and the less severe conditions, the more emphasis should be on minimizing the maintenance cost. Maintenance costs are composite costs of the superstructure and the substructure. Where traffic volumes are heavy and conditions are severe, emphasis should be on bridge systems that provide maximum durability and life expectancy. When choosing between alternatives, the choice should concentrate on what is available locally.

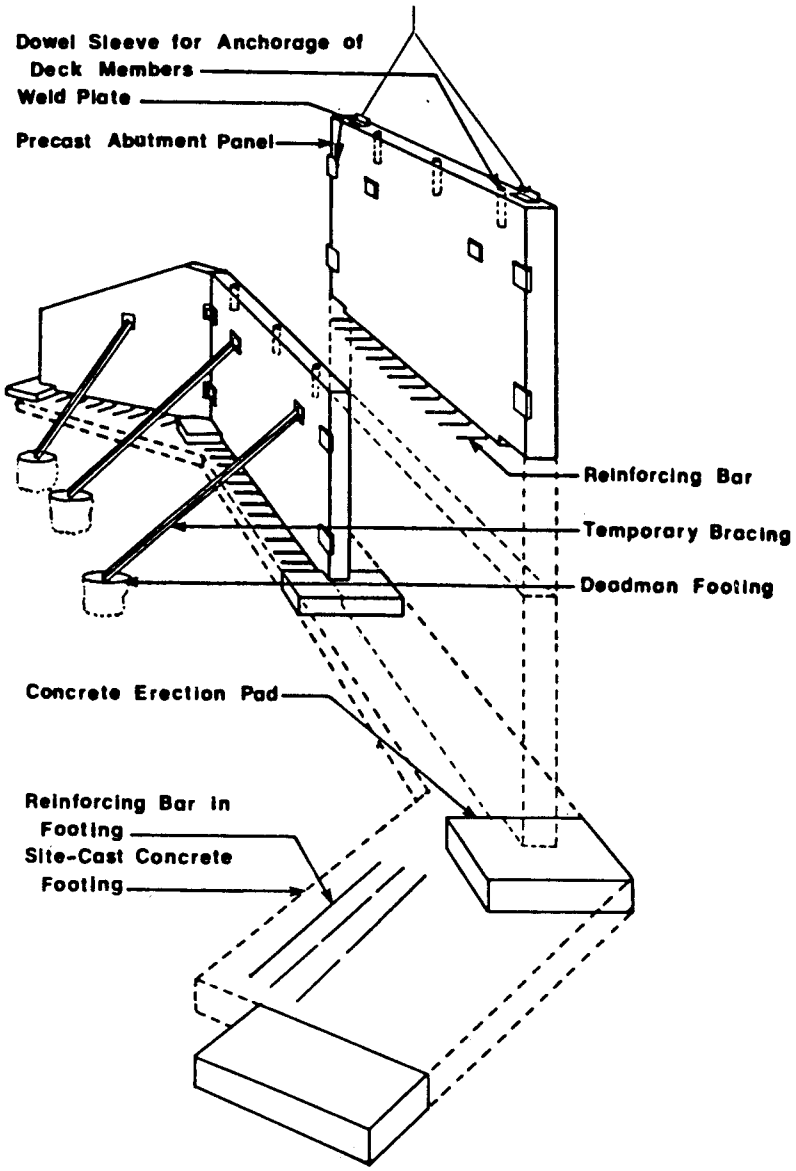

Figure 12–17 Precast abutment and wingwall.

Repair Procedures

Among the factors to be considered in choosing the repair method to restore the structural capacity and service life are durability, anticipated future use of structure, cost and speed of repair, inconvenience to users, local labor market and availability of contractors, material availability, environmental priorities, and aesthetics. Repair materials should respond similarly to changes in temperature and the applied loading, and they should blend in appearance. The following are examples of repair work for substructures.

(a)

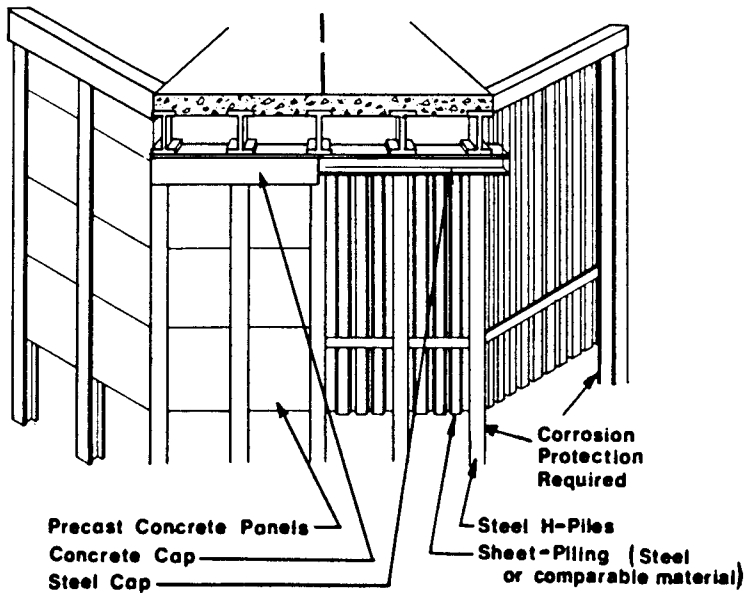

(b)

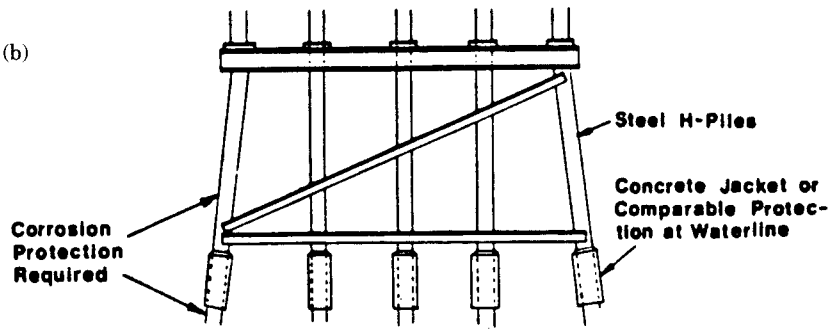

Figure 12–18 (a) Pile substructures—abutment details; (b) pile substructures—pier details.

• Figure 12–20 shows a typical repair of deteriorated timber or concrete pile and pier column by encasement in concrete using a permanent fiberglass form. The procedure may be used for piling immersed or out of water, and in principle it is similar to the strengthening process of Figure 12–9. It can be used where much of the pile cross section is lost, but some of the repair systems may be proprietary.

The construction procedure involves the following steps:

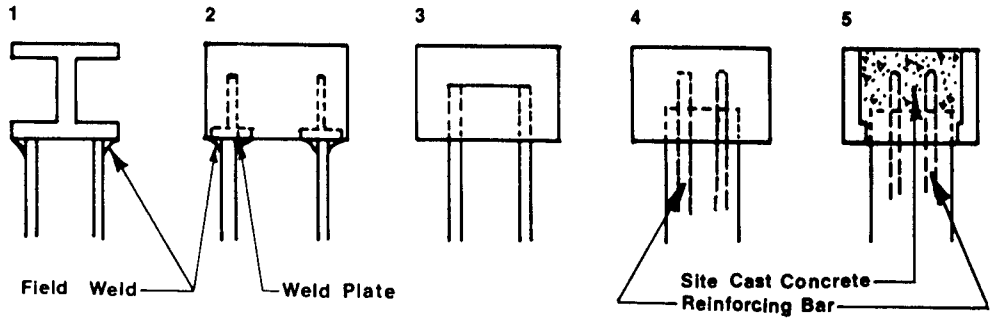

1 Steel Cap on Steel Pile
2 Precast Concrete Cap on Steel Pile
3 Site-cast Concrete Cap on Steel Pile
4 Site-cast Concrete Cap on Prestressed Concrete Pile
5 Precast Concrete Cap on Prestressed Concrete Pile

Figure 12–19 Connection details for pile substructures.

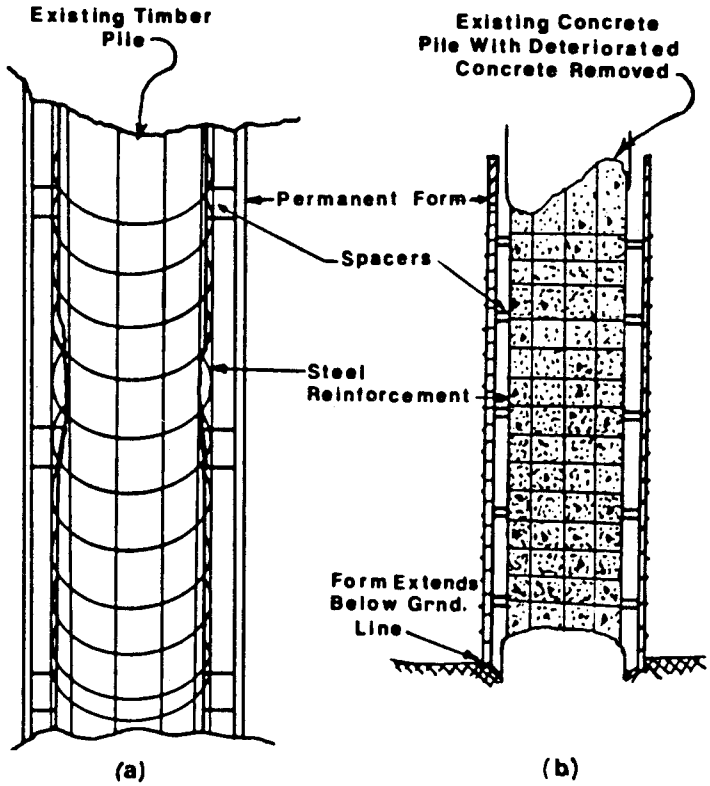

Figure 12–20 Typical technique for repairing; (a) a timber pile; (b) a concrete pile (Note that either type can be repaired above ground or below the waterline).

1. Scrape surface of the pile (or column) clean, to remove deteriorated concrete or wood.
2. Use sandblasting, if necessary, to clean the exposed reinforcement in concrete piles above the water line, and splice with new reinforcement as needed. Install steel mesh reinforcement cage around timber piles, as shown in Figure 12–20(a), or concrete pile, as shown in Figure 12–20(b). Use spacers to keep the forms in the proper position.
3. Place the forming jacket around the pile and seal the bottom of the form against pile surface, as shown in Figure 12–21.
4. Pump suitable concrete into the form through the opening at the top. Sulfate-resistant concrete should be used in salt water.
5. Finish the top portion of the repaired section. The forms should extend from above the splash zone down to sound wood or concrete. Steel piles may be protected by suitable coatings that prevent dissolved oxygen in the water from contacting the steel. Among suitable materials are epoxy coating systems and polyvinyl chloride barriers.

The resource requirements are qualified divers for underwater survey and repairs, form jackets that can be purchased or fabricated, and a concrete pump.

• An example of strengthening a weakened or settled pile bent through the use of supplementary steel H-piles and steel beam subcaps is shown in Figure 12–22. For this repair work, the traffic may have to be restricted or even stopped as necessary. The piles are driven through holes in the deck, which must be able to support the weight of pile-driving equipment. The construction procedure involves the following steps:

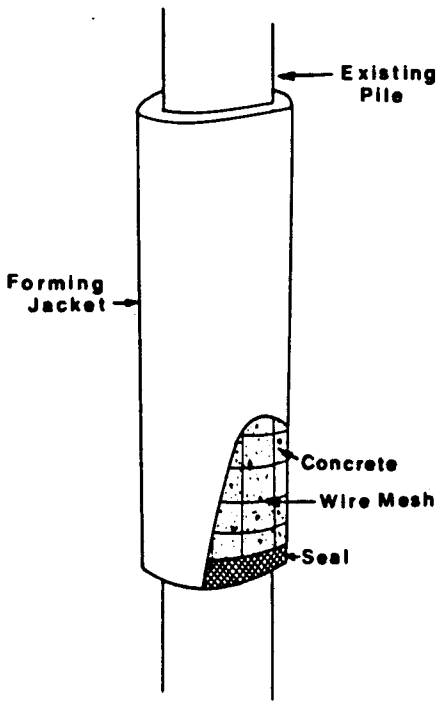

Figure 12–21 Completed repair using permanent forming jacket with bottom seal.

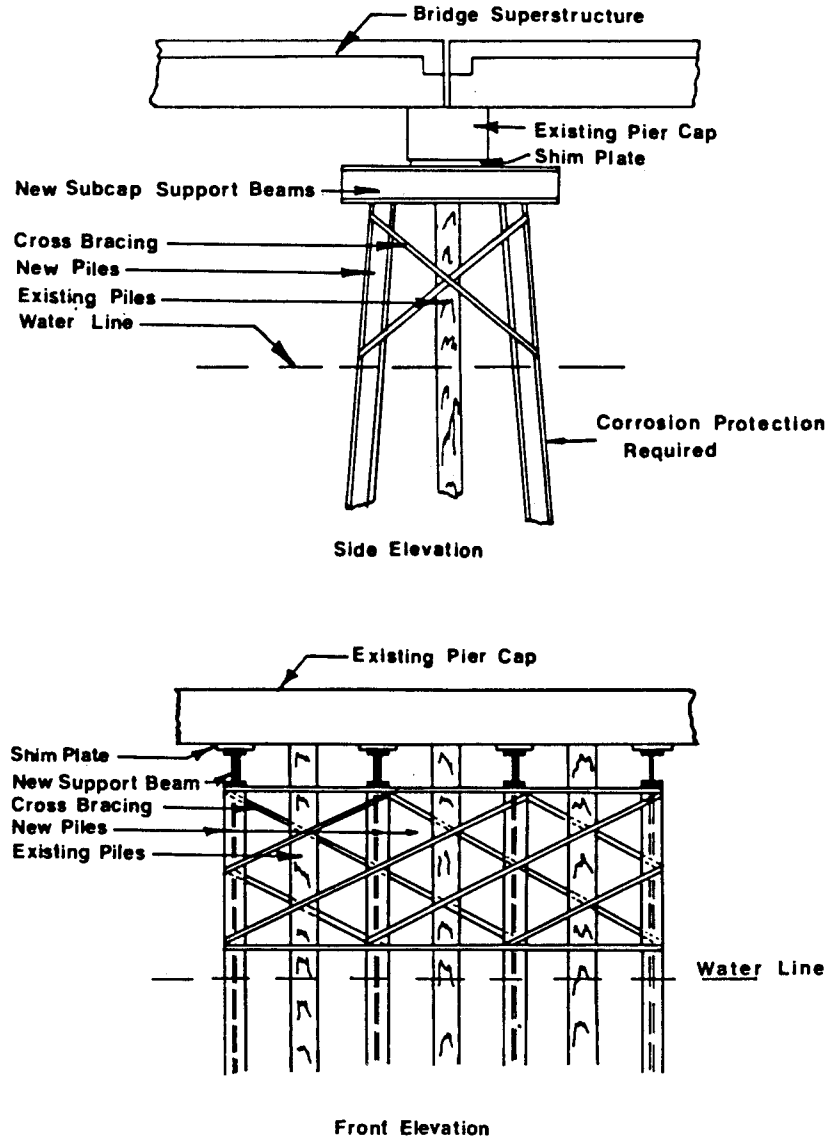

Figure 12–22 Pile bent strengthening.

1. Restrict or reroute traffic flow as required to facilitate the repair.
2. Cut holes in the deck large enough to accommodate batter piles. The holes should be close to the end diaphragm to minimize the length of the subcap.
3. Drive piles and cut off at proper level to fit the subcap support beams.
4. Install subcap support beam and weld to piles. Shim cap for fit and firm contact with existing pier cap.
5. Close deck holes and restore traffic.

The resource requirements are a pile driver and cutting equipment, properly designed, detailed, and fabricated steel members, and pavement breaking and concrete sawing equipment.

• Figure 12–23 shows a typical repair of sheared concrete beam seats. The repair of a deteriorated beam seat involves the removal of spalled concrete and replacement with new concrete using an epoxy bonding compound. This operation may be carried out under certain limitations. The area of deteriorated concrete should not be extensive, and the cause should be known and possible to deal with. Deteriorated bearings should be corrected or replaced, and high edge loads on beam seats relieved by properly designed bearings. The construction procedure involves the following steps:

1. Restrict traffic to the lanes away from the areas and sections to be repaired.
2. Construct a temporary bent for supporting jacks and blocking if jacking from abutments or pier elements cannot be accomplished.
3. Place jacks and lift beam until bearing pressure is completely relieved.
4. Remove deteriorated concrete to horizontal and vertical planes as shown in Figure 12–23 and section A-A.
5. Add new reinforcing steel where required as shown.
6. Apply epoxy bonding compound to prepared surface or sheared beam seat.
7. Form as required and cast new concrete.
8. When the new concrete has attained the required strength, remove forms, blocking, jacks and temporary supports.

The resource requirements include jacking equipment, tools to remove deteriorated concrete, forms, and necessary staging.

Note: Concrete T Beam is shown. Details are typical for other types of beams. Paint old concrete with epoxy prior to placement of new concrete.

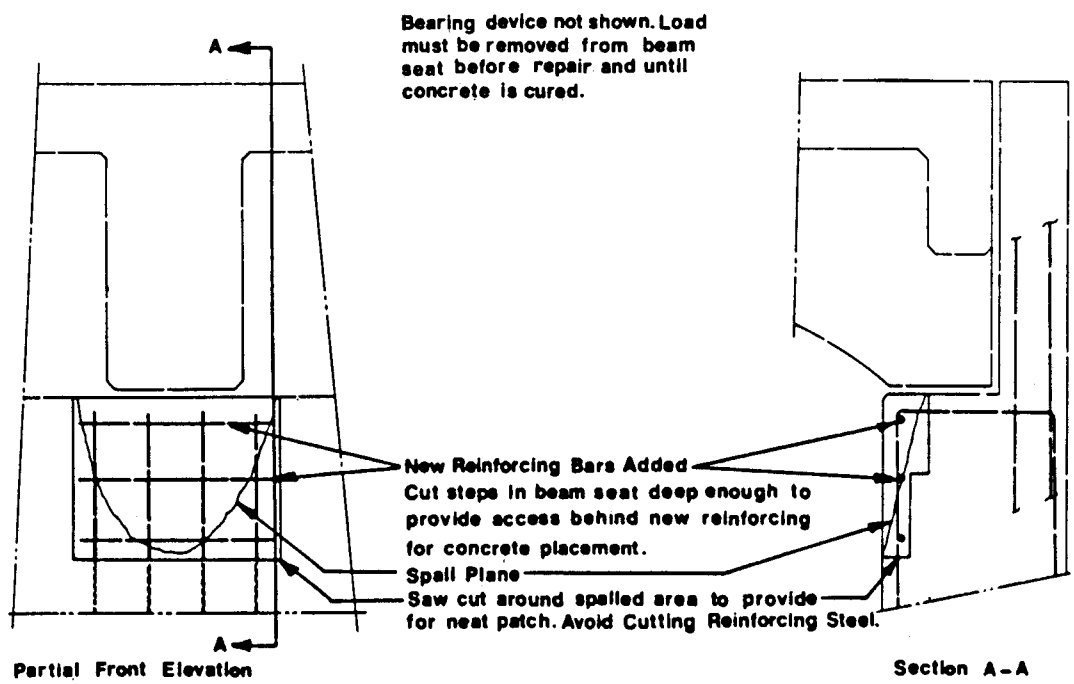

Figure 12–23 Typical repair of sheared concrete beam seats.

• A procedure for increasing the load-carrying capacity of an existing footing is shown in Figure 12–24. Because there is no real borderline between repair work and strengthening, this procedure is also used to upgrade the structural capacity of a foundation to accommodate a higher live load on the bridge. The solution is to incorporate new piles into the footing and increase its thickness to accommodate larger moments and shears. The footing must be fully excavated, and sufficient headroom should be available under the bridge for pile driving equipment. The construction sequence involves the following steps:

1. Excavate around the footing.
2. Chip concrete to expose edges of the lower layer of reinforcement as shown in Figure 12–24. In general, a thicker footing will be required because of larger moments and shears, and additional reinforcement must be provided and properly spliced with existing bars. Clean the old concrete to enhance contact with new concrete.
3. Drive all additional new piles.
4. Form the new extended footing.
5. Lap the new reinforcement to the existing bars and complete the new steel cage. If bar laps are not feasible, the steel bars may be connected with splicing devices or by welding.
6. Place the concrete and allow it to cure in the extended footing.
7. Backfill around and over the footing.

The resource requirements include excavation and pile-driving equipment, proper materials, formwork, and new piles. A complete analysis of pile ground behavior and ge-

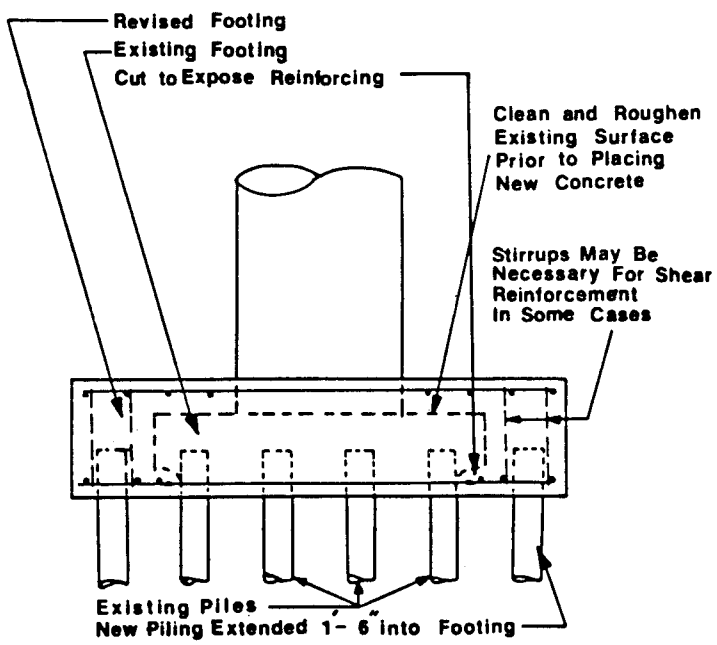

Figure 12–24 Increasing the live load capacity of an existing footing.

otechnical capacity should be carried out using procedures discussed in other sections. This solution is cost effective if there is compatibility between the remaining life of the existing piles and the new piles.

• Figure 12–25 shows a procedure for strengthening or widening an existing pier because of increased live load or to accommodate a widened deck. It can therefore be used where an analysis has determined that the present columns or pier cap are no longer structurally adequate because of distress or upgraded bridge loading. The beam seats on the existing pier cap must be in good condition and repairable for structural compatibility with the new section. The replacement of the bearing assemblies may also be part of the program. The construction procedure involves the following steps:

1. Locate the new pier columns in line with the existing pier cap.
2. Erect scaffolding around the old columns.
3. If the existing piles consist of concrete-encased steel H-piles, remove the encasement from the piling at the section where it will be embedded in the new pier cap, as shown in Figure 12–25. If the existing columns are reinforced concrete, prepare

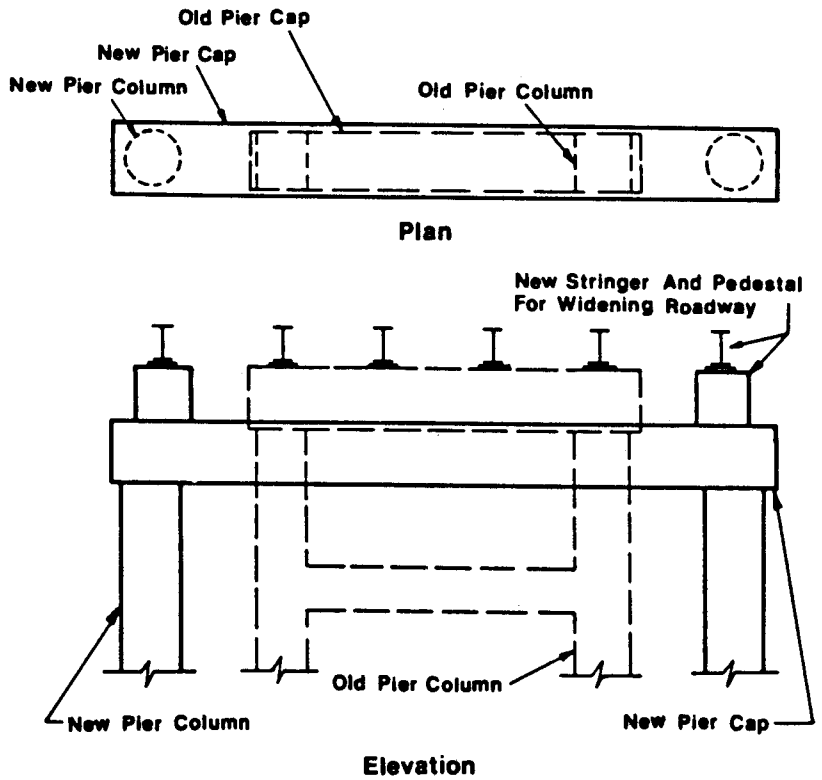

Figure 12–25 Technique for strengthening a deteriorated pier cap.

the surface of the column to be embedded so that adequate bond is provided to the new pier cap.

4. Excavate for the footing of the new columns.
5. Form and place the concrete for the new footings.
6. Drill through the existing columns to provide holes for the steel bars of the new cap, since the main horizontal reinforcement should be continuous.
7. Place the formwork and the reinforcement, and cast the new columns.
8. Remove the forms for the columns; form and place the concrete for the new pier cap.
9. In many cases the old columns may remain in place as part of the new design, or they may be removed if no reliance is placed on them.
10. Remove scaffolding and backfill where required.

The resource requirements are concrete breaking and drilling equipment, light lifting equipment, and scaffolding.

Commentary. The repair examples of the foregoing section apply to common structural and functional deficiencies of typical highway bridges. They have been used in various structures by states, and the details are generalized to meet the needs of a broad group of bridges. However, they may not cover all the deficiencies to be found on bridges on the primary and secondary system or on local roads. Invariably, a reasonable structural investigation will be necessary to assess the matter of load transfer, and distribution, settlement, and interaction of new and old members. In this process, the use of the load factor approach to assess the new structural and geotechnical capacity is highly recommended.

Repair of Accidental Damage

Most of the accidental damage to substructures is caused by the collision of heavy vehicles and by fires, and thus is noted in bridge pier columns and crashwalls. For piers in river and waterway crossings, serious damage may be caused by ships and moving barges, which is discussed in other sections.

The damage in this case may be minor, moderate, severe, or critical. Severe damage affects both the concrete and the steel reinforcement, and usually requires extensive repair supported by structural analysis. It is often necessary to restrict the flow of traffic until an assessment is available and all necessary temporary shoring is in place. Patching and epoxy injection techniques described for other forms of repair, often in conjunction with preloading, can restore the load capacity and structural integrity. Splicing may be required where steel bars have been damaged.

Critical damage affects the structural capacity and may require immediate temporary support and subsequent replacement. Likewise, it must be supported by adequate analysis during the replacement process.

The repair of fire-damaged concrete is essentially similar to the repair of impact damage, and the same procedures are generally applicable. However, the inspection and assessment of the damage can be most difficult, particularly when it requires a determination of the length of time of exposure to the fire and the temperature levels attained. A general recommendation is to sandblast the structure to remove smoke and fire stains

and loose particles and to expose possible cracking. Sounding with a hammer can disclose loose concrete remaining after sandblasting, and petrographic analysis of cores can be used if necessary to determine the extent of damage.

Changes in the coloration of the coarse aggregate provide an indication of the temperature levels, which can then be related to an assumed strength loss of the concrete. Pulse velocity tests have been used to evaluate the concrete strength, and tensile tests of sections of the reinforcing steel indicate its strength.

Pneumatically applied mortar or shotcrete has been used successfully to restore pier caps and columns when a large expanse of concrete has required variable-depth repairs. The dry mix shotcrete process is most widely used in bridge restoration. The preparation is similar to that for other patching, except that the area to be repaired must have a shape that does not entrap rebounding particles. Specialty contractors are usually retained to ensure the proper application techniques. Information on the use of shotcrete will be found in the references listed at the end of this chapter.

12.7 REPAIR AND METHODS TO ARREST CONCRETE DETERIORATION BELOW THE WATER LINE

Causes and Types of Deterioration—Usual Repair Techniques

A brief review of inspection techniques and system rating for substructures below the water line is presented in section 12.3. Interestingly, a consensus of opinion suggests that a vast percentage of concrete deterioration under water is traced to a lack of quality control during construction or to other construction and preconstruction faults. This is because high quality concrete is virtually inert in most natural environments. A further disturbing observation is that in many instances maintenance is deferred until replacement becomes the only option left to arrest deterioration.

Zones of deterioration. Experience shows that deterioration occurs most frequently above the level of low tide and below the top of the splash zone (Rissel et al., 1982). Below the level of lowest water, the concentration of oxygen decreases rapidly with depth. Water has also the effect of sealing the concrete from the ingress of oxygen when compared with the atmospheric zones. Above the splash zone there is a jack of water that is necessary to lower the electrical resistivity of the concrete and to provide additional aggressive agents. The zone between these two limits, which includes the tidal zone and the splash zone, is referred to as the primary active zone.

Deterioration at the mud line also occurs, and may be attributed to abrasion, reactive soils, or a macrocorrosion cell. This area is sometimes considered as a secondary active zone. If deterioration is confined to the primary active zone, the need for repairs is greatly simplified.

Types of deterioration. Deterioration may be grouped in types as follows:

Corrosion. This occurs essentially in the steel reinforcement and involves (1) the presence of chlorides, and (2) the decrease in electrical resistivity, or conversely, the increase in electrical conductivity of the concrete cover. The availability of oxygen influences the interaction of these factors and determines the time of corrosion initiation, the

time corrosion becomes detectable by visual inspection, and the nature and extent of damage.

Chemical Attack. As in conventional above-water concrete, chemical attack is a slow process but significant in the sense that it gradually destroys the concrete cover. At this point corrosion takes precedence.

Abrasion. This occurs in two modes. Initially, ice fluctuating with the tides can impact the concrete and cause section loss at the water line. Secondly, sand movement at the mud line can cause similar problems.

Freeze-Thaw. This mechanism is most active at the water line. It occurs when the tide drops exposing wet concrete. The water in the concrete pores freezes, expands, and creates large internal stresses locally. When the tide eventually rises, the internal ice melts and the cycle is repeated.

Deterioration stages. A rational approach to deal with deterioration is to distinguish the various stages in terms of the time the process occurs. Thus, there are three stages: (1) the initiation stage, (2) the propagation stage, and (3) the destruction stage.

The initiation stage is present when chemical and mechanical effects involve the concrete surface only.

The propagation stage is manifested by chemical and mechanical forces affecting the concrete cover. In unreinforced substructures this action simply weakens the outer concrete layers. Preexisting porosity, cracking, and sealing allow aggressive agents to reach the reinforcing steel and begin the corrosion process.

The destruction stage is reached when chemical and mechanical forces have negated the protective function of the concrete cover. Corrosion of the steel occurs now in an accelerating process. In unreinforced piers this stage is noted by the loss of the outer layer of the concrete.

Classification of repair techniques. Remedial measures can be taken before deterioration reaches the last stage. Detection procedures (see also other sections) may include cores, drillings, voltage potential readings, and chemical analyses. Once the stage of deterioration has been determined, a suitable repair method can be selected.

Risssel et al. (1982) group repair methods according to the stage of deterioration.

1. Initial stage:	Hydraulic training Penetrating Sealants
2. Beginning of the propagation stage:	Surface coatings Veneers
3. End of the propagation stage:	Wraps Jackets
4. Beginning of the destruction stage:	Crack Sealing Sacrificial concrete collar Grout repair Passive cathodic protection Active cathodic protection

The following discussion deals mainly with the repair methods associated with the destruction stage. For a complete description or repair methods at other stages, see Rissel et al. (1982) and the references listed at the end of this chapter.

Crack Sealing. A usual method of repair is by epoxy injection into a crack to restore full strutural continuity and to stop corrosion. It has been used successfully under water and for cracks as narrow as 0.002 inch.

Other resin grouts have also been developed, and provide the advantage of reacting with any water inside the crack and not simply displacing it. The result is that no water is left between the inside concrete surface and the injection material.

Sacrificial Concrete Collar. With this method, a nonstructural concrete cover is cast around the structural concrete usually at the water line, and is replaced when it deteriorates. The method is relatively expensive and increases the dead load.

Grout Repair. A variety of epoxies and concretes with modifiers or admixtures are available for the underwater resurfacing of large areas of deterioration and section loss. They may be used in conjunction with the pile jackets or formwork discussed in other sections, and may or may not include sandblasting of the reinforcing steel. With the proper grout, the combination can be an effective remedy. Grouts commonly used include (1) portland cement concrete with modifiers and admixtures, (2) latex-modified concrete slurry, (3) high alumina cement, (4) sulfur impregnated concrete, (5) epoxy mortar grout, (6) gun-applied mortar, and (7) preplaced aggregate concrete.

There is some concern as to whether permanent formwork helps to protect a repaired section or merely conceals additional deterioration.

When patching chloride-contaminated concrete with a patch of fresh concrete, if the patch comes in contact with the steel bars, a corrosion cell can be formed. In this instance, there is an increased potential for corrosion that simply shifted to the surrounding cathodic area of the same bars forming an anodic area, and corrosion then continues. This situation may be remedied by coating the exposed steel bars and the inside of the concrete cavity with epoxy bonding compound to insulate the fresh patch.

Passive Cathodic Protection. With this procedure, a sacrificial zinc anode, weighing 4 to 10 lb, is attached directly to an exposed steel bar during the underwater inspection. The method is quick and simple, and arrests corrosion of completely exposed bars for up to 2 years.

Active Cathodic Protection. Active cathodic protection of partially submerged concrete substructures is not practical on a standard basis, and this is because substructures have more complex physics. When concrete is continuous through all three zones (subterreanean, underwater, and atmospheric), the steel bars are subjected to three potentials for corrosion. However, steel piles have been successfully protected cathodically because they offer the advantage of being in direct contact with an electrolytic solution, seawater, whereas the steel bars in concrete are initially insulated from it. As the cover deteriorates and its electrical conductivity increases, that portion becomes highly active and accelerates corrosion.

Innovative Methods to Arrest Concrete Deterioration

Rissel et al. (1982) have proposed innovative methods to deal with concrete deterioration, beginning from the premise that arresting deterioration essentially means, or at least implies, interfering with a progression of events occurring naturally in a fairly defined order but at a varying rate depending on the intensity of the various factors involved. Deterioration is then analyzed as a step-by-step process, and in three separate categories: salt water (hot), salt water (cold), and fresh water.

Three main points should be considered when developing a new or improved idea to arrest concrete deterioration. First, the stage of deterioration must be established within the progression of events to be dealt with. Second, a decision must be made on how to best arrest the deterioration at that point. Third, it must be determined whether this decision is supported by economic criteria.

A main conclusion is that what helps to arrest deterioration is not a quick and easy decision but an extensive evaluation of inspection results, analysis, and economic factors. For example, if 10 percent of the piles of a bridge were to begin to deteriorate, it could be assumed that the other piles were already in the propagation stage of deterioration. In this case, an economical solution would be to consider a method that could be applied to all the piles. Extensive evaluation, however, may well raise the cost in selected piers beyond that of arresting deterioration in all piers by a sufficiently economical method. It follows, then, that an effective technology must be provided for identifying a particular stage of deterioration.

Several suggestions have been put forward by Rissel et al. (1982), but without judgment as to their potential value. These include multiple tape systems, sealants and coatings, dewatering cofferdams, sacrificial piers, and sprayers. These procedures are discussed by these investigators, and will not be repeated here. Reference to these ideas is highly recommended and may warrant further investigation.

12.8 EXAMPLE OF INSPECTION GUIDELINES: ASSESSMENT OF UNDERWATER CONCRETE

This example is intended to provide a guided, objective method to assess the threat to the integrity of a substructure from a maintenance viewpoint. It is not to be construed as an alternative to the rating system currently used to rate the substructure condition for item 60 of the FHWA SI & A manual, but rather as an adjunct to it. The SI & A rating system is applied for consistency of approach for funding eligibility from a construction viewpoint.

The example may be used as an aid in arriving at an initial assessment of a deficiency expressed as a numerical value, and this assessment in turn indicates the urgency of corrective action. The numbers prescribe the type of action to be taken in the inspection process as well as in mandatory maintenance in scheduling the work that must be performed.

Assessment process. The steps necessary in assessing deterioration are as follows:

1. First, select the description that most closely depicts the most severe example of deterioration found. The number appearing adjacent to the chosen description is the initial assessment of deterioration.
2. Document the deficiency by photographs or sketches for the purpose of introducing the inspection report.
3. Modify the initial assessment to include the threat to the structural integrity caused by the effect of supplemental or external factors. In this manner, deficiencies may first be evaluated by the suggested guidelines and then modified by conditions unique to the particular area or climate.
4. Add the assessment modification algebraically to the initial assessment to obtain a

Table 12–3 Substructure Condition below the Waterline, Urgency of Corrective Action; Maintenance Urgency Index

Maintenance Urgency Index	Maintenance Immediacy of Action	Inspection Course of Action
9	No repairs needed.	Note in inspection report only.
8	No repairs needed. List specific items for special inspection during next regular inspection.	
7	No immediate plans for repair. Examine possibility of increased level of inspection.	
6	By end of next season—add to scheduled work.	
5	Place in current schedule—current season—first reasonable opportunity.	Special notification to superior is warranted.
4	Priority—current season—review work plan for relative priority—adjust schedule if possible.	
3	High priority—current season as soon as can be scheduled.	
2	Highest priority—discontinue other work if required—emergency basis or emergency subsidiary actions if needed (post, one lane traffic, no trucks, reduced speed, etc.)	Notify superiors verbally as soon as possible and confirm in writing.
1	Emergency actions required—reroute traffic and close.	
0	Facility is closed for repairs	

maintenance urgency index. Assessment and modification numbers may be marked to articulate the guidelines used, whereas the accompanying statement documents the reason for the selection.

5. When an urgency index has been selected, the type of action to be taken is selected. This is done by referring to Table 12–3. The assessment modification chart is shown in Table 12–4. The administrative level at which the assessment modification must be approved is not discussed here.

With these guidelines, the assessment of underwater deficiencies of bridge substructures is completed in a uniformly objective fashion, and a numerical value is obtained indicating the urgency of corrective action.

12.9 EXAMPLE OF STRUCTURAL CAPACITY ANALYSIS

Figure 12–26(a) shows a pier sketch of an interior support of a two-span bridge, each span 30 feet long and simply supported. The pier cap consists of timber 12 inches × 12 inches in cross section. The piles are timber, initial diameter 12 inches, and have suffered a 1-inch section loss all around because of decay as shown. The relevant stresses in the timber members are F_c = 1100 lb/in^2 (inventory) and F_c = 1463 lb/in^2 (operating). The modulus of elasticity is $E = 1.7 \times 10^6$ lb/in^2. The live load is the standard H truck.

The dead load reaction (superstructure plus weight of cap) is computed as 2.0 kips per pile. The live load reactions for one H truck is calculated as 13.6 kips (without impact). The maximum live load reaction is calculated next for pile #2 for cases #1 and #2, shown in Figure 12–26(b) and (c), respectively.

For one truck position as shown in Figure 12–26(b), the influence coefficient is ob-

Table 12–4 Assessment Modification Chart Based on Threat to Integrity of Structure

Modification	Description
+2	No threat for minimum of 5 years and one or more of the following: 1. Deficiency condition is slowing; 2. External causes of deterioration substantially reduced or eliminated; 3. Deficiency has history in similar circumstances of being self correcting; 4. Deficiency is entirely "cosmetic" in nature and has little or no structural effect.* (Note: May be used for original rating of 2 to 6 inclusive.)
+1	No threat for minimum of 3 years and one or more of the following: 1. Deficiency condition is stable; 2. External causes of deterioration have lessened somewhat; 3. Deficiency has history in similar circumstances of growing no worse; 4. Deficiency is mostly "cosmetic" in nature and has little structural effect.* (Note: May be used for original rating of 2 to 7 inclusive.)
0	No threat for minimum of one year and one or more of the following: 1. Deficiency condition worsening at expected or "normal" rate; 2. External causes of deterioration have remained constant; 3. Deficiency has history in similar circumstances of growing worse at consistent rate; 4. Deficiency has structural effect but has not seriously reduced structural capacity. (Note: May be used for any original rating.)
−1	Threat anticipated within one year and one or more of the following: 1. Deficiency condition worsening at increasing rate; 2. External causes of deterioration are gradually increasing; 3. Deficiency has history in similar circumstances of growing worse at gradually increasing rate; 4. Deficiency has structural effect. (Note: May be used for original rating of 3 to 8 inclusive.)
−2	Threat is imminent and one or more of the following: 1. Deficiency condition is worsening rapidly; 2. External causes of deterioration are rapidly increasing; 3. Deficiency has history in similar circumstances of growing more severe at rapidly increasing rate; 4. Deficiency has severe structural effect. (Note: May be used for original rating of 4 to 8 inclusive.)

*Structural effect includes redundancy of load path and other factors.
(From Rissel et al. 1932)

tained from influence line tables as 1.3000. For two truck positions laterally placed, as shown in Figure 12–26(c), the influence coefficient for the reactions at support #2 is 1.4075. Hence, the maximum live load reaction is R_2 = (13.6)(1.4075) = 19.14 kips.

Next, we compute the structural and geotechnical (bearing) capacity for the reduced radius of 5 inches.

Radius of gyration = $r/2 = 5/2 = 2.5$ in^2

$$\text{Buckling} = \text{allowable } P/A = \frac{4.813\,E}{(L/r)^2} = \frac{(4.813)\,(1.7\times 10^6)}{(120/2.5)^2} = 3550 \text{ lb/in}^2$$

Compression = allowable stress per AASHTO = 1100 lb/in^2 (controls)

Cross-sectional area remaining = $A = \pi r^2 = (3.14)(5^2) = 78.5$ in^2

Structural capacity = (78.54)(1100)/2000 = 86.4 tons (inventory) or 86.4 × 1.33 = 114.9 tons (operating)

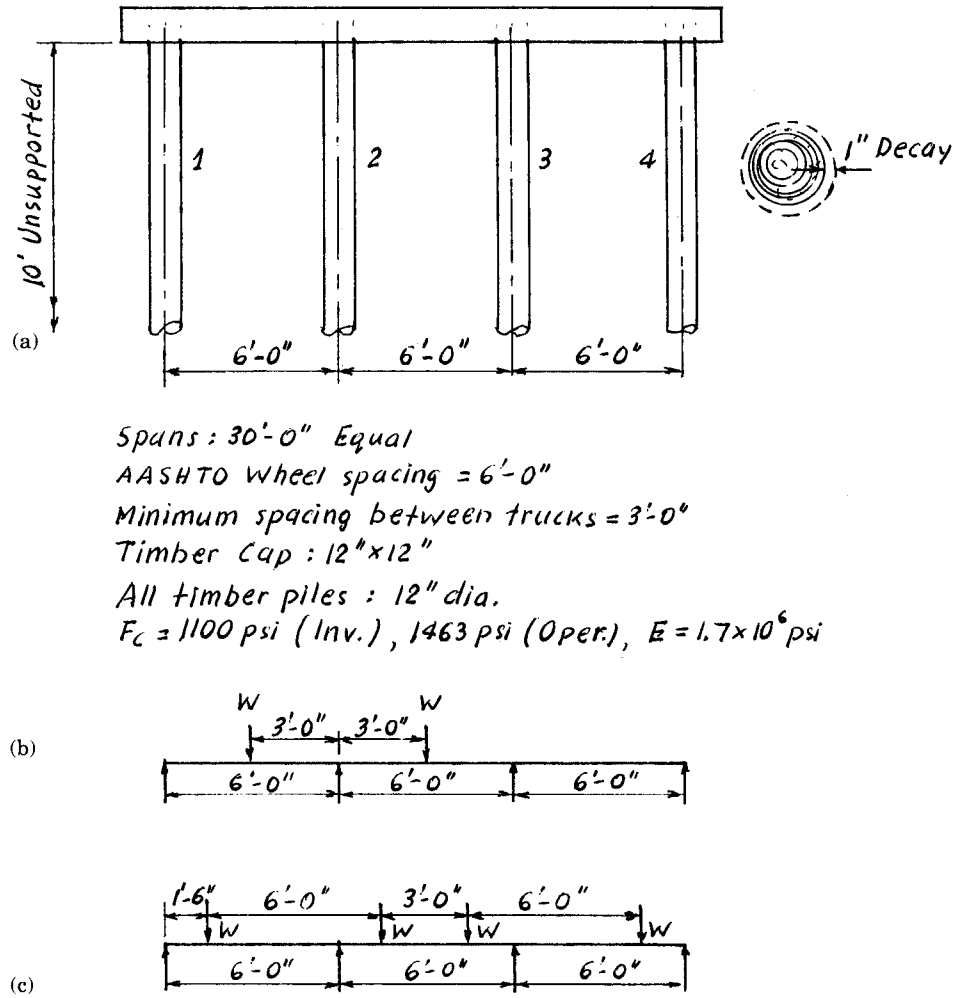

Figure 12–26 Pier of design example: (a) pier sketch; (b) loading condition, one truck; (c) loading condition, two trucks.

However, the geotechnical (bearing) capacity of the pile is determined for the reduced pile diameter (computations not shown), or

Geotechnical capacity for 10-inch diameter pile = 24 tons (inventory)
= 32 tons (operating)

Capacity available for live load = (capacity inventory − DL reaction) = 48–2 = 46 kips

Capacity available for live load = (capacity operating − DL reaction) = 64–2 = 62 kips

Next, the capacity factor is computed for both inventory and operating cases as

Capacity factor = (capacity available LL)/(live load reaction) = 2.40 (inventory)
= 3.24 (operating)

Ratio = (capacity factor operating)/(capacity factor inventory) = 3.24/2.40 = 1.35

Ratings are obtained now for operating and inventory as follows:

	Inventory	Ratio	Operating
H Truck, (inventory factor)(15)	36.0 tons	1.35	48.6 tons

12.10 EXAMPLE OF BRIDGE REHABILITATION

Description of Project

The rehabilitation program for the bridge carrying Southwest Highway (Illinois 7) over B & O.C.T. RR, Melvina and Stony Creek on the south side of Chicago included (1) a comprehensive investigation and structure report, (2) repair work, (3) strengthening, and (4) replacement, necessary to extend the service life of the structure, consistent with economic criteria of the supervising agency.

The structure consists of 25 simply supported spans, generally 50 feet long, except for two units that are 55 feet and 63 feet long, respectively. The overall length is approximately 1268 feet back-to-back of abutments. The substructure consists of reinforced concrete multicolumn rigid frame piers, except for pier 13, which is a steel bent encased in concrete wall above ground level. According to the original plans, dated 1934, all piers and abutments were supported on treated timber piles with capacity 10 to 18 tons. A complete report and details are given by Xanthakos (1981).

As of the time the investigation was carried out, the superstructure consisted of twenty-two spans of prestressed concrete box deck with wearing surface, two spans of reinforced concrete slab supported on steel I-beams, and one through girder span with floor beams, stringers, and a concrete slab.

In general, piers and abutments are aligned perpendicular to the roadway, except those abutting the railroad which are skewed to parallel the rail alignment. The deck accommodates four 11-foot lanes, two in each direction, and a pedestrian sidewalk along one side. Transverse joints are provided, with premolded joint filler at the fixed ends, and premolded fiber with steel angles at the expansion ends.

Traffic data showed an average daily traffic volume of 21,000 vehicles (as of 1981).

Brief History of the Structure

The original bridge probably dates back to 1934. The spans that now consist of prestressed box beams originally consisted of T-beam decks, removed and replaced by the box beams in the mid-1960s, while the pier caps were modified to accept the prestressed concrete box superstructure.

At the same time, the steel I-beams and girder spans had the concrete deck removed and replaced by new cast-in-place slabs, and the entire structure was treated with an I-11 asphaltic concrete overlay. Little, if any, repairs were carried out below the pier cap beams.

In 1976, numerous sporadic repairs were carried out in the lower sections of the piers, and substantial repairs were found necessary for the bearing seats of the steel spans. In order to protect the adjacent piers, steel sheeting was driven along the banks of Melvina Creek.

A bridge deck condition survey and analysis was compiled and released in 1979 by

the maintenance section of the department. The main program of this investigation focused on tests, including visual and delamination surveys, performed to determine the overall condition of component parts of the deck, and provided data regarding the best remedial action.

A main recommendation was to remove the existing wearing surface and replace it with a 3 to 4 inch low-slump concrete overlay with nominal reinforcement. Further remedial work considered necessary included joints, concrete repairs, slope protection, cleaning and painting structural steel, and replacing the existing railings with the New Jersey parapet type.

As of 1981, the structural condition was rated from the maintenance and functional point of view, and covered the entire superstructure components as well as the substructure and foundation elements. Although an aggressive rehabilitation program was recommended for the superstructure, this discussion will focus on the structural capacity and adequacy of the substructure and foundation.

Substructure and Foundation Conditions

The inspection detected sporadic repairs to the substructure, particularly in the lower sections of piers. Invariably, the substructure elements showed the signs of their age. The concrete had spalled in numerous locations, and the reinforcing steel was exposed and corroded. Apart from the visual evaluation of the physical condition, poor quality and low concrete strength was suspected in several locations. Thus, a main recommendation was to supplement the assessment of concrete deterioration by concrete cores extracted from pier columns and caps for laboratory testing.

The only information about the type of foundation was found in the original bridge plans. Evidently, the foundation consisted of creosoted timber piles. It appears that the intent of the initial design was to keep the tops of the piles below the groundwater table, hence many piers have the bottoms of their footings more than 10 feet below ground level.

Concrete Repairs

Extensive concrete repairs were stipulated for the substructure, and in many locations the use of forms was anticipated. The special provisions included over 100 items as a supplement to the mimeographed specifications. The item relevant to the repair of concrete elements is presented as an example of contractual documents. This item is as follows.

Repair Concrete Structures

This work consists of removing and replacing with portland cement mortar and pneumatic concrete (pneumatically placed mortar) at the locations shown on the plans or as specified by the Engineer, together with other necessary work as shown on the plans, for the repair of the abutments and piers.

Materials. A 1:1 sand-cement grout covering the area to be patched shall be used to bond the plastic cement to the exisiting portland cement concrete structures. The cement and fine aggregate for portland cement mortar and pneumatic concrete shall con-

form to the requirements of Section 701 and Article 703.02 of the Standard Specifications, with the following exception:

> The mixture of the portland cement mortar and pneumatic concrete for all items of repair shall consist of three (3) parts of Torpedo sand FA 2 to one (1) part portland cement.

Construction Methods. Unless otherwise directed by the Engineer, the areas shall be repaired with pneumatic concrete.

Pneumatic and portland cement mortar shall be applied so as to form a compact durable covering of the thickness desired. The Contractor shall carefully restore the original shape and contour of the repaired sections.

The cement gun for pneumatically placed mortar shall be of either the wet-mix type or the dry mix type.

The wet-mix type cement gun shall be similar to the Sprayton Gun, Model 18, or True Gun-All, Model D-2, or approved equal. The compressor shall be of sufficient capacity to provide enough air pressure to operate the concrete placing machine at its rated capacity.

The concrete placing machine shall be of the type where the water can be accurately gauged and mixed with dry materials in a mixing chamber under an air pressure of 80 to 100 pounds per square inch. The mixed material shall be fed by air pressure through a hose connected to a positive shutoff trigger type nozzle. The machine shall have a device whereby either liquid or solid additives may be added to the water or mixing tank as specified.

The dry-mix cement gun shall be of the type that is operated by compressed air and consists of an upper and a lower chamber together with an air motor operating mechanism. The mixed material in a dry state is transported through a hose, under pressure, from the cement gun to nozzle where water is added.

General Procedure of Work:

1. All exterior concrete surfaces shall be thoroughly examined by means of sounding with hammers to determine loose or defective areas that may exist.
2. Where such defective concrete surfaces exist, these areas are to be removed with an electric chisel or other mechanical tools approved by the Engineer, to a depth necessary to remove all loose and disintegrated material. All exposed reinforcing bars shall be thoroughly cleaned and undercut to a depth that shall permit a minimum of 3/4-inch of plastic cement over the reinforcing bars. The deteriorated reinforcing bars shall be removed and replaced in kind.
3. After removing the unsound concrete from the surface, the Contractor shall thoroughly clean the area involved by sandblast, airblast, or waterblast.
4. Before placing the concrete, the exposed area to be patched shall be thoroughly covered with a 1:1 sand-cement grout. The grout shall be thoroughly scrubbed into the surface to wet it uniformly, to displace air films and to incorporate any loose particles still on the surface.

   Sufficient grout for brushing may be mixed to provide material for about an hour. It shall be covered to reduce evaporation of water and remixed as it is being used. A water-cement ratio of 5.5 to 6 gallons per sack of cement will produce a grout of proper consistency for use in cool, cloudy weather. However, on hot, sunny days, grout of such consistency will not

brush out well. Under such conditions the water-cement ratio may be increased slightly to permit brushing, or the old surface may be lightly sprayed with water to permit uniform spreading of the grout.

Wetting of the surfaces shall be done carefully, and free water shall not be permitted to collect in hollows and depressions. In cloudy, cool weather the grout may be spread a considerable distance ahead of concrete placement, but in hot, dry weather the two operations will have to follow rather closely in order that the grout does not dry out excessively. Grout that has lost its water sheen is in proper condition for concreting operations.

5. The Contractor shall then proceed (while the primed surface is still moist and tacky) to repair the areas with mortar and/or pneumatic concrete.

Wherever large, deep patches are to be repaired, or when directed by the Engineer, the Contractor will be required to reinforce said patches with 2" × 2" No. 14 gauge welded wire fabric anchored to the existing concrete by means of 1/4" expansion hook bolts spaced 30" maximum in each direction to provide substantial support for the plastic cement. The minimum pneumatic concrete coverage of the mesh shall be 3/4-inch.

Curing. Curing shall be done in accordance with the applicable portions of Section 625 of the Standard Specifications and as directed by the Engineer.

Membrane curing compound will also be permitted and shall comply with the requirements as stated under Article 718.04(a) of the Standard Specifications. The Contractor shall begin curing operations as soon as the concrete has hardened sufficiently to prevent marring the surface.

The above specified work shall be paid for at the contract unit price per square foot for REPAIR CONCRETE STRUCTURES, which price shall include all labor and materials (including joint fillers, welded wire fabric, expansion hook bolts, and reinforcement bars) necessary to complete the work in place.

Epoxy Crack Sealing

This work shall consist of furnishing all labor, materials, tools, and equipment necessary to seal all cracks in accordance with the Standard Specifications, as shown on the plans and as specified in this Special Provision or as ordered by the Engineer.

The work includes all preparatory work required prior to starting the pressure sealing of joints and the furnishing of materials, equipment, and labor to complete the epoxy pressure injection sealing of cracks and tie holes.

Epoxy pressure injection compound shall be Dural Internation Corporation, "Duralith-LV," or Sika Chemical Corporation, "Sikadur Hi-Mod" (Sikastix 370), crack sealing compound or approved equal.

A shallow groove (1/4-inch wide and 1/2-inch deep) shall be cut along the path of all cracks with a rotary concrete saw and all loose fragments of concrete removed by an air jet. Holes approximately 3/4-inch in diameter and 3/4-inch deep shall be drilled into the concrete at 6- to 12-inch centers on the centerline of the routed cracks. Set tire valve stems in the drilled holes and fasten with the epoxy grout compound and seal the entire length of crack with the epoxy compound. The crack shall be completely sealed with the valves furnishing an unobstructed passage into the cracks. The injection process shall be accomplished by pumping epoxy compound into the first valve until the epoxy level

reaches the adjacent valve. The injection hose is then removed and the first valve is capped, all other valves in the circuit being previously capped. Using an inert gas, a pressure as large as can be safely used without causing relative movement between parts of the structure shall be applied on the valve where the injection was just removed, to force the epoxy sealing compound into the hairline cracks. The pressure should approach 90 psi if possible and should be maintained from one to ten minutes or more. The time can be established experimentally to satisfy specific conditions. After the pressure is released, more epoxy sealing compound is pumped through the same valve until the succeeding valve overflows. The process is then repeated with successive valves until the crack has become completely filled, pressurized, and all valves capped. After epoxy pressure injection sealing compound has set, the valve stem shall be removed, the hole filled with grout, and the surface finished flush with adjoining surface.

Structural Capacity Analysis: Pile Foundations and Spread Footings

Because of the many uncertainties and unknown conditions with regard to the soil environment, several exploratory borings were requested at representative locations along the bridge. All borings indicated a dense layer of sand, gravel, and boulders 15 to 25 feet thick, beginning at an elevation of 570–575. The coarse layer is overlain by medium silty clay with an unconfined compressive strength of 0.5 to 1.0 ton/ft^2. The bottom of footing elevation ranges from 578 to 583. Considering the pile capacity requirements (18 tons maximum), it is evident that this load transfer cannot be attained unless the piles are driven into the dense granular layer and support this load mostly by point bearing. Considering further the life of the bridge (approaching 50 years), the suitability and actual capacity of the existing pile foundation was questioned, and the decision was made to pursue a vigorous foundation analysis before considering the remaining options (total bridge replacement, foundation strengthening, and superstructure rehabilitation).

The analysis of the foundation included an estimation of the actual loads carried by the piles, and for three particular service conditions: when the bridge was initially constructed, when the T-beam deck was replaced by the box beams, and under an anticipated deck rehabilitation program with a 4-inch concrete overlay and New Jersey-type parapets. Live loads and weight of piers remained unchanged.

For the 50-foot spans, the initial superstructure dead load (T-beams and concrete slab) per pier is 815 kips. When the T-beam slabs were replaced by the box beams, this weight was reduced to about 580 kips per pier. With the 4-inch overlay and the concrete parapets, this load is increased by about 92 kips, so that the new dead load per pier is now 673 kips, still considerably less than the initial dead load of 815 kips.

For the rehabilitated superstructure and the new dead load, the design calculations included the new pile loads obtained according to applicable AASHTO criteria or load combinations for allowable stress design. These are summarized as follows:

–Piers 3, 4, 5, 6, 17, 18, 19	Pile load	= 29.6 kips	(Group I)
		28.8 kips	(Group II)
		34.9 kips	(Group III)
	Allowable	= 34.0 kips	(Group I)

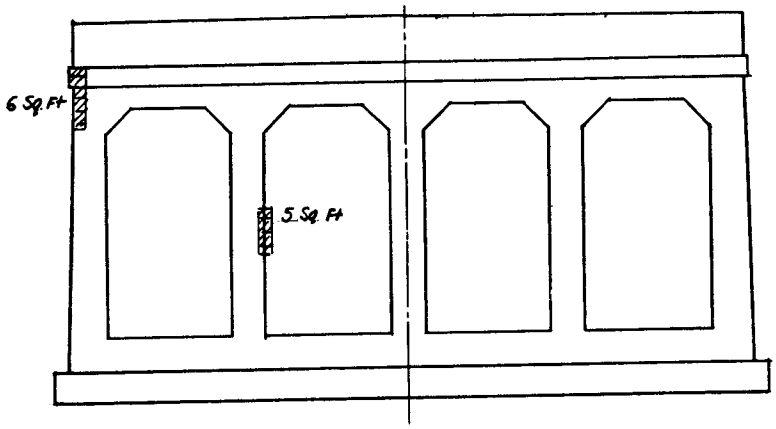

NORTH-EAST ELEVATION - PIER 3

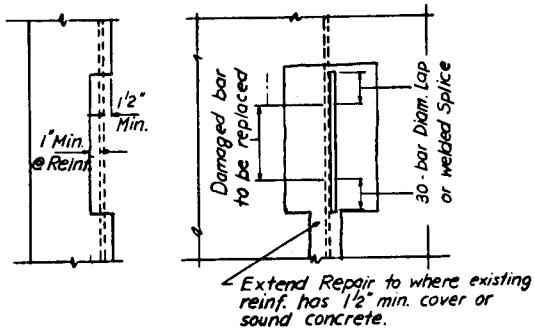

CONCRETE REPAIR DETAIL

LEGEND
Indicates Cracks
Indicates Concrete Repair with Reinf. exposed
Indicates Concrete Repair

NOTES
Exist. Reinf. bars having 10% or more of Cross Sectional Area lost to corrosion or damaged during concrete removal shall have new reinf. bars lapped or connected as shown.

Exposed Reinforcement shall be cleaned and incorporated into Concrete Patch, or new replacement Reinforcement added and spliced with existing retained Reinforcement. Fill holes at tie rod ends where Patch has spalled off and remove loose Patches.
Fill holes as specified for Repair of Concrete Structures.

Figure 12–27 Pier sketch and concrete repair details. Design example.

		42.5 kips	(Group II)
		42.5 kips	(Group III)
	Initial specified pile capacity = 34 kips		
–Piers, 1, 2, 20, 21, 22, 23	Pile load =	25.8 kips	(Group I)
		23.7 kips	(Group II)
		30.3 kips	(Group III)
	Allowable =	30 kips	(Group I)
		37.5 kips	(Group II)
		37.5 kips	(Group III)
	Initial specified pile capacity = 30 kips		
–Piers 7, 8, 9, 10, 11, 15, 16	Pile load =	32.4 kips	(Group I)
		36.2 kips	(Group II)
		39.7 kips	(Group III)
	Allowable =	36 kips	(Group I)
		45 kips	(Group II)
		45 kips	(Group III)
	Initial specified pile capacity = 36 kips		

In addition to the pile load analysis, the adequacy of the foundation was checked, assuming that the pile system might have become severely damaged or completely inoperable, an assumption confirmed later by special inspection. The allowable bearing capacity of the spread footing for this case is based on soil strength characteristics provided by the boring logs. The significant conclusion is that, ignoring the pile action completely, the footings can transfer the loads by direct bearing and with an adequate factor of safety. The suspicion that the piers were transferring the loads by spread footings rather than by the pile foundation was initially conceived considering the usual effective life of timber piles. This was later confirmed when soil investigations disclosed the occurrence of long-term consolidation of the subsoil that resulted in a uniform ground settlement of about 1 foot, with the subsequent densification of the foundation materials.

A typical pier sketch is shown in Figure 12–27 with the concrete repair detail. Each pier consists of 5 concrete columns and a massive cap. The columns have minimum cross-section dimensions 2 feet 6 inches by 3 feet, and a column spacing of 12 feet.

Because this bridge is on a highly traveled route, continuation of its service was considered essential during the major rehabilitation program of the deck. Hence, provisions were included for traffic maintenance during construction.

REFERENCES

AASHTO, 1995: "Manual for Maintenance Inspection of Bridges," 4th. ed., *American Association of State Highway and Transportation Officials,* Washington, D.C.

ACI, 1966: "Shotcreting," SP-114, American Concrete Institute.

ACI Committee 506, 1966: "Recommended Practice for Shotcreting," (ACI 506-66) (Reaffirmed 1978), American Concrete Institute.

ACI Committee 224, 1984: "Causes, Evaluation and Repair of Cracks in Concrete Structures," *Journ. American Concrete Institute,* vol. 81, pp. 211–230.

ACI, 1980: "Concrete Repair and Restoration," ACI Compilation No. 5, authorized reprint from *Concrete International: Design and Construction,* vol. 2, No. 9, Sept., p. 119.

ANDREY, D. and R. SUTER, 1986: "Maintenance and Repair of Construction Works," (Maintenance et reparation des ouvrages d'art) *Ecole Polytechnique Federale de Lausanne,* Lausanne, Switzerland, (French).

Applied Technology Council (ATC), 1983: "Seismic Retrofitting Guidelines for Highway Bridges," *Federal Highway Administration,* Final Report, Report No. FHWA-RD-83-007, Dec., p. 219.

BEAL, D. B., 1981: "Strength of Concrete Bridge Decks," FHWA Report No. FHWA-NY-RR-81-89, July, p. 36.

BEBO-International Heierli and Company, "The Reinforced Concrete Arched Bridge-BEBO System," Zurich, Switzerland.

BERGER, R. H., 1978: "Extending the Service Life of Existing Bridges by Increasing Their Load Carrying Capacity," FHWA Report No. FHWA-RD-78-133, June, p. 75.

BRICE, J. C. and J. C. BLODGETT, 1978: "Final Report—Countermeasures for Hydraulic Problems at Bridges," Vol. 2—Case Histories for Sites 1–283, Report No. FHWA-RD-78-163, *Federal Highway Administration,* September.

CHANG, F. F. M., 1973: "A Statistical Summary of the Causes and Cost of Bridge Failures," Report No. FHWA-RD-75-87, *Federal Highway Administration,* September.

CLEAR, K. C., 1980: "Cost Effective Rigid Concrete Construction and Rehabilitation in Adverse Environment," FHWA, *FCP Annual Progress Report,* September, Unpublished, pp. 13–15.

CSAGOLY, P. F. and R. A. DORTON, 1978: "The Development of the Ontario Highway Bridge Design Code," in *Transportation Research Record 665: Bridge Engineering,* vol. 2, TRB, National Research Council, Washington, D.C., pp. 1–12.

DAVIS, R. E., 1969: "Prepakt Method of Concrete Repair," *J. Am. Concrete Institute,* vol. 32, No. 2, August.

DIGEST 264, 1982: "The Durability of Steel in Concrete, Part 2 Diagnosis and Assessment of Corrosion-Cracked Concrete," *Building Research Station,* Garston, Watford, England.

DUTRUEL, F. and R. GUYADER, 1975: "Etude de la Corrosion des Canalisations en Beton," Monograph No. 7, *Center d'Etudes et de Recherches de l'Industrie du Beton Manufacture,* Epernon, June, pp. 55–64.

ESLYN, W. E. and J. W. CLARK, 1979: "Wood Bridges-Decay Inspection and Control," *Agriculture Handbook,* No. 557, Oct., pp. 20–21.

FHWA, 1979: "Bridge Inspector's Training Manual 70," Corrected Reprint, *Federal Highway Administration,* Washington, D.C.

FHWA, 1989: "Recording and Coding Guide for the Structure Inventory and Appraisal of the Nation's Bridges," *Federal Highway Administration,* Dec., Washington, D.C.

GANGARAO, H. V. S., 1978: "Conceptual Substructure Systems for Short-Span Bridges," *Transportation Engineering J.,* ASCE, New York, January.

GLASSGOLD, I. L., 1982: "Repair of Seawater Structures—An Overview," *Concrete International,* vol. 4, No. 3, March, pp. 50–52.

GREEVES, I. S., 1973: "Underwater Concreting," *Civil Engineering and Public Works Review,* vol. 68, No. 806, pp. 788–789.

Greiner Engineering Sciences, Inc., 1983: "Widening and Replacement of Concrete Deck of Woodrow Wilson Memorial Bridge," Session 187 (Modular Bridge Decks), *62nd Annual Transportation Research Board Meeting,* January, p. 16.

GEYMAYR, G. W., 1980: "Repair of Concrete in Tropical Marine Environment," *Performance of Concrete in Marine Environment,* SP-65, ACI, Detroit, pp. 535–538.

HANSON, T. A., 1972: "Systems Bridges Phase Two: Substructure," Feasibility Study for VHTRC, Charlottesville, VA., May.

HENEGHAN, J. I., 1980: "Shotcrete Repair of Concrete Structures in Marine Environment," *Performance of Concrete in Marine Environment,* SP-65, ACI, Detroit, pp. 517–518.

Highway Research Board, 1973: "Highways and the Catastrophic Floods of 1972," *Highway Research Record No. 479,* 11 Reports.

HOPKINS, G. R., R W. VANCE, and B. KASRAIE, 1980: "Scour Around Bridge Piers," Report No. FHWA-RD-79-103, FHWA, February.

HOUSTON, J. T., E. ATIMTAY, and P. M. FERGUSON, 1972: "Corrosion of Reinforcing Steel Embedded in Structural Concrete," Report No. 112-1F, *Center for Highway Research,* Univ. of Texas at Austin, March, p. 15.

JACKSON, F. H., 1932: "Resistance of Concrete to Frost Action as Affected by the Water-Cement Ratio," Proc. Part 1, *11th Annual Meeting of the Highway Research Board,* Washington, D.C., pp. 227–239.

KANNANKUTTY, R. and R. S. MORGAN, 1984: "A Policy/Program Approach to Bridge Rehabilitation Versus Replacement," *1st Intern. Bridge Conf.,* Pittsburgh, PA, June 4–6, pp. 222–227.

KITTREDGE, N. E., 1982: "Bridge Repair and Strengthening," *Master of Science in Civil Engineering Thesis,* W. Virginia Univ., Morgantown, W. Virginia, p. 112.

KLAIBER, F. W., K. F. DUNKER, T. J. WIPF, and W. W. SANDERS, JR., 1987: Methods of Strengthening Existing Highway Bridges," *NCHRP 293,* TRB, Washington, D.C.

LAMBERTON, B., 1969: "Revetment Construction by Fabriform Process," *J. Construction Div.,* ASCE, vol. 95, No. 101, July, p. 49.

LAMBERTON, JR. H. C., A. J. SAINZ, R. A. CRAWFORD, W. B. OGLETREE, and J. E. GUNN, 1981: "NCHRP Synthesis of Highway Practice 88: Underwater Inspection and Repair of Bridge Substructures," TRB, *National Research Council,* Washington, D.C., December, p. 77.

LANE, R. O., 1978: "Abrasion Resistance," *Significance of Tests and Properties of Concrete and Concrete Making Materials,* STP-169B, ASTM Philadelphia, pp. 349–352.

MANNING, D. G., 1985: "Detecting Defects and Deterioration in Highway Structures," *NCHRP 118,* TRB, Washington, D.C.

MANNING, D. G. and D. H. BYE, 1983: "Bridge Deck Rehabilitation Manual, Part 1: Condition Surveys," *Ontario Ministry of Transportation and Communications,* p. 93.

MANUEL, F. S., 1984: "Evaluation and Improvement of Existing Bridge Foundations" Rep. No. FHWA-RD-83-61, *Federal Highway Administration,* Washington, D.C., p. 192.

MCCOLLON, B. F., 1976: "Design and Construction of Conventional Bridge Decks That Are Resistant to Spalling," in *Transportation Research Record 604: Bridge Decks: Corrosion, Cathodic Protection, and Pavement Seals,* TRB, National Research Council, Washington, D.C., pp. 1–5.

MCDONALD, J. E. and T. C. LIU, 1978: "Precast Concrete Elements for Structures in Selected Theater of Operations," *U.S. Army Engineering Waterways Experiment Station,* Vicksburg, Miss., February.

MORGAN, I. L., H. D. ELLINGER, R. V. KLINKSIEK, and J. N. THOMPSON, 1980: "Examination of Concrete by Computerized Tomography," *Journ., ACI,* Vol. 77, No. 1, Jan.–Feb., p. 23.

NCHRP Report 222, 1980: "Bridges on Secondary Highways and Local Roads, Rehabilitation and Replacement," TRB, Washington, D.C.

NCHRP Report 243, 1981: "Rehabilitation and Replacement of Bridges on Secondary Highways and Local Roads," TRB, Washington, D.C.

NCHRP SYNTHESIS OF HIGHWAY PRACTICE 5, 1970. "Scour at Bridge Waterways, p. 37.

Organization for Economic Cooperation and Development, 1976: "Bridge Inspection," Paris, p. 132.

Organization for Economic Cooperation and Development, 1979: "Evaluation of Load Carrying Capacity of Bridges," Paris, p. 129.

PERKINS, P. H., 1977: *Concrete Structures: Repair, Waterproofing and Restoration,* Wiley, New York, p. 190.

POWERS, T. C., 1975: "Freezing Effects on Concrete," *Durability of Concrete,* SP-47, ACI, Detroit, pp. 1–12.

RICHARDSON, E. V. and D. B. SIMONS, 1974: "Spurs and Guide Banks: Open-File Report," *Engineering Research Center,* Colorado State Univ., Fort Collins, Colorado, p. 47.

RISEEL, M. C., D. R. GRABER, M. J. SHOEMAKER, and T. S. FLOURNOY, 1982: "Assessment of Deficiencies and Preservation of Bridge Substructures Below the Waterline," *NCHRP 251,* TRB, Washington, D.C.

ROBERTS, J., 1978: "Manual for Bridge Maintenance Planning and Repair Methods," *Florida Dept. of Transportation,* p. 282.

SHANAFELT, G. O., 1985: "Bridge Designs to Reduce and Facilitate Maintenance and Repair," *NCHRP 123,* TRB, Washington, D.C.

ROTHWELL, E. D. and J. P. BOHAN, 1974: "Investigation of Scour and Protection Around Bridge Piers," *U.S. Army Engineer Waterways Experiment Station,* Vicksburg, Miss., November.

SOLIMAN, M. I., 1985: "Repair of Distressed Reinforced Concrete Columns," *Can. Society for Civil Engineering Annual Conf.,* Saskatoon, Can., May 27–31, pp. 59–78.

STOREY, THOMAS (Engineers) Ltd., 1970: "Acrow Panel Bridge Unit Construction Bridging and Support Systems," London, p. 5.

TRB, 1979: NCHRP Synthesis of Highway Practice 57: "Durability of Concrete Bridge Decks," TRB, *National Research Council,* Washington, D.C., p. 60.

TYLER, I. L., 1964: "Concrete in Marine Environment," *Symp. on Concrete Construction in Aqueous Environments,* ACI SP-8, ACI, Detroit, pp. 2–6.

U.S. Department of Transportation, 1970: Federal Highway Administration, *Bridge Inspector's Training Manual,* U.S. DOT, FHWA, Washington, D.C., p. 181.

WAKEMAN, C. M., J. W. STORER, and O. E. LIDDELL, 1973; "179 Years in Sea Water?" *Materials Protection and Performance,* vol. 12, No. 1, January, p. 14.

WESTERBERG, B., 1980: "Strengthening and Repair of Concrete Structures," ("Forstarkning och reparation av betong-konstrucktioner,") Nordisk Betong, Sweden, No. 1, pp. 7–13 (Swedish).

Welding Design and Fabrication, 1976: "Bridge Under Repair—But Open to Traffic," Reprint, November, p. 1.

WOODS, H., 1968: "Freezing and Thawing," *Durability of Concrete Construction,* ACI, Detroit, pp. 15–20.

XANTHAKOS, P. P., 1981: "Comprehensive Report and Plans," Bridge Carrying Southwest Highway (Ill. 7) over B & O.C.T. RR," Melvina and Stony Creek, Chicago, Illinois.

YOUSHAW, R. and C. DRYER: "Underwater Non-destructive Testing of Ship Hull Welds," *National Research Council,* unpubl., pp. 4–7.

ZUK, W., 1980: "Forecast of Bridge Engineering: 1980–2000," in *Transportation Research Record 785: Bridges, Culverts, and Tunnels, TRB,* National Research Council, Washington, D.C., pp. 1–6.

Index